Preliminary Design Report

November 2007

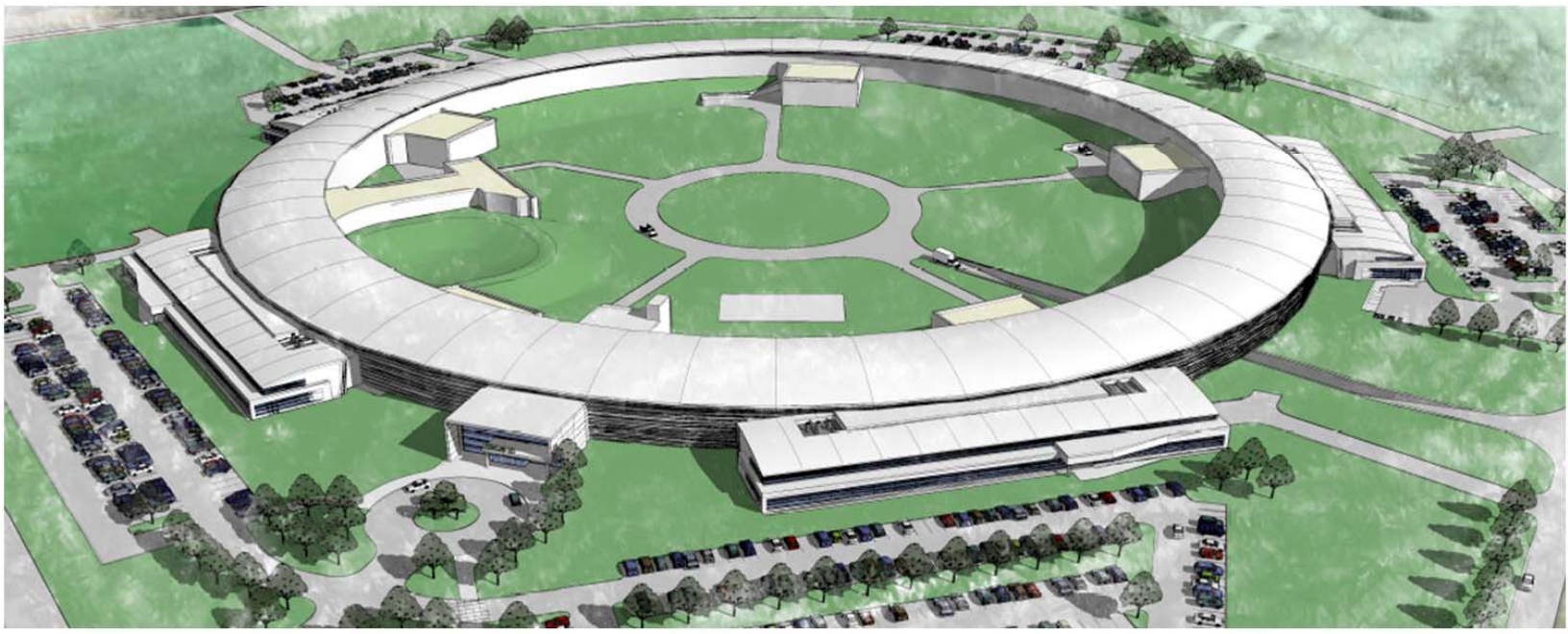

National Synchrotron Light Source II

BROOKHAVEN NATIONAL LABORATORY

CONTENTS

Part 4 Environment, Safety and Health

Chapter 1 Environment, Safety, & Health, and Quality Assurance

Chapter 2 Radiation Safety and Shielding

PROJECT OVERVIEW

1 Introduction

Following the CD0 approval (approval of mission need) of the "National Synchrotron Light Source II" (NSLS-II) during August 2005, Brookhaven National Laboratory prepared a conceptual design for a world-class user facility for scientific research using synchrotron radiation. DOE SC review of the preliminary baseline in December 2006 led to the subsequent CD1 approval (approval of alternative selection and cost range). This report is the documentation of the preliminary design work for the NSLS-II facility. The preliminary design of the Accelerator Systems (Part 1) was developed mostly based of the Conceptual Design Report, except for the Booster design, which was changed from in-storage-ring tunnel configuration to in-external-tunnel configuration. The design of beamlines (Part 2) is based on designs developed by engineering firms in accordance with the specification provided by the Project. The conventional facility design (Part 3) is the Title 1 preliminary design by the AE firm that met the NSLS-II requirements. Last and very important, Part 4 documents the ES&H design and considerations related to this preliminary design.

The NSLS-II performance goals are motivated by the recognition that major advances in many important technology problems will require scientific breakthroughs in developing new materials with advanced properties. Achieving this will require the development of new tools that will enable the characterization of the atomic and electronic structure, chemical composition, and magnetic properties of materials, at nanoscale resolution. These tools must be nondestructive, to image and characterize buried structures and interfaces, and they must operate in a wide range of temperatures and harsh environments.

The NSLS-II facility will provide ultra high brightness and flux and exceptional beam stability. It will also provide advanced insertion devices, optics, detectors, and robotics, and a suite of scientific instruments designed to maximize the scientific output of the facility. Together these will enable the study of material properties and functions with a spatial resolution of ~1 nm, an energy resolution of ~0.1 meV, and the ultra high sensitivity required to perform spectroscopy on a single atom.

In order to meet this need, NSLS-II has been designed to provide world-leading brightness and flux and exceptional beam stability. The brightness is defined as the number of photons emitted per second, per photon energy bandwidth, per solid angle, and per unit source size. Brightness is important because it determines how efficiently an intense flux of photons can be refocused to a small spot size and a small divergence. It scales as the ring current and the number of total periods of the undulator field (both of which contribute linearly to the total flux), as well as being inversely proportional to the horizontal and vertical emittances (the product of beam size and divergence) of the electron beam. Raising the current in the storage ring to obtain even brighter beams is ultimately limited by beam-driven, collective instabilities in the accelerator. Thus, to maximize the brightness, the horizontal and vertical emittances must be made as small as possible.

With the concept of using damping wigglers, low-field bending magnets, and a large number of lattice cells to achieve ultra small emittance, the performance of NSLS-II will be nearly at the ultimate limit of storage ring light sources, set by the intrinsic properties of the synchrotron radiation process. The facility will produce x-rays more than 10,000 times brighter than those produced at NSLS today. The facility, with various insertion devices, including three-pole-wigglers and low-field dipole radiations, has the capability of covering a broad range of radiation spectra, from hard x-ray to far infra-red. The superlative character and combination of capabilities will have broad impact on a wide range of disciplines and scientific initiatives in the coming decades, including new studies of small crystals in structural biology, a wide range of nanometer-resolution probes for nanoscience, coherent imaging of the structure and dynamics of disordered materials, greatly increased applicability of inelastic x-ray scattering, and properties of materials under extreme conditions.

Commissioned in 1982, the existing National Synchrotron Light Source (NSLS) provides essential scientific tools for 2,300 scientists per year from more than 400 academic, industrial, and government institutions. Their myriad research programs produce about 800 publications per year, with more than 130 appearing in premier journals. It was designed in the 1970s and is now in its third decade of service. It has been continually upgraded over the years, with the brightness increasing fully five orders of magnitude. However, it has reached the theoretical limits of performance given its small circumference and small periodicity, and only a small number of insertion devices are possible. For the productivity of the large NSLS user community to continue and even increase, and in order to tackle the "grand challenge" problems of tomorrow, it is essential that NSLS be upgraded to provide much higher average brightness and higher flux.

The combination of brightness, flux, and stability of NSLS-II will provide the world's finest capabilities for x-ray imaging. NSLS-II will enable the study of materials with ~1 nanometer (nm) spatial resolution and with ~0.1 milli-electron volt (meV) energy resolution. It will be possible to focus both soft and hard x-rays to a spatial resolution of ~1 nm and to perform spectroscopy on a single atom. With the development of novel "lens-less" imaging, it will be possible to capture x-ray images with a spatial resolution of ~1 nm. This resolution and sensitivity is unprecedented in x-ray imaging. If there is any doubt that this is needed for our future energy security, one only need remember that all the elementary steps of energy conversion (charge transfer, molecular rearrangement, and chemical reactions), both for fossil fuels and for critical renewable energy sources, take place on the nanoscale, and many of these steps involve a combination of complex physical, chemical, and often biological, transformations.

The unique characteristics of NSLS-II will enable exploration of the scientific challenges faced in developing new materials with advanced properties. These challenges include exploringthe correlation between nanoscale structure and function— investigatingthe profound effects of confinement, finite size, and proximity; the mechanisms of molecular self-assembly, which produces exquisite molecular structures in both the living and nonliving worlds; and the science of emergent behavior, one of the grand scientific challenges.

2 Scope

The project scope includes the design, construction, installation, and commissioning of the accelerator hardware, civil construction, and central facilities required to produce a new synchrotron light source. It includes a highly optimized electron storage ring, full energy injector, experimental beamlines and optics, and appropriate support equipment, all housed in a new building. Specifically, the main scope elements include:

- an electron gun and a short linac, where an electron beam is generated and accelerated to 200 meV
- the transport system to the booster
- the booster ring, where the electrons from the linac are accelerated to 3 GeV for injection into the main storage ring
- the transport system to the main storage ring
- the main storage ring, where a 500 mA current of electrons is stored at an energy of 3 GeV and sent through insertion devices and bend magnets to produce synchrotron radiation
- a suite of initial beamlines and supporting instrumentation
- the ring building, operations center, auxiliary lab office buildings, and mechanical equipment rooms, comprising the conventional facilities and supporting utility infrastructure

3 Capabilities

NSLS-II is a synchrotron with a highly optimized design that will be capable of producing world-leading levels of brightness and flux and small beams, over a very broad energy range, extending from the far IR to the very hard x-ray region. The main performance characteristics are given in Table 1.

Table 1 Main Performance goals of the NSLS-II Storage Ring.

Electron energy [GeV]	3.0
Stored current [mA]	500
Stability of average current [%]	<1
Horizontal emittance [nm-rad]: Baseline	1.0
Horizontal emittance [nm-rad]: Fully Built-out	0.6
Vertical emittance [nm-rad]	0.008
Average brightness [ph/s/0.1%bw/mm^2/mrad^2] in the 2keV to 10keV photon energy range	>10^{21}
Average flux [ph/s/0.1%bw] in the 2keV to 10keV photon energy range	>10^{16}
Horizontal electron beam size [μm]: Baseline	42
Horizontal electron beam size [μm]: Fully Built-out	32
Horizontal electron beam divergence [μrad]: Baseline	22
Horizontal electron beam divergence [μrad]: fully Built-out	16
Vertical electron beam size [μm]	3.2
Vertical electron beam divergence [μrad]	2.5
Stability of electron beam in position, size, and direction [%] of beam size or divergence	<10
Number of straight sections for insertion devices	27
Number of bend magnet sources	30

4 Work Breakdown Structure

The NSLS-II project has been organized into a Work Breakdown Structure (WBS). The WBS contains a complete definition of the project's scope and forms the basis for planning, executing, and controlling project activities. The Project WBS is shown in Figure 1. Elements are defined as specific systems/deliverables (WBS 1.3–1.5), project management (WBS 1.1), research and development (WBS 1.2) or pre-operations (WBS 1.6), consistent with discrete increments of project work and the planned method of accomplishment.

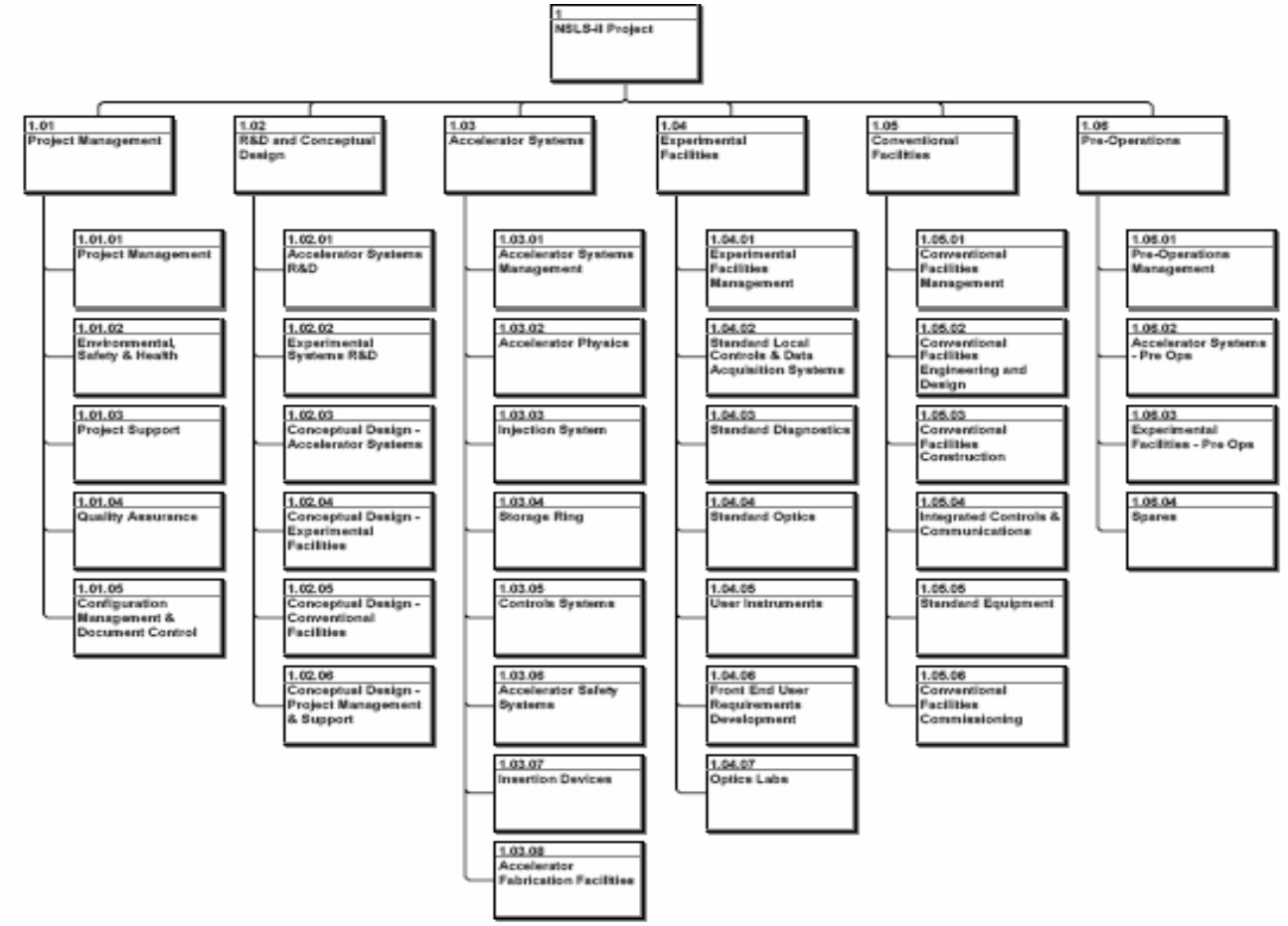

Figure 1 Work breakdown structure for the NSLS-II project:

1.01 Project Management – Project Office administrative and management activities that integrate across the entire project (management, regulatory compliance, quality assurance, safety, project controls, etc.)

1.02 Research and Development – R&D activities as necessary to support the delivery of project objectives

1.03 Accelerator Systems – All phases of design, procurement, installation, and commissioning of the accelerator systems

1.04 Experimental Facilities – All phases of design, procurement, installation, and commissioning of the suite of beamlines and instruments included in the project scope

1.05 Conventional Facilities – All phases of design, procurement, installation, and commissioning of the conventional facilities including preparation of the site and provision of all utility systems

1.06 Pre-Operations – Materials, equipment, services, etc. for integrated testing and commissioning

5 Cost and Schedule

The Total Estimated Cost (TEC) of NSLS-II is $785.4M. The Total Project Cost (TPC) is $896.2M. The schedule for construction will lead to start of operations in FY2014.

A preliminary high-level summary of the cost of the NSLS-II project, at the second level of the work breakdown structure, is given in Table 2.

Table 2 Level 2 Cost Breakout for the NSLS-II Project (fully burdened).

NSLS-II Level 2 Cost Element	Cost (AY $M)
1.1 Project Management and Support	52.5
1.3 Accelerator Systems	239.5
1.4 Experimental Facilities (includes contingency)	69.3
1.5 Conventional Facilities	240.8
Contingency (35% of TEC cost elements excl. Exp. Facilities)	183.3
NSLS-II Total Estimate Cost (TEC)	785.4
1.2 R&D	60.6
1.8 Pre-operations	50.2
Total Other Project Costs	110.8
NSLS-II Total Project Costs (TPC)	896.2

A preliminary Level 0 milestone schedule to construct NSLS-II is shown in Table 3.

Table 3 Preliminary Level 0 Milestone Schedule.

Major Milestone Events		Preliminary Schedule
CD-0	(Approve Mission Need)	4th Qtr, FY2005
CD-1	(Approve Alternative Selection and Cost Range)	3rd Qtr, FY2007
CD-2	(Approve Performance Baseline)	4th Qtr, FY2008
CD-3	(Approve Start of Construction)	2nd Qtr, FY2009
BOD of Experimental Floor Space		2nd Qtr, FY2012
CD-4	(Approve Start of Operations)	3rd Qtr, FY2015

6 Acquisition Strategy

The acquisition strategy relies on Brookhaven Science Associates (BSA), the Department of Energy Managing and Operating (M&O) contractor for Brookhaven National Laboratory, to directly manage the NSLS-II acquisition. The design, fabrication, assembly, installation, testing, and commissioning for the NSLS-II project will be largely performed by the BNL/NSLS-II scientific and technical staff. Much of the subcontracted work to be performed for NSLS-II consists of hardware fabrication and conventional facilities construction.

1 ACCELERATOR OVERVIEW

This chapter describes the main requirements and features of the NSLS-II accelerator complex, focusing on the philosophy and the approach used to select the NSLS-II ring lattice, injection scheme, and main components. Based on the considerations presented here, we believe we have arrived at an optimal, or near-optimal, design. This description is brief, and important details of the individual systems and subsystems are presented in other chapters of this preliminary design report.

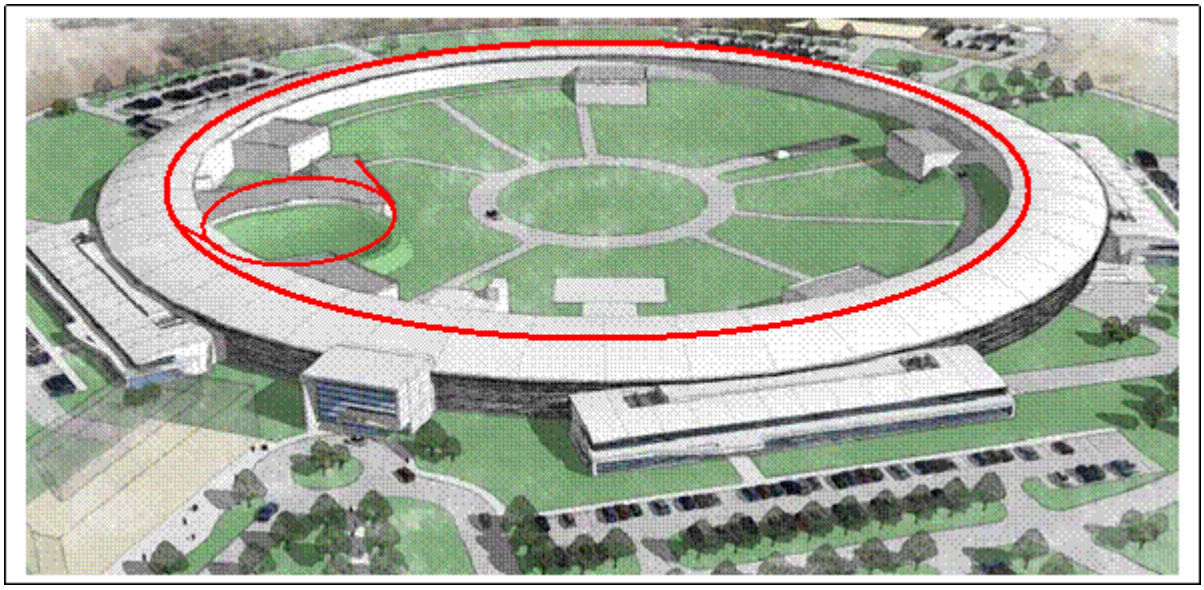

Figure 1.1.1 Schematic layout of the NSLS-II accelerators: a 200 MeV linac, a 3 GeV booster ring, and the 3 GeV storage ring.

1.1 Scope of the Accelerator Complex

NSLS-II is designed to deliver photons with average spectral brightness in the 2 keV to 10 keV energy range exceeding 10^{21} ph/mm^2/mrad^2/s/0.1%BW. The spectral flux density should exceed 10^{15} ph/s/0.1%BW in all spectral ranges and with a peak value approaching 10^{16} ph/s/0.1%BW for photon energies around 2 keV. This cutting-edge performance requires the storage ring to support a very high-current electron beam (I = 500 mA) with sub-nm-rad horizontal emittance (down to 0.5 nm-rad) and diffraction-limited vertical emittance at a wavelength of 1 Å (vertical emittance <8 pm-rad). The electron beam will be stable in its position (<10% of its size), angle (<10% of its divergence), dimensions (<10%), and intensity (±0.5% variation). The latter requirement provides for constant thermal load on the beamline front ends.

A schematic layout of the NSLS-II accelerators is shown in Figure 1.1.1. Electrons generated in the linac are accelerated to 3 GeV in the booster. The accelerated electrons are periodically added to the electron beam circulating in the storage ring to keep the stored current nearly constant in time, a process know as top-off injection. This chapter presents the main parameters of the accelerator systems and main subsystems for NSLS-II and descriptions of the considerations and process that led to their optimization.

1.1.1 Physics Design and Parameters of NSLS-II

1.1.1.1 Storage Ring

Everywhere possible, NSLS-II will use known, reliable, and cost-effective solutions for its subsystems. Examples of such subsystems extend from a simple low-energy linac to the ring and booster RF systems, which are commercially available. Subsystems that are not critical to NSLS-II performance will be based on the simplest, most robust, and best-proven technologies. Hence, all magnetic elements of the accelerators have a significant margin in their design, but are not over-designed. Only the few subsystems that are crucial for attaining the ultimate NSLS-II performance require cutting-edge technologies and engineering solutions.

The overall layout of the storage ring and beamlines is shown in Figure 1.1.2 and in more detail in Figure 1.1.3. The chosen lattice meets the challenge to provide record-low electron beam emittance. The choice of large-radius bending magnets enhances the effectiveness of damping wigglers to reduce the emittance. The lattice is optimized to meet the required performance within budget and size constraints.

As described in this chapter, the optimized storage ring lattice consists of 30 DBA cells, with straight sections alternating in length between 6.6 m and 9.3 m. There are thus 15 super-periods for the lattice. The lattice functions of one DBA cell (one half super-period) are shown in Figure 1.1.4. Each straight section is achromatic and has three quadrupoles at each end. These quadrupoles provide for appropriate matching of the optic functions (β_x, α_x and β_y, α_y) and tune advances ($\Delta\nu_{x,y}$) in the straights to compensate the strong influence of the IDs on the linear lattice [1.1.1].

In order to accommodate a number of three-pole wigglers as additional sources of hard x-rays, a 0.6-m long straight was inserted at the down steam end of all dispersion sections. In order to maintain the symmetry of these dispersion straights, the same empty spaces were also added at the up stream end of the section. Although insertion of TPWs in these non-achromatic sections will impact the effort of reducing the emittance, the impact is estimated to be about 10% for 15 such insertions around the rng.

The total number of quadrupoles per cell is 10. Each cell also has three chromatic sextupoles and seven geometric sextupoles. All quadrupoles in the SR will have individual power supplies, which will be fully utilized for high-precision, beam-based alignment and for experimental verification and correction of the linear electron optics [1.1.2]. The sextupoles will be powered by family in each pentant The main parameters of the storage ring are summarized in Table 1.1.1.

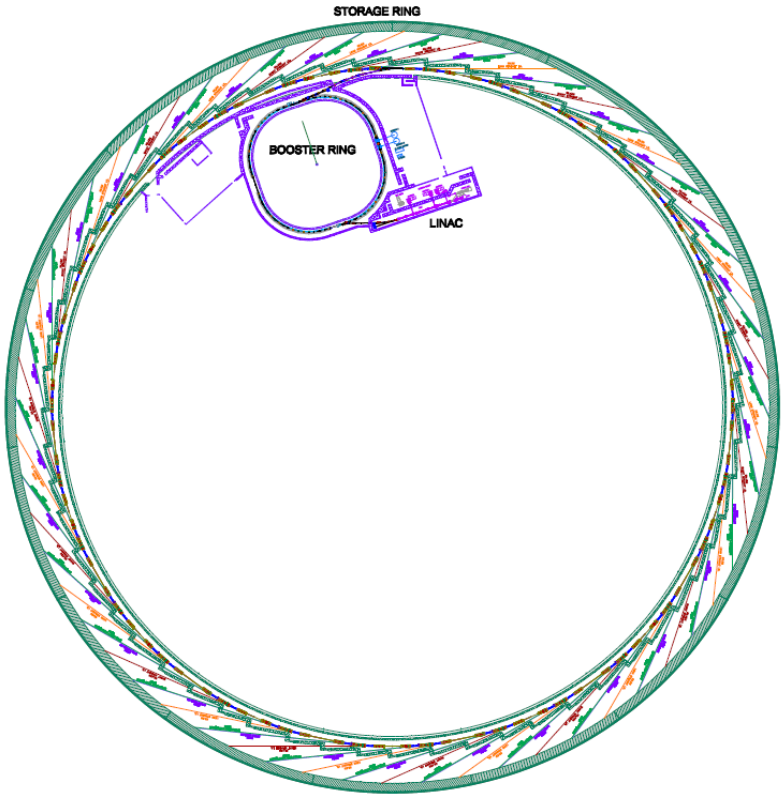

Figure 1.1.2 Geometry of the NSLS-II light source and its beamlines; green and purple lines indicate beamlines from the Three Pole wiggler and dipole, and orange and brown lines indicate those from long and short ID straights.

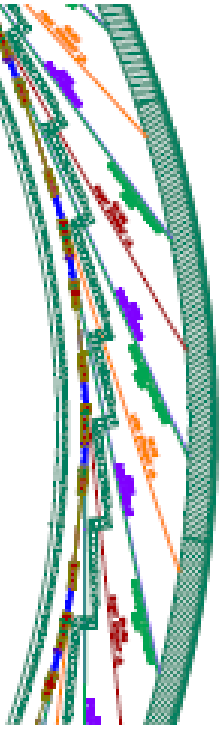

Figure 1.1.3 Three DBA cells (one and a half super-periods) with short (6.6 m) and long (9.3 m) straight sections.

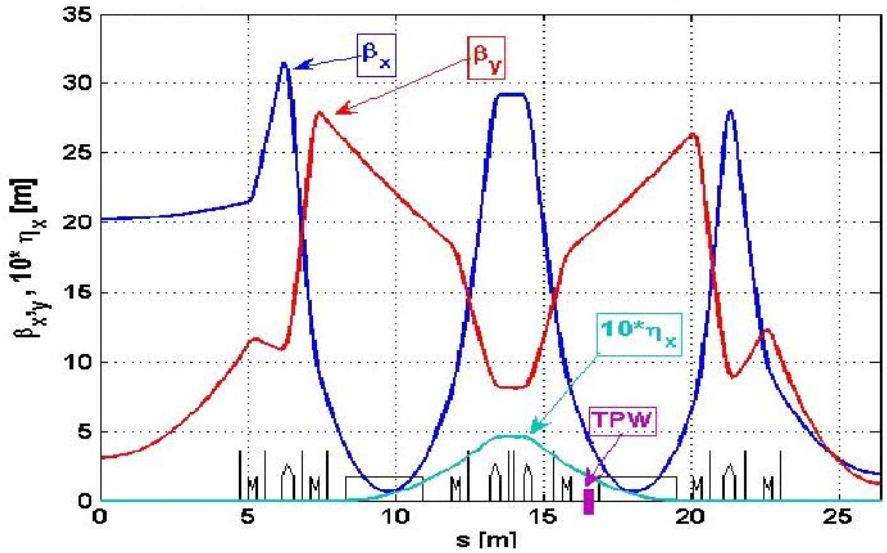

Figure 1.1.4 Lattice functions of half of an NSLS-II storage ring super-period.

Table 1.1.1 Basic Parameters of the NSLS-II Storage Ring

Energy [GeV]	3
Circumference [m]	792
Number of DBA cells	30
Number of 9.3 m straights	15
Beta-functions in the center of the 9.3 m straights: β_x, β_y [m]	21, 3.0
Number of 6.6 m straights	15
Beta-functions in the center of the 6.6 m straights: β_x, β_y [m]	2.0, 1.0
Number of dipoles	60
Number of quadrupoles	300
Number of sextupoles	300
Circulating current at 3 GeV, multi-bunch [mA]	500
Radio frequency [MHz]	499.68
Harmonic number	1320
Number of bunches at 80% fill	1040
Nominal bending field at 3 GeV [T]	0.4
Dipole critical energy at 3 GeV [keV]	2.4
Total Bending magnet radiation energy loss [keV]	286.4
Radiation energy loss per damping wiggler [keV]	129.3
Vertical emittance [nm-rad]	0.008
Horizontal emittance of bare lattice [nm-rad]	2.0
Horizontal emittance with three 7 m 1.8 T damping wigglers [nm-rad]	1.0
Horizontal emittance with eight 7 m 1.8 T damping wigglers [nm-rad]	0.6
Momentum compaction factor	3.7×10^{-4}
Bunch length, RMS, natural [mm, ps]	2.9, 10
Energy spread, RMS	0.05 –0.1%

The 3 GeV storage ring is designed to be a reliable light source of hard and soft x-rays with average spectral brightness and flux in the target energy range from ~10 eV to ~20 keV, significantly exceeding all synchrotron light sources currently operating or under construction. All of its components are designed with an operational safety margin of ~10%. The parameters of the magnets and their tolerances are specified in Section 7.1. None of the magnet parameters goes beyond well-established standards. The stability and alignment requirements are challenging but achievable (Section 6.1.2.4), as demonstrated at the Swiss Light Source. To achieve these tolerances, the clusters of quadrupoles and sextupoles will be assembled on individual girders, as shown in Figures 1.1.5 and 1.1.6. Their magnetic centers will be aligned precisely with respect to the girder fiducials using the vibrating wire technique. The pre-aligned girders will then be moved into the ring tunnel and installed. The alignment tolerances between girders (~100 microns) are less critical than between individual elements (~30 microns).

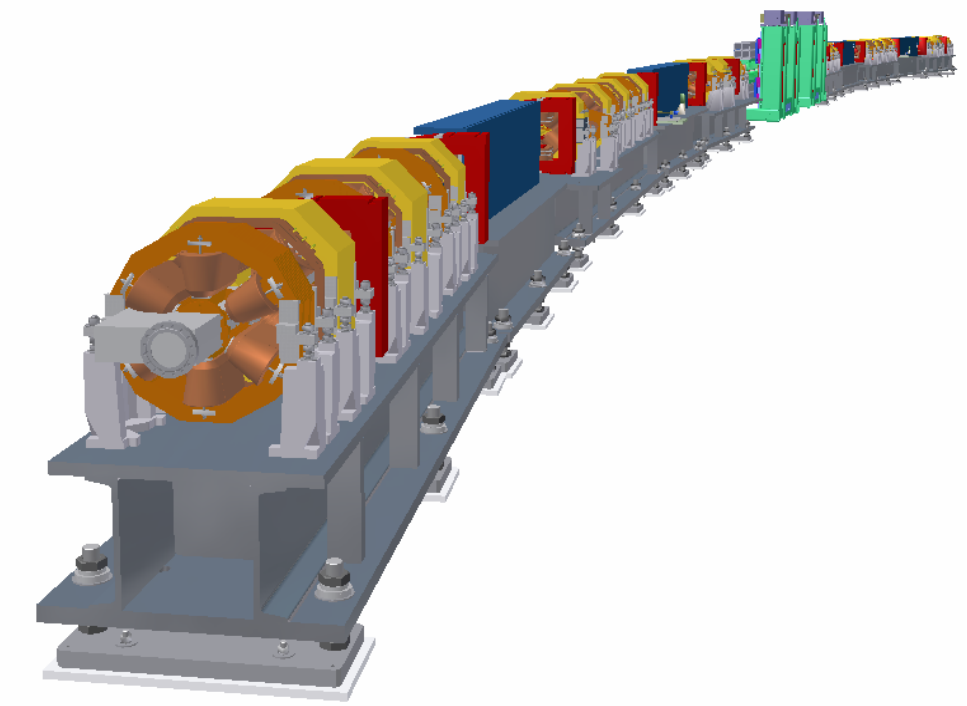

Figure 1.1.5 3D-view of the SR super-period comprised of two DBA cells and two straight sections (half of the 9.3 meter straight is shown at each end). The super-period has bilateral symmetry with respect to the center of the long or short straight section.

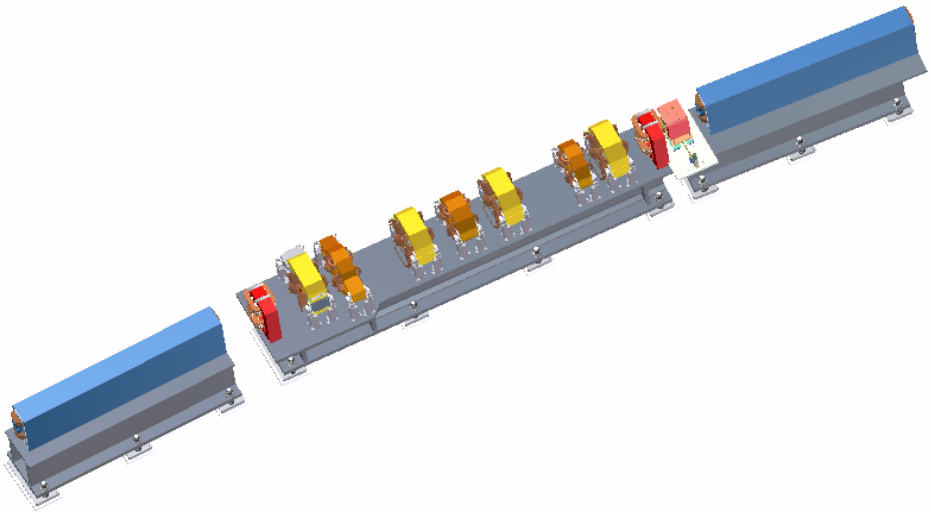

Figure 1.1.6 3D view of a standard DBA cell with bilateral symmetry. It consists of two dipoles, four quadrupoles, and five sextupoles. All quadrupoles and sextupoles are located on a single low-height rigid girder.

The girders are designed with natural resonant frequencies >50 Hz to avoid amplification of low-frequency floor vibrations. The orbit feedback system will damp beam motion at frequencies below 100 Hz keeping the orbit motion below 10% of the electron bunch transverse dimensions.

The necessity for relatively long lifetime and large dynamic aperture require the very nonlinear, sextupole-dominated, ultra low emittance SR lattice to be very robust and capable of tolerating manufacturing and installation errors. Furthermore, the presence of high-field and short-period undulators at the relatively low energy of the SR imposes an additional, very strong nonlinear component on the lattice, which changes when users change the undulator gaps. The three quadrupole families per ID provide the capability of minimizing the linear impact of these IDs, maintaining to a high degree the corrected nonlinear dynamics behavior of the beam.

The NSLS-II storage ring will be equipped with a full set of beam diagnostics and feedbacks necessary for prompt commissioning and reliable operation of this cutting-edge facility. The diagnostics will monitor

closed beam orbit position, tunes, beam current and lifetime, filling pattern, beam emittances, bunch length, positions of the photon beam in insertion devices, coherent bunch instabilities, and distribution of beam losses around the ring. It will allow for the measurement and study of parameters for the linear and nonlinear optics (including lattice functions, chromaticities, local and global coupling, momentum compaction, and magnet and RF system parameters [1.1.2]), to measure the beam energy spread as well as impedances of vacuum chambers, and to use beam-based alignment relative to the quadrupoles and sextupoles. Beam diagnostics and feedbacks will include at least the following:

- two high-precision DCCTs and two bunch-to-bunch current monitors
- beam position monitors (six BPMs with sub-μm sensitivity per cell plus two BPMs per each installed ID, with average and single turn capabilities) plus photon BPMs (1-2 per ID) paired with 120 fast orbit correctors with stainless steel chambers and 60 slow orbit correctors with aluminum chambers.
- a set of fast correctors with feedback bandwidth of 100 Hz may be provided for each ID
- monitors of both transverse tunes and synchrotron tunes
- diagnostic undulator equipped to monitor horizontal and vertical emittances of electron beam (not in baseline)
- dual-sweep streak-camera with picosecond resolution for measuring the bunch length
- beam loss monitors

All the diagnostics listed above are non-interceptive. A few interceptive diagnostics (such as flags) will be used for commissioning purposes. (See complete descriptions in Section 7.8.)

NSLS-II will use CESR-B type superconducting RF (SRF) 500 MHz cavities. In addition, passive cavities operating at the 3rd harmonic (1.5 GHz) will be used to increase the bunch length and improve the beam lifetime. Initially, the RF system will be comprised of two 500 MHz cavities and a single harmonic cavity installed in a 9.3 m straight section. A single 310 kW klystron amplifier will drive each of the main ring cavities through a 350 kW rated circulator and load (see Section 7.5 for further detail on the RF system and its cryogenics). When the facility is fully built out with insertion devices, two additional RF cavities (for a total of four) and one additional harmonic cavity (for a total of two) will be required. These additional devices will occupy one additional 9.3 m straight section.

Of the 1,320 RF buckets, only 80 to 90% will be filled. The remaining buckets will stay empty, providing a clearing gap (or gaps) for ions. Because of nonuniform beam loading in the Landau cavity, the presence of the ion clearing gap (or gaps) impacts the bunch lengths and hence the Touschek beam lifetime (see detailed discussion in Section 6.2.7).

1.1.1.2 Injection System

Due to the relatively short lifetime of the electron beam with the goal of ~3 hours, full-energy top-off injection is required. Injections will be very brief (milliseconds) and occur about once per minute. In contrast with the previous generation of light sources based on high-energy storage rings, the short lifetime of NSLS-II means that it cannot perform at its target level if the injector is not readily available. Thus, it is imperative that the injector be a very robust and reliable device. This requirement led to the selection of a full energy booster for the injector and placement of the storage ring septum and kicker magnets in the injection straight which has been carefully designed to minimize deflection of the stored electron beam.

Layout of the injection system is shown in Figure 1.1.7. It consists of a 200 MeV linac in its own shielding enclosure, linac to booster beam transport lines, 3 GeV booster in its own tunnel, booster to storage ring beam transport line, and the injection straight that is part of the storage ring. The main parameters of the injector are given in Table 1.1.2 and a detailed description is given in Chapter 5. A 200 MeV linac with thermionic triode electron gun will serve as the injector for the booster. For straightforward commissioning and reliable operation, the injector will be equipped with a full set of beam diagnostics (DC and fast current transformers, 29 BPMs, 17 fluorescent flags, and streak-camera).

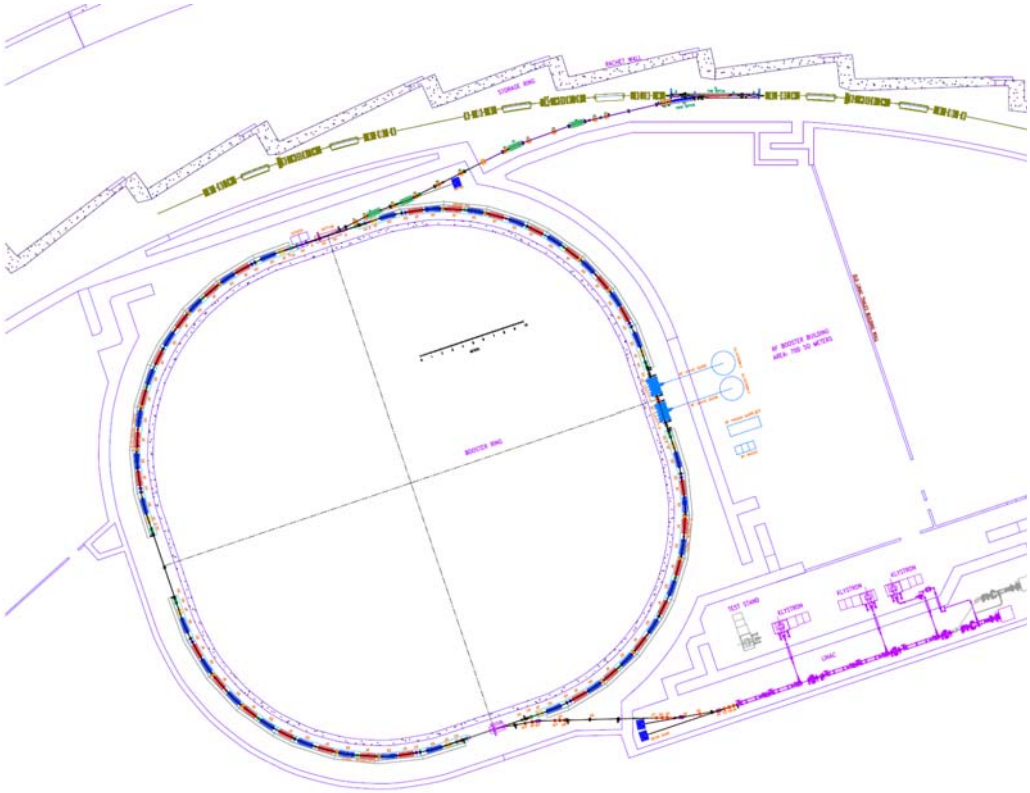

Figure 1.1.7 Schematic layout of the full energy booster.

Table 1.1.2 Main Parameters of the NSLS-II Injector

Linac	
Nominal linac energy [MeV]	200
Frequency [GHz]	2.998
Pulse repetition rate [pps]	1
Pulse charge [nC]	15
Booster	
Injection energy [MeV]	200
Nominal booster energy [GeV]	3
Circumference [m]	258.4
Ramping repetition rate [Hz]	1
Acceleration time [sec]	~0.4
Radio frequency [MHz]	499.68
Total number of superperiod	4
Total number of bending magnets (combined function)	60
Total number of quadrupoles	24
Energy loss per turn at 3 GeV [MeV]	0.625
Natural emittance at 3 GeV [nm-rad]	26.6

The booster RF system (Section 5.8) will be based on five-cell "PETRA" (room temperature, copper) cavities that will provide 1.2 MV accelerating voltage, which is sufficient for the acceleration and required energy acceptance.

1.1.1.3 Photon Sources

The NSLS-II storage ring has 27 straight sections available for insertion devices (one 9.3m straight section will be used for the injection and two for the RF system). A 9.3m straight section can also accommodate two short undulators whose radiation is separated by a local angular bump (so-called canting). NSLS-II will host a variety of different types of undulators and wigglers that will generate high brightness and high flux beams of hard and soft x-rays. A full description of these IDs and their performance, together with that of the bending magnets, is given in Chapter 8. The storage ring lattice is designed to withstand the influence of a complete set of insertion devices set to arbitrary gap (field) values in the fully developed facility (see Section 6.1.2.8).

NSLS-II will use damping wigglers (see Section 1.2) for two purposes [1.1.3]:

1. to reduce horizontal beam emittance to the desired level while minimizing the number of cells of the lattice and thus the circumference (and cost) of the storage ring
2. to serve as broadband sources of very bright and high flux x-rays superior to conventional bend-magnet sources

1.1.1.4 Mechanical Design and Magnets

Many of the mechanical designs for NSLS-II are now conventional technology for third-generation light sources. Most of the NSLS-II storage ring uses extruded aluminum vacuum chamber. Short stainless steel bellows (about 15 cm) provide space for fast feedback orbit correctors. This vacuum chamber allows for in-situ bakeout to 130°C using pressurized hot water circulated within the cooling water channel of the Al profile. Synchrotron radiation is either extracted to a user beamline or intercepted by a localized water-cooled copper absorber (see Section 7.4). All bellows in the storage ring vacuum chamber will be RF shielded to provide low impedance and low losses. The most complex are the vacuum chambers for the insertion devices, especially those for in-vacuum undulators with flexible transitions. These devices are described in Section 7.4.3. Vacuum pressure of 1×10^{-9} Torr will be provided by 240 ion vacuum pumps, 180 titanium sublimation pumps, and about 250 NEG pumps distributed around the ring, IDs, and front ends. The ring vacuum system will have 90 gate valves. The pressure and the residual gas content in the storage ring will be monitored by 270 ion gauges and by 104 residual gas analyzers.

The main parameters of the magnets for the booster and storage ring are discussed in detail in Sections 5.6 and 7.1, respectively. A number of pulsed elements (kickers and septa) are also used in NSLS-II, as described in Sections 5.9 and 7.6.2.2.

Among the most challenging requirements are those associated with the precise alignment of magnetic elements in the storage ring. Another challenge is the design of the girder system, which must be as rigid as possible to reduce vibration of the elements that results in low-frequency noise in the position and angle data from the x-ray beams. The solutions for these challenging problems are described in Section 7.2.

1.2 Optimization of the NSLS-II Design

The pre-conceptual design of NSLS-II [1.2.1] was based on 24 triple-bend achromatic cells (TBA24) with a circumference of 630 m. Further extensive studies [1.2.2] demonstrated that this lattice, with a horizontal emittance of 1.5 nm-rad, was not robust. The dynamic aperture for this lattice collapsed in the presence of realistic errors. Further studies explored possibilities of various lattices (DBA vs. TBA), radii of curvature, and circumferences, as well as damping wigglers.

The performance goals for the current NSLS-II lattice, including the effects of all realistic errors and of small gap undulators, are listed in Table 1.2.1. They are based on analyzing alternative designs for NSLS-II

and on the experience of the most advanced operational mid-energy light sources (such as the Swiss Light Source [1.2.3]).

Table 1.2.1 Goals for the NSLS-II Lattice

Beam lifetime [hours]	~3
2D dynamic aperture [mm-mrad] [2]	~25 x 25
Energy aperture [%]	~±3
Horizontal emittance at 3 GeV with 21 m damping wigglers (baseline) [nm-rad]	~0.9
Horizontal emittance at 3 GeV with 56 m damping wigglers (fully builtout) [nm-rad]	~0.6
Horizontal geometrical aperture for injection [mm]	~±20

Sextupole-dominated lattices of modern low-emittance synchrotron light sources are intrinsically non-linear and do not allow the traditional approach of designing a linear lattice and later retrofitting it with the appropriate number of sextupole families. Instead, nonlinear aspects of the lattice must be addressed from the very beginning of the lattice design through continuous iterations of both linear and nonlinear elements. Furthermore, for convergence of these iterations to a robust (i.e., operational) lattice, the following decisions are vital: the number and locations of beam position monitors (BPMs) and correctors, target BPM accuracy, the scheme for orbit correction, and methods for beam-based alignment. Details on the process of selecting an operational lattice for NSLS-II are in Section 6.1.

This process of proper lattice design is labor intensive and lengthy. As a result, only a very limited number of lattices can be studied in sufficient detail. To streamline the NSLS-II design process and to avoid dead ends such as the "zero-dynamic aperture desert," the restrictions given in Table 1.2.2 were imposed on the choices for the lattice cell in the presence of realistic errors and IDs.

Table 1.2.2 Restrictions on the NSLS-II Linear Lattice Design

Chromaticity per cell, ξ_x	≤ 3
Maximum β-functions [m]	≤ 30
Maximum η-functions [m]	>0.3
Maximum β-beating: $\Delta\beta_x/\beta_x$, $\Delta\beta_y/\beta_y$ [%]	≤5%, ≤1%
Maximum tune-spread per cell: $\Delta\nu_x$, $\Delta\nu_y$	<0.05, <0.002
Transverse alignment accuracy of quadrupoles, sextupoles and BPMs [μm]	±30
Roll-off errors for quadrupoles, sextupoles and BPMs [mrad]	≤ 0.5

Within the framework above, the following design philosophy was pursued to attain sub-nm horizontal emittance for NSLS-II:

- use a lattice with reasonable natural emittance (~2 nm-rad) and robust dynamic aperture
- keep achromatic conditions in the straight sections so IDs reduce emittance, and also to avoid additional nonlinear 3D driving terms
- use damping wigglers to reduce emittance
- limit total losses of synchrotron radiation to 1 to 2 MeV per turn to limit electrical power consumption
- increase bending radius to maximize impact of damping wigglers while keeping emittance under control
- monitor the cost

Using a larger radius for the bending magnets causes a modest increase in the ring's circumference and some increase in the maximum dispersion, resulting in reduced sextupole strengths. Our studies showed that it is possible to keep the bare emittance under control while increasing the bending radius of the dipole magnets.

Increasing the bending radius reduces the dipole field ($B_o = pc/e\rho_o$) and (in the case of the same coil cross-section) reduces the power consumption.

The approach of using damping wigglers to achieve low horizontal emittance has been used previously in accelerators designed for high energy physics, but it has not been widely used for light source designs. Usually the use of damping wigglers is associated with large synchrotron radiation losses and large consumption of RF power. This is not the case for NSLS-II – the use of a large bending radius proportionately reduces the radiation losses from both the bending magnets (U_{bends}) *and* the damping wigglers. This is a unique feature of the NSLS-II design. The emittance for a given total loss per turn from synchrotron radiation (U_{total}), i.e., for a given RF power, decreases with the increase of the radius of curvature:

$$\varepsilon_{nat} \cong \varepsilon_{bare} \cdot \frac{U_{bends}}{U_{total}};\ U_{bends} \cong 88.5\left[keV\right] \cdot \frac{E^4\left[GeV\right]}{\rho_o[m]}, \qquad U_{bends}(@3GeV) \cong \frac{7.17\left[MeV\right]}{\rho_o[m]} \tag{1.2-1}$$

where ε_{bare} is the emittance of the bare lattice (without wigglers) and ε_{nat} is the natural emittance in the presence of damping wigglers [1.2.4].

This approach to emittance control is straightforward and has a rather modest effect on the vertical dynamic aperture (see Section 6.1). The fact that the damping wigglers at NSLS-II will be also very bright, high-intensity sources of broadband x-rays makes this approach even more attractive.

Using this design approach, two promising lattices, the TBA24 (bending radius of 18 m) and the DBA32 (bending radius of 15.3 m), emerged in the early stages of the conceptual design development. Both lattices at the time of consideration had circumference ~750 meters with bare natural horizontal emittance between 1.8 and 2 nm-rad. Both could go well below 1 nm-rad with the use of damping wigglers and clearly indicated a potential for robustness.

A key advantage of lattices based on a DBA cell compared to a TBA cell is that, for lattices with comparable bare emittance, the DBA cell allows significantly more straight sections for user IDs while having a similar number of magnets and circumference. Lattices based on a DBA cell are thus preferred, and further studies were focused on selecting the optimum number of DBA cells.

Table 1.2.3 shows the key parameters used in selecting the optimum size DBA lattice. All lattices considered had a super-period of two cells, with alternating straight section lengths of ≥8 m and ≥5 m, and a bend magnet radius of 25 m (the optimum choice of bend magnet radius is discussed in the next section). A straight section length of ≥8 m is required in order to inject in a single straight, as well as to accommodate two RF cavities and one harmonic cavity in a single straight. The second straight section length of 5 m was chosen as a compromise between having longer IDs and minimizing the storage ring circumference. Shorter straights are also conducive to having smaller beta functions, and hence smaller beam sizes, as discussed in Chapter 6. Achieving very small beam sizes is especially beneficial in enabling the photon beam to be focused down to a 1 nm spot size, as discussed in Chapter 11. As discussed generally in the next section, and shown in Table 6.1.3 and Figure 6.1.3 for the choice of a DBA30 lattice with 25m bend magnet radius, eight 7m-long damping wigglers are sufficient to achieve nearly the full emittance reduction that can be achieved from damping the beam. Thus, eight of the 8m straights are assumed to be occupied by damping wigglers. Table 1.2.3 shows the resulting expected straight section utilization.

As discussed in Chapter 11, the DBA30 lattice will provide nearly the same number of beamlines, when the possibility of canting multiple independent undulators per straight is included, as exist on the present NSLS x-ray and VUV storage rings. This will enable NSLS-II to accommodate a user community comparable in size to that of the existing NSLS. The DBA30 lattice will also achieve nearly the same performance as the

DBA32. We carried out a parametric estimate of the cost savings from reducing the number of lattice cells from 32 to 24, and found a cost reduction of ~$16M (including all burdens, escalation, and contingency) per super-period (two cells). Overall, we find that the DBA30 lattice with a circumference of 780 m provides a good compromise between many competing parameters and goals (cost, length and number of user IDs, and performance). Later the circumference was changed to 792 m in order to adjust the harmonic number to 1,320, which is highly factorizable.

Table 1.2.3 Storage Ring Parameters for Number of DBA Lattice Cells Varying from 32 to 24.

Lattice	DBA32	DBA30	DBA28	DBA26	DBA24
Circumference [m]	822	780	739	697	656
Bend magnet radius [m]	25	25	25	25	25
Straight sections [n x (m)]	16x(8, 5)	15x(8, 5)	14x(8, 5)	13x(8, 5)	12x(8, 5)
Horizontal emittance, ε_x (bare) [nm-rad]	1.7	2.1	2.6	3.2	4.1
Horizontal emittance, ε_x (full set of damping wigglers) [nm-rad]	0.5	0.6	0.7	0.8	1.1
Straight Section Utilization					
8 m straights					
RF and injection	3	3	3	3	3
Damping wigglers	8	8	8	8	8
Undulators	5	4	3	2	1
5 m straights					
Undulators	16	15	14	13	12

1.2.1 Large-Radius Bends and Intrabeam Scattering (IBS) Limits

Following the choice of a DBA30 lattice, studies were carried out to determine the optimum bend magnet radius and number of damping wigglers. As the bare emittance is reduced, it ultimately becomes limited by the effects of intra-beam scattering. Therefore, an important part of our studies was related to the issue of the ultimate IBS-limited emittance for the lattice with fixed synchrotron radiation losses per turn. Even though the detailed calculations of the single and multiple intrabeam scattering on the beam lifetime and the beam emittance were performed using appropriate computer codes (see Section 6.2), the conclusions reached are very similar to those that could be derived using analytical formulae for these processes. Furthermore, such an approach allowed rapid parametric studies and avoidance of multiple, labor intensive trial-and-error lattice designs. Well-known synchrotron radiation integrals for radiation damping and quantum excitation [1.2.4] and the IBS formula for flat electron beam [1.2.5] can be used to calculate the equilibrium energy spread σ_δ and horizontal emittance ε_x:

$$\begin{aligned} \sigma_\delta{}^2 &= \tau_E\left(D_{\delta\ SR} + D_{\delta\ IBS}\right); \quad \delta = \frac{E - E_0}{E_0}; \\ \varepsilon_x\ &= \tau_x\left\langle H \cdot D_{\delta\ SR}\right\rangle + \tau_x\left\langle H \cdot D_{\delta\ IBS}\right\rangle; \\ H &= \frac{1}{\beta_x}\left[\eta_x{}^2 + (\beta_x\eta_x' - \beta_x'\eta_x/2)^2\right] \end{aligned} \tag{1.2-2}$$

where E_o is the energy of the electron beam, E is the energy of individual electrons, and τ_E and τ_x are the damping time of energy (synchrotron) oscillations and horizontal betatron oscillations, respectively. $D_{\delta\,SR}$ and $D_{\delta\,IBS}$ are relative energy diffusion coefficients caused by quantum fluctuations of synchrotron radiation (i.e., causing so-called natural emittance) and by the intrabeam scattering, respectively. The H-function is the well-known connection between emittance growth and the energy diffusion coefficients.

The energy diffusion induced by IBS can be expressed in the following terms:

$$D_{\delta\ IBS} = \frac{N_e r_e^2 c}{2^5 \pi \gamma^3 \varepsilon_x \sqrt{\varepsilon_y \beta_y(s)}\sigma_s} f(\chi_m(s)); \quad f(\chi_m) = \int_{\chi_m}^{\infty} \frac{d\chi}{\chi} \ln\left(\frac{\chi}{\chi_m}\right) e^{-\chi};$$

$$\chi_m = \frac{r_e m^2 c^4}{b_{\max} \Delta E_{acc}^{\ 2}}; \quad b_{\max} \cong n^{-1/3}, \tag{1.2-3}$$

where $\gamma=E_o/mc^2$ is the relativistic factor of the electron ($\gamma \approx 6{,}000$ for 3 GeV electrons), $N_e = I/N_b/e$ is the number of electrons per bunch, m is the mass and r_e is the classical radius of an electron, c is the speed of light, and σ_s is the electron bunch length. $f(\chi_m)$ is the scattering integral depending on the following parameters: ΔE_{acc} is the energy acceptance (in the location of scattering) and n is the density of electrons (see [1.2.5] for details of the definition). As shown in Figure 1.2.1, this function depends very slowly (logarithmically) on its parameter χ_m. For the case of NSLS-II, variations of horizontal emittance (by an order of magnitude, from 0.2 nm-rad to 2 nm-rad) change the value of $f(\chi_m)$ by only ±20%.

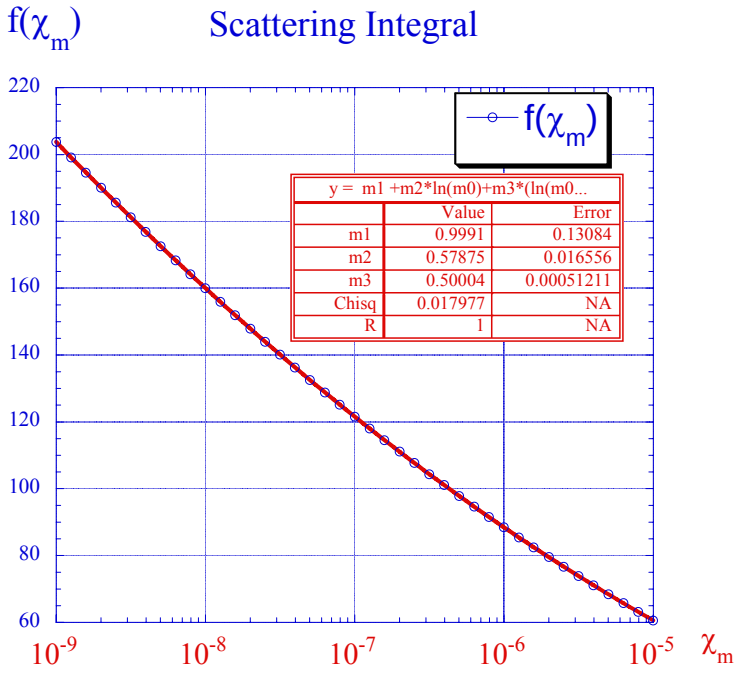

Figure 1.2.1 Dependence of the scattering integral on the maximum scattering parameter χ_m.

The NSLS-II designs have a number of parameters that are either constant or have very small variations. First, vertical emittance will be held at the diffraction level for 1 Å radiation ($\varepsilon_x \approx 8$ pm-rad). Second, both low emittance and low energy spread are paramount for the attainment of the required spectral brightness at high harmonics and in the hard-x-ray range (see Chapter 8), which led to a natural selection of a separate function lattice (i.e., there is no field gradient in the dipoles) and constant ratio of synchrotron and horizontal damping times:

$$\tau_E \cong \frac{\tau_x}{2} \cong \frac{1}{f_o} \cdot \frac{E_o}{U_{total}}; \tag{1.2-4}$$

where $T_o=1/f_o$ is the revolution time of electrons around the ring. Thus the damping time is simply proportional to the ring circumference and to the ratio between the beam energy and total losses on

synchrotron radiation E_o/U_{total}. Third, the bunch length in NSLS-II will be kept about constant (between 3 mm and 4.5 mm,) by various means, including its lengthening by harmonics cavity (see Section 6.2.7).

Equations (1.2-2) and (1.2-3) can be solved with respect to the natural emittance ($\varepsilon_{nat} = \tau_x \langle H \cdot D_\delta \rangle_{SR}$; i.e., the beam emittance in the absence of the IBS) using weak dependence of the scattering integral on the beam emittance:

$$\varepsilon_{x\ total} \cong \frac{\varepsilon_{nat}}{2}\left(1+\sqrt{1+\frac{4\varepsilon_{IBS}^{\ 2}}{\varepsilon_{nat}^{\ 2}}}\right), \tag{1.2-5}$$

where ε_{IBS} is the minimum emittance that can be achieved in a given lattice for a given current per bunch $I_b=eN_ef_o$:

$$\varepsilon_{IBS} = \sqrt{\frac{\tau_x N_e r_e^{\ 2} c}{2^5 \pi \gamma^3 \sigma_s}\left\langle H(s)\frac{f\left(\chi_m(s)\right)}{\sqrt{\varepsilon_y \beta_y(s)}}\right\rangle}\ . \tag{1.2-6}$$

The expression for ε_{IBS} (Eq. 1.2-5) can be easily evaluated for any given lattice and bunch parameters, and it naturally has very weak (square root) dependence on the bunch length, bunch current, and damping time, and even weaker (4th power root) dependence on vertical emittance. Overall, this number is a good measure of the ultimate emittance one can approach with realistic beams. For all realistic TBA24 and DBA24 through DBA32 lattices and related beam parameters under consideration (and maximum total losses limited to 1 MeV per turn), the value of ε_{IBS} was between 0.2 nm-rad and 0.25 nm-rad, thus setting the natural limit for attainable emittance. Naturally, increasing the power losses by a factor of two, to 2 MeV per turn would further reduce ε_{IBS} by $\sqrt{2}$.

The dependence of the beam emittance on the natural emittance also sets a natural scale for the bending magnet radius. As shown in Figure 1.2.2, reduction of the natural emittance below ~*(2-3)*ε_{IBS} is increasingly ineffective at reducing ε_{x_total} and is increasingly expensive as the circumference grows.

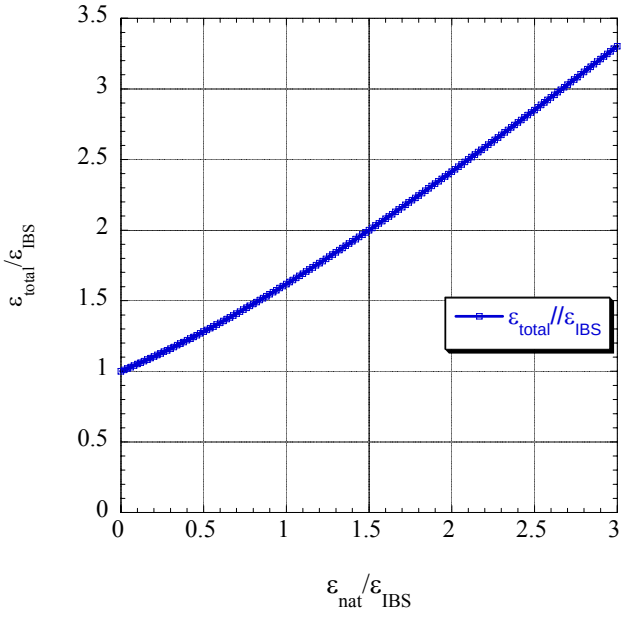

Figure 1.2.2 Dependence of the horizontal beam emittance (given by Eq. 1.2-6).

Reduction of the natural emittance by a factor of two from $2\varepsilon_{IBS}$ to ε_{IBS} (by roughly a doubling of the bending magnet radius) results in only a 33% reduction in emittance. A further doubling of the bending magnet radius only results in a 23% further emittance reduction. Hence, the optimum choice for the natural emittance is about 2 to 3 times ε_{IBS}. When combined with (Eq.) 1.2-1, this yields a simple expression for the optimum power radiated by the bending magnets:

$$U_{bends} = (2-3)U_{total}\frac{\varepsilon_{IBS}}{\varepsilon_{bare}} \quad . \tag{1.2-7}$$

For the 3 GeV NSLS-II storage ring, with total synchrotron radiation losses of 1 MeV per turn, this ratio also gives an optimum range for the radius of the bending magnets:

$$\rho_o[m] = (2.4-3.6)\frac{\varepsilon_{bare}}{\varepsilon_{IBS}} \quad . \tag{1.2-8}$$

Thus, the present DBA30 lattice with a bare emittance of ~2.1 nm-rad and ε_{IBS} ~0.25 nm-rad ($\varepsilon_{bare}/\varepsilon_{IBS} \sim 8.4$) has an optimum bending magnet radius ~25 m.

A bend magnet radius of 25 m is rather large compared to that at other synchrotrons. For example, the existing NSLS x-ray ring bend magnet radius is 6.9 m. As a result, the bend magnet critical energy at NSLS-II will be ~2.4 keV, compared to a critical energy of 7.1 keV for the bend magnets at the existing NSLS x-ray ring. As discussed in Chapter 8, this makes the NSLS-II bend magnets less attractive as sources of high flux, hard x-rays (>4 to 5 keV). However, they will be excellent sources of VUV and soft x-ray radiation. Furthermore, the damping wigglers will also serve as radiation sources for beamlines, and their brightness and flux will be about 100 times greater than would be provided by bend magnets with a small radius.

Finally, the parameters for the damping wigglers (see Chapter 8) were determined by a combination of the following effects (with the assumption that $U_{total} >> U_{bends}$):

- The wiggler magnetic field, B_w, in the damping wigglers should not be very high because it will increase the energy spread according to $\sigma_\varepsilon \propto \sqrt{B_w(T)}$, which will reduce the brightness of high harmonic radiation from the undulators.
- The wiggler period should not be too large, in order to serve as a source of very bright broadband x-rays.
- It should not be too small, to keep nonlinear effects under control.
- The wiggling angle and horizontal β-function should be limited to avoid excitation of horizontal emittance in the damping wiggler caused by $H \cong \beta_x \theta_w^2$.

As the result of optimization, damping wigglers with 1.8 T peak field and 10 cm period were selected. These damping wigglers provide synchrotron radiation losses of 18.5 keV per meter. The initial baseline configuration of NSLS-II will have three 7m-long permanent magnet wigglers. This will achieve an emittance below 1 nm-rad. All damping wigglers will have fixed gap and field and will also serve as excellent sources of user radiation. The final configuration allows up to eight damping wigglers, with which the horizontal emittance will reach a value below 0.6 nm-rad.

1.2.2 Emittance and Lifetime

Electron beam lifetime is an important parameter of the NSLS-II light source. It defines the frequency of top-off injections and, ultimately, defines the radiation environment and necessary shielding. The lifetime has a strong dependence on the energy acceptance of the storage ring. For low-emittance light sources, the energy

acceptance depends not only on the linear compaction factor α_1 (in NSLS-II, higher order compaction factors are not important, $\alpha_1/\alpha_2 \approx 3.7\times10^{-4}/4.1\times10^{-4} = 92\%$) and the parameters of the RF system (harmonic, voltage, synchronous phase), but also may depend on nonlinear coupling and the vertical gap in IDs.

Here we will focus on two unusual phenomena in the lifetime dependences for the NSLS-II storage ring, and their consequences:

- For a given energy acceptance, the beam lifetime depends very weakly on the value of the horizontal emittance (within the range from 0.2 nm-rad to 2 nm-rad).
- Lifetime dependence on the energy acceptance is approaching the fourth power of the latter.

Conventional wisdom says that lowering the beam emittance in an electron storage ring leads to a proportional reduction of the lifetime. This conclusion can be drawn from the following formula [1.2.5]:

$$\frac{1}{\tau_{Touschek}} = \frac{N_e r_e^2 c}{8\pi\cdot\sigma_x\sigma_y\sigma_s\cdot\gamma^2\cdot\delta_{acc}^3} D(\xi); \qquad \xi = \left(\frac{\delta_{acc}}{\gamma\sigma_\theta}\right)^2;$$
$$D(\xi) = \sqrt{\xi}\left\{-\frac{3}{2}e^{-\xi} + \frac{\xi}{2}\int_\xi^\infty \frac{\ln u\cdot e^{-u}}{u}du + \frac{1}{2}(3\xi - \xi\ln\xi + 2)\int_\xi^\infty \frac{e^{-u}}{u}du\right\} \tag{1.2-9}$$

where $\delta_{acc} = \Delta E_{acc}/E_o$ is the relative energy acceptance, σ_θ is the transverse angular spread (dominated by horizontal oscillation for the NSLS-II case), $\sigma_{x,y} = \sqrt{\beta_{x,y}\varepsilon_{x,y}}$ are the transverse RMS beam sizes, and $D(\xi)$ is the scattering integral causing loss of the electrons.

Nevertheless, direct use of this formula (integrated over the NLSL-II circumference) gives a lifetime dependence (shown in Figure 1.2.3) which shows very weak lifetime variation in a (0.2, 2.0) nm-rad interval, and (exponential!) lifetime growth for emittances below 0.2 nm-rad. This dependence has a very solid physics foundation [1.2.6].

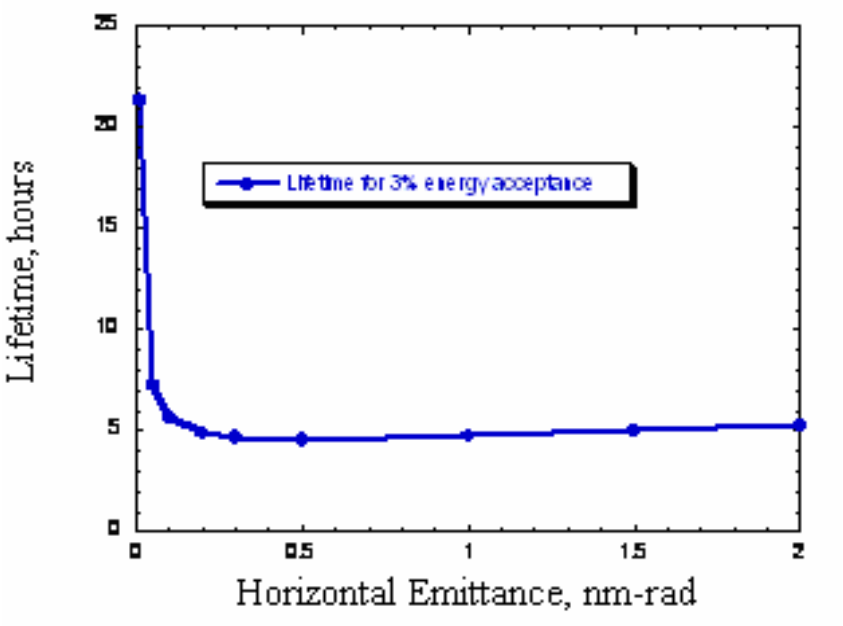

Figure 1.2.3 Dependence of the beam lifetime in NSLS-II on the horizontal emittance for 0.008 nm-rad vertical emittance and fixed uniform 3% energy acceptance.

The main loss mechanism for ultra relativistic electrons ($\gamma >> 1$, $\gamma_{NSLS\text{-}II}$ ~6000) in storage rings comes from the mechanism first described by Touschek. The simple picture can be presented as follows: In the co-

moving frame (i.e., that moving with the electron bunch), two electrons execute betatron oscillations having transverse momenta $\pm p_t$ (in the case of a flat beam, mostly in the horizontal direction: $p_x=\pm\gamma mcx'$). They then scatter on each other and transfer the momenta ($p_s=\pm\gamma mcx'$) in the direction of motion (s-direction). The Lorentz transformation into the laboratory frame gives a relativistic boost to p_s momenta by a factor of γ and generates an energy deviation of $\Delta E \approx \pm\gamma^2 mcx'$. If the energies of the scattered electrons are outside the energy acceptance ($\gamma^2 mcx' > \pm\Delta E_{acc}$), then the electrons may get lost. For most storage rings, the angular RMS spread of the electrons,

$$\sigma_\theta(s) = \sqrt{\varepsilon_x\left(1+\alpha_x^2(s)\right)/\beta_x(s) + \varepsilon_y\left(1+\alpha_y^2(s)\right)/\beta_y(s) + \eta'^2(s)\sigma_\delta^2}\,, \qquad (1.2\text{-}10)$$

is sufficient for such a process to occur (note that σ_θ is a function of azimuth s). But for storage rings with extremely low emittances (in the NSLS-II case, sub-angstrom emittances), only the far tails of the electron distribution $f(\theta) = \exp\left(-\theta^2/2\sigma_\theta{}^2\right)/\sqrt{2\pi}\sigma_\theta$ can cause such processes, and the lifetime of such beams increases with the decrease of the emittance. Formally, this dependence can be seen from a formal evaluation of the $D(\xi)$ function, shown in Figure 1.2.4.

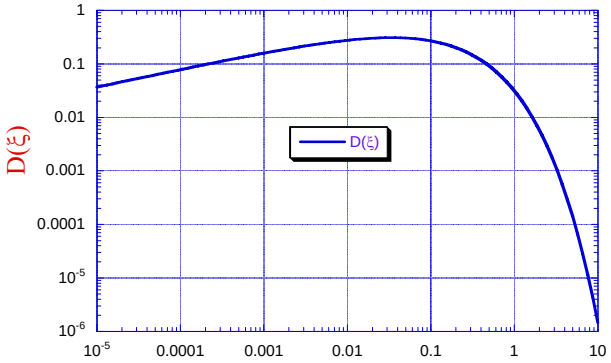

Figure 1.2.4 Dependence of the loss integral D(ξ) on the parameter ξ: D(ξ) is a rather slow function of ξ for ξ <0.01, flat in the range 0.01<ξ <0.1, and falls exponentially for ξ >0.1. (nearly a Gaussian dependence).

For NSLS-II, ξ spans the range from 2×10^{-3} to 2 (the large range is an indication of very strong variation of the β-function with s). The explanation of the lifetime dependence shown in Figure 1.2.3 is very straightforward: while reduction of the horizontal emittance increases the electron density $\propto 1/\sqrt{\varepsilon_x}$, it also increases $\xi \propto 1/\varepsilon_x$ and, as a result, increases the portion of the ring where $\xi > 0.1$ and the losses are exponentially suppressed. Figure 1.2.5 shows that for the range of NSLS-II parameters under consideration, the beam lifetime exhibits an extremely weak dependence on the horizontal emittance, but a very strong dependence on the energy acceptance. As shown by the fit in Figure 1.2.6, the lifetime of NSLS-II is proportional to the fourth power of the energy acceptance. In contrast, storage rings having larger emittances and operating in the regime of ξ <0.01 typically have a power dependence on the energy acceptance of about 2.7. This strong dependence for NSLS-II, again, comes from the fact that large values of the ξ-parameter (where losses are suppressed) are important for the reduction of the losses and increase of the lifetime of NSLS-II. This underlines the importance of a large energy acceptance for NSLS-II.

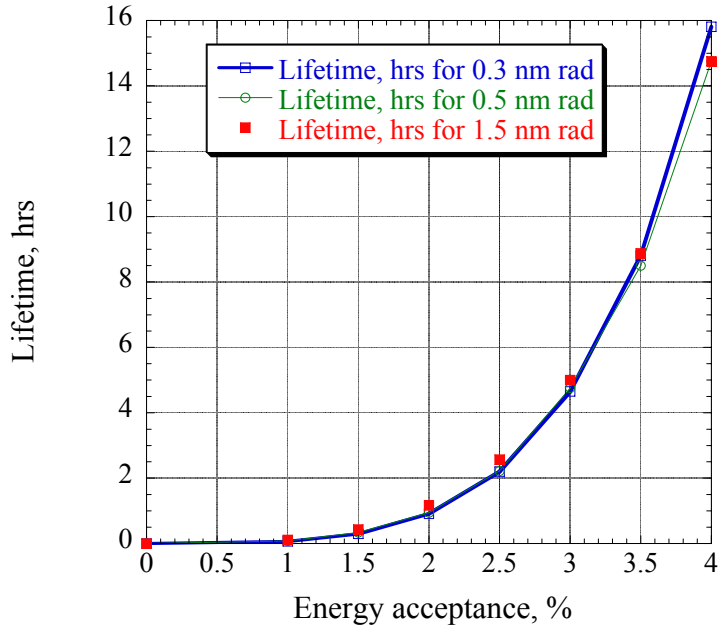

Figure 1.2.5 Dependencies of the beam lifetime on the energy acceptance for horizontal emittances of 0.3, 0.5, and 1.5 nm-rad and vertical emittance of 0.05 nm-rad. Note: the bunch length is assumed to be constant.

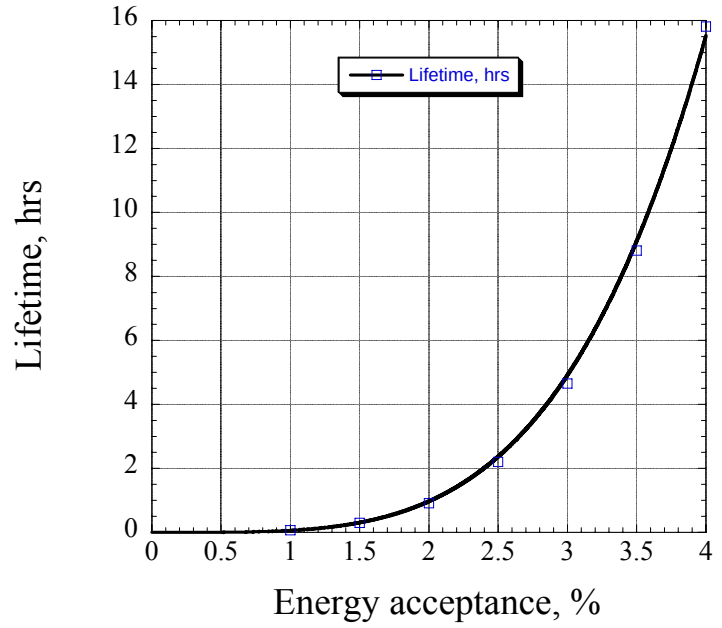

Figure 1.2.6 Fit of the beam lifetime dependence to the fourth power of the energy acceptance for horizontal emittance of 0.3 nm-rad and vertical emittance of 0.008 nm-rad.

Detailed calculations in Section 6.2.6 show features similar to those discussed in this chapter, supporting the assertion that reduction of the horizontal beam emittance at NSLS-II will not adversely affect the beam lifetime.

At the same time, any reduction of the energy acceptance for NSLS-II would have a substantial impact: a 19% reduction of the energy acceptance reduces the lifetime by a factor of two. Because of this, intense and detailed studies of the effects of the lattice and insertion devices on the beam lifetime were carried out, as reported in Chapter 6.

1.2.3 Collective Effects

Collective effects, described in detail in Section 6.2, have two distinct subgroups: instabilities and effect on the beam parameters (IBS and lifetime). We touched on the latter in the previous section. In this section, issues related to beam instabilities will be briefly reviewed.

The studies of beam instabilities were based both on well-established theoretical estimations as well as on detailed calculations of specific impedances using the code GdfidL for the most convoluted structures (such as RF cavities and ID transitions). GdfidL was also used intensively for calculating the impedance budget for the ring with resulting longitudinal impedance values of $(Z/n)_o \sim 0.4\ \Omega$.

The impedance model was used for estimating instability thresholds or their growth rate for the following: CESR-B SRF cavity, 720 m of Al vacuum chamber with ±12.5 mm vertical gap, 60 meters of copper shielding for in-vacuum undulators with gap of ±2.5 mm, and transverse (1 MΩ/m; Q = 1, 30 GHz) and longitudinal (R_s = 30 kΩ, Q = 1, Z/n = 0.4 Ω) broadband impedances to represent transitions and other imperfections in the vacuum chamber.

The studies of instabilities were performed for the most conservative case of short electron bunches (i.e., without the use of harmonic cavities). These conservative estimates predict that an electron beam with the NSLS-II parameters will be stable, with only one exception: the transverse coupled bunch instability has a threshold ~15 mA (with 500 mA required) at zero value of vertical chromaticity (see Section 6.2.3.3 for details). The studies using computer tracking predicted that increasing the chromaticity to at least +4 will stabilize the 500 mA beam. Being prudent, we include a well-known multi-bunch feedback system in the list of instrumentation for the NSLS-II storage ring. This feedback system will guarantee the suppression of this and other multi-bunch instabilities.

References

[1.1.1] T. Shaftan, J. Bengtsson and S. Kramer, "Control of Dynamic Aperture with Insertion Devices," http://accelconf.web.cern.ch/AccelConf/e06/PAPERS/THPLS091.PDF

[1.1.2] J. Safranek, "Experimental Determination of Linear Optics Including Quadrupole Rotations," http://accelconf.web.cern.ch/AccelConf/p95/ARTICLES/FAB/FAB11.PDF; also, J.A. Safranek, "Beam-Based Accelerator Modeling and Control," Proc. of Beam Instrumentation Workshop 2000, AIP Conf. Proc. 546, pp. 23–34.

[1.1.3] S. Krinsky, J. Bengtsson, and S. Kramer, "Consideration of a Double Bend Achromatic Lattice for NSLS-II," http://accelconf.web.cern.ch/AccelConf/e06/PAPERS/THPLS090.PDF

[1.2.1] NSLS-II CD-0 proposal, http://www.bnl.gov/nsls2/docs/PDF/NSLS-II_CD-0_Proposal.pdf

[1.2.2] S.L. Kramer, and J. Bengtsson, "Dynamic Aperture Optimization for Low Emittance Light Sources," http://accelconf.web.cern.ch/AccelConf/p05/PAPERS/RPAE057.PDF; and J. Bengtsson, "Control of Dynamic Aperture for Synchrotron Light Sources," http://accelconf.web.cern.ch/AccelConf/p05/PAPERS/MPPE020.PDF

[1.2.3] http://sls.web.psi.ch/view.php/about/index.html

[1.2.4] J. Murphy, *Data Book on Synchrotron Light Sources*, ver. 4, May 1996, BNL 42333, Upton, NY.

[1.2.5] J. LeDuff, "Single and Multiple Touschek Effects," Proc. of CERN Accelerator School, Rhodes, Greece, 20 Sept. – 1 Oct., 1993; Ed.: S.Turner, CERN 95–06, 22 November 1995, Vol. II, p. 573.

[1.2.6] V.N. Litvinenko, "Review of Ring-Based Light Sources," Proc. of ICFA Future Light Sources Workshop, April 2–5, 1999, APS, Argonne, IL.

2 INJECTION SYSTEMS

2.1 NSLS-II Injection Requirements

The NSLS-II injection system must meet several user requirements:

- maintain a stable level of the ring current in order to maintain a constant intensity to experiments and heat load on beamline optics
- minimize frequency of interruptions of user experiments, especially for those involving long scans that cannot accommodate interruptions in beam intensity
- minimize the disturbance of the beam during and immediately after injection due to the residual orbit perturbation from an incompletely closed injection bump and/or transients in fast magnets
- minimize bunch-to-bunch variation of current in order to minimize intensity-correlated orbit oscillations due to uneven bunch patterns [1]
- fill the storage ring from zero to full charge in a reasonable amount of time

These requirements must all be accomplished in a way that is as transparent to the users as possible. They are summarized in Table 2.1.1.

Table 2.1.1 User Requirements.

Stability of average current	<1%
Time between injections	>1 min
Bunch-to-bunch variation of current	<20%
Time to fill ring from zero to full charge	<5 min

To achieve these requirements, NSLS-II will utilize a full-energy injection system that will operate in top-off mode with minimal disturbance to the circulating beam. The technical specifications for the NSLS-II injection system are summarized in Table 2.1.2. As follows from that table, the NSLS-II injection system must supply approximately 7.3 nC of charge once per minute, assuming a lifetime of 3 hours. For single-bunch injection mode and a moderate repetition rate of a few Hz, replenishing this amount of charge would take a few seconds, occupying a significant fraction of the overall beam time. Therefore, multi-bunch injection has been adopted, leading to minimal disturbance for user experiments and lower power consumption by the injection system.

The main ring contains 1,320 RF buckets at 500 MHz. To alleviate the problems of ion trapping in the stored electron beam, approximately one-fifth of the buckets must be left empty. The exact number of buckets to fill is difficult to predict and will be determined empirically during commissioning. Feedback systems and the ultimate vacuum conditions in the ring will determine what requirements will be imposed on the bunch structure. In any case, to keep the current constant with high accuracy, considerable flexibility and accuracy must be built in to the bunch transfer timing system, the single-bunch capability, and the current and bunch structure measurement system of the main ring.

Table 2.1.2 Storage Ring Parameters Related to the NSLS-II Injector.

Parameter	Value
Energy [GeV]	3.0
Circulating current [A]	0.5
Circumference [m]	791.96
Revolution period [μs]	2.64
RF frequency [MHz]	499.68
Circulating charge [μC]	1.32
Total number of buckets	1320
Number of filled buckets at 80% filling	1080
Charge per bucket [nC]	1.22
Current per bucket [mA]	0.46
Lifetime [min]	180
Interval between top-off cycles [min]	1
Current variation between top-off cycles [%]	0.55
Current variation between top-off cycles [mA]	2.77
Charge variation between top-off cycles [nC]	7.31

2.1.1 Future Upgrades of the Bunch Pattern Formats

As described above, the NSLS-II injector must support uniform filling pattern in the storage ring starting with the beginning of operations. Two basic patterns were considered (Figure 2.1.1, two upper plots): uniform fill with the ion-clearing gap of about 20% and multiple uniform bunch trains with mini-gaps between them. Both of these bunch patterns are in the baseline design of the NSLS-II project.

Also, in response to NSLS user requests, consideration is being given to specialized bunch patterns that are not a part of the baseline design; these will be developed during later stages of the project. In addition to the nominal uniform fill, users require a single high-current bunch ("camshaft" bunch, two lower plots in Figure 2.1.1) located in the middle of the ion-clearing gap, as well as multiple camshaft bunches whose repetition rate is matched to the pulse format of modern pump lasers.

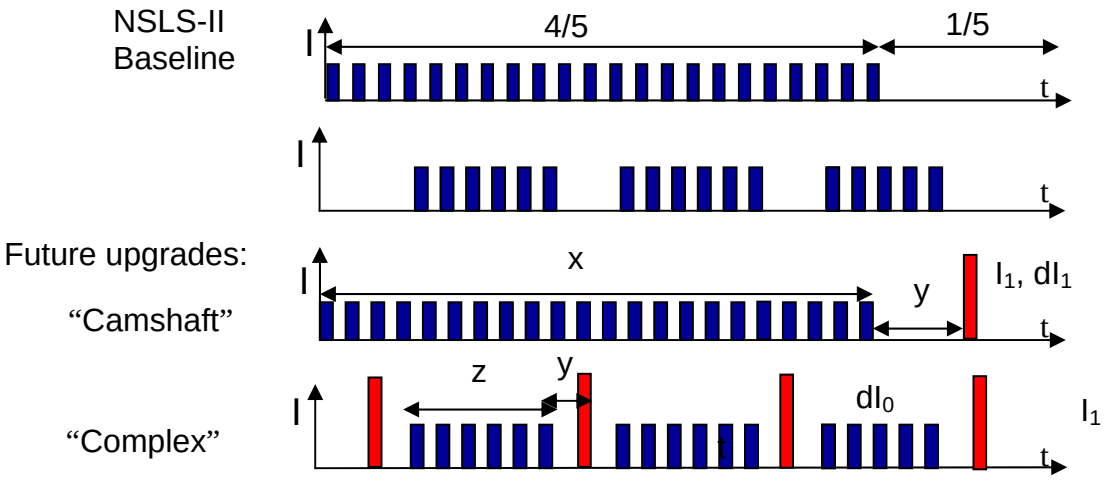

Figure 2.1.1 User requirements on the storage ring bunch patterns.

User experiments set the following conditions for the time intervals and current stability of these complex bunch patterns:

- time interval separating regular pattern from the camshaft bunch (y) more than 20ns
- number of camshaft bunches (N) is about 5
- current stability in the regular bunch pattern (dI_0) is less than 1%
- current stability in camshaft bunch(es) is less than a few percent

The maximum current of the camshaft bunch(es) will be determined by calculating thresholds of single-bunch instabilities.

For simplification of filling and maintaining current in the camshaft bunches, as well as for enhancing capabilities of the "hunt-and-peck" mode of operation, we have considered including a second gun that would operate exclusively in the single-bunch mode. Electron beam from the second gun would enter into and be accelerated in the same linac using a dog-leg merging system. This is not included in the baseline design and is slated as a possible future upgrade of the injector.

The baseline scope for the NSLS-II project includes developing an injector that will enable initial fill and maintaining of 500 mA of the circulating current in the top-off mode. Support of the complex bunch patterns is foreseen as a future upgrade.

2.1.2 Injection Sequence

The initial fill occurs at the rate of 1 Hz, and 40 bunches are transferred to the main ring, nominally, at each injection (this number can be increased to 150 bunches) to fill consecutively 1,080 of the 1,320 RF buckets available. The number of bunches in the injected train is constrained to about 40 minimum (based on beam loading physics) and a maximum of 150 (limited by the booster circumference).

Bunch trains from the injector enter the ring in sequence, starting with the front of the ring train and stepping sequentially back in time along the ring train until the end is reached, then skipping over the empty section and starting again at the head of the train, until the required current has been established.

Assuming the same amount of charge per injection (7.3 nC per bunch train) as for top-off mode, the duration of the initial fill will be about 3 minutes with the injection system running at a 1 Hz repetition rate.

Top-off operation to keep the current within 0.55% of the nominal value will be the standard operating mode of NSLS-II. The frequency of operation to keep the current within these boundaries depends on the beam lifetime and is expected to take place about once per minute. The injected bunch trains from the booster are stepped sequentially around the ring bunch structure. Users expect bunches to stay relatively constant in charge relative to each other (a difference of ±10% has been adopted). We are considering several possible techniques for providing a filling pattern with sufficient uniformity.

NSLS-II users have provided feedback regarding possible top-off formats, which is summarized in Figure 2.1.2.

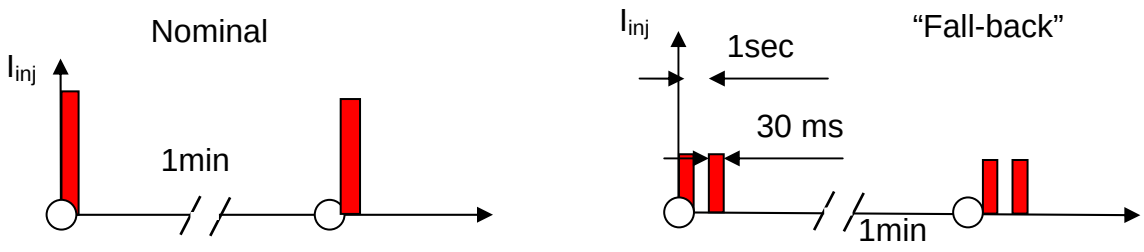

Figure 2.1.2 Format of top-off injections: Dependence of the injected beam current vs time in minutes. 30 msec corresponds to the value of the damping time, during which the stored beam will be disturbed by the injection process.

The first scenario corresponds to the nominal case, when charge increments of 7.3 nC are injected once a minute. The second scenario allows reducing the amount of injected charge in half; however, the time interval between top-off cycles (1 second given by the injector repetition rate) is unusable for the user experiments.

Other scenarios are unacceptable for users. In one scenario involving a few low-charge, consecutive top-off injections, user experiments could be disabled for a substantial fraction of the total time. Another foreseeable scenario would be maintaining the ring current at the stability level of 0.1%. In this case, unperturbed beamtime reduces down to a few seconds, which is unacceptably short for majority of users.

2.1.2 Injector scope

There are several possible basic schemes for the injection system that can meet the requirements stated above. One is to use a full-energy linear accelerator, which would require no booster synchrotron at all; another is to use a booster synchrotron fed by a small linac.

A full-energy linac would provide flexible injection operations in a single bunch mode at the repetition rate of about 50 Hz[1]. However, performance and reliability of storage ring kickers and septa at this repetition rate may present a technically challenging problem together with frequent disturbances for the storage ring current, which can lead to a charge loss. On the other hand, operating in multi-bunch mode is difficult, due to significant beam loading in the linac structures at the amount of charge that is specific for the NSLS-II injector. Another disadvantage would be the high cost for the linac and the additional cost of a building to house the linac and transport line. In addition, a full-energy linac is likely to have lower reliability and a higher operations cost than a full-energy booster. A highly reliable injection system is especially important for NSLS-II, given its short beam lifetime.

For these reasons, a full-energy booster was selected as the NSLS-II injector. Two approaches were considered for its design. In the first approach, the booster was located in the storage ring tunnel [2]. This results in a much larger circumference for the booster, but most of this is taken up by small stainless steel vacuum pipe. In the second, a "compact" booster design was evaluated [3]. Comparing both approaches [4] revealed a substantially higher total cost for the compact booster due to the extra costs of constructing and shielding a separate building to house it. However, the concerns, regarding 1) potential cross-talk between the "same-tunnel" booster and storage ring, and 2) potential schedule conflicts from installing, testing, and commissioning of both machines located in the same tunnel as well as future booster troubleshooting have lead to the choice of the compact booster as the NSLS-II injector. Therefore, the NSLS-II design employs a compact booster located in a separate tunnel.

The 200MeV linac is specified for injection into the booster. Higher injection energy is advantageous from the following points of view:

[1] Limited by an interval of few damping times in the storage ring between consecutive bunch injections

- Relatively high value of magnetic field in the booster elements at injection
- Lower losses due to booster vacuum
- Energy redundancy (if one klystron goes down, injection can still be accomplished)
- Higher energy linac produces beam with lower energy spread and emittance, which is easier to inject into the booster

Two transport lines will be constructed: one to connect the linac to the booster and a second to connect the booster to the main ring. A full set of beam diagnostics will be installed for commissioning and routine operations of the injection system.

Strategically, BNL is developing the complete preliminary design of the injector and then procuring the major components of the injector (linac and booster) from vendors. The vendors will install the equipment and jointly commission it with BNL staff. BNL will design, procure, install, and commission the transport lines and injection straight section.

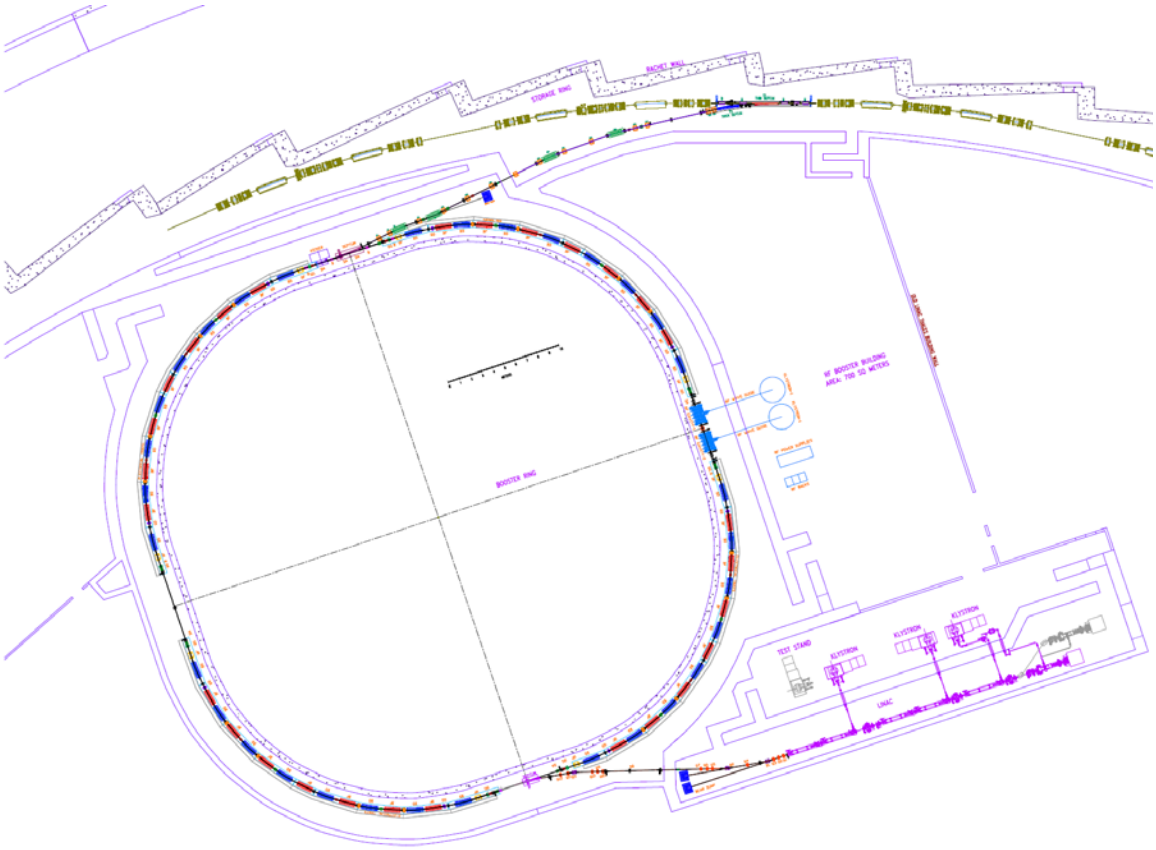

Figure 2.1.3 Layout of the NSLS-II injector.

Figure 2.1.3 demonstrates the injector layout, where the linac and booster are housed in separate tunnels and the injector service area is adjacent to these accelerators and the ring injection straight section.

In this chapter we describe all the components of the NSLS-II injection system in the following order: linac and electron gun, linac-to-booster transport line, booster with booster-to-storage ring transport line, and injector service area.

References

1 http://accelconf.web.cern.ch/AccelConf/e04/PAPERS/THPLT186.PDF

2 NSLS-II Conceptual Design report, 2006

3 T. Shaftan *et al.*, "Design of 3 GeV Booster for NSLS-II," Proc. of PAC-2005, p. 3473.

4 D. Hatton *et al.*, "Considerations of the in-tunnel versus compact booster design", NSLS-II Tech. note-2007

2.2 Linac

2.2.1 Linac Scope

The NSLS-II storage ring requires approximately 7 nC of charge to be delivered in top-off mode once every minute to replace charge lost through Touschek scattering. This charge should be delivered in a single booster cycle, so that the storage ring beam is disturbed only for the duration of the ring damping time (tens of milliseconds) each minute. Details of this will be presented later in this section. In addition, future storage ring requirements may include single camshaft bunch or timing bunches for user experiments or machine studies. To meet these requirements, two modes of linac operation are envisioned: single-pulse mode with about 1 nC charge per bunch, and multi-bunch mode, delivering bunches by tens of pC up to more than 100 pC, totaling 15 nC of charge. To inject bunch trains into a booster with a 500 MHz RF system, a 3GHz linac bunch structure must fit into the booster buckets of ~1 ns length, separated by 2 ns.

To minimize the booster cost, the aperture of the magnets is kept small. To keep the injection efficiency high given the small magnet aperture, a reasonably small emittance is required. Likewise, a small energy spread is needed to prevent beam loss in the high-dispersion regions of the booster lattice. An additional requirement is that the linac be able to provide sharp edges to the electron bunch train, to avoid injecting electrons into the ion clearing gap.

Thales and ACCEL have produced turn-key linac systems for Soleil and Diamond, respectively. The Soleil linac, using CERN "LIL" 3.5m structures, has a smaller energy spread that meets the NSLS-II design specification. An approach similar to the Soleil linac is used as a baseline and described below (Figure 2.2.1). The Diamond injector uses the DESY 2.2m accelerator structures, resulting in a slightly longer linac. To keep both options open in the preliminary design phase, the linac building has been designed to accommodate either four 5.2m tanks or five CERN 3.5m structures.

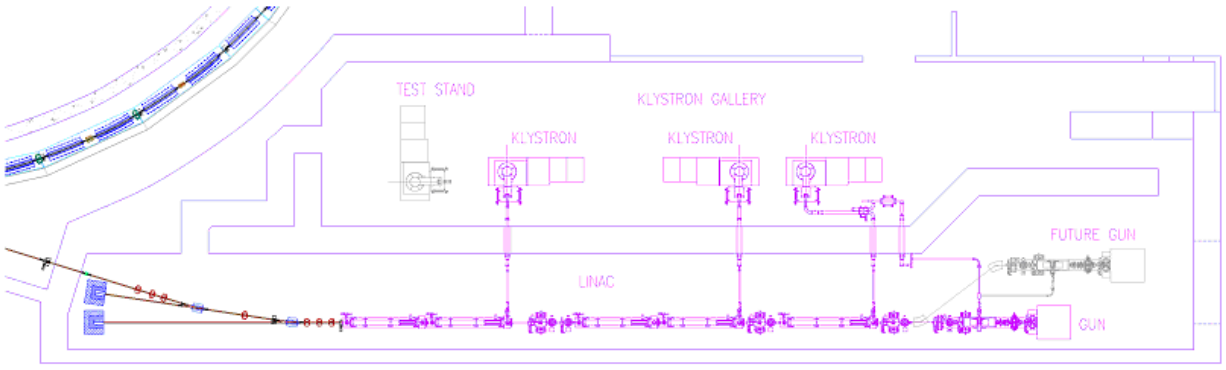

Figure 2.2.1 Layout of the 200 MeV linear accelerator.

The linear accelerator [1] consists of the following subsystems:

- 100 kV triode gun (e.g., Eimac Y-845) with a 500MHz modulation at the gun grid and a high-voltage deck
- four shielded lenses, situated between the gun and the buncher
- a 500MHz subharmonic pre-bunching cavity with ± 25 kV modulation
- a 3GHz pre-bunching cavity with ±10kV modulation (100 W power)

- a 3GHz stationary wave buncher surrounded by two shielded coils (1.2 m long, 5.5 MW, energy gain of 15 MeV)
- five traveling wave-accelerating structures at 3 GHz in the $2\pi/3$ mode and with a length of 3.5 m (flange to flange)
- a Glazer lens between the buncher and the first accelerating structure
- two focusing doublets
- three Klystrons (TH2100, 35 MW) and their modulators
- low-level RF controls

Objects colored in grey in Figure 2.2.1 represent elements of the linac that are considered as a future upgrade. As discussed in the introduction, the injector must possess sufficient flexibility in order to support complex bunch patterns. For filling and maintaining current in these, we considered including a second gun that will work exclusively in the single-bunch mode. Beam after the second gun is prebunched and accelerated in the following gun buncher system and injected in the linac at an energy of about 15 MeV using a dog-leg. Also depicted in grey is a test stand for klystrons testing.

2.2.2 Physics Design and Parameters

Although a range of parameters will meet the requirements, we focus here on a specific case of approximately 375 pC per bunch in bunch trains of 40 bunches for a total of 15 nC to provide details on the injector design. Having about a factor of two greater than the charge required in the storage ring top-off allows for faster initial fills and for losses in the injection process. Studies of booster injection and extraction losses will be included at the next design stage.

The energy spread must be controlled throughout the acceleration process. The maximum horizontal size of the beam injected into the booster (Section 2.5) is dominated by the energy spread. For ε = 125 nm-rad (2σ emittance) and maximum β_x = 12 m at the maximum dispersion, η = 0.35, and energy spread, $\Delta E/E$ = 0.5%, the maximum RMS beam size is $\Delta\sigma_x \approx \eta\Delta E/E \approx 1.75$ mm.

Recent experience at SOLEIL [2.3] has shown that industry can produce turn-key linac systems that meet these specifications. Because the approach taken may differ significantly from one machine to the next, only the salient points of a generic linac are presented.

A planar triode electron gun, the EIMAC Y845 [2.4], is used with a fast-pulser cathode driver. In single-bunch mode, the cathode is pulsed to create ~1 ns pulses of ~0.5 nC. The DC gun inherently has small energy spread. However, to compress the gun pulse for acceleration in the 2.998 GHz linac and capture it in the 500 MHz booster RF, we need to prevent nonlinearities in the RF from increasing the energy spread beyond the 0.5% (RMS) requirement. This translates into a requirement on the length of the micro-bunches exiting the linac to be less than ~11 ps.

To create these short bunches, a bunching system is required. First, a 500MHz subharmonic buncher is used to compress the charge into bunch lengths less than 1 ns to match the 500MHz booster bucket. This is followed by a 2.988GHz pre-buncher that micro-bunches the 1.5ns bunch train to $\leq$11 ps bunches within the linac buckets. A final buncher simultaneously accelerates the electrons to 3 MeV to increase capture efficiency. In bunch-train mode, the cathode is pulsed on for the duration of the train, up to 200 ns, and is bunched in the process described above. During the preliminary design phase, system performance will be confirmed by E-Gun [2] and Parmela [3] simulations, and cathode driver experiments at the NSLS electron gun test stand.

The main accelerator is comprised of 3GHz traveling wave structures, with an energy gain of:

$$E[MeV] = 12.5\sqrt{P[MW]} \tag{2.2-1}$$

The accelerating structures being considered obtain 52 MeV per tank for an input power of 17.5 MW. Using readily available 35MW klystrons, the first klystron is power split, with about 5.5 MW feeding the 3GHz pre-buncher and buncher. The latter has an energy gain of more than 15 MeV. The remaining power feeds the first linac structure. Individual waveguide phase shifters and attenuators are used for adjusting amplitude and phase between elements.

The remaining four tanks are powered by two klystrons for an energy gain of an additional 52 MeV each. Thus, a total of 255 MeV energy gain is possible. For redundancy, two waveguide switches can connect the second klystron to power the two bunchers and first tank. In this scheme, an energy of 170 MeV can be achieved if one klystron fails. This will be explored in the next design phase.

The bunch charge and train current—although not beyond that which has been achieved in other applications [4, 5]—is sufficient to warrant close attention to beam-loading issues. For traveling wave tanks, the voltage induced along the bunch train on short time scales (compared to the fill time of the cavity) is given by:

$$V_b = -ir_0 L[(1-\tau^{-1})(1-e^{-x\tau}) + xe^{-x\tau}] \tag{2.2-2}$$

where r_0 is the shunt impedance, τ the attenuation constant in nepers, L the length of the tank, and x the ratio t/t_f, where t is the time duration of the macro-pulse and t_f the fill time of the structure.

For forty 375 pC bunches separated by 2 ns (187.5 mA), this corresponds to about 1.6% in the correlated energy spread along the bunch train. There are several methods of reducing this beam loading. For a given beam current, the beam loading compensation can be achieved by sending the beam during the filling time of the second structure. This approach has been successfully implemented at SOLEIL [4] for a 300ns-long train current of 9 nC. Alternatively, the effect of beam loading can be diminished by lengthening the macro-pulse, either by simply lengthening the pulse and proportionally reducing the charge per bunch, or by pulsing the gun once every fourth, sixth, or eighth 500MHz bucket with constant charge per bunch to reduce the effect by the corresponding factor. For example, by filling 150 bunches of 100 pC each, the average current falls to 50 mA and the energy spread due to beam loading drops to 0.5%.

2.2.3 Klystron Modulators and Power Supplies

Pulsed 3GHz high-power klystrons are a mature technology and several manufacturers can meet or exceed the 35MW power requirement. The klystrons are powered by pulsed modulators. The traditional approach is to use Pulse Forming Networks with hard-tube (thyratron) switches to produce RF pulses between 2 and 4 microseconds long. NSLS has recently designed and built such a modulator for the 45MW tube installed at its DUVFEL facility. Our own experience and studies of reliability at SLAC/PEP-II and Pohang Light Source have shown that the mean time between failure (MTBF) and mean time to repair (MTTR) of the PFN/hard tube modulator dominate the linac downtime, with rates three times those of the klystron tube and its filament/core bias power supplies [6, 7]. For this reason, solid-state modulators are being explored for NSLS-II. Several competing designs have been developed for both medical linacs and the X-band International Linear Collider. One such example is the design by Scandi-nova [8], which uses a multi-turn primary pulse transformer, reducing the modulator voltage from about 40 kV to 3 kV, further increasing reliability by limiting the high voltage to only the pulse transformer and klystron cathode assembly in the oil tank [9]. These systems are also between one-half and one-third the size of similar PFN-type modulators. The decision to use a solid state or a PFN-hard tube modulator will be made during the preliminary design phase.

The 500MHz subharmonic pre-buncher requires about 6 kW (for a shunt impedance of 250 kΩ) to reach 36 kV. This is well within the range of solid-state RF amplifiers.

The 3GHz pre-buncher is a single cell with ±10 kV modulation, requiring only 100 W of RF power.

The 3GHz final buncher is a standing wave structure, requiring 5.5 MW of RF power, and delivering an energy gain of 15 MeV.

The low-level RF can be a duplicate of the DUVFEL RF system [10], with a master clock in common with the booster and storage rings driving a 2.988GHz DRO-based synthesizer whose output is split and feeds direct I/Q modulators for the amplitude and phase control of the individual klystrons. The 500 MHz will be derived from the booster RF that is synthesized in a similar way. Complimentary I/Q demodulators can be used to down-convert to baseband and close amplitude and phase loops around the cavity fields.

2.2.4 Diagnostics/Instrumentation for Linac

Table 2.4.1 shows beam diagnostics for the electron source and linac.

Table 2.4.1 Linac Diagnostics.

System	Quantity	Monitor Type	Measured beam parameter
Electron source	3	Wall current monitor	intensity, longitudinal beam characteristics
Linac	3	Fluorescent screens	position, profile
	2	Current transformers	intensity

The gun diagnostics consist of three resistive wall current monitors (WCM) to observe the longitudinal profile of the electron bunches after the gun, pre-buncher, and buncher. The WCM is formed by equally spaced broadband ceramic resistors mounted on a flexible circuit board, wrapped around a short ceramic break [11].

The bunch charge, produced by the gun and accelerated by the linac, is monitored by five fast current transformers [12]. The current transformers will monitor beam losses in the linac. Three fluorescent screens installed between the linac tanks will be used to observe the transverse profile and the position of the electron beam [13].

References

1 http://cern.ch/AccelConf/p07/PAPERS/TUPMS081.PDF

2 W. B. Herrmannsfeldt, "EGUN – An Electron Optics and Gun Design Program," SLAC 331, 1988.

3 Parmela, Ver. 3, by Lloyd M. Young , Documentation by James H. Billen, Los Alamos Nat. Lab.

4 A. Setty, et al., "Commissioning of the 100 MeV Preinjector HELIOS for the SOLEIL Synchrotron," EPAC06.

5 C. Christou, et al., "Commissioning of the Diamond Pre-Injector Linac," EPAC06.

6 C.W. Allen et al., "PEP-II Hardware Reliability," SLAC-PUB-10835.

7 S.S. Park et al., "Reliability Analysis of the PLS Klystron-Modulator System," Proc. of the Second APAC, Bejing, 2001.

8 http://www.sc-nova.com/

9 W. Crewson, "A new solid-state high-power pulsed modulator," 5th Modulator-Klystron Workshop for Future Linear Colliders MDK-2001 Geneva, 25-27 April 2001.

10 J. Rose, et al., "Radio-Frequency Control System for the DUVFEL," PAC03. http://epaper.kek.jp/p03/PAPERS/TPAB006.PDF

11 B. Fellenz, and J. Crisp, "An Improved Resistive Wall Monitor," Proc. of Beam Instrumentation Workshop 1998, AIP Conf. Proc. 451, pp. 446–453.

12 http://www.bergoz.com

13 E. Johnson, W.S. Graves, and K.E. Robinson, "Periscope Pop-In Monitor," Proc. of Beam Instrumentation Workshop 1998, AIP Conf. Proc. 451, pp. 479–484.

2.3 Booster

2.3.1 Booster Scope

The NSLS-II booster is required to produce a 3 GeV bunch train with an extracted charge of about 7.5 nC at a repetition rate of 1 Hz and a geometric emittance around 30 nm-rad. Injection in the booster ring takes place at an energy of 200 MeV. The booster magnetic field and RF voltage are ramped for 400 ms to accelerate the electron beam from the injection energy to the nominal energy of 3 GeV. At the maximum field of the ramp, the electron beam is extracted from the booster and injected into the main ring. As mentioned in section 5.2.1 we allow for a maximum beam loss of 30% during injection, a 20% maximum loss during acceleration and extraction, and 10% maximum loss for injection into the storage ring. Thus the charge to be accelerated in the booster is 10 nC which corresponds to an average beam current of 19 mA.

Since the storage ring Dynamic Aperture is limited, the injected beam quality has received serious consideration. In particular, the booster emittance may impact on the injection efficiency, which is a concern, in particular, because of frequent top-off cycles (see Chapter 4) carrying a high charge.

During the last 10 years many 3rd generation synchrotron light facilities have been put into operation. Nearly all of these facilities have chosen a full energy booster synchrotron as an infector together with a low energy linac as preinjector. The main parameters of several modern booster synchrotrons are listed in Table 2.3.1.

Table 2.3.1 Modern Boosters.

	ASP	DIAMOND	SOLEIL	SLS	ALBA	BINP
Energy, GeV	3	3	2.75	2.4	3	2.5
Tunnel	separate	Separate	separate	same	same	separate
Circumference, m	130.2	157	157	270	249.6	132
Lattice	4-fold	2-fold	2-fold	3-fold	4-fold	2-fold
Rep rate, Hz	1	5	3	3	3	1
Emittance, nm	34	144	150	9	9	50
Tunes, X/Y	9.2/3.3	6.8/4.6	6.4/4.4	12.4/8.4	12.4/7.4	9.1/9.1
Chromaticity, X/Y	-8.8/-11.5	-8.4/-6.2		-15/-12	-17/-10	-11.6/-11.4
RF freq., MHz	500	500	352	500	500	181
Damping times, X/Y/E	2.7/3.5/2.0	5.4/5.5/2.7	6.3/5.7/2.7	11/19/14	4.5/8.0/1.8	4.4/4.2/2.1
Current, mA	7	20	15	1	5	50
Source of info	[ASP]	[DIA]	[SOL]	[SLS1]	[ALB]	[BINP]

Modern boosters with energies around 3 GeV have natural horizontal emittances of the extracted beam in the 10–150 nm range. For example DIAMOND and SOLEIL boosters (located in separate buildings) have emittance of 140 nm; SLS and ALBA boosters (located in the ring tunnel) have emittances of 9 nm. The recently commissioned booster for the Australian light source (ASP) with a circumference of 130.2 m has emittance of 33 nm. The relatively low ASP booster emittance in combination with rather small circumference and conventional choice of a combined-function FODO lattice, looks attractive from the point of view of the design optimization level. A series of injection tracking simulations for the storage ring convincingly demonstrated the adequacy of the booster emittance in the range of 30-50 nm to the low-loss injection with sufficient margins for injection errors. Thus we have chosen the ASP booster model to serve as a basis for the NSLS-II booster development. To minimize the cost of the booster turn-key procurement, we are working to keep the NSLS-II booster design as close to that of the ASP booster. However, there are a few major differences between the NSLS-II and the ASP design:

- The NSLS-II booster injection energy is 200 MeV (in contrast with 100 MeV at ASP)
- The maximum dipole field is chosen to be 1 T (in contrast to 1.25 T at ASP)
- The NSLS-II booster circumference is 158.4 m (one-fifth of the storage ring circumference)
- Straight section length is 7.05 m, compared with 5.8 m at ASP
- The NSLS-II booster current is expected to be 20 mA (in contrast to 5 mA at ASP)

The booster revolution period of 528 ns restricts the length of the injected bunch train to be shorter than about 300 ns because of finite rise- and fall-time of the injection and extraction kickers. Therefore the longest bunch train generated by the linac will consists of 150 bunches.

One of the important requirements for the NSLS-II booster is in high efficiency of the charge transport through the booster. Therefore careful job must be done for optimization of the booster injection and extraction, expansion of booster magnet tolerances, design of robust orbit correction system and adequacy of Dynamic Aperture. In the next chapter we discuss the NSLS-II booster model in detail.

2.3.2 Booster lattice

The four-fold symmetry lattice is designed with five identical cells together with two modified cells containing dispersion suppressors. This results in a sufficiently low horizontal emittance of 26.5 nm-rad at the nominal energy of 3.0 GeV. The booster lattice is presented in Figure 2.3.1.

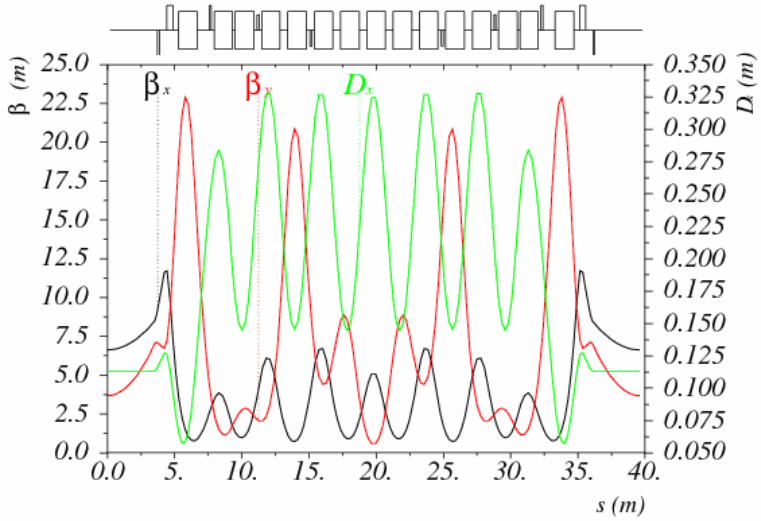

Figure 2.3.1 : One-quarter of NSLS-II booster lattice.

The lattice consists of four long (7.05 m) straight sections with low dispersion (less than 12 cm) suitable for the installation of RF cavity, injection, and extraction systems. Low lattice emittance results in the low level of dispersion and stronger focusing, which increases natural chromaticity (horizontal: -13.8, vertical -18.9), and thus sextupolar gradients integrated in the combined function dipoles. Beta-functions are limited to 25 m, which corresponds to the maximum injected beam size of about 1.7 mm RMS in the vertical plane.

The lattice is composed of two families of combined-function dipoles, together with three families of quadrupoles: QF, QD and QG (Figure 2.3.2). Three separate power supplies for the booster quadrupoles provide freedom in optimizing the lattice and controlling tunes, dispersion, and chromaticity.

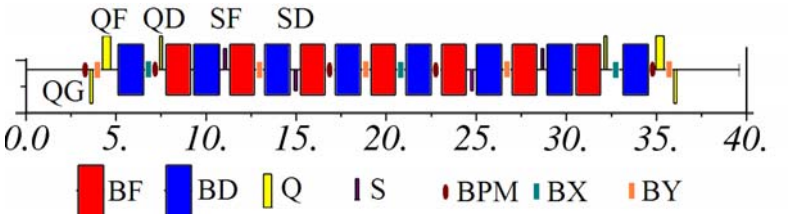

Figure 2.3.2 Elements in one-quarter of the NSLS-II booster lattice.

Chromaticity correction is implemented by introducing sextupolar gradients into the dipole pole tips. In addition, four discrete sextupoles are introduced in every booster quadrant, shown as SSF and SSD in Figure 2.3.2. Separate power supplies for both sextupole families enable independent adjustments of horizontal and vertical chromaticity.

Table 2.3.2 Part count/Magnetic Element Parameters.

Parameter	ASP Booster	NSLS-II Booster
Dipole parameters		
Number, BF/BD	28/32	28/32
Length, BF/BD	1.35/1.15 m	1.35/1.4 m
Angle, BF/BD	3.43/8.25°	3.43/8.25°
Injection energy	100 MeV	200 MeV
Field, BF/BD (inj)	0.015/0.042 T	0.030/0.069 T
Field, BF/BD (ext)	0.443/1.25 T	0.443/1.00 T
Quadrupole K1, BF/BD (ext)	0.82595/-0.66977 m^{-2}	0.82800/-0.63831 m^{-2}
Sextupole K2, BF/BD (ext)	3.54/-4.925 m^{-3}	4.10/-5.65 m^{-3}
Quadrupole parameters		
Number, QF/QD/QG	8/8	8/8/8
Length, QF/QD/QG	0.25/0.15 m	0.45/0.15/0.15 m
Quadrupole K1, QF/QD/QG (inj)	-0.0784/0.0133 m^{-2}	0.1229/0.0581/-0.0869 m^{-2}
Quadrupole K1, QF/QD/QG (ext)	-2.351/0.400 m^{-2}	1.8442/0.87119/-1.3028 m^{-2}
Sextupole parameters		
Number, SF/SD	8/8	8/8
Length, SF/SD	0.2/0.2 m	0.15/0.15 m
Sextupole K2, SF/SD (ext)	50/-30 m^{-3}	40/-40 m^{-3}

Table 2.3.2 illustrates the main parameters of the booster elements in comparison with them in the ASP booster lattice [ASP]. Reducing the booster cost we kept parameters of the focusing dipoles to be close to the original design (see Figure 2.3.3). Defocusing dipoles are similar to the ASP ones but longer (1.4 meters versus 1.15 meters), which shall require reworking hardware for the lamination stacking. Increasing the injection energy from 100 to 200 MeV significantly increased the magnet fields at injection, which simplifies achieving required field quality of the combine-function dipoles.

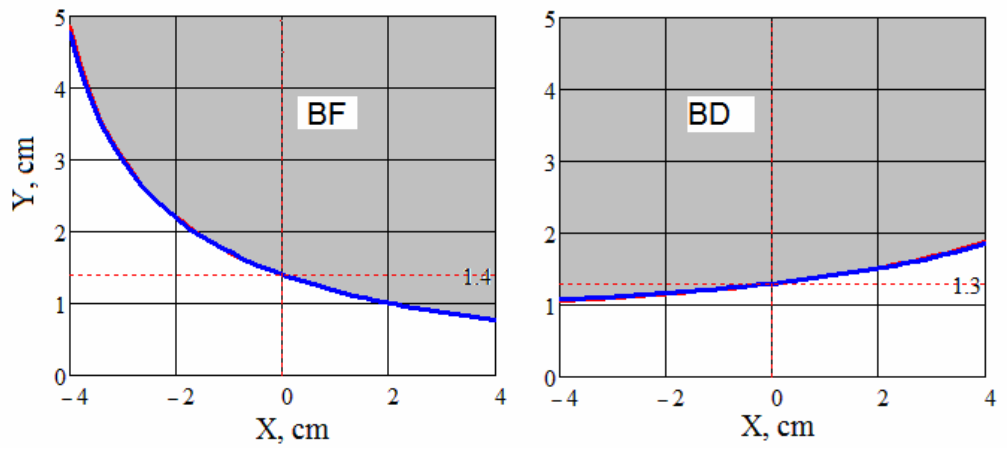

Figure 2.3.3 Magnet pole tip profiles[1], red – original ASP, blue – NSLS-II.
Left plot corresponds to the focusing dipole; right plot corresponds to the defocusing dipole.

The main parameters of the chosen booster lattice are summarized in Table 2.3.3. The parameters of the ASP booster are also listed, for comparison.

Table 2.3.3 Booster Parameters.

Parameter	ASP Booster	NSLS-II Booster
Emittance, nm	34.4	26.6
Circumference, m	130.2	158.4
Booster current, mA	<5	<28
Revolution time, ns	434	528
RF frequency, MHz	499.654	499.68
RF voltage, MV	1.2	1.5
Harmonic number	217	264
X/Y tune	9.2/3.25	10.91/6.69
X/Y chromaticity	-8.83/-11.5	-13.8/-18.9
Expected X/Y coupling	5%	10%
Corrected chromaticities	+0.83/+0.87	+1.7/+1.7
Momentum Compaction	0.0098	0.0072
Energy loss per turn, keV	743	625
X/Y/E damping time, ms	2.7/3.5/2.0	5.4/5.1/2.5
Damped energy spread, %	0.094	0.078
Damped bunch length, mm	19	13.9

The developed lattice is close to the original ASP one; however all of the requirements listed in previous introductory section are fulfilled.

In particular, attention has been paid to increase tunability of the booster lattice in the tune space. In particular, this is important for the tune adjustment at injection and tune correction during energy ramp. Including the third quadrupole family provided with large footprint in the tune space (Figure 2.3.4). While developing this footprint we constrained maximum beta-functions to stay below 20 meters for horizontal and 30 meters for

[1] Thanks to S. Mikhailov (Duke University) for his magnet design program.

vertical. This, in turn, has constrained the booster emittance to be below 50 nm for the whole upper half of the tune footprint (right plot on Figure 2.3.5). As follows from Figure 2.3.4, two defocusing quadrupole families are redundant with respect to each other, in the sense that there exist solutions (not necessarily optimal), which may be accomplished by only a single defocusing family.

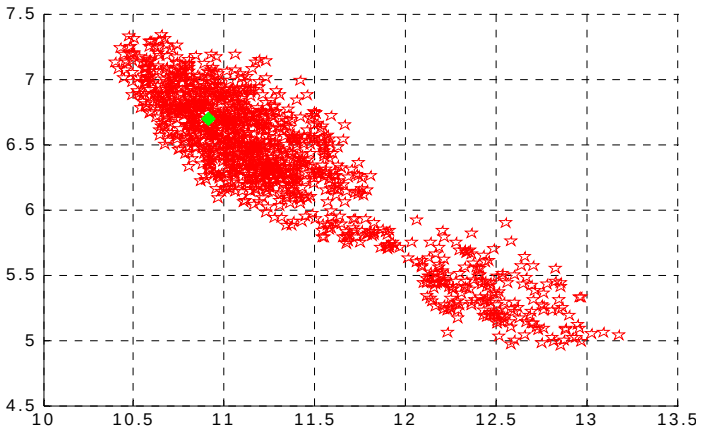

Figure 2.3.4 Tunability of the booster lattice. The plot shows a footprint of the existing lattice solutions under constraints imposed on beta-functions. Green point points the working tune location.

Large tuning range of the booster optics is also beneficial from the Dynamic Aperture optimization. The left plot on Figure 2.3.5 exhibits tune scan for DA optimization. In the peak the booster DA reaches ±10 mm in both planes, which should be sufficient for low-loss injection. We will continue optimizing the DA on the next stage of the design.

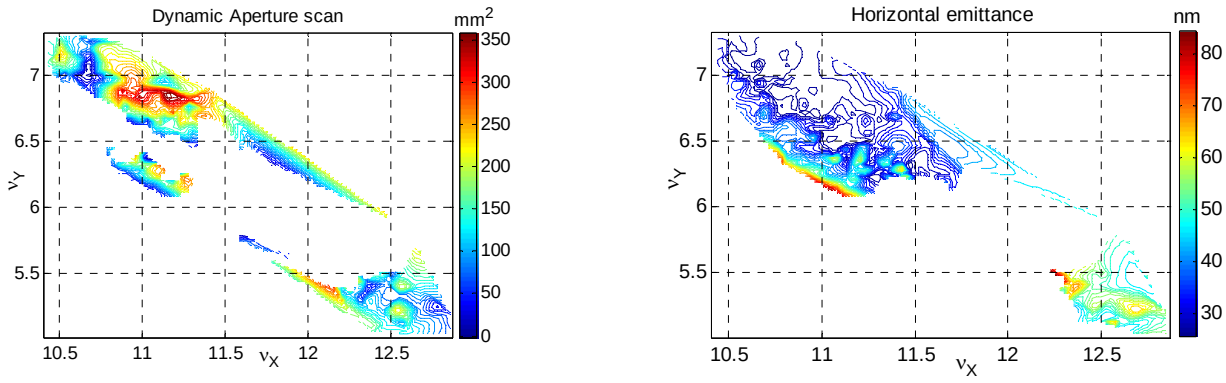

Figure 2.3.5 Tune scan for Dynamic Aperture in mm^2.
Left: abscissa – horizontal tune, ordinate – vertical tune. **Right:** corresponding emittance scan in nm·rad (right plot).

Preliminary consideration has been given to evaluation of the magnet tolerances and orbit correction system. The following tolerances for the magnet alignment and fields were assumed (Table 2.3.4). Tolerances on the magnet parameters were developed using analytical estimates that assumed normally distributed random errors in all magnets.

Table 2.3.4 Magnet Tolerances.

Source of error	Tolerance
Dipole length (relative)	0.1%
Dipole field (relative)	0.1%
Dipole long. displacement	1mm
Dipole transverse misalignment	0.1mm
Quad transverse misalignment	0.1mm
Quad gradient (relative)	0.2%

Orbit correction is implemented using 20 beam position monitors and 20 horizontal and 12 vertical trim magnets. The trim fields will follow the energy ramp, enabling orbit correction at all energies. The developed trim–BPM arrangement allows correcting the booster orbit down to a mm maximum deviation in each plane (Figure 2.3.6). This requires below 0.75 mrad (maximum value) in the corrector strength, making its design simple, with low magnet weight and size. This orbit correction system results in alignment tolerances for the dipoles and quadrupoles summarized in Table 2.3.4. These tolerances can be relaxed further by further optimizing the trim arrangement and adding one more vertical trim per quadrant.

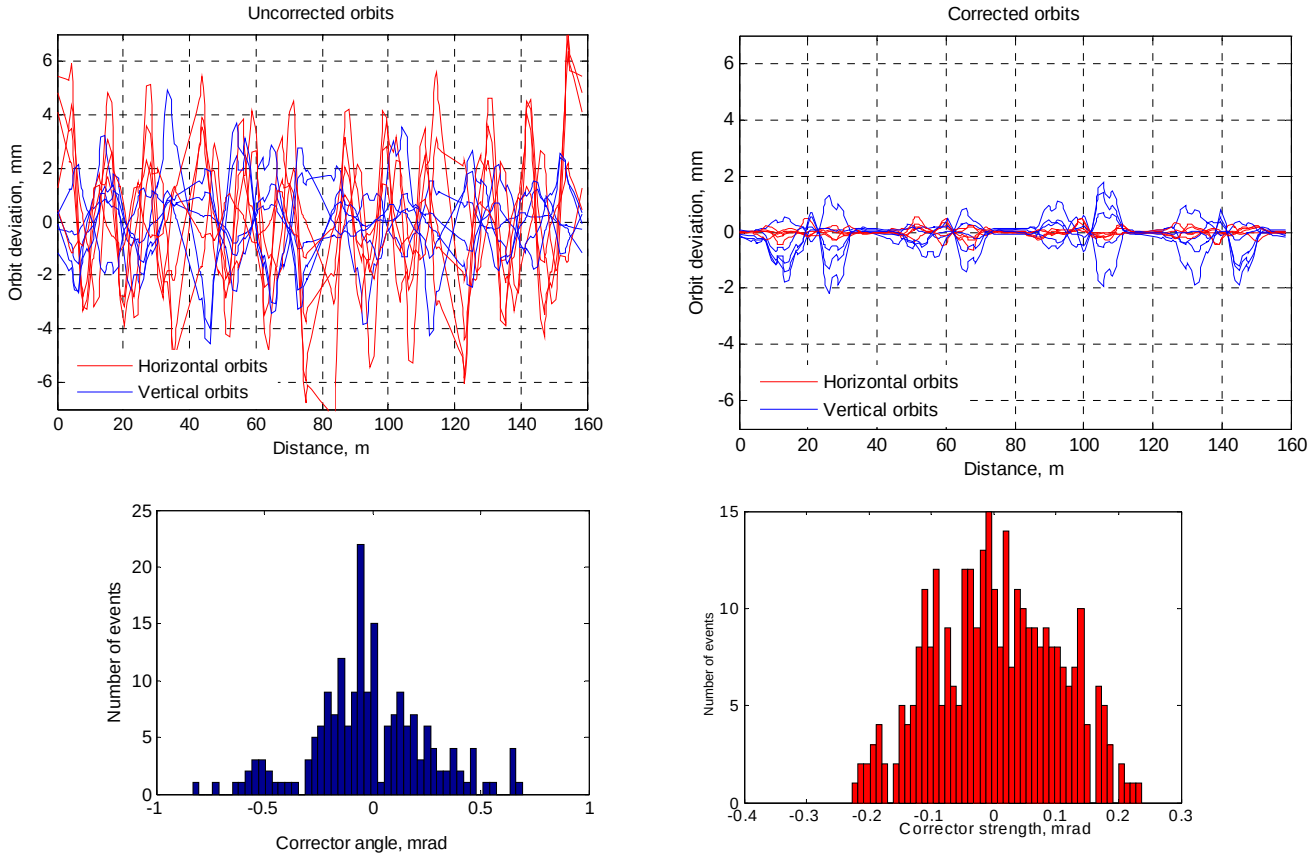

Figure 2.3.6 Uncorrected (left upper plot) and corrected (right upper plot) booster orbits. The two lower plots correspond to the statistics of the corrector angles. Red and blue traces and histograms correspond to horizontal and vertical orbits and and correctors, respectively.

Figure 2.3.7 shows envelopes of the beam injected from the linac. Linac beam parameters were chosen according to values in chapter 2.2. Electron beam phase space ellipse was matched to that of the circulating beam at the booster injection point.

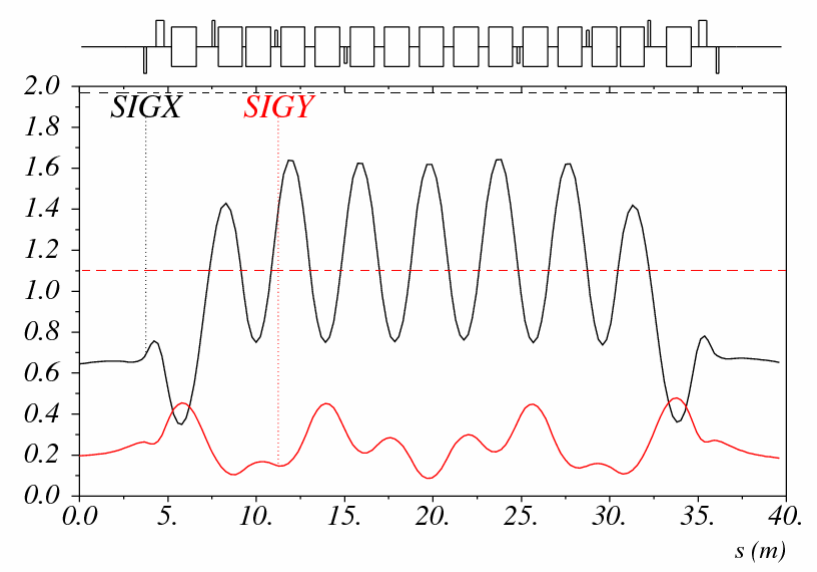

Figure 2.3.7 RMS injected beam envelopes in mm (solid curves). Dashed lines show approximate location of the dipole vacuum chamber (magnified ten times).

Short damping time at the maximum booster energy leads to the fully damped beam at the end of the ramp (Fig. 2.3.8). Here we assumed a sinusoidal ramp profile with the injection point "on the fly", i.e. on the rising slope of the energy ramp.

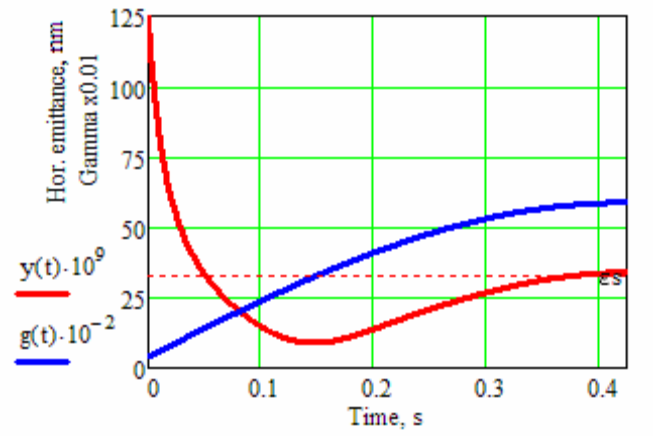

Figure 2.3.8 Booster energy ramp (in units of γ/100, blue curve) and dependence of the horizontal booster emittance versus ramp time (in nm·rad, red curve). Dashed line shows damped value of the booster emittance at 3 GeV.

Figure 2.3.9 shows the estimated beam loss throughout the energy ramp due to residual gas (mainly elastic scattering on the gas nuclei). Total relative charge loss is expected to be about 0.2% at the average value of the booster vacuum of 10^{-7} torr. We estimate the beam lifetime at the injection energy of 200 MeV to be around 10 seconds.

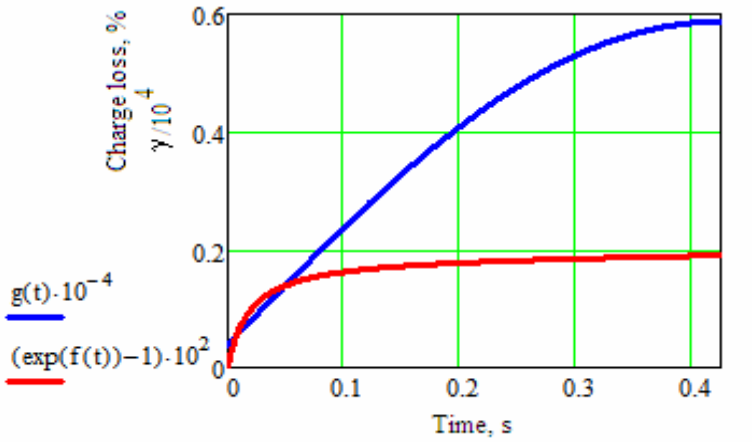

Figure 2.3.9 Relative gas-scattering losses in % of the charge throughout energy ramp.

For an estimate of the chromaticity driven by eddy currents (Figure 2.3.10), we used a formalism developed in [Edd]. For the given lattice parameters, the estimated maximum value of the sextupolar moment is 0.085 m^{-3} at 1 Hz of repetition rare. Corresponding calculated values of chromaticity are +0.5 horizontally and –1.4 vertically, which is much smaller than the natural chromaticity and can be compensated by local modification of the sextupole ramp.

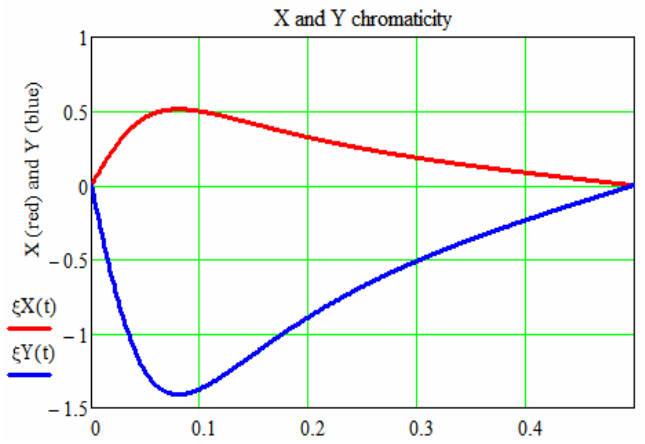

Figure 2.3.10 Eddy-currents induced chromaticity during the energy ramp

Concluding this section, we note that the developed booster design is close to the existing ASP booster except for a few important differences between the two designs that are specific for the NSLS-II and were discussed in the introduction. These were realized in the current booster layout and the overall design appears to be feasible and cost-effective.

In the line of future work, we will pay close attention to the optimization of the Dynamic Aperture and perform modeling of the ring at injection and particle tracking, for evaluating and mitigating potential injection losses. In addition we will explore high average current effects that may be of interest at the maximum value of the booster current.

2.3.3 RF Acceleration System

The booster RF acceleration system must capture the bunch train injected from the 3 GHz linac, accelerate a beam charge of 10 nC (19 mA average current) to 3 GeV, and transfer the bunch train to the storage ring 500 MHz RF buckets (Table 2.3.5). At maximum energy a bucket height of 0.85% is necessary (see Figure 2.3.12) which translates into a necessary accelerating voltage of 1.5 MV. At injection energy this rf voltage can provide a much larger bucket height so that the energy spread of the accepted beam is limited by the physical aperture and/or the transverse off energy dynamic aperture of the lattice and not by the rf system.

Table 2.3.5 RF and Beam Parameters for the Booster.

RF frequency [MHz]	499.68
Loss per turn (3 GeV) [keV]	625
Overvoltage	2
Accelerating voltage [MV]	1.5
Momentum compaction	0.0072
Bunch charge [pC]	1375
RF acceptance %	0.85
Number of bunches	40-150
Nominal beam current [mA]	
Nominal beam power at 3 GeV [kW]	12

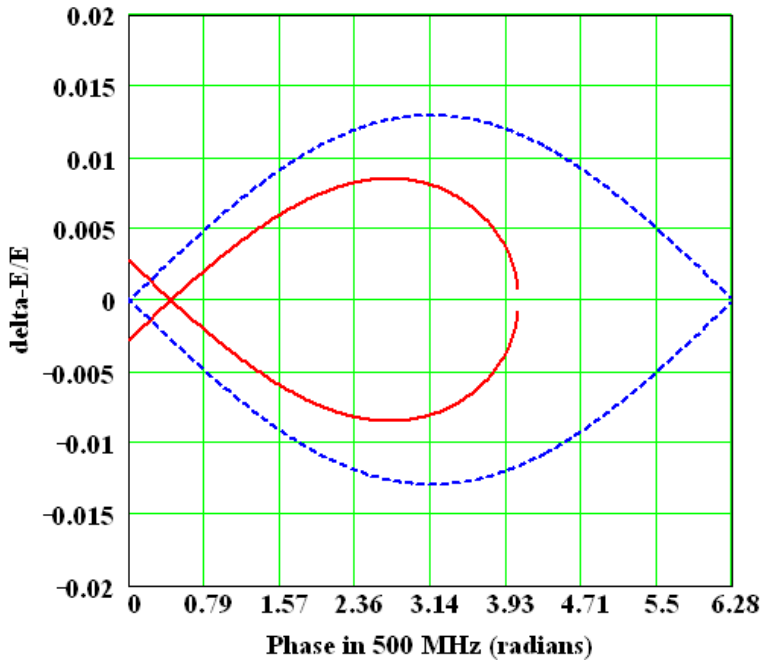

Figure 2.3.11: RF separatrix for 1.5 MV RF field at 3 GeV, with radiation losses (red curve) and the stationary bucket without losses (blue curve). The separatrix provides an energy acceptance ot 0.85% at 3 GeV.

As the rf voltage requirement of 1.5 MV is significantly more demanding compared with the beam power requirement of 12 kW a multicell cavity is the appropriate choice, e.g. the PETRA type 5-cell cavity with a shuntimpedance of 15 MOhm. With a single PETRA type cavity the total necessary rf power (cavity wall losses, beam power, 10% transmission losses and safety margin) is in excess of 100 kW. For this reason two PETRA 5-cell cavities will be used. The geometry of this cavity is shown schematically in Figure 5.3.11

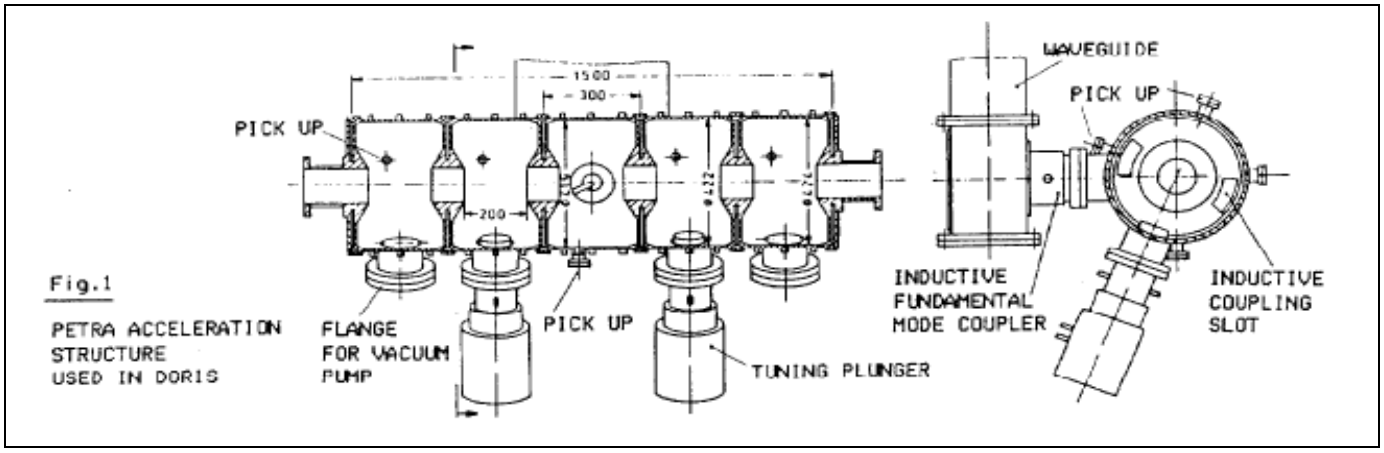

Figure 2.3.12 The five-cell PETRA cavity.

Klystrons and inductive output tubes (IOT) are available as rf power sources at 500 MHz to generate the necessary rf power. In the power range from several ten kW to 80 kW the klystron market became rather small in recent years as these tubes have been replaced by IOTs for TV applications with the consequence of significant increase in cost. IOTs have a higher efficiency (typically 65%) than klystrons and tube cost are about 30% lower as compared to klystrons. For these reasons the baseline power source will be a modified broadcast IOT transmitter capable of 80 kW output power at 499.68 MHz. Since a few years such transmitters are in use at several synchrotron light source facilities. Similar as klystrons IOTs can operate safely only under matched load conditions. Therefore a circulator is necessary between the transmitter and the cavities. Figure 2.3.13 shows a footprint of the cavity section and the IOT transmitter system including the rf power feeding line and the circulator.

The IOT transmitter utilizes a broadcast IOT tube. Several tubes are available to provide 80 kW at 500 MHz, including the THALES TH793, E2V e2v2130, and Communication and Power Industries K5H90W. Tube parameters for the TH793 are given in Table 2.3.7.

Table 2.3.7 Tube Parameters for TH793 IOT.

Beam voltage [kV]	36
Beam current [A]	3.2
Maximum output power [kW]	90
Maximum collector dissipation [kW]	70

For the HV power supply of the transmitter two technical options are in use to provide the DC power to the IOT transmitter: a standard broadcast transformer-rectifier or a Pulse-Step-Modulated switching power supply. The PSM supply has lower ripple, which results in lower residual modulation of the beam and a lower stored energy. These attributes, combined with the fast turn-off capability, eliminate the need for a hard-tube crowbar circuit.

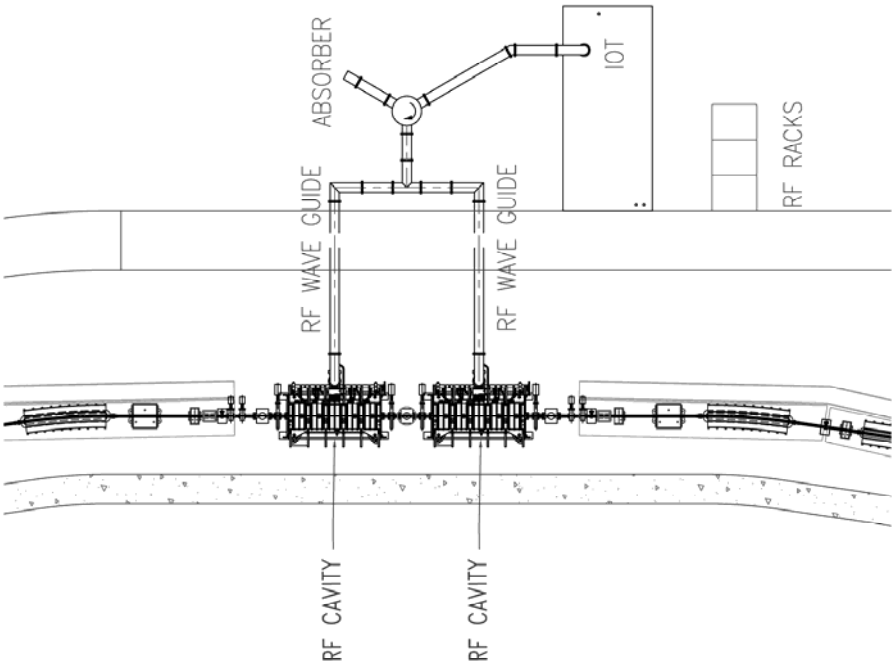

Figure 2.3.13: Footprint of the cavity section and the IOT transmitter system including the rf power feeding line

2.3.4 Booster Injection System

The booster injection system consists of the pulsed septum and kicker with their power supplies (Figure 2.3.14). It is a simple single turn on-orbit injection, allowing a maximum of about 150 consecutive bunches to be injected into the booster RF buckets. The bend angle of the septum is 140 mrad and that of the kicker is 10 mrad, making the total bend angle the same as that of the other LtB TL dipoles. This solution is viable and gives very reasonable field values for the pulsed magnets.

Separation of the trajectory of the injected beam orbit at the end of the septum and the closed orbit of the booster is 20 mm, placing the inside edge of the injection septum at 16 mm from the nominal booster orbit.

Thought is also being given to making the kicker angle larger, thus allowing the septum to be placed further away from the circulating beam in the booster and possibly replacing the pulsed septum with a well-shielded DC magnet.

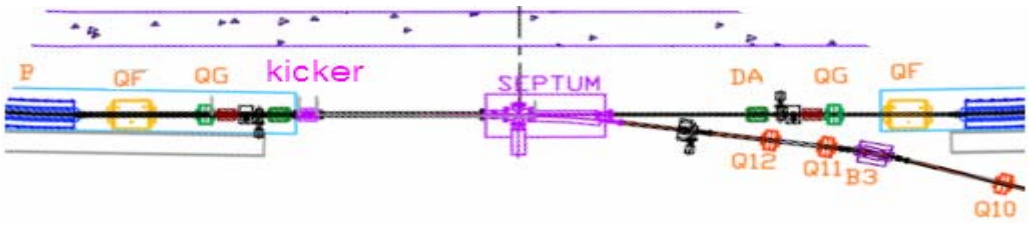

Figure 2.3.14 Booster injection system layout.

The basic magnet parameters are shown in Table 2.3.8.

Table 2.3.8 Booster Injection System Pulsed Magnet Parameters.

Injection Energy 200 MeV	Booster Injection Septum	Booster Injection Kicker
Magnetic Field (T)	0.0933	0.02
Magnetic Field (T)	0.0933	0.02
Length (m)	1.0	0.3
H x V (mm x mm)	20 x 15	50 x 25
Bend angle (mR)	140	10.0
Inductance (μH)	1.676	0.754
Peak Current (A)	1200	450
Drive Capacitor (μF)	340	70 m transmission line
Voltage (kV)	0.08	5.4
Pulse Shape	75 μsec half sine	100 nsec risetime, 300 nsec flat-top
100 nsec fall time Magnetic Materia	¼ mm Si steel	CMD5005
Ceramic chamber Coat	N/A	2 – 3 Ω/□ Ti

The capacitor banks or transmission line PFN's are charged with voltage regulated DC power supplies with up to, at least for the extraction system and ring injection system, 16-bit resolution voltage regulation. The transmission line for the injection kicker is terminated with a de-Q'ing circuit to pull the current/field down before the head of the injected bunch train re-enters the kicker after completing a booster orbit. The system impedances need to be matched carefully to prevent excessive ringing, although the requirements for the booster injection system are not very stringent. Damping during the ramp will erase all memory of injection abnormalities; these will not be translated into extraction orbit displacements.

While searching for ways of reducing charge requirements on the NSLS-II linac we are considering the possibility of the booster injection system to allow stacking of the low-energy beam at the maximum linac repetition rate of 10 Hz. Tracking calculations are in progress for attempting to stack two consecutive bunch trains (separated by 0.1 seconds or more) transversely in the booster by injecting them with ~½ of the nominal kicker strength. Recharging the capacitor banks/transmission line for 10Hz operational capability may require high current supplies and will most likely run more cost effectively at a slower rate to allow the power supplies to settle at the required voltage. As mentioned above, a larger angle for the kicker may allow replacement of the pulsed septum and its large capacitor bank with a DC magnet, eliminating this problem. Further optimization is in progress.

2.3.5 Booster Extraction System

The booster extraction system consists of four slow orbit bumpers, pulsed septum and kicker (Fig. 2.3.15). The orbit of the circulating bunch train is moved out toward the extraction septum over several hundred turns by the slow orbit bumps and is kicked into the extraction septum by the extraction kicker. The arrangement is shown in the plan view below, and the pulsed magnet specifications are outlined in Table 2.3.9.

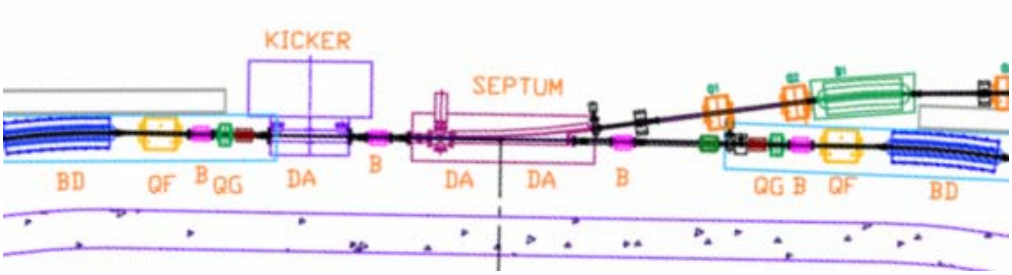

Figure 2.3.15 Booster extraction system layout. B -- orbit bumps.

Table 2.3.9 Booster Extraction System Pulsed Magnet Parameters (at the Extraction Energy of 3 GeV).

	Extraction Septum	Slow Bumps	Extraction Kicker
Magnetic Field [T]	0.8	0.4	0.05
Magnetic Field [T]	0.8	0.4	0.05
Length (m)	1.75	0.2	1.0
H x V [mm x mm]	20 x 15	50 x 25	50 x 25
Bend angle [mR]	140	7.5	5.0
Inductance [μH]	2.932	201	2.513
Peak Current [A]	10,000	400 in 20 turns	1.0
Drive Capacitor [μ])	125	505	65 m transmission line
Voltage [kV]	1.465	0.3	19.75
Pulse Shape	60 μsec half sine	1000 μsec half sine	<200 nsec risetime, 300 nsec flat-top
Magnetic Material	¼ mm Si steel	¼ mm Si steel laminate	CMD5005
Ceramic chamber Coat	N/A	N/A	0.5 Ω/□

The slow orbit bumps use 20 turns of conductor carrying a current of up to 400 A. Consideration to power these in series is under discussion at the moment. The steel laminations will be made of grain oriented heat-treated Si transformer steel with thin insulating coating on one side to reduce eddy currents. A 1.1 T septum with a 75μsec half-sine wave excitation has been running at NSLS for many years.

The extraction septum entrance is 16 mm outside of the central closed orbit of the booster; during extraction the displaced orbit is pushed to coast as close to the extraction septum as possible without incurring beam loss.

The kicker is a full-aperture device producing a field of 500 Gauss, and will be driven by a circuit similar to the one shown below (Figure 2.3.16). It turns on and reaches full flat-top field during the gap in the booster bunch train.

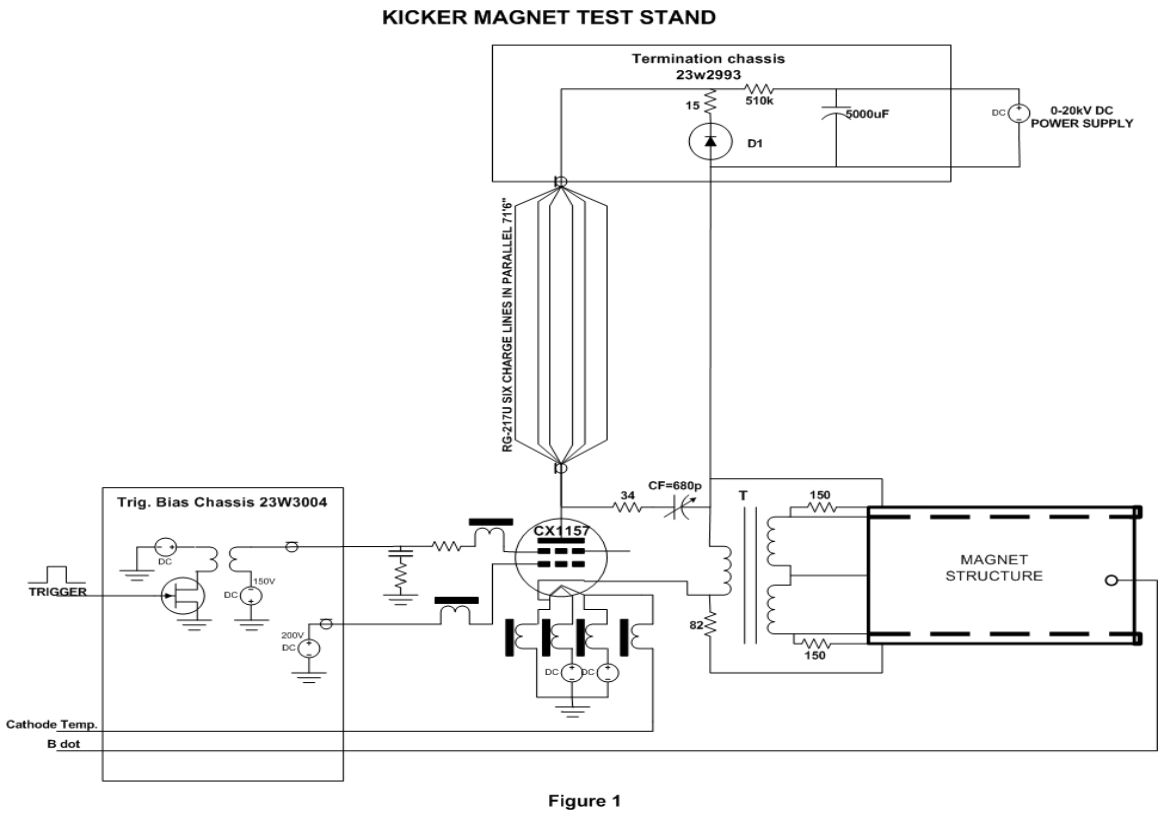

Figure 2.3.16 Booster extraction system layout.

2.3.6 Booster Diagnostics and Instrumentation

This section describes diagnostics and instrumentation for the booster ring. The following parameters will be monitored:

- orbit
- working point (tunes in both planes)
- circulating current and filling pattern
- emittances
- bunch length

Booster diagnostics are summarized in Table 2.3.10.

Table 2.3.10 Beam Diagnostics for the Booster Ring.

Monitor	Quantity	Beam parameter
DC current transformer	1	Beam current
4-button pick-ups	20	Beam position
Fluorescent screens	6	Injection position, profile
Stripline set and amplifier	2	Betatron tune and bunch cleaning system
Fast current transformer	1	Filling pattern
Optical beamline with streak-camera	1	Bunch length
Firewire camera	1	Beam position, profile

Six fluorescent screens will be used to observe shape and position of the injected electron beam during the first turn. The screen material will be YAG:Ce. This was chosen because it results in an excellent resolution of the beam image and exhibits high sensitivity and high radiation hardness.

The booster orbit will be monitored with 20 pick-up electrodes instrumented with Libera receivers. The receivers are the same as used for the storage ring and have the specifications shown in Table 2.3.11 [ite]:

Table 2.3.11 RF BPM Specifications.

Beam intensity range [dB]	>70
Input signals	0 dBm –70 dBm, 50 Ω
Operating frequency [MHz]	500 MHz
Noise RMS for k=10 mm [μm]	<3 (1.15 MHz BW) @ -20 dBm
	<15 (1.15 MHz BW) @ –44 dBm
Beam current dependence 0…-50 dBm [μm]	1
Fill pattern dependence 100%-20% [μm]	1

The booster current will be measured with a parametric current transformer, such as the one manufactured by Bergoz [ber1]. Its radiation-hardened sensor head is equipped with 30 m cable and its inner diameter of 115 mm is sufficient to fit over the flange. The parametric current transformer has the following specifications:

Table 2.3.12 Booster Current Monitor Specifications.

Full scale ranges	±20 mA, ±200 mA, ±2 A, ±20 A
Range control	2 TTL lines
Output [V]	±10
Output bandwidth (–3 dB)	8 kHz in 20 mA range, 10 kHz other ranges
Response time (at 90%) [μs]	<50
Resolution [$\mu A/Hz^{1/2}$]	<5
Output accuracy [%]	±0.1
Linearity error [%]	<0.1
Output impedance [Ω]	100

The filling pattern will be monitored with a fast current transformer. For example, the Bergoz FCT has the following specifications [ber2]:

Table 2.3.13 Fast Current Transformer specifications for measurements of the filling pattern.

Turns ratio	20:1
Nominal sensitivity [V/A]	1.25
Rise time (typ.) [ps]	200
Droop [%/μs]	<6
Upper cutoff frequency (–3 dB typical) [MHz]	1750
Lower cutoff frequency (–3 dB) [kHz]	<9.5
Position sensitivity [%/mm]	<0.2
Minimal L/R time constant [μs]	17
Maximum charge per pulse (pulses<1 ns) [μC]	0.4

We will evaluate a design of an in-flange version of FCT from the vacuum point of view and perform analysis of the wake-fields. If the design will be found unsatisfactory then the FCT will be placed over ceramic break equipped with RF shield.

The synchrotron radiation from one of the bends will be used for bunch-length measurements with the help of a streak camera [stca].

The fractional tune measurement system will be based on real-time spectral analysis of the signal induced on the strip-lines by the electron beam. Electron beam motion will be excited by broadband noise generator with fixed cutoff frequencies. The real-time spectrum analyzer will be used to observe tune evolution along the ramp. Tune measurement system based on the PLL will also be considered.

The synchrotron radiation from the bending magnet will be used for beam observation with CCD cameras. The beam image will be analyzed for the emittance measurements and also will provide information on the beam position and stability during the ramp.

2.3.7 Beam Chambers and Vacuum System

2.3.7.1 Vacuum System Scope

The booster ring vacuum system includes all vacuum chambers, vacuum pumps, vacuum instrumentation and diagnostics, vacuum controllers, and connecting wiring. The vacuum chamber design, materials, and processes are described in Section 2.3.7.2. The estimated gas load, pumping scheme, and expected pressure distribution in the booster are given in Section 2.3.7.3. The vacuum monitoring and control are explained in Section 2.3.7.4.

An average pressure below $1x10^{-7}$ Torr (see Section 2.3.2) is needed within the booster to minimize the beam loss and bremsstrahlung radiation due to beam-residual gas scattering. The booster vacuum system will be designed with sufficient pumping capability to achieve vacuum pressures in the 10^{-8} Torr range. Most booster vacuum chambers will be constructed from seamless stainless steel tubing and will utilize Conflat flanges.

2.3.7.2 Vacuum System Design

The booster vacuum will be divided into eight sections isolatable with radiation-resistant EPDM-sealed gate valves. The four (4) arc sectors will be ~ 33 m each and the four (4) straight sections of ~6 m each. Each arc sections will have 15 bending chambers of ~ 1.5 m long for BF and BD magnets, and short straight pipes for multipole magnets, bellows and side ports for appendage components such as gauges, valves, ion pumps, etc. The four straight sections will house injection, extraction, RF cavities and beam diagnostics. Conventional ultra high vacuum technology will be implemented. High vacuum will be achieved with small sputter ion pumps distributed around the booster ring.

The booster will accelerate the 200MeV bunch train from the linac to the full energy of 3 GeV at 1 Hz repetition rate. To minimize the eddy currents during the fast ramping fields (and the associated sextupole effect), the vacuum chambers will be made of thin-wall stainless steel. A wall thickness of about 0.7 mm is sufficiently strong for a bending chamber with an elliptical cross section of 24 mm (V) × 40 mm (H), while having sufficiently low eddy currents. The 60 bending chambers will be about 1.5 m long with bending radii of 10 m and 23m for defocusing and focusing chambers, respectively. They will be made from seamless stainless tubing, drawn and pressed into elliptical shape, then roll-curved to give the required bend angles. The ends of the bending chambers will be tapered from elliptical to round cross-section and welded to Conflat flanges. The maximum stress and deflection of the bending chamber under the external atmospheric pressure occurs at the top and bottom of the chambers. Using finite element analysis, the stress and deflection are found to be 11000 psi and 0.2 mm, respectively (Figure 2.3.17), which is well within acceptable ranges with large safety margins.

The straight drift pipes between bending chambers will have an inner radius of 20mm and made of thin wall stainless steel. Each drift pipe is approximately 0.8m long consisting a section for multipole magnets, a precision machined block for mounting of the four BPM buttons, a cross for vacuum pumps and gauges, and a short bellows. Conflat flanges (size DN38) will be used throughout the booster ring.

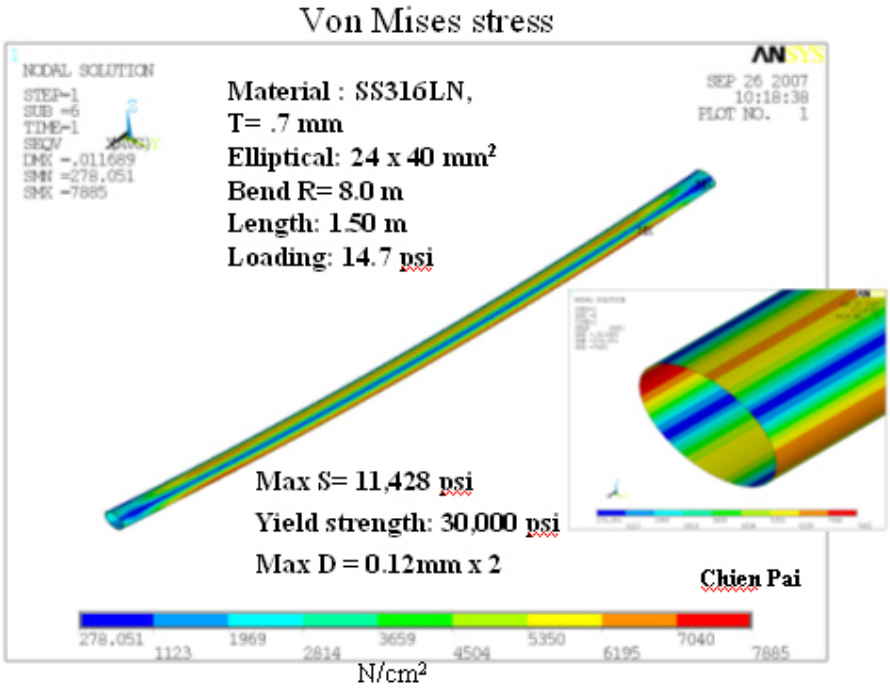

Figure 2.3.17 Calculated stress of the thin-wall bending chamber under vacuum load. The high stress is at the side of the tube along the horizontal plane with maximum stress of less than 11kpsi. The calculated deflection is ~0.2 mm.

After proper chemical cleaning, the completed chambers and drift pipes will be vacuum degassed at 450ºC in a vacuum furnace for several days to remove any trace of surface contaminants and to reduce outgassing, eliminating the need for in-situ baking. The chambers and the pipes are then assembled into the magnets, welded with end flanges, and tested prior to installation in the tunnel. Once they are installed and connected to other beam pipes, two gate valves will be mounted at the end of arc sections, so each section can be pumped down to high vacuum.

2.3.7.3 Vacuum Pumping and Pressure Distribution

The thermal outgassing of the clean stainless chamber surface will be less than $1x10^{-10}$ Torr-l/s/cm^2, 24 hours after pumping down. This is equivalent to a total thermal gas load of ~$2x10^{-5}$ Torr-l/s for the whole booster ring, excluding the contributions from RF, injection, extraction, and diagnostics. The pressure in the booster will be

dominated by the synchrotron radiation-induced desorption during the filling of the storage ring. This effect will be much less pronounced during the topoff injection mode due to low duty factor. Assuming a 25 mA multi-bunch beam accelerated to 3.0 GeV in the booster during the 0.4 sec acceleration cycle, the average synchrotron radiation power on the vacuum chamber wall will be less than 2000 W for the whole ring, concentrated at the downstream end of the dipole chambers, with a linear power density less than 40 W/m. No observable temperature rise at the chamber wall is expected.

The average photon flux during acceleration is approximately 1×10^{19} photons/sec. Assuming a PSD yield of $\eta = 2\times10^{-4}$ molecules/photon, the total photon-desorbed gas load will be about 1×10^{-4} Torr-l/s, which is much higher than the thermal desorption gas load. Desorption yield of $\eta = 2\times10^{-4}$ mol/ph can be achieved with an integrated dosage of 10^{19} ph/meter, reached in a few hours of continuous booster operation. Both the thermal- and photon-desorbed gas load will be handled with the 30 l/s ion pumps at the downstream end of each bending chamber. The pressure distribution in booster arc section can be estimated using standard linear conductance formulae and super imposing photon stimulated desorption over the thermal desorption. The pressure distributions of a 10 m long arc section for three different pumping schemes are plotted in Figure 2.3.18, with one 30 l/s ion pump downstream of each bending chambers (~ 2.2m pump spacing); with one 100 l/s ion pumps downstream of each bending chamber; and with one 30 l/s ion pump at every other bending chambers (~ 4.4m pump spacing). The average pressure for 1st case is about 1.2×10^{-7} Torr and 25% lower with 100 l/s ion pumps. Due to the limited conductivity of the small-diameter beam pipes, the average pressure will improve with shorter pump spacing, rather than with larger ion pumps, as illustrated in the 3rd case, where pressure increases by factor of 3 when number of pumps is halved. The average pressure will improve rapidly to mid 10^{-8} Torr within a week, since η decreases with integrated beam dose and thermal outgassing decreases with time.

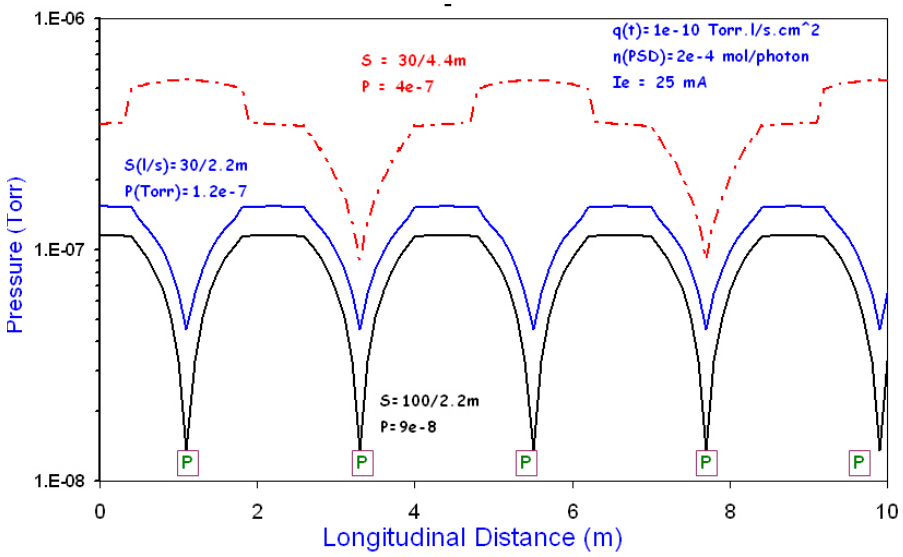

Figure 2.3.18 Pressure distribution in booster arc sections from both thermal desorption and photon-stimulated desorption. Each arc sectionl will have fifteen (15) 30 l/s ion pumps, at downstream end of each bending chamber. Due to the limited linear conductance of the small diameter beam pipes, the average pressure only decreases by 25% if 100 l/s ion pumps are used in place of the 30 l/s pumps. The average pressure will increase three folds if only one ion pump is installed for every two bending chambers.

The booster ring vacuum sectors will be roughed down from atmospheric pressure with portable turbo-pumps (TMP) backed with dry mechanical pumps before transferring to the sputter ion pumps. Two right-angle, all-metal valves will be mounted at each vacuum sector for roughing, bleed-up, and for other vacuum diagnostics. The TMP stations will have their own vacuum gauges and an electro-pneumatic valve to isolate the TMP from the vacuum section in the event of pump or power failures. The TMPs will be manually isolated with valves, once each booster ring sector is at high vacuum. Large ion pumps of about 200 l/s, identical to those deployed in the storage ring, will provide sufficient UHV pumping speed at the straight sections for RF cavities, injection, extraction, and diagnostics.

2.3.7.4 Vacuum Monitoring and Controls

Power supplies and controllers for linac and booster vacuum systems will be located in the satellite electrical racks in the Injector service area. Commercial dual ion pump controllers and vacuum gauge controllers with local and remote capabilities will power, monitor, and control the ion pumps and vacuum gauges, and interface with the PLC and control computers. Ion pump currents and the vacuum gauges will provide information on the pressure distribution in the booster ring.

2.3.7.4.1 Vacuum Monitoring

The booster vacuum will be monitored and interlocked with the ion pump current and the vacuum gauge readings. Each arc vacuum section will have a convection-enhanced Pirani gauge (TCG), two inverted-magnetron cold cathode gauges as the primary gauges, and 15 30 l/s ion pumps. One set of vacuum gauges and two large ion pumps will be installed at the short straight sections to handle the extra outgassing from RF cavities, kickers, septums and diagnostics. Residual gas analyzer heads will also be installed at short straight sections for diagnostics during operation and maintenance periods. A residual gas analyzer head may be mounted on the portable TMP stations to assist the pumpdown and troubleshooting of arc vacuum sections. Table 2.3.14 presents a list of booster vacuum devices, together with those for linac and beam transport lines.

Table 2.3.14 List of Vacuum Components for the Linac and Booster Vacuum Systems.

	IP (30 l/s)	IP (200 l/s)	TCG	CCG	TMP	RGA	GV
E-gun	2	2	2	2	1	1	2
GtL		2	1	2	1		2
Linac		8	4	8	1	1	2
LtB	4		2	4	1		2
Booster	60	8	8	12	4	3	8
BtSR	6		1	2	1	1	2
Total	72	20	18	30	10	6	18

2.3.7.4.2 Vacuum Controls

The vacuum control system will interface with vacuum devices while being part of the machine control. Due to the high radiation levels in the tunnel, all the vacuum devices will be located at the satellite control racks. These vacuum devices (such as gauge controllers, ion pump controllers, RGA, etc.), with local and remote capabilities, will communicate with the machine control system through RS232 or Ethernet links for remote monitoring, operation, and control. The low-level vacuum control will consist of dedicated vacuum programmable logic controllers. Each PLC has both digital and analog I/O modules with inputs from various vacuum devices, and provides the logic for the operation of the sector gate valves, the interlocks for other subsystem devices, and generation of the beam permits. For the gate valve control, a voting scheme with inputs from the setpoint contacts of several ion pumps will be used to initiate the interlock functions, therefore minimizing false triggering due to the failure of a single pump.

2.3.8 Booster PS

Since the booster system is foreseen as a turn-key procurement, power supplies will be design to match our requirements on the booster magnet lattice. Given that our magnet design is close to that at the existing ASP booster we expect that the dipole and quadrupole power supplies specifications will be close to that at the ASP (Table 2.3.15).

Table 2.3.15 Preliminary specifications for the booster power supplies.

Name	Number	Io, A	Vo, V
Dipole BF	1	900	220
Dipole BD	2	900	400
Quadrupole QD	1	100	50
Quadrupole QF	1	200	50
Quadrupole QG	1	100	50
Sextupole SXV	8	21	73
Sextupole SXH	8	18	45
Corrector	32	12	25

2.6.8.1 Power Supply Interlocks

All power supplies will have sufficient interlocks to prevent the power supply from damage due to changes in cooling conditions, AC power disturbances, and out-of-range setpoints. All magnet coils will have an over-temperature interlock if damage can occur due to a change in cooling or operating conditions. All power supplies will have an electrical safety interlock that will prevent the power system from turning on if the machine safety system requirements so warrant.

2.6.8.2 Electrical Safety

All power supplies will conform to the latest BNL safety requirements, especially concerning arc flash protection. Whenever possible, NRTL-listed equipment will be used.

2.6.8.3 Cable Tray

The cable tray for the magnet circuits will be located inside the main tunnel, on the ceiling. All cables will be tray-rated. Power cables will be arranged to minimize pickup from other circuits. All power cables will be separated from signal cables. All cables and trays will meet NEC requirements.

2.6.8.4 Power Supply Instrumentation

Redundant DCCTs or shunts will be used to confirm the power supply current reproducibility. High-precision DMMs and scanners will be used to monitor the power system current, the redundant current sensor, and the analog current setpoint. This equipment will ensure long-term stability and reproducibility. Temperature monitoring of the magnet coils and power system environment will be accomplished using low-cost digital temperature sensors. With such system, a problem can be identified before it becomes an emergency, making it possible for repairs to be scheduled more conveniently and economically.

2.6.8.5 Power Supply Controls

Each booster power supply circuit will require a Waveform Function Generator. These VME device cards will be located in a control system's VME chassis, mounted in one of the power supply system racks. The WFGs will generate the reference current profiles, input analog data, and perform digital state control and status readbacks. A timing system will be needed to synchronize all the WFGs. The output of the WFGs is connected via fiber optics to a Power Supply Interface. The PSI has a precision digital-to-analog converter for generating the reference current, and a multi-channel analog-to-digital converter for inputting power system signals. The PSI also has digital IO for state control and status readbacks of the power supply.

The other controls will include the operation of the high-precision DMM and scanner, and readout of the digital temperature sensors.

2.3.9 Injection System Service Building

In the following we briefly describe the injector service building layout (Figure 2.3.19). The service area will contain all injector equipment including that for the linac, transport lines, booster and the SR injection straight section. It will also include rooms for utility distribution system, workbenches and local control room.

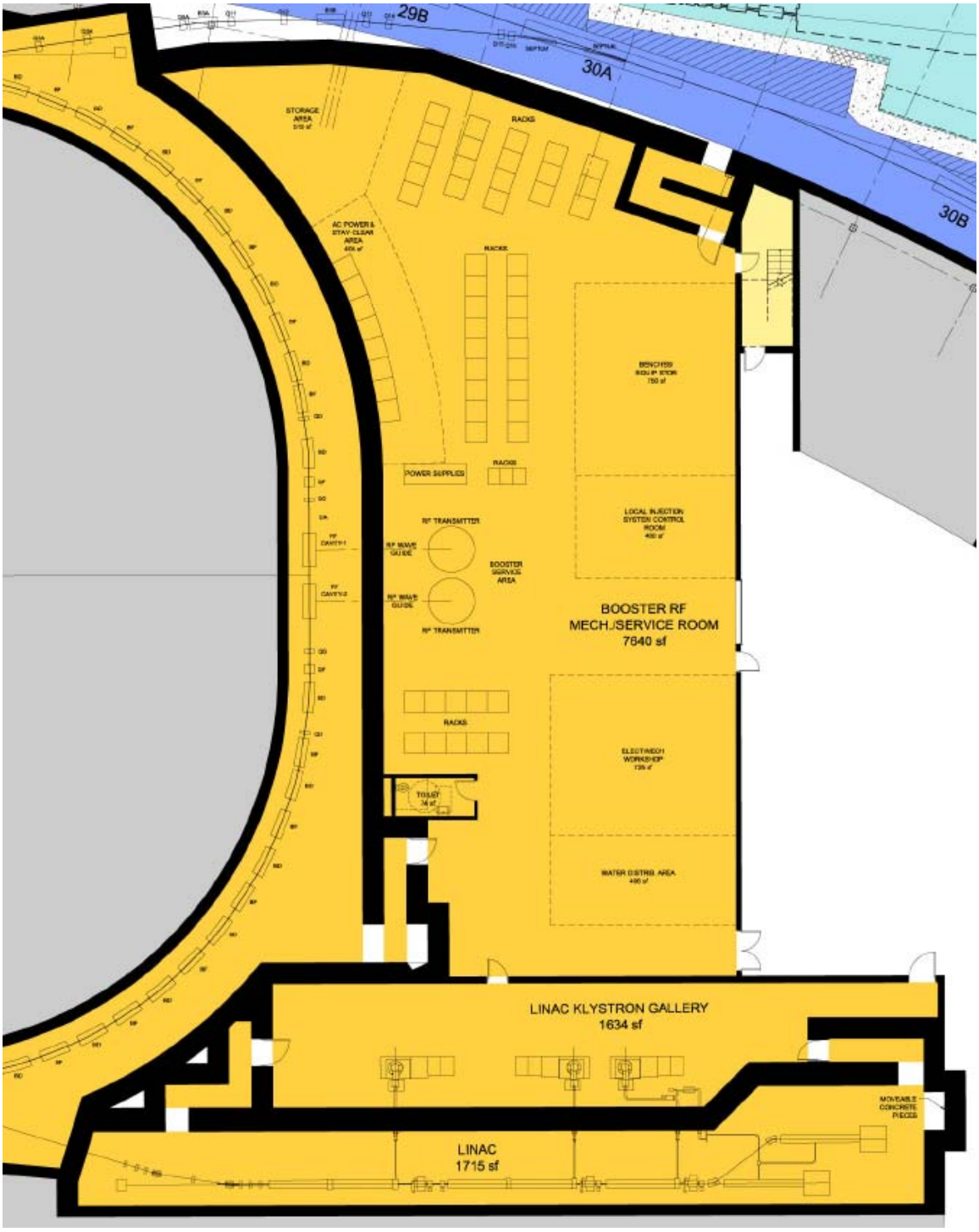

Figure 2.3.19 Layout of the injector service area

Service areas in the injector service building are listed below.

1. Booster service area
    - three dipole power supplies
    - three quadrupole power supplies
    - two sextupole power supplies
    - 40 corrector power supplies
    - vacuum power supplies
    - Injection Pulsed Magnets
    - Extraction Pulsed Magnets (bumps, kicker and septum)
    - Diagnostics: two racks
2. LbTL Service Area

    Nine racks altogether
3. B-SR TL Service Area (all areas with power supplies, vacuum equipment and diagnostics)
    - Storage ring injection system Area
    - Timing System
    - B-SR: ten racks altogether
    - SRIS: four racks (bumps), three racks (septa)
    - TS: two racks
4. AC power disconnects/ switch gear + stay-clear area
   eight panels + stay-clear area during switch operation
5. two entry labyrinths
7. bathroom
8. local Injection System Control Room
10. equipment storage area (spare parts and test instruments)
11. electronic/mechanical workshop
12. water and air distribution area (linac)
13. booster RF area

Total for building **610m^2**

2.3.10 Linac and Booster Utilities System

The cooling water for both the linac and booster ring will be provided from one of the Mechanical Equipment Rooms (MERs), whose process water system will be sized such that it will supply the necessary capacity for the linac and booster, as well as the MERs' respective copper and aluminum systems. The total heat load for this MER will be ~1.2 MW, with the linac requiring cooling for ~100 KW and the booster needing ~400 KW cooling capacity.

Both a supply and return pipe will originate from the MER and travel to both the linac and booster, at which point the necessary connection points will be supplied so as to allow their respective components to be connected to the process water. The process water will have the following thermal hydraulic parameters:

- supply (inlet) pressure ~ 120 psig
- supply (inlet) temperature ~80 F
- supply (inlet) temperature stability ± 1°F
- The booster piping will be sized for ~212 gpm and the linac piping will be sized for ~53 gpm; this results from a temperature differential across the components of ~13°F.
- The water will be clean with a resistivity of ~ 1 MOhm-cm.

Compressed air is expected to serve only for a few applications, such as, powering the phosphor screens and will be discussed in details during the next stage of the design.

References

[asp] http://ieeexplore.ieee.org/iel5/10603/33511/01591747.pdf?arnumber=1591747 asp
[dia] http://accelconf.web.cern.ch/AccelConf/e02/PAPERS/TUPRI097.pdf
[sol] http://ieeexplore.ieee.org/iel5/10603/33511/01591041.pdf?arnumber=1591041
[sls] The SLS booster synchrotron, W. Joho, M. Muñoz and A. Streun,
Nucl. Instrum. and Meth. A**,** Vol. 562-1, pp. 1-11
[alb] http://epaper.kek.jp/e06/PAPERS/THPLS057.PDF
[binp] http://ieeexplore.ieee.org/iel5/10603/33511/01590651.pdf?arnumber=1590651
[Edd] M. Munoz and V. Joho, Eddy current effects in the SLS booster:
http://**sls**bd.psi.ch/pub/**sls**notes/tmeta9810/**eddy**.html
[ite] http://www.i-tech.si/products.php
[ber1] http://www.bergoz.com/products/NPCT/PCT-downloads/files/NPCTflyer.pdf
[ber2] http://www.bergoz.com/products/FCT/d-fct.html
[stca] http://www.optronis.com/

2.4 Transport Lines

2.4.1 Linac-to-Booster Transport Line

2.4.1.1 Scope

The main function of the linac-to-booster (LtB) transfer line is to transport the 200MeV electron beam from the linac to the booster. A schematic diagram of the transport line in relation to the booster is shown in Figure 2.4.1.

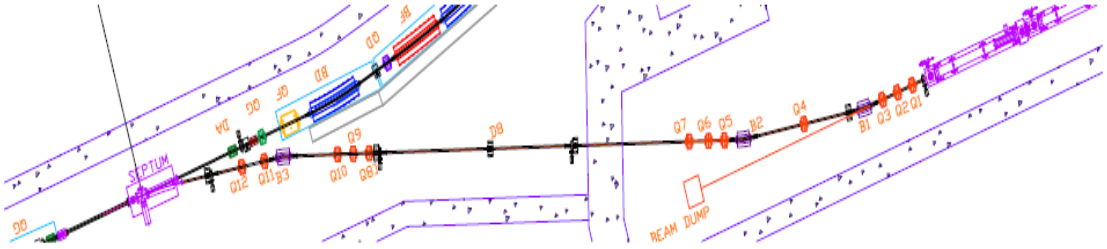

Figure 2.4.1 Schematic diagram of the LtB beam transport line. The beamline starts at the exit of the linac (30 cm upstream of Q1 shown in the figure) and ends at the exit of the injection septum which is part of the booster synchrotron. A section of the booster is shown at the left side of the figure.

The LtB line is defined between the exit point of the 200MeV linac, located 30 cm upstream of Q1, as shown in Figure 2.4.1, and the "booster injection point," located at the exit of the injection septum, shown also in same figure. The beamline has been partitioned into three sections, which are briefly discussed below.

- *The linac to achromatic section:* This section of the beamline transports the beam from the exit of the linac to the beginning of the "achromatic section." It consists of four quadrupoles and two dipoles, which each bend the beam to the right by 150 mrad. The beam is achromatic at the exit of this section.
- *The achromatic section:* The transported beam in this section is achromatic, and consists of six quadrupoles.
- *The Injection-matching section:* This is the last section of the line, and matches the transported beam to the circulating beam of the booster at the injection point, which is located at the exit point of the septum (Figure 2.4.1). This section of the line consists of a "bend to the left" dipole of 150 mrad, the injection septum, which also is a 150mrad "bend to the left" dipole, and two quadrupoles.

2.4.1.2 Beam Constraints along the LtB Line

The main beam constraints of the LtB line is to transport the extracted beam from the exit of the linac to the booster injection point, and match the beam parameters of the beam at the booster injection point to those of the circulating beam in the booster. The beam parameters [SOLL] at the linac's exit and booster injection point are shown in Table 2.4.1. The values of vertical dispersion and angular dispersion functions at these two points are zero.

Table 2.4.1 Beam Parameters at the Linac Exit Point and Booster Injection Point.

	α_x	β_x ,m	η_x ,m	η'_x	α_y	β_y, m
Linac exit point	-1.7	40.0	0.0	0.0	-1.7	40.0
Booster Injection point	7.212	8.027	-0.128	0.0	-0.523	3.043

The following additional constraints are also imposed on the LtB transport line.

- The maximum values of the horizontal and vertical beta function along the line should be less than 100 m ($\beta_{x,y}$<100 m). Similarly, the absolute values of the horizontal dispersion should be below 0.5 m ($|\eta_x|$<0.5 m) at any point along the line. This will make the size of the beam along the line compatible with the physical aperture of the line. The geometrical projected beam emittance is 50π mm·mrad in both the horizontal and vertical directions.
- The "achromatic section" of the line is designed to provide an achromatic beam in both the horizontal and vertical directions. This section of the line will be used to characterize the transported beam by measuring its projected emittance and the beam parameters at any point upstream of this section. The beam characterization can be performed by utilizing the "nominal" settings of the quadrupoles that are used to transport the beam or by altering the settings of the quadrupoles.

2.4.1.3 Beam Optics of the LtB Beam Transport Line

The beam optics of the LtB line must satisfy the constraints mentioned earlier. The beam optics were calculated with the MAD computer code, Version 8b.

The calculated values of the beta functions ($\beta_{x,y}$), and dispersion function (η_x) are plotted in Figure 2.4.2. The horizontal and vertical beam envelopes that correspond to geometrical projected beam emittances ε_x=50π mm·mrad and ε_y=50πmm·mrad are plotted in Figure 2.4.3. The projected beam emittances ε_x and ε_y correspond to two standard deviation of the beam intensity.

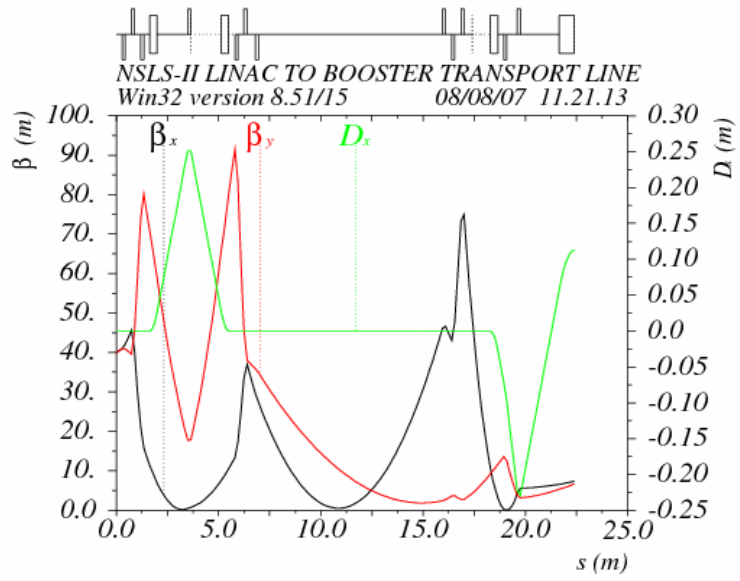

Figure 2.4.2 The $\beta_{x,y}$ (black and red lines) and η_x function (green line) at the beginning and the end of each magnetic element. The large black rectangles shown on the top of the figure represent the dipoles, and the thin black rectangles represent the quadrupoles.

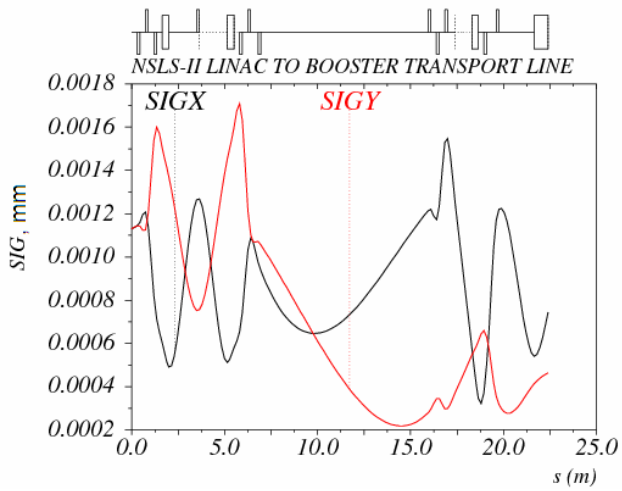

Figure 2.4.3 Half of the horizontal and vertical beam envelopes (black and red lines) that correspond to $2\sigma_{x,y}$ beam emittance. The black rectangles at the top of the figure represent the dipoles and the quadrupoles magnets.

2.4.1.4 Magnetic elements of the LtB beam transport line

In this section we provide a table with the geometry (length, aperture) and the strength of the dipoles and quadrupoles of the LtB line. Table 2.4.2 shows all the main magnetic elements of the LtB line that are used to generate the line's first-order optics, discussed in the previous section. Each magnetic element has its own power supply.

Table 2.4.2 Length, Aperture and Strength of the Main Magnetic Elements of the LtB Line.

Element Name	Type	L [m]	Gap/Rad[cm]	Strength [rad] or [m^{-1}]	Power Supply
Q1	Quadrupole	0.150	2.0	-0.09548	P Q1
Q2	Quadrupole	0.150	2.0	1.02667	P Q2
Q3	Quadrupole	0.150	2.0	0.90802	P Q3
B1	Dipole	0.350	3.0	0.150	P B1
Q4	Quadrupole	0.150	2.0	1.17679	P Q5
B2	Dipole	0.350	3.0	0.150	P B2
Q5	Quadrupole	0.15	2.0	-1.04264	P Q5
Q6	Quadrupole	0.150	2.0	1.15803	P Q6
Q7	Quadrupole	0.150	2.0	-0.04559	P Q7
Q8	Quadrupole	0.150	2.0	0.32202	P Q8
Q9	Quadrupole	0.150	2.0	-0.95966	P Q9
Q10	Quadrupole	0.150	2.0	1.10812	P Q10
B3	Dipole	0.350	3.0	-0.150	P B3
Q11	Quadrupole	0.150	2.0	-1.09038	P Q11
Q12	Quadrupole	0.150	2.0	1.70708	P Q12
BUMP	Dipole	0.350	3.0	-0.150	P BUMP

2.4.1.5 Linac-to-Booster Power Supplies

The LtB power supplies are connected to dipoles, quadrupoles, and vertical/horizontal correctors. The supplies will stay at the nominal setpoint only during the ring fill. For energy savings, it is anticipated that the supplies' output will be lowered during the dwell time in top-off mode and brought back to the operating point slightly before the fill cycle.

2.4.1.5.1 Power Supply Control

Each transfer line power supply will be set by its analog programming interface. Either a micro-controller or PLC could be used to control the supply. Analog output voltages from the control system will be used to control the current setpoint of the supply, and the digital-to-analog converter will have a resolution of at least 16 bits. Both supply output voltage and current will be read back by medium-speed analog-to-digital converters with a resolution of 16 bits. Monitoring of the supply outputs should be able to detect transients as short as 1 ms. Long-term monitoring of drift will be done by an independent external shunt connected to a high-precision analog channel.

2.4.1.5.2 Interlock

An external power distribution unit will be installed in each power supply rack and will contain a primary contactor that can be controlled remotely and independently. This contactor will be controlled by the Personnel Safety System and will be independent of the power supply controller. Each power supply will have its own circuit breaker and power receptacle. The breaker will be sized to withstand turn-on in-rush power and to limit steady-state current to the line cord rating.

2.4.1.6 Allowed Misalignment Error of the Magnetic Elements of the LtB Transport Line

The placement of the magnets along the LtB line is subject to misalignment errors: the transverse and longitudinal placement errors DX, DY, and DS; the angular placement errors about the transverse axes DPHI and DTHETA; and angular error about the longitudinal axes, DPSI.

The results of a study to determine the maximum allowed error of each geometrical misalignment appear in Table 2.4.3. In the study we assumed that any misalignment error should not generate transverse beam displacement larger than ±1.5 mm nor measurable beam coupling effects.

Table 2.4.3 shows the upper limits of the allowed errors in the placement of the magnetic elements of the LtB line. The first three quantities DX, DY, and DS, correspond to the lateral and longitudinal position error. The last three quantities, DPHI, DTHETA, and DPSI, correspond to the rotation error about the transverse axes.

Table 2.4.3 Upper Limits of the Allowed Error in the Placement of the Magnets.

	DX [mm]	DY [mm]	DS [mm]	DPHI [mrad]	DTHETA [mrad]	DPSI [mrad]
Dipoles	±1.0	±1.0	±1.0	±2.0	±2.0	±0.5
Quadrupoles	±0.5	±0.5	±2.0	±2.0	±2.0	±5.0

2.4.1.7 LtB Transport Line Instrumentation and Diagnostics

The beam instrumentation that will be used for the commissioning and normal operation of the LtB line are the horizontal and vertical corrector dipole magnets (HC,VC), the beam position monitors (HBPM, VBPM), the Fluorescent screens (FS), the current transformer (CXF). The relative location of these devices along the LtB line is presented in Table 2.4.4. The first column contains the location of the beam instrumentation, which is identified in the second column.

Table 2.4.4 Beam Instrumentation (Column 2) at Various Locations (Column 1) along the LtB Line.

Location	Instrumentation	Comment
UpStrm of Q1 line	FS1, HC1, VC1, HBPM1, VBPM1	Fluor. Screen Retractable

DownStrm of Q4	FS2, HC2, VC2,	Fluor. Screen Retractable
DownStrm of Q7	FS3, HC3, VC3, HBPM2, VBPM2	Fluor. Screen Retractable
UpStrm Q8	FS4	Fluor. Screen Retractable
UpStrm B3	HC4, VC4	
DownStrm B3	HC5, VC5	
UpStrm BUMP	FS5, HC6, VC6, CXF, HBPM3, VBPM3	Fluor. Screen Retractable

Any deviations of the actual beam trajectory from the ideal trajectory due to magnet misalignment errors will be corrected with the six horizontal and six vertical dipole correctors.

The first dipole in the LtB achromatic bend is used to steer the beam either to the booster or emittance measurement setup and also serves as an energy spectrometer. Two fluorescent screens provide for coarse and fine (with switched-off achromatic quadrupole) measurements of energy spread. The beam dumps can include Faraday cups for charge measurement. With the first dipole switched off, the electron beam is directed to the emittance measurement system.

Two additional fluorescent screens after the second dipole of the achromatic bend will be used to measure electron beam size and position. The beam trajectory during normal operations is monitored by three pick-up electrodes equipped with Libera beam position monitors (BPM) [ber3, itc]. An integrating current transformer will measure the amount of charge passing through the transport line.

2.4.1.8 Shielding

The radiological study of the NSLS-II building complex is documented in [shie]. In this study, three radiological enclosures separate the linac, the booster and the storage ring. The radiological enclosure that separates the linac from the booster partitions the LtB line into two sections. The partition of the LtB line by the radiological enclosure occurs at the straight section between quadrupoles Q7 and Q8, as shown in Figure 2.4.1. The wall thickness of the enclosure that separates the linac from the booster is sufficient to attenuate any radiation levels that can be produced by a fault condition in the linac enclosure, to radiation levels less than 2.5 μSv/h at the area of the booster enclosure.

It is therefore possible for personnel to occupy the booster area while the linac is operating, under the condition that the safety devices of the LtB line (see next section) are fully functioning and the critical devices of the LtB line have been LOTO'ed (Lock-out Tag-out).

2.4.1.9 Linac-to-Booster Critical Devices

The linac-to-booster radiation transport will have two critical devices to stop the electron beam from entering the booster, to protect personnel from prompt radiation hazard in the booster area. This redundant pair of stops will consist of a shutter mechanism and a bending magnet.

The stop will be constructed of a block of material engineered to effectively stop all the radiation produced by the linac when the block is placed in the beam path. The stop will be redundantly monitored by the interlock system using two switches. The switches monitor the closed position of the shutter: one switch for chain A, and one for chain B. When in the closed position, the stop will block all radiation from entering the booster ring.

The bending magnet upstream of the stop will provide another safety function: when it is not powered, it allows the beam to follow a straight path into a beam dump area. This will prevent the electron beam from entering the booster tunnel area. When it is safe to allow beam in the booster area, the magnet will be powered and will bend the beam into the booster ring. The magnet will be redundantly monitored by the interlock system: for current by chain A, and voltage by chain B. In the event of the stop or bending magnet failing to reach a safe state when required to do so, the interlock system will reach back and shut off the linac and gun.

5.4.2 Booster-to-Storage Ring Transport Line

2.4.2.1 Scope

The main function of the booster-to-storage ring (BtS) transport line is to transport the 3GeV electron bunches from the booster to the storage ring (SR). A schematic diagram of the transport line, in relation to the booster and storage ring, is shown in Figure 2.4.4. The BtS line is defined between the "booster extraction point," which is located at the entrance point of the "BR1" local beam-bump-dipole, and the "storage ring injection point," which is located at the exit of the injection kicker "IS." Both magnets, BR1 and S1, are shown in Figure 2.4.4.

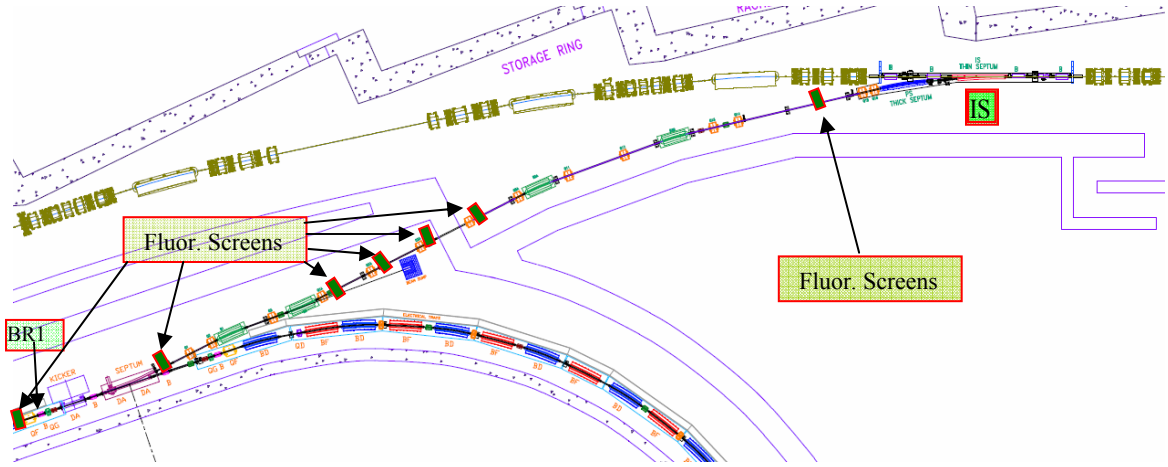

Figure 2.4.4 Schematic diagram of the BtS beam transport line. The arc at the bottom of the figure is a section of the booster, and at the top of the picture the green elements are part of the storage ring. The dark green rectangles on the BtS line are the fluorescent screens/ visual flags (VF).

For reasons, of easing the optical design, the beamline has been partitioned into three sections, which are briefly discussed below.

- *The extraction section:* This section of the beamline contains, the extraction devices, (extraction bumps, and extraction kicker, and extraction septum), two dipoles of 120 mrad bend each, that both form a horizontal "dogleg", and three quadrupoles. The two 120 mrad dipoles which form the horizontal "dogleg" and the three quadrupoles serve to generate an achromatic beam and also adjust the beam parameters, at the end of the extraction section.
- *The achromatic section:* This section of the beamline follows the extraction section, and consists of five quadrupoles. The transported beam in this section is achromatic. The secondary function of this section is to be used for measuring the projected beam emittance and the beam parameters, with the help of four visual flags installed along this section.
- *The injection section:* This is the last section of the line, and matches the transported beam to the circulating beam of the storage ring at the injection point which is located at the exit point of the Injection kicker SI. This section of the line consists of two "bend to the right" dipoles of 120 mrad each, the injection septum and the injection kicker, both bending to the right. It also includes six quadrupoles for the required beam matching at the injection point.

2.4.2.2 Beam Constraints along the BtS Line

The main beam constraints of the BtS line is to transport the extracted beam from the Booster to the Storage ring and match the beam parameters of the beam at the Injection point to those of the circulating beam. The beam parameters at the extraction and injection point are shown in Table 2.4.5. The values of vertical dispersion and angular dispersion functions of booster and storage ring lattices at these two points are zero therefore do not appear on the Table 2.4.5.

Table 2.4.5 Beam Parameters at the Booster Extraction Point, and Storage Ring Injection Point. The values of the vertical dispersion and angular dispersion functions of the booster and storage ring lattices at these two points are zero.

	α_x	β_x ,m	η_x ,m	η'_x	α_y	β_y ,m
Booster extraction point	0.0	5.0	0.1	0.0	0.0	3.0
Storage ring injection point	0.0	5.0	0.0	0.0	0.0	3.0

The following additional constraints are also imposed on the BtS transport line.

- The maximum values of the horizontal and vertical beta function along the line should be less than 100 m ($\beta_{x,y}$<100 m). Similarly the absolute value of the horizontal dispersion function should be below 2 m ($|\eta_x|$<2 m) at any point along the line. This will make the size of the beam along the line compatible with the physical aperture of the line. The geometric projected beam emittance is 27π nm-rad and 3π nm-rad in the horizontal and vertical directions respectively.
- The "achromatic section" of the line is designed to provide an achromatic beam in both the horizontal and vertical directions. This section of the line will be used to characterize the transported beam by measuring its projected emittance and the beam parameters at any point upstream of this section. The beam characterization can be performed by utilizing the "Nominal" settings of the quadrupoles that are used to transport the beam or by altering the settings of the quadrupoles.

2.4.2.3 Beam Optics of the BtS Beam Transport Line

The beam optics of the BtS line must satisfy the constraints mentioned earlier. The beam optics was calculated with the MAD computer code, version 8b.

The calculated values of the beta functions ($\beta_{x,y}$), and dispersion function (η_x) are plotted in Figure 2.4.5. The horizontal and vertical beam envelopes that correspond to the geometric projected beam emittances ε_x=50π nm-rad and ε_y=3π nm-rad are plotted in Figure 2.4.6. The projected beam sizes correspond to one standard deviation of the beam intensity.

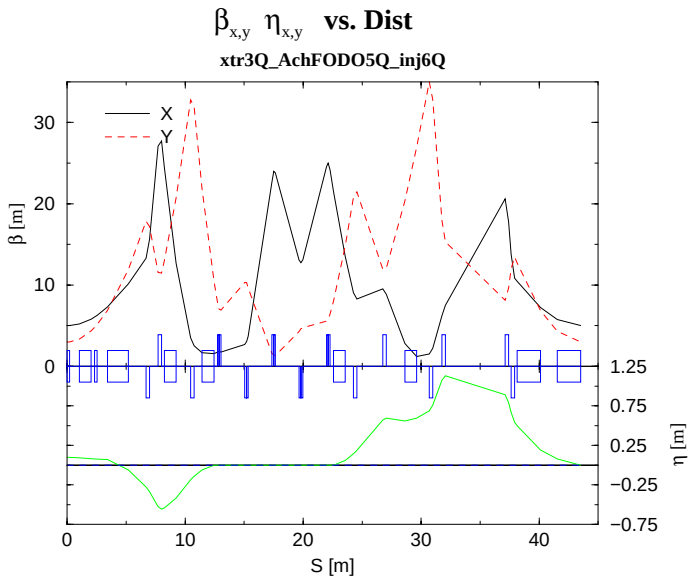

Figure 2.4.5 The $\beta_{x,y}$ (black and red lines) and η_x function (green line) at the beginning and the end of each magnetic element. The large blue rectangles represent the dipoles and the thin blue rectangles indicate the quadrupoles.

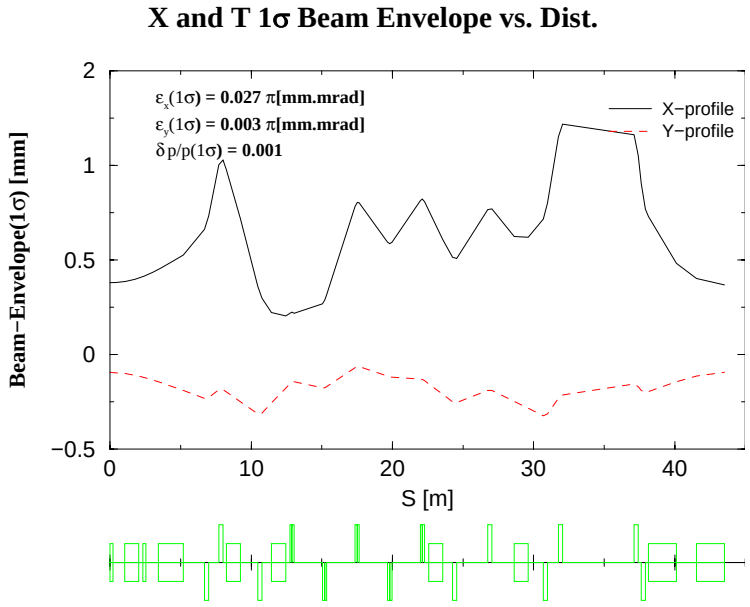

Figure 2.4.6 Half of the horizontal and vertical beam envelopes (black and red lines) that corresponds to $1\sigma_{x,y}$ beam emittance. The green rectangles at the bottom of the figure represent the dipoles and the quadrupoles.

2.4.2.4 Magnetic Elements of the BtS Transport Line

In this section we provide a table with the geometry (length, aperture) and the strength of the dipoles and quadrupoles of the BtS line. Table 2.4.6 shows all the main magnetic elements of the BtS line that are used to generate the line's first order optics which is discussed in the previous section. Each magnetic element has its own power supply except the B3I and B4I dipoles which are connected in series with a single power supply.

Table 2.4.6 Length, Aperture and Strength of the Main Magnetic Elements of BtS Line.

Element Name	Type	L [m]	Gap/Rad[cm]	Strength [rad] or [m^{-1}]	Power Supply
BR1X	Dipole	0.200	3.0	-0.080	P BR1X

KIX	Dipole	1.000	3.0	-0.005	P KIX
BR2X	Dipole	0.200	3.0	0.080	P BR2X
ESX	Dipole	1.750	3.0	-0.140	P ESX
Q1X	Quadrupole	0.300	2.0	-0.372582	P Q1X
Q2X	Quadrupole	0.300	2.0	0.5835372	P Q2X
B1X	Dipole	1.000	3.0	0.120	P B1X
Q3X	Quadrupole	0.300	2.0	-0.4201152	P Q3X
B2X	Dipole	1.000	3.0	-0.120	P B2X
Q1A	Quadrupole	0.300	2.0	0.6153693	P Q1A
Q2A	Quadrupole	0.300	2.0	-0.4201239	P Q2A
Q3A	Quadrupole	0.300	2.0	0.4269711	P Q3A
Q4A	Quadrupole	0.300	2.0	-0.350637	P Q4A
Q5A	Quadrupole	0.300	2.0	0.3244197	P Q5A
B3I	Dipole	1.000	3.0	0.120	P BI
Q1I	Quadrupole	0.300	2.0	-0.3434886	P Q1X
Q2I	Quadrupole	0.300	2.0	0.3373026	P Q2X
B4I	Dipole	1.000	3.0	0.120	P BI
Q3I	Quadrupole	0.300	2.0	-0.4447095	P Q3X
Q4I	Quadrupole	0.300	2.0	0.4081164	P Q4X
Q5I	Quadrupole	0.300	2.0	0.6599952	P Q5X
Q6I	Quadrupole	0.300	2.0	-0.6455421	P Q6X
PSI	Dipole	2.0	3.0	0.150	P PSI
ISI	Dipole	2.0	3.0	0.080	P ISI

2.4.2.5 Booster-to-Storage Ring Transport Line Power Supplies

The BtSR power supplies are connected to dipoles, quadrupoles, and vertical/horizontal correctors. The supplies will be operated around a static operating point, eliminating the need for significant voltage head room. For energy savings, we anticipate that the supply's output will be lowered during the dwell time in top-off mode and brought back to the operating point slightly before the top-off cycle. Unmodified commercial power supplies are currently used at NSLS in its transfer lines and are analog programmed by 14-bit digital-to-analog converters. The supplies are operated in current mode with shunt feedbacks.

2.4.2.5.1 Power Supply Control

Each transfer line power supply will be set by its analog programming interface. Either a micro-controller or PLC could be used to control the supply. Analog output voltages from the control system will be used to control the current setpoint of the supply, and the digital-to-analog converter will have a resolution of at least 16 bits. Both supply output voltage and current will be read back by medium-speed analog-to-digital converters with a resolution of 16 bits. Monitoring of the supply outputs should be able to detect transients as short as 1 ms. Long-term monitoring of drift will be done by an independent external shunt connected to a high-precision analog channel.

2.4.2.5.2 Interlock

An external power distribution unit will be installed in each power supply rack and will contain a primary contactor that can be controlled remotely and independently. This contactor will be controlled by the personal safety system and will be independent of the power supply controller. Each power supply will have its own circuit

breaker and power receptacle. The breaker will be sized to withstand turn-on in-rush power and to limit steady-state current to the line cord rating.

2.4.2.6 Misalignment Error of the Magnetic Elements of the BtS Transport Line

The placement of the magnets along the BtS line is subject to misalignment errors, which are the transverse and longitudinal placement errors DX, DY, and DS; the angular placement errors about the transverse axes, DPHI and DTHETA; and angular error about the longitudinal axes, DPSI.

The results of a study to determine the maximum allowed error of each geometrical misalignment appear in Table 2.4.7. In the study we assumed that any misalignment error should not generate transverse beam displacement larger than ±1.5 mm.

Table 2.4.7 shows the upper limits of the allowed errors in the placement of the magnetic elements of the BtS line. The first three quantities DX, DY, and DS, correspond to the lateral and longitudinal position error, and the last three quantities, DPHI, DTHETA, and DPSI, to the rotation error about the transverse axes (columns 5 and 6) and the longitudinal axis, (column 7).

Table 2.4.7 The Upper Limits of the Allowed Error in the Placement of the Magnets.

	DX [mm]	DY [mm]	DS [mm]	DPHI [mrad]	DTHETA [mrad]	DPSI [mrad]
Dipoles	±1.0	±1.0	±1.0	±2.0	±2.0	±1.0
Quadrupoles	±0.5	±0.5	±2.0	±2.0	±2.0	±5.0

Next, we give an example of how the corrector dipoles can be used to minimize the transverse beam displacement caused by random misalignments of the quadrupoles. Figure 2.4.7 shows the horizontal (black line) and vertical (red dashed line) displacements of the beam due to random misalignments of the quadrupoles. The possible misalignments of the quadrupoles are shown in Table 2.4.7 (columns 2 to 7), and the maximum value of each random misalignment is taken from the third row of Table 2.4.7. Figure 2.4.8 is similar to Figure 2.4.7, but with the corrector magnets excited, to minimize the horizontal and vertical displacements of the beam along the BtS line.

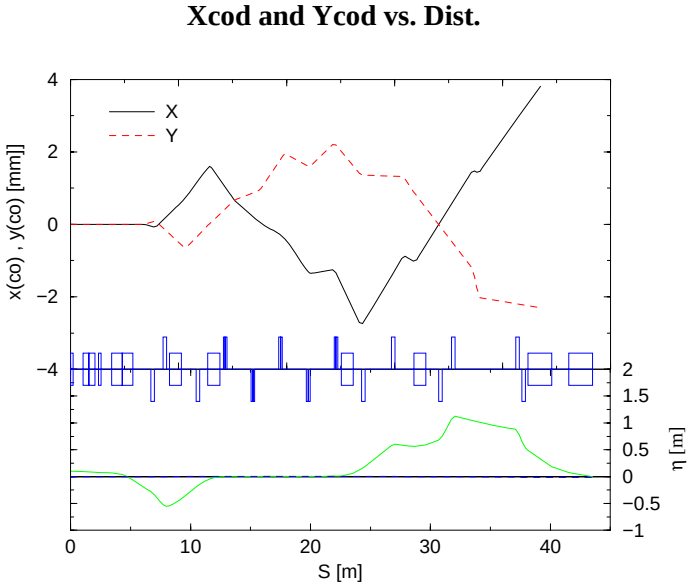

Figure 2.4.7 The X (black line) and Y (red dashed line) beam displacements along the BtS line caused by random misalignments of the quadrupoles. The possible misalignments are shown in Table 2.4.8 (columns 2 to 7) and the maximum value of a particular random misalignment is shown in the third row of Table 2.4.8.

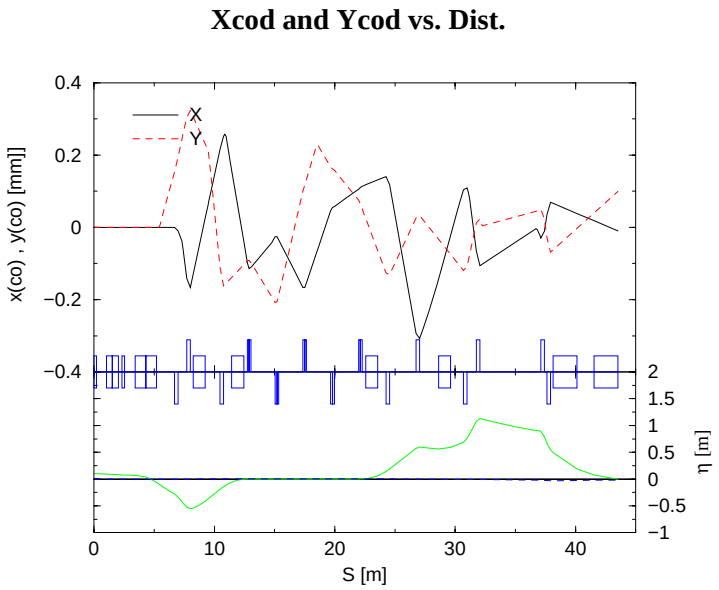

Figure 2.4.8 Same as Figure 2.4.7 but the X (black line) and Y (red dashed line) beam displacements along the BtS line are minimized by the use of the horizontal and vertical correctors.

2.4.2.7 BtS Transport Line Instrumentation and Diagnostics

The beam instrumentation that will be used for the commissioning and normal operation of the BtS line includes the horizontal and vertical corrector dipole magnets (HC, VC), the beam position monitors (HBPM, VBPM), the visual flags (VF), and the current transformer (CXF). The relative locations of these devices along the BtS line are presented in Table 2.4.8. The first column contains the location of the beam instrumentation, which is identified in the second column.

Table 2.4.8 Beam Instrumentation (Column 2) at Various Locations (Column 1) along the BtS Line.

Location	Instrumentation	Comments
Downstream of Extraction Septum	VF2, VC1, HBPM1, VBPM1	Visual Flag Retractable
Downstream of Q1X	HC1	
Downstream of B1X dipole	VC2, HBPM2, VBPM2	
Downstream of Q3X	HC2	
Downstream of Q1A	VF3, HC3, HBPM3, VBPM3	Visual Flag Retractable
Downstream of Q2A	VF4	Visual Flag Retractable
Downstream of Q3A	VF5, VC3	Visual Flag Retractable
Downstream of Q4A	VF6	Visual Flag Retractable
Downstream of Q5A	HBPM4, VBPM4	
Downstream of Q2I	HC4, HBPM5, VBPM5	
Downstream of Q3I	HC5, HBPM5, VBPM5	
Downstream of Q4I	VC5	
Upstream of Q5I	VF7, HC6, VC6, HBPM6, VBPM6, CXF	Visual Flag Retractable

Six fluorescent screens (VF), accompanied by six RF beam position monitors, will be used to measure the beam position and size. We plan to use Libera BPM receivers, which have up to 1 micrometer resolution in the single-shot mode, for processing signals from the pick-up electrodes. An integrating current transformer will be used for monitoring the injected bunch charge and injection efficiency. We are considering the possibility of installing two gated cameras with external triggers for observing the electron beam with radiation from the bending magnet.

2.4.2.8 Shielding

The radiological study of the NSLS-II building complex is documented in [shie]. In this study, three radiological enclosures separate the linac, the booster, and the storage ring. The radiological enclosure that separates the booster from the storage ring partitions the StR line into two sections. The partition of the BtS line by the radiological enclosure occurs at the straight section between quadrupoles Q3A and Q4A, as shown in Figure 2.4.1. The wall thickness of the enclosure that separates the booster from the storage ring is sufficient to attenuate any radiation levels that can be produced by a fault condition in the booster enclosure, to radiation levels less than 2.5 μSv/h at the storage ring enclosure.

It is therefore possible for personnel to occupy the storage ring area while the booster is operating, under the condition that the safety devices of the BtS line (see next section) are fully functioning and the critical devices of the BtS line have been LOTO'ed.

2.4.2.9 Booster-to-Storage Ring Critical Devices

The BtSR radiation transport will have two critical devices to stop the electron beam from entering the storage ring. These two devices will protect personnel from prompt radiation hazard in the storage ring area. This redundant pair of stops will consist of a shutter mechanism and a bending magnet.

The stop will be constructed of a block of material engineered to effectively block all the radiation produced by the booster when the block is placed in the beam path. The stop will be redundantly monitored by the interlock system using two switches that monitor the closed position of the shutter: one switch for chain A and one for chain B. When in the closed position, the stop will block all radiation from entering the storage ring.

The bending magnet upstream of the stop will provide another safety function: when it is not powered, the beam will follow a straight path to a beam dump area. This will prevent the electron beam from entering the storage ring tunnel area. When it is safe to allow beam in the storage ring area the magnet will be powered and will bend the beam into the storage ring. The magnet will be redundantly monitored by the interlock system—for current by chain A, and voltage by chain B. In the event of the stop or bending magnet failing to reach a safe state when required to do so, the interlock system will reach back and shut off the booster RF, linac, and gun.

References

[SOLL]http://ieeexplore.ieee.org/Xplore/login.jsp?url=/iel5/10603/33511/01590552.pdf?arnumber=1590552
[ber3] http://www.gmw.com/beam_diagnostics/Bergoz/bpm/pdf/GMW-DS-BPM-UHV-50_B.pdf
[shie] Technical Note "Preliminary Radiological Considerations for the Design and Operation of NSLS II Accelerator Enclosures" by P.K. Job and W.R. Casey
[sls2] http://slsbd.psi.ch/pub/slsnotes/sls1697

2.5 Storage Ring Injection Straight Section

2.5.1 Scope

The injection straight is situated in one of the "long" straight sections of the storage ring. The total straight section length is 9.3 m long from steel to steel from the adjacent magnetic elements. The injection scheme is to displace the circulating orbit a distance of 15 mm toward the septum magnet (which at its closest approach to the beam is 17 mm away from the normal closed orbit), using two pulsed orbit bump magnets, followed by two identical bumps to place the circulating beam plus the injected bunches back on the normal orbit. Ideally, if all the bumps are identical, if the current pulses are all alike, if the pulse timing is perfect and if the survey to place the magnets is perfect, this procedure should be invisible to the users except for the halo of injected electrons (horizontally) which damps down with a time constant of a few tens of milliseconds. A slightly less than ideal but still acceptable condition is when the residual orbit disturbance is below the resolution capability of the user optics and experimental apparatus. An estimate of the required precision in alignment and operation of the injection magnets was done for the SLS by C.H. Gough and A. Streun [sls2].

Some methods that may be able to compensate for the errors in alignment, variation of magnetic fields of the kickers due to magnetic material differences, excessive stray field of the injection septum are under consideration.

2.5.2 Ring injection straight section layout

At present there are commercially available pulsed magnets with their power supplies that could be procured as a turn-key system. Outsourcing of pulsed magnets is a viable option, which, together with designing and building pulsed systems in-house, received careful consideration during preliminary design. Below we discuss parameters and performance of feasible injection straight components that can be developed using either option. Their feasibility is confirmed by comparison with kickers and septa of other light sources.

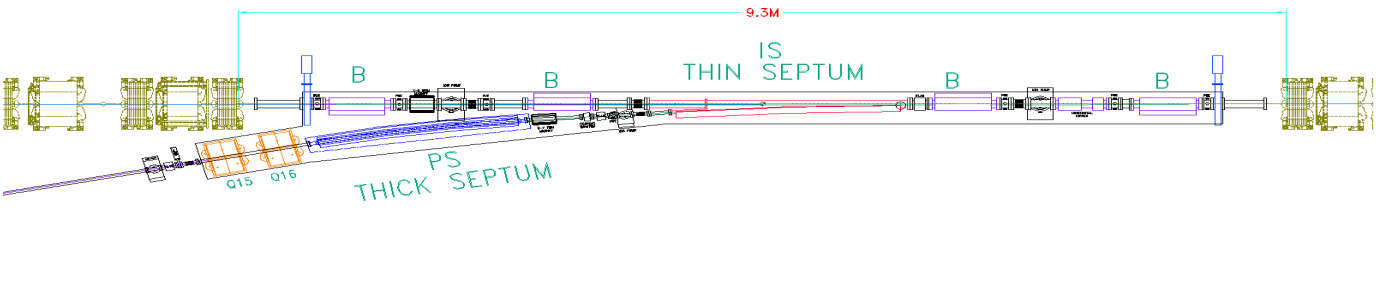

Figure 2.5.1 Injection straight layout.

The pulsed magnets contained in the injection straight are outlined in Table 2.5.1 below. These are the basic specifications required. The revolution time of the electrons in NSLS-II is 5.2 μsec, so with this configuration, the injection takes place in one turn. It is planned to inject no more than 150 bunches at one time, a train 300 nsec long. This is easily done with a 5 μsec long half sine wave pulse. However since the fractional tune for the ring is ~0.3, longer bump pulses (in units of ring revolution period) may be used, lessening the voltage requirements for the magnets and reducing the stringent timing requirements, one of the more important causes of residual beam motion caused by the injection transient. However, in this case, the beam will make several passes through the possibly not quite closed injection bump system. This may cancel some errors and lead to lower beam disturbance or it may aggravate the errors. Further studies are necessary; at this point a 5 μsec-long orbit bump is the baseline.

Table 2.5.1 Ring Injection System pulsed magnet parameters.

	Injection Septum	Thick Septum	Injection Bump
Magnetic field [T]	0.4	0.833	0.165
Length [m]	2.0	1.8	0.5
H x V [mm x mm]	20 x 15	20 x 15	60 x 23
Bend angle [mR]	80	150	8.25
Inductance [μH]	3.5	3.02	1.64
Peak current [A]	5,000	10,000	3.15
Drive capacitor [μF]	18.9	84.1	1.55
Voltage [kV]	2.1	1.9	3.1
Pulse shape	50 μsec full sine	100 μsec full sine	5 μsec half sine
Magnetic material	CMD5005 or ¼ mm Si steel	¼ mm Si steel laminate	CMD5005
Ceramic chamber coat	N/A	N/A	0.5 Ω/□

2.5.3 Residual Orbit Jitter

The stringent performance and alignment and positioning parameters of the injection components of the NSLS-II synchrotron were alluded to above. Preliminary analysis of the required parameters showed very tight tolerances in placement of the orbit bumps not only in pitch and yaw and especially in roll (which produces vertical orbit distortions) but also in transverse placement and even longitudinal position. Inhomogeneities in the magnetic material used for the orbit bumps contribute magnetic field errors. Temperature changes alter the permeability of the ferrite in unpredictable ways.

Correcting coils, orbit measurement-based feed-forward of voltages on the charge capacitors and stringent control of bump timing will be imperative. Correction trims and auxiliary windings on beam bumps will most likely be necessary and extreme care must be taken in mechanical manufacturing of bump magnetic structures, ceramic chamber coating and support structures. High resolution survey during installation and accurate placement of components will be required.

To be able to attack the residual beam oscillation problem, several capabilities should be built into the injection straight section. Provisions should be made for four dedicated correction trim bumps, up to six places for precision orbit position monitors in the straight section itself and especially at the downstream end where the orbit disturbance both in position and angle must be reduced to zero, and for winding small correction coils on the bumps to possibly compensate for unwanted field components.

The correction kickers or correction coils should be driven with current pulses that exactly mimic the drive pulses of the main bumps, possibly using operational current amplifiers controlled by signals derived from the current pulses in the main magnets. Response matrices for the correctors have to be determined and algorithms to reduce the orbit errors of the circulating beam to zero at the output of the injection straight need to be developed.

The important part is that as much of this work as possible should be done on the assembled girder before installation; For these reasons, a laboratory and electronics shop dedicated to the pulsed magnets is needed to not only verify the performance of any manufactured pulsed magnets, but also to ascertain the optimum design of these devices.

The following activities regarding pulsed magnets of the NSLS-II need to be performed so that the injection system component design and specifications can be determined and verified and further to ultimately determine performance parameters and acceptance testing of delivered components, no matter where they are manufactured:

1. Prototyping of kickers and septa for verification of pulsed magnet current, voltage, pulse length to achieve required parameters.
2. Determination of optimum (lowest inductance) pulsed magnet driver configuration.
3. Evaluation and testing of ferrite magnetic properties (permeability, loss factor, electrical conductivity).
4. Risetime, pulse shape/flat-top design verification of booster injection and extraction kicker magnets.
5. Elimination of causes of timing jitter and other noise in magnet current and field pulses.
6. Testing and evaluation of uniformity of conductive coating on inside of ceramic chambers for kicker magnets.
7. Measurement and acceptance testing of pulsed magnets received from vendor before installation in accelerators.
8. Tuning of the main ring injection straight section as a unit and setting up corrector bumps pulse shapes for minimum disturbance of circulating beam.
9. Measurements and compensation of fringing fields from pulsed components placed closely to the main ring circulating beam.
10. Training of technical staff for future upgrades and servicing of pulsed magnet systems.
11. Test bed for novel ideas in pulsed magnet technology.

The final adjustments would occur during commissioning with the actual beam, and time stability for feed-forward systems will be established.

Proposed possible correction kicker configurations are shown in Table 2.5.2 below. It is possible to wind horizontal and vertical correction windings on the same ferrite yoke, necessitating only two additional ceramic chambers in the injection straight.

Table 2.5.2 Kicker parameters for proposed correction scheme.

	Horizontal Correction Kicker	Vertical Correction Kicker
Magnetic Field [T]	0.04	0.04
Length [m]	0.2	0.2
H x V [mm x mm]	60 x 23	30 x 60
Bend angle [mR]	1	1
Inductance [μH]	0.656	0.126
Peak Current [A]	<750	1900
Drive Capacitor [μF]	3.86	20
Voltage [kV]	0.31	0.15
Pulse Shape	5 μsec half sine	5 μsec half sine
Magnetic Material	CMD5005	CMD5005
Ceramic chamber Coat	0.5 Ω/□ Ti	0.5 Ω/□ Ti

The capacitor banks for all magnets in the ring injection straight should have at least 16-bit voltage resolution and if it is feasible to use longer excitation pulses, all kickers could be driven in series due to lower voltage requirements and the pulse transmission time through the kicker string becomes a negligible fraction of the kicker system pulse length.

References

[sls2] http://slsbd.psi.ch/pub/slsnotes/sls1697.

3 LATTICE AND ACCELERATOR PHYSICS

3.1 Lattice and Beam Dynamics

The storage ring lattice is designed to provide a stable, closed orbit on which the electron beam can circulate with long lifetime and efficient injection of beam from the booster. This injection will be capable of filling the ring from zero beam current to the operating values ($\leq$500 mA) in a short time, as well as to provide top-off injection to maintain a constant level of beam current ($<\pm$0.5% variations) and thus provide a constant radiated beam power on the users' beamline components, with low thermal distortions.

The electron beam will be damped by the synchrotron radiation to a small beam emittance lower than that of any storage ring light source currently operating or under construction. The photon beams radiated from undulators will, therefore, have lower emittance and higher brilliance, surpassing any existing light sources in the 2 to 10 keV range in focused beam flux on small specimens.

3.1.1 Physics and Design Goals for the Storage Ring Lattice

The design of the NSLS-II storage ring is driven by goals required to achieve the baseline performance as well as challenge goals that will provide the potential for future upgrades of beam performance. The challenge goals will keep NSLS-II at the frontier of the field for an extended time. Table 3.1.1 lists the required and challenge goals.

Table 3.1.1 Goals for the NSLS-II Design.

Beam Property	Required Goal	Challenge Goal
Ultra low horizontal emittance [nm-rad]	$\leq$1.5 (achromatic)	$\leq$0.5
Vertical emittance [nm-rad]	0.010	0.008
Stored currents [mA]	500	750
Straights for insertion devices	$\geq$21	27
Low dispersion space for Three Pole Wigglers	$\geq$ 15	$\geq$ 15
Electron beam stability [% of beam size]	10	<5
Top-off injection current stability (Δt $\geq$2 min) [%]	<1	<1

Several lattices have been studied over the past few years. As work progressed, it became clear that the Double Bend Achromatic lattice could meet the emittance goals while providing an increased number of insertion device straight sections. To achieve our low emittance goals, we maintain achromatic arcs and install damping wigglers in the extra ID straight sections to enhance the SR power without significantly increasing the quantum excitation of the electron beam [3.1.1]. This process yields a net reduction of the beam emittance proportionally related to the ratio of dipole-radiated power to the DW-radiated power, reducing the beam emittance up to five-fold without significantly impacting the dynamic aperture performance of the ring.

The minimum emittance for a DBA lattice with 2M dipole magnets and electron energy $E_0=\gamma mc^2$ is given by

$$\varepsilon_0^{\min} = \left(7.7\times10^{-4}\, nm-rad\right)\gamma^2 / M^3. \qquad (3.1\text{-}1)$$

The achievable emittance for a realistic lattice design is about twice this minimum value. The momentum compaction is

$$\alpha = \frac{\pi^2}{6M^2}\frac{2\pi\,\rho_0}{C}\,, \tag{3.1-2}$$

where ρ_0 is the dipole magnet bending radius and C is the ring circumference. Note that the momentum compaction increases linearly with bend radius.

The emittance ε_w with damping wigglers is related to that without damping wigglers, ε_0, by $\varepsilon_w \approx \varepsilon_0 / (1+U_w / U_0)$, where U_w / U_0 is the ratio of the energy lost per turn in the wigglers to that lost in the dipoles. For NSLS-II, we chose to have a large dipole bending radius. This reduces the energy radiated in the dipoles, which means we need to radiate less energy in the wigglers to reduce the emittance by a given factor.

To be more precise, consider a wiggler of length L_w having bending radius ρ_w and period λ_w centered in the insertion section. The ratio of the fractional energy spread with the wiggler to that without is

$$\frac{\delta_w}{\delta_0} = \sqrt{\left[1+\frac{L_w}{2\pi\,\rho_0}\frac{4}{3\pi}\left(\frac{\rho_0}{\rho_w}\right)^3\right]\left[1+\frac{L_w}{4\pi\,\rho_0}\left(\frac{\rho_0}{\rho_w}\right)^2\right]^{-1}}\,, \tag{3.1-3}$$

and the ratio of the emittance with the wiggler to that without is

$$\frac{\varepsilon_w}{\varepsilon_0} = \frac{1+f}{1+\dfrac{L_w}{4\pi\,\rho_0}\left(\dfrac{\rho_0}{\rho_w}\right)^2}\,. \tag{3.1-4}$$

The fluctuation factor, f, is given by

$$f = \frac{2C_q\gamma^2}{3\pi^2\varepsilon_0}\frac{L_w\rho_0}{\rho_w^3}\left[\frac{K_w^2}{5\gamma^2}\langle\beta_x\rangle + \frac{\eta_0^2}{\beta_{x0}} + \beta_{x0}\eta_1^2\right], \tag{3.1-5}$$

where $C_q = 3.84\times10^{-13}$ m, and strength parameter $K_w = \lambda_w\gamma / 2\pi\rho_w$. The horizontal beta function is given by $\beta_x(s) = \beta_{x0} + s^2 / \beta_{x0}$, where $s = 0$ is the center of the wiggler and insertion, and $\langle\beta_x\rangle$ denotes the average value of β_x in the wiggler. We express the dispersion function in the wiggler in the form $\eta(s) = \eta_w(s)+\eta_0+\eta_1 s$, where $\eta_w(s)$ is the sinusoidal dispersion generated by the wiggler itself, and $\eta_0+\eta_1 s$ is the dispersion generated by errors elsewhere in the ring. Eq. (3.1-5) can be used to determine a tolerance on the dispersion in the insertions arising from errors.

As at ESRF, the NSLS-II lattice has alternating high and low horizontal beta function straight sections for insertion devices. A large value of β_x is desired at the injection septum. Small β_x is desired in undulators for beamlines designed to focus the radiation down to a small spot. The vertical beta function should be small in undulators to optimize brightness. In fact, it is essential that β_y not be large in any of the insertion devices. The linear tune shift produced by an undulator or wiggler is

$$\Delta\nu_y = \frac{\langle\beta_y\rangle L_w}{8\pi\rho_w^2}. \tag{3.1-6}$$

Small β_y keeps the tune shift within acceptable limits. We have bounded the straight sections with quadrupole triplets in order to provide a local correction for the modification of the betatron functions and phases due to undulator or wiggler focusing.

The tune shift with amplitude due to nonlinear undulator or wiggler focusing is

$$\frac{d\nu_y}{dJ} = \frac{\pi\langle\beta_y^2\rangle L_w}{4\lambda_w^2\rho_w^2}. \tag{3.1-7}$$

To minimize the effect of the nonlinear focusing on dynamic aperture, it is essential to have small β_y in the insertion devices.

This is the approach taken for NSLS-II [3.1.2]. A DBA with 30 cells was chosen as the lattice structure, with a natural emittance of 2.0 nm. One cell of the lattice, shown in Figure 3.1.1, comprises half a super-period with reflection symmetry about the right or left hand end of the cell. The lattice functions have been optimized to achieve achromatic arcs, low emittance and modest chromatic sextupole strengths, small Closed Orbit Amplification Factors, and desired betatron functions in the long and short straight sections, which are required for small impact on the DA of the IDs, as given by Eq. (3.1-6 and 3.1-7). The working point tune was selected for optimization of the sextupole correction of the nonlinear driving terms that limit the DA, as well as reduced COAF and instability sensitivity. The dipole magnets have been optimized (bend radius ρ_0 = 25 m, B_0 = 0.399 T at 3 GeV) to enhance the reduction of the beam emittance with the DWs. Although the bare lattice doesn't quite meet the required emittance goal (2.0 nm instead of 1.5 nm), this goal is exceeded with only one 7 m DW installed and operated at a peak field of 1.8 T.

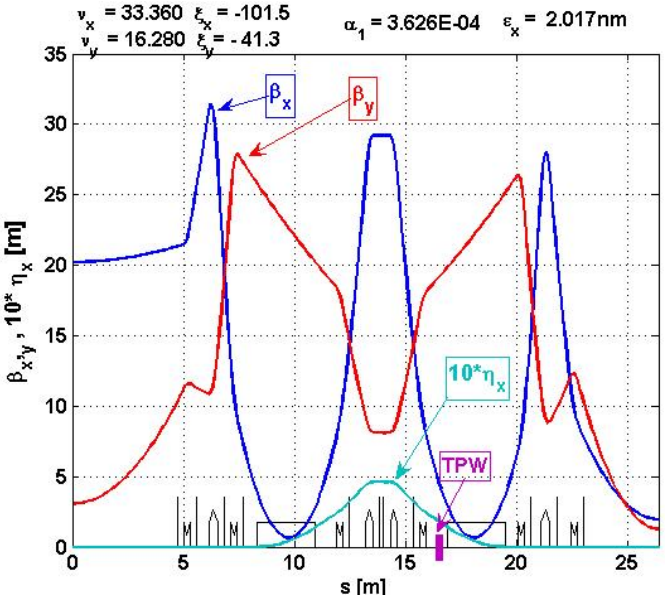

Figure 3.1.1 The lattice functions for one-half of a DBA period. A super-period consists of this cell reflected about either ID center: 9.3 m on the left-hand side or 6.6 m on the right.

The impact of DWs on the emittance and the energy spread, given by Eq. (3.1-3 and 3.1-4), is shown in Figure 3.1.2 for the designed ρ_0 = 25 m and a stronger dipole with 1.5 times the field (2/3 the bend radius). This calculation also assumes no significant spurious dispersion in the straight section, since the individual quadrupole powering in this lattice should allow the dispersion to be corrected cell-by-cell for any dipole variations. The gain in undulator brightness resulting from the smaller emittance provided by more damping

wigglers is somewhat reduced by the increased energy spread of the beam, especially at x-ray energies corresponding to higher harmonics of the undulator. Increasing the bend radius from 16.68 m to 25 m reduces both the emittance as well as the energy spread. Continuing to increase the bend radius to larger values is increasingly less effective at reducing the emittance as it approaches the IBS limit, and at the same time increasingly expensive, as it increases the circumference of the ring. As discussed in Chapter 5, a bend radius of 25 m is about optimal for NSLS-II. The installed RF power also provides a practical limit to the gain from more damping wigglers, since the beam lifetime will be reduced if the radiated power exceeds the installed power necessary for sufficient RF bucket height.

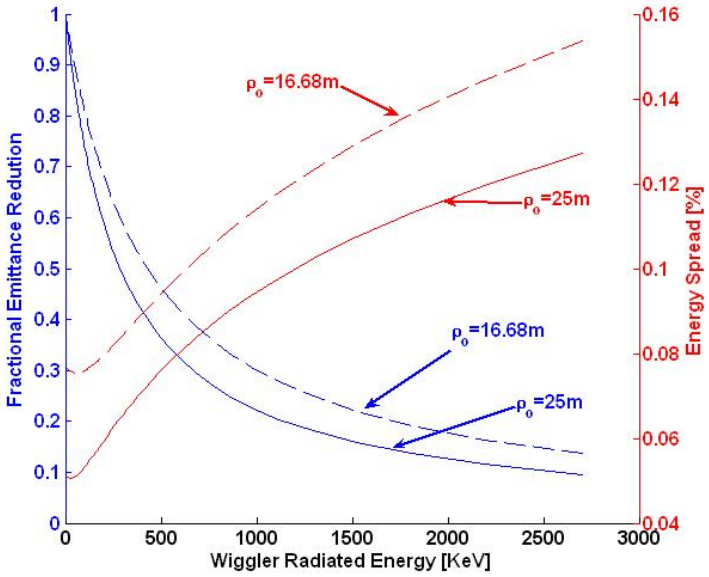

Figure 3.1.2 The fractional reduction of the ring emittance and the increase in energy spread for dipole magnets of bend radii: ρ_o = 25 m (proposed for NSLS-II) and ρ_o = 13.7 m dipole that could yield a shorter circumference lattice.

Table 3.1.2 lists the design parameters for this 15 super-period DBA (15×2) lattice. The choice of low dipole field restricts the photon beam energies radiated by the dipoles to 2.4 keV critical energy at 3 GeV. The dipole radiation will provide very bright VUV and soft-x-ray beams. Hard x-rays will be available from the installed DWs (10.8 keV critical energy) with high brilliance and flux.

Table 3.1.2 Storage Ring Parameters.

Energy [GeV]	3
Circumference [m]	791.96
DBA cells	30 (15 x 2)
Bending radius [m]	25.019
RF frequency [MHz]	499.68
Harmonic Number	1320
Momentum compaction	0.000368
Ring Tune: ν_x, ν_y	32.35, 16.28
Natural chromaticity: ξ_x, ξ_y	–103, –44.8
Maximum dispersion [m]	0.46
High-beta 9.3-m straights: β_x, β_y [m]	20.85,2.94
Low-beta 6.6-m straights: β_x, β_y [m]	2.02,1.06
Dipole radiated energy loss [keV]	286.5
Dipole critical energy [keV]	2.394

Figure 3.1.3 shows the expected reduction of the emittance as one to eight 7 m DWs are added to the ring.

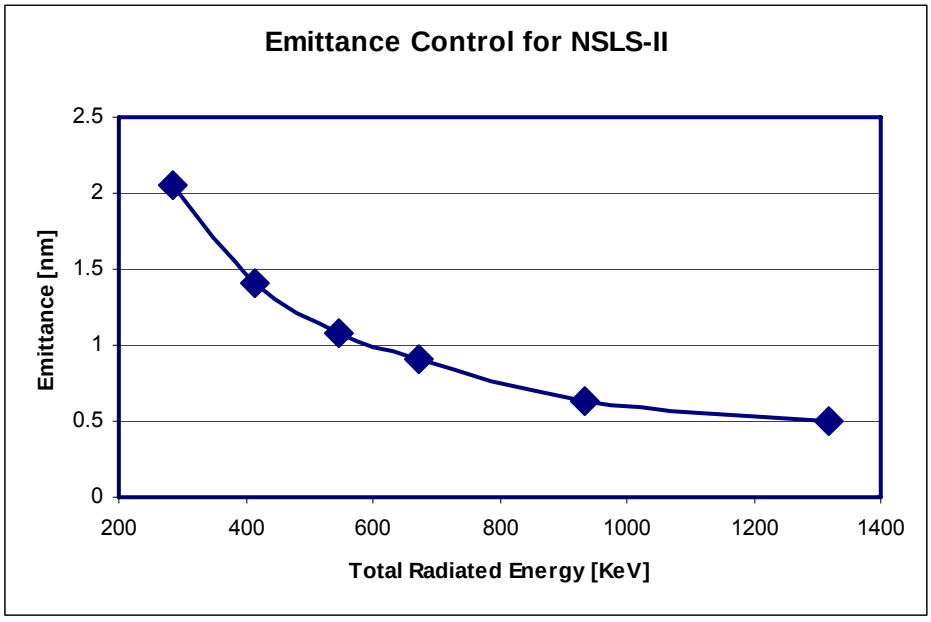

Figure 3.1.3 Emittance reduction for NSLS-II as 0, 1, 2, 3, 5, and 8 DW (7 m each) are installed and operated at 1.8 T peak field.

Table 3.1.3 compares the basic lattice properties with those obtained with 21 or 56 m of DWs installed in the ring. All of these DWs will have a fixed gap and will be available to drive user beamlines.

Table 3.1.3 Effect of Three and Eight 7 m Damping Wigglers on Beam Properties at 3 GeV.

	Zero DWs	Three 7 m DWs (21 m)	Eight 7 m DWs (56 m)
Energy loss [keV]	287	674	1320
RF voltage (3% bucket) [MV]	2.5	3.1	3.9
Synchrotron tune	0.0079	0.00876	0.0096
Natural emittance: ε_x, ε_y [nm-rad]	2.0, 0.01	0.9, 0.008	0.50, 0.008
Damping time: τ_x, τ_s [ms]	54, 27	23, 11.5	12, 6
Energy spread [%]	0.05	0.089	0.099
Bunch duration [ps]	10	15.4	15.5

The lattice shown in Figure 3.1.1, like that at ESRF, has low and high beta function straight sections. However, we have increased the length of the high-β_x straight section to provide for injection, space for RF cavities, and space for longer DWs and user IDs. The drift space between quadrupole magnets is 9.3 m. The space available for insertion devices is 7 m. The magnet layout for the Long ID straight section, with field free drift space of 9.3 m between sextupoles, is shown in Figure 3.1.4. Half the long ID is shown with reflective symmetry about the centerline (left-hand side). There are a total of six quadrupoles [(QH1, QH2, QH3)×2] and eight sextupoles [(SH1,… SH4)×2] in this ID straight section. Although they are considered as families of focusing strengths, each will be independently powered to account for magnet-to-magnet differences and for the possibility of shifting the symmetry condition for improved photon beam focusing. The three quadrupole families provide sufficient variables for correcting the local distortions of the linear lattice when IDs are installed or when the gaps are changed by the users [3.1.4, 3.1.5]. The center quadrupole (QH2) is 40cm long, while the other two are 25 cm long, in order to satisfy the maximum gradient of <22 T/m design criteria. The four families of sextupoles in this ID are required in order to correct the nonlinearity of

the lattice arising from the strong chromatic sextupoles located in the dispersive regions. For certain tunes, some sextupoles have small strengths. These might be dropped from a future optimized design.

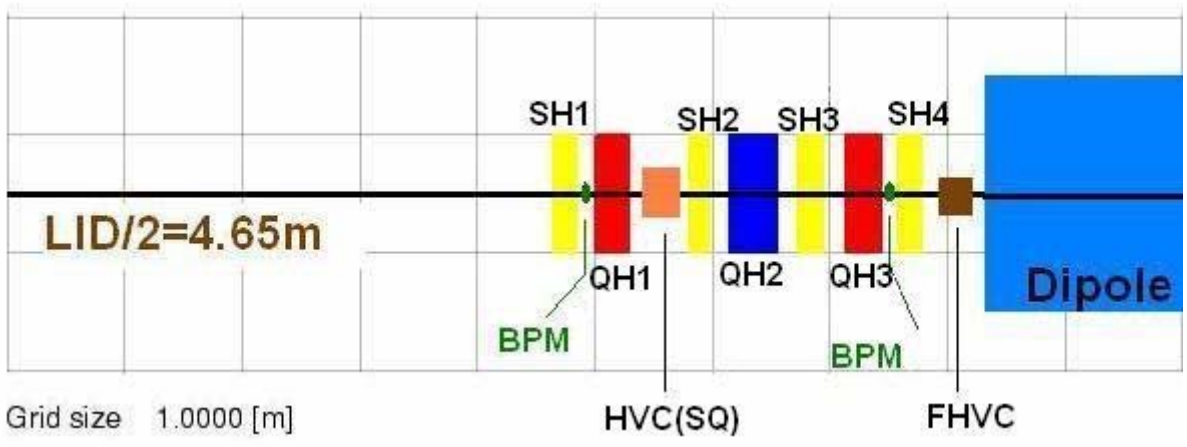

Figure 3.1.4 Layout for half of a long (high beta function-H) ID straight section, with reflection symmetry on left side.

The short ID straight section layout is shown in Figure 3.1.5. The short ID has a 6.6 m drift between the inner sextupoles and is similar to the long ID in layout of the quadrupoles and sextupole families. Differences include additional drift between quadrupoles to reduce the chromaticity, while providing the increased focusing needed for the lower beta functions. The quadrupoles are 25 cm long except for the center quadrupole (QL2) is 40 cm as in the long ID straight section. The QL2 quadrupole has the maximum gradient of the lattice quadrupoles, this magnet has a 10% safety margin of its maximum gradient to allow for tuning range for reducing the horizontal beta function in the short ID, for increase brightness of the ID source.

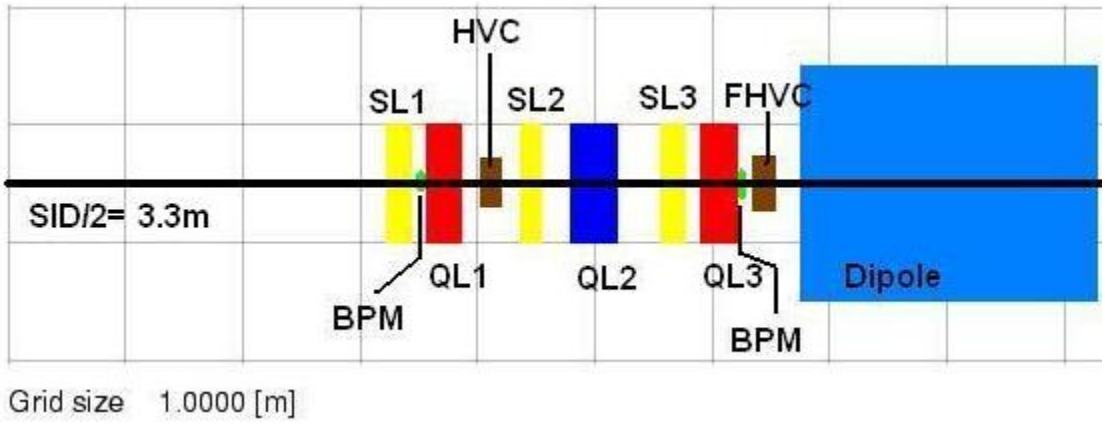

Figure 3.1.5 Layout for half of a short (low high beta function-L) ID straight section, with reflection symmetry on left side.

Two slow horizontal and vertical closed-orbit correction magnets are included in each ID straight section (some also include a skew quadrupole winding). For the purposes of this design, we assume independent corrector magnets, as shown in Figures 3.1.4 and 3.1.5. Also shown are two beam position monitors to be used for closed-orbit correction. When a user ID is installed in the ring, it is assumed that two pairs of fast horizontal and vertical correctors and a pair of user BPMs may also be installed. These will be optimized for the aperture of the ID vacuum chamber to yield increased sensitivity to orbit motion and the increased frequency of correction for fast orbit motion required for the ID beamline. To accomplish this will require

some advanced engineering, but there is adequate drift space provided. The FHVCs and UBPMs will be used as part of a global feedback system to provide submicron photon beam stability up to 100 Hz. Since the four FHVCs will provide a closed bump, the possibility of adding a photon beam position signal to the feedback system will also be available, without that signal impacting the beam for other users. Also shown in Figure 3.1.4 is a skew quadrupole in one of the HVC corrector magnets. This is one of two families of skew quadrupoles (see Figure 3.1.6 for the second family) and is used to correct the vertical coupling of the horizontal and vertical betatron phase space resulting from alignment of the dipoles and quadrupoles in the ring.

Figure 3.1.6 shows the magnet layout for the dispersion region of the lattice with the dipoles included. This region has four quadrupoles in two families and three chromatic sextupoles in two families. These magnets give some flexibility for optimizing the dispersion function for reduced chromatic sextupole strength. The two chromatic sextupoles allow the linear chromaticity to be tuned, while also reducing the 2nd order chromaticity. Space has been provided between the dipole and the vertically focusing quadrupole in order to accommodate a Three Pole Wiggler. Although the drift for the TPW is provided symmetrically around the dispersive section, only the location closest to the dipole could have a TPW installed. These TPW ($\leq$ 15) will provide source points for hard X-ray beams, for support of migrated NSLS user beamlines. As in the ID straight sections, two BPMs are included close to the quadrupoles near the ends of the girder. This is to provide improved alignment of the magnets on the girder using a beam based alignment of the BPM to the quadrupoles magnetic center. A third BPM (electrodes only) is included near the QF1 quadrupole (near the maximum dispersion point). This BPM will be used for accelerator physics measurements of the dispersion and beta functions, when needed, and could improve the orbit correction for large alignment or settlement errors. Also included are two discrete correctors (FHVC) that will be used for static and fast global orbit correction. These correctors are not symmetric about the dispersion section, in order to allow extraction of the damping wiggler beams and space for insertion of a three pole wiggler (TPW). These locations in the lattice for the TPW's will provide up to 15 possible beam sources for hard X-ray beam lines that can be migrated from the existing NSLS-Xray ring. Also show in one of the FHVC correctors is the location of one family of skew quadrupoles for coupling correction and vertical emittance control, see Section 3.1.2.?.

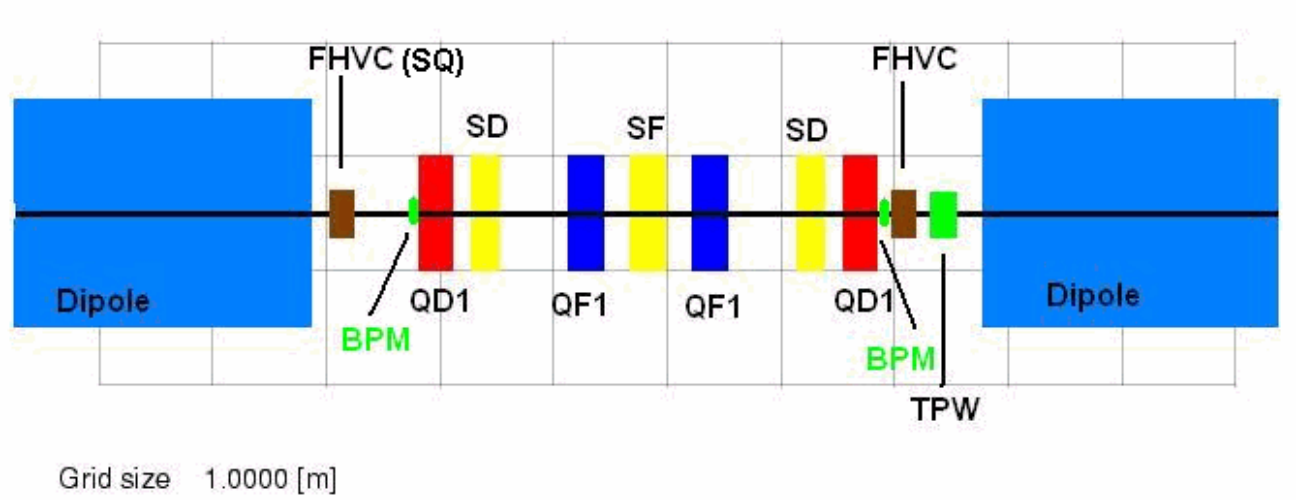

Figure 3.1.6 Layout for the dispersion section, including the two dipole magnets.

Table 3.1.4 lists a summary of the basic storage ring magnets and BPMs in the lattice design and for closed-orbit control. Also included are alignment tolerances for these magnets.

Table 3.1.4 List of Magnets, tolerances and BPMs for the NSLS-II Storage Ring.

Qty.	Magnet Type	Length [m]	B, B', B" [T,T/m,T/m^2]	Alignment Tol.
60	Dipole	2.62	0.4, 0, 0	0.1 mm, 0.5 mrad
270	Quadrupole (S)	0.25	0, 22, 0	0.03 mm, 0.2 mrad
30	Quadrupole (L)	0.40	0, 22, 0	0.03 mm, 0.2 mrad
30	Sextupole (L)	0.25	0 , 0 , 500	0.03 mm, 0.2 mrad
270	Sextupole (S)	0.20	0 , 0 , 500	0.03 mm, 0.2 mrad
180(210)	BPM readouts (positions)	0.05		0.1 mm, 0.2 mrad
120	H&V Fast Correctors(SS)	0.30	0.027, 0	0.1 mm, 0.2 mrad
60	H & V Slow Correctors	0.20	0.04, 0	0.1 mm, 0.2 mrad
150	Magnet girders			0.1 mm, 0.5 mrad

The alignment and field tolerance errors are still being studied further. However, initial testing of the lattice with tolerance that has been achieved at other light sources has shown the DA is robust for individual errors. As with most synchrotrons light sources, the **c**losed-**o**rbit **a**mplification **f**actors contribute the most significant tolerance to be handled. COAFs give the RMS closed-orbit distortion around the ring per unit of RMS alignment error (assumed to be a random Normal distribution) for all the quadrupoles in the ring. The COAF for this lattice is shown in Figure 3.1.7 for one cell and has an average value in each plane of greater than 50. This means a 100 μm RMS alignment error in the quadrupoles will yield an average closed-orbit distortion of >5 mm. This closed orbit error in the sextupoles contributes to a nonlinear focusing error in the lattice, which breaks the sextupole strength settings that yield the large DA.

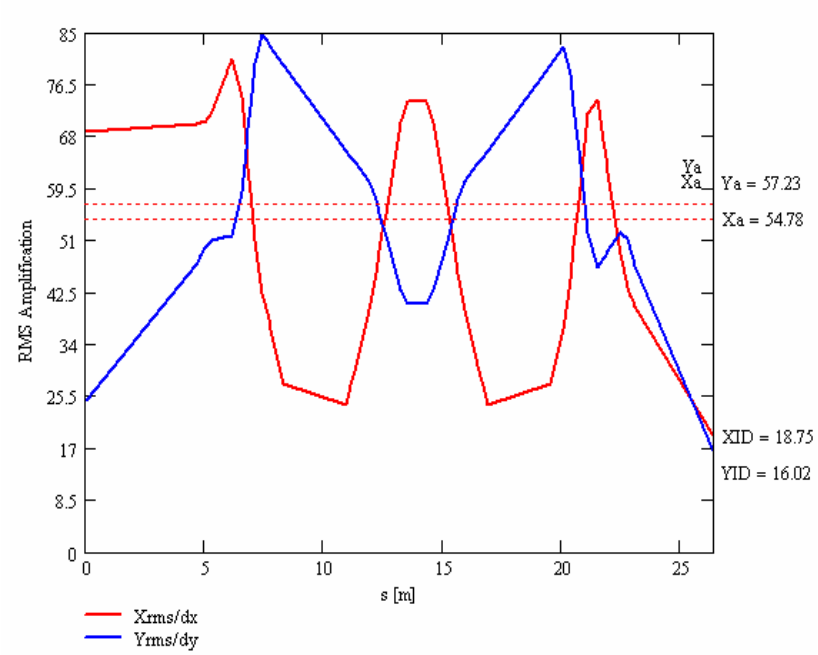

Figure 3.1.7 RMS expected closed-orbit amplification factors for random alignment errors in the quadrupoles of the lattice. Listed are the average amplification factors (Xa,Ya) and values at the short ID (XID,YID).

Figure 3.1.8 shows the impact of random quadrupole alignment errors of 100 μm that are corrected using the 6 BPMs and the 6 correction magnets per cell. We have corrected the orbit to the BPMs with an assumed no BPM noise or offset from the reference orbit. The corrected orbit DA for 20 different starting seeds (lattice layout errors) is shown with the average and RMS spread of the DA, together with the extreme values. The DA remains adequately large and is more than sufficient for injection and lifetime.

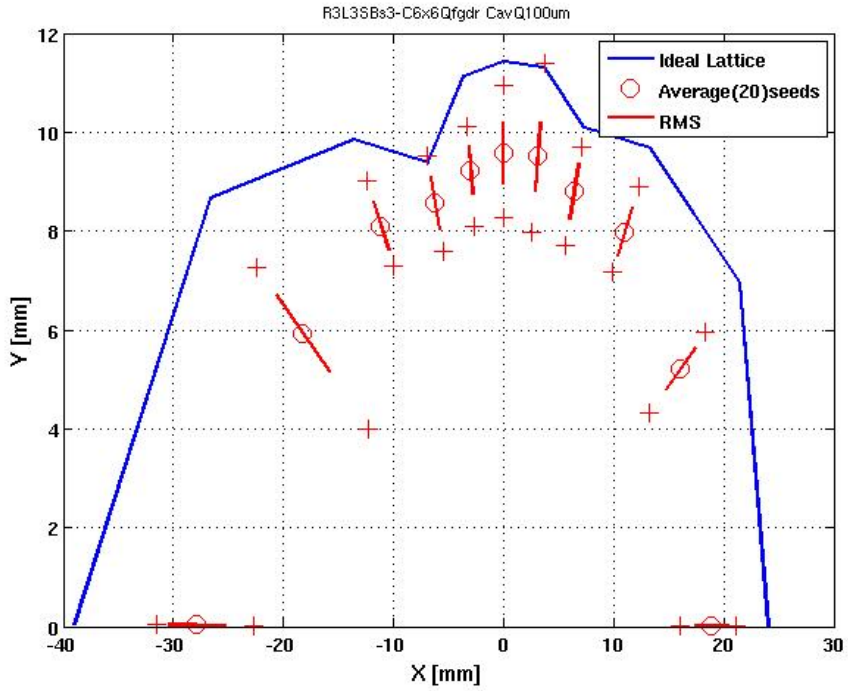

Figure 3.1.8 The DA (average, RMS and extremes values) for the lattice with 100 μm quadrupole alignment errors corrected to ideal BPMs located at the quadrupoles. It includes synchrotron oscillations, and the DA is tracked for 1 K turns around the lattice. The bare DA is also shown.

Adding a 30 μm random alignment tolerance of the BPM-to-quadrupole magnetic center yields little additional reduction of the DA, as shown in Figure 7.1.3, and is more than adequate. This random offset of the BPMs is equivalent to a BBA resolution of the BPM center relative to the quadrupole magnetic center, which could be much better than the 30 μm assumed in Figure 3.1.9, as described below.

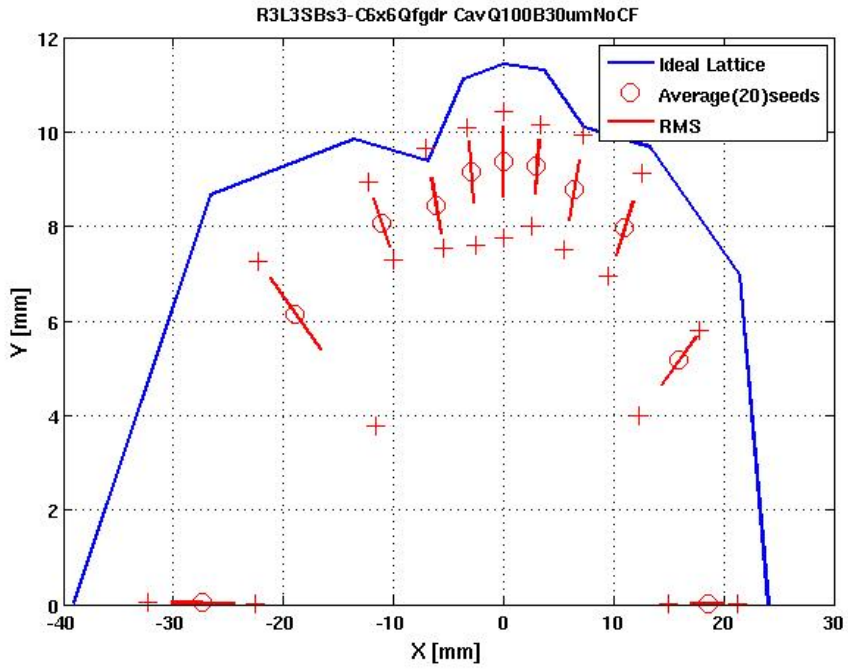

Figure 3.1.9 DA with 100 μm quadrupole alignment tolerances corrected with 30 μm BBA tolerance for BPMs (20 random seeds shown, with synchrotron oscillations).

We have assumed that the BPMs are close to the quadrupoles, since they are the source of the closed-orbit distortions in the sextupole magnets that cause the reduction of the DA. The two BPMs on a girder are aligned to the centers of the neighboring quadrupole magnetic center using the BBA procedure, which has become

common at many synchrotrons. This method uses a beam bump to vary the beam position (x, y) in the quadrupole and it's neighboring BPM. If that quadrupole has its strength modulated (ΔK_2), then the magnitude of the closed-orbit distortion measured by the BPMs is (X_m , Y_m). The BPM reading that yields a null in (X_m , Y_m) is then the magnetic center of this quadrupole, as measured by the BPM. With two BPMs on a girder, the beam can be magnetically centered to all elements on the girder using the magnetic alignment instruments: pulsed wire, vibrating wire, and/or rotating coils. Therefore we specify the alignment tolerances for the magnetic elements in terms of: 1) an alignment tolerance of centers one to another, 2) alignment of girder ends one to another and a common roll error of the girder, and 3) a BBA alignment tolerance of the BPMs to their neighboring quadrupole. The sensitivity of the closed-orbit distortion amplitude to the quadrupole modulation ($\Delta K_2 L$) and beam offset relative to the quadrupole center position, (x_c, y_c), is given by:

$$X_m(s) = \frac{\sqrt{\beta_x(s)\,\beta_x(quad)}}{2\sin(\pi Q_x)}\left(\Delta K_2\, L\right)x \geq 5.2\,\left(\Delta K_2\, L\right)x \tag{3.1.1-8}$$

and

$$Y_m(s) = \frac{\sqrt{\beta_y(s)\,\beta_y(quad)}}{2\sin(\pi Q_y)}\left(\Delta K_2\, L\right)y \geq 7.2\left(\Delta K_2\, L\right)y \tag{3.1.1-9}$$

where we assume the smallest beta function at a quadrupole and the average beta function at the BPMs. We assume that the closed-orbit amplitude is measurable to the resolution of the BPMs, ~1 μm, and the modulation is 3% of the quadrupole strength; the magnetic center should be measured in the neighboring BPM with an accuracy of better than

$$\sigma_{xc} \leq 8\ to\ 10\,\mu m \quad and\ \sigma_{yc} \leq 15\,\mu m\,. \tag{3.1.1-10}$$

Consequently, the random tolerances on the magnet-to-magnet alignment in Table 3.1.1 will be greater than the BBA resolution. However, we have assumed the BBA resolution of 30 μm in Figure 3.1.9, which is two to three times greater than achievable.

The impact of the larger values for the girder alignment tolerances were evaluated assuming that either end of the girder is aligned to an RMS level (random Normal distribution Δx, Δy). This misalignment of the girders contributes a correlated misalignment error in all magnets and BPMs on the girder. The sensitivity to this type of error is shown in Figure 3.1.10, where the Girder Amplification Factor is shown. The GAF is defined as the RMS closed-orbit distortion per unit of RMS girder misalignment. This shows a reduction in the averaged COAF (Figure 3.1.7) by a factor of 2X (H) and 3X (V). The GAF values at the center of the short straight section are 9.4 in the horizontal and 4.3 in the vertical plane, compared to 18.8 and 16.0 for the COAF, respectively. However, correcting for the assumed 100 μm girder alignment tolerances yields almost complete restoration of the DA (without BPM errors), since the correlations of the quadrupole misalignments are easier to remove by BBA alignment to the quadrupoles on the misaligned girders.

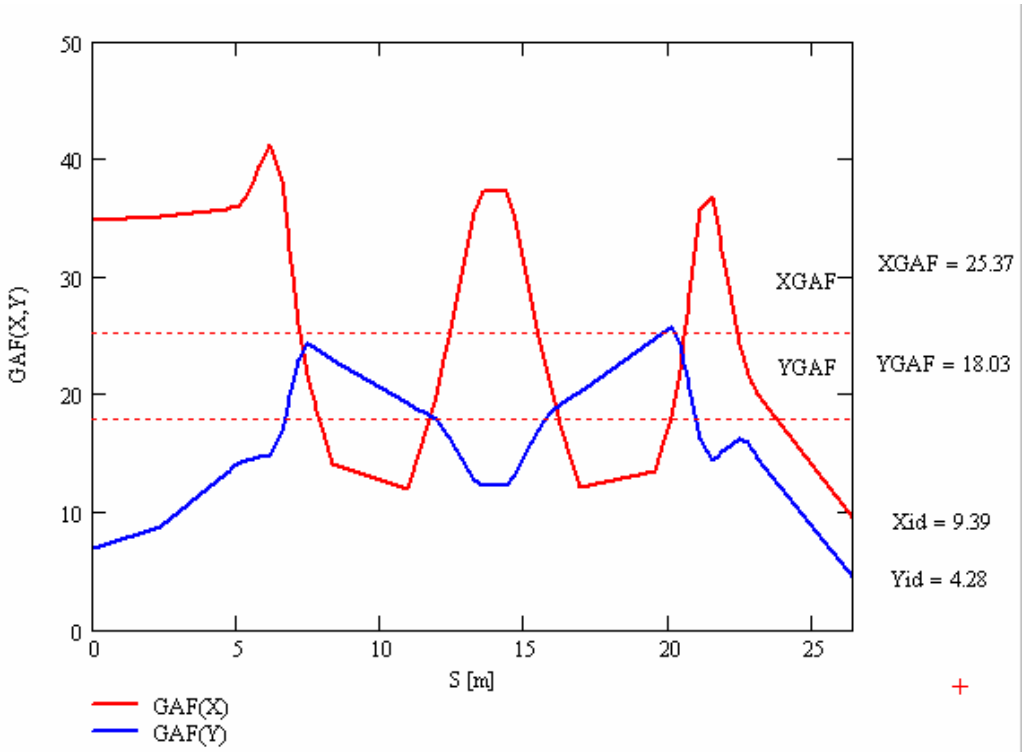

Figure 3.1.10 Girder Amplification Factors for one period of the storage ring. The average GAF values are 25 (H) and 18 (V) with values for the short ID of 9.4(H) and 4.3(V).

The corrected DA is shown in Figure 3.1.11 for 100 μm RMS random girder alignment tolerances, where no other errors are assumed in the BBA resolution for the BPMs, nor any quadrupole misalignment errors on the girder.

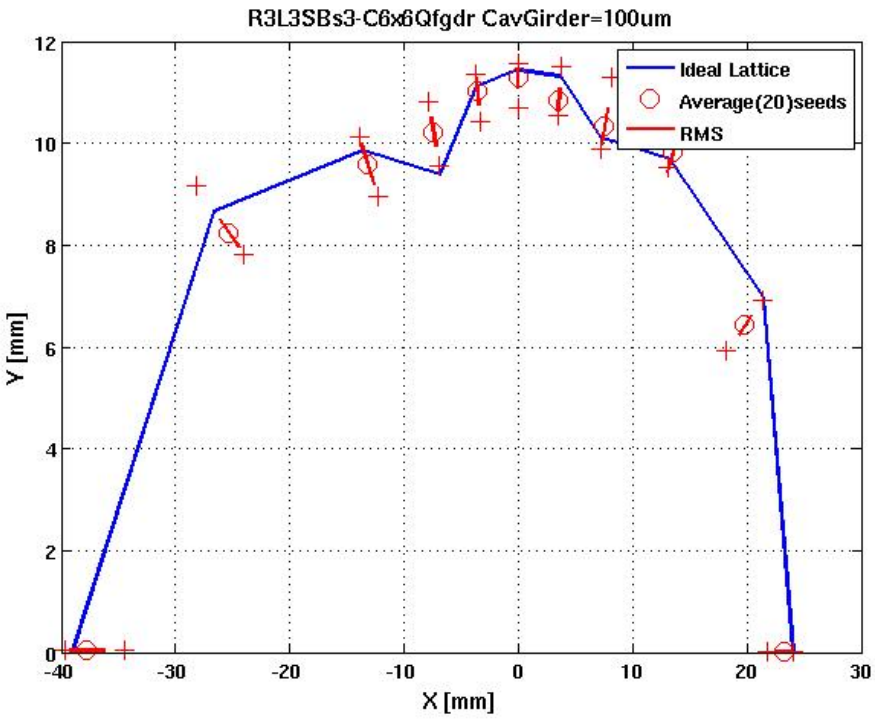

Figure 3.1.11 DA for 20 seeds (lattices) with 100 μm RMS girder alignment tolerances corrected using the BPMs with zero error in the BBA resolution.

The impact on the DA of all the misalignment tolerance, listed in Table 3.1.4 and including a 10 μm BBA resolution, as given by Eq. 3.1.1-10, is shown in Figure 3.1.12. Although there is significant reduction of the DA for this level of tolerance errors, it is well outside the physical aperture of the ring. Relaxing the alignment tolerances is still acceptable but will make the field and multipole tolerances on the magnets even tighter and will have a significant cost impact. The complete analysis of the DA with all alignment and field tolerances is presented in Section 3.1.2. The COAF and GAF presented here will also be used to estimate the orbit stability resulting from magnet vibrations in Section 7.2.2.

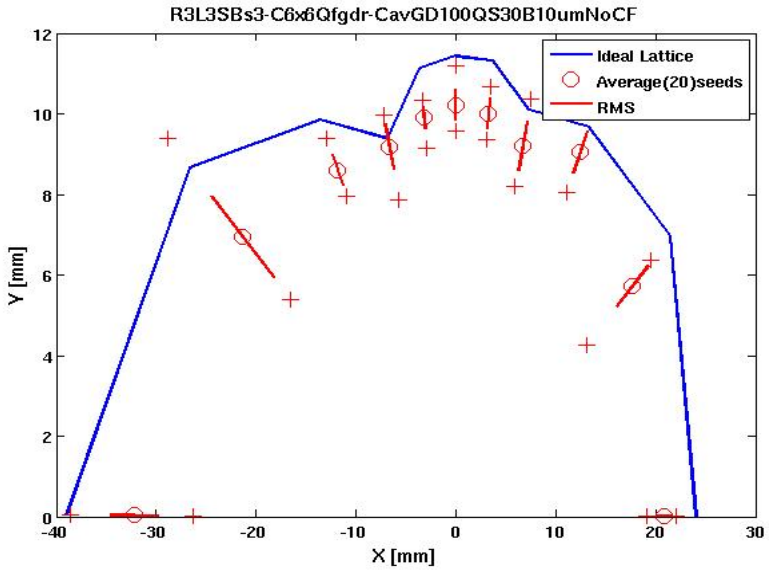

Figure 3.1.12 DA for 20 seeds (lattices) with all alignment tolerances included and using a 30 μm BBA resolution for BPMs. No quadrupole rotations are included.

3.1.2 Nonlinear Dynamics

3.1.2.1 Guidelines

One of the main design challenges for a strongly focusing lattice is to obtain adequate dynamic aperture for injection and Touschek lifetime[1]. As the required strength of the chromatic sextupoles increases, the DA can be improved by introducing extra families of geometric and chromatic sextupoles. However, once the sextupoles become too strong, this is no longer feasible. Eventually, cross terms generate higher-order terms, and when more families are introduced, the lattice will become pathological [3.1.5]. To avoid this, the following guideline has been provided for the linear optics design:

- horizontal chromaticity per cell, $\xi_x \leq 3$,
- peak dispersion, $\eta_x \geq 0.3$ m.

Similarly, we have adopted the guidelines for the DA summarized in Table 3.1.5. This is a conservative approach[2] to satisfy the requirements for the injection aperture for efficient top-off, as well as to ensure sufficient Touschek lifetime.

Table 3.1.5 Dynamic Aperture Guidelines.

	Horizontal and Vertical Dynamic Acceptance [mm·mrad]	Horizontal Dynamic Aperture [mm]	Momentum Acceptance [%]
Bare lattice (2.5 degrees of freedom[3])	~25	±20	**±3**
"Real" lattice (3 degrees of freedom[4])	~20	±15	**±3**

This also provides some leeway for magnetic alignment and field tolerances, and nonlinearities due to insertion devices, which, when included, the former perturb the symmetry of the linear optics and diminish the cancellation of the nonlinear effects whereas the latter contribute directly, reducing the DA.

3.1.2.2 Sextupole Scheme

The linear lattice has a chromaticity of $\xi_{x,y}^{(1)} \sim (-100, -37)$ and a natural momentum spread of ~0.1% leading to a tune spread of $\Delta\nu_{x,y} \sim (0.1, 0.04)$, which must be corrected[5]. The linear chromaticity is given by

$$\xi_{x,y}^{(1)} = \mp\frac{1}{4\pi}\sum_{k=1}^{N}\left[(b_2 L)_k - 2(b_3 L)_k \eta_{x,k}\right]\beta_{(x,y),k}, \tag{3.1-8}$$

[1] For medium energy rings: ~3 GeV.

[2] Based on the experience from the Swiss Light Source conceptual design, i.e., a highly nonlinear lattice [3.1.6] with straightforward commissioning [3.1.7], excellent top-off injection efficiency [3.1.8], and stability [3.1.9].

[3] With δ (momentum deviation) treated as a parameter, i.e., the adiabatic approximation.

[4] In particular, with synchrotron oscillations.

[5] Moreover, a positive linear chromaticity in the range 0–5 is required to stabilize the head-tail instability.

where *(b_2L), (b_3L)* are the integrated quadrupole and sextupole strengths, and β and η are the beta function and dispersion, respectively at the quadrupoles and sextupoles, *k*. The driving terms for linear chromaticity from sextupoles are shown in Figure 3.1.7. Two mirror symmetric chromatic families are introduced inside the dispersion section and 3+4 geometric families in the short and long straight sections, i.e., a total of 9 sextupole families. While one of the families in the latter tends to be weak, it has been left as place holders until a more comprehensive optimization has been completed. Individual power supplies for all the quadrupoles are provided, whereas the sextupole families are powered in groups of five; to allow for local optics correction [3.1.10–3.1.16] and control of residual nonlinear resonances. The latter by analyzing the betatron sidebands from turn-by-turn BPM data and controlling them with the inverted "sextupole response matrix" [3.1.17-3.1.19].

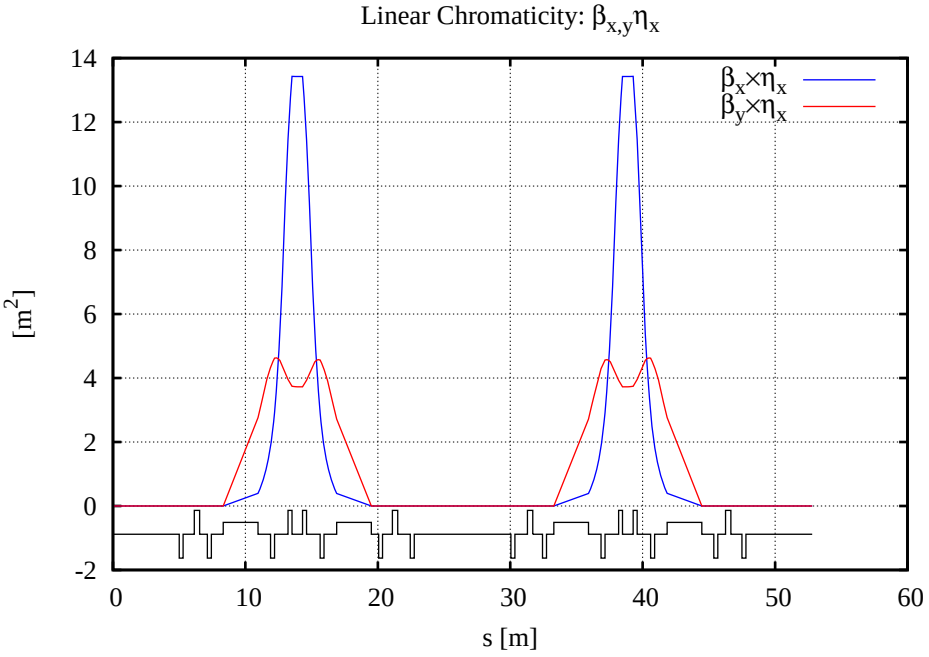

Figure 3.1.7 Driving terms for zeroing linear chromaticity with sextupoles, $\beta_{x,y}$ η_x.

After linear chromaticity has been zeroed, the residual (nonlinear) chromaticity is one of the limiting factors. The second-order chromaticity is given by [3.1.17]:

$$\xi^{(2)}_{x,y} = -\frac{1}{2}\xi^{(1)}_{x,y} \pm \frac{1}{8\pi}\sum_{k=1}^{N}\left\{2(b_3L)_k \frac{\partial \eta_{x,k}}{\partial \delta}\beta_{(x,y),k} \mp \left[(b_2L)_k - 2(b_3L)_k \eta_{x,k}\right]\frac{\partial \beta_{(x,y),k}}{\partial \delta}\right\} \qquad (3.1\text{-}9)$$

where

$$\frac{\partial \eta_{x,j}}{\partial \delta} = -\eta_{x,j} + \frac{\sqrt{\beta_{x,j}}}{2\sin(\pi\nu_x)}\sum_{k=1}^{N}\left[(b_2L)_k - (b_3L)_k \eta_{x,k}\right]\eta_{x,k}\sqrt{\beta_{x,k}}\cos\left(\left|\mu_{j\to k,x}\right| - \pi\nu_x\right)$$

and

$$\frac{\partial \beta_{(x,y),k}}{\partial \delta} = \pm \frac{\beta_{(x,y),j}}{2\sin(2\pi\nu_x)} \sum_{k=1}^{N} \left[(b_2 L)_k - 2(b_3 L)_k \eta_{x,k} \right] \beta_{(x,y),k} \cos\left(\left| 2\mu_{j\to k,(x,y)} \right| - 2\pi\nu_x \right)$$

The driving terms are shown in Figures 3.1.8 and 3.1.9. Clearly, small variations of the sextupole locations may lead to large changes of the nonlinear chromaticity[6]. In particular, the quite large momentum dependence of the optics functions $\eta_x(\delta)$ and $\beta_{x,y}(\delta)$ leads to considerable residual second and cubic terms in the horizontal chromaticity [3.1.19]. Therefore, all the sextupole families are chromatic, i.e., part of the reduction of the nonlinear chromaticity originates from the reduction of the latter with the "geometric" sextupoles, see Figures 3.1.10 and 3.1.11. The former is not reduced, because there are only two chromatic families.

[6] As noted from numerical simulations for the DIAMOND conceptual design [3.1.18].

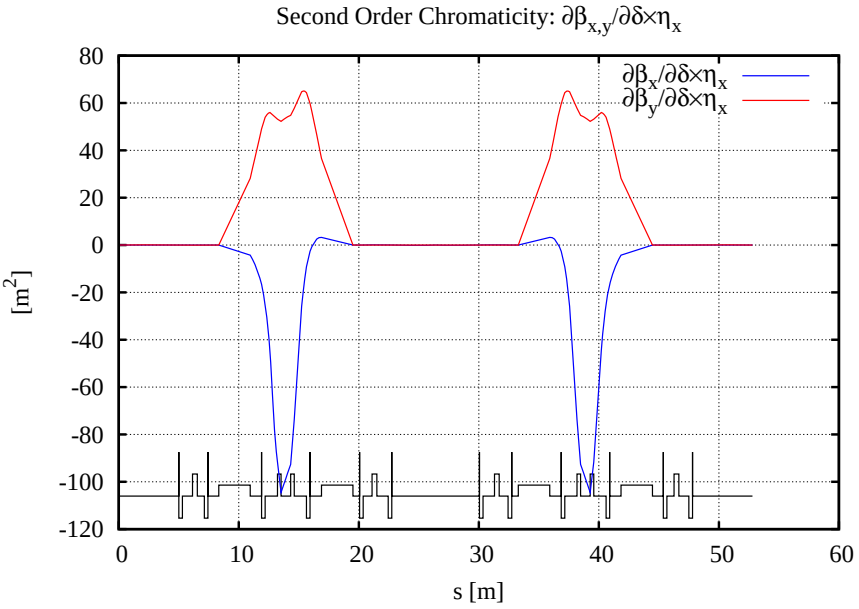

Figure 3.1.8 Driving terms for second-order chromaticity, $\partial\beta_{x,y}/\partial\delta \times \eta_x$ (no sextupoles).

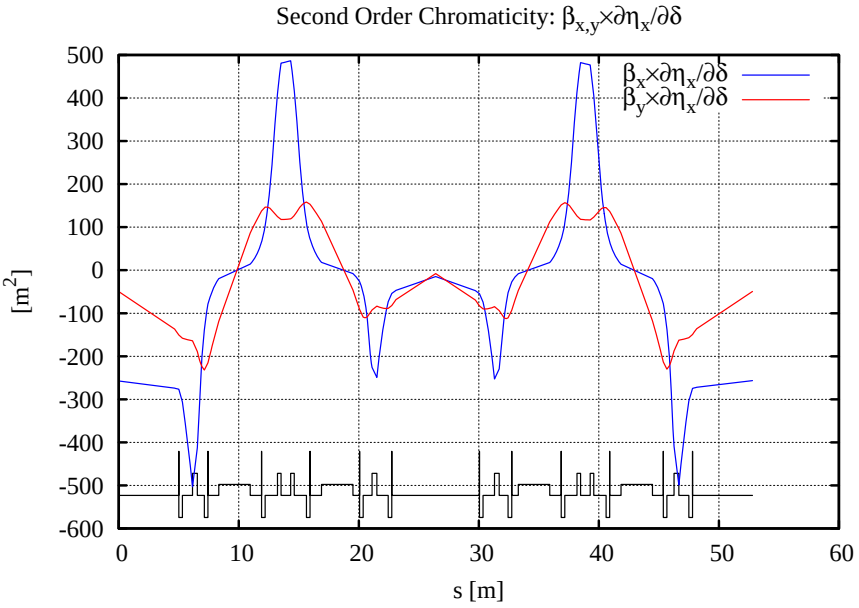

Figure 3.1.9 Driving terms for second-order chromaticity, $\beta_{x,y}\partial\eta_x/\partial\delta$ (no sextupoles).

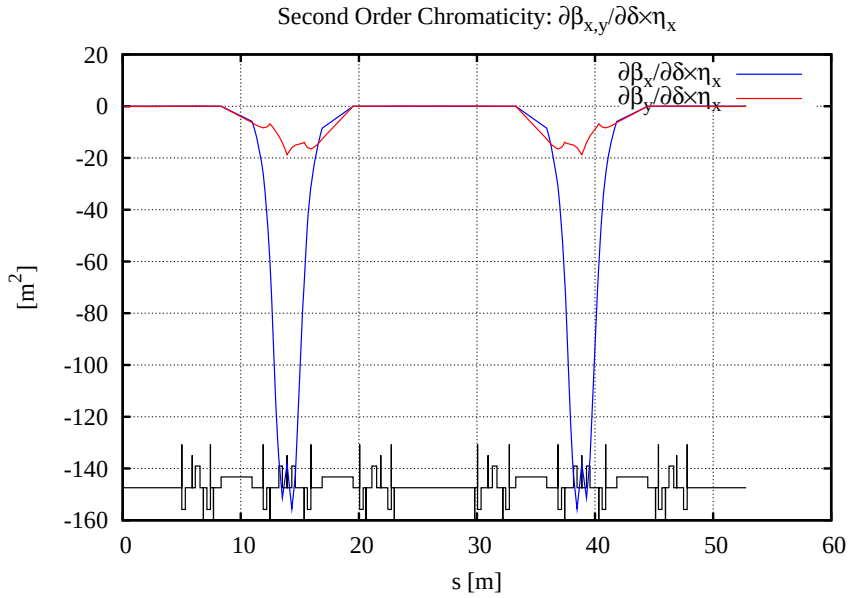

Figure 3.1.10 Driving terms for second-order chromaticity, $\partial\beta_{x,y}/\partial\delta\times\eta_x$ (with sextupoles).

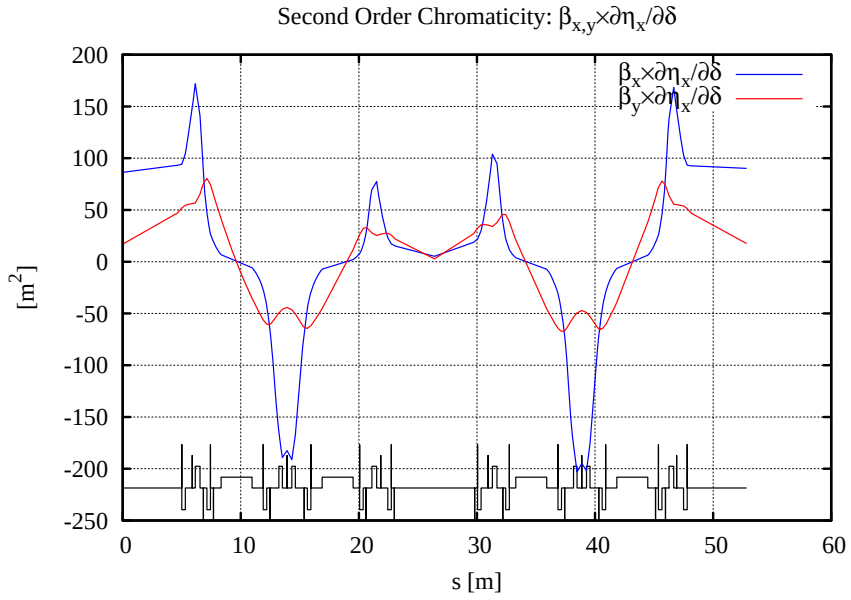

Figure 3.1.11 Driving terms for second-order chromaticity, $\beta_{x,y}\partial\eta_x/\partial\delta$ (with sextupoles).

3.1.2.3 Dynamic Aperture Optimization

The Poincaré map has the formal Lie series representation [3.1.17]:

$$\mathcal{M} = e^{:h:}\mathcal{M}_{\text{linear}} \tag{3.1-10}$$

where $\mathcal{M}_{\text{linear}}$ is the linear one-turn map, and the Lie generator h represents the nonlinear kicks parallel transported to the lattice entrance. It can be written in the normal form[7] [3.1.22]

$$\mathcal{M} = \mathcal{A}^{-1} \ldots e^{:g\left(\bar{J},\bar{\phi}\right)} e^{:k\left(\bar{J}\right)} e^{:-g\left(\bar{J},\bar{\phi}\right)} \mathcal{A} ,$$

where $\left[\bar{J},\bar{\phi}\right]$ are the action-angle variables, $\mathcal{A}$ is a linear transformation to Floquet space[8], $g\left(\bar{J},\bar{\phi}\right)$ a canonical transformation, and $k\left(\bar{J}\right)$ a nonlinear rotation. A nonlinear pseudo-invariant is obtained from

$$\mathcal{K}\left(\bar{J},\bar{\phi}\right) = e^{:g\left(\bar{J},\bar{\phi}\right)} k\left(\bar{J}\right) = \text{cst.} \mathcal{A} .$$

In particular, the terms are of the form:

$$\mathcal{K}_i \propto \frac{{J_x}^{a_x} {J_y}^{a_y}}{\sin\left(\pi\left(n_x \nu_x + n_y \nu_y\right)\right)} \tag{3.1-11}$$

where $\left[n_x,n_y\right]$ are integers, $\left[a_x,a_y\right]$, and $\left[\nu_x,\nu_y\right]$ the cell tune; note the resonance denominator. For a validation of the goodness of the pseudo-invariant as a description of the nonlinear dynamics see [3.1.23].

In contrast to the linear case, the long-term stability now depends on: $\mathcal{K}\left(\bar{J},\bar{\phi}\right)$, the cell tune, and the initial conditions. In other words, for a systematic approach, the pseudo-invariant and the working point have to be optimized simultaneously. We have implemented a generalized (partial) third-order achromat by introducing 9 sextupole families to the super-period, and minimized the coefficients of $\mathcal{K}\left(\bar{J},\bar{\phi}\right)$ over two super-periods, i.e., four DBA cells, for a range of cell tunes. At each working point with optimized sextupole strengths, we evaluated the DA by tracking. To the second order in the sextupole strengths, there are:

- 2+3+2 chromatic terms
- 5+8 geometric terms (modes)
- 3+3 tune shift with amplitude and momentum

This is a total of 26 terms[9] (see Table 3.1.6 for an inventory). These are minimized by varying the sextupole strengths using the following automated method[10] [3.1.5]:

1. For a given cell tune, the pseudo-invariant $\mathcal{K}\left(\bar{J},\bar{\phi}\right)$ and its parametric dependence on the sextupole strengths (i.e., the Jacobian) are calculated for $J_{x,y}$ and δ at the anticipated DA.
2. The norm of $\left\|\mathcal{K}\left(\bar{J},\bar{\phi}\right)\right\|$ is minimized[11] and the DA is evaluated by tracking.
3. The cell tune is changed by using a grid of working points[12] from the optics optimizations, and steps 1–3 are repeated.

[7] Recursively, i.e., to arbitrary order, by Lie series and Truncated Power Series Algebra (TPSA).
[8] Normalized phase space.
[9] The corresponding overconstrained system of nonlinear equations for the sextupole strengths can be minimized because of symmetry and the fact that the higher order terms are due to cross terms of the lower order.
[10] Feasible only because of the use of symmetry and the fact that the higher order terms appear due to cross terms of the lower order.
[11] In particular, a least-square of the individual terms.
[12] Each working point meets all the optics requirements.

The off-momentum aperture is included by using a weighted average for the DA at δ = 0, ±3%. A robust solution is obtained by establishing a broad local maximum for the DA see Figure 3.1.12[13]. The tune scan is then redone with engineering tolerances included in the tracking, see Figure 3.1.13[14], which has a broad maximum centered near $\nu_{x,y} \approx [32.87, 15.67]$. The resulting DA is shown in Figure 3.1.14, for δ = 0, ±3%. The linear chromaticity is set to $\xi_{x,y}^{(1)} \approx [2.0, 2.0]$, and the residual nonlinear chromaticity is shown in Figure 3.1.15.

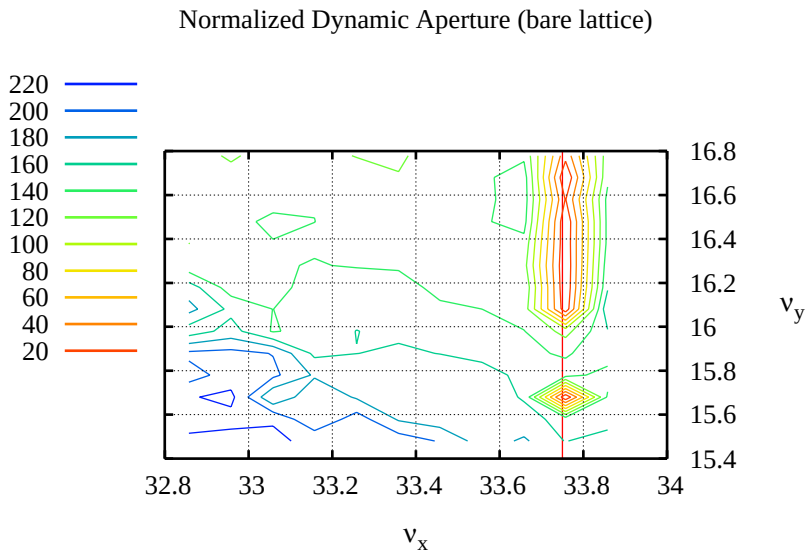

Figure 3.1.12 Normalized DA ($\text{Area}/\sqrt{\beta_x \beta_y}$) versus tune per super-period (bare lattice).

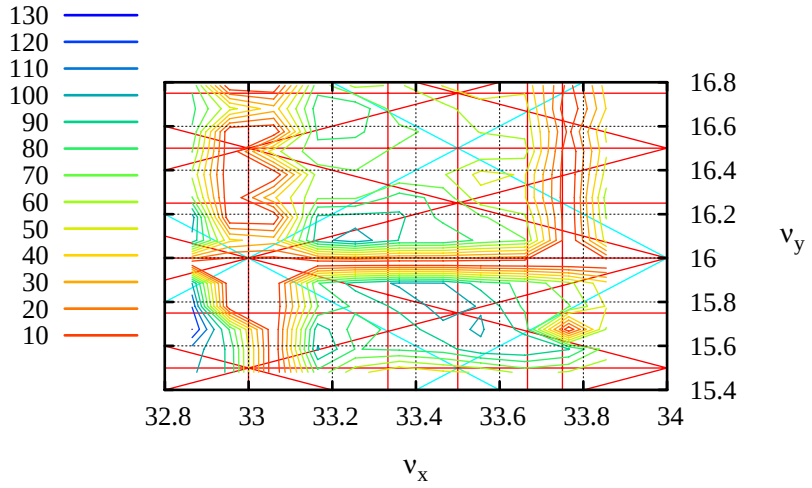

Figure 3.1.13 Normalized DA ($\text{Area}/\sqrt{\beta_x \beta_y}$) versus tune per super-period (with errors).

[13] The red line shows the (systematic) $4\nu_y = 135$ resonance.

[14] The red lines shows the resonances up to first order in the sextupole strength.

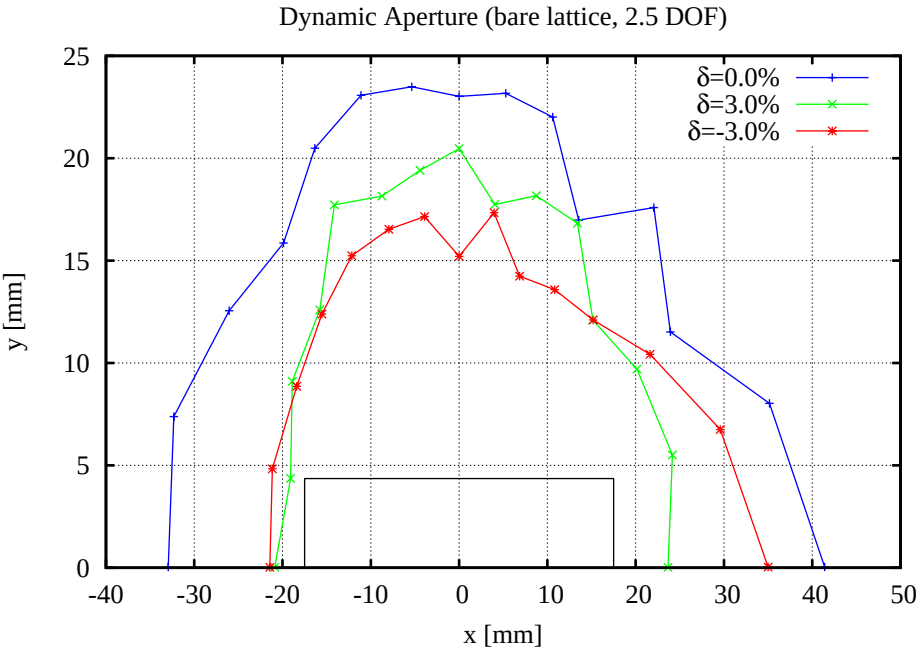

Figure 3.1.14 DA for $\delta = 0$, ±3% for the optimized tune and sextupoles at the center of the long straight section (i.e., at injection), $\beta_{x,y}$ = [20.8, 3.4] m for $\nu_{x,y} \approx [32.833, 15.616]$.

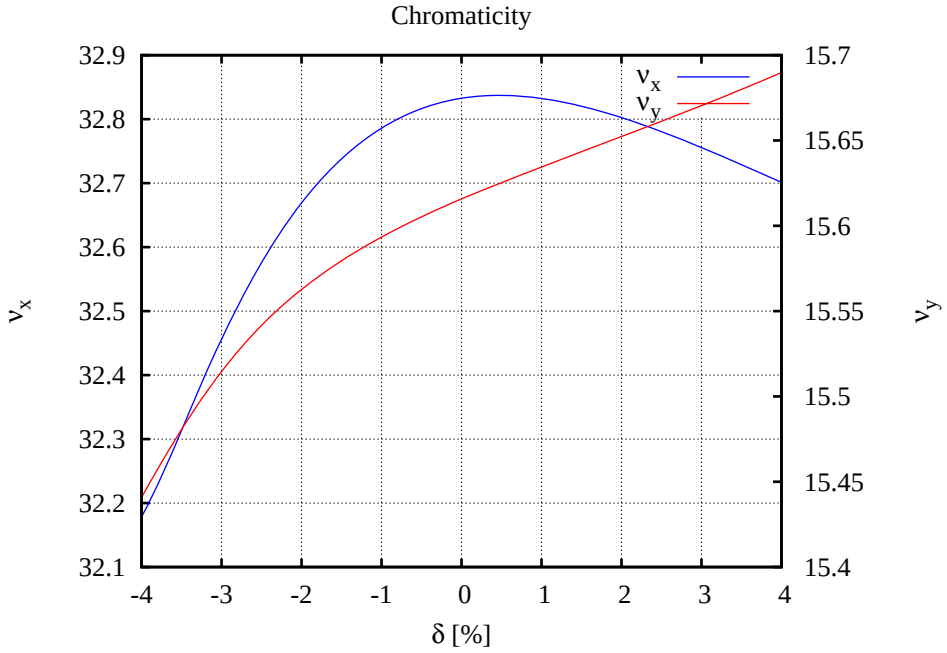

Figure 3.1.15 Residual nonlinear chromaticity for the optimized tune and sextupoles for $\xi^{(1)}_{x,y} \approx [2.0, 2.0]$.

As mentioned earlier, the horizontal chromaticity has a substantial quadratic and cubic term originating from h_{10002}, h_{20001}, h_{00201}, which generate momentum dependence of the optics function. The amplitude-dependent tune shifts are shown in Figures 3.1.16 and 3.1.17, and the balancing of the pseudo-invariant terms

is summarized by Table 3.1.3. Moreover, the crossing of the linear coupling resonances during synchrotron oscillations should be avoided (Figure 3.1.18); otherwise, the Touschek lifetime is likely to be affected.

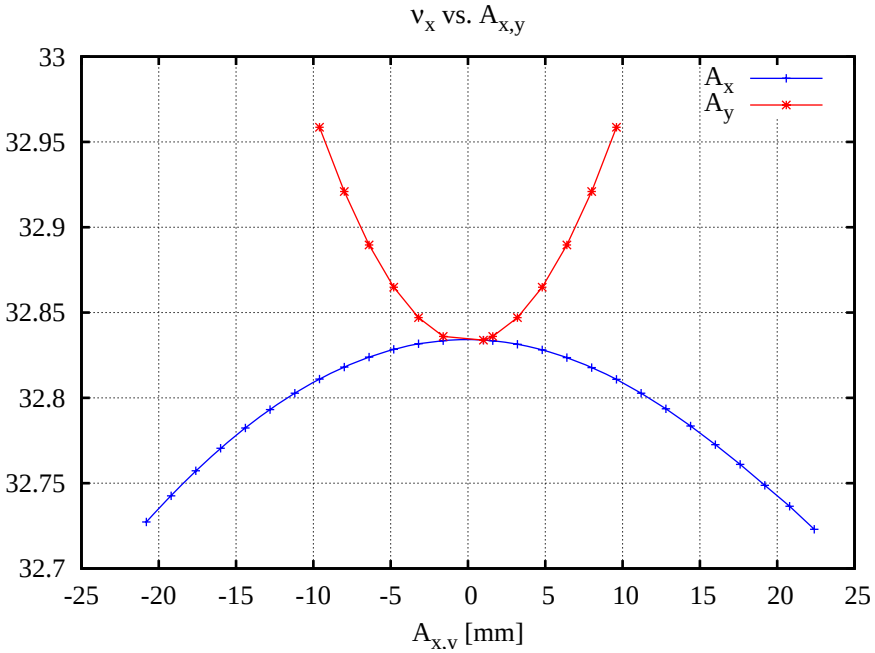

Figure 3.1.6 Horizontal tune, v_x, vs. transverse amplitude (x_0, y_0) at the long straight section for A_x = (x_0, y_0~0) and A_y = (x_0~0, y_0).

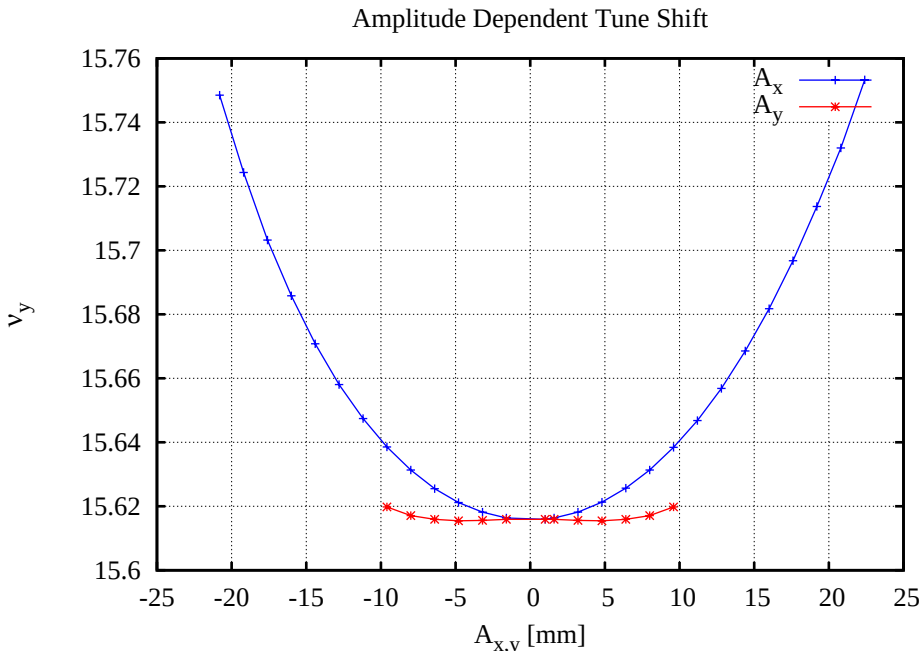

Figure 3.1.17 Vertical tune, v_y, vs. transverse amplitude (x_0, y_0) at the long straight section for: A_x = (x_0, y_0 ~0) and A_y = (x_0 ~0, y_0).

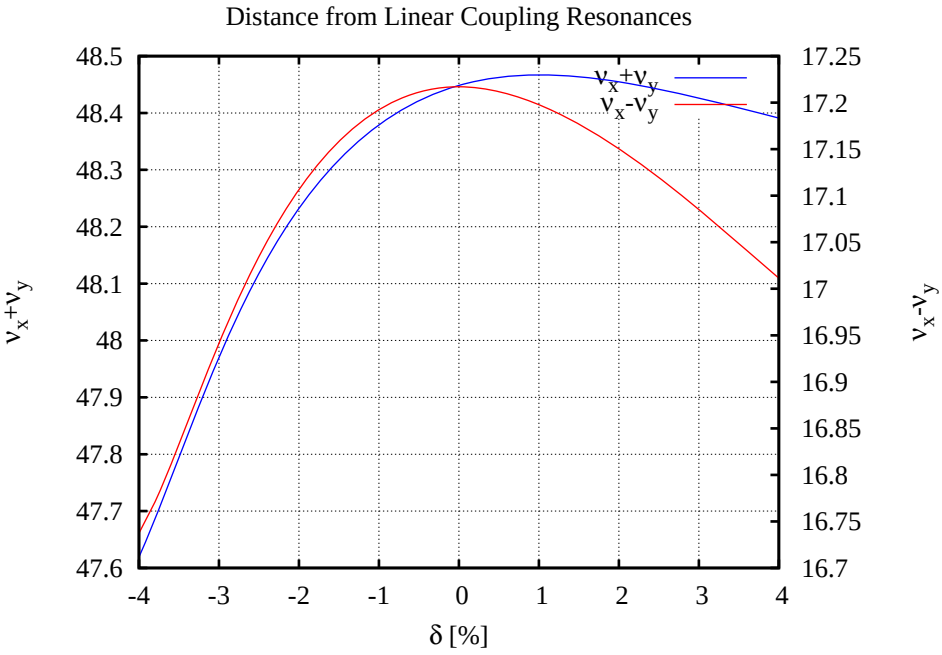

Figure 3.1.18 Distance to the linear coupling resonances.

A frequency map [3.1.15] shows diffusion rate as a function of amplitude or tunes. The diffusion rate, as defined by

$$D(\nu_x, \nu_y) = \log_{10}\left(\sqrt{(\Delta\nu_x)^2 + (\Delta\nu_y)^2}\right), \tag{3.1-12}$$

is an indicator of chaotic behavior, where $\Delta\nu$ is the tune change between the first and second half of the particle tracking with initial amplitude $J_{x,y}$. The frequency map for the optimized working point and sextupole settings for the selected linear chromaticity is shown in Figure 3.1.19, with the diffusion parameter plotted as a color-weighted value. Similarly, a frequency map for x vs. δ is shown in Figure 3.1.20; since crossing of leading order resonances for the Touschek/synchrotron oscillation/radiation damping process must be avoided.

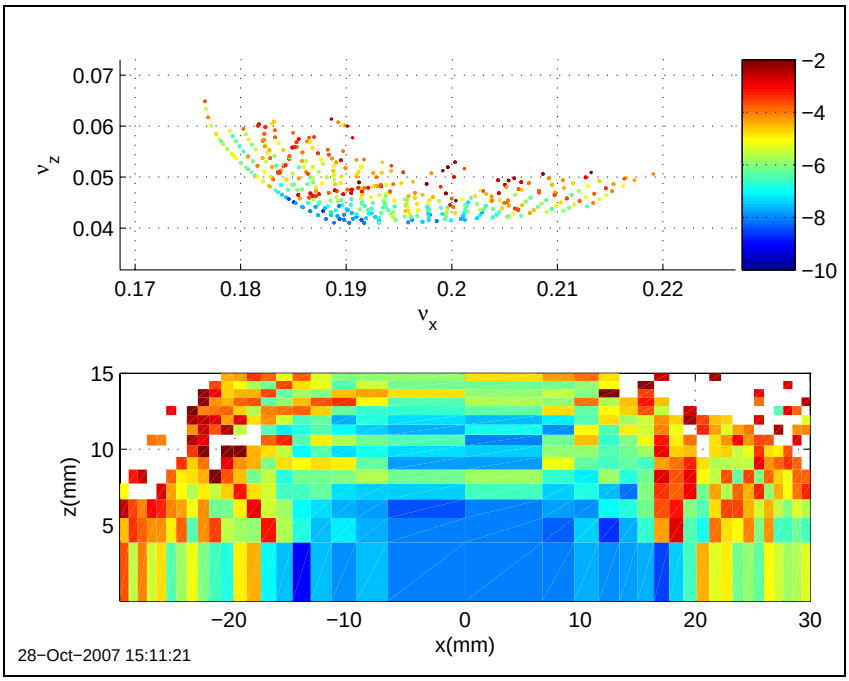

Figure 31.19 Frequency map vs. transverse amplitudes at the Long Straight Section, $\beta_{x,y}$ = (20.8, 3.4) m.

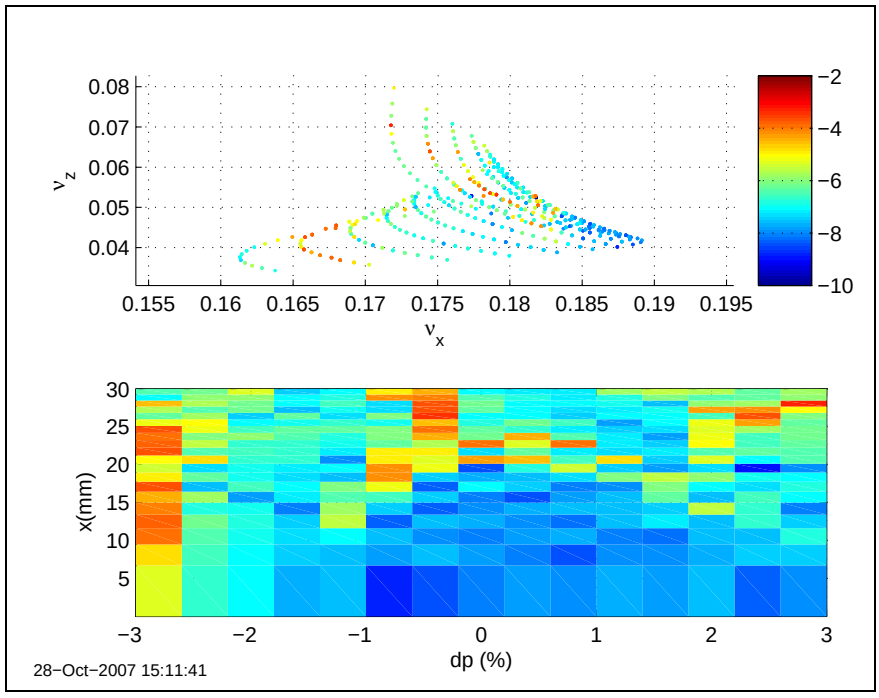

Figure 3.1.20 Frequency map vs. momentum and horizontal amplitude at the Long Straight Section, $\beta_{x,y}$ = (20.8, 3.4) m.

Table 3.1.6 Residual Normalized Lie Generators.

Lie Generator	Effect	Normalized Value
$\lvert h_{11001}\rvert$	$\partial\nu_x/\partial\delta$	5.4×10^{-7}
$\lvert h_{00111}\rvert$	$\partial\nu_y/\partial\delta$	1.5×10^{-6}
$\lvert h_{10002}\rvert$	$\partial\eta_x/\partial\delta$	2.0×10^{-6}
$\lvert h_{20001}\rvert$	$\partial\beta_x/\partial\delta$	2.4×10^{-6}
$\lvert h_{00201}\rvert$	$\partial\beta_y/\partial\delta$	1.7×10^{-6}
$\lvert h_{21000}\rvert$	ν_x	8.6×10^{-7}
$\lvert h_{10110}\rvert$	ν_x	9.2×10^{-7}
$\lvert h_{30000}\rvert$	$3\nu_x$	7.0×10^{-7}
$\lvert h_{10020}\rvert$	$\nu_x-2\nu_y$	3.7×10^{-6}
$\lvert h_{10200}\rvert$	$\nu_x+2\nu_y$	9.8×10^{-7}
$\lvert h_{20110}\rvert$	$2\nu_x$	3.1×10^{-7}
$\lvert h_{31000}\rvert$	$2\nu_x$	5.0×10^{-8}
$\lvert h_{40000}\rvert$	$4\nu_x$	7.3×10^{-7}
$\lvert h_{20020}\rvert$	$2\nu_x-2\nu_y$	1.5×10^{-6}
$\lvert h_{20200}\rvert$	$2\nu_x+2\nu_y$	5.1×10^{-8}
$\lvert h_{11200}\rvert$	$2\nu_y$	6.0×10^{-7}
$\lvert h_{00310}\rvert$	$2\nu_y$	3.9×10^{-7}
$\lvert h_{00400}\rvert$	$4\nu_y$	1.7×10^{-7}
$\lvert h_{22000}\rvert$	$\partial\nu_x/\partial J_x$	9.0×10^{-7}
$\lvert h_{11110}\rvert$	$\partial\nu_{x,y}/\partial J_{y,x}$	3.8×10^{-6}
$\lvert h_{00220}\rvert$	$\partial\nu_y/\partial J_y$	7.3×10^{-7}
$\lvert h_{22001}\rvert$	$\partial^2\nu_x/\partial J_x\partial\delta$	3.2×10^{-7}
$\lvert h_{11111}\rvert$	$\partial^2\nu_{x,y}/\partial J_{y,x}\partial\delta$	8.1×10^{-7}
$\lvert h_{00221}\rvert$	$\partial^2\nu_y/\partial J_y\partial\delta$	4.5×10^{-7}
$\lvert h_{11002}\rvert$	$\partial^2\nu_x/\partial\delta^2$	9.7×10^{-7}
$\lvert h_{00112}\rvert$	$\partial^2\nu_y/\partial\delta^2$	1.9×10^{-7}
$\lvert h_{11003}\rvert$	$\partial^3\nu_x/\partial\delta^3$	1.8×10^{-7}
$\lvert h_{00113}\rvert$	$\partial^3\nu_y/\partial\delta^3$	1.4×10^{-7}

3.1.2.4 Impact of Alignment and Field Tolerances on Dynamic Aperture

Systematic and random magnetic field errors further reduce the DA, and their impact has been evaluated by simulations. Figure 3.1.21 shows the impact on the DA as the random quadrupole gradient errors are increased for all the quadrupoles of the lattice. At a relative RMS error of $\Delta b_2/b_2 \approx 5\text{x}10^{-4}$, they reduce the DA by ~20%, which is taken as the tolerance level for the quadrupole powering errors.

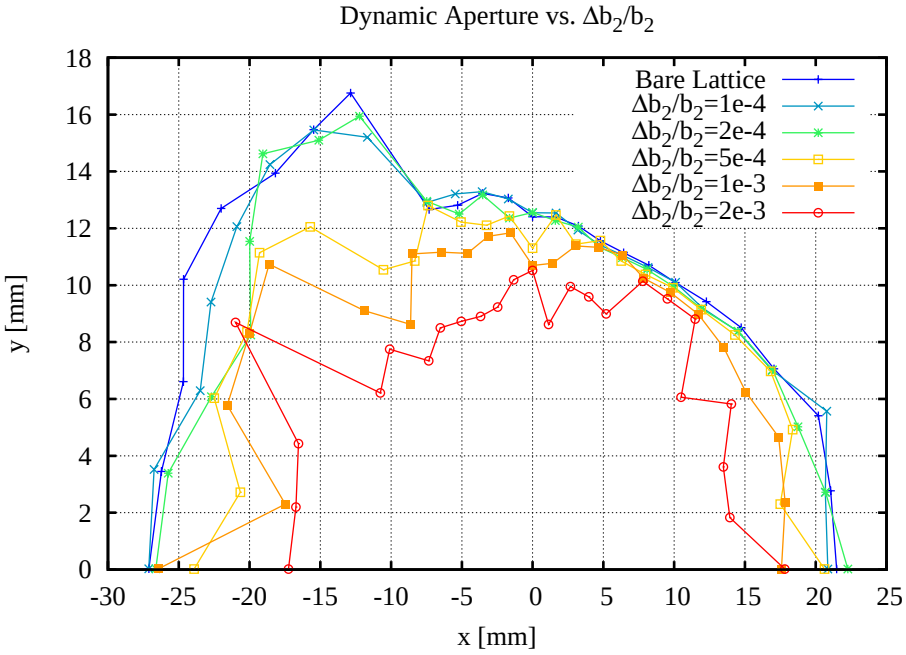

Figure 3.1.21 DA sensitivity versus the fractional gradient errors in the quadrupoles.

This reduction in DA originates from distortions of the linear optics at the sextupole magnets that perturb the influence of the carefully balanced sextupole strengths that were chosen to minimize the nonlinear driving terms. The resulting RMS beta and phase advance beats at the sextupoles can therefore be used as a tolerance level, regardless of their source [3.1.24]. These latter tolerance levels, as well as the gradient tolerance level, are listed in Table 3.1.7.

Table 3.1.7 Optics Tolerances for Robust DA of the NSLS-II Lattice.

Location	At the Quadrupoles	At the Sextupoles		
Parameter	$\left(\Delta b_2 L / b_2 L\right)_{\text{rms}}$	$\left(\Delta\beta_{x,y}/\beta_{x,y}\right)_{\text{rms}}$	$\left(\Delta\nu_{x,y}\right)_{\text{rms}}$	$\left(\Delta x_{\text{cod}}, \Delta y_{\text{cod}}\right)_{\text{rms}}$
Tolerance	$\sim 5\times10^{-4}$	$\sim(0.02, 0.03)$	$\sim(0.003, 0.01)$	$\sim(50, 50)\,\mu\text{m}$

Similarly, a tolerance level can be specified for the residual Closed-Orbit Distortions at the sextupoles, which introduce beta and phase advance beats proportional to the sextupole gradients times the COD offset. This impact on the DA was simulated by introducing random transverse alignment errors to all the sextupoles and is shown in Figure 3.1.22 vs. the RMS error. At a level of $\sigma_x = \sigma_y$ ~50 μm, the DA area is reduced by about 20%. These RMS values can be taken as the tolerance level for the misalignments and residual COD at the sextupoles that must be maintained by the global orbit correction system (see Table 3.1.7).

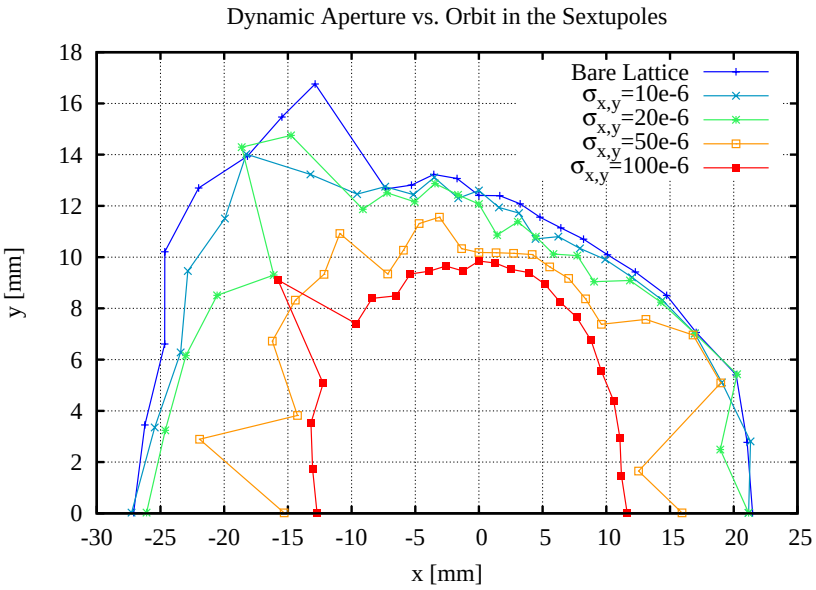

Figure 3.1.22 DA sensitivity to transverse alignment errors of the sextupoles.

Correspondingly, the required transverse magnet alignment tolerances are summarized in Table 3.1.8, assuming the COD errors are corrected using the seven BPMs and seven correctors of the lattice. Details on the global orbit correction scheme are given in Section 3.1.2.5.

Table 3.1.8 Transverse Magnet Alignment Tolerances.

	Δx RMS [μm]	Δy RMS [μm]	Roll RMS [m-rad]
Dipole	~100	~100	~0.5
Girder	~100	~100	~0.5
Quadrupoles	~30	~30	~0.2
Sextupoles	~30	~30	~0.2

The magnetic field error tolerances are specified in terms of the normal and skew multipole coefficients (b_n, a_n), defined by the normalized transverse magnetic field expansion:

$$\frac{1}{(B\rho)}\left[B_x(x,y) + i\,B_y(x,y)\right] \equiv \sum_n (b_n + i\,a_n)(x+i\,y)^{n-1} = \sum_n (b_n + i\,a_n)\,e^{i(n-1)\varphi} \qquad (3.1\text{-}13)$$

where $n = 1,2,3,\ldots$ are the dipole, quadrupole, sextupole, … components, respectively.

In particular, the multipole errors, $\Delta B_n^{(N)}$, relative to the desired field component, b_N, are normalized at a reference radius R and defined by[15]

$$\Delta B_n^{(N)}(R) \equiv R^{n-N}\,\frac{\Delta b_n}{b_N} \quad or \quad \Delta A_n^{(N)}(R) \equiv R^{n-N}\,\frac{\Delta a_n}{b_N} \qquad (3.1\text{-}14)$$

[15] Using the peak B-field for insertion devices.

where $(\Delta b_n, \Delta a_n)$ are the multipole field errors.

The tolerances for the multipole errors are given in Table 3.1.9 using values achieved at the SLS facility [3.1.25, 3.1.26]. The impact is an additional ~20% DA reduction for the lattice with the previously defined alignment tolerances. Future work will include parametric studies for a more precise specification.

Table 3.1.9 Tolerance Levels for RMS Normalized Multipole Errors.

Magnet Type	Normalized Field Error (R = 28 mm)						
Quadrupoles	$\Delta B_2^{(2)}$	$\Delta B_3^{(2)}$	$\Delta A_3^{(2)}$	$\Delta B_4^{(2)}$	$\Delta A_4^{(2)}$	$\Delta B_6^{(2)}$	$\Delta B_{10}^{(2)}$
	2.5×10^{-4}	2.8×10^{-4}	2.9×10^{-4}	1.9×10^{-4}	1.4×10^{-4}	1.3×10^{-4}	0.3×10^{-4}
Sextupoles	$\Delta B_3^{(3)}$	$\Delta B_4^{(3)}$	$\Delta A_4^{(3)}$	$\Delta B_5^{(3)}$	$\Delta B_9^{(3)}$	$\Delta B_{15}^{(3)}$	
	5.0×10^{-4}	5.2×10^{-4}	4.9×10^{-4}	3.5×10^{-4}	0.8×10^{-4}	0.5×10^{-4}	

Similarly challenging is the impact of the linear optics distortions from the insertion devices listed in Table 3.1.10. In particular, the proposed superconducting undulators will substantially affect the nonlinear dynamics in the vertical plane due to their short period (see Section 3.1.2.8). The effect of elliptically polarized undulators on the DA remains to be studied. Table 3.1.11 lists the allowed multipole field tolerances for these undulators [3.1.27]. The potential configuration includes the following IDs:

- CPMUs in the 6 m straights
- CPMUs in the 9 m straights
- DWs in the 9 m straights
- EPUs in the 6 m straights[16]

Details on the impact of these insertion devices and the control of their nonlinear terms are presented in Section 3.1.2.8.

Table 3.1.10 Insertion Device Parameters and Their Impact on the Vertical Tune.

ID	λ_u [mm]	B [T]	K_u	L_u[m]	Gap[mm]	$\Delta\nu_y$
SCU (2+1)	14	1.7	2.2	2	~5	0.002
CPMU (3)	19	1.24	2.2	3	5	0.002
DW	100	1.8	16.8	7	~11	0.028
EPU	~40	0.88	(3.3, 3.3)	~4	~6.5	TBD

[16] Presumably as 2×1 m canted devices.

Table 3.1.11 RMS Normalized Field Errors for Insertion Devices (CPMU, *R* = 20 mm).

Multipole	$\Delta B_3^{(1)}$	$\Delta A_3^{(1)}$	$\Delta B_4^{(1)}$	$\Delta A_4^{(1)}$
Random	6.6×10^{-7}	6.6×10^{-7}	2.2×10^{-8}	2.2×10^{-8}

Note: Based on tolerances from the Swiss Light Source.

3.1.2.5 Control of Closed-Orbit Distortions ("Golden Orbit" philosophy)

While essentially a linear problem, effective orbit control is crucial for robust DA[17] and orbit stability. From a DA point of view, the main objective for the global orbit correction system is to establish and maintain an orbit at the magnetic centers of the sextupoles (to avoid breaking the symmetry of the linear optics), to within ~50 μm (Table 3.1.7). As a rough guideline, the BPMs should be spaced by ~90º in phase advance and placed close to the sextupoles. With a horizontal DBA cell tune of ~1.1, about six BPMs per cell should provide good coverage. In order to center the orbit in all the BPMs, one corrector for each BPM is needed. In theory, the DA can be restored if the BPM is at the sextupole magnetic center [3.1.6]. The number of correctors can be reduced in the vertical plane, since the cell tune is only ~0.5. From the horizontal phase advance (Figure 3.1.23), it is clear that at least one BPM is required in each of the dispersive and straight sections.

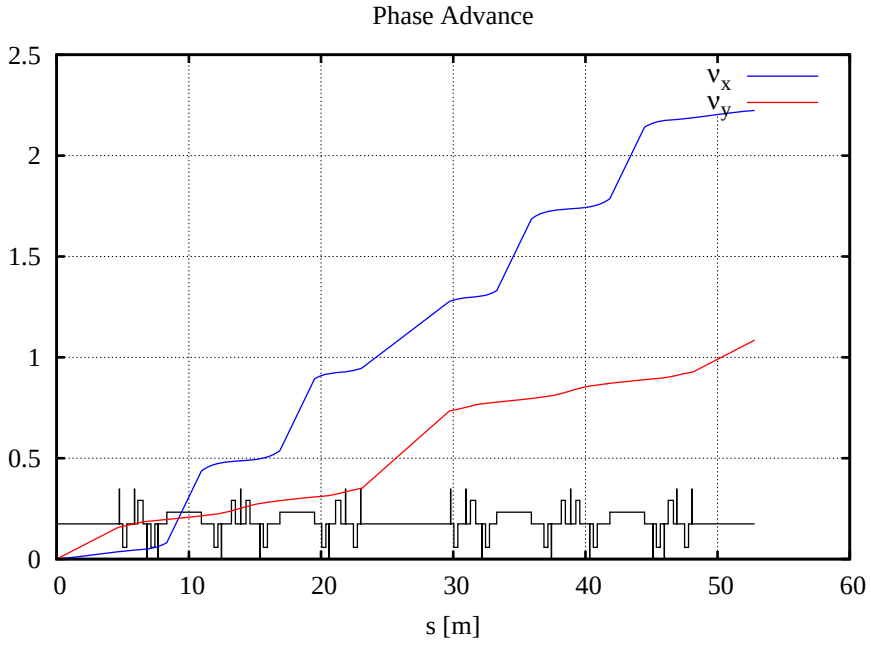

Figure 3.1.23 Normalized Phase Advance for one super-period.

Figures 3.1.24 a and b show the corrected horizontal and vertical RMS closed-orbit distortions (for 1,000 seeds) due to 100 μm RMS random horizontal and vertical quadrupole misalignment errors, with the (H-BPM×H-Corrector, V-BPM×V-Corrector) = (6×6, 6×6) baseline configuration. Clearly, the resulting orbit is well within the guidelines of Table 3.1.7. BPM buttons are included at the center of each DBA for optics checks during commissioning. Beam-based alignment [3.1.29, 3.1.30] with BPMs at the end of the girders

[17] To avoid the collapse of DA observed in the ALS CDR [3.1.26], eventually addressed by "Global Matching of the Normalized Ring" [7.1.10–7.1.15].

will make it possible to reduce orbit errors below the survey and alignment tolerances for the girders, particularly since the alignment tolerances for the magnetic centers on the girders are tighter than the girder alignment in the tunnel.

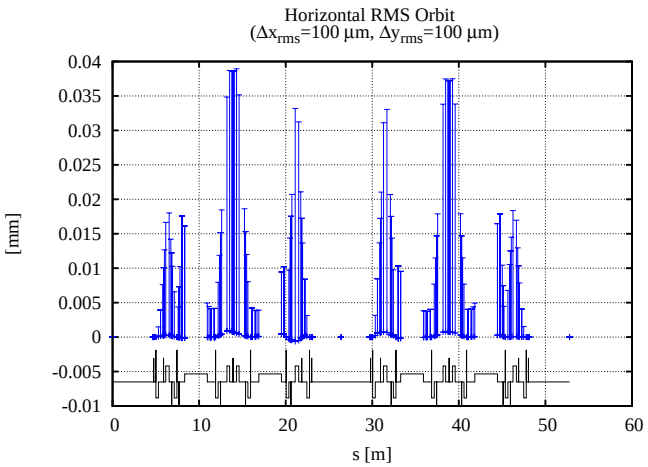

Figure 3.1.24 a Corrected horizontal RMS COD (over 1,000 seeds) for one super-period.

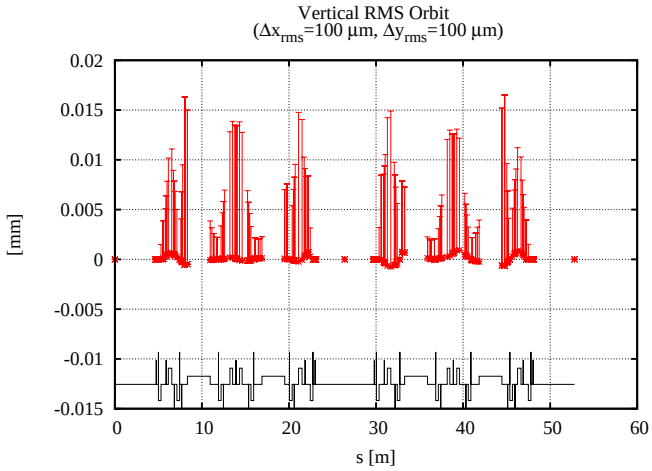

Figure 3.1.24 b Corrected vertical RMS COD (over 1,000 seeds) for one super-period.

Although placing the BPMs close to the sextupoles reduces the residual COD at the sextupoles, the BBA resolution is better for quadrupole centering (<10 μm both H and V) by at least a factor of three [3.1.27, 3.1.28]. This allows for orbit centering beyond the magnet alignment tolerance on the girder. Therefore, we have adopted the (6×6, 6×6) correction scheme, with the BPMs close to the quadrupoles for BBA with a resolution of 10 μm. The impact on the DA of the corrected COD resulting from the alignment tolerances[18] listed in Table 3.1.8 is shown in Figure 3.1.25 (for 20 random seeds). Clearly the (6×6, 6×6) orbit correction system provides adequate DA, and provides margin for error.

[18] Except for roll errors, to be treated later.

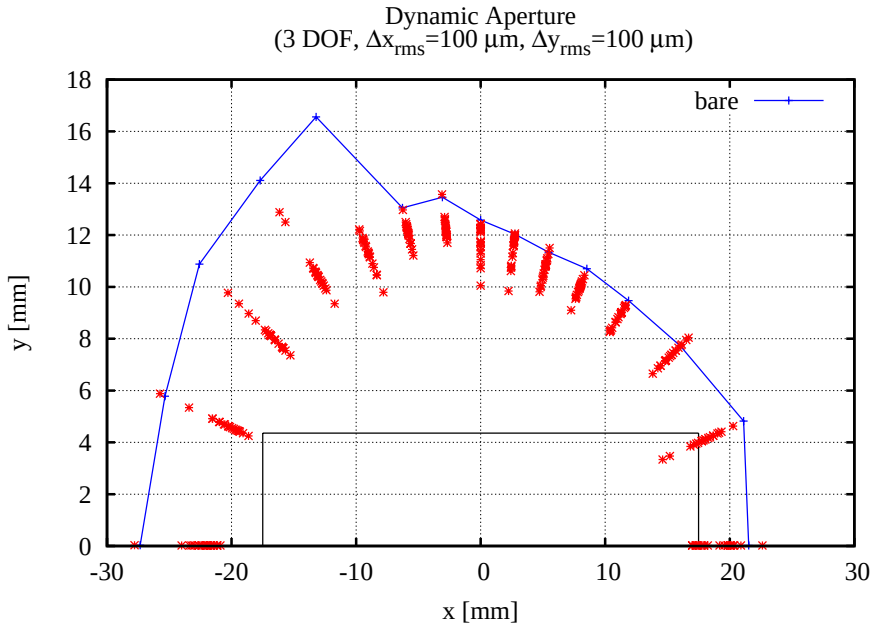

Figure 3.1.25 DA for lattice with transverse misalignment errors (20 seeds), according to Table 3.1.8. These CODs are corrected with the baseline (6×6, 6×6) system.

3.1.2.6 Control of Vertical Beamsize

The vertical beamsize is given by

$$\sigma_y = \sqrt{\beta_y \varepsilon_y + (\eta_y \sigma_\delta)^2} \tag{3.1-15}$$

where β_y and η_y are the vertical beta function and dispersion, ε_y is the vertical emittance, and σ_δ is the momentum spread. The design goal is $\varepsilon_y \sim 0.01$ nm-rad, corresponding to $\sigma_y \sim 5$ μm in the short straights. The non-vanishing vertical emittance originates from:

- linear coupling of the horizontal emittance due to roll errors of the quadrupoles and vertical orbit displacement in the sextupoles,
- and vertical dispersion due to roll errors of the dipoles and linear coupling of the horizontal dispersion.

Local control of the vertical beamsize is straightforward. In particular, by controlling the off-diagonal beam response matrix elements given by [3.1.29]:

$$\frac{\partial y_k}{\partial p_{x,i}} = -\frac{(\Delta a_2 L)_j \sqrt{\beta_{x,i}\beta_{x,j}\beta_{y,j}\beta_{x,k}}\cos\left(\left|\mu_{x,i\to j}\right| - \pi\nu_x\right)\cos\left(\left|\mu_{y,j\to k}\right| - \pi\nu_y\right)}{4\sin(\pi\nu_x)\sin(\pi\nu_y)} + O(\Delta a_2 L)^2,$$

$$\frac{\partial x_k}{\partial p_{y,i}} = -\frac{(\Delta a_2 L)_j \sqrt{\beta_{y,i}\beta_{y,j}\beta_{x,j}\beta_{y,k}}\cos\left(\left|\mu_{y,i\to j}\right| - \pi\nu_y\right)\cos\left(\left|\mu_{x,j\to k}\right| - \pi\nu_x\right)}{4\sin(\pi\nu_x)\sin(\pi\nu_y)} + O(\Delta a_2 L)^2 \tag{3.1-16}$$

for a dipole kick, $p_{(x,y),i}$ at i, due to a skew quadrupole $(a_2 L)$ at j produces an orbit change $(\Delta x_k, \Delta y_k)$ at a BPM located at k. Similarly, the local control of the vertical dispersion is done by:

$$\Delta\eta_{y,k} = -\frac{(\Delta a_2 L)_j \eta_{x,j}\sqrt{\beta_{y,j}\beta_{x,k}}\cos\left(\left|\mu_{x,j\to k}\right| - \pi\nu_x\right)}{2\sin(\pi\nu_y)} + O(\Delta a_2 L)^2 . \quad (3.1\text{-}17)$$

The driving term for the linear coupling is shown in Figure 3.1.26, whereas the driving term for vertical dispersion is similar to the one for vertical linear chromaticity, (Figure 3.1.7). Adequate control is obtained by introducing one skew quadrupole:

- in each long matching section
- in one of the dispersion cells for each super-period

for a total of 15 + 15 = 30 skew quadrupoles for the full lattice. The corresponding (linear) system of equations

$$\left[\frac{\partial \overline{\mathrm{x}}}{\partial \overline{p}_y}, \frac{\partial \overline{\mathrm{y}}}{\partial \overline{p}_x}, \Delta\overline{\eta}_{\mathrm{y}}\right]^{\mathrm{T}} = S \cdot \overline{(\Delta a_2 L)} \quad (3.1\text{-}18)$$

was solved in a least-square sense by the Singular Value Decomposition method. The vertical dispersion after correction for the coupling introduced by the roll errors in Table 3.1.8, is shown in Figure 3.1.27. It turns out that the vertical emittance can be corrected significantly below $\varepsilon_y \sim 0.01$ nm-rad. To optimize the Touschek lifetime, a vertical dispersion wave[19] is introduced to obtain the desired vertical beamsize, e.g., η_y = 5 mm $\Rightarrow \sigma_y \sim \eta_y \sigma_\delta = 5$ μm (Figure 3.1.28). Similarly, the vertical beam size and the transverse coupling angle is shown in Figures 3.1.29 and 3.1.30, respectively. Since it is straightforward to measure the beam response matrix and vertical dispersion on the real storage ring, the correction algorithm implemented for this simulation will eventually be used for commissioning as well.

[19] To avoid affecting the dynamics 0.

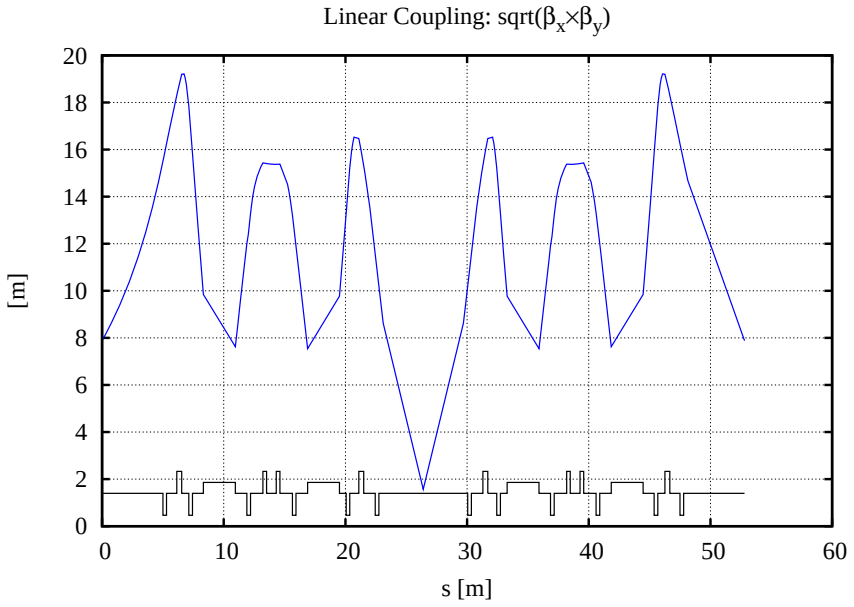

Figure 3.1.26 Driving term for linear coupling, for one super-period.

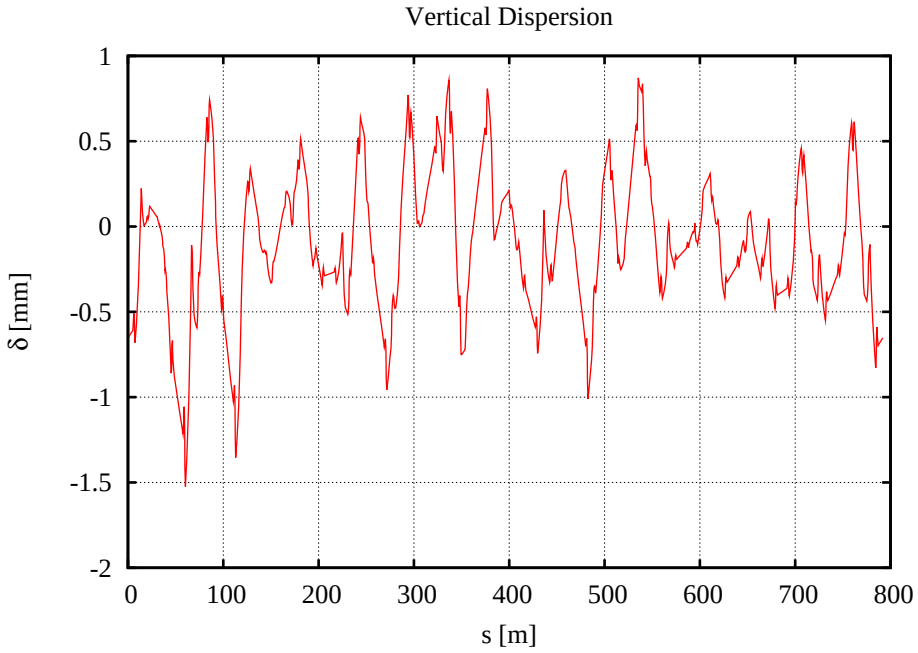

Figure 3.1.27 Corrected vertical dispersion for the quadrupole and dipole roll tolerances.

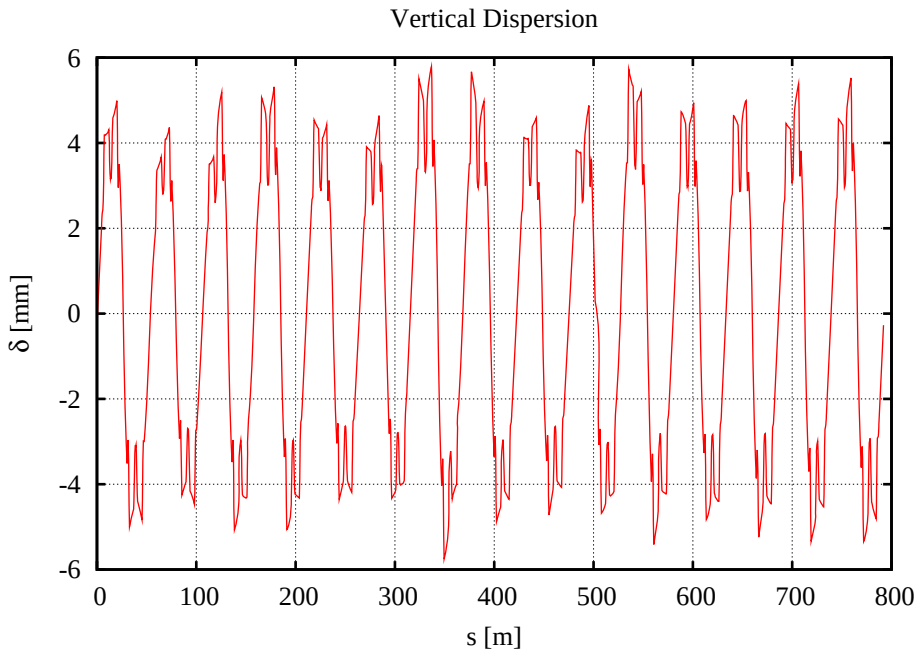

Figure 3.1.28 Corrected vertical dispersion with a residual 5 mm dispersion wave for vertical beamsize control.

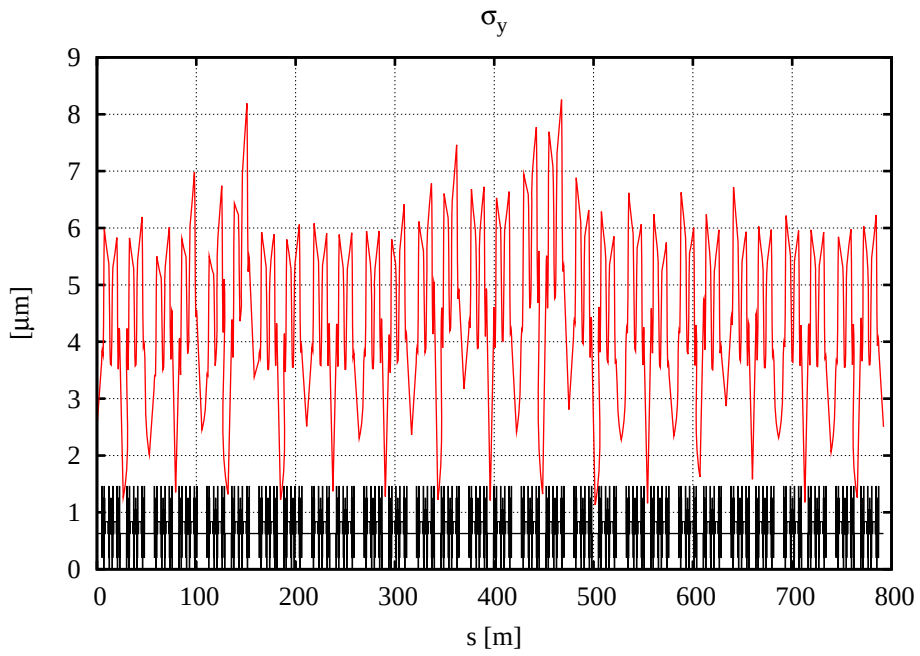

Figure 3.1.29 Vertical beam size with a residual 5 mm dispersion wave.

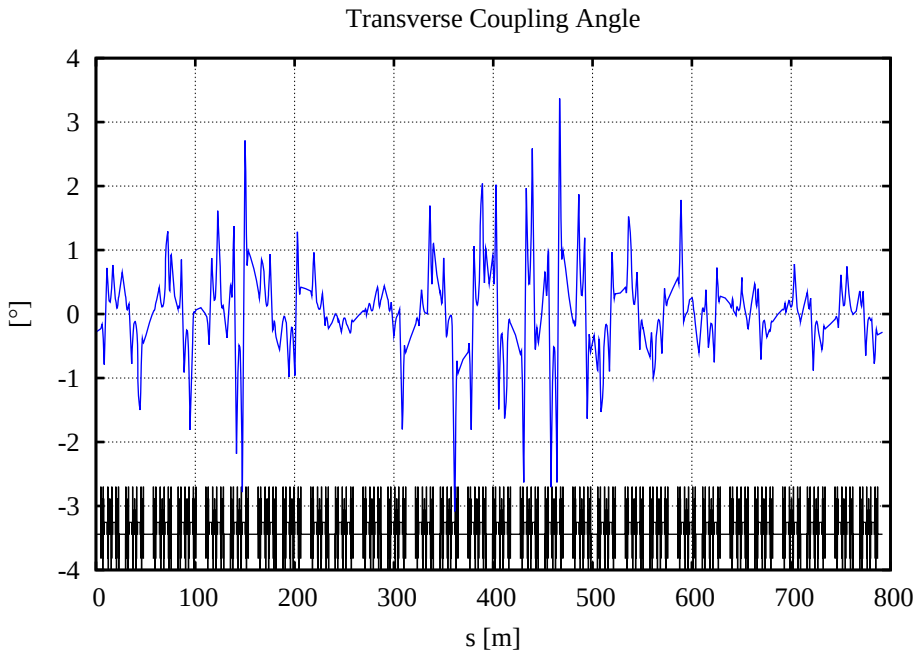

Figure 3.1.30 Transverse coupling angle around the ring with a residual 5 mm dispersion wave.

3.1.2.7 Robustness of DA

The introduction of alignment errors in the lattice leads to orbit distortions, which generate magnetic field errors due to feed-down in the multipoles. These errors are summarized in Table 3.1.12. A robust DA requires that the global orbit correction system maintains the orbit centered in the sextupoles, since feed-down leads to gradient errors. To correctly evaluate this impact, correlations between magnet-magnet alignment errors, e.g., from girder misalignments, need to be included. Also, real magnets are not pure dipoles, quadrupoles, or sextupoles, requiring systematic and random multipole errors to be included. A detailed study of the individual maximum tolerance levels of these multipole errors remains to be done, but the realistic values listed in Table 3.1.9 have been used to evaluate the impact on the DA.

Table 3.1.12 Effect of Mechanical Tolerances on the Magnetic Field Quality.

	Dipole	Quadrupole	Sextupole
Horizontal orbit		horizontal dipole error	gradient error
Vertical orbit		vertical dipole error	skew quadrupole error
Roll error	vertical dipole error	skew quadrupole error	skew sextupole error

Also, due to the nonlinear chromaticity, tracking for at least one synchrotron oscillation period is required to obtain realistic estimates of the DA, since the off-momentum particle will be slowly crossing betatron resonances, which may limit the stability to smaller amplitudes. The design goal for the RF acceptance is ±3%. To obtain a conservative estimate of the momentum aperture, an RF voltage sufficient to produce a 4% bucket height was used to evaluate the DA. The impact on the DA and momentum aperture is shown in Figures 3.1.31 – 3.1.33, where the black-outlined rectangle (Figure 3.1.31) represents the physical aperture of the lattice, propagated to the center of the long straight section. The 20 seeds shown represent 20 lattices generated with randomly distributed alignment and multipole errors having RMS values given by the tolerance values and corrected for COD, as described above. The tracked particles undergo synchrotron oscillations, but do not radiate. Since the radiation damping will also lead to the crossing of resonances, it should also be included in refined studies.

Low-emittance lattices tend to have a small linear momentum compaction, α_1, requiring the second-order term, α_2, to be included for a proper evaluation of the RF bucket, which becomes distorted and reduces the momentum acceptance [3.1.31]. The source of this distortion is a second stable fixed point, which has an energy offset given by the ratio:

$$\alpha_1/\alpha_2 \approx 3.7\times10^{-4}/4.1\times10^{-4} = 92\%\,. \tag{3.1-19}$$

Since it only becomes important for ratios <20%, it will not pose a problem for this lattice[20]. This is further demonstrated by the phase space for the longitudinal Hamiltonian (shown in Figure 3.1.34), including terms to α_3, as well as the radiation loss of 35 m of damping wigglers.

To summarize, the DA guidelines from Table 3.1.5 are easily met for the bare lattice, as well as when the impact of realistic alignment and field tolerances, listed in Tables 3.1.8 and 3.1.9, are included in the lattice model using the correction schemes described above.

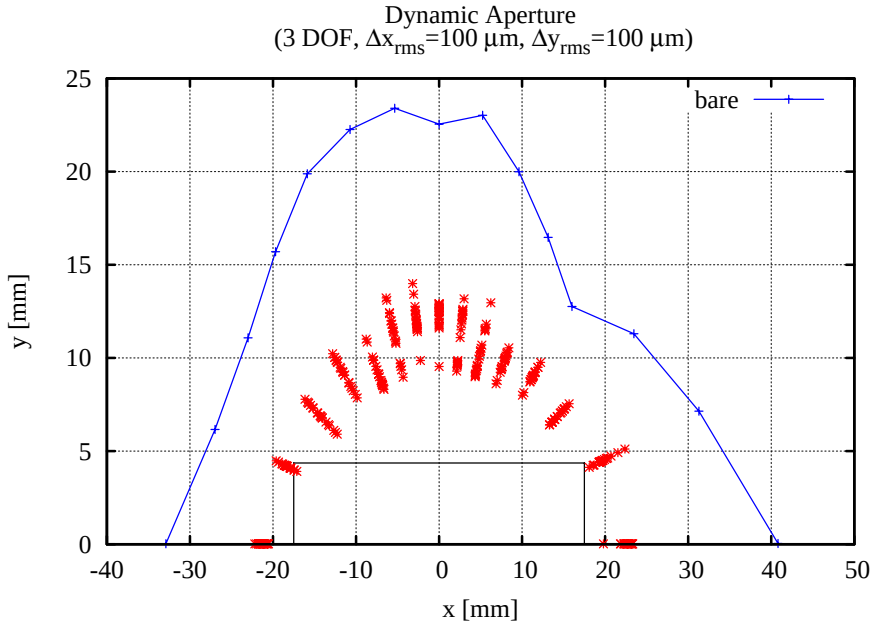

Figure 3.1.31 DA[21] for a "realistic" lattice (20 seeds) with engineering tolerances and corrections. The black outline indicates the physical aperture.

[20] An advantage of the achromatic straights for the DBA lattice.

[21] The relatively large drop to $x, y \approx [22, 12]$ mm is due to the crossing of $\nu_x = 33, 4\nu_y = 63$ at these amplitudes, see Figures 6.1.6 and 6.1.7.

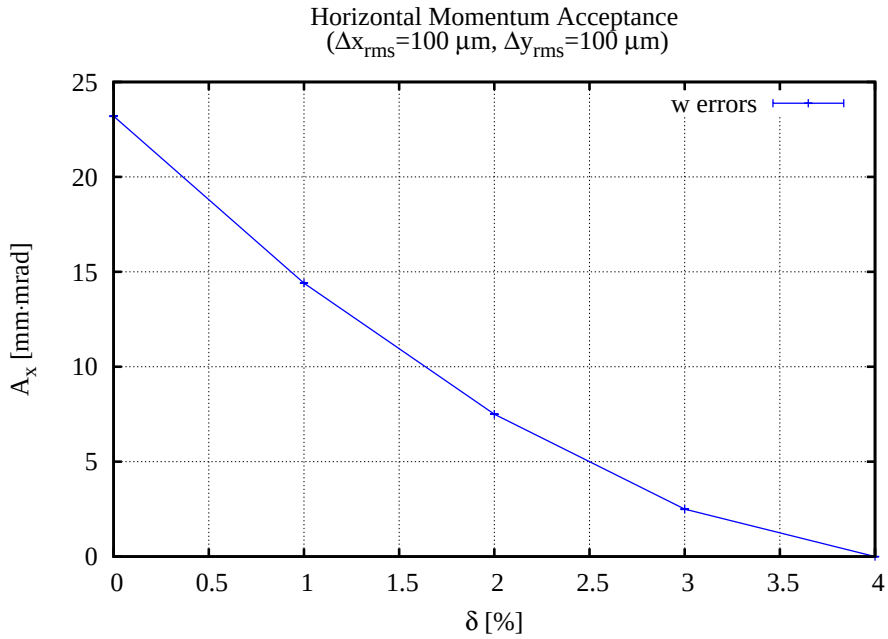

Figure 3.1.32 Average and RMS horizontal momentum acceptance for a "realistic" lattice (20 seeds) with engineering tolerances and corrections.

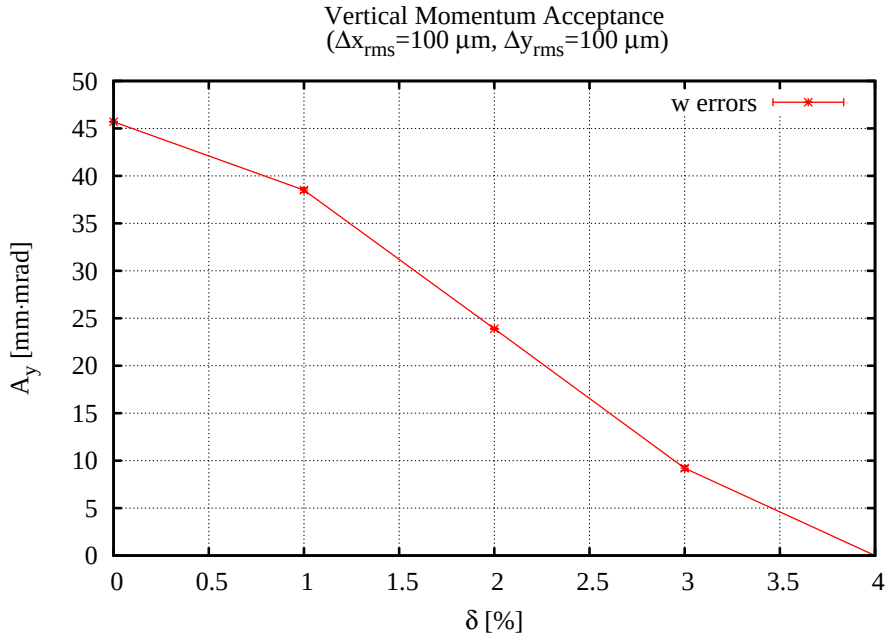

Figure 3.1.33 Average and RMS vertical momentum acceptance for a "realistic" lattice (20 seeds) with engineering tolerances and corrections.

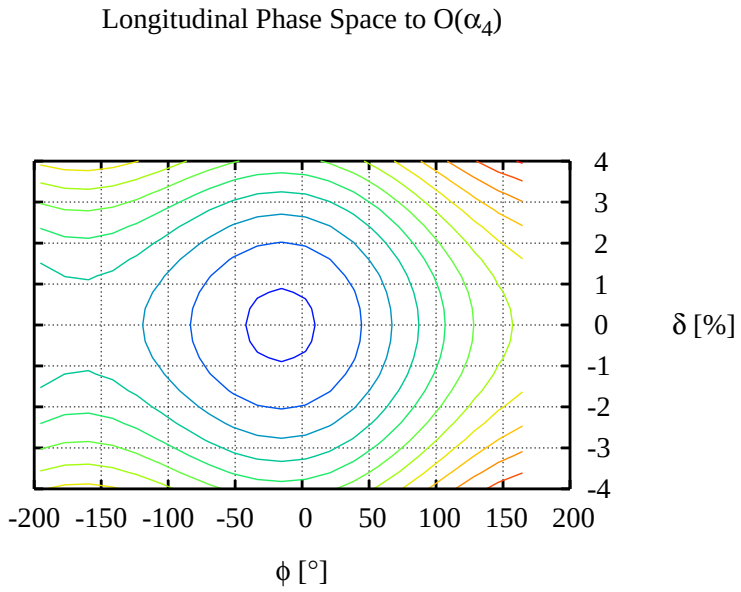

Figure 3.1.34 Longitudinal phase-space, including the radiation loss from damping wigglers.

3.1.2.8 Control of Impact from Insertion Devices

The Hamiltonian for an ID averaged over one undulator period, λ_u, is given by [3.1.36, 3.1.37]:

$$\langle H \rangle_{\lambda_u} \approx \frac{p_x^2 + p_y^2}{2(1+\delta)} - \frac{B_u^2 y^2}{4(B\rho)^2(1+\delta)} + \frac{\pi^2 B_u^2 y^4}{3(B\rho)^2 \lambda_u^2 (1+\delta)} - \delta + O\left(p_{x,y}^4\right) \tag{3.1-20}$$

with phase-space coordinates $\vec{x} = \left[x, p_x, y, p_y, \delta, c\Delta t\right]$, peak field B_u, and magnetic rigidity $(B\rho)$[22]. Note that both the leading-order linear and nonlinear effect scales with $1/(B\rho)^2$, i.e., the effect is reduced with the energy squared for a given undulator field, B_u. The term quadratic in y introduces a vertically focusing term with the integrated gradient

$$(b_2 L) \approx -\frac{B_u^2 L_u}{2(B\rho)^2} \tag{3.1-21}$$

i.e., quadratic in B_u. The beta-beat at location i due to integrated quadrupole kicks, $(\Delta b_2 L)_j$, is given by:

$$\frac{\Delta\beta_{(x,y),i}}{\beta_{(x,y),i}} = \sum_{j=1}^{N} \frac{(\Delta b_2 L)_j \beta_{(x,y),j} \cos\left(\left|2\mu_{(x,y),i\to j}\right| - 2\pi\nu_{(x,y)}\right)}{2\sin\left(2\pi\nu_{(x,y)}\right)} + O(\Delta b_2 L)^2 \tag{3.1-22}$$

where β, μ, ν are the beta functions, phase advance, and tune. Similarly, the phase-beat is given by:

[22] $(B\rho) \approx 10.007$ T-m at 3 GeV.

$$\Delta\mu_{(x,y),i} = -\sum_{j=1}^{N} \frac{\mathrm{sgn}\left(\mu_{(x,y),i\to j}\right)\left(\Delta b_2 L\right)_j \beta_{(x,y),j}\left(\sin\left(2\pi\nu_{(x,y)}\right)+\sin\left(\left|2\mu_{(x,y),i\to j}\right|-2\pi\nu_{(x,y)}\right)\right)}{4\sin\left(2\pi\nu_{(x,y)}\right)} + O\left(\Delta b_2 L\right)^2, \qquad (3.1\text{-}23)$$

and the total tune shift is given by

$$\Delta\nu_{(x,y)} = \pm\frac{1}{4\pi}\sum_{j=1}^{N}\left(\Delta b_2 L\right)_j \beta_{(x,y),j} + O\left(\Delta b_2 L\right)^2. \qquad (3.1\text{-}24)$$

The parameters for the proposed insertion devices are summarized in Table 3.1.10, and the impact of three DWs on the linear optics is shown in Figure 3.1.35, where the beta-beat is rather obvious.

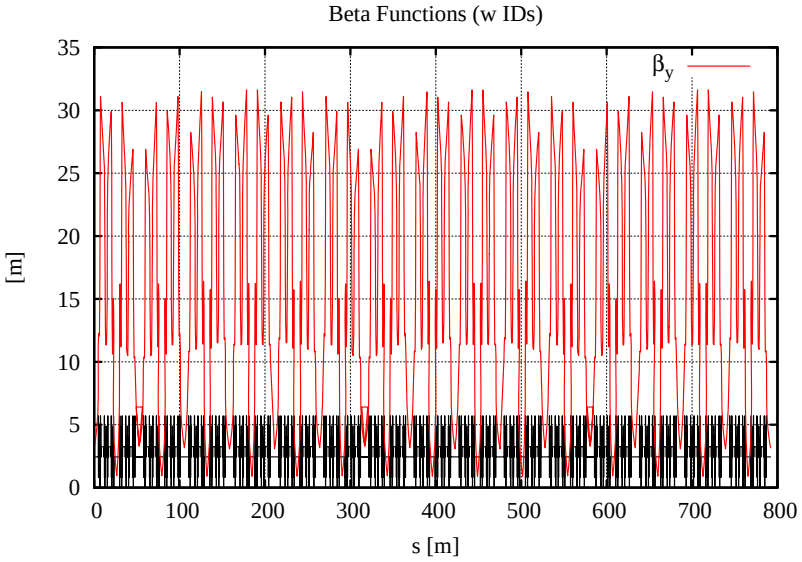

Figure 3.1.35 Perturbed beta functions of the lattice with three DWs installed.

The perturbation of the optics is corrected by adjusting the quadrupole quadruplets in the matching sections. With four quadrupole strengths as parameters, it is expected[23] that the beta- and phase advance beat can be removed in both planes. In particular, the optics deviations at all of the lattice sextupoles, *i,* are represented in a linearized system of equations that includes the focusing impact of all installed IDs $(\Delta b_2 L)_j$. These equations are given in matrix form by

$$\left[\left(\frac{\Delta\beta_{(x,y)}}{\beta_{(x,y)}}\right)_i, \Delta\mu_{(x,y),i}, \Delta\nu_{x,y}\right]^{\mathrm{T}} = A\cdot\left[\Delta\bar{b}_2\, L\right] \qquad (3.1\text{-}22)$$

which was solved using an iterated SVD algorithm[3.1.34, 3.1.35], see Figure 3.1.36. The corrected beta and phase advance beats satisfy the optics tolerances specified in Table 3.1.7.

[23] If the parameters are independent.

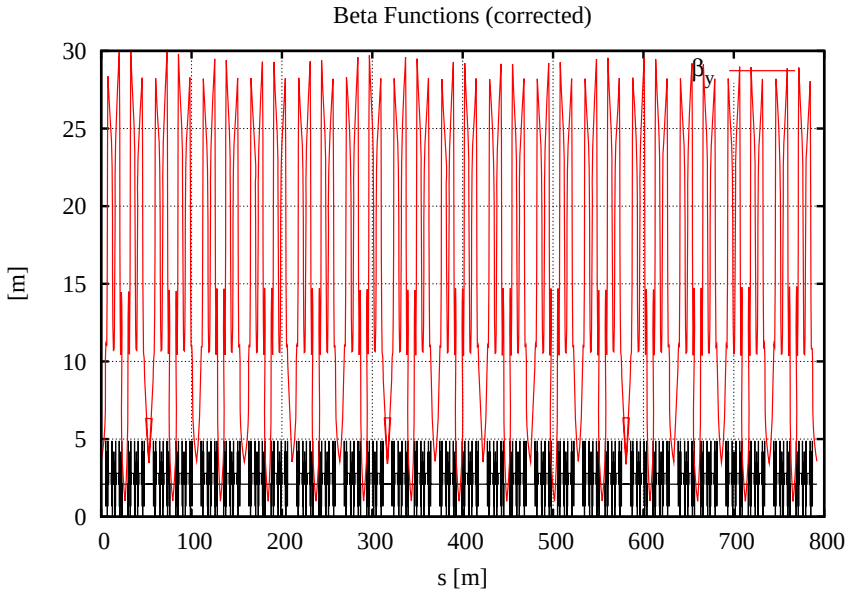

Figure 3.1.36 Corrected beta functions for the lattice with three DWs installed.

The leading order nonlinear part of the ID focusing contains an octupole-like term in the vertical plane which drives amplitude dependent vertical tune shift and $2\nu_y$ and $4\nu_y$ resonances. Table 3.1.13 presents a comparison of the magnitude of the main driving terms from the IDs with those from sextupoles in the lattice. The choice of the length for the CPMUs have been validated by tracking, see Figure 3.1.37.

Table 3.1.13 Lie Generators from the Sextupole Scheme and a Single ID.

Lie Generator	Effect	Sextupole Scheme	DW (Long Straight)	CPMU (Short Straight)	CPMU (Long Straight)	SCU (Short Straight)	SCW (Short Straight)
$\lvert h_{00220}\rvert$	$\partial\nu_y/\partial J_y$	363	609	570	1,982	641	492
$\lvert h_{00310}\rvert$	$2\nu_y$	22	72	22	976	163	251
$\lvert h_{00400}\rvert$	$4\nu_y$	1	18	57	79	43	16

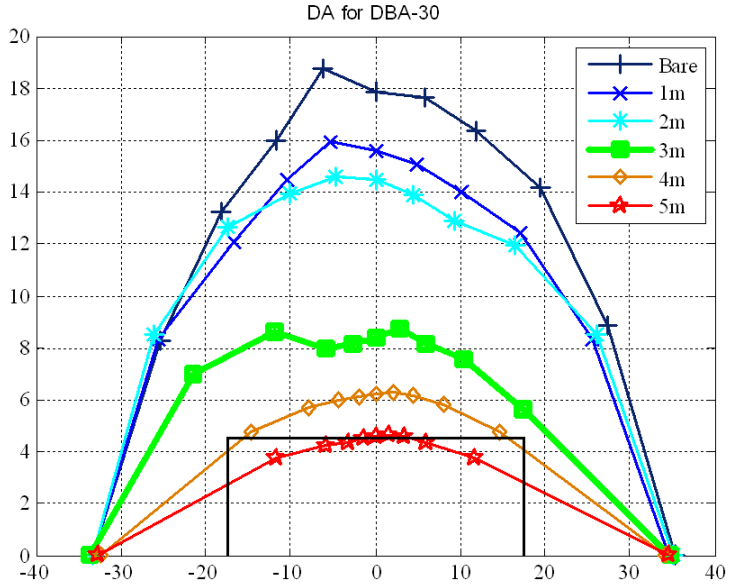

Figure 3.1.37 Impact of the length of one CPMU on the DA.

The effects on the DA and momentum aperture of a lattice with errors and 3 DWs are shown in Figures 3.1.38 and 3.1.39, respectively. The DA is reduced in the vertical to the limited physical aperture. However, there is now considerable diffusion in the interior, which will require further study. Similarly, Figures 3.1.40 and 3.1.41 show the impact of three DWs and 15 CPMUs. Again, the DA is reduced in the vertical due to the reduced vertical aperture. Also, the impact of one APPLE-II EPU is shown in Figures 3.1.42 and 31.43. It is well known that the latter are strongly nonlinear devices, and while the dynamic aperture is maintained, control of the impact of these devices may require further work. However, we have now established a realistic (numeric approach) ID model, based on RADIA kick maps [3.1.40], from which it is straightforward to extract the driving terms (analytic approach). Moreover, pioneering work to control the dynamic terns with L-shims has been developed at the ESRF [3.1.41] and BESSY-2 [3.1.42]; guided by fitted generating function techniques.

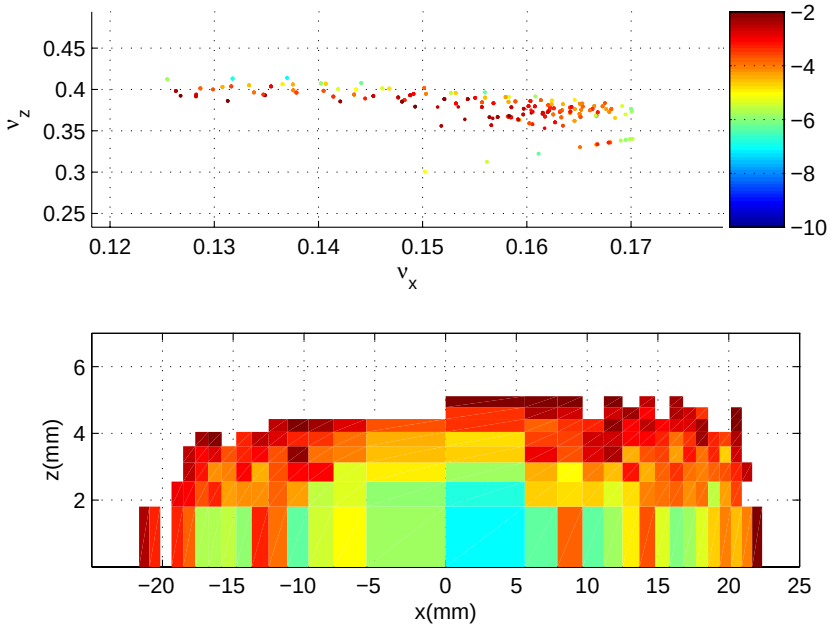

Figure 3.1.38 Frequency map vs. transverse amplitudes for a lattice with three DWs and engineering tolerances.

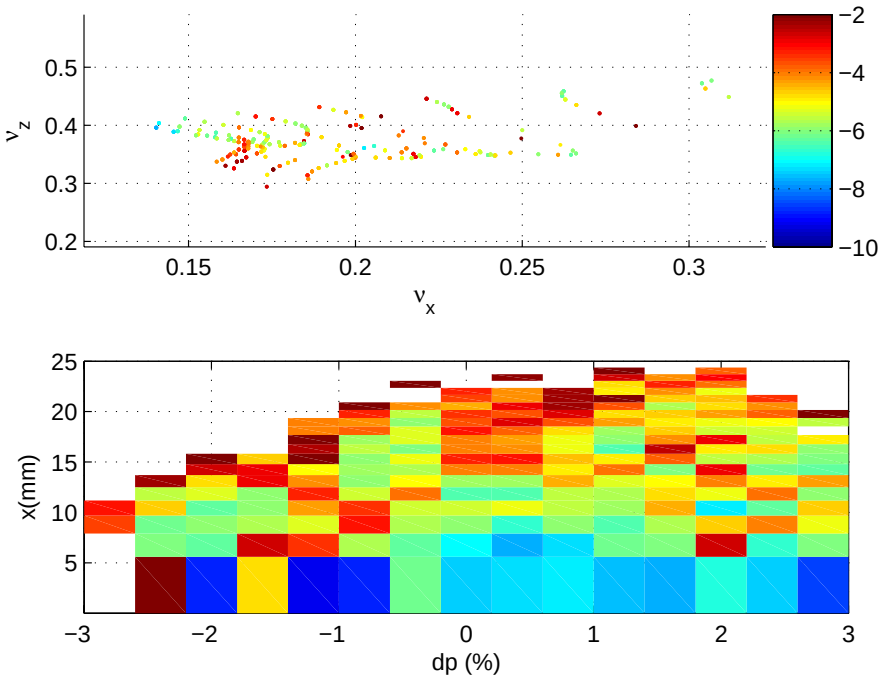

Figure 3.1.39 Frequency map vs. momentum and horizontal amplitude for a lattice with three DWs, 15 CPMUs, and engineering tolerances.

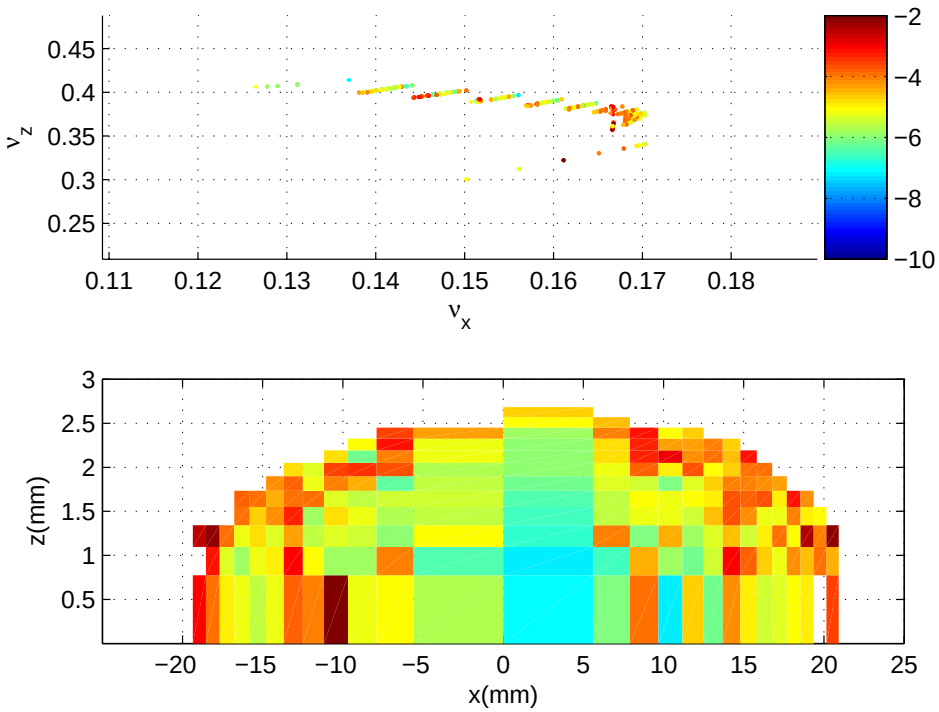

Figure 3.1.40 Frequency map vs. momentum and horizontal amplitude for a lattice with three DWs, 15 CPMUs, and engineering tolerances.

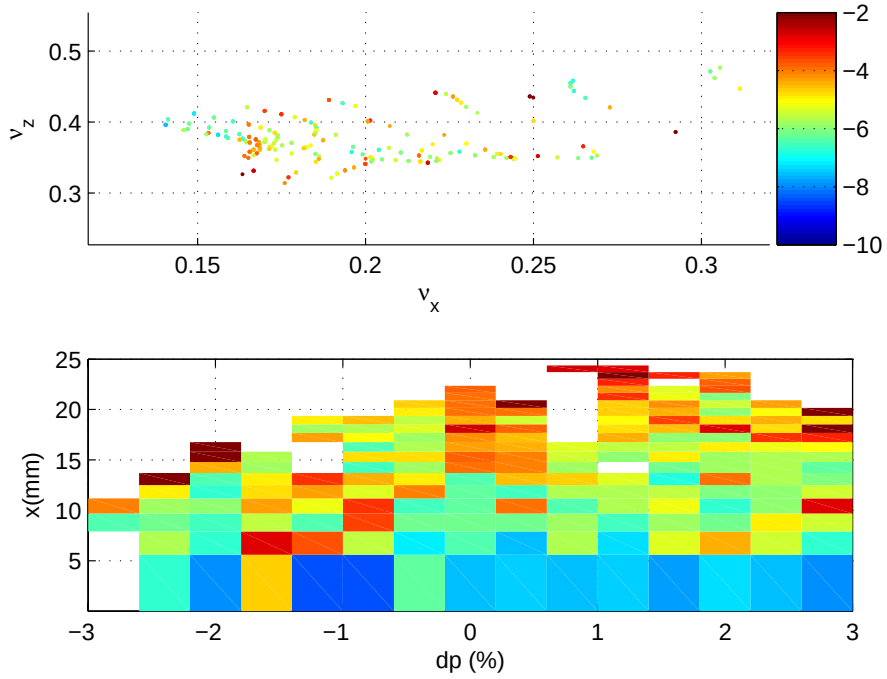

Figure 3.1.41 Frequency map vs. momentum and horizontal amplitude for a lattice with three DWs, 15 CPMUs, and engineering tolerances.

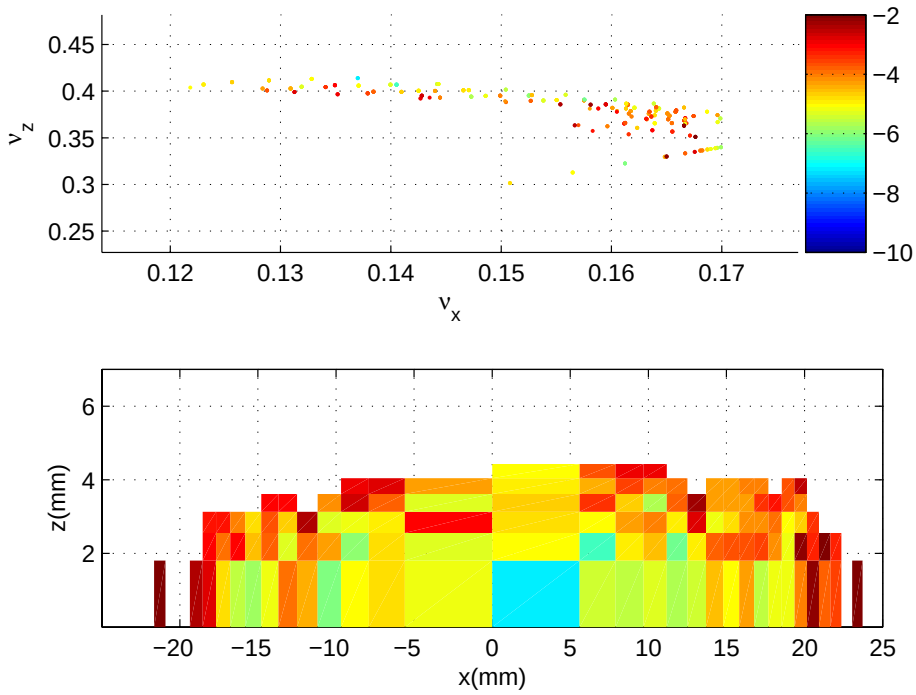

Figure 3.1.42 Frequency map vs. transverse amplitudes for a lattice w 1 EPU of APPLE-II type and engineering tolerances.

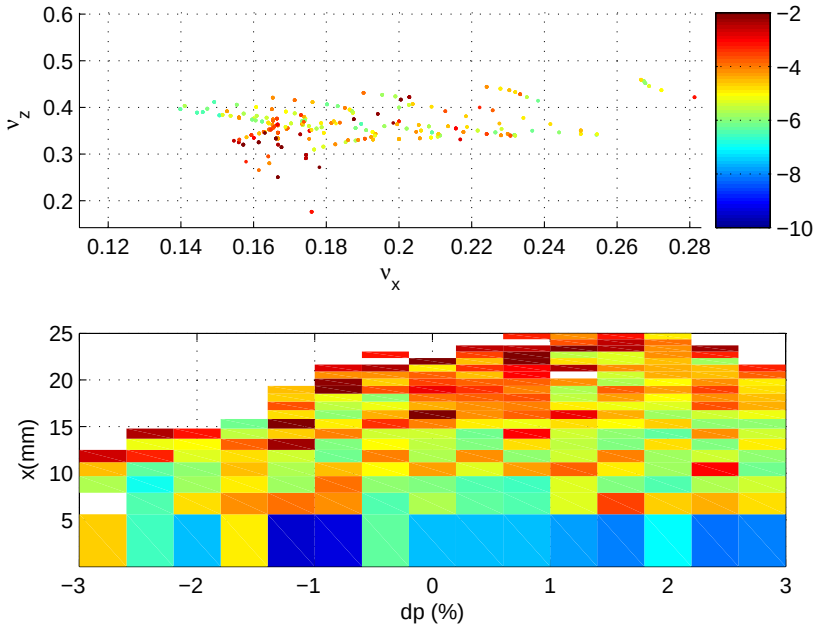

Figure 3.1.43 Frequency map vs. momentum and horizontal amplitude for a lattice w 1 EPU of APPLE-II type and engineering tolerances.

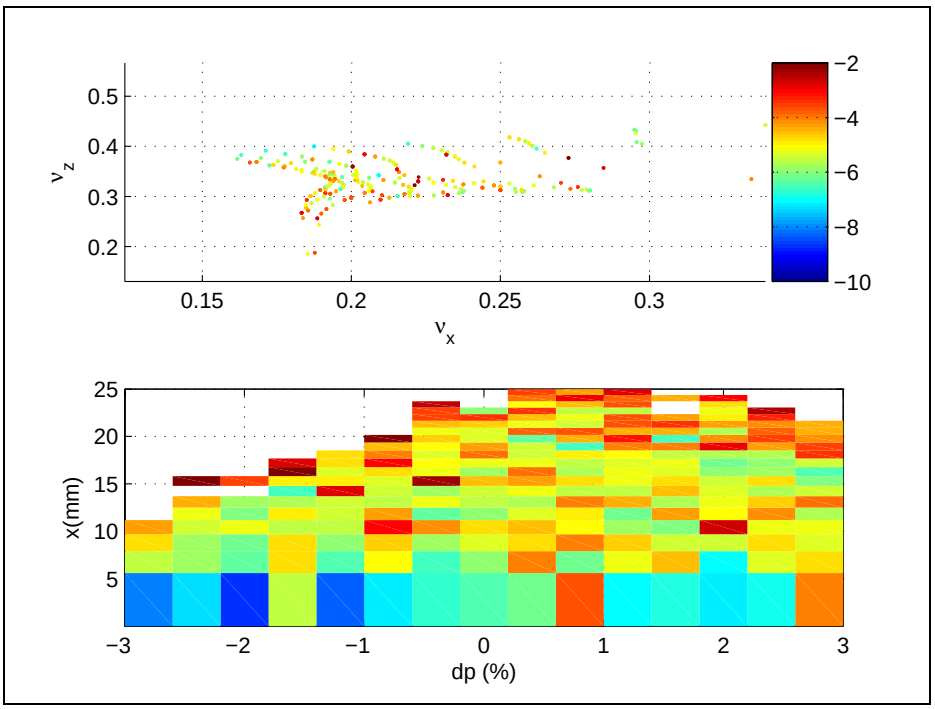

Figure 3.1.43 Frequency map vs. momentum and horizontal amplitude for a lattice w 1 EPU of APPLE-II type and engineering tolerances.

3.1.2.9 Future Work in Lattice and Beam Dynamics Issues

The work presented here shows that the lattice is robust for the errors and realistic magnets. Moreover, that the main impact from the damping wigglers is the perturbation of the optics, which can be restored, and that the dynamic aperture remains outside the physical when 3 DWs and 15 CPMUs are included. However, fine tuning of the working point is required to reduce the considerable amount of tune shift, i.e., resonances, that are observed in the interior of the DA for a realistic lattice. And, to validate the performance with a full set of IDs.

References

[3.1.1] H. Weidemann, NIM **A266**, p. 24 (1988).
[3.1.2] S. Krinsky, et. al., EPAC06, p.3487 (2006).
[3.1.3] G. Decker, and O. Singh, *Phys. Rev. STAB* **2,** p. 112801 (1999).
[3.1.4] S. Krinsky, J. Bengtsson, and S. Kramer, "Consideration of a Double Bend Achromatic Lattice for NSLS-II," pp. 3487–3489, EPAC06.
[3.1.5] J. Bengtsson, "A Control Theory Approach for Dynamic Aperture," pp. 3478–3480, EPAC06.
[3.1.6] J. Bengtsson, W. Joho, P. Marchand, G. Mülhaupt, L. Rivkin, and A. Streun, "Increasing the Energy Acceptance of High Brightness Synchrotron Light Storage Rings," *Nucl. Instr. Meth. A* **404**, 237–247 (1998).
[3.1.7] A. Wrulich, et al., "Commissioning of the Swiss Light Source," pp. 224–226, PAC01.
[3.1.8] A. Wrulich, et al., "Achievements of the SLS Commissioning," PSI. Scientific Report 2001 Vol. VII, 2002.
[3.1.9] M. Böge, "Achieving Sub-Micron Stability in Light Sources," pp. 211–213, EPAC04.
[3.1.10] J. Bengtsson, and E. Forest, "Global Matching of the Normalized Ring" Workshop on Effects of Errors in Accelerators, their Diagnosis and Corrections," Corpus Christi, TX, Oct. 3–8, 1991.
[3.1.11] J. Bengtsson, and M. Meddahi, "Modeling of Beam Dynamics and Comparison with Measurements for the Advanced Light Source (ALS)," pp. 1022–1024, EPAC94.

[3.1.12] D. Robin, G. Portmann, H. Nishimura, and J. Safranek, "Model Calibration and Symmetry Restoration of the Advanced Light Source," pp. 971–973, EPAC96.
[3.1.13] J. Safranek, "Experimental Determination of Storage Ring Optics Using Orbit Response Measurements," *Nucl. Instr. and Meth. A* **388**, 27-36 (1997).
[3.1.14] D. Robin, C. Steier, J. Safranek, and W. Decking, "Enhanced Performance of the Advanced Light Source through Periodicity Restoration of the Linear Lattice," pp. 136–138, EPAC00.
[3.1.15] J. Laskar, L. Nadolski, D. Robin, and C. Steier, "Global Dynamics of the Advanced Light Source Revealed through Experimental Frequency Map Analysis," *Phys. Rev. Lett.* **85**, 558–561 (2000).
[3.1.16] J. Bengtsson, "X-Ray Ring Optics: the Inverse Problem," NSLS Tech Note 540 (2005).
[3.1.17] J. Bengtsson, "The Sextupole Scheme for the Swiss Light Source (SLS): An Analytic Approach," SLS Note 9/97 (1997).
[3.1.18] A. Streun, J. Bengtsson, beam studies collaboration at the SLS, May 14-25, 2007.
[3.1.19] Y. Luo, M. Bai, R. Calaga, J. Bengtsson, W. Fischer, N. Malitsky, F. Pilat, T. Satogata "Measurement and Correction of Third Resonance Driving Term in the RHIC.
[3.1.20] Diamond Synchrotron Light Source: Report of the Design Specification," CCLRC (2002).
[3.1.21] S.L. Kramer, S. Krinsky, and J. Bengtsson, "Comparison of Double Bend and Triple Bend Achromatic Lattice Structures for NSLS-II" pp. 384–386, EPAC06.
[3.1.22] E. Forest "A Hamiltonian-Free Description of Single Particle Dynamics for Hopelessly Complex Systems" J. Math. Phys. **31,** pp. 1133-1144 (1990).
[3.1.23] J. Bengtsson "The Poincaré Map, Lie Generator, Nonlinear Invariant, Parameter Dependence, and Dynamic Aperture for Rings" pp. 4315-4317, PAC07
[3.1.24] J. Bengtsson, "On the NSLS-II Dynamic Aperture: Robustness," NSLS-II Tech Note 8 (2005).
[3.1.25] A. Streun, "SLS Dynamic Acceptance Degradation due to Magnet Multipole Errors," SLS-TME-TA-1998-0002 (1998).
[3.1.26] E.I. Antokhin, et al., "Multipoles of the SLS Storage Ring: Manufacturing and Magnetic Measurements," IEEE Trans. of Appl. Super. vol. 12, no. 1, 51–54 (2002).
[3.1.27] J. Safranek, C. Limborg, A. Terebilo, K.I. Blomqvist, P. Elleaume, and Y. Nosochkov, "Nonlinear Dynamics in a SPEAR Wiggler," *Phys. Rev. ST* **5,** 010701 (2002).
[3.1.28] C. Steier, G. Portmann, and A. Young, "Commissioning of the First Elliptically Polarizing Undulator at the ALS," pp. 2343–2345, EPAC00.
[3.1.29] B. Singh, and A. Streun, "Limits for Normal and Skew Sextupole and Octupole Field Errors in the First (I_1) and Second (I_2) Field-Integrals of Insertion Devices planned for SLS," SLS-TME-TA-2001-0170 (2001).
[3.1.30] "1-2 GeV Synchrotron Radiation Source Conceptual Design Report," LBNL PUB-5172 (1986).
[3.1.31] G. Portmann, D. Robin, and L. Schachinger, "Automated Beam Based Alignment of the ALS Quadrupoles," pp. 2693–2695, EPAC96.
[3.1.32] S.L. Kramer, "Beam Based Alignment," NSLS-II Tech Note (2006).
[3.1.33] J. Bengtsson, and I. Pinayev, "NSLS-II: Control of Vertical Emittance," NSLS-II Tech Note (2006).
[3.1.34] C. Steier, D. Robin, A. Wolski, G. Portmann, and J. Safranek, "Coupling Correction and Beam Dynamics at Ultralow Vertical Emittance in the ALS," pp. 3213–3215, PAC03.
[3.1.35] D. Robin, E. Forest, C. Pellegrini, and A. Amiry, "Quasi-Isochronous Storage Rings," *Phys. Rev. E* **48**, 2149–2156 (1993).
[3.1.36] L. Smith, "Effect of Wigglers and Undulators on Beam Dynamics" LBL-21391 (1986).
[3.1.37] Y. Wu, V.N. Litvinenko, and J.M.J. Madey, "Lattice and Dynamic Aperture of the Duke FEL Storage Ring," pp. 218–220, PAC93.
[3.1.38] T. Shaftan and J. Bengtsson, "Impact of Insertion Devices on the NSLS-II lattice," NSLS-II Tech. Note (2006).
[3.1.39] T. Shaftan, J. Bengtsson, and S. Kramer, "Control of Dynamic Aperture with Insertion Devices" pp. 3490–3492, EPAC06.

[3.1.40] P. Elleaume “A New Approach to the Electron Beam Dynamics in Undulators and Wigglers” pp. 661-663, EPAC92.
[3.1.41] J. Chavanne, P. Van Vaerenbergh, P. Elleaume, T. Günzel, “Recent Achievements and Future Prospect of ID Activities at the ESRF” pp. 2346–2348, EPAC00.
[3.1.42] J. Bahrdt, W. Frentrup, A. Gaupp, M. Scheer, G. Wüstefeld “Dynamics Multipole Shimming of the APPLE Undulator UE112” pp. 941–943, PAC07.

3.2 Collective Effects

3.2.1 Introduction

In this section, we discuss the effect of multi-particle interactions [3.2.1] on the electron beam in the NSLS-II storage ring. The storage ring has 500 MHz RF and a revolution period of 2.6 μs. The baseline design configuration corresponds to filling 80% (or 90%) of the RF buckets and leaving one or more gaps to allow for ion clearing. In this case we have M = 1040 bunches, each containing $N_e = 7.8\times10^9$ electrons ($N_e e$ = 1.25 nC) corresponding to a total average current $I_{av} = MN_e e/T_0 =$ 500 mA and a single-bunch current $I_0 = N_e e/T_0 =$ 0.5 mA. For an RMS bunch duration σ_t = 15 ps, the peak bunch current is $I_p = N_e e/\sqrt{2\pi}\sigma_t =$ 33 A.

Limitations on the single bunch current result from the short-range wakefield (broadband impedance). The longitudinal microwave instability depends primarily on the impedance of the vacuum vessel. The transverse mode coupling instability depends on the resistive wall impedance and the geometric impedance due to changes in the vacuum chamber cross-section.

Limitations on the total average current arise from the long-range wakefield (narrowband impedance). The longitudinal coupled-bunch instability is predominantly driven by the longitudinal higher-order modes in the RF cavity. The transverse coupled-bunch instability is primarily due to the resistive wall and the transverse higher-order modes in the RF cavity.

The most accurate approach to estimating the instability thresholds for NSLS-II is to carry out computer simulation tracking studies using the wakefields determined by numerical calculations of the wakefield for each component comprising the storage ring. This is a large effort that is now underway. Here, we shall provide estimates of the instability thresholds using a simplified model of the ring impedance, which has been developed based on impedance calculations performed to-date and on the experience at existing storage rings [3.2.2], especially APS and ESRF. We also present results of impedance calculations obtained thus far using the electromagnetic simulation code GdfidL [3.2.3].

In addition to the wakefield effects mentioned above, we also discuss intrabeam scattering. We report estimates of the Touschek lifetime resulting from single scattering, and of the increase in emittance due to multiple scattering.

We plan to use third-harmonic Landau cavities to increase the bunch length and synchrotron tune spread. Lengthening the bunch will be useful in raising the longitudinal microwave instability threshold, increasing the Touschek lifetime and reducing the effect of intrabeam scattering on the emittance. Increasing the bunch length and synchrotron tune spread improves the effectiveness of positive chromaticity in raising the single and coupled bunch transverse instability thresholds. The beam dynamics issues involved in the operation of the Landau cavities will be addressed.

3.2.2 Wakefields and Impedance

We provide a short overview of wakefields and impedance [3.2.4, 3.2.5] to clarify the approach we plan to adopt. Consider a point charge q (the drive particle) traveling very close to the speed of light in the z-direction through a vacuum enclosure displaced from the design trajectory by $\vec{r}_d$. A unit test charge travels at a distance s behind the first (Figure 3.2.1) on a trajectory parallel to the z-axis but displaced by $\vec{r}_t = (x, y)$.

The change of momentum $\Delta\vec{p}$ of the second particle, caused by the electromagnetic field of the first, is given by

$$\Delta\vec{p} = \int_{-\infty}^{\infty} dt\left[\vec{E}\left(\vec{r}_t, z, t\right) + c\,\hat{z}\times\vec{B}\left(\vec{r}_t, z, t\right)\right]_{z=ct-s}. \tag{3.2-1}$$

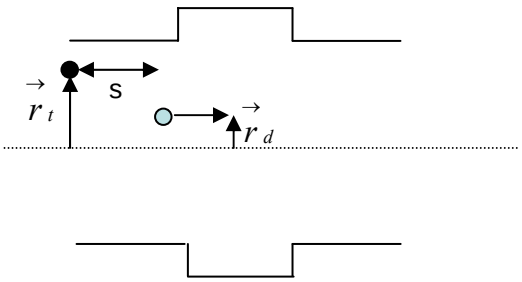

Figure 3.2.1. A drive particle *d* leading a test particle *t* through a vacuum structure.

For $\vec{r}_t = \vec{r}_d = 0$, we define the longitudinal wakefield $w_\parallel(s)$ [volt/coul] by

$$w_\parallel(s) = -\frac{c}{q}\Delta p_z = -\frac{1}{q}\int_{-\infty}^{\infty} dz E_z\left(z, t = \frac{z+s}{c}\right), \tag{3.2-2}$$

and the longitudinal impedance $Z_\parallel(k)$ [ohms] is determined by the Fourier transform,

$$Z_\parallel(k) = \int_{-\infty}^{\infty}\frac{ds}{c} w_\parallel(s) e^{iks}. \tag{3.2-3}$$

For a Gaussian bunch containing N_e electrons, the energy loss is $\Delta E = \kappa_\parallel (eN_e)^2$ and the power loss is $P = \kappa_\parallel I_0^2 T_0$, where the energy loss factor $\kappa_\parallel$ [V/C] is given by

$$\kappa_\parallel = \int_{-\infty}^{\infty}\frac{cdk}{2\pi}\,\mathrm{Re}\,Z_\parallel(k) e^{-k^2\sigma_s^2}. \tag{3.2-4}$$

The transverse wakefield [V/C-m] is

$$\vec{w}_\perp\left(s, \vec{r}_t, \vec{r}_d\right) = \frac{c}{q}\Delta\vec{p}_\perp = \frac{1}{q}\int_{-\infty}^{\infty} dz\left[\vec{E}\left(\vec{r}, z, t\right) + c\,\hat{z}\times B\left(\vec{r}, z, t\right)\right]_{t=\frac{z+s}{c}}. \tag{3.2-5}$$

The transverse impedance $\vec{Z}_\perp$ [Ω/m] is determined by the Fourier transform,

$$\vec{Z}_{\perp}\left(\vec{r}_t,\vec{r}_d,k\right)=\frac{-i}{c}\int_0^{\infty}ds\,\vec{w}_{\perp}\left(\vec{r}_t,\vec{r}_d,s\right)e^{iks}. \tag{3.2-6}$$

When the vacuum enclosure has reflection symmetry about the xz and yz planes, the transverse wakefield vanishes for $\vec{r}_t=\vec{r}_d=0$ and the first terms in a Taylor expansion yield [3.2.6],

$$w_x\left(s,x_t,x_d\right)\cong w_{Dx}\left(s\right)x_d+w_{Qx}\left(s\right)x_t \tag{3.2-7}$$

$$w_y\left(s,y_t,y_d\right)\cong w_{Dy}\left(s\right)y_d-w_{Qy}\left(s\right)y_t \tag{3.2-8}$$

where w_D is the dipole wakefield and w_Q is the quadrupolar wake. The dipole and quadrupolar impedances are determined by the Fourier transforms

$$Z_x\left(x_t,x_d,k\right)\cong Z_{Dx}\left(k\right)x_d+Z_{Qx}\left(k\right)x_t \tag{3.2-9}$$

$$Z_y\left(y_t,y_d,k\right)\cong Z_{Dy}\left(k\right)y_d-Z_{Qy}\left(k\right)y_t \tag{3.2-10}$$

The coherent betatron tune shift in a Gaussian bunch of N_e electrons produced by the transverse dipole impedance is approximately given by

$$\Delta\nu_{x,y}=\frac{e^2N_e}{4\pi E}\sum_j\beta_{x,y,j}\kappa_{x,y,j}\,, \tag{3.2-11}$$

where E is the electron energy and $\beta_{x,y,j}$ is the average value of the betatron function at the j^{th} impedance element and $\kappa_{x,y,j}$ [V/C-m] is the kick factor of the j^{th} element defined by

$$\kappa_{x,y,j}=\frac{c}{\pi}\int_0^{\infty}dk\,\mathrm{Im}\,Z_{Dx,y,j}\left(k\right)e^{-k^2\sigma_s^2}\,. \tag{3.2-12}$$

In a similar manner the quadrupolar impedance contributes to an incoherent tune spread. Some authors employ the effective impedance $\left(Z_{x,y}\right)_{eff}$ defined by

$$\left(Z_{x,y}\right)_{eff}=\frac{\int_{-\infty}^{\infty}dk\,Z_{Dx,y}\left(k\right)e^{-k^2\sigma_s^2}}{\int_{-\infty}^{\infty}dk\,e^{-k^2\sigma_s^2}} \tag{3.2-13}$$

The kick factor is related to the effective impedance by

$$\kappa_{x,y} = \frac{c}{2\sqrt{\pi}\sigma_s}\,\mathrm{Im}\left(Z_{D\,x,y}\right)_{eff}\,. \tag{3.2-14}$$

To estimate instability thresholds, we use a model in which the impedance is comprised of a broadband resonator plus the resistive wall. The analytic forms for the wakefield and impedance of these elements are summarized in Table 3.2.1.

Table 3.2.1 Analytic Expressions for Impedance and Wakefield.

Resonator	
$Q' = \sqrt{Q^2 - 1/4} \qquad k_r' = k_r Q'/Q$	
$w_\parallel(s) = \frac{ck_rR_s}{Q_s}\exp\left(-\frac{k_r s}{2Q_s}\right)\left[\cos k_r' s - \frac{1}{2Q_s'}\sin k_r' s\right]$	$w_\perp(s) = \frac{ck_rR_\perp}{Q_\perp'}\exp\left(-\frac{k_r s}{2Q_\perp}\right)\sin k_r' s$
$Z_\parallel(k) = \frac{R_s}{1 - iQ_s\left(k/k_r - k_r/k\right)}$	$Z_\perp(k) = \frac{k_r}{k}\frac{R_\perp}{1 - iQ_\perp\left(k/k_r - k_r/k\right)}$
$\kappa_\parallel = \frac{\omega_r R_s}{2Q_s} \quad (k_r\sigma_s << 1)$ $\kappa_\parallel = \frac{\omega_r R_s}{4\sqrt{\pi}\,Q_s^2\,(k_r\sigma_s)^3} \quad (k_r\sigma_s >> 1)$ $(Z/n)_0 = R_s(\omega_0/\omega_r)$	$\kappa_\perp \cong \frac{1}{\sqrt{\pi}}\frac{cR_\perp}{Q_\perp}\left(k_r^2\sigma_s\right) \quad (k_r\sigma_s << 1)$ $\kappa_\perp \cong \frac{c}{2\sqrt{\pi}\,\sigma_s}\frac{R_\perp}{Q_\perp} \quad (k_r\sigma_s >> 1)$
Resistive Wall [3.2.7]	
$s_0 = \left(2b^2/Z_0\sigma_{cond}\right)^{1/3}$	
$w_\parallel(s) \cong \frac{-cZ_0L}{4\pi\sqrt{2\pi}\,b^2}\left(\frac{s_0}{s}\right)^{3/2} \quad (s >> s_0)$	$w_\perp(s) \cong \frac{cZ_0s_0L}{2\pi b^4}\sqrt{\frac{2s_0}{\pi s}} \quad (s >> s_0)$
$Z_\parallel(k) \cong \frac{(1-i)Z_0s_0L}{4\pi b^2}\sqrt{k\,s_0} \quad (0 \le k << 1/s_0)$	$Z_\perp(k) \cong \frac{2}{kb^2}Z_\parallel(k) \quad (0 \le k << 1/s_0)$
$\kappa_\parallel \cong 1.2\frac{cZ_0}{4\pi}\frac{L}{2\pi b^2}\left(\frac{s_0}{\sigma_s}\right)^{3/2}$	$\kappa_\perp \cong 0.58\frac{cZ_0}{4\pi}\frac{2s_0L}{b^4}\sqrt{\frac{s_0}{\sigma_s}}$
Extreme Anomalous Skin Effect [3.2.8]	
$s_0 = (Bb)^{3/5}/\sin(\pi/10)$ $B = 3^{1/6}2^{-4/3}\pi^{-1/3}Z_0^{-1/3}(l/\sigma_{cond})^{1/3} \cong 3.9\times10^{-7}\,m^{2/3}$ (Cu @ 4 K, specular reflection)	
$w_\parallel(s) \cong \frac{-2cB\,Z_0L}{3\pi\,\Gamma(1/3)b}s^{-5/3} \quad (s >> s_0)$	$w_\perp(s) \cong \frac{2cBZ_0L}{\pi\,\Gamma(1/3)b^3}s^{-2/3} \quad (s >> s_0)$
$Z_\parallel(k) \cong \frac{\left(1-\sqrt{3}\,i\right)BZ_0L}{2\pi b}k^{2/3} \quad (0 \le k << 1/s_0)$	$Z_\perp(k) \cong \frac{2}{b^2\,k}Z_\parallel(k) \quad (0 \le k << 1/s_0)$
$\kappa_\parallel = 0.16\frac{cZ_0}{4\pi}\frac{L}{\pi b^2}\left(\frac{s_0}{\sigma_s}\right)^{5/3}$	$\kappa_\perp \cong 0.21\frac{cZ_0}{4\pi}\frac{2s_0L}{b^4}\left(\frac{s_0}{\sigma_s}\right)^{2/3}$

3.2.3 Estimates of Instability Thresholds

To estimate the instability thresholds, we considered an approximate model of the storage ring impedance, including the long-range wakefield due to the longitudinal and transverse higher-order modes in the CESR-B cavities. The storage ring vacuum chamber is approximated by 720 m of aluminum with a vertical half-aperture of 12.5 mm. We also included 20 in-vacuum undulators, each with 3 m copper chambers of vertical half-aperture 2.5 mm. The geometric impedance due to cross-section changes in the vacuum vessel is approximated by longitudinal and transverse broadband resonators. The parameters for the resonators are based on experience at other storage rings [3.2.2, 3.2.9], especially APS and ESRF, as well as on the impedance calculations we have performed to date. We believe the model is conservative and that it may be possible to build NSLS-II with lower impedance. The details of the impedance model are presented in Table 3.2.2, and some key parameters needed in the estimation of instability thresholds are given in Table 3.2.3.

Table 3.2.2 Impedance Model.

CESR-B cavity higher-order modes (see Tables 3.2.4 and 3.2.5.)	$\beta_x = 20m$
720 m of aluminum with half-gap of 12.5 mm and β_{av} = 7.6 m:	$\kappa_{\|\|} = 4.0V/pC \quad \kappa_y = 0.68\,KV/pC/m$
60 m of copper with half-gap of 2.5 mm and β_{av} = 2 m:	$\kappa_{\|\|} = 1.3V/pC \quad \kappa_y = 5.6\,KV/pC/m$
Transverse broadband impedance with f_r = 30 GHz, R_y = 1 MΩ/m, Q_y=1, and β_{av} = 7.6 m $\kappa_y = 19\,KV/pC/m$	
Longitudinal broadband impedance with $f_r = 30GHz$, $R_s = 30k\Omega$,	$\left(\mathrm{Im}Z_{\|\|}/n\right)_0 = 0.4\Omega \quad \kappa_{\|\|} = 35V/pC$

Table 3.2.3 Parameters for Threshold Calculations

Energy, E [GeV]	3
Revolution period, T_0 [μs]	2.6
Momentum compaction, α	3.7×10^{-4}
Energy loss, U [keV]	1172
RF voltage, V [MV]	3.7
Synchrotron tune, ν_s	0.0094
Damping time: τ_x, τ_s [ms]	13, 6.5
Energy spread, $\sigma_{\varepsilon 0}$ [%]	0.09
Bunch duration, σ_{t0} [ps]	15

3.2.3.1 Transverse Mode Coupling Instability (TMCI)

An approximate relation [3.2.10] determining the threshold of the TMCI at zero chromaticity is given by

$$\frac{\Delta\nu_y}{\nu_s} = \frac{e\,I_0^{th}}{2\,E\,\nu_s\,\omega_0}\sum_j \beta_{yj}\kappa_{yj} \cong 0.7\,, \tag{3.2-15}$$

where I_0^{th} is the threshold bunch current, β_{yj} is the average value of the vertical beta function in the j^{th} element, and κ_{yj} is its kick factor. $E = \gamma mc^2$ is the electron energy and ν_s is the synchrotron tune. Consider

a current of 0.5 mA bunch. Using the NSLS-II parameters as described in Table 3.2.3, we find that to be below the TMCI threshold requires

$$\sum_j \beta_{yj}\,\kappa_{yj} < 180\ KV/pC\,. \tag{3.2-16}$$

Using the values of the kick factors and beta functions as specified in Table 3.2.2, we find that $\sum_j \beta_{yj}\,\kappa_{yj} = 160\ KV/pC$. Therefore, 0.5 mA bunches are below the TMCI threshold for zero chromaticity.

3.2.3.2 Longitudinal Microwave Instability

At very low single-bunch current, the longitudinal density is determined by the equilibrium between radiation damping and quantum fluctuations. As the bunch current increases, the longitudinal charge distribution is modified by the wakefield. Below the threshold of the microwave instability, the energy distribution remains unchanged, and the longitudinal charge distribution $f_0\left(\tau/\sigma_{\tau 0}\right)$ is determined by the time-independent solution of the Haissinski equation [3.2.11],

$$f_0(q) = A\exp\left[-\frac{1}{2}q^2 + S\int_q^\infty dq'\int_{q'}^\infty dq''\, f_0(q'')w(q''-q')\right], \tag{3.2-17}$$

where the constant A is chosen to satisfy the normalization

$$\int_{-\infty}^{\infty} dq\, f_0(q) = 1 \tag{3.2-18}$$

In the case of a broadband resonator with shunt impedance R_s, resonant frequency ω_s, and quality factor $Q_s = 1$, the scaled current is defined by

$$S = \frac{e\,I_0\,R_s\,\omega_r}{E_0\,\nu_s\,\omega_0\,\sigma_\varepsilon} \tag{3.2-19}$$

and

$$w(q) = \exp\left(-\frac{q\omega_r\sigma_{t0}}{2}\right)\left[\cos\left(q\omega_r'\sigma_{t0}\right) - \frac{1}{2\sqrt{0.75}}\sin\left(q\omega_r'\sigma_{t0}\right)\right]. \tag{3.2-20}$$

In Figure 3.2.2, we show the Haissinski distribution for bunch currents of 0.1 mA and 0.4 mA.

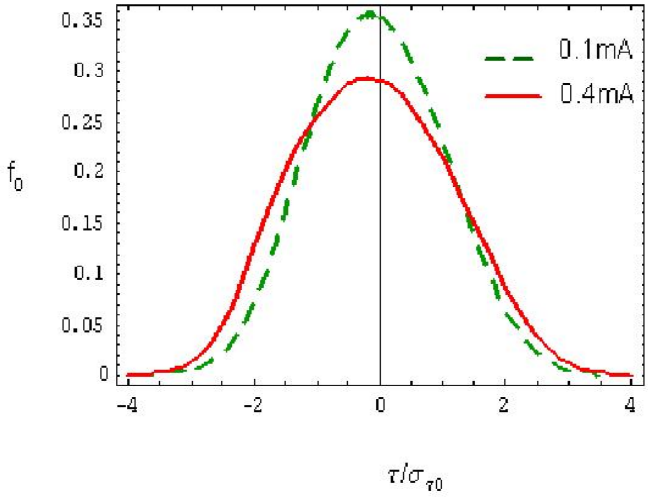

Figure 3.2.2 Longitudinal distribution as determined from the Haissinski equations.

Once the current exceeds the microwave instability threshold, both the energy distribution and the charge distribution are modified and are no longer time-independent. In the case of a broadband resonator with shunt impedance R_s, resonant frequency ω_s, and quality factor $Q_s = 1$, Oide and Yokoya [3.2.12] have shown that the single-bunch current threshold is given by

$$I_0^{th} = \frac{E \nu_s \sigma_\varepsilon}{e R_s \left(\omega_r / \omega_0\right)} S\left(\omega_r \sigma_t\right). \tag{3.2-21}$$

In Figure 3.2.3, we show the function $S\left(\omega_r \sigma_t\right)$ as determined by Oide and Yokoya (solid curve), and by tracking using the computer code ELEGANT [3.2.13] (symbols). A useful fit to the scaling function, in the regime x >0.2, is given by

$$S(x) = 11 + 9.4(x - 0.7)^2 . \tag{3.2-22}$$

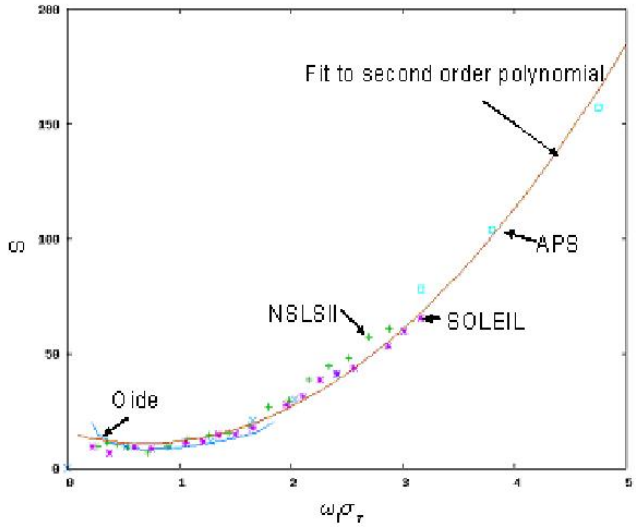

Figure 3.2.3. The scaling function $S\left(\omega_r \sigma_{t0}\right)$ as determined by Oide and Yokoya (solid blue curve) and by tracking using ELEGANT (characters). The threshold is defined to be when the energy spread has increased by 5% over the zero current value.

In the limit when $\omega_0\sigma_{t0} >> 1$, the threshold condition becomes

$$I_0^{th} = 9.4\frac{E\nu_s^2}{e\alpha\left(\mathrm{Im}\,Z/n\right)_0}\left(\omega_0\sigma_{t0}\right)^3, \tag{3.2-23}$$

where $\left(\mathrm{Im}\,Z/n\right)_0 = R_s\left(\omega_0/\omega_r\right)$. This has the same form as the Boussard [3.2.14] criterion, except that in the Boussard case, the constant 9.4 is replaced by the smaller value $\sqrt{2\pi}$. The reason that the Boussard criterion gives too pessimistic a threshold is that it does not take into account the bunch lengthening due to potential well distortion.

In Figure 3.2.4, we show the dependence of the bunch length and the energy spread as calculated using the program ELEGANT. This shows that 0.5 mA bunches will suffer negligible increase in energy spread due to the longitudinal microwave instability.

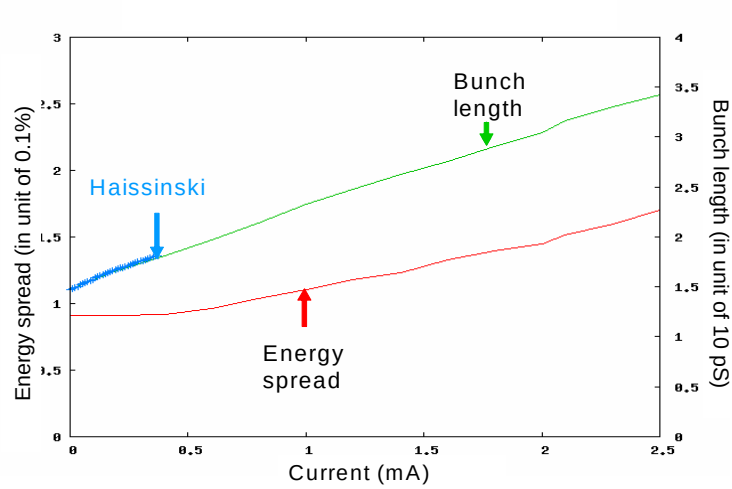

Figure 3.2.4. Bunch length and energy spread for broadband resonator. Resonant frequency f_y = 30 GHz, shunt impedance R_s = 30 $k\Omega$, and Q_s = 1. This corresponds to $(\mathrm{ImZ/n})_0$ = 0.4 Ω.

3.2.3.3 Transverse Coupled Bunch Instability Driven by Resistive Wall Impedance

As discussed in Section 3.2.3.1, the short-range part of the resistive wall impedance contributes to the single-bunch TMCI. The long-range tail contributes to the transverse coupled bunch instability. A rough approximation to the growth rate of the fastest growing transverse coupled bunch mode driven by the resistive wall impedance (at zero chromaticity) is given by

$$\frac{1}{\tau_{gr}} \cong \frac{e\,c\,I_{av}}{2E}\frac{\beta_y}{C}\mathrm{Re}\,Z_\perp^{rw}\left(\omega_0\right)\frac{1}{\sqrt{1-q}}, \tag{3.2-24}$$

where C = 792 m is the ring circumference, β_y is the average value of the vertical beta function in the resistive wall, and q = 0.28 is the fractional part of the vertical tune. Equating the growth time to the radiation damping time provides an estimate of the instability threshold. Using the model parameters given in Tables 3.2.2 and 3.2.3, we find the threshold is at a total average current of 15 mA, far below the design value of 500 mA. Running at positive chromaticity will increase this threshold value.

Particle tracking [3.2.15] has been used to estimate transverse stability thresholds for coupled bunch modes. In these calculations we include both the long-range and short-range resistive wall wakefields as well as the short-range longitudinal and transverse wakefields, as described in Table 3.2.2. To keep the problem

manageable, we assume that all RF buckets contain identical bunches interacting via a single coupled bunch mode. A single bunch is tracked and the effect of other bunches is obtained by appropriate phase shifts under the assumption that the coherent frequency shift is small compared to the characteristic frequency width in the long-range transverse impedance. This should be an excellent approximation for the resistive wall impedance, which dominates the long-range transverse wake. The resistive wall impedance is due to 60 m of Cu with vertical aperture 5 mm and average beta function 2 m, in conjunction with 720 m of Al with aperture 25 mm and average beta function 7.6 m. The broadband transverse resonator has $R_\perp$ = 1 M-Ohm/m with $Q_\perp$ = 1 and 30 GHz resonant frequency at beta function 7.6 m. A longitudinal resonator with R_s = 30 k-Ohm, resonant frequency 30 GHz, and Q_s = 1 dominates the longitudinal impedance.

Three cases were simulated. Case 0 is a "stripped" case with no longitudinal wakes, no quadrupolar wakes (also referred to as detuning wakes), and no third-harmonic RF. Case 1 has the full suite of collective effects but no third harmonic cavity. Case 2 includes a perfect third harmonic cavity. The single-bunch threshold current as a function of vertical chromaticity is shown in Figure 3.2.5. In cases 1 and 2, a chromaticity of 4 allows for an average bunch current of about 0.5 mA and hence for an average stored current of 500 mA. This demonstrates the importance of running at positive chromaticity. Note also that bunch lengthening and enhanced synchrotron frequency spread introduced by the longitudinal wakefield and the third-harmonic cavity increase the effectiveness of positive chromaticity to stabilize the beam.

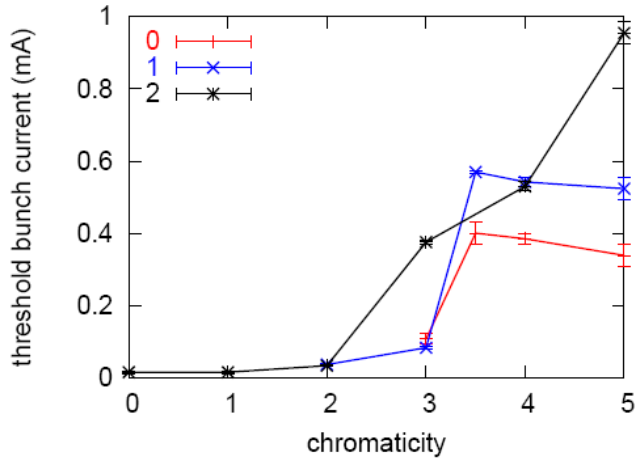

Figure 3.2.5 Threshold single bunch current vs. chromaticity for: (0) no longitudinal wakes, no quadrupolar wakes, and only fundamental RF; (1) all the impedances but only fundamental RF; (2) all impedances as well as fundamental and third-harmonic RF.

3.2.3.4 CESR-B Cavity Longitudinal Impedance and Coupled Bunch Growth Rates

The longitudinal higher-order modes (HOM) in an RF cavity can result in coupling between bunches, leading to unstable synchrotron oscillations. In the case of *M* equally spaced and populated point bunches, the coherent synchrotron frequency Ω_μ of the μ^{th} multi-bunch mode can be approximated by

$$\Omega_\mu - \omega_0 \nu_s = \frac{i e \alpha \omega_0 I_{av}}{4\pi \nu_s E} \sum_{j=-\infty}^{\infty} (M j + \mu) Z_\parallel [(M j + \mu + \nu_s)\omega_0] \tag{3.2-25}$$

and

$$(\mu = 0,1,2,\ldots,M-1). \tag{3.2-26}$$

A 3D GdfidL [3.2.3] model has been created for the CESR-B cavity [3.2.16]. The model consists of the niobium cavity with the asymmetric beam tubes, warm-to-cold transitions, and ferrite-lined HOM dampers,

and it tapers to the 25×50 mm elliptical ring beampipes. The cavity has a fluted beam tube that allows the lowest dipole mode to be coupled out to the HOM damper. This made it essential to use a 3D model for calculating the HOMs. To benchmark such a complex model, C-Fish [3.2.17] and Superfish [3.2.18] models of the cavity with complex permitivity and permeability were created. The results were compared to GdfidL and to measured data on a ferrite-lined pillbox cavity that was measured on the bench.

The Superfish model approximates the fluted beampipe by a cylindrical tube with the same cutoff frequency. An outline of the cavity geometry with the field lines of the 1586 MHz mode is shown in Figure 3.2.6.

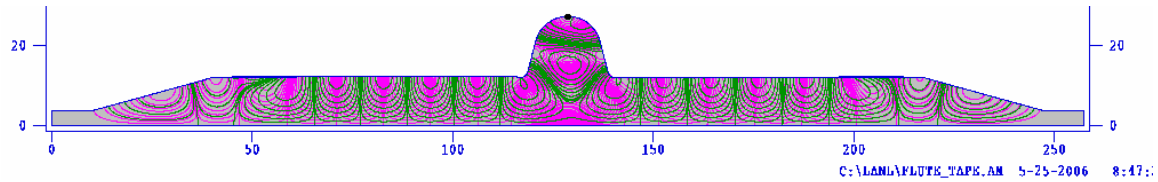

Figure 3.2.6 CESR-B cavity geometry input to C-Fish.

The first eight HOMs calculated are given in Table 3.2.4. Superfish correctly calculates the surface resistivity of niobium as a function of frequency, but only takes the complex permeability and permitivity as a single input. The permitivity of the ferrite load is relatively constant and does not contribute significantly to damping the HOM, but the ferrite permeability properties vary considerably, so specific values (Table 3.2.4) closest to the HOM frequencies were calculated. The ferrite properties were obtained from the Canadian Light Source [3.2.19]. The measurements were made at several discrete frequencies in the band of interest.

Table 3.2.4 CESR-B Higher-Order Longitudinal Modes.

Superfish			GdfidL		
Frequency (MHz)	Shunt Impedance (Ohms)	Q	Frequency (MHz)	Shunt Impedance (Ohms)	Q
952.4	112	222	950.55	8.14	350
973.32	57.07	332	976.62	54.6	420
1014.85	498	112	1014.38	505	150
1184.65	44.1	43	1181.5	13.2	60
1331.15	38.7	40	1361	65.6	20
1487.5	12.5	53	1481.5	46	40
1586.58	27.8	169	1580	7.5	30

We also performed studies of HOMs in CESR-B assembly using GdfidL code, shown in Figure 3.2.7. The studies took off from time-domain simulation of 1 pC charge passing through the structure. For the longitudinal impedance computation, the beam is moving on-axis, in comparison with the transverse impedance computation when the beam trajectory is shifted off-axis with an offset taken as 3×STEPSIZE. To get a result for the impedance, which is Fast Fourier Transforming of the wake function with higher frequency resolution, the wakepotenial is computed up to an s-value of 50 meters. Parameters of the ferrite material are taken as $\varepsilon_r = 13.4$, $\mu_r = 0.9$, $\tan\delta_\varepsilon = 0.02$, $\tan\delta_\mu = 2.33$, $\sigma_\varepsilon = 0.05\ \Omega^{-1}/m^{-1}$, and $\sigma_\mu = 46395\ \Omega/m$ at a frequency of 2.8 GHz [3.2.19].

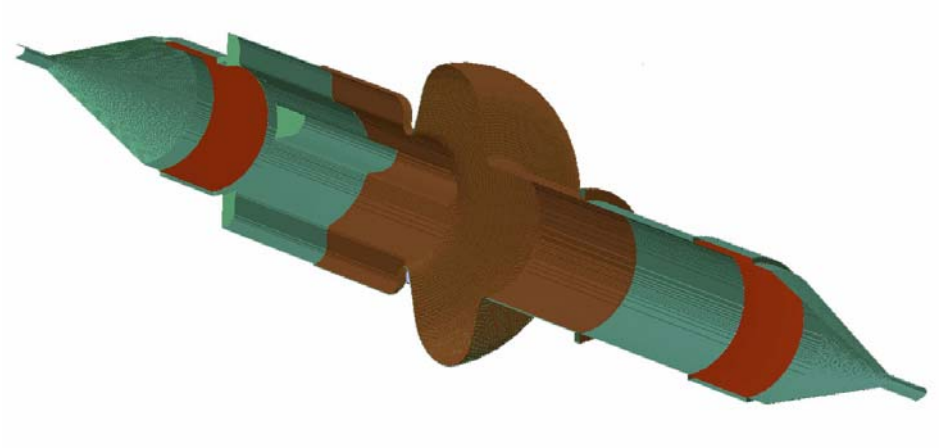

Figure 3.2.7 3D model of CESR-B cavity assembly in GdfidL.

These parameters were used in ZAP [3.2.20] to calculate the growth rates for nominal ring and beam parameters. The maximum growth time was 120 ms for the sum of three cavity impedances, much longer than the longitudinal damping time of 6.5 ms, and so the beam is longitudinally stable for cavity HOMs.

To summarize the CESR-B cavity studies, longitudinal CB growth rates were calculated for the first few HOM of the CESR-B cavity and were found to be below the damping rate, even for three installed cavities without stagger tuning. However, the combination of small-bunch length exciting higher frequency modes and ferrite loss decreasing at higher frequency could lead to unstable modes whose growth rate exceeds the damping rate, so this analysis must be extended to higher frequencies. To enable this, we are pursuing measurements of the ferrite properties to 6 GHz with Ron Hutcheon, who provided the data below 3 GHz that were used in these calculations. This work must also be extended to the third harmonic cavities.

3.2.3.5 CESR-B Cavity Transverse Impedance and Coupled Bunch Growth Rates

The transverse higher-order modes in an RF cavity can result in coupling between bunches, leading to unstable betatron oscillations. In the case of M equally spaced and populated point bunches, the coherent synchrotron frequency Ω_μ of the μ^{th} multi-bunch mode can be approximated by

$$\Omega_\mu - \omega_0 \nu_x = -i \frac{e c I_{av}}{2E} \frac{\beta_x^{cav}}{C} \sum_{j=-\infty}^{\infty} Z_\perp \left[\left(M j + \mu + \nu_y \right) \omega_0 \right], \tag{3.2-27}$$

where $\mu = 0,1,2,\ldots M-1$). The same GdlfidL model used to compute the longitudinal cavity impedances was used to compute the transverse modes. The first 15 modes are listed in Table 3.2.5.

Table 3.2.5 CESR-B Higher-Order Transverse Modes.

Time domain #	Frequency [MHz]	$R_\perp$ [kΩ/m]	$Q_{\perp,load}$
f1	608	2.2	60
f2	653	3.1	60
f3	681	15.6	70
f4	769	1.6	30
f5	864	1.03	50
f6	917	0.72	40
f7	964	0.66	30
f8	1045	0.8	30
f9	1146	1.17	30
f10	1243	2.3	70
f11	1299	0.36	160
f12	1344	0.31	40
f13	1405	0.33	70
f14	1433	0.22	100
f15	1464	0.44	70

The horizontal betatron function is 20 m at the RF cavities. These modes were used in ZAP [3.2.20] to calculate the transverse coupled-bunch growth rates. For 500 mA average current distributed uniformly in all the buckets around the ring and zero chromaticity, the coupled bunch growth time is 40 ms, which is longer than the radiation damping time of 13 ms. Therefore, the transverse cavity modes will not lead to unstable coupled-bunch betatron oscillations.

3.2.4 Impedance Budget

Extensive calculations have been performed of the wakefield and impedance produced by the storage ring components. Results of the calculations are summarized in Table 3.2.6, where we present the longitudinal kick factor (Eq. 3.2-4), the transverse kick factors (Eq. 3.2-12) and the imaginary part of the longitudinal impedance at low frequency divided by $n = \omega/\omega_0$, where $\omega_0 = 2\pi \times 384.6\,kHz$. The values given correspond to a single element. The number of times a given object is located in the ring is stated.

Table 3.2.6 Calculated Impedance for Storage Ring Components.

Object	Number of occurrences	$\kappa_{\|\|}$ V/pC	$(\mathrm{Im}Z_{\|\|}/n)_0\Omega$	κ_xV/pC/m	κ_yV/pC/m
Absorber	180	3.4×10^{-3}	9.2×10^{-6}	0.5	0.002
Bellows [1]	180	8.7×10^{-3}	124×10^{-6}	0.8	2
BPM	200	20×10^{-3}	47×10^{-6}	0.9	1.1
Cavity transitions/straight	2	3.5	14×10^{-3}	25.4	57
500 MHz CESR-B cavity	4	0.31	-----	0.17	0.17
1500 MHz CESR-B cavity	4	0.52	-----	2.6	2.6
Dipole Chamber	60	3.3×10^{-5}	0.7×10^{-7}	4.5×10^{-3}	0
Multipole Chamber	90	0.5×10^{-5}	0.1×10^{-7}	0.7×10^{-3}	0
Flange [1]	300	0.47×10^{-3}	16×10^{-6}	0.141	0.141
Injection Region	1	TBD	TBD	TBD	TBD
SCU chamber geometric	TBD	22.6×10^{-3}	0.6×10^{-3}	61	257
SCU chamber ease (2.5 m)	TBD	5.6×10^{-3}	-----	13	26
IR chamber [2]	4	0.84	2.1×10^{-3}	11.4	22.6
CPMU geometric	TBD	95×10^{-3}	1.1×10^{-3}	136	425
CPMU resistive wall (3.5 m)	TBD	66×10^{-3}	-----	112	225
720 m Al resistive wall	1	4.0	-----	272	545
Scraper (Horizontal)	2	0.22	1.4×10^{-3}	22	2
Scraper (Vertical)	2	TBD	TBD	TBD	TBD

The values for the geometric impedances were calculated using GdfidL with σ_s = 3 mm. The resistive wall and extreme anomalous skin effect estimates were made with σ_s = 4.5 mm. The bunch-length dependence of the wakefields will be determined in future work. [1]Values for bellows and flanges were calculated by Nagaoka [3.2.21] for SOLEIL with σ_s = 6 mm.[2] The values for a simplified geometry of the far-infrared extraction chamber described in section 3.2.4.3.

The Al vacuum chamber is taken to be of length 720 m with vertical half-height 12.5 mm. The copper-plated RF shield for the in-vacuum permanent magnet undulator is 3 m long with vertical half-height of 2.5 mm. The superconducting undulator chamber is 2 m long with vertical half-height 2.5 mm and is cold copper in the extreme anomalous skin effect regime [3.2.8]. The vertical resistive wall wake of the elliptic chamber is taken to be 0.8 times the value for the circular chamber and the horizontal wake is 0.4 times the circular value [3.2.22]. Results not yet determined are indicated in the table.

3.2.4.1 Insertion Device Chambers

While most of the components listed in Table 3.2.7 are fairly common and have been successfully used in many machines, we feel that significant attention is warranted for studies and optimization of the impedance due to insertion device chambers. This need is based on experience at modern light sources, where installations of small-gap ID chambers have significantly affected beam dynamics [3.2.24], as well as on the requirements for NSLS-II, which is expected to have a large number of ID chambers (~20) with gap down to 5 mm beam stay-clear. Both the resistive wall component and the geometric component due to the transitions have been studied. Furthermore, in addition to the dipole impedances, which directly cause beam instabilities, we have estimated the quadrupolar component [3.2.25], which results in incoherent frequency shift and indirectly contributes to the instabilities through the Landau damping.

For the purposes of impedance budget we consider two representative ID chamber geometries: 1) a variable-gap, in-vacuum, permanent magnet undulator, and 2) a 5 mm fixed-gap elliptical chamber (4.2 K Cu inner surface) for a superconducting small-gap undulator.

Resistive wall contribution has been estimated analytically. While the inner chamber cross-sections are either complex H-like or elliptical shapes we have conservatively used the formulas in Table 3.2.1 for round

cross-sections. It is known [3.2.22] that as the chamber gets flatter (while height is kept fixed), the longitudinal impedance passes through a minimum equal to about 90% of the round-pipe value, while the transverse impedance monotonically approaches ~80% of its round-pipe value. Copper coating and a minimum full gap of 5 mm were assumed for the estimates.

Geometric impedance contributions due to transitions [3.2.26] were calculated using EM code GdfidL [3.2.3] as well as checked against a recently developed analytical approach [3.2.25].

Table 3.2.7 Description of Components.

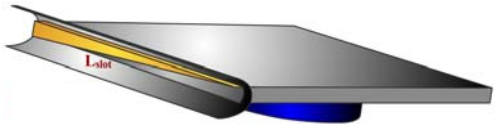	Absorber To protect the vacuum chamber and insertion devices in the ring from damage due to synchrotron radiation, photon absorbers are used. The model consists of a regular elliptical beampipe with a rectangular slot 10 mm high, 180 mm long, and 180 mm deep. A triangular copper burr is located inside the slot for synchrotron radiation absorption. It projects 5 mm inside the regular elliptical beampipe.
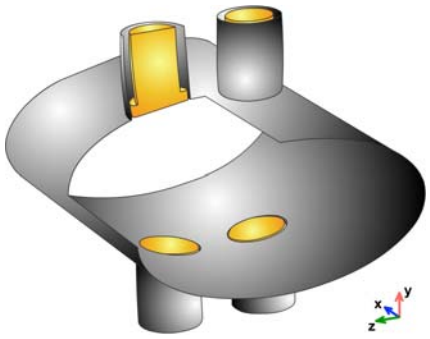	BPM Due to excitation of resonant modes in the buttons, the impedance, kick factor, and loss factor depend very strongly on the BPM button geometry. The BPM button geometry can be optimized to reduce impedance contribution and heating, without losing its resolution. To estimate BPM contribution to the transverse and longitudinal impedance, buttons designed for the SOLEIL BPM were modeled on the regular elliptic beampipe for NSLS-II. Results of the transverse impedance were compared with results for the SOLEIL BPM geometry; in both cases, 50 Ω/m was computed.
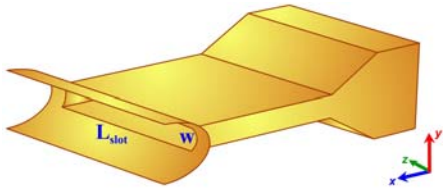	Dipole Chamber The dipole vacuum chamber for NSLS-II has an elliptical cross-section. Inside the chamber there is a slot 15 mm high. As was shown by Stupakov [3.2.23], the slot length does not affect the impedance. For this numerical computation, the slot length is taken to be 80 mm. The horizontal impedance of this geometry depends on beampipe radius and height of the slot.
	**Scraper-H** From the impedance estimations of other laboratories, horizontal or vertical beam scrapers can produce impedance comparable with that of a rectangular step or a tapered transition with a small angle of opening. Two scrapers of the presented geometry, one horizontal and the other vertical are under consideration for application in the NSLS-II ring.

3.2.4.1.1 In-Vacuum Undulator

A 3D model of the IVU [3.2.26] is shown in Figure 3.2.8 (a, top). This model is motivated by the geometry of the X13 Mini-Gap Undulator [3.2.27] currently operating at the NSLS x-ray ring and has been tailored to meet the NSLS-II requirements. The device consists of two magnet arrays of width w_m = 100 mm and thickness 34 mm, located inside a rectangular vacuum chamber of width w_{vc} = 180 mm and height h_{vc} =

170 mm. The tapered transition consists of two parts: 1) a fixed portion between the regular beampipe and the undulator vacuum chamber; and 2) a flexible-height portion with one end fixed to the interior of the undulator vacuum chamber and the other end fixed to the moveable magnet array. The flexible portion only consists of flat upper and lower conductive plates with no side walls. For simplicity in the 3D model, we used a continuous smooth taper of length 180 mm. Also, due to mesh limitations, we have shortened the magnet section length to 0.5 m.

Figure 3.2.8 (a, bottom) shows the transverse wakepotential for the considered geometry and 3 mm RMS bunch length. The wakepotential has a Gaussian-like part corresponding to mainly inductive broadband impedance, as well as a characteristic long-range tail.

The short-range wakefield in the IVU is predominantly determined by the tapers; the long-range wake depends on the cross-sectional geometry of the vacuum enclosure and the length of the magnet. The oscillations in the long-range part are due to multiple narrowband impedance resonances that are possible to characterize in terms of waveguide theory [3.2.28]. Due to limitations on the mesh, we have not yet been able to carry out a systematic study of the length dependence.

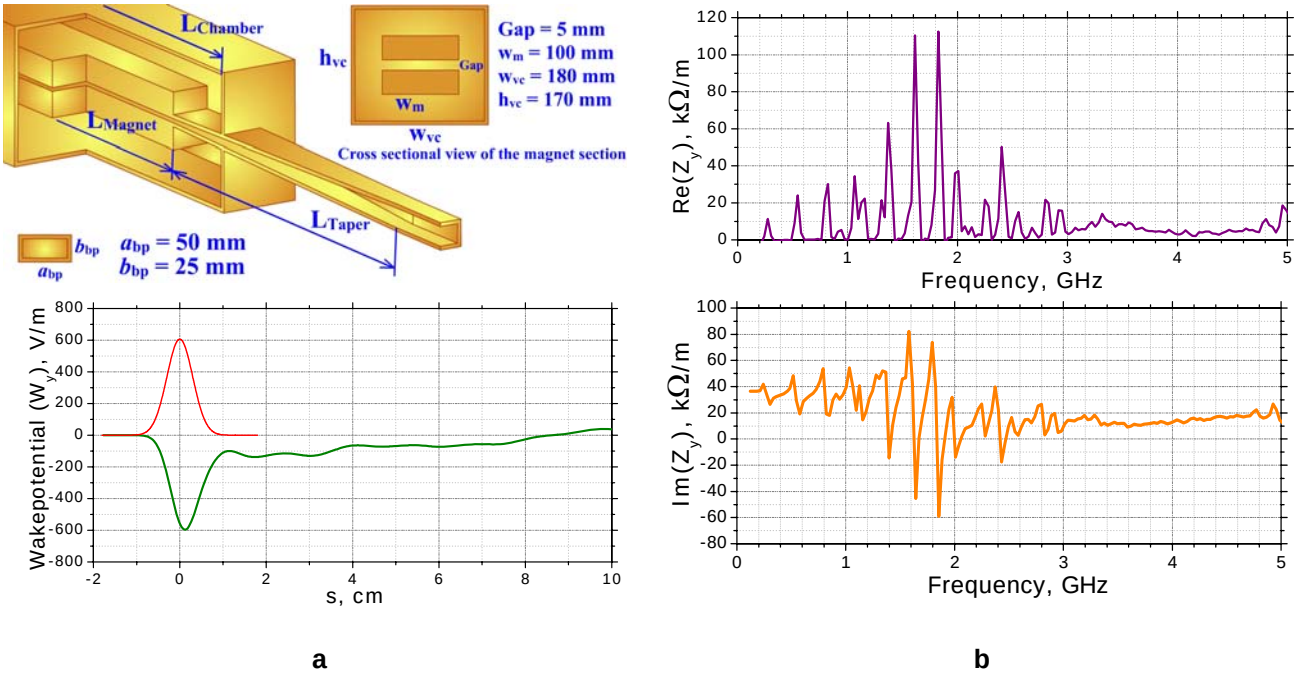

Figure 3.2.8 (**a, top**) Geometry of CPMU with L_{taper} = 180 mm; (**a, bottom**) Short-range transverse wakepotential of in-vacuum permanent magnet undulator chamber; (**c, top** and **bottom**) Low-frequency behavior of real and imaginary parts of the transverse impedance of CPMU. Impedances determined by FFT of the computed wakepotential up to s = 7 m.

3.2.4.1.2 Superconducting Undulator

Similar calculations were performed for the elliptic vacuum chamber of a superconducting undulator. The geometry of the tapered elliptic vacuum chamber is shown in Figure 3.2.9 (a, top). The small-gap magnet region of the elliptic vacuum chamber for the superconducting undulator is fixed and has major axis $2a_s$ = 15 mm and minor axis $2b_s$ = 5 mm, with a magnet section length of 2000 mm. The tapers must smoothly transition between the magnet section and the regular beampipe, which has a major axis $2a_b$ = 76 mm and minor axis $2b_b$ = 25 mm.

Transverse impedance in the low-frequency limit and the kick factor for the tapered vacuum chamber are independent of the distance between the tapers. The inner section length was reduced to 100 mm for GdfidL

calculations. The resulting wakepotential for 3 mm RMS long bunch and the taper length of L_{Taper} = 180 mm is shown in Figure 3.2.9 (a, bottom). It corresponds to κ_y = 190 V/pC/m and $ImZ_y(\omega \to 0)$ = 8.5 kΩ/m. When we increased the taper length, κ_y and $ImZ_y(\omega \to 0)$ decreased inversely proportional to L_{Taper}. The taper length of the elliptic vacuum chamber is chosen to optimize its contribution to the total impedance as well as space in the ring. Note that resonance peaks are observed inside the vacuum chamber in all cases of the transverse impedance calculations. These peaks are not resolved with a wakefield length of 0.3 m. A more detailed investigation of the electrodynamic properties of the tapered elliptic vacuum chamber uncovered the existence of trapped modes. These modes have been identified and classified [3.2.28]. In principle, these modes may affect multi-bunch dynamics and will be systematically studied.

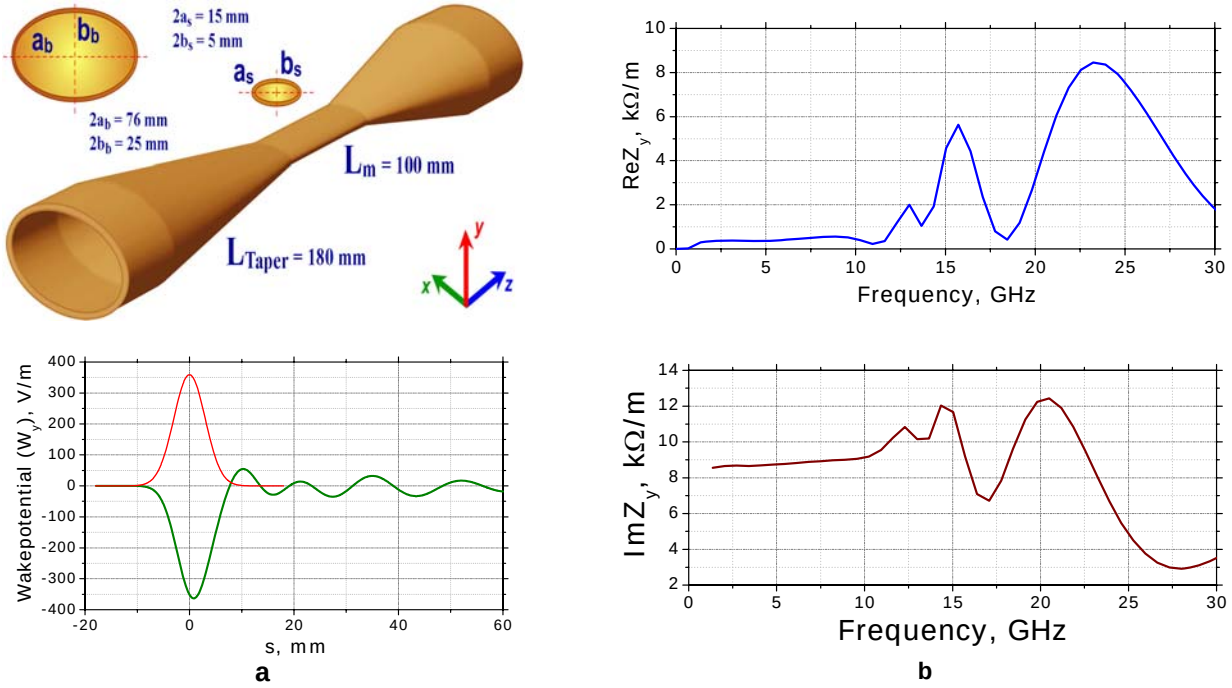

Figure 3.2.9 (**a, top**) Tapered elliptical vacuum chamber for superconducting small-gap undulator (L_{Taper} = 180 mm). **(a, bottom)** Transverse wakepotential; (**b, top**) Real part of the transverse impedance. (**b, bottom**) Imaginary part of the transverse impedance. Impedances correspond to FFT of the computed wakepotential up to s = 0.3 m.

3.2.4.2 CESR-B Short-Range Wake

CESR-B [111] type superconducting cavities are considered for acceleration of the beam in the NSLS-II storage ring. Two main 500 mHz RF cavities and one 2-cell passive 1500 MHz bunch-lengthening harmonic cavity will be fitted in one long straight section. Two long straight sections are reserved in the ring for the RF system. The complicated nature of the RF cavities requires significant computational resources, to establish the longitudinal and transverse impedances for the whole assembly. In order to avoid computational complications, the coupling impedance in the whole assembly can be estimated as a sum the impedance of cavities and transitions [3.2.29, 3.2.30].

Calculated results for the 500 M Hz main RF cavity with the attached round beam pipe of radius a=120 mm on one side and the fluted beam pipe for Higher Order Modes (HOMs) coupling on the other (Figure 3.2.10a) are presented in Table 3.2.6 (beginning of Section 3.2.4). “Perfect matched layers” (or “port” boundary condition) is used on both sides of the cavity pipe for wakefield analysis. For simplicity, the RF coupler was not included in these computations. The coupling impedance of the rectangular slot in the round

beam pipe, which will be used for matching of the input power to the cavity, can be estimated analytically or can be computed separately and added to the total impedance of the cavity.

The loss factor of the main cavity for a 3 mm bunch length (σ_s) is $\kappa_{loss}=0.31V/pC$ ($\sigma_s<<a$). Two main cavities per straight contribute the loss factor of 0.62 V/pC. It is about 6 times smaller than the value for the cavity transitions per straight.

To estimate the contribution of the harmonic cavity to the total impedance of the ring we are using a scaled model of the CESR-B main cavity at frequency 1500 MHz. The loss factor of the harmonic cavity is increased by a factor of 1.7 ($\kappa_{loss}\propto\sqrt{g}/a$, where g is the gap of the cavity) due to reduction of the cavity dimensions by a factor of 3. The kick factor of the harmonic cavity is small compared to that due to the cavity transition. Assuming a small impact from the fluted pipes, the kick factor of the harmonic cavity can be scaled from that of the main cavity as $\kappa_{\perp}\propto 1/a^3$ [222] in agreement with computed results in Table 3.2.6.

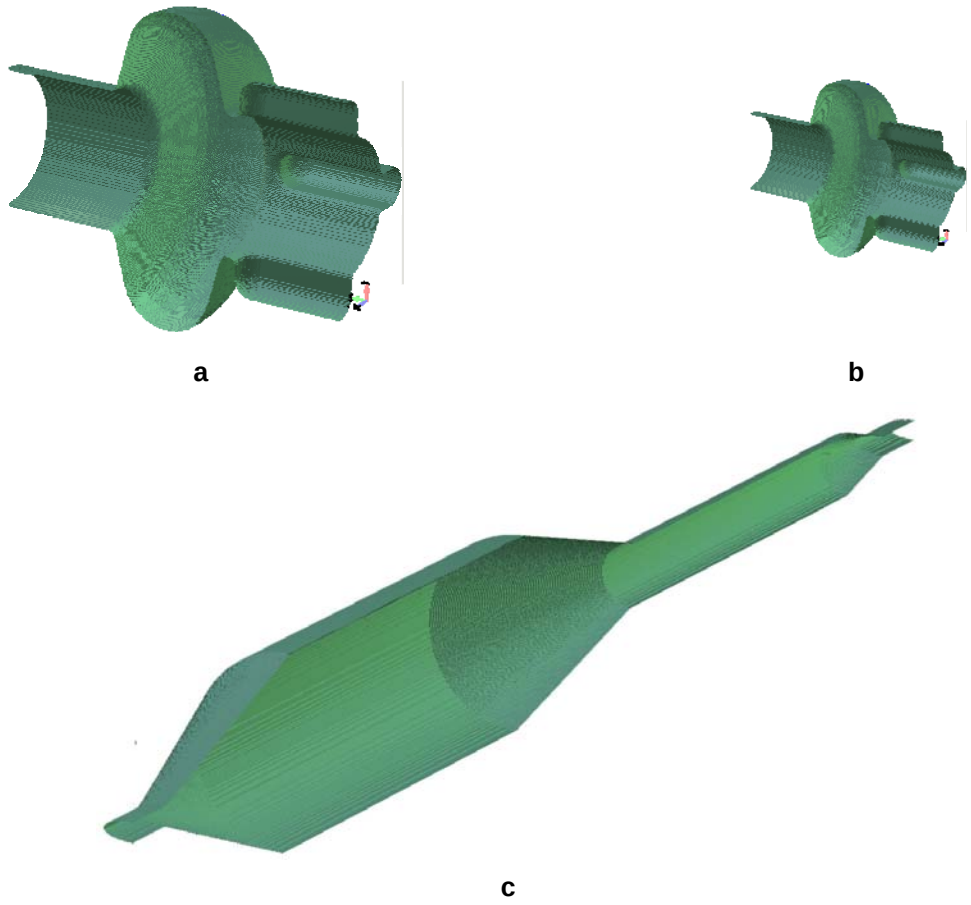

Figure 3.2.10 3D GdfidL models of the RF straight section.

a) 500 MHz main RF cavity. **b)** 1500 MHz harmonic RF cavity. **c)** Cavity transitions per straight.

Cavity transitions per straight consists of three smooth tapered transitions: regular vacuum chamber beam pipe – main cavity beam pipe, main cavity beam pipe – harmonic cavity beam pipe and harmonic cavity beam pipe – regular vacuum chamber beam pipe. Two longest tapers are taken to be 300 mm. The taper length between the beam pipe radius of the harmonic cavity (40 mm) and the regular vacuum chamber is 100 mm. For simplicity, the length of straight pipes between tapers is chosen to be 300 mm. Ferrite rings on both sides

of the RF cavities for HOM damping (narrow–band impedance) are not included in this analysis as they do not affect the short-range wakepotential (broad-band impedance).

Contribution of cavity transitions per straight to the broad-band longitudinal impedance in terms of the loss factor is significant (κ_{loss}=3.5V/pC). This value is comparable with the values for 720 m aluminum resistive wall (κ_{loss}=4V/pC) and for 200 BPMs ($\Sigma\kappa_{loss}$=4V/pC) from impedance table. Cavity itself gives a smaller contribution to the longitudinal impedance. To minimize transition impedance, taper lengths between RF cavities will be lengthened to the extent allowed by the available space.

3.2.4.3 Infrared Extraction Chamber

To take out the synchrotron radiation in far-infrared region six dipole magnets will be designed with large gap. To be able to extract the light emission ~50 mrad horizontal and ~25 mrad vertical (full radiation opening angles of the collected emission in location of the extraction mirror) within a bending magnet of ρ=*25 m* radius, the infrared (IR) chamber requires a full aperture of 67 mm vertical, 134 mm horizontal and a special trapezoidal slot extended vertically. The design of the far-IR chamber is shown in Figure 3.2.11. Since the IR-chamber has larger elliptical shape than the regular vacuum chamber (25 mm full height and 76 mm full width), smooth tapers are used to minimize the contribution to the longitudinal and transverse broad-band impedance. The IR-chamber will be installed inside of the wide-gap dipole magnet of 2.6 m long. Tapered transitions at each end of the structure, 300 mm and 100 mm long, are chosen to estimate the narrow-band impedance. They do not extend beyond the dipole magnet length and the taper length can be increased inside the dipole magnet to further reduce the broad-band impedance.

To direct the collected emission into the output port, the extraction mirror (copper color, 5 mm thick) is first modeled at the end of the trapezoid slot, 30 mm from the beam trajectory as shown in Figure 3.2.11 (zoomed part). Separation of the radiation from the electron beam is made more difficult due to the large bending radius of the NSLS-II dipoles. The mirror must be located close to the electron beam to collect the IR emission. Of particular concern is the narrow-band impedance which may be generated due to the mirror.

The narrow-band impedance computations are shown in Figure 3.2.11. The real part of the longitudinal impedance is presented for the IR-chamber with and without mirror. Set of resonant modes are generated into the chamber after the passing beam if the extraction mirror is inside. The mirror is seen by the beam and generated modes are trapped in a small pocket between the tapered transition and the mirror. These modes can cause couple bunch instability and heating of the chamber wall.

To avoid generation of resonant modes inside the chamber, we studied several variants of mirror position while maintaining the required extraction angles. One of the variants is shown in Figure 3.2.12. To avoid a pocket behind the mirror, we located the mirror at a point right after the widened cross-section had tapered back down to the regular dimensions. In this case, the extraction mirror is hidden behind the tapered transition in the region of the antechamber slot. This design eliminated the problem of resonant modes due to the mirror. It can be seen from the real part of the longitudinal impedance presented in Figure 3.2.12 (b). The narrow–band impedance of the complex IR-chamber was reduced down to the impedance of just a tapered structure.

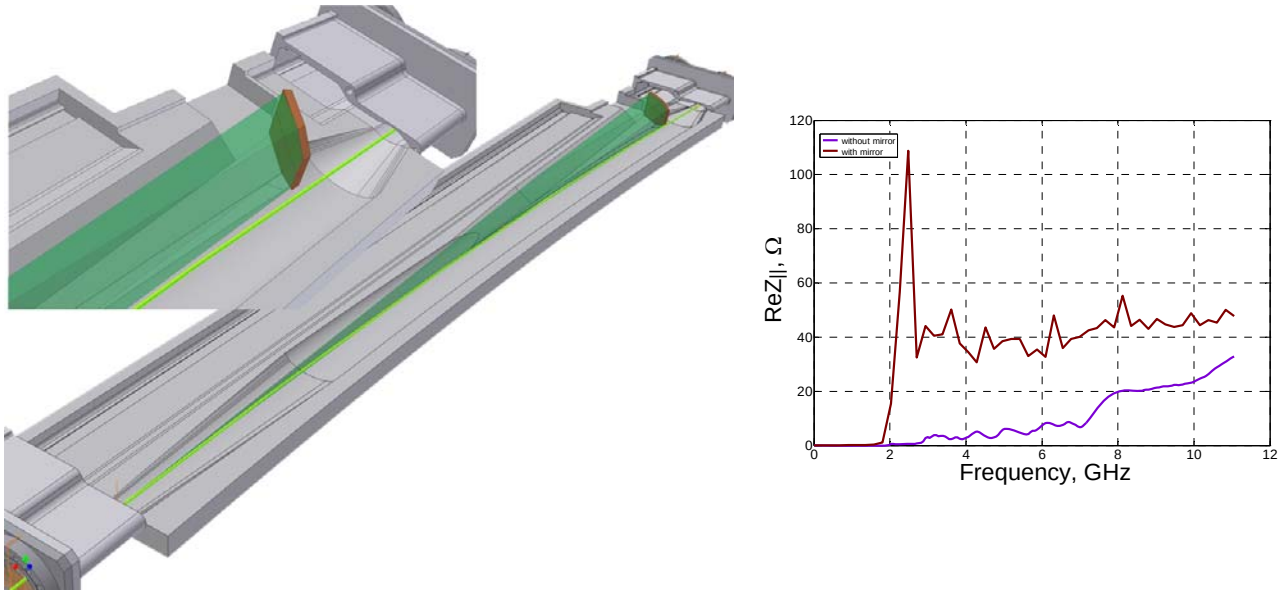

a **b**

Figure 3.2.11 Infrared extraction chamber for the dipole magnet with a large gap. **a)** Design of the IR chamber with a mirror in front of the tapered transition. The green line represents the electron beam and the green shaded region represents the IR radiation. **b)** Real part of the longitudinal impedance. Wine line and the purple line are calculations with and without extraction mirror inside the chamber respectively.

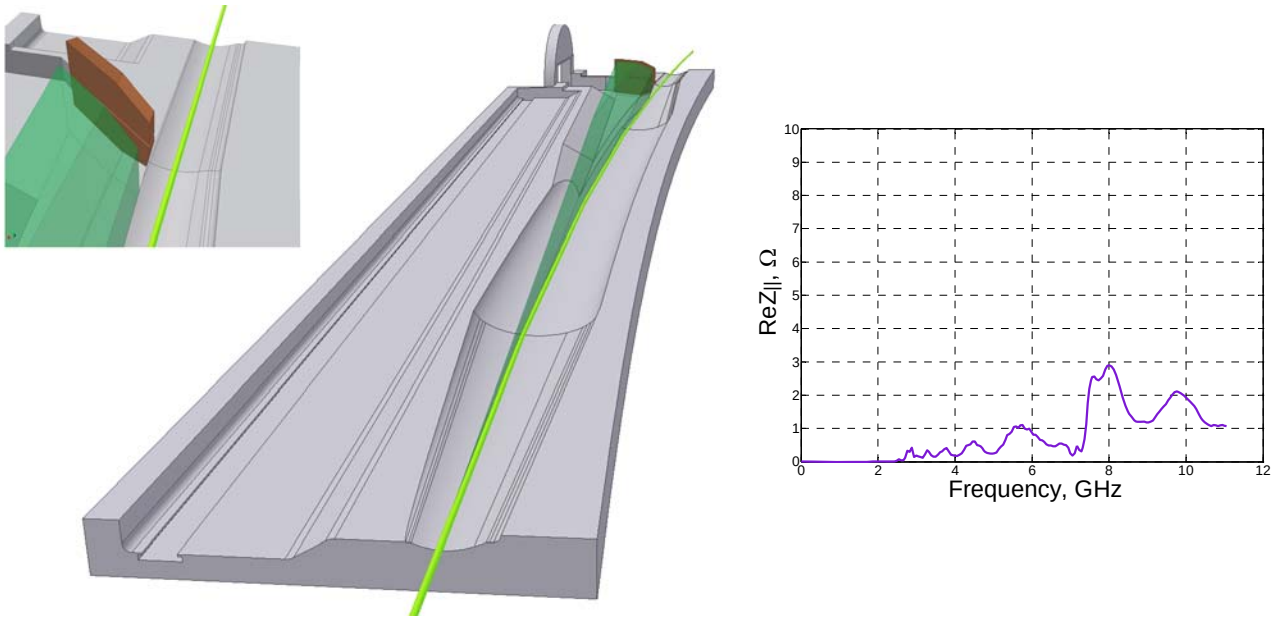

a **b**

Figure 3.2.12 Design of the infrared extraction chamber with the mirror at a point right after the widened cross-section. **a)** Mirror is located inside the regular vacuum chamber behind the tapered transition. **b)** Real part of the longitudinal impedance for the current design of the IR chamber with the extraction mirror.

To estimate the short range wake (broad-band impedance)of the IR chamber, we consider a simplified model. The full height and the full width of the tapered chamber are taken the same as for the real structure, 67 mm and 134 mm, respectively. Smooth tapered transitions, each 180 mm long, are located at both ends of

the chamber. The shorter taper length here is taken for reducing computational time. We modeled narrow and trapezoid slots, where the extraction mirror will be located. The trapezoid slot extends vertically away from the structure as shown in Figure 3.2.13 (c).

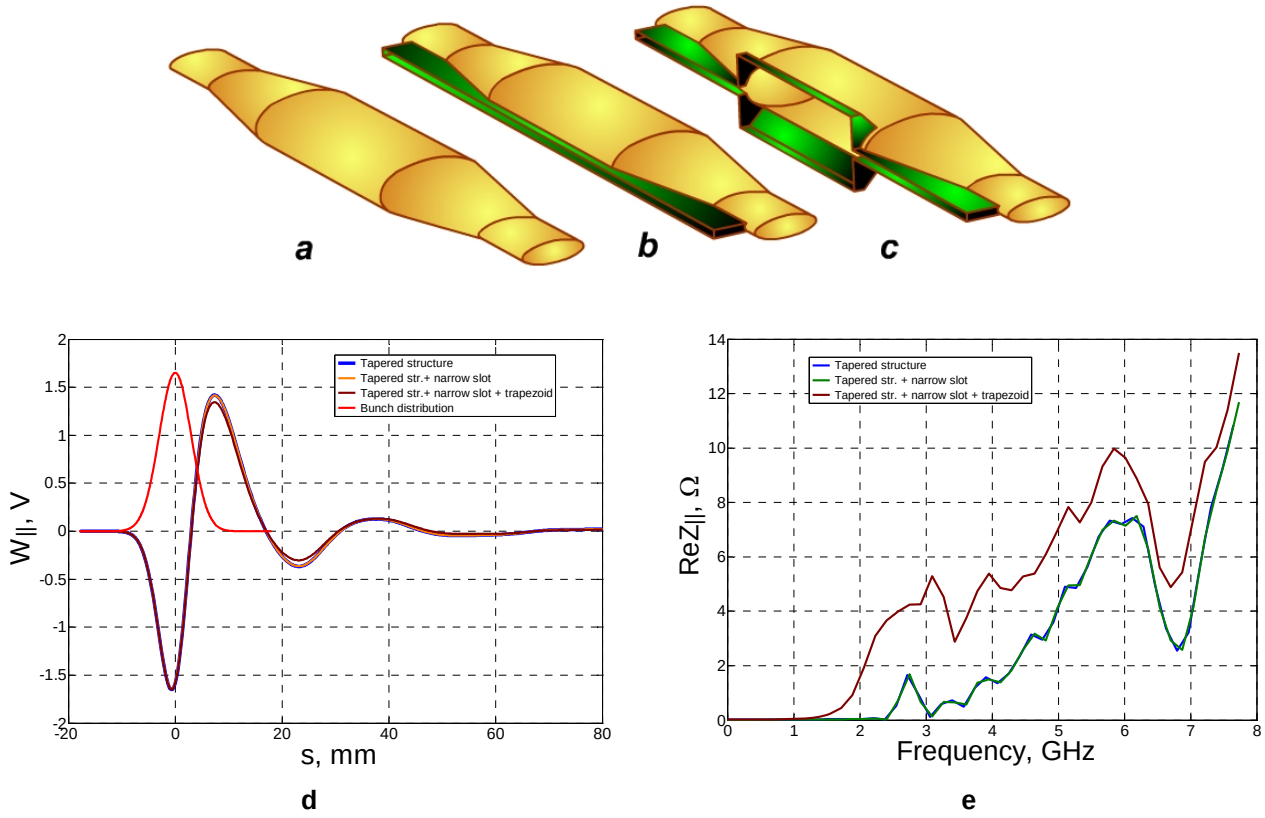

Figure 3.2.13 Simplified model of IR-extraction chamber. **a)** Tapered elliptic chamber. **b)** Tapered elliptic chamber with narrow slot. **c)** Tapered elliptic chamber with narrow slot and trapezoidal slot. **d)** The longitudinal short-range wakepotential. **e)** The real part of the longitudinal impedance.

Computations of the longitudinal wakepotential for a $\sigma_s=3\ mm$ rms bunch length show that narrow and trapezoid slots do not significantly affect the short-range wakepotential (Figure 3.2.13d) and hence the loss factor. The narrow-band impedance due to tapered transitions is similar to the impedance of the real geometry with the extraction mirror at the right location. The amplitude of the resonant peaks in the simplified geometry is slightly higher due to shorter taper length.

This analysis was concentrated on verifying of the results obtained for the real geometry, which is a more complex geometry and has a large value for numerical computations. As a first step we eliminated the resonant modes (narrow-band impedance) due to the extraction mirror. The next step needs to be done, to estimate the broad-band impedance for the actual design geometry. It requires a lot of computational time. In Table 3.2.6 we present the results computed for the simplified geometries shown in Figure 3.2.13. The loss factor for these geometries is $\kappa_{loss}=0.84V/pC$. Based on this preliminary study, the taper length for the actual design geometry will be increased to reduce the loss factor.

3.2.5 Intrabeam Scattering

Small-angle Coulomb scattering within a beam leads to the excitation of betatron and synchrotron oscillations of particles, which usually increases beam emittances in all phase planes. This effect, often called intra-beam scattering (IBS) or multiple Coulomb scattering, is proportional to the beam 3D phase-space density and depends strongly on beam energy, becoming more severe for high intensity, low energy machines.

When IBS is included, the steady-state beam properties with radiation damping are defined by

$$\varepsilon_x = \frac{\varepsilon_{x0}}{1-\tau_x/T_x}, \quad \varepsilon_y = \frac{\varepsilon_{y0}}{1-\tau_y/T_y}, \quad \sigma_p^2 = \frac{\sigma_{p0}^2}{1-\tau_p/T_p}, \tag{3.2-28}$$

where subscript 0 indicates the beam properties in the absence of IBS, $\tau_{x,y,p}$ stand for synchrotron radiation damping times, and $T_{x,y,p}$ are the IBS growth times discussed below. These equations indicate that the IBS effect becomes important when IBS rates are significant in comparison with the radiation damping rates. Because the IBS growth times $T_{x,y,p}$ depend on beam current as well as beam emittances, energy spread, and bunch length, the above equations are coupled, and solving them requires some iterative procedure. Sometimes a fourth equation is added that expresses the current-dependent relation of the bunch length to the energy spread, to account for the potential well distortion. If the vertical emittance is dominated by weak coupling (which is our expectation for NSLS-II), the effect simplifies to 2D, and the second equation is replaced by $\varepsilon_y = \kappa\, \varepsilon_x$, where κ stands for the coupling coefficient.

The basic theoretical framework of IBS effect was established long ago by Piwinski [3.2.31] and Bjorken and Mtingwa (B–M) [3.2.32] using two different approaches. These theories express IBS rise times $T_{x,y,p}$ as complicated integrals of beam parameters, such as energy and phase space density, as well as lattice properties. The B–M theory has been extended to include arbitrary vertical-horizontal and vertical-longitudinal coupling [3.2.33]. The resulting growth rates are local quantities, and have to then be averaged around the lattice. Many accelerator physics codes include some variations of the B–M approach. In addition to these general procedures which are fairly computer intensive, there exist a number of more approximate formulations of IBS effect that simplify the treatment for certain parameter regimes. For example, Bane [3.2.34] has recently shown the equivalence of the Piwinski and B–M treatments in the regime applicable for high energy machines. In this regime, Bane has found that B–M results reduce to fairly compact expressions for IBS rise times, which we have found useful for NSLS-II.

The IBS approaches mentioned above result in growth times proportional to the so-called Coulomb log factor, equal to $ln(b_{max}/b_{min})$, where $b_{max,\ min}$ are impact parameters, which are not well defined. Often, b_{max} is taken equal to σ_y . To fix b_{min}, a so-called "tail-cut" procedure was suggested by Raubenheimer [3.2.35]. He pointed out that, since IBS results in non-Gaussian beam distributions, tail particles could be overemphasized; therefore, one must chose b_{min} to eliminate interactions having collision rates smaller than SR damping rates.

The NSLS-II emittance is strongly dominated by the IDs and damping wigglers. Rather than assuming some fixed ID makeup, we have calculated IBS effects as a function of radiation losses in the machine, having ε_{x0} vary from the ~2 nm bare lattice value down to about 0.4 nm. The zero-current vertical emittance ε_{y0} was fixed at the diffraction limit for 1 Å x-rays (8 pm-rad), corresponding to κ varying from ~0.5% for bare lattice to about 2% for ε_{x0} = 0.4 nm.

Most NSLS-II calculations have been performed with the code ZAP [3.2.20], which implements the 2D procedure of the B–M theory [3.2.32], i.e., the vertical emittance is assumed dominated by coupling. We used 500 mA for the total ring current, and assumed it uniformly distributed into 80% of the 500 MHz RF buckets. As we changed the amount of radiation losses, the RF voltage was adjusted to keep the RF energy acceptance constant at 3%. Electron beam parameters in the absence of IBS, used as input to ZAP (such as horizontal

emittance, energy spread, bunch length, and radiation damping times) were calculated analytically by scaling bare lattice values by the amount of radiation losses. The results given by ZAP are shown in Figure 3.2.14.

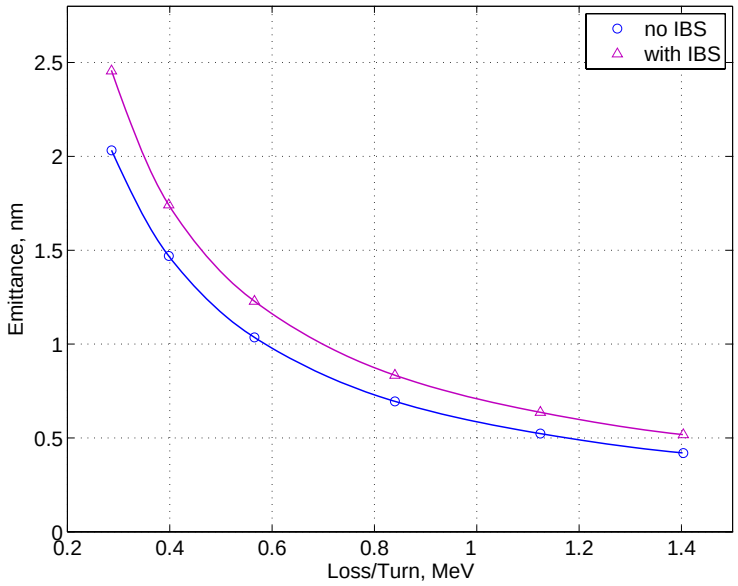

Figure 3.2.14 Horizontal emittance vs. total SR loss.

Note that the IBS-induced relative emittance blow-up does not exceed 20%, and remains fairly independent of the amount of radiation losses (and hence the emittance). This implies that for smaller emittances, increased IBS rates due to denser bunches are offset by the increase in radiation damping. This is quite contrary to a more typical situation in a storage ring light source not dominated by IDs, where decreasing the emittance by adjusting the lattice (and hence keeping the SR rates fixed) can result in an increase of IBS-induced emittance blow-up. We have also found that the IBS rise times calculated by ZAP are in reasonable agreement (better than 50 %) with the estimates we have done using Bane's formalism.

Note that the results presented in Figure 3.2.14 are based on several conservative assumptions. First, calculations are performed at zero-current bunch length, while in reality the bunch will be longer, due to potential well distortion and the harmonic RF system. At even higher single-bunch currents, used in special operating modes, the microwave instability will result in an even stronger increase in bunch length as well as energy spread, reducing the IBS effect further. In addition, the calculations of Coulomb log that are used in ZAP use $b_{max} = \sigma_x$ and do not include the tail-cut procedure. As a result, the Coulomb log value ZAP assumes for NSLS-II parameters is about 17, while more recent estimates [3.2.33] that include the cut would reduce it to about 10.

We have also done some cross-checks of the bare lattice case using the SAD code from KEK [3.2.36]. SAD has been extensively benchmarked against the experimental results from the ultra-low emittance ATF storage ring. SAD does include the tail-cut, so it results in smaller IBS induced blow-up compared to ZAP. However, when scaled for the Coulomb log, the codes are in good agreement. SAD allows for full 3D treatment of IBS and will be used in the future to study the effects of vertical dispersion for NSLS-II.

To summarize, our calculations to date indicate that under pessimistic assumptions, IBS-induced relative emittance blow-up for NSLS-II should not exceed 20% at nominal bunch intensity and therefore it should not present a problem. Furthermore, we have found the magnitude of the blow-up to be fairly independent of the NSLS-II emittance, since the increased IBS rates for denser bunches are compensated by faster radiation damping. Future studies will include accounting for a more comprehensive ID makeup, considering the effects of vertical dispersion, and further developing some models of bunch lengthening.

3.2.6 Touschek Lifetime

The beam lifetime in most modern synchrotron radiation sources is limited by the Touschek effect, which describes the collision of two electrons inside a bunch, leading to momentum transfer from the transverse (usually horizontal) plane into the longitudinal direction. If the resulting longitudinal momentum exceeds the momentum acceptance of the accelerator, these particles are lost.

The Touschek lifetime is calculated as [3.2.37],

$$\frac{1}{\tau} = \frac{r_e^2 cq}{8\pi e \gamma^3 \sigma_s} \cdot \frac{1}{C} \cdot \oint_C \frac{F((\delta_{acc}(s)/\gamma\sigma_{x'}(s))^2)}{\sigma_x(s)\sigma_{x'}(s)\sigma_y(s)\delta_{acc}^2(s)} ds, \tag{3.2-29}$$

where r_e denotes the classical electron radius, q the bunch charge, σ_s the RMS bunch length, C the circumference of the storage ring, and σ_x (s) and σ_y (s) the RMS horizontal and vertical beam radii, including the dispersion term.

$$\sigma_{x'}(s) = \frac{\varepsilon_x}{\sigma_x(s)} \sqrt{1 + \frac{H(s)\sigma_\delta^2}{\varepsilon_x}} \tag{3.2-30}$$

is the RMS beam divergence for $\alpha_x = 0$, with

$$H(s) = \gamma_x \eta^2 + 2\alpha_x \eta\eta' + \beta_x \eta'^2 \tag{3.2-31}$$

the chromatic invariant. The function F(x) is defined as

$$F(x) = \int_0^1 (\frac{2}{u} - \ln\frac{1}{u} - 2) \cdot \exp(-x/u) du. \tag{3.2-32}$$

While the Touschek lifetime depends linearly on the bunch length as well as on the vertical beamsize, its dependence on the horizontal beamsize (or emittance) is more complicated. For large horizontal beamsize, the particle density of the bunch becomes very small, thus greatly decreasing the probability of two electrons colliding. On the other hand, a large horizontal emittance results in large horizontal momenta that can be transferred into the longitudinal plane due to a Touschek scattering event. The dependence of the resulting Touschek lifetime (for a bunch length of 4.5 mm) on horizontal emittance is illustrated in Figure 3.2.15. The result is that in the region of the design emittance for NSLS-II, the Touschek lifetime is not particularly sensitive to emittance. For a variety of reasons we will discuss, this estimate of Touschek lifetime is optimistic. Even so, for the design emittance, the lifetime is below the specified lifetime of 3 hours. Increasing the bunch length with a Landau cavity can provide the extra lifetime to meet the lifetime goal.

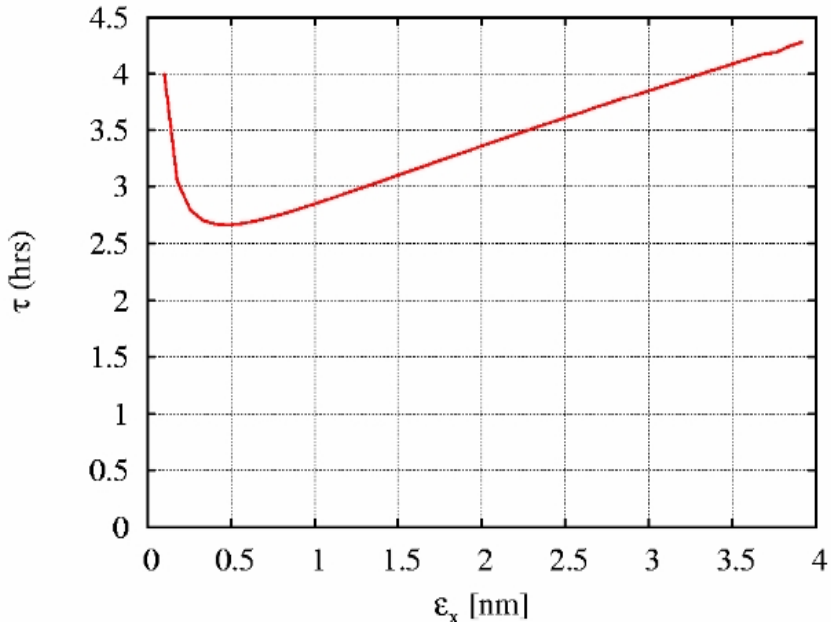

Figure 3.2.15 Touschek lifetime vs. horizontal emittance for 3% momentum acceptance and a 4.5 mm bunch length.

Experience at facilities like ALS and SLS has shown that nonlinear betatron coupling plays a significant role in limiting the momentum acceptance of the storage ring, especially in the presence of small vertical apertures due to small-gap insertion devices. Therefore, tracking has been performed using the TRACY-2 code. Since Touschek scattering occurs near the center of the bunch, the momentum acceptance δ_{acc} needs to be determined for particles starting at a longitudinal position s with coordinates $x = x' = y = y' = 0$. In general, this yields different momentum acceptances δ_{acc}^{+} for positive and δ_{acc}^{-} for negative momenta, resulting in different Touschek lifetimes τ^{+} and τ^{-}. Based on these two results, the total Touschek lifetime τ_{tot} is computed as

$$\frac{1}{\tau_{tot}} = \frac{1}{2} \cdot \left(\frac{1}{\tau^{+}} + \frac{1}{\tau^{-}} \right). \tag{3.2-33}$$

The RF acceptance has been set to ±3%. To achieve this for the bare lattice, an RF voltage of 2.5 MV is required. For the baseline case of 3 damping wigglers, a voltage of 3.1 MV is required. The RF acceptance determines the maximum achievable momentum acceptance. In fact there are a number of factors that can reduce the true momentum acceptance. Off-momentum particles below the RF acceptance can hit apertures that an on-momentum particle would not hit. This is due to the fact that off-momentum particles have a different orbit (from dispersion), and different tunes (from chromaticity). Further, as a particle executes damped synchrotron oscillations, it will sample a large region of phase space and tune space which can lead to the loss of the particle. The calculations shown here use 512 turns, or several synchrotron oscillations. Tracking for a full damping time (~ 4500 turns for 3 damping wigglers) should be performed to spot-check results. We have found that in some cases, this extra tracking time can decrease the momentum acceptance, and hence lifetime. In one case (very similar to the nominal case we present here), we found that the lifetime dropped from 2.5 hours to 2.2 hours when the number of turns was increased from 512 to 5000.

To get a realistic estimate of the momentum acceptance, a realistic lattice model is created from the design lattice and relevant non-linearities plus appropriate physical apertures are included. The lattice is non-linear due to the sextupoles, insertion devices and random and systematic higher order multipole errors. These are discussed further in the section on dynamic aperture. Here, we have taken the bare lattice and added 3 damping wigglers and 3 CPMUs, plus random and systematic multipole errors. The damping wigglers, in

addition, have higher harmonic content determined by fitting computed field maps to a Halbach basis. The systematic multipole errors come from modeling and measurements of quadrupoles and sextupoles borrowed from the SLS which are similar to our design magnets. The random errors come from measured values for the SLS magnets produced by the Budker Institute in Novosibirsk. The ID parameters used were as follows: for the damping wiggler, the peak field is 1.8 T, and the period length 9 cm, with 77 periods. For the CPMUs, the peak field is 1.2 T, and the period length 19 mm, with 160 periods.

Random misalignment and roll errors are added, including the systematic effects from the girders. The girders are misaligned randomly by 100 μ, and quadrupoles and sextupoles misaligned by 30 μ relative to the girder. The orbit is corrected by computing the beam response matrix and adjusting the corrector strengths to minimize orbit offset at the BPMs. In addition, we must correct the linear optics due to the perturbation caused by the damping wigglers. For these studies, the three damping wigglers were assumed to occur consecutively. Periodic distribution should also be considered.

The vertical emittance is determined by a combination of linear coupling and vertical dispersion. The random roll errors of 0.2 mrad for the quadruples and sextupoles and 0.5 mrad girder to girder cause coupling, but the equilibrium vertical emittance is still below the diffraction limited value of 8 pm (ε_y= 1 pm for the case used for the calculations of energy acceptance). An algorithm to increase vertical dispersion combined with coupling control/correction has been developed to control vertical emittance. The algorithm has been tested but is not included in these calculations. A vertical emittance of 8 pm is assumed here for the lifetime calculation.

After preparing the lattice by adding all the above errors, corrections and physical apertures (described below), the momentum acceptance around the ring is computed by tracking. The result for the nominal case is shown in Figure 3.2.16 (a). We see that the errors and apertures have not had a large impact and the lifetime has only dropped from 2.77 hours to 2.62 hours. Adding more insertion devices adds to the non-linearity and is expected to have an impact on momentum aperture.

As we have mentioned, beam loss can occur due to electrons hitting transverse physical apertures. Both vertical and horizontal apertures can decrease lifetime. First consider the horizontal case. A Touschek scatter in a dispersive region causes betatron oscillations throughout the ring. Considering uncoupled linear betatron dynamics, the amplitude of such oscillations is given by

$$x(s) = (\eta + \sqrt{H_0 \beta_x})\delta \tag{3.2-34}$$

with H_0 the dispersion invariant (3.2-31) at the position of the scatter, and δ the resultant relative energy change of the particle. The maximum value is approximately twice the maximum dispersion times δ. For δ of 3% this can be as large as 27 mm. Figure 3.2.16 (b) shows the effect on lifetime of varying the horizontal aperture in the maximum dispersion region. We see that below 27 mm, the lifetime decreases. This shows the importance of maintaining the stay-clear aperture. Photon absorbers are one example of elements for which it would otherwise be desirable to be closer to the beam than the stay-clear specifications.

If we expect such large horizontal betatron oscillations to be stable, then clearly any coupling will cause vertical apertures to be a concern. The smallest vertical aperture is that of the CPMU gap of ± 2.5 mm. We have varied this gap size and computed the effect on the lifetime in Figure 3.2.16 (c). Below the nominal value of ± 2.5 mm, we see a decrease in lifetime.

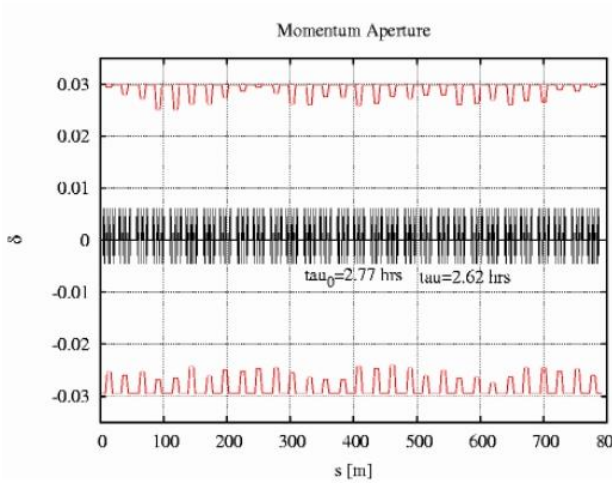

a

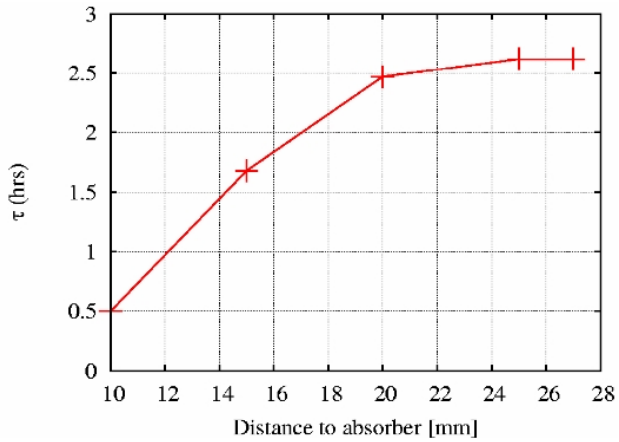

b

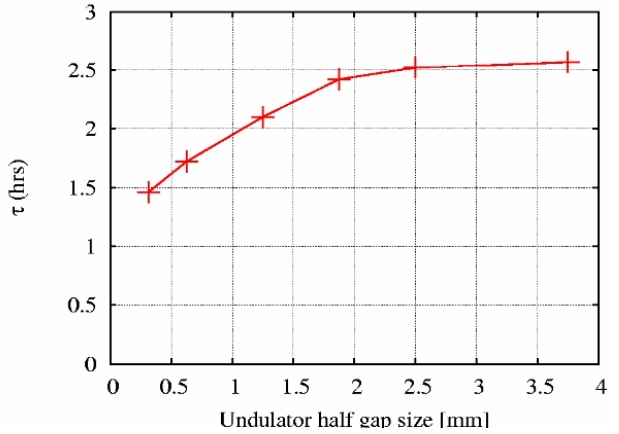

c

Figure 3.2.16

a) Momentum acceptance for baseline lattice: 3 DW, 3 CPMU;

b) Touschek lifetime dependence on horizontal aperture at peak dispersion (photon absorber)

c) Touschek lifetime dependence on vertical half-gap in CPMU.

In conclusion, a realistic storage ring model is required to estimate the Touschek lifetime, particularly in order to compute the momentum acceptance. We are developing such a realistic model to be used together with dynamic aperture calculations to analyze limits on stay-clear apertures, magnetic and alignment imperfections, and other machine parameters such as chromaticity. Such studies are ongoing and must be continually updated as the sextupole settings and tunes continue to be optimized and the lattice design continues to mature. Further effects to be explored are the impact from additional insertion devices, especially from EPUs. Also, we will study more realistic ID modeling, inclusion of the dispersion wave to get a self-consistent model, and required stay-clear apertures. We also plan comprehensive studies including multiple seeds for the random errors. Finally, we emphasize that even if the momentum acceptance of 3% is achieved, we still require the bunch lengthening effect from the Landau cavity in order to achieve a Touschek lifetime of 3 hours.

3.2.7 Landau Cavity

Let us begin by reviewing the operation of a higher-harmonic, bunch-lengthening cavity (HHC) [3.2.38]. The fundamental cavity operates at an angular frequency, $\omega_{rf} = h\omega_0$, where h is an integer and $\omega_0 = 2\pi / T_0$ is the angular frequency of revolution. Assuming the Landau cavity is operating at the n^{th} harmonic of the frequency of the fundamental RF, the voltage seen by an electron with temporal deviation τ is

$$V(\tau) = V_0\left[\sin\left(\omega_{rf}\tau + \phi_s\right) + \kappa\sin\left(n\omega_{rf}\tau + \phi_n\right)\right]. \tag{3.2-34}$$

In the ideal operation of such a cavity, one chooses to satisfy the conditions

$$\begin{aligned} U_0 &= V_0\left[\sin\phi_s + \kappa\sin\phi_n\right] \\ 0 &= \cos\phi_s + n\kappa\cos\phi_n \\ 0 &= \sin\phi_s + n^2\kappa\sin\phi_n, \end{aligned} \tag{3.2-35}$$

where energy loss (U_0) and gain are balanced, and the first and second derivatives of the waveform are set to zero, at zero phase. In this case, the voltage has the form

$$V(\tau) = \cos\phi_s\left(\sin\omega_{rf}\tau - \frac{1}{n}\sin n\omega_{rf}\tau\right) + \sin\phi_s\left(\cos\omega_{rf}\tau - \frac{1}{n^2}\cos n\omega_{rf}\tau\right). \tag{3.2-36}$$

Approximating this for small τ yields the cubic form

$$V(\tau) \cong \cos\phi_s\left(\frac{n^2-1}{6}\right)\left(\omega_{rf}\tau\right)^3 + \sin\phi_s\left(1 - \frac{1}{n^2}\right). \tag{3.2-37}$$

As we will operate the Landau cavity passively, i.e., powered only by the beam, we cannot satisfy all of the ideal conditions. A superconducting cavity, in particular, absorbs very little power, implying that ϕ_n is fixed at –π/2, a few degrees from the ideal phase. Fortunately, this phase shift has little impact on the bunch profile. Figure 3.2.17 shows an unstretched bunch (blue) plotted with a stretched bunch (red) in a uniform fill with HHC detuning at +82 kHz.

A third-harmonic Landau cavity can be used to increase the electron bunch length without increasing the energy spread. This increases the Touschek lifetime and reduces the effect of intrabeam scattering on emittance. The nonlinear voltage resulting from the use of a Landau cavity results in a large increase in the dependence of the synchrotron tune on the amplitude of synchrotron oscillations. Energy transfer from potentially unstable resonant particles within a bunch to the surrounding non-resonant particles often provides a powerful mechanism for the suppression (Landau damping) of longitudinal coupled-bunch dipole modes. Also, the increase of bunch length can increase the stabilizing effect of positive chromaticity on the transverse dipole oscillations. The increased synchrotron tune spread can also help stabilize the higher-order head-tail modes.

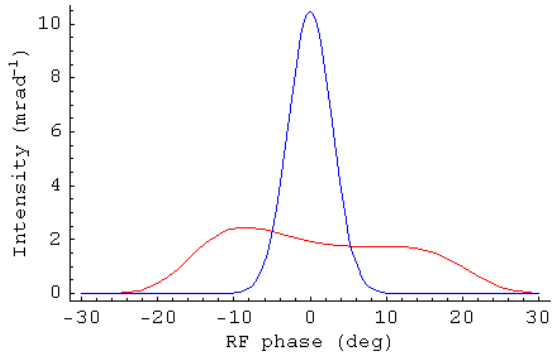

Figure 3.2.17 An unstretched bunch (blue) plotted with a stretched bunch (red) in a uniform fill with HHC detuning at +80 kHz. The bunch lengths are 14.1 and 56.1 ps, respectively.

If, as expected, there is a gap in the fill for ion clearing, then there will be a periodic transient induced in the cavity fields, causing non-uniform bunch profiles across the bunch train [3.2.39, 3.2.40, 3.2.41]. This effect is proportional to the *R/Q*s of the cavities, which favors superconducting cavities due both to their lower *R/Q* and their higher sustainable fields (requiring fewer cavities). Away from the center of the bunch train, bunches are much shorter and are peaked near the local synchronous phase, which can be a distance from the center of the nominal bucket. These peripheral bunches have shorter Touschek lifetime. This effect was found at ALS [3.2.40] to significantly reduce the overall lifetime of the beam. Figure 3.2.18 shows the bunch profiles for a 90% fill pattern, harmonic-cavity detuning of +80 kHz, and a single gap, and with the gap split into four symmetrically spaced gaps.

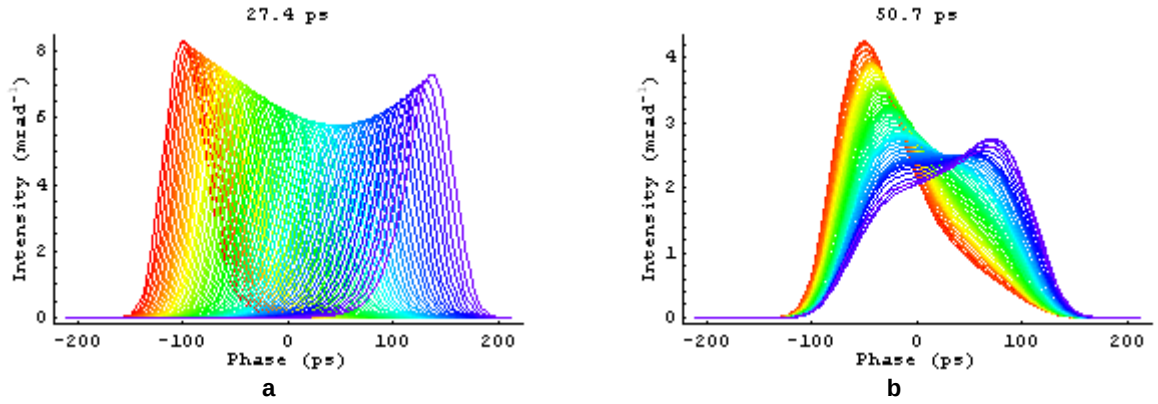

Figure 3.2.18 Bunch profiles along the bunch train for a 90% fill fraction, harmonic-cavity detuning of +80 kHz, and a) a single gap in the train, and b**)** four gaps in the train. Each plot is labeled with the average RMS bunch length of the bunches. For reference, the unstretched bunch length is 14.1 ps and the stretched bunch length in a uniform fill is 56.1 ps.

With a single ion-clearing gap, the transient is severe, even with SC cavities (Figure 3.2.18a). The bunches are dispersed in phase with only modest stretching, reducing the field the beam is able to drive in the HHCs. The increase in bunch length is less than a factor of two. In this large ring, reducing the HHC detuning to bring up the field tends to increase the dispersion before increasing the field and stretching individual bunches. But breaking up the gap into several smaller gaps makes the ring appear to the cavities to be a smaller and is effective at increasing the average bunch length. In the case of four gaps, the increase in bunch length is by a factor of 3.6. The profiles of Figure 3.2.18b with four gaps appear similar to the bunch profiles measured at ELETTRA [3.2.42], which is one-third the size of NSLS-II. With an 80% fill fraction, the bunches are even shorter (Figure 3.2.19). Bunch lengths vary smoothly with increasing fill fraction to the 56.1-ns length at a 100% fill. Smaller fill fractions aggravate the variation of bunch shapes along the train.

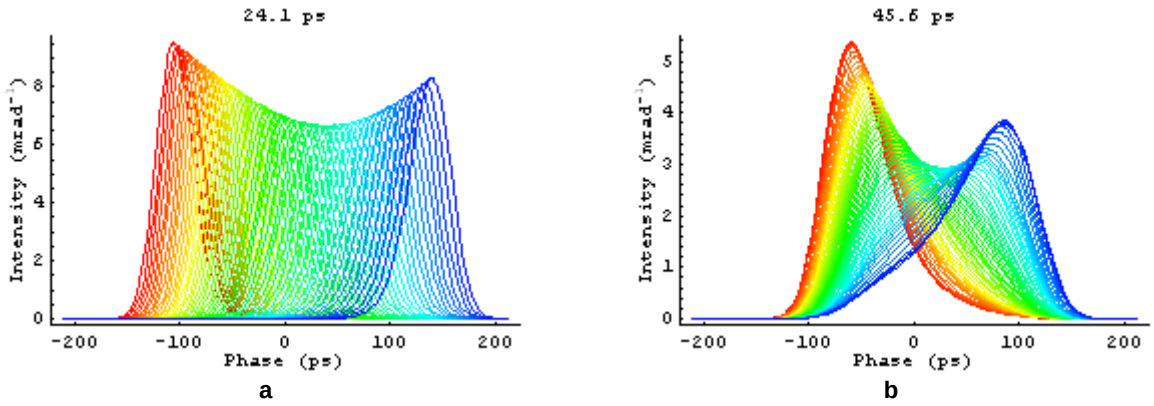

Figure 3.2.19 Bunch profiles along the bunch train for a 80% fill fraction, harmonic-cavity detuning of +80 kHz, and a) a single gap in the train, and b**)** four gaps in the train. Each plot is labeled with the average RMS bunch length of the bunches. For reference, the unstretched bunch length is 14.1 ps and the stretched bunch length in a uniform fill is 56.1 ps.

Bunch lengths vary with position along the train, and tend to be greatest near the center. In Figure 3.2.20a, each trace corresponds to a particular cavity field set by the detuning, which is from +110 (violet) to 70 (red) kHz. As HHC fields increase, bunch lengths and lifetimes tend to increase; but bunches that become double peaked, however, can show large RMS bunch length but reduced lifetime. Bunch centroid phases (arrival times) also vary with position along the train. In Figure 3.2.20b, the phase along the train is plotted for a 90% fill and the same fields as in Figure 3.2.20a. The synchronous phase is a sensitive function of local shifts in the RF wave due to the $(\omega_{\gamma} t)^3$ inflection; that sensitivity increases with increasing HHC field, even beyond the optimal HHC field.

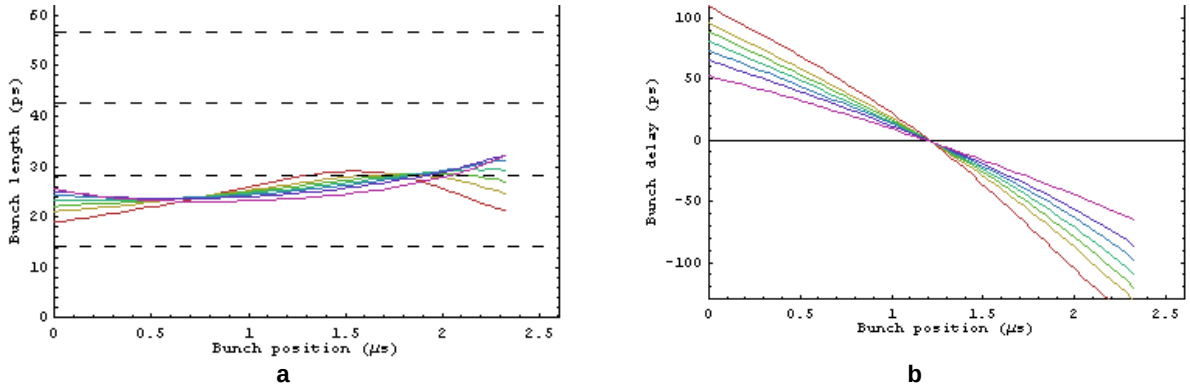

Figure 3.2.20 Bunch lengths **a)** and delays **b)** along the bunch train for a 90% fill and a single gap. Each trace corresponds to a particular cavity detuning: +110 (violet), 100, 95, 90, 85, 80, and 70 kHz (red). In a), the dashed lines are drawn at multiples of the unstretched bunch length.

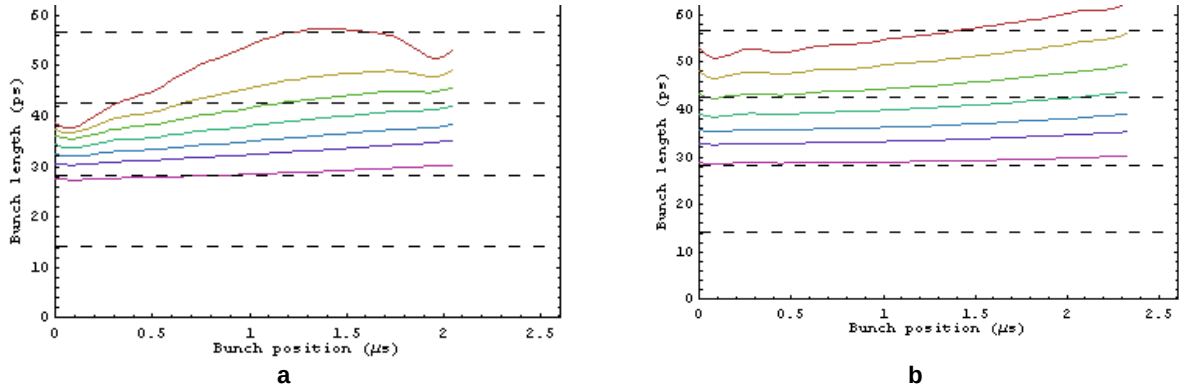

Figure 3.2.21 Bunch lengths along the bunch train with four gaps in an **a)** 80% fill, and **b)** 90% fill. Each trace corresponds to a particular cavity detuning: in **a)**, +110 (violet), 100, 95, 90, 85, 80, and 70 kHz (red), and in **b)**, +110 (violet), 100, 95, 90, 85, 80, and 75 kHz (red). The dashed lines are drawn at multiples of the unstretched bunch length.

The HHC field required for nominal bunch stretching is 1.5 MV. Since the maximum sustained fields reached in HHCs developed to date are 0.5 MV per cell in 1500 MHz cavities, three cells are required, either in three single-cell cavities, or two double-cell cavities. The performance plots above were computed assuming four cells, perhaps in two cryostats. In practice, significantly longer lifetimes are achievable by operating the HHCs at fields slightly higher than the ideal described above, as the NSLS VUV ring is operated now. The useful fields are limited by the onset of higher-order longitudinal instabilities.

The Day-1 configuration employs a reduced number of damping wigglers and consequently requires less main- and harmonic-cavity fields. Since two harmonic-cavity cells are capable of providing 1.0 MV of the 1.1 MV nominally required during this phase, most of the benefit of the HHC is obtained from this one cavity. Since the impedance is only that of two main and two HHC cells, the impact of the bunch train on bunch profiles is reduced in proportion.

Compressed bunch operation for timing experiments is possible by detuning the HHC below the RF harmonic, instead of above. The bunch length at small single-bunch currents is reduced to less than half the bunch length without a harmonic cavity. But at finite currents, potential-well distortion by the ring's broadband impedance, and microwave instability, if present, inevitably increases the bunch lengths. The short bunch lengths may also permit higher-frequency, higher-order modes in the HHC and elsewhere to drive coupled-bunch instabilities. Short-bunch operation may drive the need for longitudinal feedback.

The potential for unstable coupled-bunch modes driven by the CESR-B SC cavity in unstretched bunches was investigated in Section 3.2.3.4. In stretched bunches, Landau damping is expected to provide additional damping. This was confirmed in Vlasov simulations of stretched bunches assuming an RF potential well giving the stretched bunch of Figure 3.2.17. In each run, bunches was simulated with a single HOM present, up to 6.3 GHz, and its threshold for instability in terms of impedance determined. At all frequencies, thresholds at least a few times higher than that given in Eq. 3.2-27 were determined. Results are shown in Figure 3.2.22.

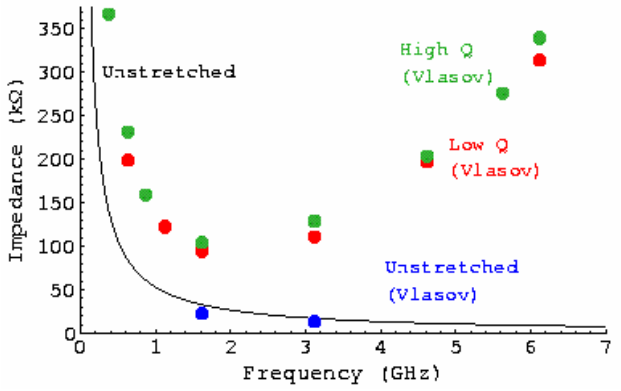

Figure 3.2.22 Instability thresholds (at 500 ma) for coupled-bunch modes in a stretched bunch expressed in terms of impedance, for a high-Q-model HOM impedance (green points) and lower-Q-model HOM impedance (red points), in the phase-four commissioning phase of the machine. The solid line is from Eq. 3.2-27, and blue points are test Vlasov runs with unstretched bunches. Thresholds were determined by Vlasov simulations.

It is useful to construct linear time-independent models of the RF system and beam, which are then plugged into comprehensive models of the RF system and used to search for unanticipated behaviors [3.2.43]. Linear models are also useful for determining RF-system specifications, such as amplifier noise specifications, from beam-based noise specifications. But the stretched bunches of NSLS-II have a multiplicity of active degrees of freedom that shape their small-signal behavior as they interact with the rf system, and the Pedersen model [3.4.44] is not adequate to model them. As an alternative, computer simulations may be used to determine beam behavior, which is realistic to the degree to which the computer model captures the physics of the beams.

In this spirit, Vlasov simulations were used to determine impulse response functions, which were then Fourier transformed to their frequency-domain representations. The beam phase response to amplitude and phase modulation of the rf, which is the motion of the bunch centroid phase in response to excitation of the RF intensity and phase, is shown in Figure 3.2.23. Although only the beam phase response is shown, beam energy, main-cavity amplitude and phase, and HHC amplitude and phase responses are also determined by a single set of simulations. Very precise rational–function fits have been obtained using MATLAB's signal processing toolbox.

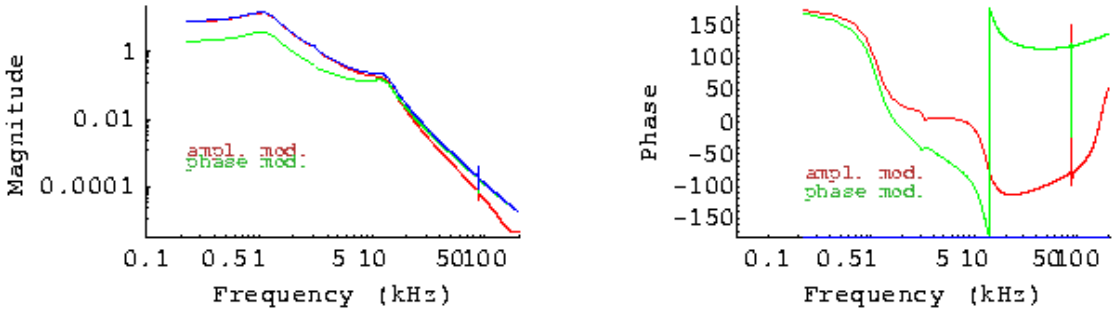

Figure 3.2.23 Beam-phase response functions to amplitude and phase modulation. Red traces are for amplitude modulation, green traces for phase modulation, and blue traces for the root square sum of the two. The left plot shows the amplitudes of the response functions, and right plots show the phases. There are four main cavities, four HHCs, HHC detuning is -4 kHz, and the loaded Q of the main cavities is set to 90 k.

There is considerable structure in these response functions starting at about 1 kHz that suggests that the problem of designing an RF controller capable of suppressing noise at significant bandwidth will be difficult. It is hoped that detailed rational-function and RF system models will provide some guidance in this area.

NSLS-II can opt to use an active HHC, i.e., HHCs that are powered by conventional amplifiers, such as was done in the NSLS VUV ring. In this configuration, resistive and reactive power are applied to control the phase of the cavity relative to the beam, almost arbitrarily. But the numerical results presented above, and the example of the VUV ring, which uses an active system to set the cavity (a NC cavity) phase to –90 degrees, show that the impact of the difference between –90 degrees and the nominal phase for stretching, even in the uniform-fill case, is insignificant. And in a fill with a significant gap, the improvement in the profiles is swamped by the effect of the periodic transient. Furthermore, an active system would require development of a cavity with an input coupler, could introduce multipacting, and could complicate HOM suppression. For these reasons, a passive cavity has been selected for NSLS-II.

3.2.8 Conclusions

Using a simplified model of the storage ring impedance, we have estimated the instability thresholds for NSLS-II. The longitudinal motion is found to be stable. At zero chromaticity, the transverse resistive wall impedance will make the beam unstable at 15 mA average current. According to simulations, increasing the chromaticity above 4 should provide stability. However, there is concern about the effect on DA at higher chromaticity; therefore, we will also use a transverse feedback system.

We have made significant progress in calculating the impedance of the storage ring using GdfidL. The results obtained thus far are within the envelope of the model we have used to estimate thresholds. Thus, we believe our model is conservative. We plan to complete the calculation of the storage ring impedance and then use the numerically determined wakefields in a tracking code to determine the instability thresholds.

Calculations indicate that the increase of emittance due to intrabeam scattering should be less than 20%. For the present state of the lattice design, the 5 mm full vertical aperture of the in-vacuum undulators reduces the energy acceptance from 3% down to 1.5% at large-dispersion locations. This results in a Touschek lifetime of 2 hrs. We plan to investigate whether further optimization of the working point can reduce the nonlinear coupling and thus increase the Touschek lifetime. Use of a Landau third-harmonic bunch lengthening cavity is planned. This will reduce the effect of intrabeam scattering on the emittance, lengthen the Touschek lifetime to more than 3 hrs, and provide enhanced longitudinal and transverse stability.

References

[3.2.1] A.W. Chao, *Physics of Collective Beam Instabilities in High Energy Accelerators* (Wiley, NY, 1993).

[3.2.2] See, e.g., K. Harkay, R. Nagaoka, J.L. Revol, and T. Nakamura, "A Preliminary Comparison of Beam Instabilities among ESRF, APS, and SPrinG-8 X-Ray Storage Ring Light Sources, Proc. EPAC2002, 1505 (2002).

[3.2.3] W. Bruns, http://www.gdfidl.de.

[3.2.4] G.V. Stupakov, "Wake and Impedance," SLAC-PUB-8683 (2000).

[3.2.5] B. Zotter and S.A. Kheifets, *Impedances and Wakes in High-Energy Particle Accelerators* (World Scientific Publishing Co., Singapore, 1998).

[3.2.6] A. Chao, S. Heifets, and B. Zotter, "Tune Shifts of Bunch Trains due to Vacuum Chambers Without Circular Symmetry," *Phys. Rev. ST-AB* **5**, 111001 (2002).

[3.2.7] K. Bane, and M. Sands, "Short-Range Resistive Wall Wakefields," AIP Conf. Proc. **367**, 131 (1995).

[3.2.8] B. Podobedov, "Extreme Anomalous Skin Effect Wakefields," unpublished.

[3.2.9] Y.C. Chae, "The Impedance Database and its Applications to the APS Storage Ring," Proc. PAC2005, 3017.
[3.2.10] See, e.g., S. Krinsky, "Simulation of Transverse Instabilities in the NSLS-II Storage Ring," BNL-75019-2005-IR.
[3.2.11] J. Haissinski, *Il Nuovo Cimento* **18**, 72 (1973).
[3.2.12] K. Oide and K. Yokoya, "Longitudinal Single-Bunch Instability in Electron Storage Ring," KEK Preprint 90-10 (1990).
[3.2.13] M. Borland, ELEGANT, http://www.aps.anl.gov/Accelerator_Systems_Division/Operations_Analysis/software.shtml
[3.2.14] D. Boussard, CERN LABII/RF/INT/75-2 (1975).
[3.2.15] M. Blaskiewicz, "The TRANFT User's Manual," unpublished.
[3.2.16] J. Kirchgessner, Part. Accel. **46**, 151 (1995).
[3.2.17] M. de Jong et al., *J. Microwave Power Electromagnetic Energy* **27**, 136 (1992).
[3.2.18] K. Halbach and R.F. Holsinger, "SUPERFISH-A Computer Program for Evaluation of RF Cavities with Cylinderical Symmetry," *Part. Accel.* **7**, 213 (1976).
[3.2.19] Mark deJong, private communication.
[3.2.20] M.S. Zisman, S. Chattopadhyay, and J.J. Bisognano, "ZAP User's Manual," LBL-21270, UC-28 (1986), 168.
[3.2.21] R. Nagaoka, "Numerical Evaluation of Geometric Impedance for SOLEIL," Proc. EPAC2004, 2038.
[3.2.22] K. Yokoya, "Resisitive Wall Impedance of Beam Pipes of General Cross Section," *Part. Accel.* **41**, 221 (1993).
[3.2.23] G. Stupakov, "Coupling Impedance of a Long Slot and an Array of Slots in a Circular Vacuum Chamber," *Phys. Rev. E* **51**, 3515 (1995).
[3.2.24] E. Karantzoulis, V. Smaluk and L. Tosi, "Broad Band Impedance Measurements on the Electron Storage Ring ELETTRA," *Phys. Rev. ST-AB* **6**, 030703 (2003).
[3.2.25] B. Podobedov and S. Krinsky, "Transverse Impedance of Elliptical Cross-Section Tapers," Proc. EPAC2006, 2973 (2006).
[3.2.26] A. Blednykh, S. Krinsky, B. Podobedov, and J.M. Wang, "Transverse Impedance for Small-Gap Undulators for NSLS-II," Proc. EPAC2006, 2973 (2006).
[3.2.27] P. Stefan et al., "Small-Gap Undulator Research at the NSLS: Concepts and Results." *Nucl. Instr. Meth. A* **412**, 161 (1998).
[3.2.28] A. Blednykh, "Trapped Modes in an Elliptic Vacuum Chamber," *Nucl. Instrum. Meth. A*.
[3.2.29] P.J. Chou, "Numerical Analysis of Higher-Order Modes for Superconducting RF Cavity at SRRC," Proc. Pac2003, 1368.
[3.2.30] P.J. Chou, J. Chen, K.-T. Hsu, C.-C. Kuo, C. Wang, and M.-H. Wang, "Collective Effects in the TLS Storage Ring after the Installation of Superconducting Cavity," Proc. PAC2005, 2360.
[3.2.31] A. Piwinski Tech. Rep. HEAC 74, Stanford, 1974; See Also A. Piwinski in A. Chao and M. Tigner, *Handbook of Acclerator Physics*, World Scientific (1999) 125.
[3.2.32] J. Bjorken and S. Mtingwa, "Intrabeam Scattering," *Part. Accel*. **13**, 115 (1983).
[3.2.33] K. Kubo and K. Oide, "Intrabeam Scattering Formulas for High Energy Beams," *Phys. Rev. ST-AB* **4**, 124401 (2001).
[3.2.34] K.L.F. Bane, "A Simplified Model of Intrabeam Scattering," SLAC-PUB-9226 (2002).
[3.2.35] T. Raubenheimer, *Part. Accel.* **45**, 111 (1994).
[3.2.36] K. Oide, *SAD User's Guide*.
[3.2.37] A. Streun, "Momentum Acceptance and Touschek lifetime," SLS Note 18/97.
[3.2.38] A. Hofmann and S. Meyers, "Beam Dynamics in a Double RF System," Proc. 11th International Conference on High Energy Accelerators, Geneva (Birkhauser Verlag, Basel, (1980), p 160.
[3.2.39] N. Towne, "Stretched Bunch Shapes in the NSLS VUV Ring," Proc. PAC1999 (1999) 2828.

[3.2.40] J.M. Byrd, S. De Santis, J. Jacob, and V. Serriere, "Transient Beam Loading Effects in Harmonic RF Systems for Light Sources," *Phys. Rev. ST-AB* **5**, 092001 (2002).

3.3 Orbit Feedback System

3.3.1 Requirements for Beam Stability

To realize the benefits of the high brightness and small beam sizes of NSLS-II, it is essential that the photon beams are exceedingly stable, assuring constant intensity after apertures, constant photon energy after monochromators, and minimal photon source size and highly precise steering accuracy for focusing on small samples. For example, in the common case of 1:1 focusing optics, positional stability of the photon beam on the sample is directly related to that of the electron beam. The position of the photon beam should be stable to a level of Δ_y/σ_y ~10%. We require beam motion of no more than 10% of beam size, particularly in the frequency range from ~10 mHz to 100 Hz. This tolerance has been adopted by many synchrotron radiation laboratories. Since the minimum vertical beta function is about 1 m, when we take the vertical emittance as $10^{-10}/4\pi$ m, the vertical beamsize is 2.7 μm RMS. Therefore, the beam position stability should be ~0.3 μm in the short straight section.

3.3.2 Fast Orbit Motion with Feedback Loop On and Off

For the NSLS-II ring with a DBA30 lattice as shown in Figure 3.1.1 (only half a super-period is shown), the performance of a fast, closed-orbit feedback system with 120 BPMs and 120 correction trims was calculated. The BPM and fast corrector positions used in this simulation are shown in Figure 3.3.1. The vacuum chamber at the fast correctors is made of stainless steel.

We averaged over 400 different sets of random numbers for positional deviation of all the quads, assuming they vibrate randomly with uncorrelated RMS displacement of 0.2 μm. The resulting beam RMS motion $\sigma_{\Delta y}$ is shown in blue in Figure 3.3.2. We used 60 out of 120 eigenvectors in this case.

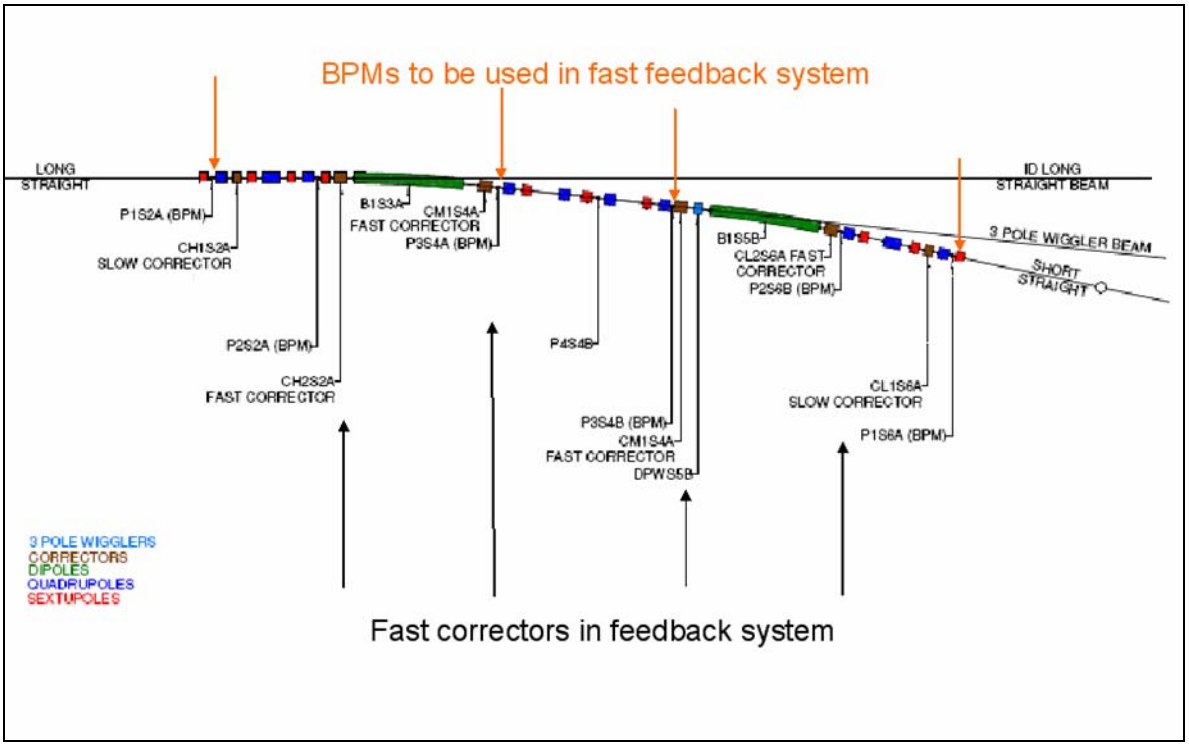

Figure 3.3.1 Positions of BPMs and fast correctors in one cell.

For each set of Gaussian random errors for the quad and BPM vibrations, all with RMS displacement of 0.2 μm, the open-loop BPM signal was calculated assuming BPM electronic noise is 0.2 μm. Then the SVD matrix was used to calculate the corrector strengths, and finally the orbit with the feedback loop closed with a gain of 100. After averaging over 400 random samples, the residual RMS beam motion shown in Figure 3.3.2 was obtained, represented by the red curve. The open-loop BPM signal and the corrector strength used in the feedback loop are marked by dark green and purple dots, respectively.

The height of the purple dots represents the RMS strength of the correctors, in units of μrad. The figure shows that the feedback loop reduces the beam motion at the center of the long straight section (z = 0) from 3 μm to 0.2 μm. The maximum RMS corrector strength is on the order of 0.14 μrad.

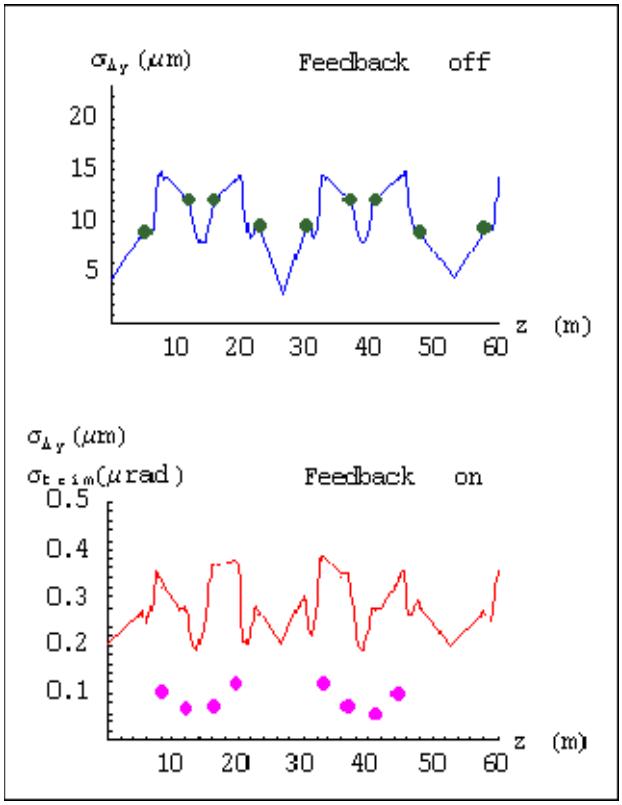

Figure 3.3.2 Open (blue) and closed-loop (red) RMS orbit motion and RMS corrector strengths (purple dots) in the feedback loop. The z- axis is the distance along the ring circumference, in meters. The green dots are the RMS motion at the location of the BPMs in the feedback loop. 60 eigenvalues out of 120 are used in this simulation.

Figure 3.3.3 gives the singular value spectrum for the 4BPM, 4 trims feedback system, indicating the possibility of using 60 eigenvectors, or using 2 trims per cell in vertical plane. Simulations confirmed that both give similar performance.

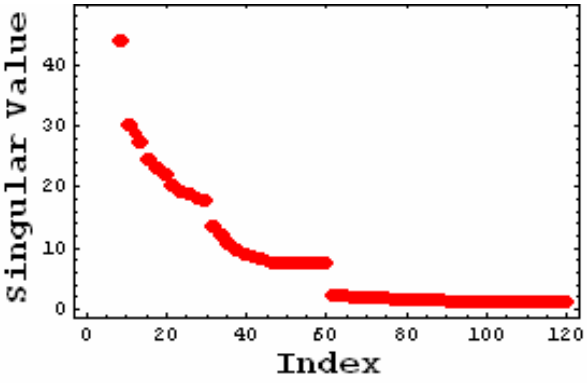

Figure 3.3.3 Singular values for the feedback system with four BPMs and four trims shows that using 60 eigenvectors should have similar performance to using all 120, and this is confirmed by simulation. It also indicates that good performance could be obtained using only two trims per cell (60 eigenvectors).

The tolerance on the floor motion required to keep beam motion within 10% of beamsize was determined using the following assumptions: 1) $\varepsilon_y = 0.1$ nm/4π, 2) all the quads and BPMs mounted on the girders have uncorrelated random vibration of 0.2 μm, and 3) the BPM electronic noise is 0.2 μm. Averaging over 400 samples gave the ratio of the vertical beam motion divided by the RMS beamsize as a function of z in the ring, shown in Figure 3.3.4. At the short straight section, the ratio of beam motion over beamsize is 6.4%. This implies that the tolerance for the quad vibration is more than 0.3 μm RMS. This calculation ignored the fact that for low-frequency ground motion, the movement of different components mounted on the girders can be correlated, since the sound wavelength at low frequency can be larger than the girder dimension. Actually, simulation for correlated movement of quads mounted on the same girder shows a reduced amplification factor, since the quads moving together tend to cancel each other [3.3.1]. The noise caused by ripples in the power supply corrector magnet current was also ignored. Compared with this effect, the orbit motion due to the vibration of BPMs is much more difficult to suppress. Actually, it is very difficult to reduce the beam motion to much less than the amplitude of the BPM vibration. Similar calculations for horizontal orbit show that if quads and BPMs have random vibration of RMS value 0.2 μm and BPM noise is 0.2 μm, the residual RMS value of beam motion is 0.14 μm at the straight sections. Since the horizontal beam size is much larger than the vertical beam size, the horizontal requirement is much easier to satisfy than the vertical.

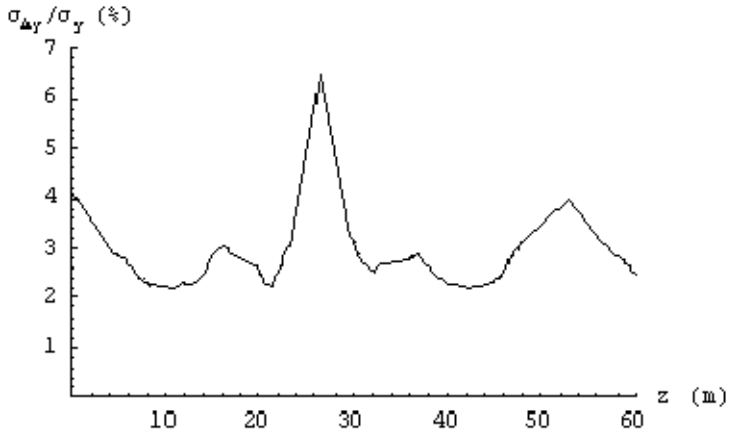

Figure 3.3.4 Closed-loop orbit deviation normalized by beam size assuming magnets random motion of 0.2 μm.

The beam motion due to power supply noise in a digital feedback system is determined by the voltage corresponding to the last bit of the power supply and the power supply current noise itself [3.3.1, 3.3.2]. Similar to the vibration simulation, we find that if we require beam motion (due to trim noise at the beam waist where $\beta_y = 1.26$ m) to be less than 0.1 μm, the RMS trim noise should be less than 4 nrad. Hence the power supply should be accurate to 4 n-rad/0.29 = 12 nrad. If the maximum trim strength is 1 mrad, we need the last digit to be less than 12 ppm and the RMS noise should be less than 4 ppm.

3.3.3 Ground Movement at the NSLS-II Site

Figure 3.3.5 shows floor vibration measurement in January 2007 at three locations: CFN, field near CFN future NSLS-II site, and NSLS beamline. This data show that due to cultural activity the noise level is higher at the current NSLS site than CFN center and the field where the future NSLS-II is located. It shows that with improved floor design and construction, the vibration noise is much lower. In Figure 3.3.6, the inverse integrated PSD of floor vibration measurement at UV ring floor near entrance using seismic sensor shows RMS vibration amplitude within bandwidth from 0.5 Hz-100 Hz is less than 0.1μm. Since the sound speed in concrete is 3 km/s, below 0.5 Hz, the ratio of sound wavelength over the storage ring diameter is sufficiently large that the effect of the vibration below 0.5 Hz is not critical.

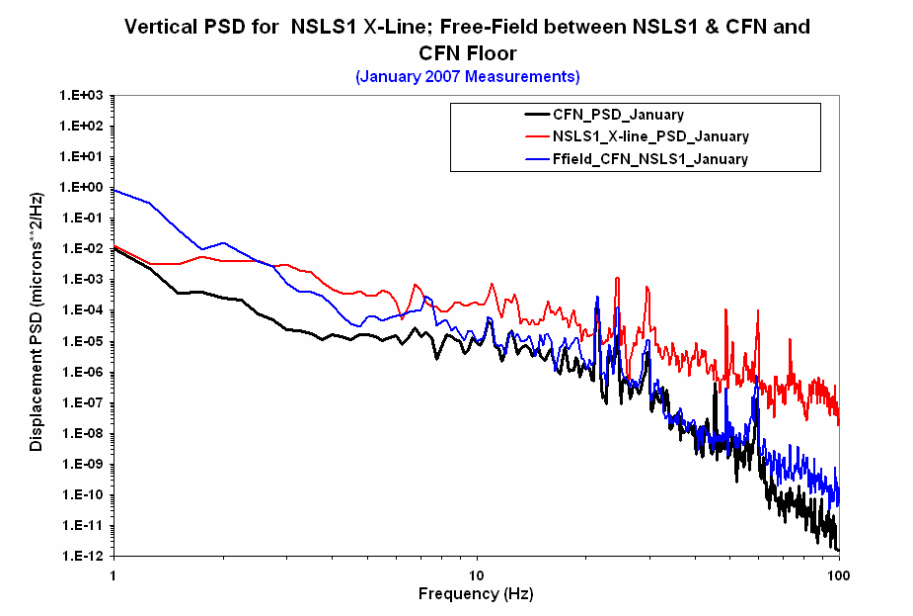

Figure 3.3.5 Floor vibration measurement at three locations: CFN, field near CFN future NSLS-II site, and NSLS beamline X1.

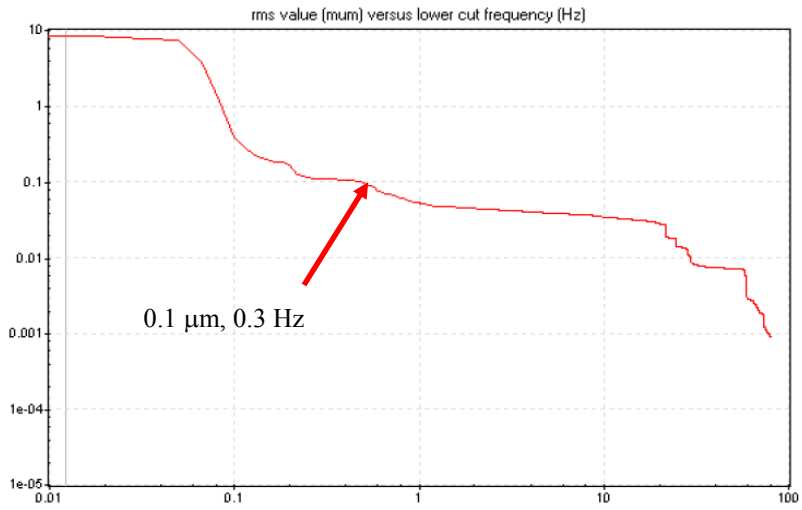

Figure 3.3.6 Inverse integrated PSD of floor vibration measurement at UV ring floor near entrance using seismic sensor showing RMS vibration amplitude within bandwidth from 0.5 Hz-100 Hz is less than 0.1 μm.

3.3.3.1 Long-Term Ground Movement

As for long-term ground movement at the BNL site, measurements carried out at RHIC between 1997 and 2002 show the coefficient A in the ATL law is $A \cong 3\times10^{-18}$ $m^2/m/s$ [3.3.4, 3.3.5]. Based on this, we estimate that the RMS movement within the 252 m diameter of NSLS-II over a half-year is about 110 μm.

We simulated the performance of the slow feedback system on long-term ground motion using the ATL law [3.3.6] at the NSLS-II site over a half year, with the same set of BPMs and correctors as mentioned in Section 3.3.2. The results are shown in Figure 3.3.7. In this specific example, the maximum ground movement was 107 μm, with an RMS value of 36 μm. The maximum relative movement between the beam and the ground was about 700 μm without feedback; with feedback, it was 48 μm with an RMS value of about 10 μm.

We averaged over 400 samples. The RMS residual movement has a mean value of 9.3 μm. This is over half a year. When we scaled according to the ATL law, the residual RMS movement within a day should be reduced to about 0.7 μm.

If the orbit is realigned every six months, then within that half year the required corrector strength for the global orbit correction is about 0.1 mrad. To leave a margin for error, the maximum strength of the corrector is specified to be 0.5 to 1 mrad. As shown in Section 3.3.2, this requires the last bit of the power supply to be 30 ppm.

3.3.3.2 Temperature Stability

As we discussed in Section 3.3.2, the most stringent requirement on orbit stability is in the 6.6 m straight sections, where the BPM motion is required to be less than 0.2 μm (see Figure 3.3.4). Due to thermal expansion of the girder and vacuum chamber support system, the air temperature stability in the storage ring tunnel is specified to be ±0.1ºC. We specify that the BPMs will move less than ±0.2 μm. To insure that in the short straight sections the orbit motion satisfy the stability requirement, we specify the BPMs at the ends of insertion devices in 6.6 m straight sections move less than ±0.1 μm with specially designed BPM supports. Our simulation shows that when those BPMs in the short straight sections move less than others, the feedback system also insure the orbit motion in those sections less than other sections correspondingly.

Feedback Loop Off

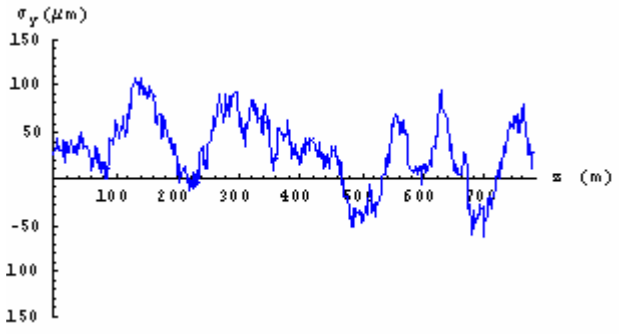

Floor motion around the ring. While the RMS of the relative displacement across the ring diameter for a large number of examples is 110 μm, in this specific example the maximum movement is 107 μm, and the RMS around the ring is 36 μm.

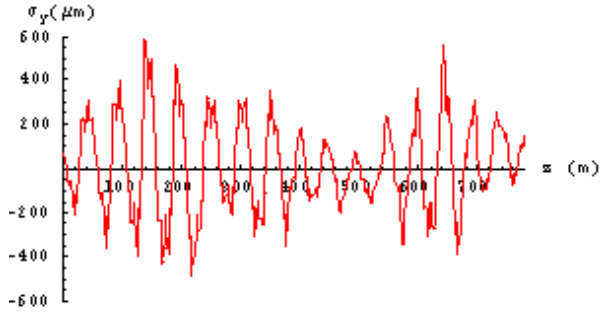

Electron beam motion (vertical) without feedback loop; maximum is 600 μm.

Feedback Loop On

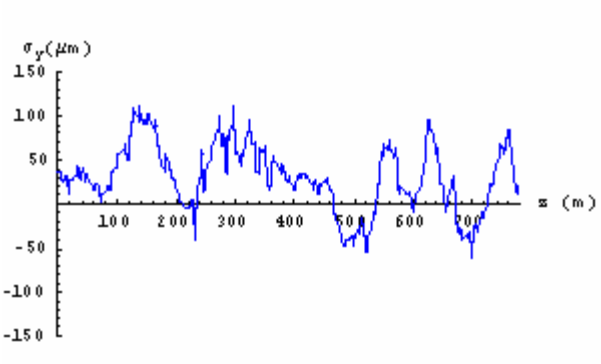

Electron beam motion with the feedback loop on follows the floor motion approximately.

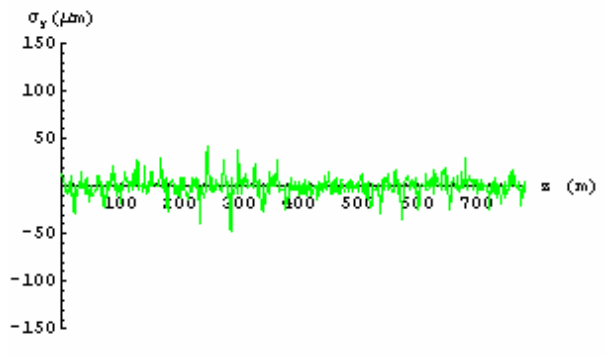

Electron beam motion relative to floor (the difference between the two plots on the left) with the feedback loop on; maximum is 48 μm, RMS 10 μm.

Figure 3.3.7 Simulated long-term ground motion and electron beam motion within half a year, with feedback system on and off. The horizontal axis is the distance along the circumference.

3.3.4 BPM Resolution and Noise Floor

A power density spectrum plot of measurement of orbit motion at NSLS using an RF BPM is reported in Figure 3.3.8, with beam motion shown in blue and the noise floor of the BPM in red. The plot shows that above 200 Hz, the beam motion is dominated by the noise floor. Hence, a feedback system with frequency higher than 200 Hz will not improve the orbit stability. The feedback system based on our BPM should have a cut-off point set below 200 Hz. Measurements at NSLS show that the vibration amplitude between 50 Hz and 200 Hz is less than 10 nm, which is negligibly small. Therefore, to relax the requirement on the feedback system bandwidth, the cut-off point is set at 60 Hz. A long-term drift test of the BPM offset is still needed, to show it is sufficiently small (lower than 0.2 μm). BPMs with better performance are available, and work in developing better BPMs is needed.

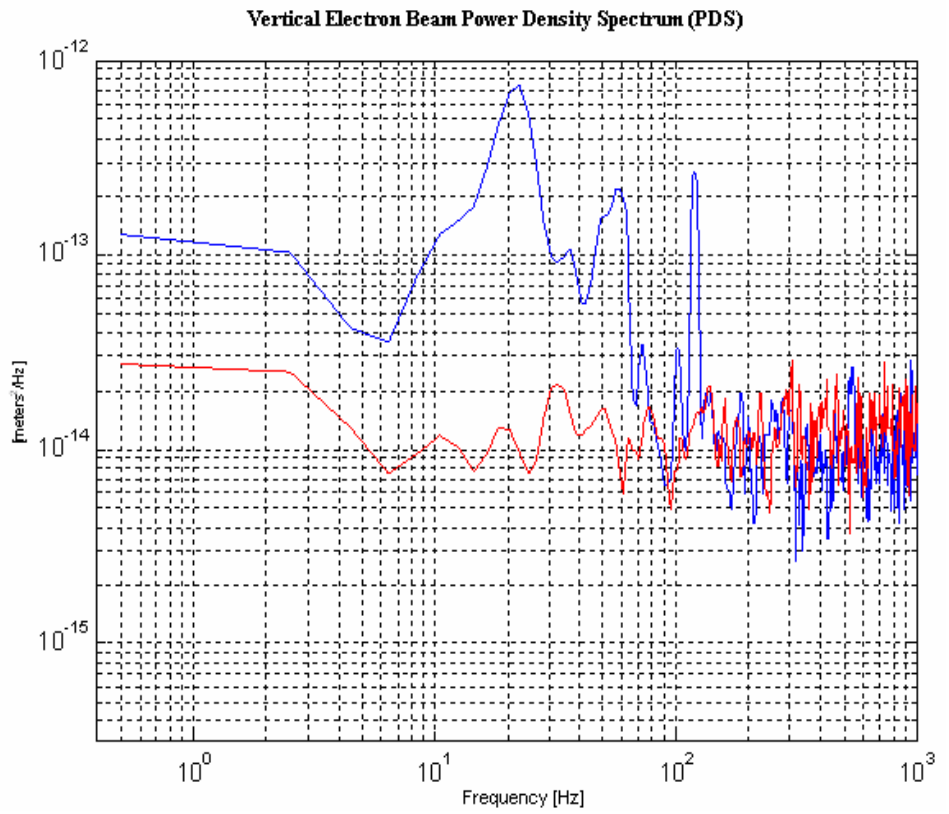

Figure 3.3.8 Power density spectrum of beam motion.

3.3.5 Requirements for the Feedback System

Based on these considerations, the ground vibration of 0.2 μm above 0.5 Hz satisfies the 0.3 μm requirement determined by the feedback system performance calculation presented in Section 3.3.2. However, the BPM motion caused by thermal expansion poses the most stringent requirement on the temperature stability, we require the ring tunnel temperature stability to be within ±0.1°C, and the BPM supports are designed such that they move less than ±0.2 μm within ±0.1°C. In particular the BPM supports at the ends of the insertion devices in the 6.6 m sections are designed to move less than ±0.1 μm within ±0.1°C.

As mentioned in Section 3.3.4, the measured beam motion coincides with the BPM noise floor for frequencies higher than 200 Hz (see Figure 3.3.8). In addition, since most of the motion comes below 60 Hz, it is desirable to design the feedback system PID circuit to reach a 60 Hz bandwidth.

Because eddy currents are proportional to the thickness and electrical conductivity of materials, only thin laminations (1 mm thickness) or air coils should be used for correctors and the low-conductive materials preferred for vacuum chambers. Eddy currents in vacuum chambers usually impose the most critical bandwidth limitation on the feedback loop [3.3.1].

When designing the feedback system bandwidth, it is crucially important to design the vacuum chamber and power supplies for all the correctors to be used in the fast global feedback system such that they have the same frequency response. Without excellent equalization, we may be forced to narrow the bandwidth of the feedback system or lower the gain of the system.

To maintain the dynamical aperture regardless of long-term ground movement requires the beam to stay within 50 μm of the center of the sextupoles. According to the simulation based on the ATL law, described in Section 3.3.2, if the ring is regularly realigned, this can be achieved. RF frequency will also be used as an additional corrector to compensate for energy drifts.

References

[3.3.1] M. Borg, PAC ’01, talk on IWBS’02, and EPAC 04 paper.
[3.3.2] J. A. Carwardine and F. R. Lenkszus, “Real-Time Orbit Feedback at the APS,” p.12, 1997 beam instrumentation workshop at SSRL.
[3.3.3] Heiko Ehrlichmann, private communication (2/2006).
[3.3.4] Vladimir Shiltsev, “Space-Time Ground Diffusion: The ATL Law for Accelerators,” DESY-MPY, Notkestrasse 85, 22603 Hamburg, Germany.
[3.3.5] Vadim Ptitsyn, private communication (7/2004).
[3.3.6] A. Walski, and N.J. Walker, Proceedings of 2003 PAC.

3.4 Canting and Decker Distortion for the NSLS-II

Canting and Decker distortion are similar in that they both require additional trim dipoles placed in the ID straight. In both cases the dispersion must be constrained in the cell. Furthermore, the sum of the additional bend angles must be zero to ensure the beam orbit stays on the center of the multipole magnets. Therefore there are three constraints at the end of the bump:

$$\begin{cases} \eta = 0 \\ \eta' = 0 \\ \sum \theta = 0 \end{cases} . \tag{3.4.1}$$

It requires three independent knobs to satisfy these constraints. In addition, we require that the perturbation to the linear lattice must be small.

Decker distortion has proven effective in reducing the stray background radiation for the photon BPMs at the Advanced Light Source [3.4.1]. Even though the stability of the photon beam is directly related to that of the electron beam circulating in the storage ring, it is also affected by other factors, such as the electron trajectory in the insertion devices. Moreover, the long beamline amplifies small jitter of the electron beam. Hence including photon BPMs to the feedback loops helps keep the photon beam stable.

The characteristic radiation angle from the NSLS-II storage ring dipole is $1/\gamma$~0.17 mr; the dipole kick from the strongest quadrupole is about one milliradian if the beam is offset by 2 mm; therefore the distortion angle is determined to be 1~2 mr.

At APS, Decker distortion was implemented after the storage ring and the beam lines were built. In their case, moving the magnet girders was easier than moving the straights and the beam lines. Their approach was to add two trims to the front and the end of a cell and then move the entire cell except the straight section. For NSLS-II, we looked at other possible options, since we can design from the beginning. Instead of moving a cell, we found it is convenient to offset the ID straight with two trims and vary the cell magnets to fulfill the constraints. The diagram is shown in Figure 3.4.1. One can vary B1, B2, the main bending magnets, M1, the trim in the straight, and all the quadrupoles to form a dispersion bump. The downstream cell is reflection symmetric to the upstream one. We examined two solutions: in the first solution we vary only the dipoles and the trims; and in the second solution we also adjust the quadrupoles, but the field in only one main dipole is changed.

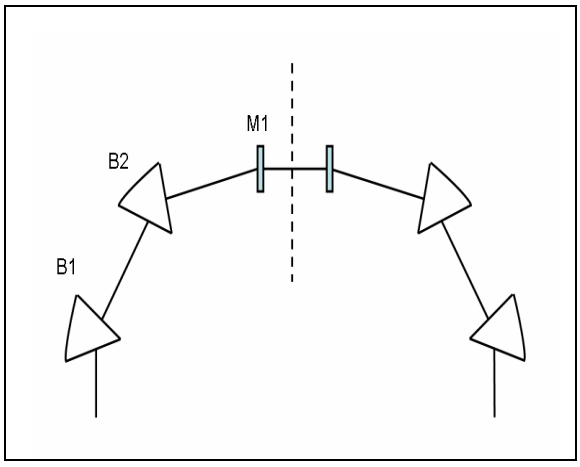

Figure 3.4.1 Diagram of Decker distortion proposed for NSLS-II.

Figure 3.4.2 shows the first solution of Decker distortion for the NSLS II lattice. In this solution only the dipoles are varied. The bend angle adjustment in the dipoles and the trim is: $\Delta\beta_1$ = –1.727 mr, $\Delta\beta_2$ = 0.727 mr and M_1=1 mr. The quadrupole settings are not changed therefore the beta functions, the emittance and the tunes are kept the same. The dispersion in the long straight is constrained to zero. The dispersion departs from zero in the short ID straight an has the value 5 mm. Because of the symmetry and emittance constraints, the effect on the beam size and the emittance growth is negligible.

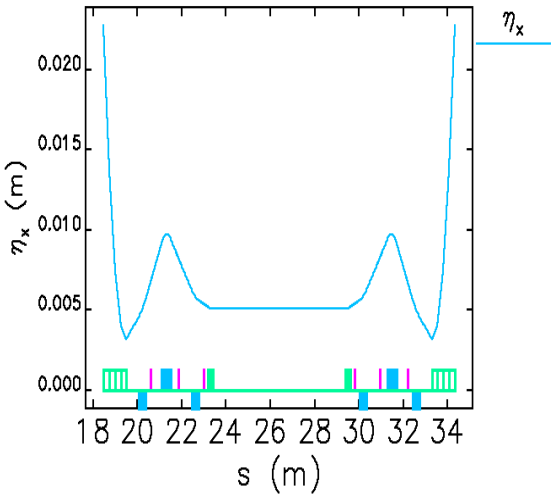

Figure 3.4.2 Dispersion function in the dipole-only solution.

The second solution with variation of quadrupoles is shown in Figure 3.4.3. In this solution there is no need to change B_1. The parameters are: $\Delta\beta_1$ = 0 mr, $\Delta\beta_2$ = -1 mr, and M_1 = 1 mr. The relative quadrupole strength changes are small, $|\Delta K_1 / K_1| \leq 0.015$. The dispersion in the long straight is zero and it is about 0.3 mm in the short straight. This scheme has an advantage in that the girder between the two main dipoles does not have to be moved.

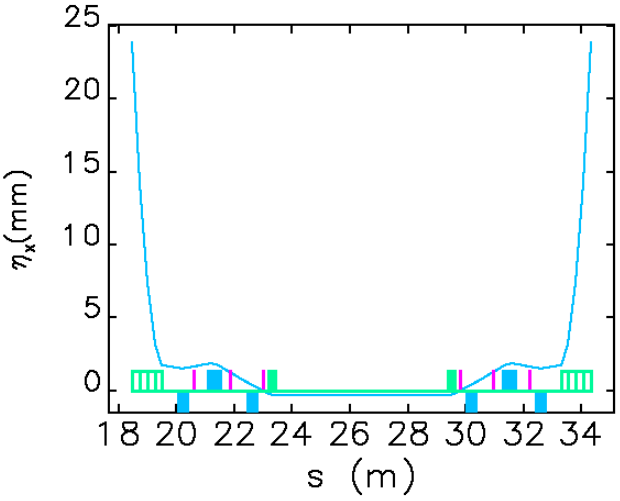

Figure 3.4.3 The second solution: varying $\Delta\beta_2$ and the quadrupoles.

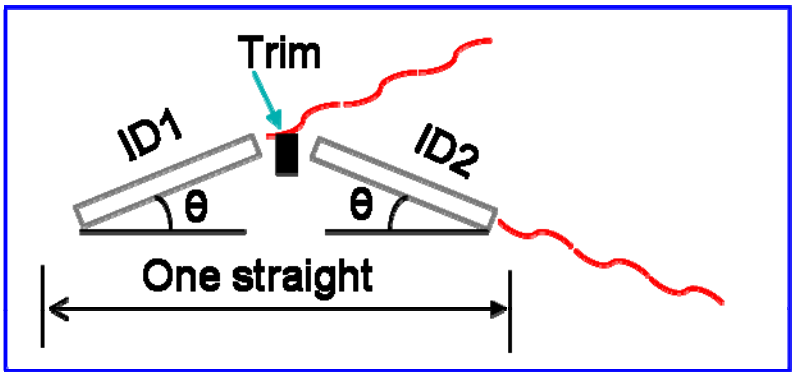

Figure 3.4.4 Diagram of canting.

The idea of canting is to split the radiation from one straight into two beam lines as is diagrammed in Figure 3.4.4. However, this also introduces external dispersion and the damping wigglers excite quantum fluctuations. The emittance growth is proportional to the dispersion invariant $H = \gamma\eta^2 + 2\alpha\eta\eta' + \beta\eta'^2$. It can be shown that if the dispersion function at the center of the straight is much less than $\beta_c\theta$, where θ is half of the canting angle; i.e., if

$$\eta_c << \beta_c\theta, \tag{3.4.2}$$

then the dispersion invariant is minimized, and

$$H_{\min} \approx \beta_c\theta^2. \tag{3.4.3}$$

Therefore the emittance growth is proportional to the center beta function and square of the canting angle.

At commissioning, NSLS-II will have three 7 meter-long damping wigglers. The relevant parameters are β_w=1.8 T, λ_w=9 cmT, cm. One calculates the opening angle to be 2θ=2.6 mr. It has been decided the maximum canting angle is 3.5 mr. With the minimized $H_{\min}$, the emittance growth is calculated as a function of the number of canted damping wigglers. The results are listed.4.1.

Table 3.4.1 Emittance Growth Due To 3.5 mr Canting.

	None canted	All canted	Growth factor
Emittance(nm)(21m)	0.9	0.96	1.068
Emittance(nm)(35m)	0.67	0.74	1.11
Emittance(nm)(56m)	0.51	0.59	1.16

The emittance growth for the baseline is only about 7% even if all three damping wigglers are canted. The emittance is less than 1 nm, which meets our design goal. Note the momentum spread is not affected by canting.

There are several choices to bend the electron orbit. A straightforward solution would be putting three trims in the straight. Such a solution is shown in Figure 3.4.5. The disadvantage of this solution is that 0.3~ 0.4 meters is needed for each trim; therefore the usable space for the insertion device is shortened.

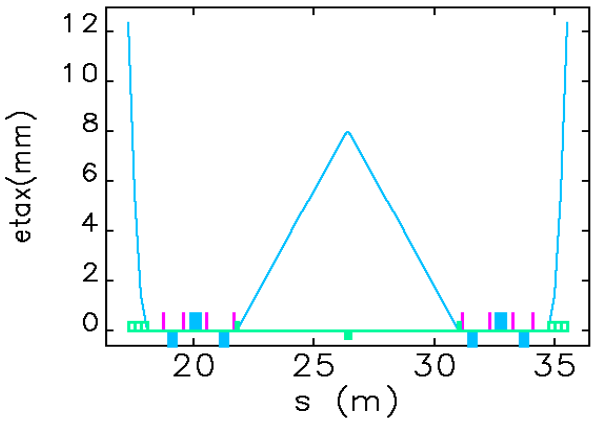

Figure 3.4.5 A straightforward solution for canting. Three trims are put in the straight as -2, 4,and -2 mr. The maximum dispersion is 8 mm.

The second option is to put only one trim in the center of the straight and vary the main dipoles and quadrupoles to satisfy the three constraints. A solution is shown in Figure 3.4.6. Note the negative dispersion in the center. This is because the dispersion invariant is minimized.

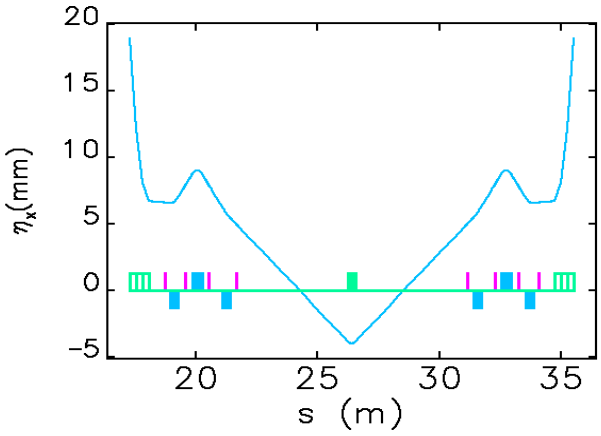

Figure 3.4.6 A solution of canting the damping wigglers. The angles or the changes are: $\Delta\beta_2 = -M_1 = -1.926$ mr. The quadrupole setting changes are
$|\Delta K_1 / K_1| < 0.01$.

A third option would be to make special poles for the damping wigglers. One pole of the damping wiggler gives about 4 mr bending to the beam. If the end poles can be made longer, then the damping wiggler itself can bend the beam. This approach looks feasible and can save both space and cost on the magnets and power supplies.

References

[3.4.1] G. Decker and O. Singh, Phys. Rev. ST Accel. Beams 2, 112801 (1999).

3.5 Extra-Long Straights

The lengths of the normal short and long straight sections at the NSLS-II are 6.6 m and 9.3 m, respectively. Some experiments, e.g., inelastic scattering experiments, would benefit from long insertion devices with length as great as 10~12 m. Such long insertion devices require extra-long straights of 12~15 meters.

A straightforward way to create such long straights is to make a few special cells; however, this approach reduces the symmetry of the lattice to the number of the longer straights and affects the dynamic aperture of the beam. In order to restore the symmetry, Hara et al. proposed a 2π transformer scheme[1]. The idea is to make the betatron phase advance a multiple of 2Π for the two matching cells and the extra-long straight; therefore the symmetry is restored. Note the periodicity number is two units less because of the excluding of the two matching cells. This idea was successfully implemented at SPring-8 in the year 2000. Four 27 m long straights were created this way.

Another issue for extra-long straights is that the vertical gap of the insertion device imposes a limiting physical aperture on the storage ring. Note the beta function in the straight is given by

$$\beta(s) = \beta_c[1 + (\frac{s}{\beta_c})^2], \tag{3.5.1}$$

where β_c is the beta function at the center of the straight.

The present physical aperture of NSLS-II is limited by the ± 2.5 mm gap of the in-vacuum undulator. In order not to diminish the physical aperture, the gap of the long undulator has to satisfy

$$h \geq 2.5\sqrt{\frac{\beta_s(L/2)}{\beta_L(L/2)}}, \tag{3.5.2}$$

where β_S and β_L are the beta functions at the ends of the IDs in the short straight and the extra-long straight. Varying β_c to maximize the aperture, one gets

$$h \geq 2.5\sqrt{\frac{L_U}{L_L}}, \tag{3.5.3}$$

where L_U and L_L are the lengths of in-vacuum undulator and the long undulator. Therefore, if the gap remains the same, an ID that is four times longer would reduce the physical aperture by two-fold. And it will be even worse if β_c is minimized for the purpose of higher brightness.

To focus the beta functions to small values while maintaining the physical aperture, quadrupole magnets can be added to the long straight to create segments. The quadrupoles are also helpful for matching the phase advance inside the long straight. Suppose the betatron phase advance of a normal straight is $\Delta\Psi$; if the phase advance of the segmented extra-long straight is $2\Pi+\Delta\Psi$, then the extra-long straight is the same as a normal straight, from the symmetry point of view.

One can show that the betatron phase advance in a magnet-free section is less than Π. Hence, to obtain 2Π phase advance, a minimum of three sections are needed. To get a better understanding of the problem, we designed a solution for NSLS-II; the beta functions are plotted in Figure 3.5.1.

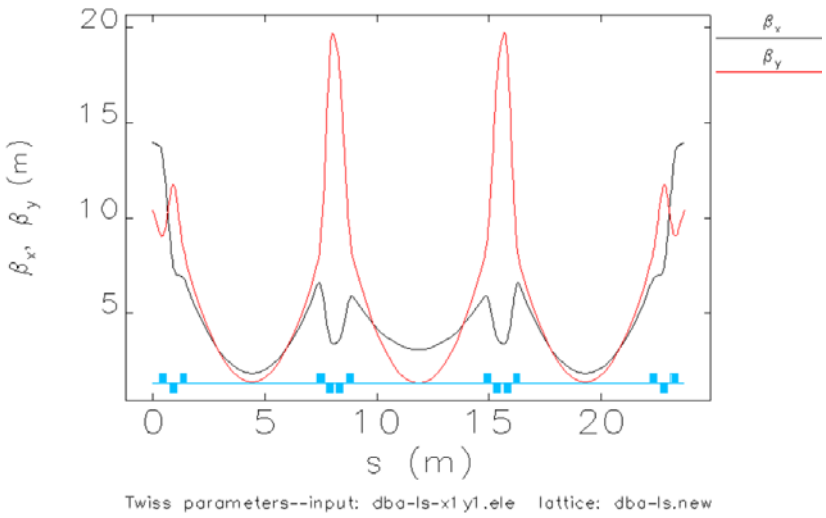

Figure 3.5.1 A segmented extra-long straight solution for NSLS-II. It starts from the last magnet in the long straight of a normal cell. The total length is 23.7 m with three equal-length straights of 5.83 m each. The generated chromaticity is $\Delta\zeta_x = -1.04$ and $\Delta\zeta_y = -3.01$. The beta functions at the center of the sections are β_x / β_y =1.8/1.4, 3.0/1.3, and 1.8/1.4 m.

Because dispersion is zero everywhere in the extra-long straights, the generated chromaticity has to be corrected by the sextupoles in the other cells. Therefore the chromaticity in every cell cannot be corrected to zero. Because of this, the extra-long straight is not transparent to the off-momentum particles. One can show that if n extra-long straights are inserted into an m-period storage ring, then the ring is n<m fold symmetric for the off-momentum particles.

Proper selection of the working point and careful elimination of the higher-order terms might restore the dynamic aperture. However, the impact of extra-long straights on the stability of the dynamic aperture of off-momentum particles could not be studied in sufficient detail before the decision on the NSLS-II footprint could be made. Furthermore, there are issues, such as the deposition of high synchrotron radiation power on the extra-long undulator beam pipes. For this reason, an alternative approach to extra-long straights is envisioned, which could be implemented into the footprint of NSLS-II.

This idea is illustrated in Figure 3.5.2. Two cells are moved aside, converting the middle straight into an extra-long straight, the maximum length of which is about 18 m for the present lattice.

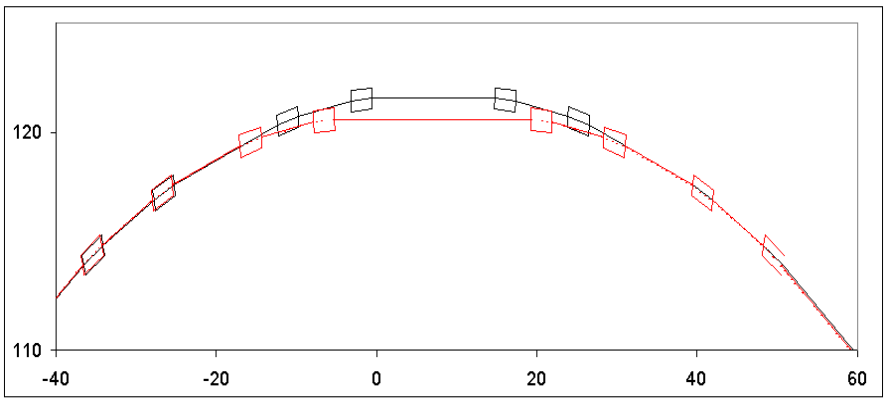

Figure 3.5.2 Moving the cells to create an extra long straight.

This scheme would allow compensation of the chromaticity and nonlinear terms in the moved cells, and they can be transparent to the off-momentum particles if all the relevant higher-order terms are eliminated. The impact of such an insert on dynamic aperture is under study.

[3.5-1] M. Hara, T. Nakamura, T. Takada, and H. Tanaka, "Use of long straight sections of SPring-8," Rev. Sci. Instrum. 63 (1), p.355, 1992.

4 STORAGE RING SYSTEM

4.1 Storage Ring Magnets

4.1.1 Parameters and Tolerances

The DBA lattice (30 cells with a super periodicity of 15) consists of 60 dipole magnets with uniform magnetic field and a maximum field of 4 kiloGauss at 3.0 GeV. The ring quadrupoles consist of a total of 300 magnets with two different lengths: 25 and 40 cm. These quadrupoles have a maximum gradient strength of 22 T/m at 3.0 GeV. The quadrupoles are individually powered, but the current lattice design assumes eight families. There are also 300 sextupoles magnets with two different lengths: 20 and 25 cm. These magnets, together with the correction magnets and BPMs, are listed in Section 6.1.1 and in Table 6.1.4.

4.1.2 Preliminary Magnet Design

4.1.2.1 Storage Ring Lattice Magnet Considerations

The magnet lattice is designed with a 30-cell DBA (double bend achromat) structure for a machine with 3.0 GeV full-energy top-off injection. The 792 m storage ring will contain more than 900 magnets. This quantity is comprised of 60 bending dipoles, 300 quadrupoles, 300 sextupole magnets, and 242 corrector magnets. To ensure acceptable dynamic aperture for the electron beam, the required magnetic field quality and alignment tolerances are the two primary considerations in the design. All the dipole magnets are connected in series and are energized by a single power supply. Individual trim power supplies will be used to provide ±3% field adjustment. All quadrupoles will be individually powered and the sextupoles will be powered in nine families. Properties of the storage ring magnets are summarized in Table 4.1.1.

Table 4.1.1 Storage Ring Magnet Specifications at 3.0 GeV.

	Dipole					
	35 mm	90 mm	Quadrupole	Sextupole	Corrector	ID Corrector
Bending angle [deg]	6	6	0	0	±0.08	±0.01
Max. Clear bore aperture [mm]	35	90	66	68	150/100	35/80
Max. Dipole field [T]	0.4	0.4	0	0	0.04	**0.01
Field gradient [T/m]	0	0	22	0	*0.36	0
Max. Sextupole field [T/m^2]	0	0	0	500	0	0
Field quality in GFR - 20 x 40 [mm]	$1x10^{-4}$	$1x10^{-4}$	$2x10^{-4}$	$5x10^{-4}$	$1x10^{-3}$	$1x10^{-2}$
Nominal operating current [A]	360	360	108	190	20	20
Cooling type	water	water	water	water	air	air
Maximum temperature rise [°C]	10	10	10	10	20	20

*Skew quadrupole component, 30 each required

** at 100 Hz

In this section, we present designs of the individual magnets. Optimization and refinements will occur during the next phase of detailed design.

The following paragraphs in this section present a partial list of lattice magnet design considerations. For the preliminary design, these considerations are global in nature and will evolve into specific design parameters for the next phase of "reference" design.

- The average current density in the coil cross-section of the storage ring magnets was selected to be less than or equal to 2 A/mm^2, with typical current densities in the copper conductor of 3.5 to 4.5 A/mm^2.
- The temperature rise of cooling water across any magnet coil will be limited to about 10ºC, with a pressure drop across each magnet of less than 4 bar.
- The magnetic alignment requirements of the multipoles exceed tolerances achievable by the normal optical survey method. Therefore, these magnets are aligned magnetically and then fixed to a rigid girder for installation in the storage ring tunnel.
- The storage ring magnet reference designs are being developed to minimize fabrication costs, provide high operational reliability, and minimize the power consumption by individual components as well as overall magnet systems.
- The magnet supports are designed so as to reduce vibration amplification by maintaining the resonance frequency of the multipole support assembly above that of the girder.
- The reference design will address a low-cost yet reliable means to integrate the multipole magnets into a vibrating wire magnet-to-magnet alignment system and a means to transfer magnetic field center locations precisely to survey targets on the magnet girder.
- Handling and rigging safety issues for magnet testing and installation will be addressed, and the reference design will comply with BNL's Critical Lift Policy.
- Electrical and all other safety issues will be addressed in the next phase of detailed design. The design of the magnets, the power cabling, and the water cooling from the magnet-to-cable connections on the girders, as well as magnet instrumentation and controls, will be fully NEC and OSHA compliant.
- Magnetic lengths were optimized and drift space between the multipoles was increased to accommodate beam position monitors (BPMs) and corrector magnets without altering the lattice.
- Electrical, magnetic, and mechanical design optimization will be performed for the reference design of the relatively low-field-strength 0.4 T dipole magnet to assure high field quality requirements for the C-type magnet cross-section.
- Extensive 3D modeling and value engineering optimization is being performed for both the 22 T/m maximum quadrupole strength and the 500 T/m^2 maximum sextupole strength. The goals are to 1) assure high field quality and extremely critical alignment requirements for both multipoles, 2) accommodate the synchrotron's x-ray extraction lines and the vacuum chamber, and 3) minimize or eliminate the effects of crosstalk between neighboring magnets and correctors.

These preliminary designs and considerations will be refined by both the Laboratory and Industrial resources during the next phase of design, resulting in a "reference" design. The final magnet design will be developed by the magnet manufacturer, and reviewed and approved by the Laboratory prior to production. Extensive 2D and 3D magnetic modeling, mechanical design, and fabrication and assembly methods have been studied, resulting in the preliminary magnet designs that are described in the following sections.

4.1.2.2 Dipole Magnet Preliminary Design

4.1.2.2.1 Scope and Physics Design Parameters

A unique attribute of NSLS-II is the use of dipole magnets with apertures of two different sizes. This requirement is necessary to accommodate a significant and growing community of users who require lower

energy infrared and THz radiation. To serve this important community, a 90 mm aperture concept has been chosen, to allow the extraction of long-wavelength light from the dipole magnet [4.1.1, 4.1.2].

The NSLS-II storage ring will be equipped with six dipole magnets that have a gap of 90 mm, and 54 dipoles that have a gap of 35 mm. Each dipole will have a magnetic length of 2.62 m with a field 0.4 T at an electron energy of 3.0 GeV. The radius of curvature of the bending magnet is 25 m; it bends the electron beam 6.0° with a sagitta of 35 mm. The dipole magnets are C-type with a curved laminated flux return yoke (Figure 4.1.2).

A new extended pole ("nose") design (Figure 4.1.3) releases a significant amount of physical space (~190 mm per magnet) and minimizes the challenges associated with a tight lattice. In most iron-dominated magnets, the magnetic length is larger than the yoke length but smaller than the coil length. The proposed NSLS-II design takes advantage of the fact that the nominal operating field of 0.4 Tesla is well below iron saturation. This allows the axial length of the iron pole to become as long as the coil length, thus making the magnetic length longer than the coil length. The proposed design makes the magnetic length larger than both the yoke length and the magnet mechanical length (including ends of the coil). The width of the iron pole is 100 mm.

Calculations of the magnetic field were made to optimize the pole contours and the quality of the magnetic field, which for a dipole magnet must have field non-homogeneity of $\Delta B/B \leq \pm 0.01\%$ over a good-field region of 40 x 20 mm (Figure 4.1.2). All computed field harmonics in the entire range of operation (up to 0.48 T) are well below one part in 10^4 at 10 mm radius.

Investigations of beam dynamics have established that the good-field region accommodates the dynamic aperture. A list of the preliminary design dipole parameters is found in Table 4.1.2.

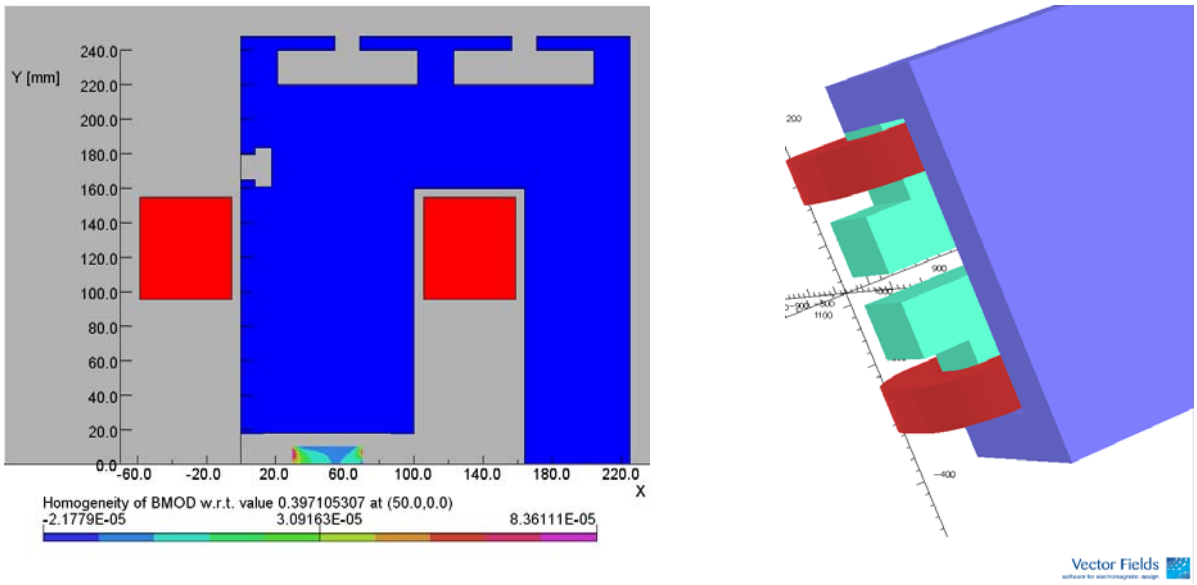

Figure 4.1.2 Magnetic model of the Ring Dipole. 2D model with relative field errors in good field aperture is shown on the left and 3D model with extended pole (nose) on the right. The proposed design makes the magnetic length of the magnet longer than the mechanical length (including coil ends), and frees significant space in a tight lattice.

The storage ring dipoles are designed so that both aperture magnets may be connected in series with a single power supply. Implementation of Decker distortion and minor differences between the two aperture magnets shall be corrected by independently powered trim coils located on each dipole The six large aperture

dipoles will be installed into the storage ring in pairs. Each pair shall comprise the adjacent bending magnets in a single cell, and there will be three cells equally distributed around the storage ring.

Table 4.1.2 Dipole Magnet Preliminary Baseline Design Parameters.

	35 mm Storage Ring Dipole	90 mm Storage Ring Dipole
Energy [GeV]	3.0	3.0
Bending angle [deg]	6	6
Clear bore aperture [mm]	35	90
Dipole field [T]	0.4	0.4
Field quality	$1x10^{-4}$	$1x10^{-4}$
Good-field region [mm]	40 x 20	40 x 20
Magnetic length [mm]	2,620	2,620
Nominal operating current [A]	360	360
Number of Ampere-turns	11,520	30,240
Number of turns / magnet	32	84
Total Inductance of the magnet [mH]	16	116
Current density in conductor [A/mm^2]	3.7	3.7
Max. temperature rise [°C]	10	10
Max. pressure drop [bar]	4.0	4.0
Voltage/magnet	11.4	32
Nom. power per magnet [kW]	4.2	11.5
Iron length Extended Pole/Return Yoke [mm]	2,585/2,415	2,530
Lamination thickness [mm]	1.5	1.5

4.1.2.2.2 Mechanical Design of the Dipole

Fabrication and assembly concepts have been studied, resulting in the preliminary magnet designs that are shown in Figures 4.1.3 and 4.1.4. The laminated magnet yokes are composed of 1.5 mm-thick dry film epoxy-coated AISI 1006 low-carbon steel sheet. The permeability of the core material deviates by about 5% from the production value. The laminations must be shuffled to ensure a uniform magnetic property. The 35 mm dipole will have a self-supporting yoke assembly.

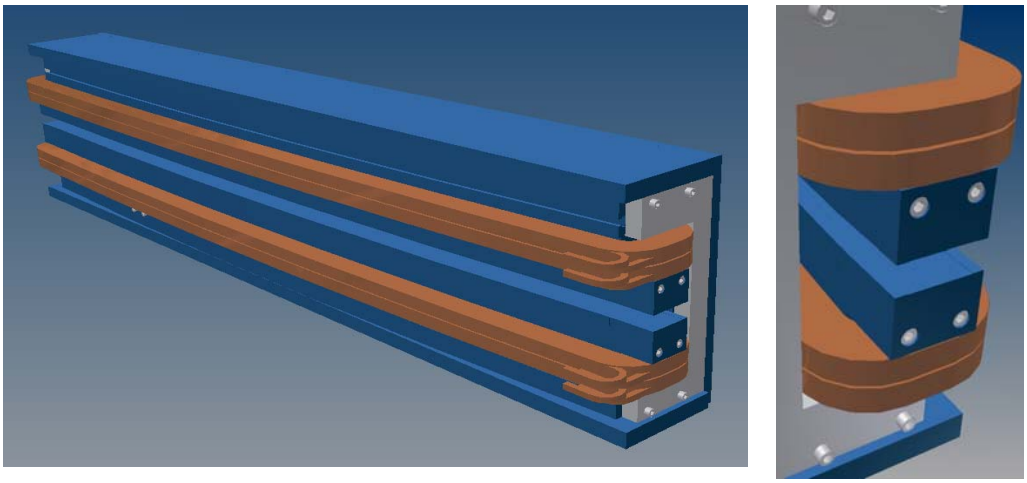

Figure 4.1.3 Views of the 35 mm storage ring dipole , with close-up of novel nose ends pinned and bolted in place.

A precision stacking fixture will be used to register all the laminations to the magnet gap. The base of the fixture will be curved to generate the 25 m nominal core radius. The dipole laminations will be stacked in parallel, and straight tie bars will be inserted through clearance slots in the laminations. Prefabricated end packs will be added to either end of the yoke assembly. The tie bars are tensioned and the yoke assembly is cured. Straight steel stiffening plates are bolted together around the top, bottom, and back of the curved laminated core. The stiffener plates are then welded to the core to form a rigid yoke assembly. The dipole end packs will be tapped and pinned in preparation for adding the nose piece.

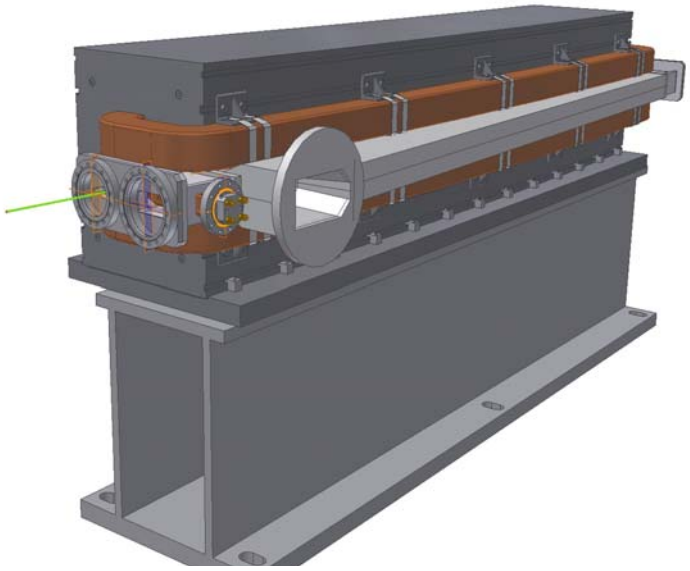

Figure 4.1.4 The 90 mm aperture dipole design concept with an IR beam extraction vacuum chamber installed.

The coils for the 35 mm dipoles are made up of square hollow copper conductors, 13 x 13 mm, with an interior diameter of 9 mm. The coils for the 90 mm dipoles are made of the same rectangular hollow copper conductors. The water channels of the hollow conductor coil "pancakes" are connected in parallel to provide cooling adequate to restrict the increase in coil temperature to less than 10°C, and in the case of the 90 mm dipoles, to reduce pressure drop in the seven-turn, six-layer coils.

Fiberglass that is vacuum impregnated with highly radiation-resistant epoxy greater than 1.0 mm thick will provide interstitial conductor insulation. An additional 1.5 mm (minimum) of vacuum-impregnated epoxy fiberglass will provide ground plane insulation. The magnet will be high-potted up to 5 kV to detect defects in the insulation.

After the coils are assembled through the gap of the 35 mm dipole and secured, the core's nose pieces will be precisely pinned and bolted to the laminated end packs at either end of the dipole yoke assemble. The nose pieces shape the dipole end fields to minimize end-field errors and to match the field profiles of the 90 mm dipole.

Dipoles of either aperture that are not used as IR sources will use a single dipole vacuum chamber design. The chamber will allow damping wiggler radiation to pass through. The larger aperture IR dipole vacuum chamber will have a minimum internal aperture of 70 mm.

The designed magnet cross-section will accommodate the vacuum chamber with a 2 mm clearance between the magnetic poles and either side of the vacuum chamber.

4.1.2.3 Quadrupole Magnet Preliminary Design

4.1.2.3.1 Scope and Physics Design Parameters

Within the 66 mm aperture of the storage ring quadrupole magnet, the field gradient homogeneity in a region 40 x 20 mm is required to be better than 0.02%. The design geometry of the quadrupole is highly constrained by several factors:

1. Field quality and magnet alignment requirements as shown in Table 4.1.3
2. The geometry of the multipole vacuum chamber, and the need to accommodate its antechamber
3. The requirement to produce a low-cost magnet with very high reliability

To provide a path for synchrotron radiation exiting insertion devices, the antechamber and extraction ports must extend beyond the horizontal mid-plane of the magnet yoke. To assure symmetry, the horizontal back leg on either side of the quadrupole has been removed to accommodate the antechamber of the vacuum chamber. Therefore, the top and bottom halves of the quadrupole are not connected with a flux-return yoke; each half is connected mechanically with nonmagnetic metallic spacers that accommodate that vacuum chamber. This figure-8 style quadrupole has been known [4.1.3] and used successfully in previous machines, such as APS and SPEAR-3; cost savings are inherent in the design.

The quality of the field gradient in the full magnet aperture has been examined through 2D and 3D modeling using the OPERA code. The poles, shims, and end chambers are optimized to produce a quadrupole field with higher order systematic multipole components that meet the requirements shown in Table 6.1.9. Further modeling will be performed to assess the effects of value engineering and structural design optimization. R&D prototype magnets will be fabricated and magnetic measurements performed, to assess the effects of fabrication errors that contribute to random and additional systematic high-order multipoles. To assure that the total multipole harmonic content of the as-built reference design will meet the requirements of Table 6.1.9, magnet pole end chamfers are being modeled and actual optimization will be performed with the prototype quadrupole laminated end packs. Table 4.1.3 lists the preliminary design parameters.

Table 4.1.3 Quadrupole Magnet Preliminary Design Parameters.

	25cm SR Quadrupole	40cm SR Quadrupole
Energy [GeV]	3.0	3.0
Clear bore aperture [mm]	55	55
Maximum field gradient at 3.0 GeV [T/m]	12.8 / 8.3	22
Field quality	2×10^{-4}	2×10^{-4}
Good field region [mm]	40 x 20	40 x 20
Magnetic length [mm]	300	400
Nominal operating current [A]	95/ 146	160
Max. Number of Ampere-turns/pole	3686 / 5778	11520
Number of turns / magnet pole	39	72
Total resistance of the magnet at 30°C [Ω]	0.0529	0.129
Total inductance of the magnet [mH]	27	135
Max. Current density in conductor [A/mm^2]	4.2	4.6
Number of parallel cooling circuits	4	4
Temperature rise [°C]	7	10
Pressure drop [bar]	4	4
Voltage / magnet [V]	5 / 7.7	19.8
Iron core length [mm]	217	367
Lamination thickness [mm]	1.5	1.5
Quadrupole alignment tolerance [μm]	30	30

3-D OPERA code modeling of the figure-8 quadrupole with chamfering of the laminated end packs is shown in Figure 4.1.5. Further modeling will ensure that the requirements for higher-order multipoles (Table 6.1.9) are met.

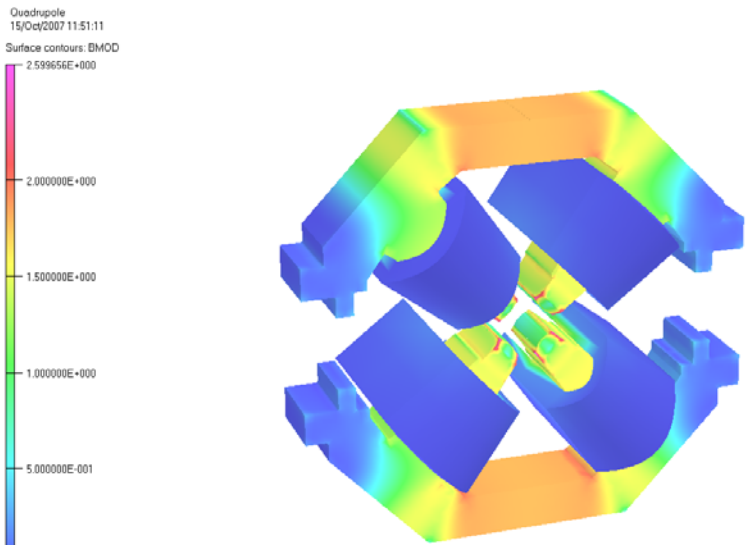

Figure 4.1.5 OPERA model of an NSLS-II storage ring quadrupole magnet cross-section, for studying the effects of pole edge chamfering.

4.1.2.3.2 Mechanical Design of the Quadrupole

Both halves of laminated iron yokes are composed of a single stamped and fine blanking lamination. The laminated magnet cores are made of low-carbon AISI 1006 steel sheet, 1.5 mm thick. A thin film of "B" staged (dry) heat-activated epoxy is applied to the lamination steel before blanking. The yoke is designed to allow the laminations to be shuffled.

End packs each having 12 laminations epoxied together are made using the Quadrupole yoke stacking fixture. The end pack stacking fixture is placed into an oven and heated until the lamination is full cured. Chamfers are precisely machined into the poles of these end packs.

The body of the quadrupole yokes are assembled using the same stacking fixture in shuffled packs about 18 mm thick. The packs are stacked with every other pack flipped in the stacking fixture. The chamfered end packs are secured to either end the center yoke section. While they are in the stacking fixture, a TIG weld bead is added to the outside of the iron to fix the packs together. The stacking fixture is compressed to a stop and heated until the epoxy between the laminations is fully cured.

The coils are wound on custom winding mandrills. Each coil has two layers of windings. For the majority of the quadrupoles, a single coil per pole is required. The conductor is a hollow square copper conductor 7.0 x 7.0 mm with a 4 mm diameter water channel and is wrapped with fiberglass.

The coil is wound in a manner that the first turn starts near the center of the length of conductor that is being wound. All NSLS-II coils are free from internal splices.

Vacuum impregnation is performed using an alumina-filled, high-radiation-resistant epoxy with a minimum thickness of 1.0 mm to provide interstitial conductor insulation. An additional 1.5 mm of alumina-filled epoxy fiberglass is applied to the outside of the coil to provide coil-to-ground plane insulation. The magnet coils will be high potted up to 5 kv to detect defects in the coil insulation system.

Value engineering of the quadrupole design to conform to lattice requirements has yielded three styles of coils. Most of the quadrupoles have four double-layer coils with four parallel water paths. Higher-field quads will have either a longer coil or additional coils per pole. Each coil shall represent an additional parallel water circuit. The increase in water temperature across any quadrupole magnet will be <1°C. Figure 4.1.6 presents the mechanical design.

The quadrupoles will be supported from near the mid-plane so thermally induced strain in the magnet's iron poles and yoke will tend to act about the magnet's axis, maintaining its pre-surveyed location to ≤10 μm over its full range of excitation. A minimum clearance of 2.0 mm is maintained between the magnet poles and vacuum chamber to effect thermal and vibrating isolation between the two devices.

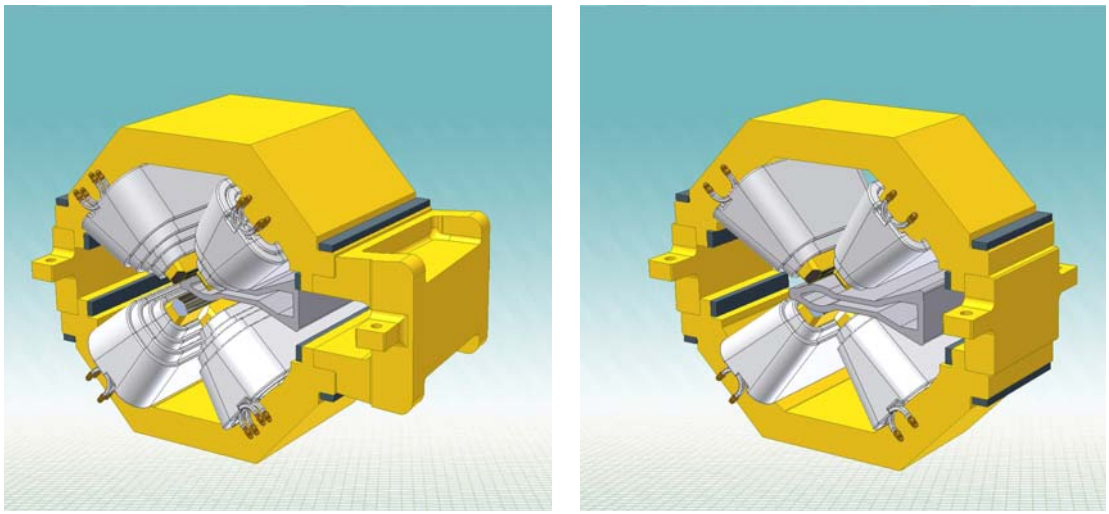

Figure 4.1.6 Preliminary designs the for NSLS-II storage ring quadrupole magnet. **Left**: A high-field quadrupole with an antechamber clearance. **Right**: a symmetric low-to-moderate field quadrupole.

4.1.2.4 Sextupole Magnet Preliminary Design

4.1.2.4.1 Scope and Physics Design Parameters

The storage ring is equipped with 300 sextupole magnets. The sextupole field homogeneity in a region 40 mm x 20 mm is required to be better than 0.05%. The geometry of the vacuum chamber determines the bore radius of the sextupole magnet. The design of the sextupole magnet is constrained by the need to accommodate a vacuum chamber's antechamber.

The poles and shims are optimized with a 2D approximation. Additional 3D modeling was performed to ensure that the requirements for higher-order multipoles (Table 6.1.9) are met.

The field quality is optimized for standard and extended sextupole models (Figure 4.1.7). The field quality is consistent with the specified sextupole field throughout the required transverse region, and all harmonics below two parts in 10^4 at 45 mm reference radius, in the entire range of operation. The bore diameter of 68 mm was determined by specifications of field quality and the spatial constraint between the vacuum chamber and the poles and coil geometry. The base of the pole is widened to prevent saturation in that area at high field excitations. In a wide-aperture sextupole, the ideal symmetry is partially broken due to nonperfect return yoke geometry, and semi-allowed harmonics (b_0, b_5, b_7, etc.) are created. We have developed a new design method that minimizes these harmonics by moving up the pole located at 90 degrees by about ~35 microns. Table 4.1.4 lists the preliminary design parameters for the sextupole magnets.

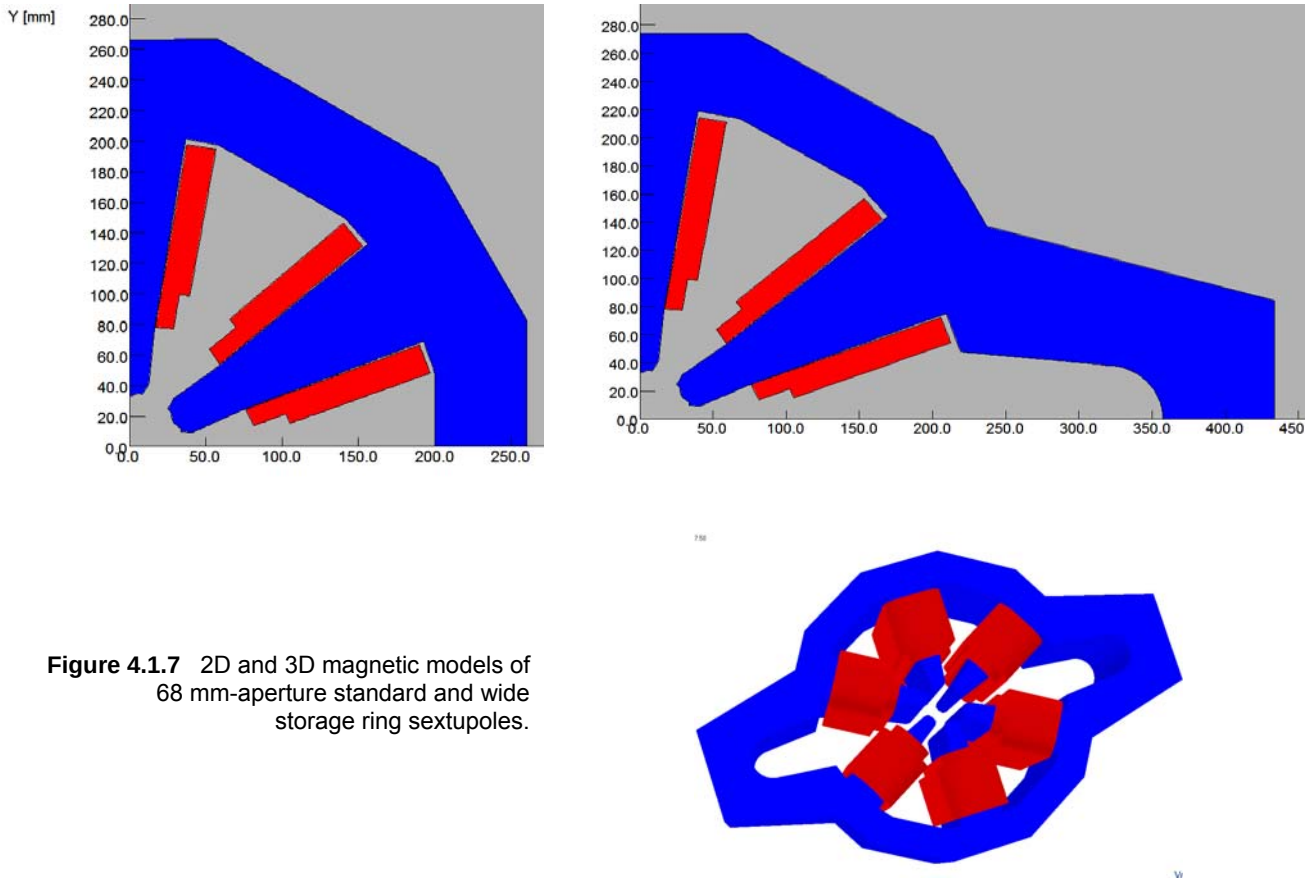

Figure 4.1.7 2D and 3D magnetic models of 68 mm-aperture standard and wide storage ring sextupoles.

Table 4.1.4 Sextupole Magnet Preliminary Design Parameters.

	20cm Sextupole	25cm Sextupole
Clear bore aperture [mm]	68	68
Sextupole field [T/m^2]	300 / 400	400
Field quality	5 x 10^{-4}	5 x 10^{-4}
Good-field region [mm]	40 x 20	40 x 20
Magnetic length[mm]	200	250
Maximum operating current [A]	123 / 164	164
Max. Number of Ampere-turns/pole	3192 / 4255	4255
Number of turns / pole	26	26
Total resistance of the magnet at 30°C [Ω]	0.0293	0.0346
Total inductance of the magnet [mH]	8.8	11.0
Temperature rise [°C]	7.5	5.1
Pressure drop [bar]	4	4
Voltage / magnet	3.3 / 4.4	5.2
Iron length [mm]	179	228
Laminae thickness [mm]	1.5	1.5
Sextupole alignment tolerance [μm]	30	30

4.1.2.4.2 Mechanical Design of the Sextupole

The sextupole magnets for the storage ring come in two lengths. Most of the sextupoles have a magnetic length of 0.2 m. The mid-cell sextupole has a magnetic length of 0.25 m.

To maintain high field quality, minimize random errors, assure the long-term mechanical stability, and not eliminate the possibility of adding steering and skew quadrupole trims in the future, the mechanical design is based on a mid-plane parting surface. To perform magnet assembly, it was determined that a removable 90-degree center pole in each magnet half is feasible (Figure 4.1.8).

A minimum clearance of >1.5 mm between the vacuum chamber and adjacent poles to maintain thermal and vibration isolation is maintained. The magnet cores are made from AISI 1006 low-carbon steel sheet. The laminations are coated with a thin film of "B" staged (dry) heat-activated epoxy. The yoke is designed to allow shuffling of laminations. The shuffled laminations are assembled in packs of ten laminations. Precision stacking fixtures are used to fabricate a series of end packs for both the two pole yoke and center-pole yoke subassemblies. After the end packs are oven cured, pin holes and chamfers are precisely machined into the pole tips. The body of the sextupole is composed of packs of shuffled laminations cured together inside a precision stacking fixture. The machined end packs are added to the mid yoke blocks in the stacking fixture. While in the stacking fixture, Tig weld beads are added to the yoke to secure the relative position of the packs.

Coils are composed of a double-layer stack of square copper conductor, 8.5 x 8.5 mm, with a 4.5 mm diameter water channel. The conductor is insulated with fiberglass. The coil is wound so the first turn starts the coil near the center of the length of conductor being wound. Vacuum impregnation is performed using alumina-filled high-radiation-resistant epoxy with a minimum interstitial conductor thickness of 1.0 mm. An additional 1.5 mm of alumina-filled fiberglass epoxy forms the ground plane insulation. The coils are high potted to 5 kv to detect defects in the insulation system. A coil center-pole subassembly is produced. A coil secured to the center-pole assembly is assembled in the yoke stacking fixture. Precision yoke end rings are assembled at either end of the sextupole core halves, and stainless steel rods with threaded ends are used to compress the yoke and end rings to precisely control yoke geometry. The end rings are used to position the center-pole relative to the two adjacent poles.

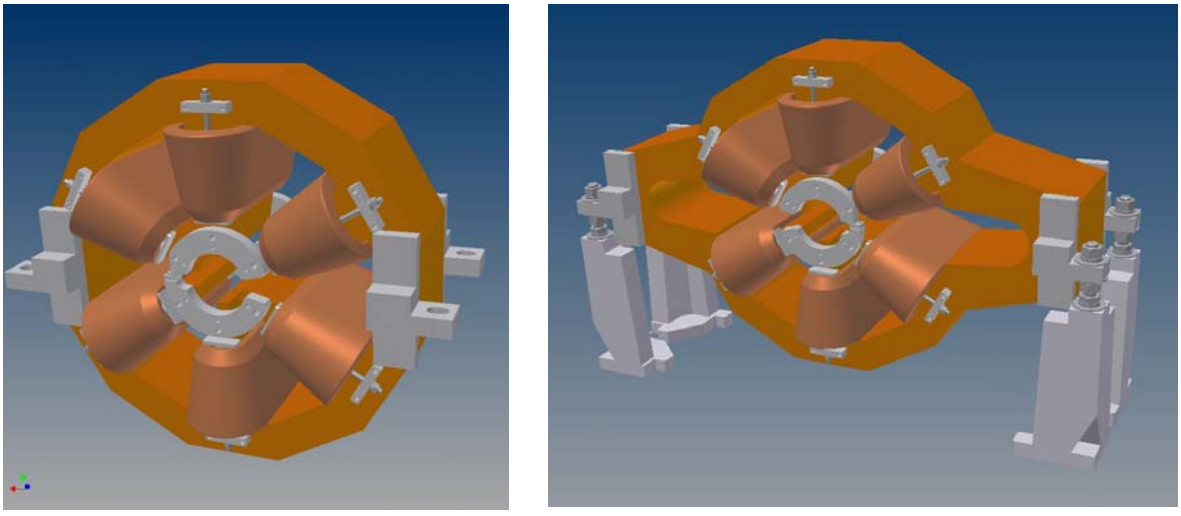

Figure 4.1.8 Preliminary design of 68 mm aperture standard and wide storage ring sextupoles.

Brackets are pinned and bolted to the yoke back legs at the mid-plane, the yokes are assembled, and the end rings are used to locate the two halves of the poles about a common center. Studs are used in the brackets to secure the core halves together. At least three parallel water circuits are used to maintain ≤10°C temperature rise in the cooling water across the magnet.

4.1.2.5 Correction Magnet Preliminary Design

In addition to the primary lattice magnets, the NSLS-II storage ring has corrector magnets. The correctors will be used to adjust the beam orbit and to correct for alignment errors. The correctors will also be used as part of both global and local feedback systems. The preliminary design calls for 242 correctors to be installed at the start of operation. Unlike other light sources where steering correction can be integrated into combined-function lattice sextupoles, the precise alignment and field quality requirements of the NSLS-II sextupoles largely prevent the use of combined-function sextupoles, making discrete correctors necessary.

There will be three types of corrector magnets. One type of global corrector will produce vertical and horizontal DC steering fields of up to 320 Gauss for ±0.8 mrad vertical and horizontal steering of the 3.0 GeV electron beam. There will be 120 of these correctors located around the stainless steel bellows assemblies at either end of the lattice dipole magnets. These correctors will produce an oscillating field component from DC to less than 100 Hz for up to ±0.1 mrad of vertical and horizontal dynamic steering. Another type of corrector, of similar design but with a smaller aperture, will be located around the aluminum vacuum chamber. A minimum of 60 of these correctors will produce both DC and an oscillating field component of greater than 5 Hz. The maximum operational frequency of these correctors will be determined as part of the NSLS-II R&D program, as we study and optimize the correctors' field interaction with the aluminum vacuum chamber. Thirty of these correctors will possess skew quadrupole windings to deliver a maximum DC field gradient of 0.36 T/m. 2D and 3D modeling studies of these correctors have been performed (Figure 4.1.9).

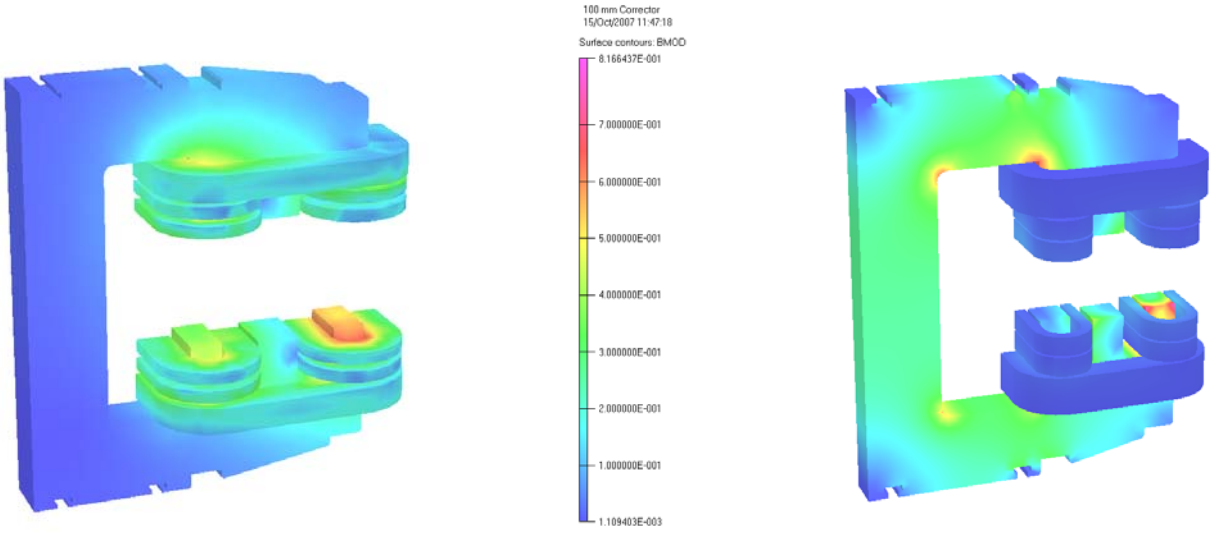

Figure 4.1.9 OPERA models of NSLS-II storage ring corrector magnets.
Left: Fast 156 mm aperture corrector. **Right**: Slow 100 mm aperture corrector.

A third type will be fast correctors, which will provide a maximum field of 100 Gauss at a frequency up to or exceeding 100 Hz. Twenty fast correctors will be used for local feedback. They will be located around stainless steel bellows or sections of stainless steel vacuum chamber at either end of an insertion device, such as an undulator. Silicon steel laminations 0.5 mm thick were selected for use in the corrector magnet flux return, to suit the charging rate. Table 4.1.5 lists the preliminary design parameters for the corrector magnets.

Many factors must be considered in the corrector magnet design. The design of a corrector magnet will be specific to its required function, the space constraints of the specific locations in the lattice, and how the corrector accommodates and interacts with the vacuum chamber design at its required location. Design options such as APS-style correctors are compact in size but tend to be rich in harmonics. Box-style correctors around the vacuum chamber have good field quality but tend not to use available space as efficiently and have larger stray fields. Analytical modeling of the C-shaped correctors revealed viable solutions for each corrector location.

Table 4.1.5 Corrector Magnet Preliminary Design Parameters.

	Fast Corrector	Slow Corrector	ID Corrector
Aperture [mm]	156	100	35/80
magnetic length [mm]	300	200	60/105
Iron core length [mm]	150	100	25
Max current at 3.0GeV	15	15	2
Max. DC voltage [V]	7.1/7.3 avg.	5.1/4.4 avg.	0.8/1.6
central field [T]	.028	0.04	0.0042
Max. NI/pole	2429/4188 avg.	2292/3360 avg.	180/360
J in copper [Amps./mm^2]	.35/1.4	.5./1.5	1.3

4.1.2.5.1 Mechanical Design of the Corrector Magnets

The connector magnets are composed of $\leq$0.5 mm, track-insulated, silicon steel (M36) sheet. The laminations are stacked and glued together in a precision stacking fixture. A single C-style lamination is used to simplify the design and minimize cost. The yokes are oven cured and then the pole tips are machined to assure precise gap spacing. The mechanical design of the six-coil baseline 156 mm-aperture fast corrector and a four-coil alternative design are shown in Figure 4.1.10.

Coils are composed of solid Pyra ML-coated rectangular, solid conductors. The coils are vacuum impregnated with alumina-filled radiation-resistant epoxy. Aluminum chill plates are added between the coils. This technique is used to eliminate water-cooled conductor and the water-to-conductor electrical isolator relying on ground plane insulation to isolate the coils from the water cooling loop. The corrector produces both vertical and horizontal fields simultaneously. The vertical field (horizontal bending) is essentially air cooled, and the horizontal field is water cooled, via inter-coil chill plates. Coils are assembled onto the yoke through the core aperture. Threaded holes in the chill plates molded into the horizontal field coils are used to secure the coil package, via long screws, to brackets on the top and bottom of the magnet yokes.

The correctors come in two apertures: 156 mm and 100 mm. Screw quadrupole excitation coils with a molded-in, water-cooled chill plate can be added to the aperture of the 100 mm corrector and can be secured to the magnet aperture in a manner similar to that of the vertical and horizontal field coils. Skew quad trim coils can also be added to the sextupole at one location per superperiod.

Tee-slotted keyways in the magnet yoke are used to secure the corrector to a wedge-style spacer between it and the top of the girder.

Injection magnets such as septum and kicker magnets are discussed in Section 5.9.

References

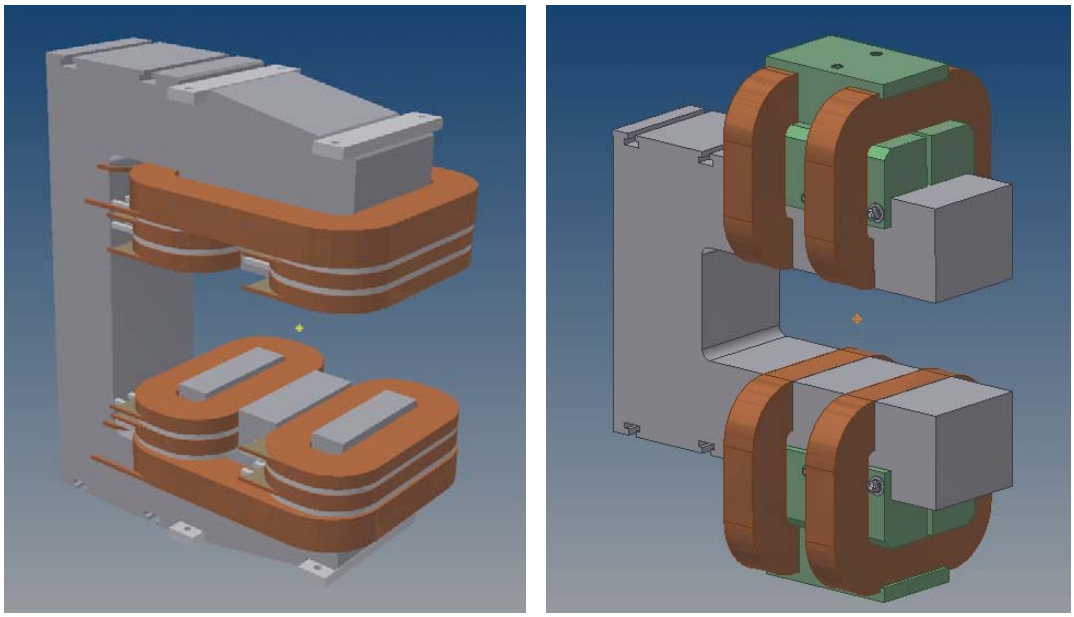

Figure 4.1.10 Preliminary designs of 156 mm aperture baseline (**left**) and alternative (**right**) corrector magnet.

[4.1.1] Creagh, D., et al., "An Infrared Beam-line at the Australian Synchrotron," SRI-2006.

[4.1.2] Katoh, M., et al., "Coherent Terahertz Radiation at UVSOR-II," SRI-2006.

[4.1.3] Danby, G.T., Jackson, J.W., IEEE Transactions in Nuclear Science, June, 1967.

4.2.3 Storage Ring Power Supplies

These power supplies are designed to stay at a fixed current except for the fast dipole correctors. The power supplies will be able to do simple ramps that will take 5 to 60 seconds from zero current to maximum current. These ramps can be software or hardware generated. The fast dipole correctors will be part of a beam-based feedback system. All power supplies will be located above the magnets in the equipment area. All power supplies will have at least a 20% margin in operating current. Listed below are the planned maximum numbers of power supplies that the storage ring will require. Some of the power supplies may have reduced quantities for day-one operation.

SR-MainDipole-PS	60 dipole magnets in a series circuit (54 small-aperture and 6 large-aperture magnets)
SR-LATrimDipole-PS	One shunt circuit to adjust current between large-aperture and small-aperture dipole magnets
SR-Quad-A-PS	150 individually powered quadrupole magnet circuits
SR-Quad-B-PS	60 individually powered quadrupole magnet circuits
SR-Quad-C-PS	90 individually powered quadrupole magnet circuits
SR-Sext-A-PS	35 pentant wide sextupole magnet circuits (7 of the 9 sextupole families)
SR-Sext-B-PS	10 pentant wide sextupole magnet circuits (2 of the 9 sextupole families)
SR-DipoleTrim-PS	60 dipole trim coil circuits – 30 planned for day-one operation
SR-SKQ-PS	30 skew quadrupole magnets circuits.
SR-BH-PS	60 intermediate speed horizontal dipole corrector magnet circuits
SR-BV-PS	60 intermediate speed vertical dipole corrector magnet circuits
SR-FGBH-PS	120 fast global horizontal correction dipole circuits
SR-FGBV-PS	120 fast global vertical correction dipole circuits
SR-FIBH-PS	120 fast insertion horizontal correction dipole circuits, 32 planned for day-one operation
SR-FIBV-PS	120 fast insertion vertical correction dipole circuits, 32 planned for day-one operation
Total slow power supplies	437 (407 planned for day-one operation)
Total intermediate-speed power supplies	120
Total fast power supplies	480 (304 planned for day-one operation)

4.2.3.1 B PS – Main Dipole Power Supply

This circuit consists of 54 small-aperture dipole magnets and 6 large-aperture dipole magnets, for a total of 60 magnets (Figure 4.2.1). The small-aperture magnets are 0.032 Ω and 16 mH. The large-aperture magnets are 0.089 Ω and 116 mH. The operating current for both magnets is ~360 A for 3.0 GeV. The cabling between magnets and the return will use 650 MCM flexible copper cables with a resistance of 0.142 Ω and inductance of 1.4 mH. The power supply load is 2.404 Ω and 1.561 H (Figure 4.2.2).

The main dipole power supply is a unipolar, two-quadrant, current-regulated supply. It will use two 12-pulse SCR converters in series with the center point connected to ground. This configuration will reduce the voltage to ground at the magnet load and reduce the voltage rating on various converter components. Each converter will have a two-stage LCRL passive filter and a series pass active filter. This is required to reduce the ripple current to low levels (Figure 4.2.2). The power supply will be able run in the invert mode while ramping down. This produces a negative voltage.

A combined digital and analog control system will control the operation of the power supply. The power supply will have a precision current regulator using a Direct Current Current Transformer as the current feedback device. The digital controls will use a feed-forward system to improve overall reproducibility. A PLC will be used for state control (on/off commands and interlocks).

The large-aperture trim dipole power supply is used to adjust the current between the large- and small-aperture dipole magnets. The purpose of the power supply is to compensate for any systematic differences between the magnetic lengths of the two different dipole magnets. The current trim is done by having a shunt circuit connected across all the large-aperture magnets (Figure 4.2.2). This power supply will be designed to float off ground. It will use the same basic controls as the quadrupole power supplies except for needed control circuit isolation.

Main Dipole Power Supply Specifications

AC input power	3-phase 460 VAC ~683 AAC
DC maximum output current – Imax	450 ADC
DC minimum output current – Imin	~1 ADC
DC output voltage	1200 VDC
operating quadrants	2: (V+, I+) & (V-, I+)
small-signal – 3 db bandwidth	500 Hz
stability (8 h–10 s) – referred to Imax	25 ppm
stability (10 s–300 ms) – referred to Imax	15 ppm
stability (300 ms–0 ms) – referred to Imax	10 ppm
absolute accuracy – referred to Imax	100 ppm
reproducability long term – referred to Imax	25 ppm
current ripple – referred to Imax	5 ppm 60 Hz and greater
resolution of reference current	18-bit ±1 LSB
resolution of current measured – fast sampling	16-bit ±1 LSB at 200 μsec
resolution of current measured – slow sampling	22-bit ±1 LSB at 16.67 msec

Large-Aperture Trim Dipole Power Supply Specifications

AC input power	3-phase 208 Vac ~ 12 AAC
DC maximum output current – Imax	13 ADC
DC minimum output current – Imin	~1 ADC
DC output voltage	300 VDC
operating quadrants	1: (V+, I+)
small-signal – 3 db bandwidth	100 Hz
stability (8 h–10 s) – referred to Imax	100 ppm
stability (10 s–300 ms) – referred to Imax	100 ppm
stability (300 ms–0 ms) – referred to Imax	50 ppm
absolute accuracy – referred to Imax	100 ppm
reproducibility long term – referred to Imax	100 ppm
current ripple – referred to Imax	10 ppm 60 Hz and greater
resolution of reference current	16-bit ±1 LSB
resolution of current measured – fast sampling	16-bit ±1 LSB at 200 μsec
resolution of current measured – slow sampling	22-bit ±1 LSB at 16.67 msec

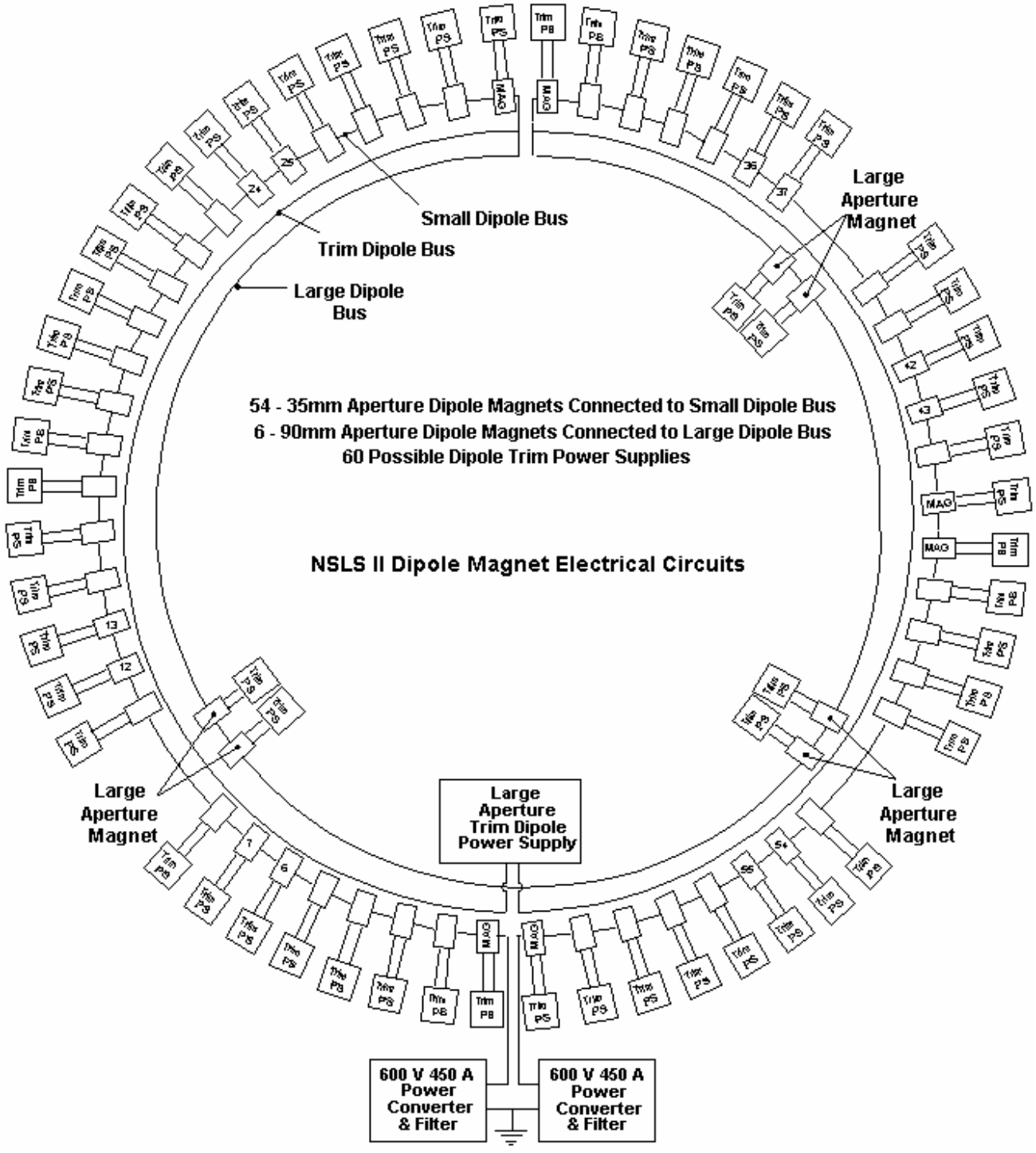

Figure 4.2.1 Storage ring dipole magnet circuit.

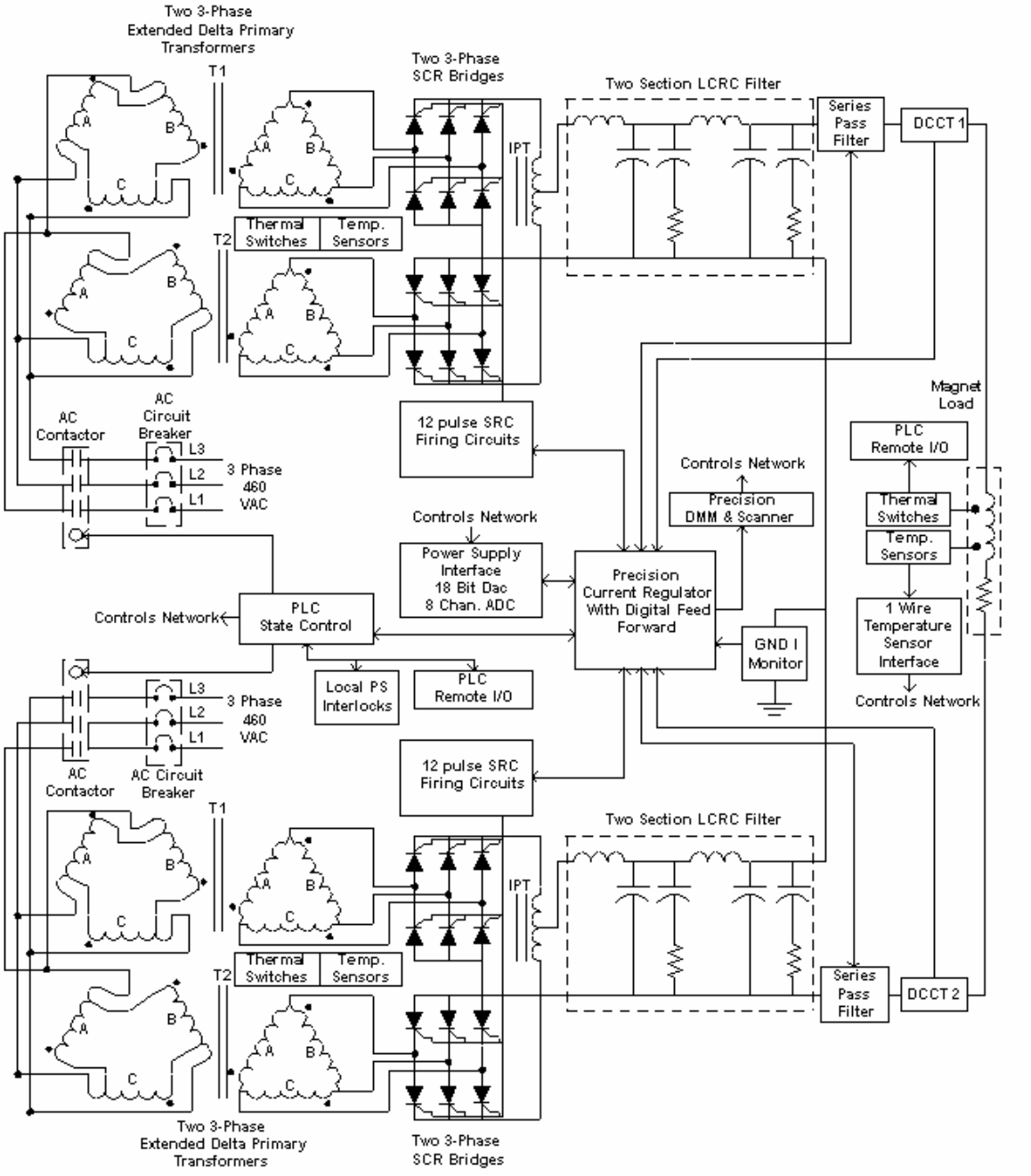

Figure 4.2.2 Dipole power supply block diagram.

4.2.2 SR-Quad-A-PS, SR-Quad-B-PS, and SR-Quad-C-PS – Quadrupole Power Supplies

These circuits will use one power supply for each magnet. The quadrupole magnet load parameters require three power supplies for the different quadrupole magnet types. There are a total of 300 magnet circuits. The following table shows which power supply is used for each type of magnet and what are the power supply loads.

PS Type	Magnet	Operating Current	Load resistance	Load Inductance	Output Cable
Quad-A	Q1L,Q3L,QF,Q3H	146 A	0.058 Ω	0.027 H	250 MCM
Quad-B	Q2L,Q2H	160 A	0.129 Ω	0.135 H	250 MCM
Quad-C	QD,Q1H	95 A	0.058 Ω	0.027 H	4/0 AWG

The cabling between the magnets and power supply will use flexible copper cables.

The power supply is a unipolar, single-quadrant, current-regulated switch-mode design. The power section is a commercial, voltage-controlled, switch-mode-programmable power supply with high output bandwidth (~0.5 kHz). These supplies have 3, 6.6, and 1.2 kW output power ratings. They fit in a standard 19-in. electronics rack and are only 3.5 and 1.75 inches high. These power supplies are air-cooled. A precision analog regulator to control the current will be developed in-house. The power supply will use a DCCT as the current feedback device. To minimize current ripple, an additional output filter can be used. An AC input module will turn the power supply on and off. A microcontroller will be used for state control (on/off commands and interlocks). See Figure 4.2.3 for a block diagram of the Quad power supply.

Quadrupole Power Supply Specifications

AC Input

PS Type	Voltage	Current	Phase
Quad-A	208 VAC	~ 11 AAC	3
Quad-B	208 VAC	~ 23 AAC	3
Quad-C	120 VAC	~ 14 AAC	1

DC Output

PS Type	Voltage	Current	Power
Quad-A	16 VDC	185 ADC	3.0 kW
Quad-B	30 VDC	220 ADC	6.6 kW
Quad-C	10 VDC	120 ADC	1.2 kW

Quadrupole Power Supply Specifications (cont.)

DC minimum output current – Imin	~0.5 ADC
operating quadrants	1: (V+, I+)
small-signal – 3 db bandwidth	100 Hz
stability (8 h–10 s) – referred to Imax	100 ppm
stability (10 s–300 ms) – referred to Imax	100 ppm
stability (300 ms–0 ms) – referred to Imax	500 ppm
absolute accuracy – referred to Imax	100 ppm
reproducibility long term – referred to Imax	100 ppm
current ripple – referred to Imax	15 ppm 60 Hz and greater
resolution of reference current	18-bit ±1 LSB
resolution of current measured – fast sampling	16-bit ±1 LSB at 200 µsec
resolution of current measured – slow sampling	22-bit ±1 LSB at 16.67 msec

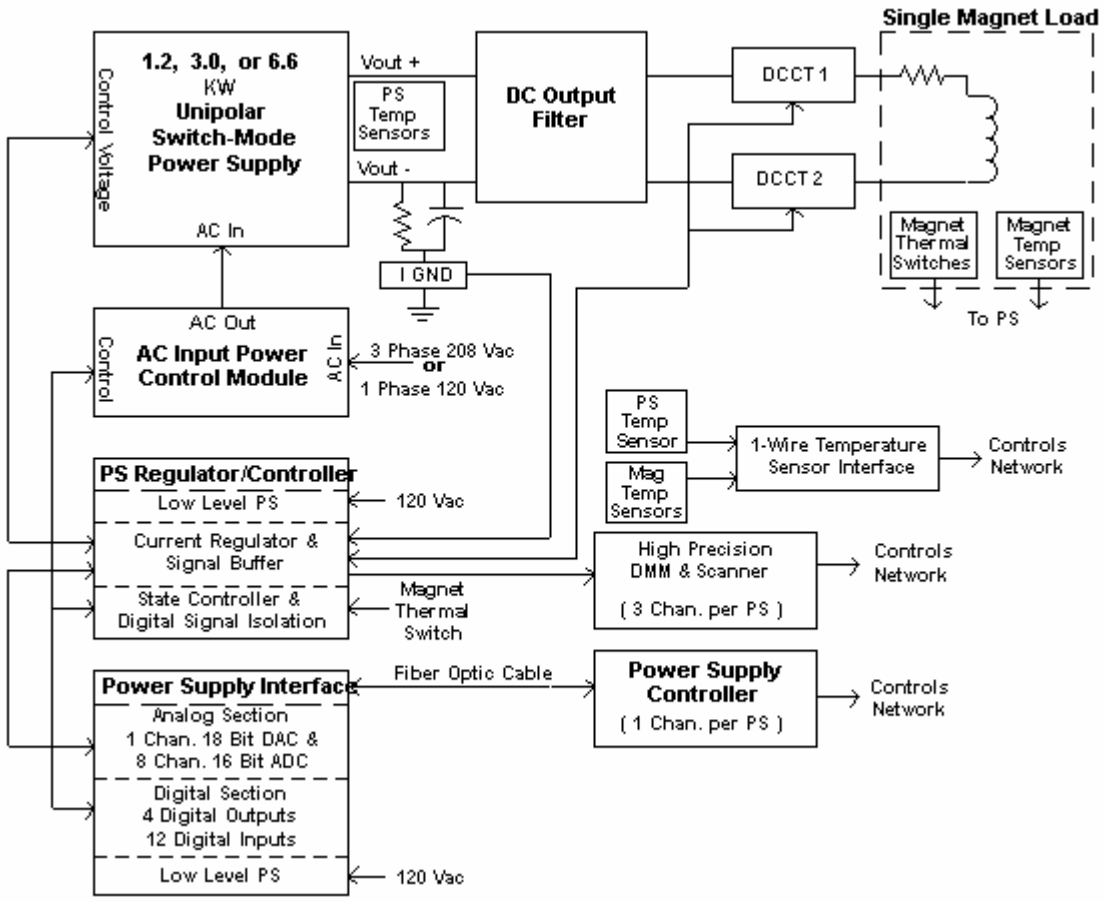

Figure 4.2.3 Quadrupole power supply block diagram.

4.2.3 SR-Sext-A-PS and SR-Sext-B-PS – Sextupole Power Supplies

These circuits will use one power supply for each family of sextupole magnets in each pentant. There are nine families in each of the five pentants. There are a total of 45 magnet circuits. The sextupole magnet load parameters require two power supply types for the different sextupole magnet families. The following table shows which power supply is used for each sextupole families and what are the power supply loads.

PS Type	Sextupole Family	Operating Current	Load resistance	Load Inductance	Output Cable
Sext-A	SL1, SL2, SL3, SL4 SH1, SH2, SH3	123 A	0.246 Ω	0.053H	250 MCM
Sext-B	SD	164 A	0.431 Ω	0.106 H	250 MCM
Sext-B	SF	164 A	0.285 Ω	0.066 H	250 MCM

The cabling between the magnets and power supply will be 250 MCM flexible copper cables. See Figure 4.2.5 for a connection diagram of sextupole families.

The supply is a unipolar, current-regulated switch-mode design, similar to that for the quadrupoles. The power section is a commercial, voltage-controlled, switch-mode-programmable power supply with high output bandwidth (~0.5 kHz). These air-cooled power supplies have an output power rating of 10 kW or 20 kW. They fit in a standard 19-in. electronics rack and are only 5.25 inches high for 10 kW and 10.5 inches high for 20 kW. A precision analog regulator to control the current will be developed in-house. The power supply will use a DCCT as the current feedback device. To minimize current ripple, an additional output filter will be used. An AC input module will turn the power supply on and off. A microcontroller will be used for state control (on/off commands and interlocks). See Figure 4.2.6 for a block diagram of the sextupole power supply.

Sextupole Power Supply Specifications

AC input

PS Type	Voltage	Current	Phase
Sext-A	208 VAC	~ 34 AAC	3
Sext-B	208 VAC	~ 68 AAC	3

DC output

PS Type	Voltage	Current	Power
Sext-A	60 VDC	167 ADC	10.0 kW
Sext-B	100 VDC	200 ADC	20.0 kW

Sextupole Power Supply Specifications (cont.)

DC minimum output current – Imin	~0.5 ADC
DC output voltage	12 VDC
operating quadrants	1: (V+, I+)
small-signal – 3 db bandwidth	100 Hz
stability (8 h–10 s) – referred to Imax	100 ppm
stability (10 s–300 ms) – referred to Imax	100 ppm
stability (300 ms–0 ms) – referred to Imax	50 ppm
absolute accuracy – referred to Imax	100 ppm
reproducibility long term – referred to Imax	100 ppm
current ripple – referred to Imax	15 ppm 60 Hz and greater
resolution of reference current	16-bit ±1 LSB
resolution of current measured – fast sampling	16-bit ±1 LSB at 200 μsec
resolution of current measured – slow sampling	22-bit ±1 LSB at 16.67 msec

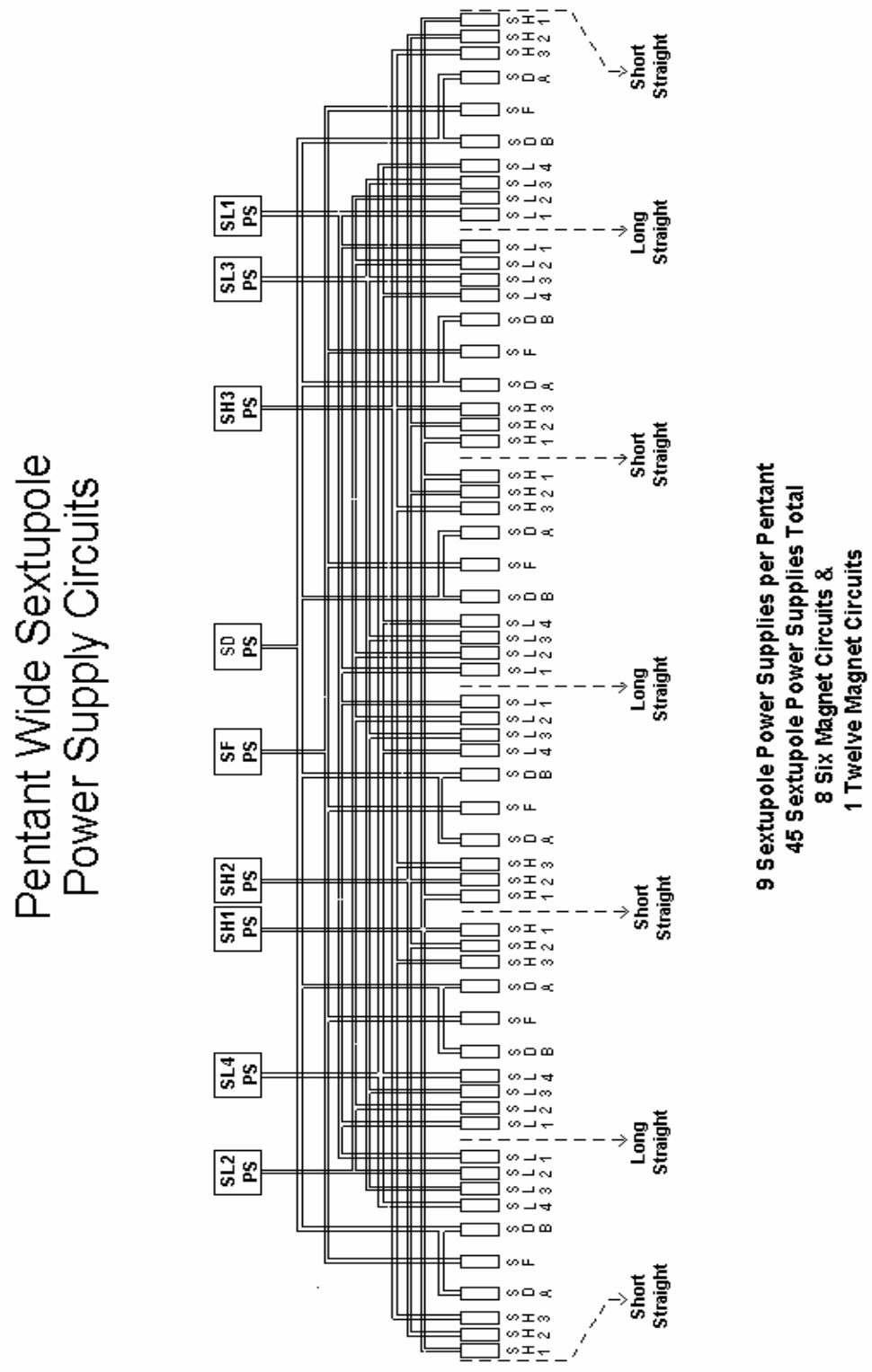

Figure 4.2.5 Connection diagram of sextupole families.

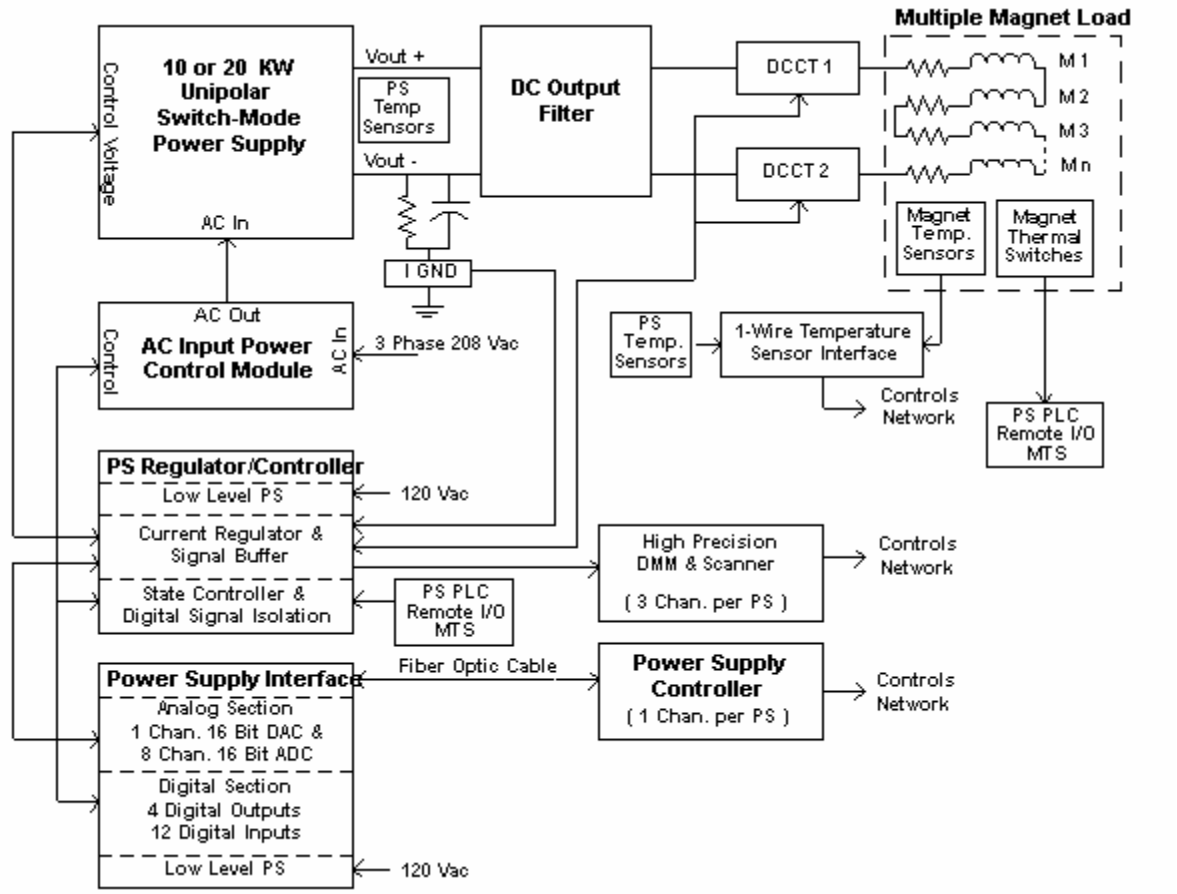

Figure 4.2.6 Sextupole power supply block diagram.

4.2.4 SR-Dipole Trim-PS and SR-SKQ-PS – Dipole Trim Coil and Skew Quadrupole Power Supplies

The Dipole Trim PS circuit consists of the trim coil sets located in the dipole magnets. The coil set is 3.11 Ω and 26 mH for small-aperture dipole and 8.67 Ω and ~90 mH. The SKQ power supply circuit consists of a corrector coil that is still to be placed in the lattice; this coil is estimated at 3.0 Ω and 5 mH. The operating current for these power supplies is ~2 A for 3.0 GeV. The cabling from the coil set to the power supply will be # 10 AWG flexible copper, routed through the tunnel ceiling into the equipment area above the main tunnel. The cabling has a resistance of 0.153 Ω and an inductance of 0.1 mH. The worst-case power supply load is 8.82 Ω and ~ 0.09 H.

The bipolar, 4-quadrant, current-regulated linear power supply fits in a standard 19-in. electronics rack and is 5.25 inches high. A precision analog regulator to control the current will be used. The power supply will use a DCCT as the current feedback device. A microcontroller will be used for state control (on/off commands and interlocks).

B1 Trim PS and SKQ PS Power Supply Specifications

AC input power	1-phase 120 VAC ~2.4 AAC
DC maximum output current – Imax	+5 ADC
DC minimum output current – Imin	–5 ADC
DC output voltage	±20 VDC
operating quadrants	4: (V+, I+), (V–, I+) , (V–, I-) & (V+, I–)
small-signal – 3 db bandwidth	10 kHz
large-signal bandwidth	~5 Hz
stability (8 h–10s) – referred to Imax	100 ppm
stability (10 s–300 ms) – referred to Imax	100 ppm
stability (300 ms–0 ms) – referred to Imax	50 ppm
absolute accuracy – referred to Imax	100 ppm
reproducibility long term – referred to Imax	100 ppm
current ripple – referred to Imax	10 ppm 60 Hz and greater
resolution of reference current	16-bit ±1LSB
resolution of current measured – fast sampling	16-bit ±1 LSB at 200 μsec
resolution of current measured – slow sampling	22-bit ±1 LSB at 16.67 msec

4.2.5 SR-BH-PS and SR-BV-PS – Intermediate Speed Horizontal and Vertical Corrector Coil Power Supplies

The BH and BV Corrector PS circuits consist of the corrector coil set located in an HVC magnet. Each coil set is ~0.34 Ω and ~25 mH. This coil set is estimated at 3.0 Ω and 1 mH. The operating current for both power supplies is ~15 A for 3.0 GeV. The cabling from the coil sets to the power supplies will be # 10 AWG flexible copper cables, routed through the tunnel ceiling into the equipment area above the main tunnel. The cabling has a resistance of 0.148 Ω and an inductance of 0.1 mH. The worst-case power supply load is 0.488 Ω and ~25 mH.

The BH and BV power supplies are bipolar, 4-quadrant, current-regulated linear PS that fit in a standard 19-in. electronics rack and are 5.25 inches high. A precision analog regulator to control the current will be used. The power supply will use a DCCT as the current feedback device. These corrector power supplies are part of an intermediate-speed beam position feedback system. A microcontroller will be used for state control (on/off commands and interlocks).

Corrector Coil Set Power Supply Specifications

AC input power	1-phase 120 VAC ~7.3 AAC
DC maximum output current – Imax	+ 24 ADC
DC minimum output current – Imin	– 24 ADC
DC output voltage	±25 VDC
operating quadrants	4: (V+, I+) , (V–, I+), (V–, I–) & (V+, I–)
small-signal – 3 db bandwidth	1 kHz
large signal – bandwidth	~5 Hz
stability (8 h–10 s) – referred to Imax	100 ppm
stability (10 s–300 ms) – referred to Imax	50 ppm
stability (300 ms–0 ms) – referred to Imax	25 ppm
absolute accuracy – referred to Imax	100 ppm
reproducibility long term – referred to Imax	100 ppm
current ripple – referred to Imax	5 ppm 60 Hz and greater
resolution of reference current	18-bit ±1 LSB
resolution of current measured – fast sampling	16-bit ±1 LSB at 200 μsec
resolution of current measured – slow sampling	22-bit ±1 LSB at 16.67 msec

4.2.6 SR-FIBH-PS and SR-FIBV- PS Fast Insertion Horizontal and Vertical Corrector Power Supplies

The FIBH and FIBV fast insertion corrector power supply circuits consist of the corrector coil set located in a fast insertion HVC magnet. These magnets are located in the insertion region on either side of an insertion device. Each coil set is estimated at ~0.8 Ω and ~ 10 mH. The operating current for the power supplies is ~2 A for 3.0 GeV. The cabling from the coil sets to the power supply will be # 10 AWG flexible copper, routed through the tunnel ceiling into the equipment area above the main tunnel. The cabling has a resistance of 0.152 Ω and inductance of 0.1 mH. The worst-case power supply load is ~0.95 Ω and 0.010 H.

The FIBH and FIBV power supplies are bipolar, 4-quadrant, current-regulated linear power supplies that fit in a standard 19-in.electronics rack and are 5.25 inches high. A precision analog regulator to control the current will be used. The power supply will use a DCCT as the current feedback device. These corrector power supplies are part of a fast beam position feedback system. A microcontroller will be used for state control (on/off commands and interlocks).

Fast Insertion Corrector Power Supply Specifications

AC input power	1-phase 208 Vac ~2.6 AAC
DC maximum output current – Imax	+ 5 ADC
DC minimum output current – Imin	- 5 ADC
DC output voltage	± 20 VDC
operating quadrants	4: (V+, I+) , (V–, I+), (V–, I–), & (V+, I–)
small-signal – 3 db bandwidth	10 kHz
large signal – bandwidth	100 Hz
stability (8 h–10 s) – referred to Imax	100 ppm
stability (10 s–300 ms) – referred to Imax	50 ppm
stability (300 ms–0 ms) – referred to Imax	25 ppm
absolute accuracy – referred to Imax	100 ppm
reproducibility long term – referred to Imax	100 ppm
current ripple – referred to Imax	5 ppm 60 Hz and greater
resolution of reference current	18-bit ±1 LSB
resolution of current measured – fast sampling	16-bit ±1 LSB at 200 μsec
resolution of current measured – slow sampling	22-bit ±1 LSB at 16.67 msec

4.2.7 SR-FGBH-PS and SR-FGBV-PS Fast Global Horizontal and Vertical Corrector Power Supplies

The FGBH and FGBV fast global corrector power supply circuits consist of the corrector coil set located in a fast global HVC magnet. This magnet is located over stainless steel bellows on both sides of the dipole magnets. This magnet serves as an alignment and fast orbit position corrector. This requires the power supply to have both high voltage and current. The operating current for the power supplies is ~15 A for 3.0 GeV The coil resistance is ~0.5 Ω and coil inductance is ~ 0.10 mH. The cabling from the coil sets to the power supply will be # 10 AWG flexible copper, routed through the tunnel ceiling into the equipment area above the main tunnel.

The FGBH and FGBV power supplies will use a switch-mode, bipolar, four-quadrant, current-regulated power supply. It will fit in a standard 19-in. electronics rack. A precision analog regulator to control the current will be used. The power supply will use a DCCT as the current feedback device. These corrector power supplies are part of a fast beam position feedback system. A microcontroller will be used for state control (on/off commands and interlocks). See Figure 4.2.7 for a block diagram of the fast global corrector power supply.

Fast Global Corrector Power Supply Specifications

AC input power	120 VAC ~14 AAC
DC maximum output current – Imax	+ 24 ADC
DC minimum output current – Imin	- 24 ADC
DC output voltage	± 45 VDC
operating quadrants	4: (V+, I+), (V–, I+), (V–, I–), & (V+, I–)
small-signal – 3 db bandwidth	5 kHz
large signal – bandwidth	100 Hz
stability (8 h–10 s) – referred to Imax	1,000 ppm
stability (10 s–300 ms) – referred to Imax	50 ppm
stability (300 ms–0 ms) – referred to Imax	25 ppm
absolute accuracy – referred to Imax	100 ppm
reproducibility long term – referred to Imax	100 ppm
current ripple – referred to Imax	5 ppm 60 Hz and greater
resolution of reference current	20-bit ± 1 LSB
resolution of current measured – fast sampling	16-bit ± 1 LSB at 200 μsec
resolution of current measured – slow sampling	22-bit ± 1 LSB at 16.67 msec

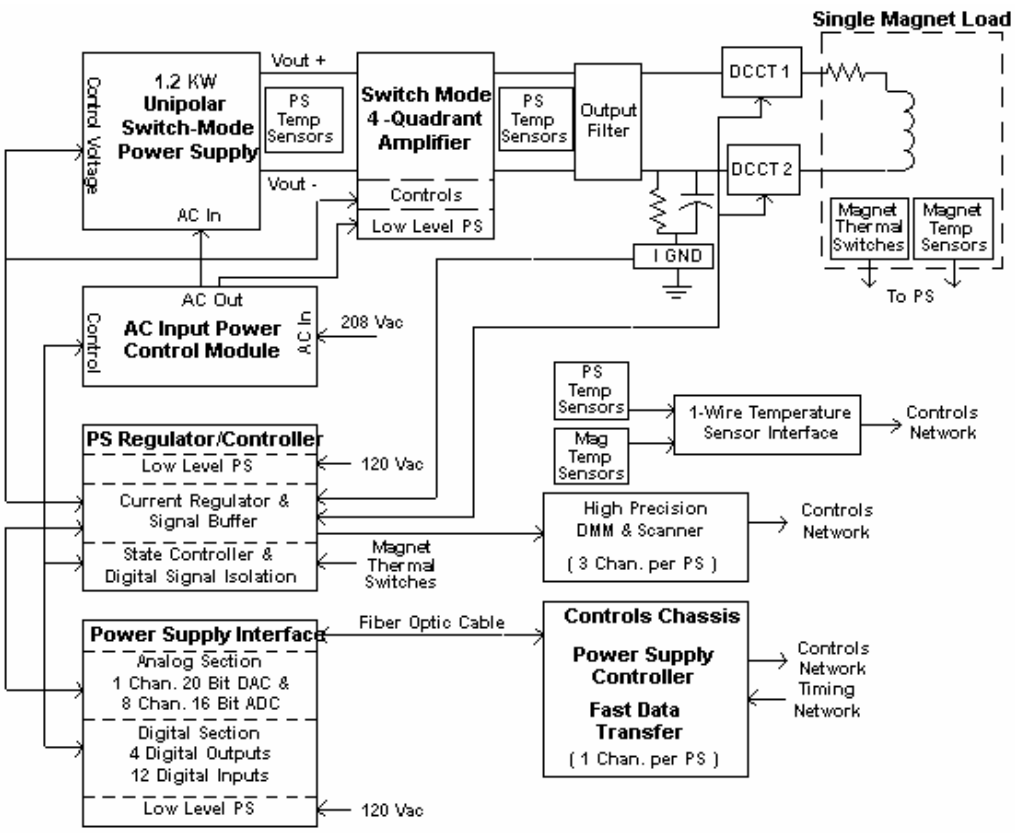

Figure 4.2.7 Block diagram of the Fast Global Corrector power supply.

4.2.8 Power Supply Interlocks

All power supplies will have sufficient interlocks that will prevent the power supply from becoming damaged due to changes in cooling conditions, AC power disturbances, and nonstandard operating conditions.

All magnet coils will have an over- temperatures interlock if there is a change in cooling and/or operating conditions. Temperature interlock for magnets that are part of ring- and pentant-wide circuits will be interfaced to a ring-wide interlock system. This system will use a PLC with remote I/O modules located in every cell. The system will monitor all the thermal switches on these magnets and route the interlock signal to the appropriate power supplies.

All power supplies will have an electrical safety interlock that will prevent the power supply from turning on if the machine safety system requires it.

4.2.9 Power Supply Instrumentation

Redundant DCCTs will be used to confirm the power supply current reproducability.

High-precision DMMs and scanners will be used to monitor the power system current, the redundant current sensor, and the analog current set point. This equipment will ensure long-term stability and reproducability.

Temperature monitoring of the magnet coils and power system environment will be accomplished using low-cost digital temperature sensors. With such systems, a problem can be identified before it becomes an emergency, making it possible for repairs to be scheduled more conveniently.

4.2.10 Power Supply Controls

The Power Supply Interface has a precision DAC for generating the reference current and a multi-channel ADC for inputting PS signals. The PSI also has digital I/O for state control and status readbacks of the PS.

A VME device card will be used to communicate between the control system and the PSI. This card will be located in a control system's VME chassis that will be mounted in one of the power supply system racks. This card will generate the reference current profiles, input analog data, and perform digital state control and status readbacks. The output of the device card is a fiber optics cable that connects to a PSI.

The other controls will include the operation of the high-precision DMM and scanner and readout of the digital temperature sensors.

4.2.11 Electrical Safety

All power supplies will conform to the latest BNL safety requirements, especially concerning arc flash protection. Whenever possible, NRTL-listed equipment will be used.

4.2.12 Cable Tray and Cable Routing

The cable tray for the magnet circuits will be located in the equipment area above the main tunnel. The cable will drop through the tunnel ceiling at two locations in each cell, where it will connect to two dipole magnets. There will also be a tray inside the main tunnel only in the area of the cell. This tray will be located over the storage ring magnets. The single cables will be installed with a twist to prevent pickup from noise sources. All cables will be tray-rated cables. Power supply cables will be arranged to minimize pickup from other circuits. All power cables will be separated from signal cables. The quadrupole, sextupole, and corrector

cables will be routed through conduit in the main tunnel ceiling. The cable going through the conduit will run in the cable tray in the tunnel until it is connected to the magnet. All cables and trays will meet NEC codes.

See Figure 4.2.8 for a block diagram of the cable and tray for one cell.

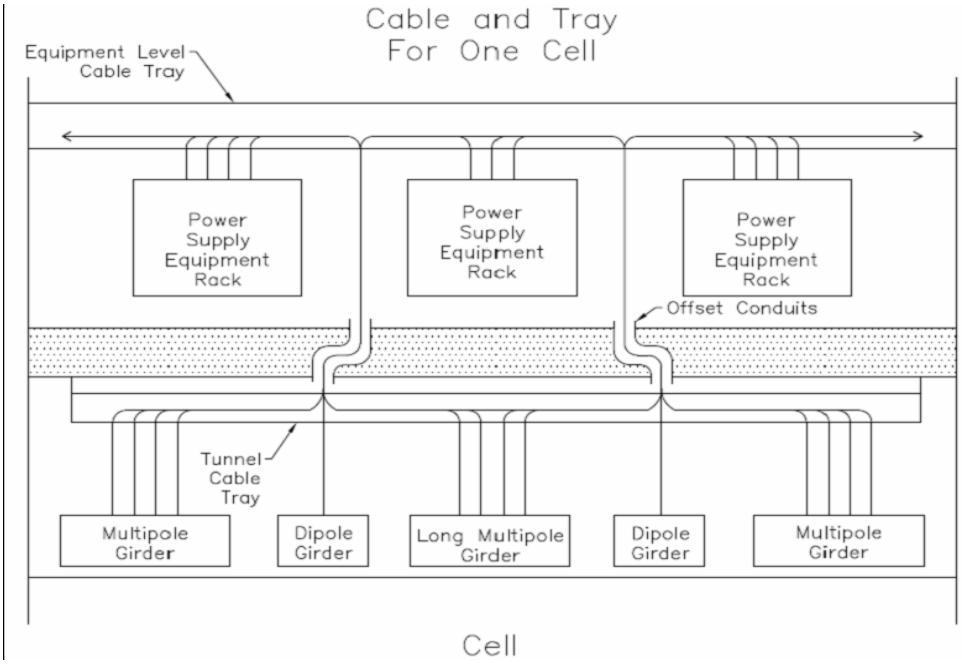

Figure 4.2.8 Block diagram of the cable and tray for one cell.

4.2.13 Power Supply Racks

All storage ring power supplies except for the dipole will be mounted in sealed Nema 12 electronics racks. These racks will have a maximum of six 3kW power supplies installed in them. These racks will also have power supply controls and instrumentation installed in them. At each cell location there are 11 power supply racks (Figure 4.2.9). The power racks will be located above the magnets they supply.

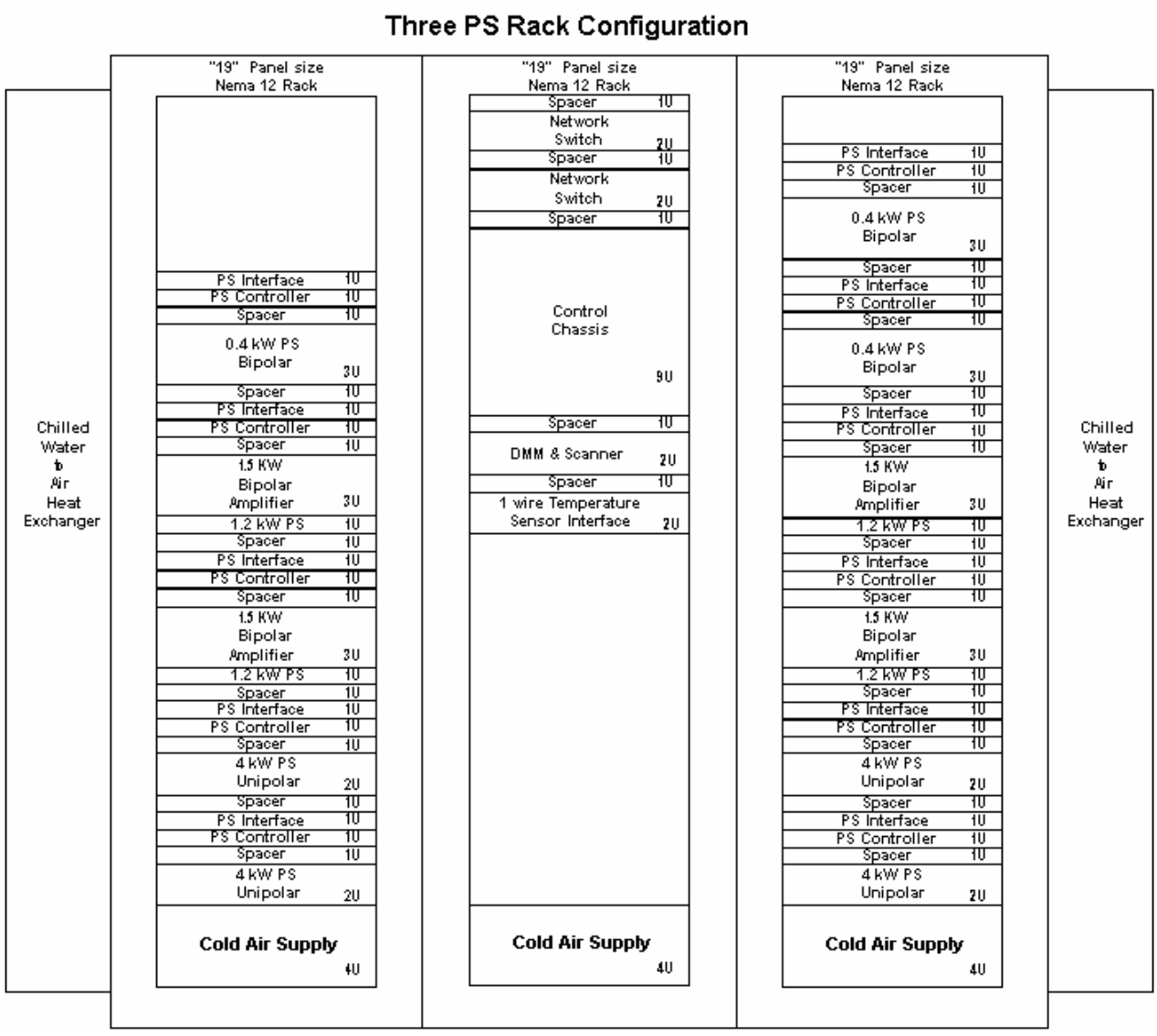

Figure 4.2.9 Magnet power supply rack layout.

A water-to-air heat exchanger will cool a set of three or four racks. Cooled air will flow through the power supplies and circulate back to the heat exchanger. The heat exchanger will use chilled water and have the outlet temperature regulated (Figure 4.2.10).

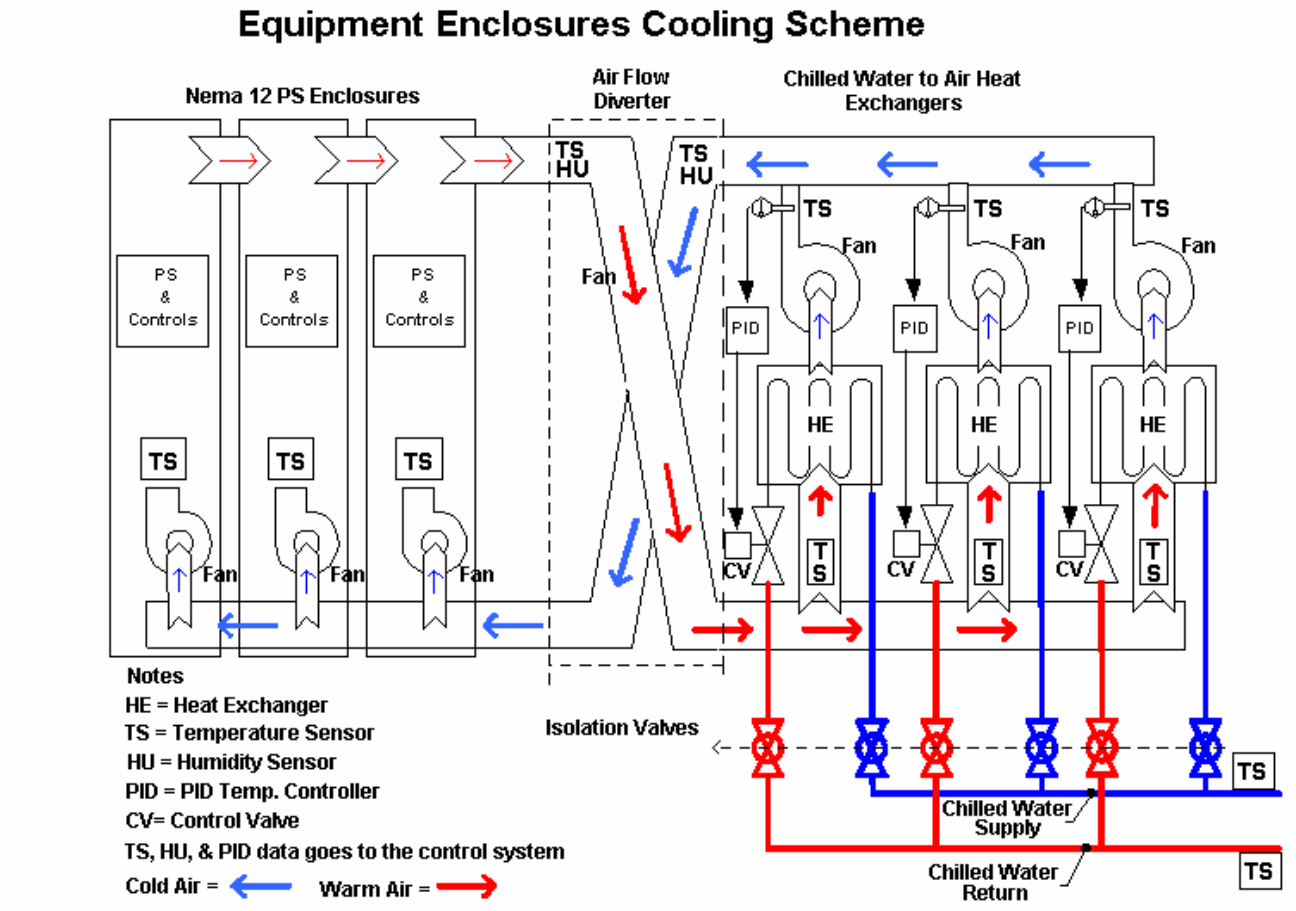

Figure 4.2.10 Rack cooling scheme.

4.3 Magnet–Girder Support System

4.3.1 Scope

This section describes alignment tolerances, stability requirements, and preliminary design of the storage ring magnet support system. Specifications for magnet alignment and stability are established from analysis of the storage ring nonlinear dynamics. Functional requirements of the girder supports are presented and design features for meeting these requirements are discussed. Various sources of ambient motion affecting the stability of the support system are identified and design solutions to mitigate their effects are discussed

4.3.2 Alignment Tolerances and Stability Requirements

The alignment tolerances for the ring magnets impact the ring performance in several ways. Magnet alignment is necessary to be able to store the electron beam with the design emittance and lifetime (i.e., sufficient dynamic aperture, DA). First, there is a relative magnet-to-magnet alignment tolerance to a line relative to the rigid girder. Second, there is an alignment tolerance specified for the transverse position of the ends of the girder and its roll angle and longitudinal position (six parameters), as it is installed in the tunnel. The girder misalignment introduces a correlated offset of the magnets. For this preliminary design, we took the achievable magnet-to-magnet alignment values from recently commissioned light sources as our specification and calculated the impact on the DA. Future studies will further explore sensitivity to these tolerances, along with the tolerance on magnetic field errors. The current tolerances are listed in Table 4.1.1. The impact of tolerance errors is discussed in Section 4.1.1.

The stability of closed-orbit position is critical to providing a constant flux in the user beamlines (i.e., intensity through slits and mirror systems). There are several sources of steering that cause large closed-orbit motion (relative to the user beamline): power supply fluctuations, energy modulations, and alignment variations due to vibrations of the magnets. We only consider the last effect here. The magnet motions that are of most concern are those of the quadrupole transverse position, dipole longitudinal position, and roll angle. This closed-orbit motion is the result of the large COAF, discussed in Section 4.1, which determined the magnitude of beam motion per unit of transverse motion of the quadrupoles, assuming that all quadrupole motions were uncorrelated in location around the ring, as well as uncorrelated in time. Here we discuss in more detail the time variation of the beam orbit due to quadrupole and dipole motion and the impact this has on the user beam.

To estimate the magnitude of the resulting orbit motion, we need to know how the quadrupoles are shifted around the ring. This depends on the noise source that generates this motion, as well as its coupling to the magnets through their support system (girders and floor). The simplest model of these magnet vibrations is just the random fluctuations of the magnet centers by a common tolerance level and assuming this impact will be the same at any frequency of vibration. This tends to overestimate the impact on the beam motion, since it ignores correlations that will smooth the distortions, as well as the synchrotron radiation damping that will damp the beam to the shifted closed orbit. This latter effect will mean that for frequencies greater than $F_{x,y} \approx 1/\tau_{x,y}$, where $\tau_{x,y}$ are the transverse damping times, the effective beam emittance will grow, while the centroid orbit shift will be reduced from that estimated from the random closed-orbit shift calculation.

We place a limit on the amplitude of magnet motion to be that which contributes to an RMS orbit shift equal to 10% of the RMS beam size in that plane. These sizes are shown in Table 4.3.1 for beam at the center of the two ID straight sections (long and short, LID and SID):

Table 4.3.1 Beam size at the center of the ID straights for 0.5 nm-rad (x) and 0.008 nm-rad (y) emittance.

Long ID	Long ID	Short ID	Short ID	TPW
σ_x, σ_y	σ_x, σ_y	σ_x, σ_y	σ_x, σ_y	σ_x, σ_y
[μm], [μrad]	[μm], [μrad]	[μm], [μrad]	[μm], [μrad]	[μm], [μm],
107.7 4.64	4.8 1.67	29.6 16.9	3.1 2.58	175 12.4

The closed orbit at the center of the short straight section for 2,000 random seeds is shown in Figure 4.3.1, for the ring quadrupoles shifted by Gaussian random values with RMS values of (ΔX = 0.157 μm and ΔY = 0.022 μm). Each point represents a different sampling of the random fluctuations of the quadrupole centers at any frequency with that amplitude, and includes all of the nonlinear elements in the calculation.

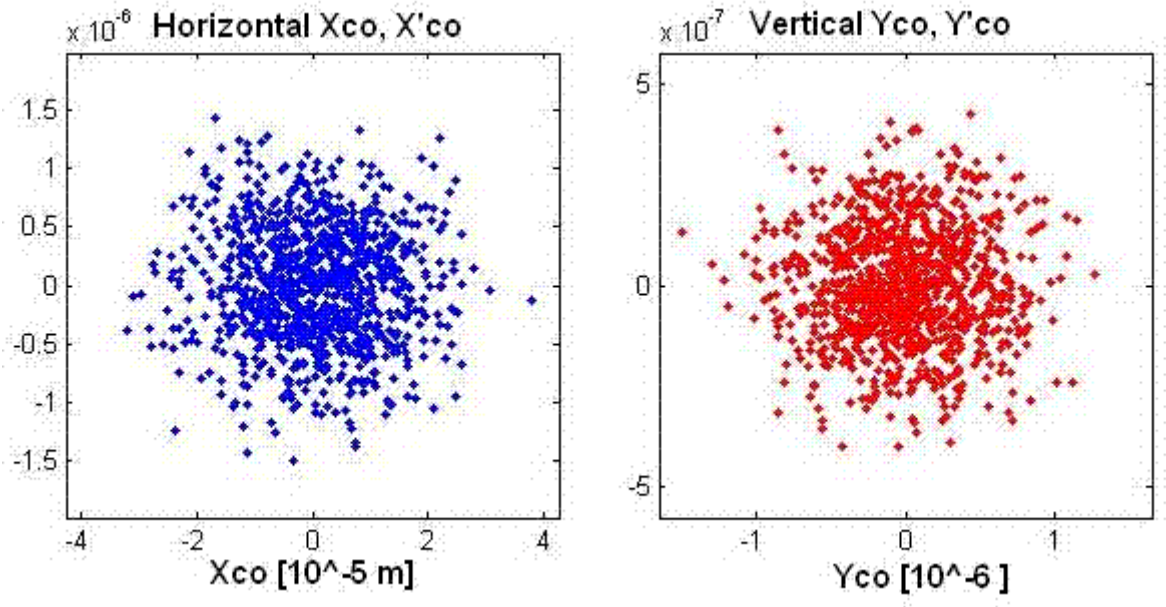

Figure 4.3.1 The horizontal and vertical closed-orbit in the LID straight for 2,000 seeds with RMS random quadrupole center shifts of ΔX = 0.157 and ΔY = 0.022 μm.

The RMS horizontal and vertical beam orbit shifts were 19.4 and 0.5 μm, respectively, or 10% of the RMS beam size in the LID. These RMS values give a very conservative tolerance for quadrupole vibration tolerances. At frequencies above the damping frequency, $F_{x,y}$, this calculation gives an estimate of the emittance dilution.

$$\Delta\varepsilon_x / \pi = \frac{1}{n}\sqrt{\sum x^2 \sum x'^2 - \left(\sum x\, x'\right)^2} \tag{4.3-1}$$

where x and x' are closed orbit and slope from each seed and the sum is over all seeds. The effective emittance dilution shown in Figure 4.3.1 is only 1% horizontal and 1% vertical of the emittance plane, or $\Delta\varepsilon_x$ = 5.1 pm and $\Delta\varepsilon_y$ = 0.09 pm, representing a small increase in the damped beam emittance.

Since the dipole magnets do not have gradients, their transverse motions have little impact on the closed-orbit motion. However, longitudinal position fluctuations of the dipoles will also create a horizontal beam

motion and the roll angle will create a vertical closed-orbit motion. Using a similar random distribution analysis, we set a tolerance level for the RMS fluctuations of the dipole longitudinal position, $\Delta S < 2$ μm, and the dipole roll angle of $\Delta\theta < 0.1$ μrad. These tolerances, together with the quadrupole levels set above, contribute increases of the RMS closed-orbit motions of 11% and the effective emittance dilution of

$$\Delta\varepsilon_x = 5.6 \text{ pm and } \Delta\varepsilon_y = 0.12 \text{ pm.} \quad (4.3\text{-}2)$$

Because the magnets are not supported independently but on girders, magnetic center fluctuations will be correlated. In Section 7.1.1 the effect of random misalignment of the girders was considered and the closed-orbit Girder Amplification Factor was computed to be 3 to 5 times less than the COAF for the quadrupoles, for independent fluctuations. The GAFs in the long ID straight sections are 34 μm (H) and 7.8 μm (V). In the short ID straight sections the GAFs are 9.4 μm (H) and 4.3 μm (V). To maintain an RMS closed-orbit fluctuation of ~10% of the RMS beam size in the LID would require random girder fluctuations of less than 0.31 μm (H) and 0.061 μm (V). The tolerances for the SID would be 0.31 μm (H) and 0.0072 μm (V). This shows the reduction in tolerance levels for vibrations coming from the correlation of the magnet vibrations, compared to the random quadrupole tolerance, and that the random model tends to yield a worst-case tolerance level estimate for vibrations.

Another model for quadrupole magnet center fluctuations attempts to include a magnet-to-magnet spatial correlation based on a ground movement model of a plane wave passing through the ring. This model was implemented in the accelerator design code BETA-ESRF [4.3.1]. The horizontal and vertical quadrupole motions are then calculated from the amplitude and wavelength (λ) of the wave. The increase in the effective emittance can be calculated from the closed-orbit shift around the ring using Eq. (4.3-1). Since there will be a dependence on the direction of the wave relative to straight sections, several phases relative to the lattice orientation have been considered, to estimate the maximum impact. The wavelength varies as a function of frequency, which depends on the knowledge of the speed of propagation. We assumed V = 270 m/sec for both S and P waves (see Section 4.3.3.5.1 for measurement for the BNL site). The impact on the beam's closed-orbit shift is then estimated by displacing the center of each quadrupole on the corresponding point of the plane wave. The effective amplitude of the closed-orbit distortion is estimated by sampling the closed orbit around the ring, instead of for different seeds. No consideration for the girders is taken, nor is there any damping of the wave or the beam assumed. Figure 4.3.2a shows the tolerance level for the horizontal (pressure, P) wave amplitude versus frequency ($f = V/\lambda$), for an effective emittance dilution that is 1% of the beam emittance, or 5 pm.

Figure 4.3.2b shows the tolerance level for the vertical (shear, S) wave amplitude versus frequency ($f = V/\lambda$), for an emittance dilution that is 1% of the beam emittance, or 0.08 pm. Clearly, as the wavelength exceeds the ring diameter of 248 m ($f<\sim2$ Hz), the entire ring moves in phase and the closed-orbit impact becomes small; the tolerance becomes quite large. Above 20 Hz (H) and 10 Hz (V), the amplitude tolerance becomes almost independent of frequency, about at the levels where $\Delta X = 0.08$ μm and $\Delta Y = 0.04$ μm.

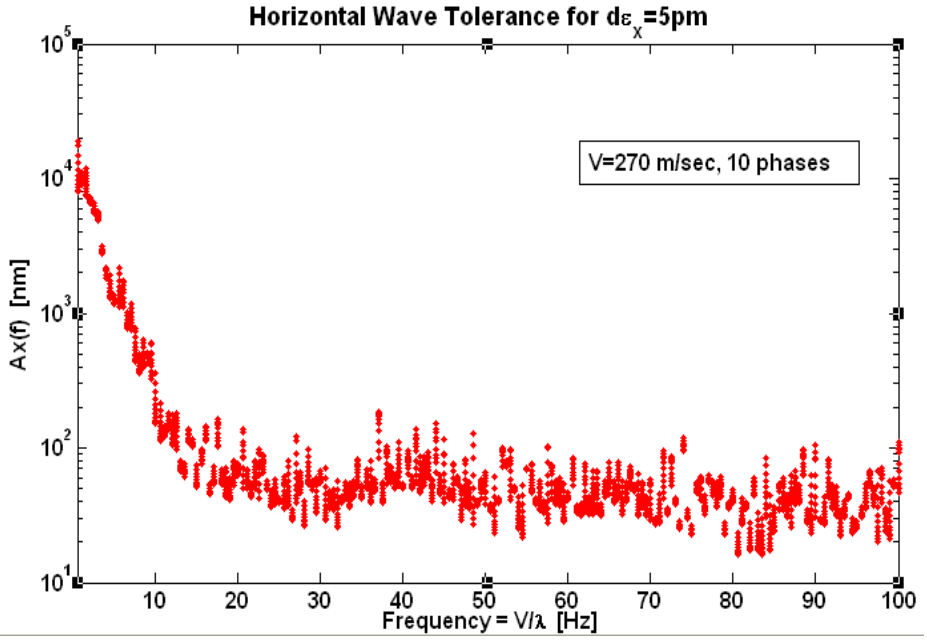

Figure 4.3.2 a The tolerance level for a horizontal wave amplitude, in nm, yielding a 5 pm emittance dilution, assuming a wave velocity of 270 m/sec.

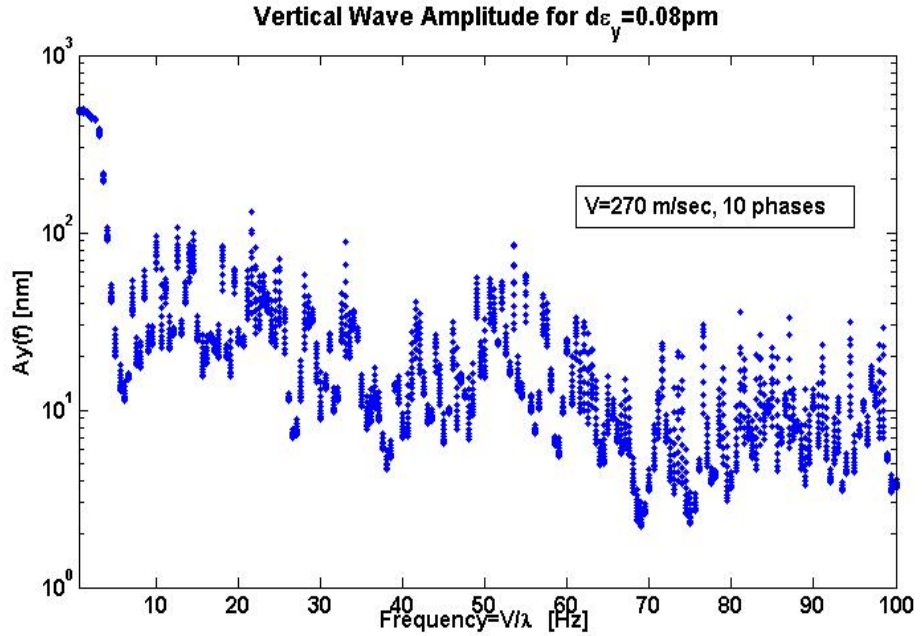

Figure 4.3.2 b The tolerance level for a vertical wave amplitude, in nm, yielding a 0.08 pm emittance dilution, assuming a wave velocity of 270 m/sec.

At frequencies below the 2 Hz level, clearly this model will yield very large tolerances, since all the ring magnets move together. In the low-frequency range (up to ~50 Hz), the global feedback system will take out most of the closed-orbit motion independent of the source term, to a level limited by the BPM and corrector electrical noise level. Above 50 Hz, the centroid motion becomes less obvious, but the beam emittance will be diluted by the effective emittance resulting from the magnet motion.

In summary, the magnet stability tolerances estimated with these models show the worst-case being the random model for the ~10% vertical beam size. However, the effective emittance contribution of this is 1% of the beam emittance and could be relaxed at least by a factor of 2, to about 0.050 μm. These tolerance limits, for the magnets only, are listed in Table 4.3.2. All other tolerances are readily achievable with careful design of girders and the accelerator floor. However, a global feedback system is planned, to ensure that orbit stability is achieved even if these tolerances cannot be achieved. Based on the calculations in Section 6.3, this feedback system will handle random quadrupole fluctuations as large as 0.3 μm vertically.

Table 4.3.2 Magnet Stability Tolerances for AC Closed-Orbit Stability, without Feedback Correction.

Tolerance Limits	ΔX RMS Quads	ΔY RMS Quads	X (LID) RMS	Y (LID) RMS	X (SID) RMS	X (SID) RMS
Random motion	<0.157 μm	<0.022 μm	10.5 μm	0.48 μm	3.2 μm	0.30 μm
Random girder motion	<0.31 μm	<0.072 μm	10.6 μm	0.5 μm	3.0 μm	0.30μm
Plane wave <5Hz	>2 μm	>0.1 μm	10.5 μm	0.5 μm	3.0 μm	0.30 μm
Plane wave >10Hz	~0.08 μm	~0.04 μm	10.5 μm	0.5 μm	3.1 μm	0.28 μm
Additional limits	**ΔS RMS Dipole**	**Δθ RMS Dipole**				
Random motion	≤2 μm	≤0.1 μrad	10 μm	0.48 μm	3.2 μm	0.30 μm

4.3.3 Preliminary Design of the Magnet–Girder Support System

4.3.3.1 Functional Requirements

The storage ring girders in a cell provide common mounting platforms for different set of magnets, as shown in Figure 4.3.3. Multipole magnets are mounted on girders in sections numbered 2, 4, and 6. Dipoles are mounted on separate girders in sections numbered 3 and 5, because of their height difference and less stringent alignment and stability requirements.

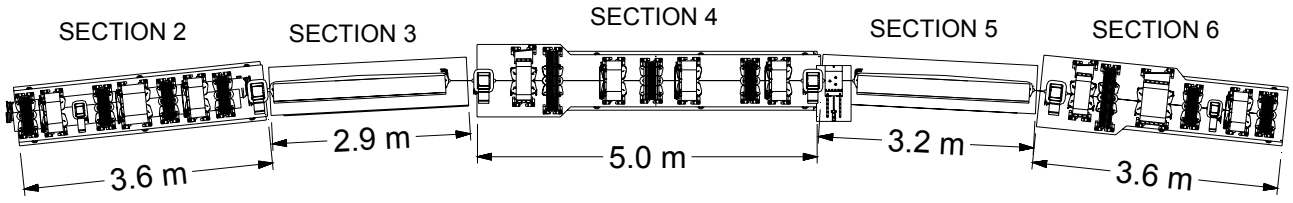

Figure 4.3.3 NSLS-II girders in one cell of the storage ring.

General functional requirements of the magnet–girder support system are given as follows:

1. Raise the centers of the magnets to the nominal beam height of 1 m. This height was chosen based on stability considerations that are discussed in Section 4.3.2.
2. Provide a stable platform for assembling and aligning the magnets outside the tunnel. The stringent alignment tolerances can only be met by precision alignment techniques (see Section 4.3.3.3) requiring out-of-tunnel assembly and alignment. The magnet alignment must remain unperturbed during the transportation and installation of the magnet–girder assemblies in the tunnel.

3. Meet girder-to-girder alignment requirements, both during the initial alignment and subsequently to compensate for long-term floor settlement.
4. Meet dynamic stability requirements under expected ambient floor motion, flow-induced vibrations, and temperature fluctuations of the tunnel air and process water.

In addition, the overall width of the magnet–girder support system must be less than 1 m, for ease of transportation and assembly in the tunnel. The support design must also be cost effective without sacrificing speed of installation and alignment.

4.3.3.2 Main Preliminary Design Features

In many recent light sources the girders have been precisely fabricated with very stringent top surface tolerances (~15 μm flatness) and with T-slot type alignment features. Magnets, built with equally tight tolerances, are fastened directly to the girder's top surface without an interface of alignment hardware. After a careful examination of this approach, we decided to design NSLS-II girders and magnets with conventional tolerances, and to use a vibrating-wire alignment technique for aligning the magnets to within ~30 μm tolerance.

A typical girder with its mounting pedestals is shown in Figure 4.3.4. The nominal length is 2.9 to 3.2 m for the dipole girders and 3.6 to 5.0 m for the multipole girders. The girders are approximately 0.8 m wide and 0.5 m high. They are fabricated by welding commercially available plates and channels of thicknesses ranging from 1 to 2 inches. After welding, the girders are stress-relieved by commercial vibratory stress-relief equipment.

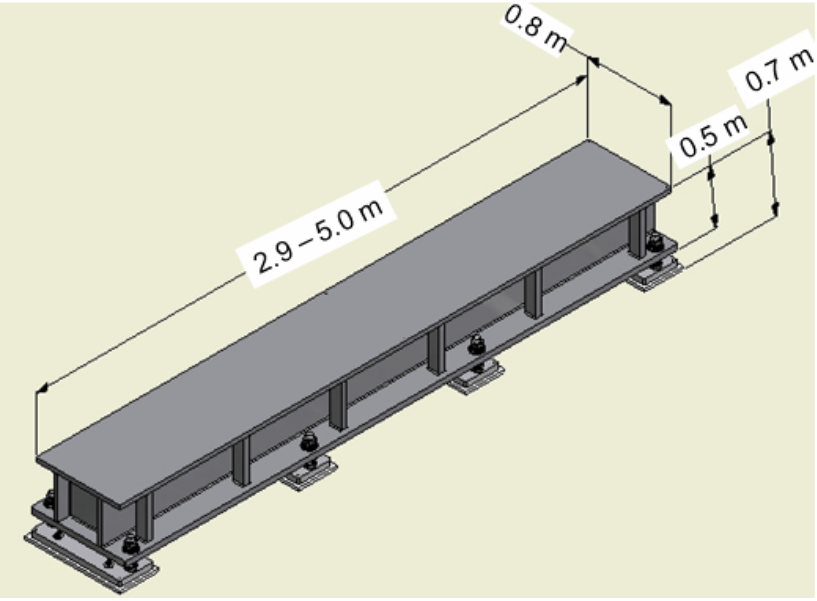

Figure 4.3.4 Preliminary design of the NSLS-II storage ring girder.

The girders are mounted on four 2-inch-thick pedestals that are grouted to the floor with nonshrinking epoxy grout. For mounting and height adjustment, eight 2 inch-diameter bolts with spherical washers are used. The girder is thus over-constrained in order to minimize static deflection and to raise the first natural frequency of the magnet–girder assembly. A similar over-constrained scheme has been used successfully at SPring-8 [4.3.2] and will be implemented at the ALBA light source [4.3.3].

4.3.3.3 Magnet–Girder Assembly and Alignment

NSLS-II lattice magnets have magnetic alignment tolerances that exceed mechanical assembly tolerances and the ability of conventional alignment techniques to locate the magnetic components within the required

tolerances. Therefore, a vibrating wire alignment technique, originally developed at Cornell University [4.3.4] and subsequently adopted at SLAC, will be used. It has been shown that this technique is capable of aligning magnets to within 10 μm with respect to an axis defined by the wire.

In this alignment technique, an oscillator drives a sinusoidal current in a thin wire (~150 μm diameter) stretched through the apertures of all the magnets on a girder while a particular magnet being measured is powered (see Figure 4.3.5).

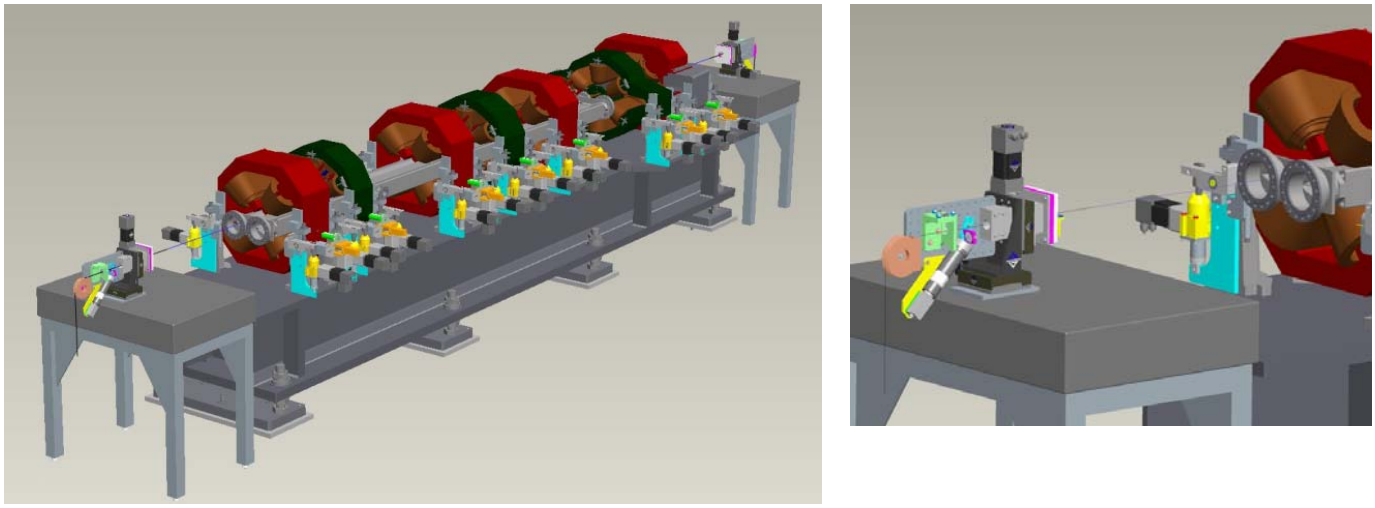

Figure 4.3.5 **Left**: Vibrating wire alignment system mounted on the girder. **Right**: Special brackets with wire movers, wire locators, and laser tracker fiducials are attached to either end of the girder.

The presence of any transverse magnetic field at the wire position exerts a sinusoidal force on the wire, causing it to vibrate. The vibrations in the wire in the transverse plane are detected by a pair of sensors (one for each axis). By carefully selecting the drive current frequency to match one of the resonant frequencies of the wire, even very small fields may produce easily detectable wire motion. For measuring average center over the length of the magnet, the resonant mode chosen is the one having an anti-node roughly at the center of the magnet being measured. The transverse field profile in the aperture of the magnet can be measured by recording the amplitude of wire motion as a function of the transverse position of the wire. In the case of a quadrupole, a linear dependence of field with horizontal and vertical position is seen, from which the magnetic axis (defined as the point where the field is zero) can be determined in the coordinate system defined by the wire translation stages. In the case of the sextupole magnets, the field profile is parabolic and the magnetic center is defined as the point where the field gradients (or equivalently, the quadrupole terms) are zero. The magnets are then moved such that the magnetic centers lie on the line joining the two end points of the wire, and are locked into place. Due to the long length (~6 to 7 m) of the wire, there is a significant sag (~600 μm) which must be precisely measured and corrected for while adjusting the magnet positions. It has been shown that the sag can be computed to sufficient accuracy from the measured fundamental resonant frequency. In the case of the quadrupoles, it may be necessary to carry out the measurements at two or more different excitation currents to eliminate any errors caused by background fields, such as the earth's field or remnant fields in the yokes of other un-powered magnets on the girder. Laser trackers are then used to transfer the positions of the wire ends (defining the axis to which all magnets are aligned) to the fiducials on the girder.

The following magnet assembly and alignment plan has been developed Upon receipt individual dipole, multipole, and corrector magnets will be subjected to an incoming test and inspection regimen. Inspections will include dimensional checks, electrical tests and magnetic measurements. Magnetic measurements shall

be performed or certified by BNL's magnet division for every lattice magnet. Magnets will then be stored until needed for girder assembly. Initially, the magnets will be installed and aligned on the girder with a laser tracker. The top-half of the multipole magnets will then be taken off and the vacuum chamber will be installed. The ends of the chamber will be sealed with Mylar caps. The caps will have small holes in either end to allow the ends of the vibrating wire to protrude through while a positive purge of dry nitrogen gas is maintained. After the top half of the magnets are reassembled, their iron cores will be supported on precisely computer-controlled positioners as shown in Figure 4.3.5. The roll angles of the magnet cores will be brought to within ±0.2 mrad tolerance by using magnet positioners and digital inclinometers. The girder is then installed in the vibrating wire test stand built in an clean temperature-controlled laboratory and all magnets are aligned to a common straight line as described above. The magnets are then tightly fastened to their supports legs.

To determine the feasibility of maintaining the magnet alignment during this fastening process, a bolting test fixture was fabricated using a Swiss Light Source magnet of the size and weight comparable to that of the NSLS-II magnets. Using electronic indicators, ten trials of positioning and then bolting the magnet were performed to replicate the procedure that will be required with the magnet mover system. Location data and time per trial were recorded. The tests proved that it is relatively quick (<10 minutes per magnet) and easy (standard fine thread hardware, no special tools nor experienced labor) to obtain a stable positioning of the magnet vertically to within 5 microns, and laterally to within 10 microns of the desired theoretically “perfect” position. Thus real magnetic alignment of the multipoles to within 20 microns on a rigid girder appears feasible.

4.3.3.4 Installation of Magnet–Girder Assemblies

A transporter system with self-contained air pads will be used to transport the girder–magnet assemblies from the alignment laboratory into the storage ring tunnel for final installation.

During the early phases of girder installation, the multipole girders will be installed prior to the dipole magnets. The wire support brackets will be left attached for the entire installation process. The air pad system will cushion any shocks to the girder during transport to prevent shifting of the magnets from their aligned positions. The girder transporter will locate the girder over the eight pedestals studs that will affix the girder to the tunnel floor.

Instrumented torque wrenches will be used in conjunction with laser trackers to precisely offload the girder from the air pads onto the pedestals’ studs. Once the girder is fixed to the floor and prior to dipole installation, in-situ vibrating wire measurements will be repeated to confirm alignment of the magnets. These measurements will be discontinued when it is established that the magnet alignment was not disturbed during transportation and alignment.

4.3.3.5 Mechanical Stability of the Magnet–Girder Support System

Sources affecting the mechanical stability of the support system include ground settlement, ambient floor motion, flow-induced vibrations, and thermal transients. These sources can be categorized in terms of the frequency range—*fast* when greater than a few Hz or *slow* when operating at frequencies lower than one Hz. Sources are also categorized based on the time-scale of the excitation, as being short (<1 hour), medium-term (<1 week), or long-term (>1 week). Short-term sources include natural and cultural ground vibrations, flow-induced vibrations, and power supply jitters. Thermal transients due to temperature changes of the cooling water or the tunnel air, as well as gravitational and tide effects, constitute medium-term sources. Floor settlement or seasonal temperature changes, which may have direct impact on the alignment of components, are considered to be long-term effects. Cultural noise or human activity is typically observed in the frequency range of 1 to 100 Hz. Ground motion from ocean waves or tides is centered at about 0.2 Hz.

4.3.3.5.1 Medium- and Long-Term Stability

Over the years, various studies have been performed at the BNL site and in the vicinity of NSLS-II to characterize the subsurface conditions. Drill-core data show that the soil at the site consists mainly of medium coarse sand with traces of silt and, in some cases, traces of clay and gravel. The shear wave velocity in the top sand layer is about 270 m/sec. The bedrock lies at a depth of approximately 430 m beneath the site. Therefore, the BNL site is classified as a very deep site with relatively soft soil. The soil consisting of glacial sands is well settled and, based on the drill-core results, exhibits limited scatter in key properties (coefficient of variation ~0.18). This is important, in that the differential movement (or settlement) in the soil supporting NSLS-II is expected to be of the order of 10 μm /10 m / year. To ensure that this is the case, a detailed study of ground settlement based on finite element analysis will be performed, taking into account both the site soil conditions and the facility layout.

4.3.3.5.2 Short-Term Stability

Short-Term Stability – Ambient Ground Motion

Ambient ground motion measurements near the NSLS-II site were taken from August 31 through September 1, 2006. Data measured at the following locations at BNL were used for a comparison of the NSLS-II site with the ALS, ESRF, and SPring-8 sites:

1. Microscopy suite of the Center for Functional Nanomaterials (CFN)
2. Foundation of a light stand near CFN, not stiffened by the presence of the building
3. A remote location near the northeast corner of BNL
4. Experimental hall of NSLS directly beneath the X1 beamline

The RMS (4–50 Hz) amplitudes of the ground motions in vertical, north–south, and east–west directions are given in Table.4.3.3. The most important value is that of the microscopy laboratory at CFN, where the RMS amplitudes are 20 nm or lower in all directions. The lower values, compared to those at the free-field at CFN and at the remote northeast BNL location, are indicative of the stiffening effect of the CFN building and the floor. The ambient ground motion at the floor of NSLS X1 beamline is considerably higher at 18 and 30 Hz, due most likely to rotating mechanical equipment.

Table 4.3.3 RMS (4-50 Hz) Ground Motion near the NSLS-II Site.

Location	Time	Vertical (nm)	North–South (nm)	East–West (nm)
Microscopy lab at CFN	7:30 pm	20	12	19
Free-Field at CFN	11:40 pm	24	41	38
Remote location near the northeast corner of BNL	Noon	21	25	26
Beamline X1 at NSLS	Midnight	71	12	13

Figure 4.3.6 shows the vertical log mean of site vibrations at the NSLS-II site expressed as PSD, compared with similar data from ALS, ESRF, and SPring-8. Shown also are PSD spectra measured at NSLS beamline X1 just after midnight, the “free-field” location near CFN, and the microscopy suite at CFN identified by the black arrow. The legend indicates the RMS amplitude using summation between 4 and 50 Hz, except for the NSLS-II log mean, which is summed with a 6 Hz lower cutoff because of contamination by the instrumentation noise floor at lower frequencies. The RMS amplitudes for ALS, ESRF, and SPring-8 were calculated in the 2 to 100 Hz band.

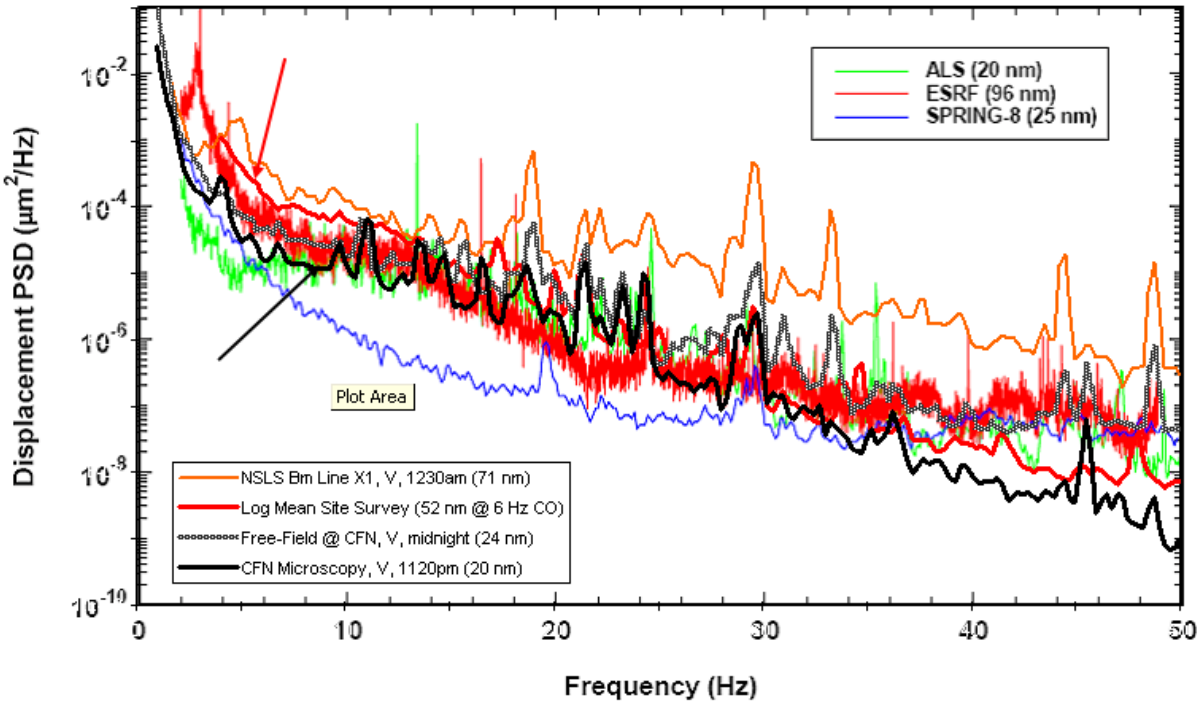

Figure 4.3.6: Comparison of PSDs of vertical ground motions at various locations near the NSLS-II site and at ALS, ESRF, and SPring-8 light sources [4.3.5].

The vibration measurements indicate the presence of local noise sources at ~18 and 30 Hz in the NSLS building. Further vibration measurements are planned to identify and eliminate these local sources of vibration. In addition, the CFN measurements show that the installation of the NSLS-II storage ring and experimental hall will significantly stiffen the site. The floor vibration levels of the NSLS-II storage ring are then expected to be comparable to those of the other light source facilities.

4.3.3.6 Resonant Frequencies of the Girder Support System

Although the NSLS-II magnet–girder assembly fastened to the pedestals is a complex dynamical system, its important design features can be understood by a simple 1-D oscillator shown in Figure 4.3.7a.

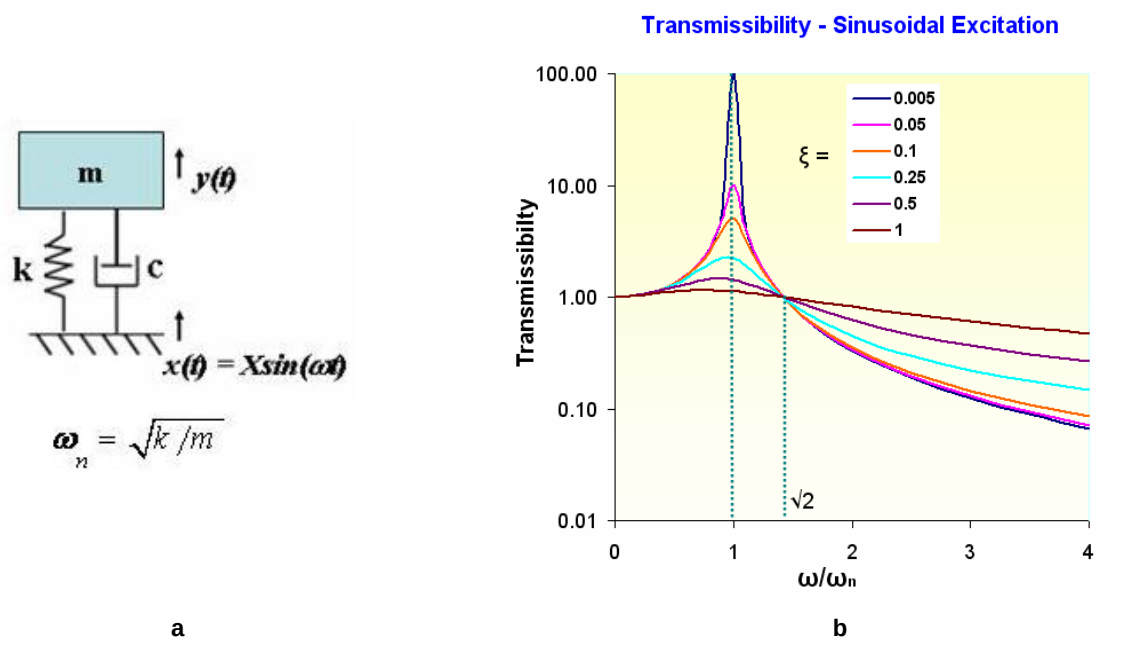

Figure 4.3.7 **a**) 1-D oscillator; **b**) transmissibility plot.

For such an oscillator, the natural frequency is

$$\omega_n = \sqrt{k/m} \tag{4.3-3}$$

and the vibration amplification (or transmissibility) is given by

$$Transmissibility = Y/X = \sqrt{\frac{4\xi^2(\omega/\omega_n)^2 + 1}{[1-(\omega/\omega_n)^2]^2 + 4\xi^2(\omega/\omega_n)^2}} \tag{4.3-4}$$

where the fraction of critical damping, ξ, is given by

$$\xi = \frac{c}{2\sqrt{mk}} \tag{4.3-5}$$

Transmissibility curves, obtained from Eq. 4.3-4 for different values of critical damping, ξ, are plotted in Figure 4.3.7b. There is no significant vibration amplification (transmissibility $\approx$ 1) when the natural frequency, ω_n, is substantially greater than the excitation frequency, ω. The ambient ground motion reduces sharply as $1/\omega^4$, as shown in Figure 4.3.6, and its amplification above 30 Hz can be ignored. Several investigations have been carried out on the dynamic response of the magnet–girder support systems using vibration measurements and finite element modal analyses. These studies have shown that it is quite difficult to raise the lowest natural frequency of the support system to greater than 20 Hz if elaborate alignment mechanisms are used either between the girder and its pedestals or between the girder and the magnets. When such alignment mechanisms are used, then the internal structural damping (ξ = 0.02 to 0.04) of the support

system is insufficient to reduce the floor motion amplification to an acceptable level. External damping devices, either active or passive, are then used, such as viscoelastic damping pads at APS and ESRF.

For the NSLS-II magnet–girder support system, a lowest natural frequency of greater than 50 Hz will be obtained by eliminating elaborate alignment mechanisms, and by lowering the beam height to 1 m. Short, stiff threaded rods will be used for height adjustment only. The alignment of the girders will be achieved by precise but removable alignment mechanisms. Finite element model analysis of the NSLS-II magnet–girder assembly shows that the lowest two natural frequencies are 58.8 Hz and 74.4 Hz. The corresponding mode shapes, rolling and twisting of the girder, are depicted in Figure 4.3.8.

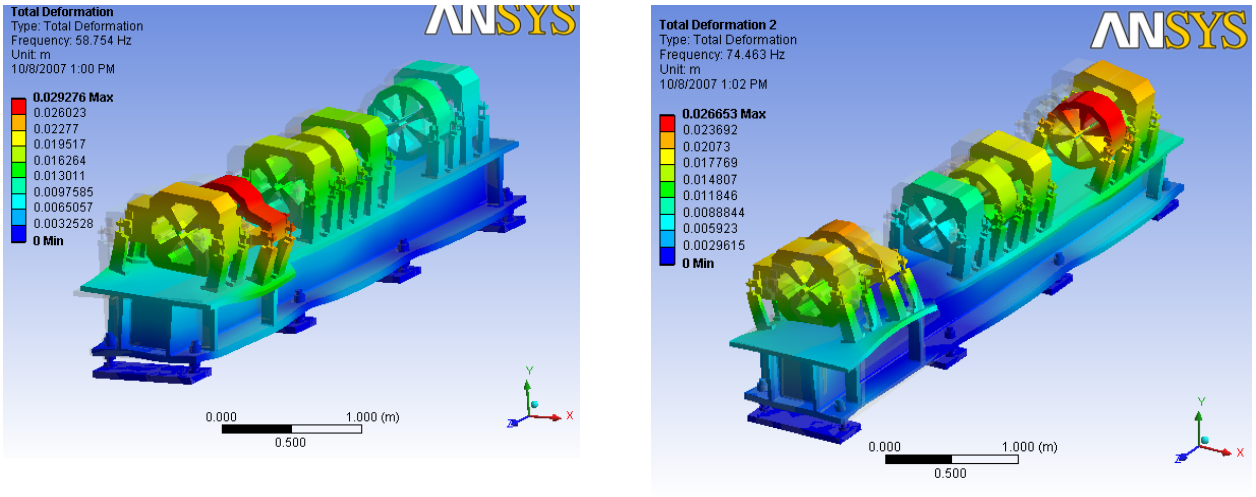

Figure 4.3.8 Mode shapes of the NSLS-II magnet–girder assembly.
Left: First mode shape, rolling, ω_1 = 58.8 Hz. **Right**: Second mode shape, twisting, ω_2 = 74.4 Hz.

4.3.3.7 Flow-Induced Vibrations

Flow-induced vibrations of the water headers can be transmitted to the magnets and the vacuum chambers [4.3.6] by flexible hoses and pipes. The effects of flow-induced vibrations will be mitigated by paying close attention to several useful design guidelines, namely:

1. Locate all rotating equipments including fans, blowers, compressors, and pumps outside the storage ring tunnel, preferable tens of meters away from the tunnel floor and ceiling.
2. Keep low flow velocities (less than 2 m/s) in the process water headers.
3. Design header supports to minimize their vibration, such as by integrating viscoelastic dampers in the headers hangers, or by attaching headers directly to the ceiling.
4. Arrange water flow circuits and connection fittings such that sharp bends are eliminated. Special attention is to be given to the routing and clamping of the hoses and tubes that connect the magnets and vacuum chambers to their respective headers.

Analytical models and vibration measurements will be employed to ensure that flow velocities required to regulate the temperature of the vacuum chambers do not induce unacceptable level of vibrations.

4.3.3.8 Thermal Stability

Ambient temperature variations will result in displacements of both the magnets on the girders and the BPMs on the vacuum chambers [4.3.7]. To ensure acceptable thermal deformations of the ring components, process water and tunnel air temperatures will be maintained to within ±0.05ºC and ± 0.1ºC, respectively, of

their nominal values, 25.0 ºC. Air-conditioning temperature cycling of ~1-hour duration will be maintained in order to take advantage of the thermal inertia of the support system. The girders will be thermally insulated to further reduce the effects of temperature transients.

Lowering the beam height from 1.4 m to 1 m would reduce the vertical thermal expansions of the assembly proportionately. In addition, over-constraining each girder to its pedestal at eight locations would minimize thermal bending effects.

To investigate the effect of temperature transients, FE thermal analyses were performed for the girder, magnets and vacuum chamber assembly. For the analyses, the fluctuations in the temperature of the tunnel air and the cooling water flowing through vacuum chamber were approximated by linear increase and decrease over 15 minuts corresponding to 1-hour temperature cycle. For modeling heat transfer by air convection, a film coefficient value of 8 W/m^2 °C and 1 W/m^2 °C was applied on all external surfaces and internal girder's surface, respectively. The lower film coefficient value was applied on the internal girder's surface to include the effect of stagnant air condition.

For modeling heat transfer by process water a film coefficient value of 15,000 W/m^2 °C was applied. For girder insulation a glass-wool material with a thermal conductivity of 0.03 W/m °C was considered in the analysis.

Figure 4.3.9 shows the temperature distribution in girder, magnets and vacuum chamber assembly. The maximum temperature change in the girder and magnets is limited to ~ 0.01ºC due to the effects of thermal mass and girder insulation. For the vacumm chamber, however, the temperature change is ~ 0.05ºC, the same as the change in the water temperature.

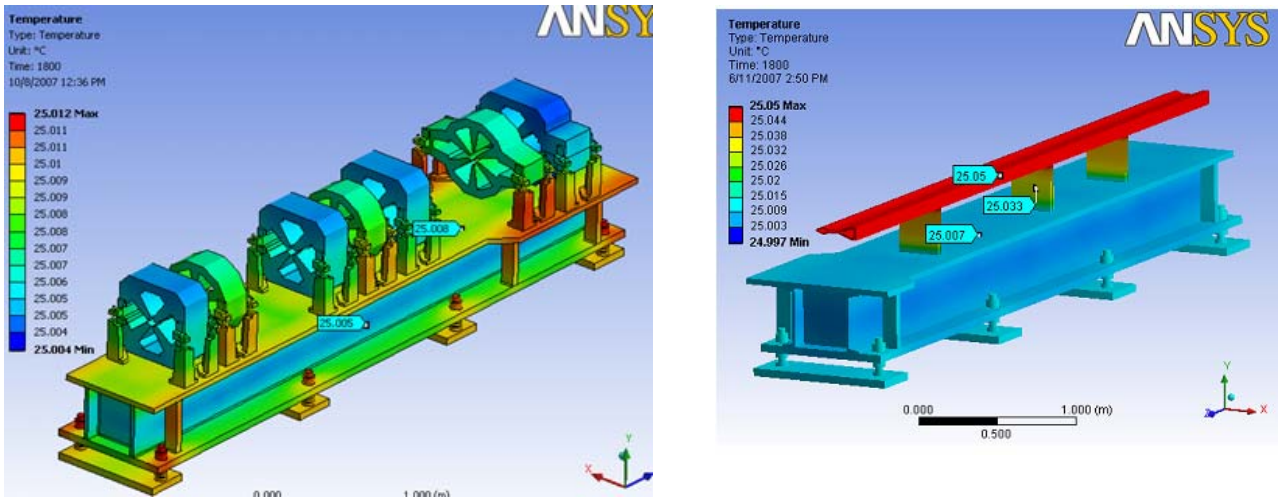

Figure.4.3.9 Temperature distribution in the girder, magnets and vacuum chamber assembly.

Vertical deformations for the girder, magnets and vacuum chamber assembly corresponding to the calculated temperature distribution are shown in Figure 4.3.10. The FEA results indicate that the RMS vertical misalignment between the magnets is 0.013 μm, which is less than the design tolerance of 0.025 μm. For the vacuum chamber, at the BPM locations next to the Invar support stands, the maximum vertical displacements are about 0.14 μm as compared to the mechanical stability budget of 0.2 μm for the chamber-mounted BPMs.

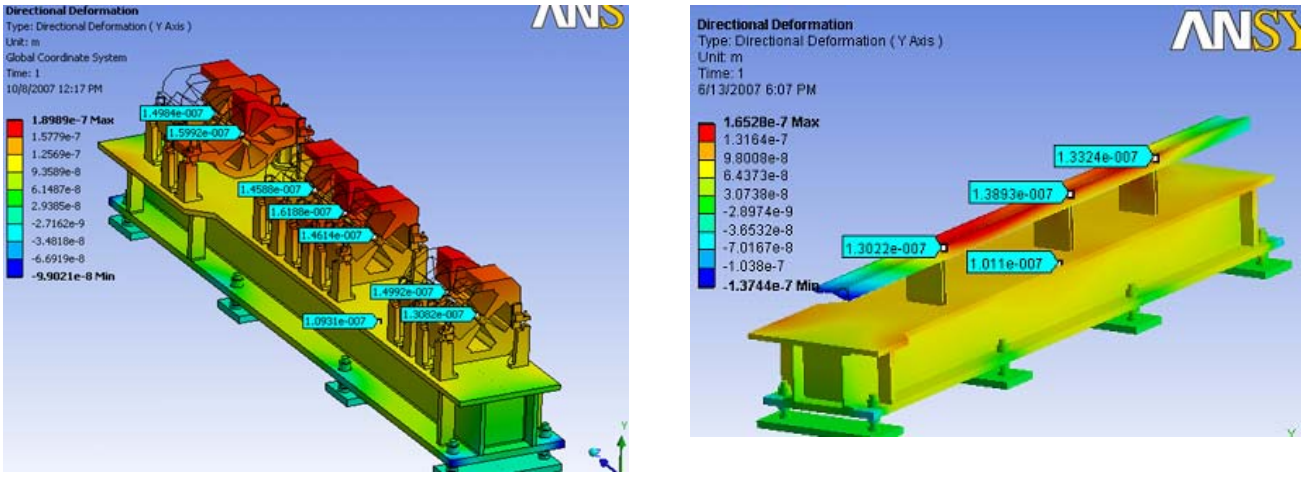

Figure.4.3.10 Vertical thermal deformations of the girder, magnets and vacuum chamber assembly.

4.3.3.9 Stability of the User BPM Support System

Compared to the chamber-mounted BPMs, the BPMs at the two ends of the insertions devices (user BPMs) as well as X-BPMS in the front ends have even more stringent mechanical stability requirements. The vertical and horizontal RMS displacements of the latter BPMs are specified to be less than 0.1 μm and 1 μm, respectively. We are considering BPM support stands made from carbon fiber composite on which the BPM blocks are supported at their mid-planes (see Figure 4.3.11). A carbon fiber composite can have thermal coefficient of expansion as low as 0.2 μm/m/ºC. With the tunnel air temperature fluctuations controlled to within ± 0.1 ºC, the vertical displacement of 1 m high support stand can be maintained to about ± 0.02 μm. The carbon fiber composites are, however, weak in the transverse (thickness) direction which can result in a system with very low natural frequency. Typical Young's moduli along the principal and transverse directions are 120 GPa and 7.5 GPa, respectively. From our preliminary discussions with vendors, we have been assured that the vendors can supply us with a 10-inch diameter carbon fiber composite that will meet the thermal design specification (< 0.1 μm) and the natural frequency requirement (> 50 Hz).

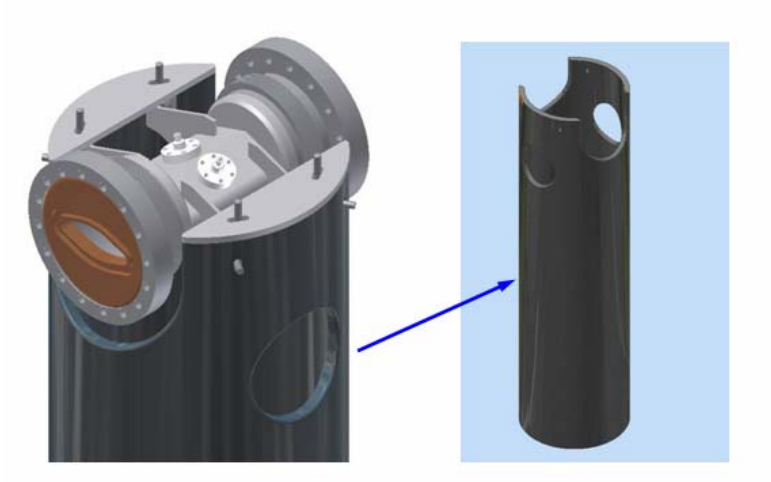

Figure 4.3.11 User BPM support stand with a BPM block mounted at its mid-plane.

A second design option for the user BPM support stands consists of a system of aluminum pipe sandwiched between two structural steel pipes. A schematic of this design is shown in Figure 4.3.12. In this design, the aluminum pipe counteracts the expansion of the steel pipes, and by carefully adjusting the lengths and diameter of each member it is possible to get zero thermal expansion at the BPM support point as indicated by the FEA thermal results (vertical displacement = 0.005 μm) shown in Figure 4.3.13.

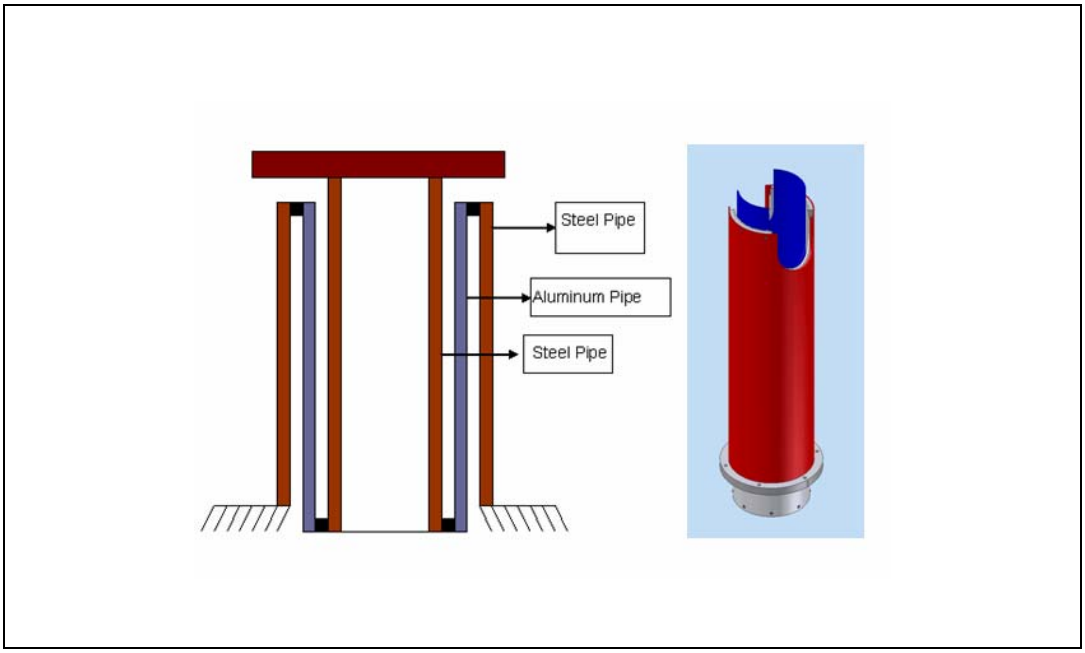

Figure 4.3.12 User BPM support stand consisting of aluminum and steel pipes

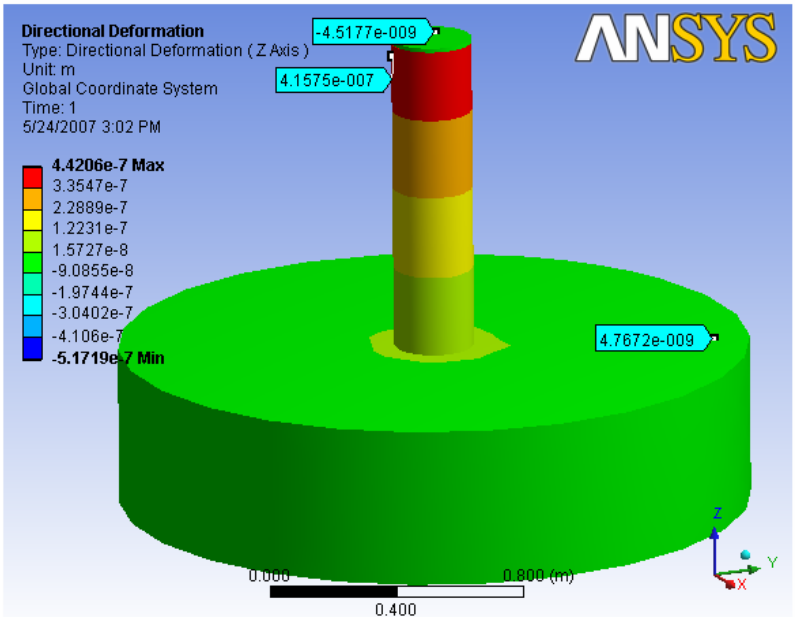

Figure 7.3.13 Maximum thermal deflection at the user BPM support point = -0.0045 microns.

Vibration FEA analysis results for this design are shown in Figure 4.3.14. The lowest natural frequency for the system is 45 Hz which corresponds to vibration (swaying) in the horizontal direction. The RMS horizontal displacement (2-50 Hz, 1σ) is calculated to be 0.026 μm as compared to the specification of 1 μm.

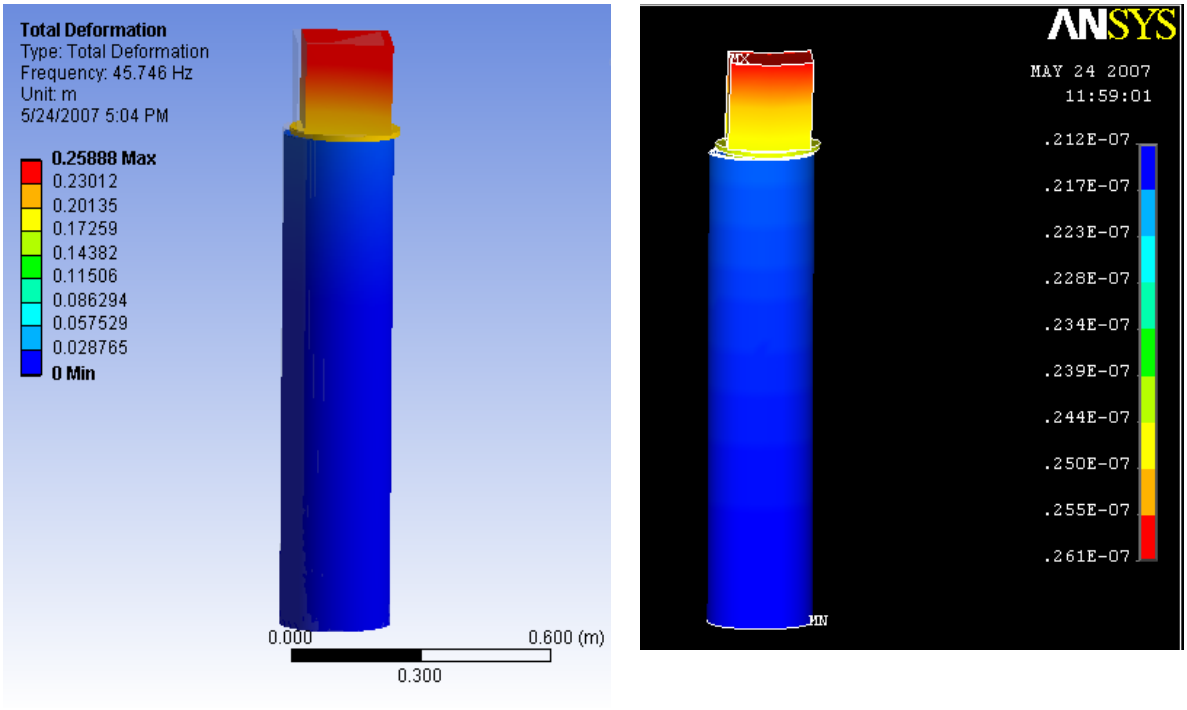

a **b**

Figure 7.3.14 **a:** Modal analysis of user BPM support stand -natural frequency = 46 Hz, **b:** Random vibration analysis of user BPM support stand-RMS displacement = 26 nm

4.3.3.10 R&D Program on Stability of the Magnet–Girder Support System

To further improve the mechanical stability performance of the girder support system, the following R&D tasks will be undertaken:

- real-time online measurements and analysis of the NSLS-II ambient ground motion.
- optimization of the stiffness of the magnet–girder assembly (A prototype assembly will be built for this purpose.)
- use of viscoelastic damping devices
- characterization and mitigation of the flow-induced vibrations of the magnets and the vacuum chambers
- investigation of the effect of process water and tunnel air temperatures on the field quality of the storage ring magnets
- assessment of insulating materials to reduce the effects of thermal transients in the tunnel

References

[4.3.1] BETA USERS' GUIDE by L. Farvacque, T.F. Gunzel, J.L. LaClare, A. Ropert.
[4.3.2] K. Tsumaki and N. Kumagai, "Vibration Measurement of the SPring-8 Storage Ring," IEEE, PAC, 2001.
[4.3.3] L. Nikitina and Y. Nikitin, private communication on ALBA girders, August 13, 2006.
[4.3.4] A. Temnykh, "The Magnetic Center Finding using Vibrating Wire Technique," CBN 99-22, Cornell University, May 26, 1999.
[4.3.5] S. Sharma, C. Doose, G. Portmann, L. Zhang, K. Tsumaki, and D. Wang, "Ground Vibration Problems at the Light Sources," 22nd Advanced ICFA Beam Dynamics, SLAC, Nov. 6-9, 2000, SLAC-WP-18, pp. 37-48.
[4.3.6] Nakazato, et al., "Observation of beam Orbit Fluctuation with Forced-Vibrating Magnets and Vacuum Chambers," MEDSI2002, Chicago, IL 2002.
[4.3.7] L. Emery, "Measurements of Thermal Effects on the Advanced Photon Source Storage Ring Vacuum Chamber," MEDSI2002, Chicago, IL, 2002.

4.4 Beam Chambers and Vacuum Systems

4.4.1 Scope

The storage ring vacuum system provides adequate and low impedance aperture for the circulating electron beam, and low pressure for long beam lifetime and low bremsstrahlung radiation. The storage ring vacuum system includes all vacuum chambers, vacuum pumps, vacuum valves, bake-out systems, and vacuum instrumentation and control. The storage ring vacuum system extends throughout the storage ring from the booster injection line-storage ring interface to the photon exit gate valve at the front end transitions to the user beamline.

During the start-up and beam commissioning of the storage ring, no insertion devices will be installed or positioned at the designated straight sections. Therefore, straight beam pipes with same cross section as the cell multipole chambers will be installed at these straight sections. Some appendage vacuum components such as rf-shielded gate valves, bellows, pumps, vacuum gauges and residual gas analyzers, will be installed at the designated straight sections together with the insertion devices after the initial beam commissioning.

Many components such as photon absorbers, beam scrappers, insertion devices, etc. require or share storage ring vacuum, but only the components whose main purpose is to maintain, monitor, and control storage ring vacuum are included in detail here. The other components are described in their respective sections.

The average pressure with beam is designed to be less than 1×10^{-9} Torr with main residue gas being hydrogen. At this pressure level, the beam lifetime due to bremsstrahlung and Coulomb scattering is longer than 40 hours. The stored beam lifetime for 500 mA operation will be limited to 2–3 hours by the Touschek lifetime due to the scattering loss of electrons in the bunch. However, localized pressure bumps will produce bremsstrahlung radiation and damage the beam line components, and have to be suppressed.

To achieve the low thermal outgassing and low photon-stimulated desorption (PSD), all the vacuum vessels and appendage vacuum components will be made from ultra high vacuum compatible materials. All the vacuum components will be carefully prepared, cleaned, and conditioned using UHV compatible processes. In-situ bake will be implemented to further lower the thermal outgassing and PSD.

4.4.2 Mechanical Design

4.4.2.1 Design Overview

There are 30 cells in the storage ring. Each vacuum cell consists of five basic chambers; an upstream matching multipole chamber, a dipole chamber, an arc section multipole chamber, a second dipole chamber, and a downstream matching multipole chamber. There are RF-shielded bellows connecting the chambers together. There is a straight section, either 6.6 m or 9.3 m long between the cells, for insertion devices and for special components such as RF cavities, injection devices, damping wigglers, and so forth. A typical vacuum cell layout is shown schematically in Figure 4.4.1. The dipole chambers are approximately three meters long and the straight chambers for the multipole magnets 3 to 5 m long. All-metal, RF-shielded gate valves will be employed to isolate each of the 30 cells and the straight sections between cells.

Most of the storage ring cell chambers will be made of extruded aluminum with a cross-section similar to that of the APS chambers [4.4.1]. Regular or bi-metal Conflat flanges with copper gaskets will be used throughout the vacuum systems, except for the flanges and seals for beam position monitor buttons, where Helicoflex delta seals will be employed. Water-cooled copper or Glidcop absorbers will be positioned in the

storage ring vacuum chambers to absorb the unused photons and heat loads, and to protect the un-cooled flanges and bellows. The entire vacuum cells will be in-situ bakeable to 130°C to remove adsorbents, such as water, and contaminants on the inner surface. Vacuum bake for the aluminum chambers will be at 120°C using pressurized hot water circulated within the cooling water channels. Alternative bakeout and conditioning approaches, such as super dry hot nitrogen flush and non-evaporable getter (NEG) strip heating, will be explored for their benefit and applicability. External heating jackets will be used for the bakeout of the appendage vacuum components.

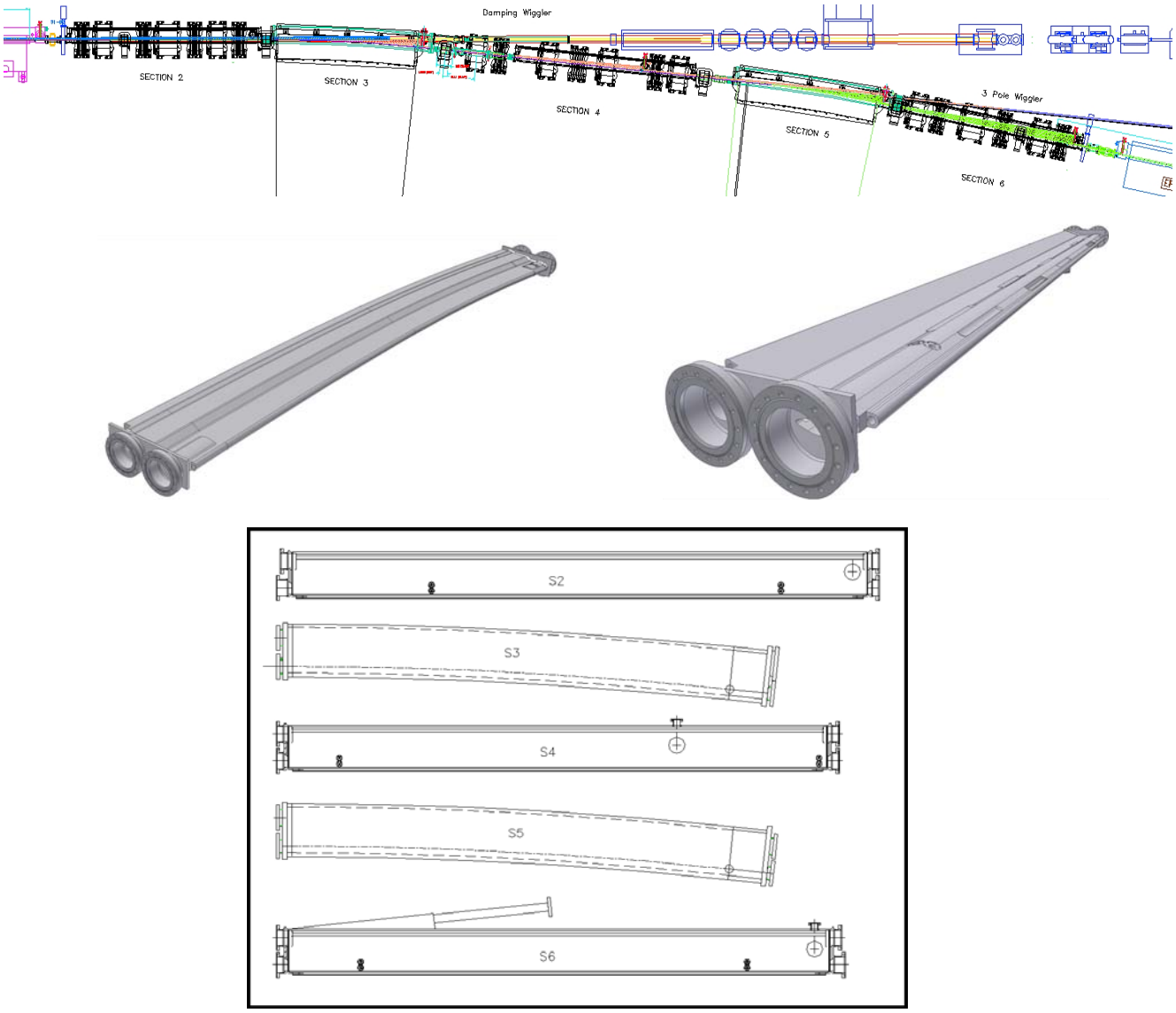

Figure 4.4.1 The layout of the five cell vacuum chambers in a typical storage ring cell with two photon exit ports; the 3D models of dipole chambers, and the arc multipole chamber; and the top view of the five chambers in each cell.

To achieve fast conditioning after intervention, sufficient pumping capacity is needed. Following rough pumping and in-situ bakeout, the vacuum cell chambers will be pumped by sputter ion pumps, non-evaporable getters (NEGs), and titanium sublimation pumps (TSP) as their main UHV pumping, The vacuum chamber design must provide provisions for stability during bakeout and with sufficient precision for accurately locating the vacuum chambers and BPM buttons after bakeout. Three chamber supports made of Invar will be employed for each cell chamber, one fixed support in the middle and two flexible supports at the

ends. The impedance of the vacuum chamber should be low enough so as not to excite higher-order mode resonances. Smooth cross-sectional transitions between components are required, as are flexible interfaces such as RF-shielded bellows between cell chambers and insertion devices.

4.4.2.2 Vacuum Chamber Design

The electron beam vacuum chambers differ according to their location within the storage ring. The vacuum chambers will provide adequate ports for heat absorbers, BPM buttons, pumps and exit ports to the front ends. A pronounced antechamber design similar to that of APS [4.4.1] will be used to allow adequate aperture for the exiting photon beams and to better distribute vacuum pumping capability. The cell vacuum chambers, as shown in Figures 4.4.2 and 4.4.3, contain two distinct but connected channels; the beam channel portion must be continuous, but the antechamber portion may be interrupted at various locations for vacuum valves, bellows, absorbers, insertion device chambers, and other devices where the mechanical requirements constrain the use of the antechamber. Ports emanating from the aluminum cell chambers will have aluminum-stainless bi-metal Conflat flanges which joint to the standard mating Conflat flanges using regular copper gaskets. The internal beam chamber cross-section will be elliptical, 25 mm vertical by 76 mm horizontal, to allow sufficient beam-to-chamber clearance, except at absorbers. The absorbers will be inserted horizontally from the antechamber side wall and positioned 22 mm to 27 mm from the beam channel center to intercept a portion of the photon fans from the bending magnets The antechamber is also sized for distributed NEG pumping and to fit within the multipole magnets.

The photon exit slot connecting the beam channel and antechamber is sized as large as possible to provide adequate aperture for photon fans and sufficient vacuum pumping conductance. However, the vertical height of this slot is restrained by magnet pole gaps and by the minimum required wall thickness under atmospheric pressure load when the chamber is under vacuum. The chamber cross sections inside the dipole, quadrupole and sextupole magnets are shown in Figure 4.4.2. There will be 2 mm clearance between chambers and magnet poles and coils at the closest points, except at corners of sextupole poles, to count in the chamber fabrication tolerances, to allow the alignment of BPM buttons and the adjustment of the chambers and supports. The extruded chamber cross sections and the cross sections after machining are given in Figure 4.4.3. The multipole chamber inside the sextupole magnets will be machined down to a minimum wall thickness of 3.1mm to accommodate the 68 mm sextupole pole gaps. The 3D finite element analysis of the stress and deflection due to atmospheric pressure load of the multipole chambers at the sextupole location are shown in Figure 4.4.4. The maximum stresses is 64 MPa, and the maximum deflections are less than 0.6 mm. The yield strength of the extruded aluminum A6063 T5 is 145 MPa, therefore providing a safety factor of > 2. The analysis for dipole chamber gives a maximum stress of 42 MPa, a safety factor of > 3, and maximum deflection of 0.55 mm.

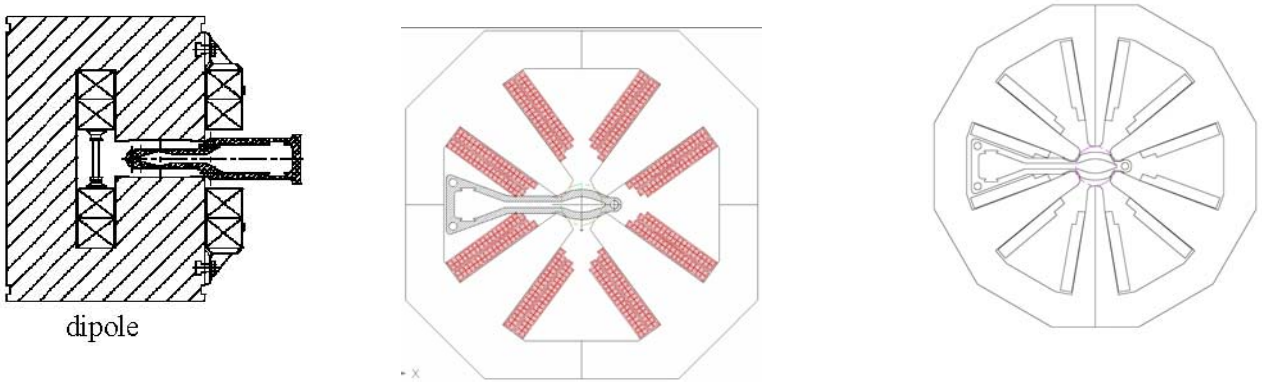

Figure 4.4.2 Storage ring vacuum chambers and magnet cross-sections at dipole, quadrupole, and sextuple interfaces. The beam channel will have an aperture of 25 mm (V)×76 mm (H). The clearance between chamber outer surface and the magnet poles will be 2 mm or more.

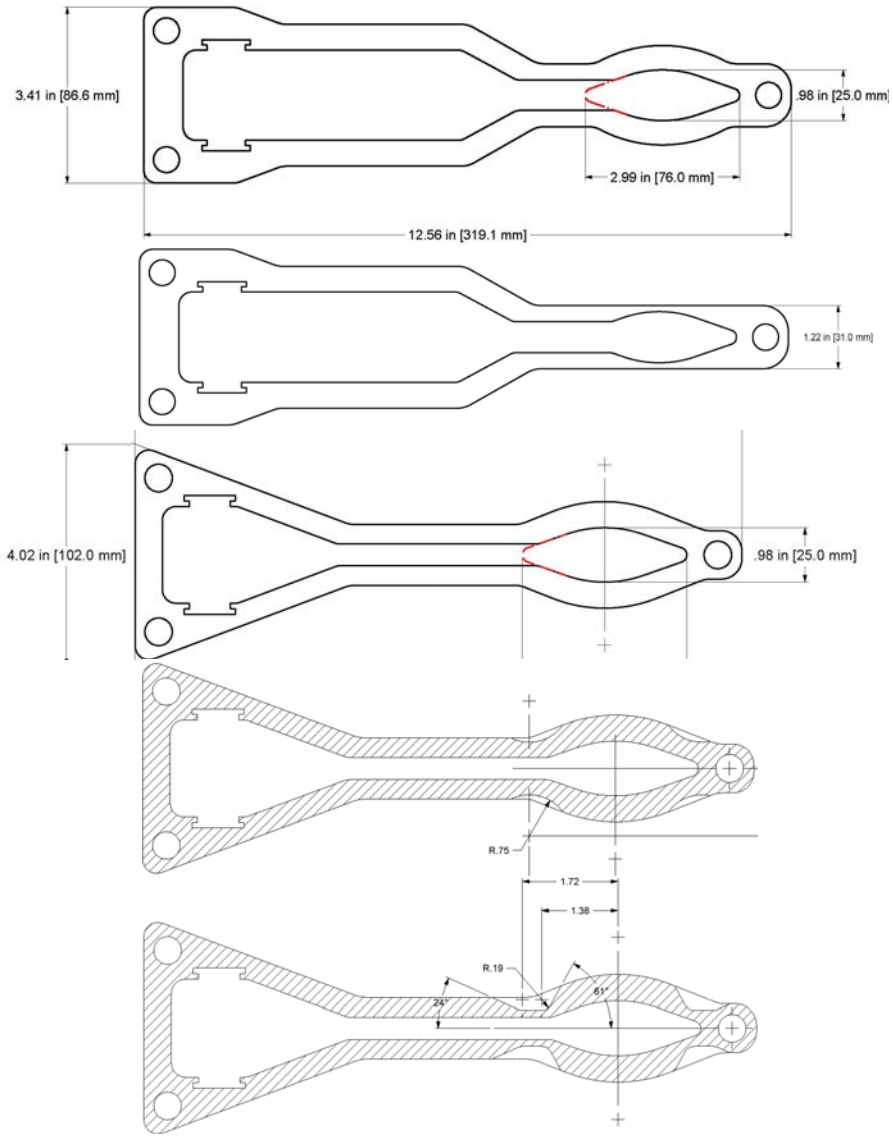

Dipole extrusion

Dipole after machining

Multipole extrusion

Multipole at quadruple after machining

Multipole at sextupole after machining

Figure 4.4.3 Storage ring vacuum chamber cross sections after extrusions and after machining, at dipole, , quadrupole, and sextupole interfaces. The minimum wall thickness at the sextupole location is ~3.1 mm, and 3 mm inside the dipole magnet.

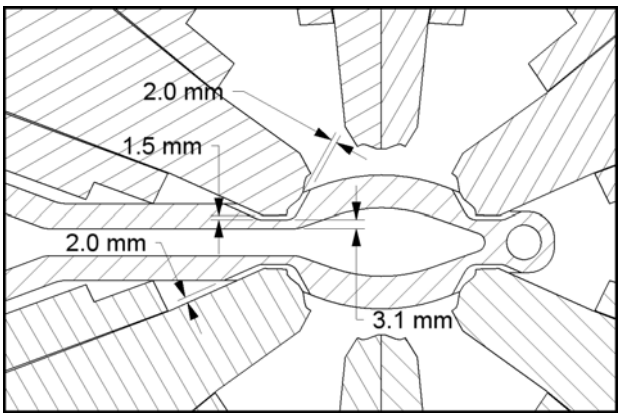

Multipole chamber cross section inside sextupole

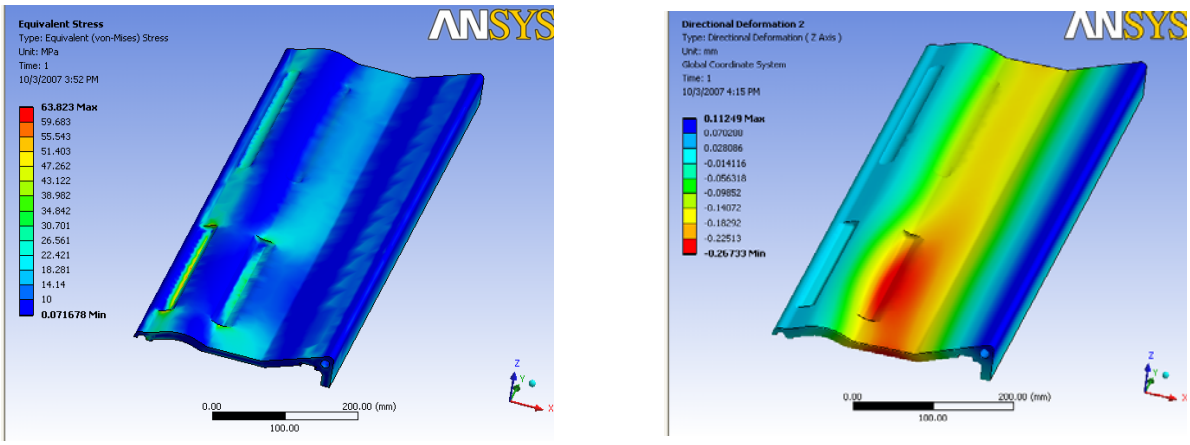

Figure 4.4.4 Top: the cross sectional view of the multipole chamber at sextupole magnet pole location: **Bottom:** 3-D finite element analysis of the deflection and stress of the multipole chamber at the sextupole pole tip locations, where the minimum wall thickness is 3.1 mm. Bottom **left:** The maximum deflection due to atmosphere pressure load is found to be 0.28 mm×2; and Bottom **right:** the maximum von Mises stress at this single point is 64 MPa, within the maximum allowable stress of 145 MPa for extruded aluminum A6063 T5.

As shown in Figure 4.4.1, there are five extruded cell chambers in each cell, named S2-S6 chambers (the straight section chambers are named as S1 chambers). The cross sections and the exact length of the cell chambers, and the locations of various absorbers within, must be developed to provide adequate apertures for both the electron beam and the photon fan, while protecting un-cooled components such as flanges and bellows. Detailed ray tracing analysis was carried out for both bending magnet radiation fans of ±52 mrad, and for damping wiggler radiation fans of ~±3 mrad. The radiation fan from other insertion devices has divergence of <<±1 mrad and will clear through the cell chambers and the connecting bellows into the front ends. Ray tracing also provides the distribution of the power and power density and the number of photons intercepted by various absorbers, allowing detailed thermal analysis of the absorbers, and pressure profile distribution in the electron beam chamber.

A portion of ray tracing at downstream end of the first bending magnet is shown in Figure 4.4.5, where ~ 40% of bending magnet fan is intercepted by the crotch absorber. Approximately 20% of the bending fan will enter the front end, together with the DW fan, through the opening in the crotch absorber. The remaining 40% of the bending fan travels downstream through the connecting bellows to S4 multipole chambers, where it is trimmed further by the two flange absorbers. The percentage of the bending fan intercepted by each absorber depends on the distance from the tip of the absorber to the beam center line, which provides

adequate protection to the downstream beam pipes, flanges, and bellows. The typical distance used for ray tracing is 25 mm; however, some are at 23 mm, 27 mm, or further, depending on the shielding requirement and dynamic aperture requirement. A list of bending radiation absorbers in a typical superperiod is given in Table 4.4.1, together with their distance from the center of the long straight, the position from the beam center, and the power and photons intercepted. The power and density are used for thermal analysis of the absorbers, while photon flux on the absorbers is used to derive pumping requirements and the pressure profile in the electron beam channel.

The DW fan passing through the crotch absorber must be clipped immediately before traveling down the front end, due to its divergence and distance (over 10 m) from the DW. This is accomplished using a DW absorber with side walls at inclined angles ~5^{o} to limit the maximum power density., and thus the temperature of the absorbers to below 300C. Depending on the canting angles of the DW, 15 – 30% radiation power (or 10 – 20 kW) will be absorbed here. The DW fan will be further clipped by fixed masks in the front end prior to entering the beamline.

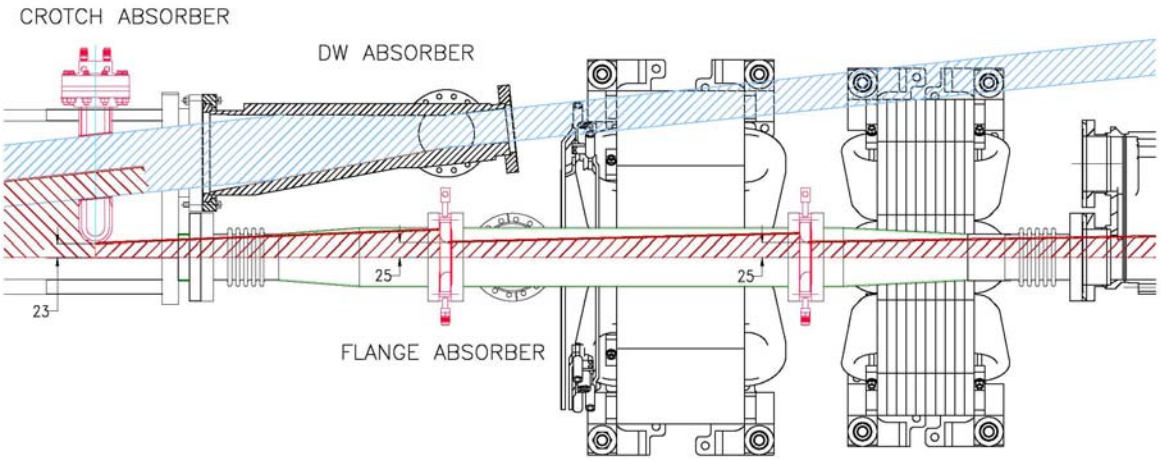

Figure 4.4.5 Chamber and absorber layout at the downstream end of the S-3 chamber (the first bending chamber), showing both the bending magnet radiation fan and the damping wiggler fan. The crotch absorber has an opening for passing the damping wiggler fan into the front end while intercepting some bending radiation.

Table 4.4.1 List of absorbers in each superperiod with their distance from the center of the long straight section, position from the beam center, angle of the bending magnet fan intercepted, total power, and the number of photons intercepted.

Section	Absorber	S	X	BM Fan	Power	# hv
#	Type	(m)	(mm)	on Absorber	3 GeV	3 GeV
S6	Stick		25	(degree)	(watt)	
S1-LS	Stick	0.00	22	0.210	84	7.1E+17
DW	Stick		37			
S3	Crotch	11.04	23	2.459	983	8.3E+18
S4	Flange	11.55	25	0.851	340	2.9E+18
	Flange	12.20	25	0.549	220	1.9E+18
	Stick	15.78	27	0.659	264	2.2E+18
S5	Crotch	20.28	25	3.611	1444	1.2E+19
S6	Stick	23.64	25	1.969	788	6.7E+18
S1-SS	Stick	24.61	22	0.086	34	2.9E+17
EPU	Stick	29.13	32	0.115	46	3.9E+17
S2	Stick	32.95	25	0.092	37	3.1E+17
S3	Crotch	36.14	23	3.366	1346	1.1E+19
S4	Flange	36.66	25	0.851	340	2.9E+18
	Flange	37.31	25	0.549	220	1.9E+18
S4	Stick	40.89	27	0.659	264	2.2E+18
S5	Crotch	45.38	25	3.611	1444	1.2E+19
S6	Stick	49.03	25	1.998	799	6.8E+18

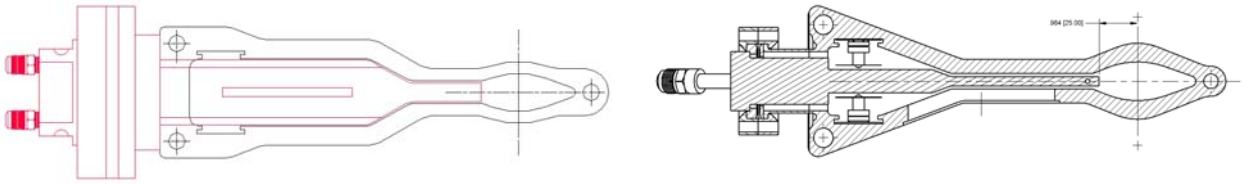

Figure 4.4.6 Conceptual design of the crotch absorbers and the stick absorbers as inserted from the side ports through the antechamber and photon exit slot. Most absorbers are positioned at 25 mm from the center of the electron beam channel, with a few positioned from 22 mm to 37 mm away.

Table 4.4.2 Types and numbers of cell vacuum chambers, absorbers, and RF-shielded bellows in the NSLS-II storage ring.

Description - Type	Length (m)	Quantity
Cell chamber – Bending – S3, S5	3	60
Cell chamber – Straight – S2	4	30
Cell chamber – Straight – S4	3.5	30
Cell chamber – Straight - S6	3.5	30
Cell – RF shielded Bellows	0.2	150
Cell - Absorber		225
ID - Absorber		45
ID chamber – EPU	~4	5
ID chamber – Damping wiggler chambers	~4	16*
ID – SRF cavity	~7	2
ID – Injection kickers + septum	~7	1
ID chamber – Empty 6.6 m straight	~5	10
ID chamber – Empty 9.3 m straight	~7	8*
ID – RF-Bellows	~0.2	~60

* Two 4 m beampipes will be used at each 9 m long straight.

4.4.2.3 Pumping at the Photon Absorbers

There are approximately eighteen photon absorbers, as listed in Table 4.4.1, in each superperiod to intercept and absorb unused photons from the two bending magnets .The absorbers are located as far from the source of the photons as practical, to reduce the power density, and thus the peak temperature on the absorber surface. Sputter ion pumps with titanium sublimation pumps (TSP) will be located at the absorbers to remove as much desorbed gas as possible, thus minimizing the amount of gas diffused back to the beam channel. The maximum gas load from bending magnet photons intercepted by each crotch absorber is estimated to be $\sim 2\times10^{-6}$ Torr-l/s, as described in Section 4.4.3.2, and can be handled with the combination of a sputter ion pump and titanium sublimation pump. The absorber for the DW radiation fan will intercept more than 10 kW of photons, resulting in a gas load of $> 3\times10^{-5}$ Torr-l/s. This high gas load at the DW absorber may be pumped by the combination of a sputter ion pump and a NEG cartridge pump, which has higher capacity than a titanium sublimation pump. Typical absorbers as inserted into the cell chambers from the side ports through the antechamber and the photon exit slot are shown in Figure 4.4.6. The crotch absorbers will be located at end of the dipole chambers where no NEG strips are present. Some stick absorbers are located in the middle of cell chambers or straight section chambers, and have to pass through the NEG strips mounted in the antechamber. Insulating coatings will be applied to the outer surface of the stick absorbers to provide electrical isolation during NEG strip conditioning and activation.

4.4.2.4 Injection Kicker Chambers

Kicker magnets require special ceramic vacuum chambers. The four ceramic chambers will be located in the injection straight section, upstream and downstream of the injection septum magnet to correct the electron beam path as needed during injection to the storage ring. These chambers will be specially designed so that they are able to 1) withstand the stresses of fast magnet actuation, 2) resist fatigue, and 3) maintain vacuum integrity. The internal surface of the ceramic chambers will be coated with a conductive film to reduce impedance for the beam image current and prevent charge buildup [4.4.2]. The film must be thin to minimize the eddy current induced by the fast-pulsing kicker field, so as not to disturb the injected beam.

4.4.2.5 Photon Exit Ports

There are two photon exit ports at each vacuum cell to extract photon beams to the user beamlines: one at straight chamber S4 for the photon beam originating from the upstream insertion device; and the second at the upstream end of straight chamber S6 for photons from the three-pole wiggler or bending magnet #2. The downstream end of these exit ports will have bending magnet photon shutters to intercept the photons before the front ends and beamlines are installed, or when the beamlines are not in use. Pneumatic gate valves will be located downstream of the photon shutters to allow vacuum isolation of the storage ring and front ends for maintenance and troubleshooting. The exit port chambers will be made of stainless steel. Sputter ion pumps with TSP will be placed at the photon shutters to remove the desorbed gas molecules. A bremsstrahlung radiation stop will be installed downstream of the gate valve prior to front end installation, to protect the equipment and personnel at the experimental floor.

4.4.2.6 RF-Shielded Bellows, Flanges, and Ports

To reduce the broadband impedance of the vacuum chamber wall and to minimize the localized HOM heating, the inner cross-section of the electron-beam chamber should be maintained as smooth as possible. High transverse impedance may cause beam instability, which might put an upper limit on the stored current. The changes in cross-sections of the beam chamber should vary smoothly, with an angle of inclination less than 1/9 for tapered transitions. The height of the steps should be less than 1 mm, in general, and less than 0.5 mm at small-aperture ducts for insertion devices. For vacuum components with cavity-like or discontinuous structure, such as flange joints and bellows, RF contact fingers will be installed to reduce the impedance and provide a smooth path for the beam image current. The opening of the thin slits of these fingers should allow enough pumping of residual gases that have been outgassed from the surface behind the slits. Calculations will be made to optimize the design of the thin slits while minimizing the impedance of the chambers. Slots or screens, if deemed necessary, will be implemented at the ion pump ports to reduce impedance and still provide adequate pumping conductance. Only commercially available RF-shielded gate valves will be used along the storage ring beam channel.

Two types of RF-shielded bellows will be studied for their finger contact force, flexibility, cost, and vacuum and RF properties: the single-finger type with hydro-formed bellows used at APS [4.4.3], and the double-finger type with welded bellows used at B-factories and a few synchrotron radiation facilities in Asia. They are shown in Figure 4.4.7. The welded bellows will allow more compression and lateral movement than the hydro-formed ones. The double-finger design may not be as reliable as the single-finger type, but does offer lower contact resistance. The magnetic permeability of both welded and formed bellows must be measured and the eddy current effect calculated, since fast corrector magnets will be mounted over the stainless steel bellows. The welded bellows will cost more than the formed ones.

Explosion-bonded bi-metal transition Conflat flanges, made from 316L stainless steel and A6061-T6 aluminum plates, will be used for the aluminum chambers throughout the storage ring. These Conflat type flanges with aluminum weld neck will be tungsten-inert-gas welded to the cell chambers using a robotic welding machine. They have the standard stainless steel knife-edge sealing face for the copper gaskets and are commercially available. They will form reliable, leak-tight joints with other bi-metal flanges and standard stainless steel flanges of adjacent chambers, bellows and other appendage vacuum components, such as vacuum pumps and gate valves. The bi-metal joints can be in-situ baked up to 250^{o}C.

a

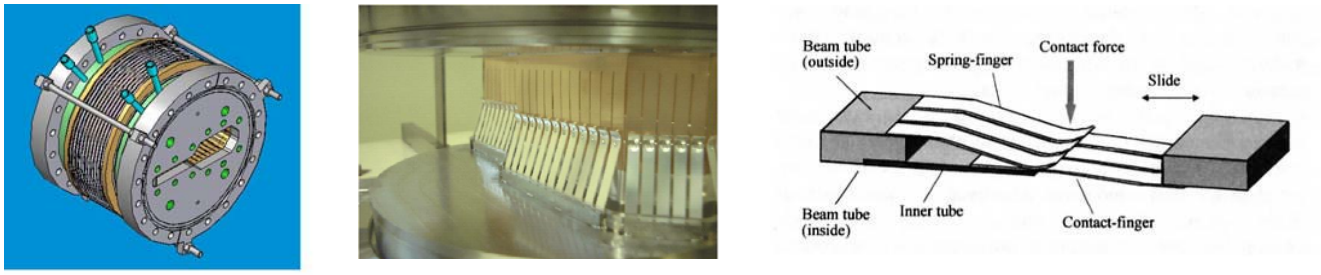

b

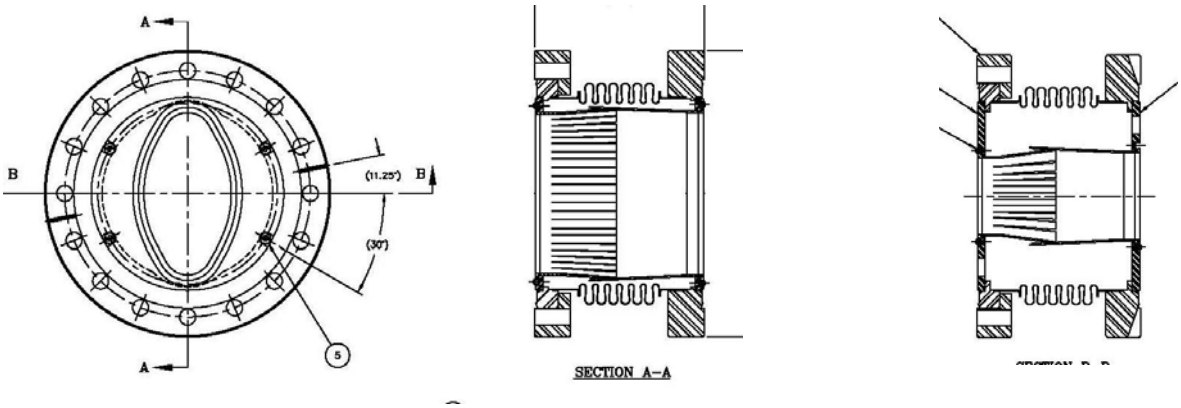

Figure 4.4.7. Two types of RF-shielded bellows: (a, upper row) the ones with welded bellows used in B-factories and BEPC-II with single or double fingers; and (b, lower row) the APS type with single fingers and hydro formed bellows.

4.4.3 Pressure Requirements and Distribution

As mentioned earlier, an average beam channel pressure of less than 1×10^{-9} Torr is needed. This pressure will provide ample beam-gas lifetime with minimal radiation and beam loss effects. Beam losses generate radiation according to electron current, energy, and vacuum pressure. At pressures greater than 10^{-8} Torr, both the stored beam lifetime and the life of many vacuum pumps will be reduced. Titanium sublimation and NEG pumps have lifetimes that are directly related to the operating pressure; therefore, maintaining this vacuum level in the storage ring improves vacuum component life, stored beam life, and minimizes the amount of radiation produced from bremsstrahlung scattering.

The beam gas scattering loss in the NSLS-II storage ring will depend largely upon the interaction of the beam with heavier residual gas molecules such as CO, CO_2, and Ar due to bremsstrahlung and Coulomb scattering. The gas density inside the vacuum chamber is determined by the installed pumping and by the surface condition of the vacuum chambers and the absorbers, which is bombarded by photons generated by the circulating electron beams. During initial ring commissioning, there are severe limitations on the achievable beam current and stored beam lifetime, caused by large pressure increases due to high photon-stimulated desorption (PSD) yield. Experience gained during early commissioning of the NSLS x-ray ring showed that residual gas spectra obtained with no stored electrons were typical of a well-baked UHV system. Hydrogen constituted approximately 95% of the residual gas at that time, and the average vacuum was in the 10^{-10} Torr range. The composition of the desorbed gases during initial operation of the x-ray ring was ~ 43% H_2, ~ 25% CO, and ~ 16% each of CO_2 and CH_4. After three months of additional beam conditioning, the

PSD rate dropped by a factor of five, and the CO, CO_2, and CH_4 peaks represented much smaller percentages of the total desorbed gas. The PSD yield versus beam conditioning dosage for copper and aluminum chambers [4.4.4, 4.4.5], as measured at NSLS, is shown in Figure 4.4.8. Typical desorption yields after 100 A.hr beam conditioning are used in the pressure simulation. The beam lifetime did not show a corresponding increase with the reduced desorption rate, mostly due to Touschek effect.

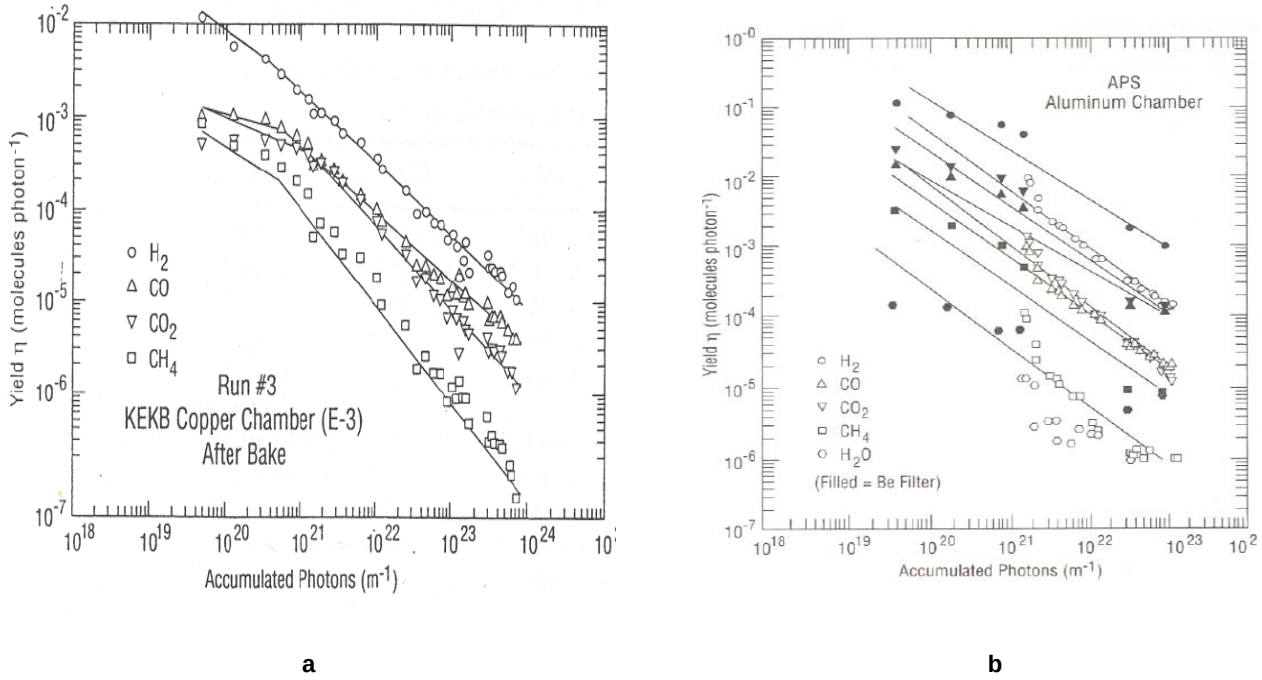

Figure 4.4.8 Comparisons of PSD yields with photon dosages for copper and aluminum. **a)** PSD yields for a 1 m pure copper sample beam chamber at KEKB. **b)** PSD yields for a 1 m extruded aluminum sample beam chamber at APS.

Most of the NSLS-II storage ring vacuum chambers will be fabricated from extruded aluminum and may be exposed to low levels of bending magnet photon radiation due to scattered photons. Almost all unused photons will be intercepted by water-cooled copper and GlidCop absorbers. After proper conditioning with photons, the PSD yields for copper, stainless steel, and aluminum will be at the same levels.

The 25×76 mm electron beam channel is vacuum pumped using distributed NEG strips in the ante chamber connected by a narrow pumping slot. Two NEG strips are installed in the extruded ante chamber and have a combined pumping speed of 240 l/s/m. The NEG pumps only chemically active gases. Sputter ion pumps (SIP) are employed to pump the inert gases not pumped by the NEGs. The SIPs are located under the photon absorbers where the majority of PSD occurs. The SIPs provide ~ 200 l/s pumping speed and are part of a combination SIP/TSP. The TSP provides an additional 500 l/s of pumping for active gases.

Linear conductance of the electron beam channel is ~ 8 l/s/m. The photon exit slot in the chamber extrusion between the ante chamber and the beam channel in dipole chamber is 15 mm high which limits the NEG pumping speed to about 135 l/s/m, in the beam channel. The slot in the multipole extrusion is 10 mm high, which yields a conductance of approximately 45 l/s/m in the beam channel.

4.4.3.1 Static Vacuum: Thermal Outgassing

The static pressure distribution in the storage ring will be determined by the amount of thermal outgassing from the internal surfaces in the vacuum chambers. These outgassing rates will depend on the construction

materials used and their preparation. After precision cleaning, the chambers will be vacuum-baked and may be glow-discharge conditioned to reduce outgassing and remove contaminants prior to their final assembly into the storage ring magnets and girders. All the chambers and vacuum components in the vacuum cell will be in-situ baked, to reduce the thermal outgassing as well as the PSD yields. Most of the internal vacuum surfaces along the storage rings are aluminum. The contribution of other materials to the thermal outgassing load is much smaller than that of aluminum wall. Vacuum-baked aluminum outgassing of 1×10^{-12} Torr-l/s/cm^2 is used for thermal gas load modeling. The thermal gas load is estimated to be 1×10^{-8} Torr-l/s/m.

4.4.3.2 Dynamic Vacuum: Photon Stimulated Desorption

During operations with stored electrons, specially designed water-cooled Glidcop absorbers will intercept most unused synchrotron radiation. The PSD rate η for vacuum-baked copper and Glidcop has been studied at NSLS [4.4.4] and at other laboratories. An η value of 1×10^{-5} molecules per photon is used for the modeling calculations [4.4.6]. The total photon flux from the storage ring dipole magnets is calculated using Np (ph/s) = $8\times10^{+20}$ [E(GeV)] [I(Amperes)]. For 3 GeV and 500 mA, the total photon flux is $1.2\times10^{+21}$ ph/s. Using these values and converting to gas load yields 3×10^{-4} Torr-l/s (or ~5×10^{-6} Torr-l/s per bending magnet). The undulator radiation will have a narrow fan. It will mostly be collimated and intercepted down at the front end and beamline, and will produce little gas load to the storage ring beam channel. In contrast, the damping wiggler radiation will have a relatively wide fan. Approximately 15% of the DW radiation will be intercepted by the crotch absorber located upstream of the S4 multipole chamber, equivalent to ~$1\times10^{+20}$ ph/s by each DW. Assuming the same η value of 1×10^{-5} molecules per photon, this corresponds to an additional gas load at photon exit port of 3×10^{-5} Torr-l/s from each DW.

4.4.3.3 Dynamic Pressure Distribution

The pressure rise with beam operation will be determined by the PSD of gases from internal surfaces of the vacuum chamber, and the amount of dynamic pumping. Most synchrotron radiation will be intercepted by water-cooled Glidcop absorbers,. The pressure distributed in a super-period of 52 m was calculated using both Molflow [4.4.7] and Vaccalc [4.4.8] software. The storage ring pressure distribution in the beam channel with with no beam current,, with 500 mA stored beam current, and with damping wigglers is plotted in Figure 4.4.9. PSD yield of 1×10^{-5} mol/ph, reached after approximately 100 amp-hours of beam conditioning, is used in the calculation. The design average pressure of less than 1×10^{-9} Torr can be reached with the current pumping scheme of distributed NEG, lumped ion pumps, and TSP. However, the DW absorber, as shown in Figure 4.4.5, does produce a sharp, but localized peak up to 10 nTorr, assuming 15% of the DW radiation be clipped here. The pressure peak will be proportionally higher if more DW fans are to be clipped here. The significant increase in bremsstrahlung radiation at this location could damage the downstream equipment and may require additional shielding. The importance of the distributed pumping by NEG strips is clearly illustrated in Figure 4.4.10. The reduction of the lumped pumping speed at the absorbers from 500 l/s to 100 l/s, due to long manifold or saturation of TSP film, only increase the average pressure by two folds. The average pressure increases by over ten folds when the NEG strip pumping is eliminated, perhaps due to saturation or fails to activate. To further illustrate this point, the NEG strips at short straight are left intact in the simulation, which generate a local pressure of ~ 0.1 nTorr.

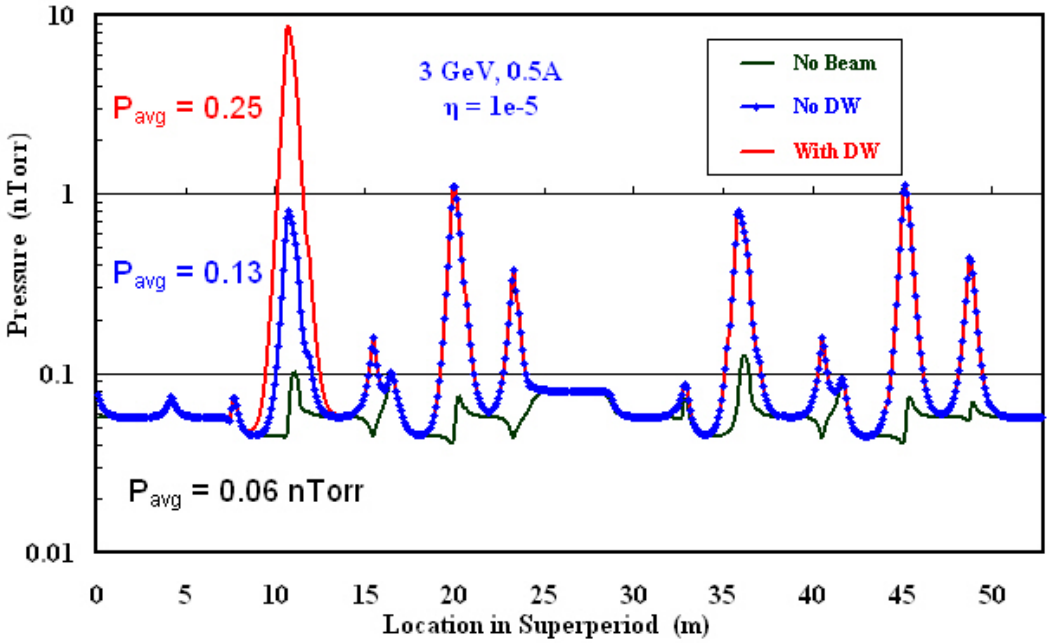

Figure 4.4.9 Pressure distribution inside the electron beam channel in one superperiod, without beam (black), with 500 mA (blue line and circles) ,and with damping wigglers (red line). The average pressure is about 0.1 nTorr without damping wiggler, ~ 0.3 nTorr with damping wiggler. However, the localized pressure at wiggler absorber is peaked at 10 nTorr.

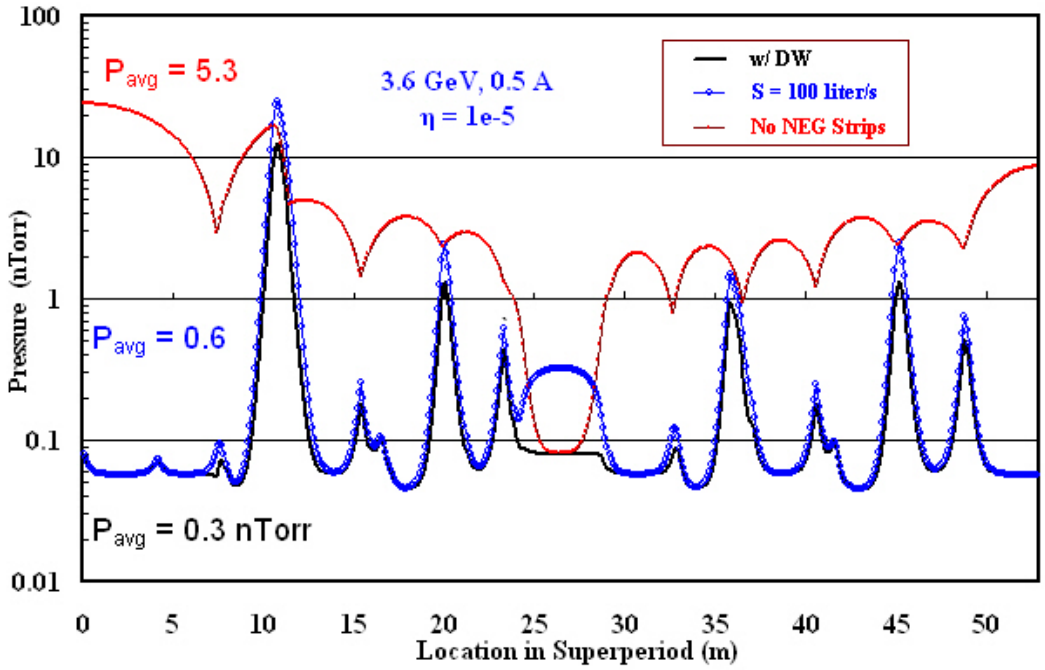

Figure. 4.4.10 Pressure distribution inside the electron beam channel in one 52 m superperiod with damping wigglers. The blue curve represents the pressure when the lumped pumping speed (IP+TSP) at absorbers is reduced from 200 l/s to 100 l/s. The red curve is when the NEG strips are not activated and the average pressure exceeds 5 nTorr.

4.4.4 Vacuum Chamber Materials, Fabrication, and Treatment

Most of the storage ring vacuum chambers will be constructed from extruded A6063-T5 aluminum. This alloy was selected based on a comparison of various properties for commonly used vacuum chamber materials for electron storage rings, as described below.

4.4.4.1 Selection of Chamber Materials

There are three common UHV materials suitable for the vacuum chambers of the electron storage ring: stainless steel, aluminum alloys, and OFHC copper, with stainless being preferred for a few new SR facilities in Europe, and aluminum for the new ones in Asia and the U.S. Copper was chosen for storage rings with high energy and high power density, such as the B-factories at SLAC and KEK, and also for its high thermal conductivity and radiation shielding properties. However, copper has the disadvantages of high material and fabrication costs. For the 3 GeV NSLS-II, radiation shielding and thermal conductivity requirements are not as critical as in the higher energy machines. Moreover, most synchrotron radiation from bending magnets will be removed by discrete copper or Glidcop absorbers. Therefore, copper has not been considered a preferred chamber material. The choice between stainless and aluminum for the NSLS-II cell chambers is based on experience at NSLS and APS, plus aluminum's vacuum and mechanical properties, ease of fabrication, and relatively reasonable cost.

One major difference between NSLS-II and other new SR facilities of comparable energy is the large bending magnet radius. The photon fan from the bending magnet will have a small dispersion and will be easily intercepted by discrete absorbers. This allows a narrow chamber geometry design; therefore, the cell chambers can be fabricated from extruded aluminum with uniform cross-sections. The need to accommodate the distributed NEG pumping also favors extruded aluminum, since an antechamber can easily be produced by aluminum extrusion. The cost of extrusion is considerably lower than that of chambers made of stamped stainless plates or machined aluminum plates, although the cost of machining the external chamber profile to fit the magnet poles and the various access ports will be significant. A few important arguments concerning the choice of material are listed and further discussed below.

Table 4.4.3 Electron Storage Ring Chamber Materials and Their Critical Properties.

Specifics	Aluminum	Stainless	Copper
Initial PSD rate	High	Low	Average
Mechanical strength	Acceptable	Excellent	Good
Thermal expansion	Large	Small	Small
Thermal conductivity	Excellent	Poor	Excellent
Weldability	Good	Excellent	Good
Beam impedance	Low	High	Low
Bi-metal flanges	Yes	No	Yes
Cooling channels	Extrusion	Brazed	Brazed
Fabrication cost	Low	Average	Expensive
Ease of in-situ bake	Good	Poor	Good
Radiation shielding	Poor	Average	Excellent

The outgassing of unbaked aluminum is higher than that of stainless, but an in-situ baked aluminum surface has similar or lower outgassing than that of stainless. The initial PSD rate of an aluminum surface is higher than those of copper and stainless. However, aluminum conditions faster and will reach the same PSD rate at a modest integrated beam dosage. The high thermal conductivity of aluminum offers distinct advantages over stainless, both during the in-situ bake and during normal operation. No conductive coatings or strips are needed on aluminum to reduce the chamber wall impedance, whereas stainless chambers may need copper strips and absorbers in certain locations and for mis-steered beam. Therefore, our preferred

material to form the cell chambers through extrusion is aluminum A6063-T5 alloy. Stainless-to-aluminum bi-metal Conflat flanges will be welded to the aluminum chambers, and standard copper seals can be used to form reliable joints between the chambers, bellows, and appendage components.

4.4.4.2 Vacuum Facility

To ensure the necessary chamber surface properties, cleanliness, mechanical quality, and leak tightness, vacuum facilities will be needed for cleaning, welding, assembling, and evaluating the vacuum chambers and other vacuum components for the storage ring and injectors. A dedicated chemical cleaning facility is required to clean the long chambers and other vacuum components. It will consist of four long, stainless steel tanks and a gantry crane capable of handling chambers up to 6 m long and 200 kG in weight. These tanks will provide ultrasonic cleaning with hot water, commercial bio-degradable cleaning agents, and de-ionized water rinse, and are suitable for aluminum, copper, inconel, and stainless chambers and materials. The exact cleaning recipe and process will be based on the chamber material and experience developed at other SR facilities such as NSLS and APS. Programmable robotic welding stations with laminar flow hoods will be set up to weld the cleaned chambers, the sub-assemblies, and the flanges. A Class 1000 clean room with ~100 m^2 floor space is needed for the assembly of the chambers with distributed NEG strips, ion pumps, gauges, absorbers, BPM buttons, and other components.

A facility with these capabilities was established at Argonne National Laboratory for the construction of the Advanced Photon Source. The NSLS-II project plans to use the ANL/APS facility for the production, chemical cleaning, and automatic welding of the cell chambers of the NSLS-II vacuum system. Should this prove impractical for some reason, equivalent facilities will be established at BNL. Even if the ANL vacuum facility is utilized, a small chemical cleaning facility is still needed at BNL for storage ring and beamline vacuum components. The clean room and vacuum bakeout/evaluation stations are still required at BNL for the final assembly and evaluation of the cell chambers. If we do not utilize the APS facility and need to establish all of the capabilities at BNL, then ~2,000 m^2 of space would be required. If the ANL facility is used for production, cleaning, and welding, then ~1,400 m^2 would be required. Building 905 at BNL has been identified as the preferred location for the BNL vacuum facility. This building has more than 2,500 m^2 of space, as well as overhead cranes, and is available for use by the NSLS-II project.

4.4.4.3 Fabrication, Assembly, and Evaluation

Most of the storage ring chambers will be made of extruded aluminum. Immediately after extrusion, the long chamber sections will be stretched to obtain the uniform cross-section and to meet the dimensional requirement. They will then be cut to the designed length. The bending chambers will be formed to the curvature on a hydraulic press with dies or rollers of correct radius. To preserve the internal cross-sections, the inner volume of the bending chambers will be filled with DI water and frozen prior to the bending/forming operation. The extruded chambers will be machined at industrial vendors to the appropriate external profiles and to add photon exit ports, access ports for BPM buttons, pumps, absorbers, and other vacuum components. The chambers will then be cleaned at the chemical cleaning facility and sealed in an aluminum bag filled with dry nitrogen gas for storage and further processing.

The aluminum chambers and flange adaptors are welded together with tungsten-inert-gas welding processes, using programmable robotic welding machines. The relative humidity of the laminar hoods over the welding zones will be reduced to less than 50% during welding to minimize oxide growth at the heat zone and to ensure weld integrity. Following welding, the vacuum chambers will be pumped down with a turbomolecular pump (TMP) backed by a dry mechanical pump, then checked for leaks using a leak detector with minimum helium sensitivity of 5×10^{-11} Torr-l/s. Specific procedures for repairing each type of weld leak will be developed to ensure that the quality of the chambers is not compromised. The cooling water channels will be leak-checked with vacuum and by sniffing while pressurized. The welded chambers are then brought

into the Class 1000 clean room for assembly of peripheral components, such as BPM buttons, NEG strips, pumps, absorbers, and gauges. The chamber end flanges will then be capped with blank flanges.

The assembled chambers will be installed at the evaluation stands for final leak checking and bakeout at 130°C using temporary ovens. The vacuum level and the residual gas composition will be closely monitored during the bakeout, using vacuum gauges and residual gas analyzers (RGA), to ensure that the chambers remain leak-tight and are free of contaminants. All the pumps, gauges, BPM buttons, absorbers, and thermocouples are to be activated and measured to ensure their proper operation during and after the bakeout cycle. The possible use of a DC glow-discharge system to clean internal surfaces with an Ar/O_2 mixture during bakeout will be investigated for its merit versus the technical complexity and cost. After bakeout, the chambers will be either at storage vacuum or back-filled with dry nitrogen for the subsequent assembly into magnets/girde and installation in the SR tunnel.

4.4.4.4 Installation, Alignment, and In-Situ Baking

During the machining of the vacuum chambers, all mounting holes for the survey fiducials will be checked against the beam channel cross-sections and the BPM mounting surfaces. To ensure precision alignment, the design of the vacuum chambers and the proposed alignment schemes will be reviewed and approved by the diagnostics, accelerator physics, and alignment and support groups. The required precision of the chamber alignment is ≤0.5 mm in general, and ≤0.1 mm for special parts such as the BPM buttons. The assembled and tested chambers will be installed into the split magnets and aligned using built-in adjustment bolts of the fixed support plates mounted on the girder. After the installation and alignment of individual chamber/magnet girders in the tunnel, the end capping flanges will be removed and the RF-shielded bellows will be installed and connected to the next cell chambers. Two sector gate valves will be mounted and supported on the end flanges of the S2 and S6 chambers of each cell. The magnet buses, cooling water lines, and vacuum equipment cables will then be connected prior to final measurement, pump down, leak check, and in-situ bakeout.

The in-situ bakeout of the storage ring cell in the tunnel will be carried out with pressurized hot water provided by the storage ring utility system. Additional heating jackets, heating tapes, and thermal insulation are needed for large appendage components, such as gate valves, ion pumps, etc., to ensure uniform temperature distribution, especially at large flange joints where uneven temperatures may result in seal failure and vacuum leaks. The supports for the chambers and the pumps must be adjusted to allow thermal expansion during the bake, while still maintaining and protecting the mechanical stability of the entire system. Three Invar plates, one fixed in the middle and two flexible at the ends, will mount and support each cell chamber on the girder. The storage ring cell will be pumped down with a turbomolecular pump backed by a dry mechanical pump during the bakeout. The vacuum level and gas composition will be continuously monitored using cell vacuum gauges and RGAs during the bakeout. The temperature of the chambers will be raised slowly by the hot water system and the heating jackets, and controlled by the bakeout programmable logic controller with inputs from the installed thermocouples on the chamber surface. The entire vacuum cell will be baked at 120°C for ~ 40 hours to remove absorbed water and other contaminants from the surfaces. The sputter ion pumps, the titanium sublimation pumps, the NEG strips, and NEG cartridges will be degassed during the bake, then activated during the ramp down of the bake. The bakeout of the whole cell will be completed in ~3 days, from Day 1 to Day 3, and can be comfortably fitted in a normal work week while still leaving sufficient time for any necessary remedial actions. The vacuum cell will be leak-checked again after the bake, using the cell RGA. The fixed support points on the chambers will be checked and adjusted to their original positions by the survey group to ensure that all the critical components, such as the BPM buttons are properly aligned.

4.4.5 Storage Ring Vacuum Pumping

The types and sizes of the pumps to be used at NSLS-II will be standardized throughout all the machine areas as much as possible, to lower the unit cost and to ease routine maintenance in the future. The selection of the pumps will be based on the experience gained from existing pumps used in NSLS and other similar SR facilities.

4.4.5.1 Roughing Pumps

A set of TMPs backed by dry mechanical pumps will be used to rough down the vacuum section from ambient pressure to high vacuum, and during in-situ bake before turning on the in-line ultra high vacuum pumps. The TMPs will be connected to the vacuum sections through small, manually operated, all-metal angle valves. TMPs with magnetic or ceramic bearings of ~100 l/s size backed by dry pumps of ~5 l/s are deemed sufficient, since the ultimate pumping speed at the vacuum chambers is limited by the conductance of the chambers, the angle valve, and the flexible hose. TMPs will be manually valved out once the sector reaches ultra high vacuum. Each of the TMP stations will be equipped with vacuum gauges and electro-pneumatic valves to quickly and effectively isolate the TMP from the vacuum section in the event of pump or power failure. A dozen TMPs will be needed during the first phase of NSLS-II construction for component testing and leak checking. These TMPs, due to limited operating lifetime under heavy usage, will be replaced with newer models during NSLS-II commissioning and operation. A list of TMPs required for the operations at the storage ring is given in Table 4.4.4.

Table 4.4.4 List of Vacuum Pumps and Gate Valves for the Storage Ring and Font Ends.

	IP 200 l/s	TSP 500 l/s	NEG Lumped 500 l/s	NEG strips*~100 l/s/m	TMP portable	Gate valves
SR	150	150	60	150	10	60
Exit port	60	60	0	0	4	60
ID	60	60	60	27	4	
Total	270	270	120	177	18	120

*Each chamber will have a pair of 3–5 m NEG strips for a total length over 1 km.

4.4.5.2 Ultra High Vacuum Pumps

After initial rough down and in-situ bakeout of the vacuum sectors, the system pumping will be transferred from TMPs to ultra high vacuum pumps, including SIPs, TSPs, NEG cartridges, and NEG strips. TSPs and NEGs have high pumping speed for active gases such as CO, CO_2, H_2O, and H_2 with equilibrium pressure down to 10^{-12} Torr; they, however, will not pump inert gases (CH_4, C_2H_6, etc.) nor noble gases (He, Ne, Ar, …). Sputter ion pumps will remove inert and noble gases as well as active gases.

Triode-type SIPs have better pumping speed for noble gases, but they tend to have higher leakage current and are harder to rebuild after electrode saturation. A few noble diode SIPs, with tantalum cathode plates and similar pumping speed as triode pumps for noble gases, will be used to supplement the regular diode-type SIPs, thus avoiding so called “argon instability.” Ion pumps of 30 l/s and 200 l/s will be used throughout NSLS-II, with the 30 l/s pumps used at conductance-limited areas such as booster synchrotron and beam transport lines; and the larger pumps at SR absorber and shutter locations. These SIPs will have large anode cells to retain sufficient pumping speeds down to the 10^{-10} Torr range. A DESY-style high-voltage feedthrough, which is less prone to radiation-induced corrosion at the brazing joint, will be used for the ion pumps. Commercial dual ion pump controllers with local and remote capabilities will power and monitor the SIP, by interfacing with the PLC and control computers, through hard wires and Ethernet linkage, respectively. Ion pump currents will supplement the vacuum gauges to provide pressure distribution over the whole ring. However, due to the buildup of leakage current in the ion pump elements, the reliable pressure

reading from ion pumps is limited to the mid 10^{-10} Torr range. A list of ion pumps for the storage ring is given in Table 4.4.4.

The large volume of active gases desorbed from the photon absorbers can be efficiently removed from the SR by localized TSPs of ~500 l/s, thus minimizing the quantity of gases diffused back to the electron beam channel. Alternatively, at absorbers for damping wigglers, with a modest increase in cost, TSPs may be replaced with NEG cartridges of comparable pumping speed but higher capacity before needing reactivations. Both TSPs and NEGs can be activated and reactivated locally or remotely. However, TSPs have the advantage of only generating a brief gas burst during their short sublimation period, while NEG activation takes longer, during which time a large amount of hydrogen is produced and should be removed by portable TMP stations.

Distributed NEG pumping in the form of NEG strips, similar to those employed at the APS storage ring, is planned for use in all cell vacuum chambers. This is deemed efficient to provide linear pumping to the beam channel through the photon exit opening. Dual strips will be mounted on the top and bottom of the antechamber. There will be sufficient clearance between the two mounted NEG strips to allow the passage of photons, even when a beam mis-steers, and for the insertion of stick absorbers. The mounting of the dual strips will be carefully designed and thoroughly tested to eliminate any potential electrical faults during in-situ bake and NEG activation. The NEG activation is at 400^{o}C for 30 minutes and will be achieved with resistive heating of the NEG strips with ~70 ampere current, carried out at the end of in-situ bakeout or during the machine maintenance period. The two NEG strips together will provide more than 240 l/s per meter pumping speed for active gases such as CO and H_2 even after pumping ~0.1 Torr-l per meter of active gases, corresponding to a few months of beam operation at 10^{-9} Torr pressure.

Some of the ID vacuum chambers will have very small gaps of a few mm, resulting in very limited linear conductance. In these cases it is not effective to simply rely on the lumped pumps located at both ends of the chamber. Sputter-coated NEG thin film has been applied to the inner surface of ID chambers at several SR facilities, notably at ESRF, where over 20 ID chambers have been coated and in operation for more than 5 years, and at Soleil, where most straight chambers have been NEG coated. For narrow-gap undulators at NSLS-II, NEG coating will be considered during the design stage; if appropriate, it will greatly simplify the pumping system design. For long straight sections that are not occupied by insertion devices, distributed NEG strips together with ion pumps and titanium pumps will be installed to maintain ultra high vacuum.

4.4.6 Vacuum Measurement and Control

4.4.6.1 Monitoring and Control Methodology

The vacuum level in the storage ring, the front ends, and the beamlines will be monitored and interlocked with the ion pump current and with vacuum gauge readings. Residual gas analyzers will also be used for online monitoring and diagnosis. Each vacuum sector will have a convection-enhanced Pirani gauge and two ionization gauges as the primary vacuum gauges. Additional vacuum gauges will be installed to protect the RF cavities and kickers. Vacuum devices such as gauge controllers, ion pump controllers, and RGA - with local and remote capabilities - can be operated through front-panel switches. Their communication with the equipment control system will be through RS232 or Ethernet links for remote monitoring and control. It is anticipated that most of the vacuum controllers will be off-the-shelf items purchased through competitive bids from qualified vendors.

Due to the high level of radiation in the SR tunnel, controllers for vacuum systems will be placed in satellite electrical racks located at mezzanine above the storage ring tunnel. Electrical power for vacuum diagnostics and controllers will be standard 115 VAC and 60 Hz. Since vacuum pumps and associated vacuum equipment surrounding the ring vacuum chambers are subjected to synchrotron and bremsstrahlung radiation, radiation-resistant cables and appropriate routing will be employed to minimize radiation damage.

4.4.6.2 Vacuum Gauges

One primary vacuum gauge, a convection-enhanced Pirani gauge, will be installed in each vacuum sector to provide pressure readings ranging from atmospheric pressure down to 10^{-4} Torr. It will also be used for other vacuum equipment protection and interlocking. Two ion gauges, either Bayard-Alpert ion gauges or inverted-magnetron cold cathode ion gauges, will be installed at each SR vacuum section as the primary UHV gauge. The same type of ion gauge will be used for injectors, beam transport lines, front ends, and user beamlines. Both types of ion gauges have a useable pressure-sensing range down to 10^{-11} Torr and they have been implemented successfully at various synchrotron radiation facilities. CCGs have the advantage of overlapping the lower end of the Pirani gauge range and can be operated through long cables for signal transfer, thus eliminating the needs of locating electronics nearby. CCG tubes do not have built-in hot filaments and are therefore less susceptible to mishandling and filament breakage during startup and commissioning. The accuracy of CCG readings is normally at ±50%. Moreover, it is difficult to degas CCGs once they are contaminated. CCGs are still our choice at this point in the design process. The numbers of vacuum gauges in each area of the storage ring are listed in Table 4.4.5.

Table 4.4.5 Number of Gauges and Residual Gas Analyzers in Areas of the Storage Ring.

	TCG*	Ionizing Gauge	Residual Gas Analyzer
SR	30	60	34
Front end	30	60	60
ID	30	60	10
Total	90	180	104

*TCG = convection-enhanced Pirani gauge

Interference with the gauge readings due to the presence of copious electrons, photons, and photoelectrons has been observed at many SR facilities. Therefore, if practically achievable, the gauge tubes will be mounted on elbows at shielded ports on the antechambers to minimize interference and erroneous pressure readings. The gauge tubes will also be installed in areas with minimal stray electrical and magnetic fields. Radiation-hardened material such as Kapton-insulated cables will bridge the short distance between the chamber gauge ports and the cable tray to ensure system reliability. Kapton cables are bakeable up to 200^{o}C. Microprocessor-based multi-gauge controllers will be used to power the vacuum gauges and to provide system monitoring and control through RS232 or an Ethernet bus. The gauge controller will be hardwired to PLCs to interlock gate valves, other beam components and subsystems.

4.4.6.3 Residual Gas Analyzers

Quadrupole-type RGAs will be installed to measure the partial pressures of residual gas species at selected locations in the injectors, storage ring, front ends, and user beamlines. Their use will help to identify sources of residual gases, including photon-desorbed gas from chamber walls and absorbers, air leaks, cooling water leaks, oil back-streaming, specialty gases back-streamed from the beamlines, and other contaminants. RGAs, with electron multiplier, will have partial pressure sensitivity down to the 10^{-13} Torr range. Due to the high cost, RGAs may only be installed at some vacuum sections during the initial phase of NSLS-II operation. The RGAs' quadrupole mass filter RF box, which contains sensitive electronics, may be located near the head and needs to be shielded from synchrotron radiation. The PC-based control units for RGAs, however, will be located at the satellite control racks, to allow easy access for online analysis and maintenance. The number of RGAs estimated for the storage ring and front ends is listed in Table 4.4.5.

4.4.6.4 Vacuum Control and Equipment Protection Systems

The vacuum control system has to 1) monitor and control all the vacuum equipment including gauges, pumps, valves, etc., to ensure that they are operating properly in their appropriate ranges; 2) collect and

archive the data for instant display and alarm and for off-line analysis; and 3), most importantly, interlock and protect the storage ring and injector from harm before damage develops.

The vacuum control system will interface directly with each vacuum device, and as part of the storage ring equipment control and protection systems (EPS). Due to high radiation levels in the storage ring tunnel, all the vacuum devices and the vacuum control system will be located at the satellite control racks. They will be backed by uninterruptible power supplies. Vacuum devices include gauge controllers, ion pump controllers, chamber and absorber temperature readouts, cooling water flow sensors, and gate valve solenoids. They can be operated via front-panel switches and with the machine control system through RS232 or Ethernet links for high-level monitoring and control. The low-level vacuum controls, consisting of several dedicated PLCs with digital and analog I/O modules, take inputs from the vacuum devices and send out commands through dry contact circuits. The PLCs, with their own microprocessors and operating systems, will be programmed by vacuum system experts and provide the logic for the operation and control of the vacuum devices.

For gate valve control, the PLCs will use a voting scheme, with inputs from the setpoint contacts of several gauges and pumps, to initiate valve interlock and closure, therefore minimizing false triggering due to the malfunctioning of a single gauge or pump. The PLC for the water flow and temperature monitoring system, with direct inputs from thermocouples and flow meters, will read and compare those with the pre-set values. An out-of-range alarm from this PLC will trigger an output to the EPS to abort the beam, thus preventing overheating of the chamber wall or absorbers, due to either the malfunction of the cooling water system or abnormal beam steering. The PLC outputs for the flow meters, the temperature readouts, and gate valve status will be part of input arrays to the EPS, which will be used to determine if conditions are unacceptable. When warranted, the EPS will initiate a fast beam abort by interrupting the low-level RF power to the accelerating cavities. The stored beam would coast inward to a scraper and be lost in a fraction of millisecond.

References

[4.4.1] J. Noonan, J. Gagliano, G.A. Goeppner, R.A. Rosenberg, and D.R. Walters, “APS Storage Ring Vacuum System Performance,” Proc. PAC97, p 3552-5 (1998).

[4.4.2] C. Doose, L. Emery, and S.H. Kim, “Investigation of the Surface Resistivity Tolerance of the Kicker Ceramic Vacuum Chamber at APS,” Proc. PAC01, p1491-3 (2001).

[4.4.3] J. Jones, S. Sharma, and D. Bromberek, “APS SR Flexible Bellows Shield Performance,” Proc. PAC99, p 3095-7 (2000).

[4.4.4] C.L. Foerster, C. Lanni, and K. Kanazawa, “Measurements of photon stimulated desorption from thick and thin oxide of KEKB collider copper beam chambers and a stainless steel beam chamber,” *J. Vac. Sci. Technol. A* **19**, 1652 (2001).

[4.4.5] C.L. Foerster, C. Lanni, J. Noonan, and R.A. Rosenberg, “Photon stimulated desorption measurements of an extruded aluminum beam chamber for the Advanced Photon Source,” *J. Vac Sci. Technol.* A14, 1273 (1996).

[4.4.6] V. Anashin, et al., “Photodesorption and Power Testing of the SR Crotch-Absorber for BESSY-II,” Proc. EPAC98, p. 2163 (1999).

[4.4.7] R. Kersevan, “MOLFLOW User’s Guide,” Sincrotrone, Trieste Technical Report, ST/M-91/17 (1991).

[4.4.8] M.K. Sullivan, “A Method for Calculating Pressure Profiles in Vacuum Pipes,” PEP II AP Note No. 6-94, March 1994. (Vaccalc is a software using the finite differential method for pressure calculation.)

4.5 Beamline Front Ends

4.5.1 Scope

The beamline front ends connect the storage ring to the user beamlines and provide radiation protection to personnel. Most of the front-end components generally reside within the storage ring's shield wall, outboard of the dipole vacuum chamber. The major components of the beamline front-ends are photon masks, shutters, heat absorbers (such as beam-defining apertures and/or slits), fast valves (or other shock wave protection devices), vacuum isolation valves, pressure isolation sensors, and diagnostics. Vacuum chambers are also included; however, the chambers are often part of the individual front-end components. Other components, such as filters, may be included depending on the application. The front end usually starts at the exit to the dipole vacuum chamber and extends to a beryllium window or a differential pump, where the user vacuum is isolated from the machine vacuum. If a beryllium window is used, it generally is positioned as close as is practical to the outer end of the storage ring shield wall. Also to be considered as important front-end components are radiation shields, i.e., safety shutter shields and bremsstrahlung shields. Vacuum pumps, vacuum sensors, and diagnostics (e.g., for Residual Gas Analysis, to activate fast valves, etc.), heater tape and provisions for bakeout, as well as the vacuum valves, are included in the front ends—even though these components are generally considered part of the vacuum system. Support tables and stands made of structural steel are provided to support the front-end components at the nominal 1m beam height.

Only six beamline front ends will be installed in the initial scope of the project: three in-vacuum undulators (IVUs), two damping wigglers (DWs), and one elliptically polarized undulator (EPU). The project scope also includes engineering and design effort for the bending magnet (BM) and three-pole wiggler (3PW) front ends. The preliminary design of the front end described below can be adopted, with appropriate modifications for beam power and beam size, to all front ends.

4.5.2 Standard Front End Design

Figure 4.5.1 shows the preliminary layout of a typical front end with its main components and their approximate locations from the center of a long straight. The first component is a bending magnet photon shutter (BMPS) which intercepts bending magnet photons when there is no front end or when a front-end is under maintenance. A slow gate valve (SGV) is the next component provided to separate the storage ring vacuum from the front-end vacuum. Until a complete front end is available for installation, the BMPS and SGV are locked in closed position, and an out-of-vacuum lead stop is provided downstream of the SGV to stop bremsstrahlung radiation.

The next component is an e-beam deflector (EBD), which prevents the injected beam from accidentally entering the beamline hutch during top-off injection. The EBD consists of permanent magnet blocks that provide a vertical field of 1.1 T over a 20cm length with a pole gap of 14 mm. The EBD is designed to deflect a 3GeV beam horizontally into the stationary tungsten blocks of the safety shutter (see below), located at ~7 m downstream. The beam is deflected at this location by 15 cm, which is 5 cm more than the horizontal beam aperture provided in the tungsten blocks.

A pair of photon BPMs (XBPM-1 and XBPM-2) is used to deliver a stable beam to the user's end station by providing beam position data to the global feedback system. Next to XBPM-1 is a lead collimator (CO), which collimates the angles of bremsstrahlung radiation to minimize the size of tungsten blocks required in the safety shutter (SS) and the amount of supplemental lead in the ratchet wall (R-WALL). The uncooled tungsten blocks in the safety shutter are protected by a water-cooled photon shutter (PS) that is inserted in the beam path before the safety shutter is actuated. A fast gate valve (FGV) in the front end is provided to intercept the pressure shock wave in the case of a vacuum breach in the beamline. Another slow gate valve is

usually provided downstream of the ratchet wall collimator (RWC) to separate front end vacuum from the beamline vacuum. Some front ends will be provided precision X-Y slits between FGV and XBPM-2, at the request of beamline users. All components of a front end requiring actuation (SGV, FGV, PS, SS, and X-Y slits) will be remotely operable.

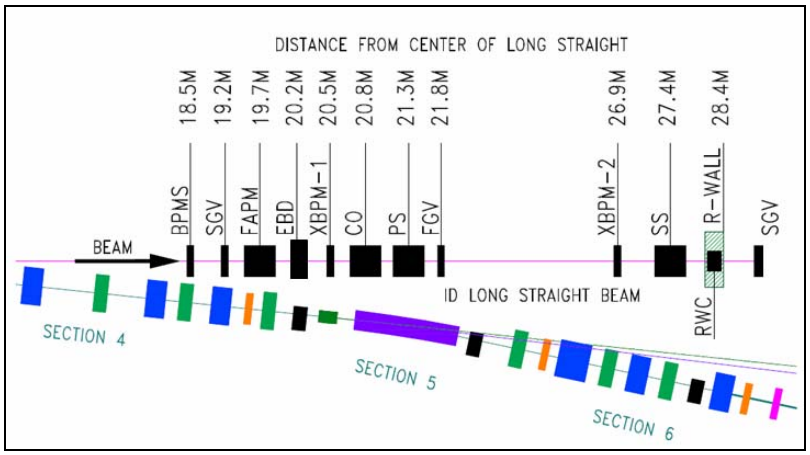

Figure 4.5.1 Typical layout of a front end. From left to right: bending magnet photon shutter (BMPS), slow gate valve (SGV), fixed aperture photon mask (FAPM), e-beam deflector (EBD), first photon BPM (XBPM-1), lead collimator (CO), photon shutter (PS), fast gate valve (FGV), second photon BPM (XBPM-2), safety shutter (SS), ratchet wall collimator (RWC), and slow gate valve (SGV).

The power densities of the NSLS-II insertion devices, shown in Table 4.5.1, are lower than those at the APS Undulator-A (130 kW/mrad^2 at 100 mA). We plan to adopt the APS designs of the front end components with appropriate modifications for the aperture requirements of each beamline.

Table 4.5.1 On-axis power densities of NSLS-II insertion devices (3 GeV, 500 mA).

	Name						
	U20	U19	U45	U100	DW-1.8T	SCW	3PW
Type	IVU	CPMU	EPU	EPU	PMW	SCW	PMW
On-axis power density (kW/mrad$^{2)}$	62.33	77.86	40.03	26.33	55.30	25.60	0.28

Figure 4.5.2 shows the typical APS designs for the three critical components: FAPM, PS, and SS. The heat-absorbing surfaces of the FAPM are designed from a single, solid piece of Glidcop, ~0.5 m long, to handle the high heat flux of the insertion devices. Water-cooling channels are gun-drilled in Glidcop block before machining for the beam aperture with 4° taper and brazing of the Conflat flanges. The design of the PS is very similar to that of the FAPM except that its downstream end can be lowered by an actuator to intercept the photon beam. In the design of the APS safety shutter, two independently movable tungsten blocks are lowered to interlock with the fixed tungsten blocks, thus closing the beam aperture and as well a line-of-sight escape for bremsstrahlung radiation. Only one set of tungsten blocks is being considered in the NSLS-II design, with the provision of redundant position switches for the movable tungsten block, and more restrictive access to the beamline hutches.

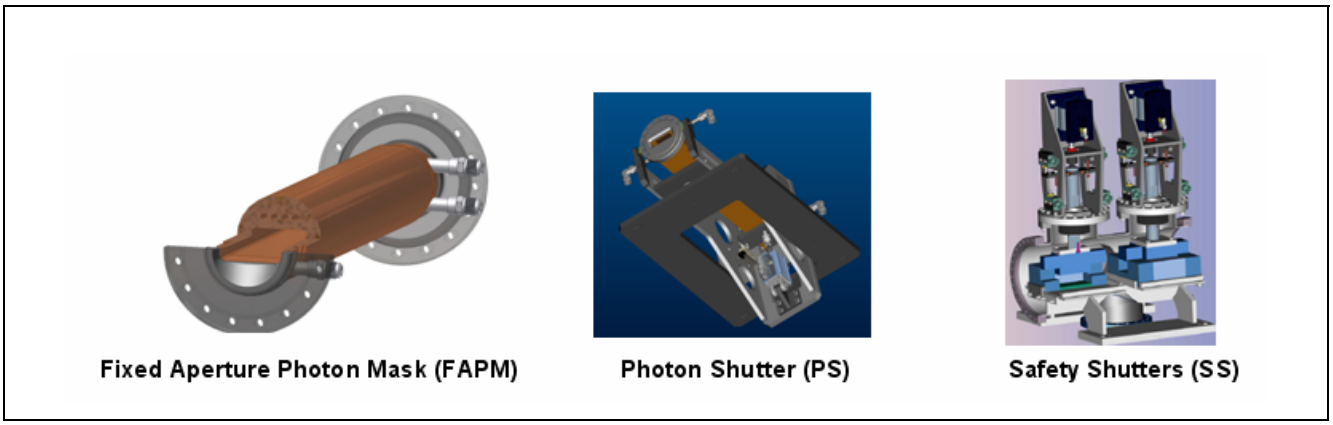

Figure 4.5.3 Typical designs of the APS front end components. Left to right: fixed aperture photon mask (FAPM), photon shutter (PS), and double safety shutter (SS).

FE analyses were performed for all front end components. The most critical component is the photon shutter which is located at ~20 m from the center the IVU in the short straight. It intercepts x-rays at an incidence angle of 4º. The analysis results (Figure 4.5.4) show a maximum temperature of 303 ºC is at the center of the beam footprint. In comparison, the acceptable temperature rise in Glidcop is ~400ºC, based on its thermal fatigue life.

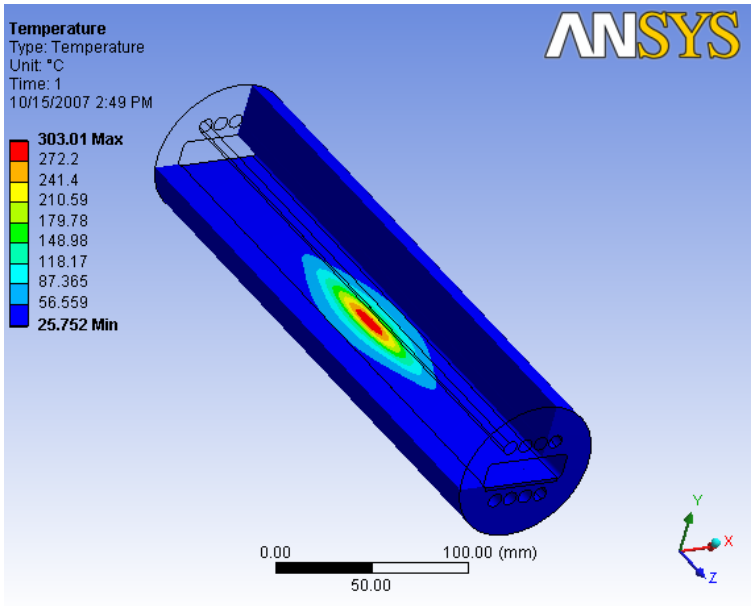

Figure 4.5.4 Temperature profile in the photon shutter located at 19 m from the center of an IVU.

4.5.3 Vacuum Components/Enclosures

The front end vacuum chambers and ducts will be constructed from 304L stainless steel and will be joined to adjacent components using commercially available Conflat flanges, copper gaskets, and UHV hardware. Fabrication of chambers and ducts will be from stainless steel utilizing TIG-welded construction.

Because the front ends share the storage ring vacuum, front-end and SR vacuum pressures must be compatible. A pressure of 10^{-9} Torr therefore must be maintained in the beamline front ends during machine

operations. To achieve these pressures, we will use a combination of UHV components and procedures, in addition to bakeout of the front-end subsystem. The chambers and beam ducts will be designed to withstand a bakeout temperature of 200°C, to accelerate the release of gases. We expect that an integral bakeout system will be incorporated in the beamline front end, to enable the capability of in-situ bakeout.

Only all-metal commercially available gate valves will be used in the front ends. An all-metal right-angle valve will be located between the photon shutter and the fast-closing valve. Attached to this valve will be a fitting with both an ion gauge and an RGA to monitor the total and partial pressures of the front-end vacuum. At the remaining port of the cross, a valve will be installed (to be used in combination with the right-angle valve) to allow for venting and pump-down when replacing either the ion or RGA gauge filaments. Additionally, installation of a vacuum valve between the fast-closing valve and the XBPM-2 is planned, to allow for separate venting/pump-down of the downstream portion of the front end. The fast gate valve should close in less than 15 msec and have a leak rate of less than 7.5×10^{-10} Torr-l/s when closed. Two ion pump/titanium sublimation pump combinations are planned, located strategically in each beamline front end. To minimize any residual gas species generated by the photon beam impinging on a surface, a 400 L/s ion pump/TSP pair will be installed near the photon shutter locations. An additional 400 L/s ion pump/TSP pair will be installed at the safety shutter, due to the relatively long distance (~5 m) between the photon shutter and safety shutter.

4.4.3.2 Radiation Protection

At times during storage ring operations, it will be necessary to access the experimental hutch (for example, to set up equipment and change samples). The remotely actuated safety shutter device is provided (see Figure 7.5.1) to stop brehmsstrahlung radiation, thus providing protection from ionizing radiation for personnel downstream of each shutter. From calculations, a thickness of 20 cm of tungsten is required to attenuate the brehmsstrahlung radiation in the forward direction. Ray-tracings will be done to determine the transverse dimensions of the tungsten shielding. Additionally, lead collimators will be provided in each front end to confine the radiation cone in the downstream experimental area. From calculations, a thickness of at least 30 cm of lead for the collimators will be required to attenuate the brehmsstrahlung radiation in the forward direction. As with the tungsten shield of the safety shutter, ray-tracings will be performed to determine the minimum transverse dimensions of lead required.

A byproduct of the brehmsstrahlung/lead collimator interaction is the production of neutrons that ultimately must be shielded. The concrete used in the shielding wall is a very effective neutron shielding material; however, there will be beampipe penetrations through the shield wall that must be considered. Void volumes between the shield wall and front-end beampipe penetrations will be filled with concrete and lead, to terminate the transit of photons and neutrons beyond the shield wall. For exit ports with no front end, the shield wall window will be completely filled with concrete.

4.4.3.4 Interlocks

The Personnel Protection System (PPS) will monitor the position of the safety shutter to provide personnel at the beamline safety from prompt radiation. The Equipment Protection System (EPS) will control the sequencing and control of front-end devices and prevent damage from occurring. The EPS will prevent damage to front-end components by sensing position, water flow, and vacuum, then taking action by operating components or dumping the beam, when appropriate.

To protect the storage ring vacuum from any inadvertent pressure rise due to front-end or beamline component failures, various interlock sequences will be implemented. Two possible scenarios in which an air-to-vacuum leak in the front end would corrupt the SR vacuum are mentioned here as examples: 1) a slow air-to-vacuum leak due to faulty bellows or a leaking weld in a vacuum chamber, and 2) a catastrophic vacuum leak due to a failure in a beamline.

If monitoring of the vacuum quality indicates a slowly increasing pressure, the origin of this pressure rise will be investigated and repaired during a regularly scheduled maintenance period. Should the pressure in the front end reach the ion gauge set point of approximately 5×10^{-7} Torr, the EPS will first signal the insertion device on the offending beamline to open its gap, thereby eliminating the high heat flux on any front-end components. The bending magnet photon shutter will then be actuated to provide dipole radiation protection to the uncooled isolation valve when it has been moved into the closed position. Finally, first the photon shutter and then the safety shutters will be the last devices instructed to close. With the storage ring isolation valve in the closed and sealed position and PPS in place, ring operations will be allowed to continue unhindered by the vacuum leak in the front end. The front end or beamline experiencing such vacuum difficulties would be repaired during a regularly scheduled maintenance period. Note that all of these front-end actions will be taking place in the background while facility operations continue unhindered.

In the case of a catastrophic leak, once the fast-closing valve is triggered by a pressure exceeding 5×10^{-6} Torr in the front end or beamline, the EPS will send the appropriate signals to dump the stored electron beam. Triggering of the FV will simultaneously close the BMPS, isolation gate valve, and safety shutters. Operations may resume when proper sealing of the isolation gate valve has been verified and the vacuum leak in the front end or beamline has been isolated from the SR vacuum.

4.6 Storage Ring RF Systems

The large dipole radius (25 m) and the medium energy (3 GeV) of NSLS-II result in very low radiated energy from the bending magnets (288 keV/turn). This increases the effectiveness of eight damping wigglers to reduce the bare emittance of 2.1 nm-rad to 0.5 nm-rad. The RF system power requirement for NSLS-II is determined primarily by the power radiated by the damping wigglers. This makes it possible for us to stage the RF system installation to parallel the installation of damping wigglers and user insertion devices.

The small momentum compaction (0.0037), an RF frequency of 500 MHz, and high RF voltage result in small bunch lengths of ~4 mm. This contributes to a short Touschek-dominated lifetime of <2 hours. To improve lifetime to greater than 3 hours, a third harmonic bunch lengthening cavity is included in the baseline design.

The storage ring RF system consists of the 500 MHz Superconducting RF cavities, their associated klystron tube amplifiers and power supplies, the passive SCRF third harmonic Landau (bunch lengthening) cavity, the liquid helium cryogenic plant, and the master clock, frequency synthesizers, digital cavity controllers, and RF distribution system that make up the low-level RF.

4.6.1 Physics Requirements and Design Parameters

The RF system must provide sufficient momentum acceptance (bucket height) so as not to be the limiting factor in the storage ring acceptance. In addition, with the small momentum compaction of the low emittance lattice leading to very short bunches, and the accompanying short lifetime, a third harmonic (1500 MHz) RF system is used to lengthen the bunches to increase the Touschek lifetime from <2 hours to >3 hours. The Landau cavity also increases the dependence of the synchrotron tune on the oscillation amplitude providing Landau damping, which can suppress bunch instabilities. The required RF power is the sum of the beam radiated power in the dipoles, damping wigglers, and user IDs. There is no unique approach to meeting the RF requirements; in fact, the frequency choice of 500 MHz is within a broad range of frequencies in which RF sources and cavity designs exist and that would meet the physics requirements. Three frequencies within this broad range, 352 MHz, 476 MHz, and 500 MHz, have been used successfully in third-generation light sources. The operating frequency of 500 MHz has been selected here due to the availability of existing SCRF cavity designs, commercial RF transmitters, and the large number of 500 MHz systems in use at light sources around the world. This translates into mature technologies and lower development costs. A summary of the ring parameters related to the design of the RF system is shown in Table 4.6.1.

Table 4.6.1 RF and Beam Parameters for the NSLS-II Storage Ring.

RF frequency [MHz]	**499.68**
Circumference [m]	792
Harmonic number	1320
Loss per turn (assuming 5 undulators, 21 m of DW, and dipole losses) [keV]	816
RF acceptance [%]	3
Accelerating voltage [MV]	3.3
Momentum compaction	3.7×10^{-4}
Bunch charge [nC]	1.25
Number of buckets filled with charge	1056

The radiation from dipoles and an assumed complement of five undulators and 21 m of damping wigglers result in an energy loss per turn of 816 keV, corresponding to 408 kW power loss at the design current of 500 mA. A 3% momentum acceptance ($\Delta p/p$) is specified to ensure sufficient Touschek lifetime of the storage

ring. For 816 keV/turn energy loss, this corresponds to an RF voltage of 3.3 MV (see Figure 4.6.1). As insertion devices and damping wigglers are added as the user program is built out, the loss per turn increases to more than 1.6 MeV, and a voltage of 4.8 MV is required to maintain the 3% bucket height.

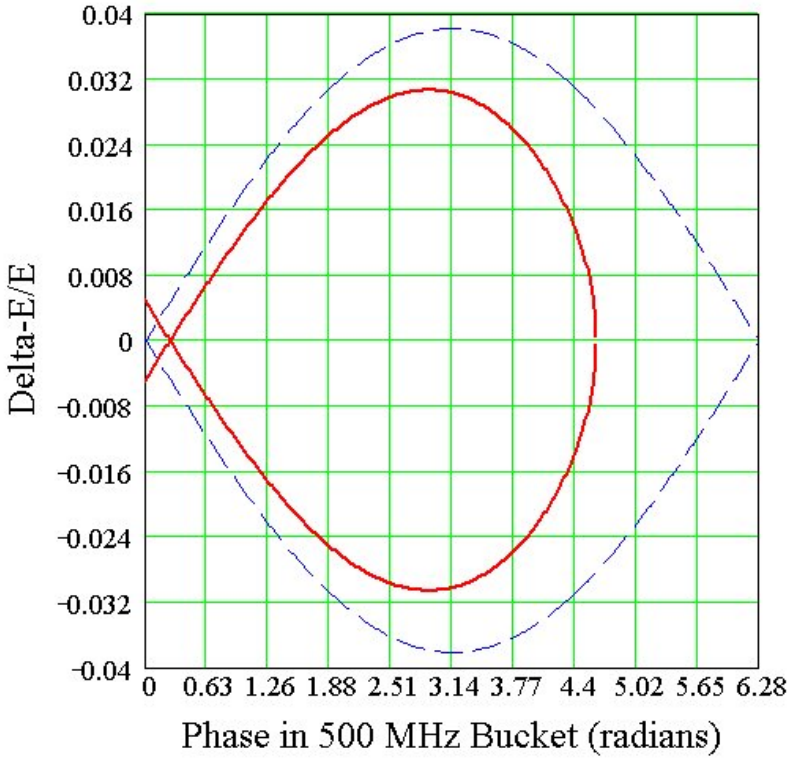

Figure 4.6.1 RF seperatrix for 3.3 MV RF field with (red trace) and without (blue trace) 816 keV/turn radiation losses. The 3% RF acceptance is easily met with two CESR-B cavities.

Thus, the evolution of the RF power requirements over the life of the facility must be taken into account. Table 4.6.2 outlines the initial machine configuration, the capabilities of the RF system, and a reasonable extrapolation as to how this might evolve as insertion devices are added. The exact scenario will be driven by the user requirements and is not fixed at this stage of the machine design.

Table 4.6.2 RF Power Requirements for Dipole Losses and Various Example Insertion Device Configurations for one, two, and four RF systems installed.

	Phase 1: Capability of installed RF (270kW/cavity)		Phase 2: Adding 2nd cavity plus purchase 300-kW Transmitter		Phase 3: Add 3rd and 4th RF station (cavity + transmitter)	
RF power requirements	**#**	**P (kW)**	**#**	**P (kW)**	**#**	**P (kW)**
Dipole	-	144	-	144	-	144
Damping wiggler (9.23 kW / m, 7 m each)	0	0	3	194	8	517
IVU (2.7 kW/m, 3 m each) [CPMU] (3.77kW/m, 3m each)	3	24	[6]	66.6	[10]	111
EPU (4.1 kW/m, 4 m each)	1	12	4	48	5	60
Total		180		452		832
RF power available for additional ID's		90		88		248
Total Available RF power		270		540		1080

The initial RF system will consist of two CESR-B cavities, each powered by a 310 kW transmitter. Three cavities will be purchased with the third cavity to be used as a spare in the event of a cavity failure. Two installed cavities can provide up to 5 MV, which exceeds the voltage requirement of 4.8 MV even for the full complement of insertion devices and the 56 m of damping wigglers envisioned for NSLS-II. However, the power coupler is capable of delivering only ~270 kW of beam power, and so the ring is limited to four damping wigglers and 10 user IDs (or equivalent) by the initially available RF power. Installing a third cavity and transmitter will support a full complement of eight damping wigglers, resulting in the ultimate horizontal emittance of 0.5 nm-rad. Two 500 MHz cavities and one 1500 MHz harmonic cavity (to be described in Section 4.6.3) fit into a single 8 m straight. A second RF straight is reserved for the third and potentially fourth CESR-B cavity and second 1500 MHz cavity, to meet the evolving power requirements of NSLS-II as more user IDs are added.

4.6.1.1 Impedance Analysis and Beam Stability

The high beam loading due to 500 mA average stored current requires highly damped structures to prevent beam instabilities. In this regard, the B-factory cavity designs of KEK, PEP-II, and Cornell are attractive and have been studied in detail.

The narrow band cavity impedances have been calculated using the codes GdfidL, SUPERFISH, and CLANS [4.6.1, 4.6.2, 4.6.3]. These codes calculate the longitudinal shunt impedance as

$$R_{sh} = \frac{\left[\mathrm{Re}\left(\int E_z(z) e^{ikz/\beta} dz\right)\right]^2}{2P}, \tag{4.6-1}$$

where P is the power dissipated in the cavity, E_z is the longitudinal electric field either on axis (monopole modes) or displaced with a radial offset corresponding to a dipole mode, quadrupole mode, etc. Here, k is the wave number (ω/c), and β is the ratio of beam velocity to that of light.

The cavities also have transverse impedances that can couple strongly to the beam. The transverse shunt impedance of a cavity is given by the integral of the force acting on the beam, as

$$Z^{\perp} = -i\left(\frac{\int_0^L (\vec{E} + \vec{v} \times \vec{B})_{\perp} ds}{\beta \cdot I_{av} \cdot a}\right), \tag{4.6-2}$$

where L is the cavity length, I_{av} is the average bunch current, and *a* the offset of the beam from the cavity axis. The beam must couple energy into the higher-order transverse mode through the electric field ;hence, there is a relation between the longitudinal and transverse impedances. The broadband impedance model uses the Panofsky-Wenzel relation,

$$Z_{\perp} = \frac{c}{\omega \Delta^2} \cdot Z_{\parallel}^{(\Delta)}, \tag{4.6-3}$$

where Δ is the offset at which the longitudinal impedance is calculated. The cavity impedances have been calculated for the PEP-II, KEK-B, and CESR-B cavities [4.6.4, 4.6.5, 4.6.6]. All three cavity designs can meet the NSLS-II requirements in terms of attainable voltage and beam power delivered. The SCRF approaches of KEK and Cornell result in lower installed RF power requirements and more efficient operation, attain much lower HOM impedances, and require fewer cavities to achieve the voltage specification. This is particularly important when additional insertion devices are installed that will increase the RF voltage

requirement to ~5 MV. The choice for NSLS-II has been narrowed to either the KEK-B cavity or the Cornell CESR-B cavity. Further studies on cost, reliability, and future upgrade potentials in the preliminary design phase will lead to the final choice. For the purposes of this document, the CESR-B cavity is baselined in order to present self-consistent calculations of system parameters such as RF power and cryoplant requirements, coupled bunch growth rates, system mechanical layouts, and cost. Details of the HOM impedances and coupled bunch growth rates are given in Section 6.2.3.

To meet the initial requirements of 3.3 MV accelerating voltage and 408 kW beam power, two RF cavities with individual klystron transmitters are to be installed. A third cavity to be used as a test cavity / spare will be purchased as part of the baseline machine. It is expected that this cavity will be installed in a future upgrade as additional insertion devices increase the beam power requirement to beyond 2×270 kW, a soft limit of the power couplers in the CESR-B cavities. The CESR-B cavity parameters are given in Table 4.6.3.

Table 4.6.3 CESR-B Cavity Parameters.

Frequency [MHz]	499.68 +/- 0.2
Electric field (normalized to 0.3m) [MV/m]	>8 MV/m
Accelerating Voltage (beam energy gain) [MV]	>2.4 MV
Unloaded Q (at 8MV/m)	$>7*10^8$
Static heat losses [W]	<30 W
Dynamic heat losses (at 4.5k and 8MV/m) [W]	<120 W
Maximum power transferred to beam [kW]	>250 kW
Loaded Q	1×10^5

In addition to coupled bunch instabilities caused by higher order modes in the cavities, the fundamental and harmonic RF systems can cause instabilities where all of the bunches oscillate in unison, the so-called Robinson instabilities. The classical Robinson analysis [4.6.7] is particularly relevant for short and compressed bunch operation of the machine. The resistive Robinson instability is not excited by the cavities. This is due to the fact that the main cavities are detuned below resonance to compensate for beam loading, which strongly damps phase oscillations, while the harmonic cavities' very high quality factor greatly reduces the resistive part of their impedance at the synchrotron frequency, and hence their excitatory (or damping) influence on phase oscillations.

The second observation concerns the reactive Robinson instability. In this instability the static bunch distribution is an unstable fixed point of the longitudinal dynamics, and a perturbation of the bunch pushes it with some growth rate away from that distribution, subsequently damping to one of two stable distributions. In the absence of harmonic cavities, the bunch is marginally unstable. The addition of inductively detuned harmonic cavities for stretched bunches tend to suppress this problem; capacitively detuned harmonic cavities for compressed bunches aggravate the instability. In unstretched or compressed operation, however, the unmitigated instability results in only a small phase shift of the bunch due to the narrow potential well. But for stretched bunches the potential well is wide and flat, and the instability results in gross distortion of the bunches, which must be addressed. A simple cure, first recognized by Miyahara [4.6.8], is to introduce a small-bandwidth feedback of the RF system to the beam. Simulations also show that a reduction of the main-cavity impedance using RF feedback suppresses the instability, although too much feedback excites a higher-order oscillatory instability.

Although glossed over in the discussion to this point, with stretched bunches the classical Robinson picture is not so simply applicable; more involved analyses, such as those by Bosch et al. [4.6.9], and numerical simulations are required to assess the stability of higher-order modes of these bunches. As was just mentioned, the use of RF feedback, which allows the adjustment of the impedance of the main cavities, is a means by which some manipulation of bunch stability is possible. Our experience with the NSLS VUV ring

also shows that short-range wakes can have an impact on the stability of stretched bunches, which is further complicated by the varying bunch profiles along the train.

4.6.2 500 MHz RF System

4.6.2.1 500 MHz Cavities

The CESR-B cavity consists of a bulk niobium SCRF single cell with waveguide coupler, a special fluted beampipe to extract the lowest frequency dipole modes, warm-to-cold transition spool pieces for thermal isolation, water-cooled C48 ferrite HOM dampers, and long tapers to transition from the 240 mm cavity bore to the elliptical beampipe. The CESR-B cavity is a "single-mode" cavity. All higher-order modes with the exception of the TM110 dipole mode propagate through the cylindrical beampipe. A fluted beampipe at the opposite end of the cavity has a lower cutoff frequency to allow the TM110 to propagate to the ferrite load. This has only a small effect on the fundamental mode. This allows a shorter attenuation length in the beam tube and a more compact cavity. The cavity assembly is shown in Figure 4.6.2. The layout of two CESR-B cavities plus a single Super3HC harmonic cavity in a single straight is shown in Figure 4.6.3.

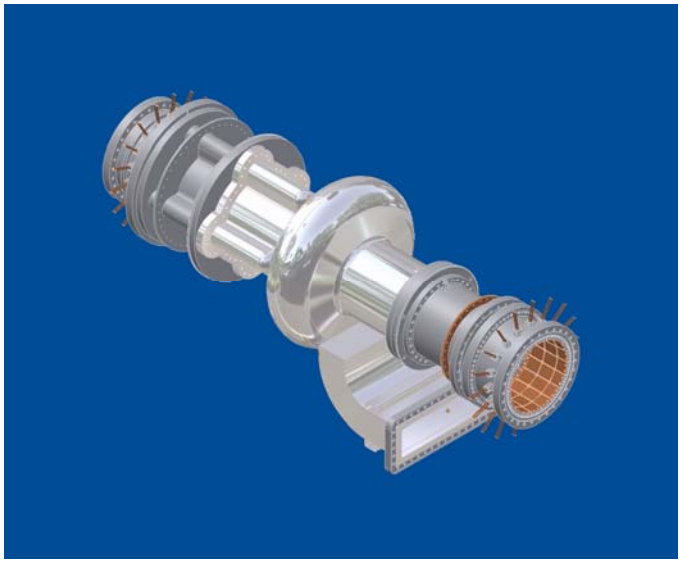

Figure 4.6.2 The CESR-B bare cavity assembly.

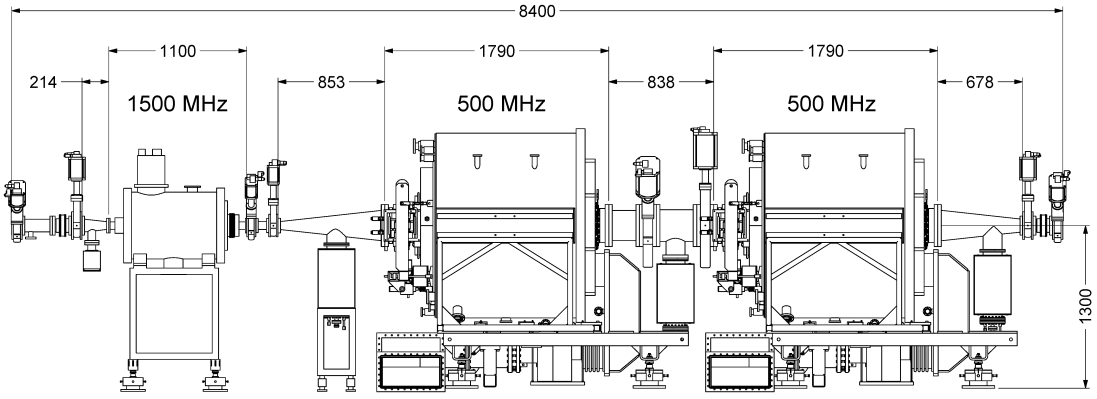

Figure 4.6.3 Layout of two 500 MHz cavities plus one 1500 MHz Landau cavity in a single straight. The tapers from the large cavity beampipe to the ring beampipe are 678-853 mm long, limited by the available length in the straight of 8.4 m. A second RF straight is reserved for additional cavities.

4.6.2.2 HOM Damper

The HOM damper consists of C48 ferrite tiles brazed to water-cooled copper backing plates that form a spool piece outside the cryostat. The ferrite is several 500 MHz attenuation lengths away from the SC cavity. There is power dissipated in the ferrite from two sources. First, there is dissipation of the fundamental 500 MHz field driven by the transmitter. This has been calculated with CFISH [4.6.2, 4.6.10] to be less than 100 W at 2.5 MV cavity voltage. Second, the beam also loses energy from wakefields. This loss is given by

$$P_{loss} = k_{\|} \cdot I_0^2 \big/ n \, T_0 \,. \tag{4.6-4}$$

For NSLS-II, $T_0 = 2.6$ μs, $I_0 = 0.5$ A, and $k_{\|}(\sigma_s = 4\text{ mm}) = 3.6$V/pC, resulting in a $P_{loss} = 2.3$ kW. In the worst case, all of this power is lost in the ferrite, which is still a factor of 4 lower than the design limit.

4.6.2.3 KEK-B Cavity Option

The superconducting cavities developed for the KEK-B factory are being considered as an option for NSLS-II, for several reasons. The most significant advantage is the higher power per coupler, which has been demonstrated at KEK to be greater than 400 kW. In principle, two KEK cavities could meet the power requirements for the full complement of damping wigglers and user insertion devices, ~800 kW. The waveguide feed at the top of the cryostat makes the tunnel installation easier, and the coupling can be optimized for various beam currents and cavity voltages by simple spacers on the antennae coupling mounting flanges, as opposed to the fixed coupling of the waveguide feed for the CESR-B approach. A layout of two KEK-B cavities in an 8 m straight is shown in Figure 4.6.4.

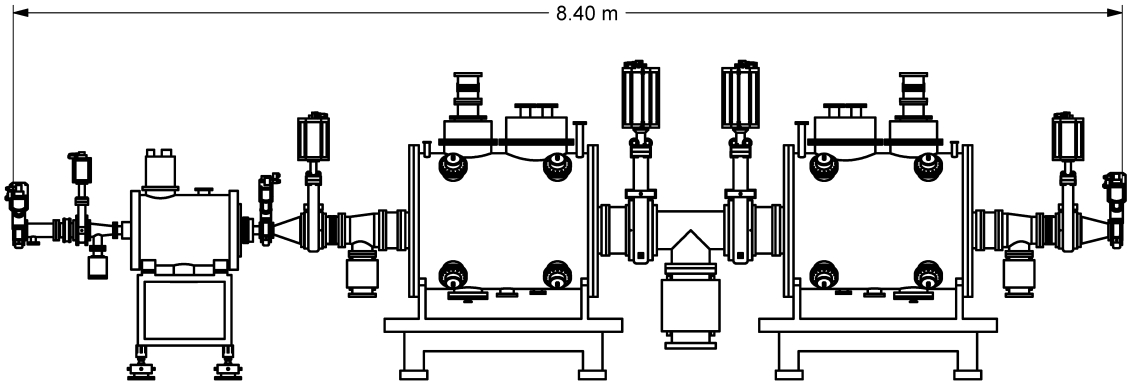

Figure 4.6.4 Installation of two KEK-B SCRF cavities in an 8.4 m (available length) straight.

4.6.2.4 RF Transmitter

The power couplers for SCRF cavities have a wide statistical variation in their power handling capability. Although they have been engineered for high power handling by proper thermal and electrical design, they are prone to multipacting, a resonant electron-avalanche effect that can impose a hard limit on power transmission and cause failure by local heating due to electron loading. The multipacting depends on the secondary-emission coefficient of the surface, which in turn depends on the properties of the bulk material, usually copper or niobium, and surface contaminants, which are usually cryo-pumped organics from the machine vacuum. These contaminants can be present at start-up or accumulate over a period of time, degrading performance and requiring, in the worst case, the cavity to be warmed up with a mild bake to drive off the condensed gases. Experience with the CESR-B cavities has shown transmitted power per coupler in the range of 250–330 kW. A transmitted power of 270 kW is assumed for meeting machine requirements and placing a limit on installed RF power. In addition to the energy losses due to radiation in dipoles, damping

wigglers, and undulators, the RF power transmitter and coupler must provide for the HOM losses that are excited by the beam. We are exploring ways of increasing the power per coupler, and will factor this into the preliminary design and choice of transmitter power.

The coupling of the waveguide to the cavity in the ideal case is adjusted so that the cavity presents a matched load to the RF source at the normal operating current and energy. Since there is a phased installation of cavities and insertion devices, this optimal coupling varies over the life of the machine. The KEK-B cavity has an adjustable antennae coupler that, in principle, can be changed to follow the optimal coupling. In practice, this must be done in a clean room environment and may be of limited value.

For an aperture-coupled cavity such as the CESR-B, coupling is set during the design and manufacture. Usually coupling is set so the generator is matched to the cavity at the highest expected beam-loading (beam power) of 270 kW. This minimizes the requirement on installed RF power. For the staged installation of insertion devices (RF power required) and RF cavities there is not a single minima, and it is necessary to balance the mismatch over the different phases. For an approximate match to the conditions in Phase 3 in Table 4.6.2, the maximum reflected power in the other three phases is ~10.5 kW. Alternatively, we can choose the coupling to be slightly over-coupled in the case of the highest beam-loading, and accept In order to reduce the residual reflected power during commissioning and staged insertion device installation, we have the option of installing a 3-stub waveguide tuner between the circulator and the cavity.

There will be variation of the impedance presented by the cavities to the beam at different times of the machine's life due to the varying number of cavities and insertion devices. RF feedback can be used to reduce (or increase) this impedance; this option is being studied and system layout designed to minimize loop delay to allow its implementation. A minimum transmitter power of 275 kW is required to meet the sum of the radiated, HOM, and reflected power demands. To allow for the case of coupler improvement (coupler is limited by multipacting, not power limitations) or system aging (degradation of klystron output power), the transmitter will be designed for a minimum of 310 kW, allowing up to ~280–300 kW per coupler.

A single 300 kW klystron amplifier will drive each of the main ring cavities through a 350 kW rated circulator and load. Klystrons that meet or exceed this power level are available from three vendors: CPI, Toshiba, and Thompson. The klystron beam power will be provided by a Pulse Step Modulation switching power supply at 55 kV and 12 A. The PSM switching power supplies have the benefit of low stored energy, and fast turn-off capability of the IGBTs eliminating the need for a crowbar circuit to protect the klystron. The power supply will have redundant switching cards built in, and will operate at full capacity even with several card failures. The RF transmitter will have local control via PLC, with system parameters and control available to the main control system via an Ethernet link. The PLC will also monitor the PSM switch modules, so that failed modules are logged and transmitter repairs can be scheduled for the next maintenance period. The main ring power systems with a rating of 300 kW are beyond the power limit of air-cooled coaxial cable, and will be implemented in WR1800 waveguide. A layout of the RF straight with the associated RF transmitters is shown in Figure 4.6.5.

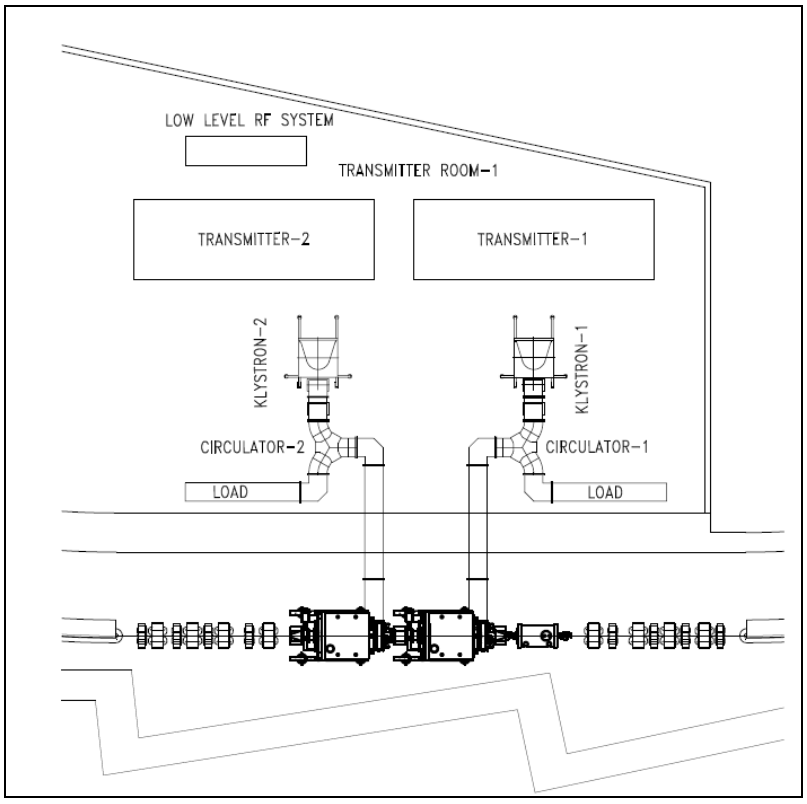

Figure 4.6.5 Layout of an RF straight section with two 500 MHz cavities and their klystron transmitters and a single 1500 MHz harmonic cavity.

An alternative approach of combining several Inductive Output Tube (IOT) amplifiers to obtain the necessary RF power has been developed at other facilities [4.6.11, 4.6.12]. IOT systems have higher efficiencies and some limited failure tolerance. Likewise several hundreds of high-power transistors can be combined to provide the required power. SOLEIL has recently commissioned such a system at 352 MHz [4.6.13]. Both of these options will be explored in detail during the R&D phase.

4.6.3 1500 MHz Harmonic Cavity System

A passive 1500 MHz SCRF cavity, such as the BESSY scaled CESR-B [4.6.14] or Super3HC [4.6.15] scaled SOLEIL cavity, has been studied for the Landau cavity in NSLS-II. Both of these cavities can achieve ~0.5 MV per cell, with the BESSY cavity containing a single cell, and the Super3HC containing two cells per cavity. The details of the impact of the Landau cavity have been discussed in Section 6.2.7 on collective effects. Here we will discuss the hardware and system configuration. For this purpose, two cells (1 cryo-module) of the Super3HC design is in the baseline design.

The nominal voltage and phase of the harmonic cavity is that which cancels the slope and second derivative with respect to time of the total RF field. This results in bunches lengthened by approximately the ratio of the harmonic-to-main cavity frequencies. The field required of the harmonic cavity is approximately the reciprocal of that ratio times the main-cavity field, although slightly less due to the non-zero main-cavity synchronous phase that is a consequence of the beam's radiation loss. In practice, this harmonic-cavity field is pushed slightly higher to provide additional stretching, striking a balance between improved lifetime and the eventual onset of longitudinal instabilities. Furthermore, the use of a gap in the ring's fill pattern for ion clearing results in perturbations of the potential wells that vary along the train. As a result, the lengths of most bunches are shortened by these perturbations and the average lifetime is reduced. For these reasons, the harmonic-cavity field and phase require further investigation. Simulations shown in Section 6.2.7 give a

maximum in bunch length for ~1.1 MV of third-harmonic voltage for the initial fundamental cavity voltage of 3.4 MV. This can be met with a single Super3HC cavity. As the number of damping wigglers and user insertion devices increases, the fundamental mode voltage increases to 4.8 MV and an additional third-harmonic cavity will be necessary for optimal bunch lengthening.

4.6.4 Low-Level RF and Beam Control

The specifications of the RF system amplitude and phase requirements are derived in part from the user requirements that the transverse motion of the photon beam is to be <10% of the RMS beam size, and the increase in photon beam size due to emittance dilution of the electron beam is to be <10%. The relation of the photon beam size and jitter to electron beam size and jitter is influenced by the design of a particular insertion device and beamline, which might impose a tighter tolerance on the electron beam stability. The stability required from the RF system to limit the transverse jitter of the electron beam to 10% beam size is derived below. This will be expanded to study the effect on the photon beam in the next phase of design.

4.6.4 Low-Level RF and Beam Control

The specifications of the RF system amplitude and phase requirements are derived in part from the user requirements that the transverse motion of the photon beam is to be <10% of the RMS beam size, and the increase in photon beam size due to emittance dilution of the electron beam is to be <10%. The relation of the photon beam size and jitter to electron beam size and jitter is influenced by the design of a particular insertion device and beamline, which might impose a tighter tolerance on the electron beam stability. The stability required from the RF system to limit the transverse jitter of the electron beam to 10% beam size is derived below. This will be expanded to study the effect on the photon beam in the next phase of design.

4.6.4.1 RF Tolerances Imposed by User Experiments

Timing experiments, such as the IR experiments run at NSLS currently, require that the timing jitter of the bunch be less than 5% of the RMS bunch length over the frequency range of 500 Hz to 50 kHz. This corresponds to a phase error of 0.16 degree for a 10 ps bunch, or a corresponding momentum jitter of 0.005% due to synchrotron motion.

The majority of users are not concerned with timing experiments but require small and stable photon beam size. The vertical photon beam divergence for a experiment using a higher harmonic of an Insertion Device (ID) is given by[1]

$$\sigma_{y'}^2 = \frac{\lambda_n}{2L}\sqrt{1+16n^2N_w^2\sigma_\delta^2} + \varepsilon_y \Big/ \beta_y \,, \tag{4.61}$$

where n is the harmonic of the ID being used, N the number of periods, L the length of the ID, σ_δ the momentum deviation, ε_y the vertical emittance of the electron beam, and β_y the vertical beta function of the lattice at the insertion device location.

For NSLS-II, ε_y ~8 x 10^{-12} nm·Rad and β_y ~1 m at the ID straights, L ~3 m, N ~100. Because of the n^2 dependence, the worst case is for n >>3, where the two terms on the right hand side of Eq. (1) are comparable. Thus, using Eq. (4-5.1), for a 10 % increase in beam size, the momentum jitter must be 44% of the inherent momentum spread—or equivalently, a phase jitter of 1.4 degrees.

A third limit on momentum spread is due to longitudinal energy oscillation leading to filamentation and increase in beam size. With a momentum kick Δp/p to the bunch, an electron would have a longitudinal oscillation:

$$\delta(t) = \left(\Delta p \big/ p\right) \sin \upsilon_s \omega_0 t + \delta_0 \sin \upsilon_s \omega_0 (t + t_0) . \tag{4-5.2}$$

Because of the longitudinal tune spread the two terms will de-cohere and become

$$\delta(t) = \left(\Delta p \big/ p\right) \sin \upsilon_s \omega_0 (t + t_1) + \delta_0 \sin \upsilon_s \omega_0 (t + t_2) , \tag{4-5.3}$$

where t_1 and t_1 are two random numbers. Averaging over t_1 , t_1 and δ_0 we arrive at

$$\sigma_\delta = \sqrt{\frac{1}{2}\left(\frac{\Delta p}{p}\right)^2 + \sigma_{\delta,0}^2} = \sqrt{1 + \frac{1}{2} f^2 \sigma_{\delta,0}} , \tag{4-5.4}$$

where $f = (\Delta p/p)/\sigma_\delta$ is the relative kick factor. For a 10% increase in σ_δ, f ~ 0.65 or $\Delta p/p = 6.5 \times 10^{-4}$. The corresponding phase jitter is given by

$$\Delta\phi = \frac{h\alpha_c}{\upsilon_s} \Delta p \big/ p , \tag{4-5.5}$$

where h is the harmonic number (1320), α_c is the momentum compaction factor = .00037, ν_s ~0.0087, and $\Delta\phi$ = 2 degrees.

The transverse electron beam size and position are related to the momentum spread and average momentum, respectively. The beam size is given as

$$\sigma_{x,y} = \sqrt{\beta_{x,y}\varepsilon_{x,y} + \left(\eta_{x,y}\sigma_\delta\right)^2} . \tag{4-5.6}$$

The residual dispersion η_y is of the order 1 mm and the second term is negligible in beam size. Vertical position is given as $y = y_0 + \eta_y \langle\delta\rangle$. The allowed centroid jitter is 10% of the beam size or 0.3μm; therefore, the average momentum jitter should be less than 3×10^{-4}, with a corresponding phase jitter of 0.95 degrees. These limits are summarized in Table 4.6.1.

Table 4.6.1 Longitudinal beam stability requirements

	Phase jitter (°)	Momentum jitter (ΔE/E x10^{-4})
Timing-dependent experiments	0.16	0.5
Vertical divergence (from momentum jitter	1.4	4.4
10% increase in σ_δ due to filamentation	2.0	6.5
Vertical centroid jitter (due to residual dispersion)	0.95	3
Dipole, TPW Beam lines (Position stability due to momentum jitter)	0.32	1

Due in large part to the near zero dispersion in the ID straights which mitigates the effect of momentum jitter, the tolerance on the RF is dominated by the IR timing experiments.

The magnitude of the effect on the beam of RF phase and amplitude noise depends on whether the source of the RF jitter is random or harmonic (systematic). Sources of noise are broadly classified into continuum sources possessing a continuous and slowly varying (with respect to frequency) spectral density, and spurious sources that possess spectral lines, possibly varying in time. Examples of the former are the continuum component of synthesizer phase noise, amplifier shot noise, and the continuum components of other active devices in the RF system. Examples of the latter are line related and power-supply switching noise, microphonics, and vibration. To assess the impact of, and derive tolerances for, RF-system noise sources, we need to determine the beam's sensitivity to noise from identified sources and derive a tolerance budget. The sensitivities are to be determined by modeling the RF system's linear response to these sources. Noise magnitudes in existing machines are a starting point for noise intensities, from which sensitivities are used to determine where noise tolerances need to be tightened. This work is in progress, and will be expanded in the preliminary design phase. Digital low-level RF systems have achieved less than 0.1 degree phase and 0.1% amplitude stability [4.6.16], these tolerances should be sufficient for NSLS-II.

4.6.4.2 Master Oscillator and Ring Frequency Synthesizers

The low-level RF and beam control design is at a preliminary stage of defining specifications and architecture. Unlike the power systems, which stay relatively static over long periods of time during the life of the machine and should be transparent to the user, the LLRF and beam control requirements may change several times as the machine evolves, so the design must be flexible. To this end a digital architecture is used.

An ultra stable Master Oscillator at the fundamental RF frequency is distributed to the storage ring, booster and linac RF stations as well as other systems such as bunch feedback systems and beam diagnostics. The Master Oscillator is software tunable to allow for a radial (frequency) loop to stabilize the beam orbit against slow drifts caused by diurnal or annual variations in machine circumference. The RF frequency is nominally 499.68 MHz ± 20kHz to cover seasonal variations, machine studies (measurement of chromaticity, etc). For the sake of clarity in the description of the low level RF it will be assumed to be 500 MHz. The Master Oscillator is mixed with an IF frequency generated from the same master oscillator. The (RF+IF) frequency is used as a local oscillator for the up/down conversion of the 500 MHz RF signals. An example of such a system is shown in Figure 4.6.6. An IF frequency of 50 MHz is chosen resulting in a 550 MHz LO frequency. This has the advantage of having a common subharmonic in the ring revolution frequency (F_{rev}) of 379KHz for both the RF (÷1320) and LO (÷1452). Thus, the F_{rev} can serve as a synchronization clock on system power-up for all of the ring, booster, and linac controllers as well as serve as a bunch zero clock for timing. The 10 MHz frequency standard for the Master Oscillator will be available as an external time base for other systems.

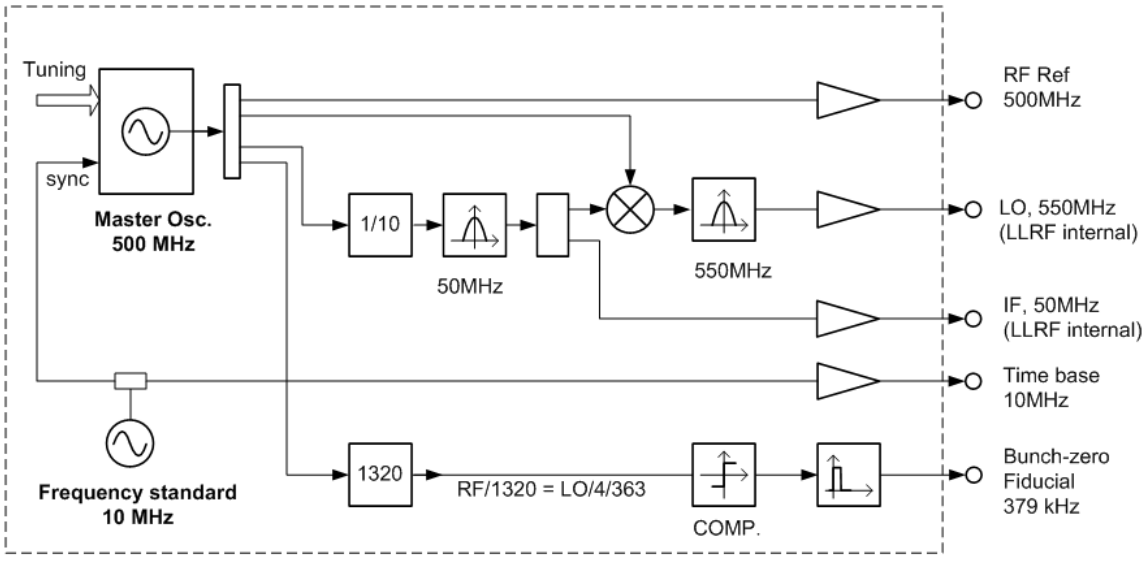

Figure 4.6.6 Master oscillator.

4.6.4.3 Cavity Controllers

The cavity-amplifier system has several nested feedback loops to control the amplitude and phase of the RF cavity fields in the presence of beam-loading, mechanical perturbations to the cavity, and residual klystron noise due to power line/DC power supply ripple. The innermost loop is the tuner loop, which tunes the cavity resonance in order to present a purely resistive impedance to the klystron, thus minimizing klystron power. This loop, which is closed around a mechanical tuner, is slow—on the order of 1 Hz. Next is an RF feedback loop that is used to adjust the impedance of the main-cavity accelerating mode. In order to stabilize the cavity fields against fast perturbations, an amplitude and phase loop around the klystron-cavity chain is implemented. Although these can be independent loops, it is more effective to combine them in a common In-phase and Quadrature (I/Q) modulation loop, due to the coupling of the loops by cavity detuning for beam loading.

In addition to the above RF, amplitude, phase, and tuner loops, it may be necessary to implement other loops. A loop for zero-order coupled-bunch-mode feedback from the beam to the RF system to damp Robinson or higher-order longitudinal instabilities may be necessary. A klystron scalar phase loop to reduce the DC power supply induced the klystron, and possibly a feed-forward loop on the anode modulation of the klystron for maximizing klystron efficiency under different operating conditions, may also prove useful.

With the exception of direct RF feedback, the above loops can be implemented in either analog or digital hardware. Analog systems have the advantage of being simpler and less expensive to produce, and have higher speed and bandwidth. Their disadvantages include the lack of flexibility in changing loop characteristics for varying beam loading, slightly less phase and amplitude accuracy, and DC shifts that are more difficult to control. Digital implementation has the advantage of flexibility, in particular of being able to synthesize the loop filters digitally so that the feedback loops can be programmed for different machine states. Higher accuracy can be achieved, and DC drifts are easier to control. This comes at the price of higher complexity, and requires an additional skill set in high-speed digital design. Careful attention must be paid during the design stage to design in “digital probes” and other debugging tools to monitor and allow trouble shooting of the digital feedback loops.

To maximize the performance of the RF system and allow simple optimization and upgrades over the life of the machine, a digital implementation is our choice for NSLS-II.

The low-level RF cavity field control will be via a digital I/Q modulator-demodulator incorporating up and down conversion, ADCs and digital-to-analog converters (DACs) interfaced to the digital baseband signal processing, a Field Programmable Gate Array (FPGA) state machine, and interface to the control system. Similar systems have been designed for both hadron and electron machines in recent years [4.6.18, 4.6.19].

Although the booster and linac RF systems are simpler since they do not have the tight RF specifications of the storage ring, and harmonic cavities are easier because they are passive with only tuner control, we will use identical ring controllers throughout, with up and down conversion from 500 to 1500 and 3000 MHz. The only difference will be how the control loops are programmed and their control system graphical user interfaces. This makes the control system integration easier to manage with I/O, yet memory buffers for fault analysis, development tools, and maintenance identical.

The controller is derived from the LBNL LLRF4 design [4.6.20]. Five RF input channels support measurement of the forward, reflected, transmitted, and reference phase RF signals plus a beam pickup signal. The 14-bit input ADCs are clocked at 68.75 MS/s derived by a divide by eight from the 550 MHz LO. Two Direct Digital Synthesizers (DDS) built into the FPGA provide two output IF frequencies via DACs clocked at 137.5 MHz (LO divide by four). These are up-converted to the cavity drive and an RF calibration signal.

A conceptual design of the digital controller is shown below in Figure 4.6.7.

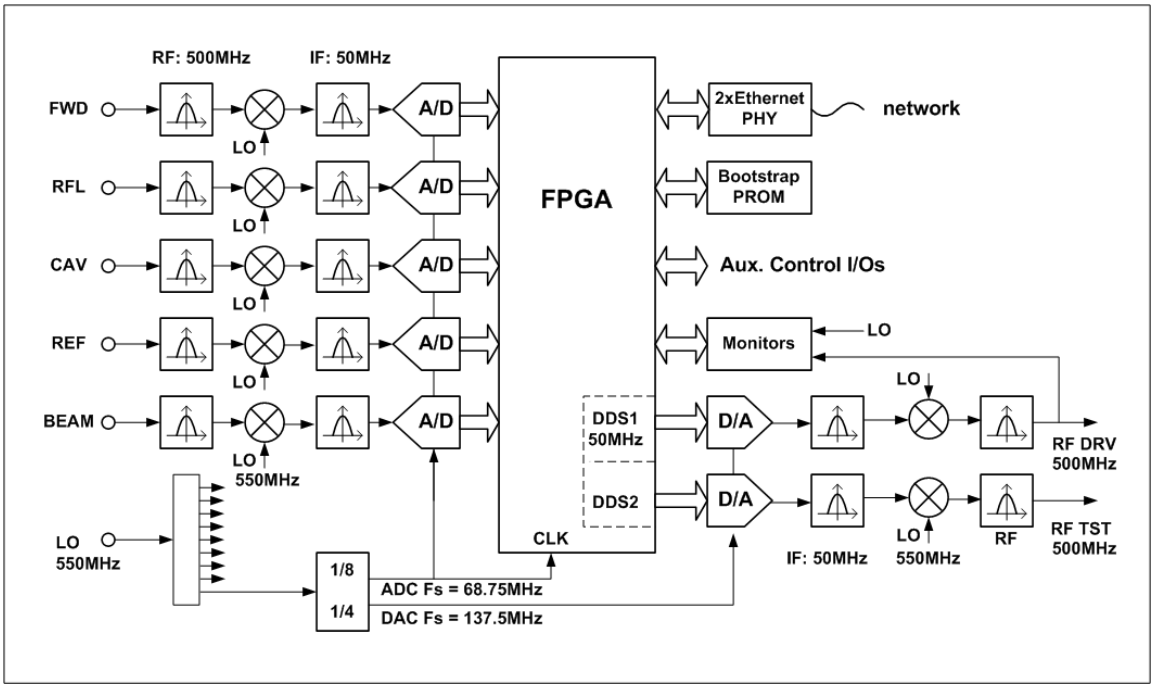

Figure 4.6.7 500 MHz Cavity controller.

Feedback algorithms within the FPGA logic will provide low frequency stabilization of the RF fields., with the phase auto-zeroed to the phase reference line. It will also adjust the fundamental RF cavity dynamic impedance for maximum stability, using information from a beam phase pickup and from the landau cavity fields.

In addition to the fast RF loops, a slower cavity tuning loop measures the phase shift between the cavity input and output, and adjusts the cavity tuner for optimum phase (usually coinciding with minimum reflected RF power). The landau cavity, since it is a passive cavity, has only this tuner loop. In order to use the same cavity controller, an additional LO frequency of 1000 MHz (2x RF frequency) will be used to down-convert

from 1500 to 500 MHz, from which point the hardware will be identical to the fundamental system. A fully built-out RF straight is shown in Figure 4.6.8 below.

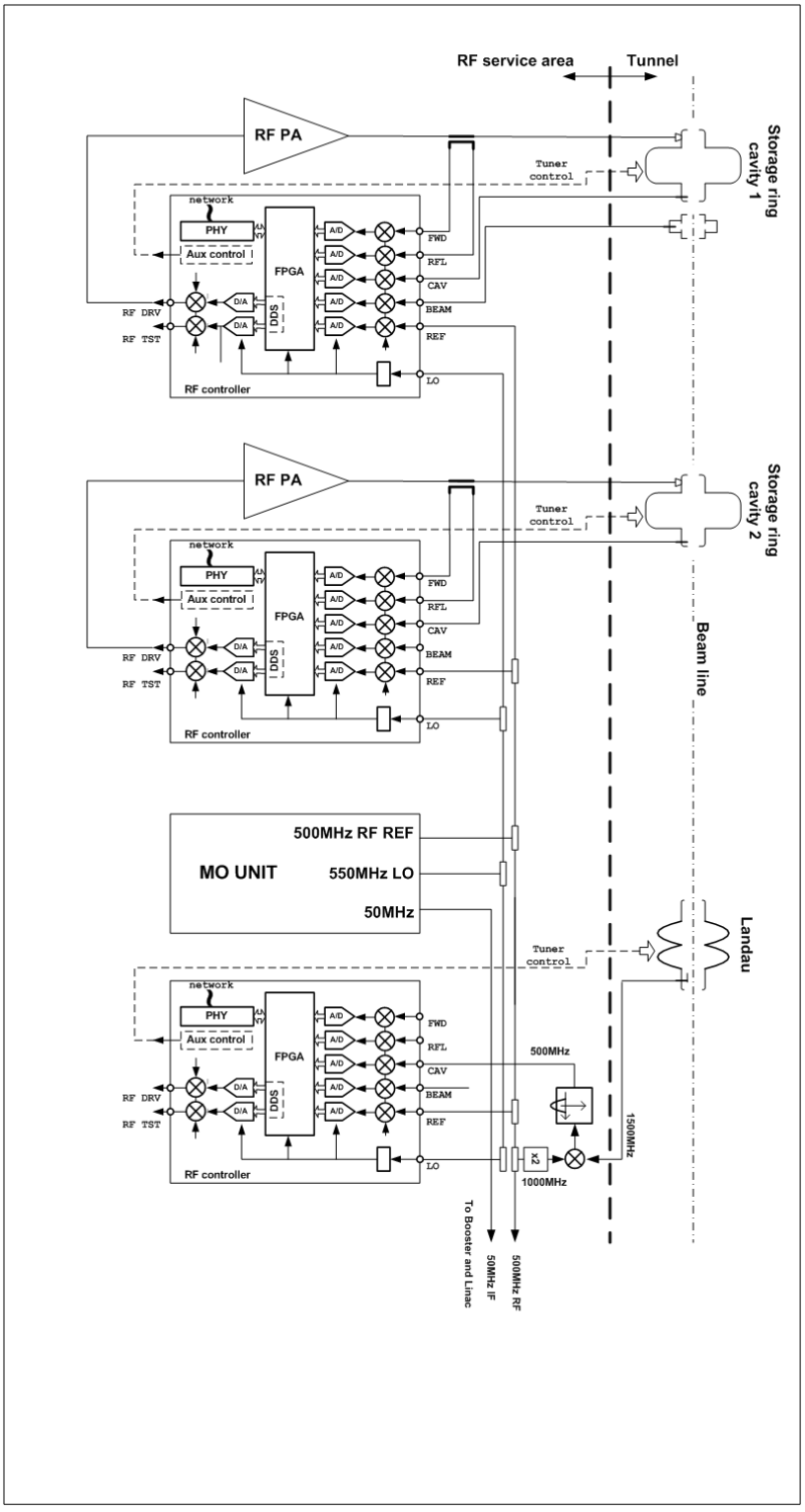

Figure 4.6.8 Storage ring system configuration.

The booster RF is very similar to the ring RF, with the exception that beam phase feedback is not expected to be included. Since the 500 MHz RF reference and the 50 MHz LO are distributed from point to point, the 550 MHz LO must be generated at the booster. It is shown in Figure 4.6.9. Identical up/down conversion from 50 MHz IF to 500 MHz RF will be used, as in the storage ring.

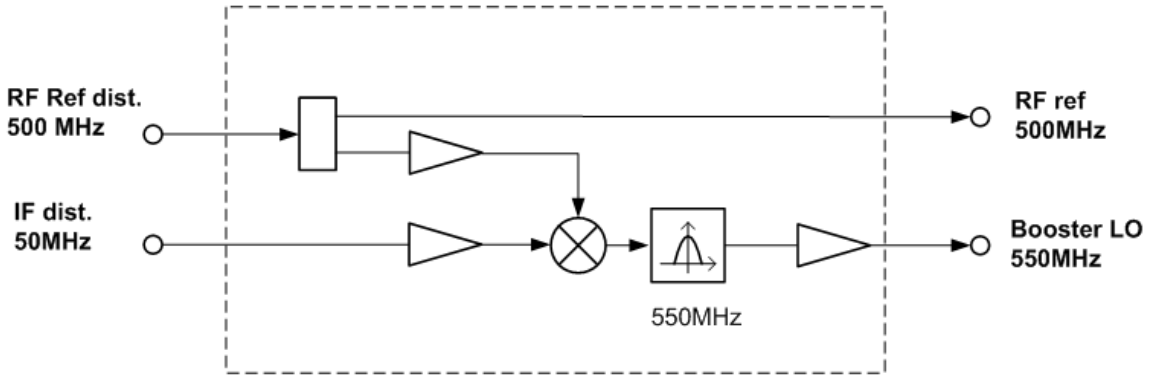

Figure 4.6.9 Booster LO generation.

The linac consists of a 500 MHz subharmonic buncher, a 3000 MHz pre-buncher with independent amplifier (and hence controller), and three klystron amplifiers. The first klystron output is split and drives a final buncher through a high-power attenuator/phase shifter and the first accelerating structure directly. The second and third klystrons drive their respective accelerating structures directly. Thus, one 500 MHz and four 3000 MHz systems need RF control. Again, to use identical RF cavity controllers the 3000,MHz signals are up/down-converted with a double conversion using 2500 MHz and 550 MHz LO frequencies. The LO generation is shown in Figure 4.6.10.

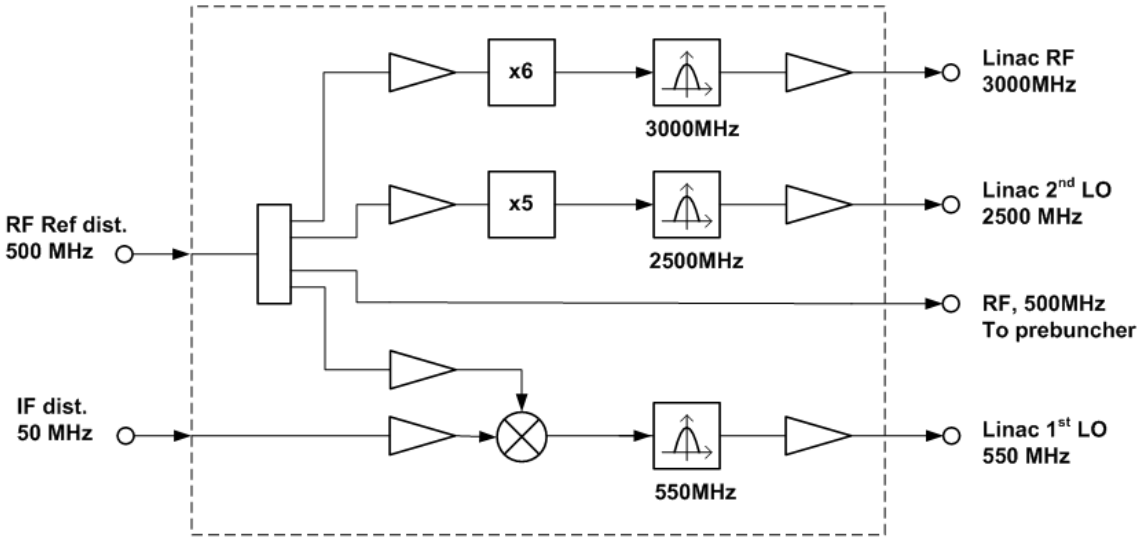

Figure 4.6.10 Frequency synthesis at the linac.

The controllers' 50 MHz IF frequency is first up-converted to 500 MHz using the 550 MHz LO, as in the 500 MHz systems. Then it is up-converted to 3000 MHz using the 2500 MHz LO. A system schematic is shown in Figure 4.6.11.

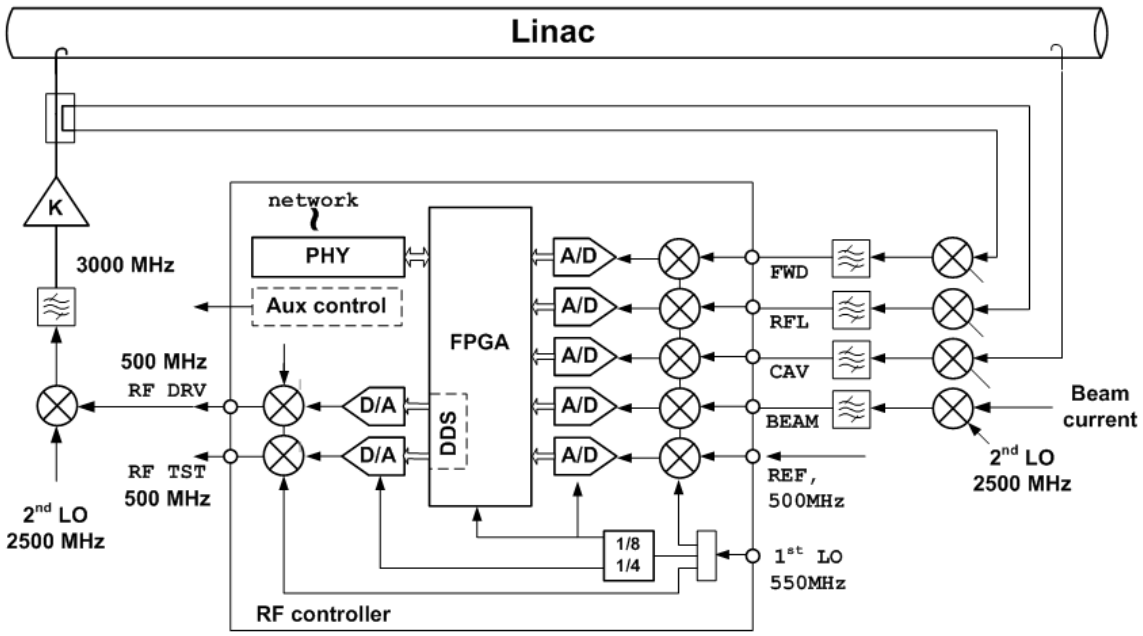

Figure 4.6.11 Linac up/down conversion and controller architecture.

References

[4.6.1] W. Brauns, www.gdfidl.de

[4.6.2] K. Halbach and R. F. Holsinger, "SUPERFISH - A Computer Program for Evaluation of RF Cavities with Cylindrical Symmetry," Particle Accelerators **7** (1976) 213-222.

[4.6.3] D. Myakishev, "CLANS2 - A Code for Calculation of Multipole Modes in Axisymmetric Cavities with Absorber Ferrites," Proceedings of the 1999 Particle Accelerator Conference, NYC.

[4.6.4] R. A. Rimmer et al., "An RF Cavity for the NLC Damping Rings," Proceedings of the 2001 Particle Accelerator Conference.

[4.6.5] S. Mitsunobu et al., "Status and Development of Superconducting Cavity for KEK-B," Proceedings of the 1997 Particle Accelerator Conference.

[4.6.6] J. Kirchgessner, Part. Accel. 46(1):151 1995.

[4.6.7] K.W. Robinson, CEAL-1010, Cambridge Electron Accelerator, Cambridge, MA (1964).

[4.6.8] Y. Miyahara et al., "Equilibrium Phase Instability in the Double RF System for Landau Damping," NIM A-260 (1987 p 518-528.

[4.6.9] R.A. Bosch et al., "Robinson Instabilities with a Higher-Harmonic Cavity," Phys Rev ST-AB **4**, p. 74401 (2001).

[4.6.10] M. de Jong et al., J. Microwave Power Electromagnetic Energy, **27**:136-142, 1992.

[4.6.11] M. Jensen et al., "First Results of the IOT Based 300 kW 500 MHz amplifier for the Diamond Light Source," PAC 2005, Knoxville, TN.

[4.6.12] F. Perez et al., "New Developments for the RF System of the ALBA Storage Ring," EPAC 2006, Edinburgh, Scotland.

[4.6.13] P. Marchand, et al., "High Power (35 kW and 190 kW) 352 MHz Solid State Amplifiers for the SOLEIL Synchrotron," PAC 2005, Knoxville, TN.

[4.6.14] Hanspeter Vogel, ACCEL. Private communication.

[4.6.15] M. Svandrlik, et al., "The Super-3HC Project: An Idle Superconducting Harmonic Cavity for Bunch Length Manipulation," EPAC 2000.

[4.6.16] S. Simrock, "Digital Low-Level RF Controls for the Future Superconducting Linear Colliders," PAC 2005, Knoxville, TN.

[4.6.17] C.W. Horrabin, and D.M. Dykes, "Diamond Low Power RF System," EPAC 96.

[4.6.18] J.M. Brennan et al., "RHIC RF beam control," EPAC-2001.

[4.6.19] M. Liepe, S. Belomestnykh, et al., "A New Digital Control System for CESR-C and the Cornell ERL," PAC 2003, Portland, OR.

[4.6.20] http://recycle.lbl.gov/llrf4/

4.7 Cryogenic Systems

4.7.1 Cryogenics System Overview

A helium closed-cycle cryogenic system is necessary to provide liquid helium to the Superconducting Radio Frequency (SRF) cavities. Baseline operation will require two 500 MHz (fundamental) and one double cell, 1500 MHz (harmonic) SRF modules which must be maintained at approximately 4.5K during operation of the storage ring. An identical configuration will be required for full operation at later date. Therefore, the cryogenic plant is sized versatile to accommodate sufficient cooling capacity for eventual full operation, four 500 MHz and two 1500 MHz SRF modules. The cryogenic system includes a refrigerator/liquefier cold box, a main compressor and a recovery compressor with oil removal systems, One LHe dewar, one valve box, liquid helium (LHe) and liquid nitrogen (LN2) transfer lines, gaseous helium (GHe) storage tanks, and a GHe management system, instrumentation, controls, and safety devices. Each 500 MHz and 1500 MHz module has 500L and 60L storage capacities, respectively, and runs with 400L and 50L He during operation.

4.7.2 Factors Influencing Cryogenic System Design

4.7.2.1 Single versus Multiple Refrigerators

The refrigeration system needs to have high reliability with near-zero unscheduled downtime. Using risk and failure analysis criteria, a study to determine the source of unavailability was undertaken in the past by the TESLA collaboration at DESY, with results shown in Table 4.7.1 in the order of their occurrence frequency.

Table 4.7.1. Rating of refrigerator system unavailability.

Rating	Topic	Example	Multiple Refrigerators
1	External Utility Failure	Electrical power, cooling water, instrument failure	No advantage
2	Blockage by frozen gas or impurities	Air and/or water vapor	Somewhat larger risk tolerance provided
3	Operational problems	Operators, controls, instrumentation,	Greater risk due to more system complexity
4	Single component failure not leading to total plant shutdown	Electrical motor burnout, compressor bearings, leaking oil pump seal, turbine bearing trouble	No advantage over component redundancy within a single refrigerator
5	Catastrophic component failure leading to plant shutdown	Loss of insulation vacuum, rupture of heat exchanger, oil spill into cold process piping	Would have a positive effect

The information in this table suggests that major downtimes are likely to occur as a result of catastrophic component failure; the effect of any of the other four occurrences is relatively negligible. Therefore, we selected a single refrigerator with a full inventory of spare critical components. Also, we will develop procedures that follow the manufacturer's recommended maintenance schedule.

4.7.2.2 Partial versus Full Loads

The reliability factor is increased by designing refrigerators that are capable of operating efficiently at partial load. When the accelerator is operated at reduced load, or when all modules are not in use, the electrical power and utility usage will be proportionally reduced. This could be achieved in two ways, operating the cold box (CB) without a LN2 pre-cooler during the baseline operation and by automatically

varying the speed of the compressor (and therefore mass flow rate of the main compressors) by incorporating a variable frequency driver (VFD) system.

4.7.2.3 With or Without Gas Purity Monitoring System

Gas impurities have an adverse effect on R/L efficiency. Air, for instance, solidifies at approximately 50K. Small solidified air particles can damage the expansion turbine, which runs at a high rotational speed; thus the concentration of impurities in the helium gas must be maintained at less than 10 ppm. The R/L internal dual 80K absorbers, coupled with a constant gas purity monitoring system, will serve as the main source of purification and as the feedback system. No external purifier has been considered, since a redundant internal adsorber with automatic reactivation and switch-over features is judged to be cost effective and the reliability is not compromised.

4.7.2.4 Heat Load Budget

There are two types of heat loads: static which come from thermal conduction and radiation, and dynamic which result from beam operation. The static heat loads of the SRF cavity cryostats are based on measured values of similar cryostats in other synchrotron facilities. The dynamic heat loads are calculated based on physics requirements. Heat loads associated with transfer lines, valve boxes, dewar losses, and other components are combination of estimated values based on information provided by vendors, engineering calculations, and professional judgment. Table 2 itemizes the estimated static and dynamic heat loads of the superconducting cavities and associated cryogenic components at 4.5K for both baseline and full operation.

The projected LN2 required by the R/L pre-cooler heat exchanger and other components heat shields is listed in Table 4.7.2 for both the initial and full system.

Table 4.7.2 Liquid nitrogen consumption estimates.

Component(s)	Per Cavity [L/hr]	Two Cavities + 1 Harmonic [L/hr]	Four Cavities + 2 Harmonic [L/hr]
500 MHz cavity	10	20	40
Harmonic cavities	10	10	20
Cold Box		23	45
RF valve box	_	12	24
Transfer lines (1 W/m), 50 m	-	2	4
Subtotal		67	133
Margin (20% of subtotal)		14	27
Total		81	160

The waveguides of each 500 MHz and 1500 MHz cavity require 0.134 g/s and 0.174 g/s of cold helium for cooling, respectively (Table 4.7.3). These are the liquefaction load to the R/L, and are equivalent to 4 L/hr and 5.2 L/hr of liquid helium. Therefore the liquefaction loads for the baseline and full operation are 13.2 L/hr and 26.5, L/hr, respectively.

Table 4.7.3 Heat loads budget and refrigeration sizing.

Cryo-Plant Heat Load Baseline Budget	Per Cavity	2 Cav. + 1 harm	4 Cav. + 2 harm
		(Baseline)	(Full Operation)
Number of Harmonic 1500MHz RF (X)	1	1.00	2
Number of 500MHz RF (Y)	1	2.00	4
Total Number (Z)	1	3.00	6
500MHZ Cavity Operation		3.3MV/2	5MV/4
Q (*10^9)		0.75	0.75
Background Heat Load			
Cavity beamtubes (RBT + FBT)*Y	13.8	27.60	55.2
Cavity Waveguide (conduction)*X	5.3	10.60	21.2
Waveguide cooling (0.134 g/s)*X	13.4	26.80	53.6
Cavity Rad. LN2 to Lhe (No MLI)*X	8.1	16.20	32.4
Harmonic (17.0W + 0.171 g/s)*Y	34.1	34.10	68.2
40, 80m Xfer Lines *(0.2W/m)*	*8.0*	*8.00*	*16.0*
2*1.6*Y*5m Xfer Line *(1.6W/m)*	*16.0*	*48.00*	*96.0*
Dewar Loss (static, Dynamic)	5.0	10.00	10.0
(Z*5W) SRF Valve Box; He only	5	15.00	30
Background TOTAL	108.7	196.30	382.6
150% background TOTAL	163.1	294.50	573.9
Dynamic Heat Leak			
V^2/(89*Qo), 10^9)		81.60	93.6
Harmonic Cavity	*22.0*	*22.00*	*44.0*
TOTAL	22	103.60	137.6
150% TOTAL	33	155.40	206.4
Standby/CD, Beam-off Load, W	108.7	196.30	382.6
Margin, 900 W R/L OP. W	791.3	703.70	517.4
Margin, 900 W R/L OP. Percent (%)	728.0	358.50	135.2
Available Liquefaction, LPH	197.8	175.90	129.4
Recover 400 Litters, Hours	2.0	2.30	3.1
Standby/CD, 150% Beam-off Load, W	163.1	294.50	573.9
Margin, 900 W R/L OP. W	737.0	605.60	326.1
Margin, 900 W R/L OP. Percent (%)	452.0	205.70	56.8
Available Liquefaction, LPH	184.2	151.40	81.5
Recover 400 Litters, Hours	2.2	2.70	4.2
Beam-on Grand Total Load, W	130.7	299.90	520.2
Margin, 900 W R/L OP. W	769.3	600.10	379.8
Margin, 900 W R/L OP. Persent (%)	588.6	200.10	73.0
Available Liquefaction, LPH	192.3	150.00	95.0
Recover 400 Litters, Hours	2.1	2.70	4.2
Beam-on, 150% Grand Total Load, W	196.1	449.90	780.3
Margin, 900 W R/L OP. W	704.0	450.20	119.7
Margin, 900 W R/L OP. Persent (%)	78.2	50.00	13.3
Available Liquefaction, LPH	176.0	112.50	29.9
Recover 400 Litters, Hours	2.3	3.60	13.4
100% Refrigeration, W	900.0		
100% Liguefaction, g/s (Linde)	7.5		
100% Liquefaction, 1ph (Linde)	225.0		

4.7.4 Design Approach

The main storage ring RF systems will initially consist of two 500 MHz (fundamental) cavities and one 1500 MHz (harmonic) Superconducting RF cavity. The cryogenic system must operate continuously for at least a full year before scheduled downtime. The design goal, therefore, was to provide a highly reliable and stable cryogenic system supported with required monitoring, alarms, interlocks, safety devices, and control system. As the cryogenic system must supply LHe to all of the RF cavities, redundancy of vulnerable components was considered, to ensure that continuous operations can be maintained effectively.

Total refrigeration cooling requirements were based on two sets of operating conditions: an initial baseline, and eventual full operations. Note that the cooling requirements for the full operation condition is approximately doubled compared with the baseline, since identical static loads are the dominant factor (Table 4.7.2). Therefore, the cryogenic system must minimally provide refrigeration power of 299.9W during baseline operation and 520.2W for the eventual full operating conditions. The Refrigerator–Liquefier (R/L) is oversized (150% margin) to enhance reliability and account for contingencies on additional heat loads that may develop during detail design.

The SCRF modules are planned to be situated in two neighboring straight sections of the storage ring, 50 m apart in two groups of three SRF cavities: two 500 MHz fundamental cavities and one 1500 Mhz harmonic cavity.

The SRF cryogenic system General Arrangement (GA) shown in Figure 4.7.1 depicts the full operating condition with capability to run at baseline. The design approach is primarily based on commercial helium R/L CB, main and recovery compressors, Variable Frequency Drivers, oil removals, helium dewars, and gas management systems. The design of the transfer lines, warm pipes, valve box, and control system will be defined during detailed system design.

General Arrangement considerations define distribution lines of equal length, locating the source LHe dewar at the approximate center of the 50 m (i.e., 25 m laterally from each module group). The distribution/return lines are listed in Table 4.7.4.

Table 4.7.4 Distribution of Source/Return Lines

Lines Description	Source/Return
Liquid Helium, 4.4K saturated	LHe dewar
Helium Vapor Return	Cold Box
Liquid Nitrogen, saturated at 25 psig	Phase Separator
Cool-down/Recovery:	
Warm-up, power failure	Cold Box or Ambient Vapr
W Pump and Purge, utility vacuum	Utility Vacuum System
LP Warm Return, e.g., vapor cooled	Compressor Suction
Nitrogen exhaust, vents to atmosphere	Valve Box Vent

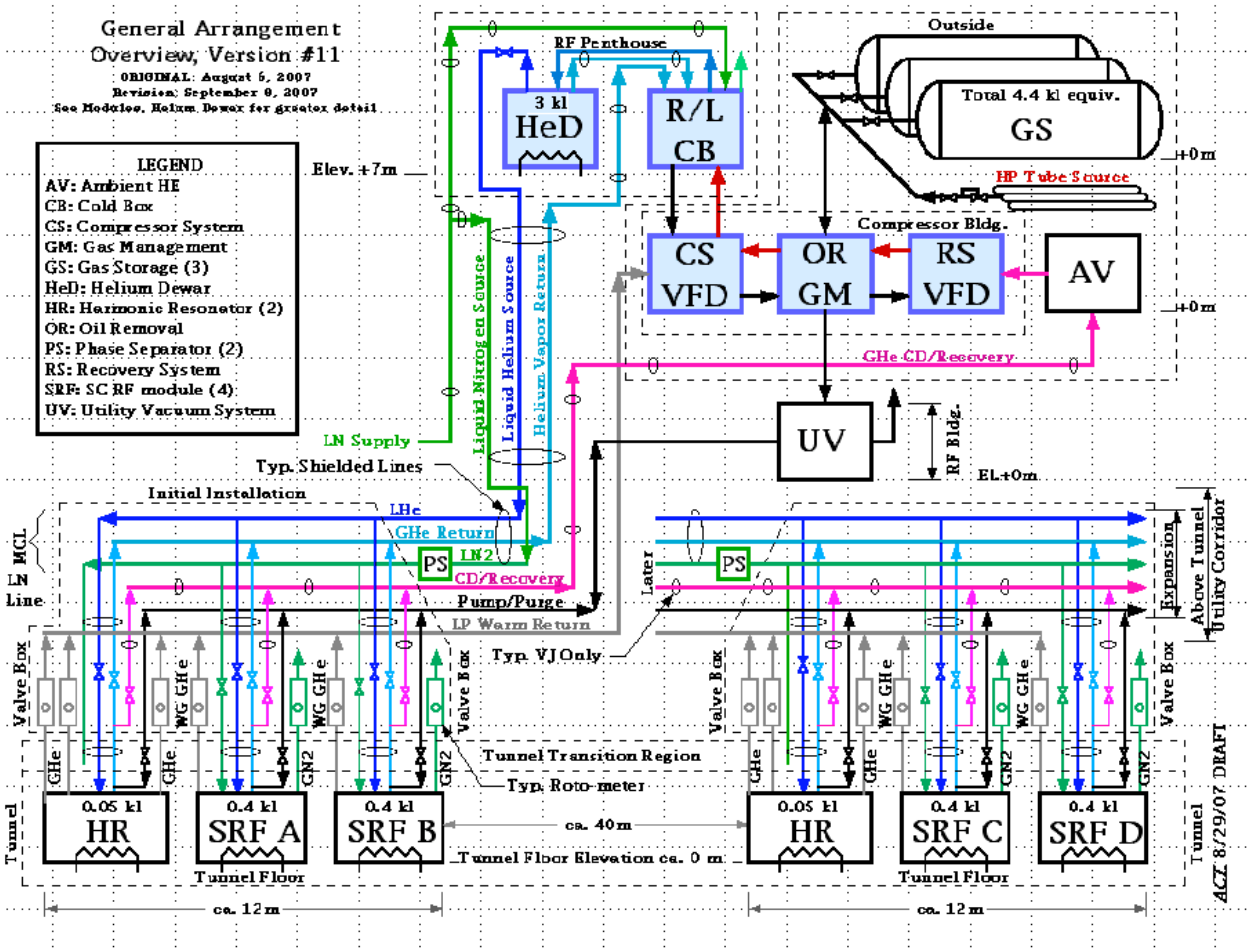

Figure 4.7.1 SRF Cryogenic, General Arrangement (GA)

Lines a, b, and c are arranged so the liquid nitrogen flow radiation-shields the He lines, and all are contained in a common insulating vacuum jacket. The CESR creators of this arrangement have dubbed this configuration, as implemented with VCR and Conflat fittings at the ends of each section, the Multi-Channel Line (MCL).

The Cool-down and Recovery line, d, provides for temporary flows and may be efficiently provided as a standard, standalone, and relatively inexpensive vacuum-jacketed transfer line commonly used for liquid nitrogen. The recovery flows (loss of power, rapid warm-up), are diverted from the cold box to an ambient vaporizer (which may be augmented with an electrical heater for extreme cold weather conditions) to assure that the recovery compressor suction stays sufficiently warm.

The Pump and Purge line, e, will be sized for efficient pumping speed with the specified Utility Vacuum System pumping speed. The Utility Vacuum System vacuum pump will be, for line size considerations and costs, located in the RF building near the tunnel straight section middle.

The Low Pressure (LP) return line, f, collects and returns GHe from the waveguide and other warm-return flows to the compressor suction.

The cryostats' LN2 shield is vented to the outside tunnel with a gaseous nitrogen exit temperature sensor and a modest flow control.

Isolation and removal of a warmed module from an otherwise cold system in standby situation will requires absolutely tight shutoff valves and the necessary procedures to verify their tightness. The safe

installation and operation procedure will be developed during detail design. However, clearly, all of the Valve Box valves will be normally in closed position, i.e., “fails closed” in the event of loss of signal or power. The operation of all essential components (such as control valve signals) will be hooked to the emergency power system in case of main power failure. Full descriptions of each subsystem are given in the following sections.

4.7.5 SRF Modules, System Layout

The two 500 MHz (fundamental) and one double-cell 1500 MHz (harmonic) SRF modules will occupy a single straight section. A designated space in the adjacent long straight section is planned for identical configuration for the fully built-out machine. These two neighboring straight sections are near the linac and the control room.

The cold box and the LHe dewar is planned to be located in a mezzanine deliberately placed almost at equal distance from each straight section. The valve box(es) will be located on the tunnel’s roof, connected to the LHe via MCL and the modules via single VJ lines.

The compressor room, gas management buffer tanks, and LN2 dewar will be in a area detached from the main building to isolate induced vibration and noise.

Another room adjacent to the cryogenic and power supply rooms is planned for testing SRF modules prior to installation, for troubleshooting, and for R&D purposes.

Currently, four rooms are dedicated to the RF power supplies and cryogenic systems. These rooms will be adjacent to the RF straight sections, minimizing the waveguide length and heat load from the helium transfer lines between the cryogenic room and SRF modules. Two power supply rooms are directly adjacent to each RF straight section. The cryogenic room houses the refrigerator, LHe dewar, inter-connecting transfer lines, multi-channel distributing manifolds, and local control system. The adjacent RF test room is dedicated for pre-installation testing and R&D purposes.

4.7.6 Refrigerator-Liquefier (R/L) Cold Box

For long term reliability with minimum maintenance, commercial R/L with gas bearing turbines will be used. Furthermore, the R/L shall be capable of operating over a large range of loads as required by the project. Comprehensive interaction with the potential vendors during this design stage has been conducted to insure best match between the system performance and operation requirements. The Linde LR280 R/L, shown in Figure 4.7.2, together with a variable frequency driven compressor (ESD441), is found to meet the present application and is used for illustration. Other potential vendors also have R/Ls of very similar characteristics.

As shown in Table 4.7.2, the expected heat load is 520 W for eventual full operation, to run four 500MHz and two 1,500MHz cavities simultaneously (with a 1.5 safety factor, the load could be 780 W). Thus, a 900W refrigerator is considered the best commercially available R/L system. For baseline operation, the expected heat load is 300 W (450 W with a 1.5 safety factor). The 900W refrigerator must be turned down to 450 W during baseline operation and to preferably to as low as 300 W in order to minimize operating costs. The excess refrigeration that can’t be turned down must be “burned” by a heater added to the LHe dewar to provide an artificial load; this is admittedly an inefficient solution.

Figure 4.7.2. Typical R/L cold box.

The Linde LR280/ESD441 is a 900W cooler at 4.4K, with three-turbines whose refrigeration can be turned down to 640 W by turning off the LN2, and by another 50% to 320 W by the use of a Variable Frequency Drive (VFD). The capacity curve for refrigeration vs. liquefaction is given in Figure 4.7.3. That almost meets the refrigeration requirements outlined above and seems an acceptable refrigeration turndown solution. However, a serious consideration has been made for the liquefaction component of the load, and especially in any case without LN2 (elaborated below). Note that the large, single R/L system solution is the most cost effective of all those considered, provided that it can demonstrate a successful (operational and cost effective) turndown capability.

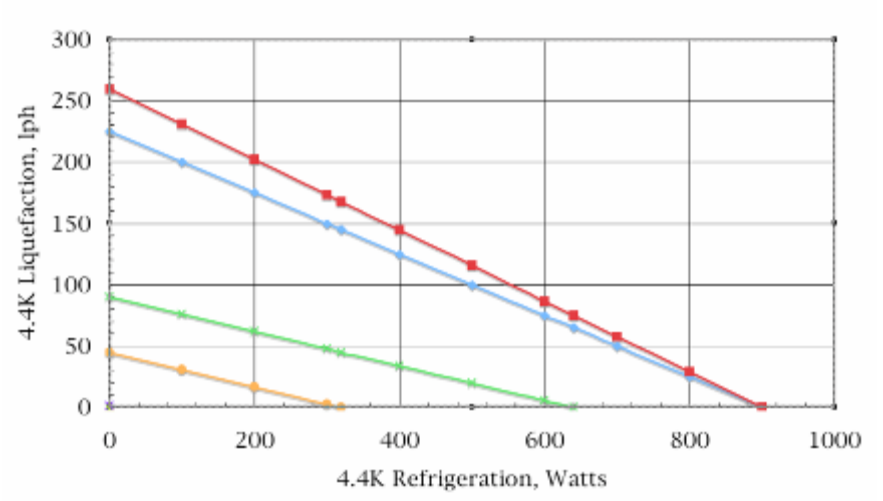

Figure 4.7.3 Liquefaction vs. refrigeration for LR280.

Red represents R/L with LN2 and assumed 100 W/g/s.

Blue represents R/L with LN2 and supplied data by Linde.

Green represents R/L without LN2 and data supplied by Linde.

Orange represents R/L without LN2 at 50% VFD, estimated by Linde.

4.7.6.1 Special Turndown Consideration

The turndown refrigeration capability of the R/L is very desirable in the current application to efficiently address the initial half-system operation. Unfortunately, a major turndown mechanism, the removal of the LN2, seriously cripples the liquefaction capability in the face of a small yet substantial liquefaction load. That means that the sum of the liquefaction loads presented to the R/L operating without LN2 is a far greater burden than that operating with LN2.

A possible solution of modulating (load tracks) of the LN2 pre-cooling with the load for turndown (rather than just turn it "off"), will be examined during the detailed design. The first order approach to modulated LN2 cooling would be to leave the LN2 "on" while turning the VFD down. the 900W unit should be able to turn down to ~450 W (VFD to 50% speed/flow) in that way. A similar VFD turndown to 40% (assuming it is possible to turn down from 60 Hz to 24 Hz) speed/flow might get close to 360 W. At the 360W level, the excess refrigeration available in the half-system will be quite small in full operation, and the excess power costs too small to be of concern.

4.7.6.2 Main Compressor System

All potential suppliers of the R/L use an oil screw compressor manufactured by Kaeser (Figure 4.7.4). Two ESD441 type compressors (one as hot standby) will provide the required 80 g/s flow at 15 bar absolute for the 900W R/L. The compressor skid consists of a bulk oil separator, a gas cooler, two stages of coalescers, an adsorber, and an oil cooler. The oil cooler is used to cool oil from the bulk oil separator for re-injection to the compressor.

Each compressor will be equipped with a Variable Frequency Driver (VFD), housed in an external cabinet. The drive motor of the compressor package is capable of varying speed between 20 Hz to 60 Hz (corresponding to one-third to full flow).

The screw compressors are low-vibration machines that normally do not require massive foundations. Vibration dampers, however, will be identified and implemented at the time of installation. All compressors will be housed in a separate building away from the main building to eliminate any possible vibration transmittal.

4.7.6.3 Recovery Compressor System

A smaller screw compressor, 12 g/s mass flow, will be used to pump boil-off helium to storage tanks in case of a power failure. This recovery compressor is to be equipped with uninterrupted power supply and automatically start. This compressor will have same pressure characteristics as the main compressor. The start time of emergency power will be about 20 s, to avoid the difficulty of starting at high suction pressure.

Figure 4.7.4 Typical Kaeser helium compressor.

4.7.7 Liquid Helium Dewar

The LHe dewar is the repository of the stored LHe heat of vaporization and concurrently the cooling source for the LHe cooled loads. Most of the R/L load is a refrigeration load; the condensed liquid is evaporated at the load and the returned cold vapor is utilized to create new liquid in a continuous R/L loop. A small portion of the R/L load, the waveguide heat intercept of the 500 MHz cavities and all the beam tube conduction and radiation cooling of the 1500 MHz cavities are in liquefaction loads (i.e., LHe is evaporated, warmed to room temperature and returned directly to the compressor suction).

The He dewar capacity has been set at 3,000 liters to 1) contain liquid inventory needed at any one time; 2) store liquid for limited period deficit (loads larger than the available refrigeration of rapid filling) operations; and 3) as a repository for recondensed and accumulated liquid in anticipation of its protracted, excessive, use. Helium operating inventory is 400 liters per SCRF CESR-B and an assumed 50 liters per Harmonic Resonator module, for a total of 1,600+2(50) = 1,700 L. An operating storage level of 500 to 1,000 L would provide the space for a 3,000L dewar to recover the entire cavity inventory as liquid (desirable in a short-term scenario), with a margin for the significant mass of saturated He vapor in a mostly empty dewar. See Table 4.7.4 for the system inventory.

Table 4.7.4 Helium system inventory.

Nominal inventory, liquid helium (liters equiv.)	250 psig ASME gas storage	3,000 liter 1% LHe dewar	4+2 cryostats cap. = 1.7 kl	HP Source, standby trailer
Warm	>3,500	0	0	$\geq$1,200
Standby	1,000	2,500	0	$\geq$1,200
Operate	1,000	800	1,700	$\geq$1,200
Shutdown	>3,500	0	0	$\geq$1,200

The He dewar will be specified as a required part of the R/L vendor supply to include the R/L connecting lines, an auxiliary inlet/outlet(s) (for feeding the dewar from an external source, should this be necessary), the dewar's heat leak rate, heaters, and instrumentation and control system. See Figure 4.7.5 for a schematic of a LHe dewar.

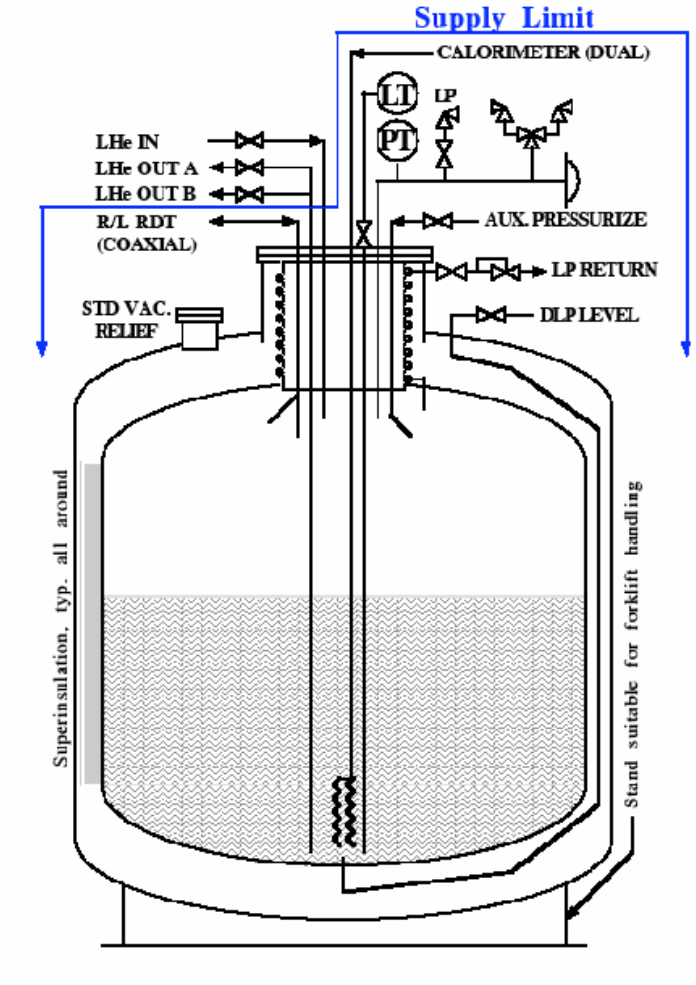

Figure 4.7.5 Schematic of the LHe dewar.

4.7.8 Liquid Nitrogen Dewar

A 10,000-gal LN2 dewar will supply LN2 to the SRF cryogenic plant. This dewar will be filled from the facility's LN2 storage tank via a vacuum-jacketed line with automatic fill control system. A LN2 Phase Separator will assure a single-phase flow to the SRF module at a constant pre-set pressure to support steady SCRF module shield and intercept cooling flows. The single phase and isothermal cooling at a constant (phase separator regulator controlled) pressure will contribute to predictable and reliable module liquid nitrogen cooling performance.

4.7.9 Gaseous Helium Storage Tanks

The warm gas storage water volume of about 6,250 scf (46,875 gal) will be sufficient to provide storage for an equivalent of 3,500 LHe to 14 bar pressure. Two 30,000 or three 20,000-gal tanks will have sufficient volume with room to spare. The total capacity of either these options is 14*60k/7.5/25 = 4,480 liquid liters equivalent.

These tanks will be designed for an internal pressure of 20 bar and external pressure of 1 bar. The maximum operating pressure is about 15 bar and the minimum operating pressure is estimated at 2 bar. The design specifications will include all appropriate ASME Boiler and Pressure Vessel Codes, Section VIII,

Divisions I (Unfired Pressure Vessels) and IX (Welding and Brazing Qualification), and Safety Relief Valves. Material and other geometric features will be detailed before purchasing.

One 30,000-scf HP gas trailer (capacity ~1,200 liquid liter equivalent) can serve as a continuous warm (no maintenance) standby storage.

4.7.10 Gas Management

Helium inventory in the refrigeration system is automatically adjusted by the gas management system as the refrigeration/ liquefaction load changes. The gas management system will consist of typically two control valves. One valve automatically sends excess helium to the buffers (for example, during quenches or warm-ups) One valve adds helium to the system from the buffer tank when the liquefaction capacity is higher than flow recovered from loads.

These two valves work in concert with the bypass recycle valve, which automatically recycles excess flow from compressor discharge to suction. These two valves maintains proper amount of helium in the system according to variation in liquefaction or refrigeration rate of the R/L. A frequency driver will reduce the total cycle mass flow rate in case of excess flow from the compressors.

Pressure transmitters and indicators with analog or digital output will be installed on both the discharge and suction lines near the main compressors. Similar transmitters will be installed near the suction side of the distribution valves boxes. Safety relief valves shall be installed in both the suction and discharge line of the compressor.

Sufficient instrumentation ports with shut-off valves will be placed on both the discharge and suction lines in the compressor room and also on the high-pressure line near the refrigerators/liquefiers. The makeup/recovery control valves will be in the compressor room. Several other smaller ports will be located on both the discharge and suction lines of the compressors and oil removals for gauges, sensors, and gas sampling purposes.

4.7.10.1 Vacuum-Jacketed (VJ) Liquid Helium Transfer Lines

Single Channel Line (SCL) and Multi-Channel Lines (MCL) vacuum-jacketed cryogenic transfer lines will be used to transfer liquid or cold GHe among various components such as to/from the main LHe dewar, SRF distribution valve box, and SRF modules. These vacuum-jacketed lines will be constructed of high-quality seamless stainless steel tubing. The lines and mating connections will have minimum heat leak and will resist damage from thermal expansion and contraction.. The use of copper tubing to carry LN2 for cooling radiation shields will be permitted, provided the design conforms to all applicable codes.

In addition to combined pump-out/burst ports, the line will have pressure and temperature transmitters with digital or analog output signals for monitoring and interlock purposes.

4.7.10.2 Vacuum-Jacketed Liquid Nitrogen Transfer Lines

Different sizes of the LN2 transfer lines will require transferring appropriate flow rate among inter-connecting components. The fill line between the outside main LN2 tank and the SRF LN2 dewar located near cryogenic plant will be vacuum jacketed (reduce the cool-down consumption and added enhance safety) capable of handling large flow rate of 400 L/hr at 4 bar head pressure. The interconnecting lines between the SRF LN2 dewar and cryogenic equipment (L/R, valve box, LHe transfer lines, heat shields, SRF modules) will be designed as rigid and flexible lines with heat leak to be less than 0.5 W/m at 80K (exclusive of valves

and bayonets). The insulating vacuum space of the lines will take into account the relative humidity factor, dew point, and seasonal temperature variations to ensure it is condensation free at all times.

Suitable keep-full valves will be installed along the fixed lines to ensure single-phase liquid flow to designated components when pressure stability is essential (e.g., SRF modules). An insertion of a LN2 phase separator before the SRF modules will insure pressure stability requirements of cavities. Similar to LHe transfer lines, these lines will also have pressure and temperature transmitters with digital or analog output signals for monitoring and interlock.

4.7.10.3 Warm Piping

In addition to vacuum jacketed lines, there are three sets of piping for warm helium:

- One suction line to transfer low-pressure helium gas from SRF modules (waveguides), valve boxes, to compressor's suction.
- one discharge line to transfer high-pressure helium gas from the main/recovery compressors to oil removals, and to either the refrigerators/liquefiers cold box or gaseous storage tanks
- one makeup/recovery line between suction/discharge of the compressors and GHe storage tanks.

These lines will be sized and designed according to the flow rate, allowable pressure drop and operating pressure and temperature conditions. Seamless Stainless Steel tubing/pipes, 304 or 304 L, will be used and constructed in conformance with all applicable codes.

4.7.10.4 Power Failure Considerations

Cryogenic systems are susceptible to damage from abrupt power losses. Loss of electrical power could cause an unexpected system shutdown which would require continuous operation of the recovery compressor to recover generated boiled-off GHe to the helium storage tanks. The recovery compressor, main helium dewars, cryogenic distribution valve box, and the cryogenic electronics of the SRF modules require a sufficient source of emergency power, as does the Oxygen Deficiency Monitoring systems, which must have an Uninterruptible Power Supply (UPS) system. A 50 KW emergency power generator is dedicated to the cryogenic system.

The demands of He inventory recovery in the case of a protracted (greater than 10 minutes) power failure is shown in Table 4.7.5.

Table 4.7.5 He inventory recovery demand during protracted (>10 min.) power failure.

LHe, Cool Time	Units	500 MHz	1500 MHz	LHe dewar
Operating Volume	Liters	400	50	800
Quant. LHe liters	Liters	1600	100	800
HOV Available	Joules	3.65E+06	2.28E+05	1.82E+06
Unit LHe Load	Watts	40.6	34.1	5.0
LHe Load, total	Watts	162.4	68.2	5
Self Cooled	Hours	6.24	0.93	101.33

4.7.10.5 Ambient Vaporizer

Power outages are most likely to create the largest recovery flow rates. An Ambient Vaporizer (AV), capable of handling ~288 l/h (~10 g/s) cold GHe flow to warm-up the temperatures for safe operation of the compressors will be used.

4.7.10.6 Valve Boxes

Two valve boxes are eventually required for full operation condition. One located near each RF straight sector location. One MCL (two total) will transfer both LHe and LN2 to each of the two VB(s) (one for the baseline condition). Individual transfer lines, most likely flexible type, will be provided between each VB and the individual SRF modules.

A tentative 15 valve-arrangement package in a horizontal rectangular enclosure is shown in Figure 4.7.6. A total of 12 valves, three LHe feeds, three GHe returns, three helium cool-downs, and three LN2s is required per GA at this stage.

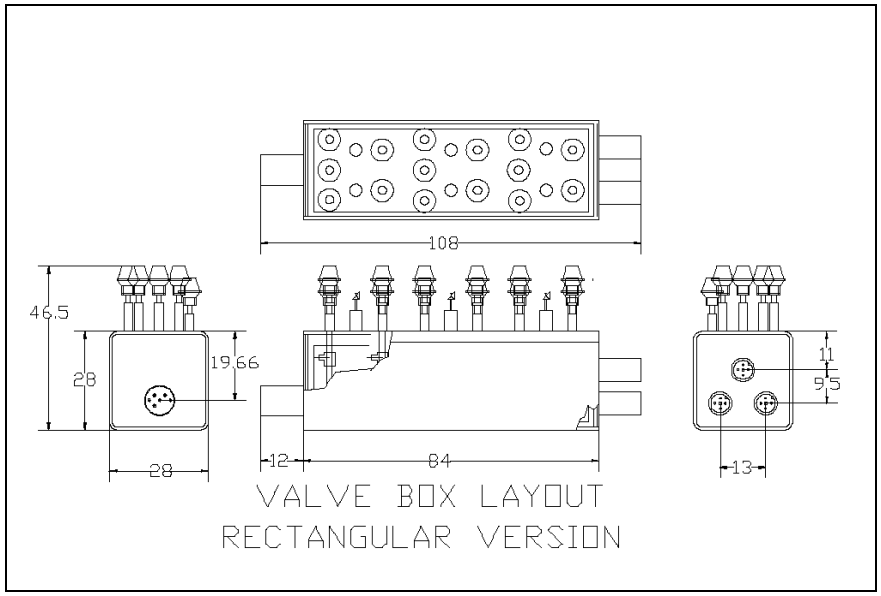

Figure 4.7.6 Tentative valve box arrangements.

4.7.10.7 Operating Modes

Process provisions for the complete installation/operation cycle must support the SCRF module operating modes as follows:

1. Independent Module Connection
2. Independent Pressure Test and Leak Check
3. Independent Pump and purge
4. Independent Liquid Nitrogen Cool-down
5. Independent Liquid Helium Cool-down and Fill
6. Independently Establish Readiness for Stable Operation
7. Independent Isolation and/or Warm up

4.7.10.8 Independent Module Connection

Although the SCRF modules have common feed and return manifolds, their inline isolation valves within the valve box (fully closed and secured) can create a complete isolation from all other modules. All transfer lines between the modules and the valve box will have separate vacuum with mating bayonets for installation.

4.7.10.9 Pressure Test and Leak Check

Each module upon complete connection shall be pressure tested and leak checked for safe operation. Only when these operations are successfully accomplished can a module considered ready for pump and purge.

4.7.10.10 Pump and Purge

Each module shall be pumped and purged to strict criteria to protect the system from impurities. System contamination can dramatically undermine and/or preclude the designed performance of an otherwise reliable system.

4.7.10.11 Liquid Nitrogen Cool-down (To about 200K)

The LHe cool-down is accomplished by activating the module's liquid nitrogen shield and intercept flows. The radiation shield isolates, and the intercepts reduce, the conduction to the He temperature cold mass from the ambient world, providing cooling. After ~48 hours (in the case of routine CESR operation of a similar system), the module can be cooled to 200K by this arrangement. The cooling progress slows dramatically below 200K. That temperature value is the suggested benchmark to initiate the second and final stage He cool-down to 4K. Finally, the module is filled with liquid helium and the operating level is established and continuously maintained in automatic mode.

4.7.10.12 Liquid Helium Cool-down to 4.5K and Fill

The standard cool-down procedure accumulates liquid using the available liquefaction capacity and then consumes the liquid heat of vaporization and sensible heat (where appropriate) to cool the load. If the cool-down rate consumes liquid at a rate greater than liquid can be produced by the R/L, the main compressor pumps the excess mass to warm gas storage for later liquefaction. To put the issue in quantitative terms, the excess consumption over liquefaction could easily reach as high as 200 L/h, or about 6.7 g/sec, well within the recovery compressor's capability.

The recovery compressor can be seen to connect to provide cool-down and recovery directly via the CD/Recovery line and an ambient vaporizer outside of the gray dotted lines, as shown in the Figure 4.7.7 block diagram.

If the recovery compressor is to do a lot of standby or variable flow pumping it should be fitted with a VFD that simply reduces the RPM whenever the bypass valve opens and increases the RPM when it is closed. Supervisory logic can decide when it is useful to turn it on and off outside of the hard-wired power failure recovery function.

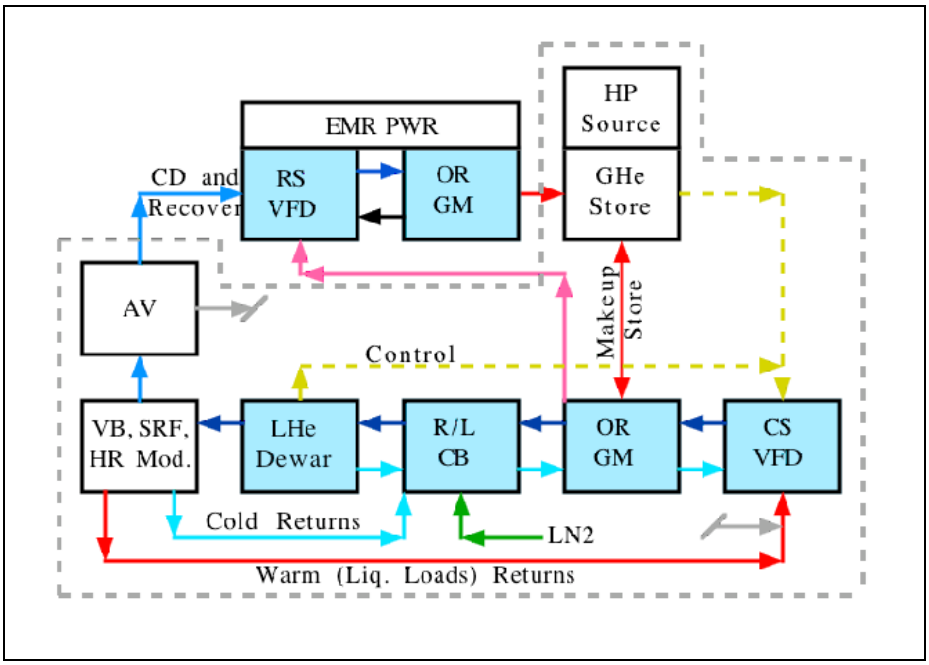

Figure 4.7.7 Compressors and gas management block diagram.

4.7.11 Establish Readiness for Stable Operation

Upon completion of cool-down to 4.5 K, each module is filled with 400 L of liquid helium or 80% of total volumetric capacity. The helium vessel's pressure, temperature and liquid level will be maintained at operating values and controlled by the local control system with monitoring and set-points accessible from the EPICS accelerator control system. The system is ready for operation when all pre-set parameters have been met and all safety interlocks are fully operational.

4.7.11.1 Independent Isolation and/or Warm up

300 K main SRF modules warm-up

This process isolates and warms-up the main SRF modules to ambient temperature, while the Main Cryogenic plant is cold. The liquid helium of the main SRF modules will boil-off by using cryostats DC (within 3 hrs) and recovered to the cold return line via the cryogenic distribution valve box and R/L cold box back to the compressor suction and gaseous helium tanks. The warm-up may include the cryogenic distribution valve box and main modules feed lines.

10-20 K main SRF modules warm-up

The main SRF modules is warmed in the same manner as the 300K warm-up, but only up to 10K to get rid of the magnetic flux trapping in the superconducting state by warming the niobium bulk cavity temperature higher than its critical temperature or up to 20K for RF window conditioning. The liquid nitrogen in the radiation shield flows continuously.

300 K Main Cryogenic Plan and main SRF modules warm-up

The main SRF module and Main Cryogenic Plant are both warmed to room temperature. The LHe dewar will, in general, continue to store liquid helium, but may be warmed as well.

300 K Main Cryogenic Plan awarm-up, cold main SRF modules

The Main Cryogenic Plant may be quickly warmed and then colled down to operating temperature again while the main SRF module is kept cold by liquid transfer from the liquid helium dewar.

4.7.12 Equipment Elevations

A study of He System Head vs. Location for locating the R/L,d LHe dewar and the valve box either at floor level or elevated to the tunnel roof was conducted, with results shown in Table 4.7.6.

Table 4.6.7 Various Equipment Location options.

Item/Case	Cold Box	LHe dewar	Valve Box	SRF Cryostat
Case A	HB Floor	HB Floor	HB Floor	Beam
Case B	HB Floor	HB Floor	Tunnel Roof	Beam
Case C	Tunnel Roof	Tunnel Roof	Tunnel Roof	Beam
Case D	Penthouse	Penthouse	Tunnel Roof	Beam

In the first case, A, the equipment is located on the High Bay (HB) floor. The second case, B, puts only the valve box on the tunnel roof. The third case, C, puts the cold box and the He dewar on the tunnel roof along with the valve box. The last case, D, puts the cold box and the LHe dewar on the penthouse level and keeps the valve box on the tunnel roof.

The cold box and LHe dewar can be at an elevated level, centralized between two straight sections, to provide a large (in LHe terms) LHe dewar liquid head (Figure 4.7.8). The elevated location allows gravity to help transfer LHe from the dewar to the valve box and cryostat below, without the need to significantly pressurize the dewar, as would otherwise be required.

The valve boxes will be located on the tunnel roof directly above each straight section joined to the LHe dewar independently, by independent MCL(s).

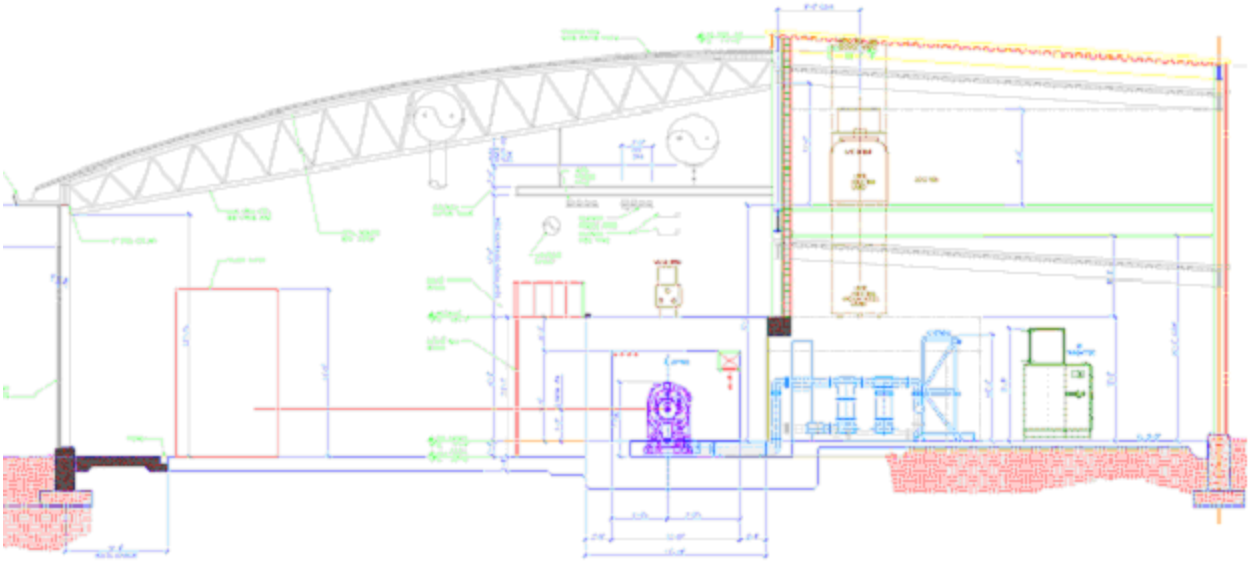

Figure 4.7.8. SRF Cryogenic system, elevation view.

The He dewar system head vs. different locations possibilities are tabulated in Figure 4.7.9. As a case in point, the dewar liquid head (see last entry in the first data column) of 1.531 psi is reduced by the cryostat liquid head (see the last entry in the cryostat column) of 0.240 psi, to provide the dewar-to-cryostat head of 1.291 psi. This is a respectable and constant LHe transfer pressure difference. Consequently, the R/L, LHe dewar, and valve box are planned to be on an elevated mezzanine with (sufficient overhead clearance), due to the highly technical advantage that case D represents. An alternative to this elevated equipment arrangement is to use a subcooler for stable LHe transfer throughout the system.

NSLS-II He System Head vs. Locations

Reference	Units	Dewar L	Dewar G	Cold Box	Cold Box	Valve Box	Cryostat
Helium		4.424K	4.424	313K GHe	300K GHe	4.424K	4.424K
Pressure		1.2	1.2	1.05 atm	13 atm	1.2	1.2
Density	g/cc	0.12080	0.02053	0.00016	0.00210	0.12080	0.12080
Density	kg/m^3	120.800	20.530	0.164	2.101	120.800	120.800
Normalized		738.665	125.536	1.000	12.847	738.665	738.665
Location		HB Flr	HB Flr	HB Flr	HB Flr	HB Flr	Beam
Service El.	m	1.500	1.500	2.600	2.600	1.500	1.397
Ref. Head	kg/m^2	181.200	30.795	0.425	5.463	181.200	168.758
Ref. Head	psi	0.257	0.044	0.001	0.008	0.257	0.240
Location		HB Flr	HB Flr	HB Flr	HB Flr	Roof	Beam
Service El.	m	1.500	1.500	2.600	2.600	5.640	1.397
Ref. Head	kg/m^2	181.200	30.795	0.425	5.463	681.337	168.758
Ref. Head	psi	0.257	0.044	0.001	0.008	0.968	0.240
		Tunnel	Tunnel	Tunnel	Tunnel	Tunnel	Beam
Location		Roof	Roof	Roof	Roof	Roof	Tunnel
Service El.	m	5.640	5.640	6.740	6.740	5.640	1.397
Ref. Head	kg/m^2	681.337	115.793	1.102	14.161	681.337	168.758
Ref. Head	psi	0.968	0.165	0.002	0.020	0.968	0.240
		Pent	Pent	Pent	Pent	Tunnel	Beam
Location		House	House	House	House	Roof	Tunnel
Service El.	m	8.917	8.917	10.017	10.017	5.640	1.397
Ref. Head	kg/m^2	1077.151	183.062	1.638	21.045	681.337	168.758
Ref. Head	psi	1.531	0.260	0.002	0.030	0.968	0.240

Figure 4.7.7. Helium system head vs different locations.

4.7.13 Instrumentation and Control

The functional analysis, consisting of the startup, shutdown, and regular and exceptional operating modes of the refrigerator will be written by the cryogenics engineer and then translated into the PLC logic for control of the refrigerator. This PLC must communicate with the PLCs embedded in the cold box, compressor, and cryo-module systems. In addition, there must be a seamless integration with the EPICS control system, allowing full control, monitoring, and history logging.

4.7.13.1 Oxygen Deficiency Hazard Monitoring and Control System

Oxygen Deficiency Hazards are present when atmospheric oxygen content falls below 19.5% by volume. The BNL Standard Based Management System has strict guidelines in compliance with the Occupational Safety and Health Administration Respiratory Protection Standard 29CRF1910.134, Table 4.7.8.

The main potential sources of reduced oxygen are from unplanned discharge of cryogens into confined spaces. Liquefied gases such as helium and nitrogen have the potential to cause ODH conditions, since expanded gases can displace air rapidly when released to the atmosphere.

For NSLS-II, a complete ODH analysis is required for each area (tunnel, cryogenic room, and compressor room), for all possible scenarios, in order to plan and put appropriate controls and measures in place. For the purpose of this report, an ODH classification of 1 is assumed, which among several requirements mandates the implementation of personal oxygen monitoring systems.

Table 4.7.8. ODH Control Measures.

	ODH Class				
Environmental Controls	**0**	**1**	**2**	**3**	**4**
1. Warning signs	■	■	■	■	■
2. Ventilation			■	■	■
3. ODH-Qualified Personnel Controls					
4. Medical approval as ODH-qualified		■	■	■	■
5. ODH training	■	■	■	■	■
6. Personal oxygen monitor		■	■	■	■
7. Self-rescue supplied atmosphere respirator		■	■	■	
8. Multiple personnel in communication			■		
9. Unexposed observer				■	■
10. Self-contained breathing apparatus					■

Gas monitoring systems, such as Safe T Net 410 (up to four channels), have been considered for installation in each area. These microprocessor-based controllers are designed to accept up to four combustible oxygen transmitters. Features include digital readout display, LED alarm indication, 4 to 20 mA output, individual low and high alarm, and relay signals for interlock purposes.

4.7.14 Preventive Maintenance Programs

The overall availability of the cryogenic system is defined as the ratio of the actual delivery time to the scheduled operating time. Synchrotron light source facilities are normally operated continuously, 24 hours per day, seven days a week, excluding short studies or maintenance periods and one or two extended periods of machine maintenance per year when the facility is shut down for preventative maintenance, upgrades, and repairs. This is necessary to decrease the number of unscheduled breakdowns. Routine preventive maintenance must therefore be conducted according to the manufacturers'

4.8 Beam Scrapers and Photon Absorbers

4.8.1 Beam Scrapers

Two pairs of electron beam scrapers will be used for accelerator physics measurements of the aperture and beam lifetime limits. The thickness must be ~$5X_o$ (radiation lengths) for the electron beam. The horizontal blades must be in the same plane and adjustable from full open (vacuum chamber width) to the chamber centerline with a resolution of ~1 μm and a reproducibility of ~5 μm. One location for the horizontal scrapers is in one of the dispersion regions next to the BPM and the SF2 sextupole, where there is high β_x and dispersion. The second location for horizontal scrapers is in the SID between the QL2 and SL2 sextupoles, the maximum β_x for the ring. The two vertical scrapers will be placed near the high β_y in the dispersion region (drift space at $\Delta\mu_y \sim\pi/2$ from the injection septum) and the LID (drift space at $\Delta\mu_y \sim 2\pi$ from the injection septum). These scrapers will provide controlled physical apertures to prevent large-amplitude particles (from the injector) from hitting the small-gap undulators, later in the ring. The scrapers will also provide defined apertures for understanding the dynamic aperture and lifetime in the ring.

4.8.1.1 Preliminary Design

To maximize their effectiveness as well as to simplify their engineering design, the two pairs of beam scrapers required will actually consist of four separate units: two horizontal and two vertical scrapers. These scrapers will serve as protective devices for the IDs. They will also be used as diagnostic tools during the commissioning phase and during machine studies.

Previous reports [4.8.1] have indicated that Touschek scattering is the dominant source of ID damage. Work done at APS has shown that scrapers should be located in a low-emittance lattice to effectively protect the IDs. This suggests that the horizontal scrapers should be installed where there is adequate dispersion at the scrapers as well as a large horizontal beta function. Touschek scattering presumably not only imparts a large energy deviation, but also induces large betatron oscillations for the scattered particles. A significant concern, however, is that the scrapers may compromise injection efficiency—or worst yet, may even produce more ID damage if the injected beam hits the scrapers, creating a shower that propagates to the IDs. To address this concern, we will carefully study the development work done at APS.

All four units planned for NSLS-II will share the same engineering design and be built identically—the horizontal and vertical scrapers differing only in the final mounting and installation. Each unit will have two jaws or blades that can move independently from one another, each being driven by precisely controlled stepping motors. The blades will be made of Glidcop, a dispersion-strengthened copper with excellent thermal and electrical properties at elevated temperatures. Each of the blade assemblies will have a water-cooling circuit to minimize thermal expansion of the blades when they are hit by the dipole radiation fan.

Furthermore, to minimize impedance problems, the shape of the blades will be determined by detailed numerical simulation. These studies are still in progress and the results are preliminary. Figures 4.8.1 and 4.8.2 show two views of the design of an existing scraper at APS. The NSLS-II scraper design will be based on this APS design, with appropriate modifications to match the chamber geometry. Figure 4.8.3 shows a preliminary layout of the possible NSLS-II scraper.

Each scraper unit will be mounted directly on the vacuum chamber and the adjustable blades can be repositioned remotely. Once they are in the desired position, however, they must stay in place within the required tolerance.

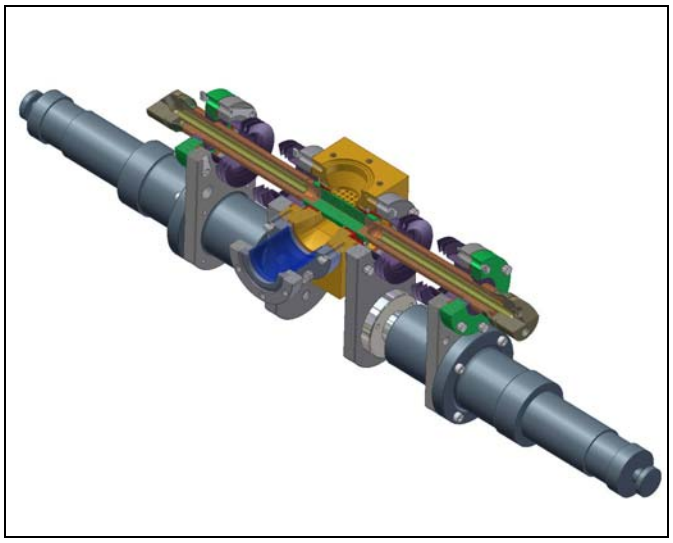

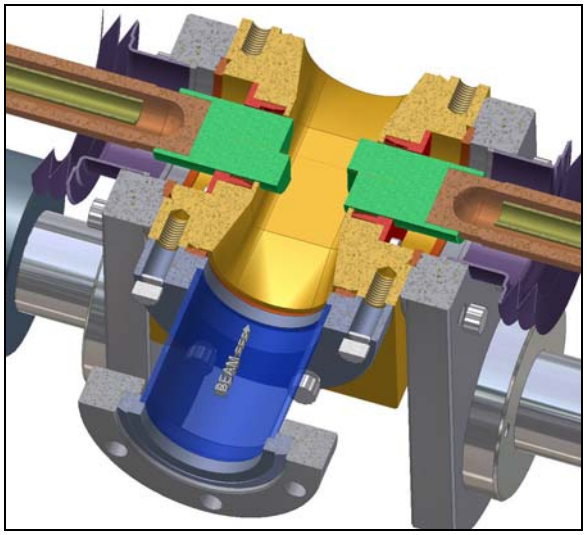

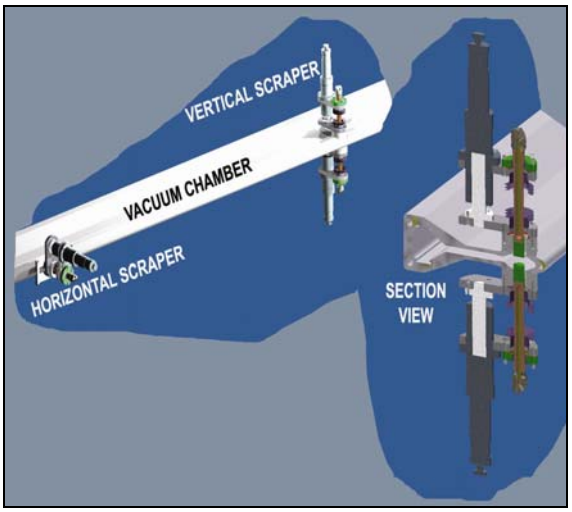

Figure 4.8.1 (top left) Sectional view of APS scraper assembly, round blades (closed).

Figure 4.8.2 (top right) Sectional view of APS scraper assembly, blades partially opened.

Figure 4.8.3 (right) Preliminary layout of NSLS-II scraper (two views)

4.8.2 Photon Absorbers

Discrete photon absorbers will be installed in the vacuum chambers to protect their uncooled surfaces from the radiation fans of the bending magnets and IDs. Shielding the vacuum chambers from radiation fans also minimizes their thermal distortions and leads to better thermal stability of the BPMs attached to the chambers. To protect the chambers from exposure to unintentional beam deviations, BPM interlocks at insertion devices will be set at ± 0.25 mrad [4.8.2]. The positional error budgets consisting of orbit error, mechanical, and survey tolerances will be set at ±2 mm.

The peak power densities of the bending magnets, damping wigglers, and the in-vacuum undulators (IVU) are 0.088 kW/mrad^2, 55.30 kW/mrad^2, and 62.33 kW/mrad^2, respectively, for a 500 mA beam at 3 GeV. The power density of the BM is uniform in its horizontal fan of 104.7 mrad (6º) except at the edges. For the DW and IVU devices, the vertical and the horizontal power density profiles are shown in Figure 4.8.4 and Figure 4.8.5 respectively.

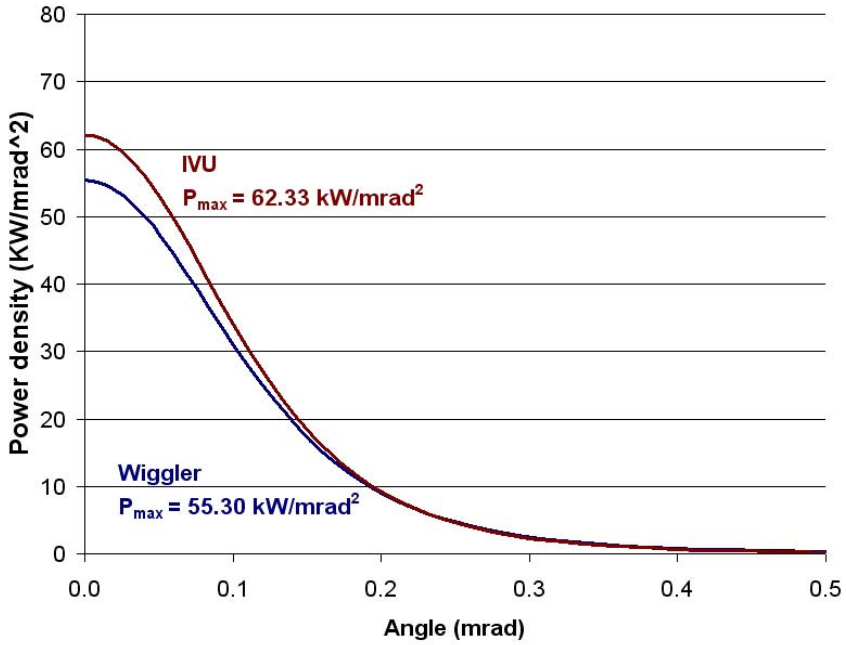

Figure 4.8.4 Vertical power density profiles, P/P_{max}, of damping wiggler and IVU. P_{max} is obtained at 500 mA beam current.

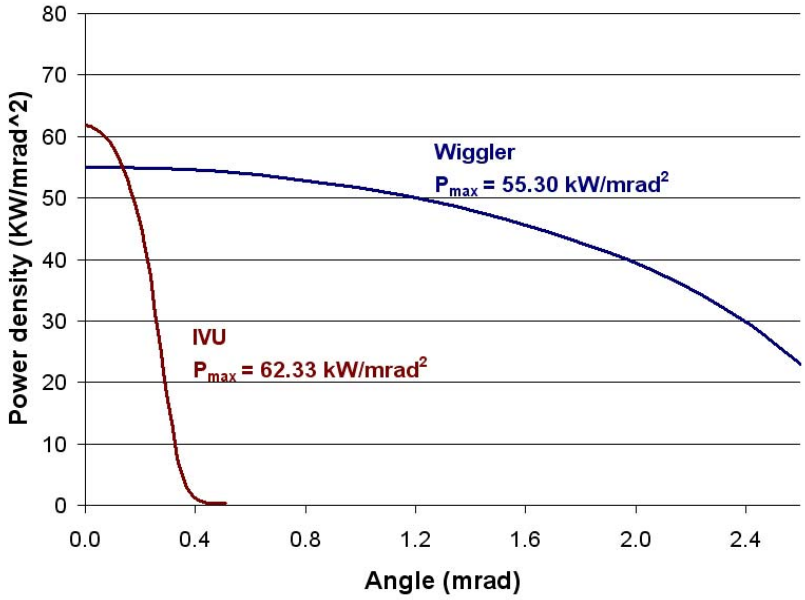

Figure 4.8.5 Horizontal power density profile, P/P_{max} for damping wiggler and IVU.

The IVU radiation fan is narrow in both directions and can be extracted with adequate clearance through the 76 mm (H) × 25 mm (V) apertures of the straight vacuum chamber in Section 2 and the 15 mm slot of the dipole chamber in Section 3. The BM and DW radiation fans in at the downstream end of Section 3 dipole chamber, however, require clipping by two absorbers, namely, a crotch absorber and a wiggler absorber (see Figure 4.8.6). Because of the high power density of the DW radiation, these absorbers clip the outer edges of the DW horizontal fan just enough to allow the clipped fan to be extracted to the front end.

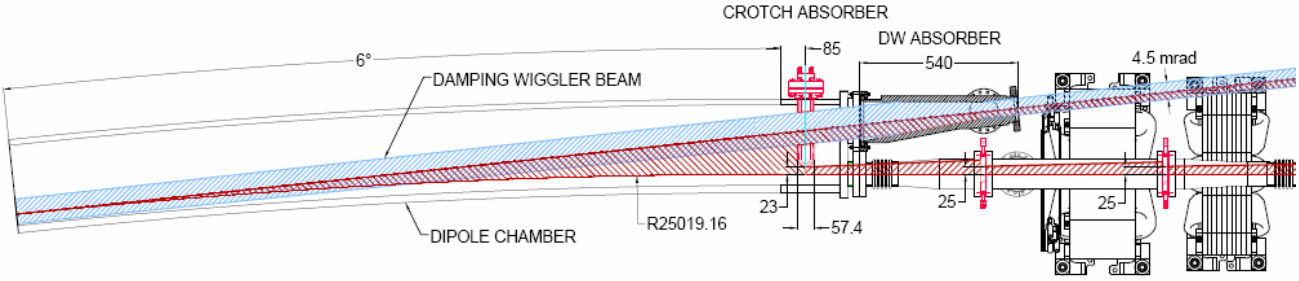

Figure 4.8.6 Clipping of BM and DW x-ray fans by crotch and wiggler absorbers in at the downstream end of the Section 3 dipole chamber. The BM radiation fan (blue color) partially overlaps the DW radiation fan (red color).

4.8.2.1 Preliminary Designs of Photon Absorbers

Figure 4.8.7a shows a 3D model of the crotch absorber inside the vacuum chamber. The absorber is made from a Glidcop® block with brazed water-cooling channels of OFHC copper. Also brazed to the Glidcop block are a stainless-steel flange and a water manifold. A rectangular slot in the center of this block allows DW or IVU radiation fans to pass through without interception.. The crotch absorber is inserted into the downstream aperture of the dipole vacuum chamber in Section 3 such that its nose tip is 5 mm inside the aperture (i.e., 30 mm outboard from the center of the aperture). The tip intercepts a total of 840 W of beam power with a maximum power density of 12 W/mm^2. A thermal analysis of the crotch absorber was carried out using ANSYS software. The results, plotted in Figure 4.8.7.b, show a peak temperature of 200ºC, which is lower than the maximum allowable temperature of 400ºC for Glidcop.

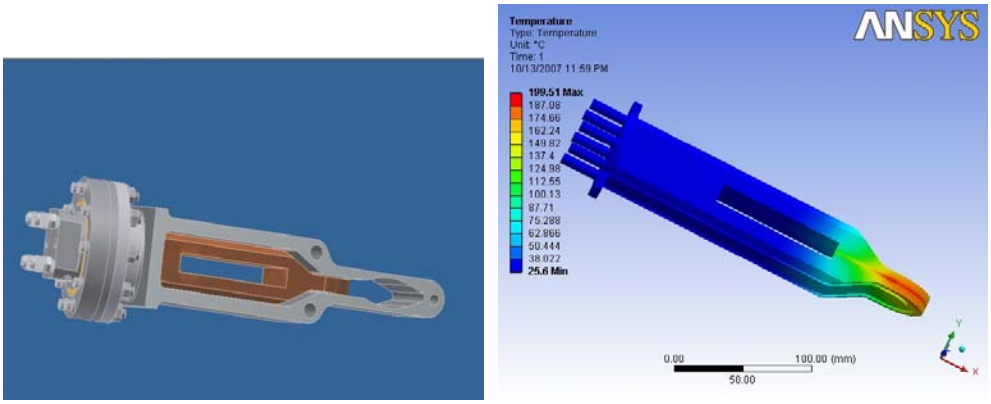

Figure 4.8.7 Crotch absorber. **a**) a 3-D section inside the vacuum chamber. **b**) temperature contours from an ANSYS FE analysis with a peak temperature of 200ºC.

The damping wiggler absorber, shown in Figure 4.8.8a, fits in the ~ 600 mm space between Section 3 and 4 on the outboard side. The upstream end of the absorber is brazed to a flange that mates with the flange of the chamber in Section 3. The downstream end is cantilevered inside a bellows assembly to allow for thermal expansions of the chambers during bakeout. Two water cooling channels are provided on each vertical side of the Glidcop block to absorb power from the outer extents (0.35x2 mrad) of the horizontal DW x-ray fan (5.2

mrad) at a grazing incidence of 6º. The total power intercepted by the two vertical sides is 4 kW, with a peak power density of 22 W/mm^2.

An ANSYS FE thermal analysis of the wiggler absorber predicted a peak surface temperature of 214ºC. The temperature profile, plotted in Figure 4.8.7b, shows high temperatures directly under the beam footprint.

Assuming a water flow of 2 GPM in each of the cooling channels, the average bulk water temperature rise will be 5.5ºC.

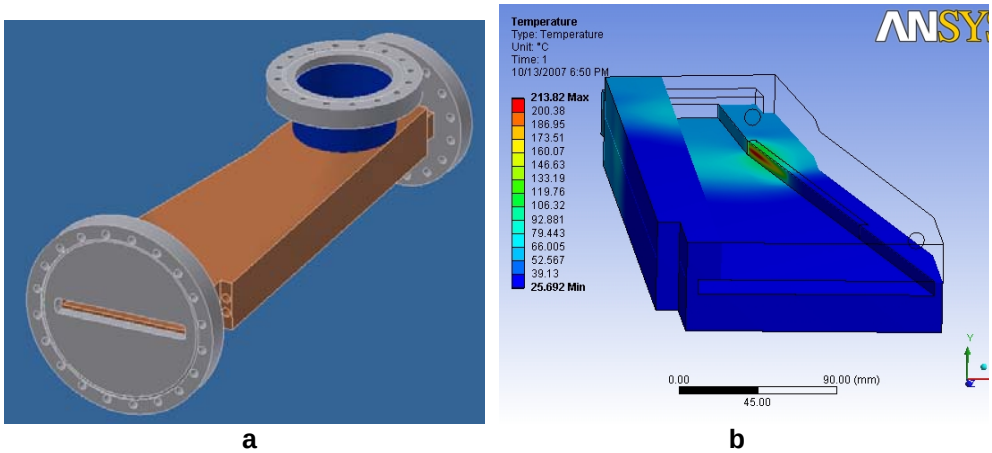

Figure 4.8.8 Damping wiggler absorber. **a**) 3D model showing Glidcop block and flanges. **b**) Temperature contours from an ANSYS FE analysis with a peak temperature of 214ºC.

Another crotch absorber will be used in Section 5 with a slot width that will allow the user-specified width of the dipole radiation fan to exit to the front end. Additionally, counter-flow and flange absorbers (Figure 4.8.9) will be used in Sections 2, 4, and 6 to intercept unused dipole radiation fans.

Figure 4.8.9 Counter-flow and flange absorbers for the storage ring vacuum chambers.

References

[4.8.1] Borland, M. "ID Protection with Fast-Moving Scrapers," OAG-TN-2004-050, November 11, 2004.

[4.8.2] V. Ravindranath, S. Sharma, B. Rusthoven, M Gosz, L. Zhang, and J. Biasci, "Thermal Fatigue Life Prediction of Al-15," proceedings, MEDSI-2006 Workshop, SPring-8, Himeji, Japan, May 24-26, 2006.

4.9 Storage Ring Diagnostics and Instrumentation

4.9.1 Introduction

State-of-the-art advanced diagnostics and instrumentation systems are required for a smooth and rapid commissioning and for productive and successful operation of the NSLS-II storage ring. This section provides a list of the monitored parameters, technical solutions with some alternative variants, and the required specifications to achieve these goals. Table 4.9.1 shows a summary of these various instrumentation components.

Table 4.9.1 Beam Diagnostics and Instrumentation for Storage Ring.

Monitor	Quantity	Function
4-button pick-ups	188	Beam position, dispersion, response matrix, turn-by-turn dynamics
Photon BPMs	1 per installed undulator	Photon beam position
DC current transformer	1	Beam current, lifetime
Emittance monitor	1	Transverse emittances
Fast current transformer	1	Filling pattern, beam current
Transverse feedback system	1	Suppress beam instabilities, tune monitoring
Pinhole camera	1	Transverse beam size, energy spread
Optical ports for visible radiation	2	To provide light for streak camera, FireWire camera, fill pattern and beam current
Streak-camera	1	Bunch length, beam dynamics
FireWire camera	1	Transverse beam characteristics
Fluorescent screen	1	Injection position, profile
RF-drive stripline and amplifier	1	Betatron tune
Beam oscillations monitor	1	Frequency components of longitudinal and transverse beam motion
P-i-n diodes loss monitors	60	Beam loss pattern
Scintillator loss monitors	10	Beam loss
X and Y beam scrapers	2	Machine studies, halo
Diagnostics undulator	1	Energy spread, beam divergence, momentum compaction factor

As a basic policy, whenever possible, we will pursue the utilization of commercial off-the-shelf devices to reduce cost as well to achieve better reliability. Most of the existing diagnostics equipment today already satisfies the basic requirements for NSLS-II and only a few, if any, need further development.

Full utilization of the micron-size electron beam requires sub-micron resolution of the orbit monitoring system, to provide the required position stability. Priority consideration will be given at the earliest stages of design to provide instruments for the detection and remedy of factors that affect beam quality.

4.9.2 Physics Design and Parameters

The following beam parameters will be monitored during regular operations:

- closed orbit (accuracy better than 10% of beam size)
- working point (tune for both planes with 10^{-4} resolution)
- circulating current (0.1% accuracy) and beam lifetime (1% accuracy)
- injection efficiency
- filling pattern (1% of maximal bunch charge)
- emittance for both planes (10% relative accuracy)

- energy spread
- individual bunch length (2 psec resolution)
- position of the photon beam for the insertion devices
- coherent bunch instabilities
- distribution of beam losses around the ring

During beam studies the following parameters will be measured:

- linear optics, including β-functions (1% accuracy) and betatron phase advance ($2\pi \times 10^{-3}$ or better)
- dispersion for both planes (1 mm accuracy)
- chromaticity for both planes (with accuracy 0.1
- coupling (0.05% absolute accuracy)
- momentum compaction (1% relative accuracy)
- beam-based alignment of quadrupoles and sextupoles (30 microns or better)
- synchrotron frequency
- RF system parameters (cavity voltages and phasing)
- vacuum chamber impedances

4.9.3 Intercepting Diagnostics

A fluorescent screen in the injection straight will provide information on the shape and position of the injected beam and will assure proper matching of the beam optics. It is included in the baseline design. The screen will have two positions. The first position will be used to observe the incoming beam from the booster. In the second position, a special hole will allow the injected beam to enter the storage ring, and the beam shape will be observed after one turn. The screen material will be cerium-doped yttrium aluminum garnet (YAG:Ce), which has excellent resolution (about 30 μm) and radiation stability [4.9.1]. The estimated horizontal beam size coming from the booster is $\sigma_x = 360$ μm, and vertical size for 10% coupling is $\sigma_y = 95$ μm. If the spatial resolution of the YAG:Ce flag is found to be inadequate, then optical transition radiation can be used.

To avoid impedance problems, the screen assembly will be designed to ensure a smooth vacuum chamber wall when the screen is fully retracted. Spring-loaded RF-fingers will be used to provide electrical contact in order to avoid trapped modes for the wake fields. A typical screen assembly used at APS is shown in Figure 4.9.1, and the RF fingers are shown in Figure 4.9.2. To use this design we will need only to modify the vacuum chamber aperture to match the NSLS-II geometry.

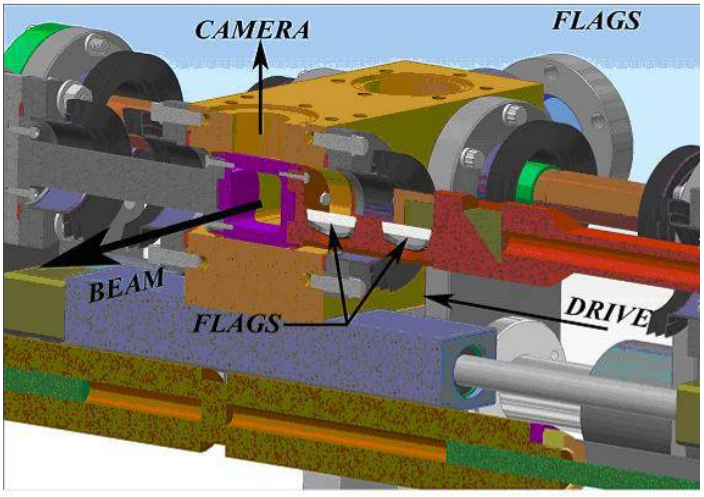

Figure 4.9.1 Design of the screen used for the diagnostic of the electron beam injected into the storage ring at APS. We will modify the vacuum chamber aperture to match the NSLS-II geometry.

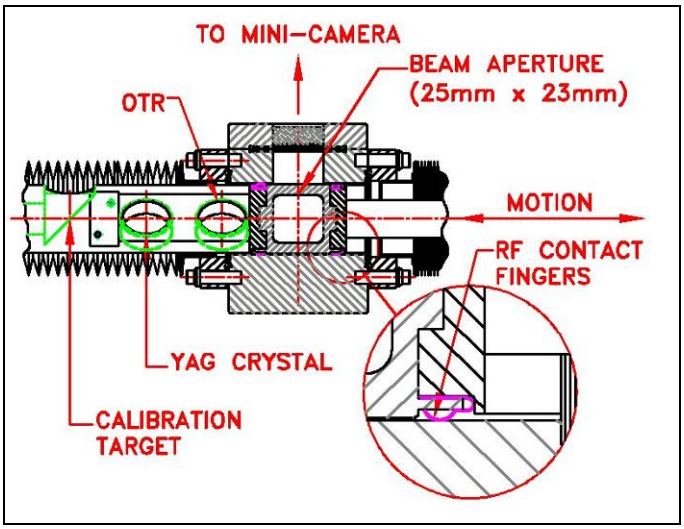

Figure 4.9.2 Spring-loaded RF fingers (see detail) provide smoothness in the vacuum chamber. Electrical contact avoids trapped modes for the wake fields.

4.9.4 Circulating Current

4.9.4.1 Filling Pattern Measurement

To maintain uniform fill and to mitigate dependence of the BPM receivers on the filling pattern, a fast current transformer (FCT), included in the baseline design, will provide electrical signal proportional to the charge of individual bunches. Figure 4.9.3 shows a typical FCT that can be directly mounted on the beam chamber with a ceramic break. FCT-WB-082-20:1 model by Bergoz has 1.75 GHz bandwidth with a 200 psec rise time [4.9.2]. The FCT will be placed over a ceramic break and provided with RF-shielded housing. Fast ADC sampling of the voltage with 500 MHz on the top of each pulse will make charge distribution available to the control system. The information obtained will be used in the top-off algorithm. The signal from the FCT can be used as input for the top-off safety interlock, based on the monitoring of circulating current. Summing found charges for all bunches will provide an alternative means for measuring total beam current.

Figure 4.9.3 Bergoz Fast Current Transformer.

4.9.4.2 Measurement of Circulating Current

A DC current transformer will monitor the stored current in the baseline design. The Bergoz New Parametric Current Transformer (NPCT) is the latest evolution of the Unser transformer [4.9.2], commonly known as DCCT, developed at CERN in 1966 by Klaus B. Unser. It is shown in Figure 4.9.4.

NPCT has large dynamic range and high bandwidth, making it a versatile device for measuring lifetime and injection efficiency. It is insensitive to a synchrotron revolution frequency and bunch fill pattern, with residual modulator ripple being eliminated, thus enabling full bandwidth operation down to a very low current.

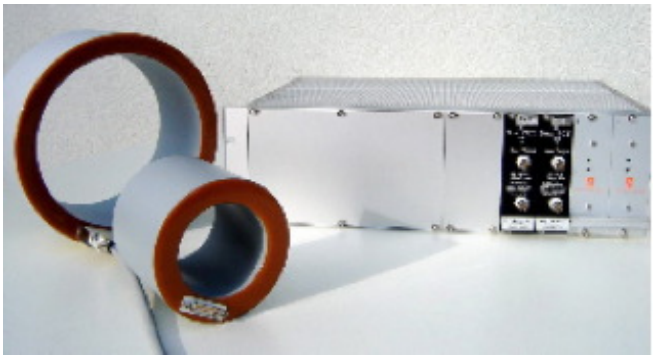

Figure 4.9.4 Bergoz NPCT (New Parametric Current Transformer).

The NPCT-115-C30-HR-H model has a radiation-hardened sensor and four ranges (±20 mA, ±200 mA, ±2 A, ±20 A) with remote control by TTL signals. Wide operational range allows utilization of NPCT starting at commissioning and during regular operations without compromising the requirements for accuracy. Its resolution is better than 1 $\mu A/Hz^{1/2}$. Such a small noise will allow measurement of the expected 60 hours lifetime for 25 mA circulating in one minute with 2% accuracy (assuming a 1 Hz sampling rate). The high bandwidth of the DCCT will allow measurements of the steps in the current after injection, and therefore provide a means of continuously monitoring injection efficiency.

The DCCT will be placed in the dedicated enclosure, providing shielding for RF noise as well as magnetic fields. The microwave absorbers and ferrite will be placed inside in order to suppress wake fields produced by the circulating electron beam.

4.9.5 RF Diagnostics

4.9.5.1 RF Beam Position Monitors

The optics of the NSLS-II storage ring are shown in Figure 4.9.5. In the baseline design there will be six beam position monitors (BPMs) equipped with receivers for each cell. Straights with insertion devices, however, will be provided with two additional instrumented BPMs.

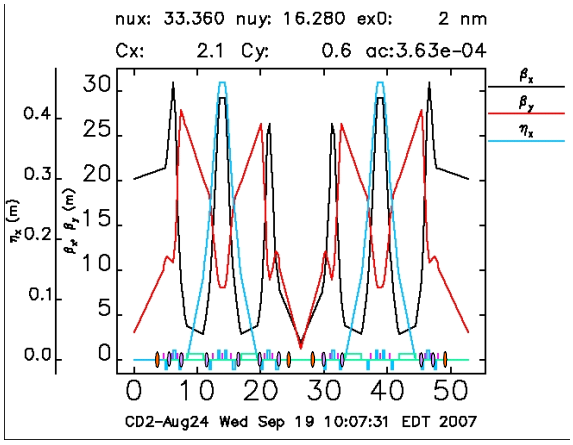

Figure 4.9.5 NSLS-II superperiod. Baseline BPMs are shown as lavender ellipses and user BPMs as orange ellipses.

The high-precision pick-up electrodes will utilize button design and will be diagonally incorporated into the aluminum extrusion vacuum chamber. Figure 4.9.6 shows the cross-section of the basic construction of the four-button pick-up electrodes. An average current of 500 mA circulating in the storage ring is expected to produce –1.1 dBm signal into 50 Ω load at 500 MHz. This estimate is done for a button, shown in Figure 4.9.7, with 5 mm radius and capacitance of 4 pF. The buttons are spaced with a distance to the beam of 20 mm. The scaling parameters for both vertical and horizontal directions are estimated to be around 10 mm for the present geometry; more precise sensitivities will be established during preliminary design.

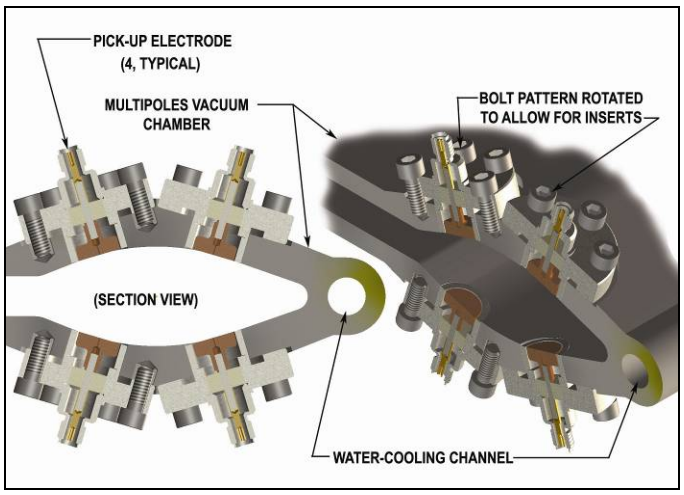

Figure 4.9.6 Four-button, two-plane pick-up electrodes mounted on the vacuum chamber.

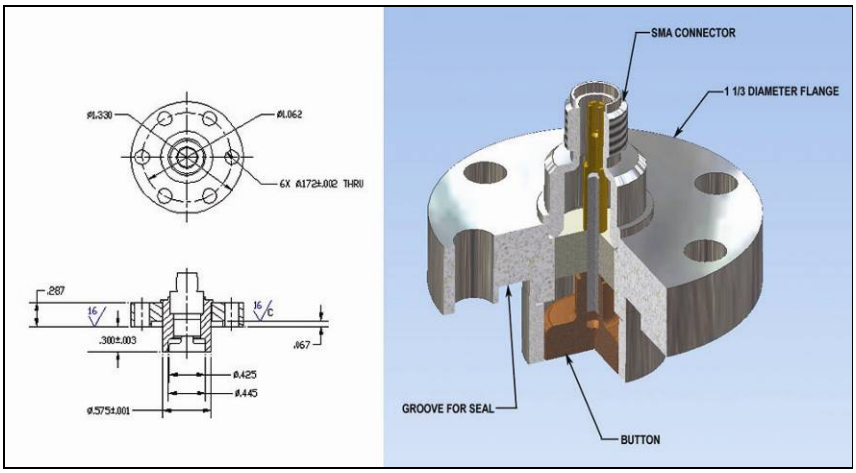

Figure 4.9.7 Design of the BPM button for the storage ring.

Libera Brilliance modules, manufactured by Instrumentation Technologies [4.9.3, 4.9.4] and shown in Figure 4.9.8, can be used to process the signal from the BPM buttons. The RMS uncertainty of the beam position is expected to be below 0.2 μm in 1 kHz bandwidth for the geometry shown. The digital design of the receivers provides the possibility of turn-to-turn beam position measurements with 1 μm accuracy. The chamber with BPM buttons will be mounted on a girder by precisely machined supports, to provide high stability. Small alignment errors, as well as electrical offsets and errors in the BPM system, will be accounted for at the commissioning using beam-based alignment, which will be straightforward, thanks to the individual power supplies.

Figure 4.9.9 Libera Brilliance by Instrumentation Technologies.

The NSLS-II storage ring utilizes very strong sextupoles. This makes it very important to have the orbit of the circulating beam as close as possible to the magnetic centers of the sextupoles. We will rely on highly accurate relative alignment of the sextupoles and quadrupoles on the same girder. In addition, a beam-based alignment procedure will be used for the sextupoles.

To provide the necessary beam stability, not only electrical noise in the BPM electronics should be considered but also mechanical motion of the vacuum chamber. For the most demanding beamlines, the high-stability BPMs will be placed on special, extra-stable posts (Figure 4.9.9), which will minimize positional changes of the vacuum chamber caused by changes in the ambient temperature. Shielded bellows will relieve the tension from the adjacent vacuum ducts. A more detailed description can be found in Section 4.3.2.

Figure 4.9.9 Design of the high-stability BPM support.

4.9.5.2 Tune Monitor

In the baseline design, the vertical and horizontal betatron tunes will be monitored using a network analyzer [4.9.5, 4.9.6]. The analyzer's source will be connected to the excitation striplines through the buffer amplifiers. The signal from the receiver pick-up electrodes will be combined with hybrids to produce vertical or horizontal signals, which will be down-converted below the revolution frequency and fed to the input of the network analyzer (Figure 4.9.10). Such an approach allows utilization of the maximal driving strength of the striplines and makes measurement of the tunes less sensitive to changes in the revolution frequency.

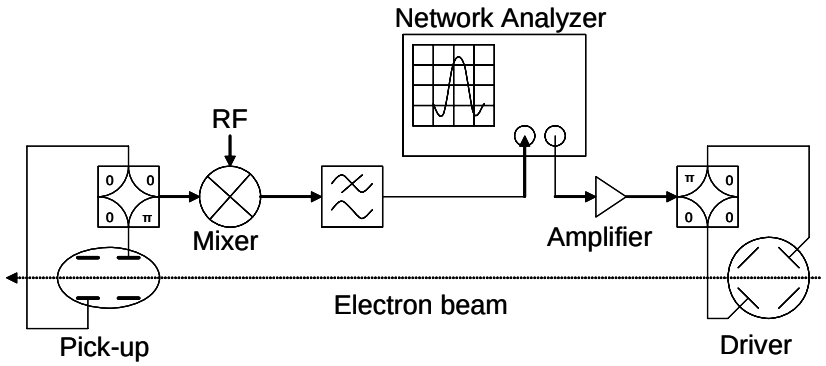

Figure 4.9.10 Layout of the tune measurement system.

As a back-up, we can use the turn-by-turn data provided by the orbit monitoring system with electron beam being excited by the pingers located in the injection straight. Another solution that can be implemented after ring commissioning is utilizing the phase-locked loop.

The tune monitor should provide betatron frequency resolution of 10^{-4} (or better) to obtain 1% accuracy in the β-functions, with up to five-fold difference in the β-functions for different planes with 0.05 allowable tune change. High precision of the tune measurements will facilitate beam-based alignment of the sextupoles, as well. Such parameters need to be reached even with chromaticities as high as 5.

4.9.5.3 Beam Oscillations Monitor

The signal from a dedicated set of pick-up electrodes will be connected to an RF spectrum analyzer (Figure 4.9.11). The sidebands observed can be used to analyze electron beam motion. Summing the signal from opposite electrodes helps to eliminate components with transverse oscillations, while maintaining the signal with phase motion of the electron bunches, which allows measurement of the synchrotron frequency. The difference signal will be used to observe transverse oscillations of the electron beam. This diagnostic instrument is included in the baseline design due to its usefulness during commissioning.

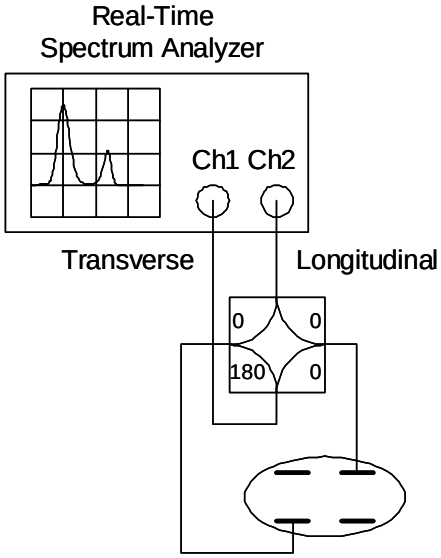

Figure 4.9.11 System for the observation of beam oscillations.

4.9.5.4 Transverse Feedback System

The resistive wall wake can destabilize the electron beam in the storage ring. Increasing the chromaticity may not be sufficient, due to limitations on sextupole strength resulting from loss of the dynamic aperture required for beam lifetime and injection. The required stability can be provided by a digital bunch-by-bunch transverse feedback system [4.9.7, 4.9.8]. A broadband signal measuring the position of the individual bunches will be provided by the button-shaped pick-up electrodes. It will be sampled with a fast ADC (sampling rate 500 MHz). A digital filter will calculate the desired correction signal, which is generated by a DAC. The correction kicks are fed through a broadband amplifier and drive the electron beam using the second stripline. We are considering using a Libera Bunch-by-bunch system as an integrated unit, which provides all necessary analog-to-digital and digital-to-analog conversion with FPGA processing [4.9.8] (Table 4.9.2). In the baseline design the transverse feedback will be employed only for the vertical plane. However, the design can be easily expanded for the horizontal plane by the addition of another processing module.

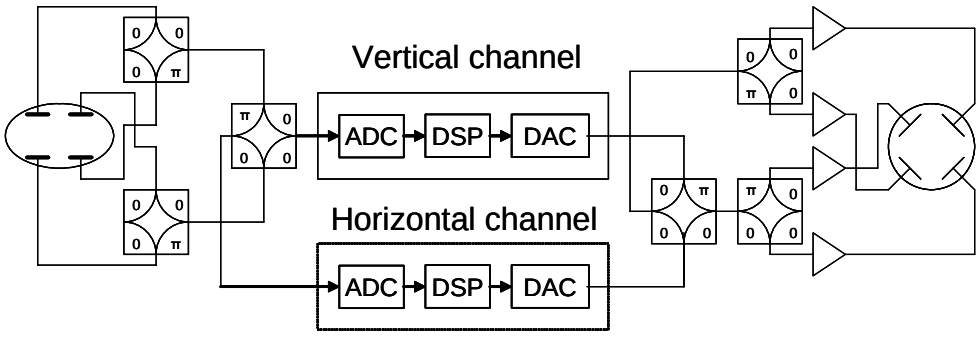

Figure 4.9.10 Conceptual layout of the transverse feedback system.

Table 4.9.2 Parameters of the transverse feedback.

Feedback parameters	vertical	horizontal
Measurement range	±0.15 mm	±1.5 mm
Resolution	0.3 micron	0.5 micron
Kick strength per turn	0.5 microrad	0.3 microrad
Minimal damping time τ_{min}	90 microsec	2.6 msec
Added noise for $\tau=\tau_{min}$	0.01 microns	0.09 microns

The length of the 50 Ω striplines will be 15 cm (one-quarter of the RF wavelength). The striplines will be installed in the drift space on the arc where β_x=4.6 m and β_y=19.1 m. 100 W amplifiers will produce and electric field of 5 kV/m on the 38 mm vertical gap. Together with the magnetic field, the stripline will produce a deflection angle of 0.5 microradians for 3.0 GeV electron beam.

4.9.6 Synchrotron Radiation Diagnostics

4.9.6.1 Overview

This section describes diagnostics for the NSLS-II storage ring that utilize visible and x-ray synchrotron radiation generated in a bending magnet and an x-ray undulator. Table 4.9.3 shows the types and quantities of diagnostics for the storage ring.

Table 4.9.3 Complement of the Optical Diagnostics for the NSLS-II Storage Ring.

Monitor type	Quantity	Function	Range	Resolution	Bandwidth
Emittance monitor	1	Horizontal emittance Vertical emittance	0.5-2.5 nm-rad 8 pm-rad	5 pm-rad 1 pm-rad	100 Hz
Streak-camera	1	Bunch length	10 – 50 ps	2 ps	8 Hz
Pinhole camera	1	Beam size Energy spread	10x30 microns 0.2 – 2%	4 microns 0.01%	30 Hz
Photon BPM	1 per beamline	Position of ID radiation	10 mm	0.001 mm	2 kHz
Diagnostics undulator with pinhole camera	1	Horizontal emittance energy spread momentum compaction factor	0.5 – 2.5 nm-rad 0.2 – 2% 10^{-4}		
FireWire camera	1	Beam profile		640x480	120 fps

4.9.6.2 Emittance monitor

For measuring the ultra low vertical emittance of the storage ring, we included in the baseline design the direct imaging of the electron beam with two zone plates. This method was developed at KEK [4.9.9] for measuring ultra small beam sizes. A double crystal monochromator selects the observation wavelength, λ. The first zone plate focuses the monochromatic beam to small spot, while the second zone plate magnifies the image, making it suitable to observe by X-ray CCD camera. The optical setup is shown in Figure 4.9.11.

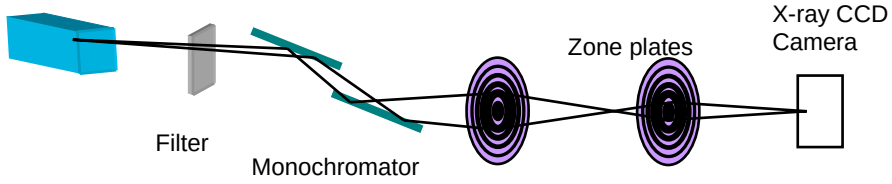

Figure 4.9.11 Layout of emittance monitor utilizing two zone plates.

4.9.6.3 Bunch Length Measurement

A double-sweep streak-camera Optronis model SC-10 [4.9.10], shown in Figure 4.9.12, will be used to measure the longitudinal beam dynamics. Its versatility and high sensitivity make it an excellent choice for monitoring the bunch length with high resolution and studying beam instabilities. The streak camera will be equipped with IOV-10 input optics. The bialkali photocathode with 8 mm × 2 mm area provides low dark noise (below 50 $e^-/cm^2/s$). The parameters of the streak camera are shown in Table 4.9.3. The synchroscan feature provides low-phase jitter for synchronous summing of signals and tracking phase dynamics. The dual sweep is also available. The readout will be performed with a fiber optically coupled CCD camera (ANIMA-PX/25).

The OptoControl software will enable us to access all streak camera parameters and to control the camera operation. A 100 MHz Ethernet (TCP/IP) interface is integrated with the control system. For additional image analysis, the OptoAnalyse software is available. This program allows the use of sophisticated image acquisition algorithms and provides various tools for temporal or spatial analysis. The photon counting combined with drift and jitter correction makes possible long-term measurements with high sensitivity and high temporal resolution.

Table 4.9.3 Optronis SC-10 Streak Camera Parameters.

Spectral response characteristics [nm]	350 to 700
Synchroscan frequency (factory setting) [MHz]	40 – 250
Temporal resolution (FWMH) [ps]	2
Sweep range	300 ps to 4 ns
Camera resolution [pixels]	1360x1024
Frame rate [Hz]	8
Dynamic range [bit]	12

The streak camera will be shared with the booster. An optical beamline from the booster will be used to transport a beam of synchrotron radiation from the booster bending magnet to the streak camera. An alternative solution is to use C5680 synchroscan streak camera by Hamamatsu.

Figure 4.9.12 View of the SC streak camera family.

4.9.6.4 Photon Beam Position Monitors

Photon beam position monitors (PhBPMs) manufactured by FMB-Berlin (shown in Figure 4.9.13) are being considered for monitoring radiation from the insertion devices [4.9.11]; the blades, of course, will be designed and optimized to suit the requirements of NSLS-II. The PhBPMs are based on a development by Dr. Karsten Holldack at BESSY. The information obtained on the position of the photon beam will be incorporated into the orbit feedback system to provide the beam stability required for user applications. In the baseline design we have one PhBPM per beamline. The PhBPM assembly will be mounted on a stable post and its location (elevation and transverse position) will be adjusted with 2D translation stages (Figure 4.9.14). Similar devices at APS enable pointing stability of the photon beam with peak-to-peak drift of less than 2 μrad over six days [4.9.12].

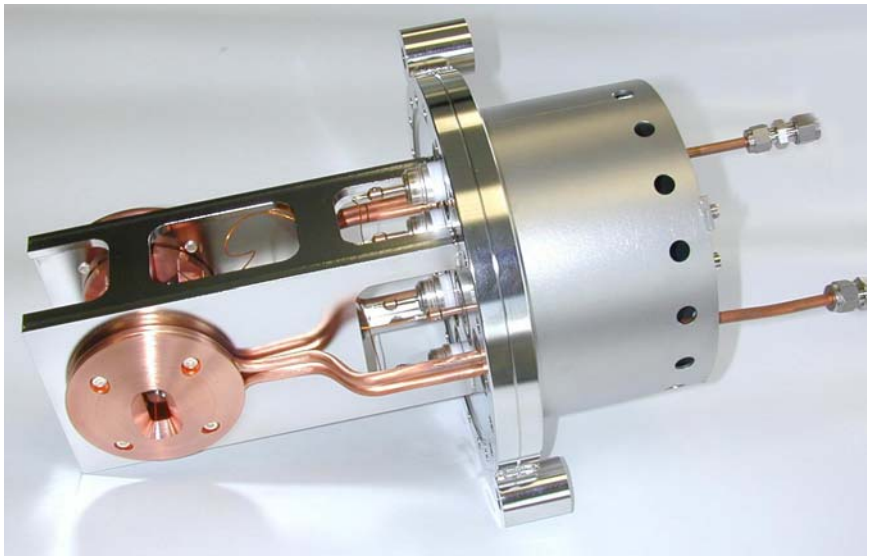

Figure 4.9.13 Photon beam position monitor.

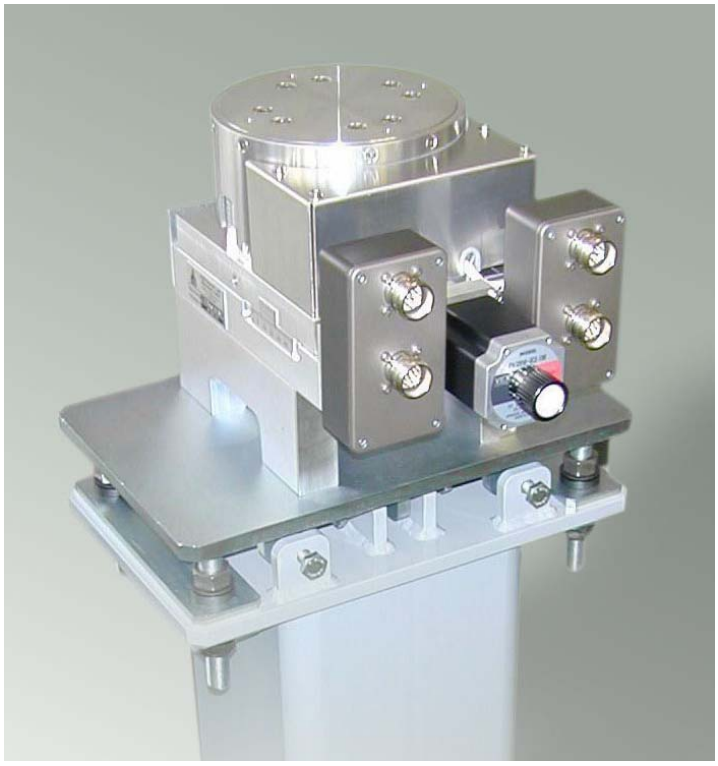

Figure 4.9.14 Photon beam position monitor on the support column with motorized stage.

4.9.6.5 Diagnostics with Visible Synchrotron Radiation

An IEEE1394 camera will be used to observe the visible radiation from the electron beam. Such an approach eliminates the need for a frame-grabber and makes display of the beam on the control computer straightforward. The camera has an external trigger capability and exposure control from 10 μsec to 5 sec.

Position-sensitive photodiodes which provide signal based on the location of the center of gravity of the optical beam can be incorporated into the orbit feedback system to monitor beam stability for IR users, as well as results of image processing. The model S2044 (the smallest object in Figure 4.9.15) has 0.6 μm sensitivity and 0.3 μsec rise time.

Figure 4.9.15 Position-sensitive diodes by Hamamatsu.

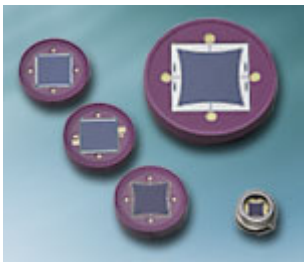

4.9.6.6 Diagnostics Undulator

The diagnostics undulator will allow independent measurement of the energy spread and horizontal emittance. The momentum compaction factor can be also measured. We plan to utilize one of the user beamline undulators in a 5m straight; therefore, this tool is not included in the baseline design.. This beamline will be equipped with an additional high-resolution fluorescent screen and a retractable pinhole (Figure 4.9.16). Use of the radiation from the undulator for diagnostic purposes will be restricted to periods when it is not needed by the users.

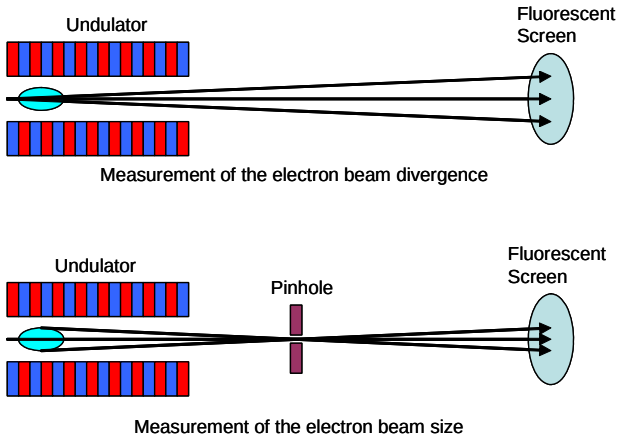

Figure 4.9.16 Beam diagnostics with undulator radiation.

The β-functions in the straight are $\beta_{xmin} = 2.5$ m and $\beta_{ymin} = 1.2$ m. The U20 undulator that we propose to use has a 20 mm period and 3 m length. To measure the divergence of the electron beam, the transverse profile of the undulator radiation will be monitored. To increase system resolution, small undulator K values will be utilized. These will also help to minimize the power from higher harmonics and avoid distorting the power profile. For $K = 0.3$, the power density of the 3rd harmonic is two orders of magnitude below the power density of the main harmonic. For this value of K, the fundamental wavelength of the undulator radiation will be 0.29 nm and the divergence due to a diffraction will be $\sigma'_{ph} = \sqrt{\lambda / L} = 9.8\,\mu\text{rad}$, which compares favorably with the horizontal divergence of the electron beam: $\sigma'_e = \sqrt{\varepsilon_x / \beta_x} = 14.1\,\mu\text{rad}$ for 0.5 nm-rad emittance.

Inserting a pinhole, which can be realized as a slit, will enable measurement of the horizontal beam size. Knowing the divergence and beam size will enable us to directly measure the beam emittance, independent of the β-function.

Analysis of the width of the undulator spectrum provides information on the energy spread of the electron beam. It is also possible to measure the momentum compaction factor by observing the shift of the undulator spectrum with revolution frequency [4.9.12].

4.9.7 Other Diagnostics

4.9.7.1 Beam Loss Monitors

NSLS-II will utilize a distributed beam loss monitoring system based on p-i-n diodes, which are commercially available from Bergoz [4.9.2] (Figure 4.9.17). Two beam loss monitors per cell will be used for monitoring the spatial distribution of beam losses.

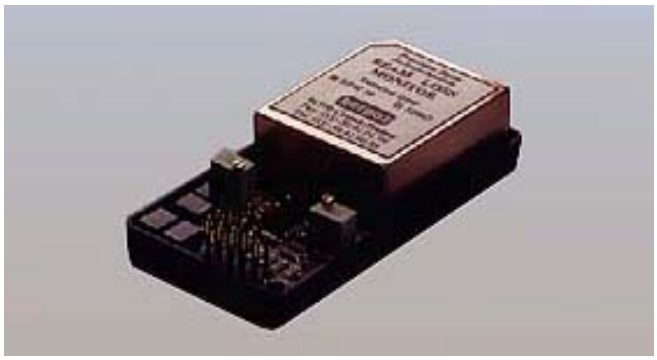

Figure 4.9.17 Beam loss monitor by Bergoz.

The loss monitors have a pulse output (one pulse per lost particle) and are insensitive to the synchrotron radiation photons. The monitors are small and can be easily relocated to the region of interest. CosyLab has developed interfaces for easy integration with the control system [4.9.13].

For the temporal distribution of the lost particles (on the scale of one turn) we plan to use ten scintillation detectors (Figure 4.9.18). They can be also be used for monitoring the losses of injected electrons near the injection and RF straights.

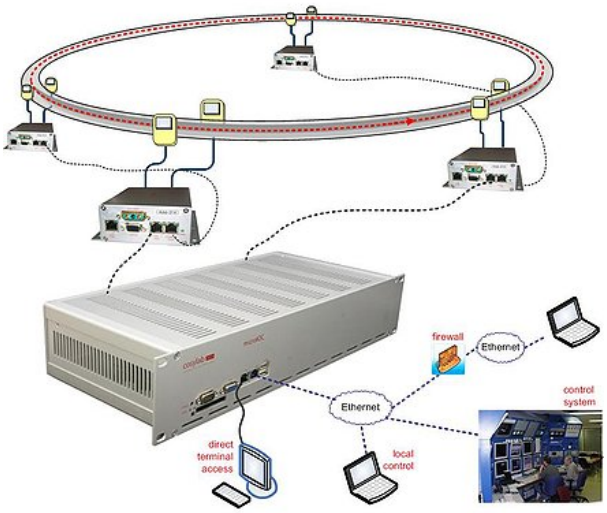

Figure 4.9.18 MicroIOC with signal conditioners for Bergoz beam loss monitors.

4.9.7.2 Scrapers

Two pairs of two-plane adjustable-position scrapers will be installed on the ring to be used both as protective devices as well as diagnostic instruments for accelerator studies. More details are described in Section 4.7. One set of scrapers (horizontal and vertical) will be installed in the dispersive section to measure the energy distribution of the electron beam. Another set will be installed in a straight section with zero dispersion in order to have information on the transverse size of the electron beam, and to eliminate possible beam halos capable of affecting the insertion devices.

4.9.7.3 High-Level Accelerator Modeling

Extracting data on the storage ring lattice from the experimental data [4.9.14] requires high-level accelerator modeling, described in the control system section. High-level accelerator modeling will also be used in the development of a real-time orbit feedback system and for coupling correction. Such high-level applications will necessitate a storage ring simulator for the offline testing and debugging of the software being developed.

A procedure was developed and experimentally verified for measuring accelerating voltage in the RF cavity [4.9.15]. The method is based on the observation of a phase shift between the electron beam and electrical field in the cavity when amplitude of the field varies. This procedure also makes it possible to measure relative phases between multiple cavities installed on the storage ring.

References

[4.9.1] E.D. Johnson, W.S. Graves, and K.E. Robinson, "Periscope Pop-In Beam Monitor," Proc. of Beam Instrumentation Workshop 1998, AIP Conf. Proc. 451, pp. 479–484.

[4.9.2] http://www.bergoz.com

[4.9.3] R. Ursic et al., "Holy Trinity of the Instrumentation Development," Proc. of the 11th Beam Instrumentation Workshop, Knoxville 2004.

[4.9.4] U. Mavric, "Innovative RF Design Unites Benefits of Multiplexed and Multichannel System," Proc. of the 11th Beam Instrumentation Workshop, Knoxville, 2004.

[4.9.5] A.S. Fisher, "Instrumentation and Diagnostics for PEP-II," Proc. Beam Instrumentation Workshop 1998, AIP Conf. Proc. 451, pp. 95–109.

[4.9.6] A. S. Fisher, M. Petree, U. Wienands, S. Allison, M. Laznovsky, M. Seeman, and J. Robin, "Upgrades to PEP-II Tune Measurements," Proc. of Beam Instrumentation Workshop 2002, AIP Conf. Proc. 648, pp. 267–274.

[4.9.7] M. Dehler, R. Kramert, P. Pollet, and T. Schilcher, "Commissioning Results of the Multi Bunch Feedback System at SLS," Proc. of EPAC 2004, pp. 2508–2510.

[4.9.8] J.M. Koch, G. Naylor, E. Plouviez, and F. Epaud, "Beam Diagnostic Features of the ESRF Multibunch Feedback," Proc. DIPAC 2007.

[4.9.9] K. Iida, et al., "Measurement of an Electron-Beam Size with a Beam Profile Monitor Using Fresnel Zone Plates," Nucl. Instr. and Meth. A506 (2003), pp. 41-49.

[4.9.10] http://www.optronis.com

[4.9.11] G. Decker and O. Singh, "Beam Stability at the Advanced Photon Source," Proc. of PAC 2005, pp. 3268–3270.

[4.9.12] B. Yang, M. Borland, and L. Emery, "High Accuracy Momentum Compaction Measurement for the APS Storage Ring with Undulator Radiation," CP546, Beam Instrumentation Workshop 2000, American Institute of Physics, pp. 235–241.

[4.9.13] http://www.CosyLab.com

[4.9.14] J.A. Safranek, "Beam-based Accelerator Modeling and Control," Proc. of Beam Instrumentation Workshop 2000, AIP Conf. Proc. 546, pp. 23–5.

[4.9.15] I. Pinayev, Characterization of the RF System of NSLS X-ray Ring, Proceedings of PAC'07.

5 Radiation Sources

This chapter describes the radiation sources to be provided in the NSLS-II baseline configuration. Continuing the tradition established by the existing NSLS, they span a very wide spectral range, from the far IR, down to 0.1 meV (equivalent to 1 cm^{-1}), to the very hard x-ray region, more than 300 keV. This is achieved by a combination of bending magnet sources, covering the IR, VUV, and soft x-ray range, three-pole wiggler sources extending into the hard x-ray range, and insertion device sources, covering the soft x-ray through very hard x-ray range. They will achieve world leading levels of time average brightness and flux from the far IR through to ~20 keV, only being surpassed above ~20 to 25 keV by the performance of synchrotrons operating at higher energy (6 to 8 GeV).

As discussed in elsewhere in this report, the NSLS-II lattice contains 30 DBA cells, or 15 superperiods with alternating straight section lengths. The beta function values at the centers of the shorter straight sections will be quite low, especially in the vertical plane, and the longer straights will have somewhat higher beta function values. The resulting horizontal and vertical electron beam sizes and divergences in the center of the two types of straights, as well as in the center of the bend magnets and three-pole wigglers, are given in Table 5.1.1. These beam sizes and divergences are very small, especially in the insertion device straight sections. The beta functions also determine the allowed minimum vertical gap of an undulator and non-linear dynamic effects constrain the maximum length of the undulator, L. The minimum undulator gap and the undulator lengths for the devices described in this chapter were all chosen to satisfy these constraints.

All of the source properties described in this chapter assume a fully-damped horizontal emittance value of 0.5 nm-rad. This is the performance value for the NSLS-II storage ring when operating with a full complement of eight 7 m damping wigglers. The initial emittance value will be greater than this value, owing to operation with fewer damping wigglers, as discussed in Chapter [xx].

Table 5.1.1 Electron Beam Size and Divergence at NSLS-II.

Type of source	Low- straight section (6.6m)	High- straight section (8.6m)	0.4T Bend magnet	1T three-pole wiggler
σ_h [μm]	28.	99.5	44.2 (35.4-122)	136
σ_h' [μrad]	19.	5.5	63.1 (28.9 – 101)	14.0
σ_v [μm]	2.6	5.5	15.7	15.7
σ_v' [μrad]	3.2	1.8	0.63	0.62

5.1 Insertion Devices

The goal in choosing the set of principal insertion device parameters is to provide a wide overall spectral coverage with insertion devices that target the photon energy ranges of interest for the experimental programs. It is expected that other parameter choices besides those outlined here may be specified to meet the needs of the science program as it evolves over time.

The set of insertion devices described included in the baseline configuration of NSLS-II consists of hard x-ray and soft x-ray undulators, x-ray damping wigglers, and high-energy superconducting wigglers. Their spectral brightness, flux, power, spatial and angular output properties, and polarization performance are described. These IDs produce high-brightness radiation spanning a large photon energy range, from the soft x-ray (~200 eV) to the very hard x-ray (~300 keV). An R&D program focused on developing the required magnetic and mechanical design of these devices is presented in Chapter [xx]. Their effects on the properties of the NSLS-II storage ring and other accelerator physics issues are presented in Chapter [xx].

Table 5.1.2: Insertion Devices included in the Baseline Configuration of NSLS-II

Type of Device	Purpose	Usage	Quantity
Damping Wiggler: 90 mm period (DW90), 1.8T, 2 × 3.5-m long	Broadband	Machine/User	3
In-Vacuum Undulator (IVU): 20mm period (U20), 1.81T, 3-m long	Hard X-ray	User	3
Elliptically-polarized undulator (EPU): 45mm period (EPU45), 4.33T, 2 × 2-m long, canted by ~0.25 mrad	Soft X-ray	User	1
Three-Pole Wiggler: 1.0T, 20cm long	Broadband	User	≤15

The complement of insertion devices included in the NSLS-II baseline configuration is listed in Table 5.1.2. This set is not meant to be complete for the built-out NSLS-II facility. Rather, these devices represent a set that attempts to optimize the performance of the beamlines included in the NSLS-II baseline configuration. These IDs have been chosen consistent with the philosophy of building beamlines dedicated to a given technique, which requires that the source also be individually optimized for each application, as appropriate.

[[remove paragraph?? Other types of undulators and/or wigglers besides those discussed in this Chapter will also be considered during the preliminary engineering design phase of the project. These will include in-vacuum EPUs, to reach smaller magnetic gaps and thereby cover wider photon energy ranges, and quasi-periodicity, for both planar undulators and EPUs. In addition, revolver concepts, figure-8 type undulators, and long-period electromagnetic undulators will be considered. These concepts are discussed further in the description of the undulator R&D program in Chapter 12.]]

5.1.1 Planar Undulators

The hard x-ray undulators at NSLS-II will be planar designs and will produce linearly polarized radiation.

5.1.1.1 IVU – U20

The baseline NSLS-II hard x-ray undulator is an In-Vacuum Undulator (IVU) with a period of 20 mm, referred to as U20. This device will be operated at room temperature and is based on the mini-gap in-vacuum undulator design and development pioneered at NSLS and now utilized at SR sources around the world.

5.1.2 Elliptically Polarized Undulators

The NSLS-II soft x-ray insertion devices will be elliptically-polarized undulators. EPUs provide full ellipticity control of the radiated output from circular through linear, while only marginally reducing the brightness of the linearly polarized output, compared to pure planar undulators of the same period. In addition, these EPUs can also provide linearly polarized output with the polarization axis oriented either horizontally, vertically, or anywhere in between. As discussed in the soft x-ray beamline Section [xx], these properties are extremely useful for separating various contributions to a given signal in an experiment.

5.1.2.1 Soft X-ray EPU – EPU45

The total length of the EPU45 undulator is specified as 4 m, corresponding to a single long device. However, this corresponds to only one of two proposed operating modes for these devices. In fact, for the soft x-ray beamlines discussed in Chapter [xx], this 4 m total length would be comprised of two ~2 m EPUs and the appropriate steering magnets and diagnostics would be placed between the sections to allow a small (~0.25 mrad) canting angle for the electron beam between them. As described in more detail in Chapter [xx],

this configuration will allow the two undulator sections to be set to two different polarizations, e.g., left circular and right circular, or horizontal linear and vertical linear. The angular separation provided by the canting will then permit fast switching between the chosen polarizations of the two EPUs, thereby enabling various types of polarization-sensitive experiments to be performed with high sensitivity, as provided by lock-in detection methods for example. The accelerator issues associated with these, and other, canting angles are discussed briefly in Section [xx] and will be addressed in more detail in the technical design phase of this project.

5.1.3 Wigglers

Classes of experiments that require continuous x-ray spectra, sizable x-ray beams, or very hard x-rays, such as EXAFS, powder diffraction, x-ray topography, x-ray standing waves, high pressure, and x-ray footprinting, to name some, will benefit from the availability of x-ray beamlines that view damping wiggler sources. Superconducting wigglers will be the preferred source for experiments requiring very hard x-rays, up to ~300 keV. All wiggler sources at NSLS-II are expected to be in high demand.

5.1.3.1 Damping Wiggler – DW90

The damping wigglers will produce the highest flux of any NSLS-II source out to ~30 keV and will also have excellent brightness. They are expected to be the premier source for experiments above ~5 keV that do not require the ultra-high brightness and extremely small beams produced by the hard x-ray undulators.

5.1.3.2 Three-pole Wiggler – TPW

The three-pole wigglers, to be inserted just upstream of the downstream bend magnet in the super-period, will produce a very useful hard x-ray bend-magnet-like spectrum. With a critical energy of 6 keV, the three-pole wigglers will produce usable hard x-ray flux out to ~25 keV. The emitted horizontal angular fan from these devices is 2 mrad wide.

5.1.3.3 Superconducting Wiggler – SCW60

The highest energy photons will be produced by very high field, short period, wigglers. The radiation will be broadband with high power at high x-ray energies, covering the 20 to 300 keV energy range. The baseline SCW60 device has a period length of 60mm and a wiggler field of 3.5T. This combination of period and magnetic field has been demonstrated technologically at ELETTRA and MAX lab. Specifications of other high magnetic field SCWs that are currently in service at medium energy synchrotrons are listed in Table 5.1.3.

Table 5.1.3 Some Working SCWs Similar in Specifications to Proposed and Alternative NSLS-II Wigglers.

Facility	Manufacturer	Field(T)	Period (cm)	# full-field poles
NSLS X17	Oxford	6	17.4	5
BESSY II	Novosibirsk	7	14.8	13
CLS	Novosibirsk	4.2	4.8	25
ELETTRA	Novosibirsk	3.6	6.4	45
MAX lab	Custom	3.5	6.1	47

Increasing the SCW60 magnetic field will be the subject of NSLS-II R&D, so that its flux and brightness are as high as possible. A target magnetic field value is 6.0T, which represents an SCW design that pushes the limit of presently achievable current density. The SCW60 will outperform other NSLS-II radiation sources at

energies above 30 keV. The target deflection parameter, K, is chosen to be high enough to generate a large horizontal beam profile of more than 0.5 m at 50 m from the source point. This allows splitting of the fan into multiple experimental hutches.

5.2 Bend Magnets

The NSLS-II bending magnets will have a relatively low critical energy (2.4 keV), and will be excellent sources for low photon energies, below 10 keV. It is expected that the available bend magnet ports will be allocated primarily to VUV and soft x-ray uses, as well as infrared uses. Those classes of experiments that require access to harder sources of bend-magnet-like x-rays (energy >~5 keV) are better suited to three-pole wigglers (TPW), described in section 5.1.3.2 above.

The NSLS-II bend magnets and three-pole wigglers will provide very stable beams. The relatively low emitted power from these sources simplifies the cooling requirements on the optics, although it does not eliminate the need to provide cooling. The brightness provided by the NSLS-II dipole sources will be two orders of magnitude higher than that of the present NSLS dipoles (extending up to ~12 keV) and their flux will also show some improvement (extending up to ~4 keV), as shown in Table 5.2.1. Indeed, the NSLS-II bend magnets will provide almost twice the flux of the ALS conventional bend magnets (i.e., not the superbends) and offer even larger improvements in source brightness. Thus, aspects of the very successful ALS research programs based on bend magnet illumination can be developed at NSLS-II, although the distribution of beamlines and end stations will be determined by the strengths and interests of the NSLS-II user community. The NSLS-II 3 three-pole wiggler sources will have essentially the same critical energy as the present NSLS dipoles, but will be more than an order of magnitude brighter and produce a factor of 1.5 to 3 times greater flux (see Table 5.2.1).

Table 5.2.1 Comparison of Bend Magnet Sources

	NSLS-II Bend Magnet		NSLS-II Three-pole-wiggler		ALS Conventional Bend Magnet		NSLS X-Ray Bend Magnet		NSLS VUV Bend Magnet	
Energy	Flux	Brightness	Flux	Brightness	Flux	Brightness	Flux	Brightness	Flux	Brightness
1000 eV	3.3×10^{13}	1.5×10^{16}	3.3×10^{13}	2.7×10^{16}	2.1×10^{13}	1.5×10^{15}	1.4×10^{13}	1.3×10^{14}	6.0×10^{12}	1.1×10^{13}
100 eV	2.5×10^{13}	8.0×10^{15}	1.9×10^{13}	1.3×10^{15}	1.5×10^{13}	7.5×10^{14}	8.0×10^{12}	7.0×10^{13}	1.3×10^{13}	9.0×10^{13}
10 eV	1.3×10^{13}	3.7×10^{15}	9.3×10^{12}	6.0×10^{14}	7.2×10^{12}	3.4×10^{14}	3.8×10^{12}	2.8×10^{13}	7.7×10^{12}	4.4×10^{12}
1 eV	5.9×10^{12}	1.7×10^{15}			3.4×10^{12}	1.6×10^{14}	1.8×10^{12}	1.3×10^{13}	3.7×10^{12}	2.0×10^{12}
0.1 eV	2.8×10^{12}	8.0×10^{14}			1.6×10^{12}	7.3×10^{13}	8.4×10^{11}	6.1×10^{12}	1.8×10^{12}	9.4×10^{11}

ALS parameters assume top-off mode operation at 500 mA stored current. Flux is in units of ph/s/0.1%BW and brightness is in units of ph/s/0.1%BW/mm^2/mrad^2.

The special considerations required for collecting infrared radiation produced by the bend magnets are discussed in detail in Section 5.4.

5.3 Parameters and Performance of Radiation Sources

The basic parameters characterizing the IDs, bending magnet, and three-pole wiggler sources are listed in Table 5.3.1. In the case of the NSLS-II bend magnet and TPW, the total power value is actually the power per horizontal mrad.

Table 5.3.1 Basic Parameters of NSLS-II Radiation Sources for Storage Ring Operation at 3.0 GeV and 500 mA

	U20	EPU45	DW90	SCW60	Bend Magnet	Three-pole wiggler
Type	IVU	EPU	PMW	SCW	Bend	PMW
Photon energy range [keV]	Hard x-ray (1.9–20)	Soft x-ray (0.180 – 7)	Broadband (<0.010 - 100)	Very hard x-ray (<0.010 – 200)	Soft and low-energy x-ray (<0.010 – 12)	Hard x-ray (<0.010 – 25)
Type of straight section	Low-β	Low-β	High-β	Low-β		
Period length, λ_U [mm]	20	45	90	60		
Total device length [m]	3.0	4.0	7.0	1.0		0.25
Number of periods	148	89	75	17		0.5
Minimum magnetic gap [mm]	5	10	12.5	15		28
Peak magnetic field strength in linear mode, B [T]	1.03	1.03	1.80	3.5	0.40	1.12
Max K_y*, linear mode	1.81	4.67	15.20	19.61		
Peak magnetic field strength in circular mode, B [T]		0.68				
Max $K_h = K_y$*, circular mode		2.87				
Minimum hν fundamental [keV]	1.62	0.183				
hν critical [keV]			10.8	21.0	2.39	6.7
Maximum total power [kW]	9.1	12.09	64.6	34.9		
Horizontal angular power density [kW/mrad]					0.023	0.064
On-axis power density [kW/mrad^2]	65.4	40.03	59.3	26.1	0.088	0.25

*K = 0.934 B[T] λ_u[cm]; effective K values listed

5.3.1 Brightness

For many experiments, especially those involving imaging or microscopy, where, for example, the beam must be focused down to a small spot, the key figure of merit of user radiation sources is their time average brightness. This is the flux output per unit bandwidth, per unit source area, and per unit solid angular divergence. Undulators and wigglers are excellent sources of high brightness radiation. The brightness of the baseline set of radiation sources for NSLS-II is shown in Figure 5.3.1. For the undulators, the tuning curves of harmonics 1, 3, 5, 7, and 9 are shown. These tuning curves show the variation of the peak brightness of the undulator harmonics as the magnetic field strength, and hence K parameter, is varied from K_{max}, listed for each undulator in Table 5.3.1, down to K_{min} ~0.4.

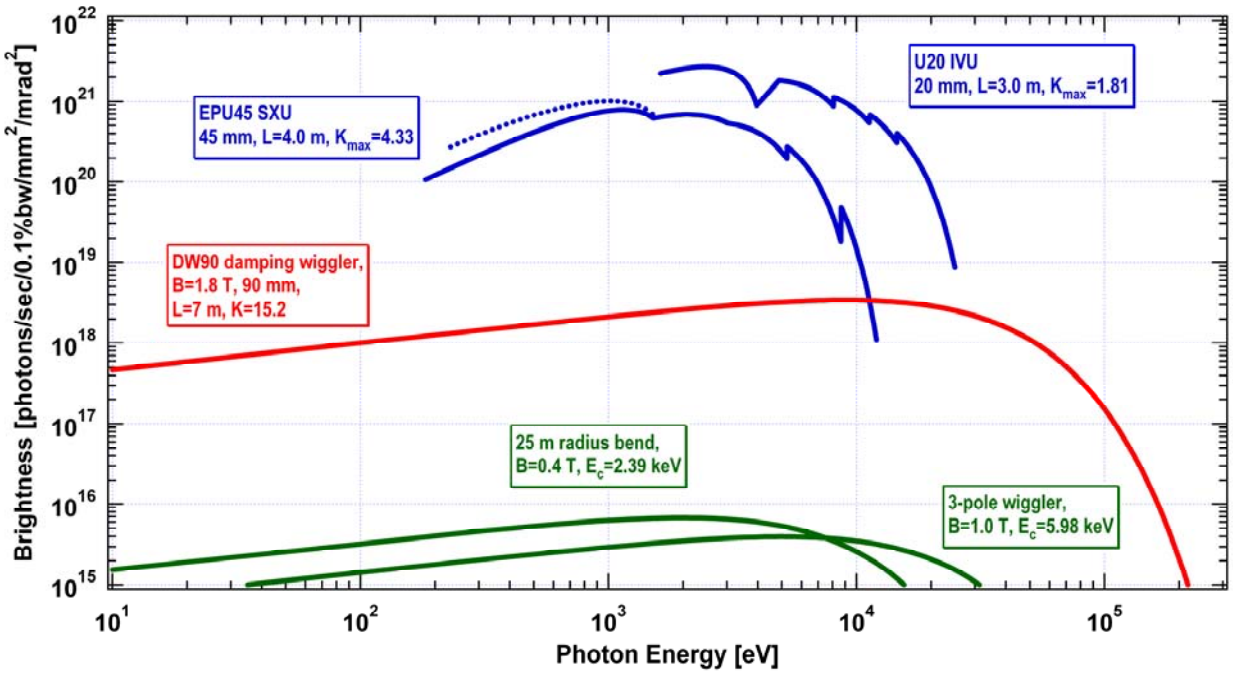

Figure 5.3.1 Brightness vs. photon energy for the baseline radiation sources at NSLS-II. Ring parameters: 3.0 GeV, 0.5 A, ε_h=0.5 nm, ε_v=0.008 nm, energy spread=0.001; Straight section parameters: low-β: β_h=2.02 m, β_v=1.06 m; high-β: β_h=20.8 m, β_v=2.94 m; $\alpha_h=\alpha_v=\eta_h=\eta_v=\eta'_h=\eta'_v=0$; Bend magnet parameters: β_h=2.62 m, β_v=20.3 m, α_h=1.75, α_v=-0.952, η_h=-0.129 m, η'_h=-0.102, $\eta_v=\eta'_v=0$; Three-pole wiggler parameters: β_h=3.87 m, β_v=35.2 m, α_h=2.01, α_v=-1.56, η_h=0.168 m, η'_h=-0.105, $\eta_v=\eta'_v=0$.

The brightness of the U20 hard x-ray undulator is the highest of any devices in the NSLS-II baseline configuration. This is due in part to the short period length of this device, thereby increasing the number of periods contributing to the flux output, and in part to the short output wavelengths compared to the soft x-ray undulator (EPU45). For diffraction-limited undulator radiation, which characterizes a good portion of the range of these two undulators, the brightness varies inversely as the square of the output wavelength. Note that the brightness of the U20 hard x-ray undulator exceeds the 10^{21} ph/s/0.1%BW/mm^2/mrad^2 level.

The wigglers provide broadband, high brightness sources of x-ray radiation. Each of the wigglers shown in Figure 5.3.1 covers nearly the entire photon energy range shown. The superconducting wiggler SCW60 is optimized for very high-energy x-ray work (i.e., above ~60 keV), while the damping wiggler DW90 is a high-flux, hard x-ray source with smooth spectral output extending down through the soft x-ray and VUV photon energy ranges.

Figure 5.3.1 shows the source brightness of the EPU45 soft x-ray undulator in two polarization modes: helical (or circular), shown as dotted lines, and linear, shown as solid lines. The circular polarized mode has intensity only in the fundamental and is slightly brighter than the linearly polarized mode at the same energy. It is expected that this mode will be used for all work below 2 keV, unless linearly polarized light is specifically required.

The NSLS-II bending magnet spectral brightness curve is also shown in Figure 5.3.1. The bending magnet spectrum is a bright source which extends from the infrared to the hard x-ray. This source will be useful up to a few times the critical energy of 2.39 keV, i.e., up to ~10 keV. The bending magnet brightness peaks at ~2 keV, making it an ideal broadband source in the soft x-ray (0.1–2 keV) and low-energy x-ray (2–5 keV) ranges.

The three-pole wiggler (TPW) source has a critical energy of 6 keV, making it a very useful continuum hard x-ray source up to ~25 keV. The TPW spectral brightness curve is shown in Figure 5.3.1. The emitted horizontal angular fan from these devices is 2 mrad wide.

5.3.2 Flux

For those experiments which do not require a very collimated and/or focused beam, the photon spectral flux is the key figure of merit. This is the number of photons per unit bandwidth per unit time, i.e. it is an angle-integrated quantity. For undulators, flux values typically quoted are integrated over the central angular cone, which contains essentially all of the usable flux from these devices. For wigglers and bend magnets, the flux value typically quoted is integrated over all angles vertically and over 1mrad horizontally. The horizontal angular dependence of bend magnets is uniform over its horizontal extent and, for wigglers, is maximum on axis and falls to zero at ±K/γ. For large-radius storage rings such as NSLS-II, the usable horizontal angular range will be determined by physical apertures in the beamline front end. The maximum horizontal angular range deliverable by NSLS-II insertion device front ends will be ~6mrad [check]. The corresponding value for bend magnets will be ~5mrad [check], whereas the three-pole wigglers will produce a 2mrad-wide horizontal angular fan. Figure 5.3.2 shows the flux for the NSLS-II radiation sources. The maximum flux is ~6×10^{15} ph/s/0.1%BW, reached by all three baseline insertion devices (DW90, IVU20, and EPU45) at the peaks of their output spectra (~0.2 keV, ~2 keV, and ~3 keV, respectively). As has been said previously, the bend magnets at NSLS-II will be superlative sources of high brightness and high flux radiation in the VUV and soft x-ray energy range. The three-pole wiggler sources are bend-magnet-like sources which extend into the hard x-ray energy range. Both the bend magnet and three-pole wiggler flux spectra peak at ~4×10^{13} ph/s/0.1%BW, per horizontal mrad.

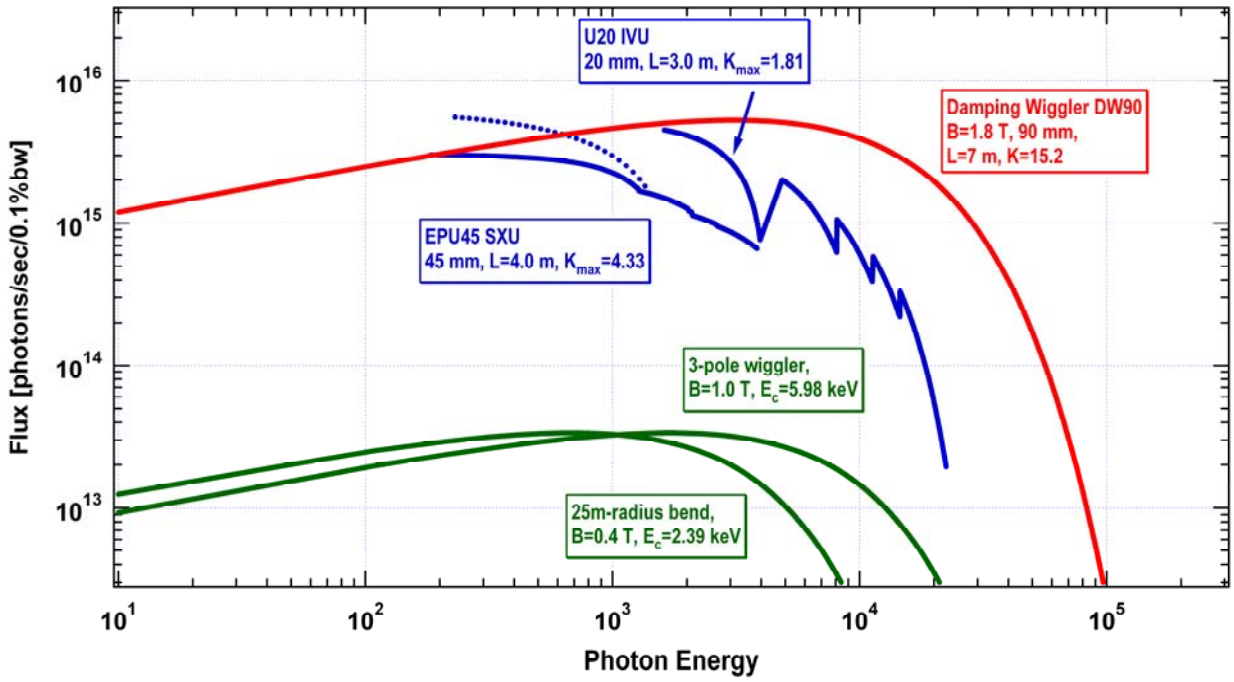

Figure 5.3.2 Flux output of baseline radiation sources at NSLS-II vs. photon energy. See the caption to Figure 5.3.1 for a listing of accelerator parameters used to calculate the flux curves shown here."

5.3.3 Power

Table 5.3.1 gives the maximum total output power of the NSLS-II radiation sources and Figure 5.3.3 shows how the total output power output of the undulators varies as their K value is changed from K_{min} (taken to be ~0.4) to K_{max}, as given in Table 5.3.1. For reference, the corresponding energy of the photons' radiation in the fundamental as a function of K is also given. The photon energy of harmonic n is n times that of the fundamental.

The total power radiated by the undulators at their maximum K settings (i.e., at minimum magnetic gap) is in the 8–13 kW range. The total power output from the NSLS-II wigglers is higher than that of the undulators, at nearly 65 kW, while that of the NSLS-II bend magnets and TPWs is very much less, at only ~23 W and 57W per horizontal mrad, respectively (see Table 5.3.1). Figure 5.3.3 also shows that the total output power at a given value of K increases by about a factor of two when operating in circular mode ($K_h = K_v \neq 0$) compared to linear mode ($K_h = 0$, $K_v \neq 0$) for the EPUs. The engineering challenges of handling the high heat loads in the insertion device front ends are detailed in Section [xx].

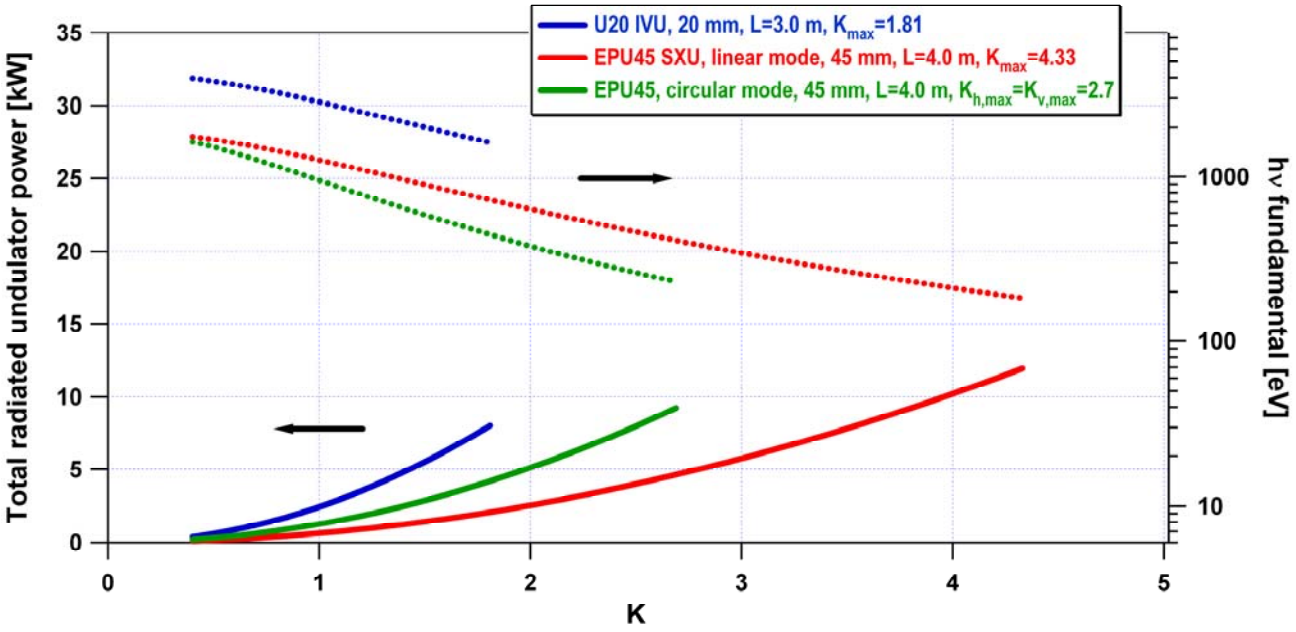

Figure 5.3.3 Total output power (left-hand axis) and fundamental output energy (right-hand axis) of the baseline NSLS-II undulators as a function of the undulator parameter, K.

5.3.4 Power Density

Table 5.3.1 gives the maximum (on-axis) angular power density of the NSLS-II radiation sources; Figure 5.3.4 shows how the maximum angular power density of the undulators varies as their K value changes from K_{min} (taken to be ~0.4) to K_{max}, as given in Table 5.3.1. For reference, the corresponding energy of the photons radiated in the fundamental as a function of K is also given. The energy of harmonic n is n times that of the fundamental. The maximum undulator angular power density radiated by the undulators at their maximum K settings (i.e., at minimum magnetic gap) varies from 40 to 65 kW/mrad^2. The wiggler angular power density output is in the 25–55 kW/mrad^2 range, while the bend magnet and TPW values are again very much less, at 88 W/mrad^2 and 220 W/mrad^2, respectively.

Figure 5.3.4 also shows that the EPU45 output angular power density in circular polarization mode is much lower than in linear polarization mode, and has a different dependence on K. This is primarily because in circular mode there are no higher harmonics, just the fundamental. An advantage of the circular

polarization mode is the lower output power density, which simplifies the design and operation of high energy-resolution beamlines by reducing the thermal deformations of the optical elements (see Chapter [xx]).

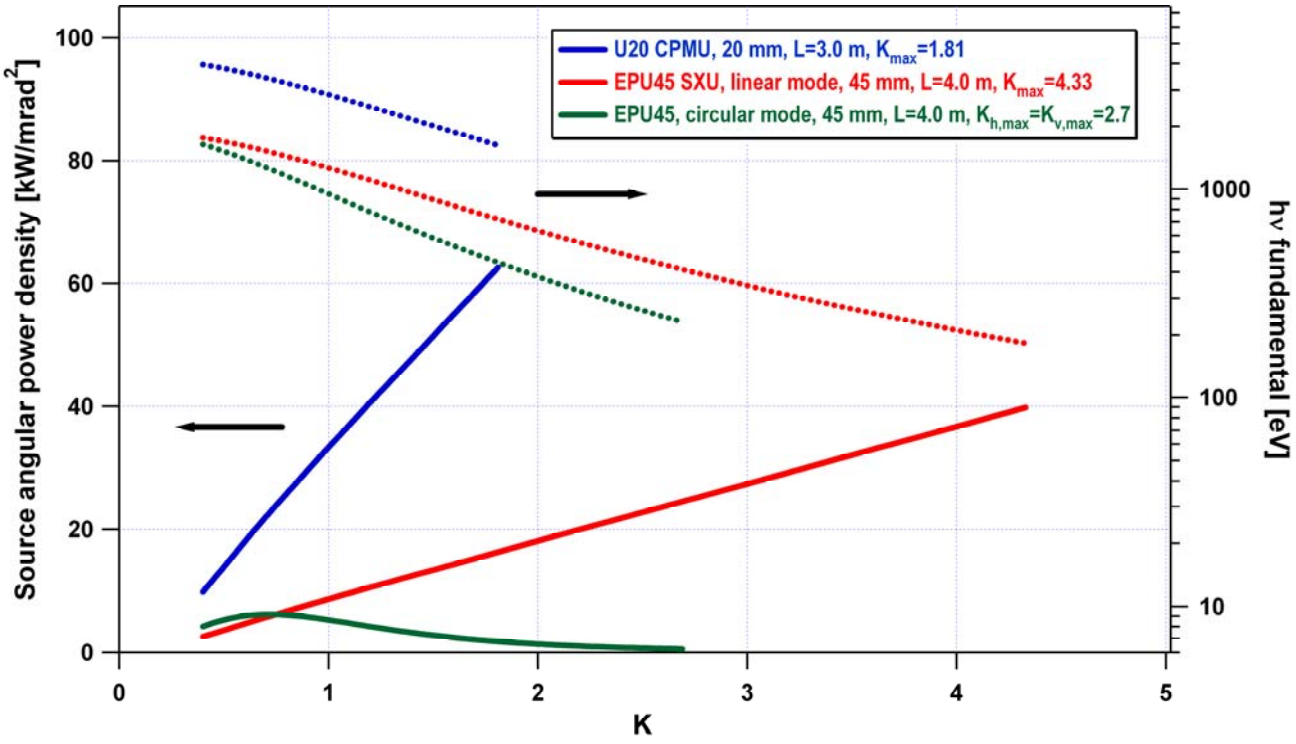

Figure 5.3.4 Angular power density (left-hand axis) and fundamental output energy (right-hand axis) of the baseline NSLS-II undulators as a function of the undulator parameter, K.

5.3.5 Photon Beam Size

The 1-σ effective photon beam size of the NSLS-II undulators is shown in Figure 5.3.5 as a function of photon energy. The lowest, straight (on a log-log graph) gray lines show the "natural" photon beam size, which is the size of a diffraction-limited photon beam for a zero emittance (and therefore zero size) electron beam. This diffraction-limited, "natural" photon beam size σ_{photon} is given by

$$\sigma_{photon} = \frac{1}{4\pi}\sqrt{2L\lambda} \quad . \tag{5.1-2}$$

One measure of the effective photon beam size, σ_{eff}, is given by the quadrature sum of the electron ($\sigma_{electron}$) and photon, σ_{photon}, contributions:

$$\sigma_{eff} = \sqrt{\sigma_{electron}^{\ 2} + \sigma_{photon}^{\ 2}} \quad . \tag{5.1-3}$$

The red and blue curves show σ_{eff} for the EPU45 SXU and U20 IVU undulators, respectively, in the vertical and horizontal planes, as labeled. Clearly, the undulator radiation is nearly diffraction-limited in the vertical plane over a wide photon energy range, from the far-infrared to ~2 keV. The deviation of the effective source size from the natural, diffraction-limited value is due to the contribution of the small, but finite, electron beam

size. The effective beam size in the horizontal plane is approximately an order of magnitude greater than the natural, diffraction-limited value at 10 keV, but at 10 eV and below is nearly diffraction-limited.

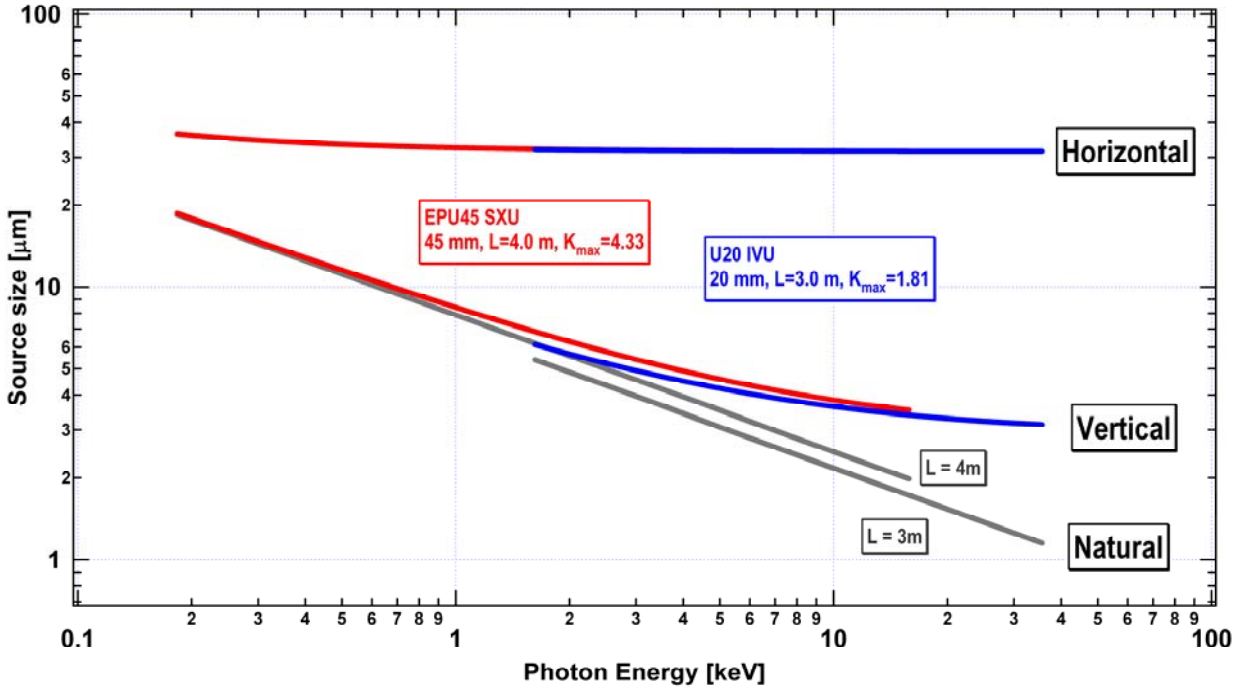

Figure 5.3.5 Photon beam source size in the horizontal and vertical directions for the NSLS-II undulators. The straight (gray) lines represent the corresponding diffraction-limited values (i.e., the zero electron beam emittance limit).

5.3.6 Photon Beam Angular Divergence

The 1-σ effective photon beam angular divergence of the NSLS-II undulators is shown in Figure 5.3.6 as a function of photon energy. The lowest, straight (on a log-log graph) gray lines show the "natural" photon beam angular divergence, which is the angular divergence of a diffraction-limited photon beam for a zero-emittance (and therefore zero angular divergence) electron beam. The diffraction-limited, "natural" photon beam angular divergence σ'_{photon} is given by

$$\sigma'_{photon} = \sqrt{\frac{\lambda}{2L}} \tag{5.1-4}$$

and the effective photon beam angular divergence σ'_{eff} is again given by the quadrature sum of the electron ($\sigma'_{electron}$) and photon (σ'_{photon}) contributions:

$$\sigma'_{eff} = \sqrt{\sigma'^{\,2}_{electron} + \sigma'^{\,2}_{photon}} \quad . \tag{5.1-5}$$

The red and blue curves in Figure 5.3.6 show σ'_{eff} for the EPU45 SXU and U20 IVU undulators, respectively, in the vertical and horizontal planes, as labeled. As in Figure 5.3.5 for beam size, Figure 5.3.6 shows that the angular divergence of the undulator radiation from NSLS-II undulators is nearly diffraction-limited in the vertical plane, and only somewhat less so in the horizontal plane, over the wide photon energy range from the far-infrared to ~2 keV. The deviation of the effective source angular divergence from the natural, diffraction-limited, value is due in part to the contribution of the tiny, but finite, beam angular divergence of the NSLS-II electron beam. In the horizontal plane, the effective beam angular divergence is

approximately a factor of 2 or 3 greater than the natural, diffraction-limited, value at 10 keV, but is nearly diffraction-limited at 10eV.

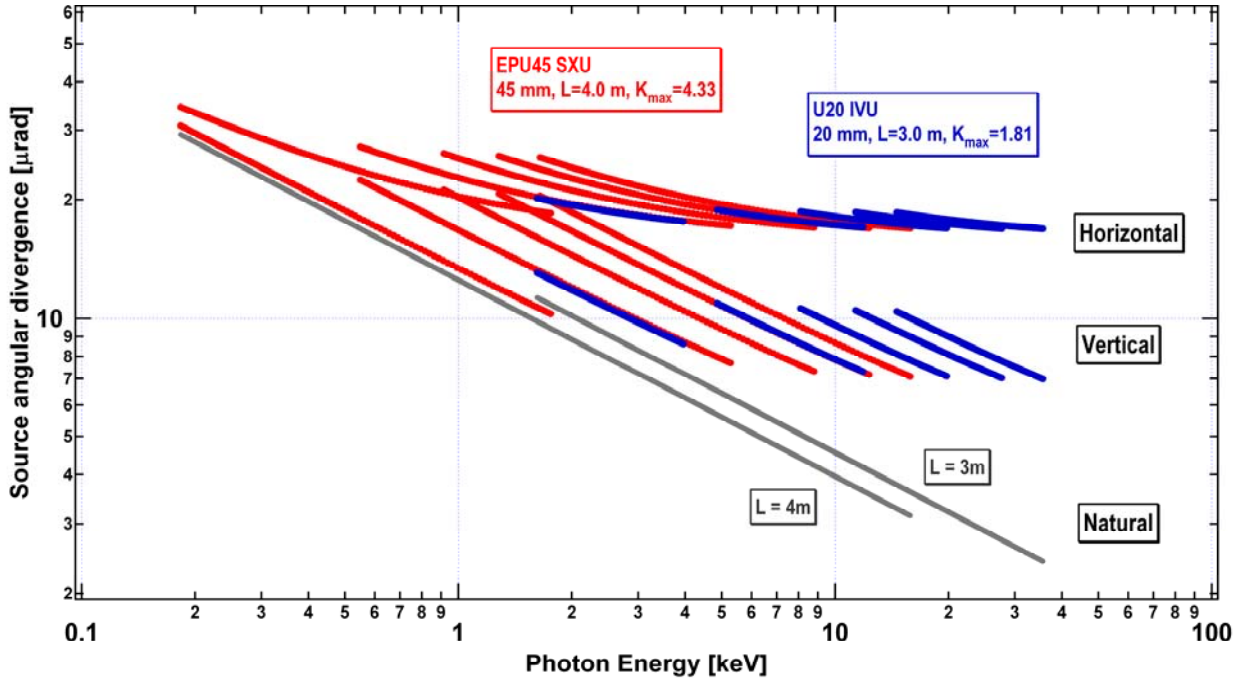

Figure 5.3.6 The angular divergence in the horizontal and vertical directions of the photon beam for the NSLS-II undulators. The straight (gray) lines represent the corresponding diffraction-limited values (i.e., the zero electron beam emittance limit).

The angular divergence is also limited by the finite energy spread of the electron beam. A noteworthy feature of Figure 5.3.6 is that the angular divergence of the various harmonics for a given undulator is approximately equal to that of the fundamental of that undulator. That is, it appears, empirically, that the angular divergence of undulator harmonic n is given by

$$\sigma_n' \approx \sqrt{\frac{\lambda_1}{2L}} \tag{5.1-6}$$

for n = 1, 3, 5, 7, or 9, in both the horizontal and vertical planes. This value is $\sqrt{\lambda_1}/\lambda_n = \sqrt{n}$ times larger than the zero-emittance angular divergence.

Thus, the limiting factor governing the vertical angular spread of the n>1 harmonics of NSLS-II undulators is the finite energy spread of the electron beam, which for the fully-damped case is $\delta E/E \sim 0.001$. This effect is stronger for the hard x-ray undulator (U20) than for the soft x-ray undulator (EPU45), but clearly affects both.

5.4 Infrared

The intrinsic infrared brightness of most synchrotron storage ring sources is determined entirely by the circulating beam current. This is certainly the case for the low emittance electron beam of the NSLS-II storage ring, and the goal of 500 mA beam current is very attractive from the standpoint of infrared performance. The ring is designed for an extremely stable beam; an important characteristic for the standard

rapid-scan interferometric techniques employed in most infrared spectroscopies. But designing an optical extraction configuration that preserves the brightness, while meeting mechanical and accelerator design constraints, can be quite difficult. Typically, the large angular collection needed to achieve an acceptable performance involves nonstandard construction geometries for the dipole chambers. These, in turn, can affect the beam impedance and lead to instabilities. A careful impedance analysis will be integral to the design of any dipole chamber intended for extracting infrared radiation, and efforts are underway to treat this issue quantitatively.

It is well known that dipole (bending) magnets produce infrared radiation by two distinct mechanisms: the conventional synchrotron radiation (bending magnet radiation) is produced in the body of the magnet, whereas edge radiation is produced as electrons enter or exit a dipole's magnetic field [5.4.1]. Infrared beamlines have been built to utilize one or the other of these source types, and sometimes both. For reasons outlined later in this section, we plan to meet most of the source requirements using bending magnet radiation, but also plan to collect and extract edge radiation. The beamline design and performance analysis described in Chapter 11 will take both source types into account.

5.4.1 Bending Magnet Source

The collection efficiency for conventional dipole bend radiation is determined by the natural opening angle for synchrotron radiation in the long wavelength limit. For a wavelength λ and bend radius ρ, the RMS half-angle is defined as:

$$\theta_\lambda = \left(\frac{3}{4\pi} \frac{\lambda}{\rho} \right)^{1/3} . \qquad (5.4\text{-}1)$$

From this expression we see that the large bending radius (ρ ~25 m) of NSLS-II dipoles causes the infrared to be emitted into angles 2.35 times smaller than for the existing NSLS VUV/IR ring (ρ ~1.9 m). Thus, the performance for NSLS-II with 38 mrad extraction would be identical to a 90 mrad extraction from the VUV/IR ring. A study of the NSLS-II dipole design indicates that a horizontal extraction of 50 mrad is achievable (plus an additional 5 mrad on the "negative side", useful for collecting edge radiation). This is based on an infrared extraction where the second dipole in a DBA cell is used in order to stay clear of any potential insertion device beamline (Figure 5.4.1). The large bending radius makes extraction increasingly difficult as one continues toward the second half of a dipole, giving rise to the 50 mrad horizontal collection limit.

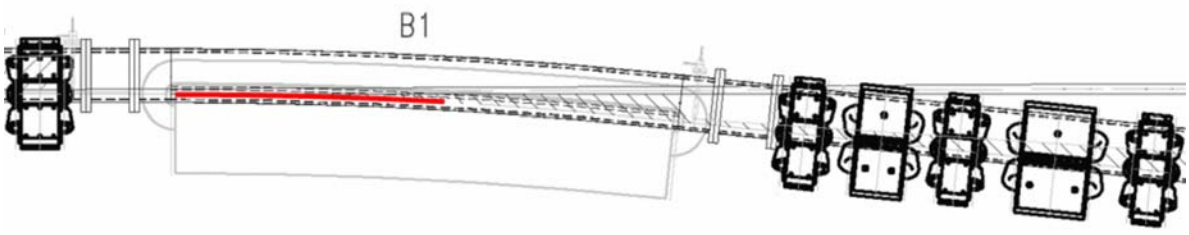

Figure 5.4.1 Drawing of the second dipole magnet in the NSLS-II DBA 30 lattice. Red line indicates the candidate IR source orbit segment. Approximately 50 mrad of horizontal collection appears feasible, including the zero degree segment for edge radiation.

The standard NSLS-II dipole bending magnets allow a vertical chamber dimension of ~25 mm and represent another constraint for infrared, limiting the vertical collection to approximately 16 mrad (the value varies from 12 mrad up to 20 mrad due to the large source depth). While this is adequate for mid-infrared spectroscopy as used in chemical imaging, it limits the performance for far-infrared spectroscopy due to the relatively large angles into which this radiation is emitted. Therefore, we are planning for a second dipole

magnet design for use on far-infrared ports. This dipole would have a ~60 mm (or larger) gap and would accept a dipole chamber providing an average 32 mrad of vertical collection (and potentially up to 48 mrad with a larger dipole gap). The need for such a large aperture port becomes even more apparent when one considers the shielding effects of a conducting dipole vacuum chamber. The subject has been treated most thoroughly by Bosch [5.4.2] who confirmed (theoretically) that bending magnet radiation is suppressed for wavelengths greater than an effective cutoff value given by $\lambda_c=(h^3/\rho)^{1/2}$ where h is the chamber height and ρ is the bending radius. The large bending radius of NSLS-II, combined with a standard chamber height of 25 mm, results in a cutoff wavelength of 800 μm, effectively removing the portion of the THz spectral range most important for magnetospectroscopy. This provides another compelling reason for a larger dipole chamber and 60 mm gap dipole magnet. Indeed, increasing the dipole gap an additional 30 mm (to accept a 75 mm vertical height chamber) would shift the cutoff wavelength to beyond 4 mm. In all cases, the detailed dipole chamber design and transitions will require careful study in terms of electron beam impedance and potential instabilities. Our initial impedance analysis for a 50 mm high chamber appears promising and suggests that an even larger (75 mm) chamber would be feasible. However, more detailed calculations will be needed for actual chamber mechanical designs to ensure no instability problems will arise.

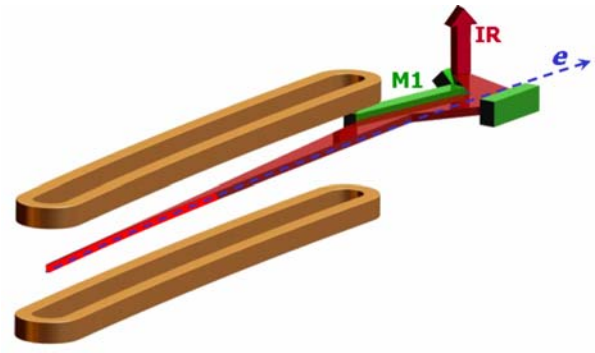

Figure 5.4.2 NSLS-II Infrared Dipole Radiation Extraction. The bright red segment marks the electron beam segment serving as an infrared source. The radiation is collected by a long mirror (M1) and reflected out of the dipole chamber by a second and third mirror combination.

The extraction arrangement for NSLS-II is proposed to have the 1st mirror optic integrated into the dipole chamber construction. The metal mirror can be made to be electrically contiguous with the chamber wall to minimize impedance effects. The oblique angle of incidence and soft x-ray spectrum from the large NSLS-II dipole bending radius limits the local power load on this optic to well under 1 kW/cm^2, such that a special slot or cooling mask may not be required (Figure 5.4.2). Finite element analysis will be performed on candidate mirror materials (e.g., aluminum or copper) to confirm that this heat load can be directly managed without significant optical distortion of the surface. Initial studies of the required optical figure for this 1st mirror suggest that a simple toroidal shape will suffice, allowing conventional diamond turning to be used in its construction (Figure 5.4.3). The remaining optical elements can be either conventional aluminized glass or diamond-turned aluminum to meet specific optical design requirements.

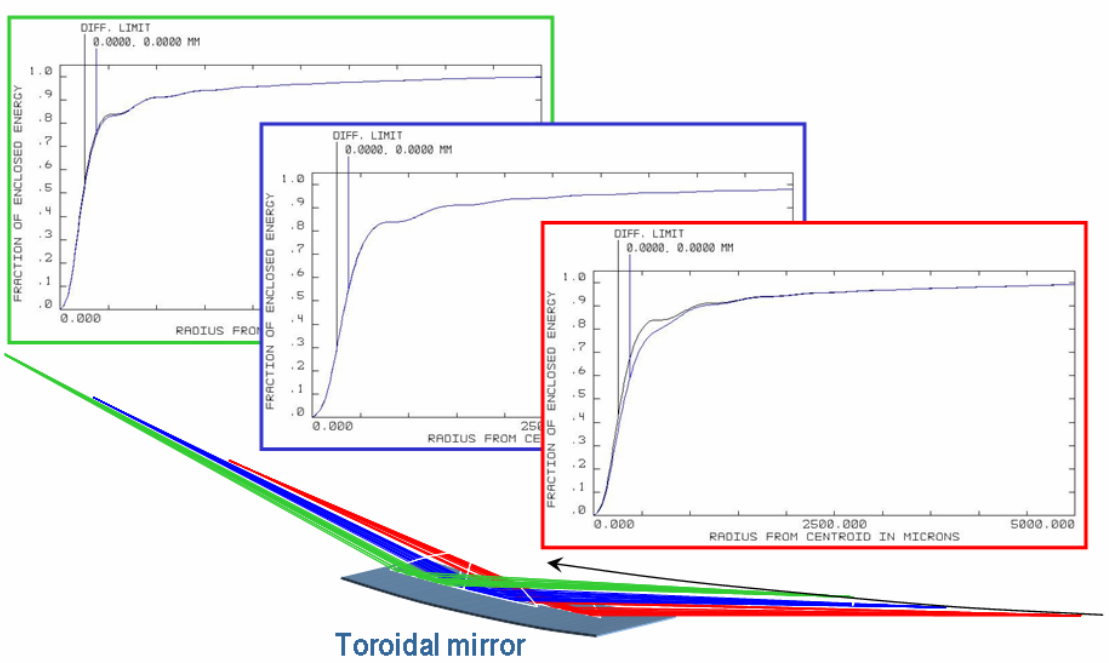

Figure 5.4.3 Extraction Optical Performance. ZEMAX optical analysis for a toroidal first mirror optic when used to focus a dipole bend/arc source at a wavelength of 6 μm (mid-infrared). Near diffraction limited performance is achieved along the entire source length.

A detailed performance comparison for these NSLS-II dipoles and the existing VUV/IR ring dipoles can be made using the standard expressions for dipole synchrotron radiation in the low frequency limit. The flux calculations can be compared to results from other synchrotron radiation source codes such as SPECTRA [5.4.3] or SRW [5.4.4] to check for consistency. Though some of these calculations are for the photon flux, they can be used for comparing brightness whenever the source's physical dimensions are smaller than the diffraction limit (the case for all IR wavelengths on NSLS-II, and IR wavelengths longer than 10 microns for the existing NSLS VUV/IR ring). We find that all three calculations agree to within 10% for the intrinsic flux of dipole radiation when multiparticle coherence and chamber shielding effects are ignored. Note that one can convert from units of ph/s/0.1%BW to watts per wavenumber, multiplying by 2×10^{-20}. Calculation results are shown in the Figures 5.4.4 and 5.4.5, along with a calculation for an existing port on the VUV/IR ring, indicating that NSLS-II can serve as a highly competitive, and indeed, world-leading, storage ring source for infrared.

Details of these calculation results show that an extraction based on a conventional NSLS-II dipole (average of 16 mrad vertical and 50 mrad horizontal) will be sufficient for mid-infrared spectroscopy, including microprobes and imaging. We envision two options for such mid-infrared extractions. In one option, the beam is divided horizontally to simultaneously serve two or three mid-infrared microprobe end stations. The three collections (in order of entering the dipole) would be (H×V) 15×12 mrad, 15×16 mrad, and 20×20 mrad. The varying vertical aperture is due to the changing distance between the first collecting mirror and the collected source segment as a function of horizontal position (angle). The performance for any of these extractions exceeds the present performance of the NSLS VUV/IR ring over most of the mid-infrared. Only at the long wavelength (low frequency) end of this spectral range are the three extractions distinguishable, with the 20×20 mrad outperforming the other two. But it should be noted that the initial 15×12 mrad collection also includes the zero-degree component, giving this the added feature of edge radiation (not included in the brightness calculation). In the other option, the entire horizontal swath is fed into a single microspectrometer end station based on a focal plane array detector for large area imaging, as

described in Chapter 11. The detailed optical system for matching the source to the instrument will be the subject of further research.

In the far-infrared, the brightness for a conventional dipole (16 mrad average vertical extraction) continues to fall away from the ideal value and below the present performance for the NSLS VUV/IR by a factor of 5 at 25 cm^{-1} (400 μm wavelength). The degradation below 10 cm^{-1} becomes even more severe when the shielding effect of the 25 mm high dipole chamber is taken into account. Note that the shielding effect for dipole radiation is a complex subject, and we have taken it into account using a simplified approach. In this approach, it is assumed that radiation unable to couple into a propagating waveguide mode of the chamber is completely lost, and is roughly equivalent to truncating the effective near-field source size to a dimension equal to the chamber height (see [5.4.2], condition 2 for strong shielding). A large-gap dipole enables greater vertical collection efficiency and also shifts the shielding cutoff to lower frequencies. This is illustrated in the brightness calculations of Figure 5.4.5, which includes curves for the standard NSLS-II dipole extraction (50×16 mrad) plus two candidate large-gap dipole extractions (50×32 mrad based on a 50 mm high dipole chamber, and 50×48 mrad based on a 75 mm high dipole chamber). Also shown is the existing performance for the NSLS VUV/IR ring's 90×90 mrad ports plus the very large port beamline at the UVSOR facility (Okazaki, Japan) that represents the most competitive far-infrared beamline elsewhere in the world. (Note: This does not take into account the coherent THz synchrotron radiation mode of operation developed at BESSY and proposed for CIRCE by the ALS/Lawrence Berkeley Lab.) The 50×48 mrad configuration would maintain the NSLS lead in the area of incoherent THz synchrotron radiation, and provide excellent ports for studying aspects of coherent synchrotron radiation production, a subject of great interest for future source development. Any of these ports would offer excellent mid-infrared performance.

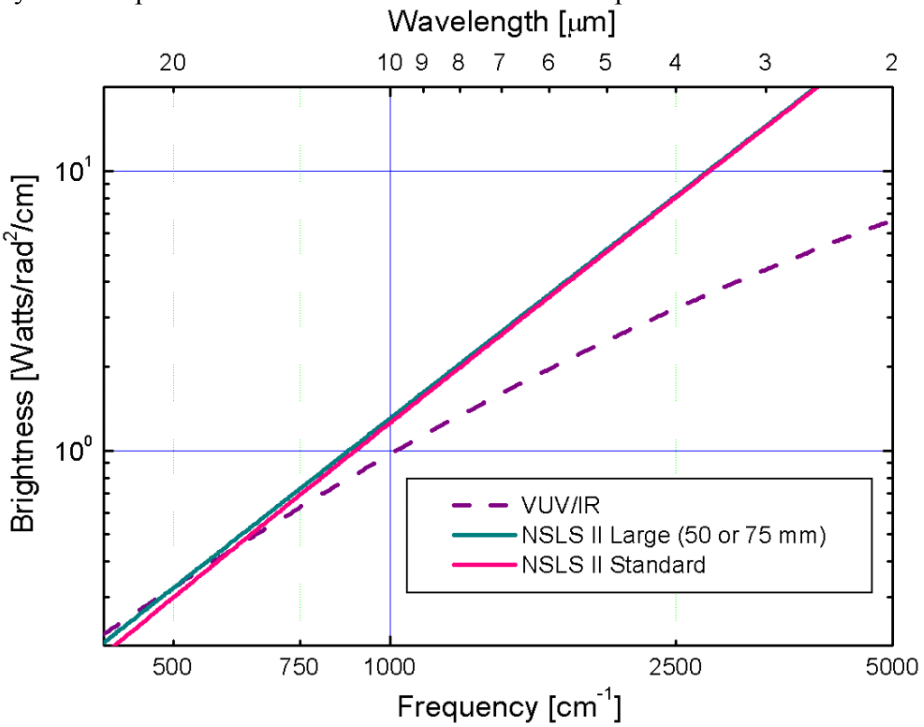

Figure 5.4.4 Calculated NSLS-II brightness for the mid-infrared spectral range, comparing the existing VUV/IR ring with the two proposed for NSLS-II extractions. Note that the lower emittance of NSLS-II leads to brightness improvements over much of this spectral range and that the standard dipole chamber height of 25 mm is sufficient for this spectral range.

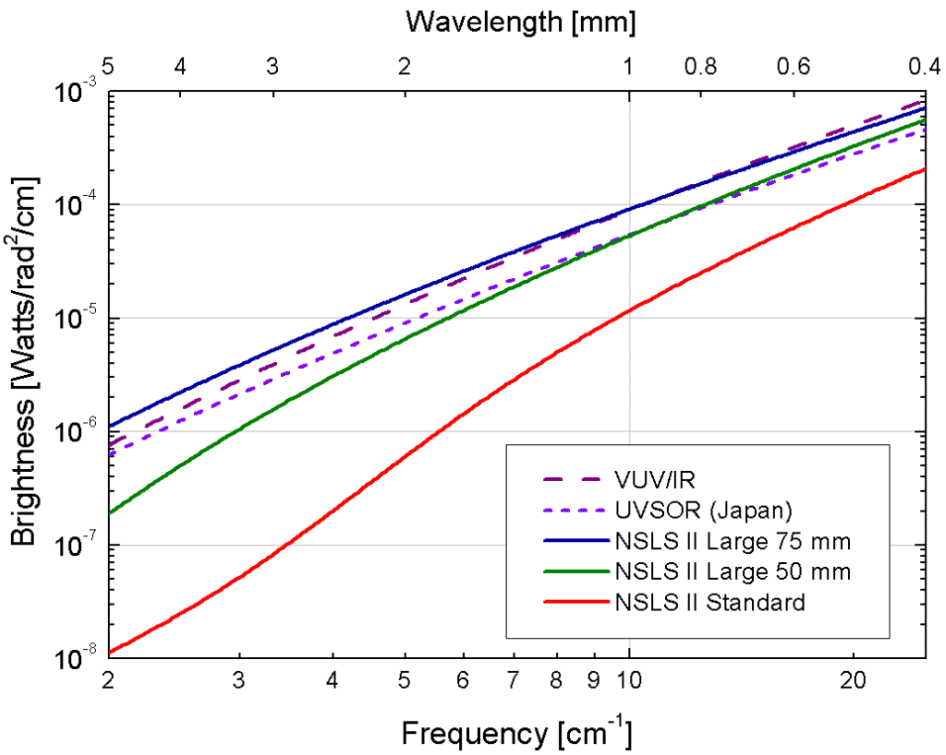

Figure 5.4.5 Calculated NSLS-II brightness for the very far-infrared spectral range, comparing the existing VUV/IR ring with three collection geometries for NSLS-II having vertical dipole chamber heights as shown, plus a high-performance beamline at UVSOR. The cutoff effect of the standard-gap dipole chamber and 16 mrad collection can be clearly seen for wavelengths greater than 1 mm.

5.4.2 Dipole Edge Source

The proposed infrared extraction geometry allows for collection of the zero-degree segment from the dipole (in line with the upstream straight section), including ~5 mrad on the opposite side. This will allow for the extraction of dipole edge radiation [5.4.1]. Dipole edge radiation has characteristics similar to transition or diffraction radiation, e.g., radial polarization. In contrast to bending magnet radiation, the far-field angular distribution for edge radiation is contained mostly within a cone of angle $\theta = 1/\gamma$. This implies an effective source size of $\lambda\gamma$ and a very long formation length of $\lambda\gamma^2$ such that computations designed exclusively for the far-field are no longer accurate. An added complication stems from the fact that dipole edges typically occur in pairs, leading to a ring-like interference pattern that depends on wavelength. The SRW code [5.4.4] includes near-field terms suitable for calculating edge radiation in the ideal case where the ring chamber has no shielding effect on the radiation. An example result from SRW is shown in Figure 5.4.6, and illustrates both edge radiation (ring-like pattern at right) and bend radiation (broad smear extending to left). The actual projection of the beam onto the first mirror optic will be stretched horizontally about a factor of 3 compared to these views (due to the 75° angle of incidence for the radiation).

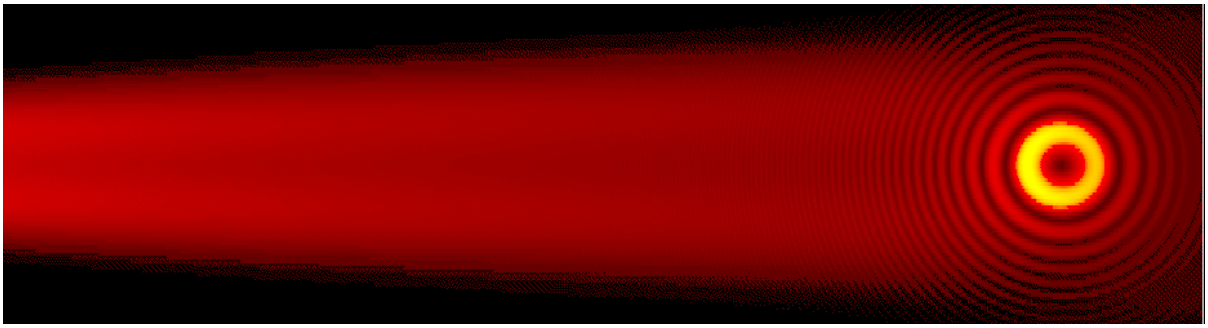

Figure 5.4.6 SRW analysis for 55 mrad (-5 to +50) horizontal and 12 to 20 mrad vertical collection of 6 μm wavelength infrared radiation produced in the leading section of an NSLS-II dipole bending magnet. The ring pattern is due to interference from the back edge of the previous dipole, located 5.6 meters upstream (distance between dipole edges in a DBA cell). The broad stripe of radiation extending to the left is the conventional bending magnet radiation.

Though a few infrared beamlines based on edge radiation exist (e.g., at ANKA/Karlsruhe, SRC/ Wisconsin, and ESRF/Grenoble), the detailed performance at long wavelengths has not been formally demonstrated. There are two reasons to be concerned about the long wavelength performance. First, the radius of the first constructive interference ring moves outward with increasing wavelength such that the collection through a finite aperture will suffer. Second, the large effective source size is expected to cause a shielding (waveguide) cutoff when the wavelength exceeds h^2/R, where h is the chamber height and R is the distance from the source to the collecting aperture [5.4.2]. Our extraction aperture would be situated approximately 3 meters away from the source point and, with a nominal chamber height of 25 mm, the cutoff would begin at a wavelength of ~200 μm such that a significant portion of the very far-infrared would be lost. Edge radiation also introduces complications for mid-infrared microspectroscopy and imaging due to its radial polarization. The source itself is point-like, making it less suitable for illuminating large area focal plane array detectors that are expected to become the standard approach for delivering large area, high-resolution images. For these reasons, our infrared extraction will be based primarily on conventional bending magnet radiation, but we will have the opportunity to exploit the unique characteristics of edge radiation where beneficial.

References

[5.4.1] R.A. Bosch et al., *Rev. Sci. Instr.* **67,** 3346 (1996); Proceedings of the Ninth Nat'l Conf. on Synch. Rad. Instrum., Argonne, IL, (1995.)
[5.4.2] R.A. Bosch, *Nucl. Instrum. & Meth. Phys. Res.* A **482**, 789 (2002).
[5.4.3] T. Tanaka and H. Kitamura, *J. Synch. Rad.* **8**, 1221 (2001)
[5.4.4] O. Chubar and P. Elleaume, *Proc. of the EPAC98 Conference*, 1177 (1998).
[5.4.5] G.L. Carr, *Vibrational Spectroscopy* **19**, 53 (1999); R.P.S.M. Lobo, et al., *Rev. Sci. Instrum.* **73**, 1 (2002).

5.5 Conceptual Magnetic Designs for the IDs

In Section 5.1 we specified the types of insertion devices that are needed to meet user requirements and to achieve the unprecedented brightness goals of NSLS-II. We presented the optical performance and spectral characteristics of these IDs. They are based on proven designs, and in some cases push the state of the art in what we believe to be rational and realizable extensions of existing technology. In this section we present conceptual magnetic designs of the various ID types that will meet the performance requirements and constraints. We also identify and describe the R&D and prototyping needed to verify each design concept, to resolve any unknowns, and to test advanced concepts for future upgrade paths. We describe novel mechanical concepts that may simplify ID designs and/or improve their performance. Finally, we describe magnetic measurement systems that will be developed to verify and optimize ID performance.

Section 5.5.1 deals with the damping wiggler, which is also used as a broadband source.

Section 5.5.5 discusses tunable, planar, hard x-ray sources, specifically the mini-gap, in-vacuum undulator (IVU) as a baseline device, and its most recent evolution, the cryo-permanent magnet undulator (CPMU).

Section 5.5.3 describes variable polarization devices for soft x-rays and vacuum ultra-violet. The baseline design is an Apple-II type machine. An alternative HiSOR-type design was considered.

Section 5.5.4 addresses using a permanent magnet three-pole wiggler (3PW) to meet the needs of the current users of hard X-ray bending magnets at NSLS.

In Section 5.6, the IDs to be installed or considered in later stages of beamline construction will be discussed. Those devices are the superconducting wigglers (both low- and high-temperature types), superconducting undulator, quasi-periodic undulator, and revolver-type undulator. Also discussed in Section 5.6 is the development of an insertion device Magnetic Measurement Facility (MMF).

5.5.1 Damping Wigglers

Earlier we defined two key parameters of the damping wigglers (DWs): the operating peak field of 1.8 T and an eventual total length of 56 m. The peak field value was chosen to be high enough to radiate sufficient power for adequate emittance damping, but not so high as to create excessive energy spread. The DWs are also useful as high-flux, high-brightness broadband sources in the hard x-ray range.

The initial installed length of DWs will be 21 m, composed of six wigglers, each 3.5 m long. A third key design parameter is the minimum magnetic gap. The estimated vertical stay-clear aperture at ±3.5 m from the center of long straight section is 9.5 mm. Allowing for beamtube wall thickness of 1 mm, plus 0.5 mm clearance between the beamtube and the magnet poles, we obtain a minimum magnetic gap of 12.5 mm. From empirical design formulas developed by Elleaume for various planar undulator (wiggler) technologies [5.7.15], we find that 1.8 T peak field can be produced at that gap by a conventional PM-hybrid wiggler with a period of 90 mm, using high-field NdFeB magnets (Br = 1.2 T) and vanadium permendur poles. However, the total radiated power from such a wiggler is less than that by the device with ideal sinusoidal field due to longitudinal higher harmonics contents. Therefore, special care is needed to optimize the field profile. Unlike users of undulator radiation, wiggler users expect a broad, dipole-like spectrum. Therefore, minimizing phase errors is not important. Shimming of DWs is concerned mainly with trajectory straightness and multipoles. In fact, gap taper, or variation in pole periodicity are sometimes introduced in wigglers intentionally to spoil coherence and to smooth the spectrum.

DWs must meet the same integrated dipole and multipole error specifications imposed on all IDs. However, since they will operate at fixed gap, these errors can be shimmed out more easily than in variable-

gap IDs, without concern about gap-dependence. The next sections discuss some additional design considerations for DWs.

5.5.1.1 Dynamic Field Integral

The integrated field seen by sinusoidally wiggling electrons [5.5.1.1] is

$$\int B_y ds \approx \frac{-L}{2k^2 B\rho} B_y(x_i) \frac{dB_y(x_i)}{dx}, \quad (5.5.1\text{-}1)$$

where L is the device length, k_w is the 2ρ/period length, ρ is the radius of curvature of the trajectory, and x_i is the horizontal displacement of the electron. This is called dynamic field integral, and it scales as ID period squared and as the derivative of the transverse field roll-off. An important aspect of optimization of long-period wiggler magnetics is how to determine the necessary transverse pole width to minimize the effect of the dynamic field integral effect while minimizing attractive force, which is proportional to the magnet area, and keeping the cost as low as possible. Beam tracking reveals the detrimental effect of this integral on the beam dynamics. However, ordinary magnetic measurement method in straight line is incapable of measuring this effect. Therefore, careful modeling effort is required for long period device.

5.5.1.2 Attractive Force and Size/Cost Challenges of the Damping Wigglers

For NSLS-II, the damping wigglers will be used as a broadband source. The design calls for 7 m of damping wiggler in an 8 m straight. In reality, it is easier to combine two 3.5 m devices. The approximate attractive force of a planar device is given as follows:

$$F_{ID} \approx \frac{B_y^2 WL}{4\mu_0}, \quad (5.5.1\text{-}2)$$

where W is the horizontal width of poles or magnets, L is the total length of the device, and μ_0 is the permeability of the vacuum. With W = 80 mm and B_{oy} = 1.8 T, the attractive force per meter is about 60 kN. A variable-gap device must have a structure that is rigid enough not to create intolerable multipole components due to defection. As this is an out-of-vacuum device, many different designs have worked properly in storage rings.

Wigglers of this type, from 2 to 4 meters in length, have been designed and build to specification by industry for many synchrotron light sources. The mechanical structures to support and control the gap of these wigglers are generally massive and expensive for variable gap device. However, NSLS-II DW is designed to operate at a fixed gap, no strict parallelness of magnet arrays is required at other gap positions. On the other hand, the available cross section of a device for NSLS-II is substantially smaller than other equivalent facility due to the lower beam height (1.0 m compared to 1.2-1.4 m for most of facilities in the world) and due to the need to have extra space in the tunnel for emergency evacuation. A detailed design study will consider alternative magnet configurations that could lessen the need for these massive structures while maintaining the structural rigidity. The goal of this project is to design a magnet configuration that can utilize a relatively compact, lower-cost magnet support system that ultimately could reduce the cost of these wigglers significantly.

5.5.1.3 Non-Sinusoidal Field Effect

Another issue for long-period undulators is the deviation from sinusoidal field, which effectively reduces the deflection parameter. (This is not an issue for wigglers, where the critical energy depends on peak field only.) We examine a hybrid undulator with side magnets and permendur poles with the parameters shown in Table 5.5.1.1.

Table 5.5.1.1 U90 Wiggler Parameters.

Period length [mm]	90
Nominal peak field [T]	1.8
Remanent field (B_r) [T]	1.20
Gap [mm]	12.5
Magnet horizontal size [mm]	140
Magnet vertical size [mm]	95
Main Pole horizontal size [mm]	80
Main Pole vertical size [mm]	75
Air gap [mm]	0.1
Chamfer (magnet) [mm]	2.0
Chamfer (pole) [mm]	1.5
Corner cut (magnet) [mm]	3.0
Gap offset (magnet) [mm]	0.25

By varying the pole thickness while keeping fixed the total period length, we have calculated the peak magnetic field (induction) and effective K_y, as shown in Table 5.5.1.2. When the pole thickness is reduced from 21 to 19 mm, the peak field increases from 1.80 to 1.85 T and effective K_y decreases from 15.2 to 15.1. This indicates that the field deviates too much from the sinusoidal form.

Table 5.5.1.2 Comparison of Peak K_y and Effective K_y with Varying Pole Width (Period Length=90 mm)

Pole Thickness (mm)	Peak Field (T)	Peak Ky	Effective Ky
19	1.85	15.6	15.1
20	1.83	15.4	15.2
21	1.80	15.2	15.2
22	1.75	14.7	15.1

The effective K value should be close to the peak K value of a sinusoidal wave of peak amplitude of 1.8T to obtain equal amount of radiated power assumed in emittance reduction calculation. The following quantity was numerically calculated over one period to compare the value with sinusoidal field.

$$P_{per} = \int_{L}^{-L} B_y^2 ds \qquad (5.5.1\text{-}3)$$

where L=period length /2. With pole thickness of 21 mm, the effective field appears to be closest to that of ideal sinusoidal field. $P_{per} = 1.01\ P_{per}$ (ideal).

5.5.1.4 Baseline Damping Wiggler Design

A hybrid structure with side magnets and permendur poles has been chosen for the NSLS-II device. Soft iron poles are significantly cheaper than permendur but produce slightly lower field. Figure 5.5.1.1 is an isometric rendering of the W90 magnet arrays by Radia. The side magnets shown in magenta have identical size; two different sized magnets are shown in green. Pieces in yellow represent permendur poles. Figure 5.5.1.2 shows the end view of the array.

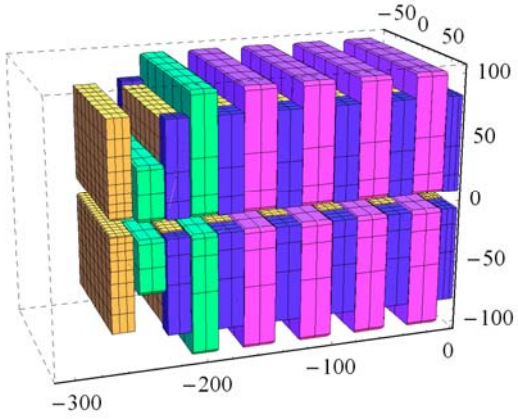

Figure 5.5.1.1 Magnet arrays of W90. Only the first few periods are shown, for clarity. Units are millimeters.

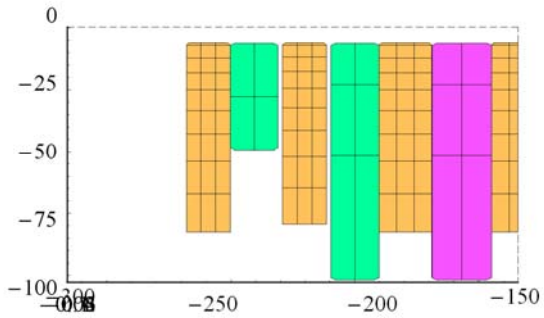

Figure 5.5.1.2 End view of W90.

The field and trajectory computed from the model are plotted in Figure 5.5.1.3, for a gap of 12.5 mm. The trajectory is calculated by a particle-tracking Runge-Kutta routine. The particle is launched with zero offset and angle (x = 0, x' = 0), and its position and angle are calculated every 2.5 mm (36 points per period). The amount of change in the first integral can be easily compensated by external coils.

a

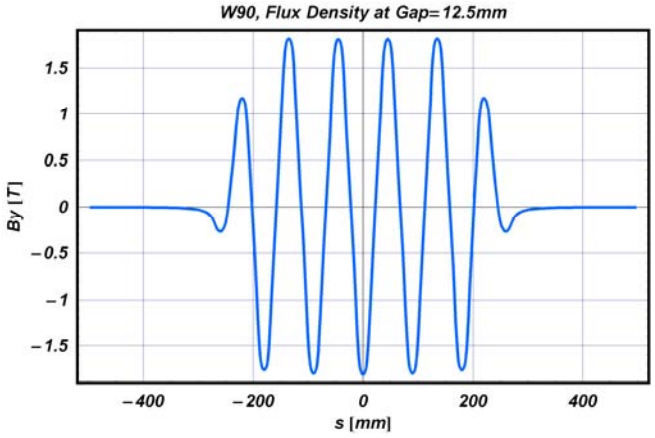

Figure 5.5.1.3 Field, angle, and trajectory plots for the five-period model of W90.

a) Vertical magnetic flux density at a gap of 12.5 mm.

b

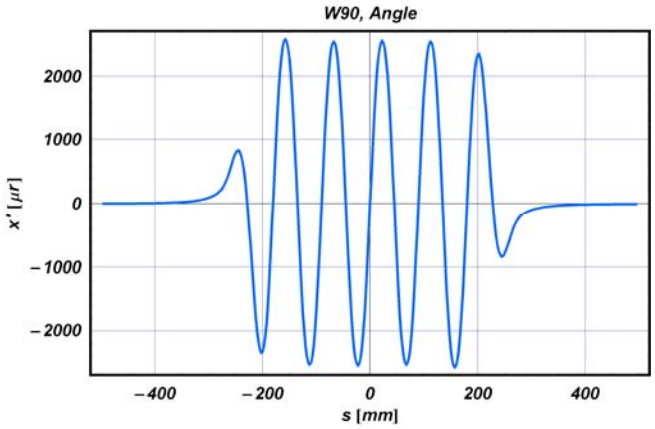

b) Horizontal angle at a gap of 12.5 mm.

c

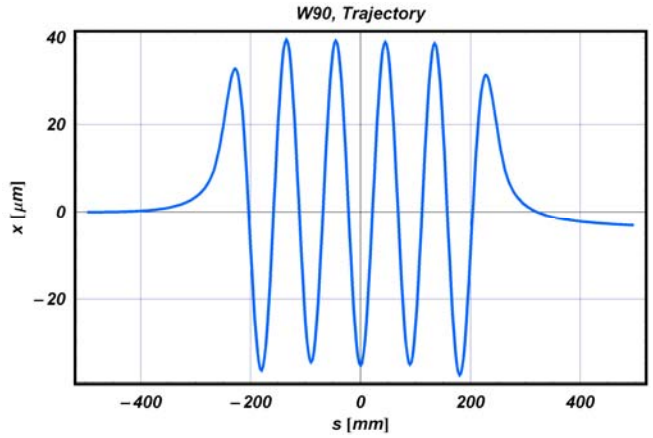

c) Horizontal trajectory at a gap of 12.5 mm.

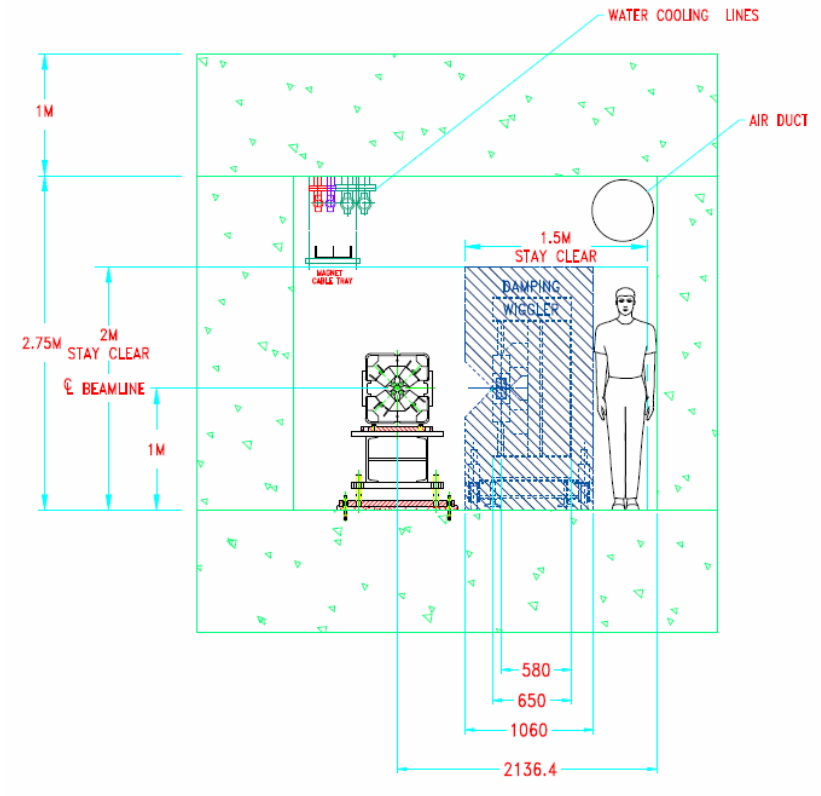

Figure 5.5.1.4 Available cross section of NSLS-II DW.

There is one challenging requirement for all NSLS-II insertion devices. That is an unusually restricted transverse cross section available for the devices. Firstly, the NSLS-II beam height is only 1.0 m compared to 1.4 m at many U.S. facilities and 1.2 m at some European and Japanese facilities. Secondly, the horizontal size is limited due to safety requirement which demand certain space in the tunnel during device transport. The external dimensions of the NSLS-II DW must conform to the envelope shown in Figure 5.5.1.4. Preliminary FEA analysis with 63 kN/m attractive force was carried out by STI Optronics, Inc. The result is shown in Figure 5.5.1.5, where the units for transition are shown in inches. These deformation translates approximately 3.9 mrad of roll angle for each strongback, which can be compensated for operating gap.

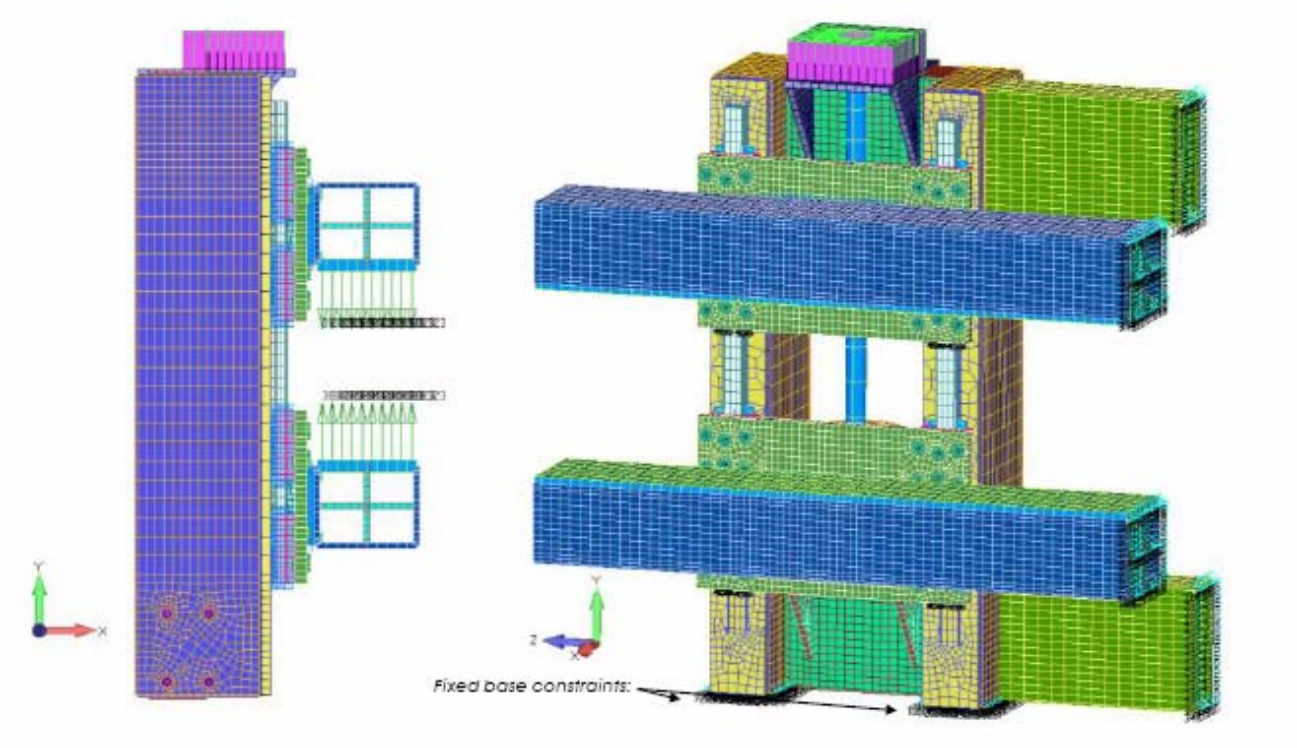

Figure 5.5.1.5 FEA analysis model

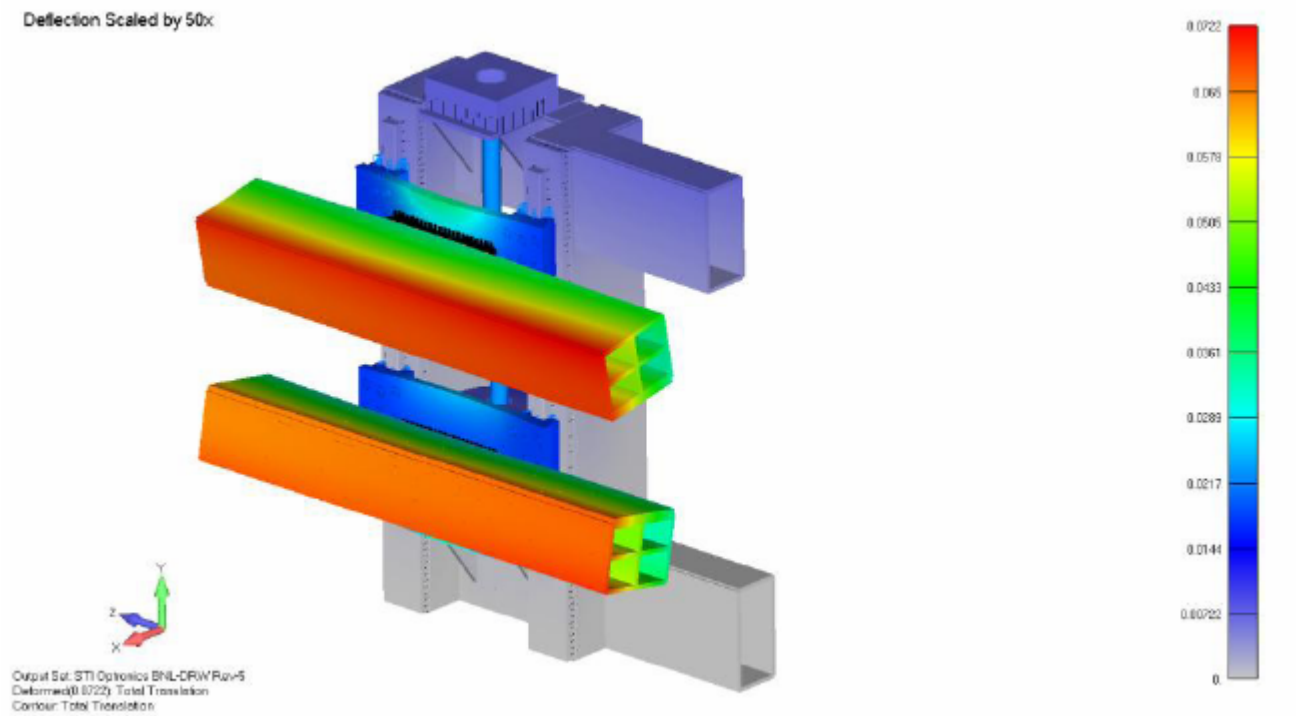

Figure 5.5.1.6 Displacement plot

5.5.1.5 R&D Elements for DW Development

Superconducting devices, especially HTS versions, can be considered as an alternative choice for DWs. However, unlike user devices, these DWs are an integral part of the light source lattice and any failure would result in the degradation of emittance, which affects all the users in the facility. Therefore, it is essential to achieve extremely high reliability for the SCWs to be considered as an alternative for PM-based DWs. Extensive reliability studies will be necessary if this option is pursued.

Another subject is a novel gap separation mechanism, which should simplify the mechanical structure of the device. Attractive force for wiggler magnets is much larger than that by an undulator, so conventional structures tend to be very rigid and heavy in order to avoid deflection. As NSLS-II DWs are presumed to be fixed-gap devices, no strict requirement for gap parallelness is required for the open position. One option is the scheme employed at the Source Development Laboratory at BNL, which utilizes inner and outer cages with roller bearings. Other possibilities will be considered.

References

[5.5.1.1] J. Safranek, et al., Nonlinear dynamics in a SPEAR wiggler, *Phys. Rev. ST*, Acc. and Beam, Vol. 5, p.010701 (2002).

5.5.2 Tunable Hard X-ray Sources

A decade ago, the hard x-ray region of the spectrum by undulators could only be covered at high-energy machines, such as ESRF, APS, and SPring-8. The advent of a mini-gap, short-period in-vacuum undulator, dubbed IVUN [5.5.1.1] in 1997 at the National Synchrotron Light Source has had a lasting impact on the design of synchrotron light source facilities all over the world. With the use of mini-gap, short-period undulators, a medium-energy ring (~3 GeV) can now produce tunable hard x-rays between 2 keV and 20 keV. Many years of successful operation of IVUs at SPring-8 [5.5.2.1], NSLS, and, more recently, at SLS and ESRF have demonstrated the reliability of IVUs. The NSLS currently has three IVUs in operation.

A long-standing concern in the ID community has been that the permanent magnets in small-gap IVUs would be gradually demagnetized and degraded by radiation, due to their proximity to the electron beam and exposure to synchrotron radiation. The conservative approach has been to use Sm_2Co_{17} magnets, rather than NdFeB magnets, because its lack of boron ought to make Sm_2Co_{17} more radiation resistant. However, after many years of successful operation at SPring-8, NSLS, and SLS without any signs of demagnetization, NdFeB IVUs with proper magnets having high intrinsic coercivity (H_{cj}) have proven to be quite radiation resistant. The newest high-remanence, high H_{cj} grades of NdFeB (such as NEOMAX AH series), developed for use in hybrid car motors, should be particularly robust and radiation resistant. We have used this high-temperature NdFeB in our most recent IVU and have based our PM ID designs for NSLS-II on this same magnet material.

Curiously, some out-of-vacuum undulators at APS have experienced localized demagnetization, particularly those with smaller aperture vacuum chambers. Detailed simulations and radiation measurements suggest that the main source of the demagnetizing radiation could be the tapered part of the aluminum vacuum chamber itself. Thus, out-of-vacuum IDs, such as the elliptically polarized undulators, may be more vulnerable to demagnetization than IVUs. Another contributing factor may be that the magnet grade used in APS undulators does not have particularly high enough H_{cj} and therefore does not withstand even localized radiation-induced heat.

Advantages of IVUs over fixed-chamber, out-of-vacuum IDs besides performance advantage are 1) that the former can be opened to provide a wide aperture during machine commissioning or beam studies, and 2) the lack of neutron-producing materials at transitions would mitigate magnet demagnetization.

A subject that needs further study is the impedance of the variable-gap IVUs. Earlier in this report, it was shown that the H-shaped space created by the gap space and the chamber forms a waveguide that contributes to transverse impedance. The RF transitions at the extremities of an ID must be properly tapered to reduce the geometric impedance. Modeling and RF measurements of real IVUs will be part of the design effort.

5.5.1 IVU (Baseline Device)

Room-temperature in-vacuum undulators are now considered to be a mature technology. Earlier concerns about demagnetization of permanent NdFeB magnets for IVUs are less of a concern now with proper magnet selection after many years of successful operation at SPring-8, NSLS, and SLS without any signs of demagnetization. The baseline design for a hard x-ray undulator for NSLS-II is based on a short-period linear undulator of the room temperature IVU type. This is the U20 device described in Chapter 5.

5.5.2 CPMU (Future Option)

For the future upgrade option, cryogenic permanent magnet undulator (CPMU) is considered. The enhancement is based on the fact that NdFeB magnet has a negative temperature coefficient of about –0.1%/K at 20°C for the remanent field (B_r), and also –0.5%/K for the intrinsic coercivity (H_{cj}). Therefore, one can expect higher field and higher radiation resistance simply by cooling the magnet array to lower temperature.

However, NdFeB exhibits a spin orientation below somewhere around 150K and its B_r starts decreasing as the temperature goes below this value [5.5.2.3]. An obvious advantage of operating NdFeB at the plateau around 150K (in addition to gaining 11 to 13% higher field), is greatly reduced sensitivity of the field to temperature gradients.

To test the effect of cooling NdFeB undulators, we measured our decommissioned 0.3 m Prototype Small-Gap Undulator in dry ice at –71°C, and demonstrated that the field increased as expected at –0.1%/°C, or about 9% when cooled down by ~90°C. However, this measurement did not reach the plateau in the B_r vs. temperature that is expected at around –120°C. Analysis of the Hall probe data showed no significant increase in phase error, or in trajectory error, except in the end terminations. We also measured a 10-pole 13.5 mm period PM-hybrid prototype in dry ice with similar results.

The SPring-8 and ESRF recently compared warm and cold measurements of a 1 - 2 m long CPMU. They found that while the fields increased as expected, magnetic field errors scaled and tracked with temperature as well. This suggests that a CPMU can be shimmed at room temperature, and it will remain optimized when it is cooled. This also supports the notion that a CPMU is inherently "fail-safe," in that it will still work well, albeit over a reduced tuning range, even if the cryocooling fails. If this result holds true for a hybrid CPMU, we will save an enormous amount of time in the magnetic shimming and spectral optimization of CPMUs by avoiding multiple cool-downs and warm-ups during the iterative shimming process. An important R&D task will be to verify by cold and warm measurements that field errors track with temperature in a hybrid CPMU as well.

5.5.2.1 "Cryo-Ready" MGU Installed in NSLS

NSLS has recently constructed and installed a 1 m long "cryo-ready" MGU for beamline X25 (18 mm period, B_y = 0.95 T at 5.6 mm gap) [5.5.2.4]. It has provision for cryogenic cooling by circulating cold He gas from a refrigerator through channels embedded in the magnet array platens. For the test we were able to cool it to 130K by circulating boil-off N_2 gas. This test demonstrated that the mechanical features designed to accommodate the large differential thermal contraction of the cold magnet arrays relative to the warm vacuum vessel worked. We mapped the undulator before and after thermal cycling and found no measurable magnetic changes.

5.5.2.2 Optical Gap Measurement

First-order gap control is performed using four external stepper motors with a linear encoder feedback system that positions each magnet girder to a mean reproducibility of 1 micron. The 1 m magnet length required multiple structural feed-throughs in the vacuum envelope to assure continuity between rigid external structural girders and the in-vacuum magnet girders. However, magnetic and mechanical measurements indicated that gap-dependent nonlinear magnetic forces, environmental temperature gradients, and operational conditions caused deflections of the in-vacuum magnet girders exceeding specifications. The external linear encoders could not measure these effects, and correction by the primary gap control system would be ineffective. The CPMU direct measurements of the magnet gap differed by greater than 1 mm with respect to the gap, as inferred by the external linear encoders. These measurements indicated that relying exclusively on a conventional external linear encoder-based control system is insufficient under extreme conditions, and a direct means of gap measurement and a secondary means of gap control are necessary to maintain micron control of the magnet girders over the full range of environmental and operational conditions. An LED-based system (e.g., Keyence LS-7030) that has a measurement accuracy of ±2 μm and repeatability of ±0.15 μm can be employed to provide a secondary means of gap control, to permit correction over the regime of these tertiary effects for up to 100 microns of nonlinear gap control. Very fine taper/bow control can be achieved by embedding temperature-controlled heaters for each post. This method successfully worked for the X25 MGU at NSLS. This feature is important even for RT-IVU to maintain very low phase errors. The effect of array deformation on phase error is examined in Section 5.5.2.4.

5.5.2.3 Optimizing the Device Design

Table 5.5.2.1 shows the possible combinations of period length, achievable peak field, and effective values of deflection parameter ($K_{y\ eff}$) at the undulator gap of 5 mm for a conventional room temperature IVU (20ºC) and cold (–120ºC) in-vacuum devices calculated by the same Radia [5.5.2.5] model used for the X25 MGU. These are all hybrid structures with vanadium permendur poles. Magnet type used in calculation for warm device is NEOMAX-32AH, Br =1.12T and Hcj =33kOe. This material was recently used for a similar device at Australian Light Source. Due to the much shorter beam lifetime and higher current for the NSLS-II storage ring than the NSLS x-ray ring, many more lost electrons will be produced as a demagnetization source. Therefore, more conservative material must be chosen compared to the NSLS MGUs. The magnet for cold type is NEOMAX-42AH Br =1.29T at 273K → 1.45T at 120K, and Hcj =24kOe at 273K → >40kOe at 120K. In this table, the effective K value for the non-sinusoidal field is calculated as

$$K_{x,y\ eff}{}^2 = 2\ \langle \gamma^2 \frac{v_{x,y}{}^2}{c^2} \rangle , \tag{5.5-1}$$

where *c* is the speed of light in vacuum, γ is the Lorentz factor, and *v* is the velocity of the electrons.

Table 5.5.2.1 Period-Length vs. Maximum Flux Density and Effective K Value for IVU at Room Temperature and 150K.

Period Length (mm)	Warm (B_r = 1.12 T) B_{peak} (T)	Warm K_{eff}	Cold (B_r = 1.45 T) B_{peak} (T)	Cold K_{eff}
16.0	0.76	1.11	0.98	1.43
17.5	1.87	1.37	1.11	1.74
19.0	0.97	1.63	1.21	2.03
20.0	1.03	1.81	1.26	2.22
21.0	1.10	1.99	1.31	2.40

All of the NSLS MGUs have severe limitations in their length. Therefore, the ideal magnetic termination at the extremities has to be compromised in order to increase the number of full-field-strength periods. Hybrid devices tend to have an inherently larger gap dependence of integrated field strength, due to the nonlinear characteristics of pole materials and anisotropy of permanent magnets. Various termination schemes that minimize the gap dependence for pure permanent magnet devices have been developed [5.7.9]. However, designs for hybrid devices have limited effectiveness. End effects tend to be less important for small-gap undulators than for large-gap, high-field wigglers.

5.5.2.4 Minimizing Phase Error

A critical requirement for short-period, in-vacuum MGUs in a medium-energy storage ring is retaining high spectral brightness, up to the 7th or even the 9th harmonic. Loss of spectral brightness is well correlated with optical phase error. Phase error can be defined as the cumulative path length difference between the electron's actual trajectory and an ideal trajectory, expressed in degrees of phase at the fundamental optical wavelength. Cumulative optical phase error of 2° RMS is considered state of the art and will be the target for all NSLS-II undulators. This is an especially challenging requirement for small-gap, short-period IDs, as shown below.

Phase error arises from three sources: 1) systematic gap error, 2) trajectory wander, and 3) random phase errors. We will next describe the techniques we have developed and use routinely to minimize phase error from these three sources.

Systematic phase error can be caused by a) bowing of the magnet arrays due to attractive magnetic forces, b) gap taper, and c) nonflatness of the magnet mounting surfaces. These are long-range gap variations, on the scale of many undulator periods, which cause a gradual variation of field amplitude, wiggle amplitude, and

therefore trajectory path length, without trajectory steering. To obtain a mechanical tolerance budget for these effects in the X25 MGU, we started with a finite-element analysis of an initial mechanical design for the magnet support beams, suspended on two hangers, under a distributed magnetic load of 8,000 N (due to the peak field of I T at a 5.6 mm gap). The resulting deflection profile was scaled to a field amplitude profile, which was numerically integrated to obtain the trajectory and, finally, a cumulative phase error profile. Figure 5.5.2.1 is a plot of the gap error (blue) and resulting cumulative phase error (magenta) vs. longitudinal position Z. The peak-to-valley deflection of 3 microns results in a RMS phase error of 0.75°. The figure shows that two supports per meter can induce a phase error of 0.75 degrees, due to deflection resulting from B = 1 T. Solid aluminum platens are assumed in this simulation.

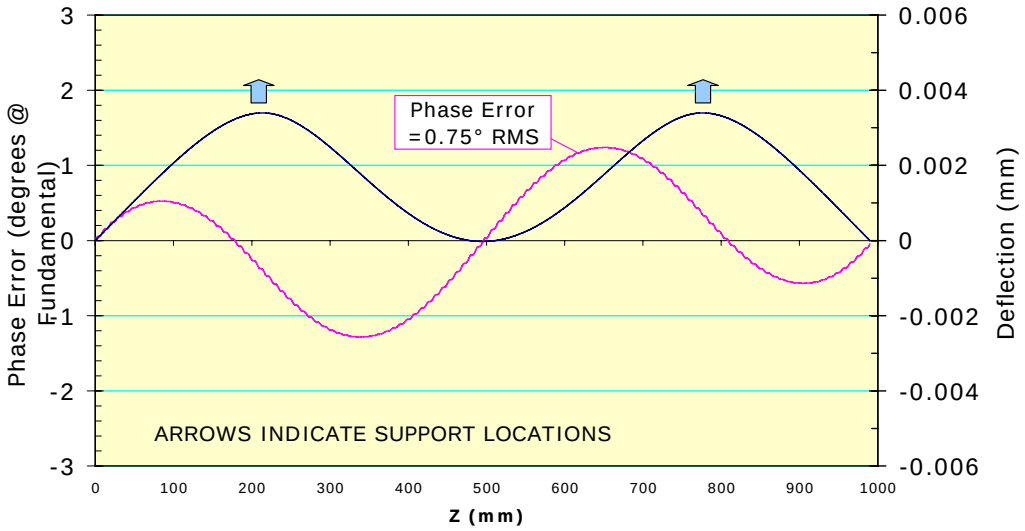

Figure 5.5.2.1 Phase error created by the mechanical deflection of aluminum magnet platens, due to the magnetic force of B = 1T.

The phase error created by 3.3 microns of linear tapering in 1 m is presented in Figure 5.5.2.2.

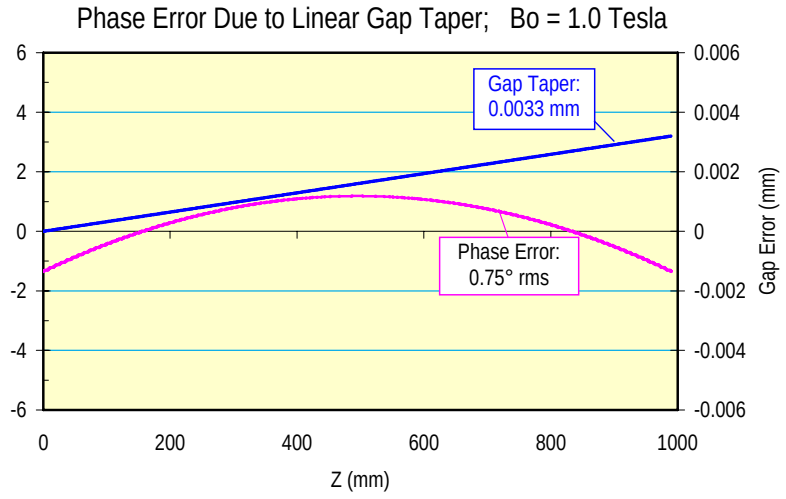

Figure 5.5.2.2 Phase error created by linear gap taper. B_0 = 1.0T.

Trajectory wander is caused by local, random field amplitude errors, which cause the trajectory to deviate from a straight line. The longer path is reflected in a phase error. Local steering errors can also accumulate over the length of the undulator as both integrated dipole (first integral error) and trajectory offset (second integral error). We routinely use the Pulsed Wire technique to quickly visualize the trajectory in undulators, identify the location and magnitude of steering errors, and apply steering shims to correct them. The pulsed

wire easily displays both the horizontal and vertical components of a trajectory, including the contribution of the Earth's field.

Random phase errors are nonsteering errors that remain following trajectory straightening and the removal of systematic phase errors. In a PM-hybrid undulator, random phase errors are mainly caused by variations in the strength of individual magnets, as well as by pole positioning errors. To minimize these, the individual magnets are first measured, then sorted, paired, selected, and assigned to specific locations in the arrays. Various manual and computer-aided sorting and selection algorithms have been developed and are considered standard practice.

Earth's field causes significant trajectory deflection in long undulators. The measured local Earth's field is about 0.4 Gauss with an inclination of about 14° from the vertical. The vertical component contributes an integrated (horizontally deflecting) dipole error of about 40 Gauss-cm/m. In a 3 m long CPMU, that adds up to a nontrivial dipole error of 120 Gauss-cm. The horizontal component is about 0.1 Gauss and oriented toward magnetic North. The effective (vertically deflecting) dipole error is <10 Gauss-cm/m and depends on the azimuthal orientation of the ID in the ring. The effect of Earth's field is readily visible on the pulsed wire as a parabolic trajectory component. It can be compensated by distributed trajectory shimming, or with external Helmholtz coils. In the X25 MGU we added a pair of 10-turn horizontal coils around the undulator vacuum vessel, powered by the end-pole trim supply from the old X25 wiggler previously residing at that location. Using the pulsed wire, we determined the optimal current to cancel Earth's field in the X25 MGU to be about 3.5 A. The small horizontal component was not compensated.

Other error specifications, such as maximum first and second integral and allowable integrated multipole requirements, will be specified before the engineering design phase.

5.5.2.5 Effect of Magnetic Field Errors on the Undulator Harmonics

The performance of real undulators is known to be poorer than the ideal case owing to magnetic field errors, despite valiant efforts to minimize such errors. It is generally accepted that the parameter which best relates magnetic field errors to spectral output is the RMS phase error ϕ. The RMS phase error ϕ is defined as the RMS path length difference between the real and ideal electron trajectories. It is calculated at the poles of the undulator and normalized to the wavelength of the fundamental harmonic (n = 1). (At higher harmonics (n >1), the RMS phase error is nϕ.) To date there has been no complete analytic treatment of the spectral effects of the phase errors. It has been argued that, for a zero-emittance electron beam, the relative on-axis brightness of the odd undulator harmonics n = 1, 3, 5, … emitted by an undulator with uncorrelated and Gaussian distributed phase errors is given by

$$B(n,\phi)/B(n,0) = e^{-n^2\phi^2} \tag{5.5.2-2}$$

where ϕ is the RMS phase error.

Recently, we have found empirically that this formula tends to underestimate the effect of phase errors for real undulators. For the two LCLS undulators discussed below, the expression above for a zero-emittance beam can be made to agree reasonably well with the result derived from magnetic measurements only if the RMS phase error is increased by ~20% from the measured value ($\phi \rightarrow 1.2\phi$). This is a large "correction" factor; more accurate results can be obtained by feeding the measured magnetic field profiles directly into undulator codes, such as UR or SPECTRA. Moreover, there is no analytical formula for phase error effects when the emittance needs to be taken into account, so we need to resort to numerical calculations.

Simulations were performed using measured magnetic field data from a set of undulators with RMS phase errors spanning a range from 2.0° to 3.7°. The measured magnetic field profiles and the storage ring parameters for NSLS-II were used as inputs to the undulator code UR in order to simulate realistic undulator spectral performance. If the results are a well-behaved function of phase error, one can then make a

determination of the maximum tolerable RMS phase error required to achieve a particular level of undulator spectral performance. As discussed below, the results confirm the intuition that achieving a 2° RMS phase error, or better, is important for maintaining high spectral brightness for the high NSLS-II harmonics (7, 9, and 11). These results also confirm the idea that the phase error effects become more significant as the ring emittance decreases.

5.5.2.5.1 Relative On-Axis Brightness for Harmonics 7, 9, and 11 vs. RMS Phase Errors for NSLS-II Undulators

Computer simulations of the relative on-axis brightness as a function of the RMS phase error were performed using the NSLS-II emittance and real measured magnetic fields of three undulators. Comparisons were made to the spectral performance of the same undulators with hypothetical ideal magnetic fields. The results are detailed below and show, for example, that the 9th harmonic undulator radiation degrades by about 15% if the RMS phase error increases from 2.0° to 3.0°.

Conditions

The NSLS-II storage ring parameters for a 5 m-long low-β insertion device straight section were used for these simulations. The following parameter values were used: emittances ε_h=0.55 nm, ε_v=0.01 nm, energy spread $\delta E/E$=0.1%, and β-functions β_h = 2.7 m, β_v=0.945 m. The resultant electron beam sizes and divergences are σ_h=38.5 μm, σ_v=3.1 μm, σ_h'=14.2 μrad, and σ_v'=3.2 μrad.

The following three undulators were studied:

- Linac Coherent Light Source undulator number 1 (LCLS #1), period length=3.0 cm, 113 periods; K and ϕ measured at 6.8 mm gap: K=3.50 and ϕ=3.54°
- Linac Coherent Light Source undulator number 2 (LCLS #2), period length=3.0 cm, 113 periods; K and ϕ measured at 6.8 mm gap: K=3.49 and ϕ=4.21°
- APS short undulator A (APS #40), K = 2.80, period length = 3.3 cm, 62 periods; K and ϕ measured at 10.5 mm gap: K = 2.80 and ϕ = 3.68°

Numerical calculations of the on-axis brightness for these three undulators were performed. In order to study the dependence on the RMS phase error, the LCLS undulator fields were scaled in both field strength (uniformly to a lower value) and period length to simulate a change of the RMS phase error (the RMS phase error decreases when the K value becomes smaller). Very minor adjustments to the on-axis view angle were applied, and as such, those fields represent real devices with true magnetic field errors. It is worth noting that for the LCLS undulators, the period length was scaled from 3.0 cm to 1.9 cm to simulate a shorter period-length undulator, such as the NSLS-II U19 CPMU hard x-ray undulator. This procedure allowed us to study undulators which have RMS phase errors covering the range 2.0° to 3.7°.

Results

The on-axis brightness of the 7th, 9th, and 11th harmonics, relative to the brightness of the corresponding harmonics of a hypothetical, ideal magnetic field undulator, is plotted in Figure 5.5.2.3 for the three undulators described above, simulated for their performance in the NSLS-II storage ring. The relative brightness of the 3rd and 5th harmonics is much closer to 100% and is not shown in this figure.

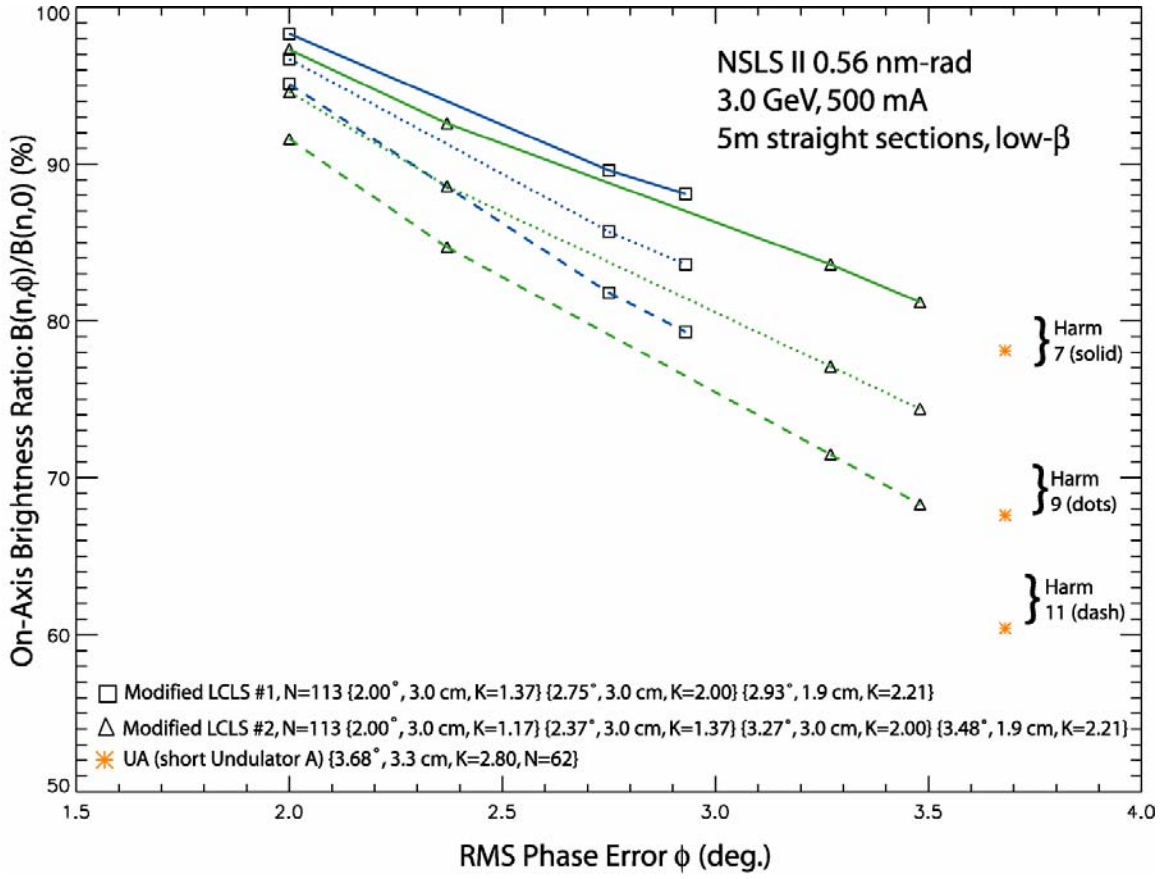

Figure 5.5.2.3 On-axis brightness of the 7th, 9th, and 11th harmonics of three undulators relative to the brightness of the corresponding harmonics of an ideal magnetic field undulator, as a function of the RMS phase error.

The key results of these simulations are as follows: improving the RMS phase error from 3.0° to 2.0° changes the relative brightness of the 7th harmonic from 86 to 98% (Δ_7 = 12% points), the 9th harmonic from 81 to 96% (Δ_9 = 15% points), and the 11th harmonic from 75 to 93% (Δ_{11} = 18% points).

Conclusions

The relative brightness of the NSLS-II undulator harmonics depends sensitively on the RMS phase error. The higher the harmonic number and the higher the RMS phase error, the faster is the rate of reduction. The rate of reduction is somewhat sensitive to the actual distribution of phase errors for real devices, but is much less sensitive to the actual K value or the undulator period length. For example, by improving the RMS phase error from 3.0° to 2.0°, the 9th harmonic would gain about 15%.

The effect of phase error becomes greater as the emittance of the storage ring decreases. For example, the performance drop for NSLS-II undulators would be 2 to 5% greater for harmonics 7–11 than for the same devices at APS, as a result of the smaller emittance of NSLS-II.

Future work on this subject should include simulations using the measured fields from recently built undulators around the world, including the 18 mm period undulator installed at NSLS beamline X25 in December 2005, which has a period length very close to the U19 CPMU proposed for NSLS-II and has a measured RMS phase error close to 2°.

5.5.2.6 Baseline IVU Magnetic Design

The base design for the NSLS-II hard x-ray planar device is derived from the NSLS cryo-ready undulator developed for X25. The X25 mini-gap in-vacuum undulator has an 18 mm period length, a minimum magnetic gap of 5.6 mm and length of 1 m, and is designed to be operated at 150 K. The NSLS-II U20 IVU will have a minimum gap of 5 mm and will be 3 m long, but most of its other requirements are similar to those for the X25 MGU. The main parameters are given in Table 5.5.2.1

Table 5.5.2.2 shows the expected mechanical tolerances of the magnetic arrays.

Table 5.5.2.2 Mechanical Tolerances.

Item	Tolerance
Magnet/pole width [μm]	±100
Magnet height [μm]	± 25
Magnet thickness [μm]	±25
Pole height [μm]	± 25
Pole thickness [μm]	± 10
Pole-to-pole flatness [μm]	±10
Period [μm]	±10
Magnet array pitch/yaw/roll (relative) [μrad]	± 25
Magnet array horizontal/vertical rack [μm]	± 5
Gap control [μm]	± 5
Gap repeatability [μm]	± 5

The phase error for the device is required to be less than two degree RMS. Slight tapering, platen bowing, and other factors must be carefully controlled to achieve this level of phase error. As mentioned above, a novel gap measurement system using a commercial, high-precision, LED-based optical micrometer was incorporated in the X25 MGU to back up the linear encoders and to correct for gap changes due to differential contraction during cryogenic operation. The system monitors the magnet gap optically through viewports at either end of the MGU, ensuring gap accuracy of ±2 μm.

Figure 5.5.2.4 shows an isometric rendering of the MGU magnet arrays by Radia. Blue magnets have identical size and two different sized magnets are shown in green. Pieces in magenta represent permendur poles.

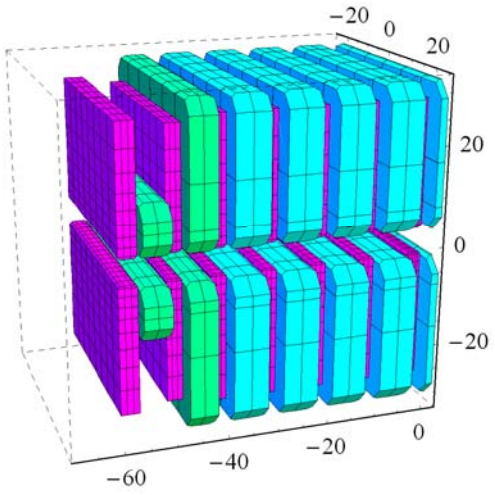

Figure 5.5.2.4 MGU magnet arrays. Only the first few periods are shown, for clarity. Units are millimeters.

The Radia simulations shown here were performed with a symmetrical model so the angular kick could be estimated. In the actual device we are likely to use an anti-symmetric structure to minimize the residual first integral. The values of magnet susceptibilities used are χ_m (para) = 0.02, χ_m (perp) = 0.42. The field and trajectory computed from the model are plotted in Figure 5.5.2.5 for gaps of a) 5.0 mm and b) 11.0 mm. The trajectory is calculated by a particle-tracking Runge-Kutta routine. The particle is launched with zero offset and angle (x = 0, x' = 0), and its position and angle are calculated every 0.53 mm (36 points per period). The gap dependence of the first integral is shown in Figure 5.5.2.6. The amount of change in the first integral found here can be easily compensated by external coils.

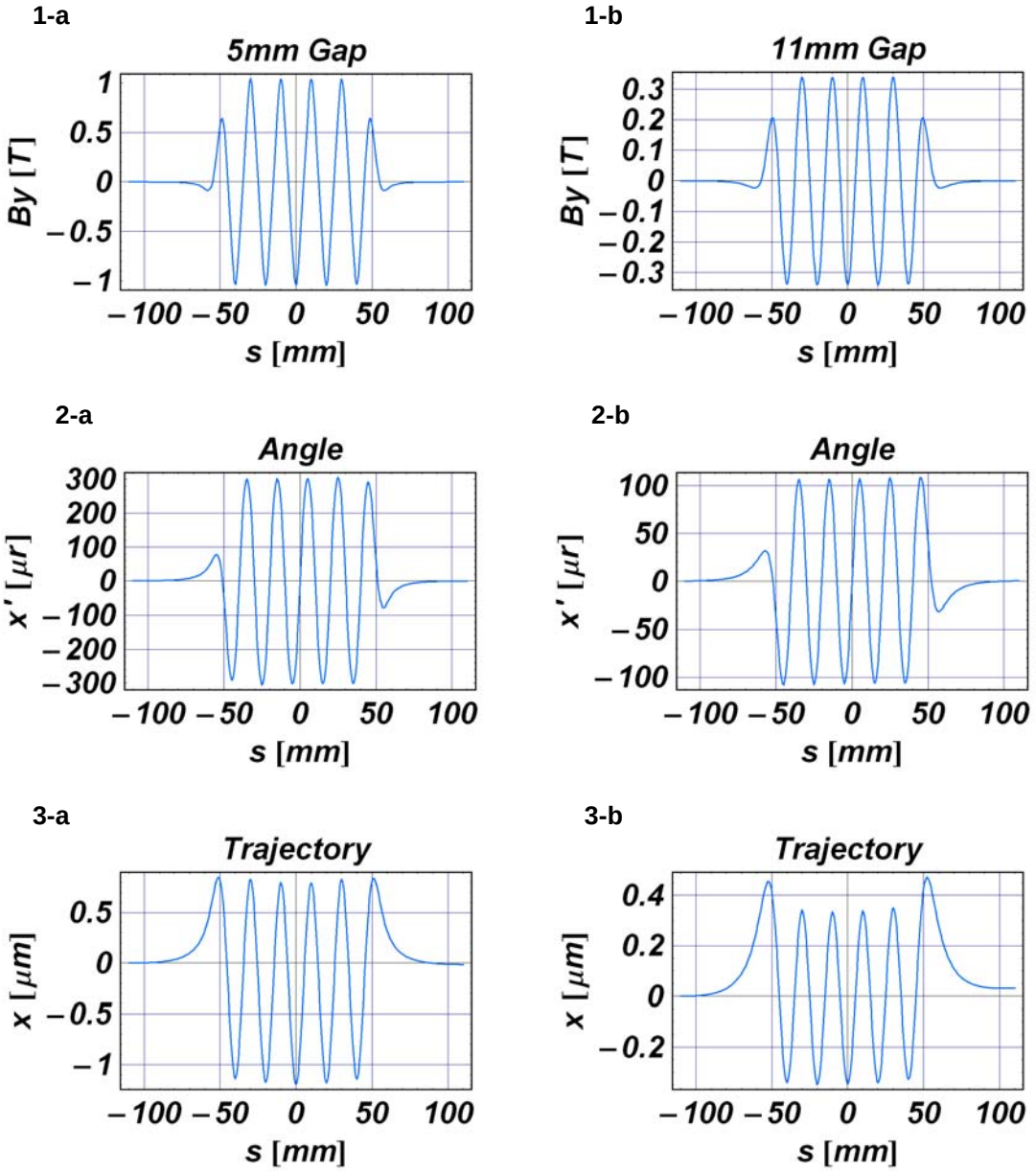

Figure 5.5.2.5 Gap dependence. Field, angle, and trajectory plots for the 7-period model for (column **a**) minimum gap (5.0 mm) and (column **b**) maximum operating gap (11.0 mm).

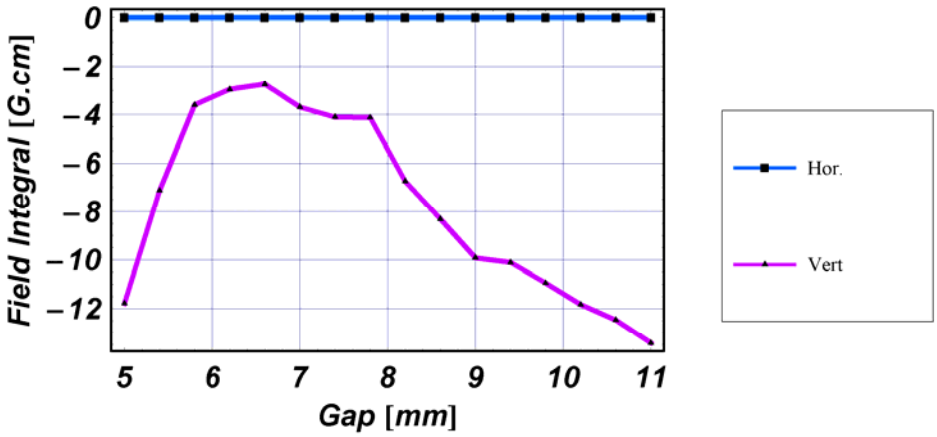

Figure 5.5.2.6 Gap dependence of the first integrals simulated for U20. Due to symmetric model structure, horizontal field integral dependence does not appear.

5.5.6 Vacuum and Mechanical Systems Development

A 3 m device will be constructed with three 1 m modules that are similar to the X25 MGU. The vacuum chamber is rectangular and opens along its length to facilitate magnetic field measurements and shimming. Most of the required vacuum components are mounted to this cover for easy access and for a cost-effective design. These components include ion pump/titanium sublimators, getter pumps, an RGA analyzer, a glow discharge cleaning system with associated pumping and view ports, an ion gauge, and bleed-up ports. The X25 system successfully achieved a pressure of less than 5×10^{-10} Torr, including magnets, after bakeout. The conceptual design in a CAD model is shown in Figure 5.5.2.7.

Techniques first demonstrated in the cryo-ready X25 MGU will be optimized and incorporated for the NSLS-II development program for the control system of the IVU. Systems such as an in-vacuum gap separation system will be modeled that can provide precision gap control with negligible effects from external temperature fluctuations and ultimately demonstrate a cost-effective alternative to more conventional gap separation and control systems.

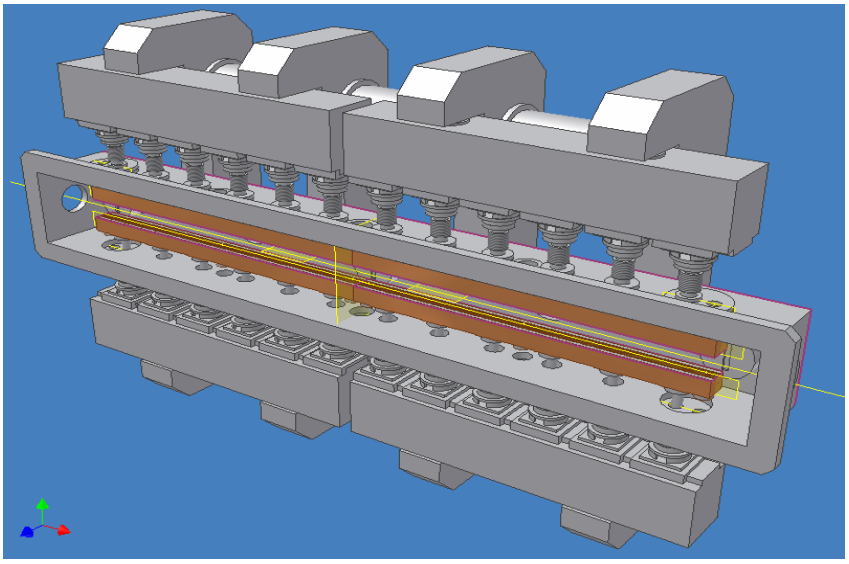

Figure 5.5.2.7 Conceptual design of U20.

References

[5.5.2.1] T. Tanabe, et al., "Development of an In-Vacuum Minipole Undulator Array for National Synchrotron Light Source In-Vacuum Undulator," *Rev. Sci. Instrum*. 69 (1), pp 18 – 24, (1998).

[5.5.2.2] H. Kitamura, "Recent development of insertion devices at SPring-8," *Nuc. Instr. & Meth. A* 467-468 (2001) p 110.

[5.5.2.3] M. Sagawa, et al., "Magnetic properties of rare-earth-iron-boron permanent materials," *J. Appl. Phys.* 57 (1985) pp 4094.

[5.5.2.4] T. Tanabe, et al., "X-25 cryo-ready in-vacuum undulator at the NSLS," AIP SRI2006 conference proceedings (to be published).

[5.5.2.5] O. Chubar, P. Elleaume, and J. Chavanne, *J. Sync. Rad*. 5, pp. 481–484 (1998).

5.5.3 Variable Polarization Device for Soft X-ray

The variable polarization undulator, also known as an elliptically polarized undulator, EPU, is becoming more popular, as its impact on beam dynamics can now be controlled to an acceptable level. Currently, no in-vacuum EPU has been constructed, because of the difficulty of having moving parts and a strong force in a UHV environment. Therefore, the baseline design for NSLS-II will be the permanent magnet out-of-vacuum EPU45 and EPU100 devices described in Section 5.1, but R&D may be carried out to investigate in-vacuum EPU designs.

Various schemes to generate variably polarized light from an insertion device have been proposed. An electromagnet-based design that switches the polarity cannot cover the required photon energy range (250 eV–2 keV). The most popular design, based on PM technology, is the Advanced Planar Polarized Light Emitter (APPLE) type [5.5.3.1]. It has been popular because it can generate all the possible polarization states with the minimum number of magnets. However, it also has a few deficiencies. Strong multipole components inherent to the design would reduce the dynamic aperture of the machine. This effect is due to the fact that horizontal field and vertical field are coupled, so static optimization for different gap and phase is difficult. In long-period devices, the electron's wiggle amplitude can be large enough for the field rolloff to affect the trajectory and result in a so-called "dynamic field integral," which is not measured by stretched wires or long coils. Recent efforts by various laboratories have mitigated these problems for limited types of operations [5.5.3.2].

There is an alternative design proposed for HiSOR by SPring-8 [5.5.3.3]. It separates the magnets for horizontal and vertical field, for ease of tuning as well as more moderate skew multipoles, at the expense of weaker achievable horizontal field. Detailed tracking studies will be carried out to decide which type of device is appropriate for NSLS-II.

Another concern for NSLS-II EPUs is the possible demagnetization of the permanent magnets by the use of the APS-style narrow gap vacuum chamber. Improvements to the vacuum chamber design will be investigated in order to minimize the source of radiation at the extremities of the chamber.

5.5.3.1 Anisotropy of Permanent Magnets

Rare-earth magnets used for insertion devices have permeability close to unity, so that, to first order, the magnetic induction from individual magnet blocks can be superposed to obtain the total field. However, more careful analysis shows that there is anisotropy in those magnets. The components of the permeability that are parallel to the preferred direction of magnetization (easy axis), and perpendicular to this direction, are different and lager than unity. The magnetic susceptibility χ_m and polarization J are defined as follows:

$$B = \mu H = \mu_0 \mu_r H = \mu_0 (\chi_m + 1) H , \quad (5.5.3\text{-}1)$$

$$J = \mu_0 \chi_m H \quad (5.5.3\text{-}2)$$

where B is magnetic induction, H is magnetic field strength, μ_0 the permeability of vacuum, and μ_r is the relative permeability defined for convenience.

The permeability can vary at different points on the hysteresis curve. For example, the value at the beginning of magnetization is termed initial permeability, and the largest gradient in the B-H curve is called maximum permeability. What is important in a magnetic circuit is the reversible or recoil permeability, which is the slope of a minor loop in the second quadrant. The recoil permeability is usually approximated by the slope of the major loop at H = 0. For NEOMAX 42AH, the susceptibility is estimated by the slope of the J-H curve around H = 0. The estimated values of susceptibilities from these curves are:

$$\chi_m \text{ (para)} = 0.02,\ \chi_m \text{ (perp)} = 0.42. \quad (5.5.3\text{-}3)$$

These values indicate that in the region where the magnetic flux lines deviate from the preferred direction of magnetization, the material can be nonlinear. For planar insertion devices, this region corresponds mostly to end sections, which determines the gap dependence of the field integral, in practical terms. However, in most EPUs, the field directions inside magnets vary greatly, depending on the array phase. For the CPMU these values will need to be measured at the operating temperature, in order to be more precise.

5.5.3.2 Advanced Options (Outside Baseline Project Scope)

In-vacuum EPU is still an R&D subject. The performance of any type of ID strongly depends on the available minimum magnetic gap. A 2.5 m long in-vacuum EPU may be developed in this program. BNL will assemble magnet and pole materials, develop in-vacuum gap separation and magnet module axial position actuators, and procure a vessel and undulator support system. Using the facilities in the Undulator Development Laboratory in Building 832, measurements and characterization of the EPU fields under various gaps and phases will be made, as well as field corrections. The in-vacuum EPU could then be installed for the X-1 beam line of NSLS I to verify performance prior to the move to NSLS-II. The goal of this development is to advance the state of the art in EPU technology, to demonstrate the first in-vacuum EPU, to resolve the uncertainty in the methods of measurement and shimming of EPUs to permit reliable and cost-effective operation, and to perfect a new class of insertion device, the in-vacuum EPU, that can be offered to meet the needs of NSLS-II users.

To switch the helicities at higher than 1 Hz, a tandem structure is needed so that light with opposite helicities is produced simultaneously for various switching schemes. In this case, each ID is located away from the center and the required beam stay-clear gap would increase. If a slower switching frequency is tolerated, one longer device with mechanical phase change is possible. Another possibility is to set up two helical undulators in tandem and have a phase shifter between them to change the resulting polarization [5.5.7.4]. In this case, two helical undulators can be in-vacuum type if limited tuning range can be tolerated. Table 5.5.3.1 shows the characteristics of an APPLE-II type EPU.

Table 5.5.3.1 Characteristics of an APPLE-II Type EPU. Assumed Br of the magnets is 1.35 T.

Period Length (mm)	Magnetic Gap (mm)	Helical ModePeak Field (Bx = By)	EffectiveKx / Ky	Linear ModeEffective Ky
40	6.5	0.87	3.2	4.87
42	8	0.77	3.0	4.76
45	10	0.68	2.87	4.67
45	11	0.62	2.6	4.38

5.3.3 EPU45 (APPLE-II) (Baseline Design)

One possibility is to install twin devices in an 8 m straight section. Assume that we can have a 5 mm vertical aperture for a 3 m device placed at the center of the 5 m straight, with vertical beta function equal to 1 m at the insertion center. In this case, the ring aperture (A) is:

$$A = \frac{gap}{\sqrt{\beta(end)}} = \frac{gap}{\sqrt{\beta_0 + (end)^2 / \beta_0}} = \frac{5mm}{\sqrt{(1+1.5^2)m}} = 2.77mm/\sqrt{m}\,. \quad (5.5.3\text{-}4)$$

We must verify that this is sufficient, but once we determine that this is acceptable, the required aperture y for an insertion device of length L placed at the center of a straight with beta-function β_0 at the center is determined to be

$$y = A\sqrt{\beta_0 + \frac{(L/2)^2}{\beta_0}} \tag{5.5.3-5}$$

For the 8 m straights β_0 = 3 m, we find the required vertical aperture is 7.4 mm at the half length of 3. 5 m. An 8 mm aperture chamber at APS allows 2.5 mm extra for the magnetic gap of their insertion device. Therefore, we will assume that the magnetic gap of the NSLS-II insertion device is close to 10 mm.

The minimum photon energy to be covered is 250 eV. An EPU45 with an APPLE-II type configuration shows the characteristics listed in Table 5.5.3.2. Here, the remanent fields of the NdFeB magnets are assumed to be 1.35 T.

Table 5.5.3.2 APPLE-II Type EPU45 Parameters.

Period length [mm]	45
Peak field (helical mode: v/h) [T]	0.68 / 0.68
Effective K	2.87
Minimum photon energy in helical mode [eV]	206
Minimum gap [mm]	10
Magnet horizontal size [mm]	50
Magnet vertical size [mm]	45
Remanent field (B_r) [T]	1.35

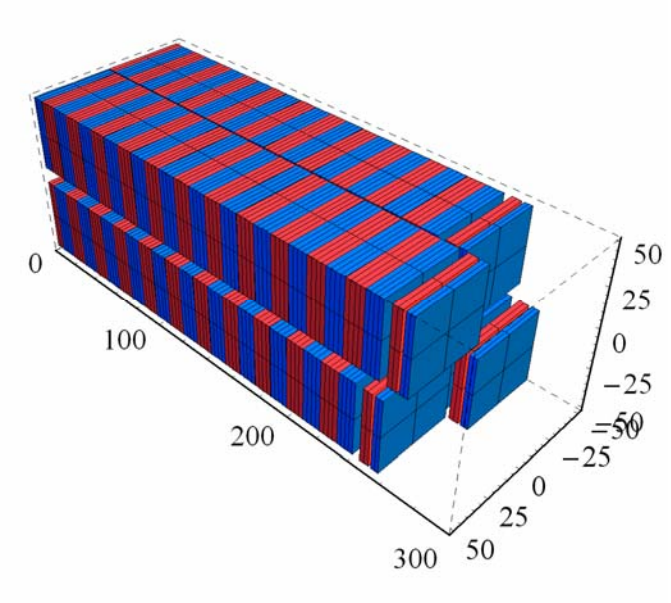

Figure 5.5.3.1 Magnet arrays of EPU45. Only the first few periods are shown for clarity. Units are millimeters. Vertically magnetized magnets are in red and horizontally magnetized magnets are in blue.

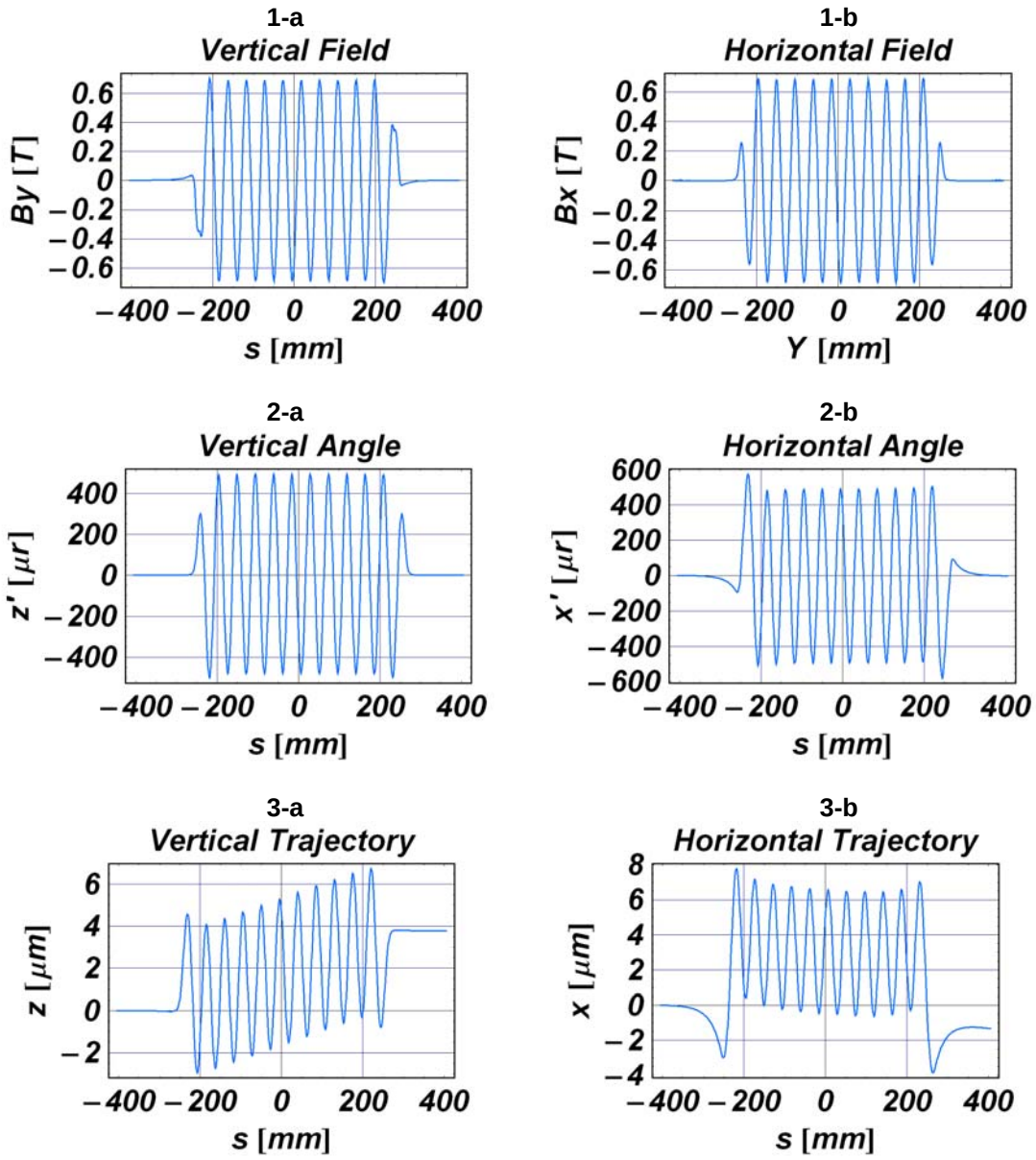

Figure 5.5.3.2 Field, angle and trajectory plots for the 11-period model of EPU45 in helical mode. **a)** vertical field, horizontal angle, horizontal trajectory and **b)** horizontal field, vertical angle, and vertical trajectory at a gap of 10 mm.

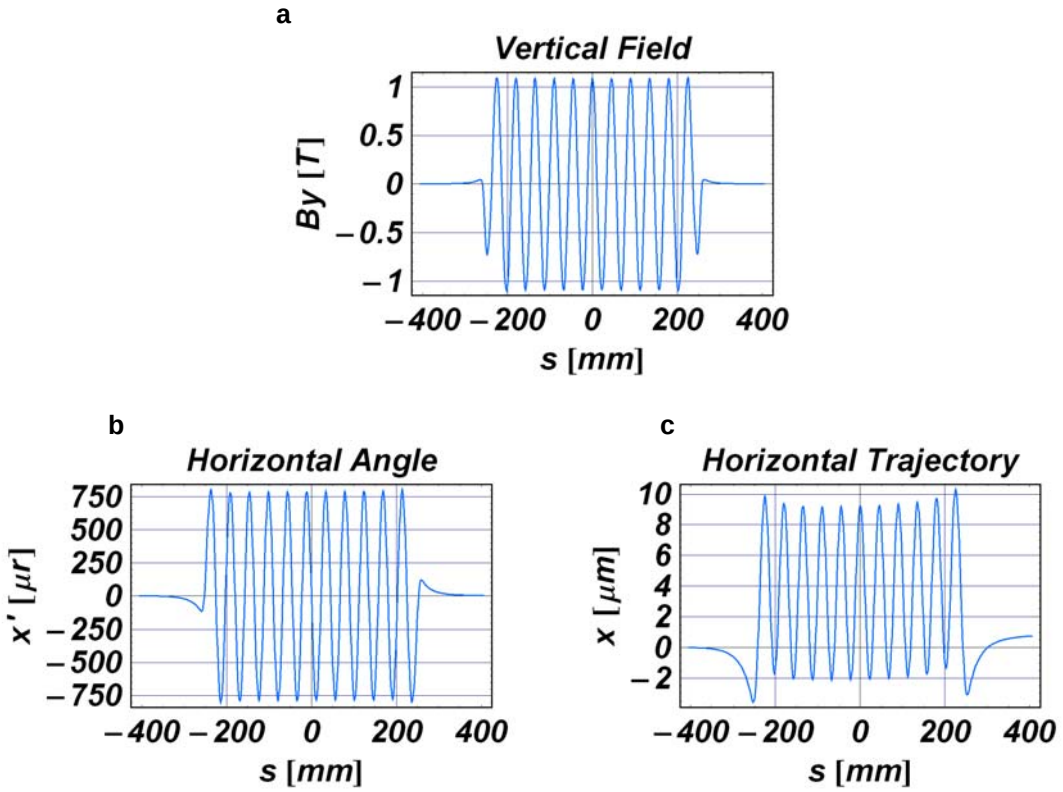

Figure 5.5.3.3 Field, angle, and trajectory plots for the 11-period model of EPU45 in linear mode. **a)** vertical field, **b)** horizontal angle, **c)** horizontal trajectory at a gap of 10 mm.

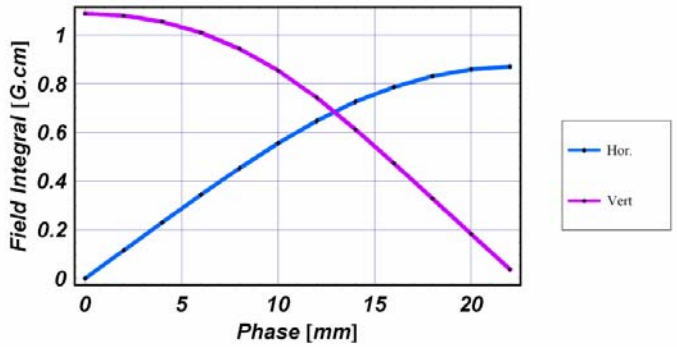

Figure 5.5.3.4 Fields vs. phase.

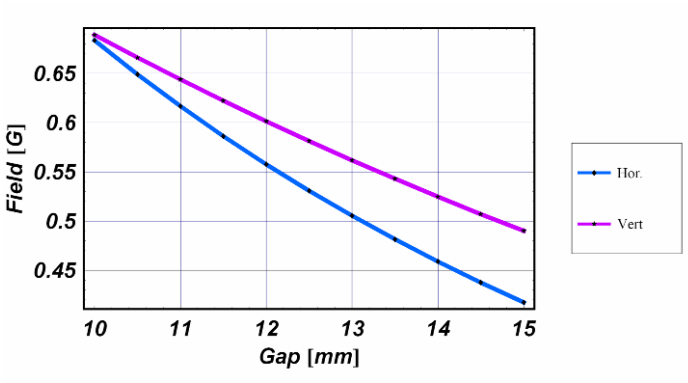

Figure 5.5.3.5 Fields vs. gap in helical mode.

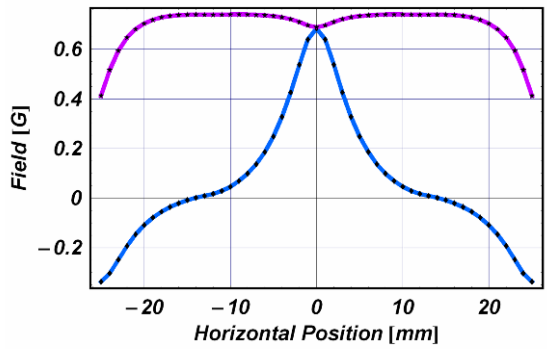

Figure 5.5.3.6 Fields vs. horizontal position at the origin in helical mode.

5.5.3.3.1. Mechanical Analysis

The small available transverse cross section of a device is also a concern for EPUs. Mechanical analyses have been conducted with slightly different parameters from EPU45. The chosen period length is 49 mm, and the minimum gap of 11 mm was selected due to cost and technical reasons. It was found that the maximum attractive force in gap direction is approximately 25000N, and that for phase direction is 15000N. The FEA analyses were done by Danfysik A/S as a part of the advanced conceptual design contract.

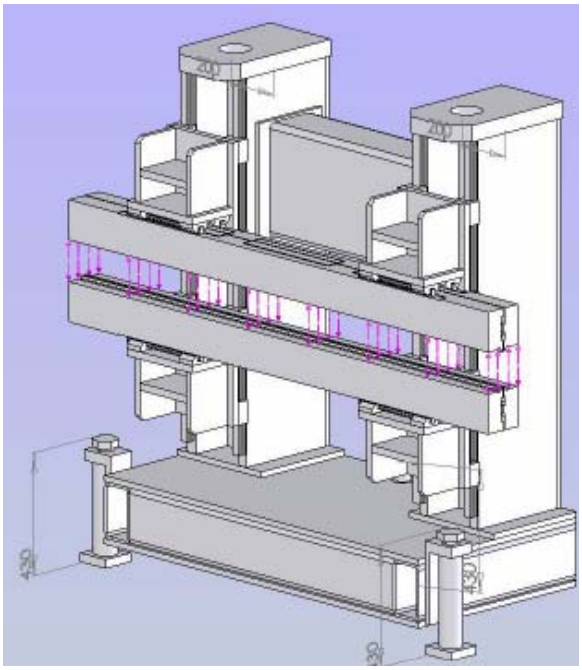

Figure 5.5.3.7 Applied force directions (magenta arrows).

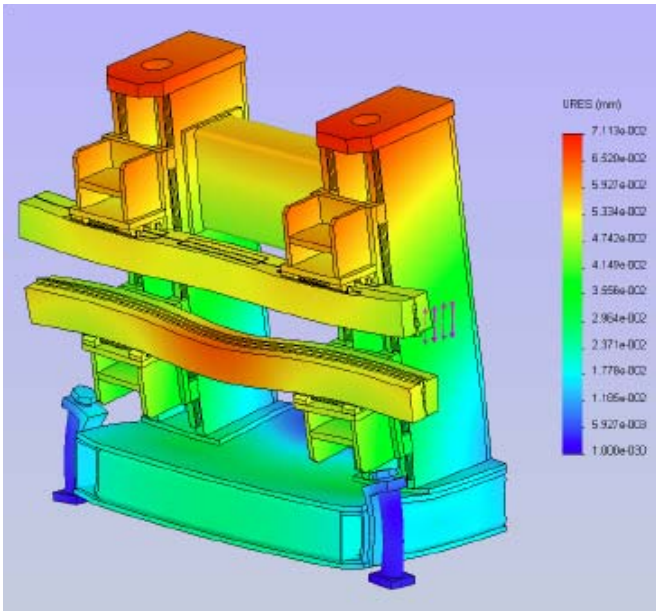

Figure 5.5.3.8 Displacement in vertical direction

Attractive force (12500N for each jaw and opposite directions)

The displacement plot shows that the maximum displacement is 0.071 mm at the top of the undulator, due to the weight of the motor and magnets. The maximum displacement between girders is approximately 0.013 mm. This amount will influence the achievable phase error in planar mode if one requires phase error better than 5 degrees, which is conventional for a commercially available Apple-II device.

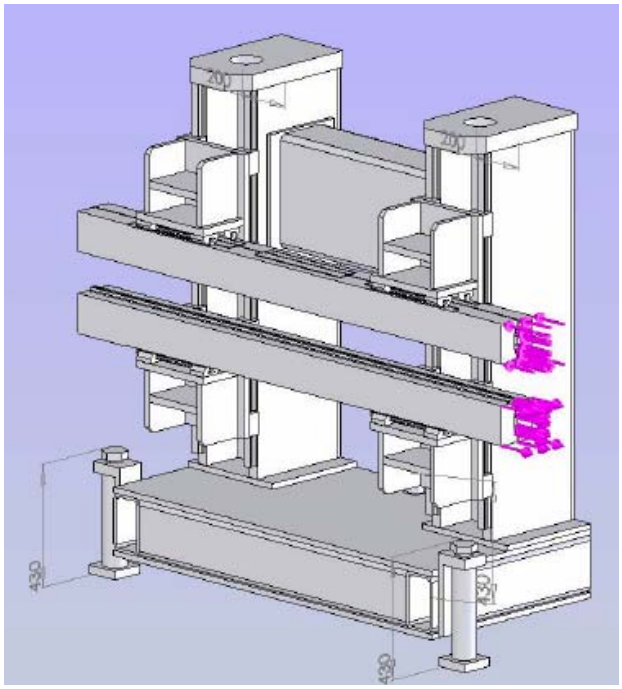

Figure 5.5.3.9 Applied force directions

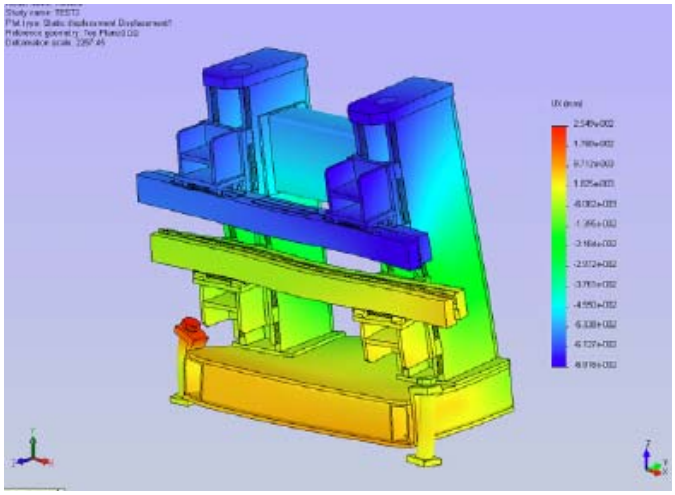

Figure 5.5.3.10 Displacement in longitudinal direction

Moment load (14700N per upper/lower jaw)

The maximum displacement in phase direction is found to be 0.062 mm. This amount can be easily compensated by the phase motion control.

5.5.3.4 EPU52 (HiSOR) Magnetic Design (Backup Option)

To alleviate a highly sharp horizontal field profile and the coupling of vertical and horizontal fields from the same magnet, a new design with three magnet arrays in each jaw has been proposed and implemented at UVSOR and HiSOR in Japan. Unlike the APPLE-II design, one array in the center produces vertical field and two arrays on the sides generate horizontal field. Therefore, each type can be separately shimmed to perfection upto lThe horizontal field profile is more benign than that from APPLE-II. The parameters for the HiSOR design are shown in Table 5.5.3.3, and a Radia drawing shows the design (Figure 5.5.3.11).

Table 5.5.3.3 HiSOR-Type EPU52 Parameters.

Period Length	52 mm
Peak Field (helical mode: v/h)	0.53 / 0.53T
Effective K	2.49
Minimum photon energy in helical mode	240 eV
Minimum gap	10 mm
Side Magnet Size (H/V)	50 / 45 mm
Center Magnet Width	14 mm
Remanent Field (Br)	1.35T

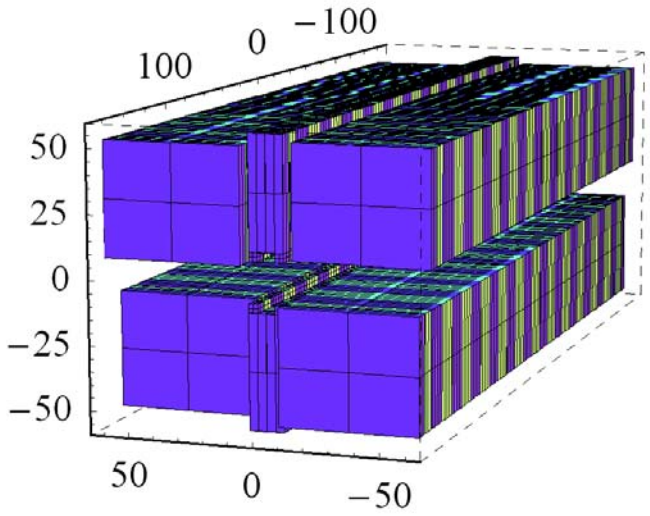

Figure 5.5.3.11 Magnet arrays of HiSOR-EPU52. Only the first few periods are shown, for clarity. Units are millimeters. Vertically magnetized magnets are in light green and horizontally magnetized magnets are in purple.

One disadvantage of the HiSOR design is that the maximum horizontal field is weaker than that of the APPLE-II for the same period length, due to the increased distance between the two arrays. Hence, slightly longer period length is required to obtain the same photon energy as with the APPLE-II design. If vertical linear polarization is needed, the vertical arrays can be shifted out of phase. However, some longitudinal components remain at the extremities, and tracking studies are needed to determine the detrimental effect.

The grooved-shape magnets in the center arrays improve the vertical field uniformity (Figure 5.5.3.13).

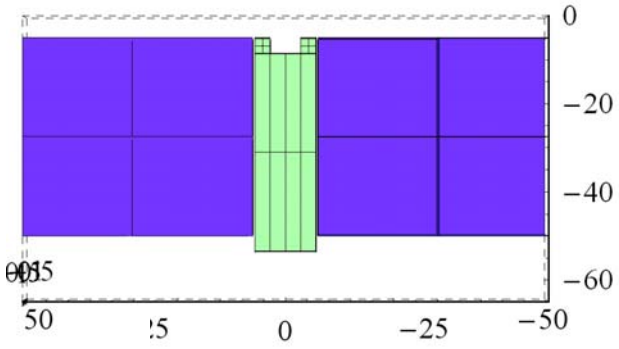

Figure 5.5.3.12 Cross-section of a magnetic array. Light green is for the vertical field and purple is for the horizontal.

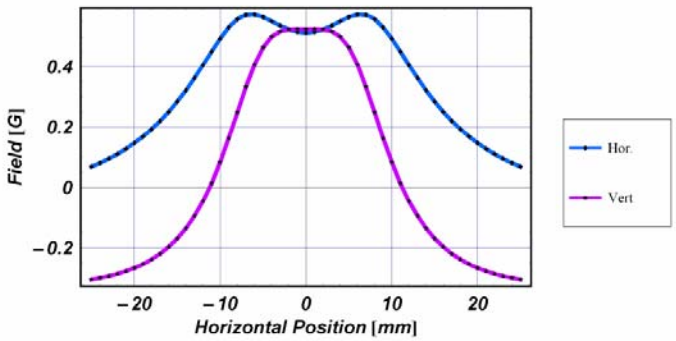

Figure 5.5.3.13 Field profile vs. horizontal position in helical mode.

References

[5.5.3.1] S. Sasaki , et al., "A new undulator generating variably polarized radiation," *Jpn. J. Appl. Phys*. 31 (1992) L1794.

[5.5.3.2] J. Bahrt, et al., "Preparing the BESSY APPLE-undulators for top-up operation," AIP SRI2006 conference proceedings (to be published).

[5.5.3.3] A. Hiraya, et al., "Undulator at HiSOR–A compact racetrack-type ring," *J. Sync. Rad.* (1998) 5, pp 445.

[5.5.3.4] T. Hara, et. al., "SPring-8 twin helical undulator," *J. Sync. Rad*. (1998) 5, pp426.

5.5.4 Three Pole Wiggler

5.5.4.1 Requirement

The NSLS-II three-pole wiggler (3PW) should be capable of producing the minimum of 2 mrad of fan angle above 1 T field. Field profile must be designed so as to minimize the emittance increase. Eq. (5.5.4.1) gives a rough estimate of emittance increase. ε_0 represents the initial emittance, N is the number of device, and B_w is the vertical field of the wiggler.

$$\varepsilon_w = \frac{\varepsilon_0 + 0.4\,N \int ds \left|B_w(s)\right|^3}{1 + 0.04\,N \int ds\, B_w(s)^2} \tag{5.5.4-1}$$

Figure 5.5.4.1 shows field, angle, and trajectory plots for the NSLS-II 3PW.

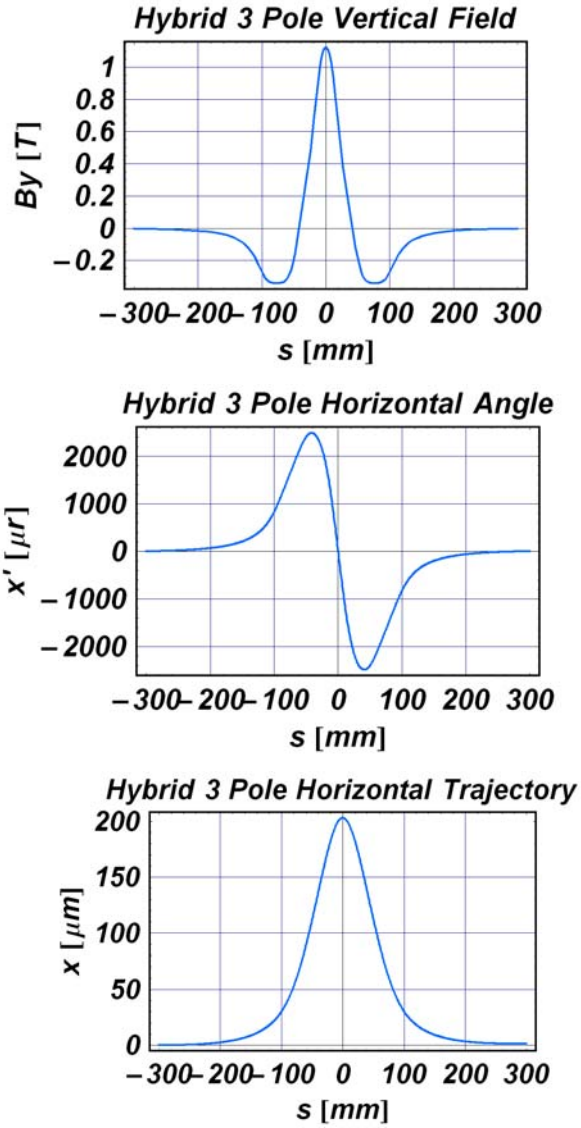

Figure 5.5.4.1 Field, angle, and trajectory plots for NSLS-II 3PW.

a) Vertical magnetic flux density at a gap of 12.5 mm

b) Horizontal angle at a gap of 12.5 mm

c) Horizontal trajectory at a gap of 12.5 mm

Figure 5.5.4.3 shows the preliminary magnetic structure of the 3PW and the distribution of magnetic flux density in the circuit. The magnetic gap in the center poles is 28 mm.

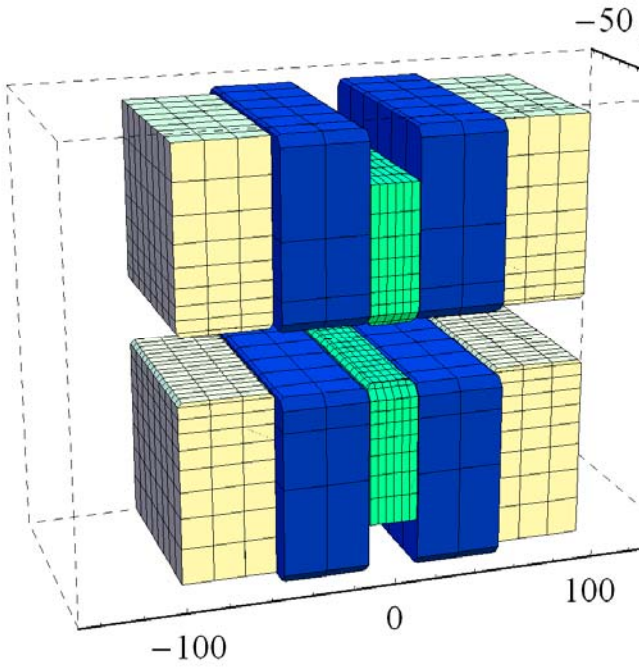

Figure 5.5.4.3 Magnetic structure of 3PW. Section in blue is NdFeB permanent magnet, green section is vanadium permendur and light yellow part is made of low-carbon steel.

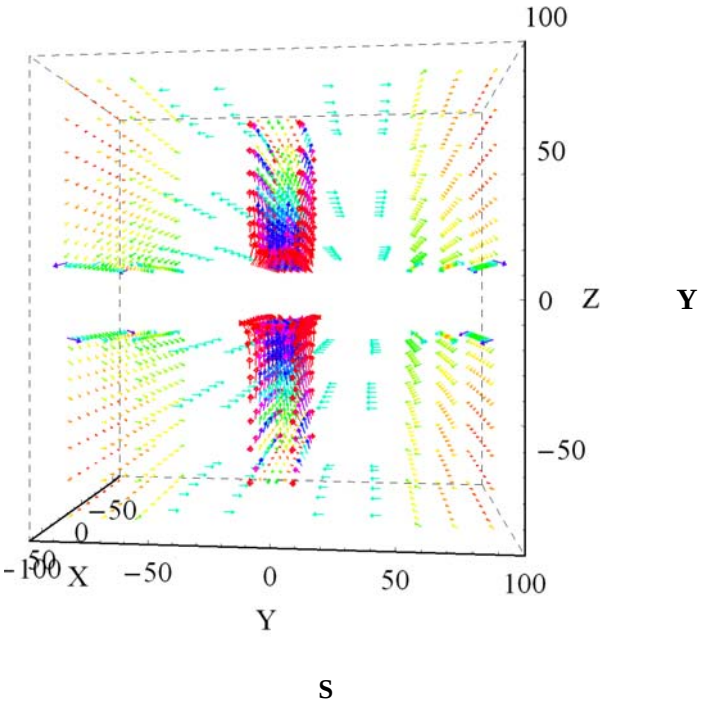

Figure 5.5.4.3 3PW magnetization vector plot.

S

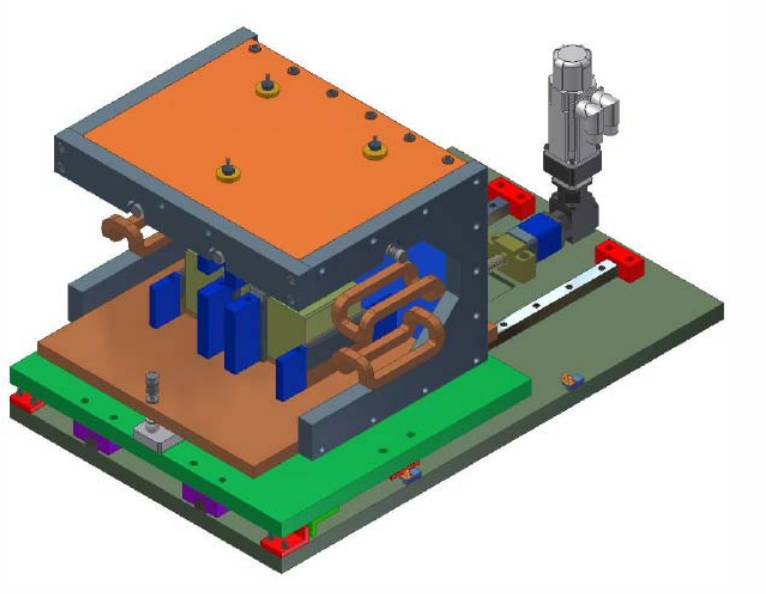

Figure 5.5.4.4
Isometric view of conceptual 3PW

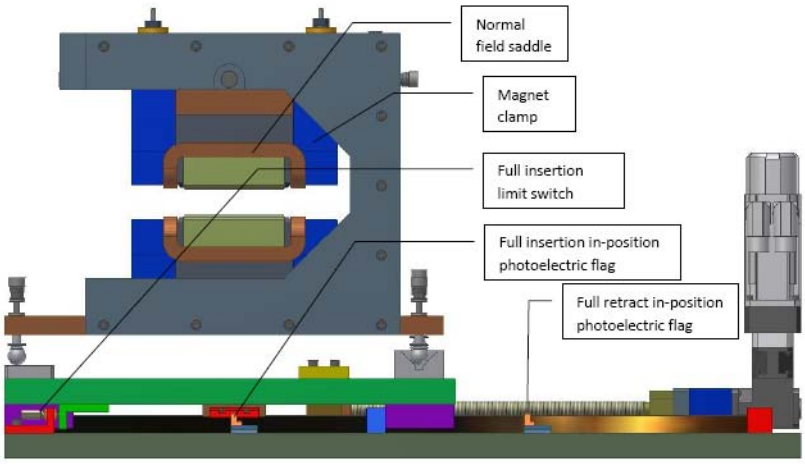

Figure 5.5.4.5
Side view of 3PW.

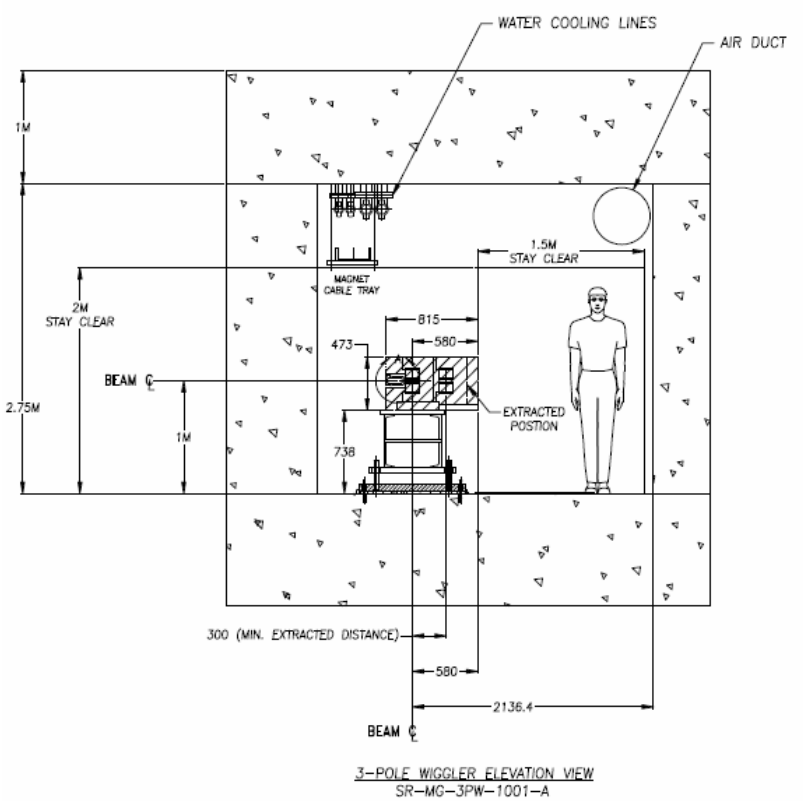

Figure 5.5.4.6 Tunnel cross section for 3PW location.

5.6 R&D Subjects and Insertion Devices for Future Consideration

In this section we briefly discuss three other types of insertion devices that will be explored in our R&D program. If these prove feasible, they would provide a number of benefits and will be considered for future installation at NSLS-II.

5.6.1 Magnetic Measurement Facility

Even though conventional insertion devices can be manufactured by industry, their ability to precisely measure the produced field is not in the state of art. Higher performance IDs to meet extremely high beam stability requirement must have very small field errors. Therefore it is essential that this project has its own insertion device magnetic measurement facility, in which each delivered device is certified and corrected if necessary. Due to handling of UHV components for IVUs, Class 10000 clean room with temperature controlled area must be secured for the measurement bench.

5.6.1.1 Requirements

Here are various requirements for the NSLS-II MMF:

1) clean area for insertion device assembly/staging
2) storage areas for insertion device parts and materials
3) temperature stabilized (± .2°C) clean-room (maybe class 10000) for magnetic survey, with gantry for overhead crane (twin 2-ton chain hoists), 7m Hall probe mapping bench, pulsed-wire test area, flowing water NMR for Hall probe calibration, and the associated electronic systems
4) machine shop, fully equipped, with storage for tooling
5) an area for winding superconducting insertion devices, with storage for parts
6) an area to setup and operate the Vertical Test Facility and also a Horizontal Test Facility for surveying superconducting insertion devices.
7) an area outside the main building—maybe an affixed structure--for bead blasting and polishing equipment, a hood for spraying paint, and an oven for curing coatings
8) office space with windows/emergency egress
9) an area for loading and unloading trucks

5.6.1.2 Building 832

Building 832 will be used to process, assemble, test and survey room temperature and cold permanent magnet undulators, and superconducting insertion devices and their associated hardware. Materials, supplies and magnet assemblies will be moved in and out of the building through the south-facing roll-up door. The large, 30 ton overhead crane will be used on occasion as required. Custom tooling/jigs for wire winding and special parts for the insertion devices and for the survey lab, will be fabricated in the shop. Parts will be polished and coated in the ‘affixed structure’ setup for that function. Areas will be set aside for the storage of permanent magnets, superconducting wire, basic hardware and other necessary ID parts and supplies. An area will be configured for winding superconducting insertion devices. In the back part of the high-bay area, the Vertical Test Facility, and later a Horizontal Test facility, will be setup for testing those superconducting designs. The permanent magnet type insertion devices will be assembled in the assembly/staging area. They will then be moved into the temperature stabilized clean-room for magnetic survey and field corrective

shimming. Cold measurement for CPMUs will also be conducted in this area. The finished devices will then be moved, maybe by flatbed trailer, to the ring for installation.

5.6.2 New Magnetic/Pole Materials

An avenue of further development of CPMUs is to investigate other rare-earth magnets that do not exhibit the spin re-orientation transition at 150K. For example, PrFeB has similar Br as NdFeB at room temperature, but its Br continues to increase further all the way down to 4K. PrFeB would permit use of liquid nitrogen to cool the CPMU to 77K and thereby attain an additional 5 to 7% increase in field. NEOMAX produced a few research samples of PrFeB several years ago, and again just recently. Although the material is not available commercially, we are discussing with NEOMAX and with SPring-8 the possibility of a funded PrFeB development project.

We will also investigate the use of exotic pole materials, such as oriented dysprosium, with a reported saturation flux density up to 3.5 Tesla at cryogenic temperatures. This opens the possibility of a CPMU built with PrFeB magnets and Dy poles, operating at 77K or lower with significantly higher performance than with NdFeB and permendur poles. This may ultimately reduce or eliminate the need for the complexity of superconducting undulators. This project will draw on the expertise in dysprosium and permanent magnet materials at the BNL Materials Science Department. If development of both PrFeB magnets and oriented Dy poles is successful, a short prototype undulator magnet module could be constructed and tested in our existing Superconducting Undulator Vertical Test Facility.

5.6.3 In-Vacuum Magnetic Measurement Systems

Two types of measurement systems are used to characterize the field quality of an insertion device at the magnetic measurement laboratory at NSLS. The first is a pulsed-wire measurement system that can be used to check the trajectories in both horizontal and vertical directions. It is also used to find the correct coil current of a Helmholz coil to cancel the earth field. The second type is a Hall probe mapping system. The Hall probe scan is done “on-the-fly,” starting from a precise home position, acquiring the desired number of samples per undulator period.

One of the challenges for CPMU development is to establish an accurate low-temperature field measurement system. For properly designed undulators, the differences in field quality between room temperature and low temperature are expected to be small. However, it is essential that the field quality be verified at the actual operating temperature. A vertically oriented cryogenic magnetic measurement apparatus for prototype undulator models up to 0.4 m in length has been developed and used at NSLS [5.6.1]. In order to measure full-length devices in a horizontal orientation, a new measurement scheme must be developed. The magnetic measurement should be done in the vacuum vessel at the cold operating temperature, but not necessarily in UHV. Figures 5.6.1 and 5.6.2 delineate the concept of an in-vacuum, in-situ Hall probe mapper based on square chamber design. It is mounted on the large rectangular front flange of the chamber. Hall probe position accuracy is maintained by a laser tracker and piezo controller. ESRF and SPring-8 have independently developed in-vacuum Hall probe mapper based on their cylindrical shape vacuum chamber. It is essential to establish our method of precise field measurement to produce the state of the art insertion device such as CPMU.

For field integral measurements, an in-vacuum moving wire system has already been developed by ACCEL and ESRF. A similar mechanism can be used for a pulsed-wire system.

There is no convenient way to make in-situ (i.e., in-vacuum) field error corrections unless a remote-control magnet adjustment mechanism is incorporated in the magnetic arrays. In the absence of this development, field error correction must be performed iteratively, where each iteration requires a lengthy series of warm-up, venting, measurement, adjustment, pump-down, and cool-down steps. Our goal is minimize the number of such iterations by 1) designing the mechanical components to minimize the

systematic field errors resulting from warm-up and cool-down, and 2) developing an efficient scheme of warm shimming and cold measurement. Ideally, field errors may track with temperature, so shimming at room temperature may suffice.

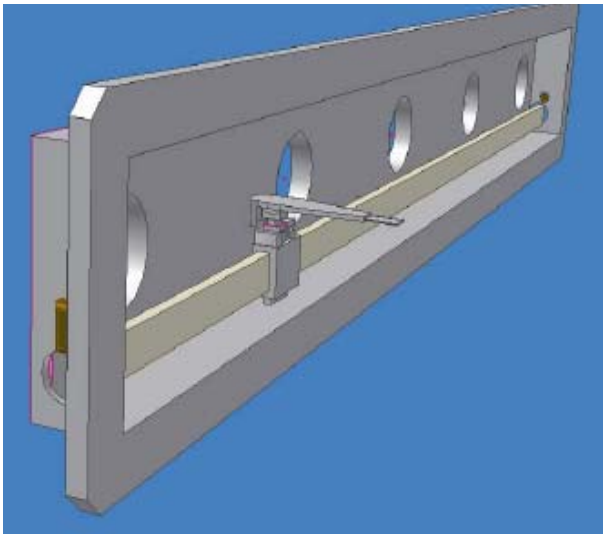

Figure 5.6.1 Hall probe mapper mounted on the flange cover.

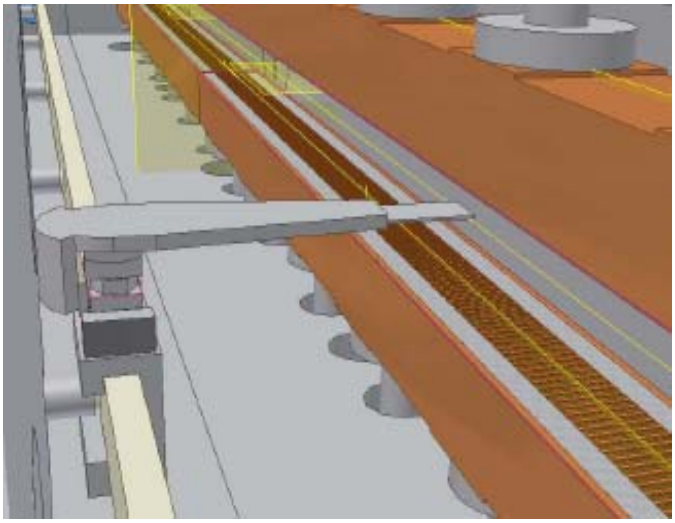

Figure 5.6.1 Mapper position with respect to the magnet arrays.

This system will be designed to be used primarily in the measurement laboratory but can also be used to perform in-situ measurements of insertion devices in remote locations such as a synchrotron tunnel. This system will incorporate a horizontal vacuum chamber that could accommodate either a CPMU or HTSCU that is 3+ m long and that demonstrates efficient installation of in-situ shimming and measurement of the magnet modules without the need for chamber reassembly. A cryogenic Hall probe, pulsed/vibrating wire, and moving wire will be investigated. The research phase will demonstrate the incorporation of an in-vacuum measuring system with the vacuum vessel and precision gap separation mechanisms.

The goal of this development is to demonstrate cryogenic undulator measurement concepts that will ultimately be used in the characterization, shimming, and in-situ measurements of all the production in-vacuum and cryogenic insertion devices.

5.6.4 Quasi-Periodic Undulator

Undulators designed to produce tunable vacuum ultra-violet and soft x-rays are of necessity long-period devices with period lengths of 40 to 100 mm or more. Because the characteristic K-parameter is proportional to the product of peak field and period, long-period undulators have necessarily high K values. Planar and elliptical undulators with high K-values produce spectra rich in harmonics (primarily odd-integer harmonics, since even harmonics are suppressed on-axis). In fact, the first few harmonics produced by high-K IDs have higher brightness and generate more SR power then the fundamental. If the user's monochromator is tuned to the fundamental, unwanted harmonics corresponding to higher orders of the monochromator pass through the exit slit unimpeded, polluting the monochromatic light and imposing an excessive heat load on optical components.

The Quasi-Periodic Undulator [5.6.2] was developed to overcome this problem. As the undulator's field amplitude pattern is altered, integer harmonics can be suppressed and replaced by noninteger harmonics. The latter do not coincide with higher orders of the monochromator and do not pass through the exit slit. The transmitted light is then purely monochromatic, and sensitive optics are protected. The monochromator must still absorb the unwanted harmonic power somewhere, but this can be accomplished by cooled absorbers at

the exit slit. As with a conventional undulator, the monochromator can be tuned to any of the noninteger harmonics of the QPU to extend the spectral coverage of the instrument.

The QPU concept has been applied to both planar and APPLE-II type IDs. In circular polarization mode, the APPLE-II generates only fundamental radiation on-axis, so the QPU is of no benefit in that case. But in planar and elliptical modes, the quasi-periodicity helps manage the harmonic power and improves spectral purity, as described above. Special care must be taken to absorb the radiated heat in vertical direction in helical / elliptical mode for long period device due to large value of K_x.

5.6.5 Superconducting Wiggler

Higher photon energies (above 20 keV) can be effectively covered by a superconducting wiggler at NSLS-II. For a field range of 3.5 T, 60 mm period length, and a 10 mm magnetic gap, low-temperature SCW technology is now well established. However, achieving 6.0 T with the same period and gap will be a challenging task. In contrast, devices based on the use of **h**igh-**t**emperature **s**uperconductors are a very promising approach for medium-field wigglers and would reduce the cost of both construction and operation. However, the current density now available for HTS wire remains inadequate to produce the necessary field. Thus, the baseline design for the NSLS-II SCW will be the SCW60 device described in Chapter 5, which is based on conventional LTS technology, but R&D will be carried out to investigate HTS wiggler designs.

5.6.6 Superconducting Undulator

The first superconducting undulator in an electron storage ring was installed at LURE, Orsay in 1979. Since then, various devices for FELs have been developed [5.6.3]. In the past fifteen years, IVUs have been the primary device for short-period undulators. One of the reasons for not using SCUs in the storage ring is the difficulty of opening the necessary gap for injection. A new SCU with a variable gap mechanism has been in operation at ANKA [5.6.4] for the past few years. It has a rather complicated two-vacuum vessel structure, one vacuum for UHV and the other for insulation. The vessels are separated by 300μm stainless steel foil. The required performance was barely achieved due to 1) excessive heat load, which reduced the critical current achievable, and 2) a structural problem that contributed to the degradation of phase errors.

SCUs with conventional NbTi wire face serious problems to reduce the heat load onto the device's cold mass to a level manageable with modern cryocoolers. Unfortunately, state-of-the-art cryocoolers have a cooling capacity of less than a few watts at 4K. What is needed is a different type of LTS wire that can withstand higher operating temperatures. One approach is to use Nb3Sn; this is being pursued by the ALS group [5.6.5]. This type of wire is best suited for high-field applications. However, it is difficult to create the precise structure required for undulators, due to the wind and react process. Another approach is to use APC NbTi wire, which is supposed to be operated at much higher current density than conventional NbTi wire. Using this approach, extra space for heat shielding may be available for a fixed-gap vacuum chamber.

Even with these developments, SCUs based on LTS technology will still have substantial thermal challenges. It may be that SCUs will not be viable until future developments in HTS technology make it possible to manufacture an HTS device. There is reason to be optimistic about this, and the NSLS-II project will monitor HTS industry developments.

Another issue for SCUs is field correction. Extra wiring to correct phase errors has been attempted, but distributed integrated multipole corrections appear to be difficult. They might require correction at the end of the device. These also are issues for future development.

The initial phase of this work was supported by two SCU-related LDRDs along with investigations to take advantage of new developments in the field of applied superconductivity.

One of the activities in this project is to demonstrate the capability for industry to produce lengths of APC NbTi and optimized Nb_3Sn superconductor that could be used to produce up to 1M long SCUs. Conductor

produced in this project can be used to produce 1/3 meter undulator prototype magnets that could be tested in the VTF.

In addition, this project will aggressively investigate films coated with high-temperature superconductors such as YBCO, MgB2, and other advanced materials, and determine the feasibility for their possible use in future SCUs and SCWs. Direct deposition methods for thick-film and multiple-layer superconducting for use in HTS magnet assemblies will be investigated in the first year. If feasible, these materials will be integrated into SCU shimming concept prototypes in the second year. This project will also investigate the design and demonstration of a superconducting EPU prototype that can be tested and measured in the VTF in year 2 or 3. The goal of this project is to demonstrate a variety of viable materials, manufacturing, and magnet design concepts for use in a NSLS-II SCU, and ultimately establish reliable superconducting insertion device technology that can be offered to meet the needs of NSLS-II users.

5.6.7 Revolver Type

If one type of magnetic array cannot satisfy the user's requirement, two or more different arrays could be used interchangeably, in a "revolver" type undulator system [5.6.6]. In-vacuum revolver type systems have also been developed. Revolver designs have been built at SPring-8 and ESRF and are operating reliably. In-vacuum revolver undulator was also developed by SPring-8 and installed at Pohang Light Source in Korea. This is a subject for future consideration, depending on the user requirements.

References

[5.6.1] D. Harder, et al., "Magnetic measurement system for the NSLS superconducting undulator vertical test facility," Proc. 2005 Particle Accelerator Conference, Knoxville, USA (2005).

[5.6.2] S. Sakaki, et al., "Conceptual design of quasiperiodic undulator," *Rev. Sci. Instrum*. 66 (2), p 1953 (1995).

[5.6.3] G. Ingold, et al., "Fabrication of a high-field short-period superconducting undulator," *Nuc. Instr. & Meth. A* 375 (1996) p. 451.

[5.6.4] A. Bernhard, et al., "Planar and Planar Helical Superconductive Undulators for Storage Rings: State of the art," Proc. 2004 European Particle Accelerator Conference, Lucerne (2004).

[5.6.5] S. Prestemon, et al., "Design and evaluation of a short period Nb3Sn superconducting undulator prototype," Proceed. 2003 Particle Accelerator Conference, Portland, U.S.A. p 1032 (2003).

[5.6.6] H. Kitamura, et al., "Recent developments of insertion devices at SPring-8," NIM-A, 467, (2001), pp 110.

6 CONTROL SYSTEM

6.1 Introduction and Scope

The control system for NSLS-II is designed to convey all monitor, control, model-based, and computed data from all accelerator, facility, experimental, safety, and operations subsystems to accomplish supervisory control, automation, and operational analysis. The scope of the control system extends from the interface of the equipment being controlled through to the designers and operators of the accelerator facility, as well as synchrotron beamline experimenters and staff. The control system includes all hardware and software for global systems such as timing, deterministic data communication, network communication, control room operations, automation and optimization. The control system includes the computers and software required to implement and integrate all subsystems including: diagnostics, power supply control, low level RF, vacuum, personnel protection, equipment protection, undulator, experimental beamlines, and conventional facilities

To provide this comprehensive monitoring, control, and automation, the NSLS-II control system must scale to support 100,000 physical I/O connections and 350,000 computed variables that can be correlated to analyze events and provide data for all control aspects. It must support 1 Hz model-based control, 110 kHz power supply digitization, 500 MHz RF control, 5 KHz orbit feedback, and 20 millisecond equipment protection mitigation. It also must provide 5 Hz updates to operators of up to 1,000 chosen parameters, provide coherent turn-by-turn orbit data for up to 2^{10} = 1,024 consecutive turns (for FFT), archive up to 6,000 parameters at a rate of 0.5 Hz continually, latch the last 10 seconds of data from all parameters in the storage ring when a fault is detected in the Machine Protection System (MPS), archive up to 1,024 consecutive turn by turn data for 1,000 parameters at a rate of 10 Hz, and provide pulse-to-pulse beam steering in the linac at 1 Hz.

Our proposed client-server architecture is depicted in Figure 6.1.1. Different levels of access and control reside at distinct layers. At the highest layer (layer 3), access is provided for activities that do not involve moment-by-moment control or monitoring of the accelerator. Layer 3 includes high level physics modeling, making use of live data and data stored in the site Relational Database (RDB in the figure). Experimental activities that do not require synchronization with the ring also reside at layer 3. Layer 2 contains accelerator operation and monitoring activities. Layer 1 contains dedicated equipment controllers, which in turn interface to specific equipment through point-to-point protocols (event system, deterministic data communication hardware for Fast Orbit Feedback. Layer 0 contains remote, slow, independent, reliable control that requires synchronization with the accelerator no faster than 2 Hz such as facility control, vacuum control, or Personnel Protection.

Communication between subsystems takes place via four distinct buses as indicated. Fast Feedback, MPS, and Global Synchronization buses supply information as implied for the needs in a deterministic and reliable fashion of these control operations. Asynchronous information flow which does not require specific transfer rates is achieved by Channel Access Protocol. This is the most global communication standard in the system and, accordingly, most devices in every layer are identified as channel access clients, servers, or both.

The standard two-layer client server architecture ensures scalability and avoids performance limitations. NSLS-II controls must be built upon a proven tool kit with well-defined interfaces at both the server and client to enable integration and development. It should enable the use of hardware and software already developed for specific light source requirements. The core of the Experimental Physics and Industrial Control System (EPICS) has been chosen as the basis for the control system. The advantages in three key areas drove this decision: large user base in the accelerator community, functionality for accelerator-related systems, and support for the required hardware interfaces.

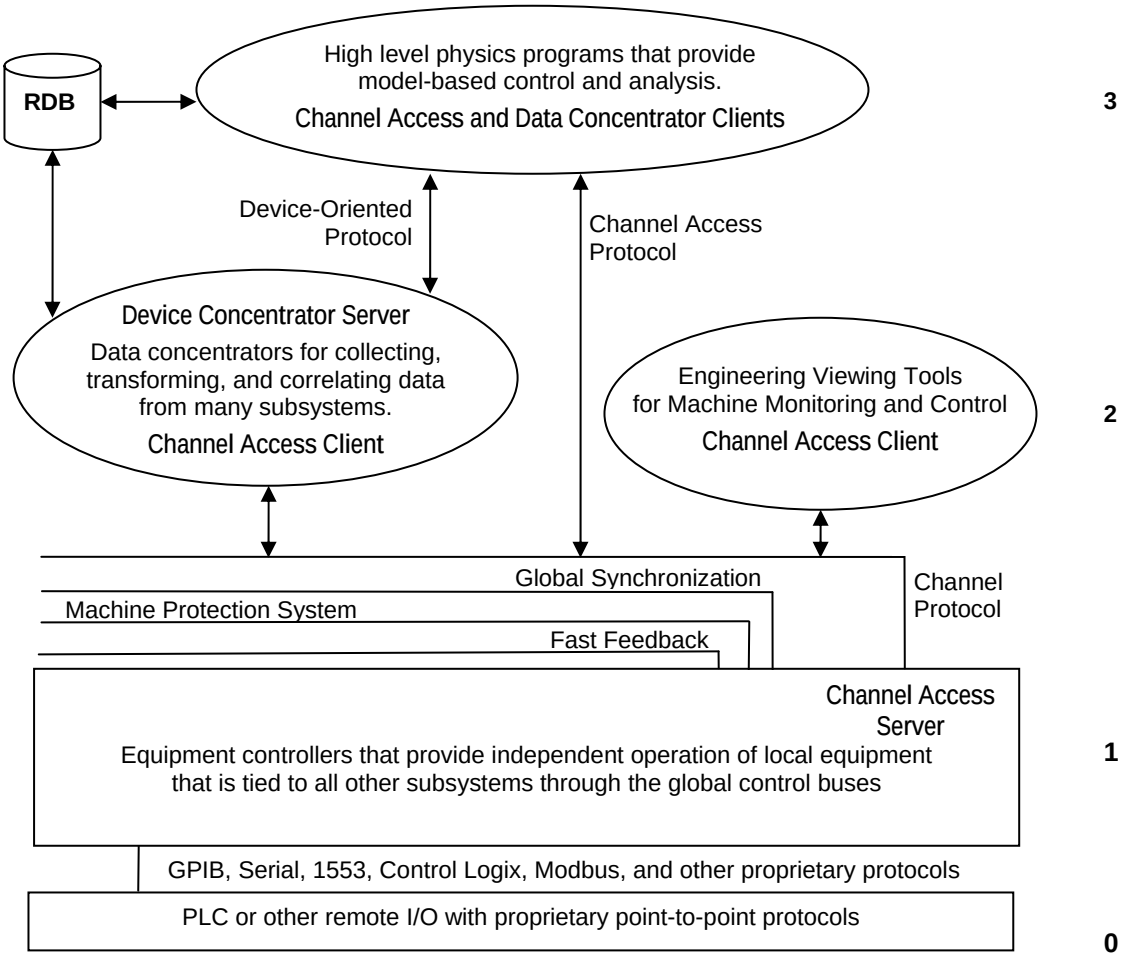

Figure 6.1.1 NSLS-II software architecture.

6.2 Control System Requirements

6.2.1 Technical Requirements

The control system must be modular, incrementally upgradeable, scaleable, and extendable. Expansion of the control system to accommodate the build-up of the accelerator and beamlines from early testing, through installation and commissioning, and during the life of the facility, should not impact the performance. The control system must be available to support all aspects of the project schedule, from component tests during prototyping to beam characterization and optimization at commissioning. To achieve this, the NSLS-II control system is based on open standards and commercial off-the-shelf equipment, whenever possible. Developments needed by NSLS-II are to be accomplished in a manner that meets the project schedule, budget, and performance needs, with consideration for knowledge transfer to the wider accelerator community.

Machine Control

Machine control supports linac control that is synchronized to the master timing system to fill the booster ring with 80 nanosecond pulse trains made up of 40 micro bunches of 2 ns length each. Pulse-to-pulse timing jitter will be less than 80 ps at the 1 Hz rate. The pulse is ramped up to the correct energy in the booster ring over 400 ms. It is then injected into the storage ring. The revolution rate for the booster and storage ring is 2.6 μs. Manual control of orbit trims, quadrupoles, sextupoles, and insertion devices is asynchronous. These are controlled by the operators, accelerator physicists, high level applications, or users. In particular, ~10 Hz write/read is suitable for "turning knobs" for a power supply. The only "fast" process is the fast orbit feedback system with 5 KHz bandwidth (and feedback systems for coherent bunch instabilities of order MHz). To summarize, the beam bunches in the ring and the injection process are synchronous to the RF, but everything else has its own time scales. Model-based control is used to correct steering, the orbit, tune, linear chromaticity, optics, etc. in the storage ring at 1 Hz.

System Reliability

The control system must have 99.99% availability, 24 hours per day, 365 days per year. Control system modifications that add new functionality will be performed during scheduled down times. New functionality for the operational facility will be tested on equipment test stands before installation. The cryogenic control must achieve even higher standards. Failures or modifications to the cryogenic control system must not result in the loss of temperature control for greater than 15 minutes. Subsystems will be designed to meet system reliability goals using high reliability technology, where required. This includes the use of an uninterruptible power supply, programmable logic controllers, battery backup, and redundant power supplies for VME crates. All subsystems will be designed to achieve operational reliability goals.

Security and Integration across Operator Base

The system must manage access requirements for the different classes of user. It must also incorporate appropriate tools to guarantee security of its computers and network systems. The source of the data should be irrelevant from the point of view of any software designer or user. For example, it should be possible to display data from the control system, from the associated relational database and from an accelerator model on one full-screen synoptic.

6.2.2 Software Requirements

Control system applications must be designed to enable future upgrades to be incorporated economically. Well defined interfaces to support the modular upgrade/replacement of code is a key component for this requirement. The EPICS architecture provides these interfaces at all levels implemented in EPICS. The software used to implement Fast Orbit Feedback (FPGA code) and the software used to implement High Level Applications will attempt to accomplish this same level of modularity.

Code Maintenance

All code, control system tools, and applications will be placed under source/release control. A standard tool will be used to control the version of software running and to keep previous versions and an audit trail for changes to released and commissioned software. Accelerator components and signal lists such as: magnetic lengths, min/max currents, calibration coefficients for currents vs. gradients, diagnostics channels, and configuration parameters also will be kept and their versions managed. The data that are also needed by accelerator models are to be kept in a similarly controlled relational database.

Open Standards, Integration, and Ease of Use

The control system will use open standards and an open architecture. The long life expectancy of an accelerator complex implies that the control system will need to evolve to incorporate upgrades and new technology. The control system must enable seamless integration of systems at both the server and client side through well-defined APIs. It is beneficial for the applications that comprise the NSLS-II control system to have a consistent look and feel. Related functions should be linked, to reduce the number of mouse clicks a user has to perform. For example, trends could be accessed by clicking on a process value hotspot displayed on a plant synoptic value. All control system facilities that need to be accessed directly will be accessible via menus, where the menu titles give a clear indication of the facility being called up. It should never be necessary for a user to remember the name of a program or of data files in order to use the system.

Context-sensitive online help facilities should be designed into the system, where feasible. Conscientious attention to common-sense ergonomics during application development will clearly pay dividends for long-term ease of use and will minimize familiarization and training costs for new operators. Production of a concise Style Guide document at an early stage in the development cycle of the project will provide a good ethos for addressing these issues.

6.2.3 Architecture Requirements

The four-layer EPICS-based client-server architecture illustrated in Figure 6.1.1 implies further design considerations for its implementation:

Network

The connection of the control system layers will use standard network components. These should be in a redundant configuration and include provision for network evolution, i.e., the development to the latest network standards. Control system network security is to include physical security that limits access to the control network from outside, using gateways and firewalls. It requires appropriate types of password and key protection within the control network with access control to manage who is controlling which operation.

Operator Interface

The operator interface will be either workstations or PCs running Linux. The control system should seamlessly integrate with office systems through a gateway process to maintain security.

Equipment Interface

The equipment interface will provide the physical connection to the equipment being controlled through a variety of interfaces. The preferred standards will include VME because of physical and electrical performance, Compact PCI where higher performance backplanes or lower point count make this more cost effective, and PLC I/O for applications where equipment safety is required and speed is not. The control system includes all VME crates and processors, any network hardware required for integrating instrumentation, the timing/event system, all hardware used for fast feedback, and all the crates and processors used to integrate the I/O. Except where noted, the intelligent device controllers, I/O, and PLCs are provided by the subsystem. The notable exceptions are the controllers for the undulator equipment and the non-BPM diagnostics in the Storage Ring. The network cables and cables to implement the global buses are the responsibility fo the control system.

Relational Database

The control system must include a relational database as a central repository for all configuration information. This should include all static information about accelerator components such as coefficients to calculate field magnetic strength from current. Consideration should be given to extending the database to include all technical information to enable subsequent support and maintenance. At the application level, there should be a unified and seamless interface to both the static and dynamic data.

6.3 Identification of Control System User Groups

The control system must support several user groups, each with varying requirements.

Accelerator Operators

Accelerator operators are the principal managers and users of the control system. It must be a complete and consistent interface for them to perform any function in the accelerator complex. The data and interfaces must be consistent in how data is presented and how equipment is seen to behave. The operation of the accelerators requires real-time control and monitoring of the equipment, archiving, alarm handling, sequencing, backup and restore for routine operation. For these users, alarm and error messages should be supported by information regarding recommended courses of action. The control system should allow the automation of plant operating tasks. It should provide applications that encourage and facilitate the keeping and passing of operation logs, particularly from shift to shift.

Accelerator Physicists

The accelerator physicists' requirements for the control system include all the routine operations of the control system together with the ability to integrate programs developed to support different accelerator models. Functionality is required to allow easy acquisition of data produced as part of an experimental run, and to provide the ability to switch between different accelerator models. Data retrieved from the control system must be acquired with sufficient time accuracy to enable accurate correlation.

Technical Groups

The technical groups require diagnostics to enable maintenance such as calibration and fault finding. Access to the control system is required in the main Control Room, local to the equipment, and potentially in the offices, laboratories and off-site. Applications must provide all diagnostic information necessary to assist in commissioning and debugging of equipment. They must provide useful fault diagnosis facilities to assist with plant equipment maintenance and maintenance of the control system itself (both hardware and software). An easy interface to databases of equipment properties, manufacturers, documentation, cabling data and fault histories is required, as well as access to information clearly identifying the geographical location of equipment and a system of fault prediction facilities to allow for scheduled maintenance of components likely to fail.

Beamline Staff and Experimenters

The end users of the experimental station require a straightforward graphical interface to the control system. They also require good integration of control system parameters with the experimental control and data acquisition systems. This is particularly necessary in the case of synchronizing scanning of a sample with changing a parameter on an insertion device in the storage ring, e.g., the gap of an undulator. Experimenters require clear information on light source status, performance, and timing signals, and may require remote access (i.e., from off site) to experiments and beam-lines.

Control System Engineers

Control system engineers require current and archived data on the status and behavior of the entire control system. Information required includes CPU loading, network loading, application monitoring (for frozen/crashed applications), connectivity status, and reports of any control system faults.

Facility Managers

The control system should be capable of producing operating reports and statistics in a form that can then be imported into software applications (i.e., spreadsheets, web-based tools, etc.) used by management. Information required could include the number of hours of beam time supplied to users and unplanned beam dump statistics – how often these events occur, time taken to restore beam, reason for beam dump, and signs of common modes of failure.

Public Users and Staff

A wide range of other groups will require information from the control system. These include technical and scientific groups on and off site. These groups should be served through a web service as the user interface.

6.4 EPICS Toolkit

EPICS is the result of a collaboration of control groups, across a number of research organizations, to produce a tool kit to build distributed control systems. The resultant tool kit reduces software development and maintenance cost by providing: configuration tools in place of programming, a large user base of proven software, a modular design that is expandable, and well defined interfaces for extension at all levels.

Worldwide, EPICS has a very large user base for a variety of accelerators, detector systems, astronomical projects, and industrial processes. Most recently, EPICS has been successfully deployed at the Diamond Light Source, the Spallation Neutron Source at ORNL, and the Australian Synchrotron Project. It is being used for the LINAC Coherent Light Source at SLAC, the Shanghai Light Source, and the multi-faceted accelerator facility JPARC at Jaeri.

The use of EPICS on a diverse range of projects means that there is a large base of drivers and hardware support already available. The existence of these makes interfacing of the underlying systems less dependent on software development.

The EPICS tool kit is supported through the collaboration with software distribution and documented through the web. There are EPICS training courses run each year by many groups in the collaboration, and there are two EPICS workshops rotating through the U.S., Europe, and Asia each year; a number of individuals and companies are also available to provide support and training.

6.4.1 Structure of an EPICS Control System

EPICS embodies the standard client server model for a distributed control system, and shown in Figure 6.4.1. The user consoles are one class of client that receives and processes information. The servers are the source of information and in the general case, the interface to the equipment being controlled. The clients and servers are physically connected using network technology and they communicate with the EPICS protocol Channel Access.

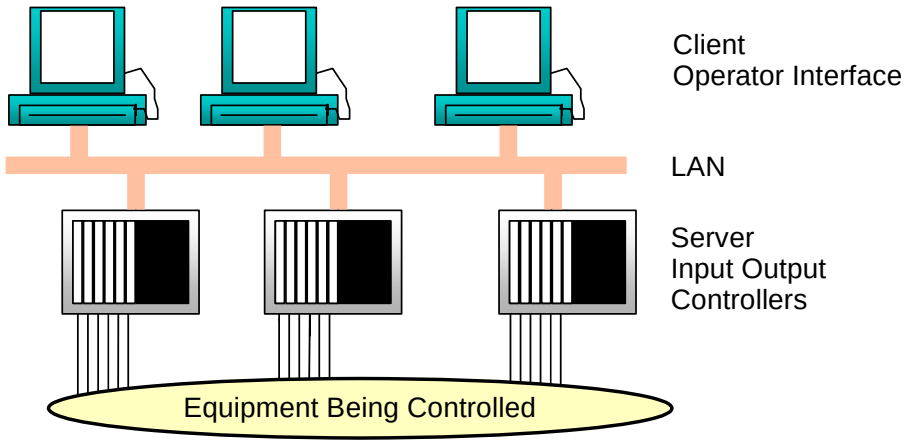

Figure 6.4.1 EPICS model.

6.4.2 EPICS Servers

The physical realization of EPICS servers is typically as multiple embedded VME systems, which are called IOCs, Figure 6.4.2. IOCs interface to the equipment being controlled, for which EPICS supports a large range of physical interface standards, protocols, and devices. IOCs also support the use of an event timing signal, to time-stamp transactions and enable synchronous acquisition or control across multiple IOCs.

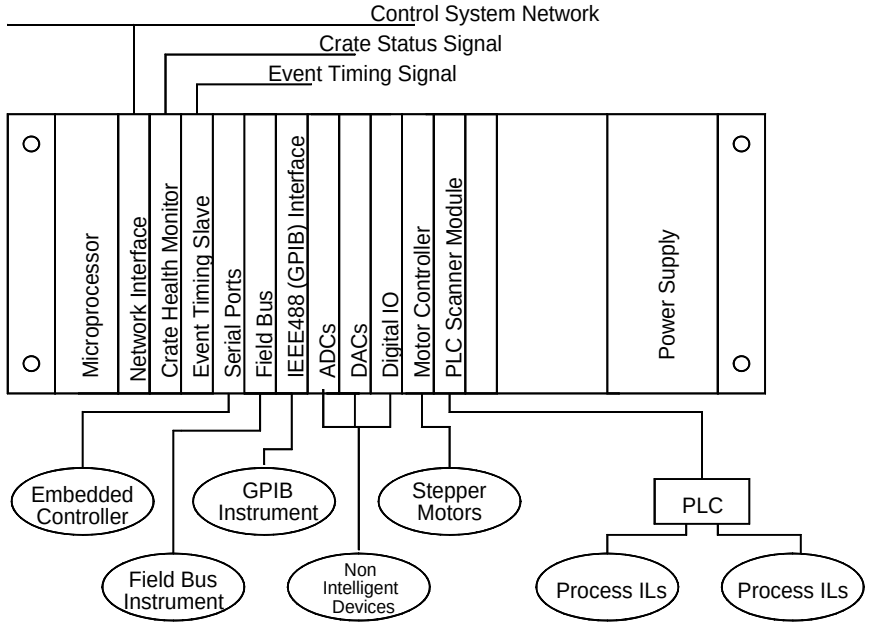

Figure 6.4.2 Example EPICS IOC.

6.4.3 Server Side Processing

Within the IOC, the CA server communicates with the Process Database, which uses the Record Support, Device Support, and Driver Support layers to interface to the plant, Figure 6.4.3. The communication from the EPICS client, over CA to the database, can be by synchronous call and reply or by the client establishing a monitor whereby the server asynchronously serves the data. The update of monitors can be on a periodic basis, on change of data, or on external event.

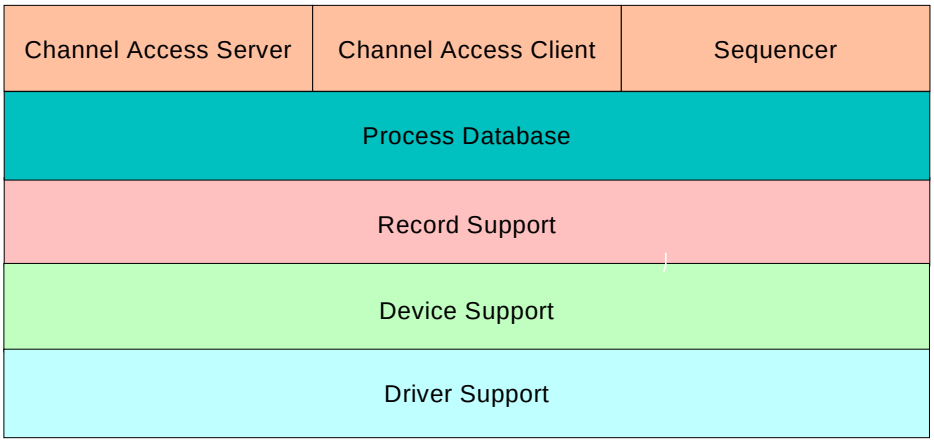

Figure 6.4.3 EPICS IOC data model.

The process database is a memory resident database that defines the functionality of the IOC. The database uses the Record Support layer to perform the processing necessary to access IO, perform data conversion, check alarms, and update monitors. The IO operations are carried out through the Device Support layer, which handles equipment specific protocols, and through the Driver Support layer, for the hardware interfaces. The structure provides support for interfacing to embedded controllers, field buses, IEEE488 (GPIB), DACs, ADCs, Digital IO, stepper motors, PLCs, power supplies, and a range of instrumentation.

Within the Input/Output Controller there is also a CA client to facilitate IOC-to-IOC communication. This is realized by linking process information from one process database to a process database on another IOC.

An IOC also contains a Sequencer to perform Finite State Machine control on the process database. The sequencer logic is defined as SNL, which is compiled to C code, then to an executable to run on the IOC. This allows for easy production on complex sequences, such as switching through the steps in bringing on a piece of equipment.

A standalone version of the CA server is available, which can be integrated into other systems without the process database and support layers. This facilitates integration of self-contained systems into EPICS, one example being the integration of LabView systems.

6.4.4 EPICS Clients

The client side of EPICS is realized on either Unix workstations or PCs running Windows and is called the OPerator Interface (OPI).

In the standard EPICS model, the OPI application programs interfaced directly to the CA client. This has limitations in that it only provides access to the dynamic control data through the CA API and so limits seamless integration of data from other sources, e.g., a RDB. The EPICS toolkit provides a suite of applications for the OPI. Among the choices for the core tools are: a synoptic user interface for control and monitoring (EDM), an Alarm Handler, an Archiver for recording and retrieving the historical state of the control system, a backup and restore facility to take snapshots of parameter settings, a knob manager to provide attachment of physical knobs to parameters and a parameter plotting tool. There is support within EPICS for the scripting languages Jython, Matlab, Tcl/Tk, Perl, and LabView. Data can be further served up to web pages through a CGI server.

6.4.5 EPICS Development Environment

The functionality of a control system built with EPICS is defined in three places: the Operator Interface, the Process Database, and the Sequencer logic. EPICS provides a number of tools to develop each of these which do not require software development. The OPI applications can be produced by a number of interface-generating tools, one of which is EDM. These tools allow for control objects to be placed on pages and animated with a connection to the control parameters. There are both text and graphical tools to produce the Process Database, which involves selecting records and drivers, and linking them to process data and alarms. The Sequencer logic is produced from SNL, which can be defined as text or, more recently, in a graphical form.

6.4.5.1 Distributed Development

Each developer will work on either a Linux PC or a Windows PC. These will be networked to a development file server providing read-access to all the necessary development tools and applications (VxWorks, RTEMS, Matlab, XAL EPICS base and extensions, configuration and database files, etc.), see Figure 6.4.4.

Modifications will only be made to local copies of applications, which will then be checked in to a branch of the CVS repository to enable any changes to be backtracked. When the application has been fully tested and is stable, this branch will become the main development branch for the control system.

A central boot server will be used to provide all the necessary files required by the local IOCs for booting. These files will be generated from the CVS repository. This will ensure that all IOCs are running a consistent and stable version of the control system. The contents of the central boot server will be mirrored on boot servers located in the control room, which will provide local booting of the IOCs.

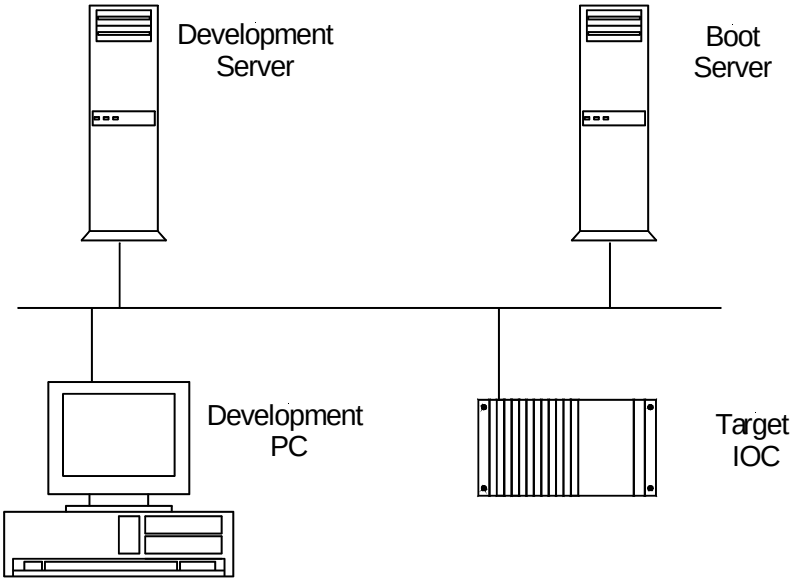

Figure 6.4.4 Distributed development structure.

File Management with CVS

CVS [6.5] is a version control system for keeping track of all modifications to project source code files. CVS is widely used in both open source and proprietary software development projects, and is generally

considered to be the best freely available, full-featured version control tool. Two features make CVS particularly suited to collaborative development across any network, including the Internet:

- Multiple developers can edit their own working copies of files simultaneously. CVS then deals with combining all the changes and notifying developers when there are conflicts.
- Developers have remote access to source code file repositories. Project members can obtain and modify project files from virtually anywhere.

CVS is a client-server system. The CVS repository is maintained on a server; clients run on users' machines and connect to the server via the network (or Internet). Clients are available for nearly all platforms, including Unix, Windows, Macintosh, and any Java-based platform. CVS allows project members to:

- Check out source files and directories
- View differences between versions of files
- View change log history and comments
- Commit changes made in their local copies of the source files to the main source code repository
- Update their local project files when they want to remain in sync with changes committed by other project members

CVS has proven very beneficial to many other accelerator projects in the world, and there is a very large CVS knowledge base within the EPICS community.

6.4.5.2 Application Development

Most application requirements can be met through the standard tools discussed in this section. Where more intelligence is required at the application level, there are EPICS interfaces to all the popular programming languages. The preferred solution will be to use C/C++, Java, or scripting languages to minimize the number of supported languages.

C/C++. C, and C++ are high-level programming languages that have become the de facto standard for portable open systems solutions on Unix/Linux platforms, with C++ usage increasing due to the popularity of Object-Oriented design and programming. Both languages have been widely used both for the EPICS baseline product and for driver software and other applications built on top of the baseline. For the NSLS-II Control System, the emphasis will be on re-use of existing software. Improvements are expected to meet NSLS-II requirements.

Tcl/Tk, Python/Jython. Tcl and Python are widely-used open-source scripting languages. They have simple and programmable syntax and can be either used as a standalone application or embedded in application programs. Tk and Python are Graphical User Interface toolkits that can be used for rapid development of powerful GUIs. Tcl/Tk and Python are highly portable, running on essentially all flavors of Unix (Linux Solaris, IRIX, AIX, *BSD*, etc.), Windows, Macintosh, and more. Tcl/Tk and Python are well supported and extensively used on many EPICS-based projects, particularly for GUI development.

Java. Java is an object-oriented interpretative programming language with a built-in Application Programming Interface that can handle graphics and user interfaces. Java can be used to create standalone applications. However, a more important use is in the development of applets, programs that can be embedded in a Web page. The growth of the Internet, together with Java's hardware independence, has made the language essential for web-based developments.

Currently, Java performance issues mean its usage will only be considered for applications where response time is unimportant. Generally, though, Java solutions providers are seeking to improve performance with developments such as just-in-time compilers and Java processors. If these developments yield effective

performance improvements during the development phase of the NSLS-II project, then Java's importance to the project will increase.

6.4.5.3 Server Development

Development of EPICS at the server level is required potentially in three places, namely record and device support, database, and state notation language.

6.4.5.4 Record and Device Support

While there is extensive record and device support available for EPICS, addition of unsupported hardware will necessitate the development of Device and possibly Record Support layers. The EPICS toolkit provides well-defined interfaces to each of these layers and examples to aid development. Device development is carried out in C within the standard EPICS development environment.

Building and developing EPICS requires either the VxWorks [6.6] or RTEMS development environment. VxWorks is currently only available for Windows or Solaris. However, given that the development environment is based on the GNU tool chain, it should be possible to run the RTEMS tools on Linux. The preference will be to standardize on one operating system for development, preferably Linux.

Database Configuration Tools

There are several Database Configuration Tools available. These DCTs allow designers to create EPICS databases by implementing them visually with a "block diagram and link wire" approach, similar to that used in electronic schematic design packages.

NSLS-II will use VisualDCT [6.7] as its database configuration tool. VisualDCT is an EPICS database configuration tool written in Java. It can therefore run under any operating system that supports a Java Runtime Environment. It was developed to provide features missing in existing configuration tools and to make databases easier to understand and implement.

The database development cycle will involve importing the EPICS runtime database into the central relational database to have a single repository of all control system information. VisualDCT has a powerful database parser, which allows existing DB and DBD files to be imported with ease. The parser detects syntax errors in databases, as well as defective visual composition data or its absence. Faults in DB files are safely handled and do not raise any critical errors. VisualDCT automatically lays out all objects that have no visual composition data and saves all visual data as comments to maintain backward compatibility. The output from VisualDCT is also a DB file, with all comments and record order preserved.

Visual DCT has been written within the EPICS community specifically to support EPICS, and is available free to EPICS database developers. However, some development of VisualDCT required to add some missing functionality will need to be undertaken.

State Notation Language / Sequencer Tools

The sequencer is a tool within EPICS that allows the implementation and control of one or more state machines on the IOC. The state machines are created using EPICS SNL. SNL has a C-like syntax, with constructs for building state machines. Once the SNL source code has been written, a SNC pre-processes it into "C" code and then compiles it to create an object file which the sequencer runs in the IOC.

6.4.5.5 Client Tools and Middleware Data Servers

Client tools are available at level 2 of the control system architecture. Clients at this level can directly access all channels in the control system through the Channel Access protocol. These data are time stamped by the Event System for reconstruction of accurate time sequences or correlation of events. At this level, client tools can use data from the IOCs directly, use control system data along with accelerator equipment information for model-based physics applications, or provide computed or correlated data to other clients.

6.4.5.6 Console Applications

The EPICS software package offers comprehensive operator display applications, which include:

- Extensible Display Manager
- Channel Archiver and Archive Viewing Tools
- Strip Chart Tool (StripTool)
- Array Display Tool (ADT)
- Parameter Display Page (DP)
- Alarm Handler
- Knob Manager (KM)
- Operator Electronic Log (CMLOG)

These applications will be used to supply operator display facilities, which will include the following functions.

Operator Menu Bar

This will provide rapid single-click access to all key operator facilities.

Plant Synoptics

These full-screen plant schematic diagrams will provide operators with an at-a-glance indication of plant conditions. Each process value displayed on a synoptic will constitute a “hotspot”; clicking on a hotspot will produce a pull-down menu providing access to further information and control actions relevant to that process value. Typically, a text description of the signal, the units of measurement, alarm limits, maximum and minimum, trend, alarm history, wiring information, operator comment and web access to online help might be provided. By this means, plant synoptics will act as the launch platforms which allow operators to access a wide variety of data in a seamless manner.

Ease of navigation will be considered during the detailed design stage for plant synoptics. An overall Synoptic Menu will be provided, which lists all synoptics grouped by functional area, presenting a clear hierarchy. In addition, where appropriate, plant synoptics will contain links to other associated synoptics. The design aim will be that operators should be able to navigate around the hierarchy without the constant need to return to the Synoptic Menu. Plant synoptics will be designed to have a simple, uncluttered appearance so as not to present more information to the operator than can reasonably be taken in.

Control Panels

Usually sized smaller than full-screen, control panels will be available with a wide variety of control widgets (radio buttons, slider bars, data entry fields with data validity checking, etc.) to allow users to apply control actions to the plant.

Control panels can be configured such that a single slider bar is used to control simultaneously a number of control outputs. Mathematical functions are available to define how these combined control outputs operate in relation to one other.

User-Configurable Tabular Displays

Operators will be able to configure their own sets of tabular displays showing closely-related accelerator parameters. Facilities will be provided to save these user-configured displays with a user-chosen name, and to recall the display from a list presented in a pull-down menu.

System Status Indicators

These schematics will show the status of IOCs, operator monitors, printers, etc. They will also display the health of key applications—so that, for example, operators are made aware quickly if alarm processing stops due to an alarm server program crash.

Operator Comments Facility

This will allow operators to enter lines of text comment for any plant input—to record, for example, when an input is not reading correctly due to a known fault. The presence of an operator comment for a process variable will be clearly indicated on any synoptic which displays that process variable. Individual comments will be easily readable via a suitable control panel, and it will also be possible to collate lists of comments (e.g., all operator comments entered during a shift).

Signal Information Panel

Only a subset of the process variables will be displayed on plant synoptics. However, operators require rapid access to information about any process variable and the Signal Information Panel satisfies this requirement. The panel will provide a Search section and a Display section. The Search section will enable the user to carry out a name search on the relational database, using a name mask to search for either an EPICS database record name or an EPICS record descriptor. Clicking on one of the returned search results will enable the user to request further information (e.g., trend, alarm history, operator comment, etc.).

Message Logging

The CMLOG package available with EPICS will be used to provide a distributed message logging system. This package can be used by any application or system that needs to log messages to centralized log files and display distributed messages to users. The CMLOG package supports C++, C, and CDEV application interfaces for logging messages and has C++ application interfaces for searching/retrieving messages from a dedicated logging server. Applications may send a selection rule to the server to select a subset of log messages for viewing; these rules can be in a form similar to C logic syntax or in a form similar to SQL.

A sample Message Log Browser (an X-Windows Motif application) is included with the CMLOG package. An additional browser will be developed using the supplied application interfaces once detailed requirements are established during the detailed design phase of the project.

6.4.5.7 Alarm Handling

The EPICS Alarm Handler package will be used to provide the following facilities:

An alarm list allows the users to view and manipulate current plant alarms. The alarm list will incorporate the following facilities:

- Indication of alarm acknowledgement state.
- Alarm message which includes EPICS record name, descriptive text, alarm value and date/time of alarm generation.
- Removal of acknowledged alarms from the Alarm List when they are no longer in the alarm state.
- Access to a menu-based set of facilities from each alarm in the Alarm list. The menu would give access to further information about the alarmed signal, including:
  - Trend
  - Alarm history
  - Access to a synoptic which includes the alarmed signal.
    - Web access (e.g., a link to a text page with more details about the alarm condition and possible corrective action)
    - Operator-selectable alarm inhibition to prevent use of the Alarm List from being disrupted by non-genuine alarms (e.g. “flickering” alarms being generated by a faulty switch). The names and descriptions of inhibited signals will be viewable on a separate list, from where it will be possible to de-inhibit each signal.
    - Association of each alarm with a plant area, along with the ability to display only alarms for a particular plant area.
    - Color indication of alarm severity.

All alarm messages will be logged to a text file for interrogation and archiving purposes. An alarm log viewer will be available, with various filtering options such as date/time, alarm severity, input name, etc. Provision will be made for audible alarm tones, driven from software using wav files. A separate alarm tone will be available for each alarm severity. An alarm banner window will be available to display a configurable number of recent alarms in a dedicated window at the top or bottom of the screen. Alarms can be acknowledged via the banner without having to call up the main Alarm List.

6.4.5.8 Archiving

The EPICS software toolkit offers comprehensive short, medium, and long-term data collection, archiving and retrieval through the EPICS Channel Archiver package. This package will be used to provide the following facilities. For long-term archiving, the archiver provides support for:

- Data retrievable in tabular and trend form
- A data quality indicator associated with each item of data
- Data compression to minimize the size of archive files
- Dumping of data to removable storage media, for long-term storage
- Loading of archive data from removable storage media for data analysis
- Timely warning to operators when archive data collection is compromised by a “disk full” condition on the archive server
- Variable data collection intervals for archiving
- A mechanism for easily configuring large numbers of process variables for archiving (e.g., by use of name masks)
- Facilities for collecting data in user-definable data sets, where data sets can include files as well as process variable data

The Historical Data Collection provides for short- to medium-term data collection offering the following features:

- Data retrievable in tabular form and trend form
- Data quality indicator associated with all data
- Variable data collection intervals
- Mathematical functions (e.g., averaging, MIN-MAX, etc.) applicable to historical data

A wide variety of data retrieval and data management tools are available with the standard Channel Archiver package, including:

- Retrieval via scripting tools, provided by the Channel Archiver Scripting Interface. Tcl, Python or Perl can be used to develop automation of archive handling.
- Retrieval via native tools, with Xarr/Striptool for UNIX-based systems and WinBrowser for Win32 systems. WinBrowser also provides data export in spreadsheet format or in a format suitable for the Matlab data analysis and modeling package.
- Retrieval via a web server plug-in, offered by the CGIExport client, which allows users to browse the archive via any web browser. File download in spreadsheet or Matlab format is supported by this plug-in.
- Command-line tools provided by the ArchiveExport/ArchiveManager component, providing commands to manage archives and to export data to a spreadsheet, to Matlab or to the GnuPlot plotting utility program.
- The Archive Engine component of the Channel Archiver package includes a built-in Web server. By using this feature, current operational parameters can be viewed and interactive configuration can be carried out via any Web browser.

6.4.5.9 Plotting

The StripTool program will be used for displaying trends of current and archived data. The key features of the StripTool program are:

- A StripTool chart displaying recent live data can be scrolled back to view archive data.
- Data acquisition via both Channel Access and CDEV, thereby allowing trending of both EPICS and non-EPICS data on the same axes.
- Ability to drag signals from synoptic diagram (drawn using MEDM) into a graph window.
- Flexible configuration options, including logarithmic and linear transformations, sampling rate, graph refresh rate, plot colors, grid lines, graph legend coloring, and plot line width. The trend can also be easily reconfigured to make one or more plot curves invisible without removing the plot configuration information for that curve.
- Trends can be printed and trend data saved to file.
- Trends are customizable via X resources, giving access to a wider set of configuration options than those offered by the standard StripTool configuration facilities.

6.4.5.10 Automatic Sequencing

For increased operational efficiency, and in support of a demanding accelerator availability requirement, the control system will include the capability of automatic sequencing, including decision making. These sequences could include automatic run-up procedures, automatic fault-recovery sequences, and automatic data-taking routines. The system will provide simple tools for defining sequences as experience is gained and will be capable of monitoring the status of automatic sequences, annunciating problems encountered in sequences, and intervening or overriding sequences if necessary.

6.4.5.11 Data Server

Computed data and aggregate data are to be done with consideration to overall performance metrics. Where it is reasonable, these data are to be created once in a server and provided to other clients in the control system. Examples of this are first turn data, ring current, and emittance measurements.

6.5 Physics Applications Rapid Prototyping

Rapid prototyping of physics applications is supported through a number of programming language interfaces to the Channel Access protocol. These include: analysis packages such as Matlab, Labview andMathmatica; scripting languages such as Jython, Pearl, Tcl/TK, and SWIG; and programming language interfaces such as: Java, C, and C++. Applications that are prototyped in this environment can be migrated into the standard EPICS front end controllers and the XAL environment for operations. (Figure 6.5.1).

6.5.1 Model-Based Physics Applications

Model-Based Physics applications must be available for all phases of commissioning. The system should be capable of operating in online and predictive modes. A RDB must contain the model parameters needed for the model based control (Figure 6.5.1). A physics modeling system will be needed to provide an interface between the control system and standard codes such as Tracy2, Elegant, or RING. These codes can mathematically model the behavior of various accelerator systems. They can be used to aid understanding of the machine, as well as being a vital tool for optimizing and operating a complex accelerator.

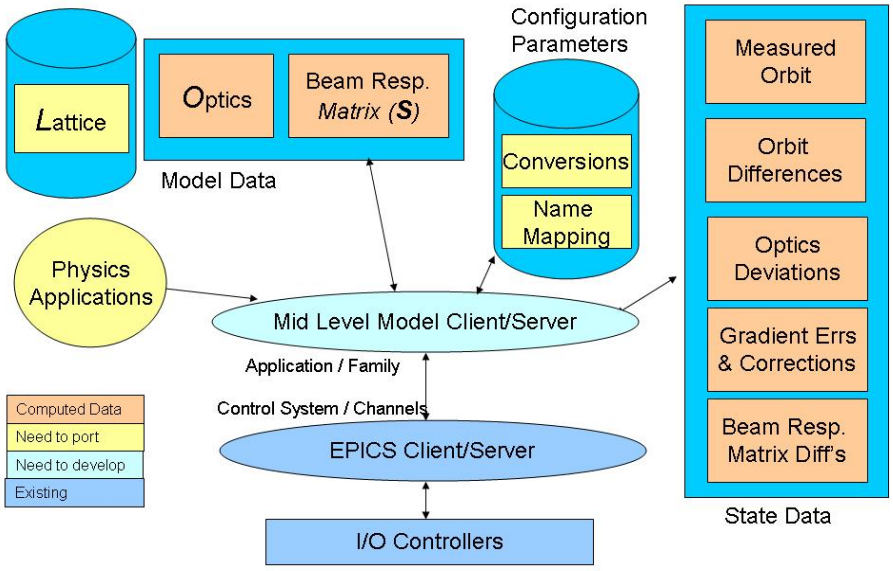

Figure 6.5.1 High-level application architecture.

Matlab Midfdle Layer Toolkit

Initial model based control is to be implemented using the Matlab Middle Layer Toolkit in conjunction with an accelerator simulation running through the EPICS process database. This provides an environment to develop commissioning tools that can be tested well in advance of the presence of any equipment.

Online Mode

Real-time magnet and RF data will be passed to the modeling system. Computed values of Twiss parameters, Q values, chromaticity, momentum compaction factor, etc. will be made available to the rest of the control system or to Accelerator Physics applications.

Predictive Mode

In this mode, offline magnet and RF values are supplied to the modeling system rather than real-time data. This will allow predictive and "look-and-see" experiments to be performed using the machine model to predict the behavior of the accelerator.

Middleware Data Servers

Middleware data servers will be provided to separate the data collection from the visualization layers. All client applications that collect data from the control system that result in the production of new data will be served to multiple, distributed clients. The distribution of this data is done over a standard protocol such as DDS or Croba. Alarm information, orbit, archive data, and emittance are some examples of data that may be produced by clients and served to other clients. The goal is to define a narrow interface that supports the reuse of clients of the API.

XAL – the Model-Based Control Framework

NSLS-II will use the new Middleware Data Servers to create applications for commissioning and operation. Operational tools are to be derived from commissioning tools. They will be modified for ease of use and clarity, maintainability, and revision control. Many of these tools are expected to be from the XAL toolkit in use at the SNS.

6.5.2 High Level Application Tools

High level tools include: system queries by physics devices or computed values, correlation plots, beam trip displays, machine protection first fault displays, and others as identified by the commissioning and operations teams.

6.6 Relational Database

MySQL will be used as the main data store for all beamline component information that is needed for model-based control. The IRMIS Entity Relationship Diagram will be used to describe all component and wiring data. It will be extended to support the Lattice information early in the project. Tools will be provided to enter this data, produce reports, and create files needed for all aspects of the project. These tools are to be developed early in cooperation with the users.

6.7 I/O Controllers / Equipment Interfaces

The I/O controllers and equipment interfaces must support the wide range of applications that are encountered in an accelerator control system. To minimize integration, training, and maintenance costs, this hardware should be limited to a solution that can meet each class of hardware integration needed. The front-end computers will run a Real-Time Operating System. The RTOS candidates are vxWorks and RTEMS. Although vxWorks runs on a wide variety of CPUs and provides much functionality, it does not provide

source code without a prohibitive investment. RTEMS is an open-source RTOS that requires more man-power to wield. Several EPICS sites now support RTEMS. Control at this level of the architecture can be done at the rate of 1 kHz with latencies of 33 μsec. Dedicated data and timing buses are required to achieve this level of performance over distributed controllers.

6.6.1 High-Speed Signals

High-speed signals such as RF, image diagnostics, and beam position signals may be processed with an FPGA to produce results that are used by the control system at a slower rate. These devices may operate on data into the MHz range and be used to analyze high-speed signals from LLRF, Beam Position Monitors, and Power Supply Controllers. These may be implanted as single device controllers that are equipped with dedicated processors to run EPICS and provide the interface to the control system, an FPGA to process the signal, a high-speed interface between the FPGA and the control system, and an interface to the timing system. These device controllers may control a single device or a set of devices. A standard architecture that includes a Power PC with a PCI or PCI interface in the Coldfire format is a candidate for this application.

6.6.2 Low Latency Response I/O

I/O that requires the control system to respond in the minimum time (known as high-density I/O) requires an instrumentation bus that provides interrupts on an external trigger and reasonable data transfer times between I/O boards. This can be implemented using either VME or PCI.

6.6.3 High-Reliability IO

Applications such as vacuum interlocks, flow switch interlocks, and cryogenic control require high reliability control of simple processes. A Programmable Logic Controller will be provided for these applications. All data from the PLC shall be available through the control system. The Control Logix PLC in conjunction with the Flex-I/O line could provide this function at a reasonable price. In any case, one PLC family will be chosen as the NSLS-II standard. These PLCs will be integrated into the control system through an IOC.

6.7 Global Control System

The control system must provide some global communication that requires higher performance than is available in a commercial network. NSLS-II requires: an Event System for synchronizing data acquisition and control; a high-speed data network for providing beam-steering data to all ring power supplies for orbit correction; and a Machine Protection System that is a fast-response bus provided for mitigation against failures that greatly impact the operation of the facility by either producing excessive radiation or causing equipment damage. We will evaluate the systems available from other laboratories. We are also considering the development of an open-source set of functionality that provides the timing, event, and data communication needed for high speed, distributed applications such as Fast Orbit Feedback and Machine Protection.

6.7.1 Event System

The Event System, also referred to as a timing system, provides all beam and RF synchronization for all control and data acquisition. The event system provides a master pattern of events that reflect the operation mode of the machine. It provides the synchronization needed to control the beam injection into the ring for initial fill and top-off. The event system may also communicate data that are required for operation and data

correlation, as well as data communicated to the subsystems that change with the mode of the machine. Examples include time stamp/pulse ID, machine mode, and global machine status.

The timing system is required to provide control of the beam transfer from the electron source to the storage ring and provide diagnostic equipment and beamline equipment with synchronization signals. The most recent light sources [8] have made use of commercial equipment and built on equipment designed by other light sources, often in collaboration with industry; it is envisaged that the same approach will be adopted for NSLS-II.

6.7.1.1 Fast Timing

The task of a timing system is to synchronize all the relevant components in an accelerator complex. One part of this task is to control the injection by triggering the particle source and firing the transfer line components, such as injection- and extraction-pulsed magnets, at the correct times. Also, beam diagnostic components such as beam position monitors and current transformers must be synchronized to the passage of the beam. This has to happen with fine time resolution, to RF frequency, clock precision, and low jitter, and is termed Fast Timing.

6.7.1.2 Event System Signals

Other tasks for the timing system are related to synchronizing components where the resolution is more relaxed. Examples include triggering the magnets for an acceleration ramp, triggering operational sequences such as the filling of the storage ring, BPM acquisition, feedback timing, insertion device control, and supplying the distributed control system with time synchronization for control and correlation of data. The time resolution for these tasks is less demanding; these tasks are often termed Events. Event Signals will be produced with a precision set by the storage ring revolution period and with predictable jitter.

6.7.1.3 Timing System Components

In designing the accelerator timing system, it is important to consider what has been used at other recently constructed sources and the integration into the EPICS control system. The time-stamp system already exists within the EPICS infrastructure and can be used in conjunction with the Event System, which was developed at APS [6.9] and enhanced by SLS and, more recently, DIAMOND (Table 6.7.1). The APS/SLS Event System can be used to meet all slow timing requirements. The Event System is fully EPICS compatible and the required VME modules are available.

Table 6.7.1 Diamond Version of the SLS Version of the APS Event System Specification.

Events	8-bit code – 255 events
Resolution	8 ns
Event TX trigger	Hardware input, software, Event Ram Clock.
Event RX output	Hardware output, software (EPICS record process)
Transmission medium	Gigabit Ethernet

The requirements for fast timing are more specific to a particular accelerator dimensions and operation. Two options (Table 6.7.2) are available for the hardware for fast timing, the KEK TD4V as a VME module delay generator and the Stanford Research DG535 as a self-contained instrument. Each is available with EPICS drivers to provide the controlled delays.

Table 6.7.2 Fast Timing Hardware Options.

	KEK TD4V	Stanford Research DG535
Form	VME 6U	Bench / Rack mounting
Delay	16 Bit / RF clock	0 to 1000 s – 5 ps steps
EPICS Support	Yes	Yes, via GPIB
Channels	1	4
Jitter	4.5 ps at 508 MHz	<60 ps

6.7.1.4 System Structure

Figure 6.7.1 gives an overview of the Event System and Fast Timing control. The Event Generator receives a start signal from the RF clock gated with a line frequency component. Events are then sent to all IOC Event Receivers for timestamp synchronization and to output relevant event signals or process EPICS records. The fast-timing IOCs will require a fast clock and trigger derived from the RF source, but fast sequences can also be initiated upon receipt of an event.

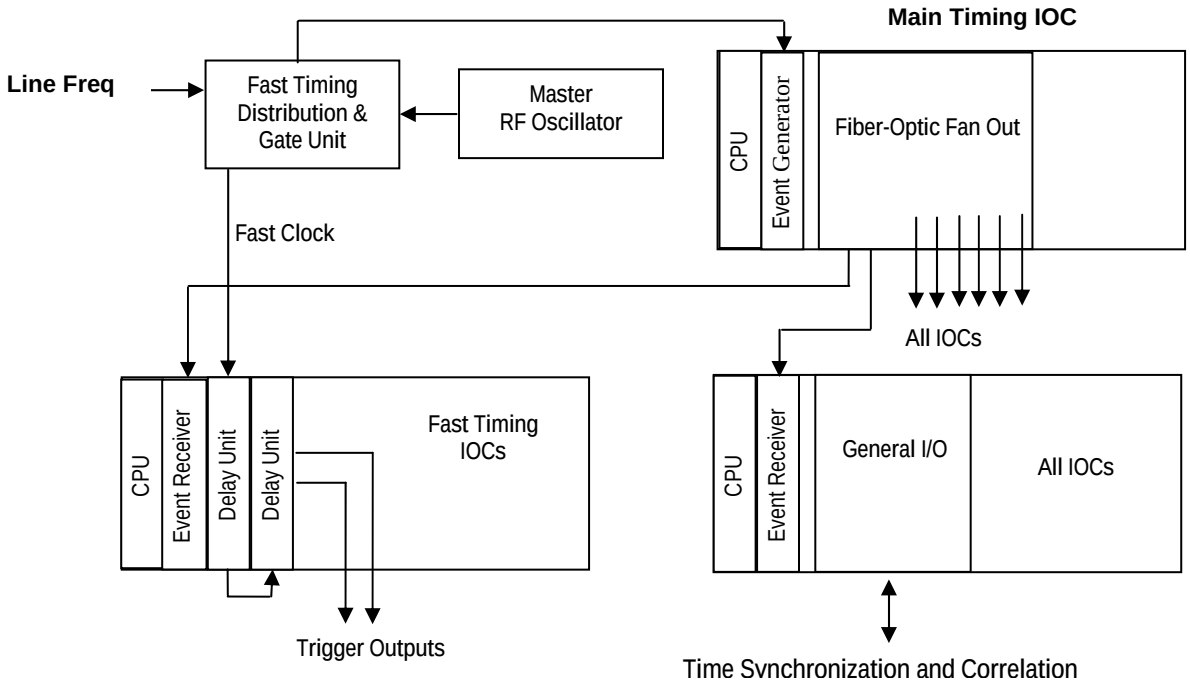

Figure 6.7.1 Block diagram of the Event system and Fast Timing system.

6.7.1.4 Signal Distribution

The Fast Timing and Event signals will be distributed over fiber-optic cable for reasons of noise immunity and distance capabilities. Further investigation is needed into the delay drifts that could be introduced by the fiber installation from temperature differentials and the standardization of length-induced delays in a facility the size of NSLS-II.

6.7.2 Fast Feedback

A beam position stabilizing system is required to maintain orbit stability to within 10% of beam dimension and to provide dynamic correction of low-frequency orbit disturbances. The proposals presented here are very much based on the work on Diamond, APS [6.10], ALS [6.11], and SLS [6.12].

6.7.2.1 Global Feedback

The feedback system will use measurements of the position of the electron beam in the storage ring and the photon beams in the beamline front-ends. This information will be compared against a reference orbit and the error used to calculate desired corrections to be applied to corrector magnets in the storage ring.

The response matrix relates the effect of small changes in corrector magnet fields to the resulting changes in the particle beam orbit as measured at chosen BPMs. By inverting the response matrix the relationship that maps orbit perturbations to changes in corrector magnet fields is obtained. For small orbit errors, this relationship is assumed to be linear and time-invariant. Different objectives, such as correcting the orbit in an rms sense or correcting specific locations, can be achieved by choice of BPM and corrector locations and by applying different weights to correctors or BPMs when computing the inverse response matrix.

6.7.2.2 Performance

Two global feedback systems, operating in parallel, are proposed to correct orbit errors on NSLS-II, namely a Slow system, correcting DC drift, and a Fast system, correcting beam disturbances to 5 KHz (Table 6.7.3). These systems will use data from both the electron and photon BPMs and operate on either or both of the steering magnet or fast correctors. For both systems, the BPMs need to be sampled synchronously, which will be achieved using Events distributed to the IOCs. In addition, this architecture must support the capture of beam dump failures.

Table 6.7.3 Feedback System Comparisons.

	Correcting Feedback	Update Rate Feedback
Slow	DC drift	0.1 Hz
Fast	0.2 mHz –100 Hz	5 KHz

6.7.2.2.1 Slow Correction

The Slow correction will correct the orbit at 10 second intervals, using the desired correctors and BPMs to compensate for slow changes in the orbit. This will maintain the user-steered orbit applied at the beginning of each fill. Communication to the BPM and Steering IOCs will use the EPICS CA communication mechanism. The slow correction will be realized as a dedicated application running on either a console or a computer server.

6.7.2.2.2 Fast Correction

Fast correction is not possible through EPICS CA mechanisms because of insufficient bandwidth. It will be realized at the IOC level on separate feedback processor boards dedicated to this function. This involves partitioning the correction calculation across the 30 Steering IOCs to calculate the correction values for the steering elements local to that IOC. Each steering IOC requires access to all the BPM values, to give flexibility in the correction algorithm. This requires a high speed connection to share data between the all BPM devices and 90 Steering IOCs. Two potential solutions for this are to use either reflective memory or network broadcasts.

EPICS process variables will be used to control the feedback process, by downloading algorithms to the feedback processors and setting coefficients and update rates.

6.7.2.3 Reflective Memory

Reflective memory is an off-the-shelf solution to distribute information across multiple computer systems without requiring processor time. It enables BPM data to be written to the reflective memory module in each of the BPM IOCs and appear in memory in all the Steering IOCs. In the system shown in Figure 6.7.2, an event received by all BPM devices would cause the photon and electron BPM values to be read by the feedback processor and written to the reflective memory board for each of the processors. The data would propagate to all the steering IOCs and when all values are received, the feedback calculation would be carried out on the Steering IOC to produce the new steering settings. These values would then be written to the steering elements in conjunction with the slow system values received through EPICS process variables.

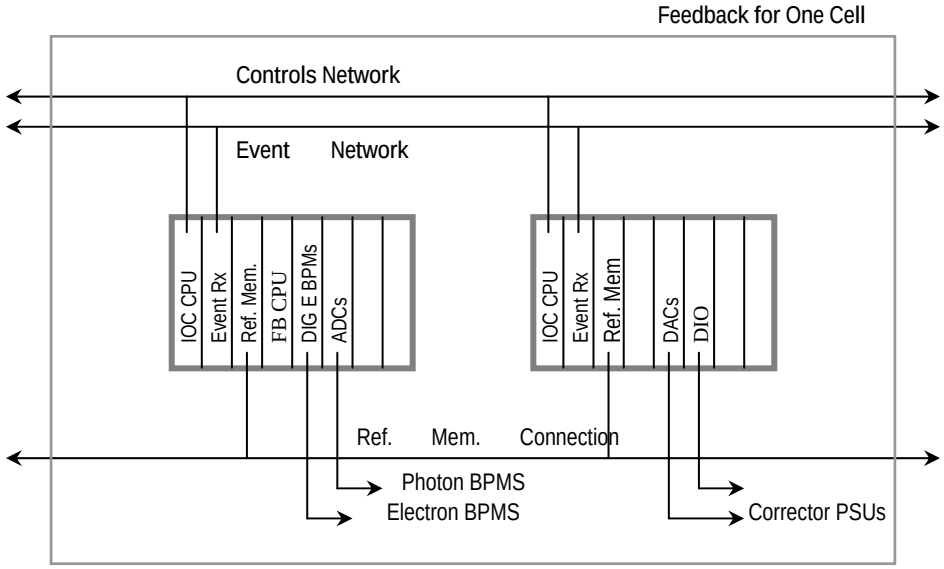

Figure 6.7.2 Reflective memory structure for one cell.

Commercially available reflective memory sizes and update rates provide for moving multi-megabytes per second across tens of boards, and so should easily meet the requirements of this application.

As the BPMs and Motor Controllers may be implemented using special FPGA boards, a second level of communication may be required to meet specifications. The architecture under consideration is show below (Figure 6.7.3).

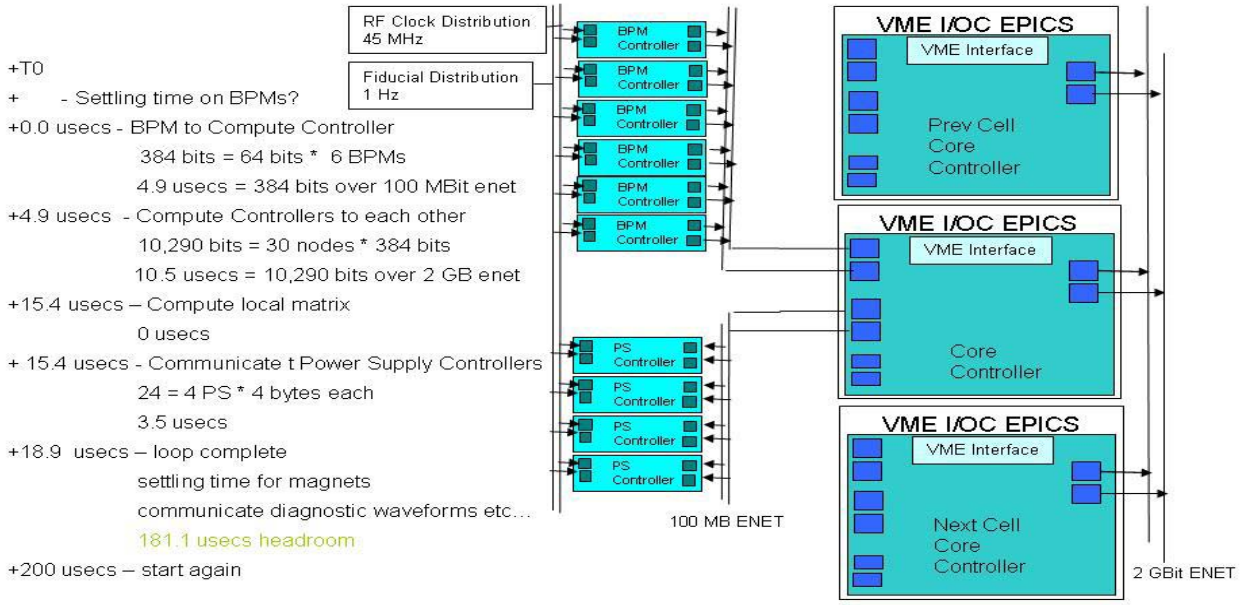

Figure 6.7.3 Architecture for the BMPs and motor controllers.

6.7.2.4 Network Broadcast

In the Network Broadcast system each of 60 feedback processors in the BPM and Steering IOCs is connected to a private network with a central switch in a star configuration. The feedback processor in each of the BPM IOCs reads the BPM values and broadcasts them over the network to be received by each steering IOC. The broadcasts take place simultaneously but do not collide, because the switch buffers each packet as it receives it. The switch then forwards the packets to all the Steering IOCs.

In the system shown in Figure 6.7.4, an event received by all BPM IOCs would cause the photon and electron BPM values to be read by the feedback processor and broadcast over the private network. When each of the 30 broadcasts has been received by all of the Steering IOCs, the calculation would be carried out on each Steering IOC to produce the new steering settings. These values are then written to the steering elements in conjunction with the slow system values received through EPICS process variables.

This option is cheaper in terms of hardware because it alleviates the need for the reflective memory boards, but incurs a development overhead to produce software for the broadcasting. The performance achievable using broadcasts also needs to be determined, to establish whether it would meet the requirements of this application.

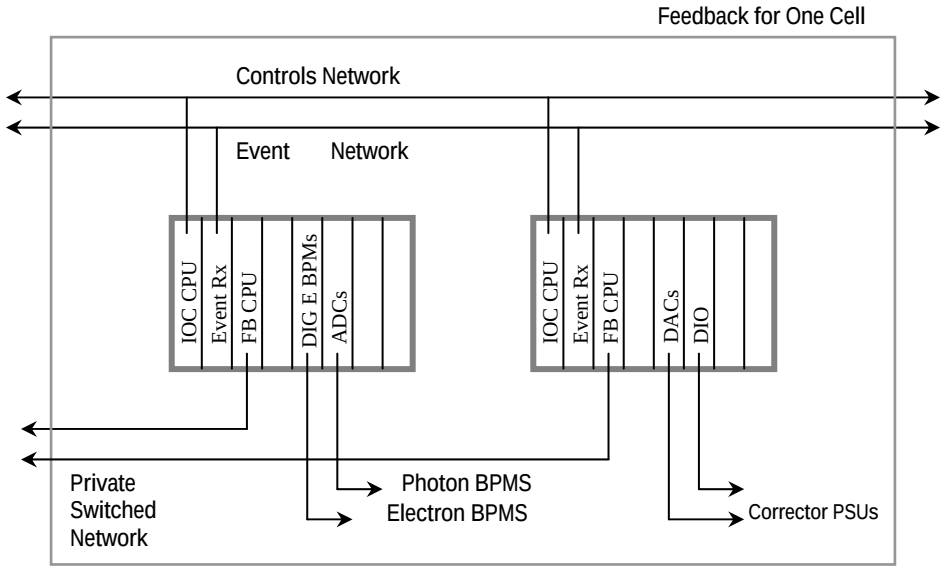

Figure 6.7.4 Network broadcast structure for one cell.

6.7.2.5 Feedback Processor

On the Steering IOC, the calculation to produce the new steering values from BPM values and the inverse response matrix needs to be carried out. The time available to carry out this calculation is dependent on the desired update rate, the time to acquire and distribute the data, and the time for the correction to propagate through the steering power supply, magnet and vessel to the beam. While the current generation of PPC processors offers similar performance as DSP processors, in terms of operations per second, they do not have the architectural feature of DSP processors for signal processing intensive calculations. However, the performance available from current PPC makes them suitable to carry out the feedback calculations at a price advantage over DSP processors.

6.7.3 Machine Protection

The control system must monitor beam envelope and other operational parameters that determine if the beam is threatening to damage equipment. Detection and reaction to dangerous conditions must be completed within 20 msec. A node on the fast feedback bus is to be used to determine if the beam is in a safe orbit.

6.8 Subsystem Control

The major subsystems being controlled are: diagnostics, power supply control, low level RF, vacuum, personnel protection, equipment protection, undulator, experimental beamlines, and conventional facilities. They fall into two distinct categories: those requiring high speed, low latency performance such as the LLRF, Diagnostics, Undulator Control, Beam Envelope Equipment Protection, and Fast Correctors, and those that do not require this such as: Slow power supply control, vacuum, personnel protection, slow equipment protection, and conventional facilities. Beamline control is a special case, in that the beam lines are a special cast in that they are run by groups outside of the NSLS II machine group.

6.8.1 High-Speed, Low-Latency Applications

High-speed, low-latency applications are integrated into the global control system through the EPICS Channel Access protocol, over Ethernet (Figure 6.8.1). This provides integration with modeling, archiving, and other operations tools. It is not adequate for response times required for FOFB at 5 KHz or machine turn-off in under 20 msecs. To meet these needs requires the event system, in conjunction with a fast, reliable, low-latency communication network. Intelligent device controllers in the front end process the signals at the 500 MHz rate and deliver data to the other device controllers over dedicated networks at the 20 KHz rate to support global feedback at 5 KHz. The intelligent device controllers also support turn-by-turn data collection, where a trip is detected and distributed over the event system.

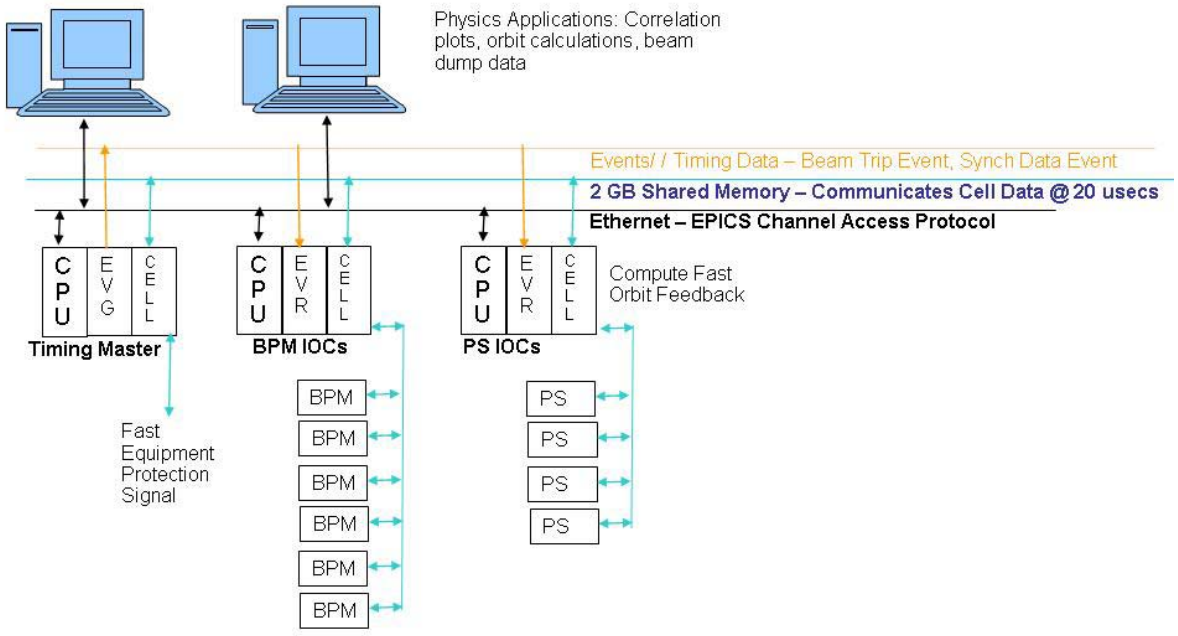

Figure 6.8.1 Control system for high-speed, low-latency applications.

6.8.2 Diagnostics Control

The slow applications, which require control and synchronization to the machine in the 60 Hz to .5 Hz range, have no need of specialized data communication buses. The event system may be used to provide triggers for synchronous data collection and time stamps for correlating events. All data communication is accomplished through the EPICS Channel Access Protocol (Figure 6.8.2). The I/O may be distributed over Ethernet or serial communication to slow, remote, controllers such as PLCs or off-the-shelve gauge controllers. This distribution of I/O reduces cable and maintenance costs. These distributed I/O are used when the data being correlated only needs to be within 500 msec. I/O requiring tighter correlation, such as slow magnets or motion controllers, are placed directly in the EPICS I/O Controller typically in a VME crate.

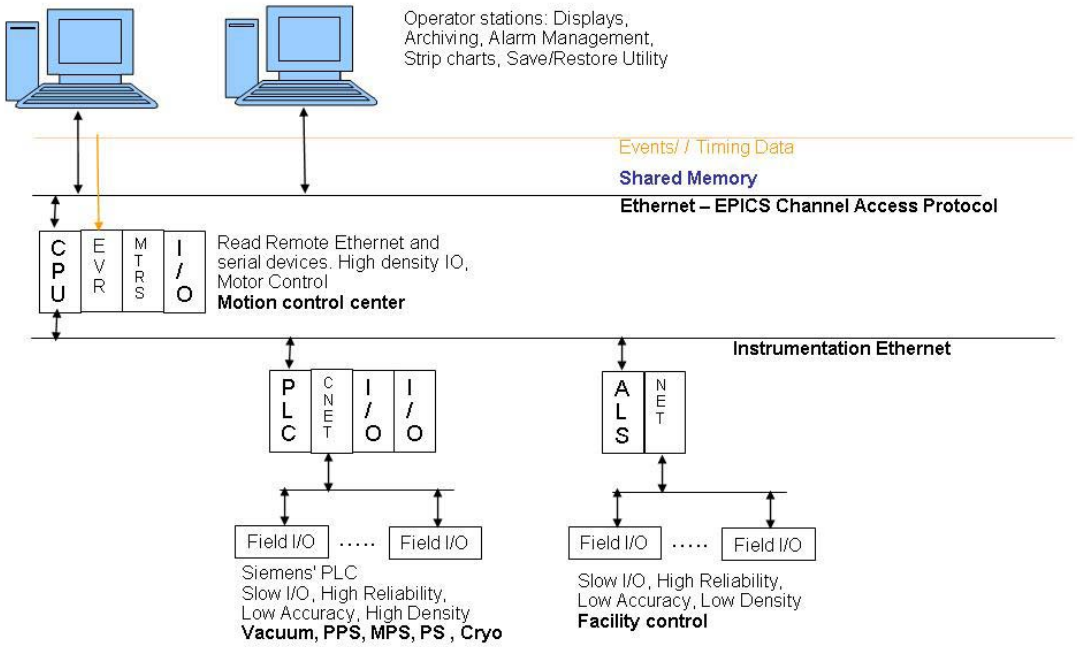

Figure 6.8.2 Control system for slow applications (within 500 msec).

6.8.3 Beamline Control

The NSLS-II accelerator control system will be in an isolated network by itself and each beamline is expected to have its own network to connect its computers and its hardware. Connections between these systems will be designed to provide the integrated flow of information between the accelerator and end stations that is needed to meet the requirements for beam monitoring and stability.

All insertion device beamlines require control of the insertion devices [6.13] which are located in the controls network. In addition beam position information, as well as numerous other signals, is needed from the accelerator control system. Similarly, beamline information, along with intensity and beam position from the beamlines, will be needed in the accelerator control system to provide continuous control of the beam.

The infrastructure needed for the exchange of information between the beamlines and the accelerator will be built into the facility. It is anticipated that single-mode fiber will be employed to connect the beamline EPICS hardware and accelerator EPICS hardware. Every beamline will be provided with a dedicated single-mode fiber bundle from the beamline to the accelerator control system racks located on top of the storage ring. In addition, there will dedicated single-mode fibers to the main control room, where some of the timing hardware is expected to be located. These single-mode fibers will be used to provide high-precision timing signals to synchronize the beamline experiments with the arrival of the x-ray beam.

Data exchange between the beamline and the accelerator EPICS systems, which do not require a very fast data rate, will be provided through an EPICS channel access process variable gateway system. This system will reside in the accelerator control system and will have an additional network connection to each of the beamline networks. This way the control, as well as data readbacks, can be accomplished with a high level of security without jeopardizing the integrity of the accelerator or beamline control systems. Such schemes have been used successfully at other facilities, such as APS and BESSY.

The development of the EPICS software for the beamline will be conducted in parallel with the accelerator to ensure that they are consistent and the exchanges of data between the two are seamless.

The beamlines will have their own computers and servers for data acquisition and control. There will be large storage capacity at the beamlines, and a central storage and backup service, with large disk farms, will be available as well. There will be 10 gigabit redundant network structure built into the facility. Each beamline network will be redundantly connected to a central computing facility, which will have a firewall to provide secure access to the outside world.

The offices in the LOBs will also have computing capability. Each LOB will be on a different network and will be serviced by a central computing facility. The LOBs will also be serviced by 10-gigabit network infrastructures. The centralization of data collected from the beamline will allow a user to retrieve data from multiple beamlines for analysis. Data reduction and analysis software will be developed by, and available from, the central computing services.

The variety of information exchange between the various control systems related to the needs of the experimental facilities is schematically indicated in Figure 6.8.3. Patterned after the system at APS [6.14], this system will be based on EPICS process variables, as discussed above.

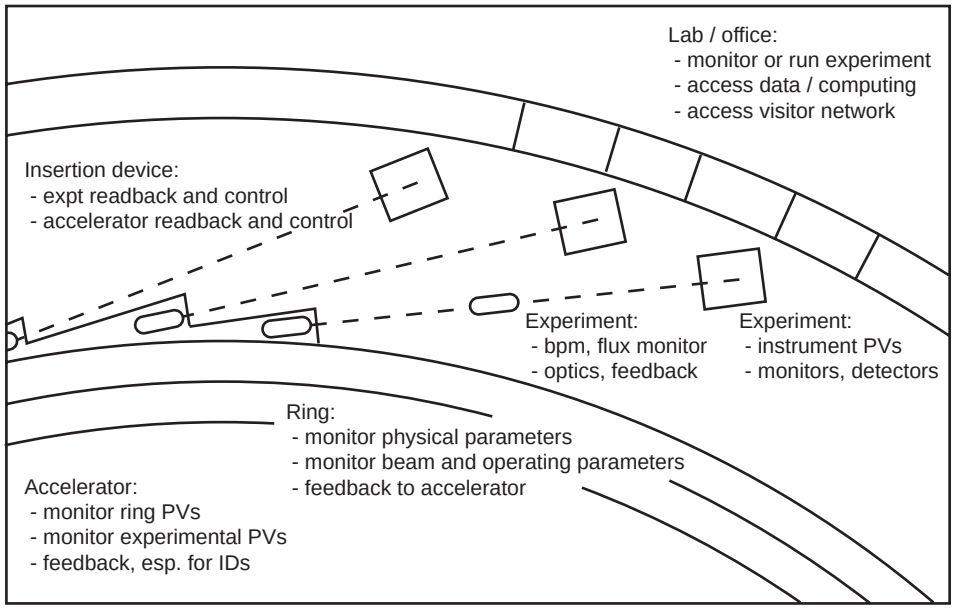

Figure 6.8.3 Activities requiring information distribution in experiment hall.

6.8.3.1 Design Concepts

From the point of view of the beamline and end station, the requirement is that every beamline have at least one dedicated EPICS IOC controlling its insertion devices and intercepting other information from the facility. For many of the hard and soft x-ray facility beamlines, EPICS will be used as a standard to control optics and beamline motors also. Specialized equipment may have different control systems, which may exist as additional EPICS clients or may in some cases be independent. It will be beneficial for the EPICS IOCs to be of a standardized hardware type. VME is a current favorite, due to its reliability, but the availability of drivers in the future and the improvements in PC-based hardware may cause the latter to be more favorable some years from now. The standardization of beamline server hardware will be assessed during the years preceding beamline commissioning and a standard will be chosen. The same requirements we have today must be satisfied. Hardware must be robust and reliable. A large basis set of scalers, motor indexers, analog and digital I/O, multi-channel analyzers, and so on must be in use. Pre-existing EPICS support for the hardware will be a third criterion.

The network as seen from the beamline is illustrated in Figure 6.8.4. As an example, a Linux PC running Medm GUIs may serve as the operator interface, while a VME CPU serves as the IOC for the beamline control system. Beam transport components with PVs that need to be available to the facility are connected to this network. (The insertion devices, on the other side of the shield wall, are networked separately.) A server acting as router, firewall, and PV gateway connects this sector or beamline network to the experimental network, to other beamlines, and to the other facility networks. The PV gateway controls all permissions necessary to establish who has control permission vs. read-only permission of the PVs.

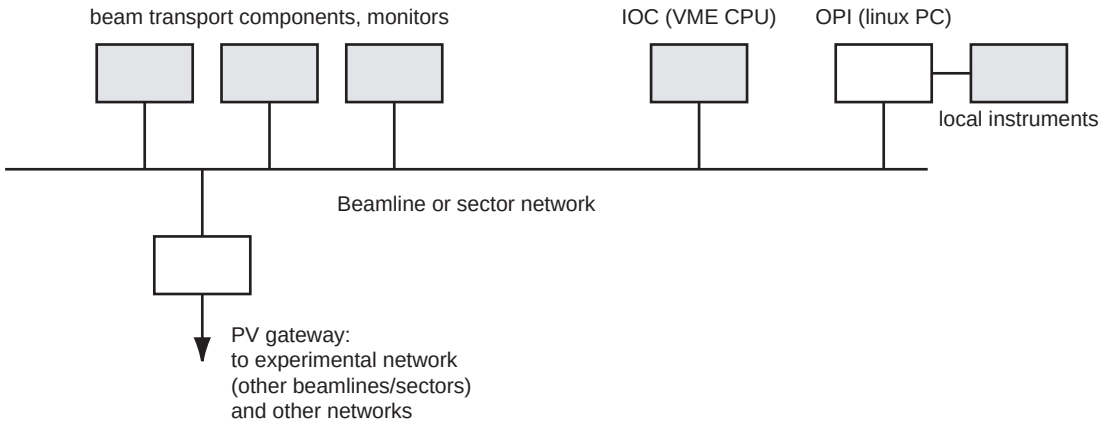

Figure 6.8.4 Sector networks make important process variables (PVs) available to the entire facility through a PV gateway. IOC=input/output controller, OPI=operator interface (as Medm GUI).

We anticipate that the system will be designed so by default read-access is available for everything, everywhere. This way, there will be no need to make assumptions during the initial configuration as to which machines' PVs and monitor values need to be communicated between the accelerator and the experiment hall. Finally, local instrumentation can be assembled on private networks as desired by the users of the individual beamlines. Specialized detectors and other instrumentation controllers may be interfaced to the beamline controls as applicable, particularly as EPICS clients.

6.8.3.2 Considerations for Accelerator–End Station Information Exchange

The accelerator monitoring complex will have far too much information in it to be useful to users as raw PVs. The accelerator group will design simple ways of mapping and colorizing the status of the accelerator with respect to beam excursions, pressure, temperature, and other sensor readouts, and make this digested information available as a monitoring system that the experimenters will be able to use. This will allow the beamline staff and users to gauge where problems may be coming from. It will also provide a unified way for the experimental division to log local beam stability in connection with pertinent information about the ring stability. This information will be provided as part of the general control system information.

The following elements will be expected to provide useful data from the beamlines back to the operations staff:

- position monitors (beams and pipes)
- ambient conditions (pressure, temperature, cooling water flow)
- status of insertion device and recent history (i.e., feedbacks triggered)
- beam figure of merit (quality after optics as defined by the end stations' needs: divergence, angular motions, spatial motions, energy drift).

It will be beneficial to create more generalized "status" readouts for beamlines as well as for the accelerator.

6.8.3.3. Design of the Main EPICS Node at Each Beamline

Resident on the experimental network and associated with each beamline, there will be a CPU running an EPICS IOC and a Linux PC configured with control GUIs and administrative scripts for that beamline. These computers will be quite similar across the NSLS-II complex, since many upstream beam components and interfaces to the gateways and other networks will be common. These computers, and the configuration to interface with facility networks and information buses, will be centrally administered. Giving each beamline a similar, centrally managed system benefits operations by allowing a standard set of tools and debugging know-how to be applied everywhere. One important concern is cybersecurity requirements. Even if the experiment network is within a firewall, the laboratory will require certain security scans. Uniformity of the beamline machines on this network will make it easier for staff to provide patches and fixes consistent with both security and smooth operations.

EPICS tools alone are sometimes insufficient for scientific data acquisition. Synchrotron beamlines have diverse needs, such as dedicated detector drivers, reciprocal space calculation, spectroscopic tools, and visualization tools for imaging. The end station equipment will be so varied that a top-down attempt at standardization would be very harmful. Thus, each beamline is expected to instrument itself in an independent way. Still, NSLS-II users and staff will benefit from having as much common support as is reasonable to interface different experimental systems and connect them to the EPICS platforms. Many different data acquisition platforms can be clients of the EPICS system. For example, LabView and Spec are widely used control and data analysis systems.

References

[6.1] M.T. Heron, and B.G. Martlew, “A Review of Options for the DIAMOND Control System,” Proc. PAC96.
[6.2] EPICS, http://www.aps.anl.gov/EPICS.
[6.3] TANGO, http://www.esrf.fr/computing/cs/tango/tango.html
[6.4] V System, http://www.vista-control.com/
[6.5] CVS, www.cvshome.org
[6.6] http://www.windriver.com/
[6.7] VisualDCT, http://kgb.ijs.si/VisualDCT
[6.8] T. Korhonen, and M. Heiniger, “Timing System of the Swiss Light Source,” Proc. ICALEPCS2001.
[6.9] F. Lenkszus, and R. Laird, “The APS Event System,” Proc. ICALEPCS95.
[6.10] J.A. Carwardine, and F.R. Lenkszus, “Real-Time Orbit Feedback at the APS,” Proc. BIW98.
[6.11] C. Steier, A. Biocca, E. Domning, S. Jacobson, G. Portmann, and Y. Wu, “Design of a Fast Global Orbit Feedback System for the Advanced Light Source,” Proc. PAC 2001.
[6.12] M. Böge, M. Dehler, T. Schilcher, V. Schlott, and R. Ursic, “Global Orbit Feedback System for the SLS Storage Ring,” Proc. ICALEPCS 99.
[6.13] M. Ramanathan, M. Smith, J. Grimmer, and M. Merritt, “Overview of insertion device controls at the Advanced Photon Source,” *Rev. Sci. Instrum.,* **73** (2002) 1448.
[6.14] M. Ramanathan, M. Smith, N. Arnold, F. Lenkszus, R. Laird, K. Evans Jr., J. Anderson, and K. Sidorowicz, “An overview of the information distribution system at the Advanced Photon Source,” *Rev. Sci. Instrum.,* **73** (2002) 1445.
[6.15] http://hpdrc.cs.fiu.edu/Sem-DDS/documentation.html

7 Equipment Protection System

The beamlines at NSLS-II are expected to handle x-ray beams with very high power and power densities. Therefore, care must be taken to design the beamline with components that can handle these power loads. Any component that has to handle these high levels of power has to be monitored. The beamline Equipment Protection System provides a means of monitoring the components which, when jeopardized, can cause component failure. The EPS has the responsibility to act on alarm conditions by mitigating the situation that has caused the alarms. The system baseline is configured with the infrastructure to support all monitoring of cooling flows and six fully populated front ends. The baseline EPS will support all future expansion in terms of wiring, I/O and control logic. Excluded from the base line is the beamline control and monitor portion of the system, and its cost is captured in the individual beamline budget.

7.1 Functionality

Every beamline EPS will monitor and interlock the devices in the front end and the beamline.

All front ends at NSLS-II are expected to have two safety shutters, one photon shutter, and a few masks. In addition, the front end will also have vacuum inline valves to provide vacuum isolation. The front end is also expected to have a fast valve to provide a conductance limitation during a vacuum accident. Most beamlines will also have an x-ray exit window as part of the front end. These x-ray windows will provide a vacuum isolation but will transmit the x-ray beam. Certain beamlines, such as the soft x-ray beamlines, are expected to share the storage ring vacuum with the front end providing the interface. In such cases, the fast valve, along with the rest of the inline vacuum valves, provides the isolation needed in case of accidents.

Due to the large power loads, all components in the front end that intercept the beam will have water cooling. These components are typically the fixed mask, photon shutter, and exit windows. The water flow will be monitored by flow meters and the signals will be fed to the EPS. All vacuum valves will be pneumatically operated. All vacuum valves will be operated by the EPS and have their positions monitored.

Most beamlines are expected to have some beam conditioning optics upstream of their monochromator. The beam conditioning optics will see the large power of the beam and as such will be interlocked by the EPS. Beamlines are also expected to have vacuum valves, which will also be controlled by the EPS.

It is expected that the beamline portion of the EPS system will be customized to suit the condition of the specific beamlines.

7.2 Design Specification

The design of the EPS is expected to be robust. The system will be based on programmable logic controllers (PLCs), which provide excellent customization capability and also extensive diagnostics.. The hardware used will be the same as used in the beamline Personnel Protection System and the Accelerator Personnel Protection System (for both topics, see Chapter 8).

Each beamline will have its own EPS system, with the sole function being to provide protection from damage of equipment due to synchrotron radiation. As such, the EPS will consist of only one PLC per beamline. The EPS system will consist of three parts: front-end EPS, beamline-specific EPS, and command/ control of PPS components such as shutters and station doors. The front-end portion of the EPS is expected to be similar on most beamlines, while the beamline portion of the EPS will be customized to each beamline. Similarly, for the command/control of PPS components, the front-end shutters will be identical in all beamlines; however, additional shutters on the beamline will be beamline specific.

All front-end components that intercept the synchrotron beam will have water cooling of the components. The water flow of the components will be monitored by the EPS via flow meters. The EPS will be in alarm state if the flow drops below a specified setpoint. Depending on the location of the component it monitors, it will command the photon shutter to close and – for cases where the flow is upstream of the photon shutter – it will request the stored beam to be dumped.

All vacuum valves in the front end will also be controlled by the EPS. Setpoints from vacuum controllers that are provided to the EPS will be used to determine when it is permissible to allow opening of the valves. The EPS will determine when it is necessary to close a valve, and will do so if it senses a vacuum alarm based on the vacuum setpoint to the system.

For specific beamlines, the EPS will be customized based on the user requirements for that beamline. Besides monitoring the water flow and controlling the vacuum valves, the EPS system may be used on beamlines to monitor other variables, such as temperature, position, and so forth.

The EPS will be used to control the actuation of the shutters. It will monitor the status of the PPS for each shutter and, when a permit is available, it will accept requests to open the shutters. The EPS will be responsible for sequencing the shutters in cases that involve a combination of photon shutters and safety shutters. All station doors that are automated will also be operated by the EPS.

7.3 Interface

The EPS will have human Interfaces (HMI) located at the main location of the hardware, which is expected to be located directly above the front end on top of the storage ring tunnel. In addition, there will be a minimum of one HMI per beamline at the beamline stations.

The EPS provides the command and control functionality for the beamline PPS. It receives the status information of the PPS and, based on that, can operate the shutters. The PPS, in addition, can request the shutter to close and the EPS will then command the shutter to close. In the event the shutter does not close within a specified time, as determined by the PPS, the PPS will initiate an emergency shutdown (ESD) situation.

The EPS will have an EPICS interface to the control system. The EPICS interface will provide both the main control room and the beamlines a complete overview of the status of each beamline. The data from the EPICS interface will also be logged and archived by the central computing systems.

The EPICS interface to the EPS will be both read and write. The write functionality will be controlled by the EPICS Channel Access Security. This is essential, to isolate the possibility of accidental control of the wrong beamline EPS via the control system.

8 Personnel Protection System

8.1 Beamline Area PPS

NSLS-II will produce intense light from IR, UV, and hard x-rays. Beamlines are designed to use either the bending magnet radiation or the radiation from insertion devices located in the straight sections of the storage ring. Beamlines may have more than one station along the beamline for every port. These stations are expected to work in parallel or sequentially.

The Personnel Protection System (PPS) is an engineered system that provides a means to ensure that personnel are not exposed to the radiation in the beamline. At NSLS-II, the role of the PPS is specifically to protect personnel from prompt radiation that is present only when there are stored electrons in the storage ring. The PPS is an engineered interlock system and is expected to monitor the various devices installed in the beamline for personnel safety and to provide emergency shutdown in case of breach of the interlock.

The PPS system, along with the required shielding in the beamlines, is expected to provide personnel safety during routine operation of the facility.

8.1.1 Functionality

Beamlines will consist of stations where synchrotron radiation is expected to be admitted. The beamline stations are expected to be made of lead-lined walls and roof, as appropriate for the particular radiation characteristics. These stations will house beamline optical components or beamline experimental equipment. The stations are expected to be large enough for personnel to work with the equipment inside.

The beamlines will have one or more shutters based on the particular layout, which is expected to vary from beamline to beamline. However, the functionality of the shutters, from the Personnel Protection System perspective, is expected to be the same and they will be monitored by the PPS. All x-ray beamlines will have shutters in the front-end area inside the storage ring shield wall (see Section 7.4). The bremsstrahlung radiation emitted by the synchrotron can only be stopped by heavy metal elements such as tungsten or lead. The heavy metal device that stops the bremsstrahlung radiation is referred to as the safety shutter. For the sake of safety, the shutter is expected to be redundant. The synchrotron beam, consisting of very high total power and power density, will be stopped by a device that is water cooled, made of copper or alloys of copper, and referred to as the photon shutter. These three devices, the two safety shutters and the photon shutter, will form a shutter cluster and their positions are monitored by the PPS.

Along the beamline are beamline optical elements that will condition the beam, including, for example, monochromators and mirrors. These devices change the characteristics of the synchrotron radiation. The radiation passing through the monochromator will, in most cases, be displaced in either the vertical plane or the horizontal plane from the incident radiation and only a small fraction of the incident radiation with a band pass (of about 0.1% or less) will be passed, with little or no power. In such cases the shutters, located downstream of the monochromator, will be called monochromatic shutters. They will be made of heavy metal and will be much shorter than the safety shutters. Once again, these monochromatic shutters are expected to be redundant for safety and will be monitored by the PPS.

A major role for the PPS will be to provide a means of ensuring that no personnel are inside beamline stations when the station is opened to synchrotron radiation. Prior to admitting the synchrotron radiation inside these stations, a search of the area has to be performed by a human. It is expected that the station search will be performed by one person only. There will be PPS devices called “search boxes” inside the station which must be visited as part of the search. Search boxes are strategically placed to ensure that during the

search all parts of the station are either visible or visited by the search personnel and no person is left behind inside the station. The search is completed when the station door is closed. The PPS will then lock the door.

Once the search process is started the PPS will start a beacon and audio signal inside the station, warning all personnel to exit. This signal is expected to last for some time, on the order about 20 to 30 seconds after the station door is closed. The function of the beacon and audio signal is to warn any personnel overlooked by the search person of impending danger. There will be very distinct emergency shutdown buttons placed inside the station which, when pressed, will instantly remove the presence of the prompt synchrotron radiation hazard. In addition, there will be also emergency egress buttons inside the station to unlock and open the door.

8.1.2 Design Specifications

The PPS will be designed to be robust and provide the emergency shutdown functionality to provide personnel safety from prompt radiation. Like the EPS, the PPS is expected to be based on programmable logic controllers. PLCs have numerous advantages over the relay logic scheme of interlocks. They can be reprogrammed to reflect changes in configurations and also have numerous diagnostics. The use of PLCs in safety system is very common now.

All devices attached to the PPS are expected to be designed to be fail-safe—that is, in case of failure the device will fail in such a manner as to either remove the hazard or remove the permit to generate or maintain the hazard.

Every beamline PPS will be designed under the same guidelines. The PPS will consist of two PLCs, referred to as chains A and B. The two PLCs will provide redundancy and will independently monitor all the devices.

All shutters will have two switches, one for chain A and one for chain B. There will be switches to monitor the closed and open positions. Similarly, all station doors will be monitored with two switches, one each for chains A and B.

At beamlines, there will be circumstances when a device such as a mask or photon beam stop is provided to absorb the power of the beam, while the radiation safety is provided by lead shielding as collimators or radiation stops. In such cases, the integrity of the masks and beam stops cannot be compromised, as they, in turn, protect the lead shielding which provides the personnel safety. In these cases, the mask or beam stop will be monitored by the PPS to ensure that it is not compromised. In most cases, the water flow to these components will be monitored independently by chains A and B of the PPS.

All PPS equipment will be clearly identified, and secured in locked cabinets. Cabling for the PPS equipment to field devices will be on separate closed raceways, which will be used exclusively for the PPS. All power to the PPS will be provided by uninterruptible power supplies, which will be backed up by generators.

8.1.3 Interface

The PPS must interface with numerous systems. The primary functionality of the PPS is to monitor and provide emergency shutdown.

To provide emergency shutdown, the PPS interfaces to the Accelerator Personnel Protection System. The PPS will remove a permit to the APPS to operate the storage ring. In the event of the removal of the permit by the PPS, it is the responsibility of the APPS to remove the hazard by dropping the dipole power supply and the RF to the storage ring systems.

The APPS will monitor the positions of the front-end shutters located inside the storage ring shield wall. The APPS will fan-out the status of the shutters to the PPS. There will be a provision in the APPS to remove

the PPS interactions for a specific beamline. This is expected to be in the form of a Kirk Key in an interface box between the PPS and APPS for each beamline. The APPS will monitor the closed positions of the front end shutters when the PPS is not available and will remove the storage ring permit if it experiences any "not closed" activity. When the PPS is available, the APPS will ignore the status of the shutters. This scheme will allow installation, maintenance, and validation of the PPS to take place while the machine is in operation.

All PPS functions will be monitored and data archived using the control system at NSLS-II. It is expected that EPICS will interface to the PPS PLCs to monitor their functionality. The EPICS interface will be read-only; there will be no writing to PLCs from the EPICS interface. Changes to the PLC operating codes will be possible from the field devices or when the PLC software is downloaded to the PLCs during routine validation of the system.

All command and control functionality for the PPS will reside with the EPS for the beamlines and front ends. The EPS will interface to the PPS and will receive signals from the PPS prior to operation of the shutter. In the event the EPS malfunctions, the ESD procedure of the PPS will activate and will remove the permit for the machine to operate. The PPS will only provide the ESD functionality and hence it expected to be simple and easy to maintain and validate.

8.2 Accelerator Personnel Protection System

As it relates to personnel protection, the NSLS-II facility consists of an electron gun and linac enclosed in a shielded area, and a main storage ring and booster enclosed in a heavily shielded tunnel. There are also numerous beamline experimental stations located on the perimeter of the accelerator tunnel. Protection from beamline radiation will be provided by the Personnel Protection System (discussed in the previous section), from linac radiation by the Linac Personnel Protection System (discussed in this section), and from radiation from the main ring and booster by the Accelerator Personnel Protection System (also discussed in this section).

8.2.1 Linac/Gun Personnel Protection System

The Gun/Linac area will contain linac accelerating sections where electrons emitted from the gun will be accelerated to an energy level for injection into the booster. The radiation hazards present during linac operation are two-fold, resulting from: 1) a high level of RF present in the linac sections that can accelerate free electrons and produce ionizing radiation fields, and 2) the acceleration of electrons to the full linac energy. RF power is supplied through klystron amplifiers powered by pulse modulators. Turning off the RF power will stop the production of radiation.

The Linac Personnel Protection System is specifically designed to protect personnel from radiation which is present only during linac operations. The LPPS is an engineered interlock system and is expected to monitor the various devices installed in the linac for personnel safety and provide emergency shutdown in case of breach of the interlock.

8.2.1.1 LPPS Functionality

A major role for the LPPS is to provide a means of ensuring that no personnel are inside the linac when the gun is on or the klystrons are pulsing. Prior to Linac operation, a search of the area has to be performed by a human. It is expected that the linac search will be performed by one person only. There will be LPPS devices called "search boxes" inside the linac, which must be visited as part of the search. The search boxes are strategically placed to ensure that during the search all parts of the linac are either visible or visited by the search personnel and no person is left behind inside the linac area. The search is completed with the closing of

the linac door. The person searching will lock the door when the search is completed and use a Kirk Key system to complete the search process.

Once the search process is completed, the LPPS system will start a beacon and audio signal inside the linac, warning all personnel to exit. This signal is expected to last on the order of about 60 to 120 seconds after the linac door is closed. The function of the beacon and audio signal is to alert any personnel who have been overlooked by the search person and trapped inside.

Emergency shutdown buttons which are very distinct will be placed inside the linac; when pressed, a shutdown button will instantly remove the radiation hazard.

8.2.1.2 LPPS Design Specifications

The LPPS will be designed to be robust and provide the emergency shutdown functionality for providing radiation safety to personnel in the linac area. The LPPS is expected to be based on programmable logic controllers. PLCs have numerous advantages over the relay logic scheme of interlocks. A PLC can be reprogrammed to reflect changes in configurations and also has numerous diagnostics. The use of PLCs in safety systems is very common and is an accepted practice at accelerator facilities across the United States.

All devices attached to the LPPS are expected to be designed to be fail-safe—in case of failure the device will fail in such a manner to either remove the hazard or remove the permit to generate/maintain the hazard.

The LPPS system will consist of two PLCs, referred to as chains A and B. The two PLCs will provide redundancy and independently monitor all the devices. To immediately stop the production of radiation, power to the modulator power supplies will be removed redundantly. This will be accomplished through the use of AC contactors, one for chain A and one for chain B.

Two critical devices will prevent radiation from entering the main ring from the linac: 1) the linac-to-main-ring stop, and 2) the bending magnet located upstream. The linac-to-main-ring stop will have two switches to monitor the closed and open positions, one switch each for chains A and B. The bending magnet upstream of the stop will be redundantly monitored for current and voltage by both chains. When the magnet is not powered it will prevent electrons from entering the accelerator tunnel area. All linac doors also will be monitored with two switches, one tied into each chain.

All LPPS equipment will be clearly identified and secured in locked cabinets. Cabling for the LPPS equipment to field devices will be separated in raceways. All power to the LPPS will be provided from an uninterruptible power source, backed by generators.

8.2.1.3 LPPS Interface

All LPPS functions will be monitored and data will be archived using the NSLS-II control system. It is expected that EPICS will interface to the LPPS PLCs to monitor their functionality. The EPICS interface will be only read-only; there will be no writing to the PLCs from the EPICS interface. Changes to the PLC operating codes will only be possible locally.

8.2.2 Storage Ring and Booster Personnel Protection System (APPS)

The storage ring and booster will coexist inside the same tunnel. The Accelerator Personnel Protection System interlock will be required to serve both the storage ring and booster. Radiation hazards during normal operations and conditioning are produced from multiple sources under different operational conditions. Operation of the RF accelerating cavities, both booster and main ring, can produce high radiation fields from secondary emissions that are accelerated by high RF fields. This radiation can be produced without electrons injected or stored in either ring.

The electron beam injected from the linac is another hazard, and, finally, stored beam in either the booster or main storage ring will produce synchrotron and bremsstrahlung radiation. The APPS must protect personnel from all conditions.

8.2.2.1 APPS Functionality

The APPS protects personnel from radiation hazards by 1) ensuring that no one is left inside the ring enclosure before operations that will produce radiation and 2) by providing a means of emergency shutdown of components, enabling personnel to stop the production of radiation in an emergency.

The ring enclosure is physically very large and will be divided into six searchable sections. Each section will be separated by a physical barrier in the form of a gate. Before operations begin, each section will be physically searched by a human. Once the search process is completed, the APPS system will start a beacon and audio signal inside the section being secured, as a warning to any overlooked personnel to exit. This signal is expected to last on the order of 60 to 240 seconds after the section gate is closed.

Emergency shutdown buttons, which have a very distinct appearance, will be placed inside the tunnel. When pressed, a shutdown button will instantly remove the radiation hazard.

The gates, along with Kirk keys, will be part of a system to allow controlled access to parts of the ring under defined conditions while other sections remain secured. With the APPS, beam will be dumped to allow authorized personnel controlled access to the ring sections while ensuring that no electron beam can be injected. Access will be monitored via a remote TV camera hookup to the control room. Each person entering the ring must remove a Kirk key; this inhibits the radiation source. A physical search of the section will be required before operations and radiation production can be resumed.

The first application of this concept defines an area around the RF accelerating cavities. The booster and storage ring cavities will need to be powered with RF for conditioning but without injected electron beam. The APPS will ensure no personnel are in the vicinity of the RF cavities during conditioning, while inhibiting electron beam from being injected into the ring. If the area is breached, the RF power source will be immediately shut off, redundantly.

During injection, while the linac-to-main-ring stop is open, if the storage ring area is breached the APPS interlock must dump stored beam and reach back to the LPPS to shut down the linac modulators.

The APPS may also be required to monitor conditions required for top-off operation of the injector. These conditions have not been determined but could include requiring a minimum stored current before top-off mode is enabled and requiring the dipole current to be at the proper energy level.

The APPS will also monitor the status of the front-end ports and will dump the beam if a port is open and the PPS detects a breach of an experimental station.

All APPS conditions and access modes are displayed and controlled from a dedicated rack in the control room.

8.2.2.2 APPS Design Specifications

The APPS will be designed to be robust and provide the emergency shutdown functionality to ensure personnel safety for the storage ring/booster area. The APPS is expected to be based on programmable logic controllers. PLCs have numerous advantages over the relay logic scheme of interlocks. A PLC can be reprogrammed to reflect changes in configurations and also has numerous diagnostics. The use of PLCs in safety systems is very common and is an accepted practice at accelerator facilities across the United States.

All devices attached to the APPS are expected to be designed to be fail-safe—in case of failure the device will fail in such a manner to either remove the hazard or remove the permit to generate/maintain the hazard.

The APPS system will consist of two PLCs, referred to as chains A and B. The two PLCs will provide redundancy and will independently monitor all the devices. To immediately stop the production of radiation, power to the RF plate power supplies and low level RF will be removed redundantly both for storage ring RF and booster RF. This will be accomplished through the use of AC contactors, one for chain A and an RF switch for chain B. The redundant means for dumping beam will also shut off the main dipole power supply through the AC contactor with both chains A and B.

The storage ring tunnel circumference is large; to avoid ground loops and EMC effects on APPS signals, fiber optic transmission of bus signals (one for each chain) will connect field I/O blocks around the ring to the main PLCs located in the control room. The control room PLCs will also connect to the RF and dipole power supply via a fiber optic I/O bus to avoid interference and corruption of signals.

The system will be designed for testability and will have built-in test features. The concept of diversity will be applied where possible.

The APPS main ring doors, emergency stops, and section gates have two switches, one each for chains A and B. All APPS equipment will be clearly identified and secured in locked cabinets. Cabling for the APPS equipment to field devices will be separated in raceways. All power to the APPS will be provided from an uninterruptible power source, backed by generators.

8.2.2.3 APPS Interface

The PLC program will incorporate a circular buffer of each scan that is triggered by an interlock breach. The buffer will be retrieved via EPICS to troubleshoot problems. All APPS functions will be monitored and data will be archived using the NSLS-II control system. It is expected that EPICS will interface to the APPS PLCs to monitor their functionality. EPICS will read data from a dedicated group of registers that reflect conditions and I/O points in the PLCs. The EPICS interface will be separate from the I/O bus. The EPICS interface will be only read-only; there will be no writing to the PLC from the EPICS interface. Changes to the PLC operating codes will only be possible locally.

9 GLOBAL SUPPORT SYSTEMS

9.1 Survey and Alignment

9.1.1 Scope

This section outlines the survey and alignment requirements and the technology and tools for achieving the NSLS-II equipment positioning goals. The required alignment tolerances are defined primarily by the physics requirements of the accelerator. At this stage of preliminary design, these tolerances are not known with high precision; however, similar parameters are available for other light sources of equivalent dimension. Our preliminary design of the survey and alignment system is based on the assumption that the tolerance requirements for NSLS-II will be similar to those of the APS, for example. An assessment will be performed, however, during the preliminary engineering design phase to identify any extraordinary position requirements of the accelerator systems, and the survey and alignment system will be modified as necessary to meet them. State-of-the art equipment and methods will be employed, but no new technology will need to be developed to meet the NSLS-II alignment requirements.

Survey and alignment provides the foundation for positioning the beam-guiding magnet structures in all 6 degrees of freedom within the required tolerances. Although the tools and instrumentation available for this task have changed over the years and faster and more accurate measurements are possible, only limited control of the environmental conditions is possible. This ultimately sets an upper limit for the achievable measurement and subsequent control network accuracy.

The scope of the survey and alignment work for NSLS-II includes the following:

- Provision of engineering staff to review the design of components having stringent alignment requirements. Engineering staff trained in state-of-the-art methods, software, and systems will be required to ensure that component designs are consistent with the survey and alignment systems that will be used to obtain the anticipated tight tolerances needed to achieve the desired emittance levels.
- Specification of alignment tolerances for each piece of equipment, and a determination of how to achieve them within the limitations of available equipment and hardware. Procedures, methods, and equipment will be specified.
- Procurement of alignment equipment, measurement equipment and instruments, targets, monuments, and hardware.
- Technical staff to achieve the precise alignment requirements during fabrication, assembly, and field installation. Technical staff trained in the use and calibration of state-of-the-art instruments and systems will be required.
- Provision of calibration equipment and facilities to maintain survey equipment within calibration tolerances.

9.1.2 Tolerances

The required positioning tolerances are an essential part of the survey and alignment design. Those tolerances dictate the instruments and methods necessary to obtain the positioning goals. Table 9.1.1 provides the required global tolerances, while Table 9.1.2 outlines the relative tolerances for the NSLS-II girder-to-girder positioning. These tolerances represent the most stringent requirements for the storage ring.

Table 9.1.1 NSLS-II Required Global Tolerances.

Global tolerances	± 3 mm
Horizontal positioning	± 3 mm
Vertical positioning	± 3 mm

Table 9.1.2 NSLS-II Girder-to-Girder Positioning Tolerances.

Relative tolerances	Girder to Girder
Horizontal positioning	± 0.15 mm
Vertical positioning	± 0.15 mm
Longitudinal	± 0.50 mm
Roll angle	± 0.5 mrad

9.1.3 Design Philosophy

9.1.3.1 Control Network Design

Depending on the size of the system to be constructed, a primary and secondary control network may be required to achieve these tolerances. NSLS-II covers an area of about one-eighth of a square kilometer with a radius of ~124 m and a circumference of ~780 m. The NSLS II construction methodology demands that separate tunnel segments be successively available and ready for installation purposes. This requires that each segment be fitted with an independent preliminary control network terminated by a primary monument at each end suitable for less demanding layout work such as the blue-line survey of the major beamline components, girder supports, and photon beamline layout in the front-end sections [9.1.1]. Only after all segments have been measured, processed by least squares, and analyzed will the final control network be ready for the positioning of the girders. Prior to construction, a calculation of the anticipated error propagation of the primary and secondary control network geometry will be needed.

9.1.3.1.1 Primary Control Network

The primary control network spans the entire accelerator facility and ties the accelerator enclosures into one reference system. It consists of a monument, M0, located at the center of the storage ring, a second similar one, M1, located at a convenient location in the infield close to the storage ring enclosure (Figure 9.1.1, left). Other monuments are distributed throughout the storage ring—for instance, at the beginning and end of each separate tunnel segment. The two monuments located in the infield should be very stable. Therefore, they require a deep foundation and a secondary outer shell for temperature stability [9.1.2], as shown in Figure 9.1.1(right). In this case a Kern centering plate is show that will be changed for a tribrach adaptor system currently widely in use. These monuments can also be used by the construction companies for layout and construction surveys.

The central monument usually defines the origin of the local right-handed coordinate system, while the second infield monument provides the orientation of the control network. The storage ring monuments are accessible through penetrations in the roof wall shielding. One of these should be located near the linac so no additional penetrations for the linac are necessary. Depending on the instrumentation used, all of the primary control points should be inter-visible. The spacing between storage ring penetrations is normally guided by the law of error propagation and should not exceed approximately 250 m.

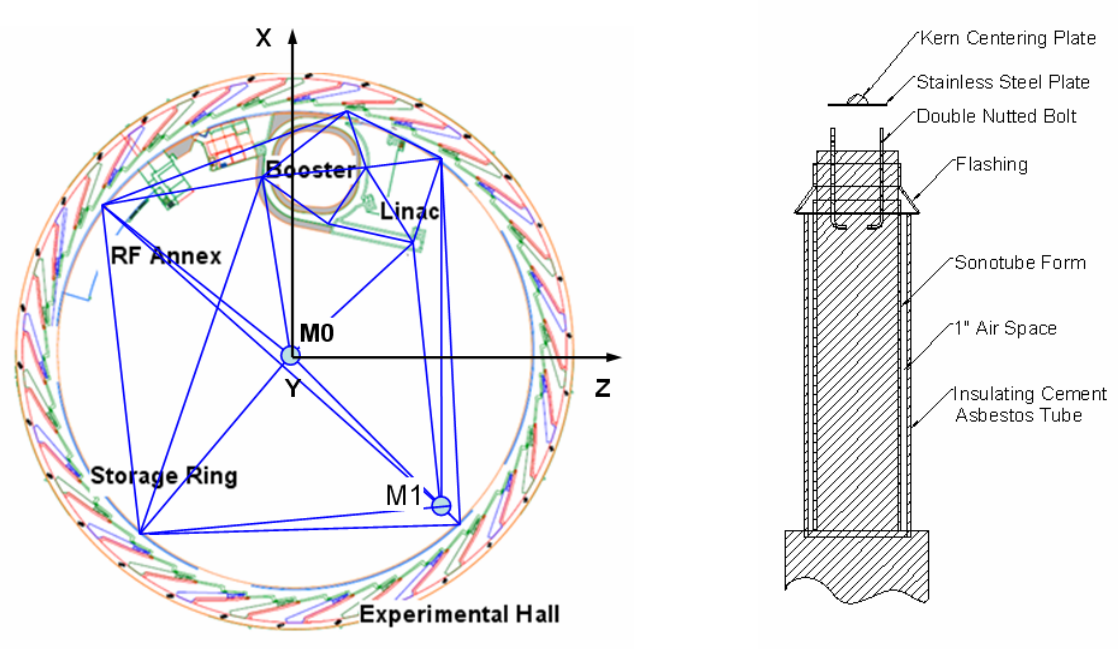

Figure 9.1.1 (Left) primary control network and global coordinate system; (Right) design of the stable monuments.

The primary control network can be measured as a trilateration network only. Current instruments are able to resolve distances to ±(0.1 + 0.1*D [Km]*) [mm], where *D* is the length of the measured distance in units of kilometer. This level of accuracy is not attainable with triangulation networks. By using a trilateration network, it should be possible to obtain a control network point accuracy of ±0.3 mm, similar to what has been achieved at the APS [9.1.3].

An alternative approach to determine the primary control network utilizes GPS observations for all primary control points. If public reference stations are not conveniently available, a local GPS reference station needs to be established at the storage ring center monument [9.1.4]. This base station supports differential GPS and would also be beneficial for the construction survey, as many survey companies have access to GPS and Real Time Kinematic (RTK) positioning technology. It is expected that utilizing DGPS, millimeter accuracies can be obtained. This approach needs to be further evaluated during the preliminary design phase to determine if it meets the requirements.

Both methods of measuring the primary network are highly dependent on the construction sequence and method, as lines of sight either between the monuments or the GPS satellites are required. This task has to be scheduled after the storage ring tunnel has been built but before the experiment hall enclosure is constructed.

9.1.3.1.2 Secondary Control Network

The design of the secondary control network is determined by the layout of the storage ring. If, as in the case of the APS, ratchet doors for each beamline are available, one can extend the secondary control network into the experiment hall (see Figure 9.1.2), providing a more stable control network design and the means to perform alignment work on beamlines while the machine is operational. The present preliminary design of NSLS-II envisions the installation of similar ratchet doors. Therefore, the secondary control network in the storage ring enclosure will be extended to the experiment hall.

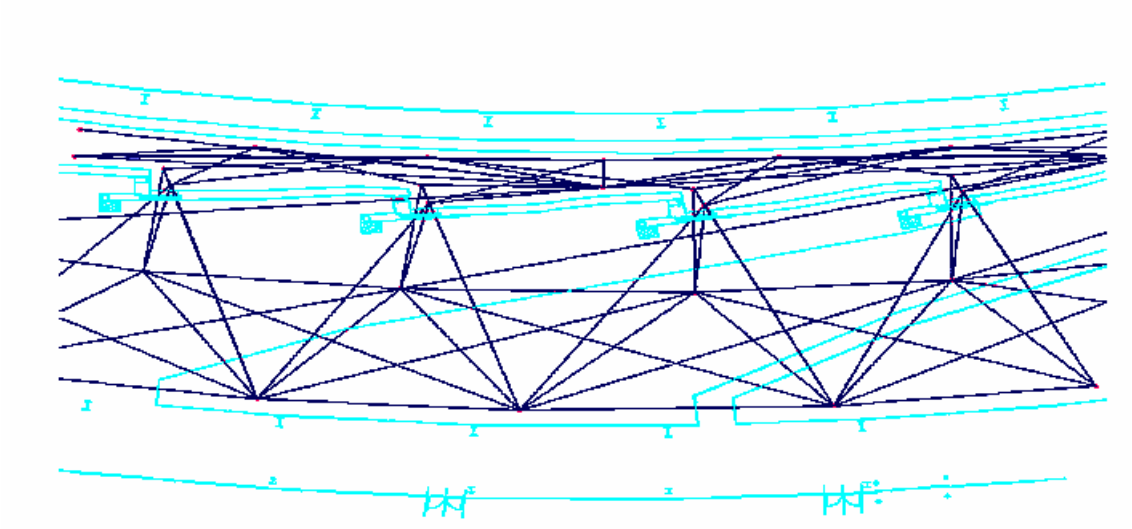

Figure 9.1.2 A secondary control network

Extending the secondary network to the experiment hall floor will benefit the layout work for the individual beamlines while the accelerator is in the commissioning phase. Each BM and ID beamline should receive two control points strategically located at an offset from the ideal beamlines and visible from the storage ring through the ratchet wall openings. Prior to the installation of the ratchet wall collimators the tie between the beamline layout in the front end and the experiment hall has to be established using optical tooling instruments. The marking of the front ends needs to be done while no girders have been placed in the tunnel and is best performed while the quadrupole and girder support locations are being laid out. Otherwise, line-of-sight to these areas will be very restricted and the markings may no longer be possible. The layout of the front-end locations is very important, as it provides the only means to extend the alignment control through the beam ports to the experiment floor.

Laser tracker instruments will be used for measuring the secondary control network, followed by a least squares analysis of the data to produce the final control points prior to setting out the machine components.

Current laser tracker systems obtain point accuracy on the order of ±0.05 mm in a spherical volume with a radius of 10 m around the instrument measurement head. For measuring the secondary control network with laser trackers, the primary control points are included in the measurement process and are part of the data analysis. This constrains the error propagation of the secondary control network to the level achieved by the primary reference network. The primary and segments of the secondary networks must be established, measured, and analyzed before accelerator equipment can be installed. However, sufficient time has to elapse for the concrete to cure before the control network monuments can be considered stable. Installing the floor monuments of the storage ring will necessitate core drilling to recess the target fixtures. The wall-mounted targets will be attached to concrete anchors with threaded inserts.

The secondary storage ring tunnel network should consist of at least four survey monuments located in cross sections of the storage ring spaced 10 m apart, as shown in Figure 9.1.3. An *a priori* error analysis needs to be performed to estimate the optimum locations for these targets and the expected point accuracy. The envisioned tunnel network creates a compact box structure to obtain a stable network geometry. Control points on the infield side of the tunnel are usually always accessible. The control points opposite the aisle should be located such that they will be visible after the girders have been positioned. The floor monuments are measured using common geometric leveling procedures to an accuracy of ±0.1 mm or better. This

information, in conjunction with the laser tracker measurements after proper analysis of the redundant data, provides the 3D control network that is used to place the accelerator components. An estimated accuracy of ±0.3 mm should be achievable for the secondary control network.

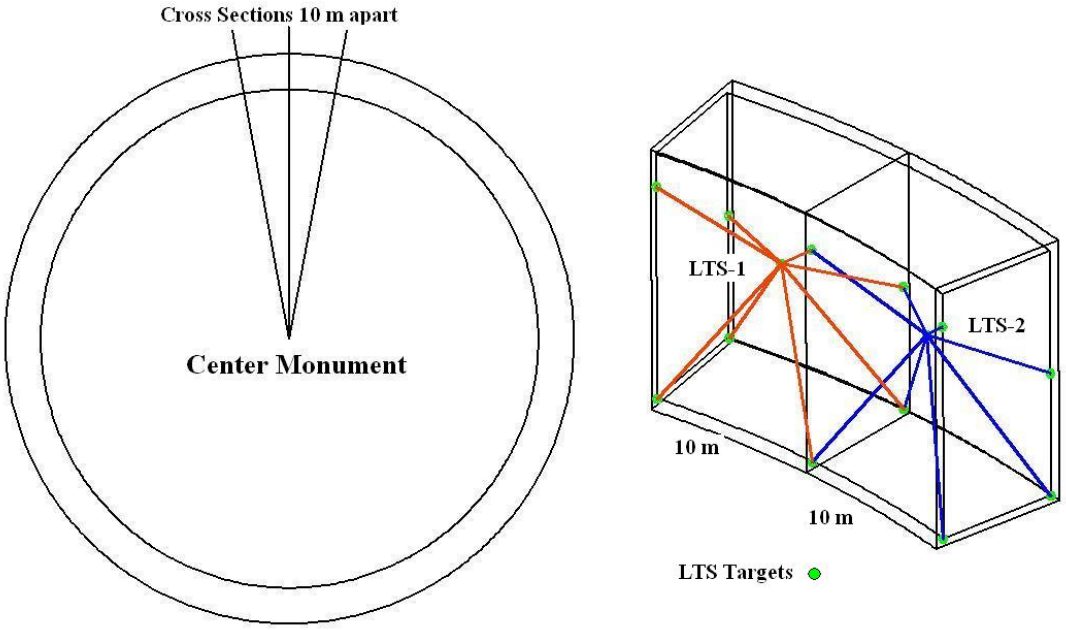

Figure 9.1.3 Sketch of a possible network design.

A variety of monuments for 1.5 inch Spherical Mounted Retro-reflectors are commercially available and can be mounted at the predetermined locations, as shown in Figure 9.1.4. This type of SMR and its accompanying receptors will be used for all survey and alignment work at NSLS-II, where possible.

Figure 9.1.4 Laser tracker 1.5 inch sphere mount.

For both the primary and secondary control network, error propagation calculations will be required before the realization of the reference network. This step provides information about the network density, optimal geometry, and minimum required measurement redundancy without diminishing the point accuracy of the control networks.

9.1.3.2 Elevation Control Network

Similar to the primary and secondary position control networks described in the previous section, we will establish primary and secondary elevation networks that are measured using common geometric level methods employing digital level instruments of proper accuracy.

Most survey instruments are referenced to local gravity. In particular, the leveling process measures elevation differences between two points with respect to the equipotential surface of the geoid. This leads to differences between a local planar system in which the accelerator is constructed and the curved geodetic reference system.

At the APS, all accelerators are located in a plane tangential to a best-fitting osculating sphere at the latitude of the center monument. The difference between this sphere and the tangential plane is on the order of 2.3 mm at 175 m from the center monument, the location of the storage ring. GEONET, the software used by APS to reduce these measurements to the reference sphere, takes local deviations into account and adjusts accordingly. In the case of NSLS-II, this may not be an issue, as the booster compared to the APS is small in size and located close to the storage ring resulting in negligible small corrections, that if necessary can be taken care of in the transfer line between the booster and storage ring injection region. This issue will be evaluated during the preliminary network analysis.

At the NSLS II components will be placed and rough-aligned first, with the components that are farthest from the tunnel entrances placed first. Care must be taken to maintain line-of-sight. To accomplish this, 3D computer graphic modeling will be used. After the heavier components are placed and aligned roughly, fine alignment will proceed using laser tracker and optical level instruments. Some settling of equipment and facilities is anticipated, and it is expected that the alignment adjustment will require checking several times during set-up, commissioning, and initial operation. Therefore, alignment equipment and expertise will have to be maintained in a constant state of readiness.

In any case, for a project the size of NSLS-II with its required high positioning tolerances, measurements for determining elevations and positions will be two distinct and separate operations. Each step requires specialty equipment designed for that purpose. Even if the existing laser trackers provide 3D point information, it is necessary to supplement the vertical information with elevation measurements derived from optical level instruments for increased accuracy.

9.1.3.3 The Lattice

In order to obtain congruence between the survey network and the lattice layout provided by the machine physicists, the datum of both of these systems must be the same. The six parameters (x, y, z, yaw, pitch, and roll) provided by the lattice for each beam component must be transferred to the Survey group and will be stored in a database that is used for all calculations to set the girders and other accelerator components. The database also contains the fiducial information of each component that needs to be placed. GEONET, a software analysis program originally developed at SLAC for this purpose and developed further at ANL and SLAC, performs these calculations and can be used at NSLS-II. However, commercial software that performs similar functions needs to be evaluated prior to starting the project and some software may need to be developed in house.

9.1.3.4 Smoothing

The initial positioning using the reference coordinate system can only be as good as the achieved network accuracy. This accuracy represents an upper limit. However, due to inherent target and instrument errors as well as environmental effects, this limit is not achievable and the actual positioning tolerance in the global system will be less than the obtained control network accuracy. Therefore a smoothing step is required.

For this part of the process, the control network is abandoned and only the local relation between adjacent girders is measured and verified. Instruments with sufficient accuracy, such as laser trackers or special offset measurement devices, can be used for this step. In particular, a comparison between the as-built and the ideal location will provide information about the relative girder position. The girder and magnet fiducial markers will be used in this step. As shown in Table 9.1.2, the girder-to-girder tolerances are relaxed in comparison to

the magnet-to-magnet requirements shown in Table 9.1.3. Nevertheless, during the fiducialization process great care has to be taken to obtain the best possible references.

Table 9.1.3 Magnet-to-Magnet Positioning Tolerances.

Relative Tolerances	Magnet-to-Magnet
Horizontal positioning	± 0.03 mm
Vertical positioning	± 0.03 mm
Roll angle	± 0.2 mrad

9.1.3.5 Fiducialization

During the fiducialization process, reference markers are determined with respect to the magnetic axis of the device. These markers are accessible after the magnet has been assembled on a girder and the vacuum chamber has been inserted. At that time, direct access to the magnetic axis is no longer possible and all positioning is performed with respect to these fiducials. Any positioning error during the fiducialization step can only be uncovered after the machine startup, with beam-based alignment methods. Unlike most of the other steps described here, this step does not provide measurement redundancy unless independent repeat measurements are performed.

For components requiring less accurate positioning, referencing to the mechanical axis may suffice. However, for the NSLS-II, the magnet-to-magnet positioning tolerances, shown in Table 9.1.3, are exceedingly stringent; therefore, a combination of magnetic and dimensional measurements is required.

Usually, rotating coils or stretched wires are used to establish the beam axis. Once the optimum position of the device is found, the information is transferred from the beam axis to the outside reference markers. This is done for each of the magnets prior to the assembly on a girder. The fiducial information is used in the assembly process. The transfer of the position information from the magnetic axis to the reference point can be performed with a 25–50 μm accuracy, depending on the method used. However, in case of NSLS-II, the accumulation of errors in determining the reference targets, the mechanical assembly of the magnets on the girder, the alignment of the magnets on the girder, and so forth may exceed the required tolerance limits. It is therefore envisioned that all multipoles will be assembled and aligned on a girder using the vibrating wire technique [9.1.5]. In this way, the intermediate steps to obtain fiducial information for each magnet separately are circumvented. After this step, the girder will be considered the smallest unit that needs to be placed in the storage ring tunnel.

The girders need to be fitted with permanently mounted SMR receptacles above each of the support feet on both the inboard and outboard side. This is required because the girder will have more than three support feet for reasons of stability and vibration damping. It is envisioned that laser trackers will be used to perform the coordinate transfer from the wire, via a touch-free probe if necessary, to the girder fiducials that are used to position the girder and to check for local deformations while aligning the girder in the storage ring tunnel. It is important that there be a defined stay-clear area around each of the girder fiducials. In particular, above each fiducial no obstructions are allowed; doing otherwise would prohibit the use of level rods on these markers.

R&D is planned to carefully evaluate this approach for the magnet alignment and fiducialization prior to construction of NSLS-II.

9.1.4 Implementation

Close coordination between the construction efforts and implementation of the control network must be maintained while NSLS-II is being built. It is also imperative that the survey and alignment team be involved

early in the design of the girder and magnet supports and moving systems, because the positioning resolution and performance are directly linked to these devices.

9.1.5 Training

At minimum, operators of survey equipment should have several years of experience in properly handling and operating instruments of that type. Instrument operators will have to work closely with the technicians who will make the required adjustments. In particular, when using laser trackers to provide real-time, online alignment capabilities, Survey and Alignment technicians will apply the required adjustments; these two steps go hand-in-hand. Most laser tracker manufacturers provide onsite training for operating their systems. For the alignment of the front ends and beamlines, optical tooling is required because space is limited. Training in the use of optical tooling instruments is commercially available. All personnel involved with the survey and alignment tasks should have experience and aptitude in the precision alignment of 3D components and hardware.

9.1.6 Component Assembly, Testing, and Calibration

Many of the instruments that are employed for survey and alignment must be tested and calibrated on a regular basis. An alignment and calibration room will be provided for this purpose. This room will be environmentally stable and will have sufficient space for secure storage of all calibration equipment (including a Coordinate Measuring Machine and one or more large surface plates), as well as for the survey instruments themselves. The alignment and calibration room will also have enough additional space to align critical assemblies. Because survey instruments are very delicate, in-house calibration is generally preferred over shipping equipment out to a vendor. Calibration procedures and training are therefore required.

The alignment and calibration room will be large enough for calibration as well as for critical assembly work to be completed in a temperature-stable environment, thus allowing alignment processes to be tested accurately before they are used for the accelerator.

9.1.7 R&D

Two important R&D tasks have been identified. The first is an error analysis of the network configuration, to determine the network layout. It is also important in that step to incorporate the anticipated construction methodology. The second important R&D task determines the magnet measurement process and its effects on the survey and alignment process. If it can be shown that the vibrating wire method can be used to position the magnets on girders, then the girder will become the smallest unit that the survey team has to contend with. However, close interaction will be required between the magnet measurement and survey groups. In particular, the girder fiducialization process needs to be established, because special equipment for the touchless wire pickup may be required.

References

[9.1.1] H. Friedsam, “The Alignment of the Advanced Photon Source at Argonne National Laboratory,” International Workshop on Accelerator Alignment, CERN, Switzerland, 1993.

[9.1.2] R. Ruland, “Synchrotron Radiation Sources A Primer,” World Scientific Publishing ISBN 981-02-1856-7.

[9.1.3] H. Friedsam, M. Penicka, and S. Zhao, “Status Report on the Survey and Alignment Efforts and Results of the Advanced Photon Source,” International Workshop on Accelerator Alignment, KEK, Japan 1995.

[9.1.4] H. Friedsam, R. Ruland, private communication.

[9.1.5] Z. Wolf, “A Vibrating Wire System for Quadrupole Fiducialization,” SLAC, LCLS-TN-05-11.

9.2 Process Water Systems

9.2.1 Scope

The NSLS-II accelerator and beamline components require a large amount of heat rejection as well as a stringent temperature stability. A number of closed-loop water systems are used that exchange heat with the water from cooling towers and chilled water from the BNL's central plant. The preliminary designs of these closed-loop water systems are described in this section. The description for the cooling tower and chilled water systems can be found in the technical design report for the Conventional Facilities.

9.2.2 Thermal Loads

The major sources of heat generation are identified in Table 9.2.1. When all beamlines are built, the total heat rejection is approximately 7.4 MW. This heat is rejected to closed loop water systems at different inlet water temperatures as shown in column 3.

Table 9.2.1: Major heat sources in the NSLS-II facility and the nominal inlet water temperature for heat rejection. The total heat rejected adds up to 7,425 kW, not including the air-conditioning load for the building.

Heat Source	Heat Rejected (kW)	Inlet Water Temperature (ºC)
Linac	100	24.0 ± 0.5
Booster	400	29.5 ± 0.5
Storage ring magnets	1400	29.5 ± 0.1
Absorber system and front ends	700	29.5 ± 0.1
RF system (klystrons)	1400	29.5 ± 0.5
Cryoplant	300	33
Power supplies and equipment	1100	7.2 ± 1.0
Beamlines (x-ray power)	250	
Beamlines (electrical)	1700	7.2 ± 1.0
Vacuum chambers	75	29.5 ± 0.05

9.2.3 Preliminary Designs of the Water Systems

There are three different closed loop water systems: (1) deionized process water systems for the copper components, (2) deionized process water system for the storage ring vacuum chambers, and (3) chilled water system for the heat exchangers of the air-cooled racks of power supplies and electronic. The first two systems are designed to exchange heat mainly with the cooling-tower water, but they can also reject partial heat load to the chilled water system on hot and humid days (wet bulb temperature of > 25 ºC).

Each of these three systems are divided into five separate unit in order to keep the pipes, pumps, valves and heat exchangers to reasonable sizes. The reduced system sizes also improve their temperature stability. The pumping stations are housed in 5 mechanical equipment rooms located on the inboard side of the storage

ring (see Figure 9.2.1). Three additional pumping stations for copper systems are provided, 2 in the RF Annex and 1 in the Booster building.

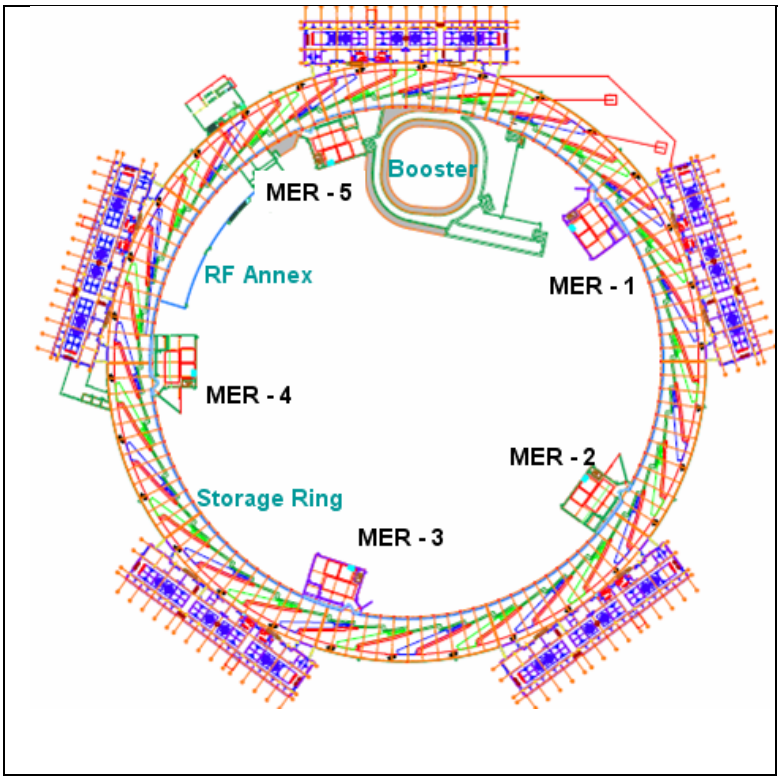

Figure 9.2.1 Mechanical equipment rooms (MERs) for the pumping stations of the closed-loop water systems. Additional pumping stations are installed in the RF Annex and Booster.

The process & instrumentation diagram (PID) for the copper water system is shown if Figure 9.2.1. The pumping station uses two 75 HP, variable frequency drive (VFD), pumps for redundancy and reliable operation. The VFD pumps, besides being energy-efficient, also provide better control over the supply-side flow, pressure and temperature. A slipstream deionizing skid keeps the resistivity and pH of the water in the specified range to minimize copper corrosion (see below).

A portion of the process water exiting from the pumps exchanges heat with the tower water in order to reject heat from magnets, absorbers, and beamline components. If necessary, heat is also exchanged with chilled water for additional cooling on hot and humid days. Mixing valves are used to regulate the water temperature to 85 ± 0.1 ºC before it is supplied to the storage ring. Another chilled water heat exchanger is used, as shown in the figure, to bring down the water temperature for the beamlines to 75 ± 0.1 ºC.

Each MER supplies process and chilled water to the equipment and components of six cells. The supply and returns pipes are branched out in the middle to serve 3 cells on each side.

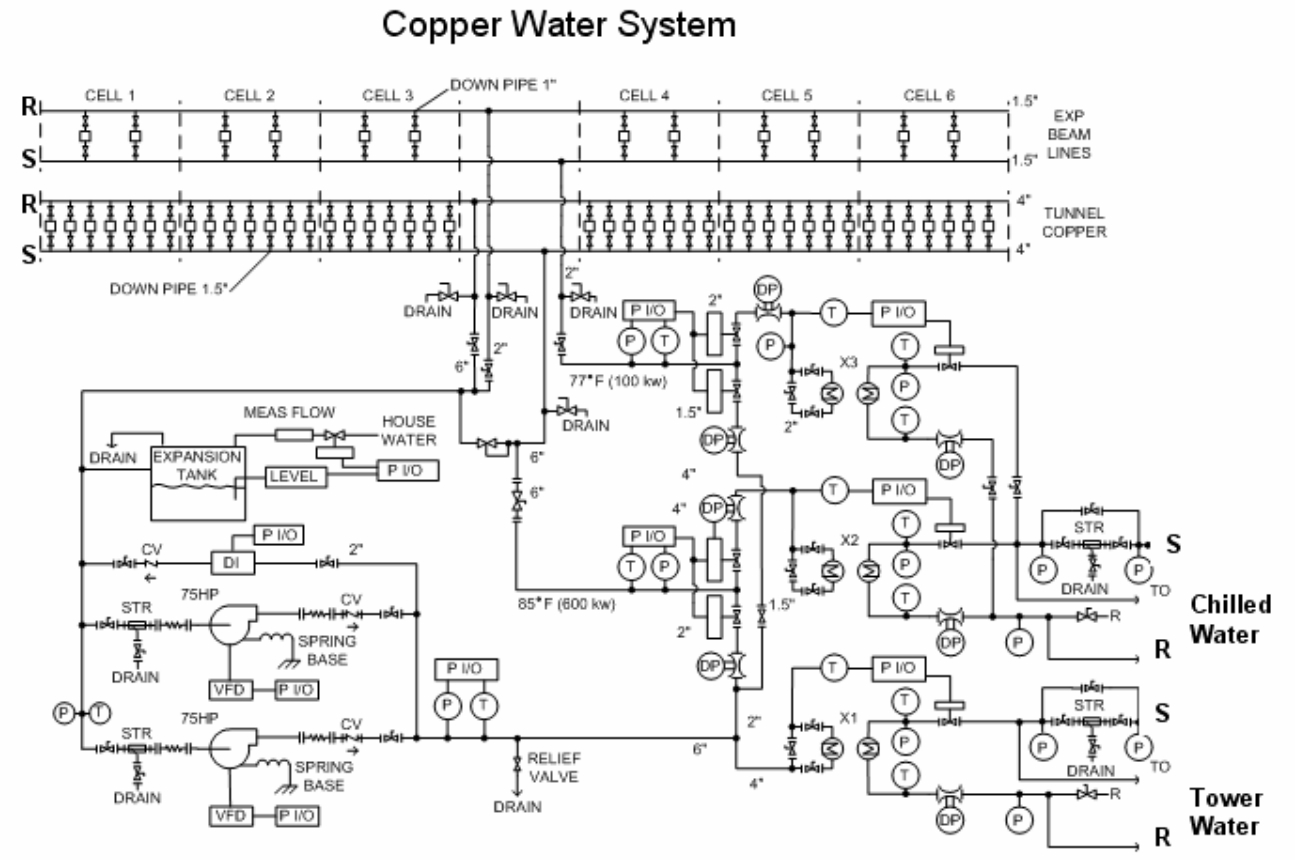

Figure 9.2.2 PID of the pumping station for the copper water system.

A similar but smaller-size pumping station with 10 HP pumps is used for the aluminum water system as shown in Figure 9.2.3. The aluminum water system is also a closed loop system which is completely isolated from the copper components and other water systems to eliminate the possibility of galvanic corrosion. The aluminum chambers of the storage ring do not directly intercept x-rays, but they do intercept x-ray power scattered from the absorbers. Another source of heat is the frictional losses from water flow through the three cooling channels of the chambers. The temperature stability of ±0.05 ºC is specified for the aluminum water system in order the keep the chamber deformations, which affect the BPM locations, to within acceptable limits.

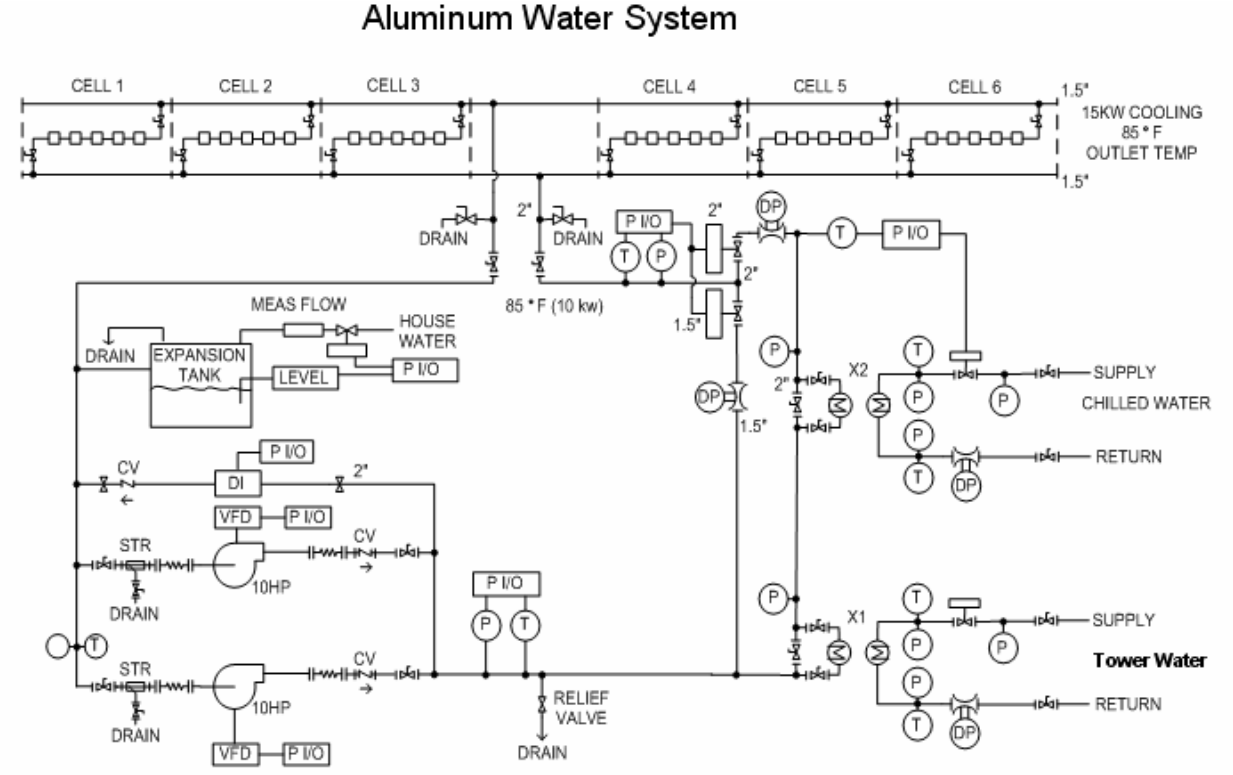

Figure 9.2.3 PID of the pumping station for the aluminum water system.

For the bakeout of aluminum chambers, the present plan is to use NEG strips or kapton heating foils. Bakeout by hot water (as is done at APS) will be considered as a less preferable option because of its complicated design and safety concerns.

The closed-loop chilled water system (not shown) exchanges heat only with the chilled water from central plant. It does not use deionizing skid and requires a moderate temperature stability of only ± 1 ºC.

9.2.4 Process Water Quality Control

Copper corrosion in the copper components cooled by deionized water remains a major concern. The main factors that affect the copper corrosion process are: water resistively, pH, dissolved oxygen and water temperature. An investigation will be made to determine the most appropriate ranges for these parameters. Bases on the experience of several accelerator facilities, the following values are selected for the preliminary design:

- Resistivity = 1 MΩ-cm ±5%
- pH = 7.5 ±0.2%
- Oxygen concentration = 6 ppb ±1 ppb
- Water temperature < 40 ºC.

1 IXS: INELASTIC SCATTERING BEAMLINE

1.1 Executive Summary

We present in this chapter a preliminary design of the Inelastic X-ray Scattering (IXS) beamline for NSLS-II. The scientific objective of the beamline is focused on very high-resolution (1 meV ~ 0.1 meV) IXS experiments as outlined in the NSLS-II Conceptual Design Report delivered in December 2006. The NSLS-II User Workshop in July 2007 provides further inputs from the user community on the scientific drivers for this beamline. The beamline as designed includes two endstations, one with 1meV and the other with 0.1meV energy resolution, both of which take full advantage of the high brightness and flux of the NSLS-II source at ~10 keV. To achieve the 0.1meV resolution goal for NSLS-II, the current design employs a newly proposed scheme based on highly asymmetrically cut Si crystal optics operating at exact back-scattering. This novel approach, albeit yet to be demonstrated in a working device for which active R&D are required, provides a unique opportunity for NSLS-II to build a fundamentally new instrument with unprecedented performance for inelastic x-ray scattering experiments that are not yet feasible on any existing instruments to date.

The scope of the present document includes the scientific objective, the radiation source, the overall beamline layout, rationales for beamline optics, the power management and the expected performance. Some design details will be presented, including the beamline vacuum system, data acquisition and motion control, and beamline components that are likely to remain the same regardless the details of the endstation design. Details on the Personnel Safety System, the Equipment Protection System, as well as additional requirements on the conventional facilities and accelerator systems will also be discussed.

Several possible configurations of the 1meV endstation will be outlined. One will be based on the same scheme as that for the 0.1meV endstation, but optimized to operate at 1meV energy resolution. This would be a logical choice as demonstrating the scheme for achieving the 0.1meV energy resolution works for 1 meV is a milestone of its own. Others are based on existing experience in building IXS beamlines that offer 1meV energy resolution at ESRF, SPring-8 and APS using Si crystal optics operating at higher photon energies. The intension here is to use crystals of lower symmetry such as quartz or sapphire which offer many possible choices of refraction with intrinsic width of the order of 1 meV at energies ~10 keV. There are concerns regarding the quality of these crystals for use as high-resolution x-ray optics. There are however substantial efforts now in making better crystals at several groups around the world. We will monitor the progress of those efforts and make a decision on the configuration of the 1meV endstation at some point in future.

The total estimated cost of the beamline based on the details of the current design stands at $9.915M, which includes the enclosures, beam transport, utilities, white beam components, high heatload optics, beam conditioning optics, Personnel Safety System, Equipment Protection System, beamline controls, and project management. The cost for the 0.1meV endstation is also included.

Finally, we would like to emphasize that the present design is still at a very preliminary stage. The final design of the beamline as well as the endstations will largely depend on the final technical details for achieving the 0.1meV energy resolution, where an active R&D program will be required and pursued. The design process will further involve consultations with the user community through workshops and with the Beamline Advisory Team (BAT) in the coming years, whereby the scientific focus of the beamline and endstations and hence their design will be further refined.

1.2 Scientific Objective

Inelastic X-ray Scattering is a momentum-resolved technique for studying dynamics and excitations in condensed matter systems. The scientific objective of the present IXS beamline is focused on very high-resolution (1 meV ~ 0.1 meV) IXS experiments for studying low-energy dynamics of a variety of systems. The NSLS-II User Workshop in July 2007 (see the breakout session on inelastic x-ray scattering at the following link: http://www.bnl.gov/nsls2/workshops/UserWorkshop_BOS2.asp) further identifies a few key scientific drivers for this beamline. They are grouped into several classes of experiments according to the required energy resolution:

- 0.1meV resolution experiments
  Examples include visco-elastic crossover behaviors of disordered systems and fluids, and new low-energy modes in complex fluids and confined systems that would require the 0.1meV resolution to be resolved. Another important area of research is in the collective dynamics of lipid membranes and other biological systems, where correlated molecular motions and density fluctuations on the meV energy scale play a significant role in determining their physical properties. The 0.1meV resolution would also be potentially useful for mapping the superconducting band gap with phonons.
- 1meV resolution experiments
  Examples include relaxation processes in disordered systems such as glasses, fluids, polymers, etc. The higher available flux promised by NSLS-II compared to existing instruments will be highly valuable for studying phonons in single crystals, surfaces, thin films, small samples down to micrometer sizes, systems under extreme pressure, phonons in excited states (pump probe), and exotic excitations in strongly correlated systems.

It is clearly recognized by the community that the 0.1meV endstation should be designed to bridge, at least partially, the dynamic gap between existing high- and low-frequency probes, which would enable new science to be done. The most exciting scientific problems requiring this energy resolution are envisaged to come from disordered systems in the forward scattering direction, where very high momentum resolution (<0.1 nm^{-1}) would also be required. For the 1meV resolution experiments, the higher available flux promised by NSLS-II should allow studies ranging from phonons in small single crystals, surfaces, thin films, to exotic excitations in strongly correlated materials, where the range of momentum transfer should cover typical Brillouin zone sizes. To take full advantage of the superior performance at ~10 keV of the NSLS-II source, the requirements and specifications for the beamline and endstations include:

- The primary beam energy is chosen at 9.1 keV near the peak of the tuning curve of a U19 undulator and also to match the proposed scheme for achieving the 0.1meV energy resolution. This energy should however be tunable over 7 ~ 12 keV to retain certain flexibility in case a different choice of refraction may be required.
- Due to the different experimental requirements for 0.1meV and 1meV resolution, there should be two endstations, one optimized for the 0.1meV, and the other for the 1meV experiments.
- The energy scan range should be on the order of 100 meV for the 0.1meV endstation, and up to about 1 eV for the 1meV endstation.
- Momentum resolution should be better than 0.1 nm^{-1} at low momentum transfer. This corresponds to an angular acceptance of less than 10 mrad for the analyzer at 9.1 keV.
- For the 1meV endstation, the momentum scan range should be up to 80 nm^{-1} in order to cover typical Brillouin zone sizes of small single crystals. This translates to a scattering angle of 120 deg at 9.1 keV.
- Beam spot size should be ≤ 5 μm (V) × 10 μm (H). This would enable studies of very small samples and samples under extreme pressure generated using diamond anvil cells.

1.3 Insertion Device

Inelastic x-ray scattering is a photon-hungry experiment. The figure-of merit for a radiation source for an IXS beamline is therefore the flux (photons per second per meV) that it delivers to the sample. The brightness or the ultimate beam spot size on the sample becomes secondary in this case, so long as it suffices to achieve the required energy resolution and be compatible with the required sample environments such as for extreme pressure. Of the devices considered in the baseline of NSLS-II, a 3m-long U19 undulator offers the best performance over 7 ~ 12 keV. Key parameters of the U19 undulator are summarized in Table 1.1.

Table 1.1. Basic parameters of a U19 undulator.

IVU specs	U19
Device type	CPMU / in vacuum
Peak field	1.14 T
Lowest 3rd harmonic energy for 3.0 GeV beam	4.4 keV
Highest harmonic to be used	7
Maximum K value – corresponding to the lowest third harmonic energy	2.03
Overall length of magnet array	3 m
Period	19 mm
Minimum magnet gap	5 mm

For further improvements that could lead to a significant increase of the incident flux, one of the options being considered is placing multiple undulators in a single long straight section. Possible choices include two 3m-long U19 or three 2m-long U14 undulators. A five-fold increase of flux is expected, for example, by using three 2m-long superconducting undulators (SCU) U14 instead of a single 3m U19 device (Figure 1.1). This assumes the ability to refocus the beam between such devices, which requires careful studies of the accelerator systems during the design phase. If the issue of refocusing can be resolved, it is obvious that the IXS beamline could make a perfect case for yet an even longer straight section for more devices.

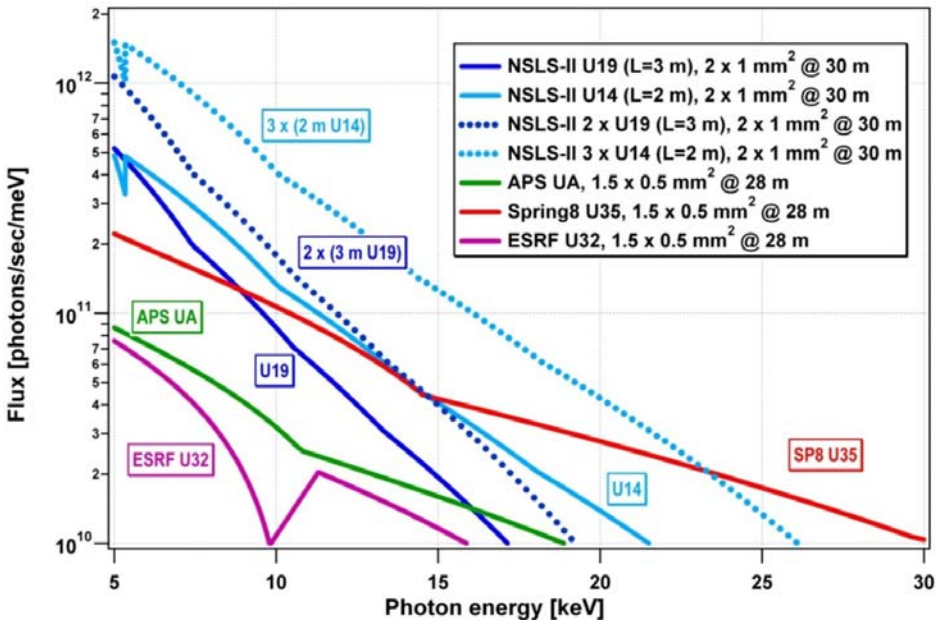

Figure 1.1. Flux comparison of various devices at NSLS-II and elsewhere, as measured in ph/s/meV. The light blue dotted curve shows the increase associated with placing three 2 m-long U14 undulators in a single straight at NSLS-II. The solid blue curve is for one 3 m-long U19 undulator.

Another option being considered is to optimize the undulator parameters to maximize the peak flux at the primary energy of the beamline. Figure 1.2 shows a comparison between a U17 and a U19 undulator of the same length. With a similar strength of the magnetic field, the U17 is expected to deliver a factor of 2 more flux at around 9 keV compared to the U19. Potentially, this type of optimization can be done for each individual beamline. There is therefore some cost implication for the additional design effort. However, the impact on the accelerator systems would be minimal.

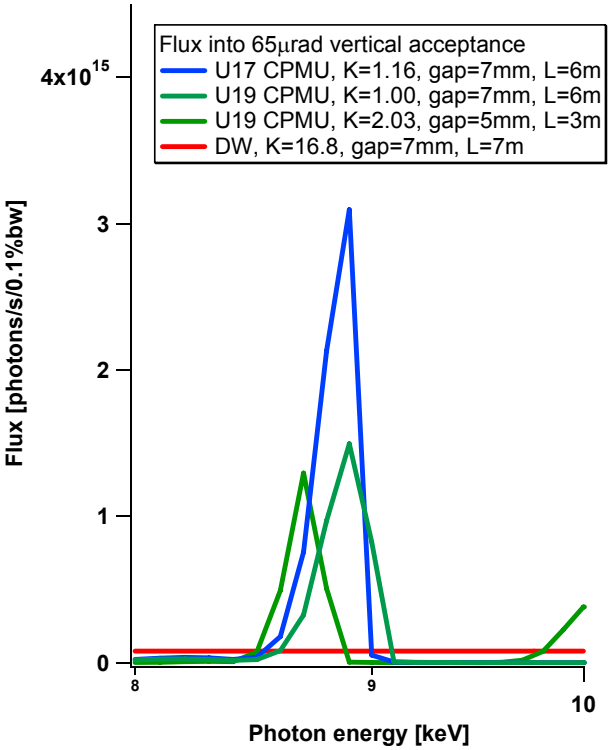

Figure 1.2. Flux comparison of various devices at NSLS-II. Here a U17 with a similar strength of magnetic field is expected to deliver a factor of 2 more flux than a U19 at ~9 keV.

In order to provide the possibility of accommodating two 3m U19 or three 2m U14 undulators, the longer 9.3m high-β straight section of the current storage ring design will be needed. Even for a single U19 undulator, there are other benefits associated with a high-β straight section for the beamline, due to the differences in the beam size and divergence between the low-β and the high-β straight section. As shown in Table 1.2, the horizontal beam size increases by about a factor of 3, whereas the angular divergence decreases by about a factor of 3.5, on moving from a low-β to a high-β straight section. This leads to a corresponding increase of horizontal source size and decrease of horizontal divergence by about a factor of 3 (Table 1.3). Consequently, the horizontal photon beam size reduces by more than a factor of 2 as a result of the reduced beam divergence as it travels downstream of the beamline. The heatload delivered onto the first optics within the central cone of the photon beam reduces also by a factor of 3 (Table 1.4). It should be noted that the flux within the central cone remains essentially the same between the low-β and the high-β straight section. Therefore, the use of a high-β straight section allows a smaller horizontal aperture with no cost to the flux. The heatload on the first optics is reduced to a manageable level, even for two U19 undulators. The smaller horizontal beam size also allows the use of shorter mirrors for the horizontal plane.

Note that a U20 is currently in the baseline device. Calculations show that there are minimal differences between the U19 and U20 in terms of their performance. The discussions in the subsequent sections will still assume the U19 device for convenience.

Table 1.2 Beam parameters assuming eight damping wigglers with 0.55nm-rad horizontal emittance.

Parameters		Low β	High β	Units	Ref.
Emittance	ε_x (horizontal) ε_y (vertical)	0.55 0.008		nm · rad	2,3
Beta function	β_x (horizontal) β_y (vertical)	1.5 0.8	18 3.1	m	3
Energy spread		0.0005 - 0.001		-	3
Beam size (sigma)	σ_x (horizontal) σ_y (vertical)	28.7 2.5	99.5 5.0	μm	Calc.
Angular divergence (sigma)	σ'_x (horizontal) σ'_y (vertical)	19.2 3.2	5.5 1.6	μrad	Calc.

Table 1.3 Source parameters of a U19 operating at several conditions in a low-β and a high-β straight section.

K	N	E, keV	Source size (σ), μm				Angular Divergence (σ), μrad			
			Low-β		High-β		Low-β		High-β	
			H	V	H	V	H	V	H	V
2.03	1	1.47	29.3	6.2	99.7	7.5	22.5	12.3	13.1	12
1.713	5	9.1	28.8	3.4	99.5	5.5	19.8	5.7	7.3	5.0
0.981	3	9.1	28.8	3.4	99.5	5.5	19.8	5.7	7.3	5.0

Table 1.4 Power from a U19 undulator in a low-β and high-β straight section delivered to the first optics at 30 m from the source through an angular aperture defined by 4σ (H) x 4σ (V) of the source divergence.

Distance, m	K (N)	Low-β			High-β		
		Ang. Aperture (HxV), μrad²	Beam Size, (HxV), mm²	Power, W	Ang. Aperture (HxV), μrad²	Beam Size, (HxV), mm²	Power, W
30	1.713 (5)	79.2 x 22.8	2.4 x 0.7	118	29.2 x 20.0	1.0 x 0.6	38
30	0.981 (3)			65			21

1.4 Sector Layout

The Inelastic X-ray Scattering beamline will occupy only the insertion device port of a sector with a long high-β straight section. Nevertheless, the required floor space to accommodate the 1meV endstation may be extended to the floor space of the adjacent beamline on the bending magnet port, which should be given due consideration regarding whether and how the bending magnet port will be used in future.

1.4.1 Front-End Layout

The current generic layout of the front-end for a long, high-β straight section is shown in Figure 1.3. As shown, this front-end layout is compatible with the current design of the IXS beamline. However, the design can be further optimized and coordinated with components planned for the first optical enclosure (FOE) of the beamline, which may provide some cost savings and allow for more efficient use of floor space in the experimental hall. For example, the space between the fast gate valve (FGV) and the second x-ray beam position monitor (XBPM-2) can be used to accommodate the X-Y slit that defines the x-ray beam for the first optical component of the beamline (i.e., the first crystal of the high heatload double crystal monochromator). Other components that should be included in the front-end include (removable) filters and screen monitors at a few locations, for diagnostics during commissioning.

A U19 undulator is expected to generate a total power of 11.2 kW and a peak power density of 77.86 $kW/mrad^2$. If two of this device are used, the total power and the power density will be doubled. The front-end must be designed to handle these power loads.

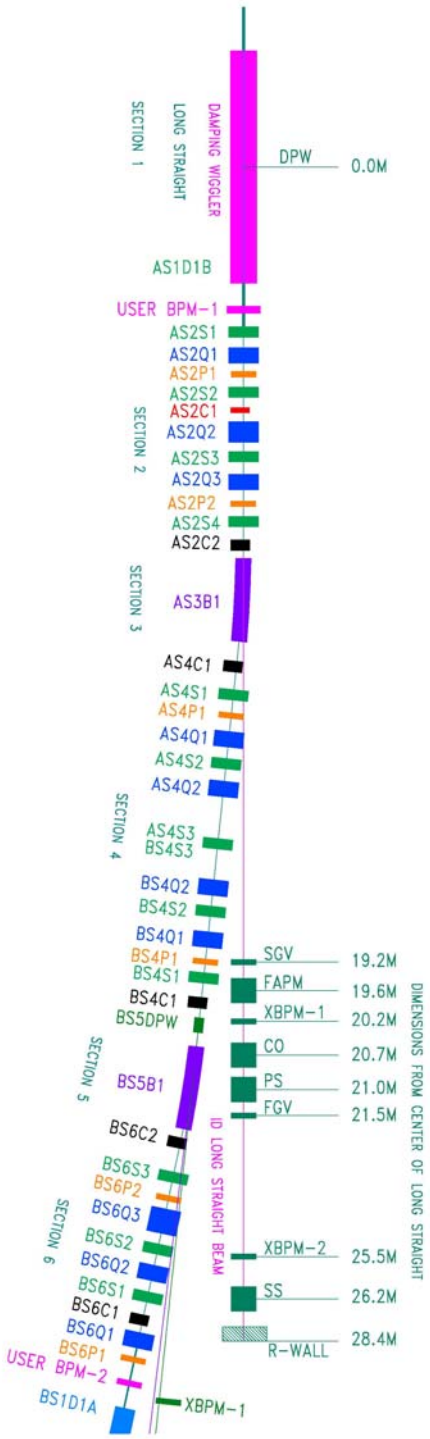

Figure 1.3 Generic layout of the front end for a long, high-β straight section. Components as shown include a slow gate valve (SGV), a fixed aperture mask (FAPM), two x-ray beam position monitors (XBPM), a lead collimator (CO), a photon shutter (PS), a fast gate valve (FGV), and a safety shutter (SS). Positions shown in meters are distance from the center of the straight section.

1.4.2 Beamline Layout

A CAD drawing of the beamline and endstations showing the general layout of the beamline is given in Figure 1.4. Functionally, there are four major optical components before each endstation. These include the high heatload double crystal monochromator (DCM), a vertical collimating/focusing mirror (VCM), a high-resolution monochromator (HRM), and a set of KB focusing mirrors. For the 0.1meV endstation, the HRM will be an inline monochromator based on the CDDW scheme [Ref]. For the 1meV endstation, the optical scheme depends on the approach we will use and will be described in more detail later. All these optical and other beamline components are housed in three enclosures. The first one (the first optical enclosure: FOE) is for the white beam components including the high heatload DCM, and the other two are for each of the two endstations. The VCM is placed in the FOE for convenience. The HRM for each endstation is considered as an integrated part of the endstation, and is therefore housed with the endstation in the same enclosure.

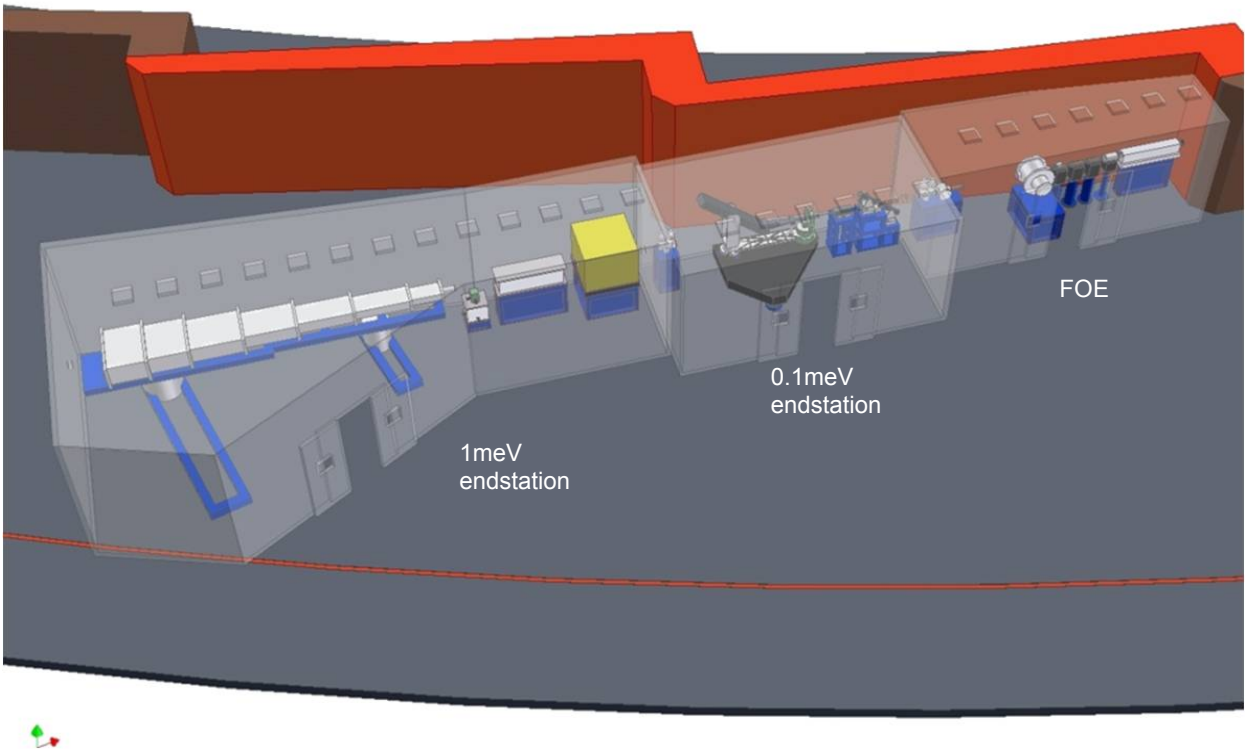

Figure 1.4. Schematic layout of the Inelastic X-ray Scattering (IXS) beamline, showing (right to left) the first optical enclosure (FOE), the 0.1meV endstation, and the 1meV endstation.

1.4.2.1 Survey and Alignment Plans

All beamline components will be surveyed and aligned in place by NSLS-II staff. To facilitate ease of alignment, all components will be fiducialized to external reference points on their table during assembly. All components are designed with a liberal tolerance allowance greater than 0.5 mm. Where necessary, laser trackers will be used which provide alignment precision to ~ 50 microns.

1.4.2.2 Utility Layouts

We will need power panels for single phase 100V and 200V rated to 100Amp each, and 3 phase 200V to 300Amp, distributed to the hutches and control areas. For each hutch, there should be de-ionized and chilled

water, compressed air, N2 and He gas distribution system. For the FOE LN2 outlet is required for the cryogenic cooling system of the DCM. The two experimental hutches will require temperature control to ±0.1 K.)

1.4.2.4 Beamline Vacuum System

The beamline vacuum will be separated from the front-end by a Be window. All beamline components will be designed to ultrahigh vacuum (UHV) standards. The beamline will be operated in most part in high vacuum level. Turbo pumps backed up by oil-free roughing pumps will be used for the pumping stations. High vacuum will be maintained by ion pumps where necessary (for concerns of vibration, for example). A rough vacuum pumping system is planned for each of the endstations for use in pumping sample chambers, flight paths, etc.

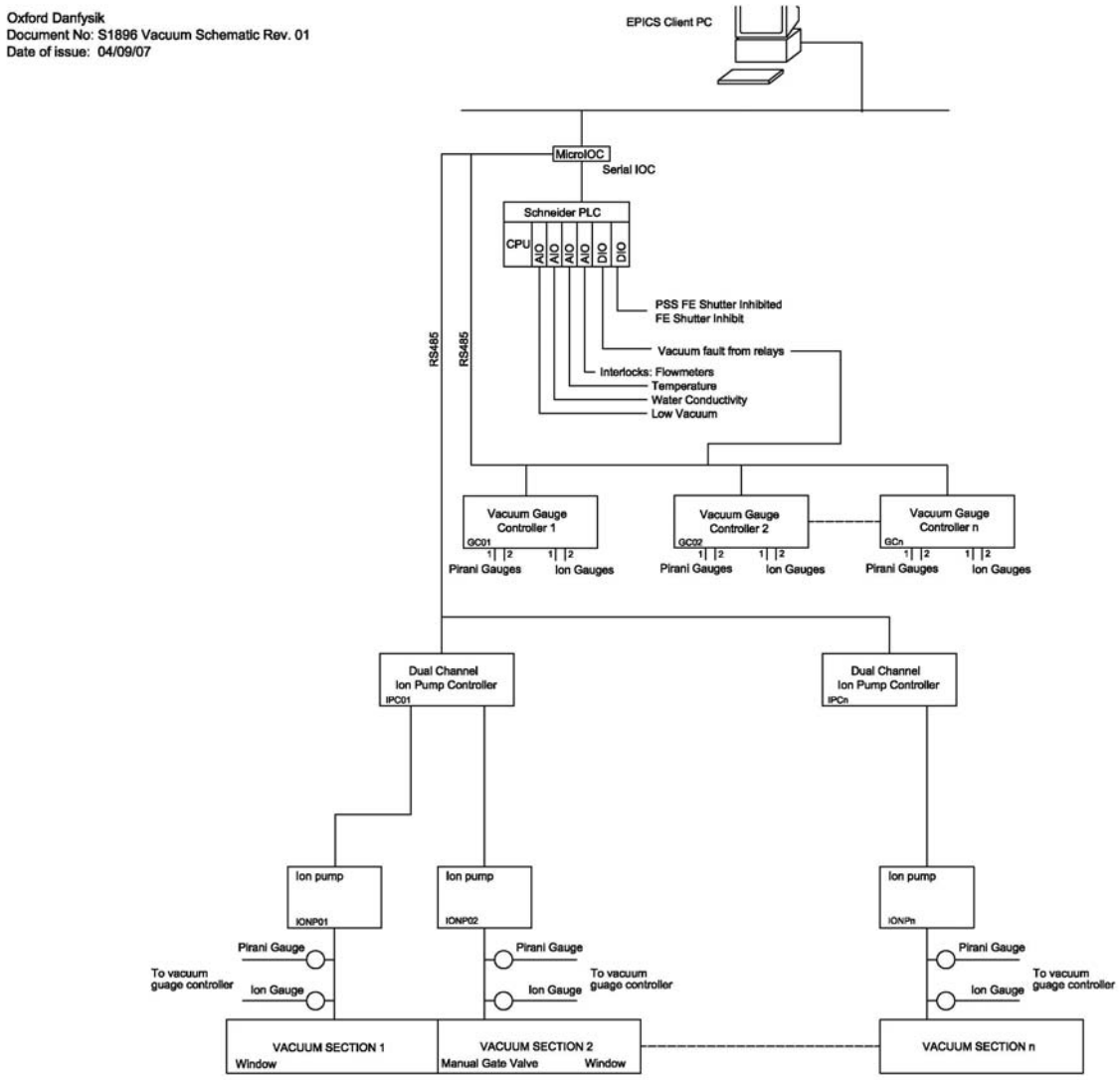

Figure 1.5. Vacuum schematic for the inelastic x-ray scattering beamline.

Figure 1.5 provides a schematic of the vacuum system for the IXS beamline. Vacuum gauge controllers are used to monitoring vacuum level measured by Pirani and ion gauges mounted on different beamline components.

Ion pump controllers provide power to each of the ion pumps used on the beamline. High-voltage splitter units are used, where necessary, to power more than one pump per output channel.

1.4.2.5 Data Acquisition System and Motion Control

The contents of the signal schematics are shown in Table 1.5. The 8-axis motion control boxes having RS232, USB, and Ethernet interfaces are customized to suit the beamline motorized axis. They also have built-in micro IOCs. Separate micro IOCs control the vacuum pump controllers, vacuum gauge controllers, DPT controllers, current amplifiers, and CCD cameras.

The EPS PLC has analog input and digital input and output, and is linked to solenoid valve actuators, fluorescent screen actuators limits, thermocouples, water flow meters, vacuum interlocks, vacuum gauge controllers, cooling water flow meters in the heat exchangers, thermocouples in the heat exchangers, and water conductivity probes.

The PSS shutter is controlled from the PSS and sends and receives status signals to and from the EPS PLC.

The micro IOC controlling the vacuum system uses RS485 protocol for communication with the pump and gauge controllers. Vacuum gauge controllers are integrated with the EPS system to monitor vacuum level in different sections of the beamline.

Piezo actuators and a bimorph mirror will need vacuum interlocks linked to the vacuum gauge controllers. The cryocooler is connected via Ethernet to a dedicated IOC, which is linked to the PSS. The Y-Z profile monitor is connected to a 32-channel electrometer.

Table 1.5. Controls schematics for the IXS beamline.

Beamline Component	No. of units	Number of Elements per Unit											
		Controlled by 8 axis Motion Control units					Controlled by EPS PLC			Controlled by micro IOC			PC
		Stepper/ Pico Motor	Server Motor	Limit/ datum switch	Encoder	Ref point	Flow meter	Thermo-couple	Solenoid valve actuator.	CCD camera	DP control unit	Current amplifier	
Beamline control system	1												1
Fixed mask	1						1	1					
Blade BPM	1	2		4			1					1	
CVD Diamond	1						1	1					
Bremsstrahlung collimator	1						1	1					
White Beam Slit (H **or** V)	2	1		2	1								
Gate Valve	16			2					1				
VFM/VCM	2	5		10	5	5					1		
HFM (bimorph)	1	5		10	5	5							
Bimorph PSU	1												
Beam shutter	3			4				1	1				
Fluorescent screen (water cooled)	1			2			1		1	1			
Fluorescent screen	5			2					1				
DCM	1	5	1	8	7	6	1	3			1		
Cryocooler	1												1
White beam / bremsstrahlung stop	1						1	1					
QBPM	5	1		2								1	
Y-Z profile monitor	1								1				
Monochromatic slits	10	2		4	2	2							

1.4.3 Beamline Components

Table 1.C.1 (see Appendix C) lists the position and size of different beamline components of the current design. Space between the main components will be filled with vacuum bellows and pipes of suitable length. The table also lists different sections of the beamline vacuum system. Positions of the beamline components are specified with respect to the center of the low-β straight section, which was used in the initial stage of the design study. It assumes the distance from the source to the external surface of the shield wall to be at 26.7m, and the distance to the end of the beamline at 66.8m.

The decision to use a high-β straight section will change the shield wall position to 28.6m, and therefore all components listed in Table 1.C.1 will need to be shifted downstream by 1.9m.

Important dimensional constraints for the high-β straight section are as follows:

- Distance from the source to the external surface of the shield wall: 28.6 m
- Maximum source to end of the beamline distance: 60.8 m

Several important considerations have been taken into account in the suggested layout of the main beamline components, which include:

- Share as many common endstation components as possible, to reduce the total cost of the project and complexity of the design.
- Reduce to a minimum the number of optical elements (crystals, mirrors, windows, etc.) put into the beam, to maximize the flux.
- Use most of the available fan of the x-ray beam, to keep the lengths of the optical elements within reasonable limits.
- Create an infrastructure and basis for further R&D that will follow the preliminary design.
- Provide enough flexibility for further beamline design based on the outcome of anticipated extensive R&D.
- For costs to be estimated realistically, include in the early design not just the main components, but all components that are not likely to be affected by further design changes.
- Fit the beamline components into the available floor space and identify any changes to the position of the walls needed to accommodate the equipment.

1.4.3.1 White Beam Slits

The white beam slits, currently planned as part of the FOE components, define the X-ray beam from the undulator source to the first optics of the beamline. If the X-Y slits are to be implemented in the front-end, this white beam slits may no longer be required.

Figure 1.6 shows the position of the white beam slits upstream of the high heatload monochromator. The slits consist of 2 L-shaped absorbers arranged in series along the beam (the downstream one being rotated by 180°) to define the aperture. Each absorber therefore defines two edges of the beam. Each absorber is moved laterally and vertically by external translation stages. There are edge-welded bellows before, between and after the two absorbers, which allow the movement of the slits relative to the beam. The slit mechanism is mounted on a synthetic granite-filled mild steel frame for stability and vibration rejection.

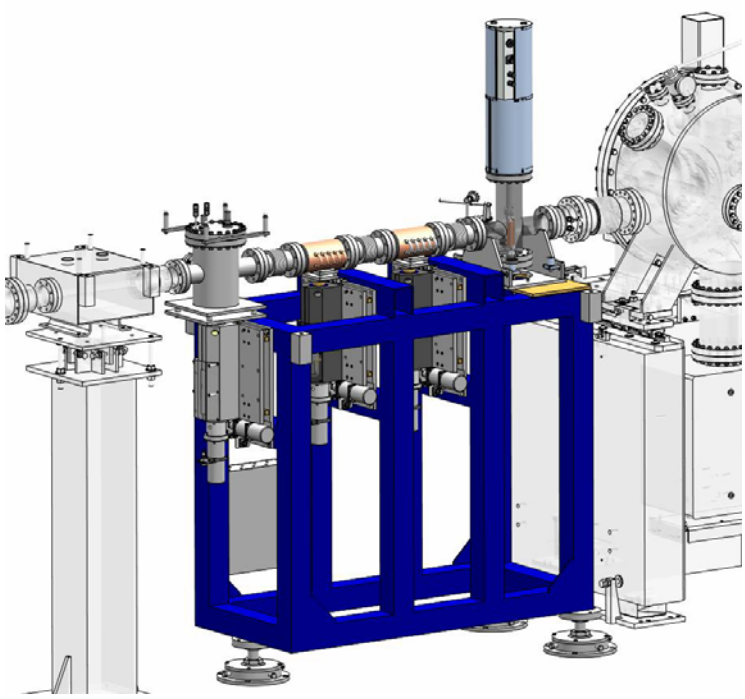

Figure 1.6. White beam slits assembly.

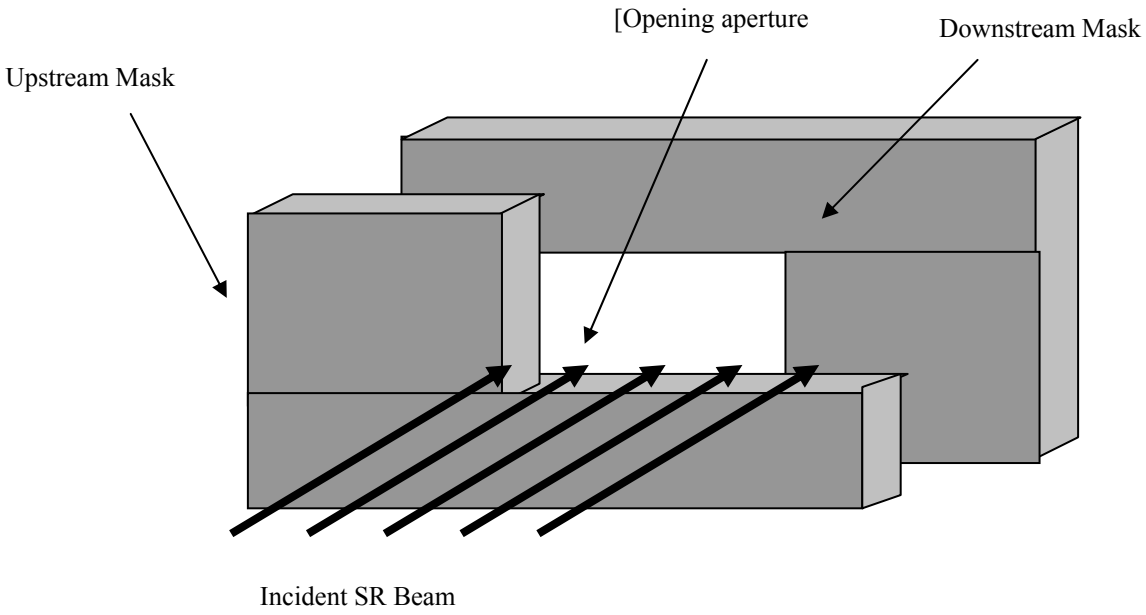

Figure 1.7. White beam slits schematic.

1.4.3.2 Bremsstrahlung Collimator and Beam Stops

The Bremsstrahlung collimators are typically made of 300 mm of lead and their dimensions are calculated from the ray tracing. We will use one of the collimators immediately after the CVD Diamond window/filter.

The Bremsstrahlung collimator is located immediately downstream the fixed mask defining the beam.

A Bremsstrahlung stop is also anticipated after the DCM. Depending on the detailed design it will be made of lead (out of vacuum) or Tungsten (in vacuum).

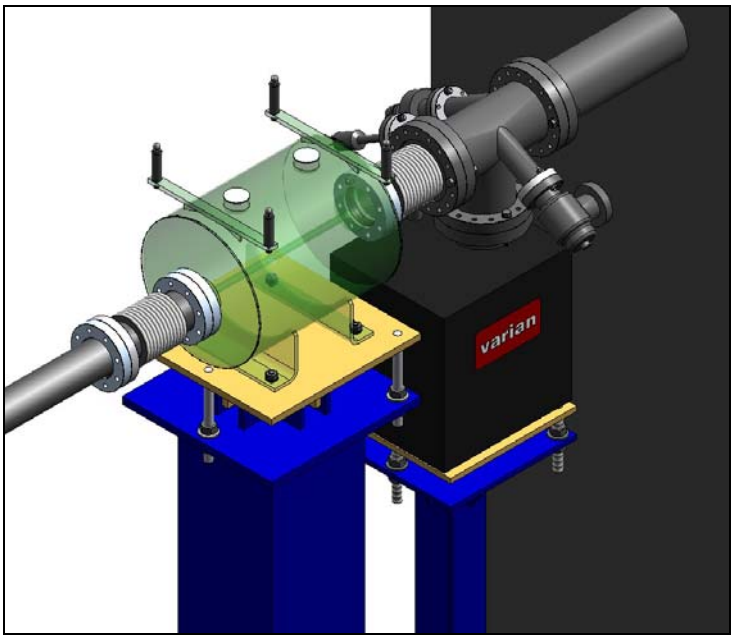

Figure 1.8. Pb collimating assembly.

1.4.3.3 High-Heatload Monochromator

A cryo-cooled Si(111) DCM with no sagittal focusing on the second crystal should provide energy resolution of ~10^{-4}, fixed exit beam height and operate across the requested energy range from 7 keV to 12 keV. Expected performance parameters of the DCM and some useful information are given in Table 1.6. We also assume 25 mm vertical offset between the incoming and outgoing beams and that beam 'walk' alone the second crystal as the energy changes will be taken by longitudinal translation of the crystal.

The results in show that

- The energy resolution is expected to be from $1.77 \cdot 10^{-4}$ to $2.45 \cdot 10^{-4}$.
- The Bragg angles are from 9.5° to 16.4°. The Bragg angle calculation assumes the lattice constant of Si(111) of 5.4309 Å.
- Perpendicular translation of the 2nd crystal over the energy range is about 0.3 mm.
- Longitudinal translation of the 2nd crystal over the energy range is approximately 32 mm.

- The footprint of the beam at the crystals of the Si(111) monochromator at all energies is less than 3.0 mm x 5.5 mm assuming 4σ (H) x 6σ (V) opening of the beam. Vertical size of the beam at the DCM position is about 1.0 mm.
- The lengths of monochromator crystals should be less than 177 mm to avoid shadowing.

The design of the DCM should meet stability requirements and be able to withstand high heat loads as discussed earlier.

It might be possible to use a water cooled DCM but more R&D is needed to prove this is a feasible. We therefore have provided a typical specification for a water cooled monochromator. The BNL water cooled system will most likely use much smaller vertical beam offset, of about 25 mm, than in the example and long second crystal to eliminate longitudinal translation and improve stability. The second crystal will be translated vertically to keep fixed offset of the beam.

The power density could however be very high, particularly when two U19 undulators will be used simultaneously in-line and at the same undulator gap as we have discussed earlier. We therefore believe that most likely a cryogenically cooled system will be needed. We therefore provide an appropriate functional specification for such a system which is being built for ASP SAXS beamline. The DCM is designed to operate at energies of 5-20 keV, has a fixed offset of 25 mm and uses a set of Si(111) crystals. The DCM is designed to achieve angular beam stability of 200 μrad that should be adequate for the current application. As the technology continuously improves using a cryogenically cooled monochromator instead of water cooled one does not create any unnecessary risk for the project.

Modifications to the standard design that should be considered include reducing the beam offset and using long high quality second crystal instead of longitudinal translation to improve stability.

Table 1.6. Performance parameters of the Si(111) DCM.

Parameters	Energy, keV		
	7	**9.1**	12
Wavelength, Å	1.7712	1.3625	1.0332
Bragg angle θ_B, deg	16.4058	12.5482	9.483
Reflectivity (double reflection)	0.85	0.91	0.94
Energy resolution			
Rocking (Darwin) width[1], μrad	39.1586	29.6027	22.2161
Bandpass due to source size	9.2×10^{-7}	1.2×10^{-6}	1.6×10^{-6}
Bandpass due to accepted angular divergence	1.2×10^{-4}	1.5×10^{-4}	2.1×10^{-4}
Resolution of the DCM	1.77×10^{-4}	2.04×10^{-4}	2.45×10^{-4}
Resolving power[2]	5649	4904	4079
Crystal size and position			
Vertical offset between incoming and outgoing beams, *D*, mm		25	
Perpendicular offset between 1st and 2nd crystals[3], mm	13.0	12.8	12.7
Longitudinal offset between the crystals[4], mm	44.3	57.5	75.9
Maximum beam footprint[5]			
transverse to the beam, mm	3.0		
along the beam, mm			6.2
Maximum length of crystals at no beam shadowing[6], mm	177		

Notes: 1) Intrinsic resolution of Si(111) is $\left(\frac{\delta\lambda}{\lambda}\right)_{cryst.}$ = 1.33 · 10^{-4} [30]. The rocking (Darwin) width is $\Omega = \frac{\delta\lambda}{\lambda}\tan\theta_B$.

2) The resolution is determined by the width of the rocking curve of the crystal, beam opening angle and size of the source

$$\frac{\Delta E}{E} = \sqrt{(\Delta\theta^2_{source} + \Delta\theta^2_{slit})\cot^2\theta_B + \left(\frac{\delta\lambda}{\lambda}\right)^2_{cryst.}},$$

$$\Delta\theta_{source} = \sigma_y / p \text{ and } \Delta\theta_{slit} = \min(\sigma_y^{'}, s_v)/p,$$

where σ_y is the vertical source size (FWHM), $\sigma_y^{'}$ is the vertical divergence of the beam (6 σ), s_v is the opening of the monochromator vertical entrance slit and *p* is a distance from the source.

Resolving power of the monochromator is reverse to the total band pass, i.e. it is $\frac{E}{\Delta E}$.

3) The distance, X, measured perpendicular to the optical surfaces of the crystals: $X = \frac{D}{2\sin\theta_B}$, where D is the constant vertical offset between incoming and outgoing beams.

4) The distance, Y, measured along the surface of the crystals: $Y = \frac{D}{2\cos\theta}$, where D is the constant vertical offset between incoming and outgoing beams. The longitudinal offset shows beam walk parallel to the surface of the crystals as the Bragg angle changes. To maintain the constant beam offset, D, the X and Y should satisfy the condition $\frac{1}{X^2} + \frac{1}{Y^2} = \frac{4}{D^2}$.

5) The beam footprint depends on the rms size and divergence of the incoming beam, DCM distance from the source and the Bragg angle so that

$$F = \sqrt{\sigma^2_{x,y} + (\sigma^{'}_{x,y}\cdot p)^2};\ F_x = F;\ F_y = F/\sin\theta,$$

where $\sigma_{x,y}$ and $\sigma^{'}_{x,y}$ are the size and divergence of the source, correspondingly, p is the distance from the source and θ is the Bragg angle.

6) To avoid shadowing of the beam at high Bragg angles, the lengths of the crystals should match the vertical beam offset.

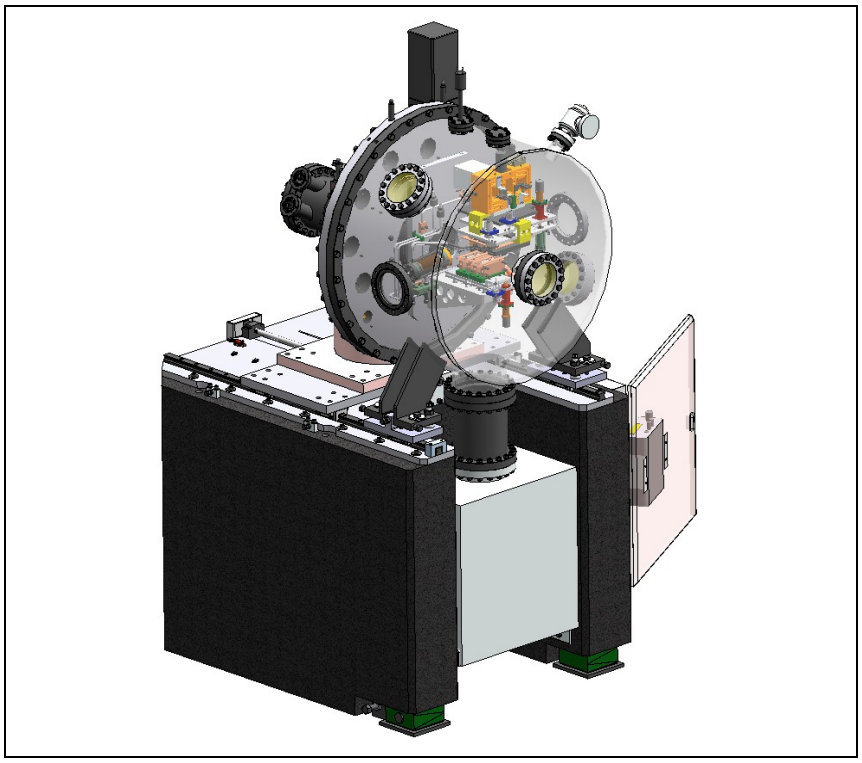

Figure 1.9. Isometric view of the Si(111) DCM.

1.4.3.4 White Beam Shutter

Special requirement for the beam shutters and their integration with the Personnel Protection System will be discussed with the vendor before the detailed design starts.

1.4.3.5 Collimating and Focusing Mirrors

As it has been discussed earlier, the beam line is expected to have few mirrors for collimating and focusing the beam in horizontal and vertical planes. Preliminary analysis shows that full energy range of 7 -12 keV can be covered without changing the angle of incidence while providing good transmission of the x-ray beam over the whole range.

Increase of the angle of incidence is favorable for reducing the cut-off energy, lengths of the mirrors and improving harmonic rejection, but the reflectivity of the mirrors decreases. We have considered using bare Si, Silica (SiO_2, less expensive option and good alternative to Si for using with monochromatic beams) and Pt, Pd and Rh coatings and concluded that Rh and bare Si or Silica are most suitable for the energy range. Pd is very similar to Rh but the latter has slightly better reflectivity. Reflectivity of Pt shows few absorption edges and it is more suitable for higher energies.

Most mirror suppliers will guarantee densities of Rh in the coatings to be better than 90% of the bulk material which is 12.41 g/cm^3 [28]. We therefore assume in this analysis the density of Rh of 11.17 g/cm^3 for calculating reflectivity of the mirror stripes. The densities are usually lower, about 85% of the bulk, for bimorph mirrors. The lower density means slightly lower reflectivity and lower cut-off energies at similar angles of incidence. The data in Figure 1.10 show that replacing Silica with Silicon as a mirror substrate increases the cut-off energy by approximately 300 eV. As the density of Rhodium decreases from 90% to 85%, the cut-off energy decreases by about 550 eV.

The density of Si, 2.33 g/cm^3 [28], is slightly higher than the density of Silica, 2.2 g/cm^3 [29]. Usually Silica is used as a substrate for making mirrors to focus monochromatic beam and silicon is used to make mirrors operating in a white beam.

Figure 1.10 shows variation of the critical angle of the mirrors versus energy for Si, Silica, Rh (and Pt). The critical angles were calculated as $\alpha_c = \sqrt{2\delta}$, where δ is a real part of the refractive index of material. Incidence angle of the mirrors should ensure that the low energy beam is not contaminated by the beam of higher energy. Also it is not desirable to make mirrors much longer than 1 m. But the reflectivity of the mirrors decreases as the angle of incidence increases. Therefore the incidence angle should be optimized taking into account these factors and ease of use.

Useful energy range is defined from 7 keV to 12 keV [2] and from the point of view of ease of use changing the mirror stripe in this region should be avoided. In that case the mirrors could be set at an incidence angle of approximately 4.5 mrad to achieve about 87-89.5% reflectivity using Rh stripe. Higher reflectivity can be obtained using Si or Silica stripe. Reflectivity of Silica, for example, at 3 mrad incidence at 7 – 9.5 keV is about 95 - 96.5%. But to cover the whole energy range of 7 – 12 keV the incidence angle should be much smaller, 2.5 mrad.

We therefore suggest operating in one of the three regimes:

- Use Rh stripe and incidence angle of 4.5 mrad.
- Use Rh stripe and incidence angle of 4.5 mrad at energies from 9.5 to 12 keV and Silica stripe and incidence angle of 3.0 mrad at energies from 7 to 9.5 keV.
- Use Use Rh stripe and incidence angle of 4.5 mrad for HCM and HFM and Silica stripe and incidence angle of 3.0 mrad for VCM and VFM.

The last option is probably a good compromise between reflectivity and ease of use. Figure 1.11 shows calculated reflectivity of bare Silica and Rh stripes.

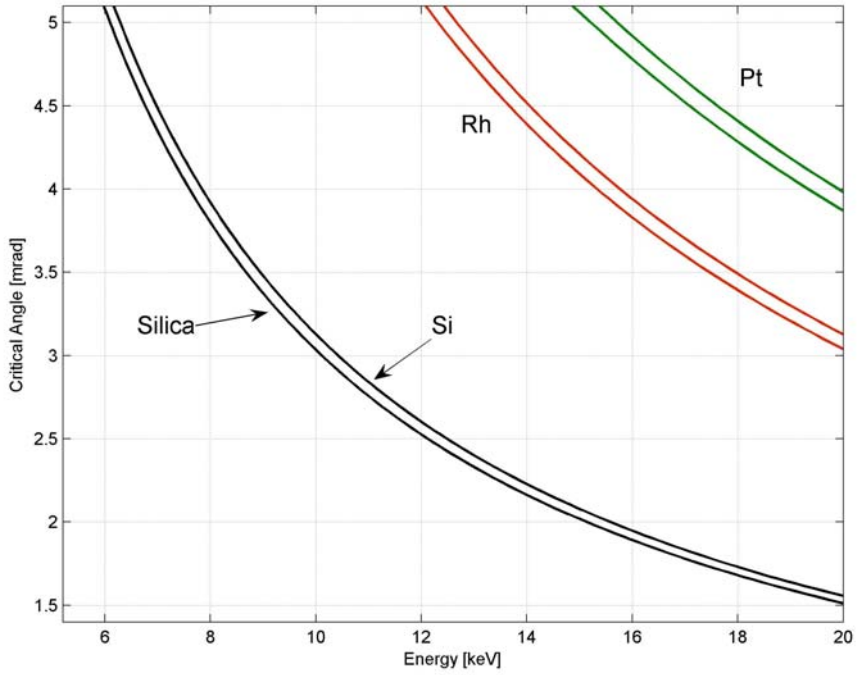

Figure 1.10 Variation of the critical thickness versus energy for bare Silica, Silicon, Rhodium and Platinum. The double lines for Rh and Pt correspond to different densities of the materials: 85% density of the bulk for the lower line and 90% for the upper line.

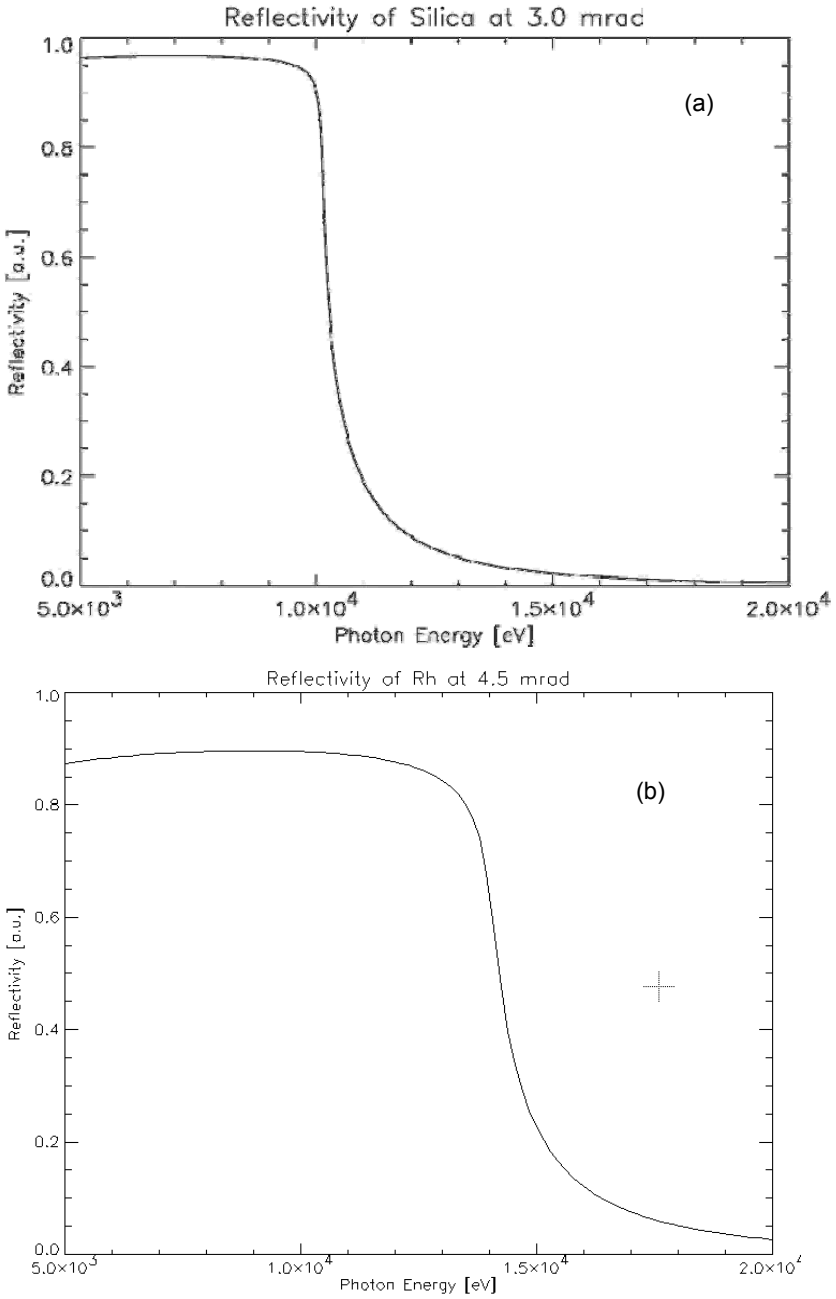

Figure 1.11 Reflectivity of Silica at 3.0 mrad (a) and Rhodium at 4.5 mrad (b)

We assume the HFM and VFM will be bent to a cylindrical shape. The lengths of the mirrors can then be calculated using the expressions given by Peatman [19]:

$$L = P\sin\left(\frac{\alpha}{2}\right)\left(\frac{1}{\sin(\theta_i + \frac{\alpha}{2})} + \frac{1}{\sin(\theta_i - \frac{\alpha}{2})}\right)$$

$$L \approx \frac{2P\sin\left(\frac{\alpha}{2}\right)}{\sin\theta_i}$$

where L is the length of the footprint of the beam on a mirror, P is a source-to-mirror distance, α is the vertical divergence of the beam and θ_i is the grazing angle of incidence of the mirror.

Estimated radii of the mirrors and some other useful characteristics are shown in Table 1.7 for the worse case in terms of beam angular divergence which is at low beta straight and ε_x =0.9 nm-rad. The VCM should have angular acceptance of 10 mrad (H) x 5 mrad (V). We have therefore increased the incidence angle to 5 mrad for that mirror to reduce its length. The cut-off energy of Rhodium at this angle will be 12.6 keV and reflectivity up to 88%. The length of the mirror depends on the amount of space required for the sample area. More accurate values of the parameters will be given after completing ray tracing analysis.

The lengths of the mirrors, particularly of the HCM and HFM ones, will decrease dramatically if the source parameters change. At ε_x =0.55 nm-rad in low beta straight the length will be 670 mm and in a high beta straight it will further decrease to 288 mm at ε_x =0.9 nm-rad and to 247 mm at ε_x =0.55 nm-rad.

Table 1.7 Parameters of the mirrors. Incident beam has angular divergence of 100 μrad (H) x 22.8 μrad (V). The *p* and *q* are source-to-mirror and mirror-to-image distances.

Mirror	Optical distance from source, m	Inci-dence angle, mrad	Coating	Beam Footprint, mm		Bent radius, m	*P*, m	*Q*, m
				Horizontal	Vertical			
VCM	31.88	2.5	Silica	3.2	291	25220	31.88	∞
VFM	39.15	2.5	Silica	3.8	291	336	- ∞	0.42
VCM[1]	40.33	5	Rh	7.6	1014	338	0.76	∞
VFM	74.46	2.5	Silica	3.8	291	516	- ∞	0.645
HFM	38.05	4.5	Rh	846	0.9	650	38.05	1.52
HCM	38.05	4.5	Rh	846	0.9	16911	38.05	∞
HFM	73.36	4.5	Rh	846	0.9	776	- ∞	1.745

Notes: 1) Footprint of the beam at VCM corresponds to angular acceptance of 10 mrad (H) and 5 mrad (V). To increase angular acceptance the VCM has Rh coating and higher angle of incidence.

The KB mirror system will include a bimorph horizontally focusing mirror and a conventional vertically focusing mirror equipped with a cylindrical bender. The bimorph mirror allows changing focus between the sample positions at the first and second endstations and reduces slope errors.

One vertically collimating (VCM) and one vertically focusing mirror will be used in monochromatic beam only. The VCM mirror systems will have capability of removing the optics from the beam delivered to the second, low-resolution, endstation using a backscattering monochromator.

The quality of the optical surface that can be achieved is being continuously improved by mirror manufacturers. We expect this trend will make it possible to purchase much better mirrors in few years time compared to those currently available on the market.

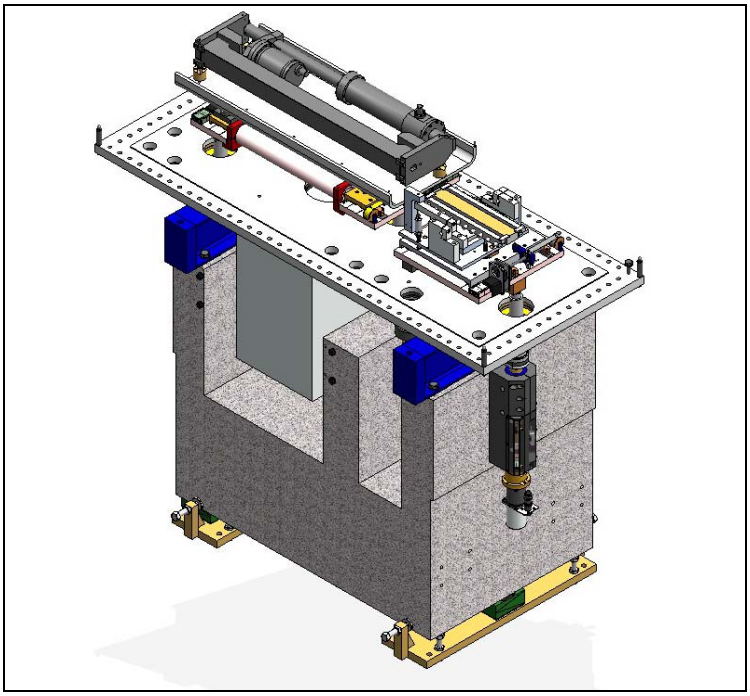

Figure 1.10. KB mirror assembly.

1.4.3.6 Monochromatic Shutter

Special requirement for the beam shutters and their integration with the Personnel Protection System will be discussed with the vendor before the detailed design starts.

1.4.3.7 Vacuum windows

Table 1.6 SiN 200nm window.

Supplier	SPI supplies
Outside frame dimensions	7.5mm x 7.5mm
Window size	1.5 mm x 1.5 mm
Membrane thickness	200 nm
Frame thickness	200 µm
Quantity	Pack of 50

1.4.4 Instruments

1.4.4.1 Endstation 1

End station 1 will have energy resolution of 0.1 meV at 9.1 keV [1]. The resolution will be achieved using novel design of high-resolution monochromator and analyzer optics exploiting an effect of angular dispersion in asymmetric Bragg diffraction predicted by dynamic theory of x-ray diffraction.

Design of the monochromator and analyzer is still subject to a debate. Significant design work and testing is required before the final working configuration becomes available. As it stays now a monochromator using this scheme consists of few Silicon crystals: a collimator, one or two dispersing elements and a wavelength selector. An inline configuration of the monochromator is preferable and the collimator and the wavelength selector could be just different sides of the same crystal, see Figure 11.5.4 in section 11.5.2.3.2 of reference [1]. To achieve a 0.1 meV energy band pass a very large asymmetry angle, of about 89.5^{o}, is required for the dispersing crystals.

The monochromator and the analyser will have an angular acceptance of 0.2-0.3 mrad in the horizontal scattering plane and 0.1 mrad in the vertical plane.

The spot size on the sample should not exceed 20-30 μm (H) x 10 μm (V). This requires a (micro) focused beam on the sample that can be achieved using a standard focusing system. The mirror to sample distance is likely to be of about 100 mm. The minimum distance is to provide some space for the sample environment.
An angular dispersive analyser similar to the monochromator will reflect the beam back to the detector. The backscattering analyser is chosen to reduce the total length of the beam line. An acceptance angle of Y^2 with Y~ 5 to 10 mrad is required. Therefore some collimating optics is needed in front of the analyser. As the asymmetry angle is large an angular acceptance of 2 to 3 mrad in the vertical plane translates into about 2 m long dispersive element length [1].

There will be a Kirkpatrick-Baez (KB) mirror system [2] with graded multilayer mirrors. This is preferred to a parabolic, or curved graded multilayer mirrors or tapered glass capillaries discussed in section 11.5.2.3 of reference [1]. The mirrors will be put after the sample but before the analyser. X-rays leaving the mirror system should match the angular acceptance of the analyser given above. Also the vertical beam size should not exceed 0.5 to 1.0 mm to restrict the length of the analyser crystals.

The spectrometer will be utilising 9.1 keV x-rays and providing an energy resolution of 0.1 meV and a momentum transfer resolution of about 0.1 – 0.4 nm^{-1}.
The energy of the photons selected by the spectrometer will be tuned by varying the temperature of the crystals. Temperature of individual segments of the segmented analyser (consisting of 8 to 10 segments 20-25 cm long) should be homogeneous to 0.5 mK corresponding to 0.01 meV energy shift [1].

1.4.4.2 Endstation 2

The vendor has considered several options for separating the beam used by the endstations. As there is significant uncertainty in the specification of the low-resolution endstation, they started by summarizing designs of the existing beamlines built at ESRF (ID28, ID16) [10,11], SPring-8 (BL35XU, BL11XU) [12-14], and ASP (3 IDC-C, IXS-CDT) [15,16] facilities. In every case there are some collimating optics in front of a high-resolution monochromator (HRM), particularly in a vertical plane. A logical conclusion is that, irrespective of the chosen monochromating scheme based on one of the known configurations of achieving high (meV) energy resolution [17-20], there will be some need for collimating the beam passing after the high

heat load monochromator and before a HRM. Therefore, we can try to use most of the optics from Endstation I at the Endstation II. That should be cost effective and allow saving some space at the second endstation.

It would be ideal to separate the beam going to Endstation II after the DCM, VCM, and HRM of Endstation I. It is unlikely, however, that the HFM can also be used as a HCM for the second endstation, as it needs to be curved to a certain radius during manufacturing. Hence the options are:

1. Design a HRM that will be flexible enough for using at both endstations. This is a risky approach, as it is unclear at present how the monochromator for Endstation II should look and if it is feasible to combine both monochromators into a single unit. To be on a safe side and keep all options open, we should assume that a completely different HRM will be designed for Endstation II. We can safely assume, however, that the HRM at Endstation I could be made capable of passing the beam straight through.
2. The HFM vessel could be used to accommodate a second mirror, the HCM, for collimating the beam at Endstation II. This option looks attractive, but some information on the design of the prospective sample area at Endstation II is needed to ensure there are no serious restrictions for pursuing this approach. It will be necessary to make specially designed gate valves with built-in windows to separate vacuum sections of the beamline so the beam is not attenuated by numerous vacuum windows before reaching the second endstation.
3. Insert a HCM for Endstation II after the high-heatload monochromator. An advantage is that a shorter HCM is needed, but it is difficult to find extra ~1.5 m space within the constraints on the position of the hatch walls. If the HCM is used for Endstation I, the HFM should have a similar length. The disadvantage of using an intermediate mirror is that about 10% of flux will be lost due to reflectivity and slope errors.
4. One option is to offset the beam horizontally using two silicon crystals, but this possibility was eliminated because of spare restrictions.
5. Offset the beam vertically using an additional vertical mirror.
6. Replace a CVD diamond window/filter with a Laue monochromator to create large angular offset between the beam paths to the endstations.

Whichever option, 2, 3 or 5, is selected, provision should be made to allow the second beam to reach Endstation II. The further upstream the mirror is, the more difficult it is to separate the beams. It might be necessary to provide translations or larger apertures to different components until the beams become sufficiently well separated. The vendor suggests implementing option 2 by putting two mirrors facing each other into a single vessel. In that case, the beam path to the second endstation becomes separated by distance x incidence angle x 4 horizontally at the HFM position and by distance x incidence angle x 2 vertically at the VFM position.

To provide enough flexibility for future developments the beamline components should be suitable for operating at energies of 7 – 12 keV. For this energy range, the most suitable mirror coating is probably Rhodium and an optimum incidence angle for the mirrors is 4.5 mrad. At low energies silicon is preferable, but a smaller (about 2.5 mrad) incidence angle is required to cover the entire energy range, and at 2.5 mrad the mirrors become too long; a good compromise is to operate at 3.0 – 3.1 mrad incidence. We would recommend using a bare silicon stripe at energies below approximately 9.0 – 9.5 keV to get about 5% higher reflectivity. As an option, the silicon stripe can be used for shorter, VCM and VFM mirrors. The diagonal offset of the beam at 4.5 mrad (assuming a Rh-coated mirror) will be approximately 20 mm per 1 m distance.

We do not know yet which configuration will be chosen for Endstation II. The options being considered include new asymmetric optics similar to Endstation I or a conventional single-bounce backscattering monochromator and a backscattering analyzer utilizing sapphire or quartz. The disadvantage of the former (or the one suggested by Baron [19]) is due to flux losses at crystals used simultaneously in Bragg reflection and transmission. The latter option appears to offer more diversity for the beamline, and there is a good chance that sufficient progress will be made over the next few years in growing high quality crystals of quartz and/or

sapphire. It sounds reasonable to use scattering in the horizontal plane as suggested in reference [1]. A proposed layout for Endstation II is listed in Table 1.C.1, but it must be noted that the layout may be subject to a major revision if the endstation is to be built on different principles.

Therefore the design of Endstation II may be similar to the recently built beamline BL35XU [13]. The points for consideration and approval include the following:

- Possible use of a pair of Si(111) crystals to shift the backscattered beam vertically by a convenient amount to separate the scattered and incident beams which are otherwise nearly parallel due to backscattering at an angle close to 90^o
- Possible need for vertical scattering analyzer
- More floor space is desirable

1.5 Additional Requirements Imposed on the Conventional Facilities

Temperature Stability

Stability requirements are determined by temperature stability and vibration (natural and self-inflicting), and were extensively discussed at the recent NSLS-II Stability Workshop in April 2007.

The beam stability requirements for different components are based on achieving less than 10% variation of the beam size. According to Shvyd'ko [22], 0.1 meV energy resolution requires <1K temperature stability inside the station. To keep broadening of the reflected beam lower than 10%, temperature variations along the dispersing elements should be within 2 mK [22].

Typical temperature variations measured at ESRF are about 0.5^o [24]. Therefore, 1K temperature stability can be achieved. For demanding beamlines, new high-flow air conditioning units (air renewal rate 20 cycles/hour) are used. Vibrations from air flow are reduced using porous ducts [23]. At the ID22 beamline at ESRF, temperature variations are $< 0.1^o$ over 24 hours [24].

Construction/conventional design measures that reduce thermal effects include choosing low-expansion materials, cooling local heat sources, thermally insulating vessels, moving all control electronics outside the hutches [24], using thermally insulated sand-filled stands, and striving for high thermal inertia [24].

1.6 Additional Requirements Imposed on the Accelerator Systems

Beam Stability

As stated above, stability requirements are determined by temperature stability and vibration (natural and self-inflicting). In terms of beam stability, the requirements for different components are based on achieving less than 10% variation of the beam size.

In addition to the temperature control measures discussed above, Shvyd'ko reports [22] that 0.1 meV energy resolution requires 0.25 μrad incident beam direction stability in the vertical plane and 0.25 μrad relative angular stability of the monochromator and analyzer single-crystal components. A similar requirement for beam stability better than 0.01 meV that would require stability of the incident beam direction (beam angle) better than 0.250 μrad is given in report [23] and its most recent updates [2]. Horizontal angle stability should be 10% of the opening angle. Horizontal and vertical position stability should be 10% of the beam size. It has been pointed out that angular vibration drifts are much worse than linear [24]. This is particularly true for long beamlines like IXS.

References [to be completed]

1-A Appendix A: Ray Tracing Using XOP and Shadow

The vendor conducted ray tracing of the beamline at 9.1 keV using the XOP and Shadow packages to analyze a combined effect of surface distortion of the first crystal of the DCM on beam size and flux at the first sample position. The assumed positions of the optical elements, DCM, VCM, HFM, and VFM, are as given in Table 1.C.1 (Appendix C). The results of the FEA analyses for several of the most important cases are given in Table 1.A.1 below and in Figures 1.A.1 and 1.A.2. Cases 2 and 4 are highlighted in the table, as the beamline is most likely to be used in a high-beta regime.

Table 1.A.1 Results of ray tracing analysis at different heat loads at first crystal of the high-heatload monochromator at 9.1 keV.

Case No.	Model (1xU19, 2xU19)	Spot size at no crystal distortion, μm	Flux at no crystal distortion, ph/s	Spot size, μm	Flux, ph/s
1	Low beta, 0.55 nm-rad, K=0.981, 1xU19, Power = 22 W	2.0 x 1.8	1.50×10^{13}	2.1 x 2.1	1.49×10^{13}
2	High beta, 0.55 nm-rad, K=0.981, 1xU19, Power= 7 W	7.0 x 1.8	1.49×10^{13}	7.0 x 2.0	1.49×10^{13}
2a	As above, but water cooled Si crystal	7.0 x 1.8	1.49×10^{13}	16 x 7.4	1.51×10^{13}
3	Low beta, 0.55 nm-rad, K=1.714, 1xU19, Power = 71 W	2.0 x 1.9	2.88×10^{13}	2.3 x 4.2	2.81×10^{13}
3a	As case 3, but base temperature is 105K to get the hot spot of the crystal at 125 K			2.1 x 0.5	2.92×10^{13}
3b	As case 3, but 2xU19, 115 W	2.0 x 2.0	5.80×10^{13}	2.9 x 5.9	5.14×10^{13}
4	High beta, 0.55 nm-rad, K=1.714, 1xU19, Power = 22 W	7.1 x 1.9	2.81×10^{13}	7.0 x 3.4	2.79×10^{13}
5	Low beta, 0.9 nm-rad, K=1.714, 2xU19, 148 W.	2.6 x 2.0	5.82×10^{13}	3.3 x 5.7	4.68×10^{13}

Corresponding heat loads are given in Table 3.4. Flux at the sample position was calculated over a 20 μm x 20 μm aperture. Mirrors were assumed to be elliptically bent, to show better spot size. The number of rays was converted into flux using the expression

$$\text{Flux[ph/s]} = \frac{\text{N}_\text{T}}{\text{N}_\text{i}} \frac{\Delta E\ [eV]}{E\ [\text{keV}]} I_0\ [\text{ph/s}],$$

where NT is the number of rays transmitted through the optical system, Ni is the number of incoming rays corresponding to the incident flux I0, $\Delta E=3eV$ is the bandwidth over which the ray tracing was performed, and E is the energy of photons in the middle of the bandwidth. The incident flux was calculated using the XUS program from the XOP package.

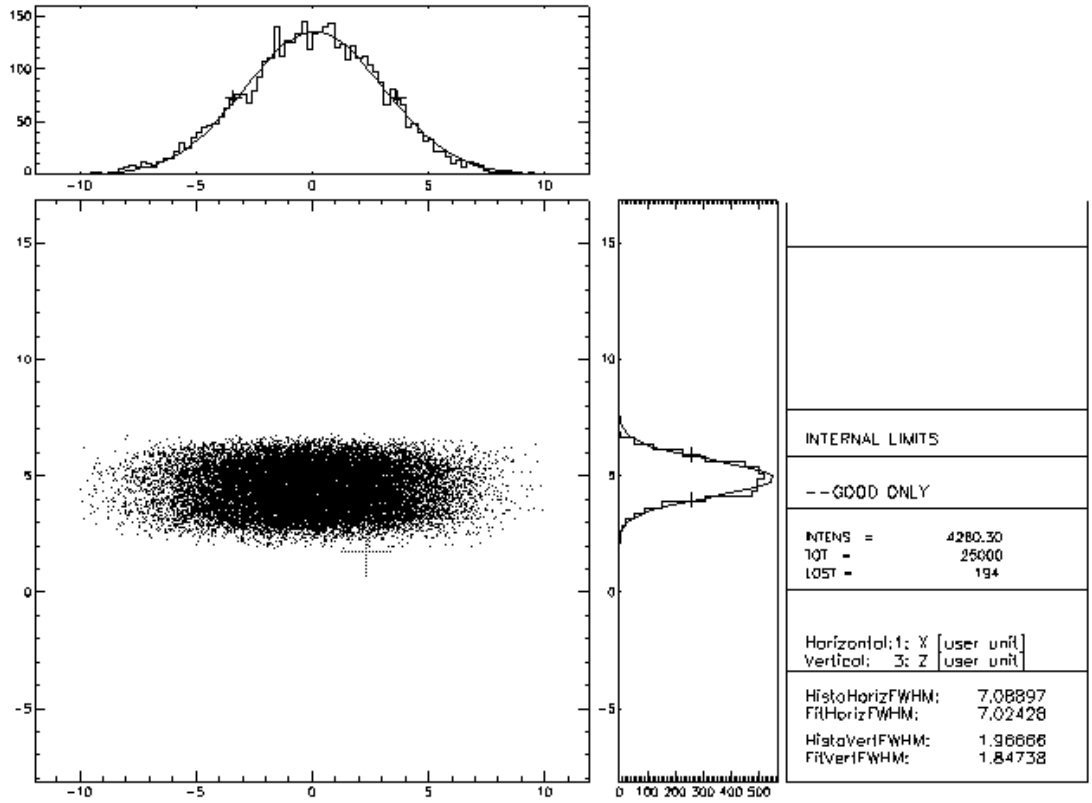

Figure B1. Beam spot at the sample for Case 2 in Table B1. Surface errors due to heating and cooling of the DCM crystal were included in the calculations.

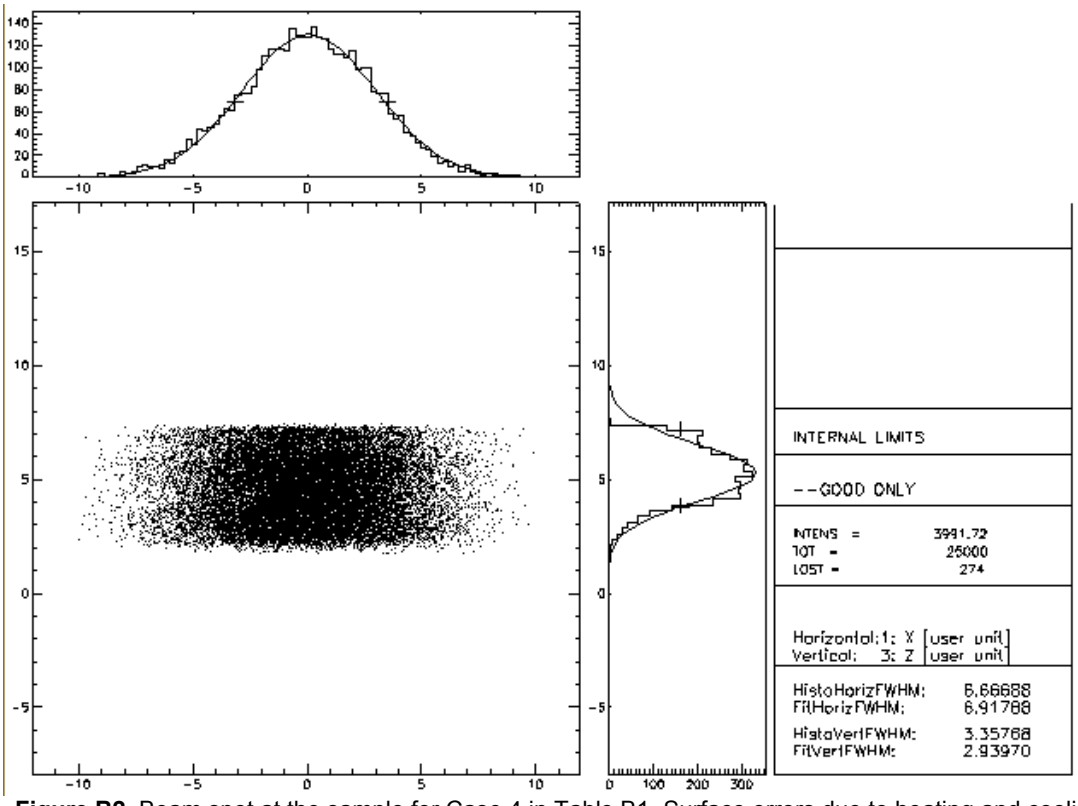

Figure B2. Beam spot at the sample for Case 4 in Table B1. Surface errors due to heating and cooling of the DCM crystal were included in the calculation.

Figure B3 shows a simulation for the same heat load as in Case 2 but for a water-cooled Si crystal. The data show significant broadening of the beam. There would be noticeable loss of flux if it were calculated over a smaller aperture than the 20 μm x 20 μm chosen here.

Results show that in the high-beta regime, the spot at the sample is sufficiently small and of a regular shape even at K=1.714 (Case 4), whereas the flux is nearly doubled compared to the case of K=0.981 (Case 2). The expected resolution of the beamline without the high-resolution optics is shown in Figure B4.

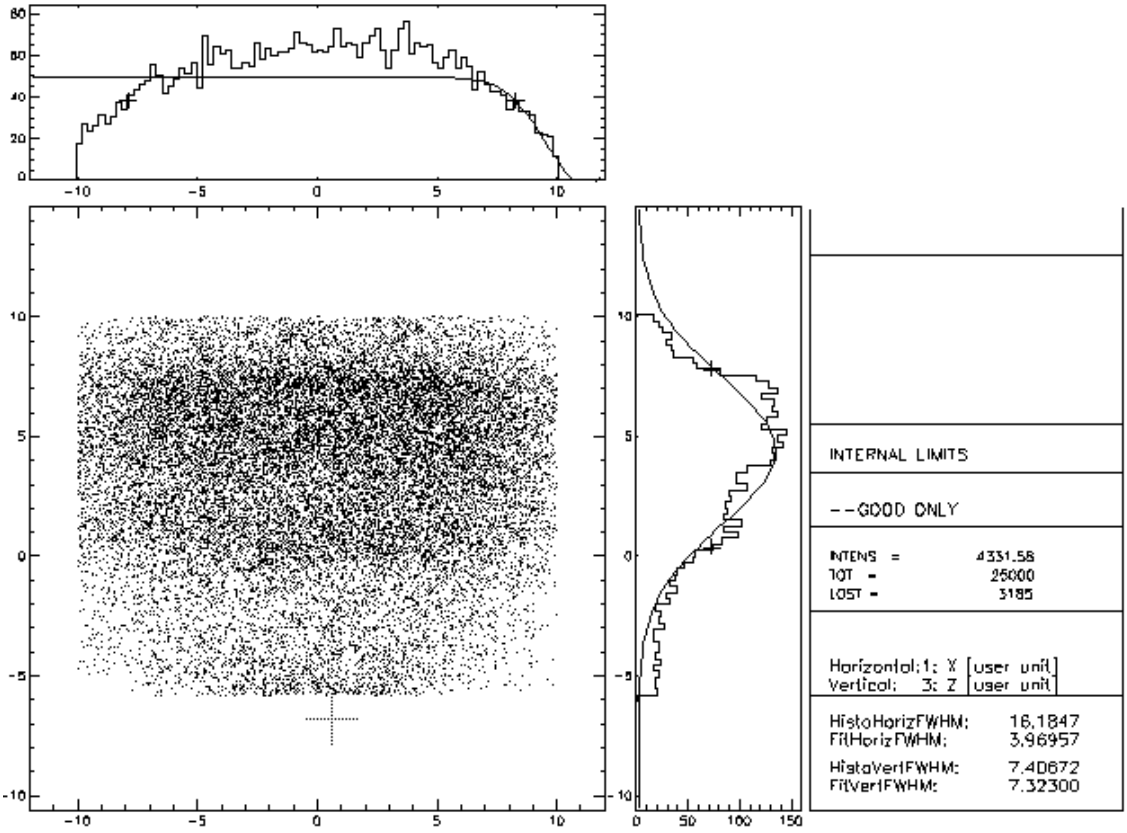

Figure B3. Beam spot at the sample for Case 2a in Table B1. Surface errors due to heating and cooling of the DCM crystal are included in the calculations. The crystal was water cooled.

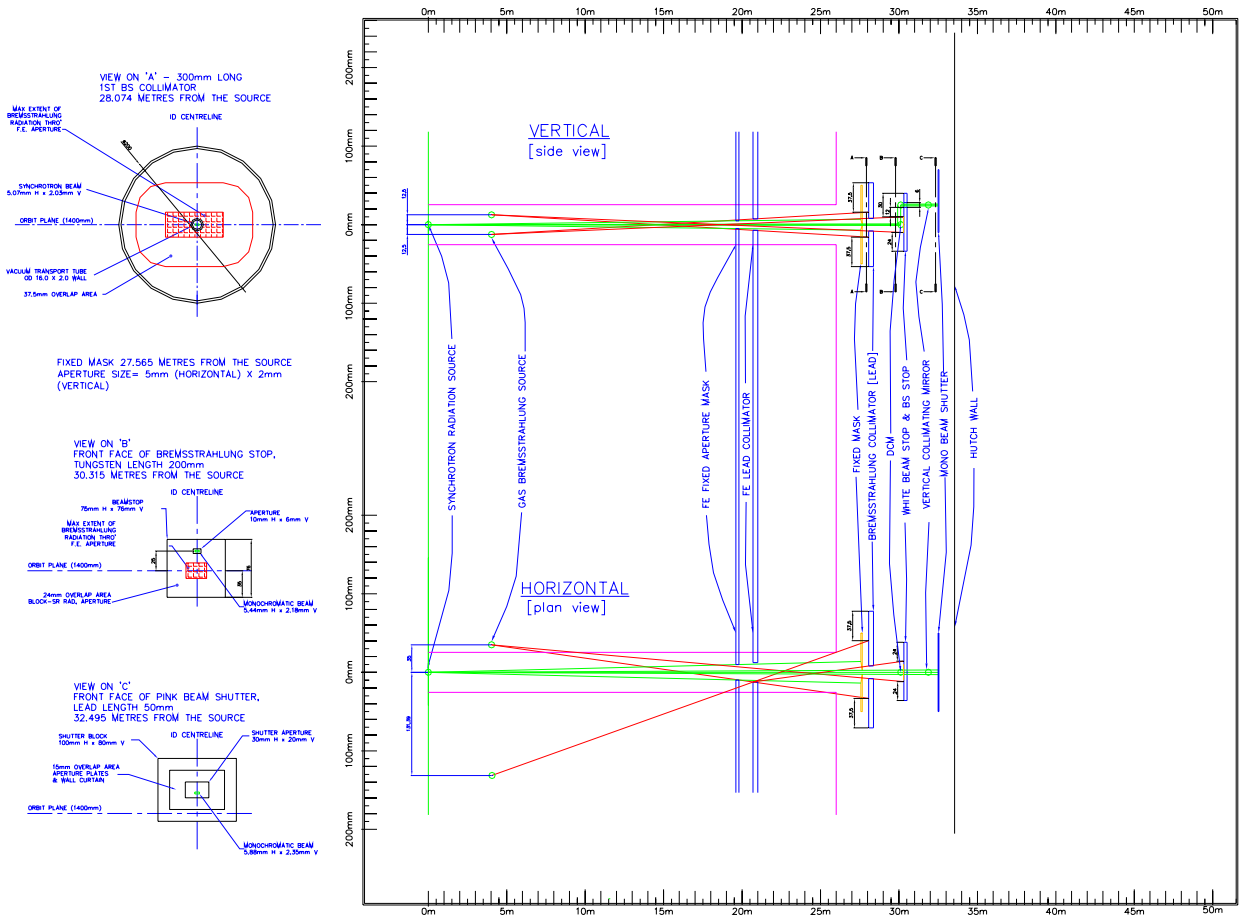

Figure B.4 Bremsstrahlung ray trace diagram for the inelastic x-ray scattering beamline.

1-B Appendix B: Beamline Layout Drawings

This is a possible layout of the IXS beamline showing a two-endstation and back-scattering monochromator configuration.

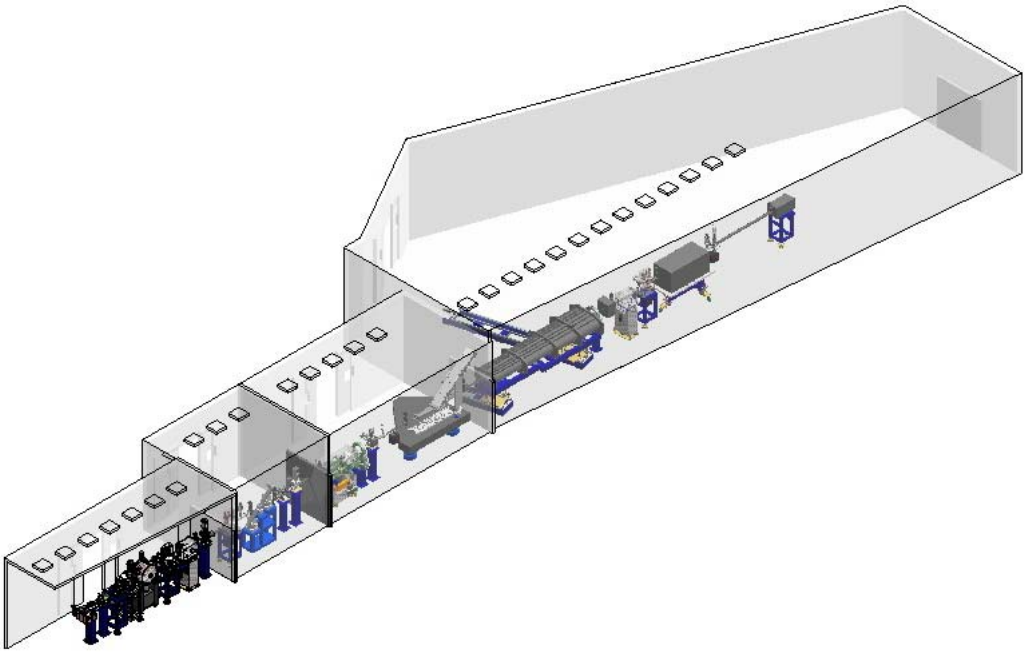

Figure B1. General view of the NSRS-2 IXS beamline and two endstations (Backscattering HRM).

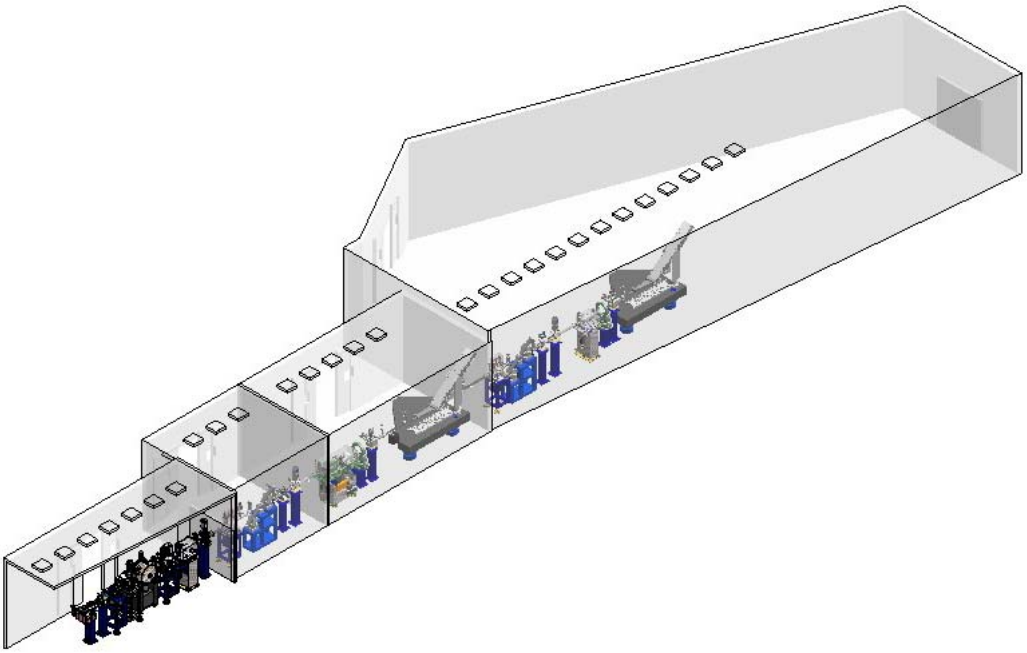

Figure B2. General view of the NSRS-2 IXS beamline and two endstations (In-line HRM) with an in-line, high-resolution monochromator.

1-C Appendix C: List of Key Beamline Components

Table 1.C.1. Proposed beamline layout based on the July 17, 2007 facility numbers.

Beamline Component	Starting position, mm	Length, mm	Vacuum section[1]	Center of Optical Element
Beamline isolation gate valve	26900	70	0/1	
Bellow	26970	175	1	
Pumping Tee	27145	420	1	
Cooled fixed mask	**27565**	**229**	1	**27680**
Bellow	27794	175	1	
CVD Diamond Window	27969	105	1/2	
Bremsstrahlung collimator	28074	388	2	
Bellow	28462	137	2	
Blade BPM	28599	319	2	
Bellow	28918	137	2	
White beam slits	**29055**	**229**	2	**29170**
Cooled Fluorescent screen	29284	211	2	
Bellow	29495	137	2	
Gate valve	29632	70	2/3	
DCM White beam / Bremsstrahlung stop	**29702**	**821**	3	**30113**
Gate valve	30523	70	3/4	
Bellow	30593	137	4	
Quadrant BPM	30730	35	4	
Monochromatic slits Fluorescent screen	30765	553	4	
Bellow	31318	137	4	
Gate valve	31455	70	4/5	
VCM	**31525**	**700**	5	**31875**
Gate valve	32225	70	5/6	
Bellow	32295	200	6	
Monochromatic beam shutter	32495	320	6	
Pipe Hutch Wall at 33.55 m	32815	600 340	6	
ENDSTATION 1				
Bellow	33415	200	6	
Monochromatic slits Fluorescent screen	33615	553	6	
Y-Z profile monitor	34168	406	6	
Bellow	34574	200	6	
Gate valve	34774	70	6/7	
High-resolution monochromator	**34844**	**1031**	7	**35360**
Gate valve	35875	70	7/8	
Bellow	35945	200	8	

Beamline Component	Starting position, mm	Length, mm	Vacuum section[1]	Center of Optical Element
Fluorescent screen	36145	300	8	
Bellow	36445	200	8	
Quadrant BPM	36645	35	8	
Monochromatic beam shutter	36680	320	8	
Pipe Hutch Wall at 37.3 m	37000	680 340	8	
Bellow	37680	200	8	
Gate valve	37880	70		
HFM	**37950**	**900**	8	**38400**
VFM	**38850**	**600**	8	**39150**
Be (150 μm) or SiN window	39450	20	8/9	
Sample position 1 (low vacuum)			9	**39570**
Be (150 μm) or SiN window	39670	20	9/10	
Monochromatic slits	39690	340	10	
Quadrant BPM	40030	35	10	
Bellow	40065	200	10	
Gate valve	40265	70	10/11	
Segmented high-resolution analyser (reflecting back at a different height) Gate valve Bellow/pipe SiN window (200 nm) Strip detector	40335 (finishes at 42835)	2500 70 300 20 600	11	**44238**
Gate valve	42835	70	11/12	
Bellow	43035	200	12	
Pipe Hutch Wall (separating Endstation II) at 46.05 m	43235	17647	12	
ENDSTATION 2 (Backscattering Monochromator option)				
Bellow	60882	200	12	
Gate valve	61082	70	12/14	
Backscattering monochromator	**61152**	**1000**	14	**61652**
Gate Valve	61082	70	14/13	
Bellow	60882	200	13	
Pipe	58932	1950	13	
Bellow	58732	200	13	
Double sided Fluorescent screen	58521	211	13	
Y-Z profile monitor	58115	406	13	
Si table	54415	3700	13	
Gate valve	54345	70	13/15	
Bellow	54145	200	15	
Monochromatic slits Fluorescent screen	53592	553	15	

Beamline Component	Starting position, mm	Length, mm	Vacuum section[1]	Center of Optical Element
Quadrant BPM	53557	35	15	
Bellow	53357	200	15	
VFM	52757	600	15	**53057**[1]
Monochromatic Slits	52692	65	15	
SiN window (200 nm)	52622	70	15	
Sample position 2 (low vacuum) Detector		446 400	16	**52451**[2]
SiN window (200 nm)	52106	70	17	

Notes: 1) Optical distance is 70.247 m from the source.
2) Optical distance is 70.853 m from the source.

2 HXN: NANOPROBE BEAMLINE

2.1 Executive Summary

The proposed beamline design follows many of the ideas presented in the December 2006 NSLS-II CDR with additional operation modes. Determining an optics plan for this beamline is complicated by the fact that the required final optics for achieving 1nm focal spots do not yet exist. The uncertainty associated with the optics requires that the beamline be designed with sufficient flexibility to provide the necessary contingency to accommodate an eventual optics solution. The challenge is to provide this flexibly without paying an excessive cost premium or the need to rebuild/replace components—allowing on-budget and on-time completion of the beamline. The design detailed here incorporates this flexibly and controls risk by utilizing well-understood front end and FOE optics components to deliver the x-ray beams generally required for illuminating any successful nano-focusing optics.

The plan is based on two focal points: one at 41 m and the other at 76 m, both supplied by a common set of upstream optics that are located in the front end and FOE. At each of these two locations a hutch will house the necessary end station equipment to support the scientific goals of the beamline. The exact location of these hutches will be determined by a number of factors, such as the characteristics of the final nano-focusing optics and details involving conventional facilities (floor space, roof line, egress, utilities, etc.). One way to look at this proposed layout is to consider the 41 m hutch a 1x location and the 76 m hutch a 2x location with regard to beam demagnification. Operationally, the focused x-ray beam can be used in only one hutch at a time. A beam stop located at the back wall of the upstream 1x hutch would allow access to the downstream 2x hutch while beam is present in the 1x hutch. Access to the 2x experimental location during x-ray operation of the 1x location will allow off line work to be performed using the end station equipment. Given the sophistication and complexity of a nano probe end station, this will provide valuable access time for instrumentation development and testing, as well as experiment setup.

The 1x/2x hutch arrangement will play a key role during the early operation phase of the project, when the main activity will be optics testing and commissioning. During this initial phase and well before the 2x hutch (and transport to it) is completed, the 1x location will serve as an early test location where various optics approaches can be evaluated and refined for eventual use in the push to 1 nm in the 2x hutch. There also exists the possibly of achieving a 1nm focal spot at the 1x location if modes such as a waveguide-coupled aperture prove feasible. The two locations can also be instrumented with complimentary end station equipment such as a full-field imaging system in the 1x location providing flexibly and agility in meeting the demands of the user science program.

The optics report section describes five optics modes: two for the 76 m 2x location, and three for the 41 m 1x location. The proposed support optics will be used to configure these five modes and are general enough to provide additional operation modes if necessary. They are also well understood today regarding both performance and cost.

Particular attention should also be given to address vibration issues with the building experimental and outbuilding floor and the principle optical items—namely, the Monochromator and Mirror systems and other key diagnostic and sample hardware. Similarly, the scanning table supports will have to be state-of-he art vibration isolated systems. Novel solutions should also be sort for BPM systems these need to be nanometer accuracy and supported upon thermally stable and vibration-free supports.

2.2 Scientific Objective

This beamline will allow the study of nanomaterials, which play important roles today in many diverse scientific fields, opening up a wide range of scientific problems ranging from studying the structure and function of catalytic nanoparticles, to the mapping of strain in buried grain boundaries, to determining the structure of single molecule devices.

This hard x-ray nanoprobe beamline will be designed and optimized to enable the production and use of a beam of hard x–ray photons with a nm beam size. As such, it will be a world-leading instrument, enabling spatially resolved versions of many powerful structural and spectroscopic x-ray techniques with unprecedented resolution. In particular, it will allow the study of nanomaterials which today play important roles in many diverse scientific fields. This beamline will take maximum advantage of the low emittance beam provided by the NSLS-II lattice.

The primary experimental techniques for this beamline will likely be scanning nanobeam techniques, but it will also have a limited full-field capability. The limited full-field capability will assist in rapidly locating areas of interest, and would thus allow more efficient use of beam time. For the scanning probe techniques, there are a variety of contrast mechanisms that allow one to extract useful information from the real-space mapping of a sample. For example, one can spatially resolve the density, elemental composition, crystallographic phase, strain, texture, chemical state, local atomic environment, and magnetization. It will operate in a number of modes, each of which will place different requirements on the detectors.

In the first mode, a fluorescence detector can be used with the sample to reveal the spatial distribution of individual elements. The second mode will use a large-area, low-spatial resolution high-sensitivity detector, such as a CCD, to obtain a spatial map of selected Fourier components of a crystallographic phase, and also a spatial map of the local strain. Third, by scanning the incident photon energy, it will be possible to access a number of spectroscopic quantities, such as the local environment from EXAFS and the local chemical state from XANES. Finally, from the back-scattered Compton scattering, one can measure the electron density. This will be especially useful for light elements such as carbon.

2.3 Insertion Device

For the nanoprobe, the over-riding design guidance is to improve the chances of attaining a 1 nm spot size. In order to do this, it is clear that the low-beta insertion section with the small source size is the right choice.

2.3.1 Undulator Power

Power density calculations have been performed for an undulator using equations presented by Kim.[1] Table 2.1 details the source, undulator, and beam parameters. Note that these calculations were prepared for a U19 cryogenically cooled permanent magnet device. We currently anticipate that the standard device for NSLS-II baseline hard x-ray undulators will be a room-temperature U20 In proceeding further with the design for this beamline, this choice should be further re-optimized and these calculations performed again.

Table 2.1. Source, Undulator, and Beam Parameters.

Source parameters	Source energy, E_s	3 GeV
	Source current, I	500 mA
Undulator parameters	Period length, λ_u	19 mm
	Number of periods	158
	Deflection parameter, K	2.03
Beam parameters	Horizontal electron size, σ_x	38.5 μm
	Horizontal electron divergence, σ'_x	14.2 μrad
	Vertical electron size, σ_y	3.05 μm
	Vertical electron divergence, σ'_y	3.22 μrad

Normalization factor, G(K). The normalizing factor is defined as:

$$G(K) = K \cdot \frac{(K^6 + 24/7 \cdot K^4 + 4 \cdot K^2 + 16/7)}{(1 + K^2)^{7/2}} \tag{2-1}$$

Substitute known values and calculate the normalization factor.

$$G(K) = (2.03) \cdot \frac{((2.03)^6 + 24/7 \cdot (2.03)^4 + 4 \cdot (2.03)^2 + 16/7)}{(1 + (2.03)^2)^{7/2}} = 0.982 \tag{2-2}$$

Magnetic field strength, B_0. The magnetic field strength of the undulator is defined as:

$$B_0 = \frac{K}{0.934 \cdot \lambda_u}. \tag{2-3}$$

Substitute known values and calculate magnetic field strength.

$$B_0 = \frac{2.03}{0.934 \cdot (19 * mm)} = 1.144 Tesla \tag{2-4}$$

Gamma of synchrotron, γ. The gamma parameter is defined as:

$$\gamma = \frac{E_s}{m_e \cdot c^2} \tag{2-5}$$

where E_s=source energy, m_e=mass of the electron (9.1095 x 10^{-28}grams) and c=speed of light (2.99792458 x 10^{10}cm/sec). Substitute known values and calculate the gamma parameter.

$$\gamma = \frac{3GeV}{(9.1095 * 10^{-28} grams) \cdot (2.99792458 * 10^{10} cm/\sec)^2} = 5871 \tag{2-6}$$

Power density distribution, $P_u(\theta, \psi)$. Power density in the forward direction is given by:

$$P_u(\theta,\psi) = 10.84 \cdot B_0 \cdot {E_s}^4 \cdot I \cdot N \cdot G(K) \cdot f_K(\theta,\psi) \quad (2\text{-}7)$$

where I = source current and N = number of periods. Based on the source, undulator, and beam parameters (Table 2.1) and the detailed functions, Figure 2.1 plots the incident vertical and horizontal heat flux distributions.

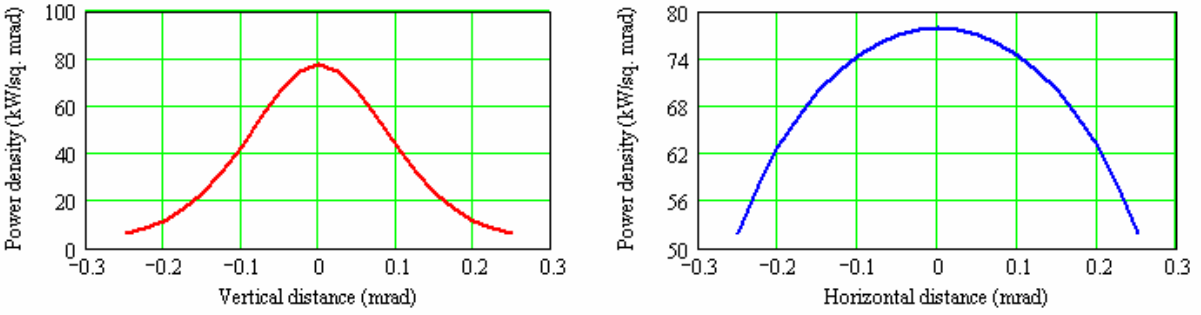

Figure 2.1. Heat flux distributions for the U20 undulator.

2.4 Sector Layout

2.4.1 Front-End Layout

In this section, the components in the front end (upstream of the ratchet wall) are discussed.

2.4.1.1 Front End Differential Pump Mask (FEDPM)

This power limiting mask will allow approximately 90% of the undulator harmonic (at 1 Å) to pass, reduces the total power to a level that is more manageable by the downstream components and protects against mis-steering of the electron beam. It will be located behind the shield wall as close to the undulator as possible with the next component (Front End Defining Aperture Mask, FEDAM) directly downstream. The vertical and horizontal location of this critical component will be defined through survey with additional motorized horizontal positioning over a restricted range to aide the initial alignment of the orbit (its front end location will make it difficult to access manual adjustors). Due to its location and size, this component is ideal for acting as the vacuum conduction-limiting aperture for a differential pump, freeing up space in the optics enclosure.

- distance from source = 14 m
- positioning = Y manual, X motorized (±0.5 mm)
- number of motors = 1

2.4.1.2 Front End Defining Aperture Mask (FEDAM)

To provide some thermal control of the central beam, motorized translation of the FEDPM and the FEDAM will be included to allow the horizontal beam size to be restricted to match the effective vertical coherent source size during nano-focusing.

- distance from source = 15 m
- aperture size = 0.3 mm (vertical) and 1.1 mm (horizontal)
- positioning = Y manual, X motorized (±0.5 mm)
- number of motors = 1
- percent harmonic (at 1 Å) = 90%
- power transmitted = 130.6W – aperture size = 0.3 mm (vertical) and 1.1 mm (horizontal)
- power transmitted = 35.7W – aperture size = 0.3 mm (vertical) and 0.3 mm (horizontal)

2.3.4.2 Beamline Layout

Figures 2.2, 2.3, and 2.4 outline the proposed beamline layout.

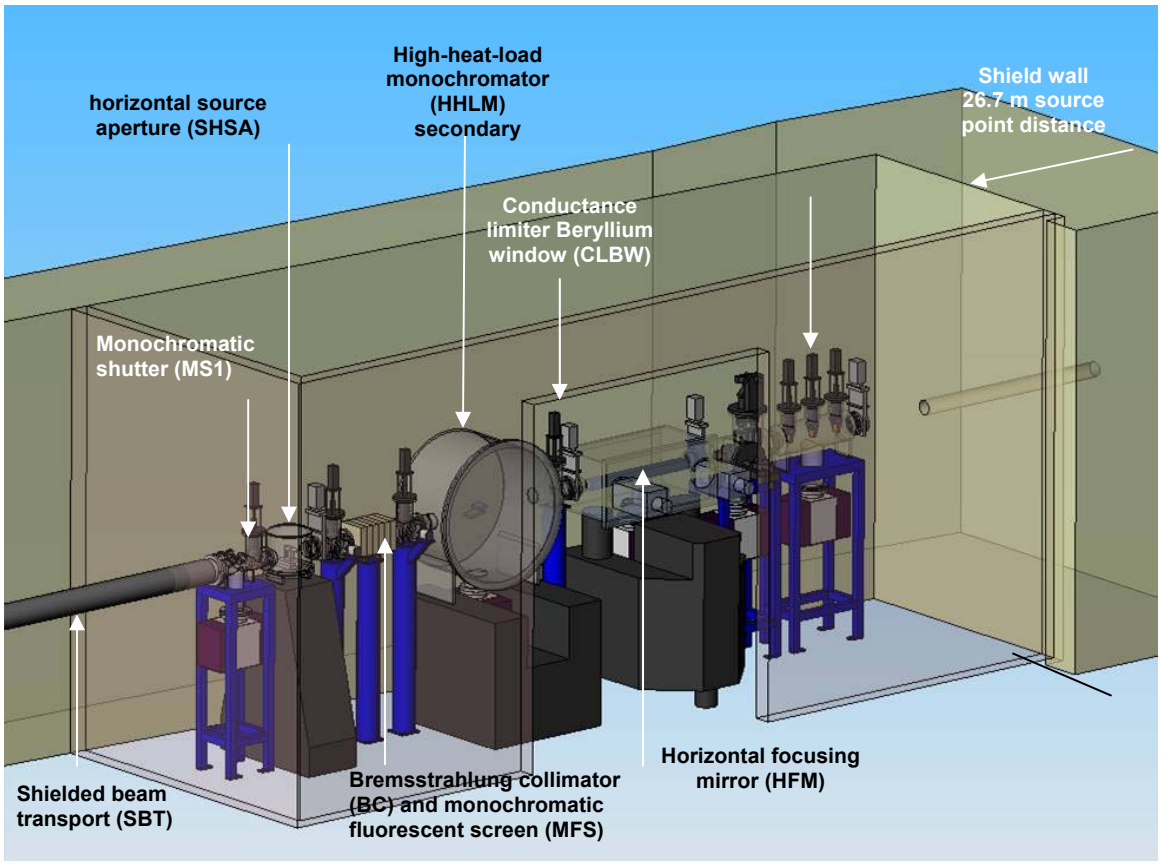

Figure 2.2. Nanoprobe beamline First Optics Enclosure (FOE).

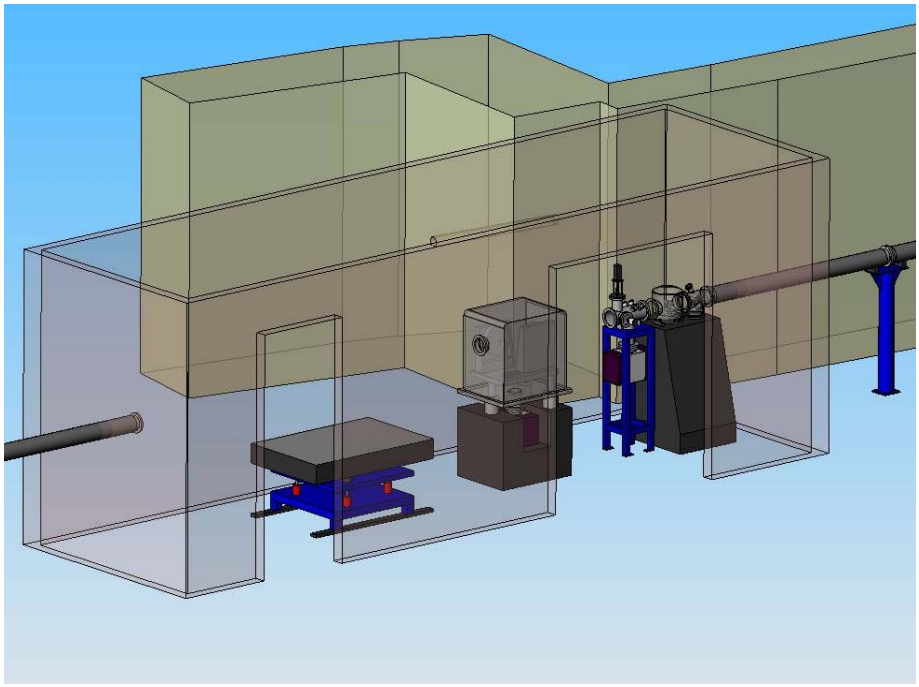

Figure 2.3. Nanoprobe beamline Station A. This station is the “x1” station and is within the experimental hall (see text).

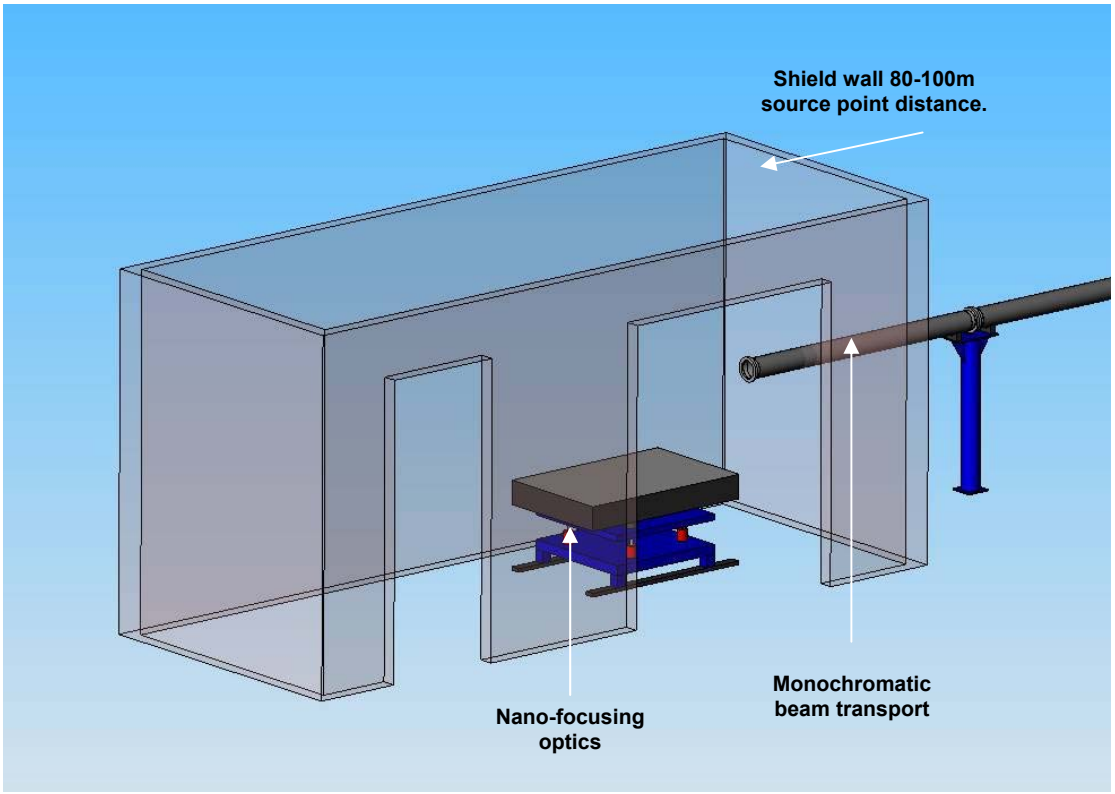

Figure 2.4. Nanoprobe beamline Station B.

2.4.2.1 Survey and Alignment

The NSLS-II nanoprobe sector should commission ~40 survey monuments on the sector, consisting of robust brass monuments countersunk into the floor. In all, there are 20 monuments located on the ID line aligned on the main ID centerline. These monuments, along with additional vertical wall marks and egress aisle locations, constitute the principal fiducial reference points for survey and alignment of the beamlines.

In addition, metallic stick-on targets will be located on the floor offset 1 meter to the main monument lines. These can be used to either establish temporary parallel lines for survey or to act as 90° turn-off points. These monuments should be surveyed relative to the two primary NSLS-II monuments per beamline. After installation, as-built precision coordinate measurements of several of the monuments will be made by the NSLS-II survey and alignment team. The locations of the monuments are shown in the main layout.

Survey and Alignment Guides

Survey monuments. Each FOE and Experiment Station will have brass monuments counter-sunk into the floor, at front and rear, plus approximately every three or four m, for each beamline.

The monuments used in NSLS-II will be compatible with the target mount for a laser tracker. The maximum error is typically ±0.3 mm. An adapter cap will fit over the monument for fitting of a 1.5-inch diameter laser retro-reflector.

Beamline centerline. A 0mrad beamline centerline will be placed in every enclosure, described with dedicated scribed brass monuments.

Beamline equipment. Each piece of beamline equipment will have mounts for laser tracker targets—typically three per piece of equipment. These should be offset to enable measurements of x-y-z and pitch, roll, and yaw adjustments.

Beamline height: 1.4 m. Each beamline will have dedicated survey targets in every enclosure. Wall-mounted targets are very useful for independent survey capability of beamline instrumentation using a Leica auto level with an accuracy capability of 10 μm.

Survey target location. Each radiation enclosure will have survey targets positioned at beam height at front and rear, plus every 3 m, for each beamline. The survey targets will be mounted on the hutch wall or concrete wall.

NSLS-II survey monuments. NSLS-II will provide a pattern of survey monument floor reference locations. These will typically be in the egress aisles plus at other key locations.

Cartesian coordinate framework. All major experimental equipment shall be kinematically mounted on the experimental floor. This will provide the ability to measure complete Cartesian coordinate reference information for experimental equipment. Provision will be made for survey reference floor markings in experiment stations, plus two target spheres on experimental equipment.

Survey Equipment

Survey equipment that has been ascertained to be available for local alignment and survey is as follows.

Beamline height instrumentation. Auto-Leveler - Nikon (accuracy of the scale division ±0.1 mm). The following upgrade may be implemented to achieve 10μm accuracy:

- NA2 Precision Auto Leveler
- GPM3 Parallel plate 10 mm for NA2
- GST-20 Tripod
- GVO-10 Short Focus lens for NA2 (1.8 m – 0.9 m)

Bragg motion axis. Survey targets are to be provided on all Bragg axes, such the device can be aligned to beam height and perpendicular to the beam centerline patch

2.4.2.2 Utility Layouts

Table 2.2 details the estimated coolant usage for the front end and first optics enclosure.

Table 2.2 Coolant Usage – Front End and FOE.

Module	Component description	Source point distance	Coolant	Required flow
1	Front End Differential Pump Mask (FEDPM)	14 m	H_20	8 L/min
	Front End Defining Aperture Mask (FEDAM)	15 m		
	Shield Wall	26.7 m		
2	White Beam Filters (WBF)	27.3 m	H_20	4 L/min
3	White Beam Slits (WBS)	27.8 m	H_20	4 L/min
4	Horizontal Focusing Mirror (HFM)	28.8 m	H_20	4 L/min
5	Conductance Limiter Beryllium Window (CLBW)	29.6 m	H_20	4 L/min
6	High Heat Load Monochromator (HHLM)	30.4 m	H_20	4 L/min
	White Beam Monitor (WBM)		LN_2	4 L/min
		30.9 m	H_20	4 L/min
			H_20	32 L/min
	TOTAL		LN_2	4 L/min

Table 2.3 details the estimated motor usage for the front end and first optics enclosure.

Table 2.3 Motor List – Front End and FOE.

Module	Component description	Source point	Number of motors	Motor	Amps / phase
1	Front End Differential Pump Mask (FEDPM)	14 m	1	Stepper	1.4
	Front End Defining Aperture Mask (FEDAM)	15 m	1	Stepper	1.4
3	White Beam Slits (WBS)	27.8 m	1 (horizontal position)	Stepper	1.4
			1 (horizontal aperture)	Stepper	1.4
			1 (vertical position)	Stepper	1.4
			1 (vertical aperture)	Stepper	1.4
4	Horizontal Focusing Mirror (HFM)	28.8 m	2 (mirror incidence)	Stepper	3.0
			3 (mirror alignment)	Stepper	2.0
			2 (mirror bending)	Stepper	2.5
6	High Heat Load Monochromator (HHLM)	30.4 m	1 (Bragg axis)	Stepper	2.5
			3 (2^{nd} crystal – roll, pitch and yaw)	Stepper	0.6
			1 (2^{nd} crystal vertical translation)	Stepper	2.5
	White Beam Monitor (WBM)	30.9 m	1	Stepper	1.4
	Secondary Horizontal Source Aperture (SHSA)	32.0 m	1 (horizontal position)	Stepper	1.4
			1 (horizontal aperture)	Stepper	1.4
	TOTAL		21	Stepper	49.8

2.4.2.3 Life Safety Code Compliance

Egress Aisles. Egress aisles are shown on the architectural layout drawing NSL-100-10-0003-A. All aisles are approximately 44 inches (1.12 m) wide.

2.4.2.4 Beamline Vacuum System

Most of the beamline components will be built to ultra high vacuum specifications with, in general, no vacuum-to-coolant joints. The exception to this are the silicon crystal mount monochromators in the ID beamlines, these will use a Cajon Swagelok VCR-type coupling connected to flexible pipes, for easy connection to the coolant supply.

To isolate the beamline vacuum from machine front end, there will be a differential pumped mask together with a Beryllium window conductance-limiter system. The nanoprobe beamline will utilize ion pumps to pump all beamline sections. In addition, gate valve pumping ports will be used to isolate the monochromator sections, to enable fast pumpdown via permanently installed turbo pump sets. Vacuum will be in the 10^{-7} to 10^{-8} Torr range. All mirror tanks will be isolated by gate valves from the rest of the beamline and will be operated in UHV (~10^{-9} Torr).

Beryllium Window Design

The main design points of the assembly are:

- At least two window thicknesses will be installed between the beamline termination window and the front end, to comply with regulations on the protection of machine vacuum. One thickness is the Be window conductance limiter and the second is the end window.
- The window material will be Brush Wellman IF1. The purity of the Be will be preferentially selected to 99.3% Be assay, with the iron and copper content less than 300 ppm, respectively.
- Coherence of the beam is a significant issue for nanoprobe experiments, so the Be windows will be polished.
- For ID beamline termination windows utilizing white beam, to protect against ozone-induced oxidization and corrosion we intend to investigate the possibility of sub-micron coating with aluminium. Alternatively, we will cap the end of the window flange with a Kapton window and flow dry nitrogen into the inter-space between the Kapton and Be to prevent corrosion. Holes burned into the Kapton due to white beam should be small, and a marginal positive pressure of dry nitrogen should suffice to keep air out and ozone production to a minimum.

Main Vacuum Sections (see also Table 2.4)

Vacuum Section 1

- Pneumatic DN200 all-metal valve (at end of the front end) 10″ CF, 8″ tube
- Tube incorporating machine protection measures: pirani gauge, cold cathode gauge, RGA, right-angled all-metal valve, 300 L/s (nom) ion pump fitted to the tube.
- Graphite Filter and Primary Slits Section – 300 L/s (nom) ion pump
- Pneumatic DN100 all-metal valve

Vacuum Section 2

- Horizontal mirror – water-cooled Si mirror
- 500 L/s (nom) ion pump, pirani gauge, cold cathode gauge, right-angled metal valve

- Diagnostics section (fluorescent screen, tungsten wire)
- Pneumatic DN100 all-metal valve

Vacuum Section 3

- Beryllium conductance-limiter window
- Double crystal monochromator – liquid nitrogen cooled
- Fitted with 500 L/s (nom) ion pump, pirani gauge, cold cathode gauge, right-angled metal valve
- Turbo dry and scroll backing pump fitted to DCM chamber
- Diagnostics section: white beam monitor and mono fluorescent screen
- GB collimator
- Pneumatic DN100 all-metal valve

Vacuum Section 4

- Photon shutter, possibly integrated gas bremsstrahlung (GB-shielding), fitted with 300 L/s (nom) ion pump, pirani gauge, cold cathode gauge, right-angled metal valve
- Secondary horizontal aperture
- Pneumatic DN100 all-metal valve

Vacuum Section 5

- White beam transport pipe 4 m long - 100mm OD tube
- Diagnostics section (fluorescent screen)
- Integrated gas bremsstrahlung/photon shutter, fitted with 300 L/s (nom) ion pump, pPirani gauge, cold cathode gauge, right-angled metal valve

Vacuum Section 6

- Quad diode BPM
- Diagnostics section (fluorescent screen, tungsten wire)
- Tube fitted with 300 L/s (nom) ion pump, pirani gauge, cold cathode gauge, right-angled metal valve
- Tertiary horizontal aperture

Vacuum Section 7

- White beam transport pipe 4 m long – 100 mm OD tube
- Diagnostics section (mono beam fluorescent screen)
- Tube fitted with 300 L/s (nom) ion pump, pirani gauge, cold cathode gauge, right-angled metal valve
- Pneumatic DN100 all-metal valve
- High-resolution monochromator
- Be window: mirror polished to less than 0.5 μm rms

Vacuum Section 8

- Nano focusing optics
- Long beam transport 29 m long

- 4*300 L/sec ion pumps, pirani gauge, cold cathode gauge, right-angled metal valve
- Be window: mirror polished to less than 0.5 μm rms; end window: Kapton foil protection
- Nano focusing optics

Table. 2.4 Vacuum Equipment Inventory.

Item	Approx Number	Comments
500 L/s (nom) ion pump	2	All major optics (mirror/DCMs)
300 L/s (nom) ion pump	5+3	Long beam transport
240 L/sec turbo and scroll set	2	Monochromators
Pirani gauges	6	Distributed down beamline 1 per vacuum section
Cold cathode gauges (IMG)	6	Distributed down beamline1 per vacuum section
RGA	1	Mirror location
Pneumatic DN100 all-metal valve	5	Distributed down beamline
All-metal right-angled valve	6	At strategic places down beamline (see flow)
Portable rough pump/leak detector	1	Not costed for, but required – assume vacuum loan pool at NSLS-II

2.4.2.5 Data Acquisition System and Motion Control

There are many combinations of control and drive electronics available for beamlines, but some general form factor decisions will reduce the options. The NSLS-II controls group will standardize on the high level control form factor.. The decision involves the balance between extra hardware and software costs verses the availability of existing controls software support (see Chapter 6, Control Systems).

Once the high-level user interface computer system has been determined, one can move down to the motor control options. Again, the synchrotron controls group will probably have a preference. The two main paths are either a simple control card (OMS) or a sophisticated intelligent controller (DeltaTau or Newport XPS). Most beamline axes are single drives that do not require any special features. However, there are exceptions, such as a diffractometer that performs trajectory scans or a monochromator that requires encoder averaging.

The final control decision is the drive amplifiers. There are a wide range on the market, with a wealth of different current ratings and features. For example, when choosing a stepper amplifier card one must chose a step size, current rating, holding current, and DC rail voltage. The choice may also be influenced by the packing density within a rack unit and the availability of spares.

2.4.3 Beamline Components

2.4.3.1 Module 1: Front End Differential Pump Mask (FEDPM)

Distance to center of undulator	14 m

A differential pump assembly will be introduced as the first component in the optics to isolate the beamline vacuum from that of the storage ring. Differential pump assembly will consist of a series of pumps separated from each other and from the UHV region by a flow-restricting aperture. The first aperture in the beamline will be fixed by the FEDPM and the FEDAM (directly downstream of the differential pump assembly), and sets the maximum acceptance of the beamline. This maximum acceptance has been set to correspond with the vertical and horizontal FWHM (full width half maximum) sizes and divergences of the

source. Based on the beam parameters detailed in Table 2.1, the maximum size of the front end aperture is given by:

$$X_1 = 4 \cdot \Sigma_x + 4 \cdot \Sigma'_x \cdot (14m) \approx 1100\,\mu m \qquad \text{Maximum horizontal opening}$$

$$Y_1 = 4 \cdot \Sigma_y + 4 \cdot \Sigma'_y \cdot (14m) \approx 300\,\mu m \qquad \text{Maximum vertical opening}$$

Using the detailed functions given in Section 2.3, the transmitted vertical and horizontal heat flux distributions are shown in Figure 2.5.

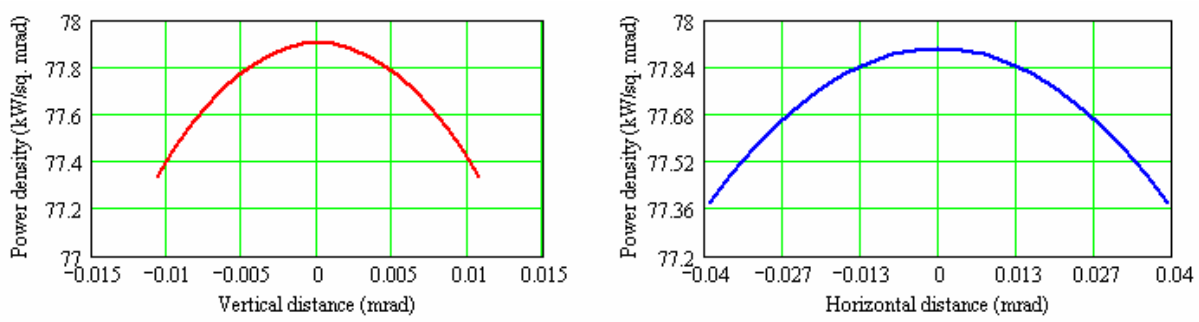

Figure 2.5. Heat flux distributions.

The radiated power for full-field operation is given by:

$$P = \int_{-\left(\frac{0.55mm}{14m}\right)rad}^{\left(\frac{0.55mm}{14m}\right)rad} \left(\int_{-\left(\frac{0.15mm}{14m}\right)rad}^{\left(\frac{0.15mm}{14m}\right)rad} P_u(\theta,\psi)\,d\theta \right) d\psi = 130.6W \ . \qquad (2\text{-}8)$$

This component is a cooled monolithic block of Glidcop AL-15 with a tapered hole terminating in a rectangular aperture with inclined absorber walls to distribute the heat load (Figure 2.6). Before the ingot is machined, it is first explosion-bonded to AISI 304L stainless steel end plates, which are then fixed to short beam tubes and front and rear entrance flanges. Explosion bonding is a bonding method in which the controlled energy of a detonating explosive is used to create a metallurgical bond between two or more similar or dissimilar materials. This joining technique was first utilized at the APS facility to enable high-strength Glidcop AL-15 materials to be used in high-heat-load components for undulator front ends[2]. The explosion bonded ingots are subjected to the standard ultra sonic tests as outlined by APS in LS 237; this is broadly based on the standard ultrasonic procedure ASTM A578, level I.

The total length, flange face to flange face, has been set at 300 mm. The entire assembly is independently mounted on its own scanning platform and can be translated as a unit by ±2 mm horizontal (motorized) and vertically (manual) adjustments to center the mask on the beam.

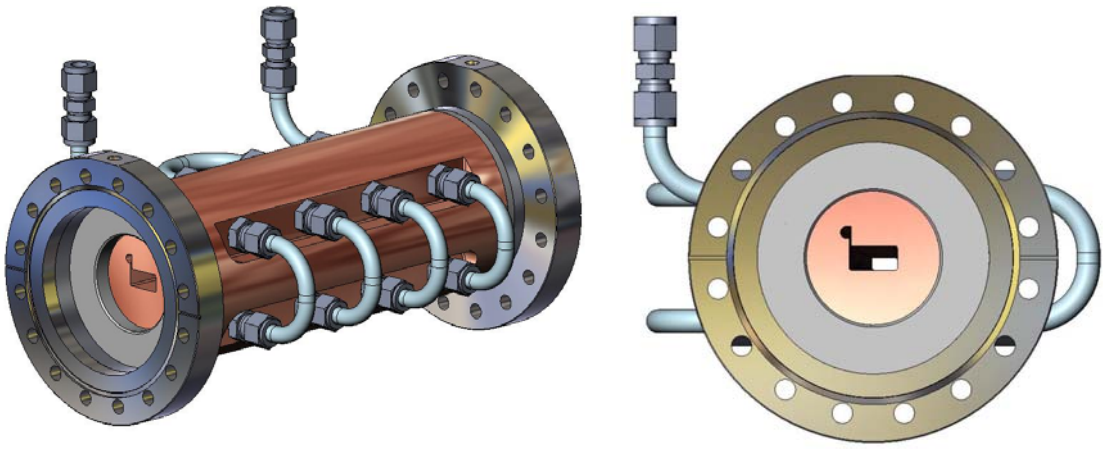

Figure 2.6. Proposed design of the FEDPM.

Motion Specification. Table 2.4 details the required motion specification for the FEDPM assembly.

Table 2.4. Motion Specification for the FEDPM Assembly.

Motion	Range	Resolution	Drive system
Horizontal motorized	±2 mm	<2 μm	Stepper motor driven variable horizontal aperture.
Horizontal manual	±5 mm	0.1 mm	Mask alignment.
Vertical manual	±5 mm	0.1 mm	Mask alignment.
Tilt Φ_X manual	±5°	0.25°	Mask alignment.
Yaw Φ_Y manual	±5°	0.25°	Mask alignment.

2.4.3.2 Module 1: Front End Defining Aperture Mask (FEDAM)

Distance to center of undulator	15 m

To provide some thermal control of the central beam, motorized translation of the FEDPM and the FEDAM will be included to allow the horizontal beam size to be restricted to match the effective vertical coherent source size during nano-focusing. The radiated power for nano-focusing operation is given by:

$$P = \int_{-\left(\frac{0.15mm}{14m}\right)rad}^{\left(\frac{0.15mm}{14m}\right)rad} \left(\int_{-\left(\frac{0.15mm}{14m}\right)rad}^{\left(\frac{0.15mm}{14m}\right)rad} P_u(\theta,\psi)d\theta \right) d\psi = 35.7W \, . \tag{2-8}$$

The proposed design for the FEDAM (Figure 2.7) is identical to that of the FEDPM, with the tapered aperture rotated through 180° along the beam centerline. By moving each aperture section independently in the horizontal direction, a variable-sized rectangular aperture can be created. The entire assembly is independently mounted on its own scanning platform and can be translated as a unit by ±2 mm horizontal (motorized) and vertical (manual) adjustments to center the mask on the beam.

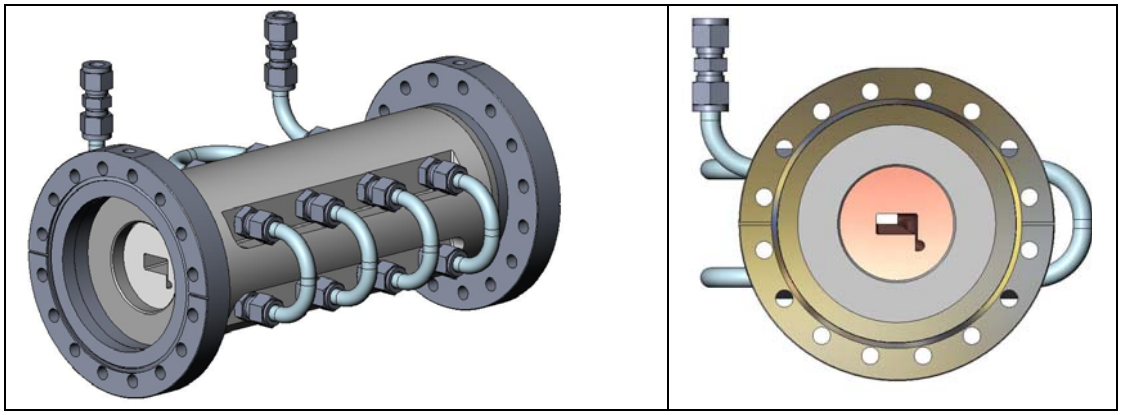

Figure 2.7. Proposed design of the FEDAM.

Motion Specification. Table 2.5 details the required motion specification for the FEDAM assembly.

Table 2.5. Motion Specification for the FEDAM Assembly.

Motion	Range	Resolution	Drive system
Horizontal motorized	±2 mm	<2 µm	Stepper motor driven variable horizontal aperture.
Horizontal manual	±5 mm	0.1 mm	Mask alignment.
Vertical manual	±5 mm	0.1 mm	Mask alignment.
Tilt Φ_X manual	±5°	0.25°	Mask alignment.
Yaw Φ_Y manual	±5°	0.25°	Mask alignment.

2.4.3.3. Shield Wall (SW)

Distance to center of undulator	26.7 m

2.4.3.4 Module 2 - White Beam Filters (WBF)

Distance to center of undulator	27.3 m

The functionality of the filter is to provide variable power absorption upstream of critical beamline components. The design incorporates three water-cooled diamond filters of different thicknesses, each mounted on independent pneumatic actuators with the facility for position translation of the filter in the beam. Diamond filter material is preferred, but there exists uncertainty regarding the degree to which this filter will preserve the source brilliance. There are a number of different types of diamond available, with the best choice for persevering coherence requiring further study. This uncertainty and the need for research and development translate into budget uncertainty. For the purpose of these specifications, commercially available CVD diamond pricing is used.

Based on the source, undulator, and beam parameters, the source spectral power distribution is shown in Figure 2.8. The transmitted spectral power distribution from a 30µm-thick CVD diamond filter is superimposed with the source distribution profile. The transmitted distribution is calculated by multiplying the source spectral distribution with the filter material absorption characteristic. The sum of transmitted

powers at each energy is then divided by the sum of the source power at each energy to give the percentage transmission from the filter. Relative to the source distribution, the power absorption for a 30μm thick CVD diamond filter has been calculated at ~4.1%. Table 2.6 shows foil thickness with calculated absorptions.

Table 2.6. Filter power variation.

Filter thickness (μm)	Transmission (W)	Absorption (W)
30	125.2	5.4
300	107.8	22.8
1000	87.1	43.5

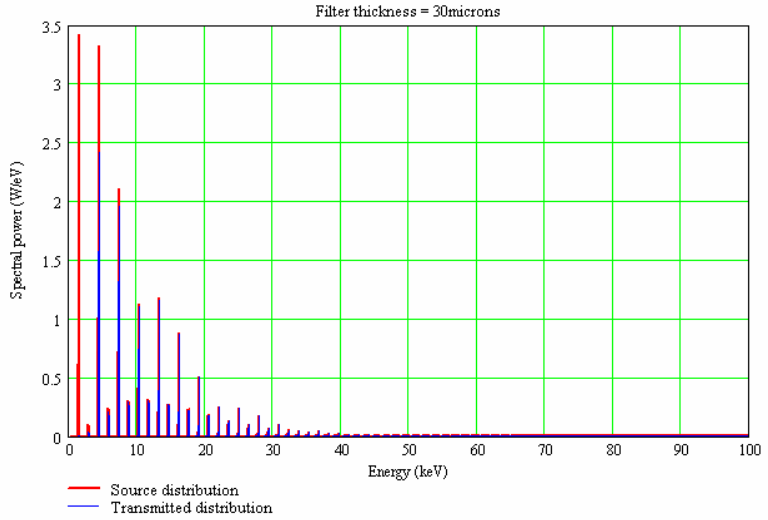

Figure 2.8. Spectral power distributions before and after a diamond filter of 30 microns.

Motion Specification. Table 2.7 details the required motion specification for the WBF assembly.

Table 2.7 Motion Specification for the WBF Assembly.

Motion	Range	Resolution	Drive system
Filter translation	50 mm	<0.5 mm	Pneumatic through vacuum actuator

2.4.3.5 Module 3 - White Beam Slits (WBS)

Distance to center of undulator	27.8 m

The functionality of the primary slits (horizontal and vertical) is to provide an upstream adjustable aperture to regulate the total thermal power exposed to the down stream components. The slits, contained within the same vessel, consist of two actuated jaws positioned serially along the beamline, one mounted horizontally and the other vertically to variably define the beam in the horizontal and vertical direction. Each pair of slits is designed with a single translation drive (up/down for vertical, left/right for horizontal) and with a second drive that adjusts the separation width of the slits (permits precise beam profile measurements with a fixed width slit).

The main design points of the assembly are:

- Each of the slits consists of an inclined block of OFHC copper with a relatively small block of tungsten mounted at the exit end of the slit. Dimensions of slit blade: 80 mm long, 50 mm wide, 30 mm high, and a ~3° incline angle.
- The tungsten edge is precision lapped so that the edge protrudes 0.1 mm above the flat on the OFHC copper incline and defines the beam with a hard edge. The tungsten can be chamfered slightly to further enhance the "hard: defining edge at high energies. The 0.1mm protrusion absorbs very little of the on-axis power density. This "knife-edge" tungsten slit concept has raised no problems in use at sector 13 and 16 at APS.[3, 4]
- The major advantage of this method is that the bulk copper takes the thermal load whilst the tungsten blade provides a hard defining edge for the x-rays.
- The cooling is through copper tubing brazed to the slit blade. No water to vacuum joints.
- The copper blades are mounted in Invar frames for thermal isolation from the support frame and vessel.
- Total length for a pair of actuators (horizontal and vertical) is <50cm.
- The end wall of the chamber can be water cooled to enable any Compton scattering from the slits to be safely absorbed in the chamber walls.
- The drive train has been extensively tested with uni-directional repeatability of 1-2µm and resolution of ~0.5µm. The slits will be equipped with encoders and precision (1micron) limit switches.

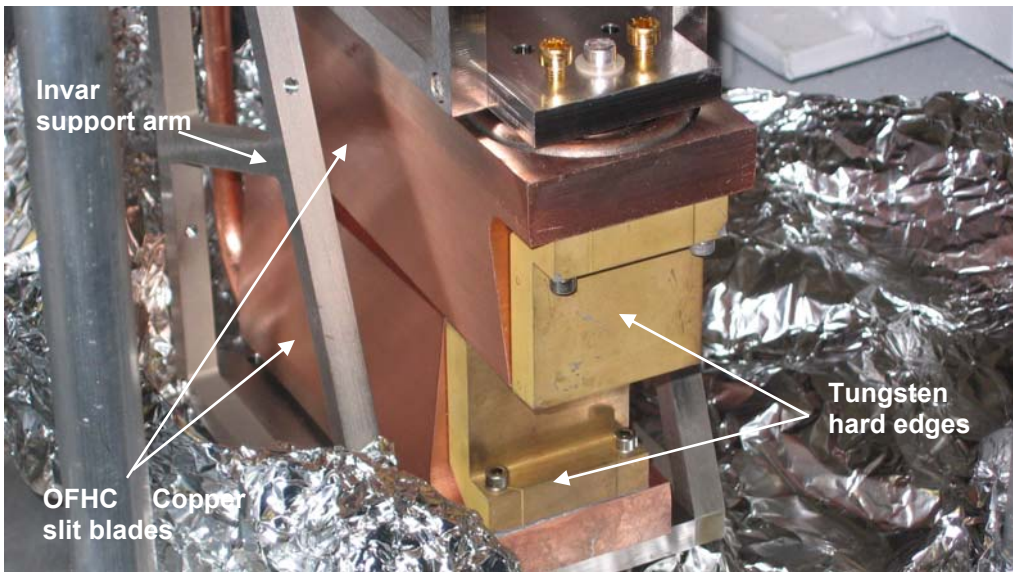

Figure 2.9. High-heat-load slits as used on HXMA ID06 beamline at CLS (designed to operate with >4kW power load).

An FEA model of the slit blade design was run to determine the structural integrity when subjected to the full thermal heat load. To improve the meshing, the FEA model was run with a finer grid than typical, to ensure accurate results. Element sizing can be characterized as fine to very fine, especially around a heat-loaded area and regions considered susceptible to high stress concentrations. The design of the horizontal and vertical slits will be identical; therefore, the incline angle of the slit blades will be fixed by the larger of the horizontal or vertical projected lengths of the beam footprint. The exit aperture of the upstream front end assembly has been set at 1.1 mm (h) by 0.3 mm (v), which at a source point distance of 14 m is equivalent to 78.6 µrad (h) by 21.4 µrad (v). Based on a source point distance of 27.8 m for the white beam slits, the

incident beam is sized at 2.2 mm wide by 0.6 mm high. Therefore, the incline height of the slit blade has been set at 4 mm to allow full acceptance of the beam (including a margin for mis-steer).

When the slit blades are aligned vertically, the incident beam footprint is at a minimum and will therefore produce the highest incident power density. This will be used as the primary design case for the FEA modeling. To apply the thermal load, a small area has been projected onto the optical surface representative of the beam footprint with an applied heat flux 5 W/mm^2 (equivalent to 131 W) to simulate the total thermal load absorbed. Figure 2.10 shows that variation of the horizontal and vertical power densities over the beam footprint are not significant; therefore, using a uniform heat loading for the FEA model is a valid assumption.

Convective cooling has been applied to the feature cut for the brazed coolant pipe. Based on a hydraulic diameter of ~4 mm and a flow rate of 4 L/min, a heat transfer coefficient of 1.8 W/cm^2 K was calculated using the Dittus-Boelter correlation. With the inclusion of thermal contact resistance, the effective heat transfer coefficient on the feature cut has been reduced to 1.5 W/cm^2 K. The results from the thermal models are then loaded into a structural model; with restraints applied to allow free expansion. The results from the FEA model are shown in Figure 2.9.

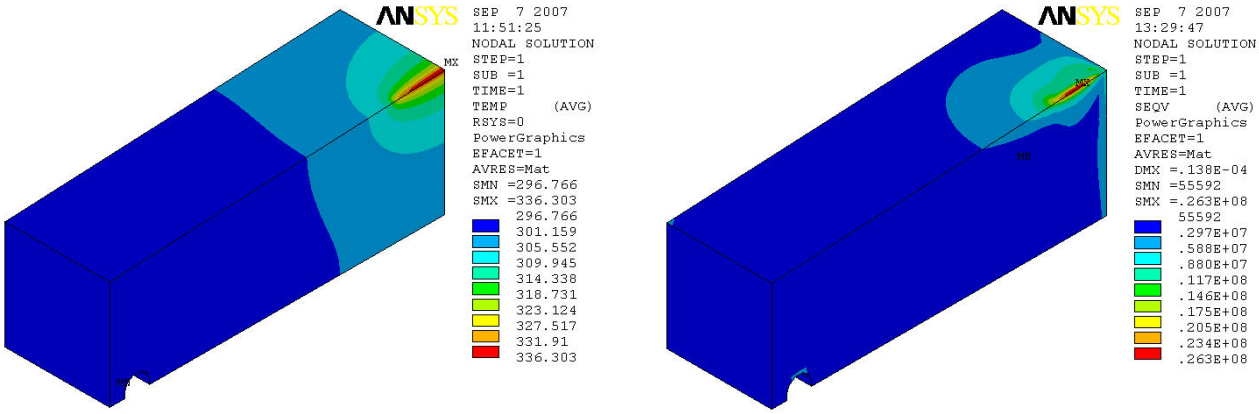

Figure 2.10. Temperature (K) and von Mises stress (Pa) distribution (left and right respectively) of inclined copper block of the white beam slits. The design fatigue stress for OFHC Copper is quoted at 215–254 MPa. The model is therefore not stress critical.

A separate analysis from the main FEA mask model has been undertaken to show the highly localized temperature rise effects on the small at the 0.1mm protrusion of the tungsten jaw into the beam. The 0.1mm element definition required makes the mesh too fine to incorporate into the main mask model. This is a valid model assumption, as the power into the 0.1mm height (by 3.1mm width) is only ~17 W, which makes the local model of the exit aperture almost entirely independent of the main mask model.

- Incident power density = 130.6 W / (2.2 mm x 0.6 mm) = 99 W/mm^2
- Beam footprint area on exit aperture = 0.1 mm x 2. 2 mm = 0.22 mm^2
- Maximum power absorbed into exit aperture = 99 W/mm^2 x 0.22 mm^2 ≈ 22W

To improve the quality of the meshing, the FEA model for the exit aperture was run with a finer grid than is typical, to ensure accurate results. For the thermal model, convective cooling was applied to the contact area between the exit aperture and the slit blade. For reasonable contact pressure exerted by screw fastening (> 4Bar), the effective heat transfer coefficient (representing inverse of thermal resistance) for indium-copper contact[5] is approximately 0.5W/cm^2/K. The bulk temperature for the convective cooling was set to 40°C, this was obtained by probing the contact area from the main FEA model of the slit blade. To apply the thermal load, a small area was projected onto the incident surface and the heat flux (99 W/mm^2) was applied to it. The results from the FEA model are shown in Figures 2.11 and 2.12.

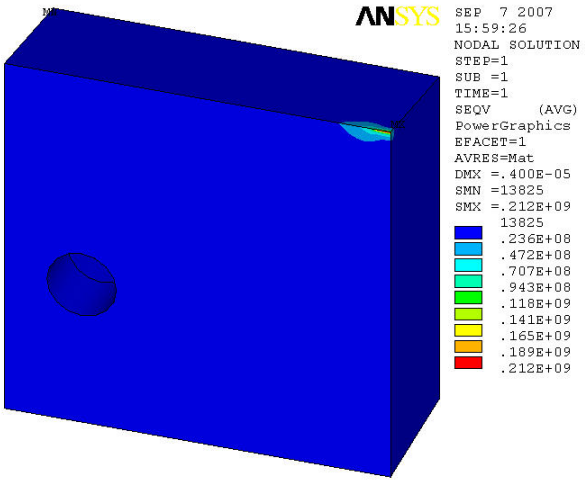

Figure 2.11 Temperature (K) and von Mises stress (Pa) distribution (left and right, respectively) of tungsten jaw of white beam slits. The design fatigue stress for tungsten is quoted at 750 MPa. The model is therefore not stress critical.

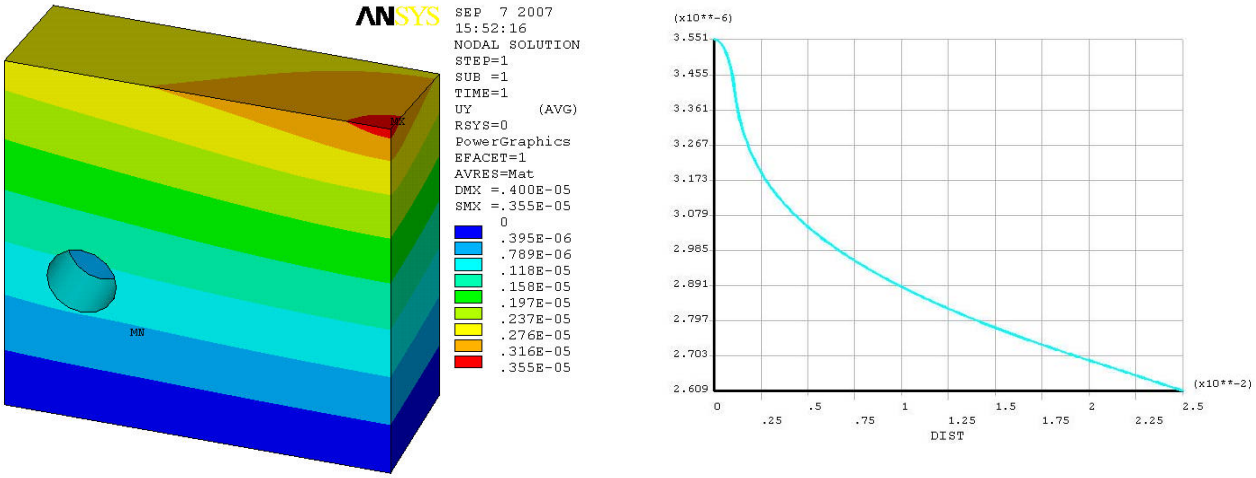

Figure 2.12 Displacement distribution (m) and hard edge displacement profile (m) of tungsten jaw – center at zero (top left and bottom right, respectively). The displacement on the cutting edge is shown to be below 4 microns.

Motion Specification. Table 2.8 details the required motion specification for the WBS assembly.

Table 2.8. Motion Specification for the WBS Assembly.

Motion	Range	Resolution	Drive system
Horizontal and vertical position	±10 mm	<2 µm	Stepper motor driven variable position.
Horizontal and vertical aperture	±5 mm	<0.5 µm	Stepper motor driven variable aperture.

2.4.3.6 Module 4: Horizontal Focusing Mirror (HFM)

Distance to center of undulator	28.8 m

Further power management of the very bright white beam is achieved through a horizontal mirror system. This will be a flat horizontally deflecting mirror used for power management and as a horizontal focusing element in full field mode. To achieve this, two independent moments are applied to either end of the mirror producing a linear moment distribution along the mirror length. The mechanical bender will allow the mirror figure to be corrected for thermal bump when producing unfocused beams as well as allow the horizontal beam to be focused either directly onto the sample or to a secondary horizontal source to be used in a compound focusing mode. In the compound focusing mode nearly the full horizontal source can be made available for full-field imaging.

The principle of the bending mechanism is shown schematically in Figure 2.13. Applying the bending forces to the mirrors through bending holes below the surface allows any distortions resulting from contact strain to dissipate before reaching the optical surface.

The x-ray mirror has two independent functions; suppression of the high energy section of the radiation spectrum and horizontal focusing of the beam. It must be remembered that transmission of photon flux from the source to the sample is the objective of the beamline; therefore reflectivity through the mirror system should be high. The mirror will have an active length of 800 mm, coated with rhodium and bare silicon and operate from 0 – 3 mrad. For low energy reflection (<8 keV), silicon is shown to be an excellent candidate with high reflectivity and harmonic suppression. To maintain mirror reflectivity, a rhodium coating would be used for the operating energies from 8 keV and up.

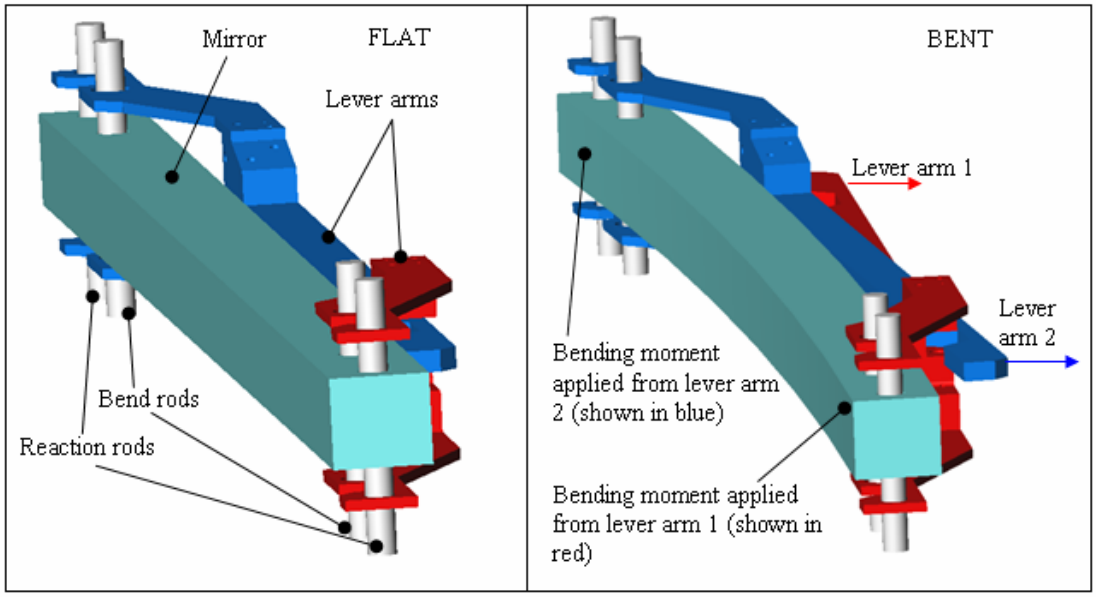

Figure 2.13 Illustrating closed-force bending principle, to be used in horizontal focusing white beam mirror.

Relative to the source distribution (i.e., upstream filters extracted from beam), the mirror power absorption when using each reflective strip is detailed in Table 2.9.

Table 2.9. Mirror Power Absorption, Grazing Angle Set at 3.0 mrad.

Reflective strip	Transmission (W)	Absorption (W)
Silicon	30.9	99.7
Rhodium	80.7	49.9

To determine the mirror displacement due to the thermal heat load, an FEA model of the mirror was run. To improve the quality of the meshing the FEA model for the horizontal mirror has been reduced to half size. Based on the maximum upstream aperture size (differential pump exit aperture), the maximum incident power on the mirror has been calculated at 354 W. To apply the thermal load, a small area has been projected onto the optical surface representative of the beam footprint with an applied heat flux of 213.5 kW/m^2 (equivalent to 130.6 W) to simulate the total thermal load absorbed. Figure 2.6 showed that variation of the horizontal and vertical power densities over the beam footprint are not significant; therefore, using a uniform heat loading for the FEA model is a valid assumption. Convective cooling was applied through the top gallium groove, with an applied heat transfer coefficient of 1 W/cm^2 K. Based on a hydraulic diameter of ~6 mm and a flow rate of 8 L/min, a heat transfer coefficient of 1.5 W/cm^2 K was calculated using the Dittus-Boelter correlation. The heat transfer coefficient value applied inside gallium grooves was lowered to account for the larger wetted area of the grooves relative to the internal area of the coolant pipe. The results from the thermal model are then loaded into a structural model; with restraints applied to allow free expansion. The results from the thermal FEA model are shown in Figure 2.14.

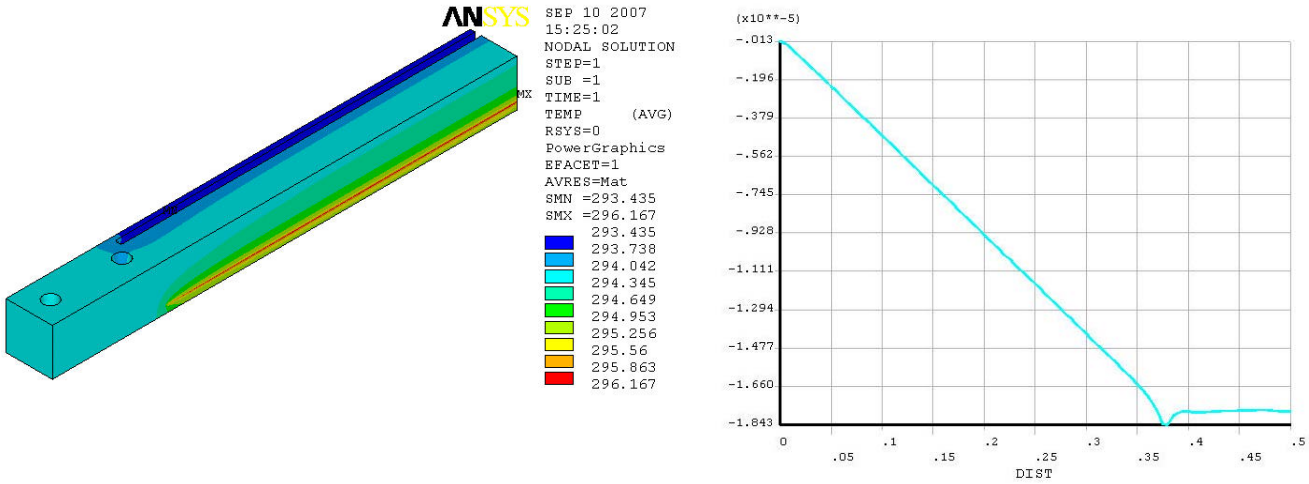

Figure 2.14. Temperature distribution (K) and thermal slope profile (radian) – center at zero (left, top, and right, bottom, respectively).

The ideal mirror bend profile is defined by the focal lengths, the incidence angle, and the optical length of the mirror. To induce the bend and achieve the required central deflection, loads are applied at either end of the mirror through the bending mechanism. However, as thermal bend should also be considered, the bending load applied that is actually applied is calculated to give the corrected mirror profile, as shown in Figure 2.15, taking into account the thermal load.

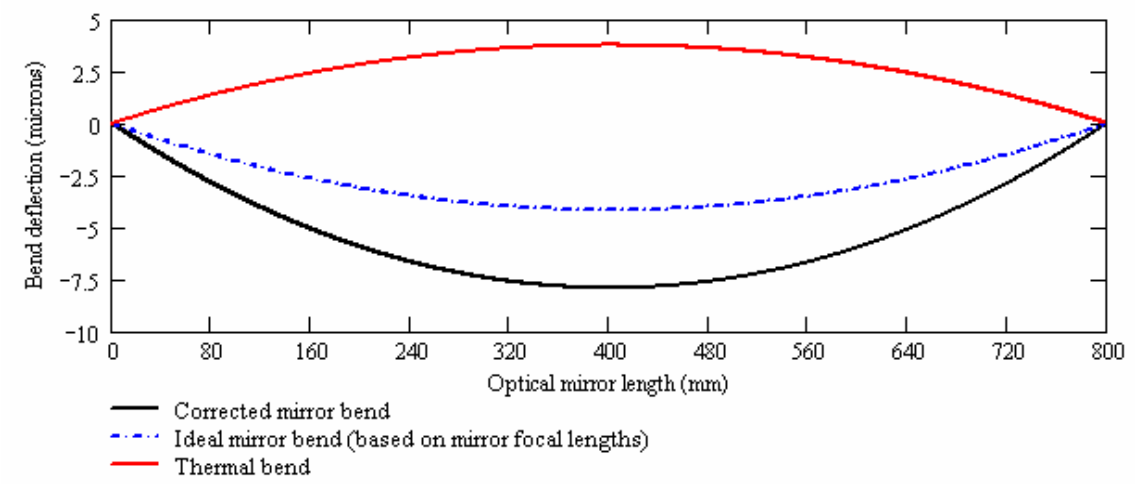

Figure 215. Corrected mirror bend profile, adjusted to include the effects of thermal load.

Since the optical axis normal is perpendicular to the gravity vector (or alternatively expressed, the reflecting optic plane lies parallel to the gravity vector), the requirement for self weight sag appears to be nil. Evidence from previous installations of bent planar mirrors has shown no focus distortion due to possible self weight sag. Based on the corrected mirror bend profile (black line), the deflection at the mid span point along the mirror length was determined. A required bend load of 77 N was then calculated, to give the required deflection at the mid span location. Figure 2.16 superimposes the mirror bend profile (bending loads and thermal bend) with ideal profile based on the mirror's focal length.

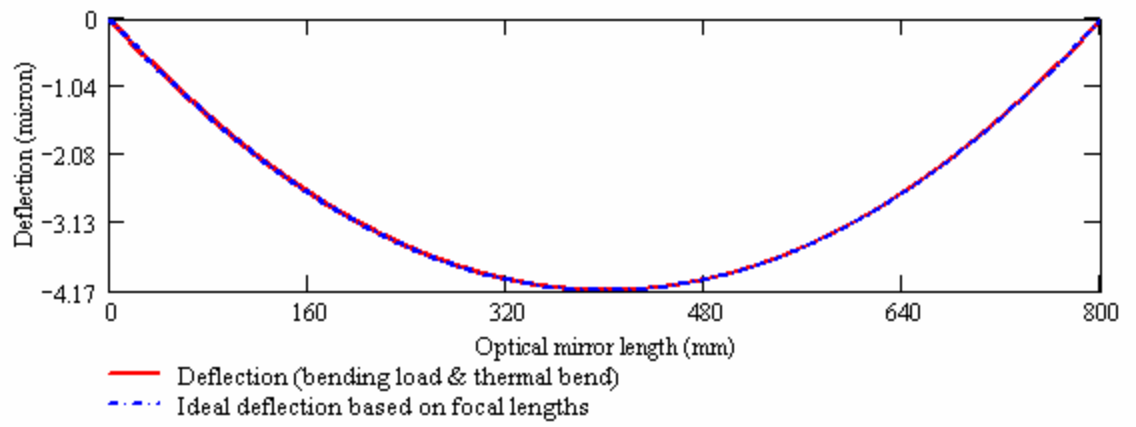

Figure 2.16 Comparison of mirror profiles.

The residual (uncorrectable) slope error is defined as the difference between the mirror slope profile (given by differentiation of its calculated displacement profile) and the slope formed by differentiation of the ideal bend profile (Figure 2.17). The residual slope error of the optically active surface has been corrected to give a root mean squared (RMS) value of 0.32 μrad, calculated over the illuminated length. Note that the optically active area is slightly less than the optical mirror length, due to space taken the bending holes.

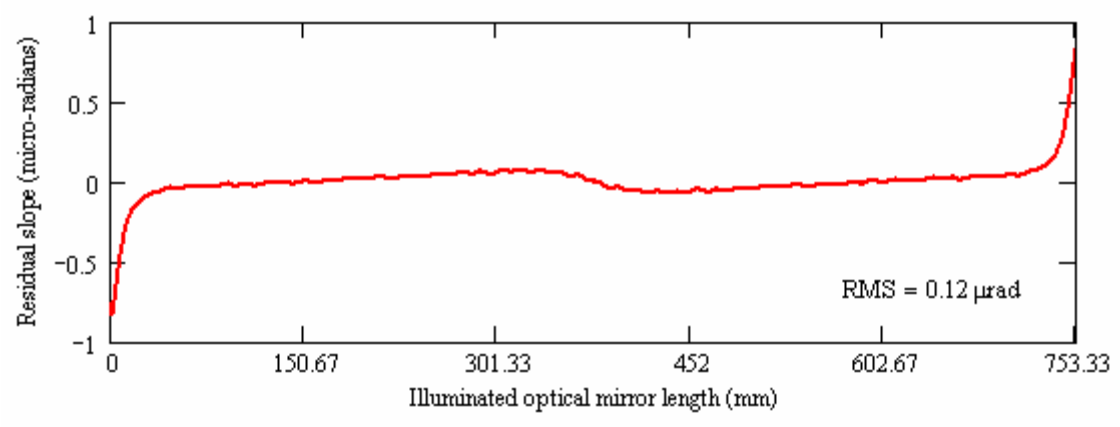

Figure 217 Residual slope error of white beam mirror.

A summary of the key criteria for mirror comparison is given in Table 2.10

Table 2.10 Horizontal Focusing Mirror, Key Criteria.

Description		Focusing mirror, reflecting horizontally
Substrate material		Single crystal silicon
Substrate dimensions		1000 mm long x 50 mm wide x 50 mm deep
Reflective coatings		Rhodium and bare silicon
Focal lengths	F_1	28.8 m
	F_2	∞
Beam acceptance		83 µrad (h) x 56 µrad (v)
Optically active length		754 mm
Incidence angle	θ	3.0 mrad
Radius of curvature	$R = \frac{2}{\left(\frac{\sin(\theta)}{F_1} + \frac{\sin(\theta)}{F_2}\right)}$	19.2 km
Calculated bending load		77 N
Calculated RMS slope error		0.12 µrad
Calculated bending stress	$\sigma = y \cdot \frac{E}{R}$	0.17 MPa

Table 2.11 details the required motion specification for the HFM assembly.

Table 2.11 Motion Specification for the HFM Assembly.

Motion	Range	Resolution	Drive system
Mirror incidence (yaw)	100 mm	<0.05µm	2 stepper motor driven through vacuum actuators.
Motorized fine yaw	±10 µrad	<0.05µrad	Through vacuum piezo driven.
Mirror alignment	±10 mm	<0.2µm	3 stepper motor driven vertical jack systems mounted to base block.
Mirror bending	-10 mm/ +30 mm	<0.2µm	2 stepper motor driven in vacuum actuators.

2.4.3.7 Module 5: Conductance Limiter Beryllium Window (CLBW)

Distance to center of undulator	29.6 m

Located directly upstream of the monochromator, the conductance limiting section is designed to act as a partial vacuum break between the high vacuum (10^{-7} to 10^{-8} Torr) regime in the monochromator and the ultra high vacuum (10^{-9} Torr and better) in the remainder of the beamline. The partial vacuum break is achieved by minimizing molecular flow between regions by providing only very narrow gap between sections, while allowing the beam to pass through (i.e., a vacuum conductance limitation). This is achieved by using an actuated beryllium window such that, when a fixed cooled mask is driven into the beam path, the gap between the frame and the upstream side of the mask is as near zero as possible (~1 mm), limiting the through conductance. There are a number of different designs for mounting the Be foil with the best choice for persevering coherence; these require further study. This uncertainty and the need for research and development translate into budget uncertainty.

Beryllium is a material that is largely transparent to x-rays, and it is therefore well suited to this task, as the beam is affected only in a very small way by passing through. Figure 2.18 shows the mass absorption characteristic for Be, and Figure 2.19 superimposes the transmitted spectral power distribution from the window with the incident distribution profile.

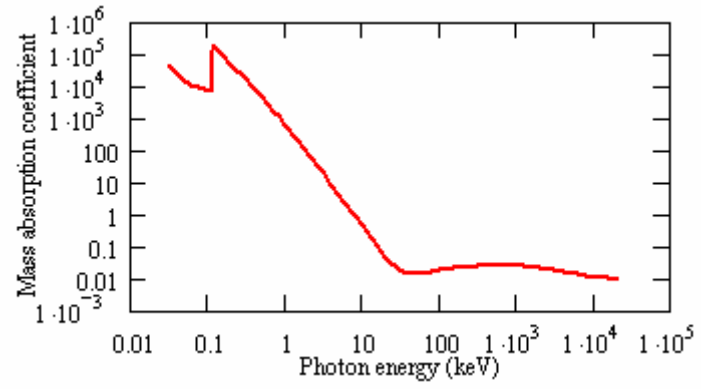

For the 0.003 to 1 KeV energy range, data were taken from:

http://www-cxro.lbl.gov/optical_constants/pert_form.html

For the 1 to 20 MeV energy range, data were taken from:

http://physics.nist.gov/PhysRefData/XrayMassCoef/ElemTab/z04.html

Figure 2.18 Mass absorption characteristic for Be.

The transmitted distribution is calculated by multiplying the incident spectral distribution by the absorption characteristic for beryllium. The sum of transmitted powers at each energy is then divided by the sum of the source power at each energy to give the percentage transmission from the mirror. Relative to the maximum incident heatload (80.7 W – heat load transmitted from the upstream mirror, see Section xx), the power transmission through the window was calculated to be 94.1%.

Motion specification. Table 2.12 details the required motion specification for the Conductance Limiter Beryllium Window assembly.

Table 2.12 Motion Specification for the CLBW Assembly.

Motion	Range	Resolution	Drive system
Filter translation	50 mm	<0.5 mm	Pneumatic through vacuum actuator.

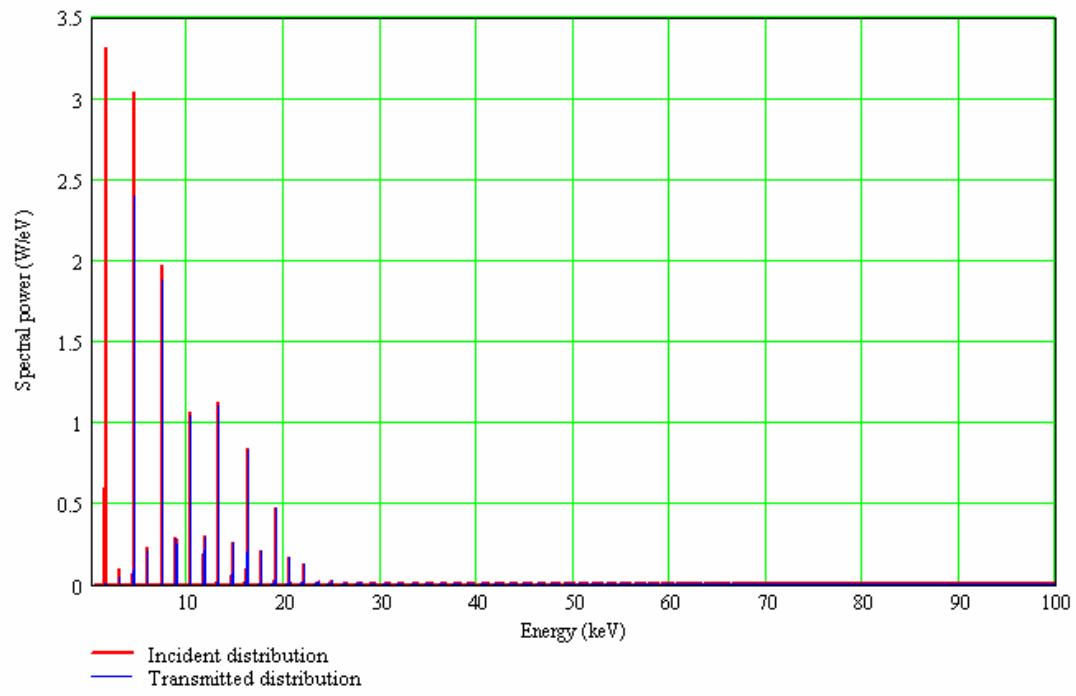

Figure 2.19 Spectral power distributions before and after Be conductance limiter. (Be density = 1850kg/m^3, foil thickness 200 μm).

2.4.3.8 Module 6 - High Heat Load Monochromator (HHLM)

Distance to center of undulator	30.4m

This will be the primary monochromator on the beamline using liquid nitrogen cooled silicon (111) crystals operating with a fixed offset of 20 mm over an energy range of 4 to 24 keV. The energy is changed by rotating the two crystals around a common axis centered on the first crystal surface plane; the output beam height is kept constant by allowing the gap between the faces of the first and second crystal to change (range of motion <1.5 mm) and the beam to "walk" along the surface of a long second crystal. Eliminating the longitudinal translation on the second crystal and replacing it with a long crystal greatly improves ease of tuning energy as well as stability, since the second crystal is more rigidly mounted. Final alignment of the lattice planes of the first and second crystals is achieved with stepper motor-driven actuators for the roll (rotation axis = horizontal axis along the beam), pitch (rotation axis = horizontal axis perpendicular to the

beam) and yaw (rotation axis = vertical axis perpendicular to the beam) adjustment of the second crystal plus a piezoelectric device for the fine pitch and roll adjustment.

Thermal and vibration stability will be of primary importance in this monochromator design. The liquid nitrogen cooling needed to maintain the thermal distortions at acceptable levels has the potential for introducing unacceptable vibration. Managing vibration issues at the level suitable for a nano focus beamline will require research and development effort, including prototypes, and therefore will increase the cost of the final instrument.

The preliminary cooling design for extracting the absorbed heat load is based on the indirect crystal cooling arrangement (similar in principle to that widely used at SPring-8). Since the incident heatload is relatively low, and to improve vibration stability, short lengths of copper braid will be used to connect the liquid nitrogen coolant pipe to the copper blocks. To provide a good thermal contact, indium foil is used between the sides of the silicon crystal and copper blocks. The indium foil has a secondary benefit of absorbing the differential expansion between the copper blocks and silicon crystal and limits the resulting stress and strain transmitted to the silicon at low temperatures. To determine the crystal displacement due to the thermal heat load, an FEA model of the crystal was run. This report shows the FEA results for the silicon crystal only. Element sizing can be characterized as fine to very fine, especially around a heat-loaded area and regions considered susceptible to high-stress concentrations.

To apply the thermal load, a small area has been projected onto the optical surface representative of the beam footprint with an applied heat flux 4.53E+6 W/m^2 (equivalent to 80.7 W – maximum heat load transmitted from upstream mirror, see Section xx) to simulate the total thermal load absorbed. Figure 2.6 showed that variation of the horizontal and vertical power densities over the beam footprint are not significant; therefore, using a uniform heat loading for the FEA model is a valid assumption.

Convective cooling was applied to the cooled contact area between the crystal and the cooled copper heat exchangers. Based the Dittus-Boelter correlation, the heat transfer coefficient through the coolant pipes is given by:

Reynolds number, Re

The Reynolds number is given by:

$$\mathrm{Re} = \rho \cdot \left(\frac{V}{\pi \cdot \left(\frac{D_h}{2} \right)^2} \right) \cdot \left(\frac{D_h}{\mu} \right), \tag{2-9}$$

where

ρ = coolant density (795.52kg/m^3 for liquid nitrogen),

V = volumetric flow rate (4 L/min),

D_h = hydraulic diameter (10 mm), and

μ = dynamic viscosity (0.001465 poise for liquid nitrogen).

Substitute known values and calculate the Reynolds number.

$$\mathrm{Re} = \left(795.52 kg / m^3\right) \cdot \left(\frac{4\, litres/\min}{\pi \cdot \left(\frac{10mm}{2}\right)^2} \right) \cdot \left(\frac{10mm}{0.001465\, poise} \right) = 46092.7 \,. \tag{2-10}$$

Prandtl number, Pr

The Prandtl number is given by:

$$\mathrm{Pr} = \mu \cdot \left(\frac{Cp}{K} \right), \tag{2-11}$$

where Cp = specific heat (2048.2J/kg K for liquid nitrogen) and K = thermal conductivity (0.14086W/m K for liquid nitrogen). Substitute known values and calculate the Prandtl number.

$$\mathrm{Pr} = \left(0.001465\, poise \cdot\right) \left(\frac{2048.2 \frac{J}{kg \cdot K}}{0.14086 \frac{W}{m \cdot K}} \right) = 2.1 \tag{2-12}$$

Nusselt number using the Dittus-Boelter correlation, Nu

For fully developed turbulent flow in smooth tubes, the Nusselt number is defined as:

$$Nu = 0.023 \cdot \mathrm{Re}^{0.8} \cdot \mathrm{Pr}^{0.3} \,. \tag{2-13}$$

Substitute known values and calculate the Prandtl number.

$$Nu = 0.023 \cdot \left(46092.7\right)^{0.8} \cdot \left(2.1\right)^{0.3} = 155.3 \tag{2-14}$$

Heat transfer coefficient through cooling channels, HTC

The heat transfer coefficient is defined as:

$$HTC = \frac{K \cdot Nu}{D_h} \,. \tag{2-15}$$

Substitute known values and calculate heat transfer coefficient.

$$HTC = \frac{\left(0.14086 \frac{W}{m \cdot K}\right) \cdot \left(155.3\right)}{\left(10mm\right)} = 2187.5 \frac{W}{m^2 \cdot K} \,. \tag{2-16}$$

With the inclusion of thermal contact resistance, the effective heat transfer coefficient on the crystal contact surface is given by:

$$HTC = \left[\frac{1}{fa \cdot HTC_0} + \sum R(Cu) + \sum R(In) + Rc \right]^{-1}, \tag{2-17}$$

where

fa = ratio of cooling channel surface area and contact surface area,

HTC_0 = heat transfer coefficient of the coolant in the cooling channels (0.83W/cm^{2}K),

$\sum R(Cu)$ = sum of the thermal conduction resistances in the copper,

$\sum R(In)$ = sum of the thermal conduction resistances in the indium and

Rc = thermal contact resistance at the interface.

As the thermal conductivity of silicon is high at cryogenic temperatures, it is useful to increase the contact surface area by oversizing the crystal height to improve heat transfer (crystal length is limited to prevent interference with the diffracted beam off the second crystal). The ratio of cooling channel surface area and contact surface area is given by:

$$fa = \frac{\text{cooling channel surface area}}{\text{contact surface area}} = \frac{6283.185 mm^2}{7000 mm^2} \approx 0.9 . \tag{2-18}$$

For thicknesses of copper and indium of 3 to 11 mm and 0.5 mm, respectively, the thermal conduction resistance through a single thickness takes the following values:

$$R(Cu) = \begin{pmatrix} 0.75 \\ 2.75 \end{pmatrix} \times 10^{-5} \, m^2 \cdot K \cdot W^{-1} , \tag{2-19}$$

and

$$R(In) = 0.62 \times 10^{-5} \, m^2 \cdot K \cdot W^{-1} . \tag{2-20}$$

Depending on the surface finish, the thermal contact resistance at the interface takes the following values:

$$Rc = \begin{pmatrix} 1 \\ 20 \end{pmatrix} \times 10^{-5} \, m^2 \cdot K \cdot W^{-1} . \tag{2-21}$$

The cooling arrangement includes three copper and two indium interfaces. We substitute known values and calculate heat transfer coefficient at contact surface:

$$HTC = \left[\frac{1}{(0.9) \cdot \left(2187.5 \frac{W}{m^2 \cdot K} \right)} + 3 \times \begin{pmatrix} 0.75 \\ 2.75 \end{pmatrix} \times 10^{-5} \frac{m^2 \cdot K}{W} + 2 \times 0.62 \times 10^{-5} \frac{m^2 \cdot K}{W} + \begin{pmatrix} 1 \\ 20 \end{pmatrix} \times 10^{-5} \frac{m^2 \cdot K}{W} \right]^{-1} \tag{2-22}$$

$$HTC \approx \begin{pmatrix} 1804.4 \\ 1243.5 \end{pmatrix} \frac{W}{m^2 \cdot K}. \tag{2-23}$$

For the FEA model, with the inclusion of thermal contact resistance, the effective heat transfer coefficient on the crystal contact surface has been reduced to 1,200 W/m^2 K. An estimation of the bulk temperature at the contact surface between the crystal and the heat exchanger is given by:

$$T_{crystal\_holder} = \frac{\Delta Q_{Cu}}{K_{Cu}} \cdot \frac{L}{S} \cdot + T_{heat\_exchanger} = \frac{80.7W}{500W/m \cdot K} \cdot \frac{20mm}{300mm^2} + 78K \approx 89K\,, \tag{2-24}$$

where

ΔQ = power dissipated through the copper braids (80.7W),

K_{Cu} = thermal conductivity of copper (500W/m K at cryogenic temperatures),

S = effective section area of braid (300mm^2),

L = braid length (20mm),

$T_{crystal\_holder}$ = temperature at interface between crystal and holder, and

$T_{heat\_exchanger}$ = temperature of liquid nitrogen coolant (78K).

To ensure good thermal contact between the cooled copper block and the silicon crystal, a contact pressure is applied to the side of the copper block, pushing it inward against the silicon crystal. Contact pressure has been set at 350 kPa; this value of contact pressure is based on an approximate relationship of 100 Pa per sq mm of contact area.[6]. This is based on a contact area of 70 mm x 50 mm.

Table 2.13 Summary of Loads Applied to FEA Model.

Case description	E=24 keV	
Thermal model loading	Beam size:	2.26 mm (h) x 0.65 mm (v)
	Heat flux loading:	4.53E+6 W/m^2
	Convection cooling:	HTC = 1200 W/m^2 K
		Bulk temperature = 89 K
Structural model loading	Results from the thermal model are loaded into a structural model, with restraints applied to allow free expansion.	
	Clamping pressure:	350 kPa

Previous thermal analysis of monochromator crystals has shown that the primary design case for selecting the crystal design is generally fixed by the optical performance at the higher energies as a result of the narrower rocking curve widths. The results from the FEA case modeled at 24 keV are shown in Figure 2.20.

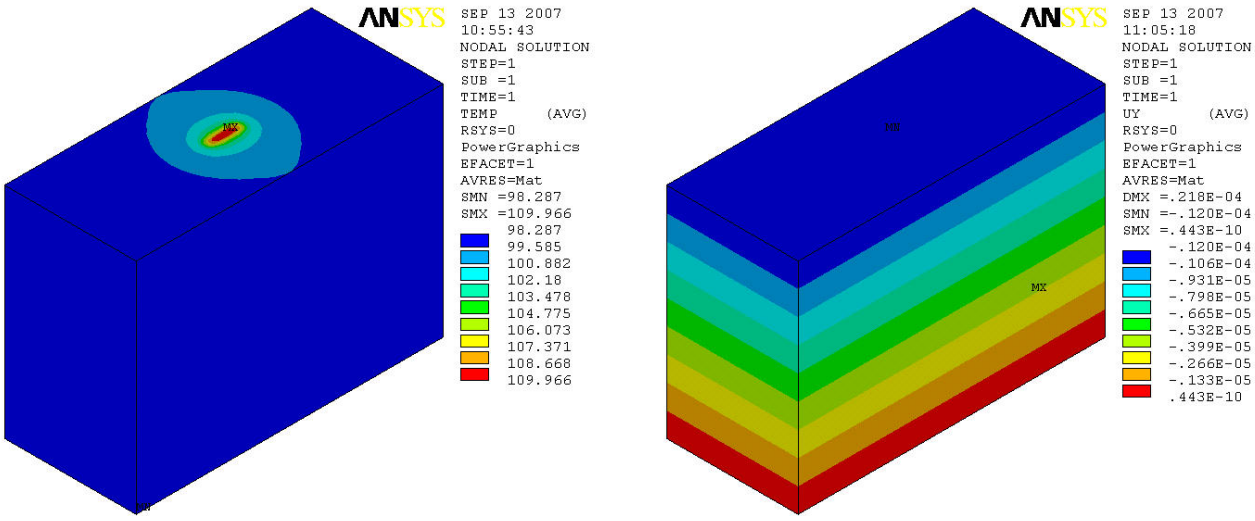

Figure 2.20. Temperature (K) and displacement (m) distribution (left and right, respectively).

To achieve an efficient photon flux transmission at the second monochromator crystal, the slope error on the first crystal should be a fraction of the rocking curve width. Since the rocking curve width is a function of energy, then the slope error for the crystal will also be dependent on the beam's energy. We use this as a basis for a conservative calculation for the first crystal's optical performance. The rocking curve width is the FWHM value for the curve that defines the peak shape on rocking the crystal in the diffracted beam. Assuming a Gaussian curve form, a relative distribution can be determined using the FWHM value. Any slope error on the first crystal surface will result in a shift of this distribution. The quantity of beam reflected is defined by the region shared by the relative distributions, as shown in Figure 2.21. For silicon (111) at 24 keV, the rocking curve width is 11.6 µrad. Based on an integrated reflectivity of 70%, the maximum allowable slope error has been calculated at 3.8 µrad. Approximately 92% of the tangential beam footprint has been shown (Figure.22) to be under the 3.8 µrad slope error limit.

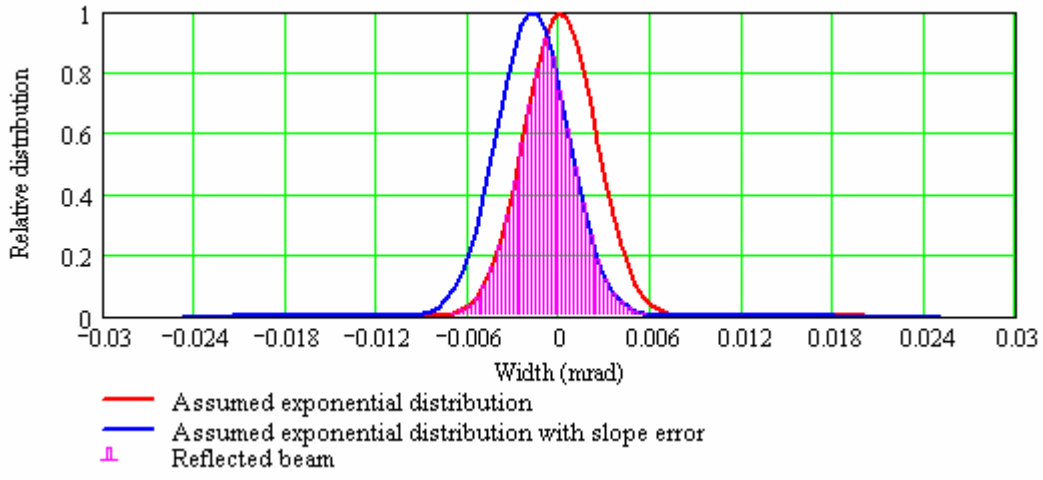

Figure 2.21 Relative distributions with slope error shift.

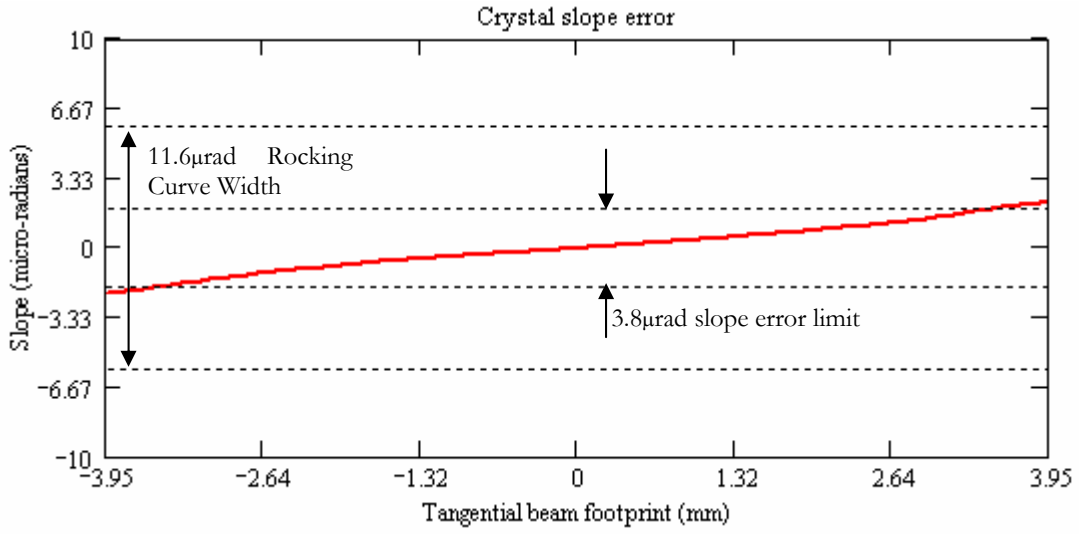

Figure 2.22 Slope profile of the first crystal with white beam incident at 24 keV.

Motion Specification. The origin for each axis will be set at the beamline source point, with the axis arrangement following the right hand rule (see Figure2.23). Some notes are provided below.

- The x-axis will be horizontal and perpendicular to the beam, in the direction away from the ring (outboard).
- The y-axis will be vertical.
- The z-axis will be horizontal and parallel with the beam, in the direction of propagation of the x-ray beam.

All rotations about a given axis are positive if, when looking along the axis in the positive direction, the rotation is clockwise.

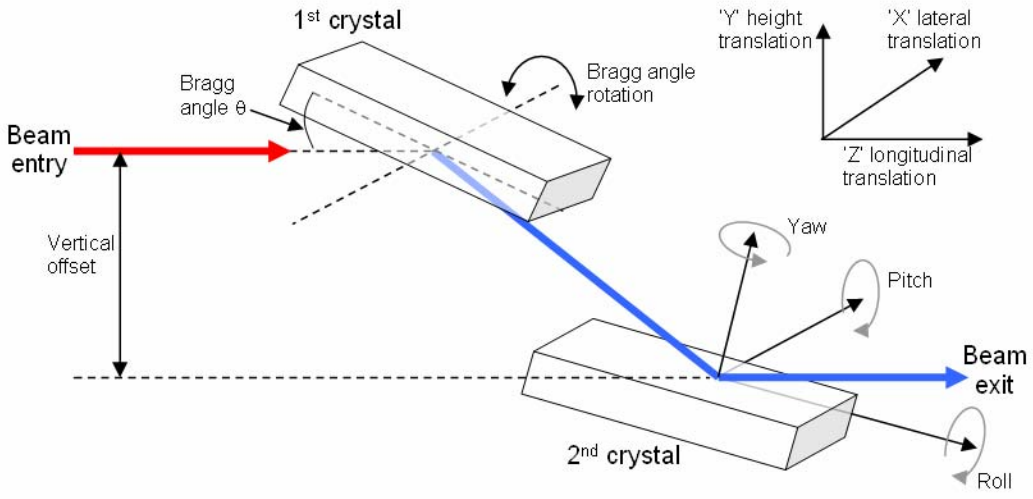

Figure 2.23 Schematic illustration of axis and angle convention.

Table 2.14 details the required motion specification for the HHLM assembly.

Table2.14 Motion Specification.

Motion	Range	Resolution	Drive system
Primary drive			
Bragg angle	-5° to 30°	<1 μrad	In vacuum stepper motor driven.
Support system			
Manual pitch (rotation about x axis)	±1°	<0.25°	System alignment.
Manual roll (rotation about y axis)	±1°	<0.25°	System alignment.
Manual yaw (rotation about z axis)	±1°	<0.25°	System alignment.
Manual lateral (x direction)	±10 mm	<250 μm	System alignment.
Manual height (y direction)	±10 mm	<250 μm	System alignment.
Manual longitudinal (z direction)	±10 mm	<250 μm	System alignment.
First crystal adjustment			
Manual roll (rotation about y axis)	±1°	<0.01°	Crystal alignment.
Manual perpendicular (Y)	±1 mm	<10 μm	Crystal alignment.
Second crystal adjustment			
Motorized coarse pitch (rotation about x axis)	±1°	<5 μrad	In vacuum stepper motor driven.
Motorized fine pitch	200 μrad	<0.05 μrad	In vacuum piezo driven.
Motorized coarse roll	±1°	<5 μrad	In vacuum stepper motor driven.
Motorized fine roll	200 μrad	<0.05 μrad	In vacuum piezo driven.
Motorized coarse yaw (rotation about z axis)	±1°	<5 μrad	In vacuum stepper motor driven.
Motorized perpendicular (to keep fixed offset)	±2 mm	<1 μm	In vacuum stepper motor driven.

2.4.3.9 White Beam Monitor (WBM)

Distance to center of undulator	30.9 m

The retractable White Beam Monitor (WBM) is a combined viewing screen and total intensity monitor for white beam (mirror in) and pink beam (mirror out), positioned directly downstream of the HHLM. It consists of a tungsten screen that is electrically isolated, water cooled, and phosphor coated. The total white and peak beam can be monitored by measuring the photo current. The beam can be visually monitored by locating a UHV window that allows a video camera to see the screen. This device will allow the position of five upstream components in succession to be optimized: 1) FEDPM, 2) FEHAM, 3) WBS, 4) HFM, and 5) HHLM. Once the alignment is complete, the WBM is retracted from the beam with a pneumatic actuator.

2.4.3.10 Bremsstrahlung Collimator (BC)

Distance to center of undulator	31.4 m

The Bremsstrahlung Collimator (BC) acts directly to restrict the size of the bremsstrahlung fan downstream. The use of external clad lead for this collimator is much less expensive than vacuum-prepared tungsten and makes best use of the limited space around this cramped area. The lead bremsstrahlung shield will comprise specially made interlocking bricks with no direct line of sight (shine path) permitted through any interspaces between the bricks. The lead will be security fastened in place to prevent removal and also will be clad in stainless steel sheet metal or Perspex covers. Connection of this standalone component is made to the beamline by flexible bellows at both entrance and exit.

The collimator is classified as a critical survey item which must not be moved once it has been set and aligned.

2.4.3.11 Monochromatic Fluorescent Screen (MFS)

Distance to center of undulator	31.9 m

The Monochromatic Fluorescent Screen (MFS) is a retractable YAG fluorescent screen that will allow the monochromatic beam to be viewed with a CCD camera for initial monochromator setup. Once the alignment is complete, the MFS is retracted from the beam with a pneumatic actuator.

2.4.3.12 Secondary Horizontal Source Aperture (SHSA)

Distance to center of undulator	32.0 m

The SHSA is an adjustable horizontal monochromatic slit intended to act as a backup secondary coherent source. The slit blades will be electrically isolated so the photo current can be measured from each blade. This will allow the SHSA to also function as a horizontal beam position monitor that can be used in a feedback mode with the HFM piezo yaw actuator.

2.4.3.13 Monochromatic Shutter (MS1)

Distance to center of undulator	32.5 m

This is a standard monochromatic shutter located close to the back wall of the optics enclosure.

2.4.3.14 Back Wall (BW)

Distance to center of undulator	33.0 m

2.4.3.15 Optics Enclosure - Incident Power Loads

Table 2.15 Summary of the Incident Heat Loads along the Optical Components within the FOE.

Component	Source Point distance	Beam size	Incident power	Transmitted power
Module 1				
Front End Differential Pump Mask (FEDPM)	14 m	1.1 mm (h) x 0.3 mm (v)		130.6 W
Front End Defining Aperture Mask (FEDAM)	1 5 m	0.3 mm (h) x 0.3 mm (v)		35.7 W
Shield Wall	26.7 m			
Module 2 Notes: Front end aperture set to 1.1 mm (h) x 0.3 mm (v)				
White Beam Filters (WBF)	27.3 m		130.6 W	
Filter thickness (μm)				
30				125.2 W
300				107.8 W
1000				87.1 W
Module 3 Note: All white beam filters removed from x-ray beam.				
White Beam Slits (WBS)	27.8 m		130.6 W	130.6 W →0 W
Module 4 Note: White beam slits open.				
Horizontal Focusing Mirror (HFM)	28.8 m		130.6 W	
reflective strip				
silicon				30.9 W
rhodium				80.7 W
Module 5 Note: Rhodium reflective strip selected on upstream mirror.				
Conductance Limiter Beryllium Window (CLBW)	29.6 m		80.7 W	75.9 W
Module 6 Note: Conductance limiter beryllium window removed from x-ray beam.				
High Heat Load Monochromator (HHLM)	30.4 m		80.7 W	0 W

2.3.6 Radiation Enclosure Design

There are several high-quality vendors for radiation hutches in Europe, as follows:

Calder-UK

Caratelli- France

Innospec-Germany

These suppliers have carried out detail design and build of radiation hutches at DLS, ESRF, SLS, and Soleil. Some of the issues the vendors need to consider are as follows:

- FOE enclosure is required to be designed as white beam enclosure.
- Stations A and B are required to be mono beam enclosures.
- The minimum shielding thickness will be in accord with NSLS-II documents.
- All the doors will be sliding doors – double for equipment and single for personnel.
- All standard enclosure heights will be 3.2 m.
- The roof of each enclosure will be surrounded by a railing to permit safe personnel access.
- Convenient access to the roof areas on the FOE, Station A, and Station B is via three access ladders.

2.4.4 Instruments

2.4.4.1 Endstation 1

Discussion of the endstation specifications and requirements is still under development.

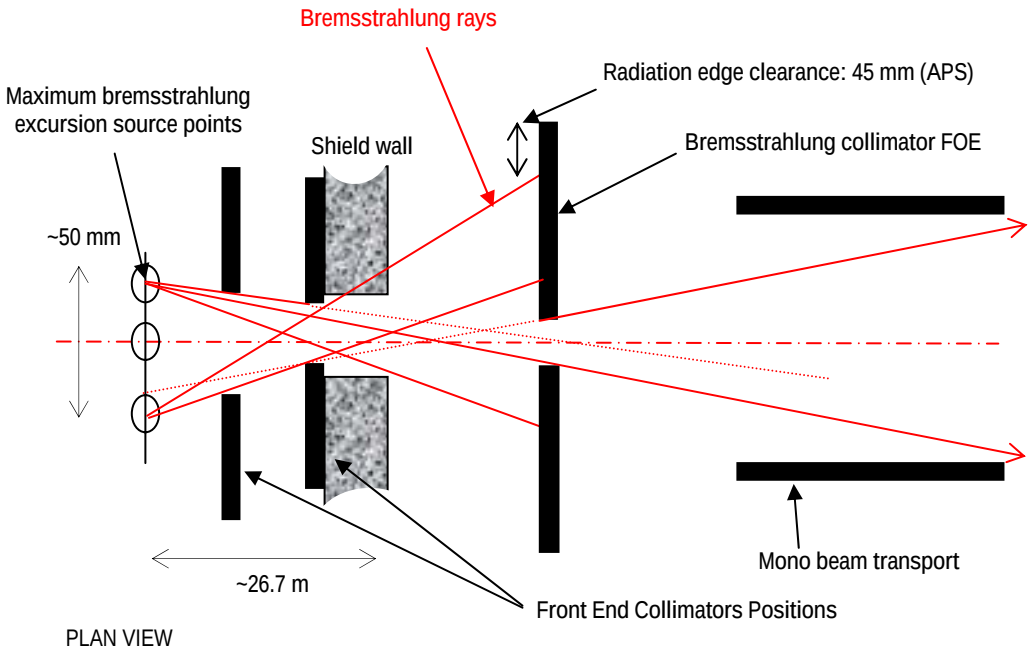

Figure 2.24. Type of bremsstrahlung anamorphic ray diagram required for effective safe beamline design.

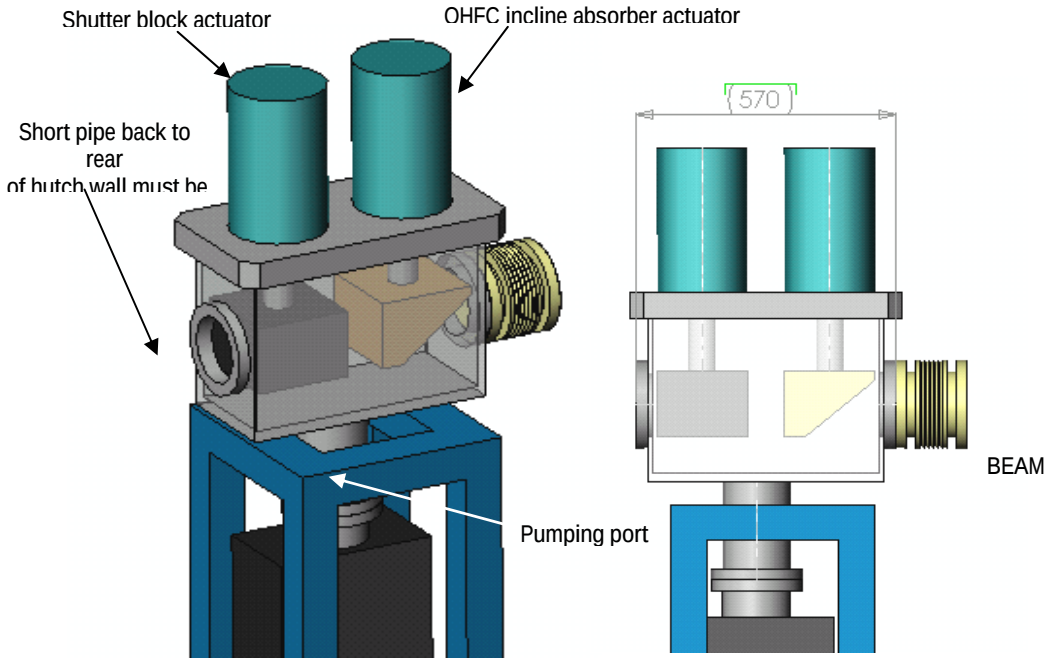

Figure 2.25 Integrated bremsstrahlung/thermal stop shutter.

2.5.3 Equipment Protection System

A Beamline Equipment Protection System (EPS) will also be required: The following table shows the preliminary fault protection logic for the beamline. The EPS protects against damage or failure due to beam heating and inadvertent vacuum let-up.

Component	Type	Action	Consequences
19-A (FOE)			
19-VALV	valve	open requested	opens valve if IMG1 ok
		close requested	closes if FE shutter closed
		air pressure fault	closes FE shutter
19-IMG01	vacuum pressure	trips high	closes FE shutter closes VALV-01 & VALV-02
19-IONP01	ion pump	on requested	turns on if IMG1 ok
19-FILT1/2/3/..	Incident Power Filter	water trips low	closes FE shutter & absorber
19-IONP02	ion pump	on requested	Turns on if IMG1 ok
19-HS1	White Beam horizontal slit	water trips low	closes FE shutter & absorber
19-VS1	White Beam vertical slit	water trips low	closes FE shutter & absorber
19-HS2	White Beam horizontal slit	water trips low	closes FE shutter & absorber
19-VS2	White Beam vertical slit	water trips low	closes FE shutter & absorber
19-VALV01	gate valve	open requested	opens valve if IMG1+IMG2 ok
		close requested	closes if FE shutter closed
		air pressure fault	closes FE shutter
19-IMG	vacuum pressure (HM mirror tank)	trips high	closes FE shutter & absorber VALV02 & 01
19-IMG	vacuum pressure	trips high	closes FE shutter closes VALV-02
19-HM	horizontal mirror	water trips low	closes FE shutter & absorber
19-IONP02	ion pump	on requested	turns on if IMG02 ok
19-VALV02	valve	open requested	opens valve if IMG2+IMG3 ok closes if FE shutter closed
		close requested air pressure fault	closes FE shutter
19-IMG	vacuum pressure	trips high	closes FE shutter closes VALV-02
19-BW1	Be window conductance limiter	water trips low	closes FE shutter & absorber
19-HHM	high heat load monochromator	water trips low	closes FE shutter & absorber
19-IONP04	Ion pump	on requested	Turns on is IMG03 ok
19-WBM	white beam monitor	LN2 trips low	closes FE shutter & absorber
19-STOP1	bremsstrahlung stop	Fixed item Possibly water cooled stop- water trips low	FIXED aperture closes FE shutter & absorber
19-MFS1	monochromatic fluorescent screen	water trips low	closes FE shutter & absorber
19-VALV03	valve	open requested close requested air pressure fault	opens valve if IMG3+IMG4 ok closes if FE shutter closed closes FE shutter
19-IMG04	vacuum pressure	trips high	closes FE shutter closes VALV-03

Component	Type	Action	Consequences
19-SHSA	secondary horizontal source aperture	water trips low	closes FE shutter & absorber
19-IONP05	ion pump	on requested	turns on if IMG04 ok
19-SHUTTER1	monochromatic shutter	open (thru) requested close (stop) requested	opens 19-FE shutter closes 19-FE shutter
19-FOE	back wall for FOE (ID-A)	trips high	closes FE shutter & absorber closes VALV03
19-SBT1	shielded beam transport	on requested	turns on if IMG ok
19-	front wall of hutch (ID-B)		
19-VALV04	valve	open requested close requested air pressure fault	opens valve if IMG4+IMG5 ok closes if FE shutter closed closes FE shutter
19-IMG	vacuum pressure	trips high	closes FE shutter closes VALV-04
19-QDBPM	quad diode BPM		
19-THSA	tertiary horizontal source aperture		
19-IONP	ion pump	on requested	turns on if IMG ok
19-MFS2	monochromatic fluorescent screen		
19-VALV05	valve	open requested close requested air pressure fault	opens valve if IMG5+IMG6 ok closes if FE shutter closed closes FE shutter
19-IMG06	vacuum pressure	trips high	closes FE shutter & absorber closes VALV05
19-IONP07	ion pump	on requested	turns on if IMG06 ok
19-HRM	high-resolution monochromator		
19-BW2	Be window		
19-NFO1	nanometer focusing optics		
19-	back wall of (ID-B)		
19-SBT2	shielded beam transport		
19-	front wall of (ID-C)		
19-NFO2	nanometer focusing optics		

Notes: Vacuum pressure trips using Inverted Magnetron Gauges (IMG) and not Piranis on each gauge cluster

Figure 2.26 is a diagram of the vacuum flow for the HXN beamline. Figure 2.27 is the EPS diagram.

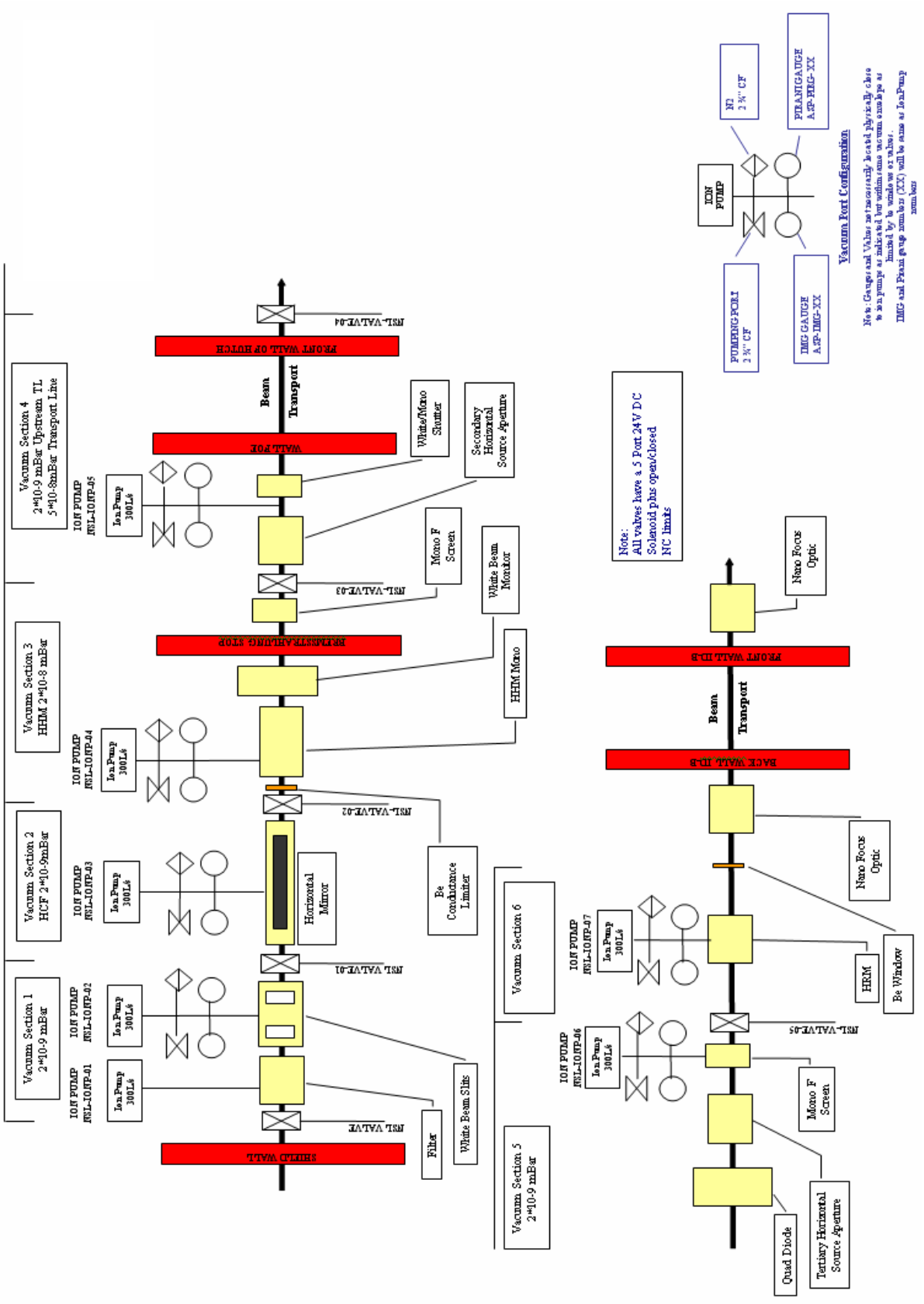

Figure 2.26 Hard X-ray Nanoprobe Beamline Vacuum Flow Diagram

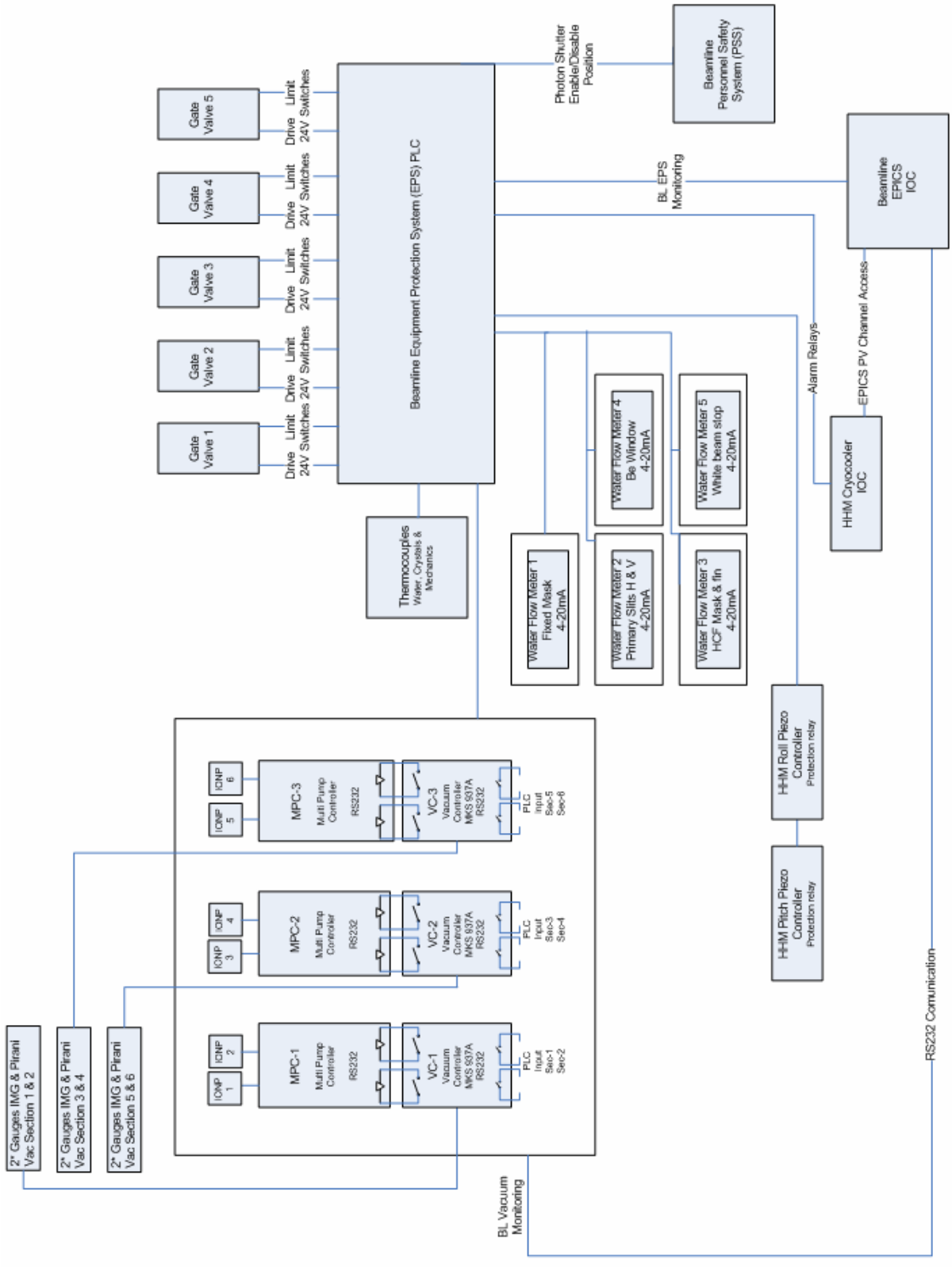

Figure 2.27. EPS Diagram.

2.6 Additional Requirements Imposed on the Conventional Facilities

2.6.1 Vibration Considerations for Synchrotron Beamlines

The beamline vibration is a mammoth subject which ranges from the influence of the distance ocean waves to the local structural resonance. This short discussion has been split in to two sections. The first section addresses vibration sources and the second section presents good engineering design practices.

2.6.1.1 Vibration Sources

Prior to beamline installation it is advisable to characterize the local experimental floor slab. The ambient displacement spectrum will be measured for an extended period of time (>24 h) to increase the likely hood that infrequent vibration sources are observed. NSLS-II should have a sitewide vibration log,, but local structures can affect the results. An example of such a case was a deformed slab at ESRF which, due to the reduced ground contact, increased the displacement amplitude by a factor of 10. The problem was resolved by the injection of grout into the interface.

The vibration source spectrum may be split into three conceptual regions, low-, medium-, and high-frequency. The sources that generate frequencies below 1 Hz (low frequency) tend to be seismic activity, ocean waves, and thermal expansion. The medium-range frequencies (1 – 100 Hz) are generated by machines, pumps, traffic, fluid flow, and mechanical resonances. The high-range (>100 Hz) frequencies are often acoustic, electro-mechanical, and well-designed mechanical resonances.

A proactive approach must be employed when addressing the vibration influence on a beamline. The low-frequency vibration amplitude will be dominated by the quality of the experimental floor and the air conditioning. The associated electron beam and x-ray beam motions may be effectively compensated by the use of closed-loop control systems on the steering magnets and mirrors. The medium-frequency mechanical sources of vibration, such as water chillers or vacuum pumps, should be identified, then moved or isolated. Care must be taken to consider even non beamline components, such as the insertion device (ID) cryostat, or automotive traffic vibrations, which may even be reduced by the removal of speed bumps and drain covers, for example. An instance of a high-frequency vibration source is an optic actuator and the respective support structure stiffness. These effects may often be reduced by the choice of good-quality drive electronics and electrical ground.

2.5.1.2 Good Engineering Design Practices

A wide range of engineering design practices have been empirically developed for synchrotron vibration management. The most basic concept is that only relative motion between the beam and the sample will be detrimental, so all the optics must be mounted from a monolithic floor slab. The most critical components are the mirrors and monochromator. The optical lever arm greatly amplifies vibration effects.

The most common form of vibration isolation within industry is the damping/isolation pad; however, the inherent position instability introduced by an elastic support element can introduce undesirable long-term position drift. For this reason, the optics are usually mounted on stiff supports that are mechanically isolated from their surroundings. Optics are usually mounted on top of a natural or synthetic granite block of high mass and low natural frequency. Granite has good vibration damping properties and a lower thermal expansion coefficient than steel fabrications. The stiffness of the granite may be increased by grouting the block to the floor, although this is often avoided for practical reasons. The upper optic assembly is then designed to be stiff with a high fundamental resonant frequency. Vibration mode analysis and FEA may be used to optimize the design. A high resonant frequency is desirable, as it is less likely to coincide with driving vibration sources and also requires more energy to be driven.

It is possible to extend the high-resonant-frequency philosophy down to the floor. Good results have been achieved using a bolted, lightweight, large cross-section metal structure instead of a massive block. The light

weight and large cross section increase the resonant frequency and the bolted interfaces provide vibration damping.

A number of methods can improve existing mechanical systems, such as the addition of external viscoelastic damping links, which take no mechanical load or tuned dampers.

A closed loop beam stabilization system is commonly employed to effectively lock the beam spot on to the sample position. The signal from a beam position monitor (BPM) is used to drive an upstream mirror or monochromator to compensate for any relative motion via a PID loop. The effectiveness of a closed-loop beam position system to remove vibration reduces as the detrimental frequency rises. In general, the greater the feedback loop frequency the higher the threshold for vibration compensation. A high-frequency, closed-loop beam position system typically runs at ~1 kHz.

It is possible to tune some unavoidable vibration sources to reduce their effect on the beam position. The pump speed and pressure of cryo-coolers may be adjusted to minimize beam influence. Software notch filters may be added to the motion control system to avoid known resonant frequencies.

In summary, vibration will be considered at each stage of beamline design installation and commissioning.

2.6.1.3 Choosing an Optical Top or Breadboard

The broadband damping characteristics are possibly the most important table specification to consider. Tables may employ tuned damping systems; however, these will become invalid as the load mass and location change. The broadband damping may be achieved with oil-based systems or solid dampers. The solid option is preferable, because oil characteristics can change over time and there is the possibility of an oil reservoir being pierced.

The current state-of-the-art system is the TMC Maximum Dry Damping, the performance of which is presented below. TMC offer their leading technology in a range of sizes, all using CleanTop II technology, which insures that fluids are not able to enter the table interior.

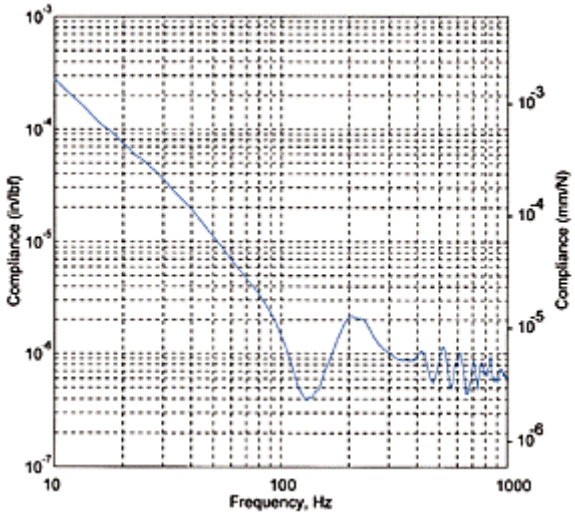

The TMC optical table top can be combined with their cutting edge STACIS active vibration cancellation system. The STACIS system provides a stiff mounting system that effectively reduces vibration in the range from 0.6 – 250 Hz. It was designed for precision microlithography and metrology. Example performance curves are given below.

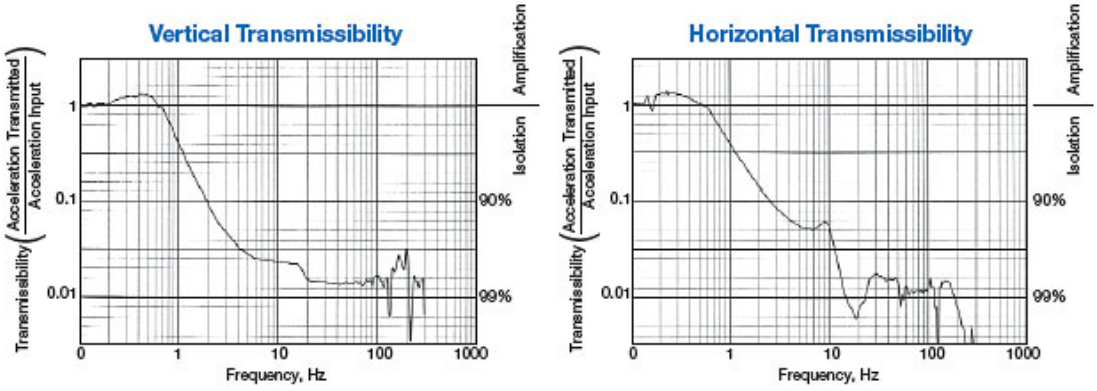

2.7 Additional Requirements Imposed on the Accelerator Systems

The current stability goals for the accelerator performance are sufficient for this beamline.

References

1 K. J. Kim, Angular Distribution of Undulator Power for an Arbitrary Deflection Parameter K, *Nuclear Instruments and Methods in Physics Research,* A246 (1986) 67-70.

2 *LS 237: Explosion Bonding of Dissimilar Materials for Fabricationg APS Front End Components—Analysis of Metallurgical and Mechanical Properties and UHV Applications,* Yuheng Li, Deming Shu, and Tuncer M. Kuzay, Experimental Facilities Division.

3 D. Shu et al. (1995). Precision white-beam a list design for high power density x-ray undulator beamlines at the APS. *Rev. Sci. Instr* **66**(2) Feb 1995.

4 M. Rivers et al. GSECARS Report, First Results from the Sector 13 (GSECARS) Undulator Beamline.

5 B. Fell, K. Fayz, Experimental Investigation of Thermal Contact Resistance for Indirectly Cooled SR Optics, MEDSI 2000.

6 Cryogenic cooling monochromators for SPring-8 undulator beamlines, *Nuclear Instruments and Methods in Physics Research A 467-468 (2001) 647-649.*

2-A Appendix A: Optical Study

2.A.1 Optics Overview

This section presents an overview of the proposed optics plan. It follows the ideas presented in the December 2006 NSLS-II CDR and suggests additional modes. Determining an optics plan for this beamline is complicated by the fact that the required final optics for achieving 1 nm do not yet exist. The uncertainty associated with the optics requires that the beamline be designed with sufficient flexibility to provide the necessary contingency to accommodate an eventual optics solution. The challenge is to provide this flexibly without paying an excessive cost premium or the need to rebuild / replace components, allowing on budget and on time completion of the beamline. The following optics plan incorporates this flexibly and controls risk by utilizing well understood front end and FOE optics components to deliver the x-ray beams generally required for illuminating any successful nano-focusing optics.

The plan is based on two focal points – one at 41 m and the other at 76 m – both supplied by a common set of upstream optics located in the front end and FOE. At each of these two locations a hutch would be constructed that is capable of housing the necessary end station equipment to support the scientific goals of the beamline. The exact location of these hutches will be determined by a number of factors such as the characteristics of the final nano-focusing optics and details involving conventional facilities (floor space, roof line, egress, utilities, etc.). One way to look at this proposed layout is to consider the 41 m hutch a 1x location and the 76m hutch a 2x location with regard to beam demagnification. Operationally, the focused x-ray beam can be used in only one hutch at a time. A beam stop located at the back wall of the upstream 1x hutch would provide access to the downstream 2x hutch while beam is present in the 1x hutch. Access to the 2x experimental location during x-ray operation of the 1x location will allow off line work to be performed using the end station equipment. Given the sophistication and complexity of a nanoprobe end station, this will provide valuable access time for instrumentation development and debugging as well as experiment setup.

The 1x/2x hutch arrangement will play a key role during the early operation phase of the project when the main activity will be optics testing and commissioning. During this initial phase and well before the 2x hutch (and transport to it) is completed, the 1x location will serve as an early test sight where various optics approaches can be evaluated and refined for eventual use in the push to 1 nm in the 2x hutch. There also exists the possibly of achieving a 1nm focal spot at the 1x location if modes such as a wave guide coupled aperture prove feasible. The two locations can also be instrumented with complimentary end station equipment such as a full-field imaging system in the 1x location providing flexibly and agility in meeting the demands of the user science program.

Below, five optics modes are presented – two for the 76m 2x location and three for the 41m 1x location. The five modes are:

- direct focusing at 76 m
- compound horizontal focusing at 76 m
- waveguide mode at 41 m
- direct mode at 41 m
- compound horizontal KB focusing mode for full-field imaging at 41 m.

The proposed support optics will be used to configure these five modes and are general enough to provide additional operation modes if necessary. They are also well understood today regarding both performance and cost. The order of presentation in this document follows the flow of the x-rays from the storage ring to the sample. The components common to all five modes will be presented first followed by discussion of each mode.

2.A.2 Critical Optics Components

In this section we discuss only optical components of primary importance to the five operation modes. For a complete component description of the please see full beamline description.

2.A.2.1 Storage ring and Insertion Devices

The first optical component to be considered in a beamline plan is the storage ring and insertion device. For this report we used the source parameters found in the NSLS-II July 2007 user workshop report. The values used are listed in Table 2.A.1 for a low-beta straight. The NSLS-II U19, 3m long undulator is an excellent source of hard x-rays. It has the advantage of effectively utilizing the storage ring's brilliance and producing hard x-rays from 2 to 30 keV that are well matched to the required optics.

2.A.2.2 Front End Fixed Mask (FEFM) and Differential Pump (DP)

This power limiting mask will allow approximately 90% of the undulator harmonic (at 1 Å) to pass, reduces the total power to a level that is more manageable by the downstream components and protects against miss-steered of the electron beam. It will be located behind the shield wall as close to the undulator as possible (~14 m) with the next component (horizontal source aperture) directly downstream. The vertical and horizontal location of this critical component will be defined through survey with additional motorized horizontal positioning over a restricted range to aide the initial alignment of the orbit (its front end location will make it difficult to access manual adjustors.) Due to its location and size this component is ideal for acting as the vacuum conduction limiting aperture for a differential pump, freeing up space in the FOE. See power management report section for thermal performance analysis.

2.A.2.3 Front End Adjustable Horizontal Source Aperture (FEHA)

This adjustable horizontal mask at ~ 14.5 m will allow the horizontal beam size to be restricted to match the effective vertical coherent source size during nano-focusing. The aperture can be opened to match the FEFM horizontal size for full-field operation mode. The aperture will be constructed as two wedges with one motor adjusting the aperture size and the other it's horizontal position. See power management report section for thermal performance analysis.

2.A.2.4 Horizontal Focusing Mirror (HFM)

This will be a flat horizontally deflecting mirror located at 28.8 m used for power management and as a horizontal focusing element for compound horizontal focusing modes. It will be water cooled with a two moment bender. The mechanical bender will allow the mirror figure to be corrected for thermal bump when producing unfocused beams as well as allow the horizontal beam to focused either directly onto the sample or over a ranged of secondary horizontal source locations from 3.2 to 9 m, resulting in demagnifications from 9 to 3.3. In compound horizontal KB focusing mode for full-field imaging at 41m nearly the full horizontal source can be collected and focused onto the sample using this mirror. The mirror will be fabricated from silicon have an active length of approximately 600 mm, coated over ½ its width with Rh and operate from 0 – 3 mrad. At its maximum incidence angle (3 mrad) working off the Rh stripe it will have an entrance aperture of 1.8 mm with an energy cut off of approximately 20 keV and capable of collecting 89% of the full horizontal undulator source. With a ½ Rh coating the bare silicon stripe can be used to achieve higher harmonic rejection for low energy operation.

Table 2.A.1 Source Parameters from NSLS-II July 2007 User Workshop.

	Based on July 2007 Workshop
Electron Energy	$E = 3GeV$
Stored Current	$I = 500\ mA$
Electron Beam Emittance	
Horizontal	$\varepsilon_x = 0.55\times10^{-9}\, m-rad$
Vertical (1.5% Coupling)	$\varepsilon_y = 8.25\times10^{-12}\, m-rad$
Betatron Function§	
Horizontal	$\beta_x = 1.5m$
Vertical	$\beta_y = 0.8m$
Electron Beam Size§	
Horizontal	$\sigma_x = 28.7\mu m$
Vertical	$\sigma_y = 2.57\mu m$
Electron Beam Divergence§	
Horizontal	$\sigma_x^{'} = 19.2\mu rad$
Vertical	$\sigma_y^{'} = 3.21\mu rad$
Intrinsic Photon Size*	$\sigma_r = 1.95\mu m$
Intrinsic Photon Divergence*	$\sigma_r^{'} = 4.08\mu rad$
Total Photon Source Size§*	
Horizontal	$\sum_x = 28.8\mu m$
Vertical	$\sum_y = 3.2\mu m$
Total Photon Source Divergence§*	
Horizontal	$\sum_x^{'} = 19.6\mu rad$
Vertical	$\sum_y^{'} = 5.19\mu rad$

§ = Low b straight.

*Quantities evaluated for 12.4 keV x-rays and a 3m long undulator.

2.A.2.5 High Heatload Monochromator (HHM)

This will be the primary monochromator on the beamline located at approximate 30.4 m, with LN2 cooled Si 111 crystals operating with a fixed offset of 20 mm over an energy range of 4 – 24 keV. The fixed offset will be maintained by allowing the gap between the faces of the first and second crystal to change (range of motion < 1.5 mm) and the beam to walk along the surface of a long (115 mm) second crystal. Eliminating the

"z-stage" on the second crystal and replacing it with a long crystal greatly improves ease of tuning energy as well as stability since the second crystal is more rigidly mounted. Thermal and vibration stability will be of primary importance in this monochromator design. The direct LN2 cooling needed to maintain the thermal distortions at acceptable levels has the potential for introducing unacceptable vibration. Managing vibration issues at the level suitable for a nano focus beamline will require R&D effort and prototypes resulting in additional cost. See power management report section for thermal performance analysis.

2.A.2.6 Secondary Horizontal Source Aperture (SHSA) + BPM

This is a high quality monochromatic aperture located at 32 m and adjustable horizontal. It will provide a secondary horizontal coherent source as well as a horizontal beam position monitor that can be used in a feedback mode with the HFM PZT pitch actuator. It will be of a relative open and center position type. The blades will be electrically isolated so that the photo current can be measured from each blade.

2.A.2.7 Quad Diode BPM (QDBPM)

This device located at 37.5 m and just inside the upstream wall of the 1 x experimental hutch. For this device the x-ray beam is incident on the face of a 1 micron thick foil generating x-ray florescence that is collected by vertical and horizontal pairs of diodes. As the beam moves on the face of the foil the solid angle of the florescence intercepted by each diode changes. The beam position is determined by computing the difference over the sum of the diode pairs. The foils are mounted on a filter wheel with six positions (one left empty) so that foil with an edge close to the beam energy can be used. Since both vertical and horizontal position information is available this device can be used in a closed loop feedback mode with the PZT's (pitch and roll) of the monochromator and or the horizontal mirror pitch PZT. This closed loop feedback can be used to stabilize the beam position. The QDBPM will be mounted on a vertical translation stage supported off the same structure as the tertiary horizontal source aperture (THSA) – see next item.

2.A.2.8 Tertiary Horizontal Source Aperture (THSA)

This is a high quality aperture located at 37.8 m that will be used to control the size of the horizontal source image produced by the HFM when operating in horizontal compound focusing mode. It will be of a relative width and center slit type with sufficient range to follow the horizontal deflected beam.

2.A.2.9 High-Resolution Monochromator (HRM)

The high-resolution monochromator located at 39 m will operate in a back scatter geometry (first crystal downstream of the second crystal) to achieve the energy resolution required for nanometer size beams. It will consist of diamond 111 crystals allowing use of higher order reflections to cover the required energy range. The crystals will be mounted on a water cooled heater stage held at constant temperature using feedback. Each crystal will be mounted on an independent high-resolution rotation stage. The first crystal rotation stage will be fixed and the second will be free to travel on a z stage so that the monochromator can be operated in fixed offset mode.

2.A.3 Optics Modes

In this section we present an analysis of five optics mode. Common to each mode is a working distance of 10 mm. A working distance of 10 mm or less is most likely needed to reach a 1nm goal. Such short working distances will severely limit the space available for items such as detectors and sample viewing optics and will require that the final focusing optic (i.e., MLL, Kinoform lenses) support structure be optimized to reduce their transverse size. Setting the working distance goal as long as 10 mm provides a safety factor should higher demagnifications be required.

The ray trace analysis presented here were conducted using a program written in IDL at the University of Chicago Center for Advanced Radiation Sources that is optimized for large and small KB optics and capable of optimally figuring both straight and tapered mirrors through the application of upstream and downstream moments. All ray-tracing is performed using realistic mirror shapes and in the case of the small KB mirrors the well established approach (see Eng et al. SPIE Proc. 3449, 145 (1998)) of dynamically figuring the mirror shape by applying two adjustable moments to a trapezoidal shaped mirror is used.

2.A.3.1 Direct Focusing at 76 m

Figure 2.A.1 shows the vertical and horizontal optics layout for the direct focusing mode at 76 m. The inserts shows scatter plots of ray traces of the source at the front end aperture and at the location of the final focusing optics. The location of the final focusing optics is defined simply by the 7.6 μm FWHM vertical source size, the 10 mm working distance, and the desired 1 nm beam size. In addition to the final focusing optics, the only other components required are the front end aperture and high-resolution monochromator. The transverse coherence angle of the vertical source at 1 Å is 6.6 μrad and is achievable with a vertical aperture at 14.5 m of 120 μm, resulting in a vertical optical aperture at 76 m of 500 μm.

In the horizontal dimension, the source is nearly 10 times larger. In order to match the vertical focus, the horizontal size of the front end aperture must be 10 μm or less. The divergence through such an aperture is defined by the size of the horizontal source and the distance to the aperture and is approximately 5 μrad. This matches well the transverse coherence angle of the new horizontal source, defined by this aperture as 5.5 μrad, resulting in a horizontal optical aperture at 76 m that is well matched to the vertical.

The scatter plots in A.2.A to the left of the front end aperture show the full beam available from the undulator. The top panel is a plot of the vertical and horizontal source, with the missing center rectangle indicating the portion of the beam that can be used by the final focusing optics. The lower panel shows a phase space plot in the horizontal direction with the vertical white band showing the portion of horizontal phase space used by the final focusing optics. To the right of the aperture are the same plots, but they now show just the transmitted beam. Figure A.x.x shows a detail view of the source that illuminates the final focusing optics, where a little less then 1% of the total undulator beam is accepted.

2.A.3.2 Compound Horizontal Focusing at 76 m

In the compound horizontal focusing mode at 76 m the horizontal focusing mirror located at 28.8 m is used to produce a secondary horizontal source at 32 m. In this mode the vertical optics are identical mode discussed above. The horizontal optics layout and ray trace scatter plots are shown in Figure A.2.x. This horizontal mirror geometry results in a horizontal demag = 9 and produces a horizontal focus with a FWHM of 7.6 μm. To be able to achieve a 1nm horizontal focus, this secondary source must be reduced to 4 μm using the secondary source aperture. The divergence of this secondary source in very large (~0.5 mrad), and the horizontal transverse coherence angle of this source is about 11 μm, requiring that nearly a factor of 50 of the full divergence be masked out of the beam that illuminates the final focusing optics. The scatter plots at the secondary source aperture show full and the masked secondary source. The scatter plots at 76 m show the beam that will illuminate the final focusing optics, showing that approximately 1 % of the total undulator beam can be made available to the optics.

One possible advantage of this mode is that the horizontal source size can be tuned by adjusting the secondary source slit. An additional advantage is that the secondary horizontal source could be stabilized on the secondary source aperture, using a feedback loop that adjusts the pitch of the horizontal mirror.

2.A.3.3 Waveguide Mode at 41 m

Figure A.2.4 shows the waveguide mode used at 41 m. In this mode primary focusing optics with a working distance of 30 mm and an aperture of 269 μm would produce a secondary source that is 50 μm FWHM. This source is then coupled to an x-ray wave guide. The waveguide will pass only a coherent source and will act as a secondary source for the secondary focusing optics. A demagnification of only 50 is now needed to achieve 1 nm focus. The secondary focusing optics would have an optical aperture of 500 μm and a working distance of 10 mm.

2.A.3.4 Direct Mode at 41 m

The direct focusing mode at 41 m is the same concept as the direct mode at 76 m. The final focusing optics would have a demagnification of 4133 and an optical aperture of 273 μm and would focus the beam to 1.89 nm at a working distance of 10 mm.

2.A.3.5 Compound Horizontal KB Focusing Mode for Full-Field Imaging at 41 m

Full-field imaging greatly benefits from the high photon flux, divergence, and small spot size produced using the compound horizontal small KB focusing mode. Figure A.2.x and Figure A.2.x show the horizontal and vertical optics layout respectively. In this mode the horizontal focusing mirror at 28.8 would focus the beam 9 m away at the tertiary horizontal aperture with a demagnification of 3.3. The horizontal beam size at this aperture is 51 μm FWHM and is re-imaged by a small KB mirror located 3.33 m away. This small KB mirror with a demagnification of 16 and a working distance of 90 mm produces a final focus of 1.4 μm FWHM. In the vertical (Figure A.2.x), only a single small KB mirror is used with a demagnification of 91, producing a vertical focus of 92 nm FWHM. The first two scatter plots in Figure A.2.x show the tertiary focal spot with the aperture fully open and set to 2 μm. The third and fourth scatter plot show the final focus produced by the small KB mirror pair for the case the tertiary aperture fully open and closed to 2 μm, resulting in a horizontal focus that ranges between 1.4 to 0.1 μm FWHM and transmitting 69% to 6% of the undulator source.

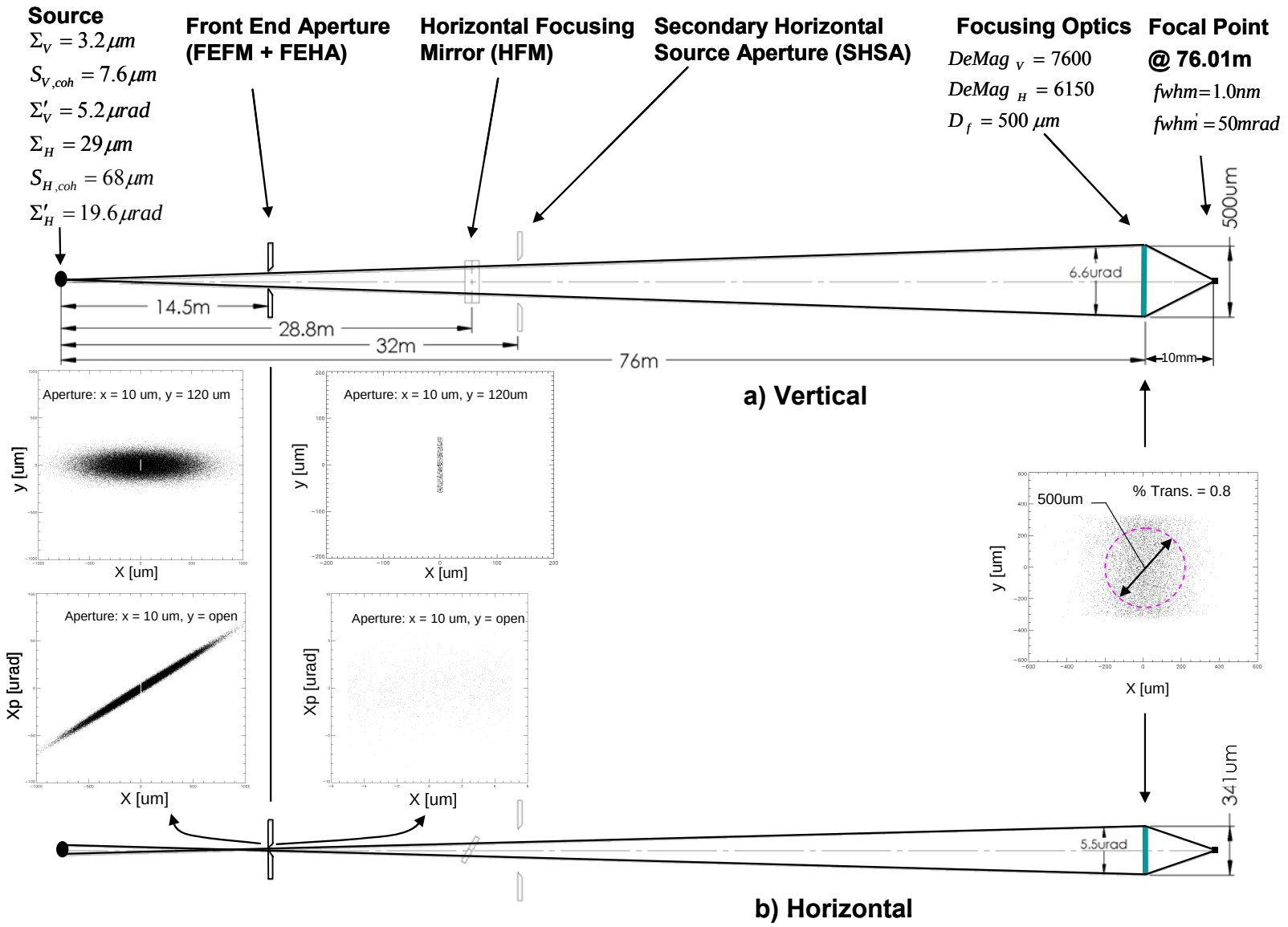

Figure 2.A.1. Optics layout and ray trace for a direct focusing at 76 m, focusing the beam to 1 nm with a working distance of 10 mm. a) vertical ray trace, b) horizontal ray trace.

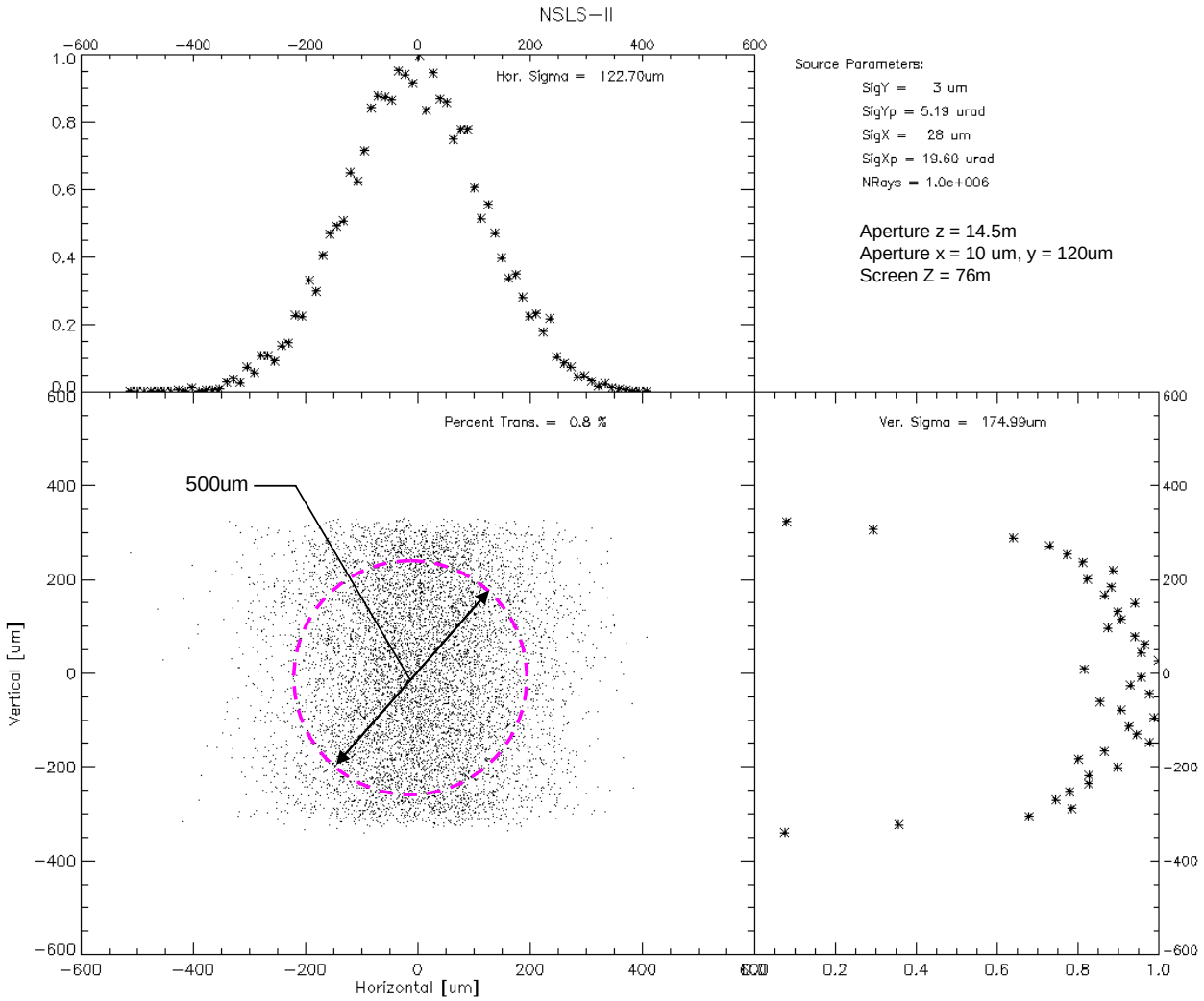

Figure 2.A.2. Scatter plot of coherent beam illuminating the nano-focusing optics for direct focusing at 76 m. 0.8 % of the total undulator harmonic is transmitted to the final optic.

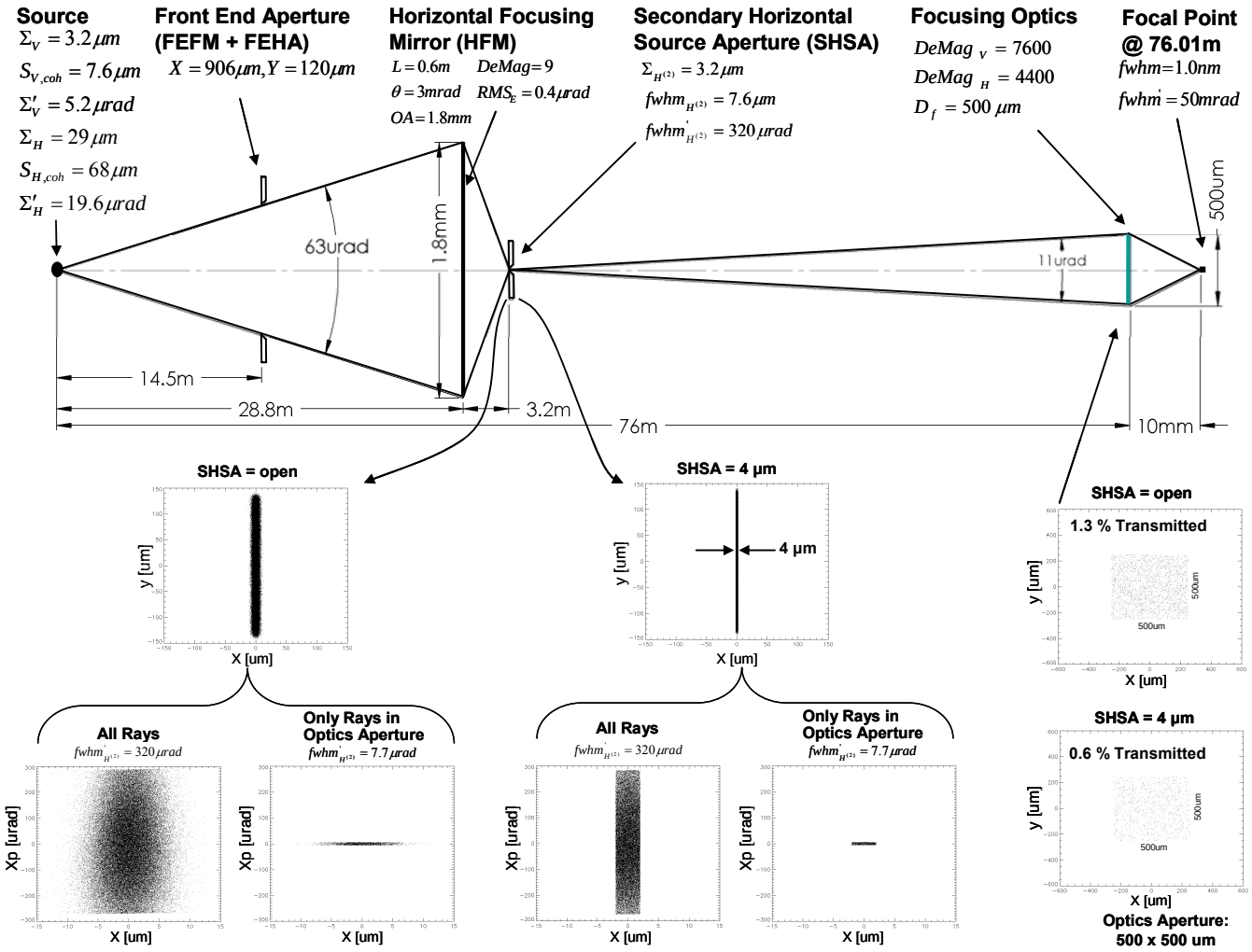

Figure 2.A.3. Optics layout and ray trace for a compound horizontal focusing at 76 m, focusing the beam to 1 nm with a working distance of 10 mm.

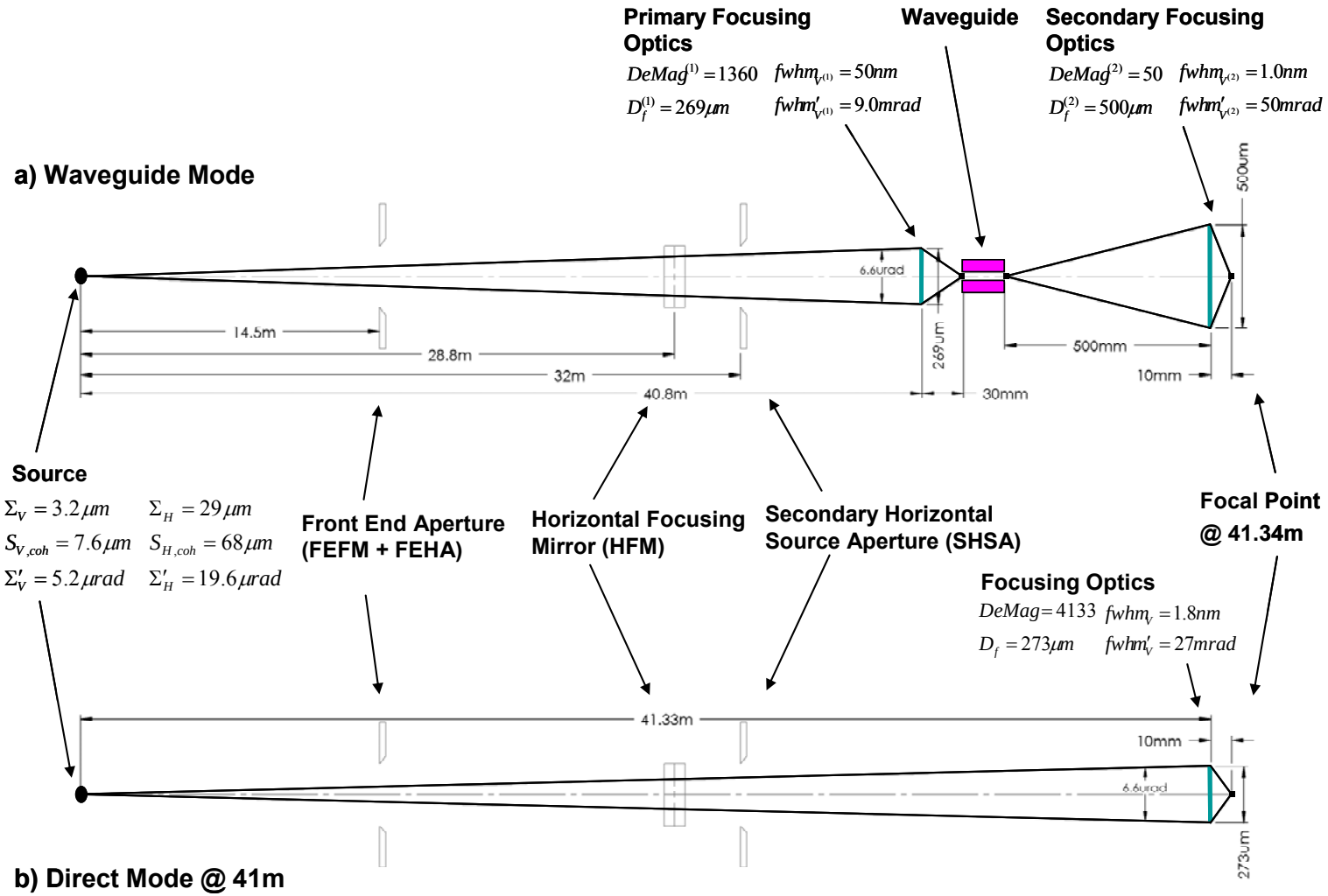

Figure 2.A.4. Optics layout for focusing at 41 m. a) Waveguide mode achieving 1 nm at 41 m with a working distance of 10 mm. b) Direct beam mode with the beam focused to 1.8 nm at 41 m with a working distance of 10 mm.

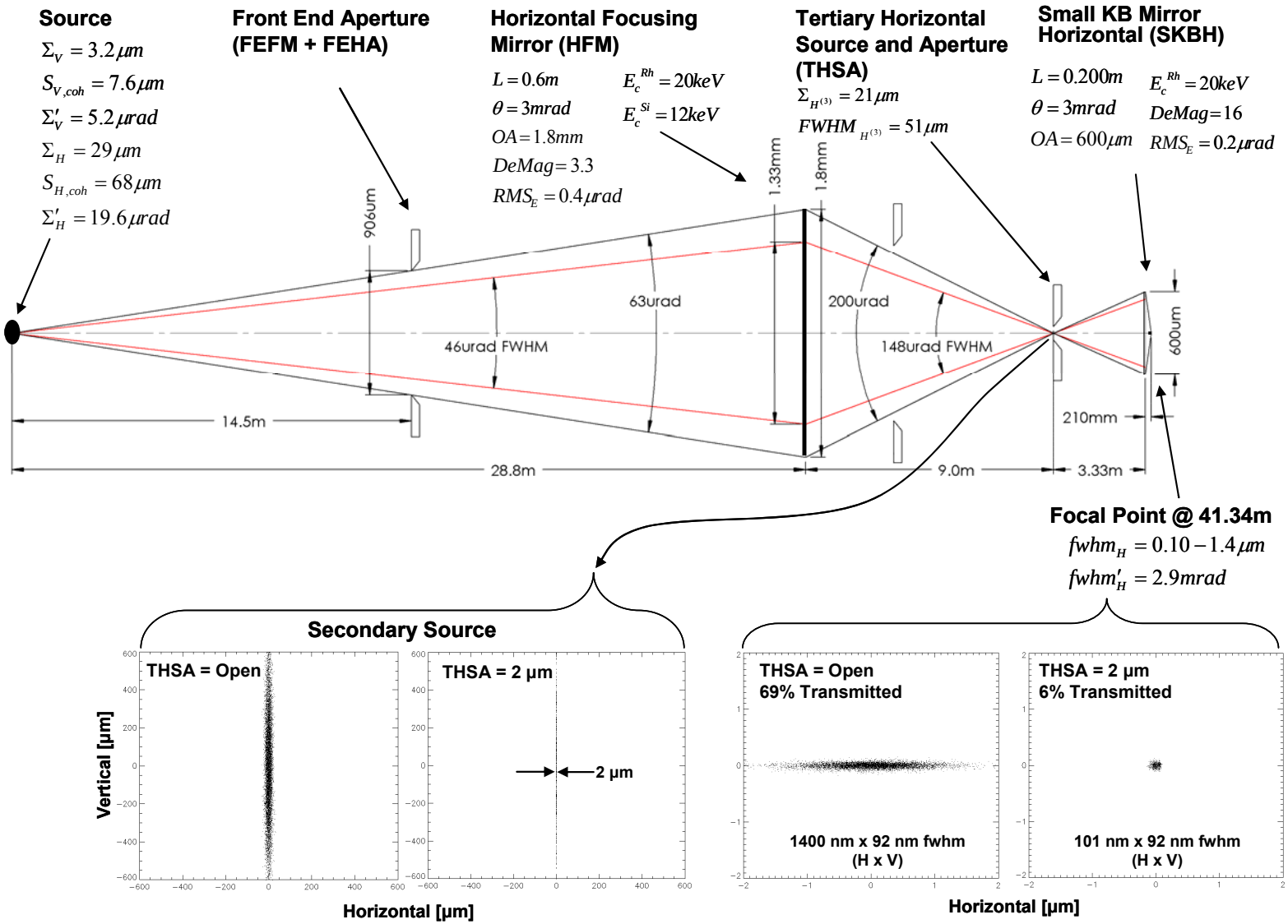

Figure 2.A.5. Optics layout and ray trace for a compound horizontal focusing at 76 m, focusing the beam to 1 nm with a working distance of 10 mm.

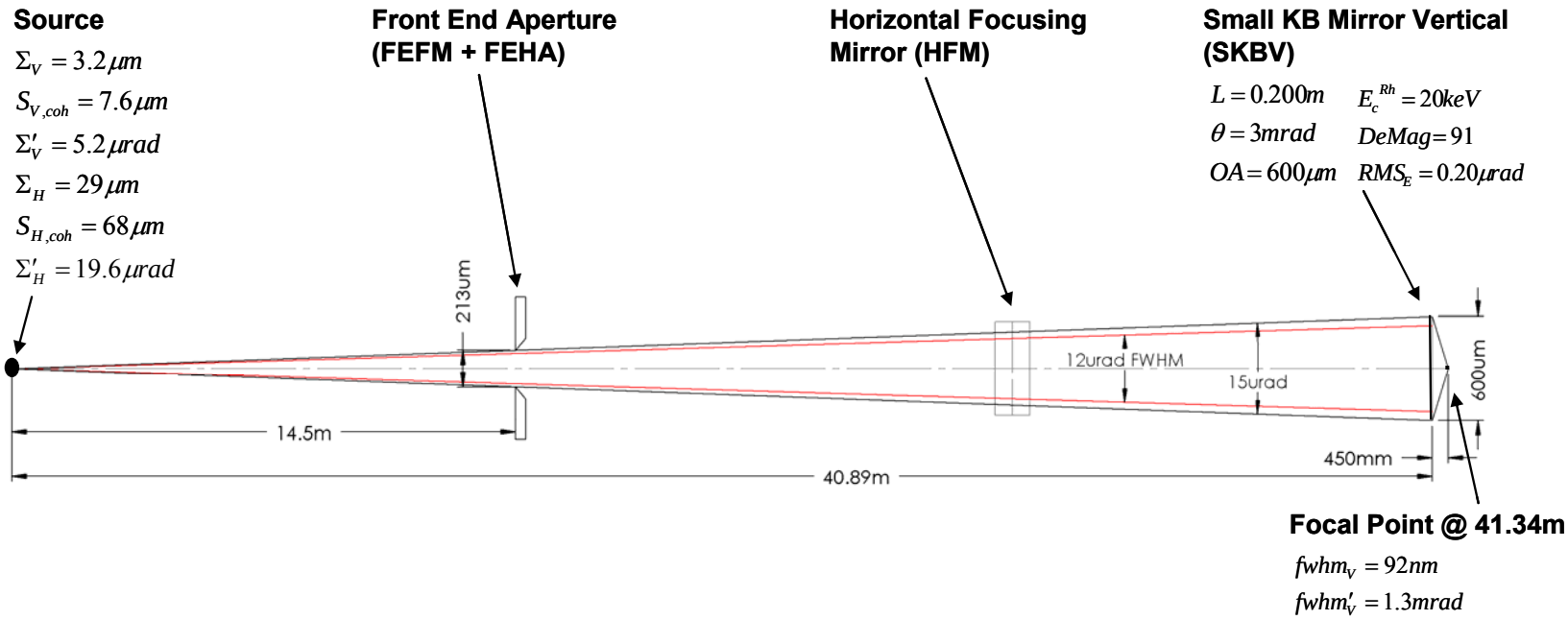

Figure 2.A.6. Vertical optics layout and ray trace for compound horizontal KB focusing mode for full-field imaging at 41m using a small vertical KB mirror, together with horizontal compound reflective optics.

3.1 Executive Summary

This section provides an overview of the conceptual design of the Coherent Hard X-Ray (CHX) Beamline at NSLS-II at Brookhaven National Laboratory.

The technique will take advantage of very high flux of the NSLS-II source. The basic concept of the proposed design of the CHX beamline is to substitute the intrinsic source with a secondary source that is controlled by the end user. A secondary source is employed only in the horizontal direction. The aim is to enlarge the lateral coherence seen at the sample position and bring the horizontal and vertical coherence lengths closer to each other [1]. The beamline design embraces two branches, the small angle branch and the coherent diffraction and large angle branch, although just one of these branches (the small angle branch) will be built as part of the NSLS-II project. The edges of the mirrors will be used to separate the branches. The main energy range for the beamline is 7 – 20 keV.

Each beamline branch will have one endstation, one for small-angle X-Ray Photon Correlation Spectroscopy (XPCS) and one for Coherent X-ray Diffraction (CXD), although only the XPCS beamline and endstation will be built as part of the project. They will be used either simultaneously (most likely and desirable mode) or sequentially, i.e. only one at a time to preserve most of flux available from the source [2]. Splitting the beam into two sections for different branches of the beam line will be done using reflecting mirrors.

The length of the XPCS beamline will be about 60 m and the length of the CXD beamline will be about 250 m.

Mirrors and monochromators should be water cooled to avoid vibration issues and simplify maintenance.

To maximize beam brilliance surfaces of the optical elements should be polished to state-of-the-art standards and the slope errors minimized.

Floor vibrations and temperature fluctuations should be minimized.

A 3 m long U19 undulator placed in a high-beta 8 m straight will be used. The minimum deflection parameter value is K=1.8. The working values for 1-sigma photon beam sizes and divergences are estimated as σ_x =100 μm, σ_y = 6 μm, σ'_x = 15 μrad and σ'_y = 12 μrad. An upgrade is being considered of adding a second undulator in-line with the first one to double the flux. It is anticipated the energy range from 7 – 9 keV will be covered using the third harmonic and a 9 – 12 keV range using the fifth harmonic.

Maximum size of the opening aperture is expected to be about 500 μm (H) x 500 μm (V) or 0.02 mrad (H) x 0.02 mrad (V).

Higher harmonics should be cut off by the mirror and lower ones by use of thin absorber. A CVD diamond crystal of approximately 100 μm thick is being considered as a suitable high-pass filter. Mirrors are expected to operate at 3 mrad incidence angle.

Scientific Objective

X-ray photon correlation spectroscopy also utilizes the very high coherent flux at NSLS-II, in this case to probe the equilibrium or steady-state dynamics of condensed matter. In this endeavor, the XPCS technique offers the significant strengths of being able to study length scales shorter than can be achieved with optical
techniques and longer time scales than can be achieved via neutron scattering. Even on optically accessible length scales, it permits the study of opaque and metallic samples, presenting new opportunities for studies of colloidal and other soft-matter systems.

XPCS involves creating a partially coherent x-ray beam, which is allowed to impinge upon a sample. The dynamics of any fluctuations within the sample are then determined by characterizing the intensity autocorrelation function, g2 = g2(Q,t), of the resultant x-ray speckle pattern versus delay time (t) and wave vector (Q). In a certain sense, this may be thought of as the time-resolved counterpart to coherent diffraction discussed above. Importantly, the quantity g2(Q,t) is related to the sample's normalized intermediate scattering function (ISF) [f(Q,t) = S(Q,t)/S(Q,0)] via g2(Q,t) = 1+A[f(Q,t)]2, where A is the optical contrast. The ISF (equivalent to the sample's Q- and t-dependent density–density autocorrelation function) is a quantity of central interest for any condensed matter system, and is usually key in comparing theory to experimental
results.

However, PCS is much more challenging with x-rays than with light. This is due to a combination of the fact that there are many fewer photons in x-ray beams from even the brightest synchrotrons than from laser sources, and the fact that x-ray scattering cross-sections are invariably many times smaller than light scattering cross-sections. As a result, the crucial aspect of any XPCS experiment is generally the signal-to-noise ratio. The XPCS SNR is linearly proportional to the source brightness.

NSLS-II will drive a revolution in the kinds of samples that will be accessible to XPCS studies. Interestingly, while the SNR scales linearly with brightness, it only scales as the square-root of the sample time (which should be a few times smaller than the sample's correlation time). It follows that for samples of a given scattering strength, meaningful XPCS measurements will be possible at NSLS-II on time scales that are about 100-1000 times faster than currently possible anywhere. Since the current state-of-the-art for diffuse scattering measurements (not from liquid crystal Bragg peaks, or surface specular reflection) corresponds to sample times of about 1 millisecond, we expect time resolutions at NSLS-II of 1 microsecond or less to be feasible, which will enable entirely new science. Indeed, with a time resolution of 0.1 microseconds, it may be possible, in favorable circumstances, to overlap with neutron spin echo measurements.

There are several classes of XPCS experiments that will be possible at NSLS-II but are impossible at current facilities. These include:

Membrane Dynamics. Studies of the dynamics of membrane-based complex fluid phases, consisting of oil–water and an amphiphilic surfactant. Such phases—including the sponge phase and the bicontinuous microemulsion phase, for example—have been the subject of intense interest over the past 20 years, not least because of their possible utility in enhanced oil recovery applications. There are detailed predictions for the equilibrium dynamics of such phases for the wave vectors most characteristic of these materials, namely wave vectors at and near the peak of the static scattering. However, these dynamics are typically too slow for neutron spin echo (NSE) measurements and occur at wavevectors that are too large for optical studies. The faster time scales made accessible by the enhanced brightness of NSLS-II will enable XPCS studies to test these predictions.

Nanoparticles in Suspension. Studies of the collective dynamics of suspensions of nanoparticles. At NSLS-II, it will be possible to study fluctuation dynamics of smaller nanoparticles than is possible

now. This will, for example, permit studies of the motions of nanoparticles confined within block copolymer matrices, or on surfaces. Such studies will be critical in understanding the processes underlying how small particles self-assemble into potentially, technologically useful structures. Especially interesting will be studies examining mixtures of differently-sized nanoparticles of differing compositions, which can self assemble into a variety of different structures, depending on their relative sizes, and which it may be possible to selectively probe via anomalous scattering methods.

Polymer Dynamics. A longstanding question in polymer science concerns so-called *reptation*, which is the process by which polymers in an entangled polymer melt diffuse. The enhanced brightness of NSLS-II will permit XPCS studies on shorter length scales than is now possible, allowing such studies to critically examine the reptation model and relaxations associated with reptation in polymer melts in a much more direct fashion—by actually looking at the polymer motion—than has been possible previously.

Surface Fluctuations. Surface XPCS studies carried out at NSLS-II will probe shorter length scales and faster time scales than are possible now and will therefore elucidate the dynamical behavior of thin liquid and polymer films, and permit definitive answers to questions concerning the role of surface roughness in quenching dynamical fluctuations, or of a polymer's radius of gyration in determining a polymer thin film's capillary mode spectrum.

Biological Applications. The increase in source brightness provided by NSLS-II presents new opportunities for XPCS measurements in systems with low electron density contrast, such as those that consist of biological materials. It is useful to note that the signal-to-noise ratio in the time correlation function obtained in XPCS measurements is proportional to the source brightness, the scattering cross-section of the sample and the square root of the fastest probed time scale. Biological samples have intrinsically low electron density contrast (e.g. the electron density contrast of proteins against water is ~0.1e/Å^3, in contrast to ~0.4e/Å^3 for Si against water). The scattering cross-section of a biological sample is therefore approximately an order of magnitude lower than an inorganic sample of comparable structure features. NSLS-II will permit accessing sub-millisecond time scales for biological samples. Such a time scale is relevant to many important biological processes. For instance, the internal motion of proteins can be described by a series of normal modes. While the high frequency normal modes can be as fast as sub-picosecond, the low frequency, global collective normal modes are on the time scale of millisecond or slower. These normal modes are related to conformation changes that are important to the proteins' function and their time scale is comfortably within the range of XPCS measurements. Membrane inclusions, such as membrane proteins and peptide induced pores, are also good candidates to be studied by XPCS. The intrinsic diffusion coefficient of lipid molecules in a fluid membrane is on the order of 1μm^2/s. The membrane inclusions are likely to have lower diffusion coefficients (e.g. 0.004μm^2/s for CFTR Cl^- channels) and the relevant length scale corresponds to scattering vector q~0.1Å^{-1}. The time scale relevant to the diffusion of membrane inclusions in XPCS measurements is therefore just below millisecond. It should be noted that this time scale is nearing what the best (longest) molecular dynamics simulations can do today. The XPCS measurements therefore could provide a validation for computer simulations. At the same time, the combined information also provides a more complete understanding of the studied system.

Insertion Device

The beamline will be using a 3 m U19 insertion device as a source of x-rays. Key storage ring and undulator parameters are summarised in Table 0.1. The parameters have been compiled from the information provided in references [1,3].

Initially one U19 undulator will be used in a high β 8.6 m straight section [1]. There will also be eight damping wigglers reducing the horizontal emittance to 0.55 nm-rad [3] from the 2.1 nm-rad specified for the bare lattice, Table 1 of reference [3]. But at the start there will only be 3 damping wigglers [2] and hence higher horizontal emittance of 0.9 nm-rad [3].

Table 0.1 Storage ring and ID parameters.

Parameters	Values	Units	Reference
Electron Energy	3	GeV	3
Storage ring current	500	mA	3
Period length	19	mm	3
Length of magnet array	3	m	3
Number of full periods	158	-	3
Field strength (max)	1.14	T	3
Maximum deflection parameter K(y)	2.03	-	3
Horizontal and vertical emittance ε_x ε_y	 0.55 / 0.9 0.008	 nm · rad nm · rad	1-3 3
Beta function horizontal and vertical β_x β_y	 18 3.1	 m m	 3 3
Energy spread	0.0005 - 0.001	-	3
Beam size (sigma) horizontal and vertical σ_x σ_y	 99.5 / 127.3 5.0	 μm μm	 Calculated Calculated
Beam angular divergence (sigma) horizontal and vertical σ'_x σ'_y	 5.5 / 7.1 1.6	 μrad μrad	 Calculated Calculated
Total power	11.18	kW	3
On-axis power density	77.86	kW/mrad^2	3

Photon beam parameters are summarized in Tables 3.1 and 3.2.

Table 0.2 Source size and angular divergence. The FWHM is calculated using σ values as $FWHM = 2\sigma\sqrt{2\ln 2}$.

A. ε_x =0.55 nm-rad

K	n	E, keV	$\sigma_{r'}$, μrad	σ_r, μm	Source size, μm				Angular divergence, μrad			
					(σ)		(FWHM)		(σ)		(FWHM)	
					H	V	H	V	H	V	H	V
1.0	3	9.0	4.79	2.29	99.5	5.5	234.4	12.9	7.3	5.1	17.2	11.9
1.73	5											
2.03	1	1.47	11.85	5.66	99.7	7.5	234.7	17.8	13.1	12.0	30.8	28.2
2.03	11	16.2	3.57	1.71	99.5	5.3	234.3	12.4	6.6	3.92	15.5	9.2

B. ε_x =0.9 nm-rad.

1.0	3	9.0	4.79	2.29	127.3	5.5	299.8	12.9	8.6	5.1	20.2	11.9
1.73	5											
2.03	1	1.47	11.85	5.66	127.4	7.5	300.1	17.8	13.8	12.0	32.5	28.2
2.03	11	16.2	3.57	1.71	127.3	5.3	299.8	12.4	7.9	3.9	18.7	9.2

Table 0.3 Effective beam size and angular divergence at different positions along the beamline. The FWHM is calculated using σ values as $FWHM = 2\sigma\sqrt{2\ln 2}$.

A. ε_x =0.55 nm-rad

Distance from sourse, m	Beam size, μm				Beam angular divergence, μrad			
	(σ)		(FWHM)		(σ)		(FWHM)	
	H	V	H	V	H	V	H	V
27.9	227.2	141.0	535.0	332.0	8.1	5.1	19.2	11.9
50	379.3	252.6	893.2	594.7	7.6		17.9	
75	558.0	378.8	1313.9	892.0	7.4		17.5	
100	738.7	505.0	1739.6	1189.3	7.4		17.4	

B. ε_x =0.9 nm-rad

27.9	271.6	142.4	639.6	335.3	9.7		22.9	

50	448.5	255.1	1056.0	600.6	9.0	5.1	21.1	12.0
75	657.4	382.5	1548.2	900.8	8.8		20.6	
100	869.4	510.0	2047.2	1201	8.7		20.5	

Figure 0.1 shows the calculated brilliance of different harmonics at values of the deflection parameter K<2.03 using the XTC program from the XOP package [6,7].

The first harmonic of the radiation is available at energies from approximately 1.47 keV to 4.5 keV, i.e. within the energy range that will not be used on the beamline. Useful undulator harmonics for the particular beam line for selecting energies from 7 to 20 keV are harmonics from 3 to 9 or possibly up to 11. Variation of K versus energy is given in Figure 0.2. Assuming the deflection parameter of the undulator, K, of any practical use will be between 2.03 and 0.4, Figure 0.2, maximum undulator gap will be less than 15 mm.

Data in Figure 0.1 show that different undulator harmonics should be used to keep maximum flux over the range of energies from 7 keV to 20 keV: the 3rd harmonic below approximately 8.1 keV, the 5th at 8.1 – 11.2 keV, the 7th at 11.2 – 13.7 keV, the 9th at 13.7 – 16.2 keV and the 11th at 16.2 – 20 keV. The most important energy range of 7 -12 keV could essentially be covered with the 3rd and 5th harmonics.

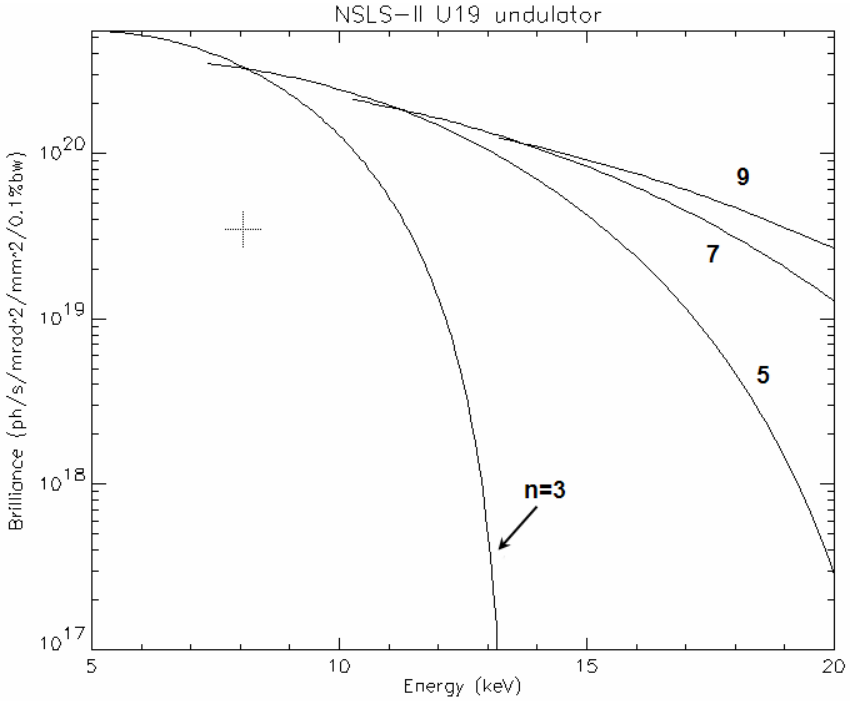

Figure 0.1 Calculated variation of the on axis brilliance of first few odd harmonics (from 3 to 9) of radiation from the U19 undulator versus energy at K<2.03.

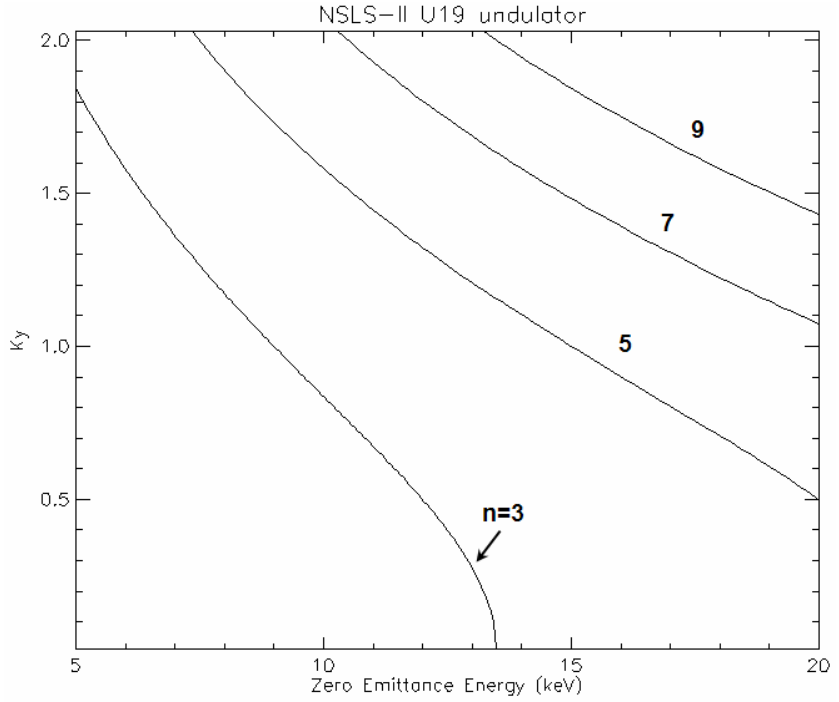

Figure 0.2 Calculated variation of the deflection parameter *K* corresponding to odd harmonics (from 3 to 9) of radiation from a U19 undulator versus energy.

Calculated heat loads for different operating modes of the U19 undulator are shown in Table 3.3. Power density distributions are shown in Figures 3.3 and 3.4. The heat load associated with a 20 μrad x 20 μrad aperture placed at 29.7 m from the souce is summarized in Table 3.4.

Table 0.4 Calculated heat loads at different operating modes of the U19 undulator. The opening angle of 100 μrad (H) x 100 μrad (V) corresponds to the size of a fixed mask. The 20 μrad (H) x 20 μrad (V) opening of the beam is the maximum opening required by experiments.

Distance from source, m	**K**	**FWHM of power distribution (H x V), μrad**	**FWHM of flux distribution[1] (H x V), μrad**	**Total Power, W**	**Power density, W/mm^2**	**Power through 0.1 (H) x 0.1 (V) mrad aperture, W**	**Power through 0.02 (H) x 0.02 (V) mrad aperture W**
27.9	1	281 x 207	20.2 x 11.9	2704	47.6	343	14.8
	1.73	490 x 217		8093	84.8	624	26.3
	2.03	579 x 218	32.5 x 28.2	11143	100.1	737	31.1

Note(s): 1) See Table 0.2, B.

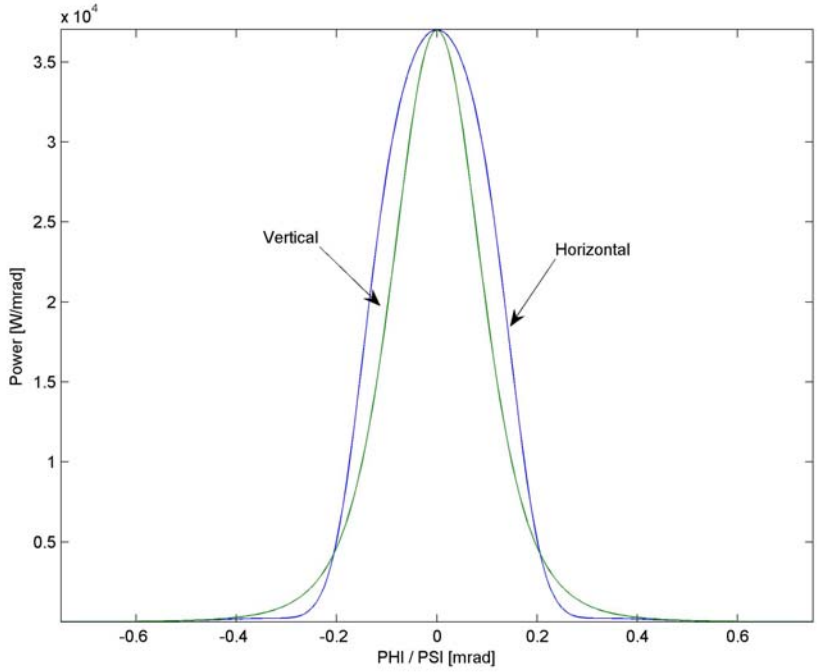

Figure 0.3 Calculated cross-section of power distribution in horizontal (FWHM=0.281 mrad) and vertical (FWHM=0.207 mrad) planes at K=1.0 and beam opening angle of 1.5 mrad (H) x 1.5 mrad (V).

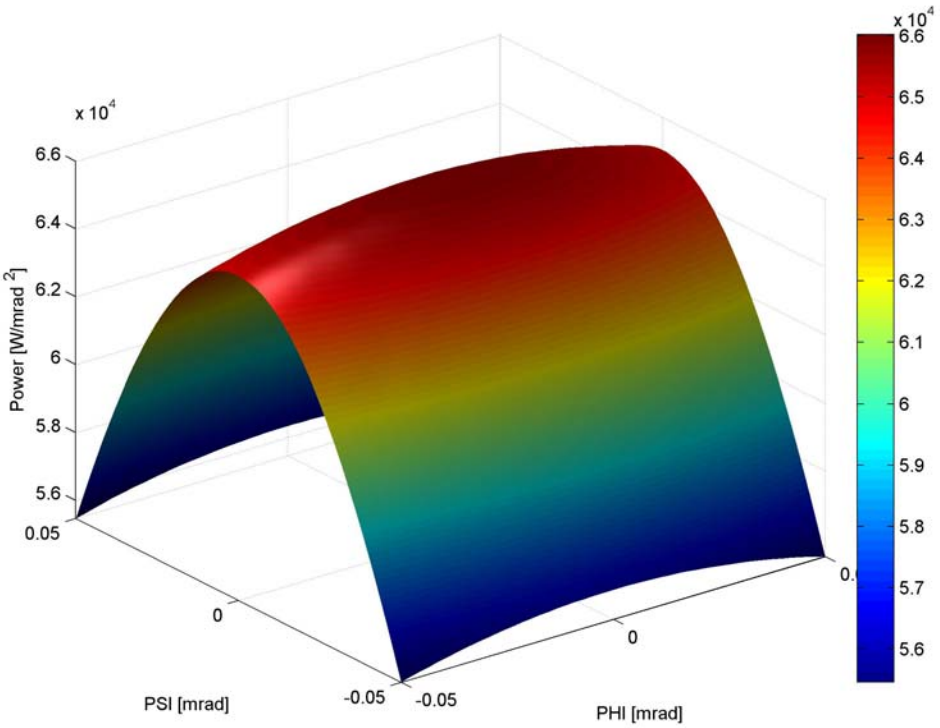

Figure 0.4 Power density distribution versus horizontal, *Phi*, and vertical, *Psi*, opening angles at a 100 μrad (H) x 100 μrad (V) aperture at *K*=1.73.

Table 0.5. Heat load at a 20 μrad x 20 μrad aperture placed at 29.7 m from the souce. The source consists of two in-line U19 undulators tuned to the same gap. Heat load is calculated without any windows/filters or mirrors and taking into account a 200 μm thick CVD diamond filter and heat loss at a Rh coated deflecting mirror at an incidence angle of 3 mrad.

Distance from source, m	**K**	**Power density, W/mm^2**	**Power, W**	**Power, W (after 200 μm CVD diamond + mirror)**	**Power through central cone $\sigma_{r'}$, W**	**Power through central cone $\sigma_{r'}$ (after 200 μm CVD diamond + mirror), W**
29.7	1.0	95.1	30	9.3	1.7	0.5
	1.73	169.7	53	29	3.0	1.6

The results in Table 0.5 show that if only coherent part of the beam is selected using slits the heat at the monochromator will only be few Watts. If however the 0.02 μrad x 0.02 μrad aperture is used, the heat at the monochromator will be much bigger, 29 W, at power density of about 170 W/mm^2.

3.2 Sector Layout

3.2.1 Beamline Layout

Table 0.6 shows the position and size of the beamline components. Space between the main components will be filled with vacuum bellows and pipes of suitable length. The table also shows different sections of the beam line vacuum system.

A CAD drawing of the beam line and the end stations showing general layout of the beam line components is given in Attachment 1.

Table 0.6 Beamline layout.

Beamline Component	Starting position, mm	Length, mm	Vacuum section[1]	Centre of Optical Element
End of shield wall	27900			
Fixed mask	**28200**	**229**	0/1	**28315**
Differential Pump	28429	420	1	
Bellow	28849	180	1	
Blade BPM	29029	319	1	
Bellow	29348	180	1	
CVD Diamond Window / Filter	**29528**	**303**	1	**29680**
Bremsstrahlung collimator	29831	388	1	
Bellow	30219	167	1	
White beam Slit (H)	30386	229	1	
Bellow	30615	167	1	
White beam Slit (V)	30782	229	1	
Bellow	31011	180	1	
Fluorescent screen	31191	340	1	
Bellow	31531	180	1	
Gate valve	31711	70	1/2	
Outbound deflecting Mirror	**31781**	**700**	2	**32131**
Gate valve	32481	70	2/3	
Bellow	32551	137	3	
Inboard White beam Slit (H)	32688	229	3	
Bellow	32917	167	3	
Inboard White beam Slit (V)	33084	229	3	
Bellow	33313	167	3	
Pipe	33480	300	3	
Gate valve	33780	70	3/4	
Inboard deflecting Mirror	**33850**	**700**	4	**34200**
Gate valve	34550	70	4	
Bellow	34620	200	4/5	
Pipe	34820	800	5	
Beam mask and white beam stop	35620	450	5	
Bellow	36070	200	5	
White Beam Shutter	36270	230	5	
Bellow	36500	200	5	
Hutch wall	36890	300		37040
Beam Transport pipe	36700	9145	5	
Beam mask and Bremsstrahlung stop	45395	450	5	
Hutch wall	45250	300		45400
Bellow	45550	200	5	
Gate valve	45750	70	5/16	
Pipe outbound	45550	295	5	
Bellow	45845	200	5	
Fluorescent screen	46045	345	5	
Gate valve	46390	70	5/6	
DCM and pink beam stop	**46460**	**745**	6	**46832.5**
Gate valve	47205	70	6/7	

Bellow	47275	200	7	
Pink Beam Shutter	47475	230	7	
Pipe	47705	604	7	
Hutch wall	48100	300		
Fluorescent screen	48309	340	7	
Quadrant BPM	48649	35	7	
Bellow	48684	150	7	
Pink beam Guard slits	48834	65	7	
Gate valve	48899	70	7/8	
VFM	**48969**	**700**	8	**49319**
Gate valve	49669	70	8/9	
Pipe	49739	290	9	
Pink beam Slits	50029	65	9	
SiN / CVD Diamond Window	50094	20 / 303	9	
Pink beam/Bremsstrahlung stop	TBD	400	14	
End station 1 equipment	TBD			
Hutch wall	60000	300		

3.2.1.1 Data Acquisition System and Motion Control

The 8-axis motion control boxes having RS232, USB and Ethernet interfaces are customized to suit the beam line motorised axis. They also have built in micro IOCs.

Separate micro IOCs control vacuum pump controllers, vacuum gauge controllers, DPT controllers, current amplifiers and CCD cameras.

EPS PLC has analogue input and digital input and output and is linked to solenoid valve actuators, fluorescent screen actuators limits, thermocouples, water flow meters, vacuum interlocks, vacuum gauge controllers, cooling water flow meters in the heat exchangers, thermocouples in the heat exchangers and water conductivity probes.

PSS shutter is controlled from the PSS and sends and receives status signals to/from EPS PLC.

Vacuum schematic is shown in a separate drawing. Vacuum gauge controllers are monitoring vacuum level measured by Pirani and ion gauges mounted on different beamline components. Ion pump controllers provide power to each of the ion pumps used on the beamline. High voltage splitter units are used where necessary to power more than one pump per output channel.

Micro IOC controlling the vacuum system uses RS485 protocol for communication with the pump and gauge controllers. Vacuum gauge controllers are integrated with the EPS system to monitor vacuum level in different sections of the beamline.

Piezo actuators need to have vacuum interlocks linked to the vacuum gauge controllers.

Table 0.7 Controls schematic of the CHX beamline.

Beamline Component	**No. of units**	**Number of elements per unit**											
		Controlled by 8 axis Motion Control units					**Controlled by EPS PLC**			**Controlled by micro IOC**			**PC**
		Stepper /Pico Motor	**Server Motor**	**Limit/ datum switch**	**Enco-der**	**Refe-rence point**	**Flow meter**	**Thermo-couple**	**Sole-noid valve actuat.**	**CCD camera**	**DPT control unit**	**Current amplifier**	
Beamline control system	1												1
Fixed mask	1						1	1					
Blade BPM	1	2		4			1					1	
CVD Diamond windows	1						1	1					
Bremsstrahlung collimator	2						1	1					
Slits (H **or** V)	12	1		2	1								
Gate Valve	14			2					1				
Horizontally Deflecting Mirror (water cooled)	2	6		10	5	5	1	1					

VFM	2	5		10	5	5					1		
HFM	1	5		10	5	5					1		
Pink Beam shutter	3			4			1	1	1				
Fluorescent screen	5			2			1		1	1			
DCM (water cooled)	2	5	1	8	7	6	1	3			1		
White/pink beam stops	5						1	1					
QBPM	2	1		2								1	
Water cooled wndows (diamond or Be)	2						1	1					

3.4.3.3 High Heat Load Monochromator

A water cooled Si(111) DCM with no sagittal focusing on the second crystal should provide energy resolution of ~10^{-4}, fixed exit beam height and operate across the requested energy range from 7 keV to 20 keV. Expected performance parameters of the DCM and some useful information are given in

Table 0.8. We also assume 25 mm vertical offset between the incoming and outgoing beams and that the beam 'walk' alone the second crystal as the energy changes will be taken by longitudinal translation of the crystal.

The results in

Table 0.8 show that

- The energy resolution is expected to be from $1.34\cdot10^{-4}$ to $1.42\cdot10^{-4}$.
- The Bragg angles are from 5.67° to 16.4°. The Bragg angle calculation assumes the lattice constant of Si(111) of 5.4309 Å.
- Perpendicular translation of the 2nd crystal over the energy range is about 0.44 mm.
- Longitudinal translation of the 2nd crystal over the energy range is approximately 82 mm.
- The footprint of the beam at the crystals of the Si(111) monochromator at all energies is less than 0.22 mm x 2.2 mm assuming 4.8 μrad (H) x 4.8 μrad (V) opening of the beam (coherent beam).If the aperture is 20 μrad (H) x 20 μrad (V) the maximum beam footprint increases to 0.9 mm x 9 mm.

The design of the DCM should meet stability requirements and be able to withstand heat loads as discussed earlier.

Table 0.8 Performance parameters of the Si(111) DCM.

Parameters	**Energy, keV**		
	7	12	20
Wavelength, Å	1.7712	1.0332	0.6199
Bragg angle θ_B, deg	16.4058	9.483	5.6732
Reflectivity (double reflection)	0.85	0.94	0.98
Energy resolution			
Rocking (Darwin) width[1], μrad	39.1586	22.2161	13.2122
Bandpass due to source size	$4.3\cdot10^{-10}$	$7.1\cdot10^{-10}$	$1.2\cdot10^{-9}$
Bandpass due to accepted angular divergence	$1.6\cdot10^{-5}$	$2.9\cdot10^{-5}$	$4.8\cdot10^{-5}$
Resolution of the DCM	$1.34\cdot10^{-4}$	$1.36\cdot10^{-4}$	$1.42\cdot10^{-4}$
Resolving power[2]	7463	7349	7067
Crystal size and position			

Vertical offset between incoming and outgoing beams, *D*, mm	25		
Perpendicular offset between 1st and 2nd crystals[3], mm	13.0	12.7	12.6
Longitudinal offset between the crystals[4], mm	44.3	75.9	126.4
Maximum beam footprint[5] transverse to the beam, mm along the beam, mm	0.22		2.21

Notes: 1) Intrinsic resolution of Si(111) is $\left(\frac{\delta\lambda}{\lambda}\right)_{cryst.}$ = 1.33 $\cdot 10^{-4}$ [30]. The rocking (Darwin) width is

$$\Omega = \frac{\delta\lambda}{\lambda}\tan\theta_B \ .$$

2) The resolution is determined by the width of the rocking curve of the crystal, beam opening angle and size of the source

$$\frac{\Delta E}{E} = \sqrt{(\Delta\theta_{source}^2 + \Delta\theta_{slit}^2)\cot^2\theta_B + \left(\frac{\delta\lambda}{\lambda}\right)_{cryst.}^2} \ ,$$

$$\Delta\theta_{source} = \sigma_y / p \ \text{ and } \ \Delta\theta_{slit} = \min(\sigma_y^{'}, s_v)/p \ ,$$

where σ_y is the vertical source size (FWHM), $\sigma_y^{'}$ is the vertical divergence of the beam (6σ), s_v is the opening of the monochromator vertical entrance slit and *p* is a distance from the source.

Resolving power of the monochromator is reverse to the total band pass, i.e. it is $\frac{E}{\Delta E}$.

3) The distance, *X*, measured perpendicular to the optical surfaces of the crystals: $X = \frac{D}{2\sin\theta_B}$, where *D* is the constant vertical offset between incoming and outgoing beams.

4) The distance, *Y*, measured along the surface of the crystals: $Y = \frac{D}{2\cos\theta}$, where *D* is the constant vertical offset between incoming and outgoing beams. The longitudinal offset shows beam walk parallel to the surface of the crystals as the Bragg angle changes. To maintain the constant beam offset, *D*, the *X* and *Y* should satisfy the condition $\frac{1}{X^2} + \frac{1}{Y^2} = \frac{4}{D^2}$.

5) The beam footprint depends on the rms size and divergence of the incoming beam, DCM distance from the source and the Bragg angle so that

$$F = \sqrt{\sigma_{x,y}^2 + (\sigma_{x,y}^{'} \cdot p)^2}; \ F_x = F; \ F_y = F/\sin\theta \ ,$$

where $\sigma_{x,y}$ and $\sigma'_{x,y}$ are the size and divergence of the source, correspondingly, *p* is the distance from the source and θ is the Bragg angle.

3.4.3.5 Mirrors (White Beam and Monochromatic)

As has been discussed earlier, the beam line is expected to have few mirrors for collimating and focusing the beam in horizontal and vertical planes. Preliminary analysis shows that full energy range of 7 -20 keV can be covered without changing the angle of incidence while providing good transmission of the x-ray beam over the whole range.

Increase of the angle of incidence is favourable for reducing the cut-off energy, lengths of the mirrors and improving harmonic rejection, but the reflectivity of the mirrors decreases. We have considered using bare Si, Pt, Pd and Rh coatings and concluded that Rh and bare Si are most suitable for the energy range. Pd is very similar to Rh but the latter has slightly better reflectivity. Reflectivity of Pt shows few absorption edges and it is more suitable for higher energies.

Most mirror suppliers will guarantee densities of Rh in the coatings to be better than 90% of the bulk material which is 12.41 g/cm^3 [17,18]. We therefore assume in this analysis the density of Rh of 11.17 g/cm^3 for calculating reflectivity of the mirror stripes. The densities are usually lower, about 85% of the bulk, for bimorph mirrors. The lower density means slightly lower reflectivity and lower cut-off energies at similar incidence angles. As the density of Rhodium decreases from 90% to 85%, the cut-off energy decreases by about 550 eV.

The density of Si, 2.33 g/cm^3 [28], is slightly higher than the density of Silica, 2.2 g/cm^3 [18]. Usually Silica is used as a substrate for making mirrors to focus monochromated beam and Silicon is used to make mirrors operating in a white beam. The data in Figure 0.5 show that replacing Silica with Silicon as a mirror substrate increases the cut-off energy by approximately 300 eV.

Figure 0.5 shows variation of the critical angle of the mirrors versus energy for Si, Silica, Rh (and Pt). The critical angles were calculated as $\alpha_c = \sqrt{2\delta}$, where δ is a real part of the refractive index of material. Incidence angle of the mirrors should ensure that the low energy beam is not contaminated by the beam of higher energy. Also it is desirable to keep the mirrors reasonably short. But the reflectivity of the mirrors decreases as the angle of incidence increases. Therefore the incidence angle should be optimised taking into account these factors and ease of use.

The useful energy range is defined from 7 keV to 20 keV [2] and from the point of view of ease of use changing the mirror incidence angle should be avoided. In that case the mirrors could be set at an incidence angle of approximately 3.0 mrad to achieve about 95% reflectivity using Rh stripe. Higher reflectivity can be obtained using Si or Silica stripe, Figure 0.6.

We therefore suggest operating at fixed angle of incidence and use bare Si (cut off energy 10.4 keV) below approximately 10 keV and Rh (cut off energy 20.8 keV) from 10 keV to 20 keV. Reflectivity of Si and Rh at 3 mrad is shown in Figure 0.7. We suggest using Silica rather than Silicon with monochromated beam.

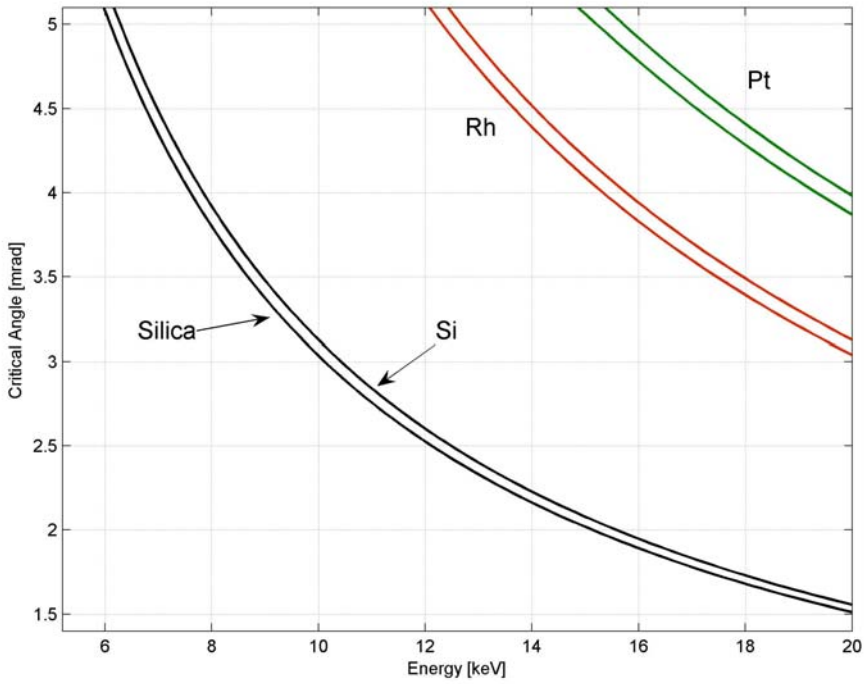

Figure 0.5 Variation of the critical thickness versus energy for bare Silica, Silicon, Rhodium and Platinum. The double lines for Rh and Pt correspond to different densities of the materials: 85% density of the bulk for the lower line and 90% for the upper line.

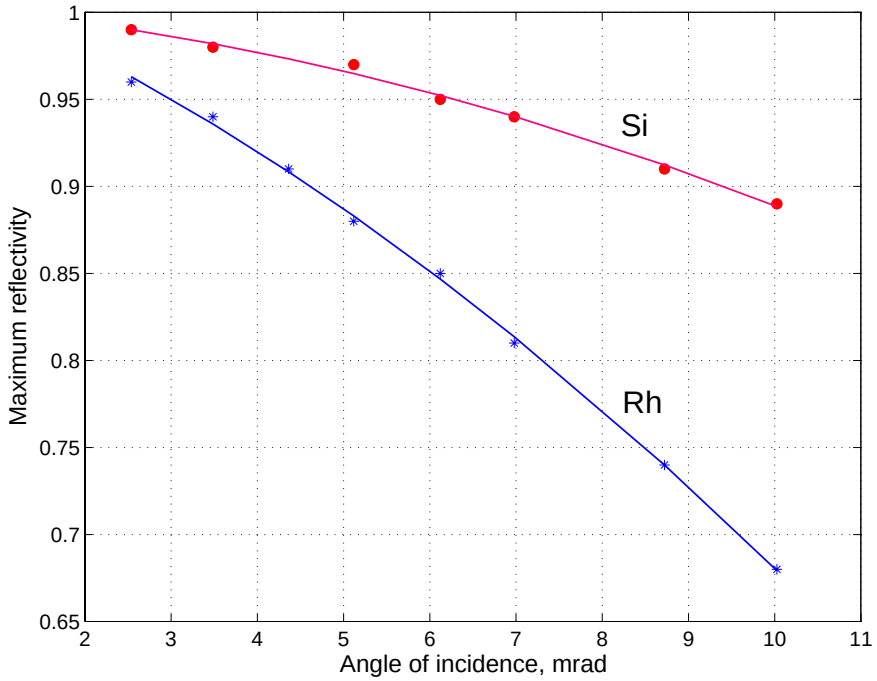

Figure 0.6 Variation of maximum reflectivity of Rh and Si versus angle of incidence.

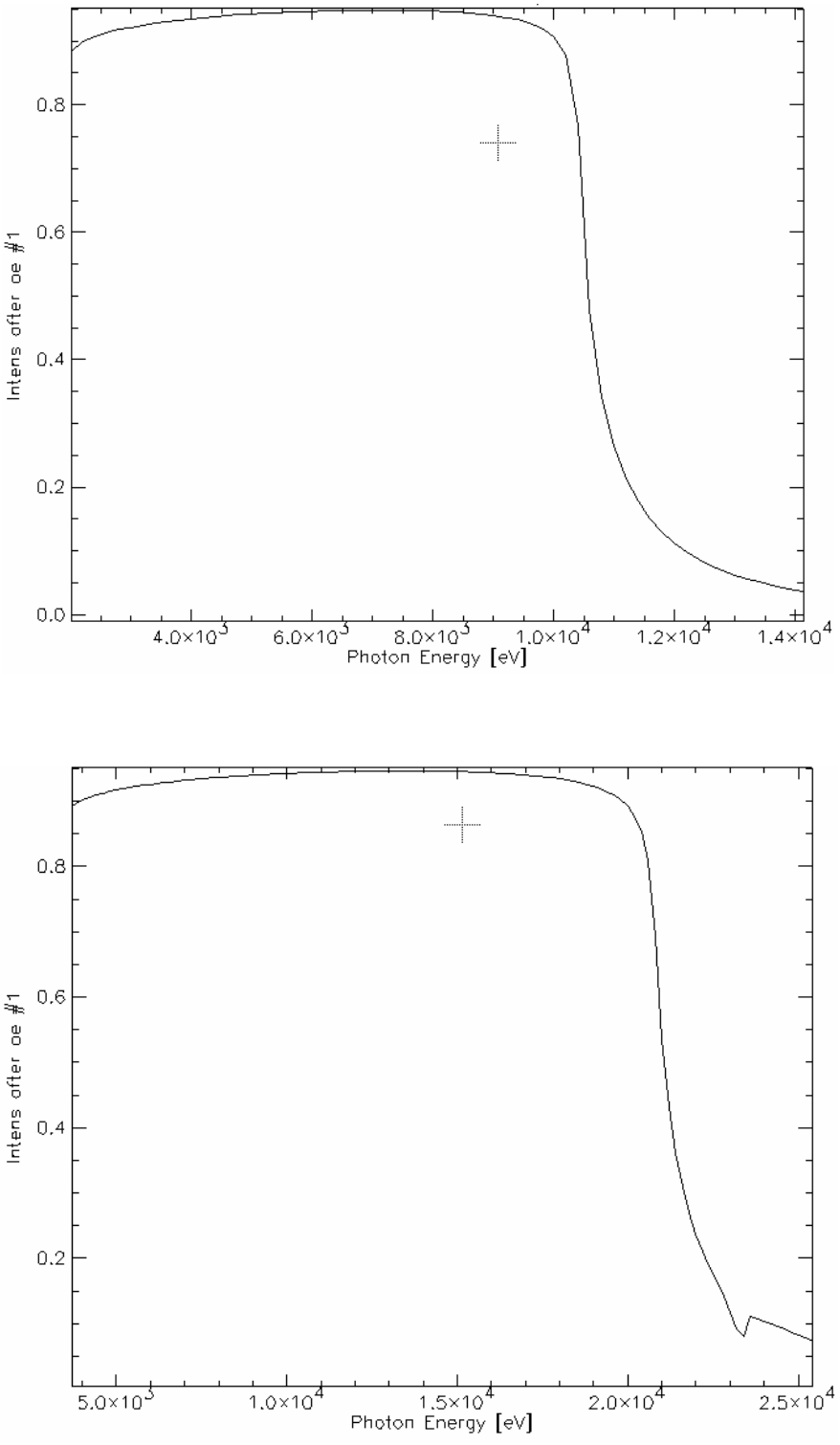

Figure 0.7 Reflectivity of Silicon (top) and Rhodium of 90% density of bulk (bottom) at 3.0 mrad.

Some useful characteristics of the mirrors are shown in Table 0.9.

The lengths of the mirrors are calculated for the case of 0.02 mrad x 0.02 mrad opening of the beam and for beam divergence of the central cone.

Table 0.9 Parameters of the mirrors. The *p* and *q* are source-to-mirror and mirror-to-image distances.

Mirror	Optical distance from source, m	Inci-dence angle, mrad	Coating	Beam Footprint, mm		Bent radius m	*P*, m	*Q*, m
				Aperture 20 µrad x 20 µrad	Aperture 4.8 µrad x 4.8 µrad			
HDM1	26.89	3	Si, Rh	179	43	N/A	-∞	∞
HDM2	28.96	3	Si, Rh	193	46	N/A	-∞	∞
VFM	47.13	3	Silica, Rh	314	75	TBD	-∞	TBD

3.4.3.6 FEA and Ray Tracing Analysis

The calculations are based on the assumptions that the horizontally deflecting mirror (HDM) at an incidence angle of 3 mrad uses a bare silicon reflecting surface and is located at 32.13 m from the source. The beam opening aperture is 0.020 mrad x 0.020 mrad. The Si(111) DCM after the deflecting mirror is at 46.83 m from the source. The primary beam is attenuated by the 200 µm thick CVD diamond window/filter located upstream of the mirror. The horizontally deflecting mirror selects 0.02 mrad of the beam to the side from the centre.

The results of the ray tracing using XOP and Shadow packages are given in Tables C1 and C2. To compensate for defocusing of the beam by slope errors at the HDM and DCM the bend radius of the HDM was optimized to achieve a single spot and maximize the intensity. Only for the Case 1 in Tables C1 and C2 representing the worse case of heat load and thermal slope errors the optimum radius was smaller than the nominal radius.

Table C1. Results of FEA analysis at different heat loads at the horizontally deflecting bare Silicon mirror (at 32.13 m, incidence angle 3 mrad) and 1st crystal of the Si(111) DCM (at 46.83 m, Bragg angle of 12.69^{o} corresponding to 9 keV). Beam opening aperture is 0.02 mrad x 0.02 mrad. The 200 µm thick CVD diamond window is assumed upstream of the mirror. Single or double U19 undulator source is operating in high-beta straight and in low emittance (0.55 nm-rad) mode.

Beamline Component	Final Case No.	Source	Max slope X, µrad	Max slope Y, µrad	RMS slope X, µrad	RMS slope Y, µrad
Horizontally Deflecting mirror	1	2xU19, K=1.731, Power= 20.5 W	2.63	0.94	1.15	0.78
	2	1xU19, K=1.0, Power= 2.1 W	0.27	0.09	0.12	0.08
	3	1xU19, K=1.731, Power= 10.0 W	1.28	0.45	0.56	0.38

	4	2xU19, K=1.0, Power= 4.2 W	0.53	0.19	0.23	0.16
DCM	1	2xU19, K=1.731, Power= 11.7 W	16.6	22.1	7.6	7.8
	2	1xU19, K=1.0, Power= 3.0 W	4.1	5.4	1.9	1.9
	3	1xU19, K=1.731, Power= 5.7 W	7.9	10.4	3.6	3.7
	4	2xU19, K=1.0, Power= 6 W	8.3	11.0	3.8	3.9

Table C2. Results of ray tracing analysis (final) of the hard coherent beamline at 9 keV. Flux was calculated over the 1000 µm x 20 µm aperture placed at the sample position at 50 m from the source. The primary beam, I_o, is assumed to be of 0.020 mrad x 0.020 mrad. The mirror is 250 mm (L) x 50 mm (W). Bending radius of the VFM was optimised by changing the focal distance. Nominal radius before any optimisation is 447.2 m.

Case No.	Incoming Flux I_o, ph/s	Spot size, µm	Flux, ph/s	Spot size, µm	Flux, ph/s	Optimised R_m (VFM), m
		no crystal distortion		Slope errors at HDM and DCM		
1	5.39×10^{14}	314 x 4.7	5.52×10^{13}	287 x 1.8	1.41×10^{13}	264.5
2	1.28×10^{14}	321 x 4.7	1.29×10^{13}	291 x 1.7	6.58×10^{12}	492.5
3	2.18×10^{14}	329 x 5.3	2.19×10^{13}	307 x 2.6	7.37×10^{12}	812.7
4	2.93×10^{14}	300 x 3.7	2.96×10^{13}	272 x 2.8	1.24×10^{13}	876.0

3.4.4 Instruments

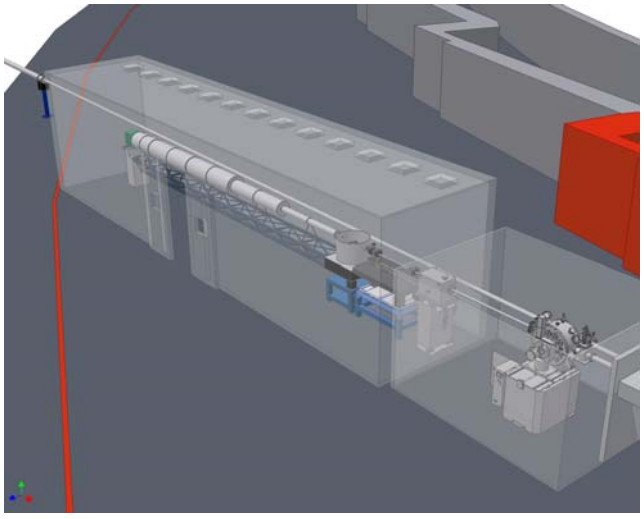

The source brightness at NSLS-II will enable XPCS experiments to study dynamics in disordered system at time scales well below milliseconds. The goal of the instrumentation in this endstation is to turn this potential into reality. To do so, the instrumentation must not compromise the superior coherence quality of the source and a state-of-art detector is needed to actually measure the intensity fluctuations in x-ray speckles that correspond to sample dynamics. Detailed requirements have already been set forth in the CDR and will not be repeated here. This document will only describe the actual instrumentation that will satisfy these requirements.

The first component inside the endstation is a vertical focusing mirror that will reduce the vertical coherent length to match that in the horizontal direction. The mirror is followed by 3 sets of slits to select coherent flux and clean up parasitic scattering from the slits. Between the mirror and slits are an attenuator and a fast shutter. The attenuator is necessary for samples that produce strong scattering. The x-ray absorbing material in the attenuator will be double-side polished silicon so that it will not introduce significant phase error to the propagating x-ray wave front. The shutter is

necessary when a CCD-type detector is being used and to avoid sample exposure to x-rays and radiation damage when data are not being collected.

The sample will be housed in a vacuum sample chamber just downstream of the 3rd set of slits. For solid samples, a hexapod will be used to position the sample into the beam and translate the sample before the expose part is damaged x-rays. The advantage of the hexapod is that an arbitrary point on the sample can be programmed as the rotation center. This is particularly useful for thin film samples that are measured in grazing incidence geometry. A rotary stage under the hexapod makes up for the hexapod's limited azimuthal rotation range. Liquid samples will be continuously flowed through a flow cell to reduce radiation damage.

The length of the flight path downstream of the sample chamber will be 10m long to produce x-ray speckles comparable to the pixels (assuming 100μm) in size. It is made up of several sections so that shorter sample-to-detector distance is possible if desired. Because of the long length of the flight path, it also needs to be large enough in diameter in order to capture enough *q*-range. With the current design of 20" tube, the highest q accessible at 12keV and 10m sample-to-detector distance is ~0.15$Å^{-1}$. The flight tube can be offset so that the beam is not centered on the exit window and higher *q*-range can be accessed on one side. The tube size is most likely larger that that of the detector itself. The detector will therefore be mounted on an x-z stage so that it can multiple images can be collected and tiled to cover the entire available *q*-range.

A beamstop assembly is located at the end of the flight path. This assembly consists of x-z-rotary stages that can position multiple beamstops (e.g. with different size or beam intensity detector) into the beam to block the direct beam and measure its intensity. A similar assembly is currently being built at beamline X9 of NSLS.

The detector group at NSLS is planning to develop a pixel array detector with auto-correlator built-in in each pixel. Such a detector will be ideal to realize the full potential of XPCS measurements at NSLS-II. In case that the development of such a detector is not successful, a pixel array detector without auto-correlators will be used instead. Specifically, a pixel array detector with 75um pixels and 10kHz frame rate is being designed by DECTRIS, who is currently marketing its 170um, 200Hz frame rate pixel array detector, PILATUS. In this case, a large computing facility must be established to store and post-process collected data.

3.5 Additional Requirements Imposed on the Conventional Facilities

Special attention must be given to stability requirements. These are determined by temperature stability and vibration (natural and self-inflicting) and they have been extensively discussed at the recent NSLS-II Stability Workshop in April 2007 [10-12].

The beam stability requirements for different components are based on achieving less than 10% variation of the beam size. To conduct different experiments like the ones mentioned by Sandy [10] or Shen [11] horizontal and vertical position stability should be 0.2 μm, vertical angle stability 0.2 μrad and horizontal angle stability 1 μrad [12]. For SAXS high beam stability (<1%) is desirable.

Typical temperature variations measured at ESRF are about 0.5^{o} [13]. At ID22 beam line at ESRF temperature variations are < 0.1^{o} over 24 hours [12]. Similar or better stability should be achieved for the beamline especially taking into consideration extremely big length of the beamline. For demanding beam lines new high flow rate air conditioning units (air renewal rate 20 cycles/hour) are used. Vibrations from air flow are reduced using porous ducts [12].

Measures allowing reducing thermal effects include choosing low expansion materials, cooling local heat sources, thermal insulation of vessels, moving all control electronics outside the hutches [13], using thermally insulated sand-filled stands, aiming at achieving first natural frequency at above 50 Hz [14] and high thermal inertia [13]. It has been pointed out that angular vibration drifts are much worse than linear [13]. This is particularly true for long beam lines like IXS.

Temperature control requires high resolution industrial grade instruments and controls with excellent repeatability. At DESY, for example, narrow span thermistor/transmitters with 0.01^{o} C sensitivity and programmable controllers with 14 bit resolution will be used [15].

Vibrations generated by water chillers, fans, compressors etc. can be reduced by selecting rotating equipment with stringent balancing requirements, using spring support for rotating equipment and inertia bases [16].

References

1. NSLS-II Conceptual Design Report, Brookhaven National Laboratory (2006).

2. BNL staff, Private communications (2007).

3. Summary of NSLS-II Source Properties, NSLS-II User Workshop 17-18 July 2007, http://www.bnl.gov/nsls2/project/source_properties.asp, 31 July 2007 (2007).

4. J. Hill, Experimental Facilities, NSLS-II User Workshop, 17-18 July 2007, http://www.bnl.gov/nsls2/07_Hill_XFD_NUW_July07.ppt (2007).

5. K-J. Kim, Optical Engineering **34**, 2, 342 (1995).

6. M.S. del Rio, R. J. Dejus, XOP Home Page: http://www.esrf.fr/computing/scientific/xop2.1/

7. M.S. del Rio, SPIE Proc. 3448, 230 (1998).

8. L. Berman, ID Beamline Optics and Damping Wigglers, EFAC May 10th 2007 (2007).

9. J.-C. Biasci, B. Plan and L. Zhang, J. Synchrotron Rad., **9**, 44 (2002).

10. A. Sandy, A hard X-ray Coherent scattering beamline for NSLS-II and …SAXS?, NSLS-II User Workshop, 17-18 July 2007, http://www.bnl.gov/nsls2/workshops/docs/UserWorkshop/BOS/coherent/Shen_Soft_Coherent.ppt (2007).

11. Q. Shen, Overview on Coherent Diffraction Imaging and Its Applications, NSLS-II User Workshop, 17-18 July 2007, http://www.bnl.gov/nsls2/workshops/docs/UserWorkshop/BOS/coherent/Shen_Soft_Coherent.ppt (2007).

12. Stability Requirements for NSLS-II Beamlines, Report of the NSLS-II Stability Task Force, NSLS-II Stability Workshop, April 18-20, 2007, http://www.bnl.gov/nsls2/docs/StabilityTaskforceReport.pdf ; updated on June 18, 2007.

13. Y. Dabin, Stability of instruments at ESRF, NSLS-II Stability Workshop, April 18-20, 2007, http://www.bnl.gov/nsls2/workshops/docs/Stability/Dabin_ESRF_Stability.ppt

14. S. Sharma and V. Ravindranath, Stability of Mechanical Systems, NSLS-II Stability Workshop, April 18-20, 2007, http://www.bnl.gov/nsls2/workshops/docs/Stability/Sharma_mechanicalSystems.ppt

15. C. Channing, Conventional Facilities. Temperature Stability, NSLS-II Stability Workshop, April 18-20, 2007, http://www.bnl.gov/nsls2/workshops/docs/Stability/Channing_CF_Tempstablity.ppt

16. J. Sidarous, Engineering Approaches to Reducing Floor Vibration at the APS and CNM, NSLS-II Stability Workshop, April 18-20, 2007, http://www.bnl.gov/nsls2/workshops/docs/Stability/Sidarous_CF.ppt

17. X-Ray Mass Attenuation Coefficients, NIST, http://physics.nist.gov/PhysRefData/XrayMassCoef/tab1.html

18. Densities (g/cm^3) of some Common Materials, LBL, http://henke.lbl.gov/cgi-bin/density.pl

19. W.B. Peatman, Gratings, mirrors and slits, Gordon & Breach Sci. Publ., Amsterdam (1997).

20. M.C. Wilson, Diamond Personnel Safety System, Proc. ICALEPCS2003, Gyeongju, Korea, 2003, http://accelconf.web.cern.ch/accelconf/ica03/PAPERS/WP515.PDF

21. A. Boron, 30ID Beamline Requirements Document for the Generation-3 Personnel Safety System (PSS) of the Advanced Photon Source at Argonne National Laboratory, Document No. 4104013001-000122004, March 2004, http://www.aps.anl.gov/asd/safetyilocks/PSS/Gen3/30id/Requirements_30ID_V00_2004_03_05%20.pdf

22. J. Hawkins, Personnel Safety System for the beamlines at the Advanced Photon Source, Rev. Sci. Instrum. 67, 3370 (1996).

23. F. Schrever, New Australian Synchrotron uses safety PLCs, http://www.industrial-embedded.com/articles/schrever/

24. M. Ramanathan, Preliminary Design Report. Inelastic X-ray Scattering CDT. Sector 30, March 2004, http://www.ixs.aps.anl.gov/IXS_PDR_final.pdf .

Appendix A: Ray Diagram

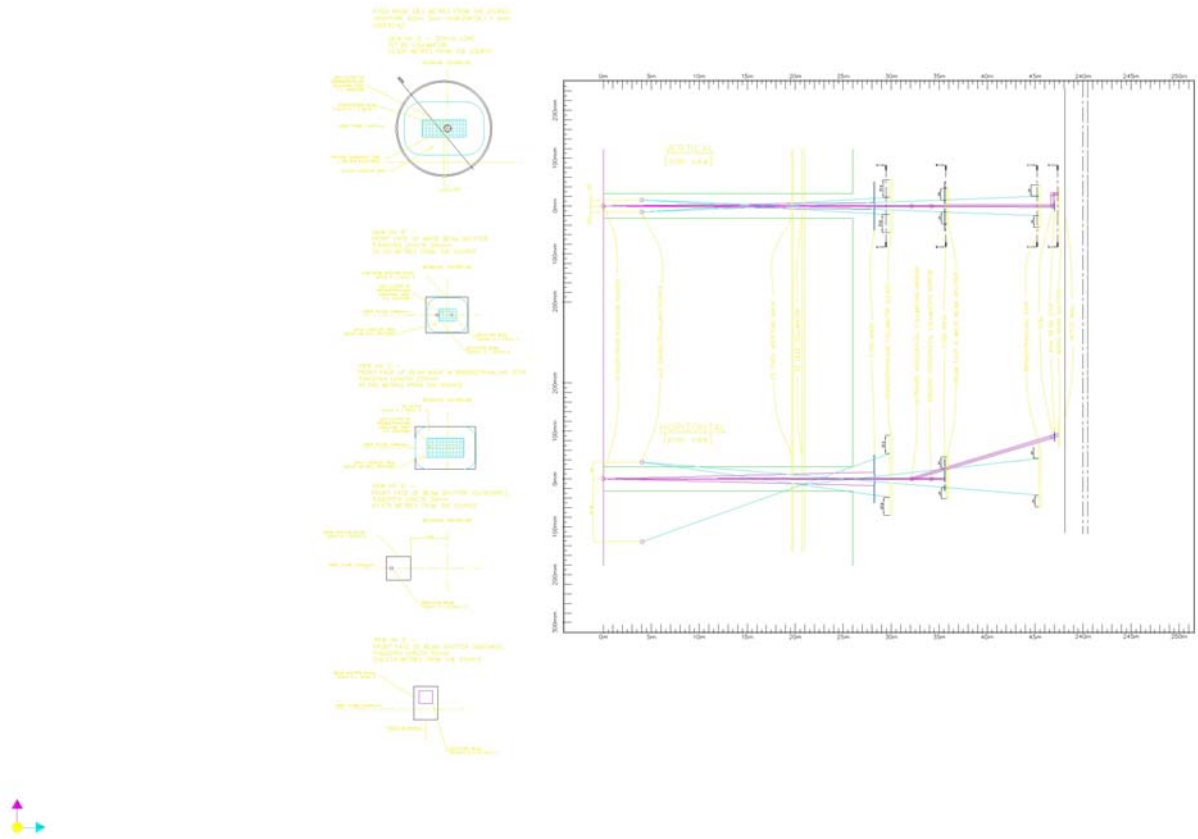

Figure A1. Bremsstrahlung and photon beam ray tracing drawing for XPCS beamline.

Appendix B: Beamline Layout Drawings

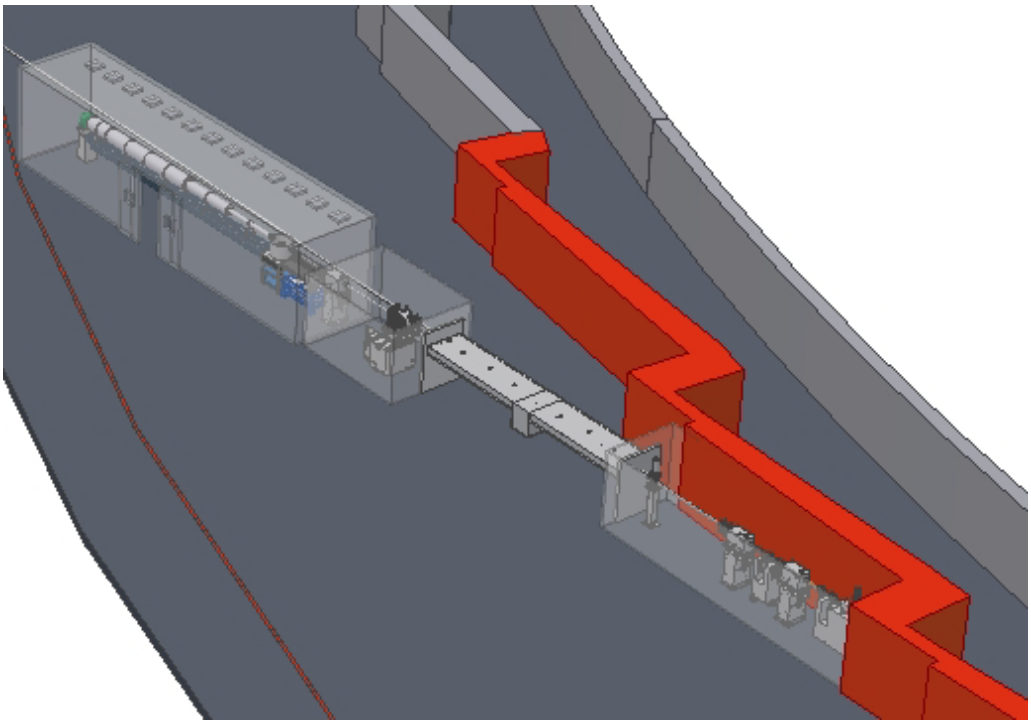

Figure A1. General view of the Hard Coherent X-Ray beamline.

Appendix C: List of Key Beamline Components

CVD Diamond Windows

Chemical Vapour Deposition (CVD) Diamond offer extreme hardness, high thermal conductivity, chemical inertness, and high transparency over a very wide spectral range. Stronger and stiffer than Beryllium, with lower thermal expansion and lower toxicity, it is ideal for UHV isolation windows in X-ray beamlines. Windows can be supplied embedded in UHV flanges and with efficient water cooling.

CVD Diamond windows, Figure 0.1, developed in cooperation with the Fraunhofer Institute of Germany and Paul Scherrer Institute of Switzerland, with the support of Argonne National Laboratory in the USA, are manufactured by Diamond Materials GmbH.

Specifications

Thickness:	200 µm
Diameter:	5 – 50mm
Vacuum performance:	<10-9mbar l/sec
Surface finish:	10nm RMS roughness

The window will be used when a monochromatic beam mode is replaced with the pink beam regime. The window will be put in place of SiN windows that are used in a monochromatic mode as last windows before the sample.

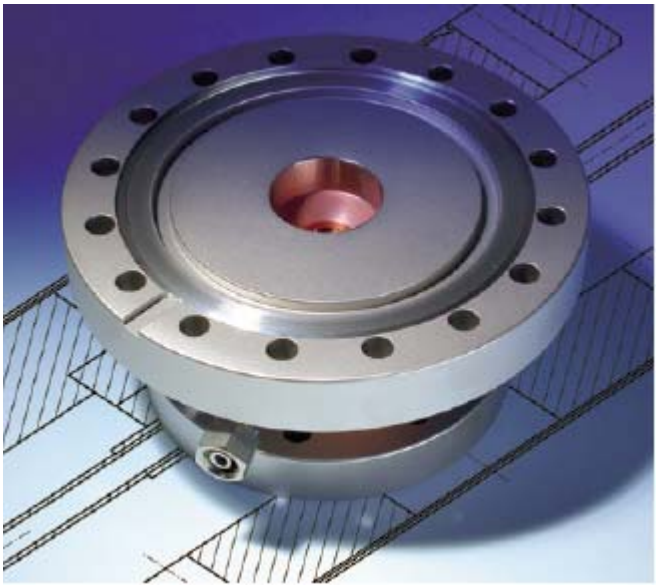

Figure 0.1 Water cooled CVD Diamond window.

Fixed mask and CVD Diamond window / filter

Description:

Window material:	CVD diamond, optical quality
Thickness:	180 µm ± 30 µm
free aperture:	10.0 mm
Surface Roughness :	R_a less than 20 nm

Mounted to a watercooled OFC copper joint with CF 63 flanges on each side and a central conical hole (20x10 mm on one side, 7.2x3.6 mm at the other side)
Assembly leak tight to a rate of 1x10e-10 Torr L/sec of He
CVD diamond window pressure tested at 1 atm pressure

Schematic drawing:

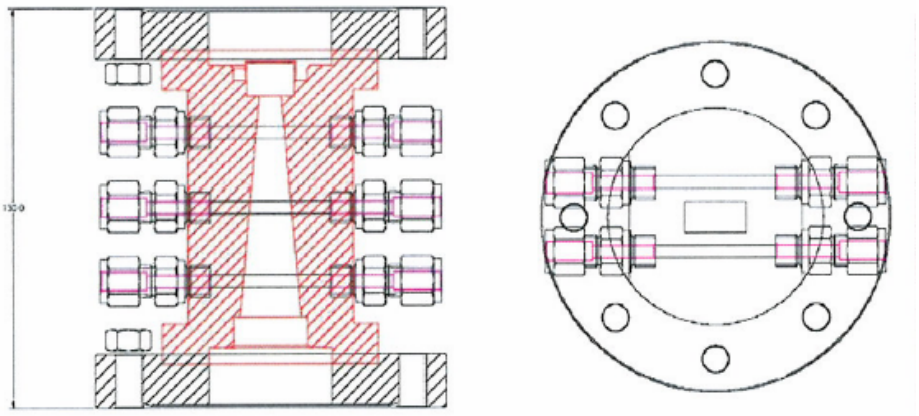

Figure 0.2 Outline specification and schematic drawing of a typical diamond window.

Blade BPM

The White Beam (BBPM) consists of a vacuum vessel containing the sensor mechanism, a support stand, and associated electronics.

The sensor mechanism consists of 2 insulated blades fixed a known distance apart in a vacuum chamber. The signals from these electrodes provide a measurement of the position of the beam.

The gap between the blades and their orientation are chosen to provide a usable current without significant disturbance to the usable x-ray beam.

Quadrant BPM

The QBPMs are available in HV and UHV configurations. The QBPMs will need to be taken out of the beam when the end station is used in a pink beam regime.

Fluorescent Screens

The screens are made in two modifications: water cooled and not water cooled. For using with pink beam water cooled option should be chosen.

Slits

High Heat Load Slits for Undulator Beams

The slit system, **Figure 0.3**, consists of 2 L-shaped absorbers arranged in series along the beam (the downstream being rotated through 180°) to define the aperture,

Figure 0.4. Each mask therefore defines two edges of the beam. Each absorber is moved laterally and vertically by external translation stages to define the beam. There are edge-welded bellows before, between and after the two absorbers, which allow the movement of the slits relative to the beam. The slit mechanism is mounted on a synthetic granite-filled mild steel frame for stability and vibration rejection.

Slits of this type will be used to define the size of the white beam.

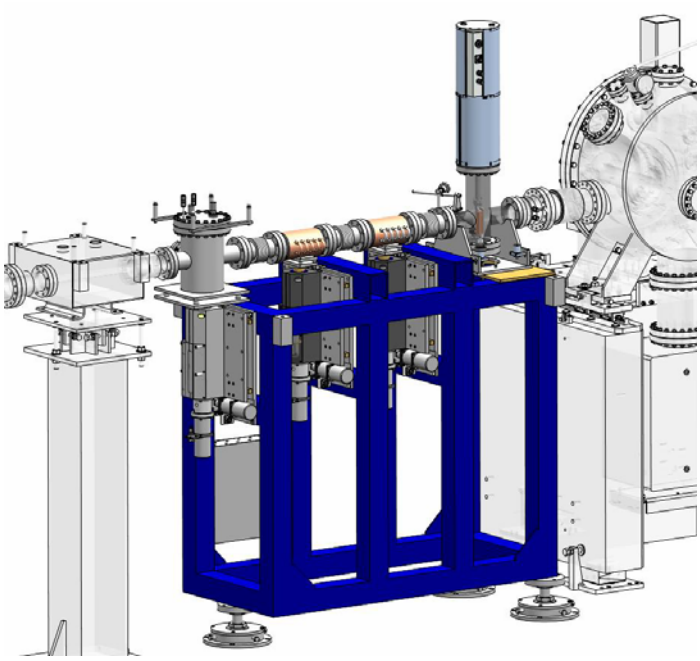

Figure 0.3 High Heat Load Slits

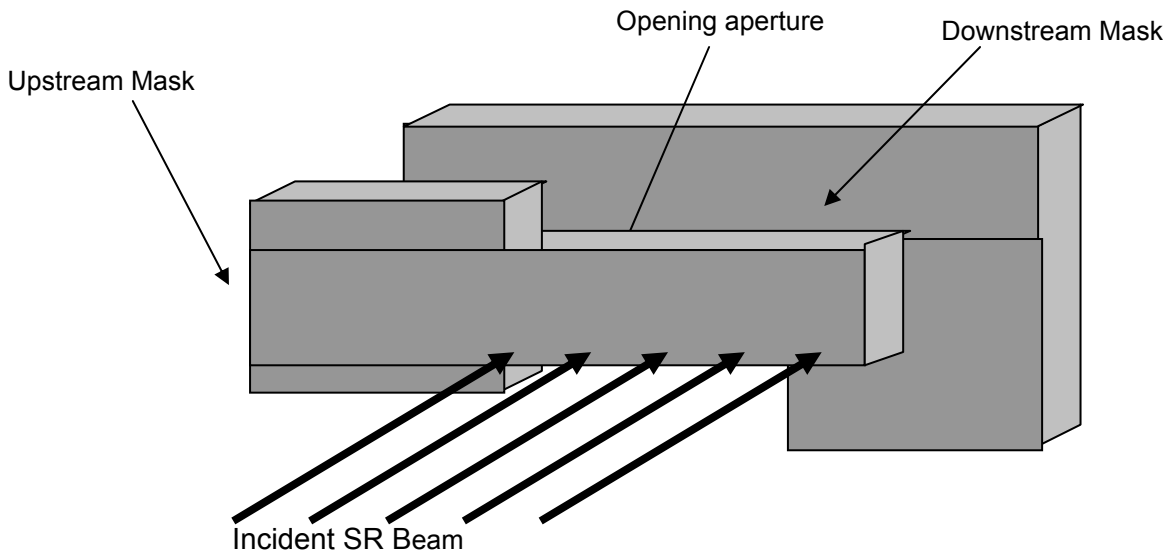

Figure 0.4 High Heat Load Slits schematic.

Pink beam Slits

The cooled Slit Unit comprises two independently actuated slit blades, mounted on the same flange. Each Slit System has a horizontal slit unit and a vertical slit unit, each of which is mounted on a flange on a vacuum vessel, one on top of the vessel and one at the side of the vessel. Each pair of blades defines either the horizontal or vertical dimension of the beam, Figure 0.5.

Each cooled slit unit consists of two slit blades, each of which is mounted onto a water-cooled Glidcop body and connected to an external actuator mechanism through a flange on the slit vessel. Indium foil is clamped between the slit blade and the copper body to enhance heat transfer by conduction, Figure 0.6. On each slit blade the edge nearest the beam is chamfered, at 3°, to produce a sharp defining (knife) edge. The chamfered face is positioned on the downstream side of the blade (on the side of the blade furthest from the source). On each cooling block the edge nearest the beam is chamfered, Figure 0.7, to reduce the power density of the beam on the block at the operating condition. The chamfered face is positioned on the upstream side of the block. An additional tungsten disaster plate is added to prevent damage over the full range of operation. The slit blades are manufactured from 5 mm thick tungsten alloy. The blade defining edge protrudes 0.5 mm above the cooling block.

The slits are specially designed for high heat loads where conventional water cooled slits can not be used.

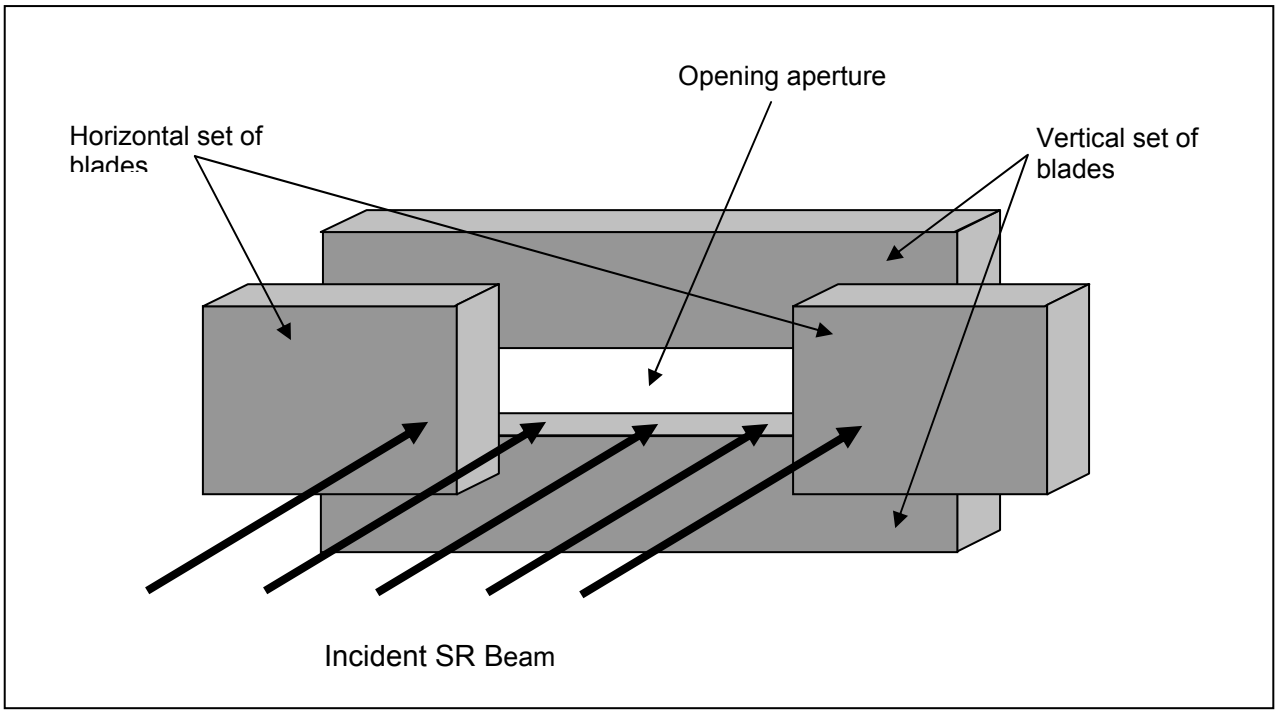

Figure 0.5 Schematic set-up of a horizontal/vertical slit system.

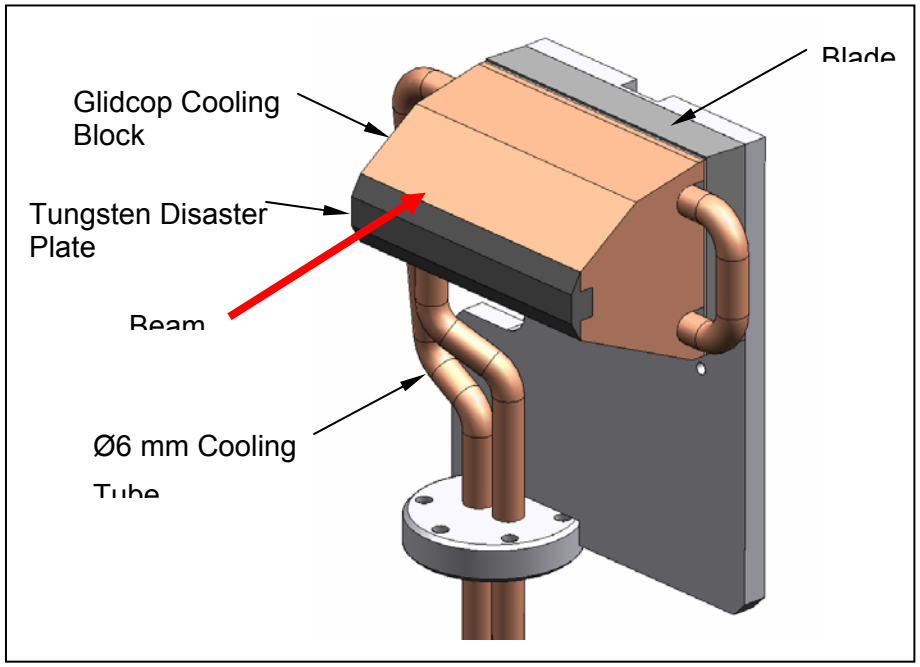

Figure 0.6 Cooling block & slit blade arrangement.

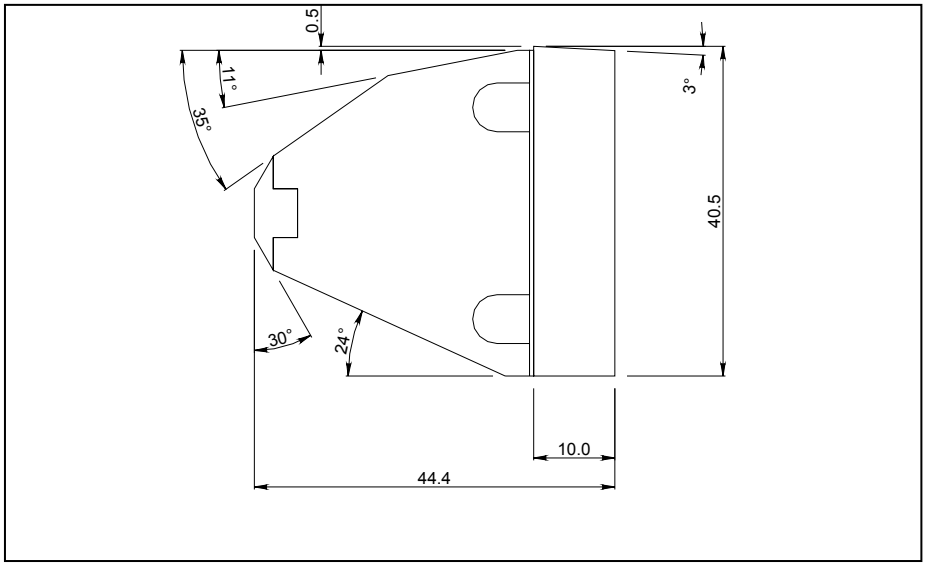

Figure 0.7 Cooling block & slit blade schematic.

Conventional water cooled slits

Each cooled slit unit consists of two slit blades, each of which is mounted onto a water-cooled OFHC copper body and connected to an external actuator mechanism through a flange on the slit vessel. Indium foil is clamped between the slit blade and the copper body to enhance heat transfer by conduction, Figure 0.8. On each slit blade the edge nearest the beam is chamfered, at 3°, to produce a sharp defining (knife) edge. The chamfered face is positioned on the downstream side of the blade (on the side of the blade furthest from the source). On each cooling block the edge nearest the beam is chamfered, at 20°, to reduce the power density of the beam on the block. The chamfered face is positioned on the upstream side of the block. The slit blades are manufactured from 10 mm thick tungsten alloy (95% tungsten or more with the remainder of nickel and iron). The blade defining edge protrudes 0.2 mm above the cooling block.

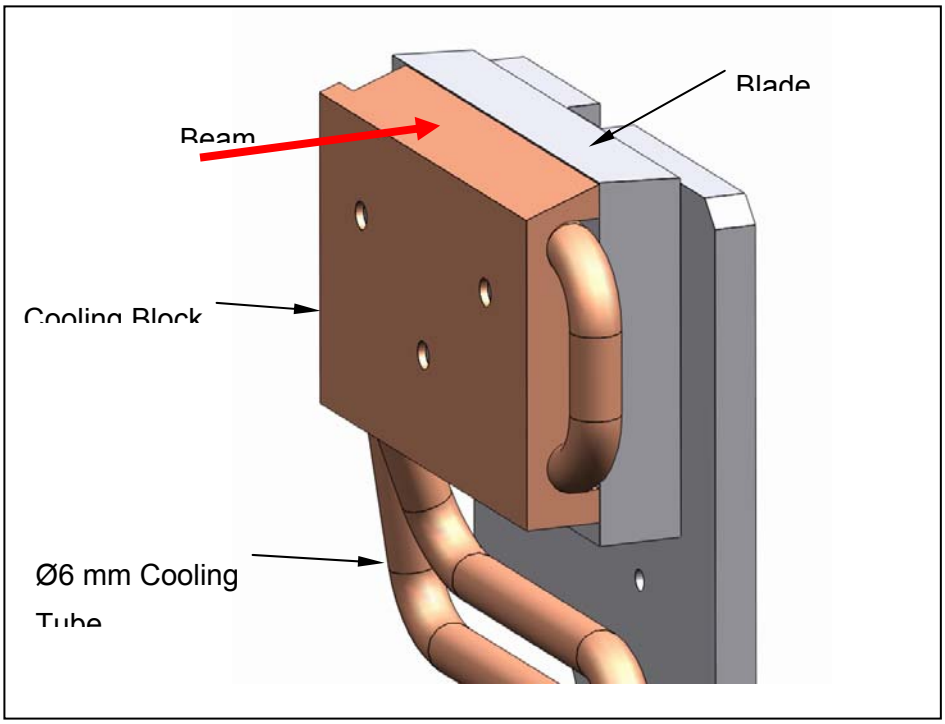

Figure 0.8 Cooling block & slit blade arrangement.

For the cooled slits a spare port is provided on the vessel. This port can accommodate an electrical feedthrough thus allowing thermocouples to be fitted to the slit blades should this be required. Thermocouples are not fitted as standard but can be retrofitted as an upgrade.

Bremsstrahlung collimator and beam stops

The Bremsstrahlung collimators are typically made of 300 mm of lead and their dimensions are calculated from the ray tracing. We will use one of the collimators immediately after the CVD Diamond window/filter.

First Bremsstrahlung stop will be specially designed to be put at the downstream end of the long beam transport pipe entering the outbound beamline. This is done to ensure sufficient separation

of the beam deflected by the mirrors. The Bremsstrahlung stop will be assembled with the water cooled beam mask.

As the end stations are designed for the pink beam Bremsstrahlung stops are needed after the sample positions. Exact location is to be decided when the end stations are designed.

Brehmsstrahlung stops are also anticipated after the DCMs. Depending on the detailed design they will be made of lead (out of vacuum) or Tungsten (in vacuum). The beam stops will need to be translated up and down when the operating mode is changed from monochromatic to pink beam mode.

Mirrors

Parameters of the mirror that will be used on the beamline are given in Table 0.9. It is not immediately clear whether bimorph mirror will offer any significant advantage. Adaptive optics for a VFM mirror can be particularly useful a water cooled DCM is used because residual slope errors could be compensated.

Plane deflecting mirrors will be water cooled and specially designed to cut out part (about one half) of the whole beam. They will operate at a fixed angle of incidence to simplify operation of the beamline. The deflecting mirrors will be made of Silicon, whereas the other mirrors can use Silica as a cheaper alternative.

The downstream vertical focusing mirror will operate in the monochromatic beam only. The mirror system will have capability of removing the optics from the beam to allow operating in pink beam regime.

Quality of the optical surface that can be achieved is being continuously improved by makers of the mirrors.

Double Crystal Monochromators

The water cooled monochromator system will most likely use a vertical beam offset of about 25 mm and a long second crystal to eliminate longitudinal translation and improve stability. The second crystal will be translated vertically to keep fixed offset of the beam.

The DCM is designed to operate at energies of 5-20 keV, has a fixed offset of 25 mm and uses a set of Si(111) crystals. The DCM is designed to achieve angular beam stability of 200 μrad that should be adequate for the current application.

Some useful characteristics of the monochromator of that type are shown in

Table 0.8.

White and pink beam shutters

Pink beam shutters will also be used. They will be positioned after the DCMs and before the hutch wall. Essentially pink shutters are made of a 15 mm thick water cooled Copper plate clamped to a 35 mm thick Tungsten block.

SiN 200 nm window

Supplier	SPI supplies
Outside frame dimensions	7.5mm x 7.5mm
Window size	1.5 mm x 1.5 mm
Membrane thickness	200 nm
Frame thickness	200 μm
Quantity	Pack of 50

4 CSX: COHERENT SOFT X-RAY BEAMLINE

4.1 Executive Summary

The coherent soft x-ray beamline design described in this chapter is state-of-the-art and will be able to fully exploit the brightness and flux provided by the NSLS-II storage ring. The source, an EPU45 Elliptically Polarizing Undulator, will allow full control of the polarization (circular and linear) of the incident photons. The beamline optics design will either preserve this polarization or, additionally, will allow fast-switching of the polarization state of the photon beam on the sample. In addition to providing very high photon flux at high energy resolution, the beam on sample will have a high degree of transverse spatial coherence.

The current design, presented here, will satisfy the requirements of "photon hungry" experiments that demand high photon flux (~10^{13} photons/sec), at high resolving power (~10^4), coherent (a few transverse modes), focused into a small spot (~1.5 μm x 3μm 1-σ).

4.2 Scientific Objective

The scientific motivation for this beamline is that its superior properties will expand the very exciting field of "photon hungry" experiments that currently are limited by their long acquisition times. This set of experiments includes any the uses the coherent part of the photon beam, such as coherent diffraction, phase retrieval imaging using coherent scattering, coherent based microscopy, phase contrast microscopy, and STXM. In addition and in particular, soft X-ray Photon Correlation Spectroscopy (XPCS) experiments demand very high coherent photon flux and have been severely limited by count rates available to date. In a different direction, but equally important, are the studies driven by a scientific case or interest in the understanding of the properties of new materials or artificially engineered systems. Examples of those systems are highly diluted materials, the study of micrometer size single crystals, nanosized-materials and interfaces. Obviously these systems could also be studied using the previously cited techniques, but in many cases other experimental techniques, so called standard, will provide with more precise information about their specific properties.

In general, either justifying the beamline from a technique or the scientific motivation point of view, a beamline working in the soft x-ray energy range will dramatically enhance its scientific capabilities with the possibility to select the incident polarization. This is a characteristic that in the past ten years has been extensively proven in the study of soft-matter and magnetic materials.

The beamline has been designed to host experiments in the soft x-rays energy range from 200eV to 2000eV requiring high coherent photon flux The current CSX beamline design provides high photon flux (~10^{13} photons/sec), at high resolving power (~10^4), coherent (a few transverse modes), focused into a small spot (~1.5 μm x 3μm 1-σ). Taken together, the CSX beamline performance is expected to be better than any other soft x-ray beamline currently operational in the US.

4.3 Insertion Device

This insertion device chosen for the CSX beamline is a pair of 45mm-period Elliptically Polarizing Undulators (EPU45's) that can operate either as one insertion device (same gap and polarization) or in canted mode, where the two EPU45's, separated in angle by ~0.16 mrad, can provide a beam with different polarization. Having two statically-canted (in horizontal angle) insertion devices allows one to control the

polarization switching rates outside the storage ring by the use of a mechanical chopper that selects beam from one of the EPU45's at a time. The switching rate for such a chopper can be quite high, up to kHz rates. Use of switching rates from 10 Hz to 1 kHz are well matched to lock-in technique detection techniques. The use of the lock-in technique has been demonstrated to be very effective in the detection of small signals from magnetic systems, especially in highly dilute samples.

4.4 Sector Layout

4.4.1 Front-End Layout

This is a soft x-ray beamline that will operate windowless and under ultrahigh vacuum conditions. Under these conditions there is no need for a differential pumping section in the front end, although one could be included in order to provide an extra degree of vacuum protection. A 15 mm-square fixed aperture will be located at 18.25 m from the center of the insertion device straight section. Non-absorbing type x-ray beam position monitors (XBPM) should be located at approximately 18.85 meters and 24.15 meters from the center of the straight. An adjustable white beam aperture should be located in the section between the fast gate valve and the second beam position monitor, to define the beam size in real time.

4.4.2 Beamline Layout

The equipment layout for this beamline allows many options. Before discussing the details of the equipment it will be helpful to have an overview of the beamline and define some names. There are three undulator configurations and two branches allowing six major modes of operation. The undulators could be configured to provide one straight beam, two canted circularly polarized beams (upstream and downsteam), two canted linearly polarized beams (upstream and downstream). It would also be possible to configure the accelerator so the beam is steered alternately though the two undulators producing a straight beam with time dependant polarization oscillations. While this case was considered, the decision was made to complete this conceptual design considering the constant **canted** and **straight** cases. For any undulator configuration the beam(s) can be directed along the **short** branch with the branching mirror retracted or along the **long** branch by deflecting off the branching mirror.

The CAD model in Figure 4.1 show an isometric overview of the beamline from the ratchet wall to the end of the short branch. Figure 4.2 shows a side view and Figure 4.3 a top view. Starting at the ratchet wall the major components are:

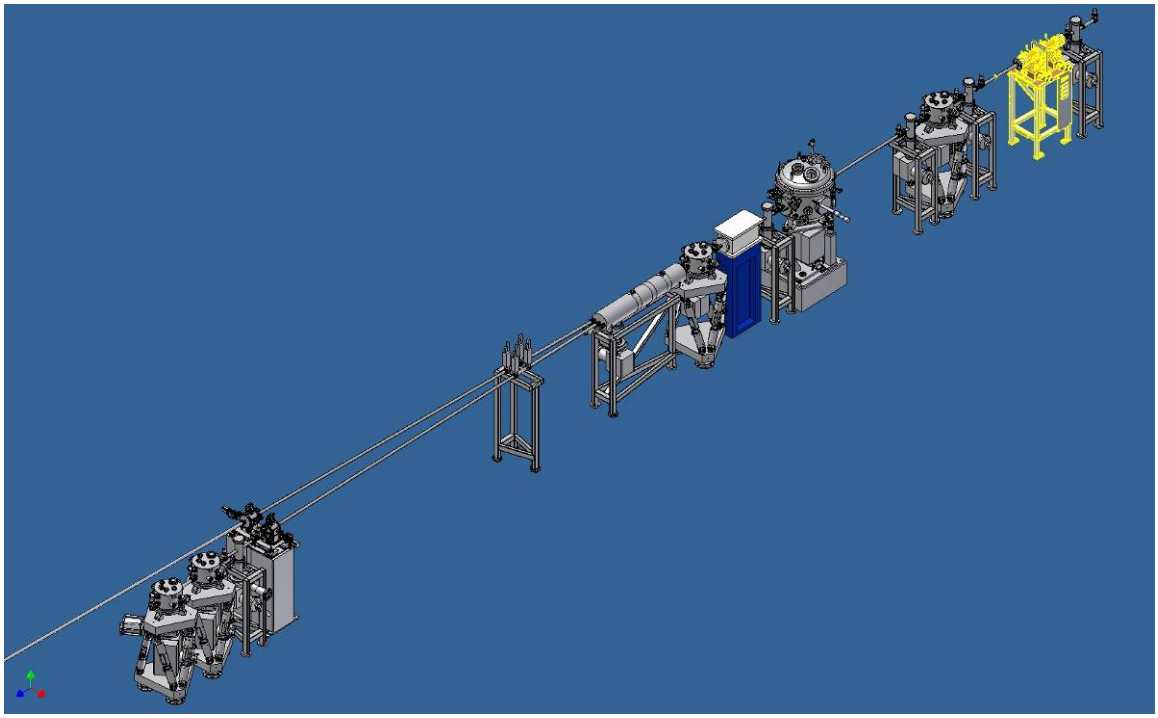

Figure 4.1

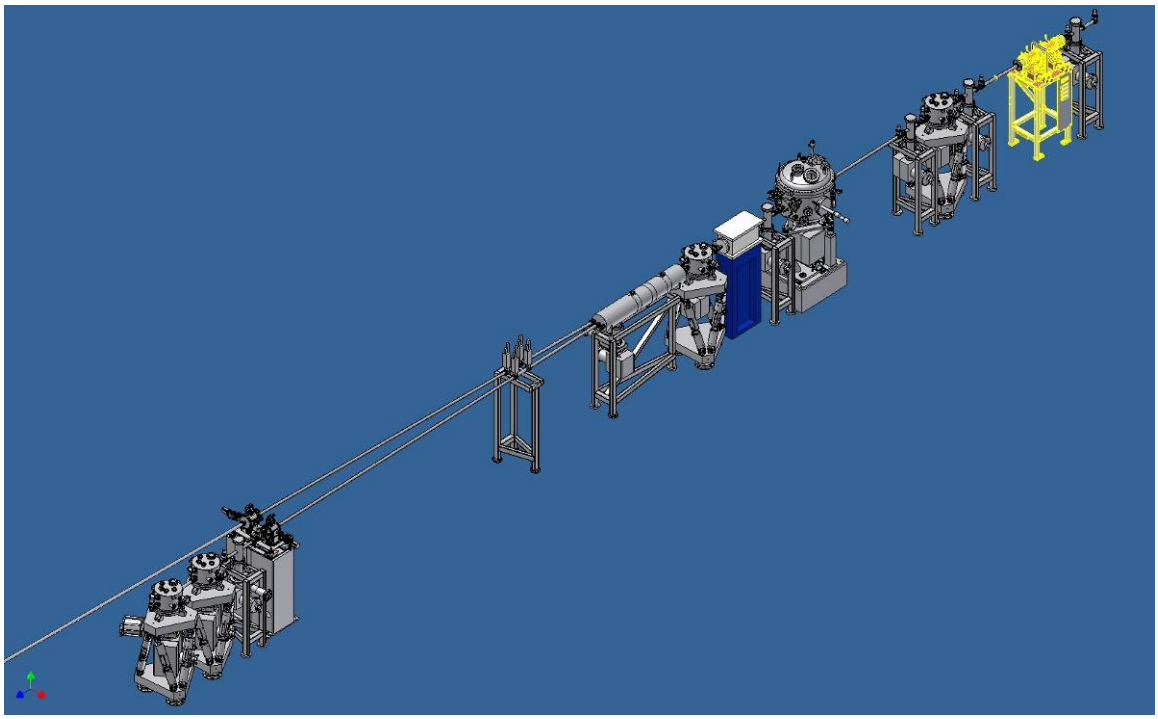

Figure 4.2

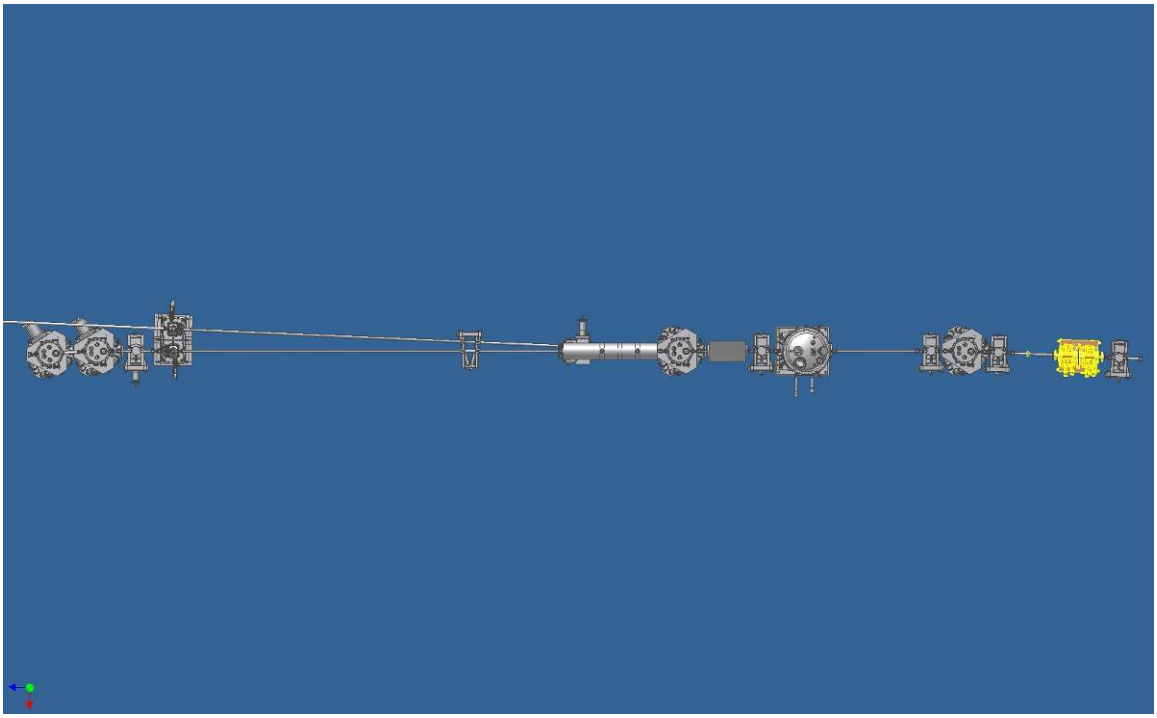

Figure 4.3

White Beam Aperture – rough beam sizing and power absorption

M1 – absorbs high energy beam reducing heat load on downstream optics and collimates the beam vertically

Monochromator – uses M2 and one of three gratings to vertically focus a selected energy on the slit

Chopper – blocks alternating polarizations when operating in canted mode

Branching Mirror – allows diverting the beam into the long branch. Each branch has the following components

Exit Slits – allows the selected energy radiation to pass to the refocusing optics

Beam Defining Slits and Gas Cell – combined chamber allow sizing of the beam, measurement of photon current, and energy calibration

M3 – Horizontal refocusing mirror

M4 – Vertical refocusing mirror

End Station

The mirrors along the beamline are supported with hexapod mounts. To the extent possible these will be made the same and share common mirror boxes. A close up of a hexapod with mirror box, pump, and valves for M3S and M4S can be seen in Figure 4.4.

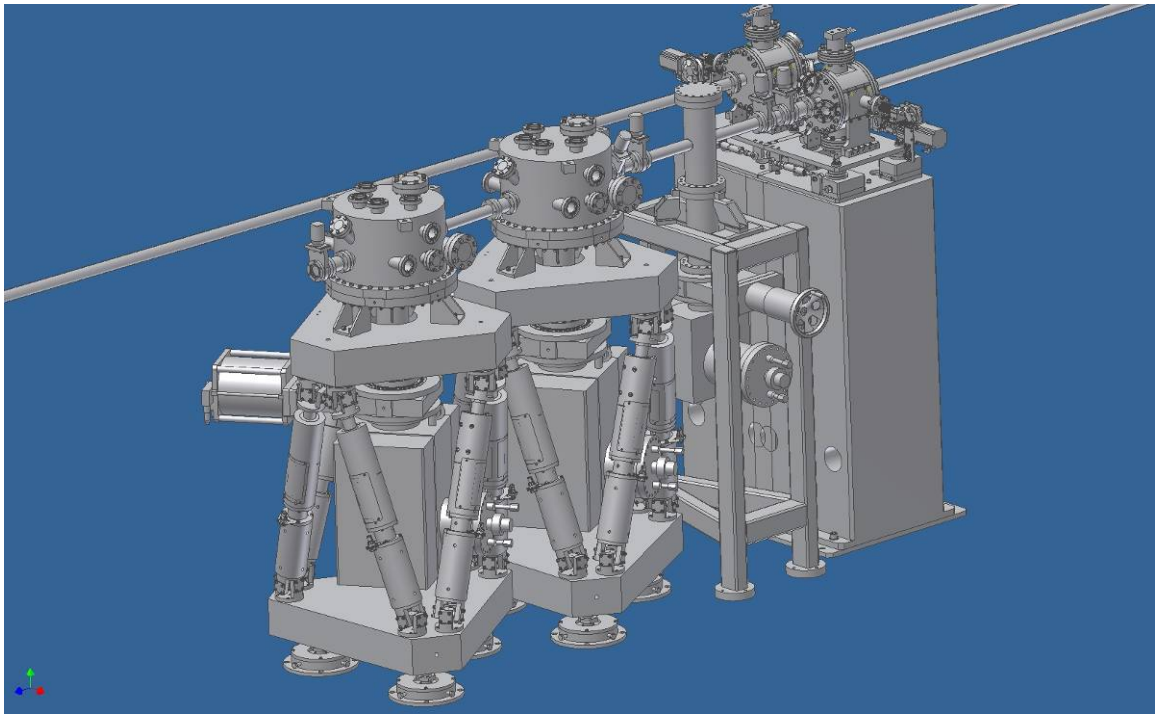

Figure 4.4

Diagnostic chambers are also standardized and placed between mirrors. in the diagnostic chambers shown in the drawings are missing many ports. The design contemplates the use of a Kimball Physics expanded sphere cube as the basic element adding the necessary equipment to the different available ports.. The space between the exit slit and the short M3 is very cramped to include beam defining slits, a gas cell, and a diagnostic chamber. The exit slit was moved as far downstream as possible to maximize the resolution and M3 was moved upstream as far as possible to maximize the space for the end station. The gas cell is included in the diagnostic chamber in front of M3. While it may be possible to fit the beam defining slits in as well, it would be more prudent to move M3 0.5 m downstream in the next design pass. In this CAD model we have only shown the beam defining slit chamber on the long line.

i) CAD model of beamline and hutch layout.

ii) Appropriate shadow model of beamline

4.4.2.1 Survey and Alignment Plans

All beamline components will be surveyed and aligned in place by the facility. In order to facilitate ease of alignment, all components will be fiducialized to external reference points on their table during assembly. All components are designed with a liberal tolerance allowance greater than 0.5 mm.

4.4.2.2 Utility Layouts

The utilities will require the coordination between the beamline and the project infrastructure. At this point in the beamline design the goal is to identify the utility requirements at a high level. Appendix C, List of Key Components, has a spreadsheet with some columns included for utility requirements. Here is a brief summary.

Cooling will be all by chilled water. The total beam heat load of about 12 kW should end up in the cooling

water. There is also the need of cooling for vacuum components including pumps and Titanium sublimator pumps (TSP). The system is envisioned to be a pressurized supply pipe of good quality water and a return pipe supplied by the lab infrastructure. This water should be low-conductivity (LC) to allow electrical isolation of cooled parts. If the water provided by the lab is not LC water, then a separate deionizing and water circulation system will be need for the beamline. The beamline will need about 24 taps into the supply and return for cooling loops. 3 of these taps would go to heat exchangers for separate temperature controlled loops for M1, M2, and the gratings. If we need to cool these below room temp a compressor-based chiller could be added to each of these loops. No cryogenic cooling is envisioned for this beamline. There will be cryogenic requirements for the end stations.

Electricity will be primarily 120 V 60 Hz, but it would be beneficial to have access to 240 V. A rough estimate is 91 duplex 120 V outlets and 9 outlets at 240 V. It would be convenient to have some clean power available in a subset of these outlets. Some of these outlets should be provided with UPS protection. Pneumatics will be required for valve actuation. This could be a pipe with local taps for valves. A rough estimate is 29 air taps. Some of these will be critical safety systems so need to be guaranteed pressure. If the project does not supply this there should be a N2 backup system to guarantee valve operation.

4.4.2.4 Beamline Vacuum System

The details of the design do not allow detailed vacuum calculations. Using the experience of Diamond I06 as a guide, each mirror box was fitted with a 500 l/s pump with TS(After consultation with Diamond beamline responsible beamline I06 does not have the TSPs and wishes they did). Smaller 150 l/s ion pumps were placed at each of the diagnostic chambers, chopper, exit slits, gas cells, and long transport lines. A valve was placed between the chambers and the pumps to allow isolation of the pumps while working on the chamber. These were cost as metal valves. Potentially some of the valves could be changed to O-ring or eliminated. In the spreadsheet of Appendix C, List of Beamline Components, there are columns detailing pump and gauge locations. Each chamber with a pump was fit with a cold cathode gauge. There is a controller for each 6 gauges. Each mirror box was fit with an RGA head. There is one RGA controller. Additional piezo axis on the mirrors may limit the bakeout temperatures to 110 C as they did at Diamond. It would be good to find a work around for this.

There are three fast isolation valves associated with this beamline. One is in the standard front end. There is one on each line between the branching mirror and the exit slit. In the final design there will need to be enough vacuum impedance down steam of these valves to allow leak detection and valve actuation before the pressure wave reaches the valve. The distances between the endstations and the branch valves are long enough that this is not expected to be a problem. The location of the valve in the front end is not defined, but the beamline will have appropriate restriction to insure 15 ms of shutting time if there is a leak in the white beam apertures. Pressure sensing switches were included in each mirror box and the white beam apertures. They should also be included in the end stations as well. The control of these valves will be through the EPS system

4.4.3 Beamline Components

The major beamline components are discussed in this section. Table QQQ covers all the optics and provides information on position, size, spot size, thermal load, and distortion requirements. In the discussion below the numbers for location are referenced from the center of the straight which is the source for the linear straight mode of operation. The mirror sizes referenced are the size of the good optical surface so actual physical size may be larger to accommodate manufacturing. Some ray tracing results are included below but the original reports from Ruben Reininger can be found in appendix A.

Mirror Summary - NSLS-II Soft X-ray Coherent Beamline

Mirror	Mirror Name	Beam from Radiation Wall	Mirror Material	Source Point	Cooling	Bend Plane	Figure Required - Length urad	Figure Required - Width urad	Heat Absorbed B 5.2mm@M1 Bend Angle 183eV Total W	Heat Absorbed B 5.2mm@M1 Bend Angle 183eV Density W/mm^2	Heat Absorbed C Beam Size - A Sigma X mm	Heat Absorbed C Beam Size - A Sigma Y mm	Heat Absorbed C 5.2mm@M1 Mirror Density W/mm^2	Heat Absorbed C 4.0mm@M1 Length Total W	Heat Absorbed C 4.0mm@M1 Width	Heat Absorbed C 7.1mmx5.2mm @M1 Shape and Properties 183eV Density W/mm^2	Heat Absorbed C 7.1mmx5.2mm @M1 Shape and Properties 183eV Total W	Heat Absorbed C 7.1mmx5.2mm @M1 Shape and Properties 183eV Density W/mm^2
M0	M0	No	No Longer in Beamline															
M1	M1		Silicon	Internal		0.25	8	966.558	0.9221	1900 @183eV		0.92			Sagital Cylinder	1160		
M1 central	M1 central		2.80	29.50	Horz			88.75	0.8644	47.617		250	50	1287.08	mm rad			
M1 upstream	M1 upstream								*0.9828*	*47.935*		250	50	1338.89	mm rad			
M1 downstream	M1 downstream								*0.9066*	*44.543*		250	50	1234.89	mm rad			
M2	M2		Silicon	Internal		0.17	3.5	101.624	0.3653	236		0.36			Planar	132		
			3.15	31.83	Vert			87.11	1.2150	17.145		380	50					
						@183eV, 150l/mm -A			*1.1331*	*21.853* @183Ev								
				31.66				88.725										
						@2.3keV, 400l/mm -A												
				31.93				84.012										
						@183eV, 1200l/mm -B												
Grating LEG	Grating LEG		Silicon	Edge		0.13	5.5	1.8125	0.0041	40		0.06			a0 l/mm	a1 l/mm^2	a2 l/mm^3	c
			5.30	32.00	Vert			87.69, 86.53	1.1267	21.425		130	25	150	0.0540	8.09E-06	~1.5	
	Grating MEG					@183, 150l/mm -A			*1.1388*	*27.340* MEG@183eV								
Grating MEG	Grating MEG			32.00				88.98, 88.47				130	25	400	0.1438	2.15E-05	~1.5	
	Grating HEG					@2.3keV, 400l/mm -A												
Grating HEG	Grating HEG			32.00				86.24, 81.78				130	25	1200	0.3018	4.51E-05	~2.2	
						@183eV, 1200l/mm -B												
BM	BM		Silicon	Edge		0.22	8.8						3	0.004				
	SLIT		7.30	34.00	Horz			88.70	1.1532	55.745		600	10	0.24	Plane			
SLIT			15.30	42.00					1.4784	0.00846								
	M3S								1.4804	0.00573								
M3S	M3S central		Silicon	None		0.17	14						0.002	2.2E-05	Plane Elliptical - Bimorph			
	M3S upstream										0.30 x 138.0 spot (+/-1 sigma)							
M3S central	M3S downstream		16.50	43.20	Horz			88.5	0.1560	69.421		350	50	22475	mm rad	189.68	mm rad	
M3S upstream	M4S								*0.2017*	*66.822*		350	50	23125	mm rad	191.51	mm rad	
M3S downstream			Silicon	None		0.37	14		*0.1417*	*68.144*		350	0.002	2.3E-05	mm rad	21825	mm rad	186.8	mm rad
M4S			17.25	43.95	Vert			88.5	0.8672	11.589		75	50	Plane Elliptical - Bimorph				
	End Station S								*0.9627*	*13.224*			0.008	18447.5	mm rad	30.463	mm rad	
											0.0038 x 0.0054 spot (1 sigma)							
End Station S			18.25	44.95					0.00188	0.00269								
									0.00205	*0.00248*								
	M3L																	
M3L	M3L central		Silicon	None											Plane Elliptical - Bimorph			
M3L central	M3L upstream																	
M3L upstream	M3L downstream		24.50	51.20	Horz			88.5				450	50	26600	mm rad	220.75	mm rad	
M3L downstream																217.54	mm rad	
	M4L		Silicon	None					*1.2742*	*75.034*		450	50	25950	mm rad	217.93	mm rad	
M4L																		
	End Station L													5600	mm rad	69.67	mm rad	
End Station L			26.50	53.20					*0.00188*	*0.00046*								
	Reference Sources - all by Ruben Reininger								*0.00164*	*0.00047*								

	A	Traces 070827.pdf	APPLE II, 85 Period, 45 mm/period, 183eV, X=46.4 um, Y=37.2 um, dX=35.1 urad, dY=
Reference Sources - all by Ruben Reininger	B	abs_M2_183eV_HEG.xls	5.2 mm square apperture at 29.5 m, 183eV, 1200l/mm (HEG), Zeiss drawing lower case
A	C	Traces 070827.pdf	APPLE II, 85 Period, 45 mm/period, 183eV, X=46.4 um, Y=37.2 um, dX=35.1 urad, dY=29.2 urad
B	D	Power deformations 070917	Various cases with different appertures and gratings
C	E	abs_M2_183eV_HEG.xls	5.2 mm square apperture at 29.5 m, 183eV, 1200l/mm (HEG), Zeiss drawing lower case
D		Power, deformations 070917	Various cases with different appertures and gratings
E		Slope Errors 070904.doc	Limits required so resolution, horizontal spot and vertical spot do not degrade by more th
		Traces 070911.doc	Canted Beam cases

4.4.3.1 White Beam Apertures

The power produced by the undulators is about 12 kW with power densities up to 40.1 kW/mrad^2. The white beam apertures, located at 28 m, would see a power density of up to 51 W/mm^2. They will have sufficient cooling to be able to absorb 12 kW at these power densities. An appropriate choice for these would be the IDT design used at Diamond. This consists are two water cooled copper cylinders with tapered square holes mounted on a translation stand. One cylinder is translated to define the bottom and right edge of the beam while the other is translated to define the top and left edge of the beam. The cylinders are water cooled but there are no water joints exposed to vacuum. This design has been used at Diamond I06 at similar power levels. The aperture needs to be adjustable to allow a spot size as large as 7.1 mm vertically (to over illuminate M2 for thermal stability) and 9.5 mm horizontally (canted beam case). The Diamond set incorporates some tungsten to help better define the beam.

4.4.3.2 M1 Mirrors

The first mirror makes a horizontal bend of 2.5° (88.75° from normal) so it absorbs a considerable amount of power passing only the softer X-rays to the downstream optics. With a 7.1 x 5.2 mm beam in the M1 plane at 29.5 m the mirror absorbs 1160 W with the undulators in the straight mode and adjusted for 183 eV. This gives a maximum power density of 0.92 W/mm2. These mirrors will be cylindrically ground to vertically collimate the beam. Thermal distortions in the length direction (meridional) beyond 0.25 μrad will increase the size of the horizontal beam spot and in the width direction (sagittal) beyond 8 μrad will decrease the energy resolution. Internally water cooled silicon mirrors have been selected for the M1s to provide the maximum thermal control. Cryogenic cooling would provide better thermal stability due to the lowered coefficient of thermal expansion (CTE) and the improved thermal conductivity of silicon at low temperatures, but with soft X-rays even a small layer of ice build up is a problem. Thermal modeling done for the Diamond I06 beamline showed expected rms slope errors of 20 μrad sagittally and 3 μrad meridionally at similar power levels (0.92 W/mm2) for an internally cooled silicon mirror. Preliminary ray tracing results have shown that this level of distortion can be compensated for by adjusting the operating angles of the monochromator and curvature of the M3 optic. Reduction of the levels of distortion may be obtained by reducing the coolant temperature enough to gain some improvements in silicon properties but not enough to produce ice build up. Both the optical correction and distortion minimization need further study to insure thermal distortions in M1 do not significantly reduce the beamline performance. The use of an M0 mirror before M1 was investigated. To split the power between the two mirrors, the M0 would need to be at a very shallow angle. This makes the mirror very large, expensive, and prone to distortion at the high power levels. There was significant cost saving in eliminating this option.

There are three M1 mirrors in this design. One for the straight operation mode and two (an upstream and a downstream) mirrors for the canted operation mode. Several options were considered to reduce the number of mirrors and some of these options may end up working. However, the three mirror option is the only one we could adequately verify during this design pass. It may be worthwhile to reopen this issue when answers to some of the accelerator related questions can be definitively answered. The three mirrors have slightly different shapes because the distance to the source varies between the operation modes. The size of the M1 mirrors was set to 250 mm long x 50 mm wide. This length is 5 σ from the expected spot size for a 5.2 mm horizontal beam size in the plane at 29.5 m. Figures QQQ, QQQ, and QQQ produced by Ruben Reininger show the expected spot on M1 with undistorted optics for the straight, canted upstream, and canted downstream configurations. Internally cooled silicon mirrors of this size with the required ~1300 mm sagittal cylindrical radius and meridional figure slope error of 0.5 μrad rms are within the normal manufacturing capability of InSync. This beamline requires meridional figure slope error of 0.25 μrad rms which may

require the addition of profile coating to the process. Detailed thermal modeling may show a longer mirror would be useful to reduce the effects of distortion at the ends of the heated stripe. The width should be enough to allow multiple stripes to be used. Wider mirrors would increase the vertical movement requirement to switch between the straight and canted modes (see below).

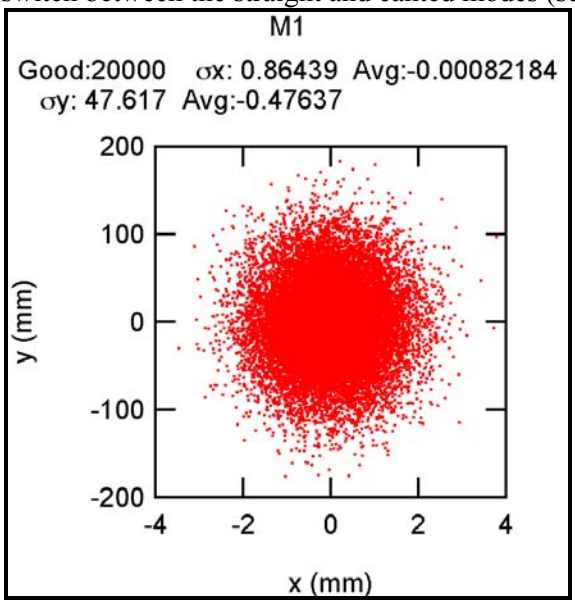

Figure 4.1. M1 illumination, undulator 183eV linear straight mode

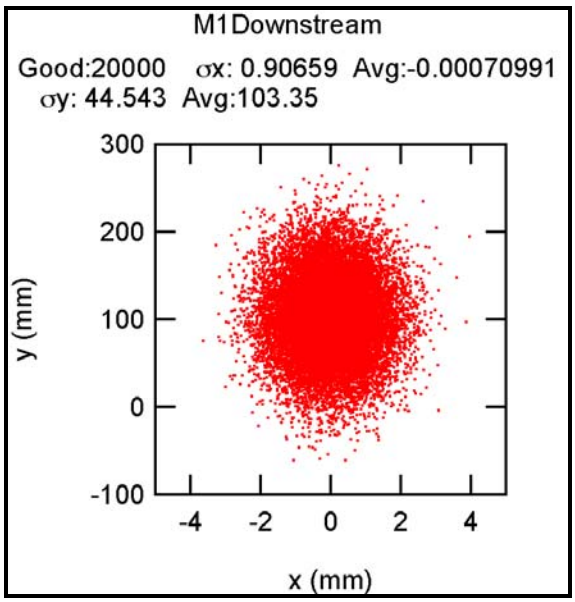

Figure 4.2. M1 illumination, undulator 230eV circular canted mode

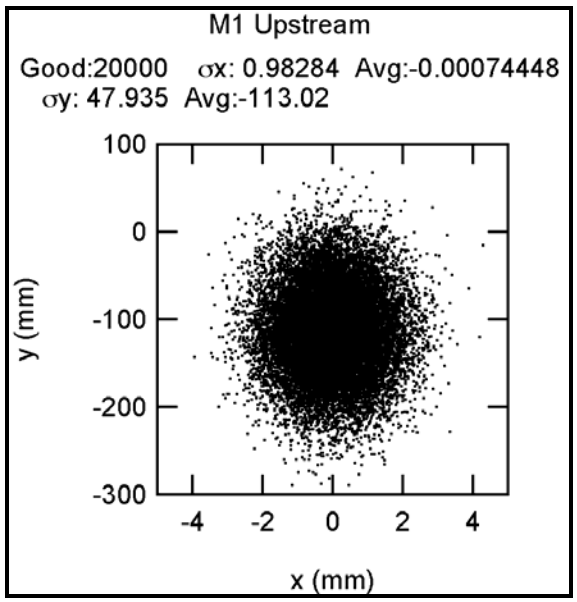

Figure 4.3. M1 illumination, undulator 230eV circular canted mode

The support system for mirrors is a hexapod system. The hexapods build by Oxford Danfysik for the Diamond I06 beamline would be a good choice. By standardizing on a flexible support the beamline will be easier to install, maintain, and operate. Controlled changes to the lengths of the six supporting legs can

Figure 2 M1 illumination, undulator 230eV circular canted mode

provide translations and rotations about convenient axis. The repeatability of motion is 1 μm and 2 μrad at the 2 σ level. This would be sufficient for single mirror alignment requirements except the bending angle. For this, additional piezoelectric axes in the vacuum chamber will be used. In the canted beam case the first mirror can be aligned with the hexapod, but the second mirror will require additional alignment. The second mirror will be fit with four in vacuum axes. With detailed study of the kinematics of the hexapod and alignment sensitivities it may be possible to reduce this number. The large translation required to change between the one mirror straight mode and the two mirror canted mode is outside the normal 25 mm range of the hexapod. A larger range can be accommodated but at some loss in repeatability. If the repeatability degradation is too large an additional vertical axis may be required. This will need additional study. The stiffness (vibration modes) of the hexapods has proven adequate for operation at Diamond I06 with similar requirements.

4.4.3.3 Monochromator

The beam enters the monochromator, makes an upward vertical bend at the M2 mirror and then another vertical bend at one of the three variable line spaced gratings. The angles of the M2 and gating are set so the beam exiting horizontally with a 15 mm vertical offset (aimed at the exit slit) is of the selected energy. The line spacing of the grating is set so the light of the selected energy hitting the bottom of the grating is exiting at a slightly upward direction and the light of the selected energy hitting the top of the grating is exiting at a slightly downward direction thus focusing the light to a minimum vertical size at the exit slit. There are three sets of grating, LEG 150 l/mm, MEG 400 l/mm, and HEV 1200 l/mm to allow a trade off between energy resolution and delivered photons. Consideration was given to adding a fourth grating position with a spherical mirror to direct a “hot pink” beam to the experiment station. The decision was made that the 150 l/mm grating could provide enough pink beam power by opening the exit slit to the desired size. This keeps the number of gratings to three allowing use of more standard monochromator designs and reduces concerns for heating of downstream optics.

The M2 mirror makes a vertical bend of 12.0° (84.01° from normal) when operating at 183eV with the HEG grating so it absorbs a considerable amount of power passing only the softest X-rays to the downstream optics. With a 5.2 x 5.2 mm beam in the M1 plane at 29.5 m the M2 mirror absorbs 102 W with the undulators in the straight linear mode and adjusted for 183 eV. This gives a maximum power density of 0.36 W/mm2. M2 is a flat mirror that does no intentional focusing. Thermal distortions in the length direction (meridional) beyond 0.17 μrad will reduce the energy resolution and in the width direction (sagittal) beyond 3.5 μrad will increase the horizontal spot size. Internally water cooled silicon mirrors have been selected for the M2 to provide the maximum thermal control. Cryogenic cooling would provide better thermal stability due to the lowered coefficient of thermal expansion (CTE) and the improved thermal conductivity of silicon at low temperatures, but with soft X-rays even a small layer of ice build up is a problem. Thermal modeling was done with Finite Element Method by Ken Kriesel. A detailed report can be found in Appendix E. The thermal load produces a raised bump on the M2 surface. This bump has the largest slope changes near the ends of its length. With a beam size of 5.2 mm square at M1 the ends of the thermal bump on M2 are still part of the active optical path and greatly degrade the vertical optical performance doubling the vertical beam size at the exit slit. Increasing the aperture to 7.1 mm vertically increases the total heat load on M2, but moves the high slope areas out of the active optical path. The remaining thermally induced distortions can be corrected. The figure change in the central part of the M2 thermal bump can be approximated by a convex radius of ≈1.8×107 mm, which means the beam incident on the grating is not vertically collimated as in the optical design. This change in the virtual source position can be corrected by operating the grating with a c value of 2.193 instead of the nominal value of 2.184 at this energy. This change in operation essentially restores the vertical size of the beam at the exit slit. While 183eV appears to be the worst case, further work needs to be done to verify that this correction method can be done at higher beam energies. The horizontal distortion of M2 increases the horizontal spot size at the end station. The plan is to correct this by changing the shape of

the focusing mirror. The M3 and M4 mirrors are planned to be bimorphs. Preliminary work suggests that this method will work. Reduction of the levels of distortion may be obtained by reducing the coolant temperature enough to gain some improvements in silicon properties but not enough to produce ice build up. Both the optical correction and distortion minimization need further study to insure thermal distortions in M2 do not significantly reduce the beamline performance.

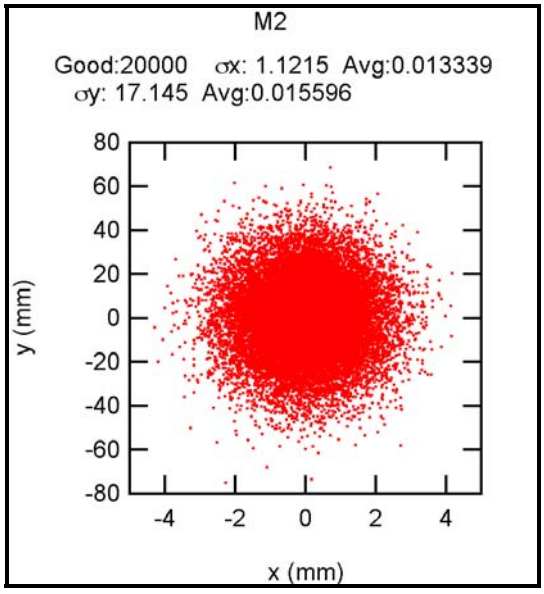

Figure 4.4. M2 mirror illumination, undulator 183eV linear straight mode

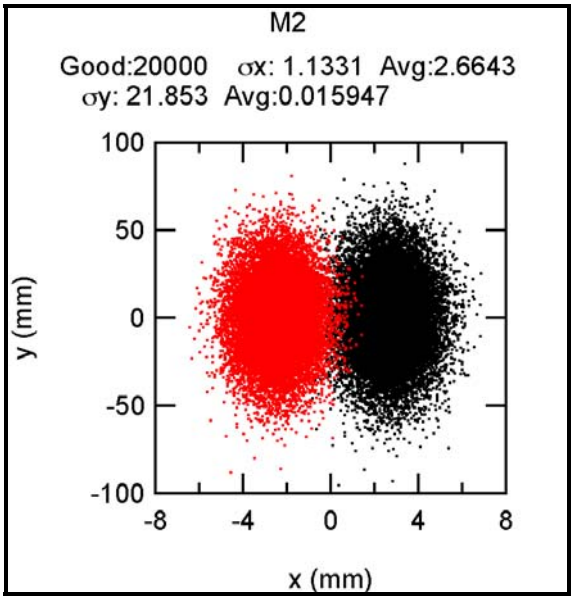

Figure 4.5. M2 mirror illumination, undulator 230eV circular canted mode

The size of the M2 mirrors was set to 380 mm long x 50 mm wide. The monochromator motion rotates M2 about a point 7.577 mm above the optical face of the grating. This changes the distance along the beamline that the center of the beam strikes the mirror from 31.66 m at 2.3 keV (88.73° from normal to beam) to 31.93 m at 183 eV (84.01° from normal to beam). This effective translation of the mirror relative to the beam helps determine the length requirement of the optic. Figures QQQ, and QQQ produced by Ruben Reininger show the expected spot on M2 with undistorted optics for the straight, canted configurations. Internally cooled silicon plane mirrors of this and figure slope error of 0.17 µrad rms are slightly pushing the current state of the art manufacturing capability of InSync. However, InSync is currently quoting 0.25 µrad rms and has produced somewhat better, without using profile coating. Addition of profile coating should allow achievement of the required figure with current technology.

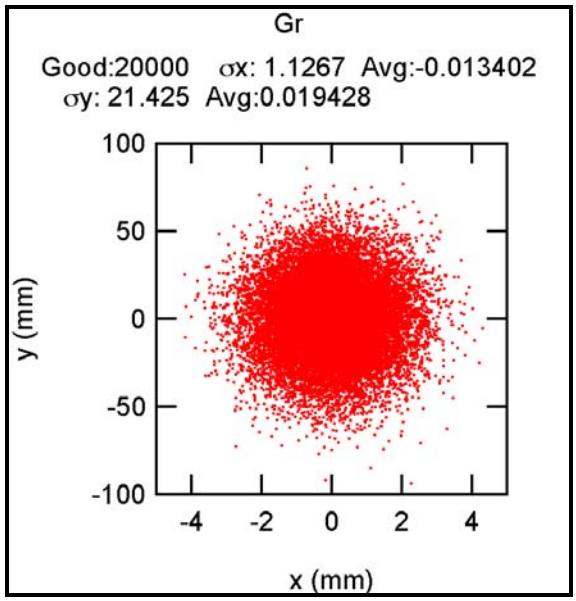

Figure 4.6. Grating illumination, undulator 183eV linear straight mode

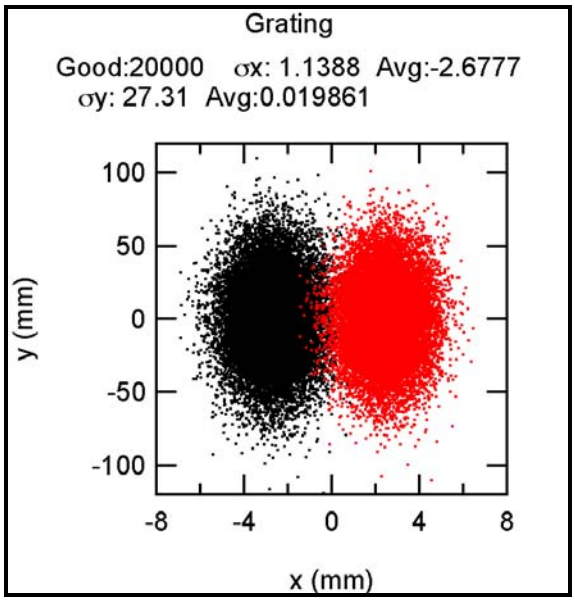

Figure 4.7. Grating illumination, undulator 230eV circular canted mode

The size of the gratings was set to 130 mm long x 25 mm wide. This length is 5 σ from the expected spot size for canted beam operation at 230eV. The monochromator motion rotates the grating about the central face of the grating and can translate the grating support to place any of the three gratings into the beam. The gratings will be edge cooled silicon because the expected heat load is less than 40 W in the worst case with a power density of 0.016 W/mm^2. Figures QQQ, and QQQ produced by Ruben Reininger show the expected spot on the gratings with undistorted optics for the straight, canted configurations. These gratings are within standard manufacturing capability.

JenOptik makes a CPGM that is suitable for this beamline. The required resolution in angle is 0.03 μrad for the gratings and 0.05 μrad for the mirror. These requirements are better than the advertised capability of the JenOptik monochromator.

4.4.3.4 Chopper

The chopper is a mechanical device with a double function, block the non-desired radiation to come down to the end stations from the two canted insertion devices and provides with the switching frequency between the two different polarizations delivered by the EPU's selecting in time the beam from one of the two canted insertion devices serving this beamline. The chopper will also have a neutral position were x-rays from both insertion devices may pass without any being blocked. The preferred location of this piece of equipment will be between the monochromator and the branching mirror. It is desired that the switching frequency of the chopper could be selected from a few Hz up to several kHz. Having the possibility to select the different frequencies will allow choose a noise free frequency without interfering with noise from other frequencies. This can be achieved utilizing a rotating blade using ferrofluidic© style feedthroughs to connect with the driving motor and the switching control mechanism located outside of the vacuum chamber. A new design of an existing chopper located at the NSLS X13A beamline, is being improved. The X13A beamline requires a chopper because of the fast switching 22Hz characteristic of its unique source an Elliptically Polarizing Wiggler (EPW).

4.4.3.5 Exit Slit

The exit slits used by the Diamond I06 beamline were manufactured by Bestec. They would also be appropriate for this beamline. The power at the exit slits is expected to be less than 10 W with a power density less than 0.24 W/mm. According to Bestec this will not require cooled slits. The two exit slits are pretty close together on the branching line, but do fit without interference. The standard stands do interfere but can be easily modified. Pictures of the spot size at the exit slits for various conditions can be found in the reports from Ruben Reininger in Appendix A, SAS Optics Reports.

4.4.3.6 M3 and M4

The final focusing mirrors, M3 & M4 are Silicon Elliptical Bimorph mirrors. The same Hexapod mounting strategy is used for these as for M1 and the branching mirrors. The heat load at these mirrors is small so they do not require cooling. Correction for the thermal distortions of the M1 mirror and M2 mirror can be made respectively by changing the curvatures of M3 and the monochromator to recover the small spot size. Preliminary investigation suggests that this could be accomplished with a simple bending of the mirrors. The bimorph technology is exciting and would allow more complete correction at a small cost premium. This cost was included. For the canted beam case there needs to be three M3 mirrors just like there are three M1s. This will require additional in vacuum axis to get precision alignment of the mirrors as with M1. Each line has just one M4. The short branch M3s and M4 are 350 mm and 75 mm long respectively. The long branch M3s and M4 are 450 mm and 350 mm long respectively. The spacing between the long branch mirrors was increased to 1 m from the 0.75 m for the short branch. The tentative distance to sample spot from the M4 is 1 m for both lines. Pictures of the spot size on the final focusing mirrors for various conditions can be found in the reports from Ruben Reininger in Appendix A, SAS Optics Reports.

4.4.3.7 Diagnostics

Diagnostics are included for vacuum, beam current monitoring, beam position monitoring, temperature and flow sensing, and energy measurement. Vacuum RGAs and cold cathode gauges are discuss in the vacuum section. Costs were included to monitor the temperatures of all 25 cooled surfaces and the flow of the corresponding 14 coolant paths. Sensor signals would be conditioned and readout over a network to the central computer. This can provide a warning for temperatures going out of range and possibly be used as input into beamline operating setting. 4 fluorescent screens are anticipated to help locate the beam. These will be housed in the diagnostic chambers. Instrumented mesh will allow measurement of beam current upstream of the exit slits. Photo diode will monitor beam current after the exit slits. These will also be housed in the diagnostic chambers. The photo current on mirror surfaces, and beam defining slits will also be monitored. These devices will also report to the network either directly or through signal conditioners. A gas cell is included on each branch to allow energy calibration. The length of these was set to 0.5 m. A decision was made to use a Kimbal Physics Expanded Sphere for the diagnostic chambers, but there was not time to include this in the CAD model.

4.4.4 Endstations

The beamline has been designed to have two branches, each of which has the capability to host one or more independent endstations, depending on user demand. The angular separation between the two branches will be 2.5° and the two branches will be of unequal length, in order to provide adequate non-interfering floor space for endstations. This beamline will be able to host a wide variety of types of endstations, including diffractometers, spectrometers, and microscopes. The only restrictions on endstation types compatible with this beamline will be space and vacuum compatibility for windowless connection to the storage ring vacuum. A very important component of the beamline equipment protection system will be interlocks that

continuously monitor the end station vacuum pressure and temperature to avoid accidental venting of the storage ring. The endstation design and hardware will provide experimental capabilities (detectors, sample environments, and sample and detector motions) with enough degrees of freedom to permit users to carry out specific experiments using focused, high-resolution, high flux, coherent soft x-rays from the beamline. The endstation will also provide pinholes and/or specific coherent soft x-ray focusing optics (e.g. Fresnel zone plates) to perform experiments using the coherent part of the photon beam.

One example of an endstation well-matched to the capabilities of the CSX beamline is a multipurpose ultrahigh vacuum compatible four-circle diffractometer that will fully utilize the energy range, high photon flux, extraordinary brightness, and polarization control provided by the beamline. Conceptually, this endstation will emphasize scattering experiments, but at the same time will have the flexibility to introduce optical elements such as pinholes, Fresnel zone plates, and polarization analyzers, allowing one to conduct an wide range of experiments. The use of pinholes of different sizes in the chamber will enable coherent scattering and/or small angle scattering experiments to be performed, depending on the pinhole size. Combining polarization control of the soft x-rays incident on the sample with the capability to analyze the polarization of the soft x-rays reflected/emitted from the sample will provide an extremely powerful tool to study orbital and spin magnetic moments and molecular orientation in crystalline and partially ordered samples.

In more detail, a multipurpose endstation would consist of a high vacuum compatible vacuum vessel containing a basic four-circle in-vacuum diffractometer, two independent concentric circles dedicated to the detector and the sample rotations. The detector arm should be able to move a wide angular range exceeding 180 degrees. It is desirable that the incident beam on the sample and the beams detected by a number of detectors be unimpeded by any other instruments in the chamber over their full intended ranges of motion. The chamber should incorporate an electromagnet, using high T_c superconducting technology that will provide with homogeneous (1% in a distance +- 5 mm from the center of the magnet) magnetic fields up to 1 Tesla in x, y and z directions. This magnet will be able to rotate together with the sample keeping constant the direction of the magnetic field relative to the sample surface, or will be able to rotate independently of the movement of the sample, without disrupting in either case the incidence of the beam on the sample. The sample stage will be mounted on a cold finger that will cover a sample energy temperature range from 4K up to 300 K. Currently it is under study the possibility to raise the temperature of the samples above room temperature, but we are aware that this could cause the quench of the superconducting magnet. The chamber it self is conceive to have a sample transfer system that will allow to transfer samples when they are cool without breaking the vacuum, reducing the down time when samples get changed.

The design of the endstation and its vessel provides space for a motorized system of pinholes or refocusing optics in the front part of the chamber to allow the use of the coherent characteristics of the x-ray beam. The design of the detector arm includes space for the future a polarization analyzer. The vessel and its ports have been designed to allow the insertion of these two instruments during a maintenance period.

The endstation will also be provided with a pressure and temperature monitoring system connected to the beamline Equipment Protection System that will protect the beamline vacuum and instruments from possible errors in the operation of the end station that could lead to loss of vacuum.

4-A Appendix A: SAS Optics Reports

Canted Beams for the Coherence Beamline.

August 23, 2007

Questions were raised about the required separation between the canted beams when the insertion devices are operated to deliver right and left circular polarized light. Since there is no horizontal focusing until the plane elliptical mirrors downstream the exit slit, the horizontal acceptance for the beams and the canting angle between them should be as small as possible. However, a too small canting angle is not desirable since the two polarizations will overlap.

Since only the first harmonic is emitted on axis when the ID is tuned to deliver circular polarized radiation, higher harmonics will be in the acceptance of the other ID. Furthermore, there could be some "at energy" flux emitted by one ID in the horizontal acceptance of the other ID.

To address these issues, we calculated the angular flux and angular power density over a wide horizontal angle when the upstream insertion device (ID) is tuned to emit circular polarized radiation. The calculations were performed with the SPECTRA code [1] at three photon energies. In the calculations we assumed that the ID center is 1.3 m upstream the center of the straight section. The machine parameters at this position are listed in Table 4.A.1. The parameters of the ID and photon energies are given in Table 4.A.2.

Figure 4.A.1Figure 4.A.2, and Figure 4.A.3 show the angular dependence of the flux density when the upstream ID is tuned to 231, 501, and 1008 eV, respectively. From these data, we obtained the integrated flux as a function of the horizontal aperture and full vertical aperture. As seen in Figure , a horizontal aperture of 0.16 mrad allows to collect practically the whole central cone flux at 501 and 1008 eV and most of this flux at 231 eV. The "at-energy" flux leaked in the acceptance window of the downstream ID was integrated from the data in Figure 4.A.1Figure 4.A.2, and Figure 4.A.3 assuming that the separation between the beams axis is equal to the acceptance angle. The leaked flux is plotted in Figure 4.A.5 for the three energies. Clearly, there is no optimal aperture for all energies. A reasonable compromise, which gives at most a 3% leak at the three energies, is a canting angle and an aperture of 0.16 mrad. A smaller leak percentage could be achieved with a canting angle of 0.2 mrad or larger and a (variable thickness) beam stop inserted in between the two beams. at high energies.

The angular power densities when the upstream ID is tuned to the three photon energies are shown in Figure ,4.A.6, Figure 4.A.7, and Figure 4.A.8. For an horizontal aperture and canting angle of 0.16 mrad the power obtained at 231 eV in the upstream ID aperture is 10.5 W and in the downstream ID aperture 22.7 W. At 501 (1008) eV the values are 45 (97) W for the upstream and 95 (71) W for the downstream.

References

1. T. Tanaka and H. Kitamura, J. Synchrotron Rad., **8**, 1221, 2001

Tables

Table 4.A.1. Machine parameters used in the calculations. Upstream ID.

Energy (GeV)	3.0
Current (mA)	500
εx (pm rad)	550
εy (pm rad)	8
βx (m)	2.61
βy (m)	2.88
αx (μrad)	0.914
αy (μrad)	1.58

Table 4.A.2: ID parameters used in the calculations.

ID type		APPLE II	
Number of periods		44	
Period length (mm)		45	
Energy (eV)	230.6	501.3	1008
kx and ky	2.69	1.67	0.94

Figures

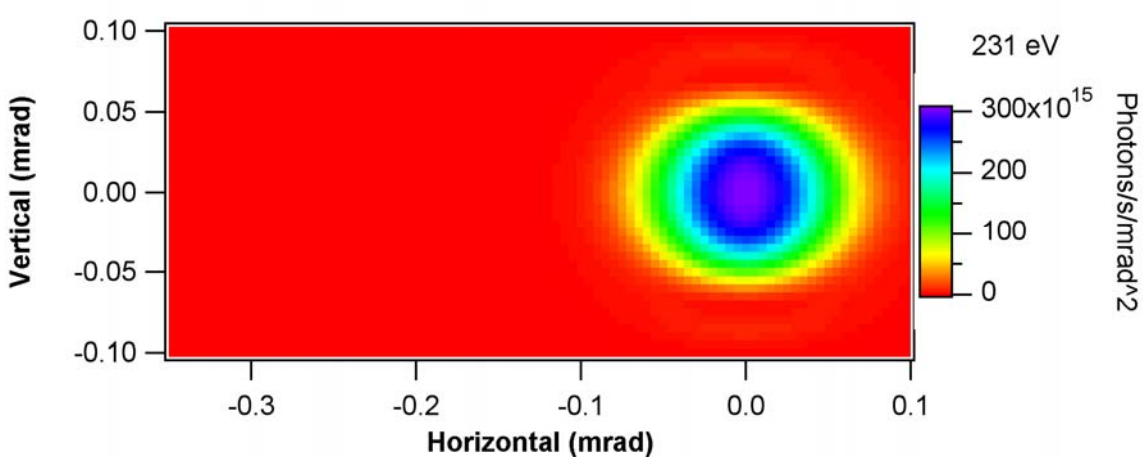

Figure 4.A.1. Angular flux density (in 0.1% BW) when the upstream ID is tuned to 231 eV.

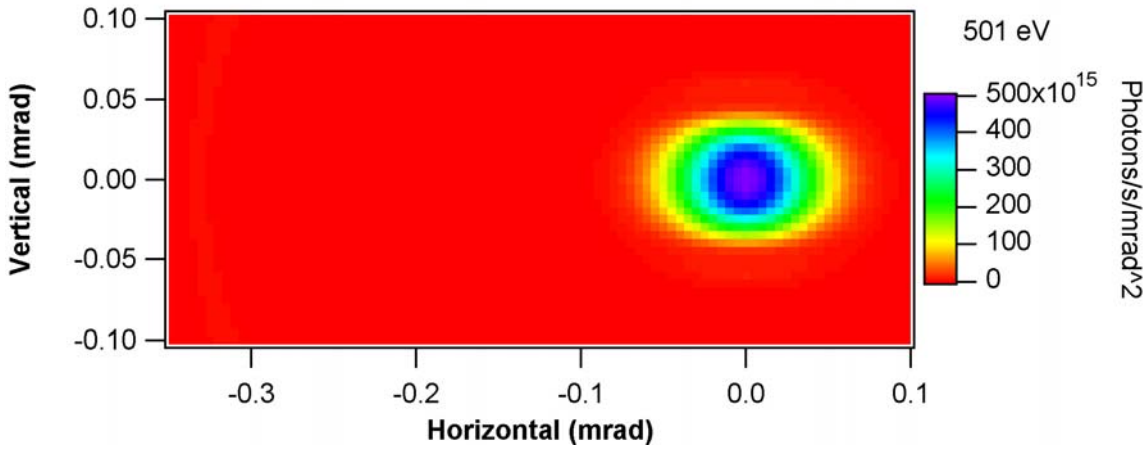

Figure 4.A.2. : As Figure 4.A.1 when the upstream ID is tuned to 501 eV.

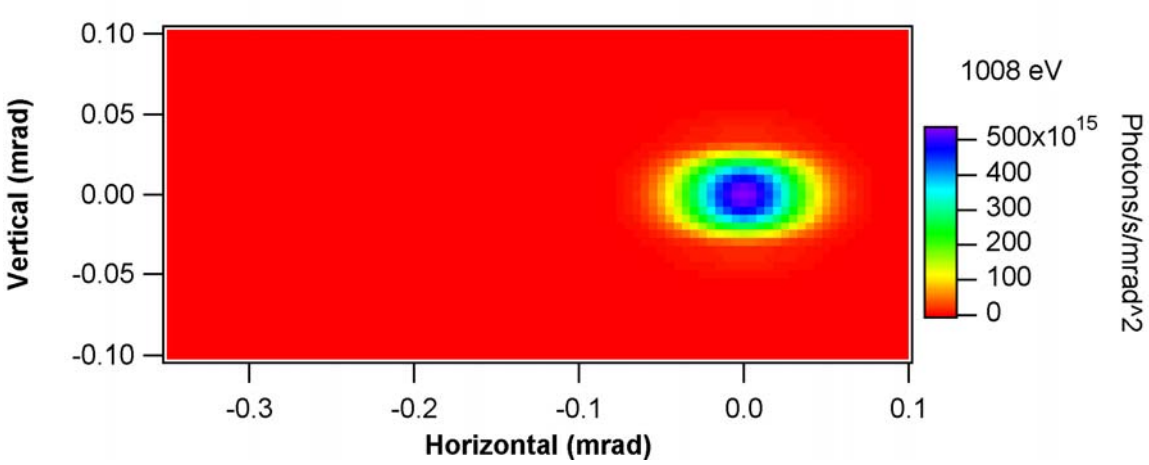

Figure4.A.3. As Figure 4.A.1 when the upstream ID is tuned to 1008 eV.

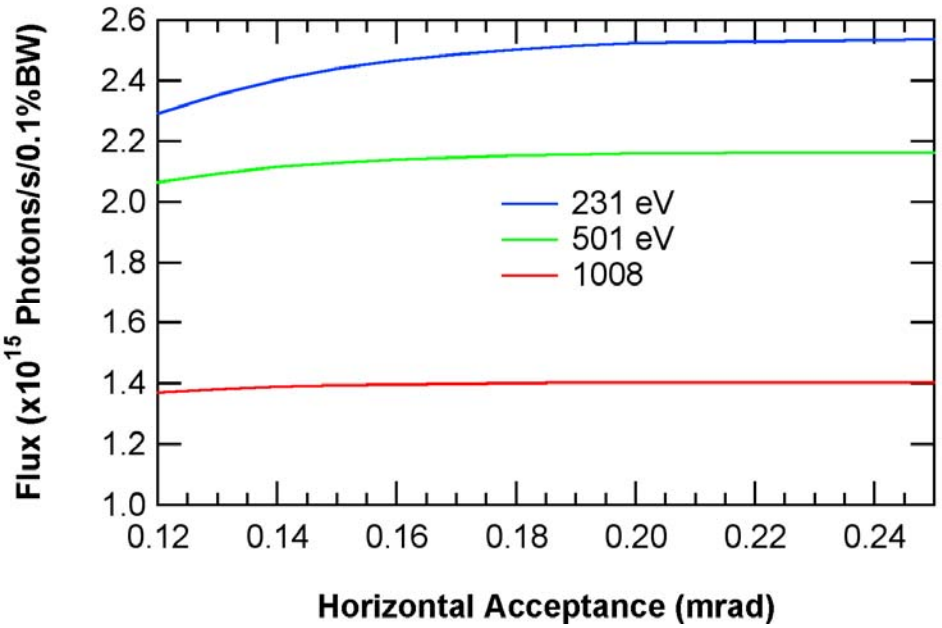

Figure 4.A.4. Flux as a function of the horizontal aperture (over full vertical aperture) for 231, 501, and 1008 eV.

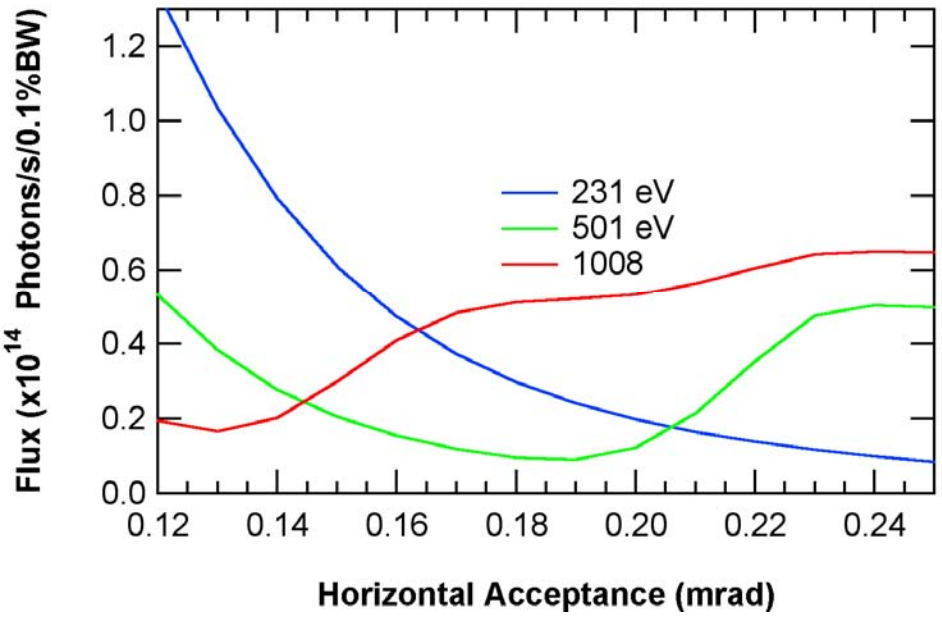

Figure 4.A.5. At–energy flux leaked onto the acceptance of the other ID as a function of the horizontal aperture (over full vertical aperture) for 231, 501, and 1008 eV. The canting angle is equal to the horizontal aperture.

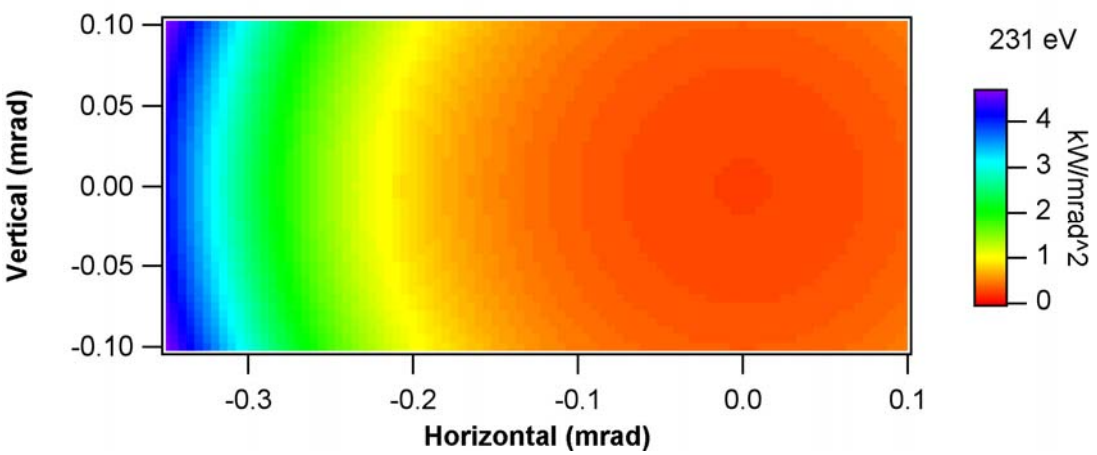

Figure 4.A.6. Angular power density when the upstream ID is tuned to 231 eV.

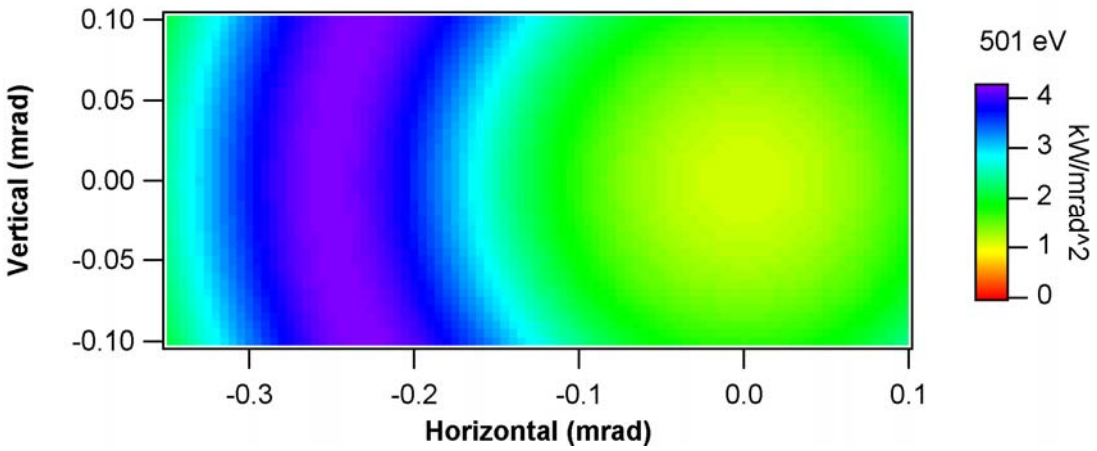

Figure 4.A.7. Angular power density when the upstream ID is tuned to 501 eV.

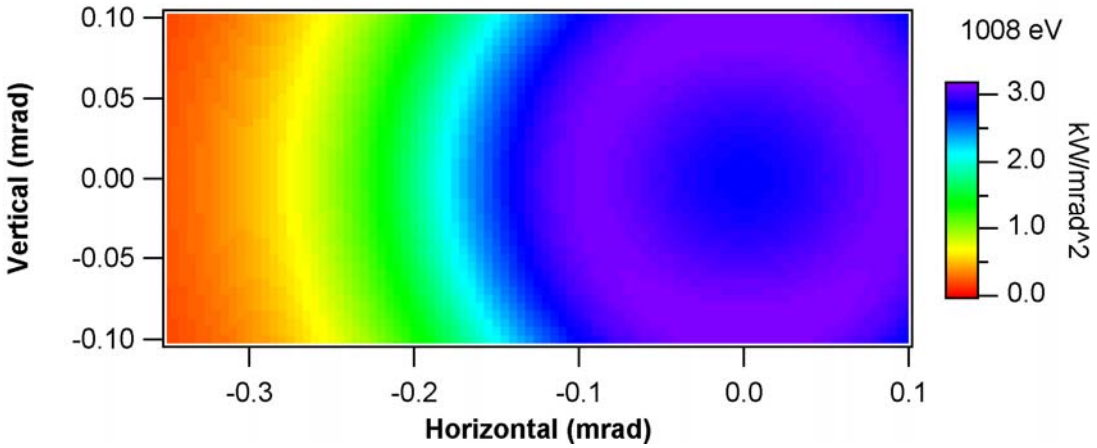

Figure 4.A.8. Angular power density when the upstream ID is tuned to 1008 eV.

4-A Appendix B: SAS Optics Reports

Preliminary Ray Tracings, Single Beam.

The purpose of this brief report is to give a first impression on the optical sizes and the size at the sample with the parameters we have discussed until now.

The machine parameters used are those at the straight center and are listed in Table 4.B.1. The parameters of the ID as well as the total source size and divergence calculated (as in our report dated July 16, 2006) at 183 eV are given in Table 4.B.2.

The distances from the source, angles of incidence, and deflection of the optical components are given in Table 4.B.3. M2 and the grating, a 150 l/mm VLS operating with c≈1.5, are tuned for 183 eV.

Figure 4.A.1, Figure 4.B.2, Figure 4.B.3, Figure 4.B.4, and Figure 4.B.5 show the illumination on M1, M2, grating, M3 and M4 with the above parameters. The ray tracings at the slit are shown in Figure 4.B.6. The spot at the sample when the slit width is set to 20 μm is seen in Figure 4.B.7. No slope errors have been assumed on the optical elements.

Tables

Table 4.B.1: Machine parameters used in the calculations.

Energy (GeV)	3.0
Current (mA)	500
σx (μm)	28
σy (μm)	2.6
σx' (μrad)	19.7
σy' (μrad)	3.1

Table 3.B.2: ID parameters used in the calculations.

ID type	APPLE II
Number of periods	85
Period length (mm)	45
Energy (eV)	183
Σx (μm)	46.4
Σy (μm)	37.2
Σx' (μrad)	35.1
Σy' (μrad)	29.2

Table 4.B.3: Distance from the source, angle of incidence, and deflection of the optical components. (183 eV, LEG)

Element	Distance (mm)	Angle (deg)	Deflection
M1- Sagittal Cylinder	29500	88.75	horizontal
M2- Plane	31851.8	87.11	vertical
Gr - Grating	32000	87.69 (inc.)	vertical
Slit	42000		
M3 - Plane Elliptical	43200	88.5	horizontal
M4 – Plane Elliptical	43950	88.5	vertical
Sample	44950		

Figures

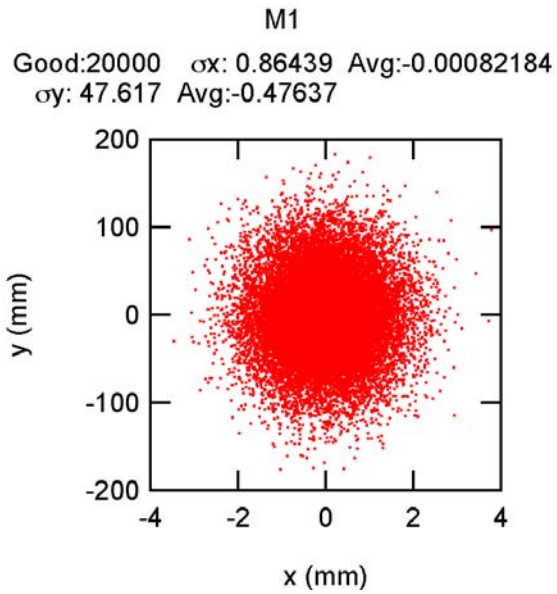

Figure 4.B.1. M1 illumination

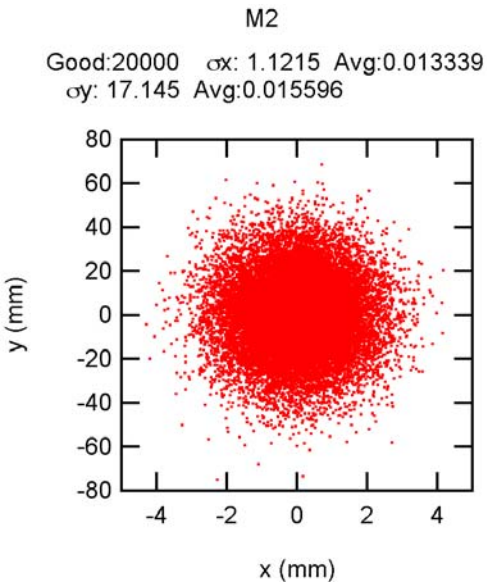

Figure 4.B.2. M2 illumination

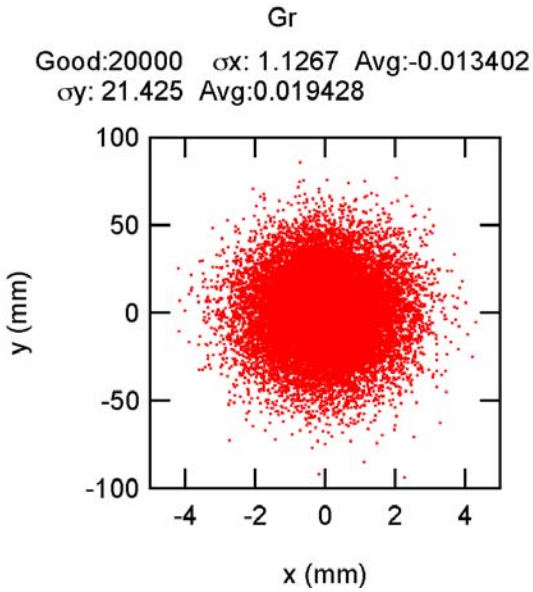

Figure 4.B.3. Grating illumination

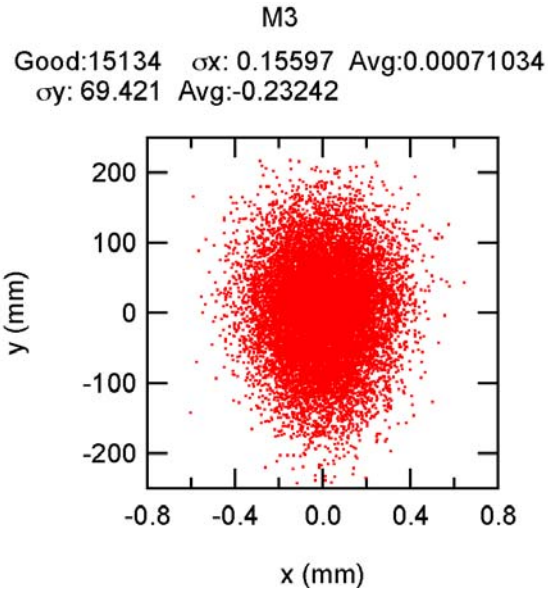

Figure. 4.B.4. M3 illumination

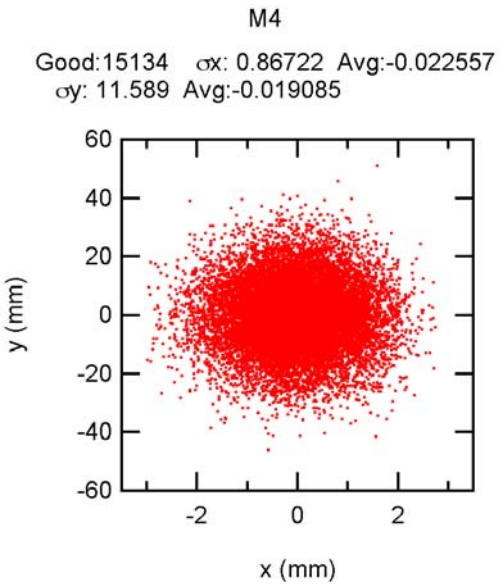

Figure 4.B.5. M4 Illumination

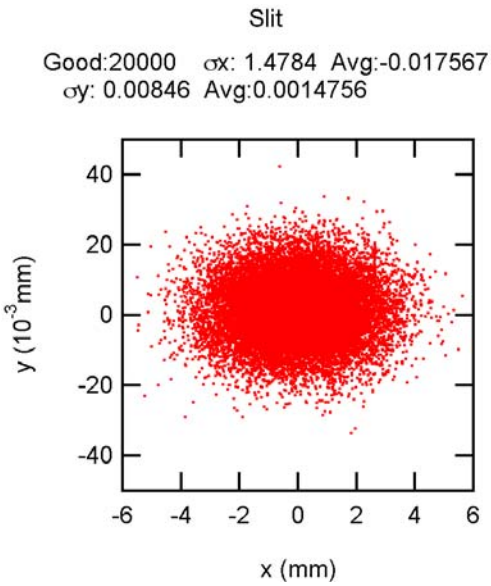

Figure 4.B.6. Image at slit

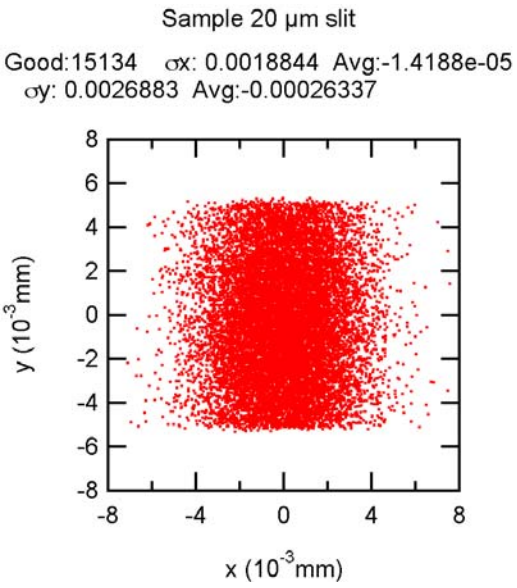

Figure 4.B.7. Image at sample position.

4-A Appendix C: SAS Optics Reports

Slope Errors on the Optical Elements.

The meridional slope errors on M1, diverting mirror, and M3 contribute to the horizontal spot size. The sagittal slope errors on M2, grating, and M4 also affect the horizontal spot size. The required slope errors were obtained from the condition that each contribution is less or equal half the minimum RMS horizontal spot size at the sample.

The meridional slope errors on M2 and the grating contribute to the resolution. The sagittal slope errors on M1 and diverting mirror also affect the resolution. The required slope errors were obtained from the condition that each contribution is less or equal half the combined resolution due to the source and a 10 μm exit slit.
The meridional slope error on M4 and the sagittal errors on M3 contribute to the vertical spot size at the sample. The required slope errors were obtained from the condition that each contribution is less or equal half the minimum RMS vertical spot size at the sample with a 10 μm slit.

The required RMS slope errors (and the condition determining it) are given in the table below.

Table 1. Maximum RMS slope errors on the optical elements

Element	Meridional(μrad)	Condition	Sagittal(μrad)	Condition
M1- Sagittal cylinder	0.25	Hor. spot size	8.0	Resolution
M2- Plane	0.17	Resolution	3.5	Hor. Spot Size
Gr - Grating	0.13	Resolution	5.5	Hor. Spot Size
Div. Mirror – Plane	0.22	Hor. Spot Size	8.8	Resolution
M3 - Plane Elliptical	0.17	Hor. Spot Size	14	Ver. Spot Size
M4 – Plane Elliptical	0.37	Ver. Spot Size	14	Hor. Spot Size

4-A Appendix D: SAS Optics Reports

Position of the Optical Elements, Optics Parameters, and Ray Tracings with Canted Beams

Position of the Optical Elements

The coordinates of the optical elements in the case of a single beam are given in Table 4.D.1. The center of the coordinate system is in the middle of the straight. The y coordinate is along the beam propagation, x is in the horizontal plane and perpendicular to y, and z is along the vertical. The distance between M3 II and M4 II was increased to 1 m.

Table 4: Coordinates of the optical elements**.**

Element	x (mm)	y (mm)	z (mm)
Source	0.000	0.000	0.000
M1	0.000	29500.000	0.000
M2	-102.583	31849.537	0.000
Grating	-109.0485	31997.621	-15.000
Slit	-545.242	41988.103	-15.000
M3	-597.586	43186.961	-15.000
M4	-662.952	43934.107	-15.000
Sample	-750.025	44929.353	28.619
Branching Mirror	-196.287	33995.717	-15.000
Slit II	-893.533	41965.275	-15.000
M3 II	-1695.366	51130.266	-15.000
M4 II	-1825.892	52121.711	-15.000
Sample II	-1956.294	53112.212	28.6193

Optical parameters

Table 2. Parameters of the optical components.

Element	Figure	Major axis (mm)	Minor axis/sagittal radius (mm)
M1 Center	Meridional Cylinder		1287.08
M1 Upstream	Meridional Cylinder		1338.89
M1 Downstream	Meridional Cylinder		1234.89
M3 Center	Meridional Elliptical Cylinder	22475.	189.68
M3 Upstream	Meridional Elliptical Cylinder	23125.	192.51
M3 Downstream	Meridional Elliptical Cylinder	21825.	186.80
M4	Meridional Elliptical Cylinder	1475.	30.463
M3 II Center	Meridional Elliptical Cylinder	26600.	220.75
M3 II Upstream	Meridional Elliptical Cylinder	27250.	223.54
M3 II Downstream	Meridional Elliptical Cylinder	25950.	217.93
M4 II	Meridional Elliptical Cylinder	5600.	69.67

Grating Parameters

The line density of the gratings is given by $k(w) = a_0 + a_1 w + a_2 w^2 + \ldots$ where w is positive towards the slit. These parameters and the c parameter are listed in Table 3.

Table 3. Grating parameters

Grating	a_0 (mm^{-1})	a_1 (mm^{-2})	a_2 (10^{-6} mm^{-3})	c parameter
LEG	150	0.05397	8.09	≈1.5
MEG	400	0.14381	21.5	≈1.5
HEG	1200	0.30181	45.1	≈2.2

Accuracy in Optics Positioning.

The resolution of the hexapods is 1μm for the translations and 1 μrad for the rotations[1]. These values are sufficient for most of the required movements besides the pitches of M1, the branching mirror, M3 and M4. Since the goal is to overlap the beams from the two IDS, lets say within 0.2 the sigma value, one needs a resolution better than 0.07 μrad on the most sensitive element, M3. We note that this resolution is 2/5 the meridional slope error specified previously for M3.

Ray Traces with Canted Beams

As in the case of the IDs emitting linearly polarized light[2], we determined the source sizes as a function of the longitudinal position using SRW. In this case, the upstream ID (located at 1.3m upstream the center of the straight) was tuned to emit circular polarized radiation at the lowest possible energy (230 eV). As seen in Figure 2, the RMS vertical size is 26 μm and it is located very close to the ID center. The vertical RMS size is 42 μm and occurs close to the ID end. The lines in the right part of the figure are linear fits to the RMS size giving RMS divergences of 32 μrad for the vertical and 34 μrad for the horizontal. In the ray tracings described below, we used these divergences and vertical RMS sizes. For the horizontal RMS size, we used the RMS beam size at the center of the ID, i.e., 45 μm.

In the canted mirrors, y=0 corresponds to the coordinates of the mirror collecting the central beam.
Figure and Figure show the illumination of the M1 mirrors collimating the upstream and downstream beams, respectively.

Figure , Figure , and Figure show the illumination of the plane mirror, the grating, and the slit plane with both beams when using the 150 l/mm grating and c=1.5. Note that the upstream beam is wider (diverging beam) but the vertical image at the slit is smaller for the upstream beam due to the larger demagnification.
The illumination of M3 with the upstream beam is seen in Figure and with the downstream beam in Figure 9. Note that due to the mirror orientation in Shadow, the y coordinates have the opposite sign. The illumination of M4 with both beams is presented in Figure 10.
The spot at the sample position with the upstream beam is displayed in Figure 11 and that of the downstream beam in Figure 12. Note that the image of the downstream beam is narrower due to the higher

[1] According to Ken Kriesel.
[2] Report "ID's Source Positions" dated September 9, 2007. The same electron beam parameters were used.

demagnification. This can be corrected by detuning the plane elliptical mirror as done in the initial beamline design.

The illumination of the mirrors of the branch line are shown in **Figure 13** (diverting mirror), **Figure 14** (M3 II upstream ID), **Figure 15** (M3 II downstream beam), and **Figure 16** (M4 II). The sample illumination with both beams is seen in **Figure 17** and **Figure 18**.

Figures

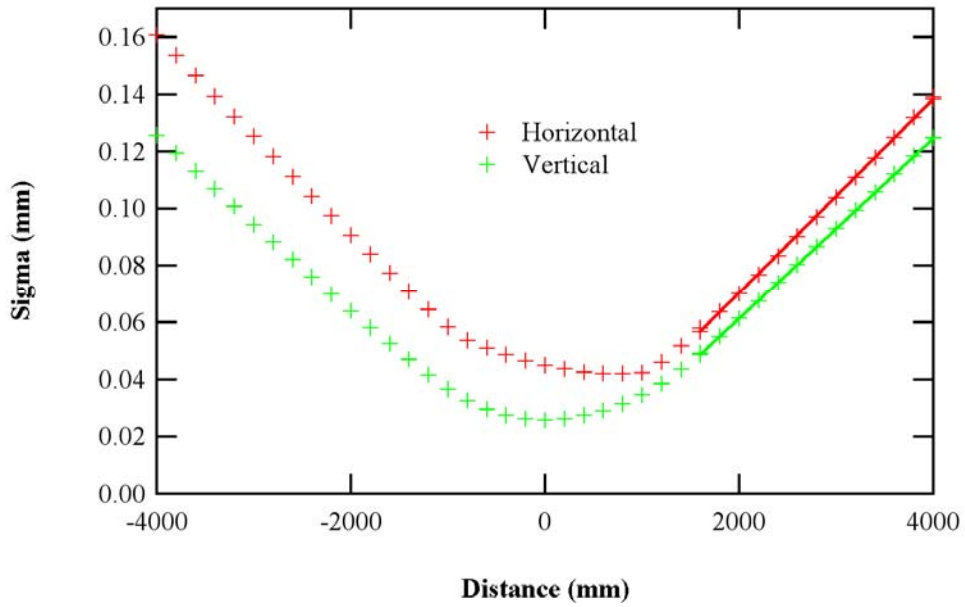

Figure 2. RMS image size of the upstream ID radiation as a function of the longitudinal position. The photon energy is 230 eV and the straight center is at +1.3 m.

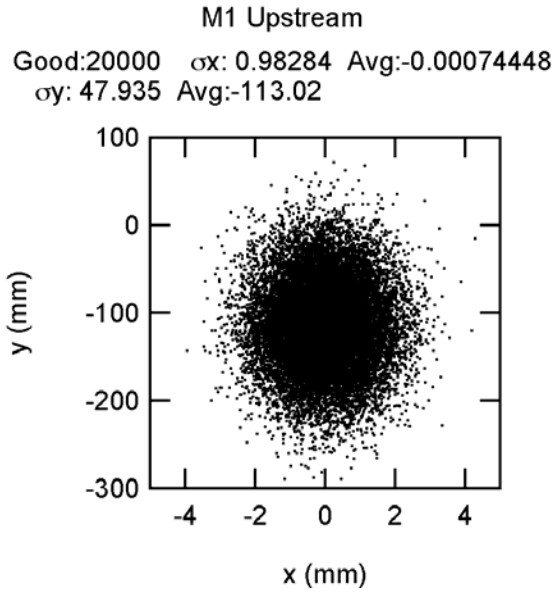

Figure 3. M1 illumination. Upstream ID.

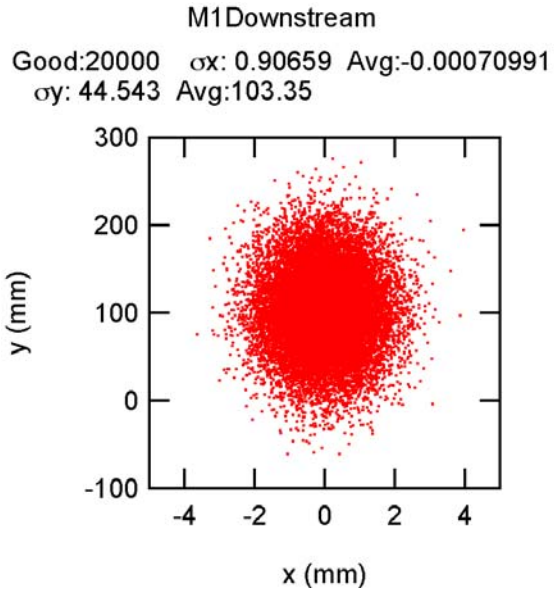

Figure 4. M1 illumination. Downstream ID.

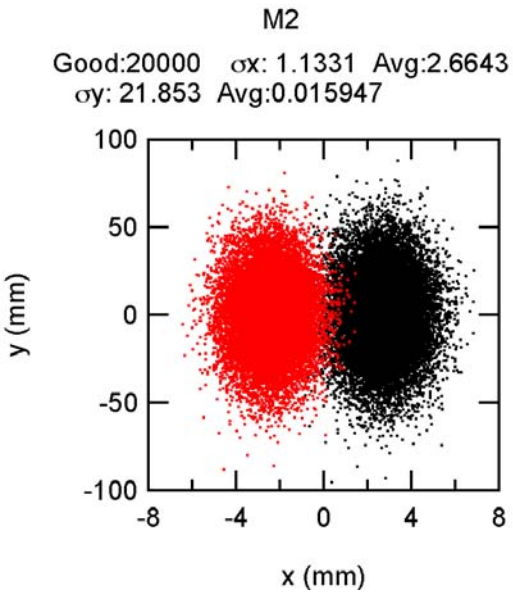

Figure 5. M2 illumination. Black: Upstream ID, Red: Downstream ID.

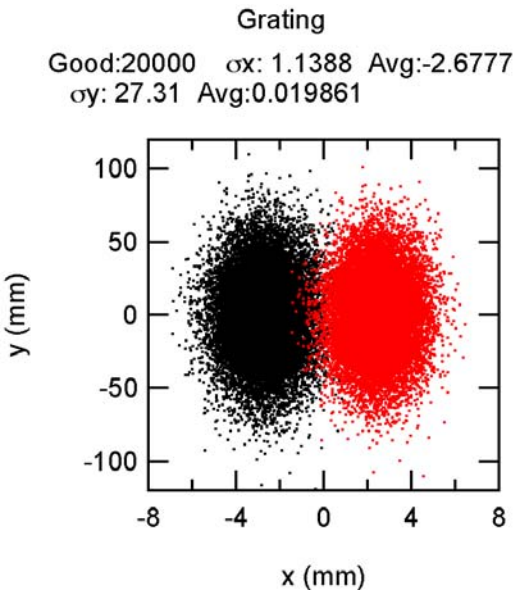

Figure 6. Grating illumination. Black: Upstream ID, Red: Downstream ID.

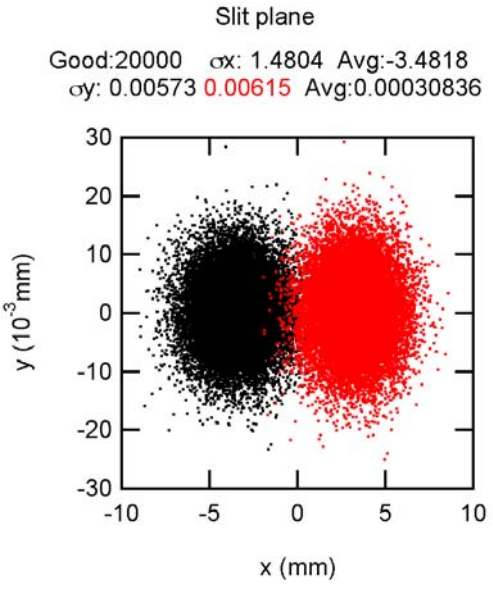

Figure 7. Slit plane. Black: Upstream ID, Red: Downstream ID.

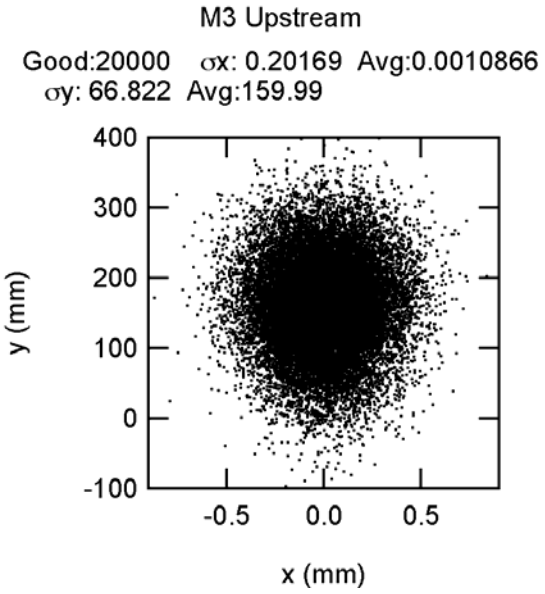

Figure 8. M3 illumination. Upstream ID.

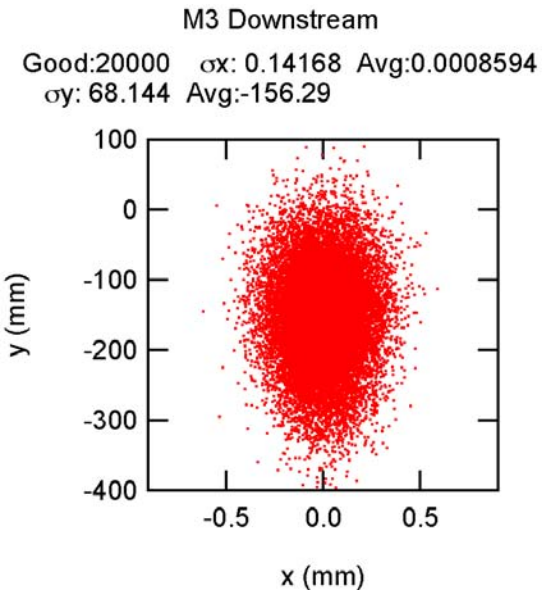

Figure 9. M3 illumination.
Downstream ID.

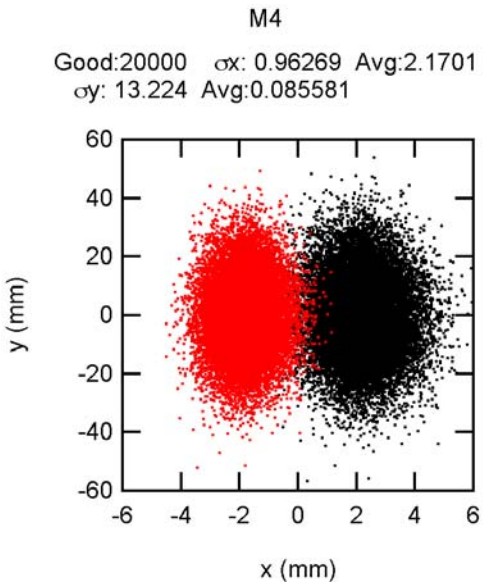

Figure 10. M4 illumination.
Black: Upstream ID, Red: Downstream ID.

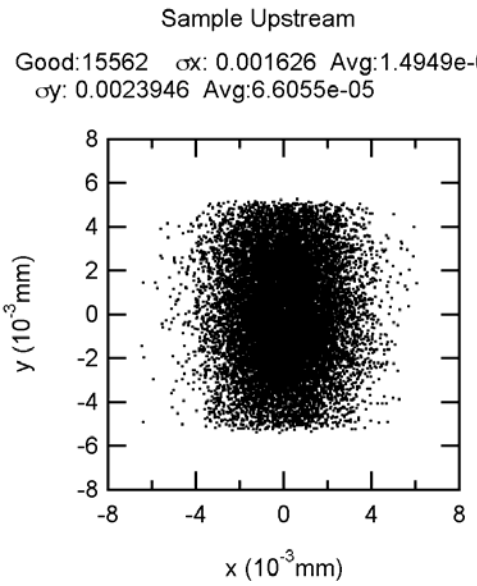

Figure 11. Sample illumination.
Upstream ID.

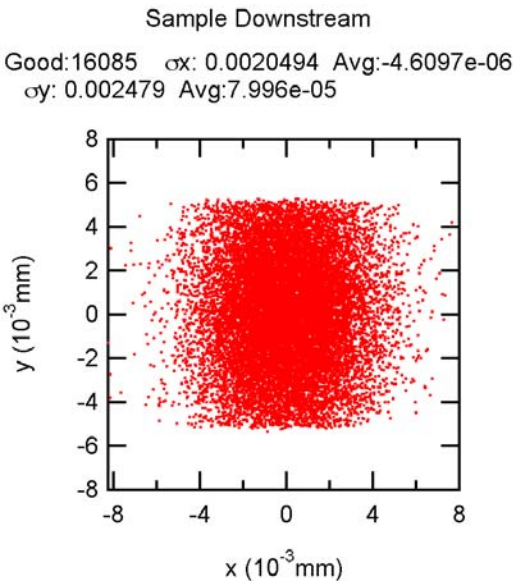

Figure 12. Sample illumination.
Downstream ID.

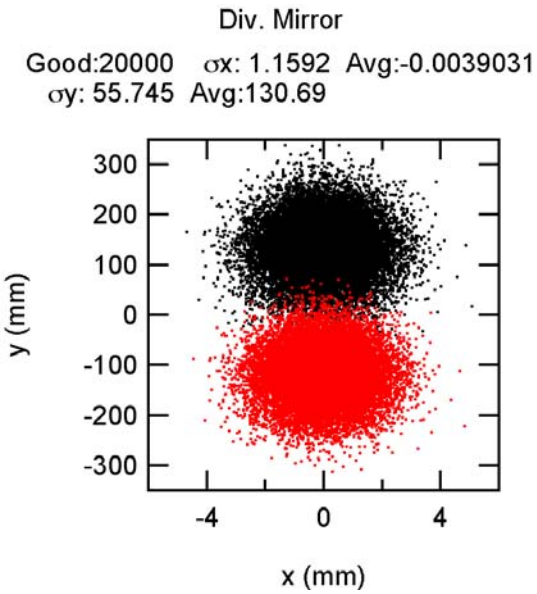

Figure 13. Illumination of the diverting mirror. Black: Upstream ID, Red: Downstream ID.

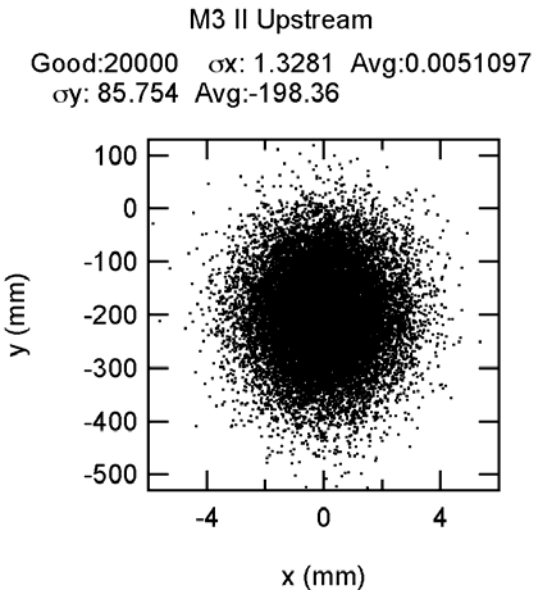

Figure 14. M3 II illumination. Upstream ID.

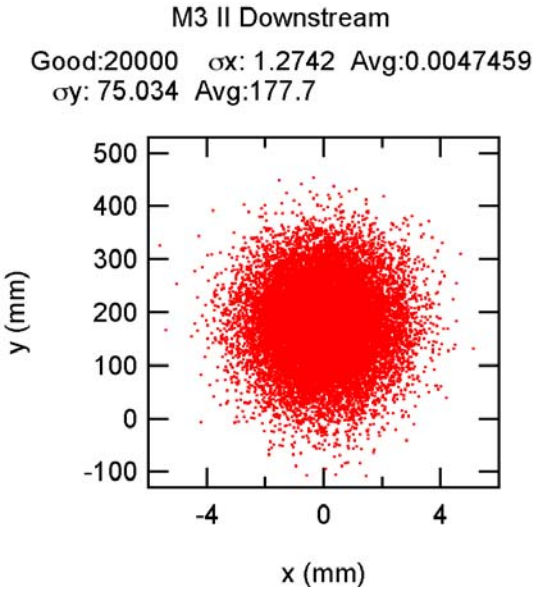

Figure 15. M3 II illumination. Downstream ID.

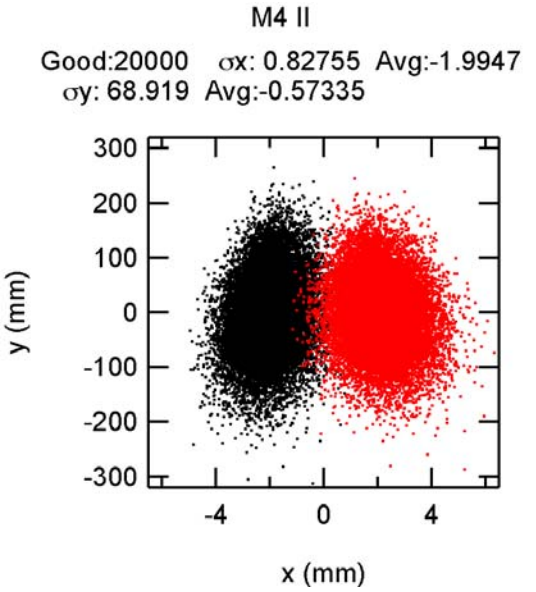

Figure 16. M4 II illumination. Black: Upstream ID, Red: Downstream ID.

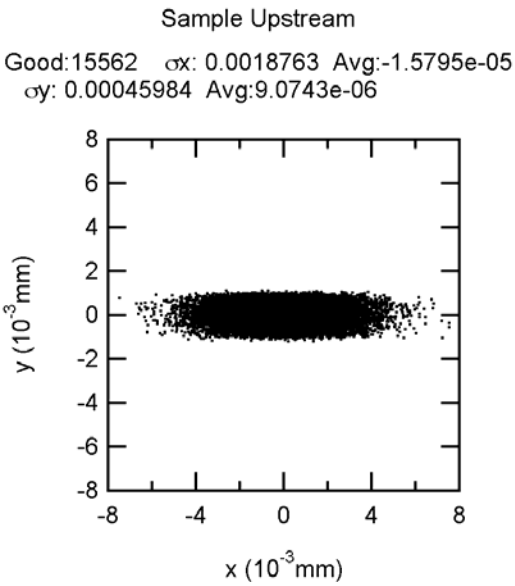

Figure 17. Sample II illumination. Upstream ID.

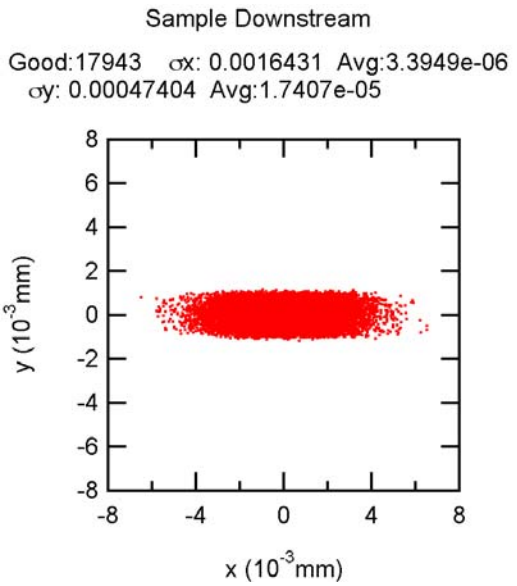

Figure 18. Sample II illumination. Downstream ID.

Power Absorbed by Optical Elements.

Corrected for the values used by Ken Kriesel on the FEA.

NOTE: Ken Kriesel corrected the illuminated length he used in the FEA of M2 in section 2 from (what I wrote) 80 mm to 68 mm. I calculated the total power on M1, M2 and the grating, for an aperture of 8×8 mm^2 at the position of M1. I added to the table (in parenthesis) the power values for the aperture used by Ken, i.e., 7.1×5.15 mm^2 at the position of M1. The effect of the reduced horizontal aperture on the slope errors along the horizontal direction needs to be investigated.

Power Absorbed by the Optical Elements

The power and power densities absorbed by M1, M2, and the grating were calculated with the IDPower routine in SRCalc with the machine and ID parameters listed in our report dated August 27, 2007. We assumed Au as the reflective coating on all optics. Table 7 summarizes the maximum power values for elements up to the slit.

The highest absorbed power and power density in M1 and M2 occur when the two IDs are operated in tandem and tuned to the lowest photon energy, 183 eV. The worst case for M2 is when it is used with the high energy grating (HEG) since its angle of incidence is the smallest, 84.0º. As described in section 2, the power incident along the length of M2 needs to extend beyond the central cone of the "good" radiation to minimize the meridional slope error. Therefore, the horizontal and vertical apertures at the position of M1 were set to 8×8 mm^2. The power densities absorbed by M1 and M2 are shown in Figure 2 and Figure 20. The total absorbed power in M1 is 1.9 kW and in M2 236 W. The maximum power densities in M1 and M2 are 0.92 and 0.36 W/mm^2, respectively.

The maximum power density on the gratings (obtained from a few cases at different energies using the LEG) is less than 16 mW/mm^2. This value was obtained with the ID tuned to 555 eV (Figure 21). The total power absorbed with the aperture mentioned above is almost 40W. The horizontal aperture could be reduced to half, which will decrease the total power to 20 W. However, this could have a negative effect on the figure of M1, which will impair the horizontal spot at the sample.

The grating efficiencies and the diffraction angles are required to obtain the power densities and power downstream the grating. Since we already calculated the monochromatic flux for this beamline with a slightly different ID (42 mm period instead of 45 mm) we used those results to estimate an upper limit for the power and power densities on those elements.

The calculated flux at the sample at 1 keV with the LEG and 10 μm slit is 5×10^{13} photons/sec, or a power of 8 mW. With an aperture of 4×4 mm^2 at the position of M1, the illuminated vertical (horizontal) size at the slit with this grating is approximately 7.2 (5.7) mm. This means that the power at the slit plane is less than 10 W and the power density is less than 0.24 W/mm^2. Approximately the same power will be incident on the diverting mirror but the absorbed power and absorbed power densities are less than 3 W and less than 4 mW/mm^2.

With a 10μm slit, the power absorbed in M3 and M4 is less than 2 mW. The total power will increase linearly with the slit width. The power densities are negligible.

The power on the chopper in the CP fast switching mode is less than 10 W and the power density is less than 0.2 W/mm^2.

Slope Errors on M2

Ken Kriesel did a FEA analysis to obtain the temperature rise and surface deformation due to the power absorbed in M2. He initially performed[3] the calculations assuming a homogeneous power density of 0.362 W/mm^2 over a length of 48 mm and a width of 5.4 mm. Ken included in the model the fact that that beam is not centered on M2 but at 307 mm from its end.

We ray traced the system up to the exit slit with the deformed surface obtained by Ken and realized that the RMS spot at the exit slit increased from 5.8 μm to more than 11 μm. The reason for the large increase is mainly due to the sharp discontinuity in the absorbed power along the mirror length, giving a large slope error in the region of the central cone.

At our request, Ken increased the length over which the power is absorbed to 68 mm. The surface deformation he obtained (assuming a constant power density instead of the small variations seen in Figure 20) is displayed as an image plot in Figure 22. From these results we extracted the surface deformation along the mirror length (at zero width) and along the mirror width (at zero length). The height profiles and the calculated slope errors are shown in Figure 23 and Figure 24.

The maximum surface deformation is actually not at the center of the beam, i.e. at 307 mm (Figure 23). As Ken pointed out, this is due to the fact that the long M2 mirror is not illuminated at the center[4]. The sharp increase in the slope error towards the edge of the region being heated by the beam is clearly seen in Figure 23. However, the beam in the central cone sees only an RMS slope error of ≈0.9 μrad and not the high slope error region.

Ray Traces with Deformed M2

The spot at the exit slit plane when the ID is tuned to 183 eV, the high energy grating is used, and there are no deformations on the optics, is shown in Figure 25. The effects of the induced figure error on M2 due to the absorbed power are evident when comparing Figure 26 to the previous one.
The figure change in the central part of M2 can be approximated by a convex radius of $\approx 1.8\times10^7$ mm, which means the beam incident on the grating is not vertically collimated as in the optical design. This change in the virtual source position can be corrected by operating the grating with a c value of 2.193 instead of the nominal value of 2.184 at this energy. The spot at the exit slit plane with the deformed M2 and the corrected c value is presented in Figure 27. The vertical RMS size is reduced to 6 μm, very close to the initial value.

The above example shows the possibility of correcting the spot size at the slit for the highest absorbed power in M2. At this energy (183 eV) the beam size is the largest. Further studies at higher energies (where the beam is smaller) need to be performed to verify that this "correction" is also possible. Still to be tested is whether the deformations along the meridional direction on M1 can be corrected with a change in the curvature of M3. FEA of this mirror are then required.

[3] I proposed that length since it is the part illuminated by the central cone.
[4] Ken Kriesel checked that illuminating the mirror center gives a symmetric deformation.

Effect of Single M1

We discussed the option of performing the fast switching of CP with the electron beam instead of canting the beams. This requires using a single collimating mirror. To assess the effect of using a single M1, we have ray traced the system when each ID has an M1 with the correct sagittal radius and when the radius is the one required when the two IDs are operated in tandem.

The ray tracings at the exit slit plane when the upstream ID is tuned to 230 eV, M1 has the correct sagittal radius, and the LEG is used, are seen in Figure 28. Changing the radius to that required for the case when the IDs are operated in tandem increases the vertical spot by almost a factor of two (Figure 29). This means that the contribution to the resolution due to the source will degrade by the same factor. Practically the same results are obtained for the downstream ID.

Table 5. Maximum power and power densities absorbed by the optical elements. Values in parentheses are for an aperture of 7.1×5.15 mm^2 at the position of M1.

Element	Power Absorbed (W)	Power Dens. Abs (W/mm^2)	Case
M1	1910 (1160)	0.92	183 eV
M2	236 (132)	0.37	183 eV HEG
Gr	40 (22)	0.016	555 eV LEG
Div. mirror	<3	<0.004	1 keV LEG
Chopper	<10	<0.2	1 keV CP LEG
Slit	<10	<0.24	1 keV LEG

Figures

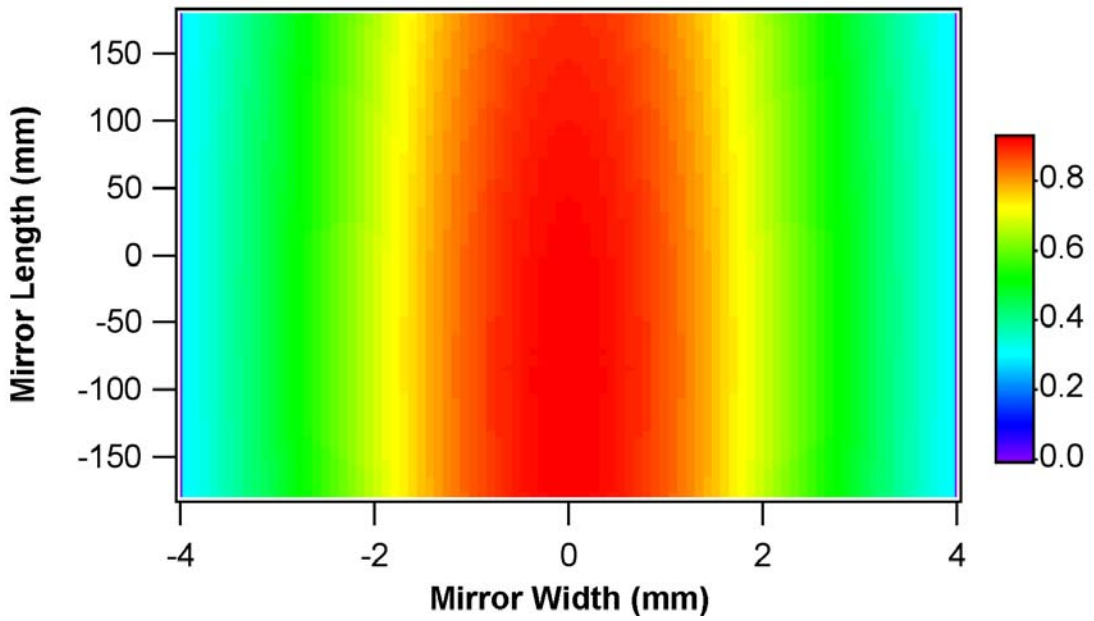

Figure 19. Power density (W/mm^2) absorbed in M1. 183 eV.

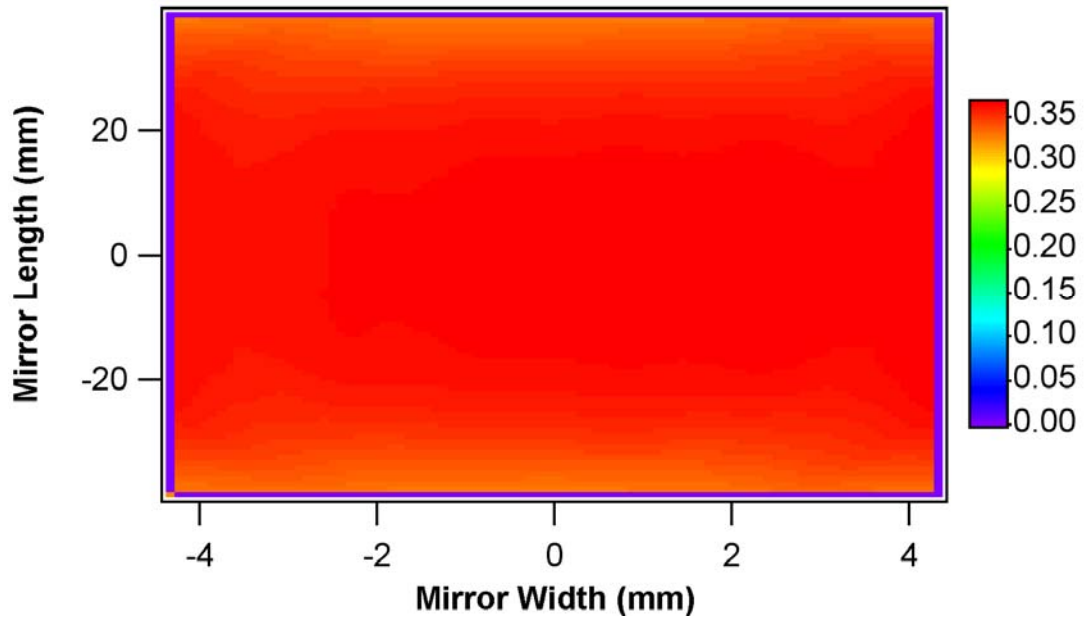

Figure 20. Power density (W/mm^2) absorbed in M2. 183 eV HEG.

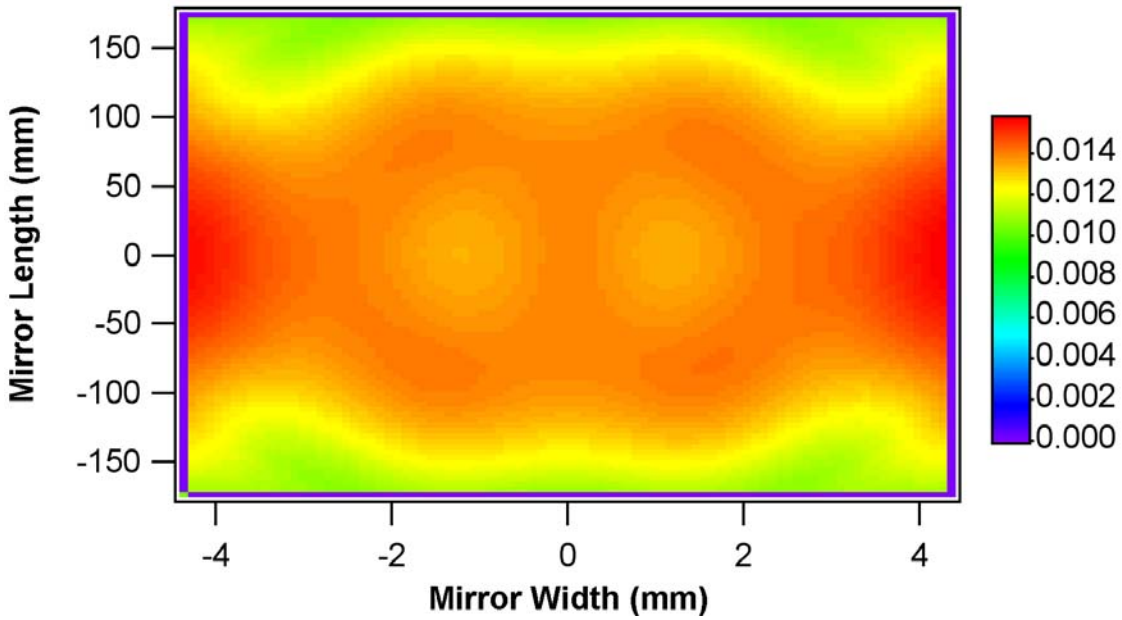

Figure 21. Power density (W/mm^2) absorbed in the LEG at 555 eV.

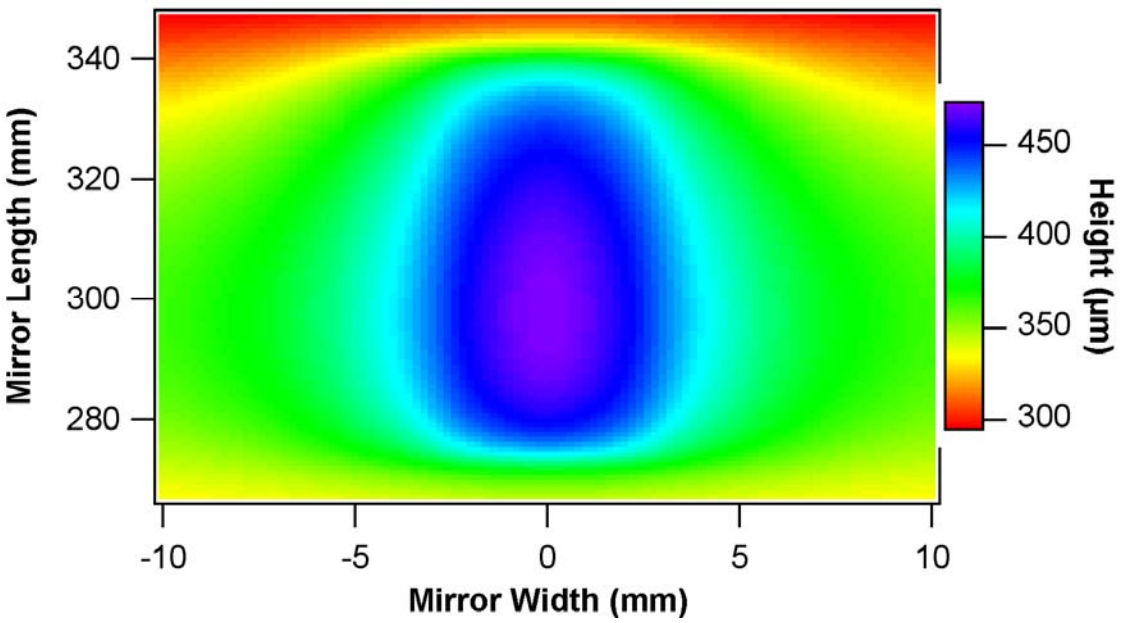

Figure 22. Height change on M2 due to the absorbed power density.

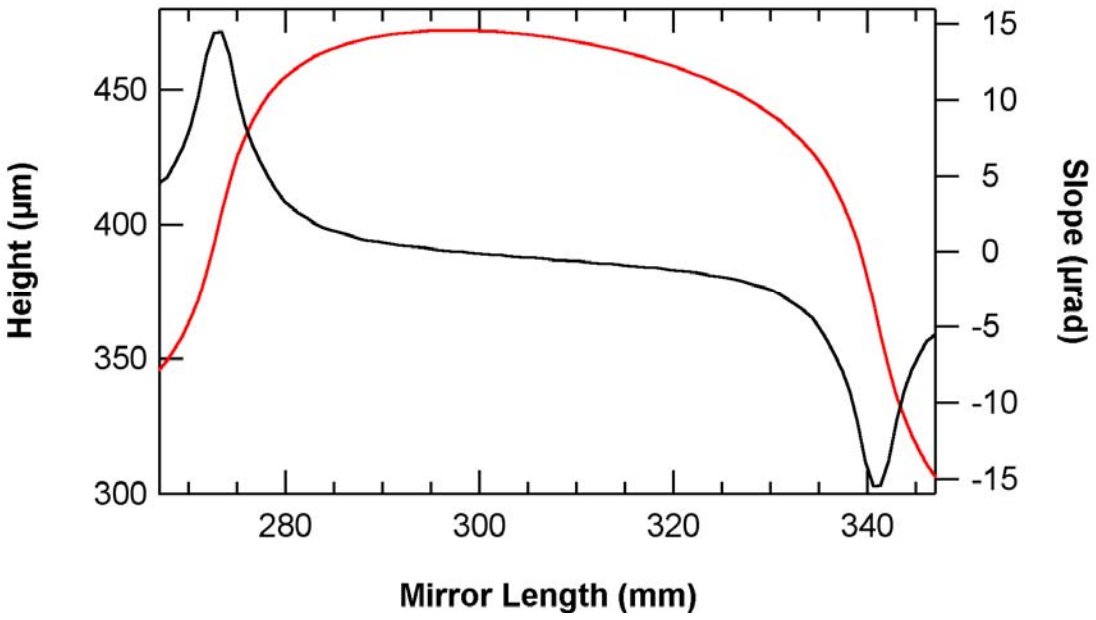

Figure 23. M2 Surface deformation (red trace) and meridional slope error (black trace) at zero width.

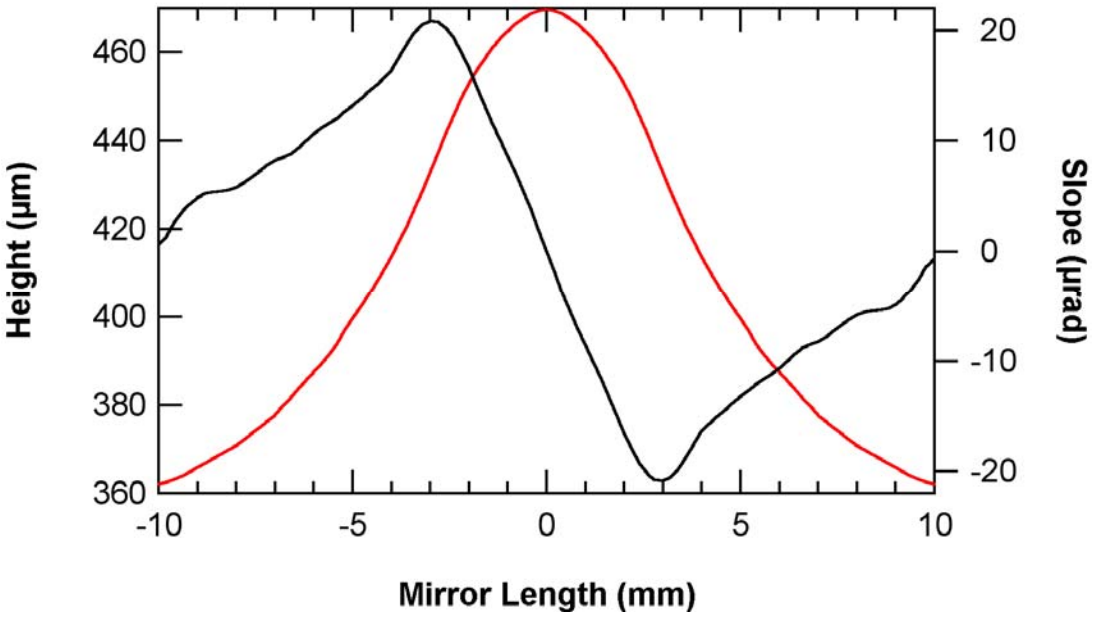

Figure 24. M2 Surface deformation (red trace) and sagittal slope error (black trace) at zero length.

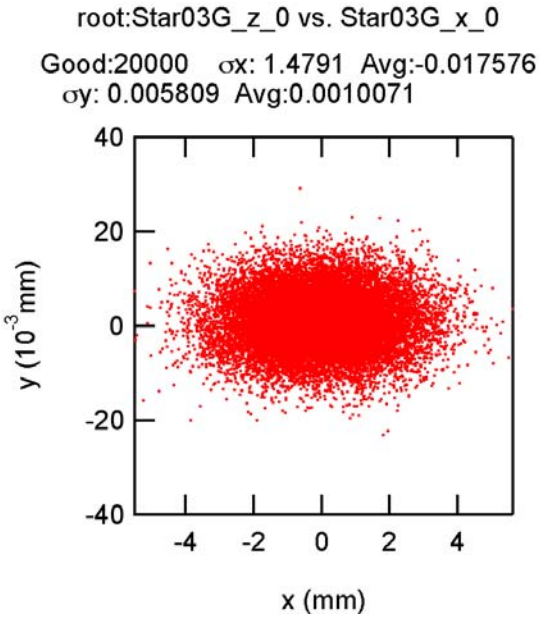

Figure 25. Ray tracings at the exit slit plane with perfect optics

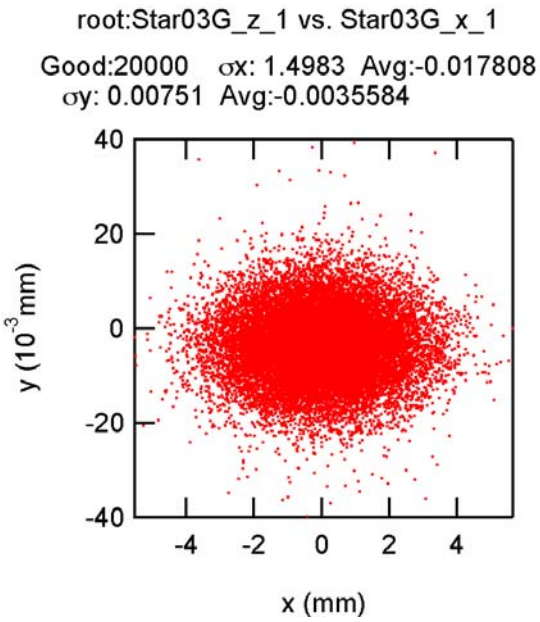

Figure 26. Ray tracings at the exit slit plane with deformed M2.

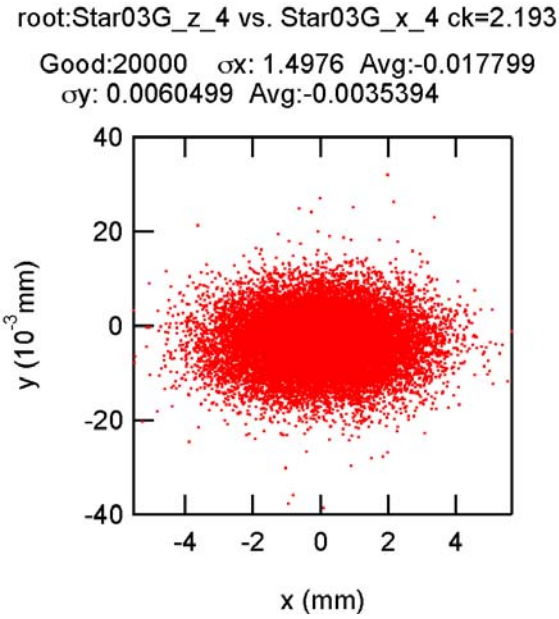

Figure 27. Ray tracings at the exit slit plane with deformed M2 and optimized c value.

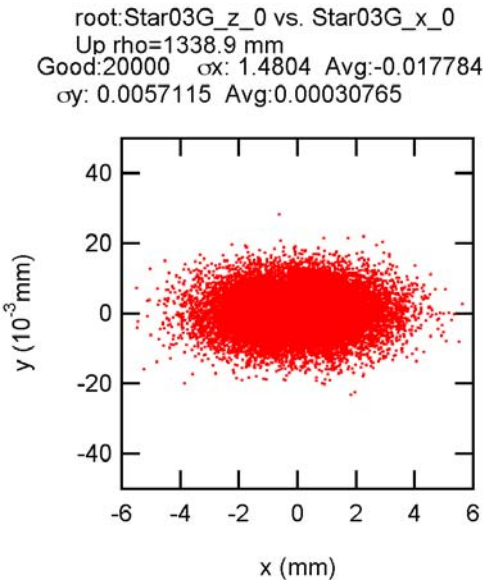

Figure 28. Ray tracings at exit slit plane for the upstream ID with correct M1 radius.

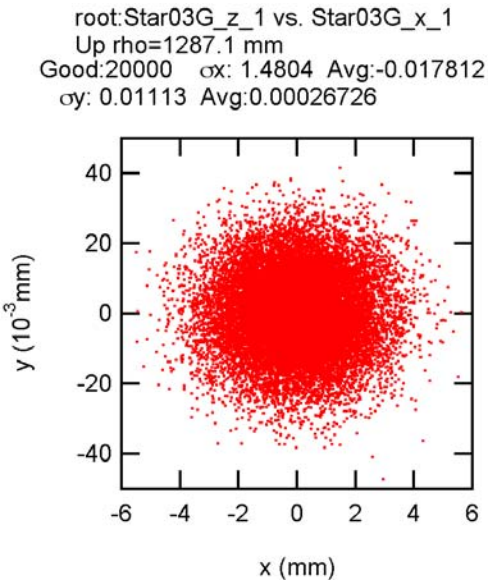

Figure 29. Ray tracings at exit slit plane for the upstream ID with M1 radius of phased IDs.

Appendix E. M2 Finite Element Analysis

A parametrically driven ANSYS input file was developed and employed for 3-D thermal-structural analysis of the M2 mirror in the NSLS2 soft x-ray coherent scattering and imaging beamline. It solves for surface deflections in two passes. The first is a thermal analysis. The second pass has the thermal solution's resulting temperature field as input along with symmetry and other structural constraints and solves for thermal stresses and deflections. It allows for temperature dependencies of some properties; varying number, dimensions, and depth below heated surface of rectangular longitudinal coolant passages; variation in overall dimensions of the mirror substrate, changes in size, location or intensity of mirror heating; and certain other variations, with single parameter value changes in some cases and modest editing of the model file in others. Currently these variations are constrained by interaction with the definition of the heat load. Further development to support significantly spatially varying power densities will allow simulation of additional load cases. This work was performed with perhaps the most demanding defined load case, single-beam 183eV operation of the beamline.

Properties of bulk single-crystal silicon were gathered. Temperature dependencies of thermal conductivity and thermal expansion coefficient[1] were included in the model file. Data[2] for directional thermal conductivity below 40 degrees K was found, showing the anisotropy disappears in the range above 30 K, so the conductivity was treated as isotropic in our range of interest. No data for directionality of thermal expansion was found. (It would seem reasonable that if structural stiffness varies with direction that there would be some variation in thermal expansion as there is in other anisotropic materials. But in the absence of directional property data, we do not model directionality of thermal expansion.)

Beginning with coolant and heat transfer parameters as well as coolant passage geometry matching the Diamond I06 beamline, some simple optimization simulations were made. Peak temperature was used as a proxy for the optical surface deformations we desire to minimize. These preliminary optimization runs resulted in a move to 1.5mm thick silicon between coolant passages and a reduction to 1mm between the optical surface and the beginning of the coolant passages. These parameters are within the range of what is workable for silicon optics manufacturers such as InSync to produce with good optical figure. A number of ANSYS FEA runs were then made using this basic set of parameters. A subset will be documented here. Initial results were compared to the closest case documented in the Diamond I06 TDR as an additional check on the modeling accuracy in this work. Several models were rerun to generate graphics files from model development to results path plots.

There are a number of simplifications and approximations in common among all ANSYS models of the M2 mirror to date. The silicon is treated as isotropic rather than orthotropic structurally. This is a significant approximation structurally (in how the silicon responds structurally to the thermally produced strains). The coolant passages as modeled run the full length of the optic, and the back of the optic is solid; a real optic will require UHV-tight end manifolding of the coolant slots and inlet & outlet connections on the back with air guarding. The optic is modeled with symmetry constraints to exploit left-right symmetry. (Because the location of the heat load in general is not centered axially, only bilateral symmetry is present in the model, not four-fold as is often modeled.) The thermal effects of the glass frit bond are treated as negligible, which is rather optimistic given the thermal resistance of the approximately 50 micron layer can equal that of several mm of silicon. The bulk temperature of the coolant is held constant at 23°C. Heat transfer coefficient is treated as constant, invariant to both silicon surface temperature and location in the flow channel. Geometric effects such as the slope increasing on the front portion of the heat bump and thereby raising its power density are minor and safely ignored; peak meridional slope of about 14 microradians change was observed at the front & back of the heat input area of 6 degrees grazing incidence, giving about ±0.013% power density change. The effect of mirror coating is trivial since the gold over chromium is nominally only 30nm thick, one millionth the substrate thickness or less. It is also likely that the thin film's conductivity being lower than that of bulk properties[3], approximates that of silicon, reducing this error further. The change in shape of the optic due to other influences including manufacturing tolerances, gravity load, support clamp loads etc. are

ignored. Structural effects of the thin coating and frit layers including residual stress and differential thermal expansion are also ignored. Differential pressure between the coolant passages and vacuum surface are ignored. Optical figure error as manufactured is ignored.

1. Basic Mechanical and Thermal Properties of Silicon, Virgina Semiconductor Inc. http://www.virginiasemi.com/pdf/Basic%20Mechanical%20and%20Thermal%20Properties%20of%20Silicon.pdf

2. Anisotropic Heat Conduction in Cubic Crystals in the Boundary Scattering Regime, Physical Review B, Volume 2, No. 10, pages 4077-4083.

3. Strain and size effects on heat transport in nanostructures, Journal of Applied Physics, Volume 93, No. 6, pages 3535-3539.

Thermal load & optic parameters were as follows.

Table 1. Parameters comparison.

Parameter	As initially described	As modeled in ANSYS
Power deposition, W/mm^2	Nearly flat at 0.354 to 0.365 (maximum variation from average is 2.36%)	Flat at average 0.36223
Size of region with power deposition	5.4 x 48.045 mm	5.4 x 48.046mm
Location of center of beam spot	307 or 307.3mm downstream of upstream end	307mm downstream of upstream end
Taper in area illuminated due to beam divergence	(not described)	Divergence treated as zero
Mirror substrate overall length mm	<380	380
Mirror substrate overall width, mm	100	60
Mirror substrate overall thickness, mm	unstated	30

Following are details of a coarsely meshed run for 5 coolant partitions ("fins") per mirror half. For modeling convenience the optic was modeled upside down as shown in the figure below. The heat load is applied on a 48.046 mm long stripe 2.7 mm wide from the origin to the slanted line shown in the figure. Note, the system of units defined & used through the simulation runs is mm, gm, second, degrees C, coulomb, newton, & joule. Consequently stresses are displayed in N/mm^2 (MPa).

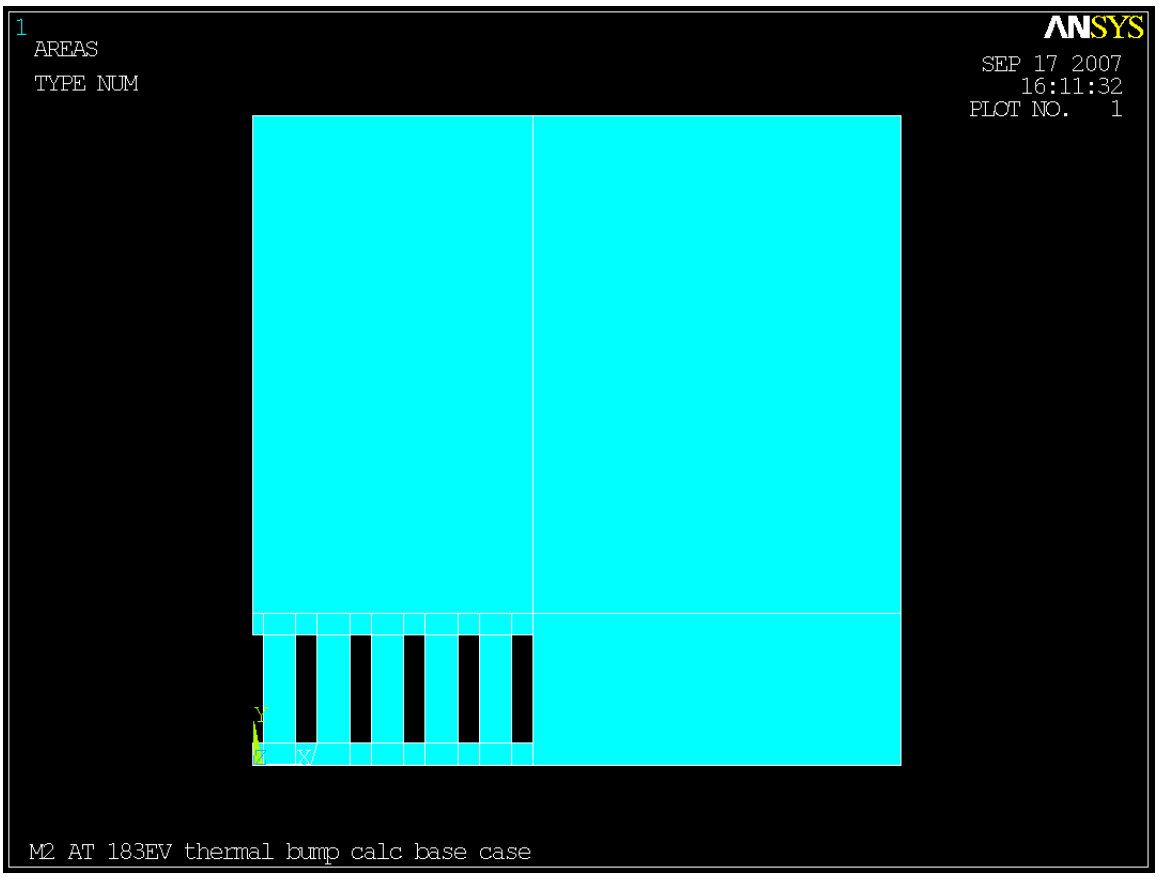

Figure 30. Silicon area shown in color; symmetry plane is at left.

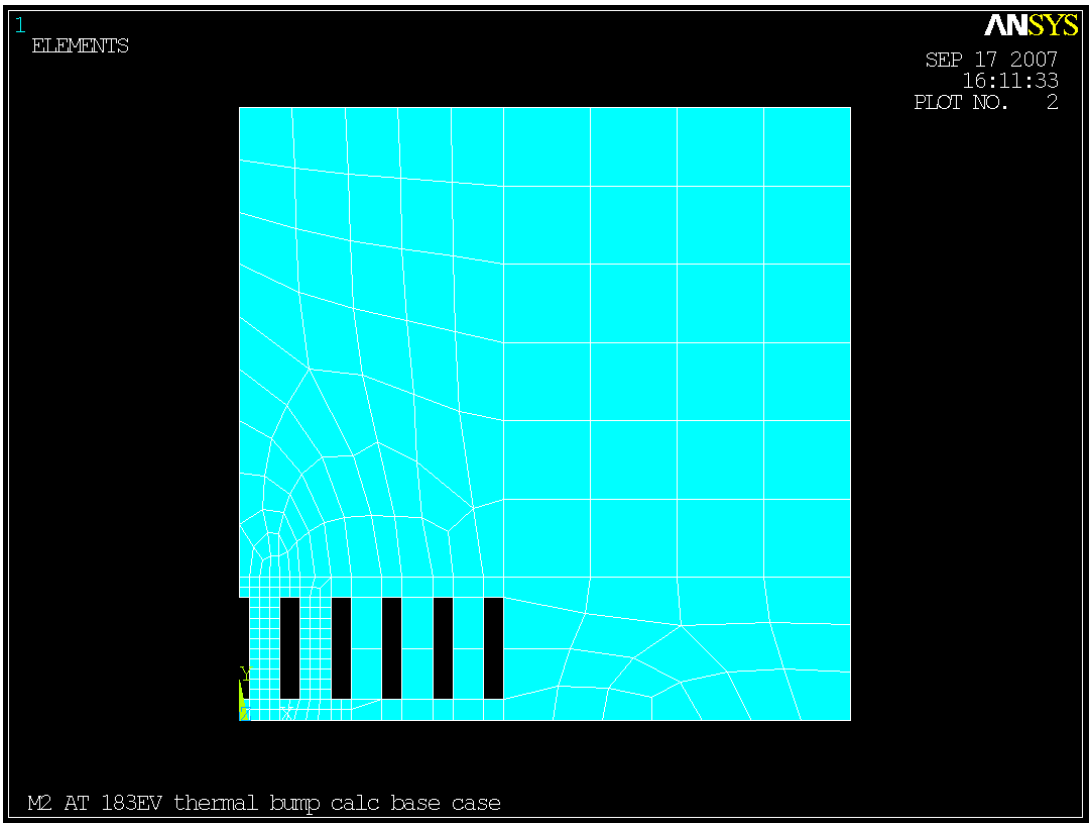

Figure 31. Initial meshing end view

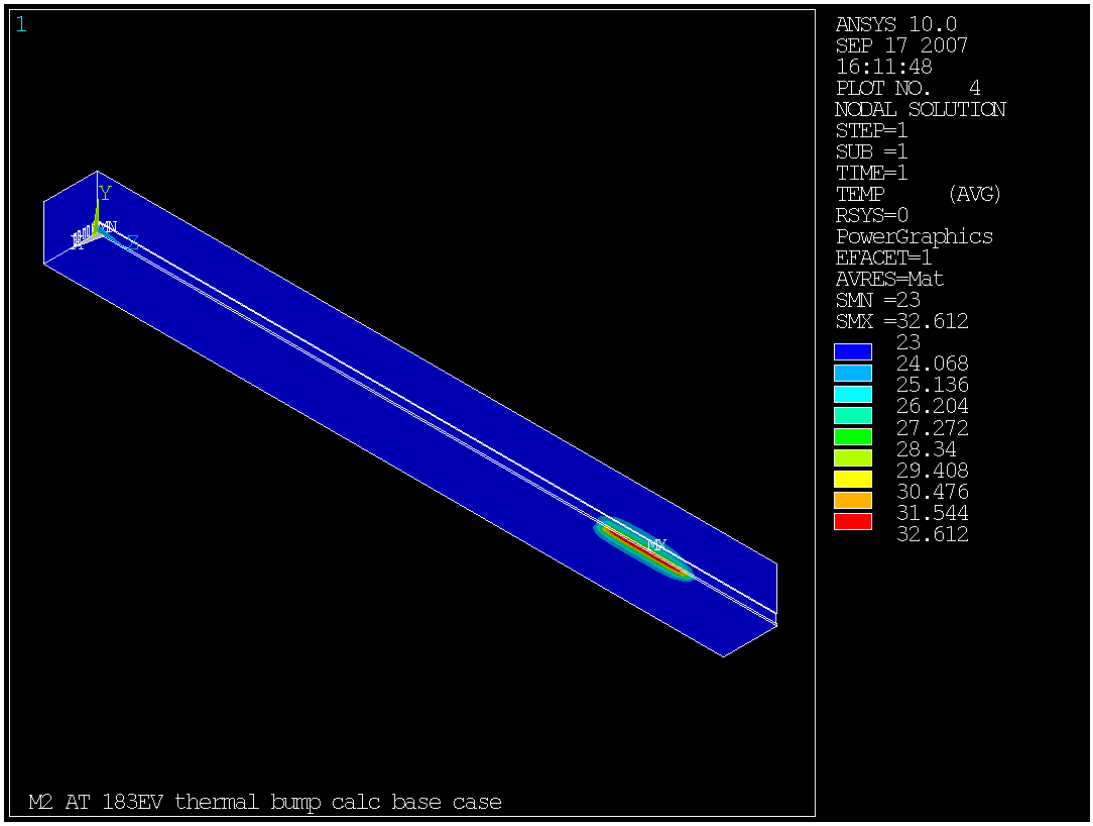

Figure 32. Thermal response, degrees C.

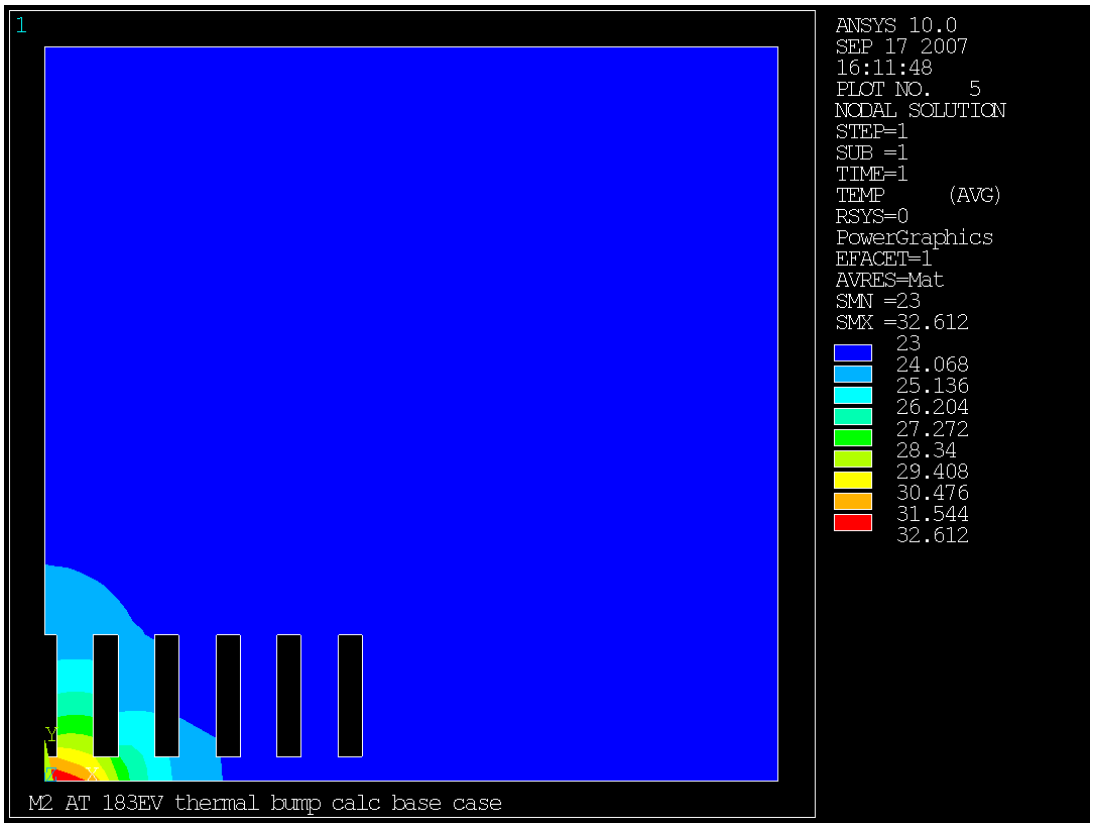

Figure 33. Thermal response at section through midpoint of heat load (Z=307mm).

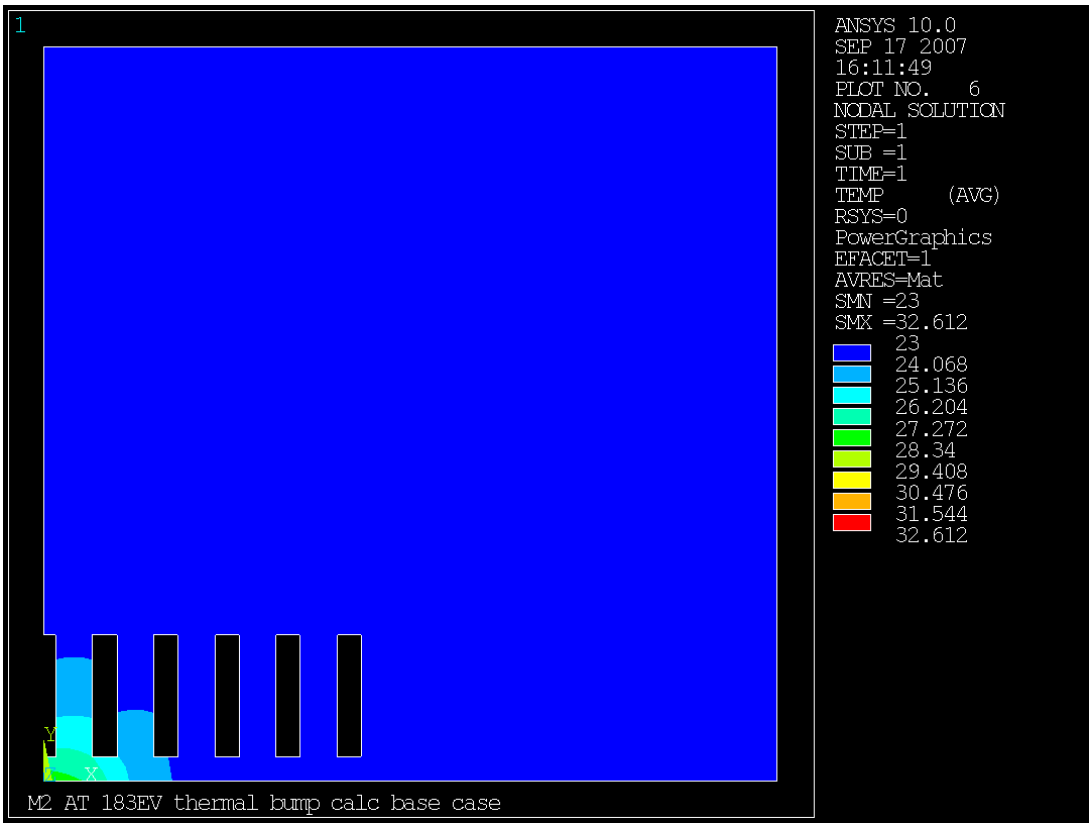

Figure 34. Thermal response, section through upstream edge of heat load (Z=283mm).

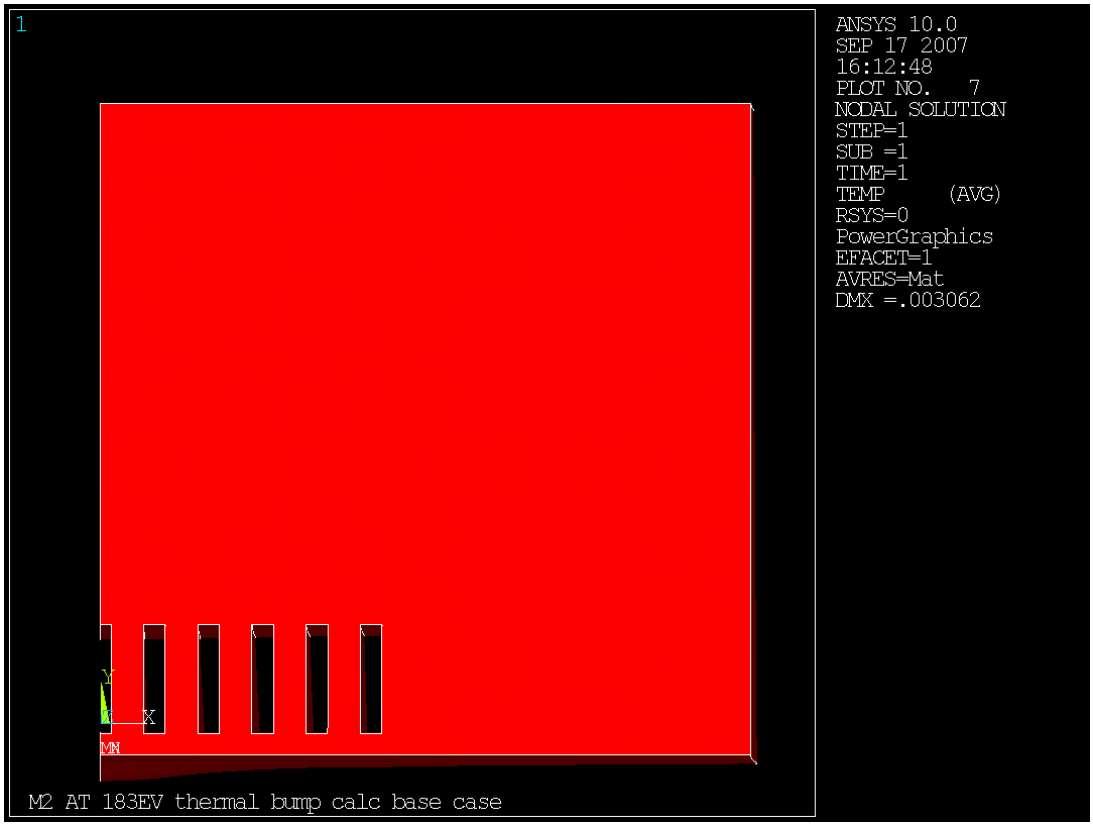

Figure 35. Exaggerated deformation end view.

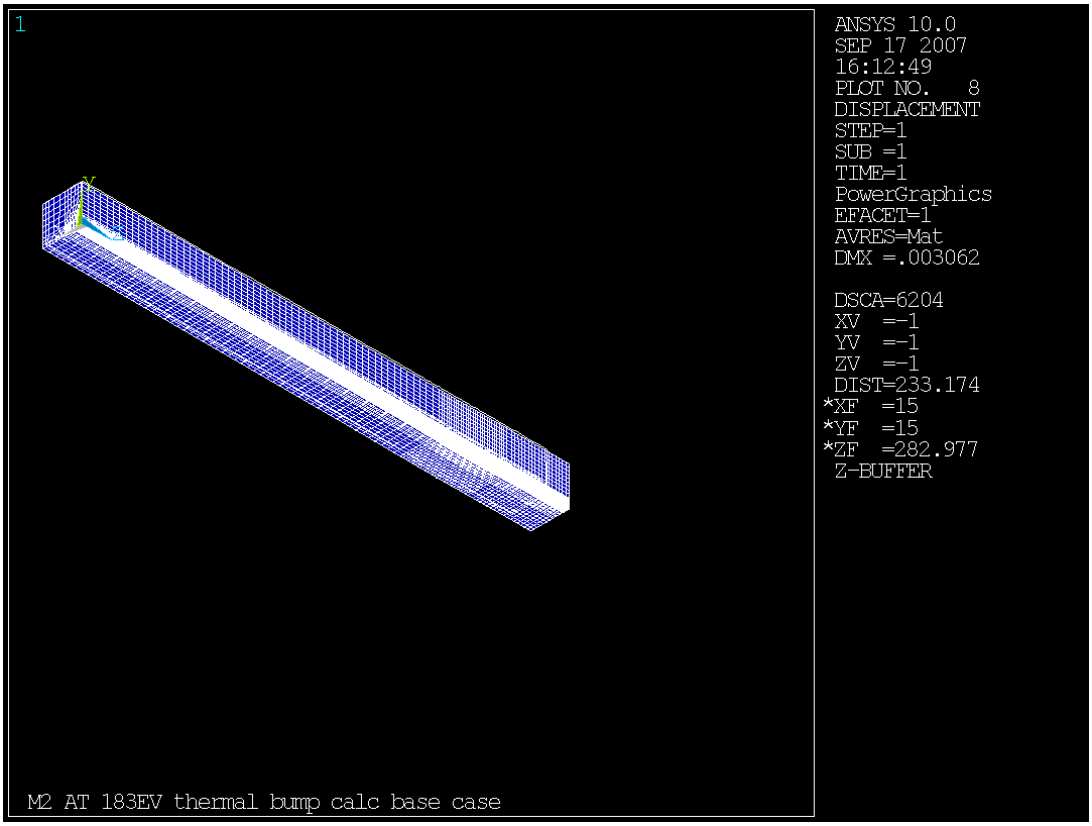

Figure 36. Displacement plot showing deformed and undeformed mesh; uniform thermal expansion dominates under the modeled conditions.

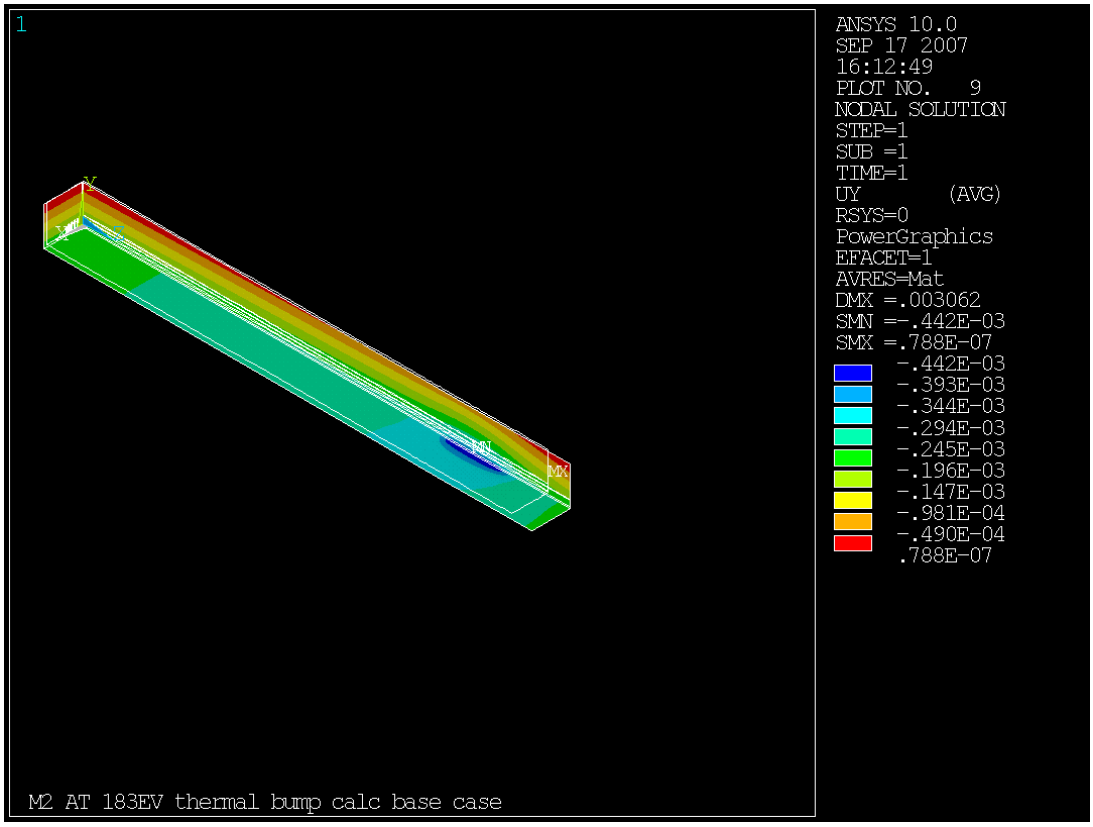

Figure 37. Displacement normal to the optical surface. Longitudinal bending and uniform thermal expansion dominate in producing the gross deflections.

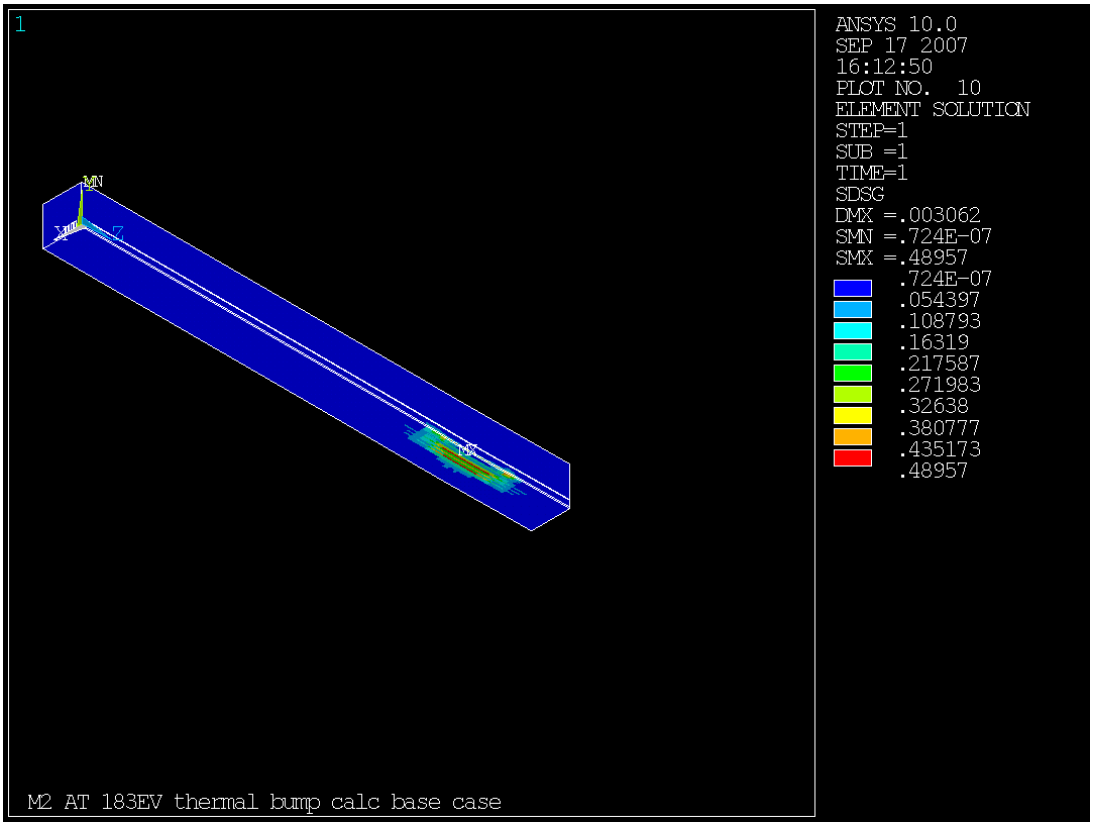

Figure 38. Absolute value of the maximum variation of any nodal stress component. Magnitude is high enough that calculated stresses should be regarded as very approximate.

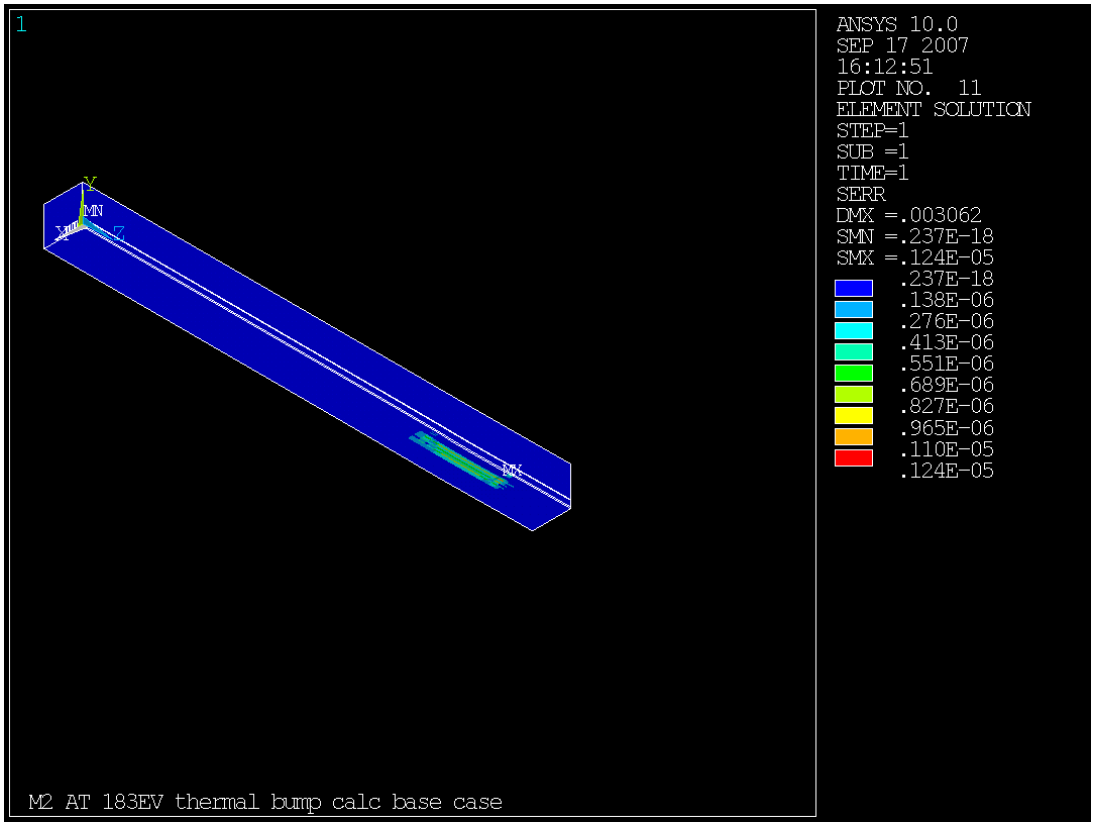

Figure 39. Energy error for the elements.

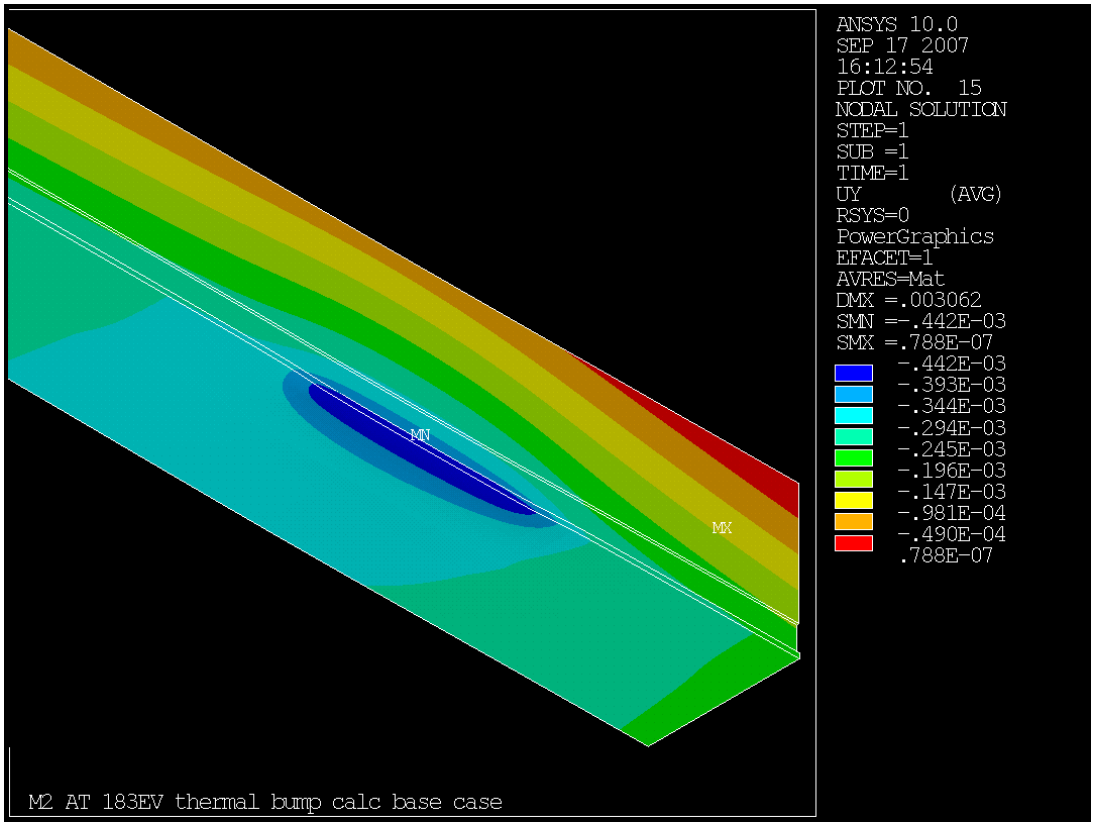

Figure 40. Displacements normal to optical surface at heat load and downstream end.

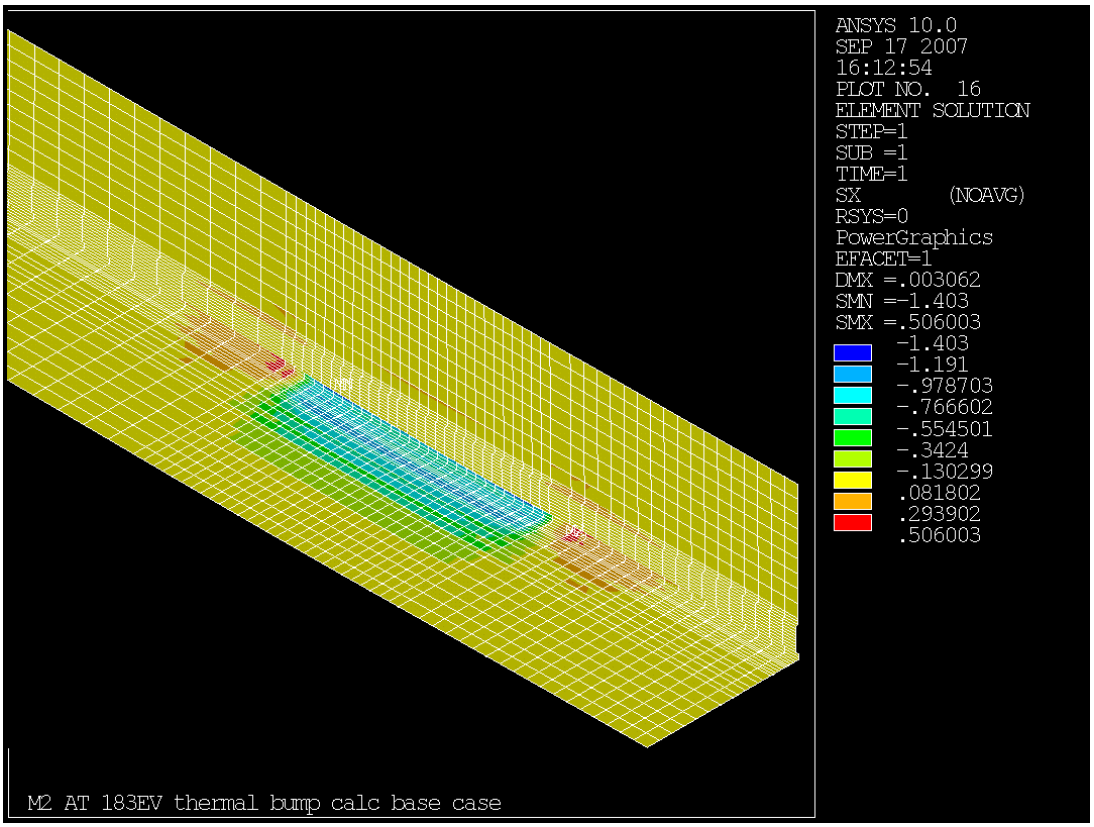

Figure 41. X axis stresses.

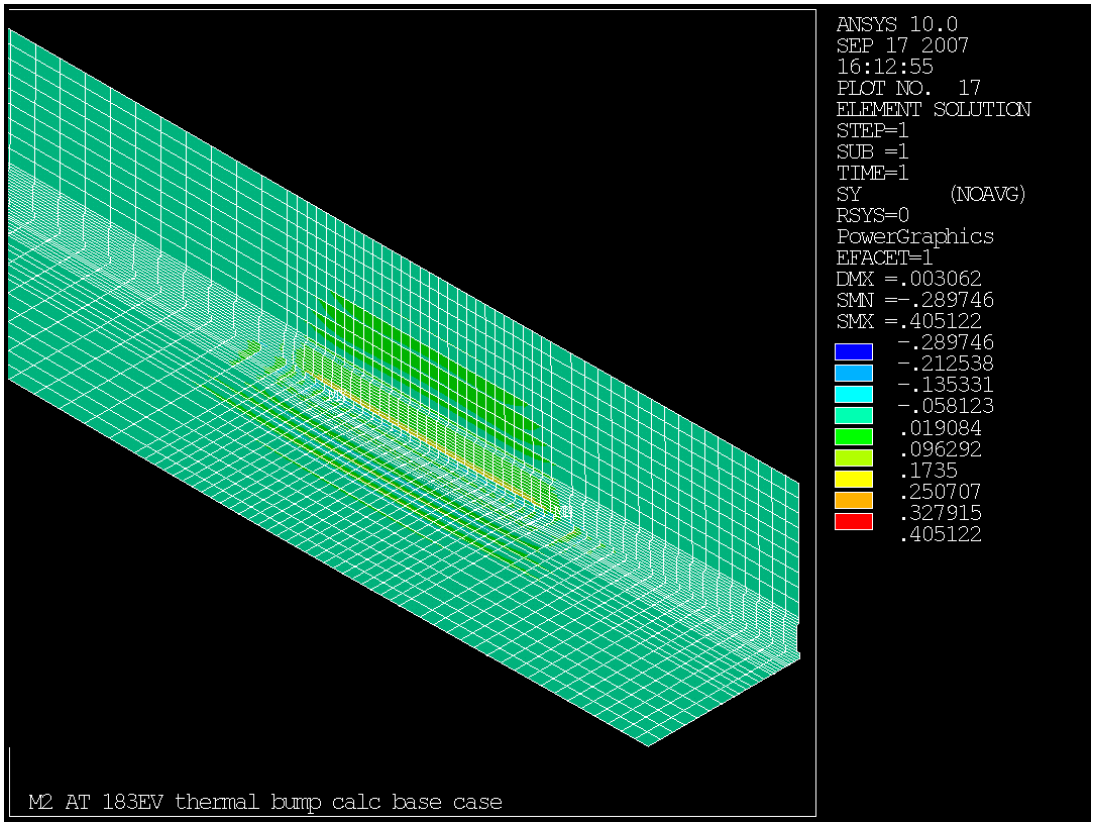

Figure 42. Y axis Stresses.

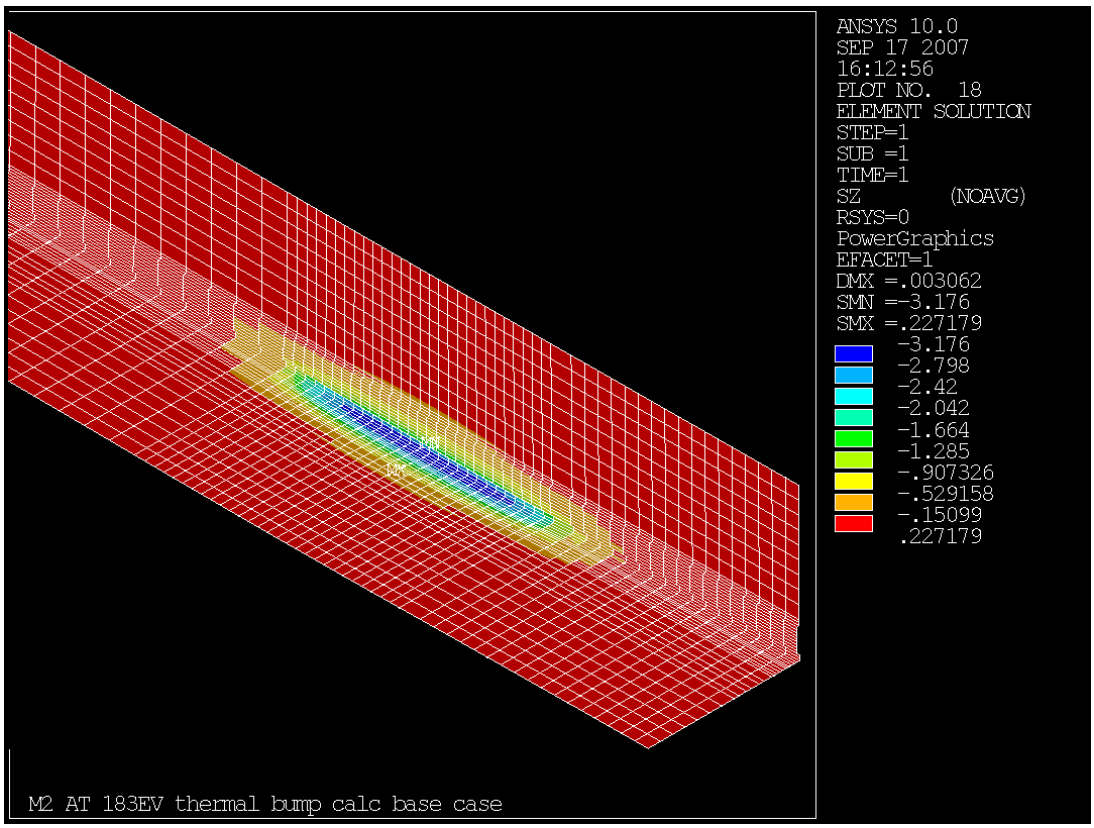

Figure 43. Z axis stresses. Contours resemble the temperature contours and the surface normal displacements.

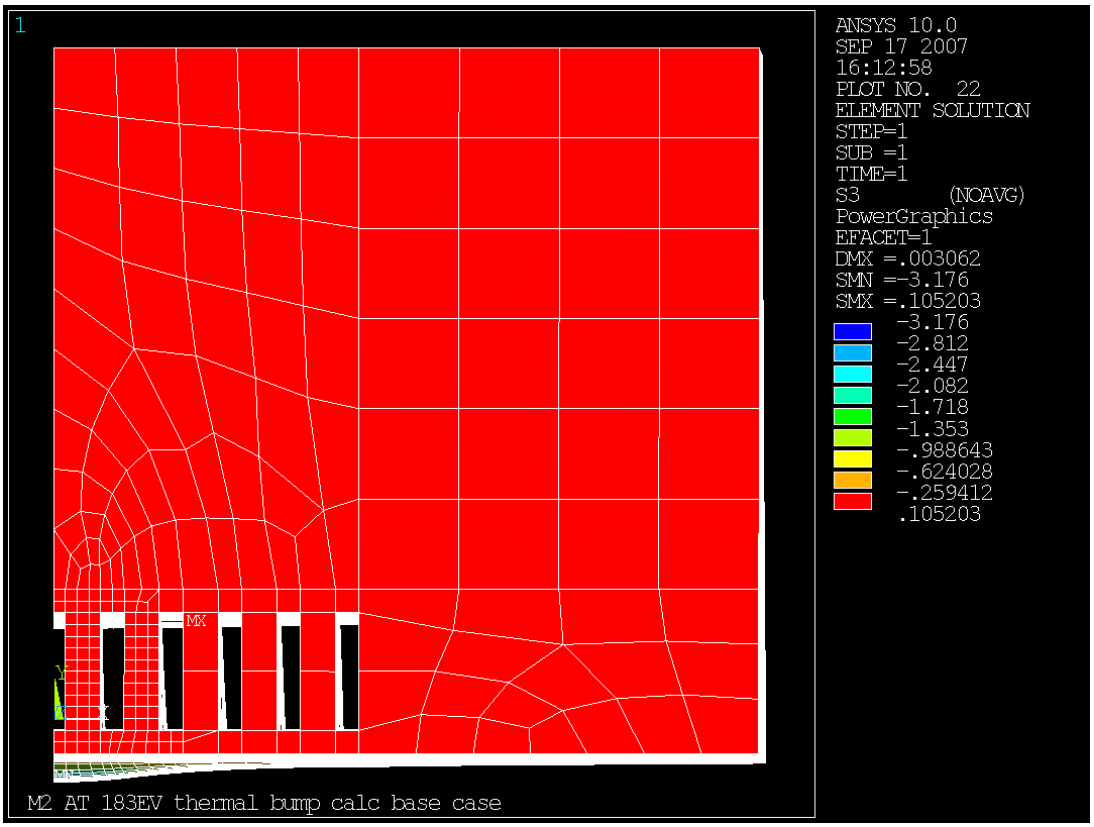

Figure 44. Third principal stress.

ANSYS path plots were generated for meridional and sagittal displacement and slope, with 380 points per meridional and 300 per sagittal plot. Small point counts (even considerably above the ANSYS default) result in the peak value of slope being understated in the path plots. The high count needed to represent the peak seems to introduce artifacts elsewhere in the sagittal slope plots.

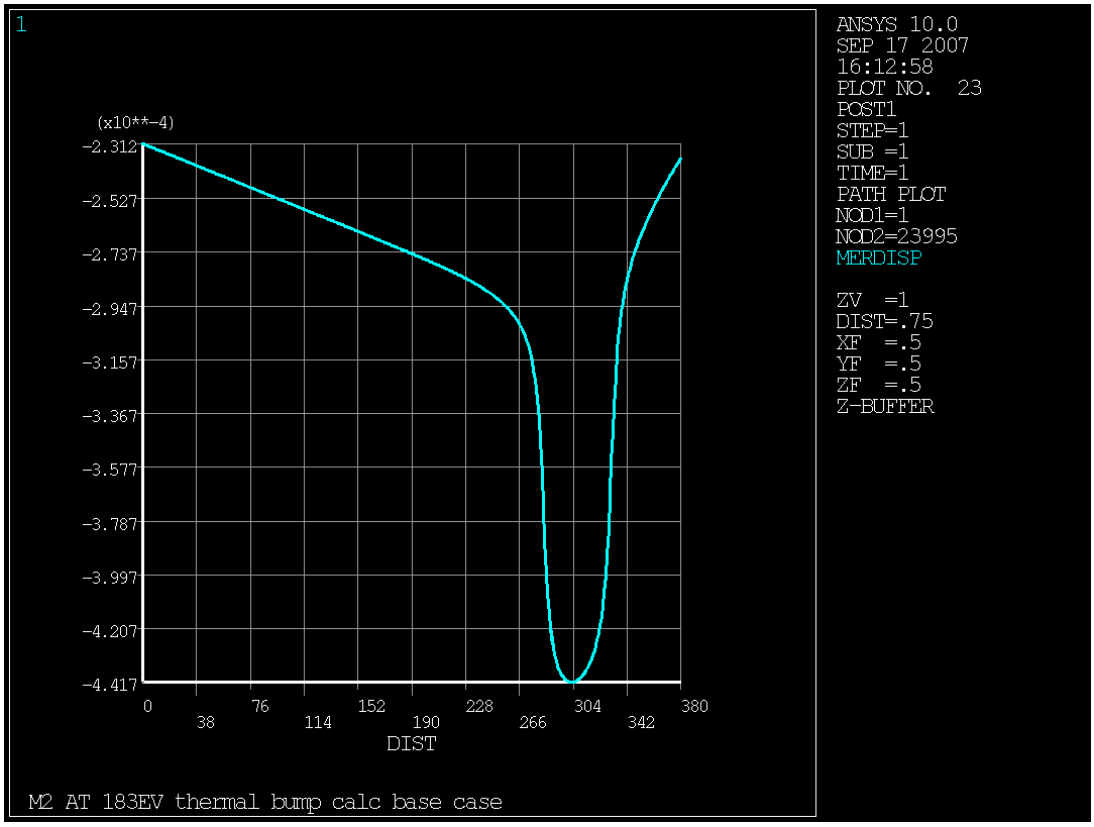

Figure 45. Meridional displacement plot, mm. Displacement is unequal at the two ends because the Z=380mm end is warmer than the z=0mm end. Peak displacement occurs shifted upstream from heat center for geometrical reasons.

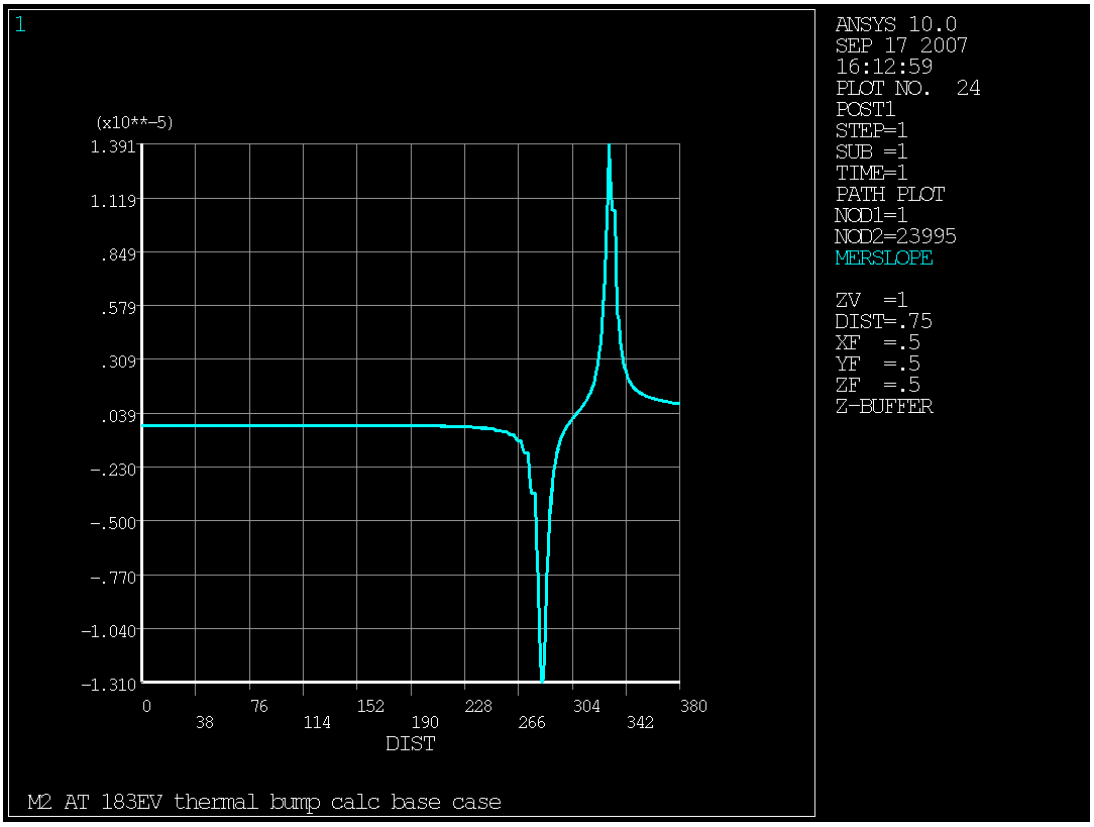

Figure 46. Meridional slope plot, radians. High curvature peaks occur at the front and back edges of the heat input area. The central slope is correctable but the end peaks are problematic.

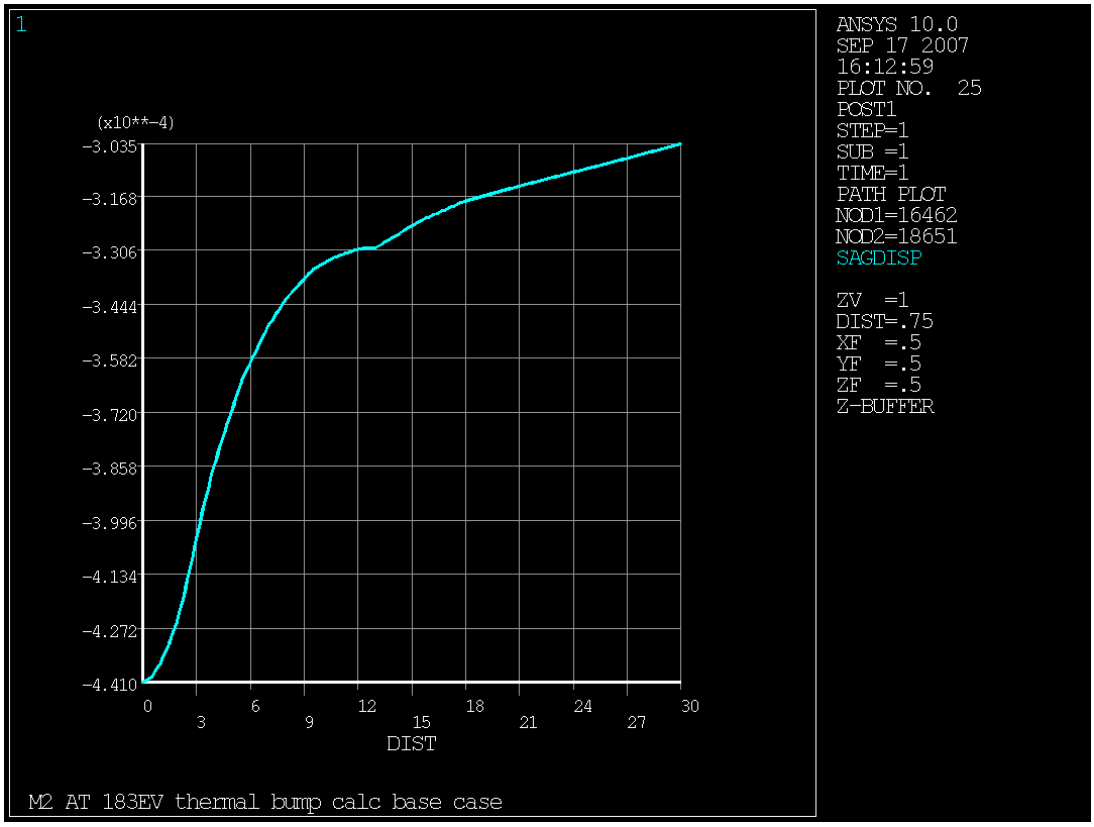

Figure 47. Sagittal displacement (mm) plot on path across midpoint of heat spot (Z=307mm). The range from 0 to 2.7mm is of interest for correction and appears highly correctable.

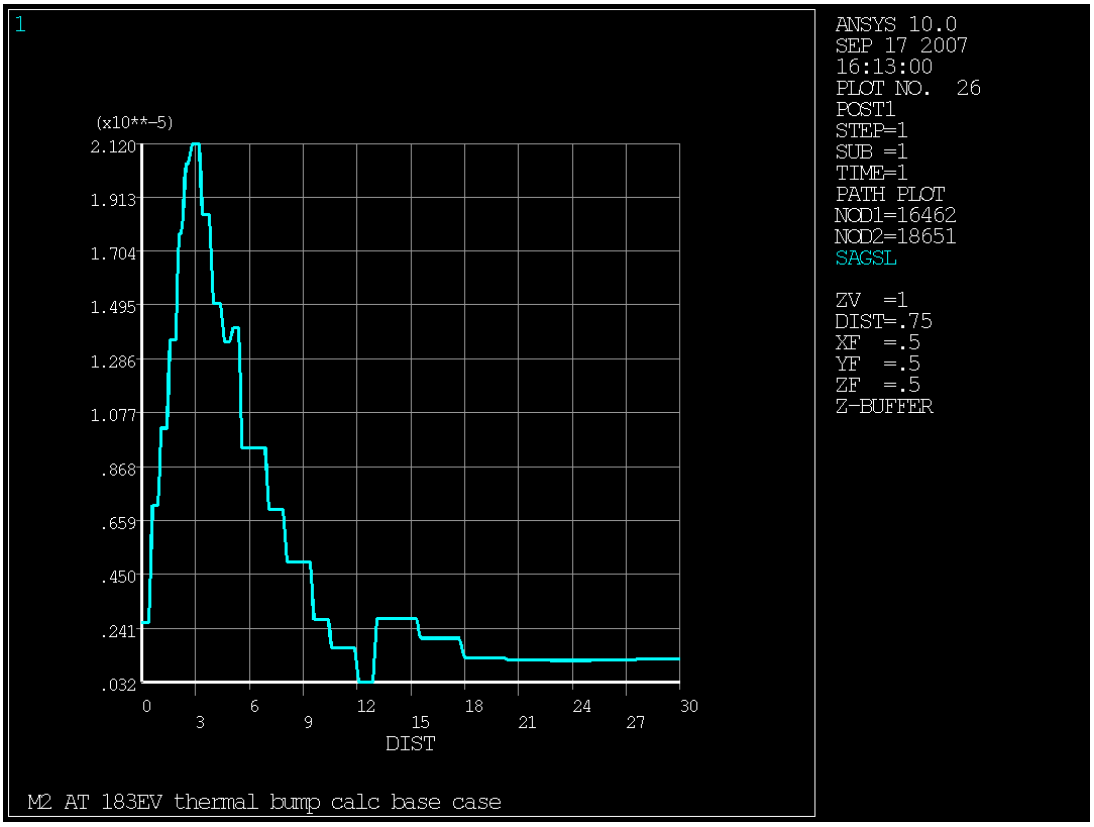

Figure 48. Sagittal slope (radians) on path through midpoint of heat spot (Z=307mm).

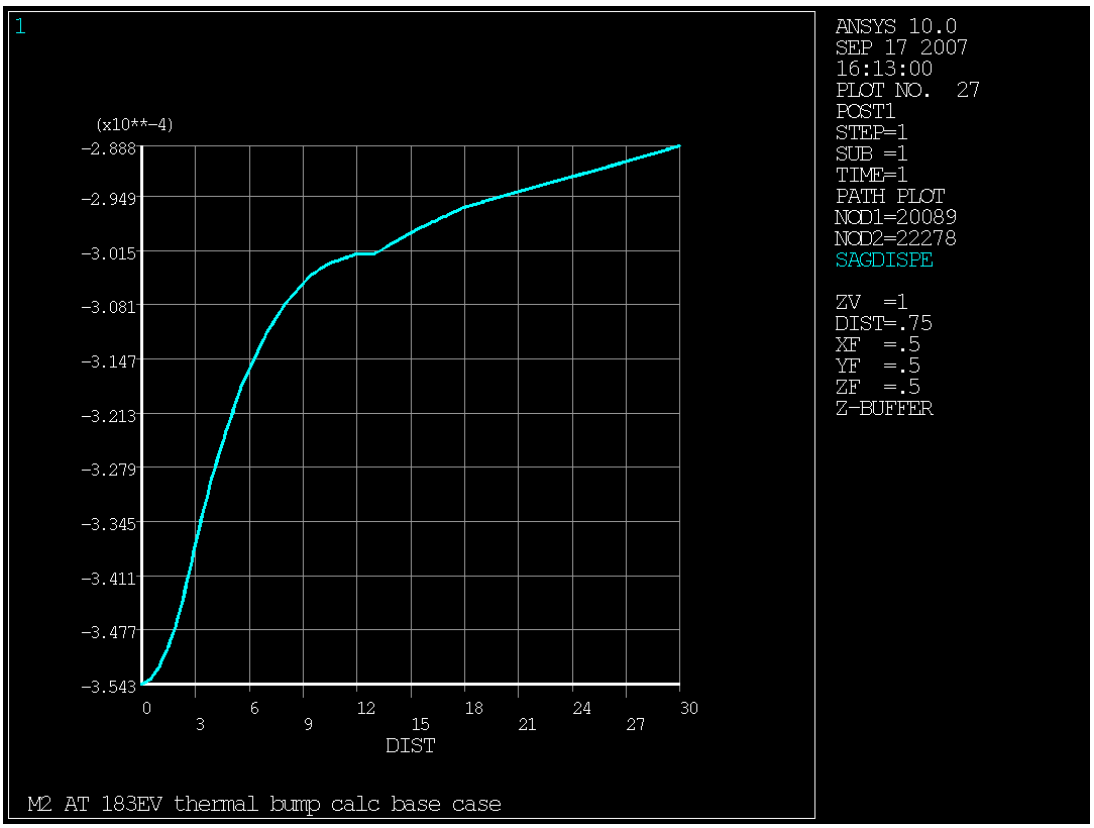

Figure 49. Sagittal displacement on path at downstream edge of heat spot (Z=331mm).

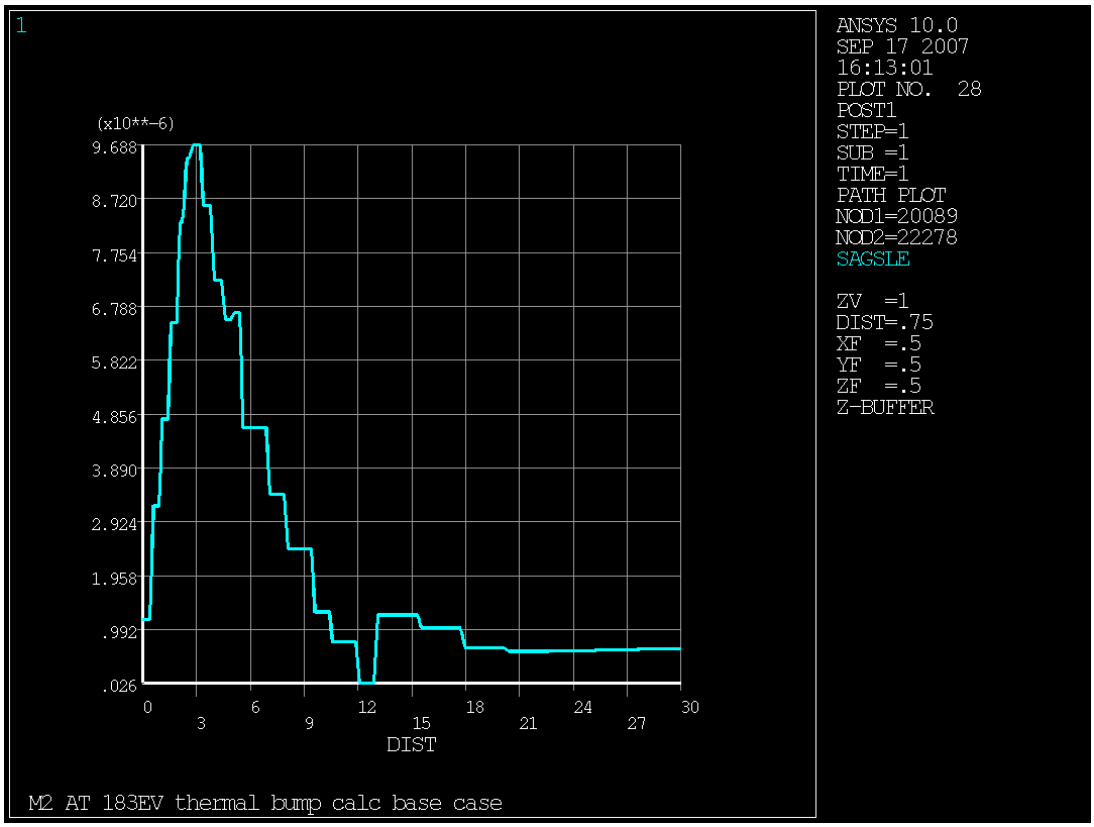

Figure 50. Sagittal slope on path at downstream edge of heat spot (Z=331mm). Note the peak slope is less than half the midpoint peak.

The resulting meridional and sagittal displacements were incorporated into a spreadsheet for analysis of slope and possibilities of compensation. It was determined the standard deviation of meridional slope after second order compensation was still several times too high, but central sagittal slope could be adequately compensated. Runs with a much thicker substrate (100 rather than 30mm) and with 3 fins rather than 5 were made. The 3-fin case showed minor changes in slope variation, with almost all parameters favoring the 5-fin case.

Subsequently a mesh refinement run was made on the base 5-fin case, and the resulting illuminated-surface displacements provided for ray tracing the deformed optic. Displacement and slope values matched within 11 percent between the base and refined runs, while temperature rise matched within one percent, giving confidence in the mesh quality. The ray tracing results predicted adverse effects on beam spot size downstream, confirming the conclusion from the spreadsheet based slope evaluation, and generating additional requests for ANSYS runs.

Some concern was expressed over the asymmetric meridional slopes and displacements such as shown in Figure 16. A model qualification run was made with the heat spot moved to centered axially at z=190mm. The resulting midpoint meridional slope was about -0.504×10^{-17} radians, 10^{-10} times lower than the absolute magnitudes of slope at z=189 and z=191mm, an excellent degree of symmetry. Some very small asymmetry is present since the difference between bulk coolant temperature and material reference temperature leads to axial expansion overall, and the structural constraint applied axially is at the Z=0mm (upstream) end. This would displace the midpoint about 0.5 micron downstream. At a rate of change of slope of 0.50295×10^{-7} radians/mm that is a tiny effect but still a much larger effect than the calculated asymmetry referenced to the midpoint. The asymmetry in slopes and displacements relative to heat spot midpoint is actually expected and necessary, as shown in the following figure.

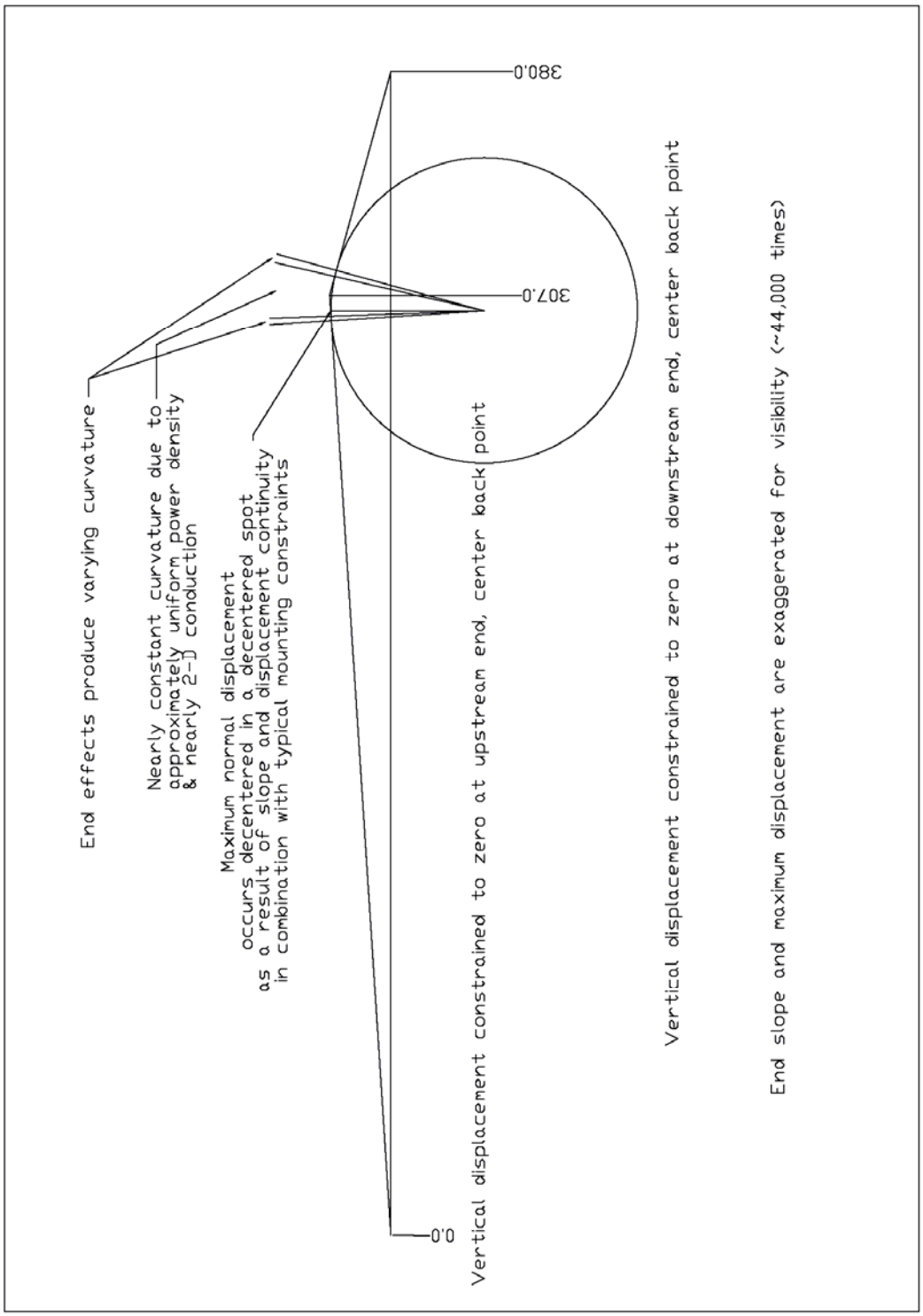

Figure 51. Asymmetric thermal load location generates asymmetric slopes and end displacements. Here the M2 optic is idealized as a slender bar with thermal bending over a segment.

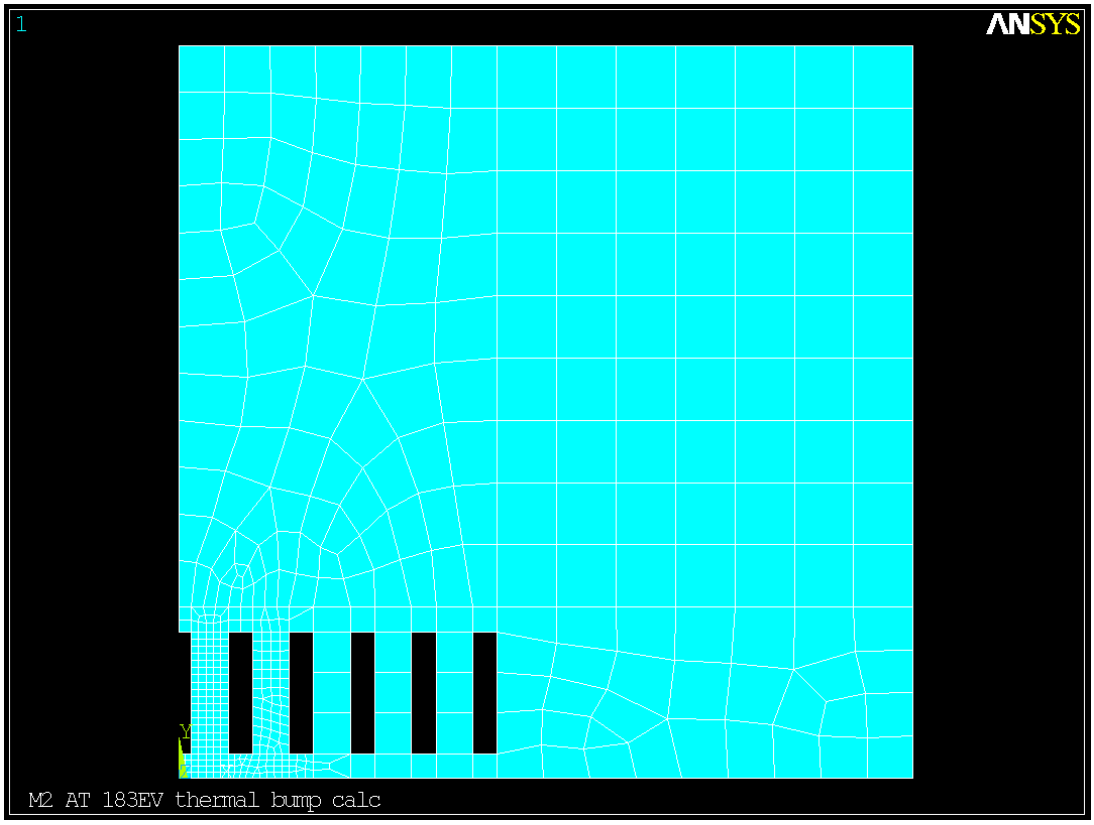

Figure 52. Refined mesh end view. The axial mesh spacing was also refined.

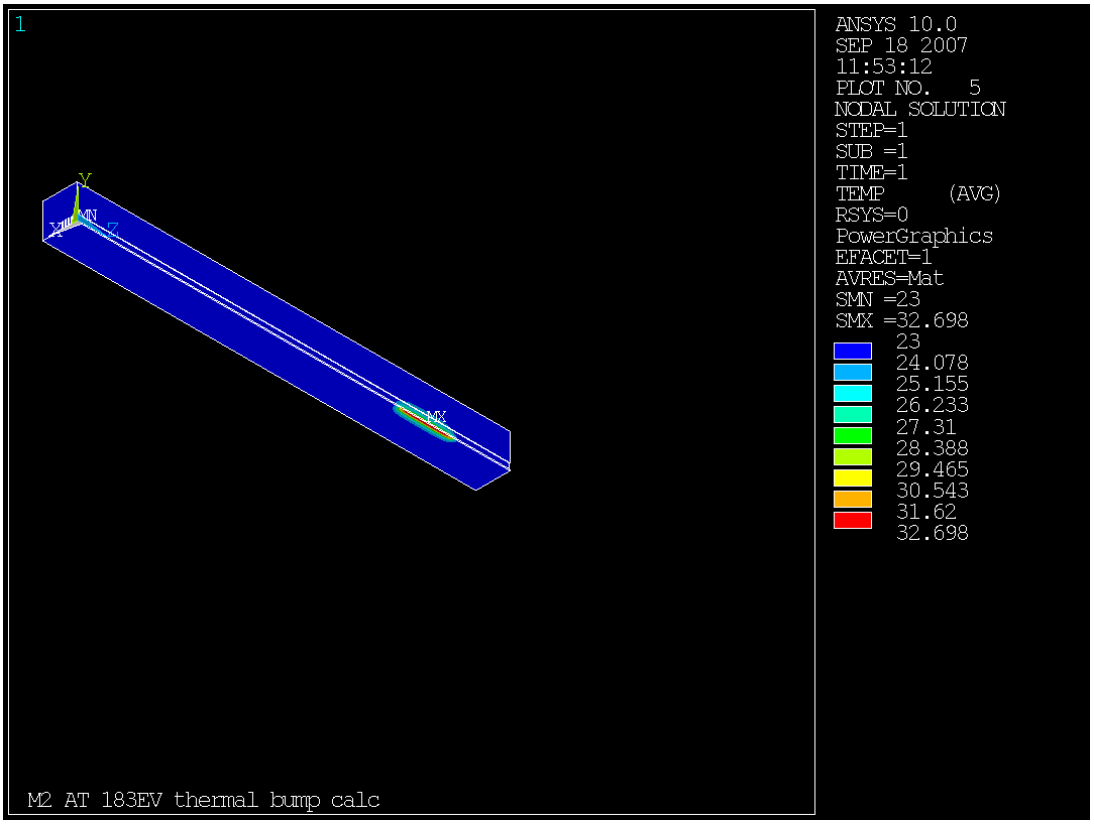

Figure 53. Maximum temperature rise above coolant bulk temperature with the refined mesh is 0.9% higher than coarse mesh run for same geometry & load case.

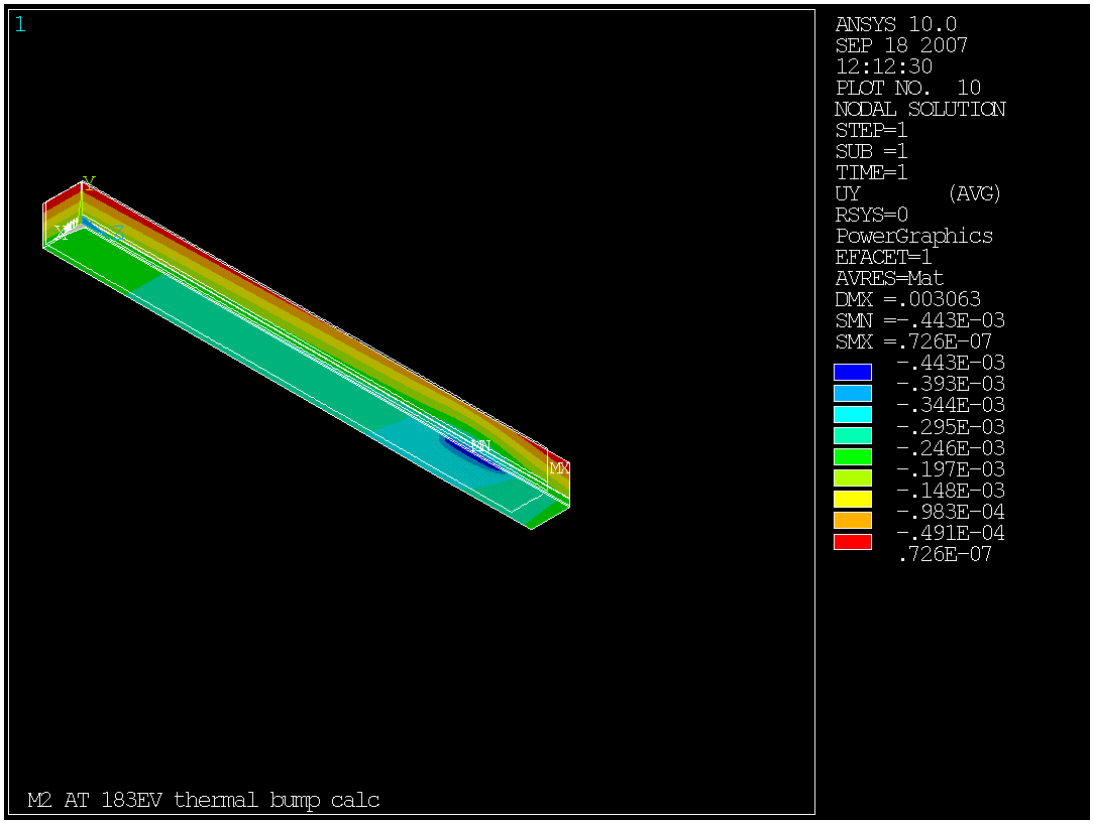

Figure 54. Refined mesh displacement in direction normal to the optical surface.

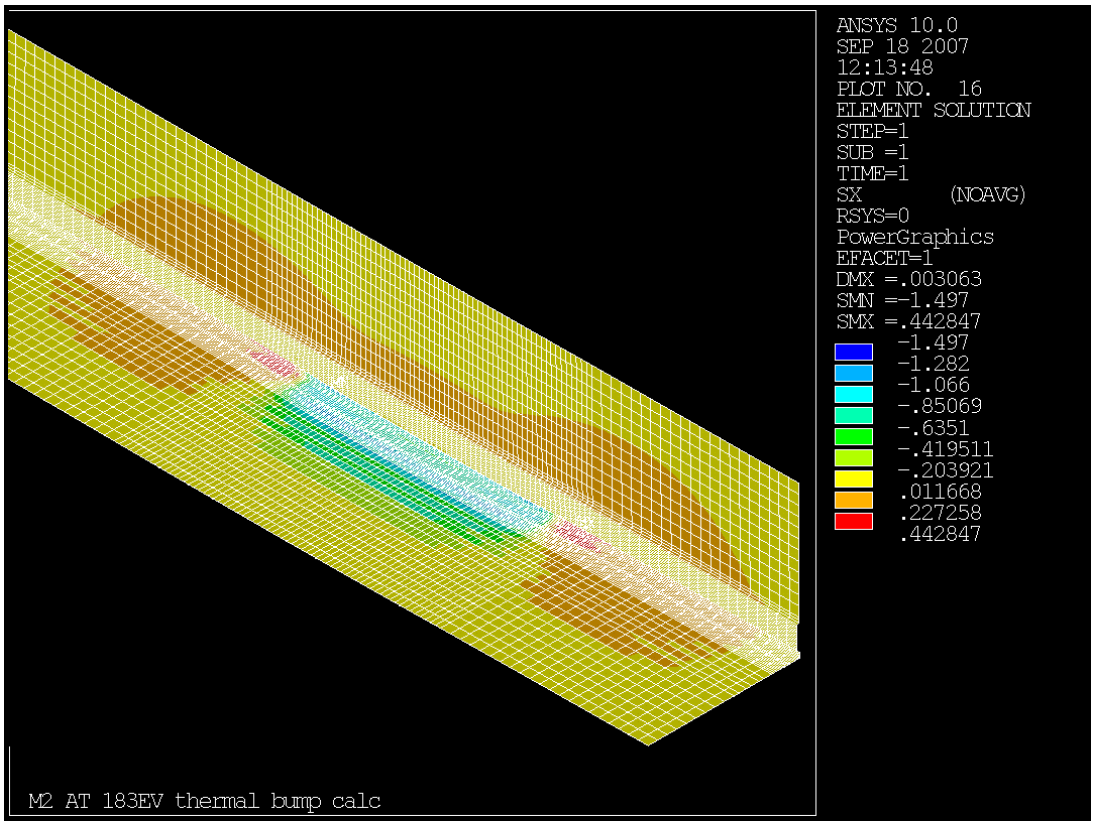

Figure 55. Refined mesh X axis stress.

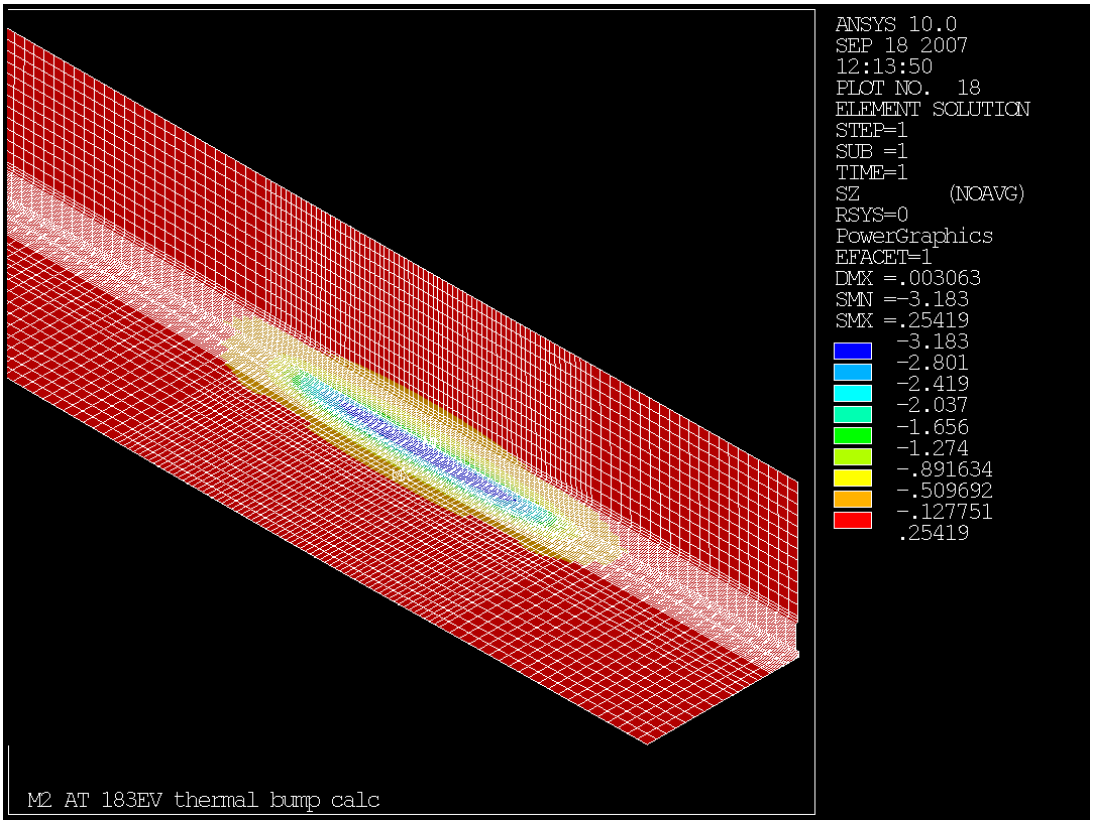

Figure 56. Refined mesh Z axis stress.

Table 2. Comparison of coarse and refined mesh 5-fin runs. The difference in slopes is largest at the edge sagittal value, at 11%.

Parameter	Coarse run	Refined run
Peak temperature, °C	32.612	32.698
Maximum displacement (which is axial), microns	3.062	3.063
Maximum normal displacement, microns	0.44175	0.44266
Maximum SDSG	0.48957	0.46697
Maximum SERR	0.124E-05	0.406E-06
SX extremes, N/mm^2	-1.403, 0.506	-1.497, 0.4428
SY extremes, N/mm^2	-0.2897, 0.4051	-0.3808, 0.3995
SZ extremes, N/mm^2	-3.176, 0.2272	-3.183, 0.2542
S3 extremes, N/mm^2	-3.176, 0.1052	-3.183, 0.0971
Meridional displ & slope, mm & microradians max	0.0004417, 13.91	0.0004426, 15.333
Central sagittal displ & slope, mm & microradians max	0.0004410, 21.2	0.0004419, 22.0
Edge sagittal displ & slope, mm & microradians max	0.0003543, 9.688	0.0003569, 10.77

Table 3. Comparison of 5-fin and 3-fin coarse mesh runs.

Parameter	Coarse 5-fin run	Coarse 3-fin run
Peak temperature, °C	32.612	32.679
Maximum displacement (which is	3.062	3.14

axial), microns		
Maximum normal displacement, microns	0.44175	0.457
Maximum SDSG	0.48957	0.69396
Maximum SERR	0.124E-05	0.146E-05
SX extremes, N/mm^2	-1.403, 0.506	-1.559, 0.4377
SY extremes, N/mm^2	-0.2897, 0.4051	-0.2710, 0.4281
SZ extremes, N/mm^2	-3.176, 0.2272	-3.156, 0.1867
S3 extremes, N/mm^2	-3.176, 0.1052	-3.156, 0.1442
Meridional displ & slope, mm & microradians max	0.0004417, 13.91	0.0004564, 13.99
Central sagittal displ & slope, mm & microradians max	0.0004410, 21.2	0.0004558, 20.86
Edge sagittal displ & slope, mm & microradians max	0.0003543, 9.688	0.0003683, 9.992

A requested run was with the length of heat spot increased from 48.046mm overall to 68mm overall. This was performed with the refined mesh.

Table 4. Comparison of refined mesh 5-fin base and extended heat spot runs.

Parameter	Refined base run	Extended spot run
Peak temperature, °C	32.698	32.719
Maximum displacement (which is axial), microns	3.063	3.111
Maximum normal displacement, microns	0.44266	0.472
Maximum SDSG	0.46697	0.45927
Maximum SERR	0.406E-06	0.421E-06
SX extremes, N/mm^2	-1.497, 0.4428	-1.476, 0.4559
SY extremes, N/mm^2	-0.3808, 0.3995	-0.3747, 0.3985
SZ extremes, N/mm^2	-3.183, 0.2542	-3.233, 0.2575
S3 extremes, N/mm^2	-3.183, 0.0971	-3.233, 0.0980
Meridional displ & slope, mm & microradians max	0.0004426, 15.333	0.0004721, 15.82
Central sagittal displ & slope, mm & microradians max	0.0004419, 22.0	0.0004697, 21.94
Z=331 sagittal displ & slope, mm & microradians max	0.0003569, 10.77 (downstream edge)	0.0004384, 21.54 (at Z=331, 10mm inside downstream edge of extended spot)

Extension of the heat spot lengthens the roughly cylindrical central portion of the normal displacements, improving the correctability of the distortions as intended. Normal displacements were provided to ray tracing to verify that.

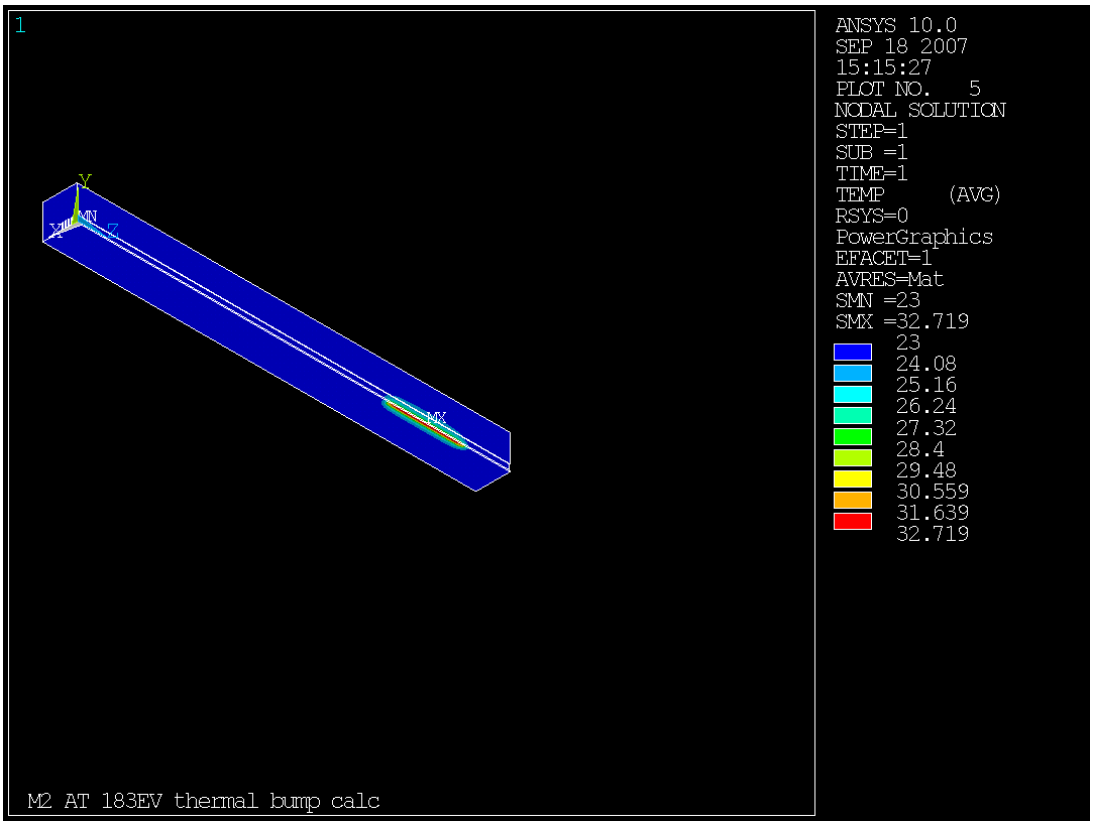

Figure 57. Temperature response of refined mesh 5-fin case with extended heat spot.

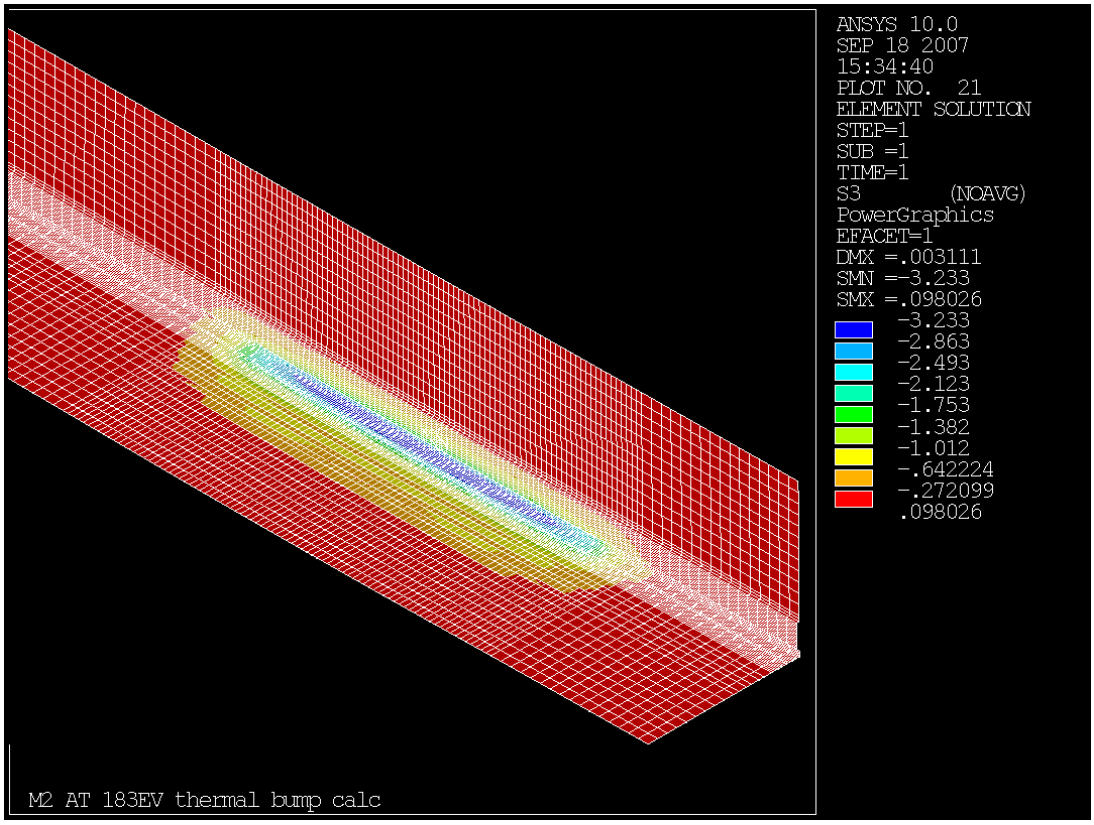

Figure 58. Refined mesh 5-fin case with extended heat load, showing third principal stress with mesh outline superimposed.

Stiffening the optic with a significantly thicker substrate appears to have only minor effects on slope, with 6% lower meridional slope and 6.3% higher edge sagittal slope.
Some results of the 100mm thick substrate case are shown below.

Table 5. Comparison of 100mm thick substrate to 30mm thick.

Parameter	30mm	100mm
Peak temperature, °C	32.612	32.604
Maximum displacement (which is axial), microns	3.062	3.149
Maximum normal displacement, microns	0.44175	0.962
Maximum SDSG	0.48957	0.5159
Maximum SERR	0.124E-05	0.109E-05
SX extremes, N/mm^2	-1.403, 0.506	-1.45,0.428
SY extremes, N/mm^2	-0.2897, 0.4051	-0.266, 0.4041
SZ extremes, N/mm^2	-3.176, 0.2272	-3.222,0.2055
S3 extremes, N/mm^2	-3.176, 0.1052	-3.222,0.0982
Meridional displ & slope, mm & microradians max	0.0004417, 13.91	0.000962, 13.08
Central sagittal displ & slope, mm & microradians max	0.0004410, 21.2	0.000962, 21.22
Edge sagittal displ & slope, mm & microradians max	0.0003543, 9.688	0.0008911, 10.30

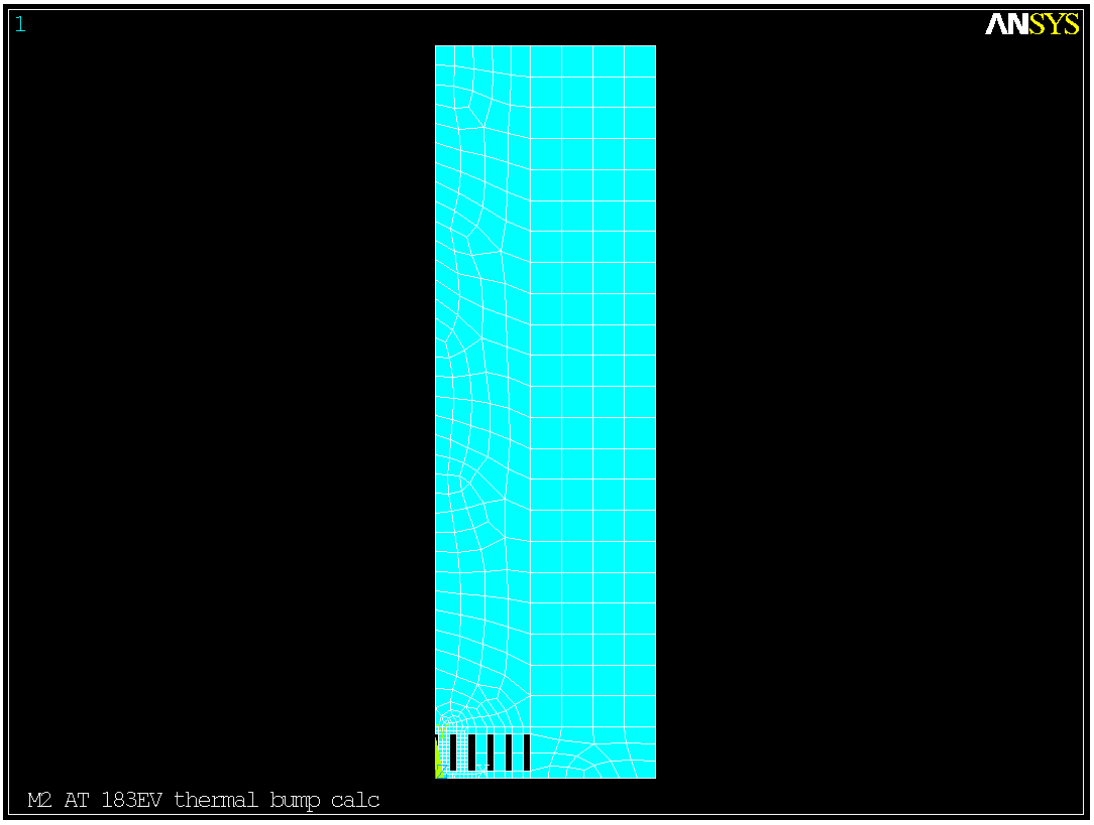

Figure 59. End view of mesh on 100mm thick case.

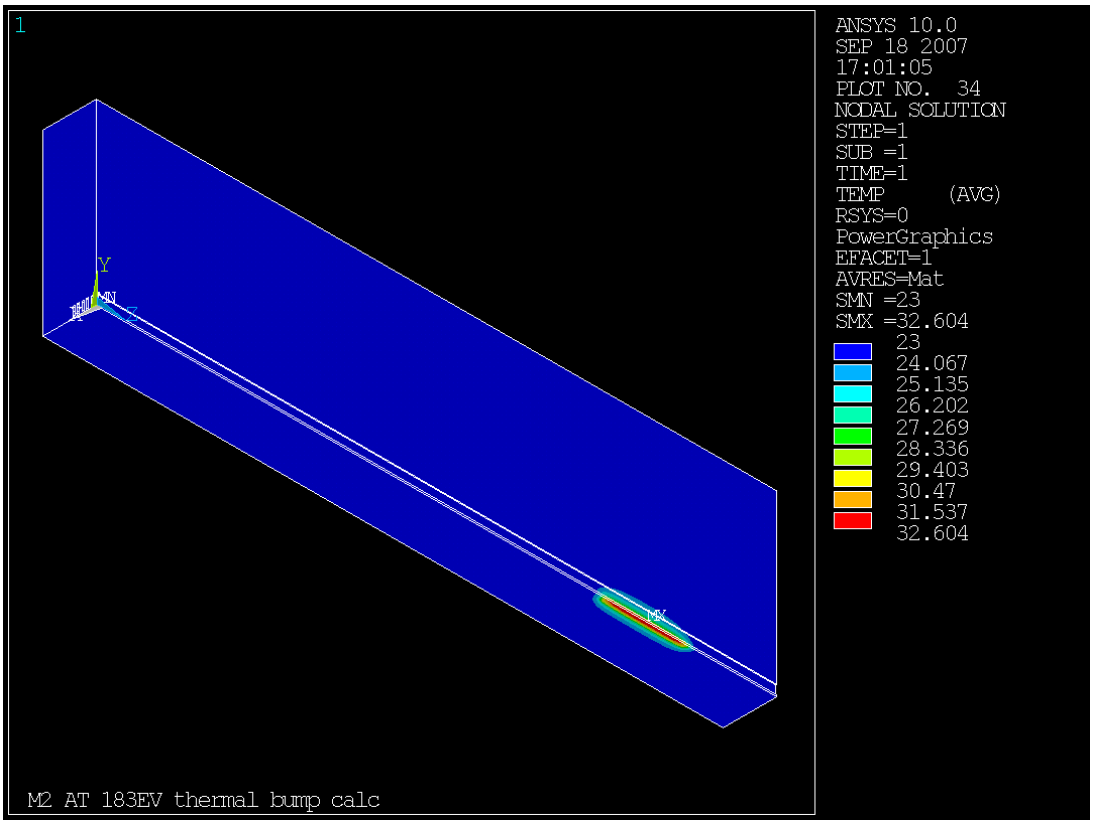

Figure 60. Resulting temperature solution.

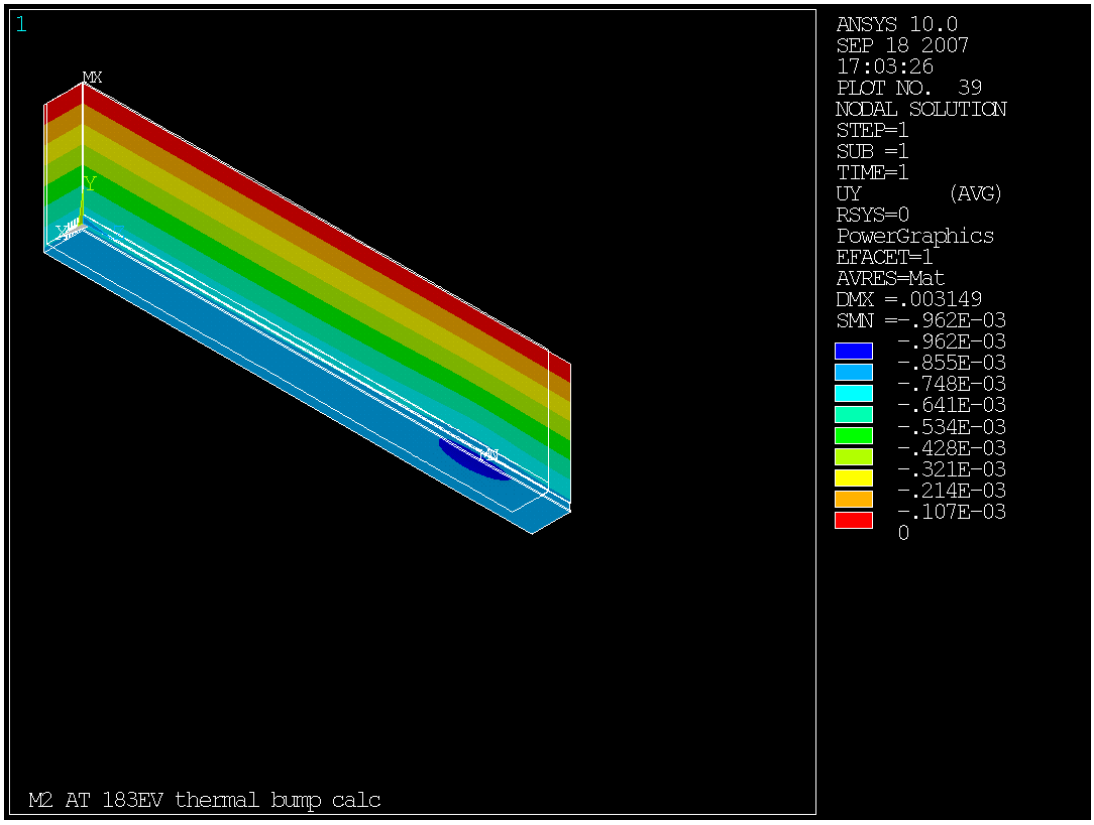

Figure 61. Displacement normal to the optical surface for 100mm thick substrate.

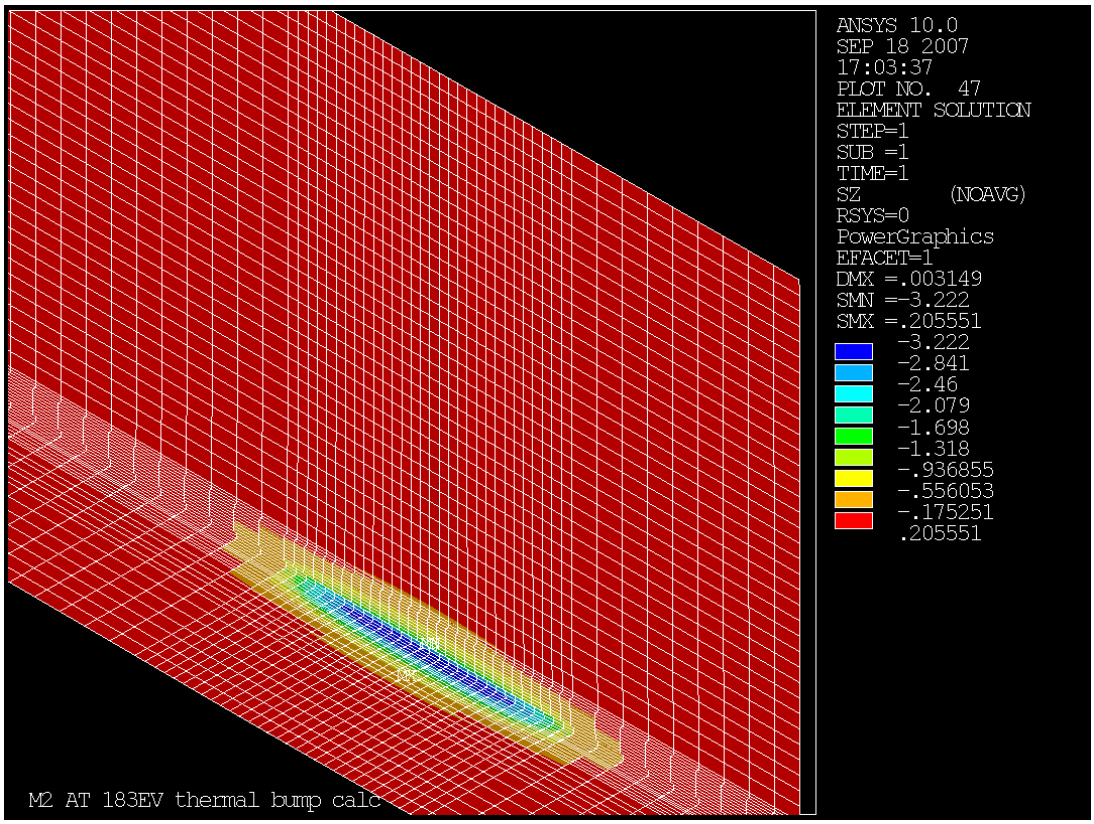

Figure 62. Z axis stress for 100mm thick substrate.

Summary

The M2 183eV operating case was selected for analysis as an expected worst case and determined to generate excessive distortion of the optical surface. A workaround was proposed, and simulated in ANSYS and in ray tracing, providing verification the workaround is sufficient to preserve optical figure at M2.

The 3-D parametric ANSYS model is adaptable to running many load and geometry cases. It still contains many approximations some of which should be removed in future design effort. With modification to handle generalized power density distributions, it will be applicable to additional optical elements in the beamline and additional beamline operating conditions. It is easily applicable to optimization studies. Variations in several variables were analyzed for effect on temperature and active optical surface shape. Evaluating surface slopes via path plots is an efficient way to forecast negative impact on ray tracing results & beamline performance.

The ANSYS outputs from differing meshes show that the temperatures and displacements reproduce well, and slopes to about 11% or better. Reproducibility of stresses is not as good; ANSYS measures of stress accuracy show that stress values from particular nodes & elements should not be relied on, as the values at a given node differ significantly among elements that have that node in common. However, the extreme values and the ranges of stress obtained reproduce reasonably well, and the extreme values are low in all cases. Peak thermal stresses obtained to date are low, below the level requiring acid etch. Stress concentrations and additional loads have not yet been examined. Uniform thermal expansion from reference temperature to (the slightly elevated) bulk coolant temperature is very significant in the overall displacement. These displacements were obtained with constraints applied at worst case locations (extreme ends of back surface) maximizing bulk expansion response and the effect of thermal bending on peak displacement. Real mirror mounting locations will straddle less than the optic's total length and so reduce the influence of thermal expansion on peak displacement. All simulation performed was steady state.

5 XAS: HARD X-RAY ABSORPTION SPECTROSCOPY

5.1 Executive Summary

This document describes the strategic need and preliminary technical design for a damping wiggler-based hard x-ray absorption spectroscopy beamline as an NSLS-II Project Beamline. It represents the synthesis of user and scientific community input, interactions with project and accelerator staff, contracted engineering reports from Accel Corporation, and technical reviews by the NSLS-II EFAC and others.

The technique of x-ray absorption spectroscopy uses each element's characteristic absorption edge(s) to obtain local (within ~10Å) information about that element. It is a non-destructive, element-specific probe of local physical and electronic structure, speciation, and chemical state. XAS measurements may be made by transmission, characteristic x-ray fluorescence, or photoelectron yield. Samples may be crystalline or amorphous, and in nearly any form (solid, liquid, gas, solution, mixture, etc.), and may be measured *in situ* under a variety of conditions.

5.2 Scientific Objectives

Mission and specifications: The mission of this beamline is twofold. One is to provide a versatile and highly productive facility for applications of hard X-ray Absorption Spectroscopy in a wide range of scientific disciplines including material science and catalysis, nanomaterials research, environmental science and geology, and life sciences and biology. This is necessary to address, from the outset of user operations, the significant demand for high-quality XAS at the NSLS. The second, and equally important, mission is to pursue cutting-edge capabilities and techniques in XAS, such as are appropriate to capitalize on the advanced qualities of the NSLS-II source. This beamline therefore is intended to outperform all currently available XAS facilities in the combined metrics of flux, versatility of spatial and energy resolution, and energy range.

Based on these objectives, beamline specifications are summarized as follows:

Source:	Damping Wiggler, length 7 m (or one of two canted 3.5-m segments)
Monochromator crystals:	LN2 cooled, flat crystals; 1st pair Si(111), 2nd pair Si(311) switchable by horizontal translation
Energy range:	~5 – 50 keV, with provisions for reaching 90 keV
Focusing:	macro: toroidal mirror, micro: K-B set
Spot size at sample:	operating values around 1mm macro- and 1 micron micro-focused, but up to 5x40 mm unfocused
Estimated photon flux at sample:	> 10^{13} – 10^{14} ph / s / 0.1% BW (10^{12} for microbeam)
Energy Resolution (standard):	dE/E 3 x 10^{-4} (Si(111))
High energy resolution mode:	1 x 10^{-5} or better, with energy-refining monochromator
Scan modes:	continuous-scan (slew) or step-and-count
Endstation 1:	microbeam XAS
Endstation 2:	bulk XAS, three sample positions: classic benchtop, controlled atmosphere, large apparatus

User need: Synchrotron XAS is a cornerstone of material and chemical analyses on the molecular scale. As such, its use has become routine and less "exciting," but not less important. A statistical analysis obtained from NSLS User Administration showed that, in FY06, 653 of 3295 on-site users at the NSLS (22.5%) were at the 8 beamlines devoted to hard XAS (and 2 beamlines performing microbeam XAS). To weigh possible overlap in these beamline-specific numbers, a manual count of unique individuals currently involved in XAS experiments yielded 505, a comparable percentage of the ~2250 current active NSLS users. These users

represent a wide range of scientific fields, are interested in nearly every element of the periodic table, and have samples ranging in size from nanometers to centimeters.

In order to benefit the greatest range of users, without compromising the more advanced capabilities and potential future directions, this beamline is equipped with versatile and adaptable endstation components founded on a solid infrastructure and beamline optics designed to deliver the highest quality (and quantity) of beam possible. These details are described more fully in the sections to follow. Efficiency is also an important aspect of productivity, so both the optical configuration and experimental setups are intended to minimize downtime. In addition, an available continuous-scan mode, rather than more typical step-and-count measurement, will significantly enhance throughput.

Scientific opportunities: Current challenges facing application of XAS in more difficult systems are signal strength, fluorescence detection, spatial and energy resolution, time, and energy range. The status of XAS as a more mature technique has left many with the impression that there is nothing new to develop. However, the unparalleled qualities of the NSLS-II open the door to considering new aspects of the technique (e.g. higher energy resolution) and new applications.

The very high flux available will make possible measurements at lower concentrations and using smaller sample mass. This is important in the study of catalysts, environmental contaminants, dispersed nanoparticles, and dilute biological systems. It will also enable “bulk” measurements of very small quantities of material, such as atmospheric particulates and marine colloids, extraterrestrial material, proteins and biological complexes, and sub-monolayer surface adsorbates.

Many problems in XAS analysis are the result of detector-limited fluorescence measurements. For example, an energy-dispersive solid state detector has intrinsic limits of energy resolution and total count rate. Samples with very low target signal and very high background will saturate the detector before enough useful signal is obtained. Interfering fluorescences can similarly overwhelm a weak signal. Increasing flux alone will exacerbate these problems. However, the considerably higher flux available here will enable the use of energy-selective detectors, such as wavelength-dispersive detectors or crystal analyzers. Historically these have not been widely used because they can only accept a very small fraction of the fluorescence emanating from the sample, and therefore required very high sample concentrations. The NSLS-II XAS beamline will provide sufficient flux to use energy-selective fluorescence detectors at trace concentrations. Recent advances in detector technology have made tremendous improvements and are expected to continue to do so. These further developments will be incorporated in the final design to add to the capabilities of this beamline.

Spatial resolution is the primary goal of the nanoprobe beamline. However, XAS experiments cover the whole range of spatial resolution from nm on up. Therefore this beamline is designed with an adaptability of spot size, from unfocused 5x40 mm down to as small as 200x200 microns in the “bulk” endstation, and down to ~1 micron in the microbeam endstation. Many XAS experiments involve processes occurring on a range of spatial scales, but have previously been relegated to separate bulk and micro facilities. Tunability of spot size at a single facility will allow users to better tailor measurements to their needs.

Energy resolution is most important for near-edge XAS structure (referred to as XANES or NEXAFS), where there may be sharp features that are highly sensitive to local electronic structure. These features, such as the pre-edge peak of hexavalent chromium (K edge 5.9 keV), the arsenate peak (As K edge at 12 keV), or pertechnetate (Tc K edge at 21 keV), are narrower than, or exhibit chemically-induced shifts of less than, the best resolution of a Si(311) monochromator. Yet methods of producing higher-resolution monochromatic beams are less efficient and naturally have lower bandpass, and thus have significantly decreased flux as compared with more typical energy resolution monochromators. The high flux and well-collimated beam available at NSLS-II afford the luxury of employing an energy-refining monochromator to accomplish these measurements even at trace concentrations.

Time-resolved experiments are naturally facilitated by high flux. While it will not be possible to move this high-heatload monochromator fast enough for true “quick” XAS (sub-second scan rate), the continuous-scan mode will collect scans on the order of one to three minutes, for time-resolved experiments on the appropriate scale.

Energy range has been a limiting factor in XAS applications. X-ray Absorption edges range from the soft x-ray regime to over 100 keV, while typical Synchrotron hard XAS facilities operate between 4.5 and 30 keV. The 5-90 keV range listed above encompasses the K edges of chromium to bismuth, and L edges of cesium through americium. There has recently been a dramatic increase in applications of "tender" (1-5 keV) XAS as facility development has made that range more accessible. Similar opportunities exist for higher energies (35-90 keV): using K edges as alternatives (or complements) to L edges, probing thick samples or buried regions, penetrating large-volume catalytic or high-pressure cells, avoiding interferences, and reducing radiation damage (e.g. in biological samples containing trace heavy elements such as mercury).

The rare-earth elements are of common interest to both materials research (optoelectronics) and geochemistry, at trace concentrations. Routine XAS work has been limited to the L edges (at 5.5 to 11.3 keV), but these often overlap and interfere (there being 48 L edges in that span). In contrast, the 16 K edges of these elements are nicely resolved over the span of 38 to 65 keV.

One other characteristic quality of NSLS-II that is of important consideration for these applications is its expected world-leading beam stability. While classic XAS experiments involved large uniform samples, most current and expected future samples are heterogeneous on varying spatial scales. These analyses require beam positional stability (e.g. better than 5 microns for a 1 mm spot) over a series of 1000-eV scans. Stable intensity (i.e. top-off injection) is critical to maintain stability of optics under high heat loads. And energy stability, the repeatability of energy calibration over a series of scans, is a prerequisite for useful high-energy-resolution measurements. The design of beamline components must then make a conscious effort to not degrade the inherent source stability.

Research programs: Specific research programs are being developed (or adapted) for this beamline by facility staff and leading user groups. Such programs will be the focus of a beamline workshop scheduled for January 16-17, 2008, following up on the NSLS-II User Workshop breakout session in July, 2007. Several of these will capitalize on the technical opportunities outlined above to address important DOE needs. The following two representative examples highlight research that will do so. In catalysis research, it is important to be able to measure the catalytic reaction *in situ* and/or in time-resolved fashion. However, in order to obtain sufficient signal quality in an appropriate time, this often requires preparation of samples with higher concentrations than are used in actual applications. These may not function the same as their dilute counterparts. The higher flux here will allow measurements at real-world application concentrations. This program will also require the capability of simultaneous XRD to more completely characterize sample systems in one run.

A similar example may be found in environmental stewardship and remediation. Of great concern to DOE is the subsurface contamination present at many of its sites, especially contamination by radionucludes and mercury. Typical concentrations in these environments, however, are below the current EXAFS sensitivity limits of most facilities. Moreover, wet sediment samples are heterogeneous, contain interfering elements, and produce high backgrounds due to fluorescence, scattering and diffraction. Yet detailed knowledge of chemical and physical speciation and processes is essential to determine appropriate courses of action for long-term stewardship and remediation of these DOE sites. The high flux, tunable spot size, energy resolution, and available energy-selective detection are all attributes which make the NSLS-II XAS beamline key in addressing this issue.

Future development and integrated facilities: The expected needs of the user community for XAS facilities at NSLS-II can not be met by a single beamline, however versatile and productive. Therefore, this beamline is part of a larger scope and long-term strategy that includes build-out of this beamline by canting the source, construction of additional non-Project beamlines, and migration of beamlines from NSLS.

The beamline design presented here explicitly includes accommodations for future canting. This is a highly desirable and cost-effective means of doubling capacity, as summarized here:

Sources:	Two canted damping wiggler segments (3.5 m each)
Separation between on-axis beams:	3.5 mrad

Inboard beamline:	microbeam, ~1 micron Acceptance up to 0.1 mrad x 0.1 mrad, on axis 1st experimental station additional optical components
Outboard beamline:	Bulk beam size Acceptance up to 1 mrad x 0.15 mrad max., on axis 2nd experimental station existing optical components

While the current project scope includes both endstations, it includes only one set of optical components for a single source. It is expected that canting of the source and addition of a second set of optics to make the two endstations independent will be undertaken at the earliest opportunity. There is very high demand, as well, for the lower energy range. This will likely be addressed by installing a complementary 1 to 5 keV bulk/micro XAS beamline at an adjacent dipole source as part of a core cluster. Additional non-Project XAS beamlines are expected to include “quick” XAS (sub-second scan time), perhaps on an undulator source, and specialized catalysis and biological XAS beamlines.

5.3 Insertion Device

XAS applications require a stable, broad energy range, non-coherent, high-flux source. The NSLS-II Damping Wiggler is an ideal source for XAS. These IDs are necessary for performance of the accelerator, and will be installed in high-beta straight sections. The standard geometry is a 7 m long device, but this can be effectively divided into two canted 3.5 m segments to provide additional capacity as described above. As shown in Figs. 5.3.1 and 5.3.2, the DW-100 source produces the highest total flux of all NSLS-II sources in the 5-35 keV energy range. Furthermore, it yields the highest brightness of the broad-spectrum sources over the same energy range. However, the spatial distribution of the generated radiation is energy-dependent. As shown in Fig. 5.3.3 and 5.3.4, the higher energy radiation is limited to the central portion of the fan. Since XAS applications require a uniform distribution as energy is scanned, this restricts use to the central on-axis portion of the fan. It also requires narrower acceptance when working at high energies, but that is naturally limited by the angular acceptance of the mirrors and monochromator. These factors make it undesirable to split a single source fan into the two experimental hutches; each application requires on-axis radiation by alternately sharing a single source (and eventually each having its own canted source).

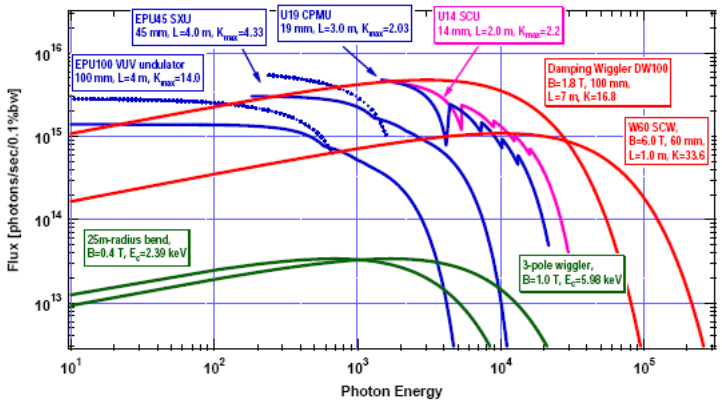

Figure 5.3.1. Flux of various NSLS-II sources.

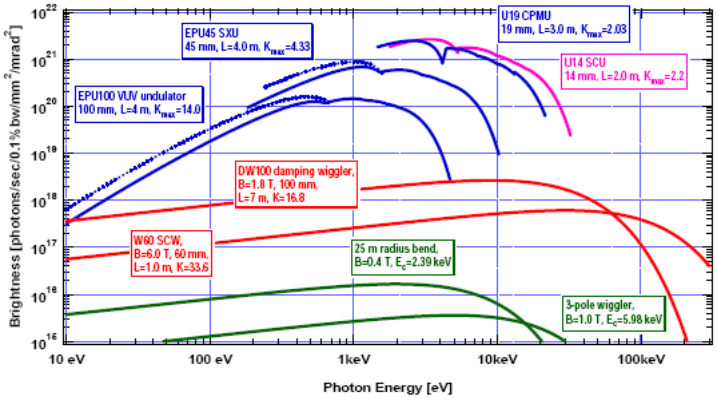

Figure 5.3.2. Brightness of various NSLS-II sources.

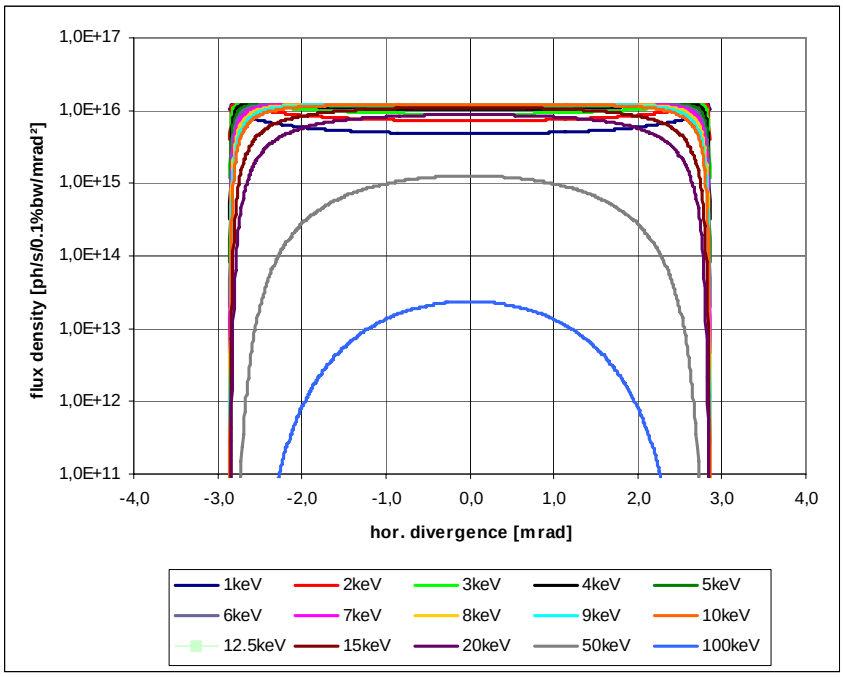

Figure 5.3.3. Horizontal distribution of flux density.

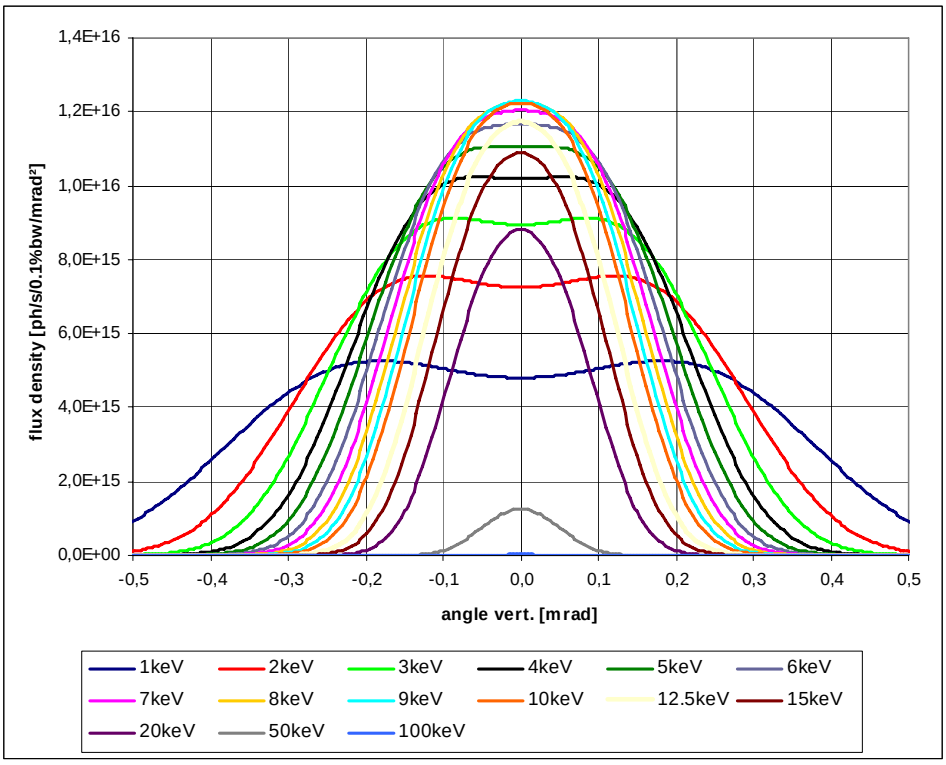

Figure 5.3.4. Vertical distribution of flux density.

The most challenging aspect of using the damping wiggler source is the unprecedented heat load. The full fan of a 7 m ID delivers approximately 65 kW of power, and even restricting acceptance to 1 mrad horizontal and 0.15 mrad vertical still delivers nearly 8 kW to the beamline optics. This maximum angular acceptance (in both dimensions) is defined by the optics (mirrors and monochromator), rather than by heatload limits. Heat load will be discussed further in the description of each component.

Current strategy for canting considers two possible paths. One is to begin operations with 7 m of wiggler in-line and introduce canting at a later stage. This has the advantage of extracting the highest possible flux during early operations when the ring current will not be at the full 500 mA, but has the disadvantage of requiring a repositioning and re-alignment of the ID, front end, and all optical components. The other path is to begin operations with two canted sections but only use one of them. This has the advantage of establishing the positions and alignments that will be used even when canting is fully implemented, and also provides the facility with an early test case for commissioning and refining canted wiggler sources. It has the disadvantage, however, of less flux initially. This second option is favored by beamline design personnel for the added reason that it reduces the heat load issue by an effective factor of two, and improves access to the lowest energy around 5 keV. In either case it is therefore unlikely that the beamline will experience full power from a 7 m wiggler at full ring current. However, component design is based on being able to handle this full heat load, so as to provide a margin of safety and to allow for potential future changes in beamline or project design.

Note that current ray-tracing, heatload and performance calculations are based on a damping wiggler with 100 mm period (DW-100). Current device design now calls for a period of 90 mm (DW-90); this will have a minor effect. Brightness and flux (within the used portion of the radiation fan) will increase slightly, as will heatload and power density. Ongoing thermal and performance modeling will take this into account as component design progresses.

5.4 Sector Layout

This sector begins with the insertion device as described above. Front End components are located within the ring tunnel, upstream of the shield (ratchet) wall. On the Experimental Floor, beamline layout consists of a first optic enclosure (FOE) containing all white-beam components and beamline optics through photon shutter, and two experimental endstations in series.

5.4.1 Front-End Layout

A standard front end layout is shown below, with specific items and their positions for this beamline in the table to follow. Note that accommodations are made now for future canting and upgrades.

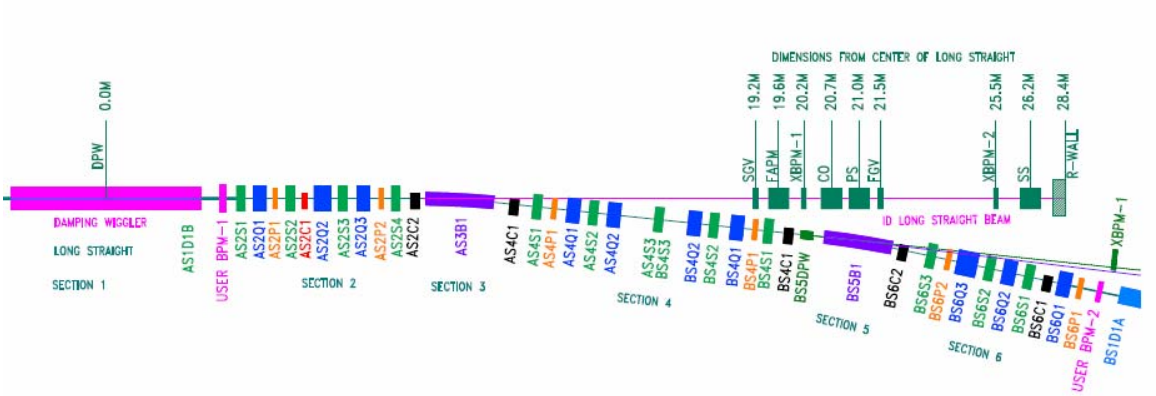

	Position (center) (m)	Acceptance (horiz x vert) (mrad)
Source	0.0	~5.5 x 0.8
Slow gate valve	19.2	
Fixed aperture mask	19.6	(-1.90/+2.35) x (+/- 0.25)
Beam position monitor	20.2	
Bremsstrahlung collimator	20.7	(-2.00/+2.45) x (+/- 0.30)
Photon shutter	21.0	
White beam slits (not shown)	22.5	(+/- 0.6) x (+/- 0.20) centered on outboard cant
room for white beam slits (second canted beam)	23.0	
room for possible future side-deflecting mirror	24.2	
Beam position monitor (removed from design)	25.5	
Safety shutter	26.2	
room for safety shutter (second canted beam)	26.7	
Bremsstrahlung collimator built into shield wall	28.2	(-2.00/+3.40) x (+/- 0.30)
Shield wall face	28.4	

A beamstop and gate valve will be initially installed at the shield wall for commissioning of the ID and front end components.

5.4.2 Beamline Layout

The following table provides a detailed layout of beamline components. Schematics and 3-D rendering of the XAS beamline follow the table. More detailed drawings can be found in Appendix 5B.

	Start	Center	Fixed Pos	Length
Shield Wall			28.4	
spool piece, gate valve, bellows	28.4			0.3
Pre-Filter, Attenuators (all water-cooled)	28.7			1.1
Bremsstrahlung collimator	29.8	30.1		0.6
gate valve, bellows	30.4			0.2
Mirror 1	30.6	31.5		1.8
gate valve, bellows	32.4			0.3
Monitoring	32.7			0.3
Steering mask and Be window	33.0			0.5
Double crystal monochromator (high heatload)	33.5	34.1		1.2
gate valve, bellows	34.7			0.2
space for monochromator, canted beam	34.9	35.5		1.2
Bremsstrahlung and white beam stop	36.1			0.5
Beam monitoring and Monochromatic slits	36.6			0.8
gate valve, bellows	37.4			0.2
High energy resolution monochromator	37.6	38.1		1.0
gate valve, bellows	38.6			0.2
Mirror 2	38.8	39.7		1.8
Gate valve, bellows	40.6			0.3
Space for Beam monitoring and Mono slits, canted beam	40.9			0.8
Space for optics, canted beam	41.7			1.6
Photon shutter	43.3	43.55		0.5
Space for Photon shutter, canted beam	43.8			1.0
FOE wall	44.8			0.4
flight tube, shielded	45.2			4.1
Experimental hutch wall	49.3			0.2
Monitoring	49.5			0.5
Exit window and slits	50.0			0.1
Sample location, Endstation 1 (incl. microfocusing optics)		51.5		2.7
Experimental hutch wall	52.8			0.2
Monitoring and slits	53.0			0.5
Sample location 1, Endstation 2		54.3		1.5
Sample location 2, Endstation 2		55.9		1.8
Sample location 3, Endstation 2		58.0		3.0
Hutch wall	59.8			0.2
End	60.0		60.0	

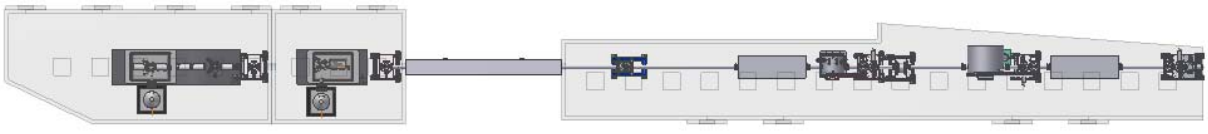

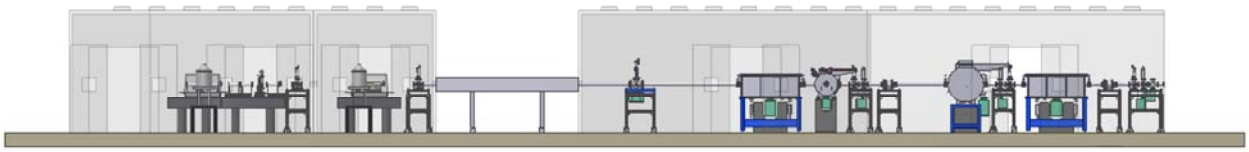

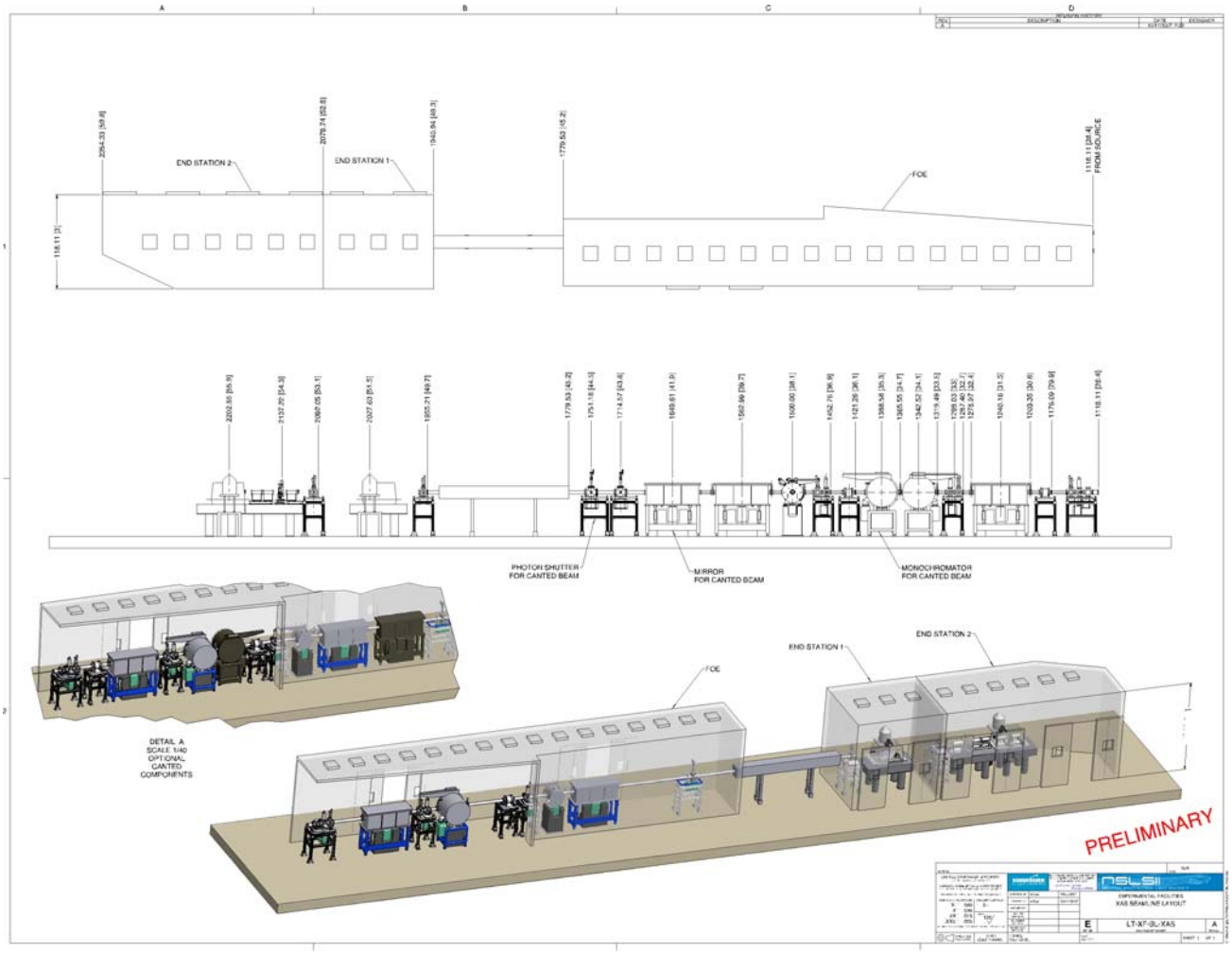

Initial ray-tracing and performance calculations are based on a beamline length of 64.3 m. Subsequent facility design refinements have decreased this to 60.0 m. Adjusting endstation positions required an increase in horizontal focusing to ~2.7:1, resulting in a marginally larger spot size and increase in vertical distortion of partly-focused beam. The ideal value is 2:1, and values of 3:1 or greater result in a decrease of horizontal acceptance of the focusing mirror to less than 1 mrad. Final design will consider this balance between layout and performance in consideration of planned optical elements. For example, it may be advantageous to place the future canted-beam monochromator downstream of this beamline's focusing mirror, thus resulting in more ideal 2.3:1 focusing with the added challenge of having adjacent white beam pass through the high energy resolution monochromator and mirror 2 chambers.

5.4.2.1 Survey and Alignment

All beamline components will be surveyed and aligned in place by the facility. In order to facilitate ease of alignment, all components will be fiducialized to external reference points on their table during assembly. These include horizontal and vertical position and angle, relative to the photon beam. All components are designed with a liberal tolerance allowance greater than 0.5 mm. Provisions will be made for laser pre-alignment of beamline optics.

5.4.2.2 Utility Layouts

This section describes the utility requirements assumed for the damping wiggler beamlines at NSLS-II. The numbers provided are estimations based on the current understanding of the beamline design; significant deviations may be possible depending on possible future evolution of the beamline layouts.

Cooling water. Cooling water is required for all high-heat-load components except the monochromator. Process water, the standard cooling water provided by the facility for this purpose, is clean de-ionized water at a temperature of approximately 20°C. Additional requirements are as follows: temperature stability within 0.1°C, pressure 60 to 100 psi, pressure stability within 5 psi, and free of pump vibrations.

The components and their requirements are listed in the following table.

Component	Number of Circuits	Consumption max.
Pre-Filter and Be-Window	2	4 l/min
Attenuator Units	4	8 l/min
Collimating Mirror and Mirror Protection Mask	1	12 l/min
Steering Mask and White Beam Monitor	2	6 l/min
Thermal Stabilization and Compton shielding of DCM	1	4 l/min
White Beam Stop	1	4 l/min
total:	11	38 l/min

If additional control is necessary, the DCMs temperature stabilization system will be separately supplied with temperature-controlled water by means of a dedicated chiller unit, thus allowing to set the flow to be set and the temperature precisely stabilized, independently from the main water supply in the hutch. This chiller will make it possible to set the water temperature in the range of 25 to 35°C and to keep it constant to ±0.1°C. It can either be equipped with its own electrical cooling system or be connected to the hutch cooling water.

Liquid nitrogen. The cryo cooler unit for the DCM requires connection to a liquid nitrogen (LN2) supply. It is recommended to have a LN2 supply tap within 2 to 3 m of the final cryo cooler position. LN2 is also needed within both experimental hutches for sample cooling and for auto-filling of detector dewars.

Compressed air. The following components must be connected to a dry, filtered compressed air supply having a pressure between 70 and 100 psi:

- the monochromatic beam shutter
- all gate valves
- attenuator units, if pneumatically driven

Electrical power. Three types of power are required: standard power for heating, pumps, etc.; low-noise power for measuring equipment; and UPS power for critical systems. Along the beamline a grounding bar is needed, to ground the beamline components. The grounding bar must be connected to the central power

distribution ground. A separate low-noise ground is also needed. Standard beamline service of 60 kW is expected to suffice. There are several distinct areas to which electrical power distribution is needed.

1. Beamline Control System Cabinets

A central 3-phase power distribution should be placed near the cabinets. In total, approx. 12 kW are needed.

2. Cryo Cooler Unit

This unit needs a single-phase power distribution of approximately 2.5 kW.

3. *FOE*

The required power in the FOE can be up to 30 kW to accommodate the extreme case where the full beamline might be pumped and baked at the same time.

4. Experimental Hutch

In the hutches, both low-noise and standard power outlets should be distributed along the length of the hutch. Total needs should not exceed 20 kW.

5. *Experimental Control Station*

The control station needs adequate power (of all three types) for computer controls, interfaces, and communications, estimated as 5 kW max.

Gases. Dry nitrogen is needed in the FOE, delivered to each vacuum pump-out port as described in 5.4.2.4. In addition, a distribution and control system is needed for local-source gases (helium, Argon, etc.) within the experimental hutches: for enclosures, ion chambers, detectors, sample cells and experimental apparatus.

5.4.2.3 Life Safety Code Compliance

Floor layout and access walkways will be arranged so as to comply with applicable emergency egress requirements. Figures 5.4.2.3a and b show initial access/egress walkways in red. Specific details will be developed in conjunction with layouts of neighboring beamlines, and in conjunction with ES&H personnel and NSLS-II policy. Exit routes will be posted and included in user training.

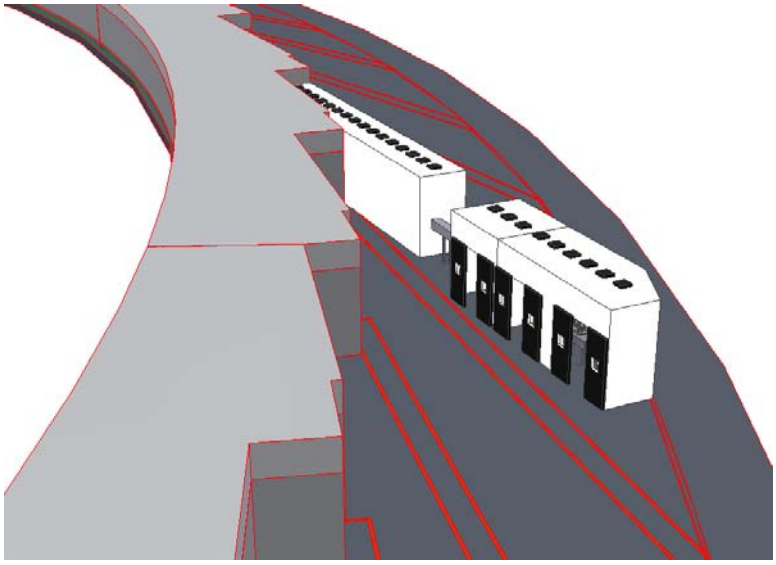

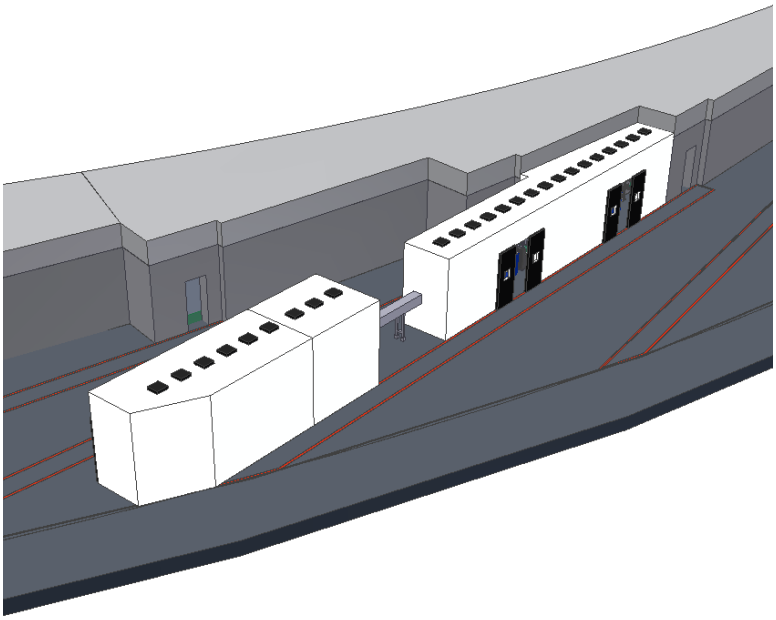

5.4.2.4 Beamline Vacuum System

There will be several vacuum sections, isolated from each other through gate valves. Each vacuum section will be equipped with an ion pump, full-range vacuum gauge, and pump-out port. Each pump-out port will consist of a rectangular, all-metal valve (CF40) to rough down the vacuum using a pump cart, and a valved connection to dry nitrogen supply to vent the section. The monochromator will also be equipped with a CF63 gate valve where an interlock-protected magnetic bearing (oil-free) turbo molecular pump will be permanently mounted.

The white beam section of the beamline will be bakeable in order to achieve a vacuum pressure below 10^{-9} torr. The monochromatic section is designed to achieve a base pressure in the 10^{-8} torr range or better.

Besides the large flanges of the monochromator doors (that are Viton sealed) and the flanges of the mirror vessels (metal-sealed for M1 and Viton-sealed for M2), all flanges will be bakeable metal-sealed Conflat standard. There will be no mechanical water-vacuum seals anywhere in this design.

The following diagram shows a general schematic overview of the vacuum and its protection system (note that the location of the water-cooled Be window has been changed from this layout):

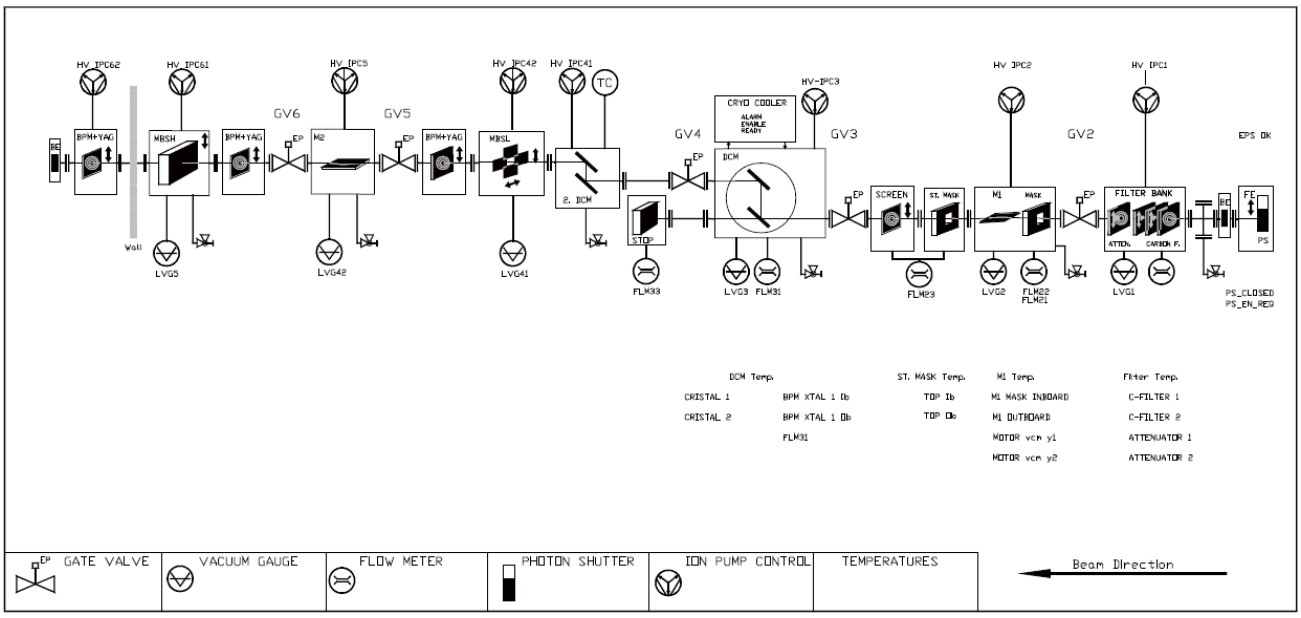

Figure 5.4.2.4

Vacuum control and Equipment Protection System sensors (pressure, temperature, water flow). All components (including valves, shutters and pumps) also have indicators of status or position.

5.4.2.5 Data Acquisition System and Motion Control

See Appendix G for general specifications of an example control system. This document was developed for several Accel components under consideration for this beamline.

5.4.3 Beamline Components

As tabulated in 5.4.2, the following items comprise the major beamline components necessary to deliver controlled monochromatic beam to the experimental hutches.

5.4.3.1 White Beam Slits

While these slits are located in the Front End, they will be under beamline control. Please refer to the appropriate chapter for detailed front-end specifications. In general, these slits will be water-cooled, accept up to 1.0 mrad horizontal by 0.15 mrad vertical, and have resolution and repeatability of better than 10 microns. The 4 independent blades will be tungsten-edged for the high energy range being used, and each capable of closing 2 mm past the centerline. Heat load modeling will need to be conducted in order to ensure that the blades can tolerate the required absorbed power. Accommodations will be made to include future blades to also define the second canted beam.

5.4.3.2 Pre Filter, Be window, Attenuators

Hard x-ray beamlines typically have a beryllium (Be) window to separate the beamline vacuum from the machine vacuum. A Be window also absorbs a significant fraction of the unused low-energy radiation, therefore reducing the overall power delivered to downstream components. However, in a wiggler beamline such as this, calculations of the absorbed power indicate that a Be window in the direct white beam would fail. Due to their high thermal conductivity and mechanical stability, carbon foils are typically used as a protective filter material in front of the Be window.

This beamline design incorporates three components, a set of graphite foil pre-filters to protect the Be window, a Be-window for vacuum isolation, and an additional attenuator package to further manage the power load on the optical components. The C pre-filter and Be window combine to absorb the lowest-energy radiation, and effectively establish the low-energy limit of the beamline's range.

The approach described here is to design a filter assembly that can be safely used whenever required in order to reduce the power levels on the optical components. Reduced power will improve the performance and stability of the white beam optical components such as collimating mirror and monochromator. Considering the high heat load which is produced by the wiggler the carbon filter unit is an essential component to maintain sustainable power levels down the beamline.

When considering the heat load absorbed by the most upstream filter, a standard water-cooled graphite filter is not able to cope with the high heat load. From experience at other facilities using similar powerful sources, there are two possible solutions:

A) Thin C foils which are only radiation cooled. In that case the foils become extremely hot (up to 1500°C or higher). This system is in place at NSLS X25, formerly a wiggler but now an undulator beamline. A stack of radiative cooled foils successfully withstand the power load (3.4 W/mm^2). They use seven foils from 5 µm up to 51 µm in thickness. After a few years operation, the foils do not show any visible damage. In addition it has been verified that the temperature of the foils is somewhat lower than calculated. This system has proven to work reliably up to temperatures over 1000°C.

B) High thermal conductivity Highly Oriented Pyrolytic Graphite (HOPG) foils, mounted in a water-cooled filter frame. This system is employed at ALS Beamline 5.0. HOPG is clamped between two water cooled copper frames and absorbs 10 W/mm^2 (250 µm). The contact pressure is finely adjusted by springs. Temperatures up to 1000 K are possible. After more than one year operation, there is no visible damage on the HOPG foil.

We have carefully evaluated the behaviour of specifically the first filter unit for the power load of the damping wiggler source; please refer to Appendix D. Both options, radiation cooled filter elements as well as contact cooled filter, are possible solutions for this beamline. A final careful FEA has to be done using the filter and source parameters for the configurations needed.

Be window and pre-filter

This component is very similar to the set-up used at different beamlines at BNL. It consists of a water cooled frame which holds the different filters. The radiation-cooled foil is hold in a Tantalum frame, since it must withstand the extremely high contact temperature, and will turn hot itself. The power then is dissipated into the surrounding environment and is absorbed by a water cooled copper surface positioned around the Tantalum frame. The Tantalum frames, together with the carbon foils, are placed in a water-cooled cartridge made of OFHC copper. The cartridge is held and mounted on a DN40CF flange. The assembly is mounted to a DN100CF base flange and fits in a DN100CF standard cross. PT100 temperature sensors (e.g. two sensors) will be installed in the copper cartridge and monitored by the control system. If any PT100 sensor exceeds a temperature limit the beam shutter will be closed. The PT100 sensors will be connected to an electrical feedthrough, the water pipe (SF-copper, Ø8x1) will be brazed on the cartridge and on a DN40CF flange avoiding water-to-vacuum joints.

A possible filter combination could be as shown:

Table 5.4.3.2 Possible pre-filter combination.

Filter no.	Filter thickness [μm]	Absorbed power [W]	Absorbed power density [W/mm²]
1	5	222	1.6
2	5	96	0.7
3	5	72	0.5
4	25	240	1.8
5	25	162	1.2
6	50	237	1.8
7	50	180	1.4
8	100	277	2.1
9	135	283	2.2
10	300	457	3.6
11	300	337	2.6

Attenuator Unit: This unit consists of a number of different filter setups, that allow tailoring the power load on the optical components to the right level of operation for each particular operational mode of the beamline. The design foreseen for your beamline is based on the one we have realized recently for other high heat load beamlines and is described in the following paragraphs. Currently, we assume that for the Damping wiggler beamlines it might be reasonable to work with two pneumatically driven attenuator units and two or even three motorized filter banks with different filters mounted.

The latest ACCEL design is based on a series of three water-cooled filters mounted on three pneumatic drives. These three carbon foils are of Annealed Pyrolytic Graphite (APG). These APG foils have a similar thermal behaviour than HOPG and are available down to thicknesses of 50μm. The foils are clamped to copper frames where the thermal contact is improved by (i) polishing the surface of the copper within the contact area and (ii) using springs that apply a well defined and well distributed contact pressure. The thermal conductivity of APG is similar to diamond. Due to its excellent mechanical properties and together with the advanced cooling each foil is designed to remove about 500 W. The power density on the first foil presents the most challenge and therefore limits the maximum thickness of the foil, while heat conduction as well as physical integrity under thermal stress define the minimum thickness of the first foil. The APG foil used in the existing system is 125 μm thick. This thickness presents a good balance between the transmission at lower energies and the still very good stability of the foil. The second foil can only be inserted in the beam when the first foil is already in.

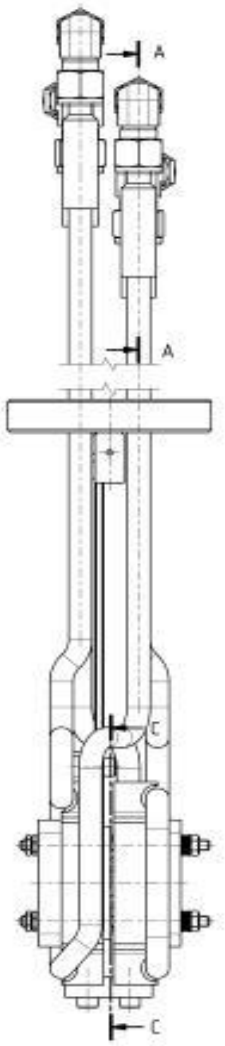

Figure 5.4.3.2a Directly cooled high power filter set-up, which can be pneumatically driven.

The fourth filter drive is motorized and consist of a cooled frame with five positions that can be used for graphite foils (Pyrolytic graphite) of different thickness to be used to further attenuate the beam. This filter design avoids water-to-vacuum joints. Water pipes are brazed to the each cooled copper frame and to the vacuum feedthrough, where edge-welded bellows permit the translation of the frames with the filters.

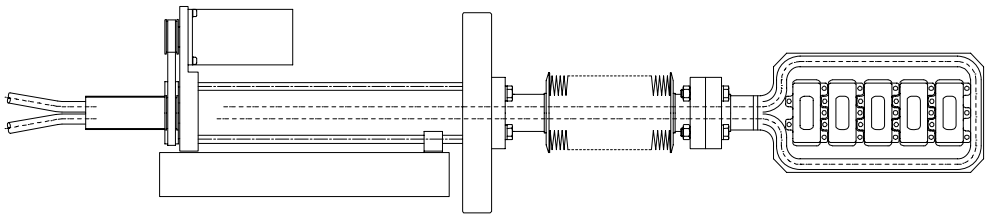

Figure 5.4.3.2b Example motorized water-cooled attenuator assembly

Please note that the filter bank must be equipped with a special protection, as the 2nd filter foil can only be introduced into the beam, when the 1st foil is already in the beam. Similarly the standard motorized filters units can only be put into the beam when both pneumatic filters are in the beam.

As an option the two first PG foils could be replaced by a 250 µm HOPG foil based on the above mentioned ALS design. Using such a design, the maximum temperature is reduced significantly and therefore we do not expect any influence by infrared radiation on the downstream optical components. On the other hand the use of HOPG will significantly reduce the flux at the sample at low energy.

The vessel of the filter assembly is equipped with view ports which permit visual inspection.

General*:*

UHV rated

Two pneumatic driven actuators:

- APG foils clamped on a double sided cooled copper frame
- 1000 W cooling capacity for each actuator
- position monitored by limit switches

Two motorized actuators:

- PG foils and metal foils clamped on a cooled copper frame
- 500 W cooling capacity
- position monitored by limit switches

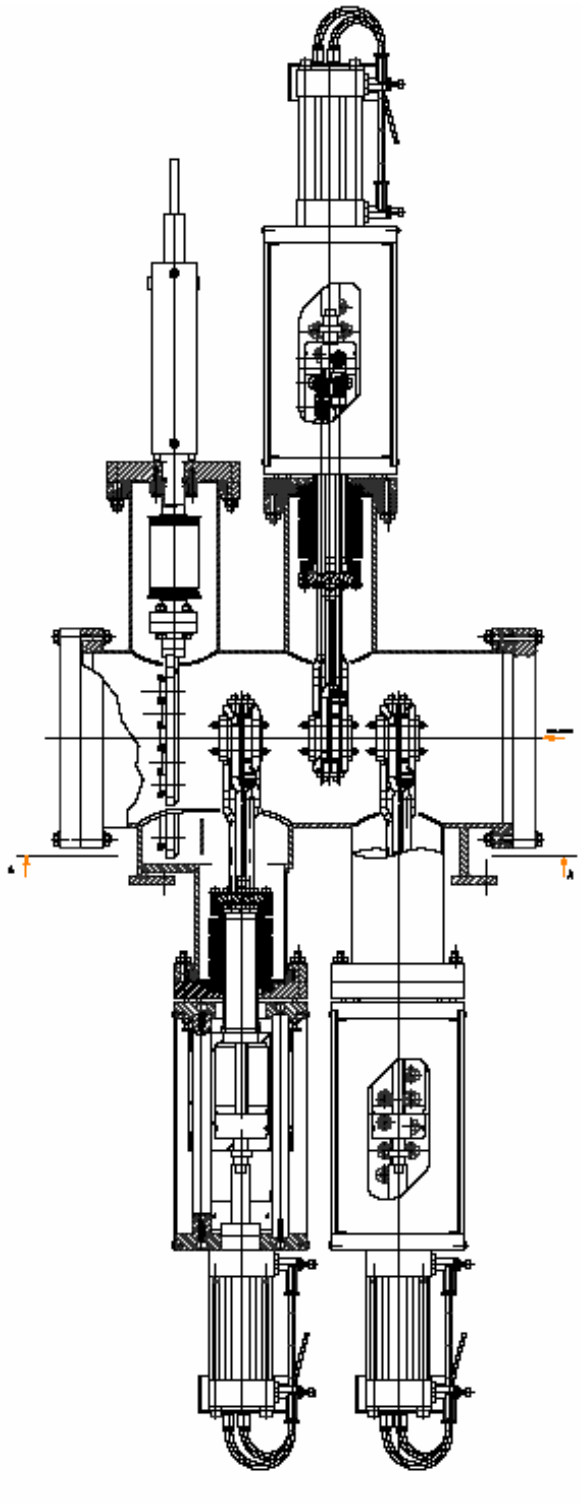

Figure 5.4.3.2c Example high heat load filter system as installed at the XAS beamline at ASP.

5.4.3.3 Bremsstrahlung Collimator

The collimator will absorb high-energy Bremsstrahlung radiation originating inside the ring and defines the extent of the remaining Bremsstrahlung extremal rays on which the dimensions of the downstream white-beam stop must be defined. The outer dimensions and dimensions of the aperture will be determined through

ray tracing. Appendix B shows the initial Bremsstrahlung ray-tracing, using two different types of collimators and stops. A lead Bremsstrahlung collimator basically consists of a rectangular vacuum pipe mounted inside a block of lead. Because of the vacuum pipe, some tolerances and the necessary clearance, the openings in such lead collimators are rather large. An in-vacuum tungsten collimator allows a much smaller beam opening and therefore much better collimation. This is the recommended option. In addition, the tungsten collimator is more compact; the absorption length for lead is determined to be 300 mm along the beam direction; for tungsten, 200 mm. The collimator assembly will sit on an adjustable support that will permit translation and tilting for precise alignment, then will subsequently be locked in place as part of the safety system.

5.4.3.4 White beam Mirror

A directly cooled Si mirror offers several advantages. This technology is in use at beamlines at NSLS and the ALS, and mirrors with the required quality characteristics can be procured. As long as the bond of such a mirror is not directly exposed to the x-ray beam, the stability of the frit-bonding seems not to be a problem, even after several years of use. This being the case, and to protect the end of the mirror from inadvertent exposure to direct beam, a water-cooled protection mask will be employed.

An additional feature required for such a high-intensity beam will be a shielding shroud over the sides and above the face of the mirror, to keep scattered radiation from heating the enclosure and positioning/bending mechanism components.

5.4.3.5 Steering Mask

A protective water-cooled steering mask just upstream of the monoichromator will serve to protect the DCM interior and any uncooled downstream surface from being hit by a miss-steered direct beam. Furthermore, a steering mask would serve as a conductance-limiting aperture for the vacuum performance between these two sections. To accommodate all operation modes of the beamline, this mask must sit on a vertical stage and will be equipped with edge-welded bellows to allow for the necessary translations.

The mask will have water channels, I.D. 8 mm, with copper tubes brazed to it (no water-to- vacuum joints are used in this design). The material will be Glidcop and the impinging area will have a suitable slope so it can withstand the high thermal stress that will be produced under worst-case conditions (i.e. full beam).

Specifications

Material	Glidcop
Total power capacity	≤ 6 kW
Maximum power density on surface	12 W/mm^2
Angle of cooled surface	Approx. 10°
Length of water cooled body	Approx 150 mm
Water flow maximum	6 l/min.
max. pressure	120 psi
Aperture size	1 mrad (h) x 0.15 mrad (v)

5.4.3.6 High-Heatload Monochromator

This component is the critical item of the wiggler-based XAS beamline. It must be able to handle the large heat load (perhaps as high as 2.5 kW) while still maintaining the requisite stability and optical quality.

Crystal design. As discussed in Appendix D, there are two ways to cool the crystals, either by direct or by indirect cooling. The monochromator designed by Accel is typically equipped with indirectly cooled crystals. This cooling method is certainly more robust and more reliable in terms of leak tightness, but is less

efficient for high heat loads. In such a case, the crystal set-up must be redesigned to accommodate direct-cooled crystals.

In-house monochromator development and design is based on the "hockey-puck" crystal geometry, and this will be pursued within the NSLS-II Project R&D program. This is the preferred option, as it is proven technology (on a smaller scale) and appears to be able to effect more efficient cooling.

Cryocooler. For cooling the crystals to LN_2-temperatures, a closed loop LN_2 cryo-system will be used. Originally developed for the ESRF, the Accel Cryotherm model is most highly regarded. Its control system is based on a PLC with an interface to a standard PC to manage the temperature controls system via EPICS.

5.4.3.7 High-Energy-Resolution Monitor

This device will be based on a high-precision version of a standard DCM. Choice of crystals, since cooling is not an issue, will be made on the basis of optimal energy range, bandpass, available crystal quality, and testing work to be performed at the NSLS.

5.4.3.8 Monochromatic Focusing Mirror

For the VFM, a configuration of two sagittal cylinders with different sagittal radii in the substrate is technically feasible; the polishing of such a mirror will be a very challenging process, but a vendor has accomplished several similar mirrors already.

The following table summarizes possible specifications for the two mirror substrates and benders, based on similar existing beamlines.

	M1	M2
Mirror Substrate	Monocrystalline Silicon	Fused Silica or ULE or Zerodur
Direction of Reflection	Downwards	Upwards
Shape	FLAT cylindrically bent to tangential cylinder	Double sagittal cylinder cylindrically bent to torus + central flat
Tangential Operational Bending Radius Range	5.0 km - flat (> 40 km)	3.5 km - flat (> 40 km)
Sagittal Bending Radius	flat (> 1 km)	(i) $R_{sag}1$= tbd mm (Pt coated) (ii) $R_{sag}2$= tbd mm (uncoated)
Substrate Length	approx. 1400 mm	
Substrate Width	~ 120 mm	~ 135 mm
Substrate Thickness	60 to 70 mm	60 to 70 mm
Optical Active Surface: Length	1200 mm	
Width	2 x 35 mm (Si & Pt)	2 x 35 mm (cylinders) polished width ~ 45 mm
Slope Error: Sagittal	< 15 µrad rms for M1 < 25 µrad rms for M2 (best effort < 15 µrad rms)	
Tangential	< 2.5 µrad rms on 1200 mm (Best effort: < 2 µrad rms)	
Micro Roughness	< 3 Å rms; best effort < 2 Å rms	
Coating	Pt> 600 Å; Cr underlayer	Pt> 600 Å; Cr underlayer Bare central flat

Cooling	YES, directly cooled	No

5.4.3.9 Beam Monitoring Elements

a) Water-cooled white beam CVD fluorescence screen: The device consists of a retractable water-cooled CVD diamond foil, acting as x-ray screen, mounted to a pneumatic drive; the fluorescent effect is based on the residual doping with nitrogen atoms. The diamond screen is transparent; i.e., beam detecting further downstream is possible. The assembly is mounted to a DN100 CF cross with one view port permitting a side view onto the screen. The pneumatic drive is equipped with limit switches. The vacuum feedthrough is made of edge-welded bellows. The water lines are brazed to the screen support to avoid vacuum-to-water joints. The foil is clamped to the cooled support.

The projection of the beam onto the 45° inclined foil will be monitored with a CCD camera. This system is capable of staying in the beam. However, because of the resulting absorption at photon energies below 10 keV, the screen should be withdrawn when not in use. Moreover, to increase the lifetime of the foil and prevent overexposure of the camera, this screen should only be used at reduced power levels—i.e., in combination with some of the carbon filters.

This screen has been installed at the high power wiggler beamline at the Australian Synchrotron Project.

General	
Screen material	CVD Diamond foil less than 0.125 mm thick
Screen slope	45°
Field of view	40 mm (h) x 20 mm (v)

These fluorescence screen monitors typically are mounted to a pneumatic drive via a vacuum feedthrough on a conflat flange. The water-cooled monitor is inserted in the beam by a stepper motor. Modeling of heat load and power absorption will be required. The flange is also equipped with a view port for the camera that provides side view of the screen. Examples can be seen below, for a water-cooled device and an uncooled device.

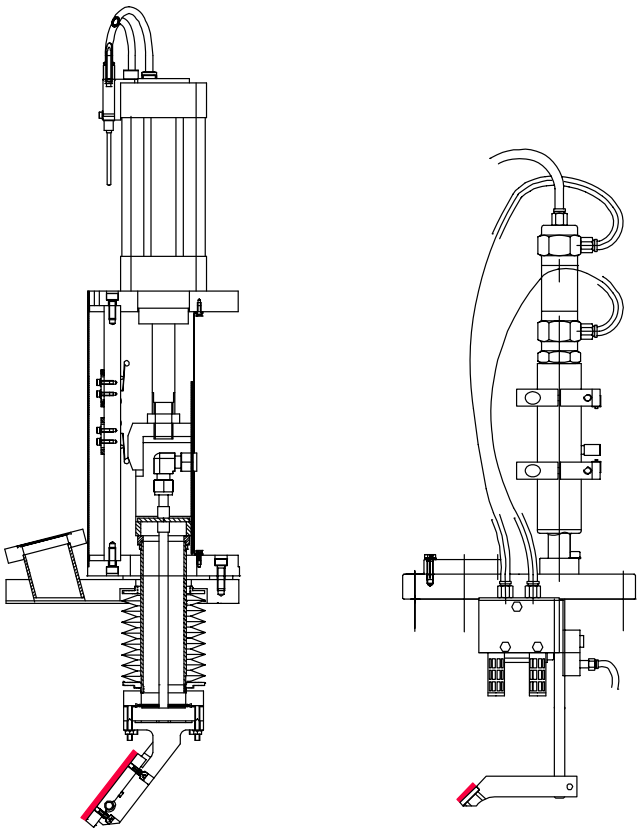

General:	Screen 1	Screen 2
Beam Size (hor. x vert.)	20mm x 15mm	≤ 40mm x ≤ 20mm
Screen Size (fluorescent region; hor. x vert.)	20mm x 20mm	50mm x 60mm
Water Cooling	yes	no

b) Quadrant diode beam position monitor (4-diode BPM): A standard monitoring device for monochromatic beams of large size is a quadrant type detector that monitors the fluorescence yield of a target foil. Beam position information is derived from the intensity ratio of one pair of diodes. The device is rated for UHV and consists of a diode holder (holding four diodes) and a fluorescence foil holder.

The four detecting silicon diodes are mounted to a vertical stage that permits a vertical positioning of the diodes which is needed to operate at different beam heights.

There are mounts for two foils, which can be of different kind, or be the same. Typically, thin chromium and copper foils are used, but silver foils might be used as well. Chromium and copper have been working up to photon energies of around 20 keV. There is an option to mount a YAG crystal underneath this foil holder. Than this YAG can be used to visualize the beam by means of a camera looking from the side onto a prism which is positioned behind the YAG.

The assembly is designed such that it mounts to a CF100 flange and fits a standard size DN100 CF cross.

The detection electronics for the diodes will consist of an integrated four-channel picoammeter.

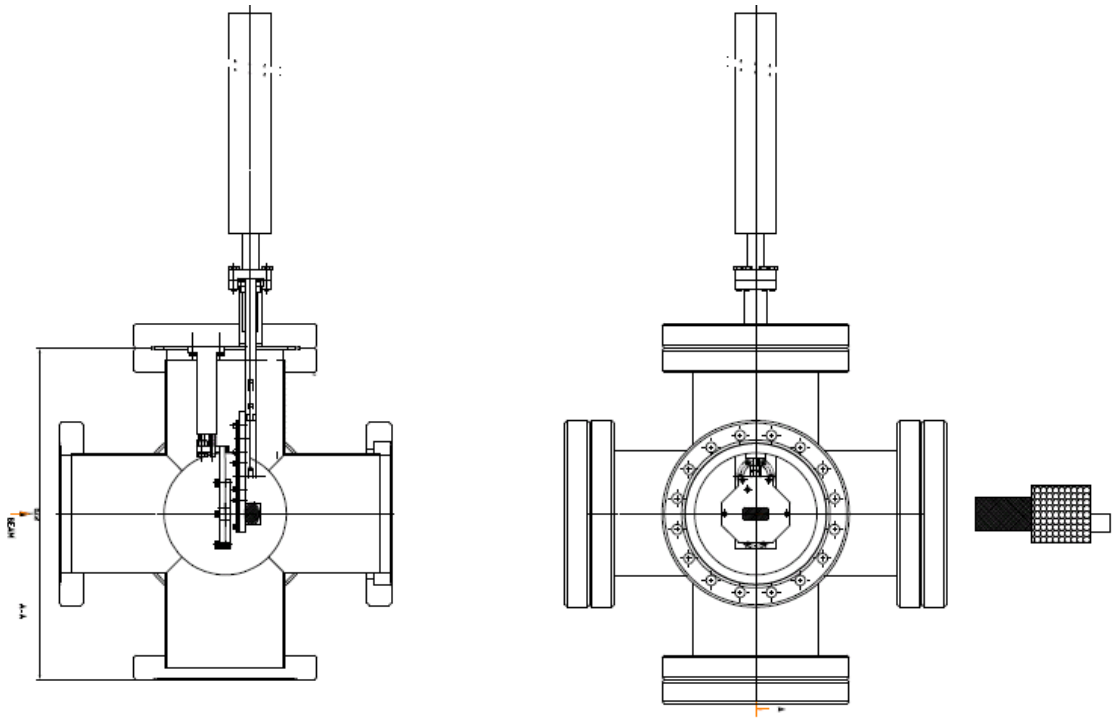

UHV rated BPM with diodes and fluorescent foil and screen

General:

Energy range	5 KeV to 25 KeV
Foils	0.5 micron Cr, Cu, or Ag
Photo current	~2 μA @ 10^{13} ph/s

Translation stages:

Stepper motor drives	linear actuator with 2-phase stepper motor and limits
Maximum stroke diodes	50 mm
Maximum stroke foils	100 mm

c) Endstation X-ray beam monitor and camera: This type of x-ray beam monitor is a commercially available visualization system for x-rays, or can be contrived with minimal effort. Such a system provides a field of view large enough to study the beam size, beam profile and the beam position stability of a focused beam in the endstation (at atmosphere), but must be removed from the beam path during data collection.

Feedback systems: electronic beam position monitors (type b above) will be strategically incorporated into at least two feedback systems.

The first of these will monitor beam position at the entrance slits for the high energy resolution monochromator. When this monochromator is in use, the BPM will be incorporated into a synchronization control loop that maintains tune between the two monochromators. While it is conservatively expected that the high-resolution mode of operation will preclude use of continuous-scan data collection (so as to allow for stabilization at each data point), this would be a desirable feature and is worth pursuing as part of final design.

The second feedback system will employ BPMs at the upstream end of each experimental hutch. These will be utilized (being highly sensitive due to the long lever arm) to control fine monochromator (and possibly mirror) adjustments to maintain beam position at the sample. This type of feedback is in place at a number of existing beamlines. While the NSLS-II source will have exemplary stability, feedback systems are likely to still be required to eliminate instabilities created by the beamline optics and their mechanisms.

5.4.3.10 Monochromatic slits and photon shutter

A standard design for in-vacuum monochromatic slits and for photon shutter will be developed for the NSLS-II experimental facilities. These designs will be used for all applicable beamlines.

5.4.4 Instruments

Instrumentation for the XAS beamline will consist of two endstations providing advanced capabilities to address cutting-edge challenges in local-scale physical, chemical, and electronic structures. The guiding philosophy for design of these endstations is to provide the widest range of high-quality XAS tools to fit current scientific needs. It is also intended to ensure a solid infrastructure that remains versatile and adaptable to both expected and unforeseen experimental needs of 2013 and forward.

A central aspect of this is detector selection. Preliminary design calls for a suite of detectors to answer the basic needs of various methods of measurement. It is expected that more detailed specifications for these detectors will be defined after further interactions with the community and through the Beamline Advisory Team process. Further technical developments are likely in the next few years; incorporation of these into final beamline design will enhance capabilities. Also, beamline design will explicitly include provisions to accommodate the subsequent addition of detectors beyond current project scope.

The following sections describe Endstation 2, the main experimental hutch for bulk XAS, and Endstation 1, the smaller upstream hutch for microbeam XAS. At initial operations, these endstations will operate from a single control station and share a single source and set of beamline optics. For efficient experimental setup, users will be able to access Endstation 2 while Endstation 1 is in use, but not vice versa. Eventually (but beyond Project scope), each endstation will operate independently, thus doubling capacity. In that arrangement, Endstation 2 will be served by the outboard of the two canted sources; Endstation 1 the inboard source.

This combination of endstations will provide a range of spot size from 5 x 40 mm to 1 x 1 micron, to cover the range of scale needed for the planned research programs. It will also complement efforts at the nanoprobe Project beamline which, combined with the planned soft x-ray spectromicroscopy facility, will pursue finer spatial resolutions.

Instrument control and data collection will include all motor drive channels, ion chamber and detector outputs, sample image capture, temperature, sample-cell and illumination control. Data collection software will include standard XAS scanning parameters, sample mapping functions (micro and macro beam), programmed sample locations and experimental control, and will also incorporate XRD data and image capture from sample cameras.

5.4.4.1 Endstation 2

This endstation will serve bulk applications at three sample positions. Each will have its own set of components to minimize downtime and effort for setting up or reconfiguring each experiment.

Sample position 1: The scientific mission of this classic benchtop style setup will be for *in-situ* analyses, grazing-incidence surface measurements, high concentration and fast-scanning applications, and use of high energy resolution fluorescence detection or simultaneous XRD.

Flow-through cells are important for *in-situ* measurement of catalysts at controlled temperature and gas flow, and for chemical (e.g. ion exchange), environmental (e.g. contaminant adsorption), and geochemical (mineral-water reactions) solution flow experiments. Flow-through cells are also important for some biological materials where a static solution may suffer radiation damage. Other *in-situ* sample cells include those for electrochemical and fuel-cell research, laser or small magnet units, or high pressure measurements.

Surface XAS is an important measurement technique that is ideally suited for the highly-collimated high-brightness beam provided by this source. Measurements are typically made in total reflection, using either the reflected beam (analogous to transmission through a thin sample) or fluorescence. The high flux at this

beamline will greatly improve the ability to measure very dilute (sub-monolayer) surface species, and the higher energy range will create additional opportunities to do so at buried interfaces or under solutions.

An important mode of data collection will be continuous-scan (slew) mode, where the monochromator is kept in continuous motion while measurements are made. Scans in this mode will take only one to three minutes each, resulting in very high throughput for more routine measurements. Time-resolved studies on this scale are thus possible.

Fluorescence detector-limited applications involve samples with low target signal but high background, or those with strong interference by overlapping fluorescence peaks (in a solid-state detector spectrum). These benefit from use of a high energy resolution or energy-selective detector, but such detectors typically accept only a very small solid angle of fluorescence from the sample. The very high flux and excellent macro focus of this beamline will make energy-selective detectors much more attractive. The wavelength-dispersive spectrometer included in this preliminary design will be useful on samples where conventional detection is unsuccessful.

Simultaneous XRD is of great interest to many of the catalysis and in-situ research programs, as well as for bulk characterization of samples in general.

Components at sample position 1 include the following (all within project scope):

- Optical table, fixed height
- Separate table for detector(s) at 90° to beam
- Beam-defining x-y slits
- Ionization chambers for I-zero, transmitted and reference measurements
- Optical rail
- Sample stage with x, y, z, rotation, and horizontal and vertical tilts
- LN2-cooled sample mount
- Stage adapter for flow-through cells
- sample temperature control
- Camera on sample position (45° to beam), with illuminator
- Compressed-helium cryostat
- Fluorescence detectors: Lytle, PIPS, and solid-state Si (e.g. the Vortex type)
- High energy resolution fluorescence detector, such as a wavelength-dispersive spectrometer
- Area detector for simultaneous XRD, to be placed downstream of sample stage
- Light-weight helium-filled flight tube to deliver beam to sample position 2 when needed

It is expected that each experiment will provide its own sample cells, but the support infrastructure (e.g. gas supply connections, flow control, temperature control and monitoring, etc.) is part of the beamline. The sample stage must have sufficient capacity to support the cryostat or other sample cell. Tilt geometries are needed for both horizontal and vertical polarization-dependent grazing-incidence measurements. Detectors will be positioned with appropriate stages. The area detector will be moved back, out of the beam path, when not in use, and may also be used in Endstation 1.

Sample position 2: The scientific mission of this station will be for low-concentration samples, hazardous radioactive or nanomaterials, and samples requiring clean environment or a controlled atmosphere. The "multi-use enclosure" employed here is designed to serve the needs of such samples. Based on designs in the planning stage at two NSLS beamlines, this enclosure would serve as a glove box, open up to operate as a fume hood, or simply be open to atmosphere. Sealed glove-box mode would be necessary for air-sensitive samples or those requiring a specific atmosphere. Examples include a variety of catalysts, redox-sensitive environmental samples, anaerobic biological samples, and atmospheric science applications. Radioactive samples, nanomaterials, and other hazardous materials require containment and often also need ventilation as in a fume hood. The enclosure would operate in that mode with the glove-bearing face opened for access. Policies and requirements as to HEPA filtration and monitoring for these materials will be more clearly defined in conjunction with ES&H personnel as the Project develops. The bottom of the enclosure will be lined with trays made of Teflon or similar materials for ease of cleaning and decontamination. Samples requiring no special care would simply be measured in air.

An important consideration for low-concentration measurements will be the requirement for a clean sample environment. Experience at NSLS X15B with ultra-low (sub-ppm) concentrations demonstrate the need to keep the sample free of dust during analysis, and to eliminate stray scatter from other parts of the hutch. This enclosure will be kept clean. Dust will not be a problem in glove-box mode; for open and fume-hood modes, an air-filtering curtain will be placed across the opening during analysis to reduce dust. As for contamination of the signal by scatter, that will be addressed by applying a collimating cone to the detector snout, and a scatter shield behind the sample.

Components at sample position 2 include the following:

- Support table, fixed height
- Separate table for detector at 90° to beam
- Multi-use enclosure (described above)
- Beam-defining x-y slits
- Ionization chambers for I-zero and transmitted beam measurements
- Sample stage with x, y, z, and rotation motion
- LN2-cooled sample mount
- Camera on sample position (45° to beam), with illuminator
- Multi-element Ge fluorescence detector, with a sealed feed-through into the enclosure
- Nose cone collimator and filter holder for detector
- Set of filters (shared)
- Light-weight helium-filled flight tube to deliver beam to sample position 3 when needed

The detector will be retractable and have height adjustment to center on beam. Experiments at this sample position can take advantage of components at position 1 for additional beam monitoring, analysis of reference samples, etc., or may employ a helium-filled flight tube to efficiently traverse position 1.

Sample position 3: The function of this position will be for any large apparatus that needs more room than is available at the benchtop position. Large magnets, catalytic cells, and large-volume high-pressure assemblies can be wheeled into the hutch in this position.

Components at sample position 2 include x-y slits, available channels for motor control, sample monitoring, and detectors, and approximately 2 x 2 m floor space.

Experiments at this sample position can take advantage of components at positions 1 and 2 for additional beam monitoring, analysis of reference samples, etc., or may employ a helium-filled flight tube as described above.

5.4.4.2 Endstation 1

As a complement to the bulk endstation (having a minimum spot size of about 0.2 x 0.2 mm), Endstation 1 will address microbeam applications for XAS, providing a very high flux (estimated 10^{12} ph/sec at 8 keV) in an approximately 1 x 1 micron spot size, and having the important ability to maintain focus and positional stability over a 1000-eV EXAFS scan. Its scientific mission will center on a) relating micron-scale elemental distribution to physical structure and chemical speciation in heterogeneous materials, and b) XAS measurements of small samples. Obtaining local information in heterogeneous samples is important for such examples as measuring micron-scale variations in catalyst systems, identifying reactive particles and local chemical transformations in environmental samples, exploring biogeochemical processes involving microbes, and relating structure and chemical processes in biological samples. This tool will also be useful for studying reaction and transport processes of nanoparticles in industrial, environmental, and biological systems.

The microbeam endstation also meets a critical need in the study of small samples, such as single crystals, small samples for grazing-incidence surface XAS, small-mass samples of atmospheric or marine particulates, and in nuclear forensics. Recent work at NSLS X27A employs orientation-dependent single-crystal XAS to examine site-dependent substitution chemistry. Atmospheric particulates, critical in cloud formation and global climate research, are naturally difficult to obtain in quantity. The field of nuclear forensics is a new application for microbeam XAS, as it becomes more important to be able to identify, on the basis of trace

particles, evidence of nuclear materials processing or weapons testing. And in high pressure research, microbeam XAS can be applied to diamond anvil cell experiments.

Simultaneous microbeam XRD and XAS is also an important aspect of this endstation, which will share an area detector with Endstation 1. Planned applications include identification of crystalline phases in heterogeneous samples to further characterize structure-function relationships, and to measure crystalline structural variations during local-scale reactions in, for example, catalytic or ion-exchange materials.

The primary mission of this microprobe will be XAS, as it is expected that other beamlines (at undulator sources) will specialize in x-ray fluorescence and XRD imaging at micron or submicron resolution. The optics and source described here are optimized for the stable energy scans required for XAS.

Components at Endstation 1 include the following:

- Support table, fixed height
- Multi-use enclosure (described above)
- Separate table for detector at 90° to beam
- Beam-defining x-y slits
- Miniature ionization chambers for unfocused and focused I-zero, and transmitted beam measurements
- Kirkpatrick-Baez microfocusing mirror set, within enclosure
- Sample stage with x, y, z, and rotation motions
- LN2-cooled sample mount
- Low- and high-resolution microscope cameras on sample position (45° to beam), with illumination
- UV illumination for sample imaging
- Light-weight helium-filled flight tube to deliver beam to Endstation 2 when needed

The sample stage will have sufficient precision for microbeam applications. Conventional K-B mirrors will be used to focus up to 0.1 x 0.1 mrad of on-axis wiggler beam to a ~1 micron spot. The detector will be retractable and have a positioning stage to center it on beam. The area detector for XRD listed in Endstation 2 may also be used in Endstation 1; in order to accommodate it outside the enclosure a large sealed x-ray transparent window will be installed on the downstream end of the enclosure.

This endstation is separated from the three sample positions in the “bulk” endstation for several practical reasons. First, it is a sufficiently different application of XAS that it will benefit from the distinction and the future opportunity to operate in an independent and optimized manner. Second, it improves efficiency to be able to take beam in the upstream hutch while setting up more elaborate experiments in the other. And third, its requirements for beamline optics (angular acceptance, heat load, and the like) differ from the bulk techniques.

5.5 Preliminary Safety Analysis

This section is concerned with Synchrotron and bremsstrahlung radiation protection.

5.5.1 Beamline Radiation Analysis

Geometrical Synchrotron and Bremsstrahlung Ray-Tracing

Please find the relevant synchrotron as well as bremsstrahlung ray tracing schemes in Appendix A. The results of these drawings were derived based on the following documents:

1. Technical Bulletin 20 of the Advanced Photon Source
2. NSLS II Technical Note no 020, Guidelines for NSLS II beamlines..
3. Document SR_lattice_frontend_longstraight_8_22_07.pdf
4. Comments in e-mail of Sushil Sharma about first aperture within the front end

For the creation of the initial ray-tracing files we used the following parameters:

Source point		center of long straight section
Fixed Aperture Mask (FAPM)	19.8 m	
First Pb collimator		20.7 m
Safety shutter position	26.2 m	
End of Front End		28.6 m
Bremsstrahlung source from center of straight section	4 m downstream	
Bremsstrahlung lateral source dimensions	+35 mm	outboard
		Inboard unknown
		Vertical ± 12.5 mm

In addition we defined the following parameters and used those in the evaluation:

Synchrotron radiation miss-steer	±2.0 mm	
Size of the First Aperture Mask:		2.5 mrad (h) x 0.5 mrad (v)

The horizontal size of the first front end aperture was assumed to be 2.5 mrad to take a practical start. We assume that the size of this aperture will be part of future discussions, since this challenging aperture has to be designed together with both ID beams and the goal is that the Front-End delivers only a fan of 1mrad (h) x 0.15 mrad (v). For our ray-tracings we have assumed that there is a further mask just outside the Shield Wall defining the beam to 1 mrad x 0.15 mrad,

Please see Appendix A for the ray-tracing files which were realized using the above input parameters. Those file can be used for detailed discussions and have to be updated when the detailed parameters of the Front-Ends are available.

Further thoughts are needed on the first collimator. Most likely concerning two ID lines (3.5 mrad apart) this collimator will be a combination of an in-vacuum tungsten together with an outside lead collimator.

As it can be seen in the horizontal schemes the size of the beamline collimator inside the FOE is still reasonable. Most interesting is the result on the vertical ray tracing. As it is typically (and practically) done at other beamlines we have placed the beam defining second aperture at the end of the front end assembly right after the ratchet wall. This allows a rather small vertical opening of the collimator in the FOE and therefore an efficient collimation of the Bremsstrahlung at the beginning of the FOE.

Our target is the smallest possible collimator aperture resulting in the smallest possible beam offset of the monochromator. The conflict arises from the requirement to provide enough absorbing material inside the Bremsstrahlung stop between the Bremsstrahlung extremal and the aperture for the monochromatic beam. In this evaluation we follow the assumption that 11 mm are necessary.

In the ray-tracings we have assumed a vertical opening of the first lead collimator in the FOE of 15mm. Under this assumption one needs at least a DCM offset of 30mm to fulfill the requirements at the beam stop. This should be possible and acceptable. By using an in-vacuum tungsten collimator and optimizing the positions one could probably reduce the vertical offset at the DCM to 25mm. But this needs further detailed evaluations based on the more detailed design of the Front-End.

Enclosures:

There will be three beamline radiation enclosures at the XAS beamline, one first optics enclosure (FOE) and two contiguous experimental hutches. The FOE contains all beamline optics, and will be shielded for white beam and Bremsstrahlung scatter. The FOE with its lead-shielded sides interfaces to the ratchet wall of the storage ring. Following the standard regulations for white beam hutches, the labyrinths to run electricity as well as media and power connections will be located on the roof. The hutch will be long enough (approx 17 m) to accommodate the optics for both the original beamline and the canted beamline to be built later. One

double door with sliding panels, large enough to accommodate larger components being moved via fork lift, will provide access to the hutch.

The beam transport between the FOE and the first EH will be a tunnel type (coffin style) transport. Such an enclosure design will provide enough flexibility to accommodate vacuum pipes for both canted beamlines. Shielding interfaces such as guillotines are included.

The FOE will be equipped with an overhead crane (1 metric ton). A summary of the specifications is as follows:

First Optics Enclosure, white beam hutch (FOE)

	Sides 17 m x 3.3 m	Downstream wall 3 m x 3.3 m	Roof 17 m x 2.5 m
Shielding requirements: Lead (mm)	23 mm	50 mm	14 mm

- one extra panel of size 1 m x 1 m x 50 mm at the downstream wall centred at 1400 mm above the floor
- one sliding double door (white beam hutch)
- 10 lockable, hinged chicanes on the roof
- one hutch crane (1 metric ton), on trolley above trace of beam
- one set of guillotine, adjustable shielding around beam pipe on downstream wall
- painted with primer

Shielded Beam Transport (coffin style, base with lid)

- lead shielding of 7 mm thickness
- dimensions: 8 m long, 0.4 m x 0.4 m cross section
- support stands every 2 m with gussets
- painted with primer

First Experimental Enclosure, monochromatic hutch (EH-1)

	Upstream wall 3 m x 3.3 m	Sides 3.5 m x 3.3 m	Downstream wall 3 m x 3.3 m	Roof 3.5 m x 3 m
Shielding requirements: Lead (mm)	6 mm	6 mm	6 mm	5 mm

- one sliding door
- three lockable, hinged chicanes on the roof, three on the sides
- one set of guillotine, adjustable shielding around beam pipe on upstream wall
- painted with primer

Second Experimental Enclosure, monochromatic hutch (EH-2)

	Upstream wall 3 m x 3.3 m	Sides 7 m x 3.3 m	Downstream wall 3 m x 3.3 m	Roof 7 m x 3 m

Shielding requirements: Lead (mm)	6 mm	6 mm	6 mm	5 mm

- one sliding double door
- one sliding single door
- seven lockable, hinged chicanes on the roof, four on the sides
- one set of guillotine, adjustable shielding around beam pipe on upstream wall
- painted with primer

Provision will be made to run cable trays and utilities inside and outside the hutches.

5.5.2 Personnel Safety System

This will be a beamline-specific application of the NSLS-II standard PSS, and will encompass hutch door interlocks, beam-stops, photon and safety beam shutters. Specific components are described elsewhere, and this beamline will utilize one touch-screen panel, one shutter control, emergency-stop and personnel-check provision for all three enclosures, and door interlocks for 1 door on FOE, two on EH1 and two on EH2.

5.5.3 Equipment Protection System

This will be a beamline-specific application of the NSLS-II standard EPS, and will include vacuum, temperature, water flow, beam status, and cryo-cooler status. Specific components are described elsewhere.

5.6 Additional Requirements Imposed on the Conventional Facilities

Endstation multi-use enclosures will need to interface with common exhaust system planned as part of facility.

6 XPD: POWDER DIFFRACTION X-RAY BEAMLINE

6.1 Executive Summary

This chapter describes the design for a damping wiggler based high-energy high-resolution powder diffraction beamline at NSLS-II. This beamline is optimized for high-energy high-resolution x-ray powder diffraction, operating in the energy range from around 20 keV and extending well above 50 keV. This facility will be the only high-resolution instrument in the United States capable of collecting data at high energies and will make it ideal for *in situ* and time resolved studies of samples held in environmental cells. The following sections give a description of the scientific objective of the powder diffraction facility and a conceptual design of the beamline and end-station layout. In proposing a beamline design which could operate effectively, considering the very high power loads that are delivered from the NSLS-II damping wiggler source, the ACCEL x-ray synchrotron beamline design company were hired to arrive at a suitable set of beamline components that would be able to manage these high heat-loads and provide the required optical functions. In this process, a range of scenarios were considered in the design. In this chapter, we highlight our current thinking for such a design, taking some of the concepts and suggestions provided by ACCEL. The scope of this NSLS-II powder diffraction beamline is to provide one high-energy high-resolution x-ray powder diffraction end-station and an additional enclosure for "routine" powder diffraction. This additional enclosure could be equipped with existing NSLS-I equipment and provide an additional facility that could ultimately be served by a canted wiggler source.

6.2 Scientific Objective

The proposed powder diffraction beamline at NSLS-II will be a tunable high-resolution facility with the ability to collect data at high energies (20 keV to 100 keV), offering exceptional capabilities such as fast (milli-second) readout rates and high angular resolution on the same instrument. This will be an outstanding research facility for studying the structure and kinetics of materials under real conditions, and will meet the needs of the powder diffraction user community. For example, there are dedicated powder diffraction facilities at ESRF (BM16, ID31), DIAMOND (I11, I15), APS (sector 16, 5-BM-C, 6ID-B,C,D, 12-BM-B, 33BM-C), SOLEIL (CRISTAL, HighPressure, MARS, SIXS), the Swiss Light Source (MS), and the Australian Synchrotrone. Powder diffraction has widespread scientific interest, such as in the fields of metallurgy, solid-state chemistry, nanomaterials, microelectronics, mineralogy, and the biological and pharmaceutical sciences. In addition, the study of condensed matter at extreme conditions is developing into a very rich field of research. In situ elastic scattering provides the data required to derive structure models, which is essential to systematic searches for new classes of materials and to rationalizing their desirable properties.

The proposed NSLS-II powder diffraction beamline will be the only high-resolution instrument in the U.S. that is capable of collecting data at high energies, which will make it ideal for in situ and time-resolved studies of samples held in environmental cells in which the pressure, temperature, and chemistry can be varied. The high-energy x-rays will be able to propagate through environmental cells, allowing for the investigation of materials made up of high-Z components, and enabling high-q accessibility, which is crucial for atomic pair distribution function analysis and high-pressure cell research. By employing a high-resolution crystal analyzer array, this new instrument will allow enhancement, through suppression of the fluorescence and Compton components (including diffuse scattering), required to evaluate technologically important disordered materials. Due to the inherent small instrumental (and source) broadening, the high resolution of

the crystal array will enable the measurement of accurate peak-profiles, thus allowing the investigation of strain, lattice defects, and micro-structure. The implementation of a fast position-sensitive strip-array detector will also allow the real-time , microsecond timescale study of phase transitions, transformations, and catalytic reactions as a function of temperature, chemical gradients, and pressure. For combinatorial science and screening, robotic sample changers will facilitate rapid sample change and high-throughput data collection.

The great interest and excitement in the proposed NSLS-II powder diffraction beamline was evidenced at the NSLS-II user workshop held on July 17 – 18, 2007, where a breakout session on powder diffraction (http://www.bnl.gov/nsls2/workshops/UserWorkshop_BOS1.asp) was attended by more than 50 people. During this workshop, ideas on the capabilities of the beamline and research areas were discussed. In these early stages of the project, a beamline access team (BAT) is beginning to form and a further workshop is to be held on November 30, 2007.

6.3 Insertion Device

The powder diffraction beamline will be located on a damping wiggler source, which is located in a high-β straight-section of the NSLS-II ring. Unlike the NSLS-II undulator, bending-magnet and 3-pole wiggler sources, the NSLS-II damping wiggler extends the range of high energy x-ray access well beyond the 50 keV region, thus allowing the study of samples under real conditions, i.e. in environmental chambers. The basic parameters for the damping wiggler source used in this design are shown in the tables below Tables 6.1

Table 6.1 NSLS-II Machine and Damping Wiggler Parameters.

NSLS-II Machine & Damping Wiggler Parameters	
Electron energy, Eo	3 GeV
Electron current, Io	500 mA
Number of periods	70
Period length, λu	10 cm
Magnetic field	1.8 Tesla
Deflection parameter, k	16.81
Critical energy	10.8 keV

Table 6.2 RMS Electron Beam Values at the Center of the High-β Straight Section.

Root-Mean-Square electron beam values at the center of high-β straight-section	
Horizontal electron beam size, σ_x	99.0 μm
Vertical electron beam size, σ_z	5.5 μm
Horizontal electron beam divergence, σ_x'	5.5 μrad
Vertical eectron beam divergence, σ_z'	1.8 μrad

We note that as a result of optimization of the damping wiggler design, the period of this device has subsequently been refined to 90 mm. This has the advantage of reducing the angular fan of the radiation, making canting two devices more practical. While this is not expected to have a large impact on the design considerations presented here, it will be necessary to reevaluate any of these issues in light of the new source design.

Figures 6.1 and 6.2 show the flux (integrated over 3 mrad horizontally) and brightness values for the various NSLS-II sources. With a critical energy of 10.8 keV, the NSLS-II damping wiggler has flux values of 1.7 x 10^{15} (at 20 keV), 3.3 x10^{14} (at 40 keV), 5.6x10^{13} (at 60 keV),1.0x10^{13} (at 80 keV) and 1.4x10^{12} (at 100 keV) ph/sec/0.1% BW/mrad. The corresponding brightness values are 2.2x10^{18} (at 20 keV), 1.0x10^{18} (at 40 keV), 5.7x10^{17} (at 60keV), 2.6x10^{17} (at 80keV) and 1.2x10^{17} (at 100 keV) ph/sec/0.1%BW/mrad2/mm^2.

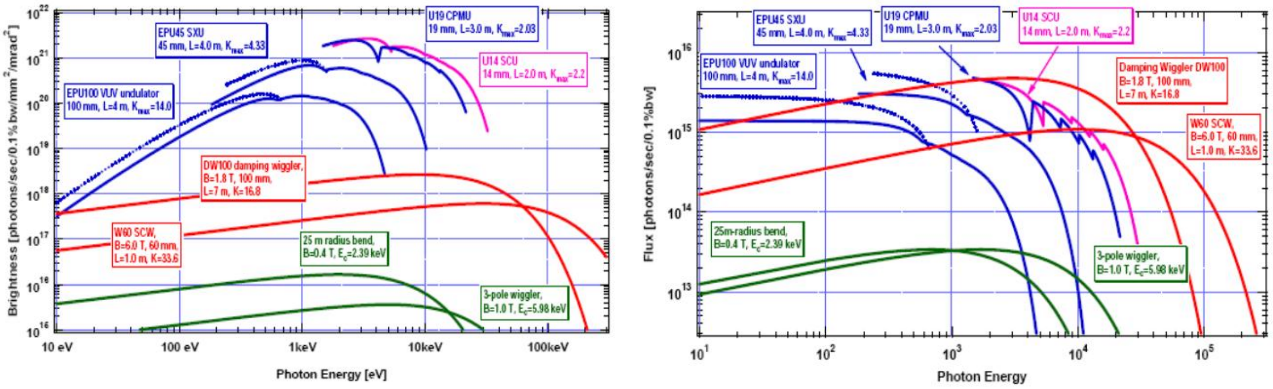

Figure 6.1 Flux and brightness curves for the various NSLS-II sources, including the 7.0m-long damping wiggler source.

Figure 6.2 shows the flux and brightness comparisons between the NSLS-II damping wiggler source and the existing NSLS X17 super-conducting wiggler (a high-pressure diffraction beamline). As is evidenced by these plots, the NSLS-II damping wiggler source exceeds the X17 source output and will make the proposed high-energy high-resolution powder diffraction beamline at the NSLS-II machine a very powerful facility.

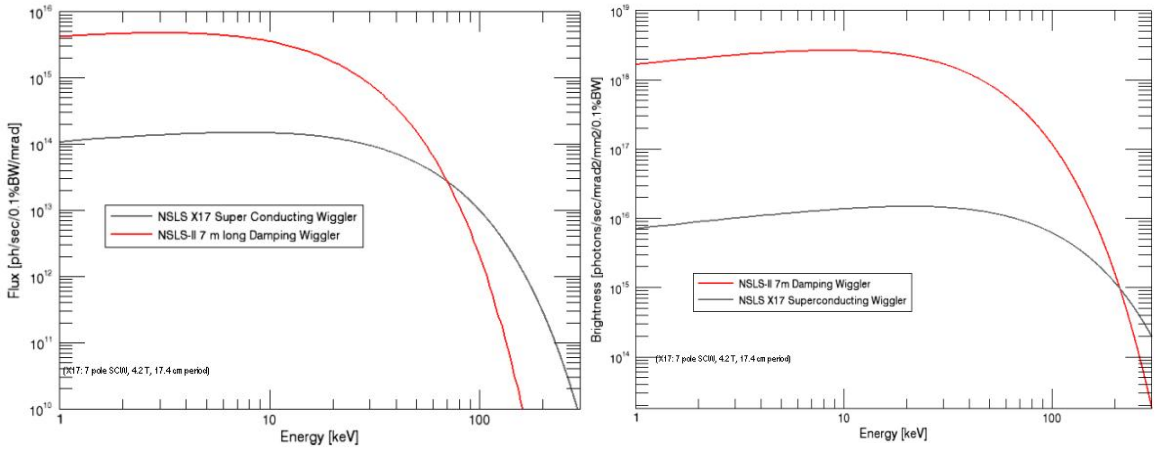

Figure 6.2 Flux and brightness comparisons between the NSLS-II 7m long damping wiggler source and the NSLS-I super-conducting wiggler.

6.4 Sector Layout

The following sections describe the conceptual configuration of the NSLS-II powder diffraction facility.

6.4.1 Front-End Layout

A layout of a typical front-end is shown below (SGV: slow gate valve; FAPM: fixed aperture mask, XBPM: photon BPM; CO: lead collimator; FGV: fast gate valve; SS: safety shutter). The components that are not shown are: 1) ratchet wall collimator (a beam pipe going through the ratchet wall and surrounded by lead), and 2) a gate valve downstream of the ratchet wall collimator (this gate valve can be removed after commissioning).

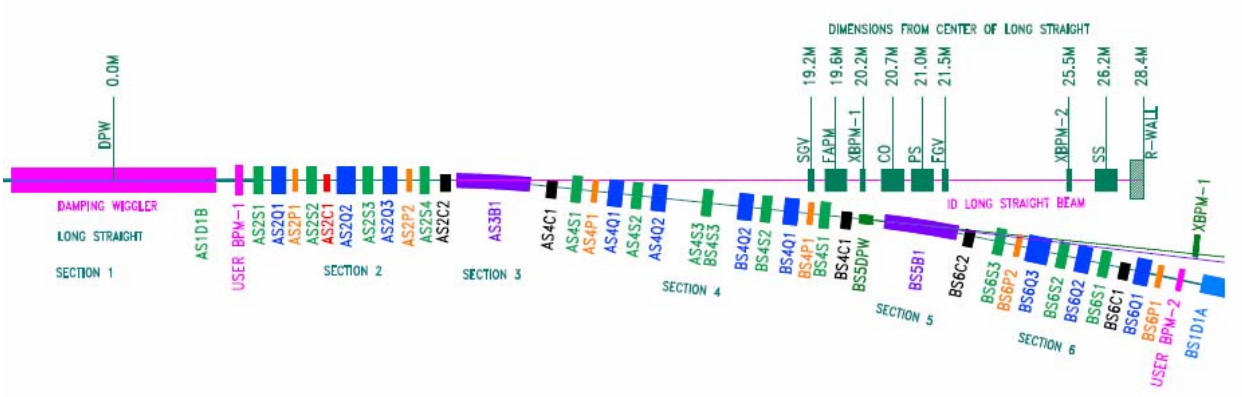

Figure 6.3 Front-end layout plan of NSLS-II.

For the NSLS-II powder diffraction beamline, the fixed aperture mask (FAPM) will limit the angular acceptance to 1 mrad (H) x 0.15 mrad (V) and reduce the power load on the downstream optical components (see Section 6.4.3). In addition, white-beam X-Y slits will be situated between the second x-ray beam position monitor (XBPM-2) and the fast gate valve (FGV), to further reduce power loads and reduce the angular acceptance, if required.

6.4.2 Beamline Layout

From discussions with the user community, potential BATs, and vendors, a conceptual design of the NSLS-II powder diffraction has been devised that would meet the requirements for a high-energy high-resolution facility. Furthermore, the beamline will be designed in way that it allows the addition of a second beamline, which could be served using a second canted wiggler in the same straight section.

Outlined in the tables below are the beamline performance, as described by the various operational modes. All flux values assume a 1mrad (H) x 0.1 mrad (V) acceptance.

Table 6.4 lists the photon flux, in units of ph/sec/0.1%BW, before and after the 1.5m-long Pt-coated vertically focusing/collimating mirror, which operates at a fixed grazing incidence angle of 2 mrad. For operations above 40 keV, where the mirror reflectivity falls considerably, it is withdrawn from the optical path. Reflected in these values are 5 mm of carbon pre-filters.

Table 6.4 Flux at and after the vertical focusing mirror, which is located in the front optical enclosure.

Energy [keV]	Flux at Mirror (with 5 mm carbon) ph/sec/0.1%BW	Flux after mirror (withdrawn for > 40 keV) ph/sec/0.1%BW
20	$4.6x10^{14}$	$3.7x10^{14}$
40	$1.7x10^{14}$	$1.2x10^{14}$
60	$3.7x10^{13}$	
80	$7.2x10^{12}$	
100	$1.3x10^{12}$	

Tables 6.5 and 6.6 detail the x-ray flux, in units of ph/sec, at the sample position (location H in the high-resolution enclosure – Figure 6.4, 57.7 m from the damping wiggler source), using both sagitally-focusing silicon-111 and -311 double-crystal Laue monochromators. The bandpass of these crystal orientations are noted in the table captions. The horizontal focused beam size (FWHM) are estimated from the ~2:1 focusing of this device and current NSLS measurements (see section 6.4.3.3). In the vertical direction, the 1.5 m long mirror in the FOE can deliver a focused 400 μm (FWHM) beam and a 3 of mm beam in the high-resolution/collimating mode, below 40 keV.

Table 6.5 Bent Laue Mode (2:1 focusing): dE/E ~$1x10^{-3}$ – Si(111). 0.5mm-thick Laue crystals and 2mm silicon pre-filter. 5 mm carbon.

Energy [keV]	**Flux at sample** [ph/sec]	**Beam dimensions at sample**
20	1.8x1013	300 μm (H) x 400 μm (V) / 3mm – mirror in
40	1.1x1014	300 μm (H) x 400 μm (V) / 3mm – mirror in
60	3.0x1013	300 μm (H) x 5 mm (V)
80	6.2x1012	300 μm (H) x 5 mm (V)
100	1.1x1012	300 μm (H) x 5 mm (V)

Table 6.6 Bent Laue Mode (2:1 focusing): dE/E ~$1x10^{-4}$ –Si(311). 0.5mm-thick Laue crystals and 2mm silicon pre-filter. 5 mm carbon.

Energy [keV]	**Flux at sample** [ph/sec]	**Beam dimensions at sample**
20	7.2x1012	300 μm (H) x 400 μm (V) / 3mm – mirror in
40	4.4x1013	300 μm (H) x 400 μm (V) / 3mm – mirror in
60	1.2x1013	300 μm (H) x 5 mm (V)
80	2.5x1012	300 μm (H) x 5 mm (V)
100	4.4x1011	300 μm (H) x 5 mm (V)

For very high-resolution powder diffraction work, the Laue crystals can be unbent to eliminate contributions to the vertical beam divergence that can be induced by the sagittal bending. In this mode, the flux and beam size values are shown in Table 6.7. To reduce the horizontal beam size, we propose to use a graded multiplayer focusing optic within the experimental enclosure. Table 6.8 shows both the x-ray flux and beam dimensions for this mode of operation.

Table 6-7 Unbent Laue – for high resolution. dE/E ~1x10^{-4} – Si(111)

Energy [keV]	**Flux at sample** [ph/sec]	**Beam dimensions at sample**
20	1.8x1012	5.8 cm (H) x 400 μm (V) / 3mm – mirror in
40	1.1x1013	5.8 cm (H) x 400 μm (V) / 3mm – mirror in
60	3.0x1012	5.8 cm (H) x 5 mm (V)
80	6.2x1011	5.8 cm (H) x 5 mm (V)
100	1.1x1011	5.8 cm (H) x 5 mm (V)

Table 6.8 Unbent Laue – for high resolution. dE/E ~ 1x10^{-4} – Si(111) + 0.5mm-long graded multiplayer optic.

Energy [keV]	**Inc. Angle** [mrad]	**Hor. Accep.** [mm]	**Flux at sample** [ph/sec]	**Beam dimensions at sample**
20	7.7	3.15	9.8x1010	14 μm (H) x 400 μm (V) / 3mm – mirror in
40	3.9	1.95	3.7x1011	14 μm (H) x 400 μm (V) / 3mm – mirror in
60	2.6	1.3	6.7x1010	14 μm (H) x 5 mm (V)
80	1.9	0.95	1.0x1010	14 μm (H) x 5 mm (V)
100	1.5	0.75	1.3x109	14 μm (H) x 5 mm (V)

The conceptual layout for the NSLS-II powder diffraction beamline is shown in Figure 6.4. The beamline consists of the following optical components:

A. a pre-filter and beryllium window – to isolate the beamline from the machine vacuum, and a filter unit to limit the power load on the downstream optical components

B. a 1.5 meter long bendable focusing/collimating mirror operating at a fixed grazing incidence angle of ~ 2mrad, which will be coated with platinum and be able to function up to 40 keV. Above this energy, this mirror will be withdrawn from the optical path

C. a sagitally focusing double-crystal Laue monochromator to provide focusing and wavelength selection, with the required band-pass

D. beam monitoring unit

E. a monochromatic photon beam shutter

F. sample position in the upstream experimental hutch (endstation equipment not in the scope of this project)

G. a horizontal focusing graded multiplayer for focusing the beam onto small samples at H

H. a sample position in the downstream experimental enclosure

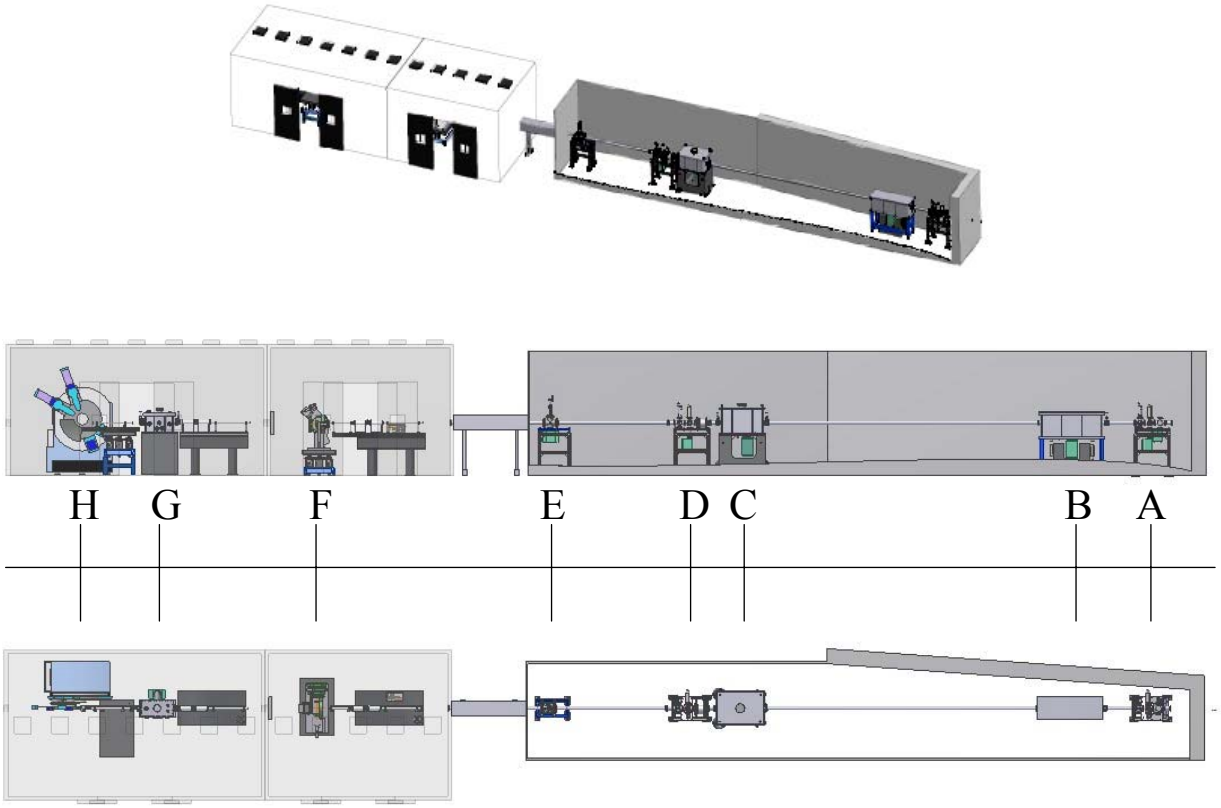

Figure 6.4 Conceptual layout for the powder diffraction beamline.

Table 6.9 Distances of the various components from the conceptual layout of the powder diffraction beamline.

Component	Distance from Source
A. Be window and Filter Unit	29.0 m
B. 1.5m-long focusing/collimating mirror	31.1 m
C. Sagitally Focusing Double-Crystal Laue Monochromator	40.0 m
D. Beam Monitoring Unit	41.36 m
E. Monochromatic Photon Shutter	45.1 m
F. Upstream Sample Position	51.3 m
G. Horizontally Focusing Graded 0.5 m long Multilayer	55.6 m
H. Downstream Sample Position	57.7 m

6.4.2.1 Survey and Alignment Plans

All beamline components will be surveyed and aligned in place by the facility. To facilitate ease of alignment, all components will be fiducialized to external reference points on their table during assembly. All components are designed with a liberal tolerance allowance greater than 0.5 mm.

6.4.2.2 Utility Layouts

Cooling water is required for all high-heat components. Requirements for the standard cooling water supply and the components and flow rates that are needed are shown in the tables below.

Table 6.10 Cooling water requirements for the XPD.

Approximate Temperature	20°C to 30°C
Temperature Stability	± 1°C
Maximum Pressure	6 bar
Pressure Stability	± 0.1 bar
Quality	de-ionized but not ultra-pure

Table 6.11 Flow requirements for the various XPD optical components.

Component	# of Circuits	Max. Consumption
Pre-Filter and Be window	1	4 l/min
Attenuator Units	4	8 l/min
Vertical Collimating/Focusing mirror and mirror protection mask	1	12 l/min
Thermal Stabilization and Cooling of Laue mono	1	Local Chiller
White Beam Stop	1	4 l/min

The cryo-cooler unit for the double-crystal Laue monochromator requires connection to a liquid nitrogen supply. It is recommended to have a liquid nitrogen supply within 2 to 3 meters of the final cryo-cooler position. The following components must be connected to a dry, filtered compressed air supply having a pressure of between 70 psi and 100 psi: the monochromatic photon beam shutter, all gate valces and the pneumatically driven attenuator filter units. There are three main areas where electrical power is required:

- Control system cabinets: A central 3-phase power distribution should be placed near the cabinets. In total, approximately 12 kW are required,
- Cryo-cooler unit: This unit needs a 1-phase power distribution of approximately 2.5 kW,
- Enclosures:

Within the hutches, two types of power outlets should be provided for each section: a low-noise outlet for measuring equipment and a standard outlet for mobile pumps and heaters. The outlets should be distributed along the length of each enclosure. The required power in the front optical enclosure could be up to 30 kW to accommodate the extreme case where the full beamline may be pumped and baked at the same time. Along the beamline a grounding bar is needed, to ground the beamline components. The grounding bar must be connected to the central power distribution ground.

6.4.2.3 Beamline Vacuum System

We have assumed that there will be several vacuum sections, isolated from each other through gate valves. Each vacuum section will be equipped with one ion pump and has one rectangular all-metal valve, CF40, to rough down the vacuum using a pump cart and to vent the section. The monochromator is equipped with one all-metal valve CF16 for venting and, in addition, with a CF63 gate valve where a turbo molecular pump will be permanently mounted. Each section is also equipped with a full-range vacuum gauge. The white

beam part of the beamline will be realized to be bakeable in order to achieve a vacuum pressure below 10^{-9} mbar. The monochromatic part is designed to achieve a base pressure in the 10^{-8} mbar range. Besides the large flanges of the monochromator doors (that are Viton sealed) and of the mirror vessels (metal sealed for the VCM and Viton sealed for the VFM) all flanges will be realized according to the Conflat standard.

The layout of a typical vacuum system for one beamline section, and a general overview of the entire vacuum and EPS systems are shown in Figure 6.6.

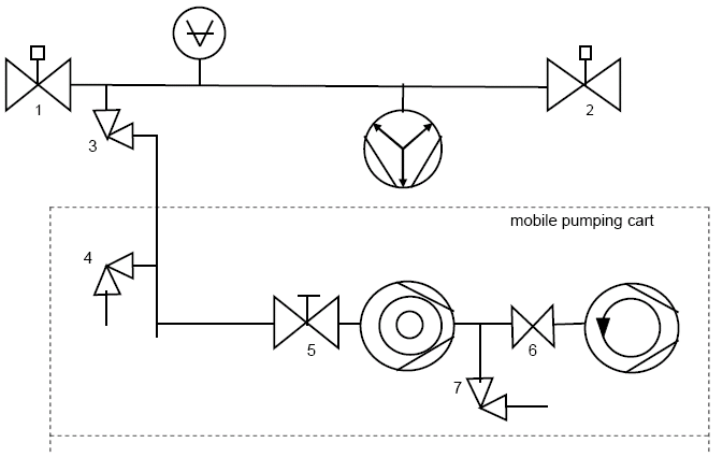

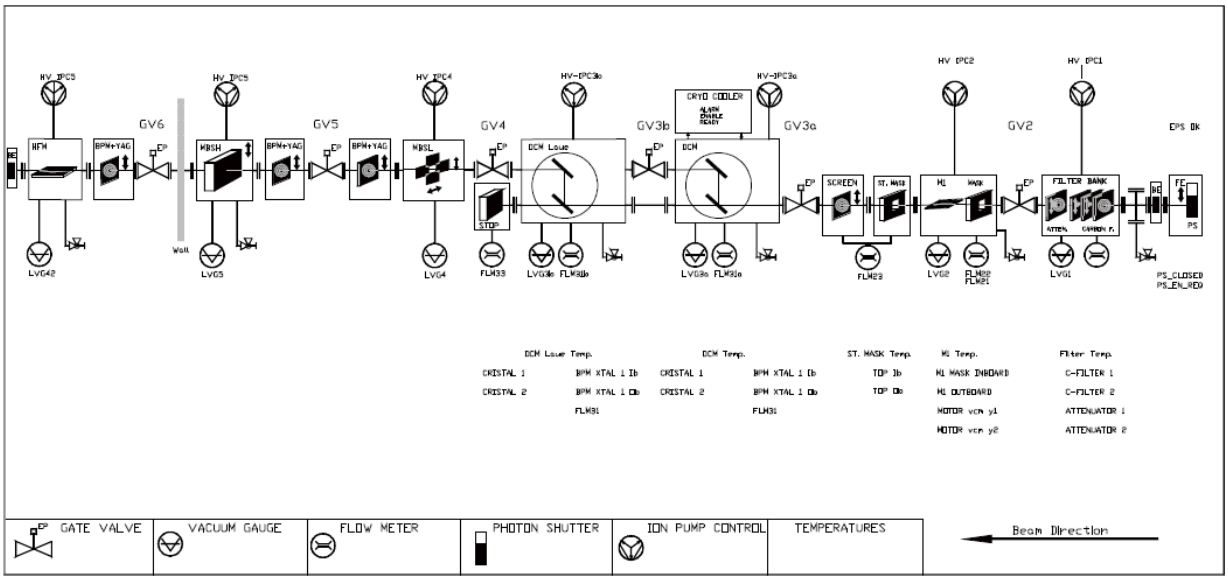

Figure 6.6 **Top**: 1,2 : Sub-section isolation valves. 3: full metal right-angled valve attached to the BL-section. 4: Right-angled valve to vent either the sub-section or the pumping station. 5: hand actuated gate valve CF63. 6: valve to separate the pre-pump from the leak detector. 7: valve to connect the leak detector. **Bottom**: General schematic overview of the entire vacuum and EPS system. The DCM indicated in the drawing is from earlier design considerations, and does not exist in the current configuration.

6.4.2.4 Beamline Control, Motion Control, and EPS

This section covers a general specification for a beamline control system, including the Equipment Protection System (EPS) and the vacuum controls as it could be realized for a NSLS-II beamline. The particular control system chosen here is based on Delta-Tau hardware and Experimental Physics and

Industrial Control System (EPICS) software. The EPS is based on a PLC unit and covers the vacuum monitoring and control as well. This document provides the specifications for the design of a typical beamline control system (BLCS). The beamline control system is the electronic hardware and software interface between the beamline operator and the beamline components. It must be versatile and robust to allow the operator reliable remote control of the beamline components and endstation hardware for the purpose of aligning the beamline and conducting experiments in a precise and yet safe and protective way. It should also have the capability of easily implementing high-end automation. The complete BLCS for the beamline consists of the software and hardware for the following subcomponents:

- control of the full beamline (through EPICS IOCs)
- motion control
- beamline diagnostics
- vacuum control
- beamline equipment protection system (BLEPS)
- control of the closed-loop cryo-cooler

The overall hardware and software architecture is determined by the use of EPICS for beamline control. Within this architecture, field I/Os (i.e., signals from beamline components, experimental stations, etc.) are concentrated in controllers called EPICS IOCs. There can be several EPICS IOCs per beamline. These IOCs communicate to EPICS channel access clients (operator workstations), other EPICS IOCs and embedded EPICS IOCs using TCP/IP. Through these IOCs, the control of the motion of the component axes, detectors, feedback, interfacing to the BLEPS, etc. is established. From an EPICS client, a user can remotely operate the beamline through operator interfaces. Previous releases of EPICS Base required that EPICS IOCs use a vxWorks operating system. However, EPICS Base Release 3.14 has allowed the configuration of operating systems such as Unix, Linux, and Windows as EPICS Soft IOCs. With this configuration, use of non-VME hardware is now possible, lending greater flexibility in the choice of control hardware.

6.2.4.5.1 Overall Beamline Control

The BLCS uses many hardware and software interfaces to establish communication between the various devices that constitute the beamline. The design of the BLCS aims to combine the advantages of having centralized control for convenience of software maintenance and upgrade and yet distributed intelligence for more flexibility, better cable management and housekeeping. All cabling from the beamline components can be routed to control cabinets located near the optics and hutch. Figure 6.7 shows a possible layout of the beamline control devices and the communication interfaces.

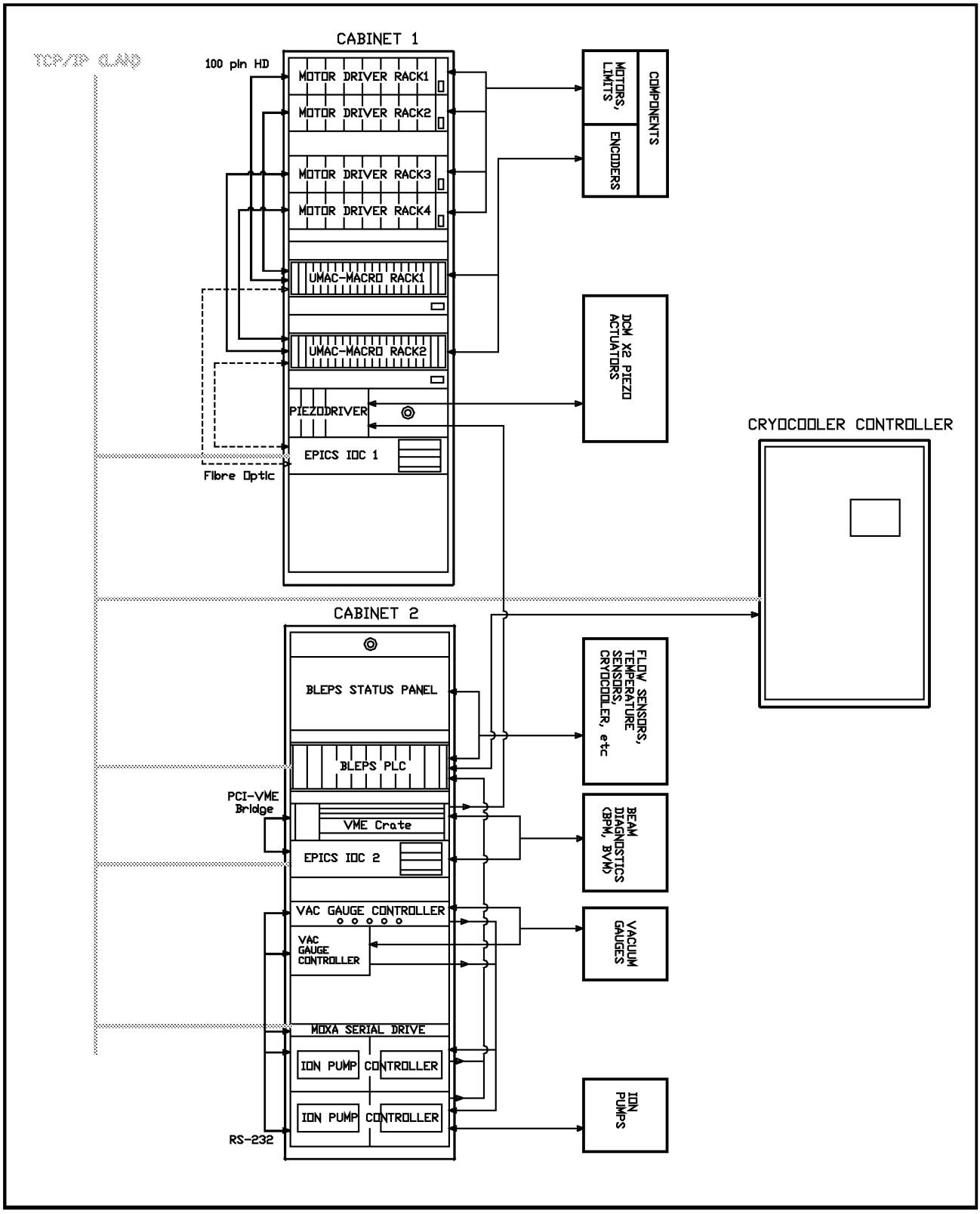

Figure 6.6 Possible layout of the powder diffraction beamline control system.

The beamline control hardware will be housed in two 19-in. control cabinets or racks. The cabinets will consist of several control crates where a crate is a 19-in., variable-height enclosure. The crate types are listed in Table 6.11.

Table 6.11 Possible Crate Control Configurations for the Powder Diffraction Beamline.

Crate	Function
EPICS IOC	A workstation PC running a Linux O/S and configured as an EPICS SoftIOC. It will have PCI slots populated with the motion controller and signal processing cards.
UMAC MACRO Crate	The distributed interface to the stepper motor drivers, encoders, motion control related DIO and AIO
Stepper driver crates	8-axes stepper driver crates
Piezo controller	Control for the piezo actuators
BLEPS	The BLEPS PLC, I/O modules and Status Display Panel
Vacuum gauge control	For readout of the vacuum gauges installed on the beamline
Ion pump controllers	Each controller serves two ion pumps. Two controllers occupy 19-in. x 3HU.
MOXA Serial Drive	Provides serial ports for communication of serial devices with the EPICS IOC. It communicates with the EPICS IOC through TCP/IP.

Each cabinet has an input power requirement of 3-phase/400VAC, 20A. The 3-phase supply is broken out into three single-phase 230VAC supplies within the cabinet which powers the instrumentation crates.

The cryo-cooler control unit will be a stand-alone unit comprising all the control electronics for controlling and monitoring the liquid nitrogen cryo-cooler. It will contain its own PLC for signal processing and alarm handling and will communicate with the beamline EPS through TCP/IP (and hardware connections, if required) to perform specific safety interlock tasks. It will also have a local control/status panel for constant monitoring independent of the network.

These are local electronics that need to be located close to components and are mounted onto the support structures of the components. Local electronics include interpolators for electronics and LVDT readouts. The LVDT readouts output 0-10 V analog signals which will be routed to an ADC readout in the control cabinet.

The beamline will be controlled through EPICS. The EPICS environment will consist of: 1) IOCs running Linux, 2) EPICS Base 3.14.7 or higher, and 3) State Notation Language/Sequencer sequence programs: MEDM and EDM, other EPICS extensions as required, and SynApps.

The control hardware used in the powder diffraction beamline should be supported through EPICS device driver and device support modules. Purely soft support modules are also required to provide useful functions such as data acquisition, scanning, save/restore, user calculations, etc. Through these modules a user, sitting at an EPICS client, can communicate with the EPICS IOCs, the EPICS IOCs can communicate with the control hardware, and the hardware components communicate with each other. The operator interfaces will be the GUIs through which a user operates the beamline. GUIs will be developed with MEDM or EDM.

Beamline motion control refers to the control of all the movable axes of the beamline, the readback of the encoding elements, and the activation of protective switches that limit over-travel. Furthermore, when incremental encoders are used, homing mechanisms should be incorporated for calibration of the absolute position of the axis. Motion control hardware includes the following: 1) motion controller system, 2) motor amplifiers/drivers, 3) connection hardware (interface panels, connectors, cable), 4) Limit/Home switch hardware, and 5) encoder hardware.

For motion control hardware, we are considering the intelligent motion controllers from Delta Tau due to their excellent performance for synchronized correlated motions and for their flexibility. The MACRO[1] distributed system consists of two 32-axis motion controllers residing in PCI slots of the EPICS IOC1, connected through fiber optics to UMAC-MACRO crates. These UMAC-MACRO crates can be customized to output signals supporting several types of motors, digital and analog I/Os, and encoder inputs.

Each 19-in. UMAC-MACRO crate can support up to 32 motorized axes. Each set of eight axes in the UMAC-MACRO connects to one eight-axis motor driver crate. The Turbo PMAC2 PCI Ultralite is a member of the Turbo PMAC family of boards optimized for interface to the system through the MACRO ring. It can command up to 32 axes through the MACRO ring. The Turbo PMAC2 PCI Ultralite is a full-sized PCI-bus expansion card. This card is capable of PCI bus communications, with or without the optional dual-ported RAM (DPRAM).

For this beamline control, the card will be delivered with the DPRAM option. Standalone operation is also possible, and communications can occur through an RS-232 port. Through the rest of this chapter, the 32 axis PMAC2 motion controller will be referred to as the PMAC. MACRO is an acronym for Motion and Control Ring Optical and is a non-proprietary digital interface developed by Delta Tau for a single-wire connection between the multi-axis motion controllers, amplifiers, and I/O through a fiber optic ring. The MACRO minimizes wiring complexity, reduces hardware, and eliminates noise in large systems. The high-speed 125 Mbits/sec transfer rate is capable of closing the servo loops across the MACRO ring, allowing the flexibility to choose distributed intelligence or centralized control. The 16-axis UMAC MACRO CPU provides a remote interface for encoders, flags, direct-PWM digital drives, analog drives, and/or digital I/O for a Turbo PMAC2 with MACRO interface. It communicates with the Turbo PMAC2 solely through the MACRO ring, but interfaces to standard drives, encoders, flags, and Opto-22 style I/O through on-board connectors. It is designed to run up to 16 motors. Through the rest of this chapter, the 16-axis UMAC MACRO CPU will be referred to as the UMAC.

An interface board between the UMAC-MACRO Crate and the Stepper Driver Crate forwards the step/direction signals and returns the limit/flag signals. Each board provides signals for eight axes and connects to the stepper-driver crate through a standard 100-pin, high-density connector. This interface board will be mounted on the rear of the UMAC-MACRO crate.

Bipolar stepper drivers will be provided to match the requirements for the specific axis in terms of torque requirements, drive currents, and micro-stepping. All motorized axes on optical components (monochromator and mirrors) and slit systems will be encoded with incremental encoders (quadrature or analog). All motorized axes will be fitted with limit switches to determine the travel range and to protect against mechanical damage caused by over-travel. These switches are externally mounted and can be adjusted to set a required travel range. The limit switch contacts are configured to be “normally closed.” Homing of the component axes, to zero the counter, is performed using the precision end switches. Table 6.12 lists typical types of cables and connectors.

Table 6.13 List of possible cables and connectors for the powder diffraction beamline.

Function	Cable Type	#CondPairsxCross-section	Connector
Motor	Facility standard	4x2x0.75mm^2 + 6x0.25mm^2 (separately shielded)	Trim-Trio Souriau e.g. UTO014-12ST
EPS SIGNALS	Unitronic LiHCH (TP)	4x2x0.25 12x2x0.25	SubD-9 (valves, flow, pressure) SubD-25 (temperatures)
Quadrature ENCODER	Unitronic LiHCH (TP)	8x2x0.25	SubD-15
Analog Encoder	Belden 8164	4x2x0.23	SubD-15
D/A/Video SIGNALS	Coxial	RG58U, RG174	BNC, Lemo

[1] Motion and Control Ring Optical

The motion control software is determined by the use of the Delta Tau motion controller and the EPICS control software. PMAC Executive Pro Suite is a Windows-based suite of programs, running on Windows XP and 2000, that communicates to the PMAC through its serial port. It allows standalone operation of the motion controller for initial configuration of the hardware and for testing of connections to the stepper drivers. It also contains tuning and plotting programs useful for performance demonstration and debugging at a lower level. Uploading and downloading of files and variable settings is possible for quick configuration and saving/restoring of settings.

The EPICS support for the PMAC2 controller will also contain a set of setup files that must be downloaded to the PMAC. These files are not EPICS specific but are required to set up the communication of the EPICS IOC to the controller. They will be preloaded to the PMAC/UMAC prior to establishing EPICS communication. As mentioned before, our design is based on control of the motion of the component motors though EPICS through the support developed for the Turbo PMAC2 PCI Ultralite motion controller currently in use at the XAS beamline at the Australian Synchrotron.

Beam position monitors will be installed along the beamline as diagnostic elements. To read out the current signals from these monitors, use of compact quad-electrometer electronics are considered. These devices are supported in EPICS and can be used to feed back the BPM signal to a piezoelectric actuator via a 16-bit DAC. They can also be used for ion chambers.

There will be beamline vacuum control and monitoring instrumentation, consisting of a vacuum gauge controller, the Pfeiffer Maxiguage TPG256A, and the ion pump controllers. The vacuum gauge controller and the ion pumps will interface to the EPICS IOC via their RS232 ports. RS232 ports are provided by the MOXA Nport5610-8 serial device server which communicates to the EPICS IOC via TCP/IP. Vacuum level readouts from the vacuum gauges will be input into the vacuum controller which will compare the readings against preset trip points. Status of these trip points are directly wired to the BLEPS as digital inputs. The status of the HV of the ion pumps is directly monitored by the BLEPS. Through EPICS, the pressures read by the vacuum gauges will be remotely available.

The primary purpose of the beamline EPS is to protect the individual beamline components against x-ray damage, loss of vacuum, loss of coolant flow (water and liquid nitrogen), and elevated temperatures. The beamline EPS communicates with the Beamline Personal Safety System (BLPSS) PLC and with the Front End EPS and Front End PSS (FEEPS, FEPSS) through specified interface signals. Communication to the EPICS IOCs is via modbusIP. The EPS hardware will be based on the Programmable Logic Controller (PLC) technique (e.g., Schneider Electric TSX Premium), including a CPU (TSXP572634M) with an Ethernet interface. The BLEPS hardware will consist of an approximately 4HU 19-in. crate (CPU and I/O modules) and a 6HU local display panel. The display panel will be an etched aluminum plate with green/red LEDs to indicate satisfactory/unsatisfactory conditions of the relevant component signal. The BLEPS PLC will be programmed to take protective actions in the case of detection of unfavorable conditions in the beamline.

Control and monitoring of the PLC will be available through GUIs and will offer the following functions: 1) Monitoring: EPS alarm status, beamline gate valve status, temperature values, flow trip points status, pressure trip point status, ion pump HV status, cryo-cooler ready/alarm/enable status, pneumatic actuator position status, and conductivity meter readings; and 2) Control: beamline gate valves and pneumatic actuator insertion/retraction.

For ease of configuration of the BLEPS, the beamline will be divided into EPS vacuum sections. The vacuum sections are defined based on the specific beamline component configuration and the need to isolate the components. Vacuum sections are bounded by gate valves. Based on information on the beamline design and requirements for communication with other sections of the beamline control system, interface signals will be determined. All relay contacts are “normally open” (N/O), 24 VDC Flag return signals. In general, the following type of beamline signals will be monitored by the BLEPS: process cooling water (PCW) flow, conductivity, critical device temperatures (filters), fixed and “disaster” masks,, monochromator crystals, vacuum, cryo-cooler status, gate valves position, pneumatic-driven filters, and beam position monitors.

The cryo-cooler controller is a stand-alone control cabinet which controls the closed-loop liquid nitrogen circuit used to cool the monochromator Laue crystals. It interfaces to the EPICS IOC for remote monitoring and control and to the BLEPS for communication of ready status and alarm signals.

6.4.3 Beamline Components

The following items describe the various beamline components for the high-energy, high-resolution powder diffraction beamline.

6.4.3.1 White Beam Slits

These components are included in the front end (Section 6.4.1), thus they do not belong to the scope of supply for the beamline.

6.4.3.2 Pre-Filter, Beryllium Window, and Attenuators

In hard x-ray beamlines, one typically uses a beryllium (Be) window to separate the beamline vacuum from the machine vacuum. Such a window has also the advantage that it absorbs a good fraction of the unused low energy x-ray spectrum, therefore reducing the overall power dumped on downstream components. However, in a wiggler beamline such as the NSLS-II DW 100 described here, calculation of the absorbed power indicates that a Be window in the direct of white beam from the wiggler simply would fail. Due to carbon's high thermal conductivity and mechanical stability, carbon foil(s) is (are) typically used as a protective filter material in front of or instead of a Be window. The combination of carbon filters and Be windows must be carefully tailored, taking into account both the absorbed heat load and the requirement for the highest possible flux transmission at lower energies. Our approach is to design a filter assembly that can be safely used whenever required, to reduce the power levels on the optical components.

Reduced power always will improve the performance of white beam optical components such as the focusing/collimating mirror and the sagitally-focusing double-crystal Laue monochromator. Considering the high heat load that is produced by the wiggler, the carbon filter unit is an essential component for maintaining sustainable power levels along the powder diffraction beamline. With respect to the heat load absorbed by the most upstream filter, a standard water-cooled graphite filter cannot cope with the high heat load. From experience at other facilities using similar powerful sources, we considered two possible solutions: 1) Using thin C foils which are only radiation cooled. In that case the foils become extremely hot – up to 1500°C and higher. 2) Using high-thermal-conductivity highly oriented pyrolytic graphite (HOPG) foils to form a filter frame, which can be safely water cooled.

In the following paragraphs some proven designs are summarized:

ALS, Beamline 5.0[2]

HOPG is clamped between two water cooled copper frames and absorbs 10 W/mm^2 (250 μm). The contact pressure is finely adjusted by springs. Temperatures up to 1000K are possible. After more than one year operation, there is no visible damage on the HOPG foil.

NSLS, MGU-undulator-beamline[3]

A stack of radiative cooled foils successfully withstand the power load from a wiggler (3.4 W/mm^2). They use seven foils, starting from 5 μm up to 51 μm. After a few years of operation, no visible damage can be observed on the foils. In addition it has been verified that the temperature of the foils is somewhat lower

[2] Private communication with D.Cambie; "Annealed Pyrolytic Graphite filter for beamline 5.0 at the ALS" - D.Cambie, C.Cork – MEDSI proceedings 2004

[3] private communication with P. Montanez and L. Bermann

than the calculated value. This system has proven to work reliably up to temperatures of 1000°C and slightly higher.

CHESS, wiggler-beamlines[4]

A HOPG foil was brazed directly to a copper block (12 W/mm^2 on 250 µm). Some cracks observed in the foil most likely were caused by the cooldown process during brazing. The system worked for some time, but failed with doubled power load. The replacement design has operated without failure for several months. The HOPG is clamped on two sites in a copper frame with improved water-cooling performance (jet-stream-cooling, very closed to the edge of the HOPG).

The consultant evaluated the behavior of the first filter unit for the power load of the damping wiggler source (please refer to Appendix D), demonstrating that both options, radiation-cooled filter elements as well as contact-cooled filters, are possible solutions for this beamline. A final careful FEA must be carried out using the final source parameters. In the beamline design they incorporated two components, a Be-window with sufficient pre-filters and an attenuator set up to manage the power load on the optical components:

6.4.3.2.1 Pre-Filter

This component is very similar to the setup already in use at several beamlines at BNL. It consists of a water-cooled frame that holds the different filters. The radiation-cooled foil is held in a tantalum frame, since it must withstand the extremely high contact temperature, and will become hot itself. The power then is dissipated into the surrounding environment and is absorbed by a water-cooled copper surface positioned around the tantalum frame. The tantalum frames, together with the carbon foils, are placed in a water-cooled cartridge made of OFHC copper. The cartridge is held and mounted on a DN40CF flange. The assembly is mounted to a DN100CF base flange and fits in a DN100CF standard cross. PT100 temperature sensors (e.g., two sensors) will be installed in the copper cartridge and monitored by the control system. If any PT100 sensor exceeds a temperature limit, the beam shutter will be closed. The PT100 sensors will be connected to an electrical feed-through. The water pipe (SF-copper, Ø8x1) will be brazed on the cartridge and on a DN40CF flange, avoiding water-to-vacuum joints. Possible carbon filter combinations are shown in Table 6.14.

Table 6.14 Possible Carbon Pre-Filter Combinations for the Be Window.

Filter no.	Filter thickness [µm]	absorbed power [W]	absorbed power density [W/mm²]
1	5	222	1.6
2	5	96	0.7
3	5	72	0.5
4	25	240	1.8
5	25	162	1.2
6	50	237	1.8
7	50	180	1.4
8	100	277	2.1
9	135	283	2.2
10	300	457	3.6
11	300	337	2.6

[4] private communication with J.Savino; "Improved high heat load graphite filter design at CHESS wiggler beamlines" – J.J.Savino, Q.Shen – SRI 2003 Proceedings

6.4.3.2.2 Attenuator Unit

This unit consists of a number of different filter setups that allow tailoring the power load on the optical components to the right level of operation for each particular operational mode of the beamline. The design being considered is based on one built recently by ACCEL for other high heat load beamlines and is described in the following paragraphs. Currently, we assume that for the DW beamlines it might be reasonable to work with two pneumatically driven attenuator units and two, or even three, motorized filter banks with different filters mounted. The latest design is based on a series of three water-cooled filters mounted on three pneumatic drives. These three carbon foils are of annealed pyrolytic graphite (APG). The foils have a thermal behavior similar to that of HOPG and are available down to thicknesses of 50 μm. The foils are clamped to copper frames where the thermal contact is improved by 1) polishing the surface of the copper within the contact area and 2) using springs that apply a wel-defined and well-distributed contact pressure. The thermal conductivity of APG is similar to diamond. Due to its excellent mechanical properties, and together with the advanced cooling, each foil is designed to remove about 500 W. The power density on the first foil constitutes the biggest challenge and therefore limits the maximum thickness of the foil, while heat conduction as well as physical integrity under thermal stress define its minimum thickness. The APG foil used in the existing system is 125 μm thick. The second foil can only be inserted in the beam when the first foil is already in place.

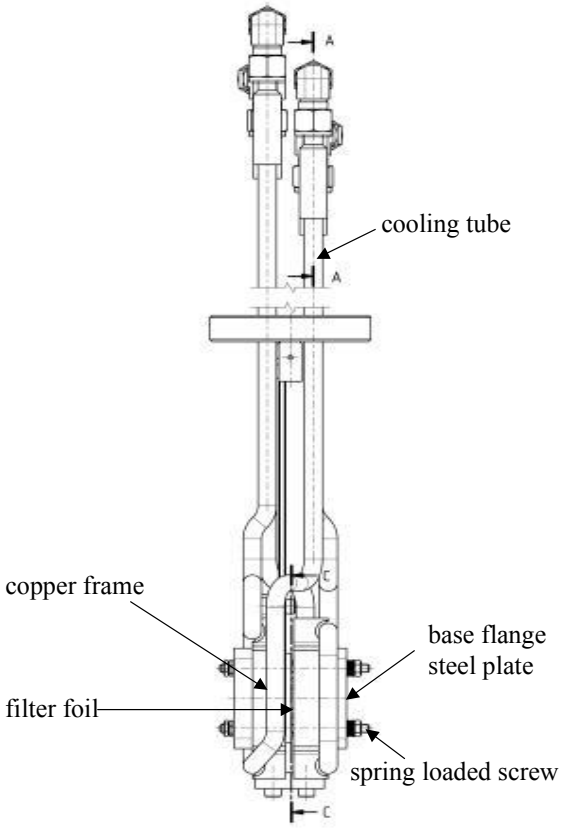

Figure 6.xx Directly-cooled high-power filter set-up, pneumatically driven.

The fourth filter drive is motorized and consist of a cooled frame with five positions that can be used for graphite foils (pyrolytic graphite) of different thickness to be used to further attenuate the beam. This filter design avoids water-to-vacuum joints. Water pipes are brazed to each cooled copper frame and to the vacuum feed-through, where edge-welded bellows allow the translation of the frames with the filters.

6.4.3.3 Sagitally-Focusing Double-Crystal Laue Monochromator

Sagittal focusing using Laue crystals was pioneered at the NSLS (Zhong et al., 2001; Zhong et al., 2002; Zhong et al, 2003). The concept is shown in Figure 1a. This new x-ray optics concept makes it possible to focus a large divergence of high-energy x-rays produced by the NSLS-II damping wiggler. The extent of such focusing is similar to that of sagittal focusing by a Bragg crystal, except for a factor related to the asymmetry angle. The anticlastic bending facilitates the use of inverse-Cauchois geometry in the meridional plane to provide better energy-resolution and to increase the photon flux by an order-of-magnitude compared to traditional sagittal focusing with Bragg crystals. Furthermore, sagittal focusing by a Laue crystal is preferred over a Bragg crystal at x-ray energies above 30 keV because, unlike Bragg crystals, the length of the beam's footprint on a Laue crystal is small and insensitive to energy. For many experiments, beam divergences of order 1 milli-radian at the sample will be tolerable. In diffraction experiments with a vertical scattering plane geometry, a larger divergence in the horizontal plane can also be tolerated.

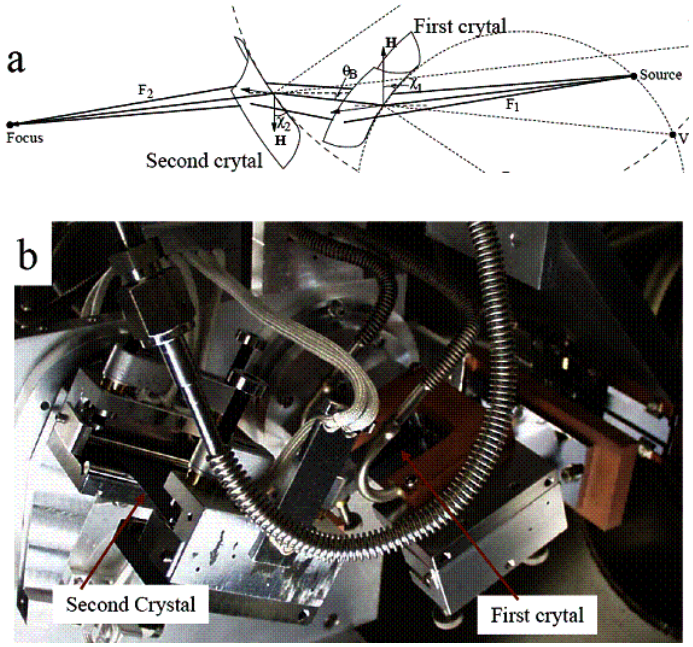

Figure 1: The mechanism of the sagittal focusing with asymmetric Laue crystals, bending of the crystals causes precession of the diffraction vector (H) around the axis of sagittal bending, and the resulting focusing of the diffracted beams. b) Photograph of a monochromator installed at the NSLS X17B1 beamline.

A double-crystal sagittally focusing monochromator, based on this concept, has been constructed and tested, and has been in use at the X17B1 beamline for two years, providing 67 keV x-rays (Figure 1b). It focuses a horizontal divergence of 3 milli-radians to a brightness-limited horizontal dimension of 0.2 mm. The x-ray flux-density at the focus was a few hundred times larger than that of unfocused x rays. Currently, using this device, flux on a small sample in a diamond-anvil cell is limited by the brightness of NSLS storage ring.

1. Z. Zhong, C. Kao, D.P. Siddons, H. Zhong, and J.B. Hastings, "X-ray reflectivity of sagittally bent Laue crystals", *Acta. Cryst. A* **59** (2003) 1-6.
2. Z. Zhong, C. Kao, D.P. Siddons and J.B. Hastings, "Rocking-curve width of sagittally bent Laue crystals", *Acta Cryst, A* **58** (2002) 487-493.

3. Z. Zhong, C.C. Kao, D.P. Siddons and J. B. Hastings, "Sagittal focussing of high-energy synchrotron x-rays with asymmetric Laue crystals, II: experimental studies", *J. Appl. Cryst.*, **34** (2001) 646-653.
4. Z. Zhong, C.C. Kao, D.P. Siddons and J. B. Hastings, "Sagittal focussing of high-energy synchrotron x-rays with asymmetric Laue crystals, I: theoretical considerations", *J. Appl. Cryst.* **34** (2001) 504-509.

After reviewing the current status of the sagitally-focusing double-crystal Laue monochromator, we do not expect any major technical difficulties to realize a final version of the device that could be integrated in the powder diffraction beamline, apart from the management of the rather large heat load expected on the set of necessary C and Si pre-filters, and also on the first crystal itself, and on the white beam stop that has to be positioned in between the two diffracting elements. In order to get a quantitative feeling of the challenges related to the large heat load inherent to the damping wiggler source, we have carried out a preliminary study focused on what could be reasonably thought to be the worst-case scenario: a full 7 m long damping wiggler and the maximum acceptance of the beamline of 1 (hor) x 0.15 (ver) mrad^2. Results are detailed in **Table 6.14 Power load on filters and crystals, on the powder diffraction beamline, for a fixed acceptance of 1 (hor) x 0.15 (ver) mrad^2.**

C Pre-filter thickness [mm]	Si Filter thickness [mm]	Power absorbed in C Pre-filter [W]	Power absorbed in Si Filter [W]	Power absorbed in first Laue Xtal [W]	Power dump in beam stop [W]
2	0	3331	0	1642	2435
2	1	3331	2246	354	1477
2	2	3331	2840	177	1060
3.5	0	4057	0	1182	2169
3.5	1	4057	1691	310	1350
3.5	2	4057	2215	159	977
5	0	4560	0	907	1941
5	1	4560	1341	271	1236
5	2	4560	1803	143	902
10	0	5578	0	457	1373
10	1	5578	724	180	926
10	2	5578	1037	102	691

and **Error! Reference source not found.** below.

Power load on filters and crystals for a fixed acceptance of 1x0.15 mrad^2 :

Table 6.14 Power load on filters and crystals, on the powder diffraction beamline, for a fixed acceptance of 1 (hor) x 0.15 (ver) mrad^2.

C Pre-filter thickness [mm]	Si Filter thickness [mm]	Power absorbed in C Pre-filter [W]	Power absorbed in Si Filter [W]	Power absorbed in first Laue Xtal [W]	Power dump in beam stop [W]
2	0	3331	0	1642	2435
2	1	3331	2246	354	1477
2	2	3331	2840	177	1060
3.5	0	4057	0	1182	2169
3.5	1	4057	1691	310	1350

3.5	2	4057	2215	159	977
5	0	4560	0	907	1941
5	1	4560	1341	271	1236
5	2	4560	1803	143	902
10	0	5578	0	457	1373
10	1	5578	724	180	926
10	2	5578	1037	102	691

As can be seen from the results, even with the thickest C shielding, it would be rather difficult to work with a single 2 mm Si filter in front of the Laue monochromator, because of the very high heat load that would not be sustainable by a single Si blade. It would then be necessary to split the overall 2 mm Si over several thinner blades, similarly to what is done with the C pre-filters. Moreover, the white beam stop after the first crystal should probably be a sloped block made of GlidCop as the total power and, mostly, the power density is still high and because of space constraints it may not be possible to design the stop with a very shallow slope to the incident beam. Finally, even with the max. shielding (10 mm C + 2 mm Si), there are still ~ 100 W dump in the first crystal and the large amount of shielding material would make the device transmission not very efficient below 30 keV. Careful attention should then be dedicated to the matching of protective material thickness vs. overall transmission and vs. power loading of all elements (filters, crystal and beam stop), unless the beamline acceptance is significantly reduced. The envisaged system design will result in an extreme stable, massive and compact system. The vacuum chamber will directly sit onto a solid U-shaped granite block avoiding efficiently amplifications from floor vibrations. Based on our approach of in-vacuum solutions the monochromator mechanics will be placed inside the vacuum vessel. As a result the design will be very compact avoiding vacuum feed-throughs for any movements and the mechanics of all movements will be placed to the crystals as close as possible. Therefore, the system will prove to be very stable and precise and will yield the following advantages: The intended design for the monochromator will permit operation in the energy range of 20-100keV with a constant beam offset of 15 mm upwards. The following adjustment units are shown in Table .

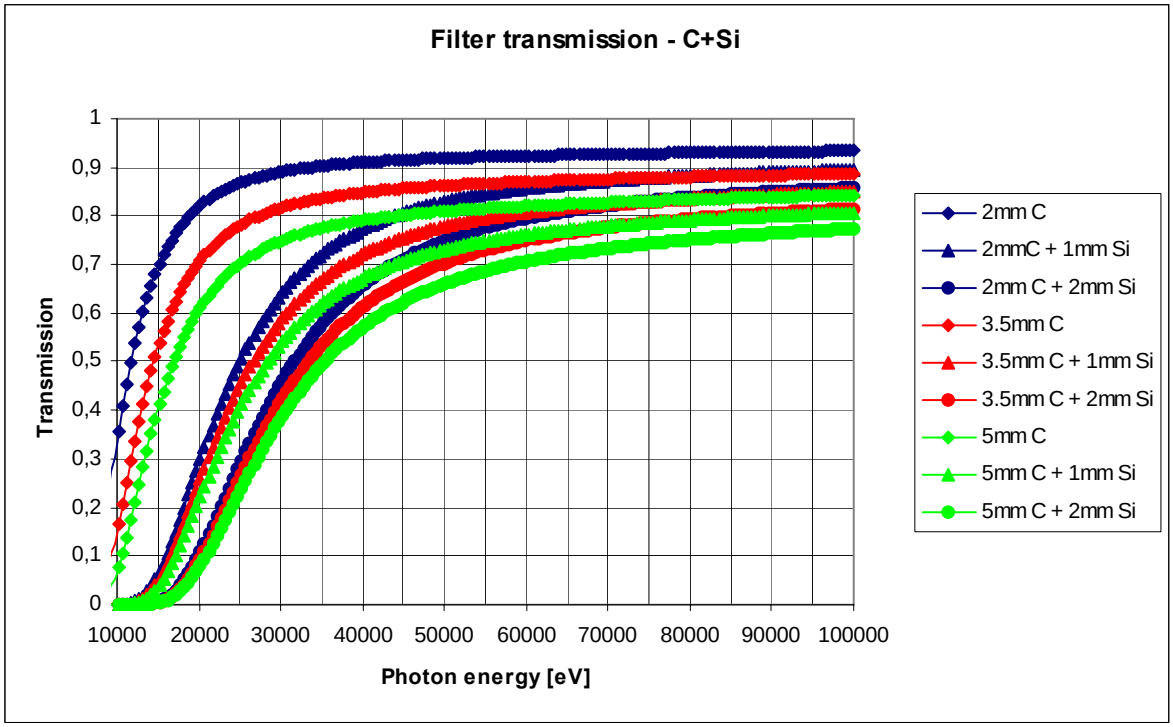

Figure 2: Transmission of various filter combinations on the powder diffraction beamline.

Table 6.15 Possible Adjustments for the Sagitally-Focusing Double-Crystal Laue Monochromator.
Bending adjustments are not shown in this table.

Movement	Range	Resolution	Repeatability
Whole optic assembly:			
Transversal (Y)	150 mm	≤ 5 µm	≤ 20 µm
1st and 2nd crystal units:			
Longitudinal (X)	500 mm	≤ 0.5 µm	≤ 20 µm
Yaw rotation (ϕ_1)	360°	≤ 10 µrad	≤ 10 µrad
Vertical (Z1)	40 mm	≤ 0.1 µm	≤ 5 µm
Roll rotation (χ_1)	-20 – 20°	≤ 10 µrad	≤ 20 µrad
Bragg rotation ($\theta 1_{coarse}$)	-5 – 35°	≤ 10 µrad	≤ 20 µrad
Bragg rotation ($\theta 1_{fine}$)	± 50 µrad	≈ 0.01µrad	≈ 0.06" (uni-directional)

6.4.3.4 White Beam Shutter

The white beam shutter is included in the front-end section (Section 6.4.1), and thus does not belong to the scope of supply for the beamline.

6.4.3.5 Vertically Focusing/Collimating Mirror

The basic design of the damping wiggler powder diffraction beamline foresees a single vertically collimating/focusing mirror placed in the front optical enclosure (white beam section), upstream of the sagitally-focusing double-crystal Laue monochromator. Nevertheless it has been decided to make provisions

for a possible upgrade of the beamline optics, leaving enough space in the beamline layout for the installation of a further horizontally/vertically focusing mirror (double toroid) downstream of this monochromator. Special attention has been paid to the cooling of the mirror, which is exposed to a significant level of absorbed power load and whose performance is rather critical in determining the ultimate energy resolution of the monochromator. An established technical solution for the mirror cooling, similar to the one that is implemented at the 7 Tesla superconducting wiggler HMI beamline at BESSY and at the Australian Synchrotron XAS beamline relies on indirectly cooling the mirror substrate with three Cu cooling blades immersed in a Ga-In eutecticum bath filling grooves machined in the optical surface of the mirror. This technical solution has already demonstrated to be able to cope with a total absorbed power load of the order of 2 kW but may fail for the even higher loads that the mirror may face at NSLS-II (Appendix D).

We have then explored two additional options that offer a better chance to withstand extreme heat loads: (i) Directly cooled Glidcop Mirror or (ii) Directly cooled Si Mirror. There is a possibility to use Glidcop as a mirror substrate material. This solution allows a direct cooling schema, which certainly has some advantages for higher power loads of a few kW (Appendix D). It should be noted that some doubts exist on the long term stability of Glidcop when exposed to the white beam and furthermore it is a more challenging material to polish than Si. A more favored direction is to use a directly cooled Si mirror. This technology is in use at beamlines at NSLS and the ALS and such mirrors can be realized with the requested quality. Provided that it is not directly exposed to the X-ray beam, the stability of the frit-bonding seems not to be a problem even after several years of use. Mirror specifications are shown in the table below.

Table 1 Specifications for the ACCEL vertically focusing/collimating mirror, for the powder diffraction beamline.

Mirror Substrate	Mono-crystalline Silicon (or Glidcop)
Direction of Reflection	Upwards
Shape	FLAT /cylindrically bent to tangential cylinder
Tangential Bending Radius	5.0 km - flat (> 40 km)
Sagittal Bending Radius	flat (> 1 km)
Substrate Length	approx. 1400 mm
Substrate Width	~ 120 mm
Substrate Thickness	60 to 70 mm**
Optical Active Surface: Length	1200 mm
Optical Active Surface: Width	2 x 35 mm (Si & Pt)
Sagittal Slope Error:	< 15 µrad rms
Tangential Slope Error:	< 2.5 µrad rms on 1200 mm (Best effort: < 2 µrad rms)
Micro Roughness	< 3 Å rms; best effort < 2 Å rms
Coating	Pt> 600 Å; Cr underlayer/ Bare central Si stripe
Cooling	Directly cooled

The ACCEL high stability mirror system mechanics is designed to be very robust, reliable and to allow easy access for maintenance and installation. A key design feature is that the mirror positioning mechanics is directly supported by a massive granite block that is mechanically decoupled from the vacuum chamber. This design allows to realize a very stable system and to greatly reduce the influence of vibrations propagating along the beamline. In order to get an as easy as possible access to the mirror, rectangular vacuum chambers are used. The chamber lid can be removed and then the entire mirror with its positioning mechanics is easily accessible.

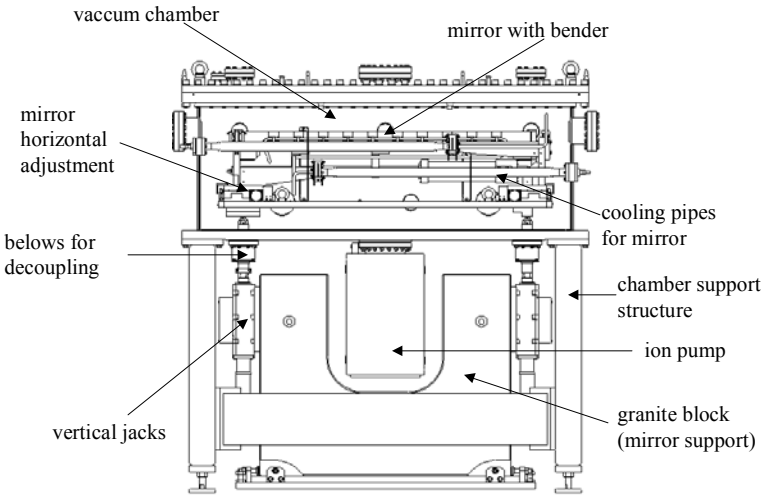

Figure 6.xx Side view of a high stability mirror system with a water-cooled bender.

Overall Technical Description. A very important design aspect of the high stability mirror systems is the complete mechanical separation between the optics and the vacuum chamber. This aims to avoid as much as possible vibration propagation to the mirrors. A massive granite block directly supports the mirrors holders/benders that are mechanically isolated from the vacuum chamber by means of edge-welded bellows. Another design guideline is to use in-vacuum actuators for the horizontal translation and its associated rotation (yaw), in order to (i) preserve the decoupling between the vacuum chamber with its support structure and the mirror with its positioner and (ii) to realize a system as compact as possible. Thus, two UHV compatible horizontal translation stages will be installed in the vacuum chamber (one at each extremity of the mirror), with one independent UHV compatible stepper motor each. Vertical translations will be performed by means of vertical jacks that also perform the two remaining rotations (pitch and roll). The mirror can thus be remotely adjusted in five independent degrees of freedom. All rotations (pitch, roll and yaw) will be realized by means of software pseudo-motors. Translations in/out of the beam will be realized by moving at the same time, of the same amount and in the same direction the three motors that act on the vertical jacks. Pitch and roll rotations will also be realized by the same three jacks. Horizontal translation (strip change) and yaw rotations will be realized by means of the two in-vacuum motors that act on the horizontal linear translation We suggest using a protective water-cooled steering mask between the mirror and the monochromator. It serves to better protect the monochromator interior or any un-cooled surface downstream from being hit by a mis-steered hot beam coming off the 1st mirror and further serves as a conductance limiting aperture for the vacuum performance between these two sections. To accommodate all operation modes of the beamline this mask has to sit on a vertical stage and will be equipped with edge welded bellows to allow for the necessary translations.

The mask will have water channels, I.D. 8 mm, with copper tubes brazed to it (no water-to- vacuum joints are used in our design). The material will be Glidcop and the impinging area will have a suitable slope so that it can withstand the high thermal stress that will be produced under worst conditions.

6.4.3.5 Beam monitoring elements

Beam monitoring elements are extremely important for beamline alignment. In this section, three such systems (as provided by ACCEL), are described: (a)Water-cooled White Beam CVD fluorescence screen The device consists of a retractable water-cooled CVD diamond foil, acting as x-ray screen, mounted to a pneumatic drive; the fluorescent effect is based on the residual doping with nitrogen atoms. The diamond screen is transparent, i.e. beam detecting further downstream is possible. The assembly is mounted to a

DN100 CF cross with one view port permitting a side view onto the screen. The pneumatic drive is equipped with limit switches. The vacuum feed-through is made of edge-welded bellows. The water lines are brazed to the screen support to avoid vacuum-to-water joints. The foil is clamped to the cooled support. The projection of the beam onto the 45° inclined foil will be monitored with a CCD camera. This system is capable of staying in the beam. However, because of the resulting absorption at photon energies below 10 keV, we advise to withdraw the screen when not in use. Moreover, to increase the lifetime of the foil and prevent overexposure of the camera, this screen should only be used at reduced power levels, i.e. in combination with some of the carbon filters. This screen has been installed at the high power wiggler beamline at the Australian Synchrotron Project.

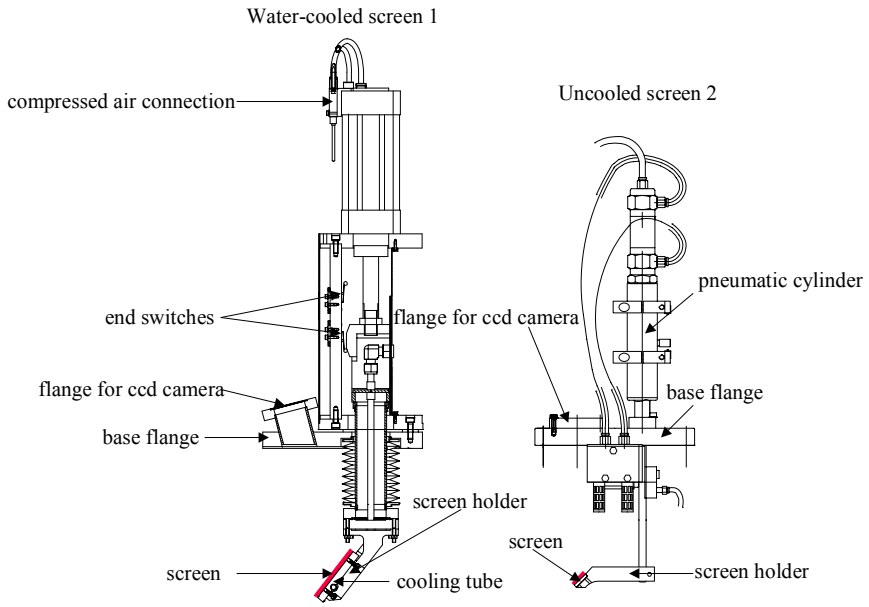

Figure6.xx Examples of ACCEL fluorescence screen beam monitors.

b) The fluorescence screen monitors typically are mounted to a pneumatic drive via a vacuum feed-through on a conflat flange. The water-cooled monitor is inserted in the beam by a stepper motor. The flange is also equipped with a view port for the camera that provides side view of the screen. Examples can be seen in Figure, for a water-cooled device and an un-cooled device.

c) Quadrant diode beam position monitor (4-diode BPM). ACCEL standard monitoring device for monochromatic beams of large size is a quadrant type detector that monitors the fluorescence yield of a target foil. Beam position information is derived from the intensity ratio of one pair of diodes. The device is rated for UHV and consists of a diode holder (holding four diodes) and a fluorescence foil holder. The four detecting silicon diodes are mounted to a vertical stage that permits the vertical positioning of the diodes which is necessary to operate the BPM at different beam heights.There are mounts for two foils, which can be of different kinds, or be the same. Typically, thin chromium and copper foils are used, but silver foils might be used as well. Chromium and copper have been working up to photon energies of around 20 keV. There is an option to mount a YAG crystal underneath this foil holder. Then, this YAG can be used to visualize the beam by means of a camera looking from the side onto a prism which is positioned behind the YAG. The assembly is designed such that it mounts to a CF100 flange and fits a standard size DN100 CF cross. The detection electronic for the diodes will be consisting of an integrated four-channel pico-ammeter with direct digital output.

d) The x-ray beam monitor is a commercially available visualization system for x-rays. Such a system provides a field of view large enough to study the beam size, beam profile and the beam position stability of a focused beam in the end-station (at atmosphere).

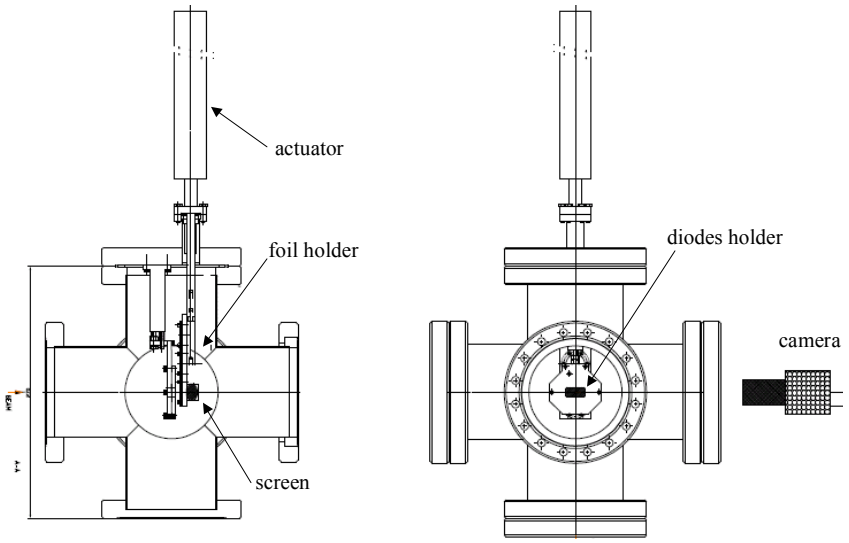

Figure 6.xx BPM (UHV rated) with diodes and fluorescent foil and screen.

6.4.3.6 Monochromatic Shutter

Although the powder-diffraction beamline anticipates using in-house fabricated monochromatic beam shutters, we include a description of the ACCEL photon shutter for completeness. These shutters consist of a high-density material absorber block, which is moved by means of a pneumatic actuator. The feed-through is mounted to a DN100CF flange. The motion of the pneumatic actuator is transferred to the absorber block through an edge-welded bellow, which has a guaranteed life time of 10^5 cycles. The absorber block is made of a Tungsten alloy having a Tungsten content of > 95% and a density of 17.5 g/cm³. The pneumatically driven actuator has a stroke of 60 mm. The pneumatic drive can be operated within a pressure range between 4 to 8 bar. The necessary magnetic valve is switched with a voltage of 24 V. The speed is adjustable by means of one-way restrictors. Each limit (upper and lower) of the stroke is indicated by two independent electromechanical switches. In case of failure (i.e. no power supply at the magnetic valve and no pressure at the pneumatic actuator), the shutter will close due to gravity. In Figure, we present a shutter that was recently designed for GM/CA-CAT (APS) and CMCF (CLS) where redundancy in form of double actuators was required.

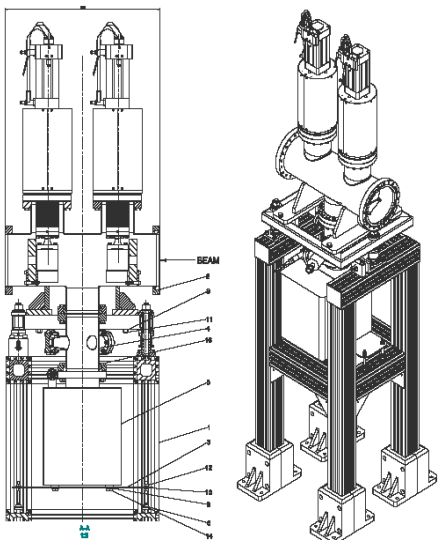

Figure 6.xx Sketch of one of ACCEL's monochromatic photon shutters.

6.4.3.7 Vacuum windows

A typical solution for the final widow in the powder diffraction beamline is to use a Be foil of appropriate aperture, diffusion bonded to a stainless steel double sided flange. The exit Be window will be carbon coated to protect the beryllium surface against oxidation in air.

Table 6.xx Specifications for the final Be window in the powder-diffraction beamline.

General:	
Material	stainless steel flange
	CF100
Foil material	Be-foil, PF-60, both sides polished
Foil thickness	0.250 mm
Aperture size of Exit window	tailored

6.4.3.8 Enclosures

There will be three beamline radiation enclosures at the damping wiggler powder diffraction beamline; one first optics enclosure (FOE) and two experimental hutches. The FOE contains all beamline optics (filter units, mirror, monochromator, beam monitoring assembly and photon shutter), and will be a white beam hutch. The FOE with its lead shielded sides interfaces to the ratchet wall of the storage ring. Following the standard regulations for white beam hutches, the labyrinths to run electricity as well as media and power connections will be located on the roof. The hutch will be very long (approx 17 m) to accommodate the optics for both the original beamline and possible optics for a canted beamline. One double door with sliding panels, large enough to move in larger components using a fork lift, will provide access to the hutch. Based on our experience with regulations at national US laboratories and following the ALARA practice we have based our evaluation for the FOE on the more conservative numbers for lead shielding that are presented in the document, NSLS-II Technical Note 014, Table 6, i.e. following the thickest lead shielding requirements for the FOE (see details below). The beam transport between the FOE and the first experimental hutch will be a tunnel type (coffin style) transport. Such an enclosure design will provide enough flexibility to accommodate vacuum pipes for beamlines. The shielding of interfaces such as guillotines etc. is included. All three

enclosures will be equipped with an overhead crane (one metric ton), several labyrinths and sliding doors. A summary of the specifications is as follows:

First Optics Enclosure, white beam hutch (FOE):

	Upstream wall 2 m x 3.3 m	Sides 17.5 m x 3.3 m	Downstream wall 3 m x 3.3 m	Roof 17.5 m x 2.5 m
Shielding requirements Lead [mm]	16 mm	23 mm	50 mm	14 mm

- one extra panel of size 1 m x 1 m x 50 mm at downstream wall centred at 1400 mm above floor
- one sliding double door (white beam hutch)
- 10 times chicane on the roof, all chicane with hinges
- one hutch crane, 1 metric ton
- one set of guillotine, adjustable shielding around beam pipe on downstream wall
- painted with primer

Shielded Beam Transport (coffin style, base with lid):

Lead shielding of 7 mm thickness.
Dimensions: 2 m long, 0.4 m x 0.4 m cross section
Support stands every 2 m with gussets.
Painted with primer

Upstream Experimental Enclosure, monochromatic hutch (EH-1):

	Upstream wall 4 m x 3.3 m	Sides 7 m x 3.3 m	Downstream wall 4 m x 3.3 m	Roof 7 m x 4 m
Shielding requirements Lead [mm]	6 mm	6 mm	6 mm	5 mm

- One sliding door
- 5 times chicane on the roof, 3 times chicane on the sides, all chicane with hinges
- one hutch crane, 1 metric ton
- one set of guillotine, adjustable shielding around beam pipe on upstream wall
- painted with primer

Downstream Experimental Enclosure, monochromatic hutch (EH-2)

	Upstream wall 4 m x 3.3 m	Sides 7 m x 3.3 m	Downstream wall 4 m x 3.3 m	Roof 7 m x 4 m
Shielding requirements Lead [mm]	6 mm	6 mm	6 mm	5 mm

- One sliding double door
- One sliding single door
- 5 times chicane on the roof, 3 times chicane on the sides, all chicane with hinges
- one hutch crane, 1 metric ton
- one set of guillotine, adjustable shielding around beam pipe on upstream wall
- painted with primer

Provision will be made to run cable trays and utilities inside and outside the hutches.

6.4.4 Instruments

This section describes the end-station instrumentation necessary to perform high-energy high-resolution powder diffraction. The scope of the powder diffraction beamline allows for one end-station (Endstation 1), that will allow high-energy high-resolution powder diffraction, with the other optical enclosure (most upstream enclosure) to be populated in the future – possibly by existing NSLS-I equipment and served by a canting wiggler source in the high-β straight-section.

6.4.4.1 Endstation 1

This section describes the high-energy high-resolution powder diffraction end-station. Our current thinking in designing this facility is to use equivalent set-ups employed at various high-energy high-resolution powder diffraction stations at other synchrotron radiation facilities. In general, the end-station consists of a highly accurate 3-axis diffractometer: One axis is used for sample orientation (or spinning), the second axis holds a fast read-put position sensitive silicon strip detector for in-situ time-resolved studies and remains essentially fixed, and the third axis is used to hold a multi-crystal silicon array analyzer system that can be rotated in the vertical diffraction plane. The scientific drivers for this particular instrument has been outlined in the first two sections of this chapter. Two high-resolution diffractometers, whichexist at various high-resolution powder diffraction beamlines, could be employed at this beamline.. We show two multi-channel crystal arrays on the drawing (Figure 14, taken from the SLS design), but a different design and large array could be easily envisaged. The resolution of the rotary stages need to be highly accurate to obtain accurate peak positions and reliable data. The Newport and RPI systems have the necessary resolution to enable the operation of this facility. The other all resolution of the system should provide peak shape resolution of < 5 milli-degrees, thus allowing accurate peak profile measurements essential in the study of strain, microstructure and lattice defects. Mython strip array detectors (PSI design) are to be installed at the DIAMOND, SLS and Australian synchrotron facilities and our design will incorporate similar technology; a 7000-element silicon strip detector array currently being fabricated at the NSLS for in-situ real time material studies. A variety of sample environments (not shown) has been included in our budget, consisting of cryostats, furnaces, laser heating and diamond-anvil cells for high-pressure research. In addition, a robotic sample chamber has been included (not shown) for high-throughput measurements for combinatorial investigation and screening purposes. The overall design is relatively standard, except for the inclusion of a graded bendable multiplayer system that will be used to focus the beam to ~ 14 microns in the horizontal for studying small samples (e.g. for high-pressure diamond-anvil cell research). This mirror is located relatively close to the sample position to minimize beam motion as the multiplayer is rotated to match the incoming x-ray wavelength.

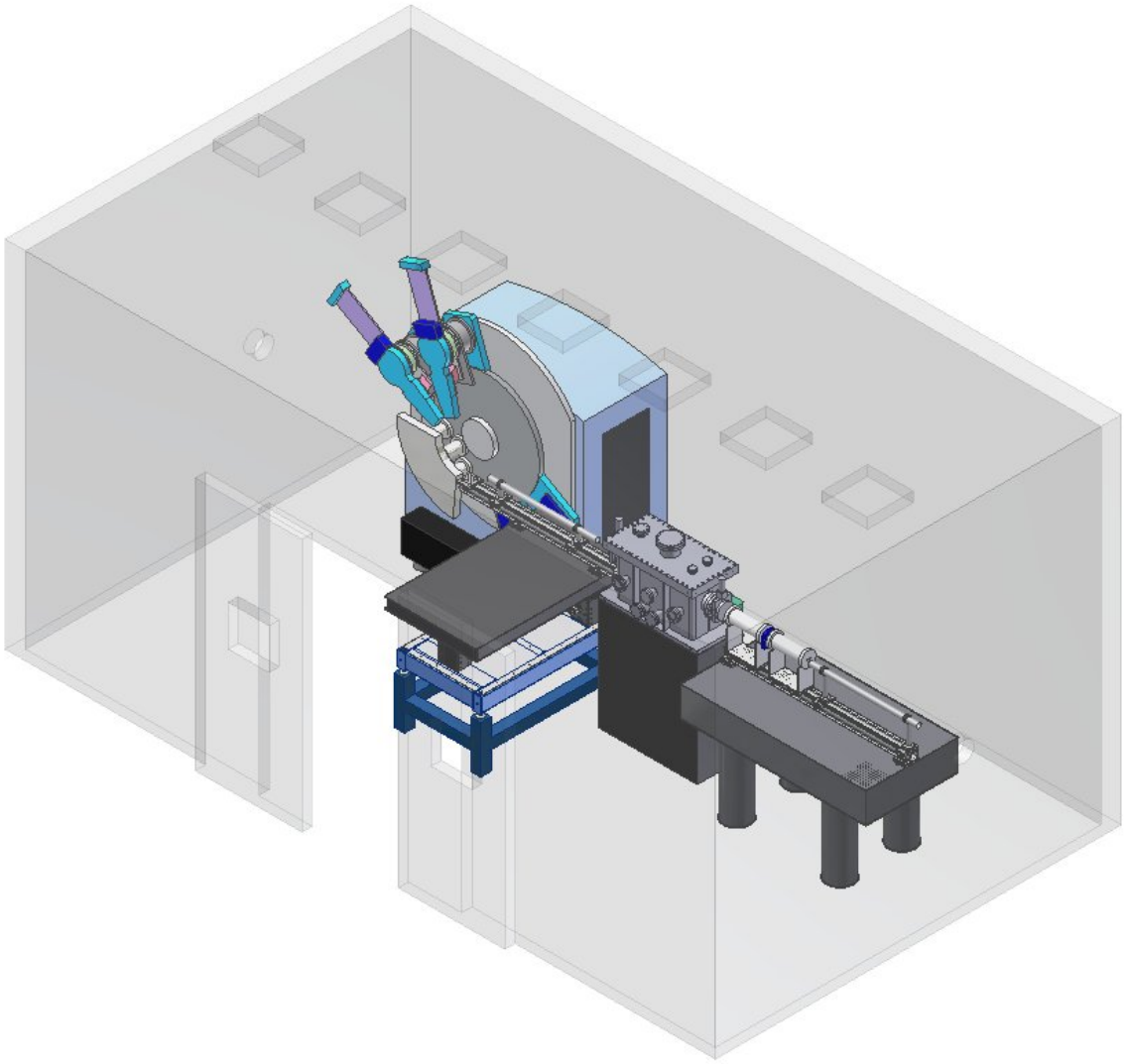

Figure 3: Conceptual design of the NSLS-II high-energy high-resolution powder diffraction beamline. For clarity, sample environments (such as crysostats, furnaces and diamond-anvil cells) and a robotic sample changer for high-through-put applications are not included in the figure.

6.4.4.2 Endstation 2

Although not in the scope of the present NSLS-II project, the most upstream optical enclosure is included to serve as a possible second powder diffraction beamline. This second beamline, which could be served by a canted wiggler source in the high-β straight section, could be populated by existing NSLS-I equipment. For example, there are many Huber diffractometers, several CCD cameras and robotic sample changers operational at NSLS beamlines at this current period of time.For example, we show in Fig XXX, a routine powder diffraction setup, with a huber diffractomer, with a ccd camera on a 2-theta arm. We anticipate such a facility would also be in high demand at the NSLS-II machine.

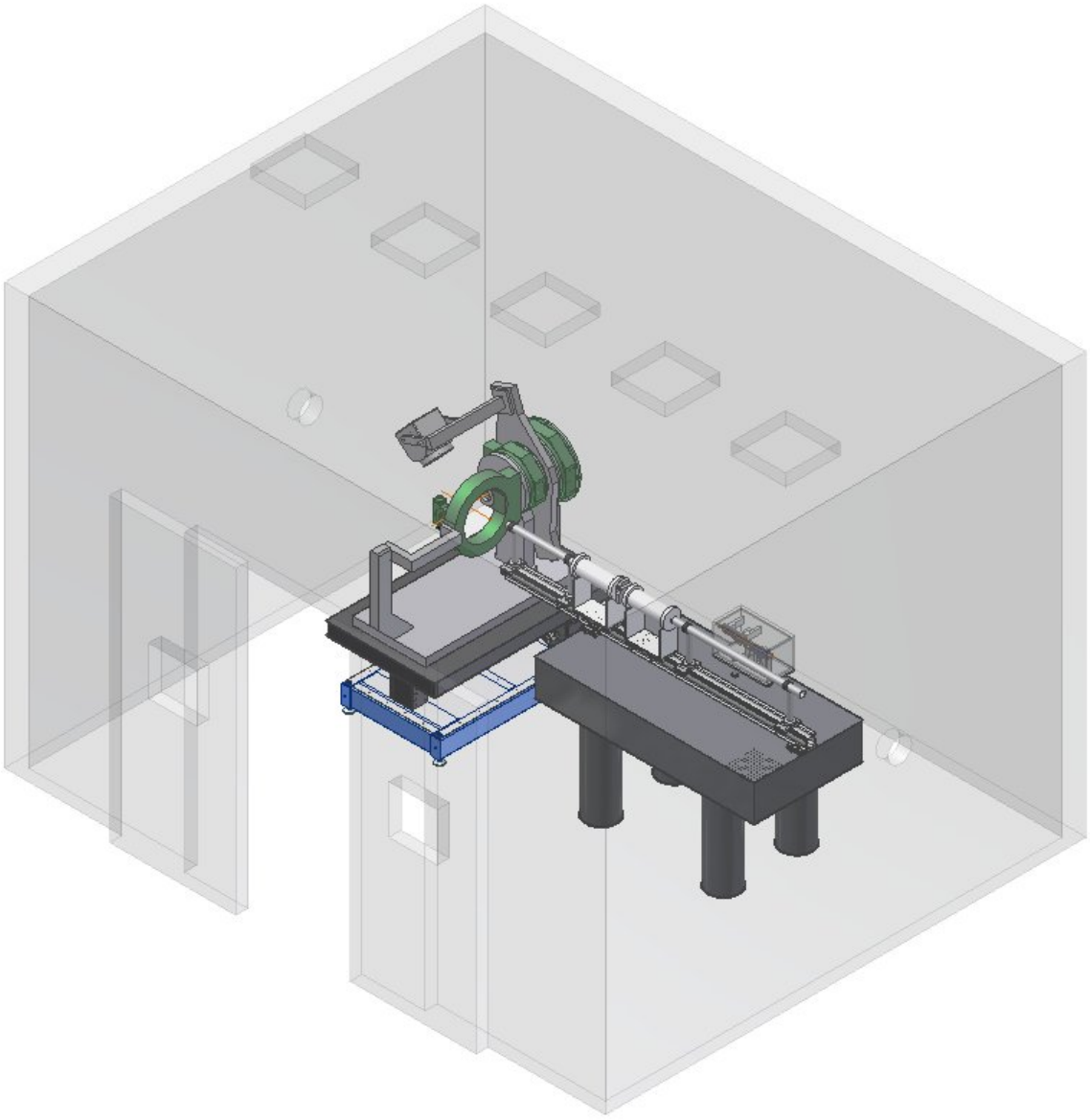

Figure 4 Conceptual layout for a second powder diffraction beamline, upstream of the high-energy high resolution NSLS-II powder diffraction beamline. Note that this end-station is not in the current scope of the NSLS-II project.

6.5 Additional Requirements Imposed on the Conventional Facilities

Powder diffraction experiments will be performed in both the high-resolution (crystal array) and area detector modes. The crystal analyzer is the most demanding in terms of angular stability, since it aims to provide high d-spacing resolution and precision. The area detector mode is primarily affected by position stability. Both modes are sensitive to beam energy changes.

In the crystal analyzer mode, the critical requirement is angular stability. A typical powder peak width using an analyzer crystal is in the range of 0.001^{o} to 0.01^{o} at 17 keV, depending on the sample quality. 0.001^{o} is unusually good. Let us consider 0.005^{o} as typical. Then, the photon beam stability should be 10% of this value i.e. 0.0005^{o}, or 8 μrad.

A related concern is the energy stability, since energy maps directly to d-spacing in a diffraction experiment. Using Si(111), it's intrinsic energy resolution, $dE/E \sim 10^{-4}$, which sets a limit on what we can achieve with a sample. If we assume we can find centroids to a few percent of this, we end up with an energy stability requirement of at least 10^{-5}. This maps to an angular stability of 1 or 2 μrad [Si(111) at 17 keV has a Darwin width of 15 μrad], and a monochromator temperature stability of 10 Kelvin.

All of the above arguments are directed in the vertical plane of diffraction.

Area detector measurements are typically 10 times or more lower resolution than using a crystal analyzer, so angular stability is not the limiting case. In contrast to the crystal analyzer mode, position stability is important, since position is used as an angle analogue. If we assume a focused beamline with a focal spot of 100 μm and a detector with similar spatial resolution, then using the '10% rule', beam stability should be on the 10 μm level. Similar arguments apply to energy stability. In this case, the spatial stability requirements are in both the horizontal and vertical directions.

TABLE OF CONTENTS

1 CONVENTIONAL FACILITIES OVERVIEW

1.1 Introduction

The NSLS-II conventional facilities will provide the structures and systems necessary to enable installation and operation of the accelerator and experimental beamlines. The conventional facilities must be designed and constructed to enable the world-leading performance objectives of the project mission. Furthermore, the conventional facilities must be constructed on an aggressive schedule that enables installation of the accelerator systems and experimental beamlines in accordance with the project schedule goals. Lastly, the conventional facilities must meet the functional and aesthetic goals of creating an economically vibrant research facility that achieves technical excellence and is adaptable to the varied and changing requirements of the user community. This report describes the scope and design considerations for the NSLS-II conventional facilities.

1.2 Project Goals

The goals of the conventional facilities portion of the project support the overall goals of the NSLS-II project. These goals provide the guiding principals for preliminary design of the conventional facilities.

- World-class scientific capability
- Promote collaborative interaction
- Flexible building capability
- Economic construction and operation
- Sustainable design
- Phase construction to allow earliest start of accelerator installation

1.3 Project Description

The NSLS-II conventional facilities will be designed to provide the buildings, services and utility infrastructure needed to support the technical scope of the project and the mission of a high technology user facility. The selected site is at the southeast corner of the present intersection of Brookhaven Avenue and Groves Street. The facility will be proximate to the existing NSLS Building and the recently constructed Center for Functional Nanomaterials, (CFN) as indicated on the site plan, Figure 1.1.

The conventional facilities will consist of a Ring Building to house the accelerator and associated beamlines, an Injection Building for the compact booster, and linac, a two story Operations Center for the control room function, three Lab Office Buildings (LOB's) for beamline staff and the beamline user community, an RF Building, and five two story Service Buildings containing mechanical and electrical equipment. Additionally, the overall building complex is being planned to include two additional future Lab Office Buildings, the Joint Photon Science Institute (JPSI) Building and possible locations for future scientific buildings. An alternate for a third floor to the Operations Center is also being considered to provide office space for NSLS-II management and accelerator scientists. These additional buildings are considered alternate or future construction and are not included in the Program or Cost of the NSLS-II project.

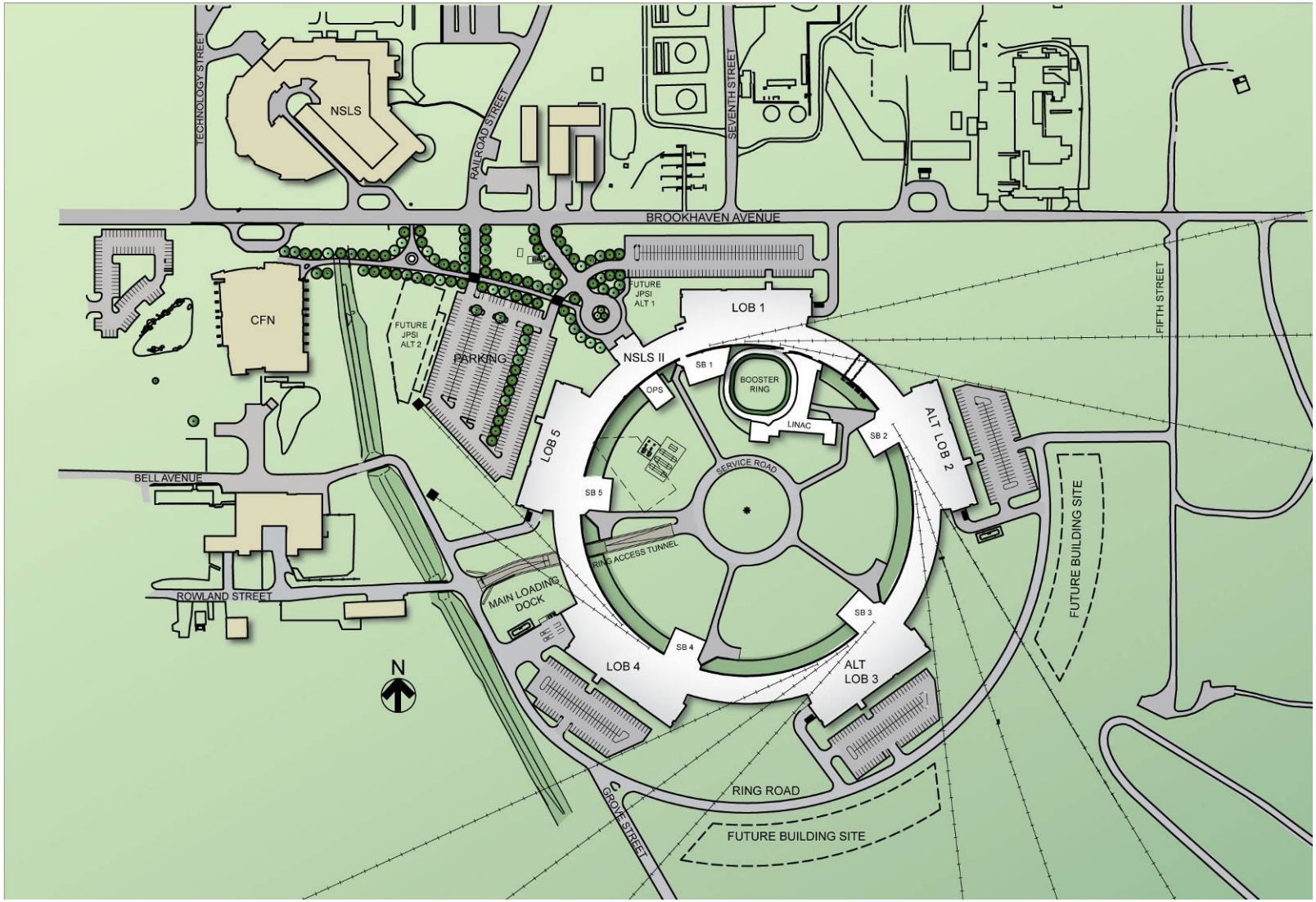

Figure 1.1 NSLS-II Site Plan.

An architectural rendering of NSLS-II, shown in Figure 1.2, indicates the preliminary design architectural theme for the facility. Figure 1.3 indicates the floor plan and functional relationships of the built-out NSLS-II complex. The approximate gross area for each of these buildings is shown in Table 1.1. The building program is discussed more fully in the Architectural Section of this report.

Table 1.1 NSLS-II Area.

Building Component	Net Area (ft^2)	Gross Area (ft^2)
Operations Center	9,232	11,600
Injection Building	17,693	24,440
RF Building	10,182	10,630
Ring Building	219,888	240,075
Service buildings (5)	48,130	53,640
Lab Office Buildings (3)	50,358	71,536
Total NSLS-II	355,483	411,921

Figure 1.2 Architectural rendering of NSLS-II.

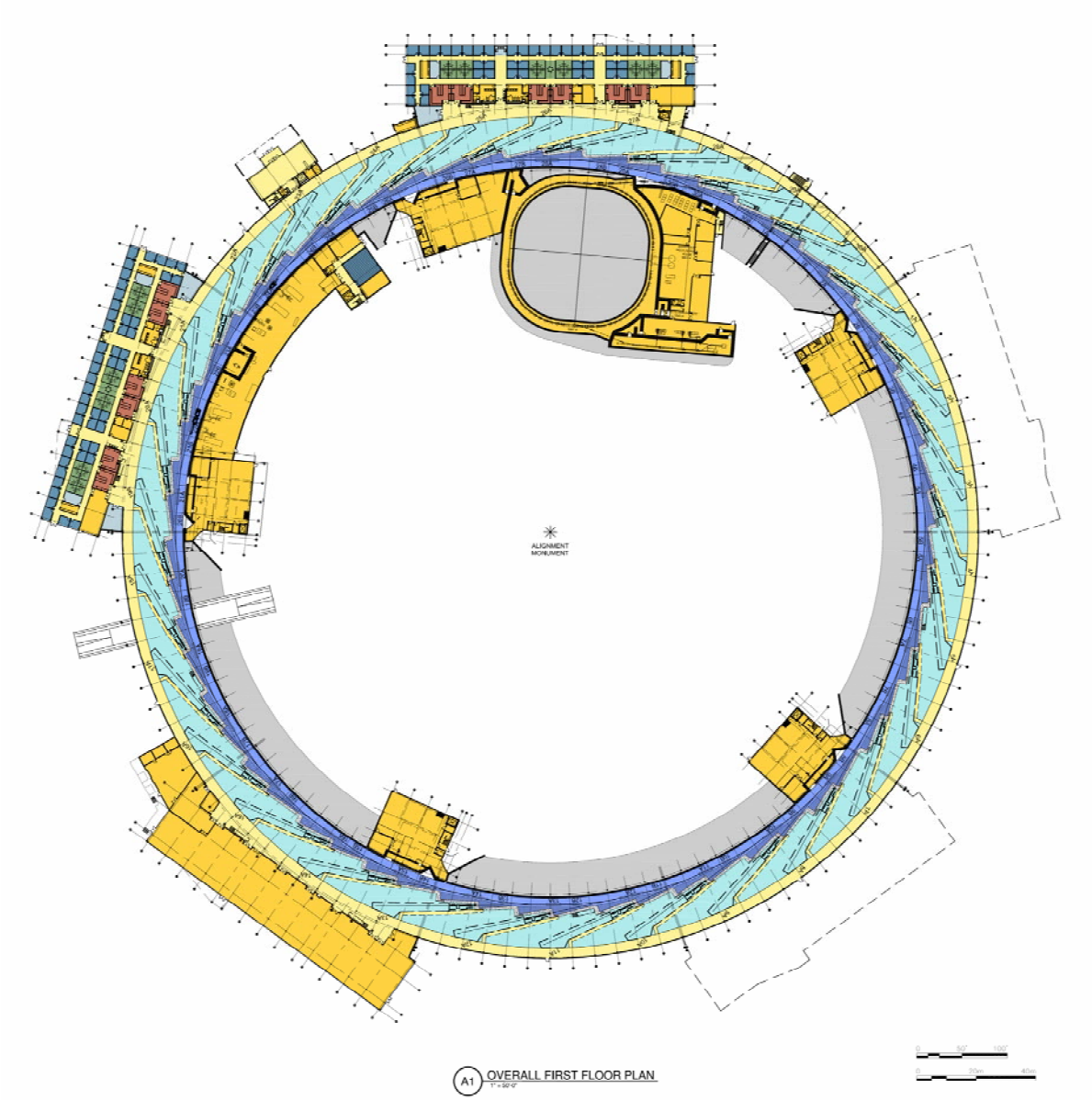

Figure 1.3 NSLS-II Complex Layout – First Floor Plan.

1.4 The Design Process

The NSLS-II site, located at the present intersection of Brookhaven Avenue and Groves Street is at the eastern boundary of the Science and Technology zone in the BNL Master Plan. It is the last parcel in the Brookhaven Avenue corridor development plan. The site is well suited to construction of NSLS-II given its close proximity to the existing NSLS and CFN buildings and has many advantages in terms of constructability including a relatively level and mostly clear site, good geologic conditions, good access to utilities and low background vibration levels.. The NSLS-II site plan comprises the following: NSLS-II Ring Building Complex - the heart of the project where scientific experiments are conducted, the loop road circling around the building, allowing access to Lab Office Buildings and connected to a vehicle tunnel for emergency and maintenance vehicle access to the inner Ring road area, and the service drive inside the ring for vehicle

access to the Operations Center, Injection Building, Service Buildings and storage ring tunnel. For planning purposes, additional elements which are not part of this project, are indicated on the site plan. These include the proposed Joint Photon Science Institute and possible future scientific buildings.

The current site design supports the need for reasonable proximity to the existing NSLS and the CFN. The existing NSLS will continue to provide office and technical support space for NSLS-II staff, thus the NSLS-II footprint has been moved as far West and North (close to NSLS) to minimize travel distance for these staff. This siting also supports anticipated collaborative interaction of the CFN with NSLS-II. The proposed landscaped walkways link all building main entrances and outdoor interaction spaces encouraging exchange of ideas among scientists. In addition Groves Street is discontinued from Bell Avenue to Brookhaven Avenue to discourage through traffic near the NSLS-II building. There will be a formal drop-off, circle drive in front of the NSLS-II main entrance lobby at the Operations Center Building which would be highly visible from the main entrances to the CFN and existing NSLS buildings.

Another important issue in development of the NSLS-II site plan was to maximize opportunities for installation of extra-long beamlines that would extend beyond the Ring Building walls and into the surrounding landscape. The NSLS-II orientation on the site, as well as the location of each LOB is influenced by the best possible location for these future extra long beamlines. Due to existing site topography and site access issues, the most preferable locations for the longest beamlines (up to several hundred meters) are in the easterly direction between LOBs 1 and 2, and southeast between LOBs 2 and 3. Opportunities for extra long beamlines of 100 – 200 meters are also available between LOBs 3 and 4 and between LOBs 4 and 5.

1.5 Work Breakdown Structure

The work breakdown structure for the NSLS-II conventional facilities is shown in Figure 1.4.

Figure 1.4 NSLS-II Conventional Facilities Work Breakdown Structure.

1.6 Method of Accomplishment

1.6.1 Design

Title I and Title II design of the NSLS-II conventional facilities will be performed by an A/E firm under contract to BNL. HDR Architecture has been competitively selected to provide design services for the NSLS-II main buildings and facilities. Title I and II design of the expansion of the Central Chilled Water Facility will be performed by Giffels Engineers. Each firm will also optionally provide Title III support services for shop drawing review, field verification and engineering support during construction.

Additional engineering support will be provided by BNL Plant Engineering Division to assure that new utility services and systems provided by NSLS-II are compatible with existing BNL utility systems and are properly interconnected.

The conventional facilities design team led by HDR includes the following firms:

- HDR Architecture, Inc.
- GEI Consultants, Inc.
- Colin Gordon Associates, Inc.
- VitaTech Engineering, LLC
- VJ Associates
- EMO Energy Solutions, LLC
- Municipal Land Survey, P.C.

1.6.2 Construction Management

Construction management of NSLS-II conventional facilities will be performed by the NSLS-II conventional facilities team with staff augmentation support services from a competitively procured construction management firm. The joint venture of Liro/Gilbane has been selected to provide design phase construction management services. Procurement of construction phase construction management services will be via a competitive “best value” process awarded prior to award of the main construction contracts.

1.6.3 Procurement & Contracting Plan

Conventional construction will involve construction of the NSLS-II complex of buildings and improvements to land and utilities including expansion of the existing Central Chilled Water Facility. These will be procured generally as lump-sum competitively procured contracts to general contractors. It is anticipated that there will be one major contract for the complex of buildings to be constructed on the NSLS-II site and a series of smaller construction packages for specialized work scope that has clearly defined interface points with the main construction contract. The anticipated construction packages are:

1. Site Preparation - Certain aspects of the site preparation work will be contracted as an early package to clear and prepare the site, reduce risk of unforeseen underground conditions and reduce overall schedule duration of the main contract.
2. Ring Building Complex -The main Ring Building contract will encompass site development and construction of all the NSLS-II buildings and on-site utilities and systems.
3. Central Chilled Water - The Chilled water contract will expand the Central Chilled Water Facility to provide cooling capacity to NSLS-II. This will be jointly funded by BNL and NSLS-II

4. Electrical Substation – The electrical substation contract will expand the main site electrical substation to provide electrical power to NSLS-II

Additional smaller packages may be issued as advantageous to the project. The contractors will be selected based on a competitive evaluated bid whereby the award is given to the firm meeting all technical, management, financial, past performance record, and safety qualifications for the project at the best value.

1.6.4 Construction Schedule

The construction schedule for conventional facilities is fully integrated with the overall resource loaded schedule for the NSLS-II project. Design and construction of conventional facilities is essentially the critical path for the project until such time as beneficial occupancy of the buildings can be accepted and installation of the accelerator systems can begin. In order to enable earliest start of accelerator systems installation, the Ring building construction will be broken into phases enabling earliest completion of pentants (or 1/5 of the Ring Building circumference) and each pentant will be accepted as early as possible. Scheduling of installation of various utility systems has been coordinated to support this phasing.

1.6.5 Construction Safety

Maintaining a safe work environment and the prevention of worker injury is paramount to the success of conventional facility construction. Specific construction safety measures are detailed in the Final Hazards Analysis and the ESH section of the project Preliminary Design Report. Among the measures that will be taken to assure worker safety are:

1. Selection of contractors based on a proven record of safety performance
2. Designation of dedicated full time safety oversight staff as part of the NSLS-II team, the construction manager and each contractor
3. Development and implementation of a robust and effective construction safety plan governing all work on the project that utilizes integrated safety management principles
4. Line management responsibility for safety and active oversight and intervention as needed
5. Use of construction safety incentives to motivate outstanding safety performance

1.6.6 Quality Assurance

The project will be conducted in accordance with BNL's site-wide Quality Assurance Program (QAP) that applies to all work conducted at BNL. The BNL QAP conforms to the requirements of Department of Energy (DOE) Order 414.1, Quality Assurance, and 10CFR 830 Subpart A, Quality Assurance Requirements. BNL's QAP consists of the following ten criteria:

- Program
- Personnel Training and Qualification
- Quality Improvement
- Documents and Records
- Work Processes
- Design
- Procurement
- Inspection and Acceptance Testing
- Management Assessment
- Independent Assessment

BNL's approach to satisfying the requirements of these criteria are delineated in the BNL Quality Assurance Program Description within the BNL Standards-Based Management System (SBMS). The NSLS-II design, construction and operation are subject to the QAP. A key element of the QAP is the concept of "Graded Approach", that is, applying an appropriate level of analysis, controls, and documentation commensurate with the potential to have an environmental, safety, health, radiological, or quality impact.

The NSLS-II QAP has been developed and addresses both the conventional and technical aspects of the project. This plan addresses project activities from design through construction, as well as commissioning and startup. The sections of the NSLS-II QAP applicable to conventional facilities address the basic design and construction of the building and utilities systems executed by the NSLS-II Conventional Facilities Division. Requirements of the NSLS-II QAP will flow down to contractors performing design and construction of conventional facilities.

1.6.7 Value Management

Value Management (VM) will be performed for this project as required under DOE Order 413.3A, "Program and Project Management for the Acquisition of Capital Assets." An independent value management team will perform VM review during Title I design. A VM report will be provided to the NSLS-II Project Director for consideration and, where feasible, incorporation into project design documents.

The VM review will be a systematic review of the mature Title I design performed by an independent team of qualified consultants. The team will comprehensively review design elements and material selections with regard to their needed level of performance and quality. Alternate methods, elements and selections that meet the necessary performance and quality will be considered. The comparative first cost and life cycle cost of these alternatives will be determined and compared to the original design. A VM report will be prepared indicating alternatives considered, their respective costs and recommendations as to which alternatives should be implemented in the project design.

A Value Engineering Workshop was conducted with Liro/Gilbane and independent VE specialist hired by BNL on Wednesday and Thursday October 3rd and 4th, 2007. The results of this workshop are not finalized as of this writing but several VE items have been incorporated into the 100% Title 1 submission. They have been incorporated in one of two ways.

- The drawings and other documents were changed to incorporate the VE item.
- A note was added to the documents that addresses the VE item with the understanding that further design and/or investigation needs to be done to fully incorporate the VE item.

1.6.8 Commissioning

An important element in the ultimate success of the NSLS-II will be proper commissioning of the facilities systems and instruments. The sensitivity of the storage ring and research beamlines requires that all systems and instruments achieve their maximum performance capability to fulfill the research mission. Additionally, any systems or equipment that can create environmental disturbance must be properly calibrated, balanced, tuned, or shielded to prevent detrimental impact to the research. During the design phase, a preliminary facility commissioning plan will be prepared to assure that appropriate commissioning requirements have been included in the NSLS-II design. The commissioning plan will:

- Present a schedule and sequence for start-up of building systems and instruments, including dependencies linked to the conventional or technical construction schedule.
- Identify safety approvals required prior to start-up
- Identify systems and instruments at the equipment level that will require commissioning.
- Identify references and sources of start-up procedures and performance, test and acceptance criteria for the instruments and equipment.

- Identify whether the equipment will be commissioned by BNL staff, contractor staff, vendor staff, or if the services of a specialty commissioning contractor are warranted.
- Identify the point at which equipment has been accepted and can be turned over to operations staff.
- Be updated during the design and construction phases as appropriate to reflect changes in equipment selection and performance.

2 SITE / CIVIL

2.1 Design Criteria

2.1.1 Codes and Standards

The latest edition of the codes, standards, orders, and guides referred to in this section will be followed, with a reference point of August 2008 being the anticipated design completion date. All work will be in accordance with BNL's Implementation Plan for DOE 413.3, "Program and Project Management for the Acquisition of Capital Assets."

2.1.2 DOE Orders

DOE O5480.4 – Environmental Protection, Safety and Health Protection Standards
DOE O413.3A – Program and Project Management for the Acquisition of Capital Assets
DOE O414.1C – Quality Assurance
DOE O420.1B – Facility Safety
DOE O420.2B – Safety of Accelerator Facilities

2.1.3 Codes, Standards, and Guides

10CFR851 Worker Safety and Health Program
Building Code of New York State (NYSBC) – 2002 Edition
American Concrete Institute
Building Code Requirements for Structural Concrete (ACI 318-99)
BNL Standards Based Management System Subject Areas
New York State and Suffolk County Department of Health Codes
American National Standards Institute
ANSI 117.1 Accessible and Useable Buildings and Facilities
American Society for Testing Materials Standards
National Institute of Standards and Technology
Occupational Safety and Health Administration (OSHA)
New York State Fire Prevention Code - 2002 Edition
ACGIH Standards
Americans with Disabilities Act Accessibility Guideline (ADAAG)
Leadership in Energy and Environmental Design (LEED) 2.2
LEED for Labs

2.2 Site Description

The location for the proposed NSLS-II site is based upon several criteria and includes the ability to comply with environmental requirements; the ability to meet research mission objectives; the physical proximity to collaborative BNL research facilities in the new Center for Functional Nanomaterials (CFN) and the existing NSLS, constructability factors related to site conditions; economic factors affecting project cost; conformance with BNL strategic planning goals and the ability to support future expansion and long beam lines. The site selected for construction of the NSLS-II meets all of the criteria indicated above. The site design also responds to these criteria. The NSLS-II site plan is shown in Figure 2.1.

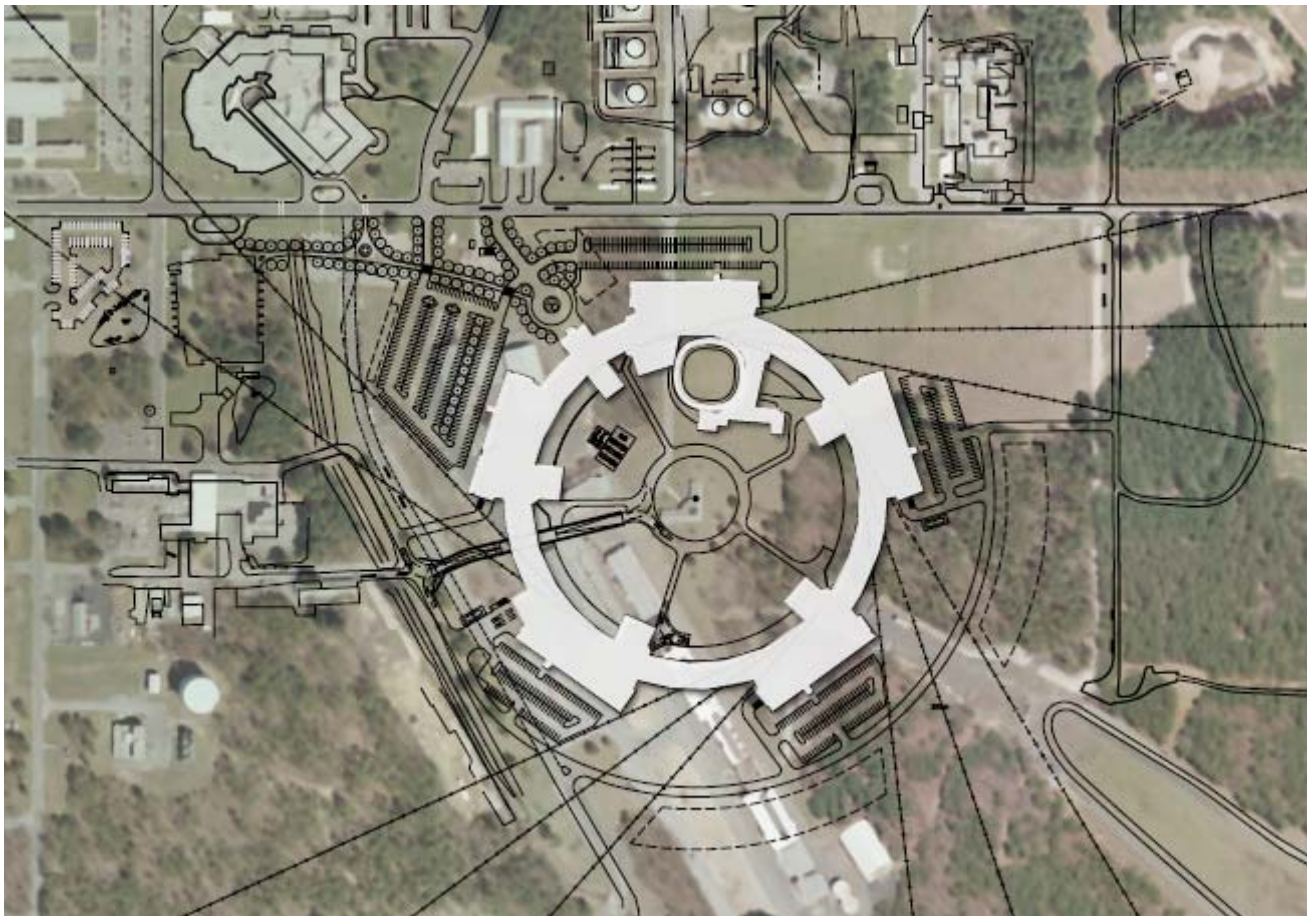

Figure 2.1 NSLS-II Site Plan.

2.3 Campus Planning

The site is approximately 50 acres located at the southeast corner of the intersection of Brookhaven Avenue and Groves Street on the BNL campus. Master planning envisions Brookhaven Avenue becoming the primary east–west arterial street through the BNL campus. Land adjacent to Brookhaven Avenue is considered desirable for current and future building projects at BNL, including NSLS-II. The architectural vocabulary along this axis is transforming in character from traditional masonry aesthetics to the west to an advanced technology image to the east.

Located at this strategic location along Brookhaven Avenue and together with the CFN, NSLS-II will form a significant “sciences” focal point, and further emphasize BNL’s commitment to newer facilities that promote leading-edge discoveries.

Locating NSLS-II here allows for future extended beamlines of up to 1000 m in length. These may eventually project eastward along Brookhaven Avenue, or have a disposition that is to the southeast or the south. The site accommodates many future options for BNL.

The adjacencies that NSLS-II will leverage at this site are highly advantageous. The existing NSLS building located diagonally across Brookhaven Avenue to the northwest, will promote ease of interaction between that building and NSLS-II. This is particularly important since many of the NSLS-II staff will office

in the existing NSLS building. This location will also simplify the relocation of equipment and staff between the two facilities. Additionally, the site is situated directly adjacent to the CFN (across Groves Street to the west). This adjacency will provide for unparalleled opportunities of collaborative research between two of the nation's premier science facilities. Locations for the potential Joint Photon Source Institute (JPSI) building have also been proposed, one near the Operations Center another in the northwest corner of the site or possibly across Brookhaven Avenue just east of the existing NSLS. This building would be a separate structure, physically disconnected from NSLS-II, but with a public space landscaped with pedestrian walkways in between the two buildings. Space for possible future scientific buildings are also shown on the site plan immediately outside of the Loop Road.

2.4 Access, Traffic, Parking

The site is bounded by Brookhaven Avenue on the north, Groves Street on the west and Fifth Street on the east. This configuration will provide easy access to all parts of the facility. The main entrance of the Operations Center Building will face the present intersection of Brookhaven Avenue and Groves Street. (Following construction of the NSLS-II Groves Street will no longer extend all the way to Brookhaven Avenue, but rather terminate at Bell Avenue.) This northwest orientation of the main entrance of the Operations Center Building achieves the objective of minimizing the walking distances to the existing NSLS. Traffic into the primary NSLS-II parking lot will be from Brookhaven Avenue, and a drop-off, circle drive will be provided at the main entrance of the Operations Center Building. Groves Street will be discontinued between Bell and Brookhaven Avenues, but will be connected to the NSLS-II Loop Road that will be constructed around most of the outer perimeter of the building site. NSLS-II will also have access points from Bell Avenue and Rowland Street. The Loop Road will serve most of the Lab Office Buildings and also provide for service road access around the site.

Parking immediately west of the Operations Center Building and LOB-5 will serve the NSLS-II, and possibly the future JPSI building. All parking will be situated an appropriate distance away from the new structures to accommodate potential security measures/guidelines.

Each of the Lab Office Buildings will have an entrance serving the occupants of that building. Approximately 100 parking spaces will be provided at each LOB within convenient walking distance. Bicycle racks will be provided near each building entrance. Fire Department access will be provided to each LOB, but said access will remain a minimum of 40 feet away from the structure (establishing a "stay clear zone").

Service vehicles will access the "center" of NSLS-II via a tunnel under the Ring Building. The tunnel will allow emergency vehicles as well as delivery of large equipment to enter this "center". It will be required to comply with NYDOT requirements, and will be at least 19 ft wide (with a minimum 14'-2" clearance as it travels under the Ring Building). The ramps in and out will have a slope not to exceed 8 percent grade.

Pedestrian traffic will be accommodated by careful placement of sidewalks between the existing NSLS, the CFN, and NSLS-II.

2.5 Vibration Survey

Pre-design vibration surveys of the building site were conducted by Colin Gordon Associates and additional site baseline vibration measurements and analysis have been performed by BNL staff. The purpose of the surveys were to evaluate the ability of the proposed NSLS-II to meet stated vibration criteria. The data and analysis indicate the site existing background or cultural vibration levels are low and that there are no particular vibration characteristics that would adversely affect the performance of the NSLS-II scientific equipment. Results indicate the site is quiet "vibrationally" and capable of meeting the proposed vibration and stability criteria. A minimum 100 foot building setback along both Brookhaven Avenue and Groves Street will be maintained from the Experimental Floor to minimize the potential negative vibration impacts of passing traffic on these roads. Specific vibration criteria for NSLS-II are described elsewhere in this

document (Section 3 – Architecture) . Additional analysis and independent technical review by the Stability Task Force have also been performed and are available for review.

2.5.1 Experimental Hall

Data were collected in mid-afternoon at six locations at the NSLS-II site and processed to obtain one-third octave band velocity spectra. Results indicate the site will easily meet all vibration criteria for VC-E, but will not meet NIST-A criteria below a frequency of 5 Hz. It is believed that the low-frequency component which exceeds NIST-A is due to nearby traffic, probably on the Long Island Expressway and the William Floyd Parkway.

It is anticipated that the heavy floor slab of NSLS-II will reduce the amplitude at most frequencies, yielding a more favorable comparison to the criteria. Additional data was therefore taken on the floor slab of the nearby CFN (partially complete at the time) in the late evening hours. The analysis indicated that the slabs of the CFN will meet NIST-A criteria during the nighttime hours. These data are thought to be representative of the eventual nighttime performance of the Experimental Hall in NSLS-II.

2.5.2 Accelerator Tunnel

To evaluate the Accelerator Tunnel, survey data were transformed to displacement Power Spectral Density (PSD) spectra. This is the desired format for storage ring vibration criteria. When calculated over the range of 4 to 50 Hz, the calculated R values do not meet the stated criteria of R less than 25 nm. However, it was noted that the data below 6 or 7 Hz was contaminated by system noise due to an instrument cable. If the criteria are modified slightly to calculate R from 6 to 50 Hz or from 8 to 50 Hz, thereby eliminating the questionable data, the R values will generally meet the stated criteria of less than 25 nm.

Supplemental data collected in the CFN microscopy lab again validates the hypothesis that the heavy building slab will make a significant difference in the vibration data. Measurements taken at 7:30 pm and at 11:40 pm both yielded results that met the RMS amplitude criteria for NSLS-II of 25 nm. Again, it is anticipated that the improvement in vibration results due to the floor slabs at CFN will translate to improvements in the NSLS-II data.

Overall, the vibration study indicates that following the installation of the floor slab for the Accelerator Tunnel and the Experimental Hall, which will significantly stiffen the site, the vibration environment will be comparable to that of other leading light source facilities around the world.

Numerical models were constructed which allow examination of such design issues as placement of the Support Building with respect to the Ring, and even the placement of equipment within the Support Building. These models were calibrated using known and measurable performance of source data at several other facilities, including APS, RHIC, CFN and SPring8.

One of the key studies involved a comparison of placing the Support Building inside the ring versus outside of it. The preliminary results at this time suggest that placement inside the ring would lead to lower vertical ring displacement, and that if the mechanical systems were placed on a structurally supported floor (rather than a slab on grade) there would be further benefit, providing placement within the building were considered. The differences are quite dramatic, as indicated below:

Table 2.1 Service Building Vibration Comparison

Service Building Location	Floor Type	Equipment Location	Vertical Ring Displacement
Outside	Slab-on-grade	Middle	16.0 nm
Inside	Structurally Supported	Inner area	15.0 nm
		Middle area	2.6 nm
		Outer area	8.8 nm

Modeling studies will continue, refining issues that have already been addressed in a preliminary way and examining additional variables.

On parameter which will be considered will be the use of polymer-modified concrete to mitigate cultural and mechanical vibrations that might be transmitted through the slab. This was employed in the CFN, and measurements there indicate that vibration attenuation with distance can be doubled by the use of a 6" topping poured over an 8" structural slab, where the topping is treated with a particular polymer admixture and fiber reinforcement.

2.6 EMI/RFI Survey

Pre-design electromagnetic interference surveys were conducted on June 14th and September 19th, 2006 by VitaTech Engineering, LLC. Several types of measurements were taken to characterize the site:

- AC Extremely Low Frequency Electromagnetic Interference (ELF EMI)
- DC Electromagnetic Interference
- Radiofrequency Interference (RFI)

The site demonstrated no ambient electromagnetic or radio frequency interference that would adversely affect the performance of NSLS-II scientific equipment. The nearby NWS Doppler radar facility does not appear to have a problematic effect with respect to RFI.

The site is generally undeveloped and therefore should be relatively free of large electromagnetic fields above the ambient background. Buried electrical power feeders running east-west along Brookhaven Avenue and north-south along Seventh Street are sources of EMI that need to be considered. A 100 foot building setback along Brookhaven Avenue will allow fields to largely decay without impacting the building's performance. The feeder along Seventh Street will be relocated away from the NSLS-II building footprint and will not impact the facility.

2.6.1 AC ELF Electromagnetic Interference

AC ELF EMI fields are substantial along Brookhaven Avenue due to the existing underground electrical feeders, ranging up to 3.36 mG. These flux densities drop off rapidly to the south, reaching approximately 0.1 mG at the 100 foot building setback line, and dropping further to essentially zero beyond that point. Likewise, flux densities peak at approximately 0.4 mG above the buried electrical power lines at Seventh Street, but drop off very rapidly to the east. As a point of reference, flux densities of up to 0.3 mG are acceptable for high-accuracy instruments such as TEMs, SEMs, and E-beam writers, which will be used in the CFN. There are currently no instruments planned for NSLS-II that will have these sensitivities.

2.6.2 DC Electromagnetic Interference

DC Electromagnetic Interference is caused by ferromagnetic masses in motion, typically objects such as elevators, trains, cars, buses, etc. There is potential for DC EMI due to regular traffic along Brookhaven Avenue to the north, as well as along Fifth Avenue to the east. Analysis by VitaTech indicates that between 40 to 130 feet south of Brookhaven Avenue the DC fields will be such that instrumentation with dB/dt

differential DC EMI and resultant RMS thresholds between 1 mG and 0.1 mG will meet the specifications. Between 130 to 200 feet, instruments with a threshold of 0.1 mG to 0.01 mG will meet the specifications (197 feet is the predicted 0.01 mG isoline). Similar separation distances will apply to north–south traffic along Fifth Street.

2.6.3 Radiofrequency Interference

The RFI site measurements indicated very low electric field strength across a range of frequencies from 100 kHz to 18 GHz. The NEXRAD Doppler weather radar that is located only 2,200 ft away operates at a frequency of 2877 MHz. The existing NSLS building has experienced RFI impacts from the NEXRAD radar, causing the need for RF shielding around select laboratory and research areas to reduce the problem. A similar remediation approach will be used at NSLS-II (if needed); shielding will be provided specifically at the hutches based on scientific requirements (rather than providing general shielding for the entire building).

Electric field strength RF levels were recorded on September 19, 2006 by VitaTech Engineering at a point approximately in the center of the NSLS-II site. Data over a broad spectrum of frequencies indicated elevated RF levels at a number of frequencies (from various sources, including the NEXRAD radar). In all cases, the electric field strength RF levels were below 1V/m, which is the typical threshold for scientific instrumentation.

2.7 Geotechnical Survey

A geotechnical survey of the preferred site was conducted in July of 2006 and additional subsurface explorations were performed in April 2007. The explorations included 15 cone penetrometer test (CPT) soundings and ten test borings. The results indicate that the site conditions are generally uniform with 2 to 12 inches of topsoil and 2 to 9 feet of existing fill lays over medium dense to very dense sands near the proposed buildings and roadways. The sand deposits will work well for spread footings and may be suitable for reuse as compacted structural fill. The existing fill material is generally suitable for use as common fill around the site outside the building footprint.

With regard to column and wall settlement it is estimated that total settlement of spread footings will be less than 1 inch, and differential settlements will be less than 0.75 inch. This settlement will occur as loads are applied and therefore these settlements will be essentially complete by the time construction is finished. This settlement is acceptable for column and wall footings and will not effect the technical systems.

The floor slab within the experimental hall will support highly sensitive scientific equipment, and settlement of the floor slab after the equipment has been installed and calibrated must be minimized. Soils beneath the floor slab will settle in response to dead and live loads. It is anticipated that settlement will be complete within about one to two weeks after load application. Settlement resulting from floor slab dead loads and fill required beneath the floor slab is expected to occur during construction, and therefore will not contribute to post-construction settlement. However, application of substantial localized live load could cause minor post-construction settlement. We calculate the total and differential post-construction settlement from the live load to be less than 0.25 inch. Differential settlement will be less than the total settlement. For sensitive equipment where heavy beamline equipment loads are applied, it may be desirable to allow a two to three week waiting period between installation and final calibration.

Soils at the site are classified as Site Class D, “Stiff Soil Profile” in accordance with the New York State Building Code. The soil is not susceptible to liquefaction. The geotechnical report is included in the Appendix for reference.

A final set of borings will be performed prior to detailed design to fully detail the geotechnical conditions of the full building footprint in its final location. These borings in concert with other engineering factors will

form the basis of the final finished floor elevation which will be optimized for building stability, cut and fill quantities and existing utility elevations.

2.8 Topographic Survey

A preliminary topographic survey was conducted in June of 2006. That survey indicated the site to be relatively flat and well-suited for the NSLS-II. A more detailed topographic survey specifically for the NSLS-II site was conducted in September 2007. Site elevations appear to vary from 10 feet above the proposed Experimental Floor elevation, to 6 feet below said elevation; however, most of the site appears to be near the proposed floor elevation. Level grades may minimize the requirement for substantial cut and fill operations, and may work to accommodate potential future long beamlines extending up to 1000 m onto adjacent ground.

2.9 Existing Site Utilities

Existing site utilities consist of electrical power, chilled water, steam, potable water, sanitary sewers, storm drainage, and dry compressed air lines. Electrical power is wheeled to the site at 69 kV by the local electrical utility company (LIPA). This tie line has sufficient capacity for NSLS-II loads. The other site utilities are generated at BNL's central utility plants and distributed underground for use throughout the BNL campus. The distribution systems for these site utilities are of sufficient capacity to serve the NSLS-II; however, additional generating capacity will be required for chilled water and cooling tower water. Additional chiller capacity and cooling tower capacity will be added at the existing central utility plant. A separate cooling tower system for process water cooling will be located near NSLS-II.

The most significant impact NSLS-II will have on the current BNL utility infrastructure is the central chilled water system which is currently at the maximum without spare capacity to meet additional loads for the NSLS-II. As part of this project, additional chilled water capacity will be added to the existing central chilled water plant. Expanding the central chilled water plant (in lieu of constructing dedicated local capacity) provides advantages in reliability and reduced costs to the project .

Existing sanitary sewers are located parallel to and south of Brookhaven Avenue (6 in. VTP) and parallel to and west of Seventh Street (10 in. VTP). The system along Brookhaven Avenue can generally remain as is and the northerly and easterly Lab Office Buildings will be connected to this sewer line. The system along Seventh Street, extending further south parallel to and east of Groves Street, must be relocated, as it conflicts with proposed NSLS-II construction.

All utilities except chilled water will be accessed from Brookhaven Avenue. These utilities have adequate capacities and connections, enabling the routing of new site utilities through a common utility vault (underneath the Ring Building floor) and into the "center" of NSLS-II. This approach provides good access for maintenance, while also minimizing the effects of noise and vibration, when compared to running utilities through the building.

The following site utilities are available at or near the site and will used for NSLS-II:

- Potable water
- Sanitary sewers
- Storm drainage
- Chilled water
- Steam and condensate
- Compressed air
- Electrical power
- Telephone/data
- Fire alarm

2.9.1 Potable Water

Existing potable water lines are located around the perimeter of the site as follows:

- Along the north side of Brookhaven Avenue (12 in. and 10 in.)
- Parallel to and west of Seventh Street (8 in.) and extending south beyond the NSLS-II site
- Parallel to and east of Groves Street (8 in.)

The 8 in. line west of Seventh Street will need to be relocated around the footprint of the building. Connection of fire protection water and domestic water for the NSLS-II loop system will be from the relocated 8 in. line west of Seventh Street and the 12 in. line at Brookhaven Avenue and North Sixth Street. Potable water for fire protection must be maintained to existing buildings 485,497 and the RADTEC area to the south of the NSLS-II site.

2.9.2 Sanitary Sewers

Existing sanitary sewer lines are adjacent to the site on two sides. A 6 in. VTP line parallels Brookhaven Avenue on the north of the site and a 10 in. VTP west of Seventh Street meets with the 6 in. line at MH-163. The sanitary line then crosses Brookhaven to a 20 in. VTP line. The NSLS-II will connect to the 6 in. line from the Operations Center and one LOB. The remaining services will be routed to a new underground pumping station and pumped into the 10 in. VTP line.

2.9.3 Storm Drainage

Storm drainage will be collected and directed on site through a combination of both underground piping and structures, as well as overland flows. Multiple retention basins will be utilized to encourage and accelerate percolation of rainfall into the ground as near as possible to the location where it falls (as encouraged by LEED). The storm drainage system will be designed to insure that historical runoffs are not exceeded in the post NSLS-II condition. Excess storm drainage runoff will collect in retention basins and/or other storm drainage structures. Calculations to determine the current capacity of the existing open drainage channel along the west side of Groves Street will be done.

2.9.4 Chilled Water

Chilled water is a BNL campus-wide distributed utility. A joint BNL and NSLS-II funded activity will expand the BNL Central Chilled Water facility (CCWF) to meet both growing BNL chilled water loads as well as the added load for NSLS-II. The plant expansion will be a four bay plant that will install two new chillers for NSLS-II loads. NSLS-II will tie into existing central chilled water lines at Rochester Street. A chilled water supply and return header will be routed underground to the Ring Building and pass under the Ring Building through the traffic access tunnel and then be routed to supply each of the service buildings and other building loads. Underground piping will be ductile iron.

2.9.5 Steam & Condensate

Steam & Condensate lines are a BNL campus-wide distributed utility. The existing BNL Central Steam Facility (CSF) has adequate capacity to support NSLS-II requirements. NSLS-II will tie into existing steam (10 in.) & condensate (4 in.) lines just north of Brookhaven Avenue. These lines will connect at MH-47. Underground piping will be insulated steel.

2.9.6 Compressed Air

Compressed air is a BNL campus-wide distributed utility that is provided with the central chilled water distribution. NSLS-II will tie into existing site compressed air at Rochester St. and will route this piping in

concert with the chilled water piping.. A 3 in. compressed air line will be routed underground to the Ring Building and pass under the Ring Building through the traffic access tunnel. Compressed air piping will be PVC coated steel.

2.9.7 Electrical Power

For a description of electrical site utilities, see Section 10, Electrical Engineering.

2.9.8 Telephone / Data

For a description of telephone/data utilities, see Section 10.10.2, Telecommunications System.

2.9.9 Fire Alarm

For a description of fire alarms, see Section 10.10.1, Fire Alarm System.

2.10 Existing Facilities

BNL has an on-going program to remove older, inefficient, non-sustainable World War II erafacilities and consolidate operations into more permanent buildings. Consistent with this program, there is a project underway to relocate BNL warehousing, shipping, and receiving operations from the WW-II era buildings at the western edge of the proposed NSLS-II site. BNL will remove buildings and structures associated with these operations prior to construction of NSLS-II.

2.10.1 Existing Conditions

A preliminary topographic survey was conducted in June 2006. That survey drawing identified 1 foot contours and major surface features. It has been the basis for the site/civil design through Title 1. A more detailed topographic survey for the specific NSLS-II site was conducted in September 2007 and will be complete in October 2007. That survey will be the basis for the site/civil design through Title 2.

The proposed construction site is relatively level with mostly open fields, previously used for recreation. As previously stated there are warehouse buildings on the western edge of the NSLS-II site that are in the process of being removed under a separate BNL project. There are also some existing trees within the NSLS-II construction site that will require removal. Additionally, there is a railroad spur running parallel to Groves Street that enters the site from the south that will need to be cut back to a point outside the NSLS-II site. This railroad spur will be available for use during construction for delivery of bulk materials (if needed). The existing tree removal and cut back of the railroad spur are part of the NSLS-II site preparation work.

Existing storm drainage is accommodated along the western edge of the NSLS-II site in an open drainage channel. However, consistent with sustainable design principles, on-site recharge/infiltration of storm drainage will be maximized with only limited overflow going to the existing open drainage channel .

2.11 Preliminary Design

2.11.1 Improvements to Land

Improvements to the land include removal of existing structures, pavements, abandoned site utilities, a railroad spur, and some unsuitable fill. Once this has occurred, grading to new finished grades, installation of all new site utilities, storm drainage, site lighting and pavements (as well as final landscaping) can take place. This WBS element will consist of two work packages:

- Site Preparation which will encompass site clearing and grubbing, isolation of utilities, and rerouting of water and electric services.;
- Site Restoration and Landscaping, which will be included in the Ring Building contract, will include site grading and earthwork, the installation of all new storm drainage features, site lighting, pavements and final seeding.

2.11.1.1 Existing Structures

Removal of the existing building structures will be performed under a separate contract prior to NSLS-II site work. Underground utilities serving these buildings will be removed back to the utility mains as part of the NSLS-II contract. An early site preparation package will be done to provide temporary services to any existing structures that are to remain.

2.11.1.2 Existing Pavements

Removal of existing pavements will be required for all of Railroad Street and Seventh Street, and parts of Groves Street. These roadways will be removed to a point that enables tie-in to new roads and parking areas constructed as part of NSLS-II.

2.11.1.3 Existing Abandoned Utilities

Existing site utility systems that are not being used or have been abandoned in place will be removed as part of the NSLS-II project. The site plan identifies several underground utility pipes that will be removed back to an approved location and terminated.

2.11.1.4 Existing Railroad Spur

The existing railroad spur that runs parallel to Groves Street will be removed to a point south of the proposed NSLS-II site. Approximately 500 feet of existing track will be removed.

2.11.1.5 Other Miscellaneous Site Work

Site clearing will be required to remove existing trees to the west of Seventh Street and in the east/southeast quadrant of the NSLS-II site. The geotechnical report indicates a one foot layer of topsoil above sand, gravel, and silt. The topsoil will be removed for construction and retained for finished grading and replacement topsoil near the end of construction. Any other unsuitable fill identified by the geotechnical report will also be removed and replaced by material from an on-site borrow pit. Final site grading will bring the site to finished grade elevations shown elsewhere in this document. The proposed finished floor elevation for NSLS-II at 70.0 feet above mean sea level (as shown/referenced in other areas of this report) was previously established following preliminary cut and fill quantity studies. These studies will be refined and recalculated during detailed designto confirm that this elevation remains the most optimum for NSLS-II.

Construction staging and access areas, as well as future lay-down yards and/or excess soil stockpile areas (out of the way of future building construction) will be designated. Construction trailers and associated contractor parking will be situated on the north side of Brookhaven Avenue. This location provides easy access to current and future construction areas, and capitalizes on existing facilities/utilities in this area previously used for this same purpose. Designated future lay-down yards and/or excess soil stockpile areas will be situated immediately south of Brookhaven Avenue (and west of Fifth Street). This location has already been mostly cleared of existing trees/vegetation (due to existing recreational ball fields here) and is relatively level. It is also adjacent to the current and future construction area, but out of the way of any actual new construction.

2.11.1.6 New Paving

New paving for NSLS-II will include:

- Curbed drives and entrances from Brookhaven Avenue and Groves Street to NSLS-II facilities
- Curbed drop-off, circle drive (with enhanced concrete paving) for the Operations Center Building's main entrance
- Parking (predominantly uncurbed) for the Operations Center Building
- Loop Road (uncurbed) around the outer perimeter of the NSLS-II site
- Access to the Loop Road from Groves Street and Fifth Street
- Parking (mostly uncurbed) for LOBs 1,4and 5 only (parking for LOBs 2 and 3 are future)
- Truck access to the main loading dock at LOB 4 and loading platforms at LOBs 1 and 5. Fire truck access must be maintained at the locations of future LOBs 2 and 3.
- Traffic access tunnel under the Ring Building into the "center" of NSLS-II
- Service drives (uncurbed) around the infield within the "center" of NSLS-II, including individual access points to each service building
- Campus sidewalks and outdoor gathering spaces (with enhanced concrete paving) in the areas between the existing NSLS, CFN and NSLS-II

2.11.1.7 New Storm Drainage

Storm water drainage from the roofs of buildings and drainage from the paved areas will be directed by either underground pipes and/or overland flow to small retention basins (as encouraged by the LEED guidelines) to achieve the maximum possible infiltration/percolation into the ground water system. For paved areas closest to the existing open drainage channel along the west side of Groves Street, some of the storm drainage will be piped directly into this feature. A retention basin will also be required within the "center" of NSLS-II, at the infield of the Ring Building. Special drainage accommodations will be required for the traffic access tunnel under the Ring Building. Both of these areas will be designed to adequately discharge all storm drainage effectively away from NSLS-II, requiring piping and/or a sump pump associated with the low point in the traffic access tunnel. The other retention basins will be situated outside the Ring Building, and generally out of the way of any future long beamlines. Collected storm water at the retention basins will be allowed to percolate into the ground following storm events as on-site soil conditions suggest percolation will be rapid. All storm water drainage systems will be designed (as required) to meet 100 year storm design criteria.

2.11.1.8 New Landscaping

After construction, all disturbed areas will be re-vegetated with a combination of native or indigenous plant materials, seeding, sod and/or wildflowers/groundcovers to minimize the negative effects of soil erosion and allow for minimal maintenance by BNL.

2.11.1.9 Erosion and Sedimentation Control

Erosion and sedimentation control systems will be installed and utilized for the duration of the construction phase of the project. Silt fencing and stabilized construction entrances will be installed prior to the commencement of construction activities. Disturbed areas within the construction site will be stabilized as soon as practical and subsequently maintained with appropriate methods to minimize erosion of exposed earth. Temporary seeding, mulching, or crushed stone will be used to achieve stabilization.

The proposed construction activities will result in the disturbance of one (1) or more acres of land. Therefore, BNL will be required to obtain coverage under a SPDES General Permit (GP-02-01) prior to the commencement of any soil disturbance. To obtain coverage under the general permit, BNL will file a

completed Notice of Intent (NOI) with the New York State Department of Environmental Conservation (NYSDEC) affirming that a Stormwater Pollution Prevention Plan (SWPPP) has been prepared for the construction site (and will be fully implemented prior to the start of construction activities). Best Management Practices (BMP's) from the New York State Standards and Specifications for Erosion and Sediment Control will be put into place to limit the negative impacts of soil erosion. BMP's include the following:

- Sediment Traps will be located as required to minimize the amount of soil loss, and to keep soil from entering existing storm drainage systems.
- Temporary Sediment Basins will be located in watershed basins and within future permanent extended detention/retention/recharge basins.
- Temporary swales (wet and dry) will be used to convey storm water during current and future construction to soil erosion and sediment control features.
- Check dams and rock dams will be located in drainage swales as required to help filter/settle out any sediment.
- Construction access points (stabilized construction entrances with wash racks) will be employed to prevent the tracking of mud from construction vehicles onto existing roadways.
- Temporary grassing will used to stabilize all areas of soil disturbance.
- Dust control will be utilized during dry conditions to minimize the nuisance of blowing of dust.

In addition to the above-mentioned BMP's, the contractor will be required to stage the work consistent with NYSDEC requirements, and will need to stabilize all land disturbing activity within 14 days. In the event that temporary grassing can not be performed due to cold weather conditions, mulching will be required instead. Temporary grassing of the site will be required by completion of work once grasses can be planted. Erosion control devices will need to be inspected at least weekly (and after each rain), and repaired as necessary. Erosion control devices will be properly installed prior to site disturbance as logistically feasible and depending on the staging of work. These will be maintained in good working condition until completion of the early site preparation package construction (and/or replaced when effectiveness is reduced to 50%). Finally, additional erosion control measures will be installed to control sediment and silt from leaving the site as determined necessary by the ESHQ Directorate.

3 ARCHITECTURE

3.1 Design Criteria

3.1.1 Codes and Standards

The latest edition of the codes, standards, orders, and guides referred to in this section will be followed, with a reference point of August 2008 being the anticipated design completion date. All work will be in accordance with BNL's Implementation Plan for DOE 413.3, "Program and Project Management for the Acquisition of Capital Assets."

3.1.2 DOE Orders

DOE O5480.4 – Environmental Protection, Safety and Health Protection Standards
DOE O413.3A – Program and Project Management for the Acquisition of Capital Assets
DOE O414.1C – Quality Assurance
DOE O420.1B – Facility Safety
DOE O420.2B – Safety of Accelerator Facilities

3.1.3 Codes, Standards, and Guides

Building Code of New York State (NYSBC) – 2002 Edition
American Concrete Institute
Building Code Requirements for Structural Concrete (ACI 318-99)
BNL Standards Based Management System Subject Areas
New York State and Suffolk County Department of Health Codes
American National Standards Institute
ANSI 117.1 Accessible and Useable Buildings and Facilities
American Society for Testing Materials Standards
ASHRAE Standard 90.1-2001 Energy Standards for Buildings Except Low-Rise Residential Buildings
Factory Mutual
National Institute of Standards and Technology
National Fire Protection Association (NFPA) Standards
Occupational Safety and Health Administration (OSHA)
Underwriters Laboratory
New York State Fire Prevention Code - 2002 Edition
Energy Conservation Code of New York State - 2002 Edition
Americans with Disabilities Act Accessibility Guideline (ADAAG)
Leadership in Energy and Environmental Design (LEED) 2.2
LEED for Labs

3.2 Architecture

3.2.1 Building Envelope

The building envelope will be designed to meet at a minimum the prescriptive requirements of the Energy Conservation Code of New York (ECCNY). Brookhaven National Laboratory is located in Climate Zone 11B

of the ECCNY. The thermal design parameters for envelope elements are dependent on the ratio of fenestration to overall wall area. The Ring Building has a window-wall ratio of less than 10 % and the LOBs and the Operations Center have window-wall ratios greater than 10%. This ratio affects the prescriptive requirements of the ECCNY, as shown in Tables 3.1 and 3.2. Window to wall ratios of 0 to 10% are considered low fenestration area buildings and ratios of 25 to 40% are high fenestration area buildings.

Table 3.1 R-Values for High Fenestration Area Buildings – ECCNY

Building Component	Prescriptive R-Value
Exterior wall	R-11
Exterior wall below grade	R-11
Glazing	R-2 (U=0.5)
Roof (continuous insulation)	R-24
Slab on grade edge	R-8

Table 3.2 R-Values for Low Fenestration Area Buildings – ECCNY

Building Component	Prescriptive R-Value
Exterior wall	R-11
Exterior wall below grade	R-11
Glazing	No requirement
Roof (continuous insulation)	R-19
Slab on grade edge	No requirement

More stringent criteria will be used in most locations as required to meet the temperature stability performance of the building and to help achieve sustainability (LEED) goals. Targeted design R-values for wall and roofing systems will match or be slightly higher than the prescriptive values shown above:

- Target R-value for Exterior wall system R-20
- Target R-value for Roofing system R-24

3.2.2 Building Occupancy

NSLS-II will be in operation 24 hours a day, 7 days a week; however, occupied hours for most staff are 8:00 AM to 5:00 PM. The overall building will be classified, per the Building Code of New York State, as a Business (“B”) Occupancy. The anticipated populations of the various areas are shown in Table 3.3:

Table 3.3 Building Office Capacity

Building	Population
Operations Center	75 (Alt 3rd floor)
Ring Tunnel / Experimental Hall	0
Lab Office Building 1	72
Lab Office Building 2	72 (future)
Lab Office Building 3	72 (future)
Lab Office Building 4	72 (future)
Lab Office Building 5	72
Booster / Linac Building	TBD
RF Building	0

3.2.3 Parking

Parking will be provided for the Operations Center, the future JPSI building and for each of the Lab Office Buildings. LOBs 1, 4, and 5 will have approximately 100 parking spaces provided for employees and visitors. The main parking area for the Operations Center and the future JPSI will provide approximately 200 parking spaces for employees and visitors. Parking at LOBs 2 and 3 will be future and added when LOB 2 and 3 are added. A drop-off loop will be provided to the entrance of the Operations Center. Each parking lot will be barrier free and provide the required number of ADA-compliant parking spaces to meet current LEED requirements. Requirements for parking spaces are as shown in Table 3.4.

Table 3.4 Parking Requirements.

Building	Parking Spaces
Operations Center & future JPSI*	210
Lab Office Building 1	100
Lab Office Building 2	Future
Lab Office Building 3	Future
Lab Office Building 4	100
Lab Office Building 5	84
Total	494
*Not part of NSLS-II Project	

3.2.4 Vibration Criteria

The vibration limits of the Experimental Hall are those criteria associated with the user-supplied research instruments, which are not well defined at this time. Therefore, the vibration requirements of this space will be established to meet general vibration criteria for similar physical science research centers. The vibration requirements of the vast majority of research equipment available today would be satisfied by a floor meeting vibration criterion VC-E or the more stringent NIST-A. The NIST-A criterion is more stringent than VC-E at frequencies less than 20 Hz. A minimum target of VC-E will be established for the Experimental Hall.

The vibration requirements for the accelerator tunnel have been provided in a much different manner. The storage ring is most sensitive to frequencies in the range of 4 to 50 Hz. The criterion for the storage ring vibration is defined in terms of R, the area beneath the power spectral density (PSD) spectrum $\Delta(f)$, between cutoff frequencies f_1 and f_2. The RMS amplitude, R, is to be less than 25 nm. R is defined as

$$R = \sqrt{\sum_{f_1=4}^{f_2=50} \Delta(f) \times \delta f}$$

where $\Delta(f)$ is the displacement power spectral density spectrum (in units such as m^2/Hz, where the frequency term in the denominator is the measurement bandwidth) and δf is the frequency resolution of the spectrum,

0.25 Hz. The lower and upper bounds of the summation are 4 and 50 Hz, respectively. Frequency components outside this range may be neglected.

3.2.5 Noise Criteria

One of the primary goals of the NSLS-II is to provide world-class research facilities. One aspect of this requirement is to provide a very quiet Experimental Hall. The facility will have two primary types of noise sources: 1) the facility's mechanical systems, such as air handlers, and 2) the user-provided research equipment. The noise control associated with the first group is within the purview of the NSLS-II design team, but the ability to mitigate noise associated with the second group is somewhat limited. It can be anticipated via passive room noise control measures incorporated into the design, but it cannot be controlled via mechanical constraints such as airflow velocities, fan selection, or silencers, concepts typically employed for the first group.

Studies carried out during the design of the Advanced Photon Source determined that final operational room noise in the Experimental Hall would be a mix of sound from both groups of sources, and that NC-60 to NC-65 would be achievable from a combination of mechanical system noise control measures on the proposed air handling system and room absorption incorporated into walls and ceiling. In the absence of absorptive material, the noise at APS was predicted to be on the order of NC-70. This assumed a degree of localized noise control (with regard to user equipment) similar to what was used in NSLS I. APS elected to require noise control to be provided by users as part of the instrumentation and/or hutches, and omitted plans for absorbent material.

In March 2007, a program of measurements was carried out at APS, determining that the mean+σ noise in operational areas of the Experiment Hall was NC-61 (67 dBA), with a total range of only 4 NC points and a σ of one point. In an undeveloped area (representing a noise contribution only from building facilities), the noise was found to be NC-56 (62 dBA).

NSLS-II will utilize absorptive material and appropriate mechanical system design to achieve NC 55 or better in the As-Built stage (prior to operation of user equipment), with a goal of providing a Mean+σ noise environment of NC-58 or better. Noise Criteria (NC) level guidelines for other spaces in the facility will be as shown in Table 3.3.5.

Table 3.5 Acoustic Noise Criteria.

Space Type	Noise Criteria (NC) Level
Office	35–40
Laboratory	45–50
Conference rooms	30
Interaction space	40
Common use areas	40–45
Accelerator tunnel	None
Experimental Hall	55 or better
Mechanical / electrical rooms	Per ACGIH TLVs

3.2.6 EMI / RFI Criteria

No universal EMI/RFI design criteria has been established for the NSLS-II facility, although individual beamlines or experiments may have specific requirements. Shielding, if required will be the responsibility of the researcher at the individual beamline or laboratory.

3.3 Functional Program

Adjacencies of the various functional areas within the NSLS-II complex have been established through detailed discussions with the Accelerator Systems Division, the Experimental Facilities Division, the Conventional Facilities Division, Plant Engineering, Environmental Safety & Health, Maintenance, and Management.

Relationships between the areas will meet the requirements outlined in the following sections.

3.3.1 Ring Tunnel

- Requires access from the Ring Building infield for tunnel equipment installation.
- Shielding is required on the inboard, outboard, and top of the ring tunnel. This can be achieved with high-density concrete, normal weight concrete, or soil. This can also be achieved with a combination of these materials. The primary shielding material will be standard weight concrete.
- Access to the tunnel from the Experimental Hall is required at each beamline. This access will be included on the initial 15 beamlines (IDs 14-29) and be through sliding shielded doors. On the remaining 15 beamlines (IDs 1-13 and 30) will be blocked up with shield block and installed when a beamline is added at them.
- Storage ring power supplies will be located on the tunnel mezzanine directly above the ring tunnel.
- Easy access from the Operations Center control room to the ring tunnel is desirable.
- Access from the Experimental Floor to the ring mezzanine will be from stairs or ships ladders running parallel to the interior ring tunnel ratchet wall at locations where there is no active beam line.
- Walls of the ring tunnel must provide radiation shielding from the rest of the facility.

3.3.2 Experimental Hall and Access Corridor

- The Experimental Hall will have 30 sectors (a sector includes a straight section and the adjacent bending magnet) and must accommodate 25 to 30 60 m insertion device beamlines and hutches and another 25 to 30 bending magnet beamlines. The Experimental Hall must be able to accommodate future beamlines that will extend outside the building.
- Floor height with respect to the tunnel must allow beamlines to be 1.4 meters above the finished floor in the Experimental Hall. The floor must be constructed to limit differential settlement, as the beamlines must be maintained at 1.4 meters along their entire length.
- The Experimental Hall must have line-of-sight access into the tunnel for beamline set-up and alignment.
- A perimeter access corridor for equipment and personnel access to the beamlines is required. Beamlines must have easy access to nearby LOBs and Operations Center.
- The access corridor should provide space for informal interaction between researchers.
- An outdoor public space with seating will be provided near LOB 1 for lunch, coffee breaks, etc. A sandwich grille with a service window to the outdoor space and into the Experimental Hall will be provided to serve light meals.

3.3.3 Operations Center

- The Operations Center should provide visitors a viewing gallery overlooking the Experimental Floor.
- The control room and small conference room, should be grouped together on the second floor with easy access to the Booster / Linac and Ring Tunnel areas.
- The computer room should be below the control room.
- Provision for future covered access to the Joint Photon Sciences Institute building should be considered.
- The Operations Center should have an entry lobby for displays and a reception area for new users and guests.

- A third floor including offices and meeting spaces will be designed as a bid alternate. The decision to accept the alternate will be made prior to construction.

3.3.4 Lab Office Buildings

- Laboratory space and offices should be near to their respective beamlines.
- LOBs needs an entrance and parking lot.
- Individual laboratories in the LOBs should have access to the Experimental Hall through double doors.
- Informal interaction space should be provided in each LOB, as well as conference rooms.
- Laboratory space within a LOB will be shared by all six sectors using the LOB.
- Laboratories will require chemicals and gases to be delivered to them. Provision for delivery and storage of these materials is required. A high hazard storage area is provided adjacent to LOB-4 adjacent to the main loading dock.
- LOBs must be configured to allow for future expansion requiring additional labs and offices.
- LOBs 1 and 5 as well as future LOBs will have an at-grade loading platform.
- The main loading dock replaces the at-grade loading platform for LOB 4.
- Each LOB will have a gas bottle storage area.
- HVAC for the LOBs will be air handling units in each LOB mechanical mezzanine.
- Each LOB will have two fume hoods. One HEPA-filtered laboratory fume hood for working with nanomaterials and the second capable of being retrofitted with HEPA filtration.

3.3.5 Service Buildings

- Service buildings will house mechanical and electrical equipment supporting the Ring Building and must therefore be equally spaced around the interior side of Ring Building.
- Service buildings require access for large equipment moves.
- Access to the ring tunnel for both equipment and personnel will be provided through the service buildings from both the tunnel mezzanine and the Ring Building infield.
- Service buildings must be located so utilities can be easily and efficiently routed to them.
- Service Buildings will have a hoist/crane located on the second floor and accessible to the outside through double doors for hoisting materials for the Tunnel Mezzanine up onto the second floor.
- The ductwork leading from the Service Building into the Accelerator Tunnel must run through a labyrinth for radiation shielding.
- Pedestrian access from the Service Building into the Accelerator Tunnel must run through a labyrinth for radiation shielding.

3.3.6 Injection and RF Buildings

- The Injection and RF Buildings must be adjacent to the storage ring tunnel.
- The Injection Building must be shielded due to radiation during linac and booster operation.
- The RF Building must have a shielded test area
- The RF Building must have a small cryo equipment enclosure nearby (but separate for vibration isolation) and concrete pad for associated Helium storage tanks.
- HVAC for the RF Building and Booster Service Building will be by roof mounted AHU's.
- HVAC for the Injection Building will be by AHUs located in rooms within the buildings. The ductwork leading into these buildings must run through a labyrinth for radiation shielding.

3.4 Space Program

3.4.1 Building Program

NSLS-II will have distinct components that make up the final building plan. They are the Ring Building, the Operations Center, the Lab Office Buildings, the Service Buildings, the Injection Building and the RF Building. Each of these buildings has separate space and utility requirements. It is also important to note that the existing NSLS will continue to be utilized to provide administrative and engineering office, workshop and technical space that will support the needs of NSLS-II. The net additional building program requirements for NSLS-II include the User and Facility beamline office and lab space, NSLS-II operations space and the physical support space to house the operating machinery, accelerator and beamlines.

3.4.1.1 Definitions

Net Square Feet (NSF): The sum of all areas that are required to meet general or specific functional needs. NSF is calculated based on the interior dimensions of the rooms and spaces.

Gross Square Feet (GSF): The total area of all spaces in the building including wall thicknesses. GSF is calculated based on the exterior face of the building spaces and includes non-assignable spaces such as building circulation, mechanical/electrical rooms, restrooms, janitor closets, and the area of interior and exterior walls.

Building Efficiency: Building efficiency is calculated as the ratio of NSF/GSF.

Table 3.6 Summary Program of Spaces.

Space Description	NSF	GSF
Operations Center	9,232	11,600
Injection Building	17,693	22,440
RF Building	10,182	10,630
Ring Building (incl. Service Buildings)	268,018	293,715
Lab Office Buildings* (3)	50,358	71,536
Total Square Feet	355,483	411,921
Building Efficiency: 86%		

* 2 additional LOBs are future

3.4.2 Operations Center

The Operations Center will be a two-story structure, with an alternate third story, that serves as the focal point of the facility. It includes a two story high entry lobby space for reception and displays. The Operations Center will contain the accelerator control room with associated conference room, lunch room, and computer room, support space and a visitor's viewing gallery located on the second level overlooking the Experimental Floor. Figure 3.1 illustrates the layout of the Operations Center first floor and Figure 3.2 shows the second floor layout.

An optional third floor will accommodate offices for administration and accelerator physicists associated with storage ring operations. This will include the area over the entrance lobby that could be used for a Director's suite or a large Conference Room.

Table 3.7 Operations Center Program of Spaces.

Room Name	Size NSF	No. of Spaces	Total NSF	GSF	Notes
First Floor					
Lobby	2,415	1	2,415		
Computer room	976	1	976		
Telecom	409	1	409		
Switchgear	655	1	655		
Break room / Kitchenette	512	1	512		
Unisex Toilet	78	1	78		
Second Floor					
Control conference room	676	1	676		
Control room	1,547	1	1,547		
Toilets & Showers	76	2	152		
Men's Locker Room	128	1	128		
Women's Locker Room	126	1	126		
Storage	108	1	108		
Bridge & Viewing Gallery	1,450	1	1,450		
Operations Center		15	9,232	11,600	
Efficiency – Operations Center: 79%					
Alternate Third Floor			132		
Private office			2,561		
Open office			2,469		
Toilets			284		
Kitchenette	126	1	126		
Directors Office	301	1	301		
Conference Rooms			943		
Director's Assistant	221	1	221		
Alternates		55	6,753	10,310	

3.4.3 Injection Building

The Injection Building (Booster / Linac) consists of spaces for the compact booster, the linac, klystron gallery and support for these in a single story building. Two Service Buildings are adjacent to the Booster ring and will provide services for it and the linac. The Booster ring and linac require shielding. This is accomplished by a combination of concrete walls and earthen berms. The layout of the Injection Building is shown in Figure 3.4.

Table 3.8 Injection Building Program of Spaces.

Room Name	Size NSF	No. of Spaces	Total NSF	GSF	Notes
Linac Room	1,715	1	1,715		
Klystron Gallery	1,620	1	1,620		
Booster Service Building - East	6,102	1	6,102		
Booster Service Building – West	1,568	1	1,568		
Booster Ring Tunnel	6,688	1	6,688		
Injection Building		5	17,693	24,440	
Efficiency: 72%					

3.4.4 RF Building

The RF Building is located inside the ring on the west side of the Operations Center and connected to the Operations Center by a double door. This building houses the RF cavities which are located on ID 22A and 24A. The space requires at least 6 meter height clearance and a crane or temporary gantry for installing equipment. There is also a concrete shielded room for doing RF testing located in this building. The RF Building layout is illustrated in Figure 3.3.

Located adjacent to this building on the inner part of the ring is the Helium tank yard that services the RF cavities and a pre-engineered pump building to serve the Helium Tank Yard.

Table 3.9 RF Building Program of Spaces.

Room Name	Size NSF	No. of Spaces	Total NSF	GSF	Notes
RF Cavity Room	9,756	1	9,756		
RF Test	426	1	426		
RF Building		2	10,182	10,630	
Efficiency: 96%					

3.4.5 Ring Building

The Ring Building, shown in Table 3.7, will consist of four main space components, the Ring Tunnel, the Tunnel Mezzanine, the Experimental Hall, and the Access Corridor. Additionally, the main loading dock, stock room and hazardous materials storage are also included in the Ring Building and located adjacent to LOB 4.

The ring tunnel, housing the booster ring and the storage ring, occupies the inner most area of the Ring Building. The beamlines used by the experimental stations extend tangentially from the ring at select locations. The Experimental Hall is designed to accommodate beamlines that are approximately 60 m long from the center of the straight section to the intersection at the access corridor. Outboard of the Experimental Hall will be the access corridor. Above the ring tunnel is the tunnel mezzanine. Power supplies for the accelerator will be located on the tunnel mezzanine with electrical power feeds dropping through the floor into the tunnel.

Beyond the ring tunnel is the experimental floor where the beamlines and hutches for the experiments are located. The floor in this area will be designed to reduce transmission of vibration and prevent differential settlement of the floor which can be detrimental to the performance of the beamlines.

Along the periphery of the experimental floor is the access corridor which is approximately 10 ft wide and designed for fork truck and pedestrian traffic. This will be a continuous aisle that runs the circumference of the Ring Building. It is from this aisle that the experimental floor and LOBs will be accessed. The access

corridor between LOB 1 and 2 will accommodate future long beam lines that will interrupt the corridor where they penetrate it. Access over the long beamlines will be accomplished by a raised steel bridge over the beamline sized for forklift traffic. The bridge will include an equipment lift on one end closest to the LOB, access lifts to each of the beam lines, and a ramp on the other end. The access corridor between the other LOBs will have a thickened slab design that will allow for installation of the raised platform in the future.

An outdoor public space with seating will be provided for lunch, coffee breaks, etc. A sandwich grille will be provided to serve light meals. It will be located on the Ring Building between LOB One and the Operations Center.

A typical Ring Building Pentant is illustrated in Figure 3.5.

Table 3.10 Ring Building Program of Spaces.

Room Name	Size NSF	No. of Spaces	Total NSF	GSF	Notes
Ring tunnel	37,300	1	37,300		
Experimental Hall	94,235	1	94,235		
Access Corridor	33,018	1	33,018		
Tunnel mezzanine	50,950	1	50,950		
Grille	257	1	257		Located near LOB 1
Loading dock	2,060	1	2,060		Located near LOB 4
Stock Room	1,618	1	1,618		Located near LOB 4
Hazardous materials storage	450	1	450		Located near LOB 4
Ring Building		8	219,888	240,075	
Efficiency: 92%					

3.4.5.1 Service Buildings

There will be five two-story service buildings located inboard of the ring. These buildings will house the mechanical and electrical equipment to service the experimental floor, the ring tunnel, and the tunnel mezzanine. The Service Building first floor will provide personnel access to the ring tunnel through a labyrinth, and equipment access to the ring tunnel at two of these service buildings through a shielded door. The other three Service Buildings will each have an opening filled with removable, pre-engineered concrete shield block to accommodate a future shielded door. The inner road access will connect to the service buildings through the first floor.

The Service Building second floor will house air handlers for the experimental floor area. The second floor will be serviced by a equipment hoist and double exterior doors located on the second floor and fire stairs from the first floor. It will provide equipment access to the tunnel mezzanine via an a double six foot wide hollow metal door. Mechanical equipment rooms for the Lab Office Buildings, Booster, and Operations center are included with their respective buildings.

The layout of a typical Service Building is shown in Figure 3.6.

Table 3.11 Service Buildings Program of Spaces.

Room Name	Size NSF	No. of Spaces	Total NSF	GSF	Notes
Service Building # 1	9,626	1	9,626		
Service Building # 2	9,626	1	9,626		
Service Building # 3	9,626	1	9,626		
Service Building # 4	9,626	1	9,626		
Service Building # 5	9,626	1	9,626		
		5	48,130	53,640	
Efficiency: 90%					

3.4.6 Lab Office Buildings

There will be three single-story Lab Office Buildings (LOB), two fully built out (LOBs 1 and 5) and one shelled (LOB 4). There will be two future LOBs that can be constructed when the beamlines are built in their area of the building. LOBs include open-plan offices for the scientists and technicians, (a VE items that eliminates all enclosed offices in LOBs 1 and 5 has been incorporated here and on the drawings by note only) twelve laboratory modules (two modules per typical laboratory) plus interaction areas, conference rooms, machine shop, and shipping/receiving and storage. The shipping/receiving area will be eliminated in LOB 4 and a stock room and main loading dock added that will service LOB 4 as well as the rest of the facility. The layout typical to LOB 1 and 5 is shown in Figure 3.7.

LOB 4 will be a shelled space in the base building work with just the exterior envelope constructed. This includes exterior walls, roofs, doors and windows. Minimum mechanical, electrical lighting and power rough-in and plumbing rough-in that provides minimum life safety for exiting and to prevent freezing of sprinkler piping in the winter.

3.4.6.1 Laboratory Design

Each built-out LOB will have six laboratories, which will be shared with all the beamlines associated with that particular LOB. These labs are based on a 12 ft wide and 20 ft long lab planning module with each lab being two modules wide. These labs will have access to the Experimental Hall through recessed double doors 6 ft wide (two 3 ft wide leaves). The labs will be accessed from the LOB by a single recessed 3 ft wide door.

At least two labs in each LOB will be wet labs, either chemistry or biology, which will require a fume hood. At least one of these hoods will be HEPA filtered in each LOB, and one more will be upgradeable with HEPA filtration. Additionally, each LOB will have the capability to provide at least one HEPA filtered fume hood designated for nanomaterials work. The other labs will be dry labs with cabinetry and equipment but a fume hood is planned for only one of the four dry labs. These labs may be equipped with elephant trunk exhausts or glove boxes as needed by the laboratory type.

Chemistry wet labs will include ventilated chemical storage cabinets incorporated into the fume hood base. Each wet laboratory will also be furnished with a safety shower/eyewash station. Floor drains will not be provided in laboratory spaces.

Since the LOB labs are going to be shared labs, it is necessary to make the labs as generic as possible while still serving the requirements of the research being performed.

Table 3.12 Lab Office Buildings Program of Spaces.

Room Name	Size NSF	No. of Spaces	Total NSF	GSF	Notes
Lab Office Building					
Private office	110	48	5,280		
Open office space	90	24	2,160		
Laboratory – Wet	480	2	960		
Laboratory – Dry	480	4	1,920		
Storage	110	1	110		
Conference room	560	2	1,120		
Conference room	220	2	440		
Lobby & interaction spaces	600	1	600		
Break rooms / kitchenettes	240	2	480		
Shipping Receiving & Storage	960	1	960		
Toilet/shower	250	2	500		
Electrical / Data	153	1	153		
Janitor Closet	63	1	63		
Access Corridor Interface	2,090	1	2,090		
Machine Shop	270	1	270		
		93	17,106		
Lab Office Buildings 1 & 5		186	34,212		
Lab Office Building 4 (Shelled)		1	16,146		
			50,358	71,536	
Efficiency: 70%					

3.4.7 Construction Alternates

Some components of the NSLS-II will be bid as Alternates to the Base Building. These will be designed as part of the Title II Design and constructed as budget allows. Other components are identified as Future construction and will not be designed at this time.

- Operations Center Floors 1 and 2 — Base
- Operation Center Floor 3 — Alternate
- Injection Building — Base
- RF Building — Base
- Ring Building Pentants 1-5 — Base
- Lab Office Building #1 — Base
- Lab Office Building #2 — Future
- Lab Office Building #3 — Future
- Lab Office Building #4 Shell — Base
- Lab Office Building #4 Fit-out — Future
- Lab Office Building #5 — Base

3.4.8 Circulation

Entry points into the Ring Building are provided around the circumference of the building both from the outside and the inside of the ring. The main entrance to the Ring Building will be from the Operations Center lobby. Other entrances to the complex are available from the LOBs and from the service buildings. Within the two-story Operations Center, two elevators will provide vertical transportation – a passenger elevator in the lobby and a service elevator inside the ring.

When the accelerator is operating, access to the ring tunnel is not allowed, for safety reasons. Doors into the ring tunnel will be interlocked with the accelerator to prevent entry into the tunnel when the beam is operating.

Primary circulation within the Ring Building will be provided by the access corridor that circumscribes the outside of the building. It will provide for both pedestrian and vehicular (bicycle, forklift, etc.) traffic. The access corridor will have points of entry from each LOB and from each laboratory within the LOBs. Emergency exit doors are located on the perimeter of the ring (both inside and outside walls) that meet the current NYS Building Code. A elevated bridge with ramps and equipment platform lift is located between LOB 1 and future LOB 2 to accommodate long beamlines being installed in this area. Provisions for elevated bridges in other area where long beamlines are anticipated in the future are included the design and sized for all anticipated traffic in these areas.

Access to the Tunnel mezzanine from the Experimental Hall will be via steel stairs located at the ratchet for the bending magnets. There will be one per pendant (approx. every 600' to meet NYSBC for travel) except that the bridge at the Operations Center will take the place of one of these stairs.

Control room personnel require ready access to the tunnel mezzanine and the ring tunnel itself. The tunnel mezzanine will provide the means of circulation around the ring from the control room. A pedestrian bridge will be provided from the Operations Center second floor across the Experimental Hall to the tunnel mezzanine. Entrance to the accelerator tunnel will be via the service buildings. Stairs in the service buildings will provide circulation between the mezzanine level and the tunnel level. Personnel will access the accelerator tunnel through a personnel labyrinth on the first level.

3.4.9 Building Floor Elevations

The floor elevation for the Ring Building (experimental floor) is the functional baseline for the elevations of the adjoining buildings and spaces. This elevation is set to minimize the need for engineered fill while also considering the balance of cut and fill on the site. The floor elevations for the components are given in Table 3.13.

Table 3.13 Building Floor Elevations.

Building Component	Floor Elevation
Experimental floor and access corridor	+ 70 ft
Ring tunnel	+ 71 ft 4 in.
Tunnel mezzanine	+ 83 ft 7 in.
Lab Office Building	+ 70 ft
Operations Center	--
First floor	+70 ft
Second floor	+ 83 ft 7 in.
Third floor	+98 ft
Service buildings	--
Lower level / Ring tunnel access	+ 71 ft 4 in.
Upper level	+ 83 ft 7 in.
Booster / Linac Building	+ 71 ft 4 in.
RF Building	+ 71 ft 4 in.

3.5 Preliminary Design

3.5.1 Operations Center

3.5.1.1 Architectural Concepts

The Operations Center lobby will serve as the front door to the NSLS-II complex. It is envisioned to be two stories in height and will provide a welcoming environment for guests.

3.5.1.2 Future Expansion

The Operations Center will be designed for an optional third floor, that will house a combination of open plan and private offices along with a large conference room and director's suite above the lobby area. The design does not provide for future expansion horizontally or vertically, however, connectivity to future adjacent buildings is possible.

3.5.1.3 Space Program

The first floor will consist of the lobby with space for displays, elevator and restroom on the front side of the ring. An outdoor seating area with coffee bar and sandwich grille will be adjacent to the Lobby. The computer room, break room switchgear and telecom rooms are on the first floor on the inside of the ring. The second floor includes the control room, a conference room, toilets and the viewing gallery overlooking the Experimental Hall, a bridge across the Experimental Hall. The alternate third floor will house a combination of open plan and private offices.

3.5.1.4 Circulation

The primary point of entry will be the main entrance and lobby that will draw in pedestrian traffic from the parking lot and drop-off loop. Sidewalks are envisioned for pedestrian traffic to and from the adjacent future JPSI and to the CFN across Groves Street and the NSLS across Brookhaven Avenue. Interaction areas will be incorporated adjacent to key circulation areas of the building. The building also provides the primary entrance into the Experimental Hall. A bridge accessed from the second floor will span across the Experimental Hall and provide access to the control room as well as the accelerator tunnel, tunnel mezzanine, Linac and RF Building. Two elevators will provide vertical circulation within the building.

3.5.1.5 Quality of Life

Building orientation, sustainable materials, and the use of natural light will be integrated into the design to promote a comfortable and productive environment. Unlike the Ring Building, the Operation Center's envelope will consist of large areas of glass, allowing for visual transparency and to provide an inviting front door to the NSLS-II complex. The lobby will be a space for informal interaction and social events. An outdoor seating area can be provided between the Operations Center and the future JPSI building as a comfortable place to enjoy coffee or lunch.

3.5.1.6 Building Construction

The exterior of the Operations Center will be constructed of an insulated metal wall panel and stud system. The wall system on the entrance lobby will be comprised of the exterior panel system to match Type A without the liner panel, exterior sheathing, air barrier, 6 in. metal studs, fiberglass batt insulation, and interior gypsum board. The minimum thermal resistance of the system will be R-20.

The wall system on the inner ring portion of the Operations Center will be comprised of the exterior panel system to match Type A without the liner panel, exterior sheathing, air barrier, 6 in. metal studs, fiberglass batt insulation, and interior gypsum board. The minimum thermal resistance of the system will be R-20.

The roof of the Operations Center will be a flat TPO membrane roofing system that meets current LEED requirements and the energy code minimum R-value. A built-up roofing system is an option in place of the TPO system but not meet LEED requirements for Heat Island, Energy Star Roofing.

The curtain wall windows at the Operations Center will consist of 1 in. clear tempered insulated glass with a low-E coating in a thermally broken aluminum frame. The thermal transmission value for the glazing will be a U value of 0.30 in the summer and 0.30 in the winter. The visible light transmission will be 69% and the shading coefficient will be a maximum of 0.44.

The exterior doors will be curtain wall aluminum insulated doors to match the windows at the entrance, and insulated hollow metal doors and frames on the inner ring portion of the Operations Center.

3.5.1.7 Interior Finishes

The Operations Center will have gypsum board walls with wood doors and hollow metal frames. The offices will have a side light or interior window to allow natural light into the interior spaces. The interior finishes are as follows:

- Floor finishes office area and conference rooms – carpet tile
- Floor finishes control room and computer room – raised floor
- Floor finishes lobby – porcelain ceramic tile
- Floor finishes toilet rooms – porcelain ceramic tile
- Exterior walls - painted
- Interior walls typical – painted
- Interior walls conference rooms – paint or wall coverings
- Interior walls of toilet rooms – ceramic tile
- Ceiling system – suspended acoustical tiles and grid
- Doors – wood, stained
- Door frames – painted
- Floor surfaces shall have a wet slip coefficient of 0.5 or greater.

3.5.2 Ring Building

3.5.2.1 Architectural Concepts

The Ring Building is the scientific and visual focal point for the NSLS-II facility. The halo-shaped building will dominate the site by its sheer breadth, although its height is not proportionally commanding.

3.5.2.2 Future Expansion

The Ring Building is designed for future expansion by the addition of LOBs or support buildings to its outer or inner periphery. It is also possible that future beamlines will be added with a length of up to 1000 m, which will extend substantially beyond the limits of the building. The facility is being designed to allow these long beamlines to be installed in the future with minimal impact on the current building. Accommodation for the long beamlines will include an elevated access corridor between LOB 1 and 2 which will enable pedestrian and forklift traffic to transit the area with the use of ramps and lifts.

3.5.2.2 Space Program

Within the Ring Building are the Injection Building, the RF Building, the Ring Tunnel, the Tunnel Mezzanine, and the Experimental Hall. Service buildings connected to the inboard side of the Ring Building will provide HVAC, mechanical, and electrical services to some building components. The Injection and RF Buildings will have their own HVAC systems.

On the exterior of the ring there will be the Loading Dock, Stock Room and Hazardous Material Storage, located adjacent to LOB four. There is also a Grill area for food vending and lunch services, this Grill will be located adjacent to LOB one between LOB one and the main entrance.

3.5.2.3 Circulation

The access corridor around the outside perimeter of the Ring Building provides the primary circulation route for the building. It will be designed to handle both pedestrian and forklift traffic. The corridor will provide access to the Operations Center, all of the LOBs, individual laboratories within the LOBs, and the adjacent Experimental Hall. Stairs from the Experimental Hall will provide access to the tunnel mezzanine and the service buildings. The pedestrian bridge spanning the Experimental Hall will allow operators to conveniently walk between the control room and the lobby. Stairs within the service building will provide a means of accessing the ring tunnel from the tunnel mezzanine level.

Egress from the Experimental Hall will be through the four LOBs, the Operations Center, across the tunnel mezzanine and through the service buildings, or through intermediate emergency exit doors spaced around the exterior perimeter of the Ring Building.

The access corridor will incorporate provisions for the long beam lines between the LOBs. This will be a raised steel ramp and corridor that will allow the beam line to run underneath it. There will be a ramp on one end and an access platform lift on the other. Running between the beamlines from this raised corridor will be platform lifts and stairs for access to the beamlines.

3.5.2.4 Quality of Life

Although the focus of the Ring Building is the enhancement of scientific inquiry, it is desirable to make the space an environment that researchers will enjoy occupying. Comfort facilities for the Ring Building are provided in the Operations Center and in the five LOBs (two in the base build) within a reasonable distance from all beamlines. An alternate for perimeter windows will bring natural lighting into the space . Exterior shading will prevent direct sunlight from impacting experimental performance.

3.5.2.5 Building Construction

3.5.2.5.1 Experimental Hall

The Ring Building exterior walls will be comprised of a built-up sandwiched pre-formed metal wall panel system with rigid insulation and interior metal liner panel. The minimum thermal resistance of the system will be R-20. The panels profiles will be Type A on the exterior side of the Ring and Type B on the inner side of the Ring Building (Tunnel mezzanine).

The roof of the Ring Building will be a curved standing seamed metal roof system. The system will be comprised of the standing seamed roof over R24 rigid insulation, gypsum board sheathing, and structural metal roof deck.

The optional clerestory windows at the Ring Building will consist of 1 in. clear tempered insulated glass with a low-E coating in a thermally broken aluminum frame. The thermal transmission value for the glazing will be a U value of 0.30 in the summer and 0.30 in the winter. The visible light transmission will be 69% and

the shading coefficient will be a maximum of 0.44. These clerestories will be included in the design and a bid alternate.

The exterior doors of the Ring Building will be insulated hollow metal doors and hollow metal frames.

Acoustical treatments will line the ceiling and walls to maintain an acceptable noise level in the Experimental Hall.

The Grill area will be of similar construction to the ring building.

The Loading Dock and Stock rooms will be of similar construction to the adjacent LOB. See the building construction for the LOBs in section 3.5.3.

The Hazardous Storage will be made of concrete or concrete block with the appropriate fire rating. The roof will be a poured concrete flat roof with TPO roofing above the concrete. A built-up roofing system is an option in place of the TPO system but not meet LEED requirements for Heat Island or Energy Star Roofing.

3.5.2.5.2 Ring Tunnel

The ring tunnel will be constructed of poured in place standard weight concrete as described in the Building Superstructure section. Additional shielding will be provided in specifically identified areas as required. A shielded door (boronated polyethylene and lead filled steel) will be provided at each beamline allowing access to the Ring Tunnel from the Experimental Hall. Where no door is provided the opening will be blocked up with radiation shield block.

The roof of the Ring Tunnel will have embedded uni-strut at four feet on center for hanging ductwork, cable tray, piping, etc.

3.5.2.5.3 Service Buildings

The service buildings' lower level will be constructed of poured in place concrete walls with a soil berm to the height of the second level. The second level exterior walls will be a built-up metal wall panel system Type B with rigid insulation and interior metal liner panel. The minimum thermal resistance of the system will be R-20.

The roof of the service buildings will be a sloped standing seam metal roofing system. It will consist of a standing seamed roof over R24 rigid insulation, gypsum board sheathing, and structural metal roof deck.

The exterior doors of the service buildings will be insulated hollow metal doors and hollow metal frames.

Each service building will be provided with an opening into the Ring Tunnel that may be filled with concrete block as portable shielding, or be used for a superdoor (radiation shield door made of boronated polyethylene and lead-filled steel door) installation. Initially two doors will be installed.,

A one ton hoist or lift will be provided at each service building for lifting power supplies and other electric gear to the mezzanine level.

3.5.2.5.4 Injection and RF Buildings

The Booster tunnel will be constructed of poured in place standard weight concrete, which will be covered with earth as additional shielding.

The Linac Building will be constructed of a combination of poured in place standard weight concrete and a built-up metal wall panel system Type B with rigid insulation and interior metal liner panel. The minimum thermal resistance of the system will be R-20.

The exterior walls of the Booster Service building and the RF Building will be a built-up metal wall panel system Type B with rigid insulation and interior metal liner panel. The minimum thermal resistance of the system will be R-20.

Interior walls shared with the ring tunnel will be concrete of sufficient thickness to provide adequate radiation shielding.

The roof of these buildings will be a TPO membrane roofing system. It will consist of a mechanically adhered TPO roof over R24 rigid insulation, gypsum board sheathing, and structural metal roof deck. Earth covered structures will include a fluid applied water proofing system.

The exterior doors of the Booster Service building, the Klystron Galley and the RF Building will be insulated hollow metal doors and hollow metal frames.

3.5.2.6 Interior Finishes

3.5.2.6.1 Experimental Hall

The Experimental Hall will have the following interior finishes:

- Floor finishes – sealed concrete with a wet slip coefficient of 0.5 or greater.
- Exterior walls – factory-finished wall panels
- Interior walls – factory finished steel or concrete or gypsum board walls – painted.
- Steel – painted
- Roof Structure – painted
- Doors and frames– painted
- Shield doors – factory finish

3.5.2.6.2 Ring Tunnel

The ring tunnel will have the following finishes:

- Floor finishes – sealed concrete with a wet slip coefficient of 0.5 or greater.
- Interior and exterior concrete walls – painted or sealed
- Concrete roof structure – painted or sealed

3.5.2.6.3 Service Buildings

The service buildings will have the following finishes:

- Floor finishes – Sealed concrete with a wet slip coefficient of 0.5 or greater.
- Exterior and interior metal wall – Factory-finished wall panels
- Interior and exterior concrete walls – painted
- Steel – painted
- Doors and frames– painted or factory finished.
- Shield doors – factory finish

3.5.2.6.4 Injection and RF Buildings

The Injection and RF Buildings will have the following finishes:

- Floor finishes – Sealed concrete with a wet slip coefficient of 0.5 or greater.
- Exterior wall – Factory-finished wall panels
- Interior walls – factory-finished steel or concrete or gypsum board walls – painted
- Steel – painted
- Roof Structure – painted
- Doors and frames– painted
- Shield doors – factory finish

3.5.2.6.5 Loading Dock, Hazardous Storage and Stock Room

These buildings will have the following finishes:

- Floor finishes – Sealed concrete
- Exterior wall Loading Dock/Stock Room– Factory-finished wall panels
- Exterior wall Hazardous Storage – Concrete or Concrete Block
- Interior and exterior concrete walls – painted
- Steel – painted
- Doors and frames– painted or factory finished.
- Overhead Doors – Factory Finished.

3.5.2.6.6 Grille

The Grille will have the following finishes:

- Floor finishes – Sealed concrete
- Exterior– Factory-finished wall panels
- Interior walls – painted, see section 3.3.5 for acoustical requirements
- Steel – painted
- Doors and frames– painted or factory finished.

3.5.3 Lab Office Buildings

3.5.3.1 Architectural Concepts

Five LOBs (three base build and two future) will be spaced around the exterior of the Ring Building. The LOBs will be the primary entrance for many researchers and beamline staff. A focus on interactive spaces will provide an environment where collaboration is encouraged.

3.5.3.2 Future Expansion

The five Lab Office Buildings are being designed with the intent of future expansion. Each LOB is being initially programmed to support six sectors, with one insertion device and one bending magnet beamline per sector. If additional beamlines are added by canting insertion device beamlines, the LOBs will need to expand to support these. The LOBs are designed to expand horizontally along the outside of the Ring Building as future need demands. Services to any expansion, including HVAC, plumbing, power, etc. will be added at the time of the expansion. They are not included in the initial scope of the project.

3.5.3.3 Space Program

LOBs 1 and 5 will contain 72 offices, 12 laboratory modules (2 modules per lab for six total labs per LOB), conference rooms, storage, a kitchenette, a machine shop and a delivery / staging space adjacent to the loading berth. The Experimental Hall will have direct access to the staging space via a six foot wide double door. The intent of the Lab Office Buildings is to provide support space for experimentation that is close to the beamlines. Each LOB will support six sectors in the Experimental Hall. The LOB will provide offices for each supported sector. The six laboratories will be shared by all six sectors to minimize duplication of space requirements and lab equipment. Each laboratory will have direct access to the Experimental Hall access corridor via double doors for moving equipment between them. There will be two wet labs per LOB which will have fume hoods. One of these fume hoods will be HEPA filtered.

LOB four will be a shelled space in the base building work with just the exterior envelope included, this includes exterior walls, roofs, doors and windows. Minimum mechanical, electrical lighting and power rough-

in and plumbing rough-in that provides minimum life safety for exiting and to prevent freezing of sprinkler piping in the winter.

Each of the three LOBs as well as the two future will be designed to be a separate control area from the Ring Building with a one hour fire separation wall between the LOB and the Ring Building. It will then be up to the NSLS-II administration to determine which of the LOBs is designated one of the three remaining Control Areas. See section 12.4.5 for the code requirements for Control Areas.

3.5.3.4 Circulation

Each Lab Office Building will be primarily one story high with an exception for an upper level mechanical attic (accesses by stairs on the access corridor side of the LOB) and have a parking lot adjacent to the building and an exterior entrance that will be the primary entrance for most researchers and visitors. Direct access to the Experimental Hall will be provided from the lobby/interaction area and will be a controlled access point. Equipment and materials will be brought into the building from a loading area that will also allow equipment to be conveniently moved into the Experimental Hall. Pedestrian traffic to other LOBs or to the Operations Center will be via the access corridor around the perimeter of the Ring Building.

3.5.3.5 Quality of Life

The Lab Office Buildings will be home to staff and visitors who frequently work long and irregular hours. The glass storefront exterior walls will bring natural light into the office space. The glass façade and the relatively small size of the LOBs will create a contrast to the massive form of the Ring Building and will break down the scale. Open space with comfortable seating will encourage cooperative interactions between research teams. A kitchenette will include a sink, refrigerator, and microwave for preparing simple meals. Comfort facilities will include toilets and a shower in each LOB. The building materials and use of natural lighting will provide the Lab Office Buildings with a pleasant work environment.

3.5.3.6 Building Construction

The exterior walls of the LOBs will be comprised of the exterior panel system to match Type A without the liner panel, exterior sheathing, air barrier, 6 in. metal studs, fiberglass batt insulation, and interior gypsum board. The minimum thermal resistance of the system will be R-20. Portions of the LOB exterior will be an aluminum and glass curtain wall.

The roof of the LOBs will be a standing seamed metal roof system. The system will be comprised of the standing seamed roof over R24 rigid insulation, vapor barrier, and structural metal roof deck. There will be an AHU mezzanine within the roof space for air-handling equipment serving the LOB.

The curtain wall windows at the LOBs will consist of 1 in. clear tempered insulated glass with a low-E coating in a thermally broken aluminum frame. The thermal transmission value for the glazing will be a U value of 0.30 in the summer and 0.30 in the winter. The visible light transmission will be 69% and the shading coefficient will be a maximum of 0.44.

The exterior doors will be curtain wall aluminum insulated doors to match the windows or insulated hollow metal doors and frames.

The laboratory walls and doors leading from the LOB to the Ring access corridor will be one-hour rated construction. Walls will be metal stud and gypsum board and the doors will be hollow metal doors and frames.

3.5.3.7 Interior Finishes

The LOBs will have gypsum board walls with wood doors and hollow metal frames. The offices will have a side light or interior window to allow natural light into the interior spaces. The interior finishes of the LOBs are as follows:

- Floor finishes, office area and conference rooms – carpet tile
- Floor finishes, laboratories – sheet linoleum
- Floor finishes, lobby – porcelain ceramic tile
- Floor finishes, toilet rooms – porcelain ceramic tile
- Exterior walls - painted
- Interior walls, offices and labs – painted
- Interior walls, conference rooms – paint or wall coverings
- Interior walls, toilet rooms – ceramic tile
- Ceiling system – suspended acoustical tiles and grid or gypsum board at high ceilings
- Acoustical treatments – see section 3.2.5 for acoustical requirements
- Doors – stained wood
- Door frames – painted
- All floor surfaces shall have a wet slip coefficient of 0.5 or greater.

4 SUSTAINABLE DESIGN

4.1 Design Criteria

4.1.1 Codes and Standards

The latest edition of the codes, standards, orders, and guides referred to in this section will be followed, with a reference point of August 2008 being the anticipated design completion date. All work will be in accordance with BNL's Implementation Plan for DOE 413.3, "Program and Project Management for the Acquisition of Capital Assets."

4.1.2 DOE and Other Governmental Orders

Executive Order 13423 – Strengthening Federal Environmental, Energy, and Transportation Management

Energy Policy Act of 2005

10 CFR Part 433

DOE O5480.4 – Environmental Protection, Safety and Health Protection Standards
DOE O413.3A – Program and Project Management for the Acquisition of Capital Assets
DOE O414.1C – Quality Assurance
DOE O420.1B – Facility Safety
DOE O420.2B – Safety of Accelerator Facilities

4.1.3 Codes, Standards, and Guides

Building Code of New York State (NYSBC) – 2002 Edition
ASHRAE Standard 90.1-2001 Energy Standards for Buildings Except Low-Rise Residential Buildings
Energy Conservation Code of New York State - 2002 Edition
Leadership in Energy and Environmental Design (LEED) 2.2
LEED for Labs

4.2 Sustainable Design Overview and Approach

Sustainable design is an approach that addresses how design decisions will impact the natural environment, building occupants, and the bottom line. Making sustainable design a priority does not mean losing sight of other program requirements such as schedule and budget. Instead, sustainable design is as an additional set of criteria on which to base design decisions.

4.2.1 Project Goals

The National Synchrotron Light Source II (NSLS-II) Facility will strive to incorporate a wide range of sustainable strategies and objectives throughout the design and construction process, while meeting the functional requirements of advanced technology and creating a workplace that is environmentally friendly, energy-efficient, and both healthy and pleasant to be in. The team was challenged to design the NSLS-II Facility not only to meet the LEED® (The Leadership in Energy and Environmental Design) requirements but also to address the new Executive Order (EO) 13423 and the clarifying guidance dated March 29, 2007. The EO 13423 titled "Strengthening Federal Environmental, Energy, and Transportation Management" was issued

on January 24, 2007 and requires all Federal agencies to lead by example in advancing the nation's energy security and environmental performance by achieving the following goals:

- VEHICLES: Increase purchase of alternative fuel, hybrid, and plug-in hybrid electric vehicles when commercially available.
- PETROLEUM CONSERVATION: Reduce petroleum consumption in fleet vehicles by 2% annually through 2015.
- ALTERNATIVE FUEL USE: Increase alternative fuel consumption at least 10% annually.
- ENERGY EFFICIENCY: Reduce energy intensity by 3 % annually through 2015 or by 30% by 2015.
- GREENHOUSE GASES: By reducing energy intensity by 3% annually or 30% by 2015, reduce greenhouse gas emissions.
- RENEWABLE POWER: At least 50% of current renewable energy purchases must come from new renewable sources (in service after January 1, 1999).
- BUILDING PERFORMANCE: Construct or renovate buildings in accordance with sustainability strategies, including resource conservation, reduction, and use; siting; and indoor environmental quality.
- WATER CONSERVATION: Reduce water consumption intensity by 2% annually through 2015.
- PROCUREMENT: Expand purchases of environmentally-sound goods and services, including biobased products.
- POLLUTION PREVENTION: Reduce use of chemicals and toxic materials and purchase lower risk chemicals and toxic materials from top priority list.
- ELECTRONICS MANAGEMENT: Annually, 95% of electronic products purchased must meet Electronic Product Environmental Assessment Tool standards where applicable; enable Energy Star® features on 100% of computers and monitors; and reuse, donate, sell, or recycle 100% of electronic products using environmentally sound management practices.
- ENVIRONMENTAL MANAGEMENT SYSTEMS: Implement EMS at all appropriate organizational levels to ensure use of EMS as the primary management approach for addressing environmental aspects of internal agency operations and activities.

Our team will evaluate five of the goals listed in the Executive Order that apply directly to new building construction:

- Energy Efficiency
- Greenhouse Gases
- Renewable Power
- Building Performance
- Water Conservation

4.2.2 LEED Point System

The LEED Rating System is a voluntary, consensus-based, national rating system developed by the U.S. Green Building Council. LEED provides a complete framework for assessing building performance and meeting sustainability goals. Its current version: LEED Version 2.2 for New Construction and Major Renovations (NC) is being proposed for this project. With this version, USGBC has launched a series of enhancements including LEED on-line which will aid in the documentation and certification process for this

project. LEED projects can now submit 100% of their documentation on-line, track Credit Interpretation Requests (CIRs), manage key project details, etc.

Consistent with the USGBC LEED program and the Executive Order the team identified five key principles that define and guide our sustainable approach. These principles will continue to be monitored throughout the design and construction and include the following:

- Site: Sustainable Site Design
- Water: Protecting and Conserving Water
- Energy: Designing for Energy Efficiency and Considering Alternative Energy Sources
- Materials: Optimizing the Environmental Life Cycle of Materials
- IEQ: Enhance Indoor Environmental Quality

The project is evaluated per each LEED criteria which is either a 'Prerequisite' or 'Credit' which results in a point score for certification:

Prerequisites: This category is based on minimum requirements and must be met. No further points will be awarded unless the minimum is achieved. There are a total of seven Prerequisites.

Credits: Credits are evaluated and result in a point score. Under LEED-NC v.2.2 there are 69 total points available.

The certifications levels are available as follows:

LEED Certified	26-32 Points
LEED Silver	33-38 Points
LEED Gold	39-51 Points
LEED Platinum	52-69 Points

4.3 Sustainable Site

- Maximizing the benefit of the existing site can be accomplished though a number of sustainable measures, one of which is stormwater management. The volume of stormwater generated on the site depends on the area of impervious surfaces and it could potentially have a negative Impact on the New York Sound Water Quality.
- To control the quantity of stormwater run-off detention ponds have been designed to capture excess and reduce the impact on the municipal system.
- The possibility of utilizing bio-retention ponds or pervious pavement to treat stormwater runoffs is proposed, in addition to controlling quantity. These strategies help to promote infiltration, and capture and treat the stormwater runoff.
- Our team identified other life Cycle Cost Savings Strategies that can reduce stormwater runoffs and provide significant savings in potable water use for the building. Rainwater Collection System if implemented could in fact contribute to achieving eight LEED Credits and reduce annual potable water usage for the building by up to 7.5 million gallons. Annual Rainwater Collection for the NSLS-II calculated based on 48" annual average rainfall (see Table 4.1 below) from 310,000 sf roof area equals 7,827,000 gal per year. The LEED Credits affected by this approach are as follows: Potable Water Usage Reduction: For 500 Occupants = 778,800 gal/yr (64,900 gal/month) = 3 Credits
- Potable Water Usage Reduction for Process Cooling = 7,050,000 gal/yr (587,500 gal/month) = 1 Innovation Credit

- Stormwater Runoffs Reduction = 2 Credits
- Irrigation = 2 Credits

Table 4.1 - BNL Monthly Average Rainwater Collection

Month	Ave. rainfall inches	Collection area sq. ft.	gal per in. sf	Recovered water %	Collected gallons
Jan	3.75	310,000	0.62	85	612,600
Feb	3.42	310,000	0.62	85	558,700
Mar	4.17	310,000	0.62	85	681,300
Apr	4.01	310,000	0.62	85	655,100
May	3.93	310,000	0.62	85	642,000
Jun	3.93	310,000	0.62	85	642,000
Jul	4.44	310,000	0.62	85	725,400
Aug	4.49	310,000	0.62	85	733,500
Sep	4.14	310,000	0.62	85	676,400
Oct	3.83	310,000	0.62	85	625,700
Nov	3.95	310,000	0.62	85	645,300
Dec	3.85	3100,000	0.62	85	629,000
Totals	48				7,827,000

Table 4.2 - Rainwater Harvesting System Design Based On One Storage Tank Per Each LOB Building.

Quantity	Description	Unit cost	Total cost
5	Storage tanks, above ground, 40,000 gal each (200,000 gal total storage)	$1.00 per gal	200,000
2500 lf	Aluminum or galvalume gutters and downspouts	$6.00 per lf	15,000
5	"First wash" equipment (piping, strainers, valves, tanks)	$800 each	4,000
5	Distribution equipment (piping, pumps, pressure tanks)	$1200 each	6,000
5	Misc. piping, valves, etc. per tank	$1000 each	5,000
1	Contingency	10%	13,000
1	Design and engineering fees	15%	21,000
TOTAL			$264,000

(Cost based on other projects.)

4.4 Water: Protecting and Conserving Water

Implementing water efficiency measures can reduce potable water withdraws, and often save building owners money. In addition, sustainable water use protects natural water bodies from contamination. To reduce potable water consumption, no permanent irrigation will be provided for the site, the plantings will be native to the region and will require little or no additional water after new growth has been established.

In addition to rain water usage, we will specify water conserving fixtures to provide savings of 20-30 percent less water than the water usage requirements under the Energy Policy Act 1992. Appropriate water treatment will be required prior to water re-use.

4.5 Energy: Designing for Energy Efficiency and Considering Alternative Sources of Energy

The impact that energy use has on the environment is broad and long-lived. Almost every aspect of conventional energy use poses some threat to the natural environment. To create energy requires fuel. Harvesting these fuel resources from the Earth, whether they are coal, natural gas, oil or wood, is destructive to natural habitats. Federal Energy Management Program (FEMP) at the US Department of Energy (DOE) released an interim final rule for new federal building energy efficiency standard that requires new buildings to achieve an energy consumption level that is at least 30% below the level achieved under the standard (ASHRAE 90.1-2004).

Implementing energy efficient strategies will include daylighting, high energy efficiency equipment, EMS optimization, ENERGY STAR roof, and commissioning. These will all contribute to a reduction off the baseline- creating a building which will perform at a higher level, ultimately reducing overall energy consumption and reducing operating and maintenance costs.

Some of the Life Cycle Cost Saving Strategy proposed to reach highest possible Energy Efficiency for this project follows:

- Solar shading
- Energy Efficient Building Envelope and Roofing System
- Daylight Harvesting and Occupancy Sensors
- Energy Efficient Lighting System
- Designed to economically turn waste heat into useful heat for loads such as space heating and domestic hot water
- Process load recovery
- Exhaust air heat recovery to be used on 100% outside air handling units.
- On-Site renewable energy sources

Design and construction project's costs associated with the above energy efficiency strategies can be defined further as the project's design progresses and LEED Certification Level is approved by the Client.

4.6 Materials: Optimizing the Environmental Life Cycle of Materials

Almost 70 percent of all energy invested in a building's construction is embodied in the materials themselves. Embodied energy is the energy required to extract, transport, process, install, recycle or dispose of these materials. Our team will evaluate the environmental impact, resource efficiency and performance of the proposed building materials. We will consider non-toxic materials from local and renewable sources.

The material selection process will focus on life-cycle issues rather than solely on aesthetic or first cost. The team is committed to maximize use of recycled content materials and those that are manufactured regionally.

Material recycling will be facilitated to reduce waste and conserve resources. The design team will provide for an area dedicated to the separation, collection, and storage of materials for recycling by the building occupants.

Construction Waste Management Plan will be required for this project. A minimum of 75% of construction, demolition and land clearing waste will be recycled and/or salvaged to meet LEED requirements.

The team is committed to specifying locally manufactured materials and recycled content materials that are durable and esthetically pleasing.

4.7 IEQ: Enhance Indoor Environmental Quality

The quality of the indoor environment has a significant impact on human health, productivity and quality of life. Sustainable indoor environments promote daylighting, natural ventilation, and interiors that are free of toxins. The result is an interior environment that safeguards occupant health, and reduces operating costs. These can include strategies such as CO2 monitoring System, low VOC and non-toxic materials, air monitoring systems.

A large contributor to the quality of the indoor environment is the indoor air quality; the development and implementation of an Indoor Air Quality (IAQ) Management Plan during construction and pre-occupancy can positively impact both the occupant and the maintenance budget.

In addition to industry standard sustainable initiatives, NSLS-II team will propose specific innovations in sustainability pertaining to IEQ and human comfort. These innovations include using furniture systems which use post-consumer recycled content and reduce harmful VOCs into the working environment. This in conjuncture with the development and utilization of simulated daylight will add to the quality of the indoor working environment providing signification benefits to human health, productivity and quality of life.

4.8 LEED Status

In order to keep track of LEED prerequisite and credit point status of the project a tracking spreadsheet has been developed and attached to this report.

A description of the columns included in the spreadsheets is as follows:

- LEED Prerequisite/ Credit. Title and Intent of each prerequisite/credit taken directly from LEED. What the credit/prerequisite is meant to achieve.
- LEED Points Available. Notes the number of points available for each LEED credit if an REQ'D appears in the column, this indicates a prerequisite for which there are no associated points).
- "Yes" / "Maybe" / "No" Status
  - "Yes" The credit can be achieved
  - "Maybe" The credit will be pursued although there is not enough information at this time to assume it will be earned
  - "No" The credit is not achievable.

To meet LEED Certified Level it is required to have a minimum of 26 points. Current design shows that we can achieve 28 Yes and 18 Maybe points. The feasibility of achieving LEED Certified is shown in the LEED Point Summary below and it is also in line with the new Federal mandates. There are minimal cost implications associated with this strategy. These costs can be defined further as the project's design progresses.

Table 4.3 - LEED NC 2.2 TOTAL POINT SUMMARY

Certified Level
Yes 28 points
Maybe 18 points
No 23 points
Total Possible 69 points
SUSTAINABLE SITES
Yes 5 points
Maybe 7 points
No 2 points
Total Possible 14 points
WATER EFFICIENCY
Yes 3 points
Maybe 2 points
No 0 points
Total Possible 5 points
ENERGY & ATMOSPHERE
Yes 3 points
Maybe 1 points
No 13 points
Total Possible 17 points
MATERIALS & RESOURCES
Yes 7 points
Maybe 0 points
No 6 points
Total Possible 13 points
INDOOR ENVIRONMENTAL QUALITY
Yes 6 points
Maybe 7 points
No 2 points
Total Possible 15 points
LEED AP AND INNOVATION CREDITS
Yes 4 points
Maybe 1 points
No 0 points
Total Possible 5 points

4.9 LEED Project Checklist

LEED-NC Version 2.2 Registered Project Checklist is included below for Certified Level.

5 STRUCTURAL ENGINEERING

5.1 Design Criteria

5.1.1 Codes and Standards

The latest edition of the codes, standards, orders, and guides referred to in this section will be followed, with a reference point of August 2008 being the anticipated design completion date. All work will be in accordance with BNL's Implementation Plan for DOE 413.3, "Program and Project Management for the Acquisition of Capital Assets."

5.1.2 DOE Orders

DOE O5480.4 – Environmental Protection, Safety and Health Protection Standards
DOE O413.3A – Program and Project Management for the Acquisition of Capital Assets
DOE O414.1C – Quality Assurance
DOE O420.1B – Facility Safety
DOE O420.2B – Safety of Accelerator Facilities

5.1.3 Codes, Standards, and Guides

Building Code of New York State (NYSBC) – 2002 Edition
American Concrete Institute
Building Code Requirements for Structural Concrete (ACI 318-99)
BNL Standards Based Management System Subject Areas
New York State and Suffolk County Department of Health Codes
American National Standards Institute
ANSI 117.1 Accessible and Useable Buildings and Facilities
AISC Specification for Structural Steel Buildings
SJI Standard Specifications for Long Span Steel Joists (LH Series) and Deep Long Span Steel Joists (DLH Series)
American Society for Testing Materials Standards
Factory Mutual
National Institute of Standards and Technology
Occupational Safety and Health Administration (OSHA)
Underwriters Laboratory
New York State Fire Prevention Code - 2002 Edition
Americans with Disabilities Act Accessibility Guideline (ADAAG)
Leadership in Energy and Environmental Design (LEED) 2.2
LEED for Labs

5.2 Soil Conditions

5.2.1 Subsurface Conditions

The subsurface explorations encountered topsoil lying above a layer of fill overlying a stratified sand deposit that extends to more than 100 ft deep. Topsoil ranging in thickness from 2 to 12 in. was encountered in

borings drilled in landscaped areas. Topsoil was not encountered in borings drilled in paved/developed areas. Each of the borings encountered fill ranging in thickness from 2 to 9 ft. This fill is characterized as silty sand or widely-graded sand. Fill was also detected within the upper 1 to 10 feet in CPT soundings made near existing roadways. Several explorations experienced refusals, indicating buried objects within the fill.

A layer of stratified sand, sand with silt, and sand with gravel was encountered below the fill in all of the borings and CPT soundings. The sand is light brown to brown, with density ranging from medium dense to very dense.

Subsurface explorations were terminated within the sand at maximum depths of about 100 ft. A 1999 report on the stratigraphy and hydrogeologic conditions at the lab prepared by the United States Geologic Survey refers to the sand as the "Upper Glacial Aquifer," and states that the thickness at BNL is about 185 ft. Confining clay units and additional sand and gravel aquifers overlie bedrock, which reportedly occurs at a depth of about 1,500 ft.

The depth to groundwater appears to range from about 21.5 to 36.5 ft below ground surface, depending on the location at the site. This is based on the boring and CPT observations, as well as data collected in 2003 for CFN.

The soil beneath the NSLS-II has an average shear velocity that classifies it as a stiff profile for earthquake design purposes as defined by the New York State Building Code. The corresponding site class is D. The soil is not considered to be susceptible to liquefaction.

It is recommended that foundations be designed as spread footing foundations with slab-on-grade floors. Fill should be removed below footings so they bear directly on the sand deposits, or on a layer of compacted structural fill placed after removal of fill. Maximum allowable bearing pressure is 2.5 tons per square foot on footings at least 3 ft wide.

The site contours indicate that the Experimental Hall floor will range from 9 ft below grade to 4 ft above grade. Floors are well above groundwater levels encountered in the explorations. It is recommended that the slab-on-grade floors bear on a minimum of 6 in. of compacted structural fill placed over the natural sand deposit. The existing fill should be removed below floor slabs due to the tight settlement tolerance. Adequate densification should be accomplished using a heavy roller for both the native sand as well as the structural fill. This will provide a base for the Experimental Hall floor and should yield a low differential settlement when combined with the floor slab design.

Soils beneath the floor slab will settle in response to dead and live loads. It is anticipated that settlement will be complete within about one to two weeks after load application. Settlement resulting from floor slab dead loads and fill required beneath the floor slab is expected to occur during construction, and therefore will not contribute to post-construction settlement. However, the 250 psf live load could cause minor post-construction settlement. GEI calculated that the total and post-construction settlement from the live load to be less than 0.25 inches. Differential settlement will be less than the total settlement.

5.2.2 Laboratory Testing

Geotechnical studies of the proposed NSLS-II building site have been performed which included 21 grain size distribution analyses on soil samples recovered from the test borings.

5.3 Design Loads

5.3.1 Live Loads:

- Laboratories: 125 psf
- Experimental Hall: 250 psf (2000 psf capacity of 15 inch SOG)

- Ring Tunnel: 250 psf (3000 psf capacity of 33 inch SOG)
- Booster Ring 250 psf (2000 psf capacity of 18 inch SOG)
- Tunnel Mezzanine: 250 psf
- Ring Building Access Corridor: 125 psf or wheel loads from fork lift trucks
- Corridors: 100 psf
- Stairs, Lobbies & Viewing Gallery: 100 psf
- Offices: 100 psf (incl. 20 psf for partitions)
- Light Storage Areas: 125 psf
- Mechanical Rooms: 150 psf or actual weight of equipment

5.3.2 Snow Loads:

- Ground snow load Pg: 45 psf
- Snow importance factor I_s: 1.0 (Category I)
- Snow exposure factor Ce: 0.9
- Thermal Factor Ct: 1.0
- Design snow load: 30 psf + drift where applicable

5.3.3 Wind Loads:

- Basic wind speed (3-second gust): 120 mph
- Wind load importance factor I_w: 1.00 (Category I)
- Wind exposure: B

5.3.4 Earthquake Loads:

- Short period acceleration Ss: 0.25g
- 1 second period acceleration S1: 0.08g
- Site Class: D
- Seismic Use Group: I
- Seismic Design Category: B
- Seismic Importance Factor I_E: 1.0 (Category I)

5.4 Structural System

5.4.1 Foundation:

Geotechnical investigation reports on the project done during the Conceptual Design Phase (August 30, 2006) and Advanced Conceptual Phase (May 25, 2007) by GEI Consultants recommend the foundation system to be spread footings bearing directly on sand deposits or compacted structural fill after removal of existing fill. The recommended maximum allowable bearing pressure is 2.5 tons per square foot.

5.4.2 Building Super-Structure:

a) Ring Building:

The overall structure for this building will be in structural steel with curved roof supported by 67'-0" span open web steel joists on columns radially spaced on inner and outer rings @ approximately 21'-0" and 25'-0" spacing respectively. For lateral force resistance, radial steel joists shall be connected to end columns by moment connections and braced frames shall be used circumferentially. The roof deck shall typically be 20 GA – 1 ½" thick steel deck.

Within the Ring Building, there will be the ring tunnel, walls and roof of which shall be constructed in cast-in place concrete. The thickness for walls adjacent to earth berming shall be 20" and the thickness for walls without earth berming shall be 32". The tunnel roof slab shall be 34" thick, designed to provide shielding and support the electrical gear. The tunnel floor slab shall be 33" thick reinforced concrete slab on grade poured in place over compacted sub-grade.

The Experimental Floor shall have 15" thick reinforced concrete slab, poured in place over compacted sub-grade. This slab shall be poured against and tied to the tunnel floor slab with rebar dowels to minimize differential settlement. Isolated from this slab, will be the 8" reinforced concrete access corridor slab, poured over compacted sub-grade near the outer ring and designed for fork lift truck wheel loads.

b) Service Buildings:

These buildings along the inner perimeter of the Ring Building shall be two story structures with concrete exterior walls at the Lower Level supporting the braced steel frames for the Second Floor above. The concrete side walls shall be designed for lateral earth pressure from the berms.

The Second Floor construction shall typically consist of 20 GA – 2" thick composite steel deck with 3" lightweight concrete topping (total slab thickness = 5") supported on framework of steel beams and girders.

The Roof will comprise of structural steel framing supporting 20 GA – 1 ½ " thick steel roof deck.

The First Floor construction shall consist of 6" thick slab on grade reinforced with 6x6 – W2.9 x W2.9 WWF over 6" compacted granular fill and vapor retarder. Vibrating equipment areas will have a structural slab with an air gap between the compacted fill below.

c) Operations Center Building:

This two story building (with alternate third floor) shall have construction similar to the Service Buildings except that the lowest story shall be framed and braced in structural steel too.

d) Lab Office Buildings

These are generally single story structures with Penthouse above the laboratories. The Penthouse floor construction shall comprise of 20 GA – 2" thick composite steel deck with lightweight concrete topping (total slab thickness = 5") supported on framework of steel beams and girders. The roof shall consist of 20 GA - 1 ½ " thick steel roof deck supported on structural steel beams and girders instead of open web steel joists (See sketch SK-6 for typical framing) The use of steel beams/girders will provide better support for the mechanical equipment and systems.

The First Floor construction shall be similar to the Service Buildings.

e) Linac and RF Buildings:

These structures are mainly single story structures with partial mezzanine/ second level floor in the RF Building. Construction of these structures in structural steel is similar to Service Buildings.

f) Access Tunnel:

There will be an Access Tunnel 20’ wide and 14’ high (clear height) that will go through under the Ring Building for service vehicles .The tunnel retaining walls shall be about18” thick reinforced concrete walls, also supporting the tunnel roof/experimental floor. This may consist of eight span continuous one way reinforced concrete slabs supported on concrete beams spanning between the tunnel walls.

g) Special Considerations:

The floor slab for the Storage Ring Tunnel, the Experimental Hall and the Booster Tunnel shall be designed to allow minimal differential settlement. Thickness of floor slabs, walls, and tunnel roof are driven by radiation shielding requirements and not gravity loads.

The floor slabs of the Storage Ring Tunnel, Booster and Linac tunnel, and the Experimental Hall shall be structurally continuous with no isolation joints or contraction joints.

5.4.3 Lateral Load Resisting System:

Lateral loads shall be mainly resisted by braced frames wherever possible, otherwise by moment frames where bracing location would become architecturally prohibitive.

5.4.4 Materials

- Concrete (normal weight, unless noted otherwise):

  Foundation and slab on grade: f'c = 4000 psi.

  Piers, walls, grade beams, slabs and stairs on grade: f'c = 4000 psi.

  Light weight concrete for Second Level/Mezzanine Floors: f'c = 4000 psi.

- Reinforcing steel:

  Deformed: ASTM 615, Grade 60.

  Welded wire fabric: ASTM A185.

- Structural steel:

  Wide flanges and tees: ASTM A992, Fy = 50 ksi.

  Channels, angles and plates: ASTM A36, Fy = 36 ksi.

  Steel pipes: ASTM A53, Type E or S, Grade B, Fy = 35 ksi.

  Structural tubes: ASTM A500, Grade B, Fy = 46 ksi.

  Anchor bolts: ASTM F1554, 3/4" dia. min.

  Bolts: ASTM A325, 7/8" dia. min.

- Steel Joists:

  Chord and web sections: ASTM A36, Fy = 36 ksi ; or ASTM A588 Fy = 50 ksi

6 MECHANICAL – HVAC SYSTEMS

6.1 Design Criteria

6.1.1 Codes and Standards

The latest edition of the codes, standards, orders, and guides referred to in this section will be followed, with a reference point of August 2008 being the anticipated design completion date. All work will be in accordance with BNL's Implementation Plan for DOE 413.3, "Program and Project Management for the Acquisition of Capital Assets."

6.1.2 DOE Orders

DOE O5480.4 – Environmental Protection, Safety and Health Protection Standards
DOE O413.3A – Program and Project Management for the Acquisition of Capital Assets
DOE O414.1C – Quality Assurance
DOE O420.1B – Facility Safety
DOE O420.2B – Safety of Accelerator Facilities

6.1.3 Codes, Standards, and Guides

Building Code of New York State (NYSBC) – 2002 Edition
American National Standards Institute
ANSI 117.1 Accessible and Useable Buildings and Facilities
American Society of Mechanical Engineers
American Society for Testing Materials Standards
American Society of Heating, Refrigeration, and Air Conditioning Engineers (ASHRAE) Design Guidelines
ASHRAE Standard 90.1-2001 Energy Standards for Buildings Except Low-Rise Residential Buildings
American Water Works Association
ANSI/ASHRAE Standard 62-2001 Ventilation for Acceptable Indoor Air Quality
ANSI/AIHA Z9.5-2003 Standards for Laboratory Ventilation
ANSI/ASHRAE 110-1985 Method of Testing Performance of Laboratory Fume Hoods
Factory Mutual
Mechanical Code of New York State
National Institute of Standards and Technology
National Fire Protection Association (NFPA) Standards
Sheet Metal and Air Conditioning Contractors' National Association (SMACNA) Standards for Ductwork Design
Occupational Safety and Health Administration (OSHA)
Underwriters Laboratory
New York State Plumbing Code - 2002 Edition
New York State Fire Prevention Code - 2002 Edition
Energy Conservation Code of New York State - 2002 Edition
Americans with Disabilities Act Accessibility Guideline (ADAAG)
Leadership in Energy and Environmental Design (LEED) 2.2
LEED for Labs

6.2 Design Conditions

6.2.1 Outdoor:

Summer - 95 °F dry bulb,
76 °F wet bulb

Winter - 0 °F, 15 mph wind

6.2.2 Indoor:

Table 6.1 Indoor Design.

Area Designation	Design Temperature ºF		Accuracy ±ºF	Relative Humidity %		Accuracy ±%RH
	Winter	Summer		Winter	Summer	
Ring Tunnel	78	78	0.18	30	50	10%
Experimental Hall	75	75	1.0	30	50	10%
Booster Ring Tunnel	78	78	1.8	30	50	10%
Linac	72	75	1.8	30	50	10%
Klystron Gallery	72	75	1.8	30	50	10%
RF Building	72	75	1	30	50	10%
Offices	72	75	5	30	50	10%
Laboratories	72	75	5	30	50	10%
Conference Rooms	72	75	5	30	50	10%
Support Spaces	72	75	5	30	50	10%

6.2.3 Air Filtration:

Table 6.2 Air Filtration.

Area	Pre-filters	Final Filters
Tunnel	30%	95%
Laboratories / shops	30%	95%
Experimental Hall	30%	95%
Linac & RF	30%	95%
Offices, lobby, support	30%	90%

6.3 Utility Systems

6.3.1 Chilled water

1. Twenty inch supply and return chilled water pipes will be connected from the existing underground site chilled water system to the building. The chilled water temperature supplied by the Central Plant is 46°F. The flow and supply/return water temperature difference will be measured for cooling energy calculations. Estimated cooling load of the building is 2400 tons. The total chilled water flow is 4100 GPM using 14 °F temperature rise. Chilled water will serve air handling units, electrical power supply units, and miscellaneous cooling equipment. Since the chilled water pumps at the central plant have adequate capacity and head, no chilled water pumps

will be provided in the building. Chilled water will also be used for temperature control trim and redundancy for process cooling water systems located in the service buildings.

6.3.2 Steam

Steam is available at the site from the Central Utility Plant at 125 psig.

The estimated peak steam load of the new building is 17,000 lbs/hr, and the estimated size required for the underground steam supply pipe is 8 inch. The condensate will be collected at a duplex condensate receiver and returned to the central plant in a separate conduit using a 3 inch Schedule 80 carrier pipe. Condensate pumps will be sized for 2.5 times the maximum condensate flow and for 40 psig head. Steam flow will be measured for energy calculations.

6.3.3 Process Cooling Tower Water

Cooling towers located at the building and operating year around will provide cooling for the process system. The estimated cooling load of 2700 tons will be handled by three cooling towers of 1350 ton each, one of which will operate as stand-by. The system will be sized for 11°F temperature difference and 84°F tower leaving water temperature.

6.4 HVAC Systems

6.4.1 General Laboratories

In laboratories, a minimum of 12 air changes per hour will be used, providing 2 cfm/sq. ft based on 10 ft ceiling height. Assuming no external heat gain, 1.5 W/sq. ft for lighting, and 165 sq. ft /person for people load, this design will allow 9.5 W/sq. ft miscellaneous heat gain from equipment. After the equipment heat gain and the number of fume hoods are further defined, the supply and exhaust air requirement of the laboratories will be finalized. In order to minimize the systems energy usage, coil loop heat recovery will be provided as an alternate. It consists of glycol heat recovery coils in the air handling units and in the exhaust system. Duplex pumps, each sized for 100% of the maximum capacity will circulate glycol between the coils to transfer heat from the exhaust air into the outside air in the winter. Depending upon outdoor conditions, the system can also be used in the summer to pre-cool the outside air. The Fire Department will have the ability to control the ventilation system to exhaust smoke. The control will be at the fire alarm system panel in the main lobby of the Operational Center and each of the LOB buildings.

6.4.2 Accelerator Tunnel

The Accelerator Tunnel HVAC systems consist of five constant volume custom packaged air handling units located along the tunnel in five service buildings. The AHU's will have 2inch double wall construction, galvanized steel inner lining, and stainless steel condensate drain pan. Each unit will include prefilter, silencers, steam preheat coil, cooling coil, dual supply and return fans, 95% final filter, steam humidifier, hot water reheat coil, and a duct mounted low heat density electric reheat coil for final accurate temperature control with SCR controller. The supply and return fans will have Adjustable Frequency Drives (AFD) to compensate for filter loading, allow future flexibility, and provide ease of adjustment during balancing. Supply air will be cooled to 50°F for dehumidification and reheated by the fan heat and hot water reheat coil to 0.9°F (0.5°C) below the required discharge temperature. The final discharge temperature to the tunnel will be controlled by the electric reheat coil to ±0.18°F (0.1°C) accuracy. Four high precision temperature sensors per air handling unit will be located in the tunnel. Their accuracy will be ±0.018°F (0.01°C). Temperature will be controlled by any individual sensor or by the average of the four. Cooling coil discharge temperature

will be reset based upon the tunnel relative humidity to maintain RH set point with minimum energy consumption.

6.4.3 Experimental Hall

The Experimental Hall HVAC systems consist of ten variable air volume packaged air handling units located in the service buildings, two units per pentant. They will be variable volume terminal reheat type utilizing hot water for reheat. The units will have 2 inch double wall construction with stainless steel condensate drain pans and galvanized steel interior liner. Unit components include return fan, relief and outside air sections, 30% prefilters, silencers, steam preheat coil, cooling coil, supply fan, and humidifier. The supply and return fans will have adjustable frequency drives. Cooling coils will be sized to cool the air to 50°F for dehumidification. Return air will be partially ducted. Return registers will be located above the accelerator tunnel in order to remove the heat generated by the equipment. Hutches will be served by constant volume air terminal units with hot water re-heat coil and two exhaust registers to remove the contaminants. The hutch exhaust systems will be sized for future exhaust requirements and will have 100% redundant fans. One general exhaust system, serving toilets, janitor closets, and other areas requiring exhaust, will be provided for each sector. The Fire Department will have the ability to control the ventilation system to exhaust smoke. The control will be at the fire alarm system panel in the main lobby of the Operational Center and each of the LOB buildings.

6.4.4 RF Service Building

The Service building will be served by a rooftop mounted HVAC unit sized for the total sensible equipment load. Depending on the final load, one or two CRAC units will be installed for stand by. Ventilation and humidity control will be provided by a 2inch double wall air handling unit sized for 6 AC/HR but normally delivering 2 AC/HR 100% outside air. The added capacity will also allow the unit to be used for smoke evacuation.

6.4.5 Booster Ring Tunnel

The tunnel will be served by a constant volume custom packaged air handling unit, located in the service building. The AHU's will have 2inch double wall construction, galvanized steel inner lining, and stainless steel condensate drain pan. Each unit will include pre-filter, silencers, steam preheat coil, cooling coil, supply and return fans, 95% final filter, steam humidifier, and hot water reheat coil. The supply and return fans will have Adjustable Frequency Drives (AFD) to compensate for filter loading, allow future flexibility, and provide ease of adjustment during balancing. Supply air will be cooled to 50°F for dehumidification. The Fire Department will have the ability to control the ventilation system to exhaust smoke. The control will be at the fire alarm system panel in the service building.

6.4.6 Booster RF Service Room

The Service Room will be served by a variable volume packaged air handling unit located on the roof. The AHU will have 2 inch double wall construction, galvanized steel inner lining, and stainless steel condensate drain pan. The unit will include pre-filter, silencers, steam preheat coil, cooling coil, supply and return fans, 95% final filter, steam humidifier, and hot water reheat coil. The supply and return fans will have Adjustable Frequency Drives (AFD) to compensate for filter loading, allow future flexibility, and provide ease of adjustment during balancing. Supply air will be cooled to 50°F for dehumidification.

6.4.7 Linac and Linac Klystron Gallery

The Linac and Gallery will be served by a constant volume packaged air handling unit located in Booster RF Service Room. The AHU will be a constant volume re-heat type with 2 inch double wall construction, galvanized steel inner lining, and stainless steel condensate drain pan. Unit will include pre-filter, steam preheat coil, cooling coil, supply and return fans, 95% final filter, steam humidifier, and hot water reheat coil. The supply and return fans will have Adjustable Frequency Drives (AFD) to compensate for filter loading, allow future flexibility, and provide ease of adjustment during balancing. Supply air will be cooled to 50°F for dehumidification. Constant volume air terminal units will be utilized for individual space temperature control.

6.4.8 Operations Center

The Operations Center will be served by a variable volume packaged air handling unit located on the roof of the building. The AHU will have 2inch double wall construction, galvanized steel inner lining, and stainless steel condensate drain pan. Unit will include pre-filter, silencers, steam preheat coil, cooling coil, supply and return fans, 90% final filter, steam humidifier, and hot water reheat coil. The supply and return fans will have Adjustable Frequency Drives (AFD) to compensate for filter loading, allow future flexibility, and provide ease of adjustment during balancing. Variable air volume air terminal units with hot water re-heat coil will be utilized for space temperature zone control.

The computer room and control room will be served by chilled water computer room air conditioning (CRAC) units complete with 90% efficiency filter, humidifier and hot water heating coil.\

The lobby entrance will be served by a constant volume packaged air handling unit located in the mechanical room, complete with 90% efficient filter, cooling coil and hot water heating coil.

6.4.9 Lab Office Building

The building will be served by two air handling units located in the penthouse, one to serve the office area and the other to serve the laboratory area. The office area AHU will be a variable volume unit and the laboratory area AHU will be a constant volume unit. Both AHU's will have 2inch double wall construction, galvanized steel inner lining, and stainless steel condensate drain pan. The office air handling unit will include pre-filter, silencers, steam preheat coil, cooling coil, supply and return fans, 90% final filter, and steam humidifier The laboratory air handling unit will include pre-filter, steam heating coil, heat recovery coil, cooling coil, supply fan, 95% final filter, and steam humidifier. Both AHU's will utilize Adjustable Frequency Drives (AFD) to compensate for filter loading, allow future flexibility, and provide ease of adjustment during balancing. Variable volume air terminal units with hot water re-heat coil will be used for office area temperature zone control and constant volume air terminal units with hot water re-heat coil will be used for laboratory area temperature zone control.

6.5 Air Handling Units - General

All air-handling units will have access sections between the various components to allow efficient airflow through the units and adequate space to perform inspection and maintenance. All units will be installed in draw through configuration providing good dehumidification and even air flow through the cooling coils.

Supply and return fans will be housed centrifugal, belt-driven and will have high efficiency airfoil blades and AMCA label. In order to minimize their vibration, all fans will be dynamically balanced after installation on the job site. Air pre-filters and final filters will be replaceable cartridge type with filter efficiencies based on NBS Atmospheric Dust Spot Method. Their sizes will be standardized 24 x 24 and 12 x 24 inch where possible.

Energy efficient electric motors will be compatible with AFD's.

6.6 Air Distribution

6.6.1 Ductwork

All ductwork will be constructed in accordance with SMACNA standards. Supply air ducts will be galvanized steel, and be insulated on the exterior. High-pressure duct upstream of the terminal units will be built to 6 inch WG pressure standards and will be sized for medium velocity. Low-pressure ducts constructed to 2 inch WG will be used from terminal units to diffusers. Flexible run outs to diffusers will allow ease of installation and provide final sound attenuation of terminal unit and duct-generated noise. Exhaust and return ductwork will be low and medium pressure construction sized for 0.075 inch WG/ 100 ft friction loss and/or 1800 FPM velocity maximum. It will be un-insulated except in areas where condensation on duct surfaces may occur. In supply ducts, no internal lining will be used. Galvanized steel will be used for all lab main exhaust ductwork and stainless steel for all exposed branch ductwork.

6.6.2 Air Terminal Units

Temperature control of individual spaces will be by constant and variable volume terminal units with reheat coils. Heating coils will have copper tubes with bonded aluminum fins. Separate terminal units will be provided for areas requiring individual temperature control. Offices with similar thermal load, maximum four, may be served by one terminal unit.

6.6.3 Diffusers, Registers and Grilles

Four-way, louvered faced supply diffusers and perforated face return and exhaust registers will be used in laboratories and administrative offices.

In noise and vibration sensitive areas, high volume diffusers will be considered. Air devices in large open areas will be sized to provide good air distribution and maximum noise criteria of NC 35.

6.6.4 Pressurization

A negative pressurization of 100 cfm per door will be maintained in the laboratories by exhausting more air from the rooms than is supplied.

In toilets, janitor closets, and other less critical areas, negative pressurization will be maintained at 50 cfm per door. The entire building will be kept at positive pressure.

6.6.5 Ventilation

Ventilation will be provided as follows:

- Offices, conference rooms and other occupied areas will be provided a minimum of 20 cfm per person.
- The Experimental Hall will be provided 20 cfm per person.
- Laboratories will be provided 6 air changes per hour minimum.
- The Ring Tunnel will be provided 6 air changes per hour.
- The Booster Tunnel and Linac will be provided 6 air changes per hour.
- Service Buildings will be provided 6 air changes per hour.
- The RF Building will be provided 6 air changes per hour

6.7 Exhaust Systems

6.7.1 Exhaust fans will be provided for the following:

- Fume hoods
- General laboratory exhaust
- Toilet rooms
- Mechanical and electrical rooms
- Process equipment
- Hazardous storage
- Beamline hutches via a common exhaust system
- Other areas requiring exhaust

6.7.2 Chemical Fume Hoods

Chemical fume hoods will be designed for a maximum airflow based upon a 100 fpm air velocity with the sash open to 18 in. height. All hoods shall have flow alarms. The Laboratory HVAC system will be a constant volume design utilizing air valves. Fume hoods identified for nanomaterials research will be provided with bag-in bag-out HEPA filtration rated at 99.97% efficiency, with gel seal type filter housing. At least one such hood will be furnished for each LOB. Wet laboratories will also be provided with ventilated chemical storage cabinets integral to the fume hood. All fume hoods shall be configured to be retrofitted with HEPA filtration in the future. Hoods shall be tested in the "As-Installed" condition.

6.7.3 Bio-Safety Cabinets

The need for these is yet to be determined.

6.8 Distribution Systems

6.8.1 Steam Distribution

The building will be served with 125 psig high pressure steam from the central plant which will be reduced in the main utility vault to 15 psig. Two pressure reducing valves, one used as standby, will be provided. The 15 psig steam will be routed underground inside the ring and distributed to the individual service buildings. Steam will be used in preheat coils, heat exchangers, domestic water heaters, humidifiers, and other miscellaneous heating devices. Condensate from the individual service buildings will be pumped to a main condensate receiver located in the central mechanical equipment room. From there, condensate will be returned to the Central Plant. Flash steam from high pressure condensate will be recovered in a flash tank and utilized in the low pressure system.

6.8.2 Heating Hot Water

In order to minimize the building's energy consumption, the primary source of hot water for space heating will be heat pumps located in the individual service buildings. They will recover heat from the process cooling system, utilizing it as the energy source for space heating. Excess heat from the process

system will be directed to cooling towers on the site. An alternate to this approach is to use the process cooling water directly as a heat exchange medium. As a back up to the heat recovery system and to provide supplementary heating if necessary, the hot water will be circulated through steam fired heat exchangers located in the individual service buildings. The hot water will be used for terminal reheat coils, reheat coils in air handling units, and in miscellaneous heating devices such as fan coil units, unit heaters, and finned tube radiation. Duplex heat exchangers will each be sized for 100% of the heating load, while redundant circulating pumps will each be sized for 66% of the full flow. Control valves will be two-way type, with three-way valves used at the end of long runs to assure adequate system circulation and minimum 25% flow through the circulating pumps. Isolation valves will be provided for future maintenance, and piping will be designed in a reverse return configuration to simplify balancing.

6.8.3 Chilled Water

The pumps at the central plant have adequate capacity to serve the building. Consequently, no local chilled water pumps will be provided. Chilled water will be supplied directly to cooling coils and miscellaneous cooling equipment such as fan coil units. Cooling coils will be selected for 12-14 °F waterside temperature difference. In general, two-way control valves will be used at the air handling unit chilled water coils to achieve flow reduction at low loads, while three-way valves will be provided at the end of long runs to maintain minimum flow. For the electrical power units' cooling, a secondary cooling system will be provided consisting of duplex plate heat exchangers and duplex circulating pumps each sized for 100% of the cooling load.

6.8.4 Process Cooling Water

The 18 inch main condenser water supply and return piping will be routed underground inside the ring. It will be distributed to each service building to serve process water for aluminum and non-aluminum system heat exchangers.

6.8.5 Humidification

For humidification, steam from the central plant will be utilized by humidifiers in the air handling units to maintain the required humidity levels. Multiple manifold stainless steel humidifiers will be located downstream of final filters and will be selected to minimize vapor trail. Humidity sensors will be located in the return air ducts.

6.8.6 Piping Systems

Water and steam piping will be schedule 40 black steel with screwed joints through 2inch and welded joints 2-½inch and up. Schedule 80 black steel will be utilized for condensate return pipe to provide a longer life. Steam and condensate piping shall be pre-insulated with galvanized or epoxy coated steel jacket. Pipe will be provided with fiberglass pipe insulation and all-service jacket with self-sealing lap. Hydronic piping systems will be sized for a maximum velocity of 8 feet per second, and a maximum pressure drop of 4 ft WG per 100 ft. In noise and vibration sensitive areas, velocity will be limited to 4 feet per second. Chilled water piping insulation will be provided with vapor barrier jacket to prevent condensation. In-line circulators will be used for pumps under 1/2 HP. Pumps 1/2 HP and larger will be base mounted end suction or vertical/horizontal split case type. Motors 3 HP and over will be premium efficiency. Strainers, check valves, and temperature and pressure gauges, water treatment system, air and pressure control will be provided. Clean steam supply and condensate return pipes will be stainless steel.

6.9 Miscellaneous Heating/Cooling Devices

Fan coil units will be provided in stairways and lobbies for heating, cooling, and humidity control. Unit heaters will be used in mechanical and electrical equipment rooms. Finned tube radiation will be used to offset the "cold wall" effect of exterior walls and windows in offices and other areas.

6.10 Energy Conservation

In order to minimize the building's energy consumption and comply with LEED certification criteria, various energy conservation techniques will be evaluated during the design and will be incorporated if analysis is favorable.

6.10.1 Energy Saving Measures

For air handling units with 100% outside air, coil loop heat recovery will be provided. The filters and heat recovery coil will be bypassed during non-recovery periods to minimize exhaust fan energy.

The building heating system will utilize heat pumps to recover heat from process cooling.

Discharge temperature of heating hot water will be reset during the summer to minimize heat loss.

Adjustable Frequency Drives (AFD's) will be used for all major air moving devices and pumps. This will provide considerable energy savings for the variable volume air and hydronic systems. For constant volume air handling units serving the laboratories, AFD's will simplify initial balancing, accommodate future changes, and save energy by allowing adjustment as filters become loaded.

High efficiency equipment and high efficiency motors will be selected for all applications.

Non-critical air handling units will utilize optimum start-stop energy management software.

Insulation of piping systems will exceed the applicable energy codes.

6.11 Automatic Temperature Control

Direct digital controls compatible with the existing Building Automation System will be utilized. Except for air terminal units, control valves and dampers will have pneumatic actuators. A duplex control air compressor, air dryer, and filter will be installed in the lower level mechanical room.

Air handling units with return fans will have airside economizer, allowing the utilization of 100% outside air for free cooling. A signal from the fire alarm system will shut down all air-handling units. The Fire Department may manually activate a smoke purge.

6.12 System Testing and Balancing

6.12.1 Waterside

System will be leak tested, and pumps and other equipment will be checked for alignment and proper operation. Flow through pumps will be measured and properly adjusted. Motor amperage will be read and recorded.

6.12.2 Air Side

High-pressure supply ducts and all hood exhaust duct systems will be tested for leaks. System fans will be checked for proper rotation and balance, and all drive sheaves will be adjusted for proper airflow. Motor

amperage will be read and recorded. Airflow at all terminal units, diffusers, registers, and grilles will be adjusted to specifications and recorded.

6.13 Vibration

Minimization of vibration caused by rotating equipment is a primary concern for the NSLS-II facility. Several strategies will be used to accomplish this goal.

1. Rotating equipment will not be located adjacent to the Ring Tunnel or the Experimental Hall. Separation is a primary strategy for reducing the impact of vibration on the machine performance.
2. Mechanical equipment will be isolated from distribution systems using flexible connectors where possible.
3. Major equipment items will be specified at a higher quality level (not commercial standard).
4. Major rotational equipment will be factory balanced.
5. Rotating equipment will be mounted using vibration isolation supports and where applicable, inertia bases will be used.
6. Distribution systems such as piping and ductwork will be supported using vibration isolators.

6.14 Commissioning

Due to the size and complexity of the project and in compliance with LEED requirements, a commissioning contractor will supervise and document performance of all equipment startup, balancing, testing and verification.

Table 6.3 NSLS-II Estimated Cooling Load.

	Chilled Water Loads											
Load	Linac	Linac / Klystron Galley	Booster RF	Booster Ring Tunnel	RF Service Building	Tunnel Mezzanine	Ring Tunnel	Experimental Hall	OPS Center	Lab Office Building	Process Chilled Water	Process Cooling Tower
EQUIPMENT (KW)												
Transformers						59						
RF power usage	40	40	16		264							2734
Booster controls			1									
Storage Ring controls					4						36	
Cryogenic Plant												1000
RF diagnostics	1				1							
Controls & Instrumentation	13		64	12				65			30	
Vacuum								24			219	
Interlock						32					32	
Tunnel Magnets							229					
Tunnel Leads							95	231				1872
Power Supply								34			651	
Equipment Leads						189						
Sub-total (KW)	54	40	81	12	269	280	324	354	0	0	968	5606
Sub-total (MBH)	183	137	277	40	918	957	1106	1208	0	0	3304	19132
Walls & Roof (MBH)	7	7	16	-	13	478	-	1910				
Lights (MBH)	17	16	53	34	69	348	195	1349				
People Sensible (MBH)	1	1	5	9	9	34	34	137				
OA Sensible (MBH)	1	1	4	9	10	101	44	303				
People Latent (MBH)	2	2	5	9	9	34	34	135				
OA Latent (MBH)	2	2	5	10	10	213	149	446				
Fan Heat to SA(MBH)	47	36	79	19	227	409	265	1036				
TOTAL LOAD (MBH)	260	202	443	129	1265	2572	1825	6525				
TOTAL LOAD (TONS)	22	17	37	11	105	214	152	544	48	577	275	1594

TOTAL CHILLER LOAD (TONS) 2002 TOTAL COOLING TOWER LOAD (TONS) 1,594

Assumptions:

Fan heat based on 4.5 deg. F rise.

Lab office bldg is based on Calculated Load

OPS Center is based on Calculated Load

Equipment load is based on BNL spread sheet and meeting comments.

Wall & roof load based on calculated skin load

Outside air at 20 cfm/person based on BNL estimated people occupancy.

7 MECHANICAL ENGINEERING - PLUMBING

7.1 Design Criteria

7.1.1 Codes and Standards

The latest edition of the codes, standards, orders, and guides referred to in this section will be followed, with a reference point of August 2008 being the anticipated design completion date. All work will be in accordance with BNL's Implementation Plan for DOE 413.3, "Program and Project Management for the Acquisition of Capital Assets."

7.1.2 DOE Orders

DOE O5480.4 – Environmental Protection, Safety and Health Protection Standards
DOE O413.3A – Program and Project Management for the Acquisition of Capital Assets
DOE O414.1C – Quality Assurance
DOE O420.1B – Facility Safety
DOE O420.2B – Safety of Accelerator Facilities

7.1.3 Codes, Standards, and Guides

Building Code of New York State (NYSBC) – 2002 Edition
American National Standards Institute
ANSI 117.1 Accessible and Useable Buildings and Facilities
American Society of Mechanical Engineers
American Society for Testing Materials Standards
American Society of Heating, Refrigeration, and Air Conditioning Engineers (ASHRAE) Design Guidelines
ASHRAE Standard 90.1-2001 Energy Standards for Buildings Except Low-Rise Residential Buildings
American Water Works Association
ANSI/ASHRAE Standard 62-2001 Ventilation for Acceptable Indoor Air Quality
ANSI/AIHA Z9.5-2003 Standards for Laboratory Ventilation
ANSI/ASHRAE 110-1985 Method of Testing Performance of Laboratory Fume Hoods
Factory Mutual
Mechanical Code of New York State
National Institute of Standards and Technology
National Fire Protection Association (NFPA) Standards
Sheet Metal and Air Conditioning Contractors' National Association (SMACNA) Standards for Ductwork Design
Occupational Safety and Health Administration (OSHA)
Underwriters Laboratory
New York State Plumbing Code - 2002 Edition
New York State Fire Prevention Code - 2002 Edition
Energy Conservation Code of New York State - 2002 Edition
Americans with Disabilities Act Accessibility Guideline (ADAAG)
Leadership in Energy and Environmental Design (LEED) 2.2
LEED for Labs

7.2 Plumbing Systems

The NSLS-II facility will require the following plumbing systems:

- Domestic cold water
- Domestic hot water
- Sanitary sewer
- Tempered water (for emergency eye wash and shower)
- Storm (rain) water drainage

These services will be distributed within the Operations Center, the LOBs, the Experimental Hall, and the Booster / Linac and RF Buildings.

7.3 Preliminary Design

7.3.1 Plumbing Systems

7.3.1.1 Potable Water

Scope/Major elements	Water heaters
	Piping and accessories
	Safety showers/ eye washes
Redundancy	Two mains, with multiple connection points to the site system will connect to form a looped system feeding the building.
Cold water supply temperature	Ambient
Hot water supply temperature	See Narrative below
Coverage	Experimental Hall
	Operations Center
	LOB
Service buildings	
Materials of construction	
Piping	3 in. and over: Ductile iron, cement lined (buried)
	3 in. and under: Copper (above ground)
Valves	Ball, globe or gate, bronze
Pumps	Stainless steel impeller, shaft
	Mechanical seals
	Ductile iron casing
Tanks	Galvanized steel (storage)
	Stainless steel or glass lined (water heaters)
Remarks	Disinfected to code requirements

Single 3 inch domestic water services with valves will be extended from the site water main to the Service Buildings as described below. The available pressure has not been verified at this time. Flow data will be obtained during Title II. Installation of a booster pump is not anticipated.

Supply for the domestic water systems shall originate from the water main loop on the interior (courtyard) side of the Ring Building. This interior loop shall be fed from an exterior (road side) loop water main in two locations. In turn, the exterior loop is also fed from two locations from the water mains on the site. (See Civil discussion for additional information on the water distribution plan.)

A domestic service shall enter each of the Service Buildings and supply the water system for the Service Building, adjacent LOB, and approximately 20-percent of the Ring Building. The service will be provided

with two (2) full size ASSE 1013 listed reduced pressure backflow prevention devices piped in parallel. Potable water serving the facility will be used for both the domestic and laboratory plumbing fixtures and equipment.

Laboratory faucets will incorporate integral vacuum breakers, and make-ups to mechanical and laboratory equipment will be provided with appropriate backflow prevention devices.

Domestic hot water will be provided at each laboratory building mechanical equipment room and include a circulated piping system. Hot water will be produced by a storage type electric water heater. The hot water will be stored at 140°F and distributed to lavatories and laboratory fixtures at 120°F through a thermostatic mixing valve.

A tempered (85°F) water distribution piping system will be provided through a thermostatic mixing valve and used as the source for the eyewash / safety showers located throughout each laboratory building. The system will be circulated.

Type "L" copper tubing with wrought copper or cast brass fittings and solder joints will be the pipe material. The pipe joints will be formed with 95-5 tin-antimony solder or code approved "lead free" solder and flux having a chemical composition equal to or less than 0.2-percent lead. Piping 2 in. and smaller may be joined with fittings utilizing a copper crimping system such as the Rigid/Viega ProPress System. 2½ in. piping and over may be schedule 40 galvanized steel with threaded or mechanical couplings (Victaulic style connections). The piping will be insulated with fiberglass pipe insulation having an all service jacket and self-sealing lap.

7.3.1.2 Sanitary

At a minimum, each LOB and Service Building will have a sanitary sewer connection to the site sanitary sewer. Due to the anticipated elevations of the site sanitary sewers, several of the LOB's will need to have sewage ejectors. The remainder will be gravity flow. (See Civil Discussion for additional description of the site sanitary sewers.)

The sanitary drainage system will provide drainage facilities for the toilet fixtures and mechanical room drains. The piping will typically be 4-inch where water closets are served, and 3-inch otherwise. The associated vent piping will be 2-inch and 1 1/2-inch respectively.

Horizontal collection into the building drain will occur below the slab of the First floor and generally exit by gravity to the site sanitary sewer.

To facilitate maintenance and reliability of service, cleanouts will be provided throughout the drainage system. Generally, these will be in accordance with Code requirements, however, consideration of placement will also address accessibility and disturbance to the ongoing functions of the facility. Cleanouts will be the same size as the pipe to which they are connected up to 4-inch, and for larger sizes the cleanout will not exceed 4-inch. Long sweep ells, or wye and 1/8th bends will be utilized to transition from the cleanout to the pipe to permit easy entry for maintenance.

Service weight cast iron soil pipe and fittings was selected as the piping material for this system. Cast iron piping has repeatedly proven its dependability of service. Two methods of joining the pipe and fittings are available. The gasketed bell and spigot joint using a neoprene gasket will be used for the portions of the system placed underground. The no-hub clamped joint using a one piece neoprene gasket, and stainless steel shield with retaining clamps will be used for the above ground portions where the possibility of modifications exist.

7.3.1.3 Storm (Rain) Water Drainage

Storm water will be collected utilizing commercially available drains of style, size, and quantity consistent with the area being drained. Sizing of the drains and collection piping will be based on using a rainfall rate of 3 inches per hour for a storm of 1 hour duration and 100 year return for the primary roof drainage system. Where required, emergency overflow drains and piping will be provided. The piping will generally be routed vertically from the drains to below the First floor slab where it will be collected horizontally and discharge by gravity to the site storm sewers.

Cleanouts will be provided and will follow the same parameters described for the sanitary drainage system.

The pipe materials will be the same as those selected for the sanitary drainage system.

8 FIRE PROTECTION

8.1 Design Criteria

8.1.1 Codes and Standards

The latest edition of the codes, standards, orders, and guides referred to in this section will be followed, with a reference point of August 2008 being the anticipated design completion date. All work will be in accordance with BNL's Implementation Plan for DOE 413.3, "Program and Project Management for the Acquisition of Capital Assets."

8.1.2 DOE Orders

DOE O5480.4 – Environmental Protection, Safety and Health Protection Standards
DOE O413.3A – Program and Project Management for the Acquisition of Capital Assets
DOE O414.1C – Quality Assurance
DOE O420.1B – Facility Safety
DOE O420.2B – Safety of Accelerator Facilities
10 CFR 851

8.1.3 Codes, Standards, and Guides

Building Code of New York State (NYSBC) – 2002 Edition
American National Standards Institute
ANSI 117.1 Accessible and Useable Buildings and Facilities
American Society for Testing Materials Standards
Factory Mutual
Mechanical Code of New York State
National Institute of Standards and Technology
National Fire Protection Association (NFPA) Standards
Occupational Safety and Health Administration (OSHA)
Underwriters Laboratory
New York State Fire Prevention Code - 2002 Edition
Americans with Disabilities Act Accessibility Guideline (ADAAG)

8.2 Preliminary Design

8.2.1 Fire Zones

The NSLS-II complex is divided into five fire zones, corresponding to the ring pentants.

8.2.2 Fire Protection System

Scope/Major elements	Fire water main
	Hydrants
	Piping, sprinklers and accessories
Redundancy	System loop is fed from two connection points to the site system
Capacity	Per Code
Coverage	Entire NSLS-II complex
Hazard classifications	Ordinary Hazard Group 1 unless noted otherwise
Accelerator tunnel	See narrative
Experimental Hall	See narrative
Office / Public spaces	See narrative
Utility areas	See narrative
Gas cabinets	See narrative
Chemical storage areas	Extra Hazard Group 2
Fire hose allowance	Per NFPA 13
Fusible link rating	As required for application
Minimum supply pressure	TBD
Materials of construction	
Piping	Ductile iron, cement lined (buried)
	Schedule 40 black steel (above ground)
Valves	Butterfly or OS&Y – Supervised
Pumps	Not required.

Within each fire zone a single fire service will be extended from the site water main to the Service Buildings as described below. The available pressure has not been verified at this time. Fire flow data will be obtained during Title II from the BNL Fire Protection Engineering Group. Installation of a fire pump is not anticipated.

Supply for the fire protection systems shall originate from the water main loop on the interior (courtyard) side of the Ring Building. This interior loop shall be fed from an exterior (road side) loop water main in two locations. In turn, the exterior loop is also fed from two locations from the water mains on the sight. (See Civil discussion for additional information on the water distribution plan.)

A fire service shall enter each of the Service Buildings and supply the four (4) combined sprinkler and standpipe systems for the Service Building, adjacent LOB, and approximately 20-percent of the Ring Building. The service will be provided with two (2) full size Underwriters Laboratory and Factory Mutual listed reduced pressure principle backflow prevention devices piped in parallel. Downstream of the service entry there will be a wet alarm valve assembly for the combined sprinkler and standpipe systems. The combined sprinkler and standpipe systems are: the Service Building with the area above the Mezzanine floor, the remained of the Experimental floor, the Tunnel, and the LOB. Each floor within a system shall be individually annunciated and provided with a supervised zone control valve. The header will have two (2) fire department Siamese connections. One connection shall be located on the front face of the building, and the other on the interior face (courtyard) of the building. Each shall be located near an entry point into the facility. A water motor gong connected to each wet alarm valve assembly will be provided. The water motor gong shall be located adjacent to the entrance on the exterior interior ring wall.

The multiple wet sprinkler systems will be designed to provide 100-percent protection of the facility. A 2 inch capped pipe fed from the Experimental floor sprinkler system shall be provided by each of the beamline entrances for protection of hutches. Where the piping installation will be subject to freezing temperatures, dry sprinklers will be employed.

Interior piping will be Schedule 40 steel pipe. No other piping material will be acceptable. The piping will be joined by welding, threaded fittings, or roll-groove fittings and couplings. Pipe and fittings used in dry pipe portions of the system will be galvanized inside and outside.

Unless otherwise indicated, the entire sprinkler system will be designed as an Ordinary Hazard Group 1 occupancy with 0.15 GPM/SF density. The remote hydraulic area for each system shall be calculated at 2500 square feet.

A fire standpipe system is not required for this facility based on the Building and Fire Codes of New York State. However, per BNL's requirements, a fire standpipe system will be provided that will serve 2-1/2 inch fire department valves. These valves will be located in the Ring Building approximately every 200 feet around the Experimental Hall. The 2-1/2 inch fire department valves will have 2-1/2 x 1-1/2 inch reducers. Additional fire department valves will be located in stairs and at all other entrance as required to achieve total coverage. Hose valves in stairs shall be located on the floor level and not the intermediate level stair landing.

Fire hydrants will be located along the Loop Road outside of the Ring Building and along the Service Road inboard of the Ring Building at distances meeting DOE and local code requirements, but not more than 300 ft from all building entrances. Hydrants will not be located less than 50 feet from the building.

9 PROCESS SYSTEMS

9.1 Design Criteria

9.1.1 Codes and Standards

The latest edition of the codes, standards, orders, and guides referred to in this section will be followed, with a reference point of August 2008 being the anticipated design completion date. All work will be in accordance with BNL's Implementation Plan for DOE 413.3, "Program and Project Management for the Acquisition of Capital Assets."

9.1.2 DOE Orders

DOE O5480.4 – Environmental Protection, Safety and Health Protection Standards
DOE O413.3A – Program and Project Management for the Acquisition of Capital Assets
DOE O414.1C – Quality Assurance
DOE O420.1B – Facility Safety
DOE O420.2B – Safety of Accelerator Facilities

9.1.3 Codes, Standards, and Guides

Building Code of New York State (NYSBC) – 2002 Edition
American National Standards Institute
ANSI 117.1 Accessible and Useable Buildings and Facilities
American Society of Mechanical Engineers
American Society for Testing Materials Standards
American Water Works Association
ANSI/AIHA Z9.5-2003 Standards for Laboratory Ventilation
Factory Mutual
Mechanical Code of New York State
National Institute of Standards and Technology
National Fire Protection Association (NFPA) Standards
Occupational Safety and Health Administration (OSHA)
Underwriters Laboratory
New York State Plumbing Code - 2002 Edition

9.2 Preliminary Design

Process systems will be provided to NSLS-II to meet the needs of the accelerator, beamlines, and laboratories. The following process systems are included:

- Nitrogen
- Liquid nitrogen
- Compressed air
- Deionized water
- Process Cooling Water (provided by Accelerator Systems)

9.2.1 Nitrogen

Scope/Major elements	Site nitrogen skid, evaporator
	Piping and accessories
Redundancy	None*
Supply pressure	100 psig
Coverage	Experimental Hall
	Lab Office Buildings
Materials of construction	
Piping	Type L hard-drawn copper, oxygen cleaned
Valves	Ball, full port, brass, 3-piece, oxygen cleaned

*System redundancy is initially not provided, however the system will be configured to add an additional nitrogen tank and vaporizer in the future as beamlines are added and demand increases.

The source for gaseous nitrogen will be vaporizers installed at the liquid nitrogen tank. Primary distribution will occur in the Ring Building. Secondary mains serving the lab/office buildings will be valved to permit isolation for maintenance and modifications. Branches serving individual laboratory modules will be valved.

Piping material will be type L copper tubing with wrought copper fittings and solder joints utilizing 95-5 tin-antimony solder.

The gaseous nitrogen distribution system will be designed to maintain a maximum pressure drop of 10-percent from the point of discharge to the farthest outlet.

9.2.2 Liquid Nitrogen

Scope/Major elements	Site nitrogen skid
	Piping and accessories
Redundancy	None*
Coverage	Experimental Hall
	RF Building
Materials of construction	
Piping	Vacuum jacketed

*System redundancy is initially not provided, however the system will be configured to add an additional nitrogen tank and vaporizer in the future as beamlines are added and demand increases.

Liquid nitrogen will be stored in a centrally located tank between LOBs 4 and 5. Primary distribution will occur in the Ring Building with connection points available for beamline use and the RF cryo systems area. Filling stations will be provided at each lab/office building to permit dewars to be filled.

The piping distribution system will be through vacuum jacketed piping with either a dynamic or static vacuum. The piping shall contain an inner carrier tube and an exterior jacket. The annular space shall be under vacuum and have appropriate spacers. The system components (piping, fittings, valves, etc.) shall be products manufactured by, or provided by, a single manufacturer and not built up assemblies.

9.2.3 Clean Dry Compressed Air

Scope/Major elements	Filter / dryer skids
	Piping and Accessories
Redundancy	Oil free back-up compressor / dryer skid
Capacity	TBD
Supply pressure	100 psig from site system
	95 psig after regulator
Quality	Clean (Oil free), dry air
Moisture	-20°F dew point
Particulate	1 micron
Coverage	Experimental Hall
	Central Lab Office Building
	Lab Office Buildings
	Service buildings
Materials of construction	
Piping	Hard-drawn copper, brazed
Valves	Ball, full port, brass

The source for the laboratory compressed air will be the site wide 100 psig system. The site system is oil free, filtered, clean, and dried to minus 20°F dew point.

To assure clean, dry compressed air delivery to the laboratories, the incoming service will be provided with a 1 micron coalescing filter to collect moisture and/or particulates originating in the site distribution piping. The filter will be designed to remove all particulates 1 micron and larger, and 100% of liquid water. A pressure regulator will be installed downstream of the filter and set for a discharge pressure of 95 psig. Individual connection points for personnel use will be provided with a regulator set limiting the pressure to 30 psig.

Piping for the system will be Type L copper tubing (ASTM B819) with wrought copper fittings and brazed joints. All components including valves will be cleaned for oxygen service and capped and/or bagged by the manufacturer for delivery to the site for installation. Assembly will be with brazing filler alloy without the use of flux.

Note: During the detailed design phase the need for both a GN2 system and compressed air system will be evaluated. It may be feasible to just utilize GN2 in lieu of compressed air service. The compressed air main will be run to the NSLS II site as part of the connection to the central chilled water system and will be available if deemed necessary.

9.2.4 Deionized Water

Scope/Major elements	DI water
	Point-of-use systems
Redundancy	
Capacity	
Supply temperature	78 F
Supply pressure	
Make-up water source	Potable water make-up system
Coverage	Lab Office Buildings Laboratories
Water quality	
Resistivity	1 mega-ohm/cm (min)
Materials of construction	
Piping	Sch. 80 polypropylene
Tanks	GRP, stainless steel
Valves	Diaphragm or ball, polypropylene
Pumps	Stainless steel

Each Lab Office Building that requires DI water as a consumable will be provided with a separate point-of-use water system. The system will include polishing, storage, and distribution components. Point-of-use polishing units will be installed in the laboratory designated for “wet use” in each LOB.

9.2.5 Process Cooling Water

The deionized process cooling water systems for the Booster, Linac, Storage Ring and beamlines are included in the Technical Construction portion of the NSLS-II project. These systems will be located in designated space in the Service Building and the equipment areas of the Injection and RF Buildings. Conventional Facilities will provide process cooling tower water and chilled water to these systems.

The process cooling tower water system will reject the majority of the process loads captured by the process water systems. Chilled water will be used to finely control the cooling water temperature. Plate and frame heat exchangers located in the mechanical equipment room spaces will reject heat to both the process cooling tower water system and the chilled water system. Process cooling water piping will be distributed around the perimeter of the Ring Building. Chilled water piping will be insulated to prevent condensation at low supply water temperatures. Cooling tower water and process cooling water systems will not require insulation.

10 ELECTRICAL ENGINEERING

10.1 Design Criteria

10.1.1 Codes and Standards

The latest edition of the codes, standards, orders, and guides referred to in this section will be followed, with a reference point of August 2008 being the anticipated design completion date. All work will be in accordance with BNL's Implementation Plan for DOE 413.3, "Program and Project Management for the Acquisition of Capital Assets."

10.1.2 DOE Orders

DOE O5480.4 – Environmental Protection, Safety and Health Protection Standards
DOE O413.3A – Program and Project Management for the Acquisition of Capital Assets
DOE O414.1C – Quality Assurance
DOE O420.1B – Facility Safety
DOE O420.2B – Safety of Accelerator Facilities

10.1.3 Codes, Standards, and Guides

Building Code of New York State (NYSBC) – 2002 Edition
National Electrical Code, NFPA 70, 2008.
Standard for Electrical Safety in the Workplace, NFPA 70E, 2004
National Fire Alarm Code, NFPA 72, 2002
Life Safety Code, NFPA 101, 2006
Emergency and Standby Power Systems, NFPA 110, 2005
29 CFR 1910, Occupational Safety and Health Standards
29 CFR 1926, Safety and Health Regulations for Construction
Energy Conservation Code of New York State - 2002 Edition
Americans with Disabilities Act Accessibility Guideline (ADAAG)
Leadership in Energy and Environmental Design (LEED) 2.2
LEED for Labs

10.2 SITE UTILITIES

10.2.1 Relocation and/or Demolition of Existing Utilities

The scope of relocation and/or demolition of existing electric and communication utilities will be based on a utility survey and the final building footprint. Existing utilities around the perimeter of the site that are active will remain, while utilities that cross the site and are abandoned will be removed where they cross under the footprint of the building.

10.2.2 Building 603 Substation Expansion:

The Building 603 campus substation will be expanded to include a fourth transformer (Transformer #0) to support the NSLS-II project. Plans and specifications associated with this work and modifications within

Building 603 will be provided in a separate package to allow early construction to begin in advance of the NSLS-II building package.

The existing 69 kV substation yard will be modified to allow the new equipment to be installed. The two existing 69 kV potential transformers will be relocated. A new 69 kV SF6 breaker and a new 20.0/26.7/29.9 MVA, 66.0-13.8 kV transformer will be provided. A new fire separation wall will be provided between the existing Transformer #3 and the new transformer. The exterior of Building 603 adjacent to the Transformer #0 will be sprayed with an exterior grade fire proofing material.

Within Building 603, the existing walls around the storage room will be removed and a new 275 ft2 addition with a roll-up door will be provided to house the relocated supplies. Existing utilities above the proposed location of the new switchgear line-up will be rerouted.

The new Bus #0, 15 kV, SF6 metal-clad switchgear will be located over the existing cable trench and adjacent to the existing Bus #2 switchgear.

The Bus #0 switchgear will include a 2000 A main breaker, three 2000 A tie breakers to Bus #1, Bus #2, and Bus #3, one 1200 A outgoing breaker to feed the NSLS-II project, and three cells for future 1200 A outgoing breakers.

A new 2000 A tie breaker will be provided in each of the existing Bus #1, Bus #2, and Bus #3 switchgear lineups.

A new 1200 A outgoing breaker will be provided in one of the empty cells in the Bus #2 switchgear to provide redundant service to the NSLS-II Project.

Modifications to existing switchgear will match their respective manufacturer’s standards.

2000 A, 15kV busway will be utilized between the new transformer and the new switchgear, and to interconnect the new switchgear to each of the existing lineups.

10.2.3 Campus Distribution:

Two 1000 A feeders will be provided to serve the NSLS-II Project. The primary feeder will originate at the Bus #0 switchgear in Building 603. An alternate for a back-up feeder will be included which will originate at the Bus #2 switchgear.

Each feeder will consisting of two sets of 3-1/C, 1000 kcmil, 15 kV, MV-105, 133% EPR copper conductors and will be routed through a new manhole and duct bank system from Building 603 south along North Sixth Street, and west along Brookhaven Avenue to the NSLS-II site. The duct bank will be a 6-way 6 in. concrete encased duct bank.

The manhole and duct bank portion of this work will be included in the Building 603 substation upgrade package. The feeder cables will be included in the NSLS-II building package.

10.2.4 NSLS-II Site Distribution:

The site distribution system will be configured in a primary selective scheme with all unit-substations connected to the primary feeder.

A 6-way 6 in. concrete-encased duct bank will be routed from a manhole at Brookhaven Avenue to a manhole in the infield of the Ring Building via the basement utility room. A 6-way 6 in. duct bank will then be routed around the infield interconnecting all the unit-substations. Each 1000 A feeder consisting of two sets of 3-1/c, 1000 kcmil, 15 kV, MV-105, 133% EPR copper conductors will be routed to the “A” and “B” switches receptively of each unit-substation.

One unit-substation will be located at each Service Building #1 through #5 and at the Linac / Booster Building. Two unit-substations will be located between the Cryo Plant and the RF Building..

Each unit-substation will consist of primary switchgear, a 13,800-480Y/277 V, oil-filled substation type transformer, and a secondary air terminal section. The primary switchgear will be 15 kV outdoor, non-walk-in metal-enclosed switchgear with a key-interlocked duplex switch in series with one set of fuses. Each 2000 or 2500 kVA transformer will be triple rated 55˚ OA, 65˚ OA, and 65˚ FA. A duct bank and secondary feeder will be extended from the secondary air terminal cabinet to the 480 V switchgear located in the main electrical room of each service building. In lieu of a secondary air terminal cabinet, the unit-substations serving the Cryo Plant and RF Building will include outdoor walk-in 480Y/277 volt switchgear for distribution of feeders to loads within the Cryo Plant and RF Building.

An outgoing 480 V feeder in two 4 in. ducts (minimum one spare) will be provided from switchgear #2 to the process cooling tower facility on the north side of Brookhaven Avenue.

10.2.5 Voice/Data:

A new four-way 4 in. concrete-encased ductbank will be provided from existing manhole MH-84 to the BDF room in the Operations Building. The ductbank will be used for both copper and fiber optic cables.

Copper cables will be routed from Building 537 to the BDF via manholes MH-85 and 84.

Fiber optic cable will be routed from Building 515 near the intersection of Brookhaven Avenue and Rochester Street through existing ductbanks and manholes MH-14B, 14H, 87, 86, 85 and 84 and through a new 4-way 4” duct bank from MH-84 to the BDF.

10.2.6 Street Lighting:

New street lighting, matching the Brookhaven standard, will be provided along Brookhaven Avenue between Groves Street and the last vehicle entry point into the site, and along Groves Street between Brookhaven Avenue and its last vehicle entry point into the site. Pole mounted full cut-off fixtures will be provided to comply with LEED and Dark-sky requirements. The street lights will be circuited to building lighting panels via the building low-voltage lighting control panels.

10.3 Interior Power Distribution

10.3.1 Service Building Power Distribution:

A 3000 or 4000 amp, 480Y/277 V, 3-phase, 4-wire switchgear will be located in each of the five service building main electrical rooms. Each switchgear will include a main breaker section, and two or more distribution sections. The main sections will contain a drawout power air circuit breaker, CTs, digital meter with communication, and surge suppression equipment. Feeder devices in the distribution sections will also be drawout power air circuit breakers.

480 Y/277 V distribution panels will be located in the mechanical rooms on both levels to serve lighting and mechanical equipment. Receptacle panels will be located adjacent to each mechanical panel to serve receptacles and other 120 V equipment.

Electrical power loads are shown in Table 10.1 at the end of this section.

10.3.2 Tunnel and Tunnel Mezzanine Power Distribution:

Most of the equipment that supports the storage ring is located on the mezzanine above the tunnel and operates at 120 or 208 V. Power to this equipment will be distributed on a per cell basis with 6 cells served by

each of the five Service Building switchgear line-ups (each cell serves two beamlines). A separate 480Y277 V feeder will serve one distribution panel at each cell. This panel will in turn sub-feed five 208Y120 V panels via separate transformers. A separate transformer and double section panel will be provided for each of the three single magnet power supply racks. A fourth transformer and double section panel will be provided to serve the vacuum instrument racks. A fifth transformer will serve Experimental Hall equipment.

To reduce arc-flash hazard, transformer sizes will be limited and remote controlled electrically operated molded case circuit breakers will be provided in the 480Y/277 V panel.

Future branch circuits can be routed from the panels to the racks in conduit or cable tray supported by a support grid mounted above the Mezzanine.

Lights and miscellaneous receptacles will be circuited to panels located in the adjacent service building.

10.3.3 Experimental Hall Power Distribution:

A fifth transformer and single section panel will be provided at the tunnel mezzanine to serve Experimental Hall equipment. These panels will sub-feed two single section panels at the mezzanine level, one above each ratchet wall to serve equipment associated with that beamline.

Future branch circuits can drop out of these panels and be routed across the Experimental Hall on a support grid to equipment located along the beamline. Distribution panels for future beamlines between LOB2 thru LOB 4 will be provided with future beamlines.

Lights and miscellaneous receptacles in the Experimental Hall will be circuited to panels located in the adjacent service building.

10.3.4 Injection Building Power Distribution:

One 3000 A switchgear line-up will be located in the mechanical / service room. This switchgear will be dedicated to Linac and Booster equipment within the Injection Building.

10.3.5 RF Building/Cryo Plant Power Distribution:

Two 3000 A outdoor walk-in switchgear line-ups will be located at each unit-substation in the electric yard between the RF Building and the Cryo Plant. One line-up will serve loads within the RF Building. The second line-up will serve loads associated with the Cryo Plant.

10.3.6 Lab Office Building Power Distribution:

Each Lab Office Building will be provided with a 480Y/277 V panel fed directly from the switchgear in the associated service building. These panels will sub-feed two additional panels, one in each third of the building. These panels will serve lighting and mechanical equipment within the Lab Office Building, and sub-feed 208Y/120 V panels to serve receptacles in the labs and office areas.

Within each lab, two-compartment surface mounted raceway will be provided at bench tops and around the perimeter of the lab. Equipment in the center of the room will be served by surface-mounted raceways mounted on overhead ceiling-mounted service carriers.

10.3.7 Emergency Power:

Because of the building’s large size, two generators will be provided, one each at Service Building #2 and at the RF Building. The assumed size of each generator is 250 kW. A sub-base fuel tank in compliance with

Suffolk County Article 12 will be provided with a 12-hour full load operation capacity. To reduce noise and vibration, a weatherproof, sound attenuated reach-in enclosure will be provided.

Two automatic transfer switches will be provided; one to serve code required emergency loads, and one to serve optional standby loads. The emergency loads include egress and exit lighting, the fire alarm system, fire suppression system, smoke exhaust fans, selected lab exhaust and make-up systems, and select HVAC control systems. The emergency loads will be reenergized within 10 seconds of sensing a power outage.

The optional standby loads are not defined, but will likely include selected laboratory equipment, one switched light fixture in each lab, and the communication and security systems. Optional standby loads may be delayed to limit motor starting kVA.

10.3.8 Uninterruptible Power Supply (UPS):

A UPS will be provided to support the Control Room and Computer Room. The preliminary size is 30 kVA.

If uninterruptible power is required for a specific piece of lab or experimental equipment, point-of-use UPS units will be provided by the users.

10.3.9 Voltage Utilization:

- Site distribution – 13,800 V, 3-phase, grounded wye distribution system.
- Building lighting - 277 V
- Motors 1/2 horsepower and larger - 480 V, 3-phase
- Motors less than 1/2 horsepower - 120 V
- Equipment – As required by nameplate, except special voltages and frequencies including 220 V, 230 V, 240 V, 380 V, DC, 50 Hz, 400 Hz, 415 Hz, etc. will require user provided point-of-use transformers and/or frequency converters.

10.3.10 Voltage Drop:

Voltage drop will be limited to 2% in feeders and 3% in branch circuits.

10.3.11 Feeders and Branch Circuits:

All conductors will be copper installed in conduit. Conductors #3 and smaller will have THWN insulation. Conductors #2 and larger will have XHHW insulation.

Conductors #10 AWG and smaller will be solid. Conductors #8 AWG and larger will be stranded. Minimum size conductors will be #12 AWG for branch circuits, #14 AWG for control wiring and #18 for signal cables.

All feeder and branch circuit conductors will be provided with color coded insulation throughout their entire length.

Separate neutral conductors will be provided for each receptacle circuit. Insulation of neutrals will be provided with three colored strips matching their associate phase conductors. Insulation of neutrals serving two or three pole circuits will be solid.

All feeders and branch circuits will be provided with a green insulated equipment grounding conductor.

All branch circuits serving sensitive electronic laboratory receptacles and equipment will be provided with a green with three yellow strips isolated equipment grounding conductors.

Generally, conduit will be electrical metallic tubing with compression fittings. Conduit below grade will be concrete encased schedule 40 PVC. No conduit will be imbedded within slabs on or above grade.

10.3.12 Arc-Flash Hazard Analysis:

An arc-flash hazard analysis will be performed during design to compare different distribution system configurations and again during construction using installed component characteristics to determine actual incident energy levels and recommended boundary information and PPE category.

10.4 Grounding

10.4.1 Grounding Electrode System

The grounding electrode system will consist of underground metal piping, building steel, concrete encased 250 kcmil Ufer ground within all exterior wall foundations with direct buried cross connecting 250kcmil conductors 100 ft on center, and 10 ft ground rods spaced at approximately 100 ft on center around the perimeter.

A ground grid will be provided at the Building 603 substation expansion, and at each unit substation transformer at the project site to reduce earth resistance and to limit step and touch potential.

All underground connections will be exothermically welded.

The ground grid shall be designed to provide <5 ohms of resistance to earth.

A main ground bus will be located in the main electrical room at each service building. The grounding electrode conductors, interior metal pipe grounds, and the telecommunication ground will be connected to the main grounding bus.

10.4.2 Power System Grounding:

All power system grounding will be in accordance with the NEC.

The secondary of each 13,800-480Y/277 V substation transformer will be grounded at the substation. The grounded neutral will be re-bonded at each switchgear main breaker.

The generator neutral will be grounded at each generator. Four-pole automatic transfer switches will be provided.

The secondary of each 480-208Y/120 V transformer will be connected to the nearest building steel via a local power system ground bus.

Ground fault protection will be provided at the switchgear main and all feeder breakers.

A separate green insulated equipment grounding conductor will be provided in all feeders and branch circuits.

Branch circuits serving sensitive electronic equipment will be provided with a green with yellow strips isolated equipment grounding conductor in addition to the green equipment grounding conductor.

10.4.3 Instrument Reference Ground:

An instrument reference ground bus will be provided at each beamline to be used by users only for the purpose of grounding sensitive electronic communication circuits. The bus will be connected directly to the grounding electrode system and bonded to the local transformer(s) which provide power to that beamline equipment. The instrument reference ground bus will be considered the beamline's single point ground for all user equipment. Reference grounds within the hutches will be connected to the beamline's single point ground.

10.4.4 Telecommunication grounding:

Telecommunication grounding will be provided in accordance with EIA/TIA 607 including providing a ground conductor in all telecommunication cable trays.

10.4.5 Lightning protection:

A complete lightning protection system will be provided in accordance with NFPA 780 and UL 96A.

10.4.6 Cathodic protection:

Cathodic protection will not be provided.

10.5 RFI and ELF EMI Mitigation

No specific provisions are needed to mitigate radio frequency interference or extremely low frequency (60 Hz) electromagnetic fields.

10.6 Vibration Isolation

The generators will be provided with spring isolators as recommended by the vibration consultant. All transformers will be mounted on neoprene pads. No conduit will be installed under or within vibration isolation slabs.

10.7 Radiation Protection

Conduit penetrations in to the tunnel will be limited in quantity and located only through the tunnel roof or the service building labyrinth. All penetrations will include an off-set to eliminate line of sight through the roof concrete. Spare penetrations will be provided for future use

10.8 Exterior Lighting

Exterior illumination levels will be as indicated in DOE/IES standards, LEED 2.2 SS Credit 8 and Dark-sky requirements.

Parking lots, loop and interior roadways will be lit by 175 watt metal halide full cut-off fixtures mounted on 20 foot aluminum poles.

Walkways will be lit by 100 watt metal halide cut-off fixtures mounted on 12 foot aluminum poles and 50 watt metal halide bollards.

Building mounted exterior lighting will be provided at entrances and exits and at the loading dock. Equipment yards will be lighted with spill light from the adjacent access drive fixtures and by 100 watt metal halide full cut-off fixtures mounted on 12 foot aluminum poles.

No architectural/façade lighting will be provided.

Site lighting will be circuited to building panels and controlled by photocell to provide on/off operation.

10.9 Interior Lighting

Lighting design will be accomplished with energy efficient fluorescent lamps and electronic ballasts. Downlights and accent lights will be provided by compact fluorescent lamps.

Fluorescent lamps for troffers and pendant type fixtures will be a combination of T5 28 watt, T5HO 54 watt and T8, 32 watt lamps with a color temperature of 4100K with a CRI of at least 75. The T5 and T5HO lamps are provided to maximize energy conservation by using the highest efficiency lamps in the highest efficiency fixtures.

Fluorescent ballasts for T5, T5HO and T8 lamps and compact fluorescent lamps will be electronic type with a ballast factor of 0.85 minimum and total harmonic distortion of less than 10%.

Compact fluorescent lamps will be used in downlights and wall wash fixtures.

Exit lights will be LED type.

Fluorescent fixtures in labs will be controlled by a low-voltage control system with low-voltage switches at the entrances.

Occupancy sensors will be provided in enclosed offices and in open office areas, corridors, restrooms, and in support spaces.

Footcandle levels will be in accordance with DOE standards where applicable and with the IES Handbook for other spaces:

- Storage Ring Tunnel: 30 FC.
- Mezzanine: 30 FC.
- Experimental Hall: 30 FC.
- LINAC: 30 FC.
- Booster Ring Tunnel: 30 FC.
- Booster/LINAC Support Building: 30 FC.
- RF Building: 30 FC.
- Laboratories: 50-75 FC general with 75 FC on work surfaces.
- Offices: 30-50 FC general with 50 FC on work surfaces.
- Operations Center: 50 FC.
- Conference rooms: 30 FC.
- Attended support spaces: 30 FC.
- Unattended support spaces: 15 FC.
- Corridors, Stairs: 10-15 FC.
- Restrooms: 10-15 FC general with 30 FC at the mirror/sink area.
- Mechanical/electrical equipment rooms: 15 FC.
- Telephone/communication rooms: 50 FC.

Fixture types are tentatively defined as follows:

- Tunnel: Surface mounted enclosed and gasketed.
- Mezzanine: 2-lamp industrial fluorescent with 10% uplight.
- Experimental Hall: 250 watt metal halide with glass reflectors. Because of the restrike time of metal halide fixtures, wall mounted fluorescent fixtures will be provided on the outside wall for egress lighting.
- Laboratories: Pendant mounted direct/indirect fixtures with a single row of T5HO lamps.
- Enclosed offices: Recessed volumetric type fluorescent troffers with ribbed acrylic lens under each T5 lamp.
- Open office areas: Recessed volumetric type fluorescent troffers with ribbed acrylic lens under each T5 lamp.
- Conference rooms: Pendant mounted direct/indirect fixtures with a single row of T5HO lamps.
- Support spaces: Recessed volumetric type fluorescent troffers with ribbed acrylic lens under each T5 lamp.
- Corridors: Recessed volumetric type fluorescent troffers with ribbed acrylic lens under each T5 lamp.
- Stairs: Direct/indirect fluorescent wall brackets.
- Restrooms: Recessed linear fluorescent wall washers mounted along the back and front walls.
- Mechanical/electrical equipment rooms: 2-lamp industrial fluorescent with 10% uplight.
- Telephone/communication rooms: 2-lamp industrial fluorescent with 10% uplight.

Egress and exit lighting will be provided in accordance with NYSBC and NFPA 101.

10.10 Special Systems

10.10.1 Fire Alarm System:

A complete manual and automatic, supervised, fire detection and voice evacuation system will be provided. It will be a non-coded, addressable, microprocessor-based fire alarm system with initiating devices, notification appliances, and monitoring and control devices. Initiating and appliance circuits will be Class B. The fire alarm system will be in accordance with DOE requirements and NFPA 72.

There will be five (5) fire alarm control panels. The fire alarm control panels will be located adjacent to the exterior doors of the service buildings. The panels will be Grinnell/Simplex model 4100U fire alarm panels. The panels will be connected together by fiber cabling. Seven (7) remote fire alarm annunciation panels will be located. at the main entrance of the operations building, adjacent to the truck dock by each of the Laboratory Office Buildings, at the exterior door where future Laboratory Office Buildings will be connected, and at the Linac. The remote fire alarm annunciation panels will be connected to the fire alarm panel via fiber cable. A central fire alarm annunciation workstation will be located in the control room in the operations building.

Manual stations will be programmable and located at all building exits, at all exit stairs, and at 300 foot intervals in egress corridors.

Photoelectric area smoke detectors will be located in each lab and in elevator lobbies, shaft and machine room. Provisions will be made for smoke detectors to be located within the future hutches. Smoke detectors in elevator lobbies, shaft and machine room will initiate elevator recall. Duct smoke detectors will be provided in air handling systems as required by NYSBC and NFPA 90A.

An air sampling smoke detection system will be provided throughout the Tunnel and Experimental Hall including the Tunnel Mezzanine. Each air sampling system can cover up to 20,000 sf. Therefore each Pentant will be provided with one air sampling system in the Tunnel and three air sampling systems in the Experimental Hall. The air sampling system will be Fenwal Protection System model AnaLaser-II.

Heat detectors will be located adjacent to sprinkler heads in elevator shafts and machine room and will de-energize elevator power in accordance with ANSI 17.1, Elevator Code.

Wet sprinkler valves assemblies, sprinkler/standpipe water flow and tamper switches, and pre-action and dry-pipe systems will be monitored.

Combination audio/visual and/or visual only devices will be provided throughout the facility. A minimum of two indicating circuits will be provided in each area with devices connected alternately. A visual device will be located on the exterior of the building adjacent to each entrance where a fire alarm control panel is located to guide the Fire Department to the activated panel.

Notification appliance circuit power supplies will be distributed throughout the facility to provide power for the audible/visual appliances and to reduce voltage drop. The power supplies will be located in easily accessible locations.

Common alarm and trouble signals will be transmitted via fiber optic cable to the campus fire alarm system.

10.10.2 Telecommunication System (Voice, Data and Video):

A complete pathways, spaces, and structured cabling distribution system will be provided that consists of telecommunication rooms, plywood backboards, racks, cabinets, cable tray, conduit, back boxes, copper cable, fiber optic cable, connectors, cover plates, termination blocks, cross connect cables, patch panels, and all necessary accessories and will be provided in accordance with applicable EIA/TIA standards.

The Building Distribution Frame room will be located in the Operations Building. The BDF room will also serve as the Intermediate Distribution Frame room for the Operations Building.

One IDF will be located in each Service Building and in each Lab Office Building. The Service Building IDF will serve outlets in that Service Building and in the adjacent Experimental Hall. The Lab Office Building IDF will serve outlets in the associated lab office areas.

Cable tray will be provided above the Mezzanine to interconnect the BDF with all the IDF’s. This tray will carry backbone cables and station cables serving the Experimental Hall.

Cable tray will be provided at lab and office corridors to route station cables to outlets in the lab office areas.

Conduit will be provided between the cable tray and each outlet or raceway.

Each voice/data outlet will be provided with one Cat 6 voice jack and one Cat 6 data jack.

Each data outlet will be provided with one Cat 6 data jack.

Voice and data riser cabling will be provided from the BDF to each IDF. Voice riser cables will be multi unshielded twisted pairs, 24 gauge, solid copper and terminated on the terminal block in each closet. Data riser cabling will be 12 multi mode and 12 single mode fiber optic cables terminated at each end in a patch

panel with a type SC connector. Voice will be terminated directly on rack-mounted termination panels. Patch panels will be mounted in 19 in. equipment racks.

Station cabling from each voice/data will consist of two four-pair Category 6 cables terminated at the devices and on the rack mounted telephone terminal blocks. Cables will be labeled at each device, terminal block, and patch panel.

10.10.3 Security System:

The security system will consist of a card reader access control system with limited security camera feed to the Security Center at Building 50.

Card readers will be located at each building entrance, and at each entrance to other selected spaces such as the control room, control computer room and electrical switchgear rooms.

CCTV systems will be provided for limited property protection areas such as the control room and control computer room. To match campus standards, security equipment components (card readers, controllers, locks, door contacts, etc.) will be owner furnished, contractor installed. Door exiting device, power transfer hinges, etc. will be coordinated with the door schedule. Security system cabling will be contractor installed and terminated by the owner.

Table 10.1 Electrical Loads.

	Equip. kW	VA/SF	SF	kVA	df	kVA / Pentant	Total kVA
Storage Ring Equipment: (uniform load)							
Storage Ring	3211.9						
Insertion Devices	204.0						
Experimental Hall Equipment:							
Beam Lines	401.8				200% spare		805
Lab Office Buildings: (5 LOBs)							
Lighting		2	20000	40	1.0	40	200
Mechanical		5	20000	100	1.0	100	500
Receptacles		3	12800	38	0.6	23	115
Labs		25	2880	72	0.6	43	215
25% Spare						52	260
						258	1290
Experimental Hall and Service Buildings:							
Lighting		2	64000	128	1.0	128	640
Mechanical		6	64000	384	1.0	384	1920
Receptacles		1	64000	64	0.6	38	190
25% Spare						138	690
Storage Ring Point loads:						688	3440
Storage Ring Equipment (point load):							
SR Dipole (assumed at Sector #2)	460.0						
RF, Cryo Plant, Injection Loads:							
Linac Equipment:							
Source	11.6						
LINAC	29.6						
LINAC RF	200.0						
Booster Ring Equipment:							
Booster Ring LEBT	51.8						
Booster Ring Booster	1075.0						
Booster Ring HEBT	70.8						
Booster RF	170.0						
Linac, Booster Ring :							
Lighting		2	32000	64	1.0		64
Mechanical		6	32000	192	1.0		192
Receptacles		1	32000	32	0.6		19.2
25% Spare							69
RF Building Equipment:							344
Main Ring RF	2850.0						
Cryogenic Plant	500.0						
RF Controls and Diagnostics	40.0						
RF, Cryo Plant :							
Lighting		2	8000	16	1.0		16
Mechanical		6	8000	48	1.0		48
Receptacles		1	8000	8	0.6		4.8
25% Spare							17
							86
			Building Lighting, Misc Receptacle, Mechanical and Spare =				5963
Total Equipment Load	9276.5						9277
Loads for 3 GeV Energy Level					Total Building Load (kVA) =		15,239

11 ENVIRONMENT, SAFETY AND HEALTH

11.1 Scope and Content

The scope and intent of this Environment, Safety and Health analysis is to:

1. Identify codes and standards applicable to conventional facility design.
2. Identify specific criteria for design of the conventional facility building and systems that meet the requirements of the applicable codes and standards, particularly those criteria that address the hazards identified by BNL in the Preliminary Hazards Analysis.
3. Define concepts for the conventional facility building and safety systems design to mitigate the identified hazards.

This ES&H analysis includes the following sections:

1. Building Code Analysis (BCNY)
2. Other Codes and Standards
3. Preliminary Hazards Analysis
4. Fire Protection
5. Pressure Safety
6. Industrial Hygiene
7. Other ES&H Issues

This document will be used as a reference by the design team and BNL throughout subsequent phases of the project.

11.2 Building Code Analysis

The preliminary building code analysis is attached to the end of this report.

11.3 Other Codes and Standards

The following DOE Orders and Guidelines will govern design and operation of the facility. Specific requirements in each order or guideline that are applicable to the facility design are summarized.

Where specific requirements conflict, or conflict with the Building Code of New York State, the more stringent requirement will govern.

11.3.1 DOE O 420.1B – Facility Safety

a) Fire protection system design

b) Natural phenomena hazards mitigation

11.3.2 DOE O 420.2B -Safety of Accelerator Facilities

a) Beamline safety systems (access control, beamline shutoffs/ interlocks, search confirmation system)

b) Electrical safety

c) Cryogenic and oxygen-deficiency hazards

d) Ionizing and non-ionizing radiation

e) Experimental activities

11.3.3 10 CFR 851 – Worker Safety and Health Program

a) Fire protection

b) Pressure safety

c) Industrial hygiene

d) Biological safety

e) Electrical safety

f) Nanotechnology safety

11.3.4 BNL Worker Safety and Health Program

a) To be confirmed during detailed design

11.4 Preliminary Hazards Analysis

BNL has developed a Preliminary Hazards Analysis (PHA) which identifies hazards related to facility construction and operation. This analysis will be updated to a Final Hazards Analysis for submission at Critical Decision 2 (CD-2).

The Hazards Analysis is used to identify design and operation strategies to mitigate potential hazards. Relevant findings and requirements from the Preliminary Hazards Analysis are incorporated into the following sections.

A summary of the risk assessment from the Preliminary Hazards Analysis, with pre-and post-mitigation risk categories, is presented in Table 11.1 for reference. A full description of the design and operation mitigation strategies is provided in the PHA.

Table 11.1 Preliminary Hazards Analysis

PHA Hazard Identifier	Hazard	Pre-Mitigation Risk Category	Post Mitigation Risk Category
NSLS-II PHA - 1	Construction	High	Moderate
NSLS-II PHA – 2	Natural Phenomena	Low	Routine
NSLS-II PHA – 3	Environmental	Moderate	Low
NSLS-II PHA – 4	Waste	Moderate	Low
NSLS-II PHA – 5	Fire	High	Low
NSLS-II PHA – 6	Electrical	High	Moderate
NSLS-II PHA – 7	Noise	Moderate	Low
NSLS-II PHA – 8	Cryogenic	Moderate	Low
NSLS-II PHA – 9	Confined space	Moderate	Low
NSLS-II PHA – 10	Ozone	Low	Low
NSLS-II PHA – 11	Chemical/hazmat	High	Moderate
NSLS-II PHA – 12	Vacuum, cooling water, air	Moderate	Low
NSLS-II PHA – 13	Ionizing Radiation	High	Moderate
NSLS-II PHA – 14	Non-Ionizing Radiation	Moderate	Low
NSLS-II PHA – 15	Material Handling	High	Moderate
NSLS-II PHA – 16	Experimental Operations	High	Moderate

This section of the Title I design narrative addresses, directly or indirectly, all of the hazards identified in the Preliminary Hazards Analysis except construction hazards and natural phenomena hazards. The latter are addressed in the civil, structural, and architectural chapters of this narrative. Construction hazards will be addressed separately.

11.5 Fire Protection

11.5.1 Requirements

For the purposes of this analysis, “Fire Protection” includes the following elements as defined in DOE Order 420.1B – Facility Safety:

a) Water supply

b) Fire-rated construction and barriers

c) Automatic extinguishing systems

d) Redundant fire protection systems for vulnerable safety class systems

e) Emergency egress and illumination

f) Fire department access and standpipe systems

g) Containment of fire fighting water

Requirements and criteria for fire protection are derived from the following codes and orders:

a) Building Code of New York State (2002)

b) Fire Code of New York State (2002)

c) DOE O 420.1B – Facility Safety

d) DOE O 420.2B – Safety of Accelerator Facilities

e) 10 CFR 851 – Worker Safety and Health Program

Design mitigation strategies are also identified in the PHA under PHA-5.

11.5.2 Codes and Standards

The following codes and standards will apply to design of fire protection systems.

a) DOE STD-1066-99 – Fire Protection System Design Criteria

b) NFPA 70 – National Electrical Code (2005)

c) NFPA 70E – Standard for Electrical Safety in the Workplace (2004)

d) NFPA 101 – Life Safety Code (2006)

e) NFPA 90A – Standard for Installation of Air-Conditioning and Ventilating Systems (2002)

f) NFPA 780 – Standard for Installation of Lightning Protection Systems (2004)

g) NFPA 72 – National Fire Alarm Code (2007)

h) NFPA 14 – Standard for the Installation of Standpipe and Hose Systems (2003)

i) NFPA 45 – Standard on Fire Protection for Laboratories Using Chemicals (2004)

j) NFPA 13 – Standard for the Installation of Sprinkler Systems (2002)

11.5.3 Compartmentation

The BCNY requires fire rated barriers at the following locations, as indicated in Section B - Building Code Analysis:

a) Occupancy separations

b) Control area separations

c) Vertical exit enclosures

d) Horizontal exit enclosures

DOE Order 420.1B also requires construction of fire rated barriers to limit maximum possible fire loss (MPFL) from a single fire event to $50 million, or installation of redundant fire protection systems where the MPFL exceeds this limit.

The MPFL is defined as the value of property (excluding land), within a fire area, including the replacement cost of equipment and property and any applicable decontamination and clean-up costs following a fire event. This loss assumes the failure of both automatic fire sprinkler systems and manual fire fighting efforts. A waiver from the DOE will be required to allow the experimental hall and tunnel to be constructed without intermediate fire barriers since the MPFL value of these spaces exceeds the established limit.

For the NSLS-II facility, fire rated barriers are proposed at the following locations:

a) 1-hour fire rated separation between the experimental hall and each LOB

b) 1-hour fire rated enclosure around stairwells in the service buildings and the operations center

c) 2-hour fire rated separation between the operation center (portion inside the ring) and the ring building

d) no fire barrier separation within the experimental hall or the tunnel

e) no fire barrier separation between the experimental hall and the service buildings, RF service building, or booster ring building

11.5.4 Fire Department Access

The Fire Code of New York State requires a Fire Department access to be a minimum of 14 feet high and 20 feet wide. This will accommodate the BNL Fire Department's largest response vehicle (22 tons, 37 feet long, 13 feet high, and 11 feet wide). The Fire Department will be able to reach NSLS-II by road from the north, west or south.

Access to the NSLS-II building complex will be provided from Brookhaven Avenue to the main facility entrance, to the west end of the facility perimeter road (bypassing the main parking areas), and directly to the perimeter road east entrance. Additional points of access to the west side of the perimeter road will be from Bell Avenue and Rowland Street, and to the south from Princeton Street via Weaver Drive or Groves Street. Each LOB is accessed from the perimeter road. The main entrance is accessed directly off of Brookhaven. Access to the service buildings, RF Building, and Injection Buildings will be from the inside of the main ring building via a tunnel from the perimeter road. The tunnel will be sized to accommodate the largest BNL firefighting vehicle and will have a maximum 8 percent slope.

There is the potential for construction of long beamlines in the southeast quadrant of the building that could cross the perimeter road. Any changes in perimeter road grade will be limited to a maximum 8 percent slope.

There will be 10 primary entrances for emergency responders to the NSLS-II building, six from outside and 5 from inside the ring building. These primary entrances are:

a) Main entrance to the Operations Building

b) Main truck dock entrance to each LOB

c) Service building (access from inside the ring)

d) Exterior door where Alternate LOB will be located.

Because of the size of the facility, a means of easily identifying emergency responder access points during daytime and nighttime hours will be provided. This will be further developed during detailed design.

11.5.5 Fire Protection Water Supply

DOE Standard 1066-99 specifies requirements for fire protection water supply, including hydrant demand. This standard also requires that an additional, independent source of fire protection water be provided when the Maximum Possible Fire Loss (MPFL) is in excess of $100 million.

For the NSLS-II facility, fire protection water will be supplied by BNL's potable water system, which is supplied by several deep wells and is stabilized by two elevated water storage tanks (one with a capacity of 1 million gallons and another of 350,000 gallons). The system can sustain three days of domestic supply and a maximum fire demand (4000 gpm for 4 hours) for BNL when two of the system's largest pumps are out of service and one storage tank is unavailable. The piping distribution network is well gridded to reduce the impact to any one building from a single water main break.

Five (5) potable water/fire water services will be extended from the site water mains to the service buildings. Each feed into the building will be hydraulically sized to handle the total combined requirements for water supply of the domestic and automatic sprinkler/standpipe systems.

Each service will be provided with two reduced pressure backflow prevention devices. The potable water supply will be protected against backflow from the automatic fire sprinkler and standpipe systems by an Underwriters Laboratory and Factory Mutual listed reduced pressure principle backflow preventor as required by Section 608.16.4.of the Plumbing Code of New York State (PCNY).

11.5.6 Fire Protection

BCNY Section 903 defines fire protection requirements applicable to the NSLS-II facility.

DOE Standard 1066-99 specifies that sprinkler systems must be designed in accordance with NFPA Standard 13.

DOE Standard 1066-99 also specifies the following fire protection system requirements to limit loss potential. Implementation or waiver of both of these requirements will need further review with the DOE.

a) A redundant fire protection system that, despite the failure of the primary fire protection system, will limit the loss to acceptable levels as determined by the AHJ (when the MPFL exceeds $50 million)

b) A redundant fire protection system and a 3-hour fire barrier when the MPFL exceeds $150 million

Neither the FCNY nor DOE Standard 1066-99 require standpipes for buildings less than 3 stories in height, unless deemed necessary for facilities with “extensive and complex interior layouts” by the DOE Fire Protection AHJ. Where standpipes are installed they shall be designed to NFPA Standard 14.

DOE Standard 1066-99 indicates that hydrants should be provided so that hose runs to all exterior portions of a protected building are no more than 300 feet, and that hydrants are located not closer than 40 feet to buildings. Hydrant water supply should be per the FCNY for the most severe facility fire risk, reduced as allowed for building automatic sprinkler protection.

For the NSLS-II facility, a combination sprinkler/standpipe system meeting the requirements of NFPA 13 “Standard for Installation of Sprinklers” and NFPA 14 “Standard for the Installation of Standpipe and Hosepipe Systems” will be designed to provide 100-percent protection of the facility. Where the piping installation will be subject to freezing temperatures, dry sprinklers will be employed; this will be further evaluated during detailed design. Means of adding water conditioning chemicals to the sprinkler system to combat corrosion will be provided.

Two Fire Department connections for each of the five fire (5) zones. One connection shall be located on the front face of the building, and the other on the interior face (courtyard) of the building. Each shall be located near an entry point into the facility. Each pair of FDC will serve a single fire zone and will be interconnected with the automatic sprinkler and standpipe systems.

Fire hydrants will be located along the Loop Road outside of the Ring Building and along the Service Road inboard of the Ring Building at distances meeting DOE and code requirements and not more than 300 feet from all building entrances.

11.5.7 Detection and Alarming

Specific requirements for fire detection and notification in the BCNY/FCNY will be detailed in the next phase of design.

DOE Standard 1066-99 requires that fire alarm systems comply with NFPA 72 - National Fire Alarm Code and have the following features:

a) Retransmission of signals to the site Fire Department alarm center

b) Local alarms for the building or zone(s) in alarm.

c) Visual alarms.

d) Location of a fire alarm control panel near the main entrance or other protected location as determined by the AHJ. For buildings with multiple zones, a zone alarm panel or graphic is required at the main entrance.

e) Supervisory devices except for locked valves.

f) Water flow alarm at each sprinkler riser.

g) Means of manual fire notification.

For NSLS-II, a complete manual and automatic, supervised, fire detection and voice evacuation system meeting the requirements of NFPA 72 will be provided. It will be a non-coded, addressable, microprocessor-based fire alarm system with initiating devices, notification appliances, and monitoring and control devices. Initiating and appliance circuits will be Class B. The fire alarm system will be in accordance with DOE and NY State Code requirements.

Smoke detection will be provided in laboratories in the LOBs, in the control room, in all electrical rooms (including switchgear rooms in the Service Buildings), in telephone and data communications rooms, and in elevator lobbies, shafts and machine rooms. Provisions will be provided for connecting future smoke detectors located within the future experimental hutches. Smoke detectors in elevator lobbies, shafts and machine rooms will initiate elevator recall. Duct smoke detectors will be provided in air handling systems as required by BCNY and NFPA 90A. Manual pull stations will be located at each building exit.

High sensitivity smoke detectors (HSSD systems) will be provided in four (4) areas: the Experiment Floor, the Tunnel Mezzanine area, the accelerator ring tunnel and the booster tunnel.

Heat detectors will de-energize elevator power in accordance with ANSI 17.1 Elevator Code.

Sprinkler system water flow will be monitored and the system will supervise the sprinkler valves and the installed detection systems.

Combination audible/visual alarm and/or visual only annunciation devices to alert the occupants will be provided throughout the ring, the corridor system, in each laboratory, in each hutch, and in most rooms, other than single person offices. Fire alarm and supervisory signals will be transmitted via dedicated fiber optic cable to the BNL Fire Rescue Group in Building 599 monitors and to a secondary monitoring station at Security (Bldg 50) via the Site Fire Alarm System. All fire alarm signals will also annunciate in the control room. The main fire alarm control panel will be located at the facility entrance, with repeater panels located at the entrance to each LOB and each Service Building.

Spot smoke detection will be arranged to have a “pre-alarm” signal (permissible by NFPA 72 with the approval of the Authority Having Jurisdiction). This “pre-alarm” signal from single smoke detector(s) will be displayed in the control room and transmitted to the BNL Fire Rescue Group without immediately activating the fire alarm audible/visual devices. Notification devices will be activated automatically within a fixed time period unless the facility operators in the main control room do not put the system on hold.

11.5.8 Smoke Control

No code requirements have been identified that would require installation of a means of smoke control for the tunnel, experimental hall, or lab office buildings. However, BNL has indicated a need for smoke control from the experimental hall, the accelerator ring tunnel, and the booster tunnel to further enhance the ability to quickly evacuate personnel from this space in a fire emergency and to limit the spread of fire/smoke beyond the point of origin. The Fire Department will have the ability to control the ventilation systems to divert recirculated air to the outdoors. Fresh air would not continue to be supplied from the activated GHVAC system. The control panel will be at the fire alarm system panels.

11.6 Pressure Safety

11.6.1 Requirements

Requirements and criteria for pressure safety are derived from the following:

a) 10 CFR 851 – Worker Safety and Health Program

11.6.2 Applicable Codes and Standards

The following codes and standards will apply to the design and fabrication of pressure systems.

a) ASME Boiler and Pressure Vessel Code (2007)

b) ANSI B31.3 – Process Piping (2002)

c) ANSI B31.9 – Building Services Piping (1996)

d) CGA S-1.3 – Pressure Relief Device Standards Part 3 – Stationary Storage Containers for Compressed Gases (2005)

11.6.3 Design Requirements

Specific requirements for implementation of pressure safety-related codes and standards will be defined in the next phase of design. These requirements may include, but not be limited to, the following.

a) Incorporation of applicable codes and standards into the relevant construction specifications.

b) Location of compressed gas cylinder racks in areas protected from potential damage or potential sources of energy that could cause an overpressure condition.

c) Specification and selection of appropriate relief valves and other protective devices on mechanical and process services under pressure.

d) Routing of relief valve and rupture disk discharges to safe locations, away from potential personnel travel pathways.

e) Routing of pressurized services away from exposure to damage from mobile equipment, hoists, etc.

11.7 Industrial Hygiene

11.7.1 Requirements

Requirements and criteria for industrial hygiene are derived from the following codes and orders:

a) Building Code of New York State (2002)

b) DOE O 420.2B –Safety of Accelerator Facilities

c) 10 CFR 851 – Worker Safety and Health Program

Design mitigation strategies are also identified in the PHA under the following:

a) Waste Hazards (PHA-4)

b) Noise and Vibration Hazards (PHA-7)

c) Cryogenic Hazards (PHA-8)

d) Confined Space Hazards (PHA-9)

e) Ozone Hazards (PHA-10)

f) Chemical and Hazardous Materials Hazards (PHA-11)

g) Accelerator/Beamline Hazards (PHA-12)

h) Ionizing Radiation Hazards (PHA-13)

i) Non-Ionizing Radiation Hazards (PHA-14)

j) Material Handling Hazards (PHA-15)

k) Experimental Hazards (PHA-16)

11.7.2 Codes and Standards

The following codes and standards will apply to design of facilities and systems related to the hazard areas identified above.

a) Building Code of New York State (2002)

b) NFPA 30 – Flammable and Combustible Liquids Code (2003)

c) NFPA 55 – Standard for the Storage, Use, and Handling of Compressed Gases and Cryogenic Fluids in Portable and Stationary Containers, Cylinders, and Tanks (2005)

d) OSHA 29 CFR 1910 – Standards for General Industry (2007)

e) ANSI Z136.1 – Safe Use of Lasers (2000)

f) ANSI Z9.5 – Standard for Laboratory Ventilation (2003)

g) CGA V-6 – Standard Cryogenic Liquid Transfer Connections (2000)

11.7.3 Hazardous Material Storage and Handling

a) Allowable Quantities

The maximum allowable quantities of hazardous chemicals and gases (unused chemicals and gases, materials in use, and waste) are dictated by the BCNY for any control area in a B-occupancy building. These are indicated in Tables 11.2 and 11.3.

Table 11.2 – Allowable Quantities of Chemicals

Maximum Allowable Quantities per Control Area		
Material	Allowed Storage(1)	Allowed Use (Open System)(2)
Flammable Class 1-A	120 gal	20 gal
Flammable Class I-B	240 gal	30 gal
Flammable Class I-C	360 gal	40 gal
Combined Flammables	480 gal	60 gal
Water Reactive Class 1	No limit	No limit
Water Reactive Class 2	200 lbs (3)	20 lbs (3)
Water Reactive Class 3	20 lbs	2 lbs
Oxidizer Class 1	800 gal	200 gal
Oxidizer Class 2	50 gal	10 gal
Oxidizer Class 3	4 gal	0.4 gal
Oxidizer Class 4	0.2 gal	0.02 gal
Unstable (Reactive) Class 1	No limit	No limit
Unstable (Reactive) Class 2	200 lbs	20 lbs
Unstable (Reactive) Class 3	20 lbs	2 lbs
Unstable (Reactive) Class 4	2 lbs	0.25 lbs
Toxic	500 lbs	125 lbs
Highly Toxic	40 lbs	3 gal
Corrosive	2,000 gal	200 gal

Notes:
1. Increased as allowed for automatically sprinklered spaces and use of approved storage cabinets.
2. Aggregate quantity of storage and in-use shall not exceed allowable quantity for storage.
3. Assumes sulfuric acid. Equivalent to 20 gallons in storage and 2 gallons in open use.

Table 11.3 – Allowable Quantities of Hazardous Gases

Maximum Allowable Quantities per Control Area		
Material	Allowed Storage(1)	Allowed Use (Closed System)(2)
Flammable	2,000 cf	2,000 cf
Pyrophoric	100 cf	20 cf
Highly Toxic	40 cf (3)	40 cf
Toxic	1,620 cf	1,620 cf
Oxidizing	3,000 cf	3,000 cf

Notes:
1. Increased as allowed for sprinklered spaces.
2. Aggregate quantity of storage and in-use shall not exceed allowable quantity for storage.
3. In approved gas cabinets only.

Definitions of “highly toxic” and “toxic” gases, as defined in the Toxic Gas Ordinance (TGO), are as follows:

"Highly Toxic" (Class I): material that has a median lethal concentration in air of 200 ppm or less by volume, when administered by continuous inhalation of one hour to albino rats weighing between 200 and 300 grams each

"Toxic" (Class II): material that has a median lethal concentration in air of more than 200 ppm but less than 3,000 ppm by volume, under the same conditions

For mixtures, the classification as "highly toxic" or "toxic" depends on the mole fraction of the toxic material in the mixture. For purposes of this analysis, it is assumed that all gases will be pure.

If the volume of any hazardous chemical or gas in storage or use exceeds the amount listed in Tables 11.2 or 11.3, the area in which it is stored and/or used in excess of these amounts must be H-occupancy.

b) Hazardous Material Storage Areas

The design criteria for hazardous chemical and gases storage areas are prescribed by the BCNY. There are criteria applicable to storage within control areas in B occupancies (within the maximum allowable quantities) and additional criteria applicable to rooms or buildings for storage of quantities exceeding the maximum allowable quantities per control area (H-occupancy storage rooms or buildings).

For storage of materials in less than or equal to the maximum allowable quantities in control areas, code requirements include the following.

i) Separation of the control area by 1-hour fire barrier from adjacent control areas with minimum 2-hour rated floor construction for levels above ground

ii) Where storage cabinets are used to increase maximum allowable quantities of materials, which is reflected in the amounts listed in Table 11.2, cabinets shall be constructed per code and a liquid-tight floor to minimum of 2 inches

iii) Where gas cabinets are used to increase maximum allowable quantities of materials, which is reflected in the amounts listed in Table 11.3, cabinets shall be constructed per code and ventilated to maintain negative pressure with respect to the surroundings. No more than 3 cylinders may be housed in a single cabinet.

iv) For exhausted enclosures where necessary per code or where provided to increase maximum allowable quantities, enclosures shall be ventilated at negative pressure relative to surrounding areas, and provided with automatic fire extinguishing system if flammables are stored therein.

For H-occupancy rooms or buildings intended for storage of hazardous materials in quantities exceeding the amounts allowed per control area, the following additional code criteria apply:

i) Liquid storage cabinets may not exceed 120 gallons of total storage capacity, with no more than 60 gallons of Class I or Class II liquids.

ii) A minimum aisle width of 4 feet is required between adjacent liquid storage racks and a minimum 8-foot main aisle must be maintained.

iii) Rooms for storage of liquids shall be ventilated and maintained negative to surrounding spaces.

iv) An automatic sprinkler system is required.

v) Spill control and secondary containment is required to contain a spill from the largest vessel plus 20 minutes of fire protection water flow over the minimum system design area or room area (whichever is smaller).

vi) Non-compatible materials shall be stored in separate, approved enclosures.

A central chemical storage building will be provided adjacent to the LOB-1 loading dock. This building will be designed as an H-occupancy building and will be subdivided by partial non-combustible partitions to separate oxidizers, water reactives, acids, bases, and toxics. If any highly toxic liquids are intended to be used in the NSLS-II facility, a separate room with 1-hour fire barrier would have to be constructed. This will be evaluated further during detailed design.

The chemical storage building will be constructed of non-combustible materials. No explosion venting panels will be provided. Spill containment per BCNY and FCNY requirements for H-occupancy spaces will be provided for these rooms, with leak detection systems capable of alarming to the facility control room.

A separate building will be provided for 90-day storage of waste chemicals at the same location outside LOB-1. Waste chemicals will be stored in individual containers in chemical storage cabinets in the room. The waste room will be divided by non-combustible partitions as required to provide segregation by chemical type (oxidizers, water reactives, acids, bases, and toxics). The room will be designed the same as the chemical storerooms.

Each chemical storeroom will be provided with an exhaust ventilation system with a minimum of 1 cfm per square foot of floor area. The system will be designed to operate continuously and exhaust to the outside without recirculation. Each room will be conditioned to a temperature range of 55 to 85 F.

Each chemical storeroom will be provided with an automatic sprinkler system. A combination safety shower/eye wash station will be provided in each storeroom.

Chemicals and wastes used in laboratories or in beamline hutches will be stored in approved enclosures, ventilated where required by code. It is anticipated that only small volumes of chemicals for immediate use will be stored outside the central chemical storage room.

Treatment chemicals for closed-loop water systems (e.g., scale and corrosion inhibitors and biocides for use in the cooling towers) will be stored in drums or portable totes, depending on the anticipated rate of consumption. These chemicals will be stored in suitable enclosures at the point of use.

Gas cylinder storage areas will be provided near the loading dock in each LOB. Space will be provided for storage of gas cylinders in delivery to the final points of use, and for empty cylinders awaiting collection. No central storage of gas cylinders will be provided for NSLS-II; these will be delivered on a “just-in-time” basis.

Cylinder racks will be segregated by gas type, e.g., flammables and oxidizers. Appropriate cylinder restraints will be provided. The need for cages or other form of security for new or empty cylinders will be further evaluated during the next phase of design.

c) Hazardous Material Distribution

The design criteria for fixed distribution of hazardous chemicals and gases are prescribed by the BCNY. These criteria include:

i) Piping system construction

ii) Automatic shutoff valves

iii) Pressure relief

iv) Backflow prevention

v) Leak detection

Other than chemicals for closed loop system conditioning and liquid nitrogen (addressed in a separate part of this section), no piped distribution of chemicals is anticipated.

Piping systems for treatment chemicals will be compatible with the chemical and will be provided with containment and leak detection.

For chemicals used for experimental purposes, liquid transfer of materials having an NFPA 704 hazard ranking of 3 or 4 will be by safety cans complying with UL 30. Liquid containers exceeding 5 gallons will be transported on a cart or truck. In addition, containers with materials that have a hazard ranking of 3 or 4 per NFPA 704 will be transported on a cart or truck, unless no more than two containers are hand carried in safety containers. The cart or truck will be capable of containing a spill from the largest single container being transported.

It is anticipated that inert gases will be piped directly from cylinders to the equipment using the gas, with the cylinders located near to the point of use and manually changed when required. If demand dictates that multiple cylinders can be in use for a particular purpose, or if automatic change-over from empty to full cylinders is required for uninterrupted operation, fixed gas manifolds with distribution piping to the point of use will be provided. This will be further evaluated during detailed design.

Wherever hazardous gases are used, these will be housed in approved gas cabinets and piped via contained piping systems from the cylinder manifold to the point of use. Hazardous gas piping systems will be provided with leak detection, excess flow protection, and automatic shutoff as required by applicable codes. This will also be further evaluated during detailed design.

d) Safety Showers/Eyewash Stations

OSHA (29 CFR 1910.151(c)) requires "where the eyes or body of any person may be exposed to injurious corrosive materials, suitable facilities for quick drenching or flushing of the eyes and body shall be provided within the work area for immediate emergency use." “Suitable facilities” is defined by OSHA as meeting current industry standards. ANSI Z358.1-2004 is the recognized industry standard. ANSI's definition of "hazardous material" includes caustics and additional substances and compounds that have the capability of producing adverse effects on the health and safety of humans. This standard requires the following:

i) Installation of eyewash and shower equipment in appropriate situations when employees are exposed to hazardous materials.

ii) Location of emergency showers and eyewashes within 10 seconds travel distance of and no greater than 55 feet from a hazard, located on same level as hazard, and with a travel path free of obstructions including doors.

iii) Shower valves of simple operation, turn off to on in one second or less, and providing hands-free operation once activated.

iv) Flushing fluids shall be tepid.

v) Showers can be either plumbed or self-contained.

vi) Flow alarms should be installed in shower supply piping to indicate when the unit is being used.

vii) Pressure and minimum flow requirements as provided in the standard.

For the NSLS-II facility, safety shower/eyewash stations will be located in the following areas:

i) Chemical and waste storage areas.

ii) Laboratories containing fume hoods.

iii) Experimental hutches where chemicals are used.

Water for safety showers and eyewashes will be either a central tepid water loop (potable water maintained at required temperature) or from local hot and cold potable water services with local mixing valve at each appliance. These alternates will be evaluated further during detailed design. Safety showers will not be fitted with flow switches. Safety showers in areas subject to freezing will be provided with suitable freeze protection.

Other Wastes

The types and volume of wastes that will be generated and transported by NSLS-II are not anticipated to differ markedly from those generated and transported by the existing NSLS. During a typical year of operation, NSLS-II will generate 3,000 to 5,000 pounds of wastes. The following are estimates of the types of wastes (in addition to waste chemicals):

i) Industrial Waste: oils and oily rags, cutting fluids, resin recharge rinse waters, and photographic wastes; oils and rinse water are the major components of industrial waste

ii) Radiological Waste: sources and other radioactive materials; eliminated by decay-in-storage when possible and disposed of as hazardous waste.

iii) Mixed Waste: eliminated by decay in-storage when possible and disposed of as hazardous waste

iv) Regulated Medical Waste: the Medical Department will dispose of syringes, needles, pipettes, vials, and razor blades

Storage areas meet appropriate code requirements will be provide at each LOB for non-chemical wastes. These areas will be B-occupancy.

11.7.4 Cryogenics Storage and Handling

Bulk storage of liquid nitrogen and liquid helium will be required at the new facility. These cryogenic fluids are used for cooling of magnets and other ring components, and for cooling of experimental apparatus.

Storage vessel and pressurized distribution piping system design and construction is governed by the ASME Boiler and Pressure Vessel Code (2007) and by ANSI/ASME B31.3 – Process Piping (2002). All piping systems and storage systems will be designed and installed to comply with applicable ASME and ANSI standards. Some specialized accelerator components that do not fall within code parameters will require engineering analysis to assure reliability.

The predominant hazard associated with distribution and use of cryogenic liquids is oxygen depletion in the event of a cryogen spill with subsequent flash to vapor (the expansion ratios for liquid nitrogen and liquid helium are 696 and 754 respectively, at 70° F). This hazard is present anywhere cryogenic liquids may be used in the facility, including the RF service building, tunnel, experimental hutches, and laboratories, and can result from a piping system failure, dewar leak, or similar occurrence. A lesser hazard is the potential for burns; this is typically mitigated by procedure and PPE.

The OSHA Respiratory Protection Standard 29 CFR 1910.134 defines an oxygen deficient atmosphere as an atmosphere containing less than 19.5% oxygen by volume. BNL has procedures in place to determine the Oxygen Deficiency Hazard (ODH) classification of any space where cryogenic liquids are used, and has established ODH control measures applicable to each hazard class. These control measures include ventilation (minimum one volume change per hour) for spaces with hazard class of 2 or greater, use of a personal monitor and availability of a self-rescue respirator for hazard class 1 or greater, and provisions for SCBA near the hazard area for spaces with hazard class of 4.

Determination of ODH hazard classes will be made during detailed design, when the scope of cryogen distribution and use is more firmly established. All spaces where cryogens may be used will be ventilated to at least one air volume change per hour. It is anticipated that the following additional control measures will be required:

a) Installation of local oxygen concentration monitors at locations where dewars may be used (e.g., in laboratories and experimental hutches). Monitors will be linked to local alarm lamps and sounders to provide warning alarms when the oxygen concentration falls to pre-determined levels. Warning lamps will be placed inside potential hazardous spaces and outside any entry to the space.

b) Dewar vessel filling stations will have interlocks to prevent flow of cryogenic fluid until the dewar is properly vented.

The need for emergency venting of enclosed spaces where cryogens are used will be evaluated during detailed design.

11.7.5 Material Handling

The new NSLS-II facility will be designed to accommodate delivery and movement of experimental equipment, facilities equipment components (e.g., pumps and motors) for service and maintenance, chemical containers, gas cylinders, dewars, water treatment ion exchange vessels for off-site regeneration, and other consumables for offices and laboratories from the loading docks to the points of use.

Accelerator and storage ring component installation will be addressed separately.

BNL has determined that there is no requirement for installation of a permanent bridge crane in the experimental hall. Provisions will be made for use of portable hoists. The requirement for permanent attachment points to structure will be determined during detailed design, along with method of personnel access to the attachment points for fixing hoists prior to use.

The need for permanent cranes or hoists in the service buildings will also be evaluated during detailed design.

Hoists will comply with applicable codes and standards, including the following:

a) ANSI/ASME B30.16-2003 - Standard for Overhead Hoists (Underhung)

b) ANSI/ASME B30.21-2005 - Standard for Manually Operated Lever Hoists

The following provisions will be made for material transport to and within the facility:

a) Roadway access to the inner ring with sufficient turning radii for an articulated tanker to make the initial helium delivery and for box van or flatbed truck for loading and unloading of equipment to the service buildings.

b) Roadway access with turning provisions for a box van or flatbed truck delivery to LOB loading docks for delivery of equipment, chemicals, gases, and other consumables. The main loading dock (at LOB-1) will be elevated and provided with dock levelers.

c) Roadway access suitable for an articulated tanker to make deliveries of liquid nitrogen to the storage tank between LOB-4 and LOB-5 and the future tank near LOB-2. The roadway layout will allow the tanker to unload without blocking other traffic to the LOB docks. Nitrogen storage tanks will be oriented away from personnel to reduce noise and fog exposure.

d) Bollards will be provided where necessary to protect equipment adjacent to roadways.

e) A nominal 10-foot wide circulation aisle will be maintained around the perimeter of the experimental hall to allow access to the beamlines from the LOB docks. The aisle will be suitable for forklift access for movement of heavy experimental equipment. Overhead services will be maintained at least 10 ft above the aisleway.

f) For beamlines which extend into the perimeter aisle and beyond, ramps will be provided with maximum slope to accommodate a forklift. Where the ramps are too steep for manual movement of liquid nitrogen dewars, automatic dewar fill stations will be provided at the LOBs on either side of the ramp(s).

g) An access aisle will be maintained at the perimeter of the mezzanine level.

11.7.6 Ionizing Radiation

Protection against ionizing radiation is addressed in DOE O 420.2B - Safety of Accelerator Facilities as well as in 10 CFR 830 Subpart B - Safety Basis Requirements of the Nuclear Safety Management Rule and 10 CFR 835 - Occupational Radiation Protection.

Shielding of the accelerator, storage ring, and beamline systems will be addressed elsewhere as part of the accelerator and storage ring systems design.

Beam interlocks, including exclusion zone search system interlocks, will also be addressed as part of the accelerator and storage ring systems design. These will be provided with the accelerator/storage ring installation.

11.7.7 Non-Ionizing Radiation

Regulatory requirements for control of exposure to non-ionizing radiation, including lasers and radiation in the radio frequency and microwave frequency regions, shall meet the Threshold Limit Values of the American Conference of Governmental Industrial Hygienists. The requirements for shielding will be addressed along with ionizing radiation shielding as part of the accelerator and storage ring component design and installation.

There is the potential for use of Class 1, 2, 3a, 3b, or 4 lasers as part of the beamline or laboratory experiments. BNL regulations regarding installation and user lasers will be applied to this project, including the requirement for failsafe laser interlocks for Class 4 lasers. This will be further evaluated during detailed design.

11.7.8 Process Exhaust

ANSI/AIHA Z9.5-2003 - Standard for Laboratory Ventilation and ANSI/AIHA Z9.2-2001 - Standard for Fundamentals Governing the Design and Operation of Local Exhaust Ventilation Systems are the governing standards for design of process exhaust systems for laboratory and experimental operations. These standards will define the criteria for process exhaust systems for NSLS-II. ANSI/AIHA Z9.2 is also referenced in OSHA 29 CFR 1910.94.

Laboratory fume hoods and corresponding process exhaust system(s) will be in accordance with Standard Z9.5. Evaluation of compatibility of exhaust streams to determine if multiple hoods can be manifolded will be made during detailed design. When chemical storage cabinets are integral with a fume hood, the chemical cabinet will be ventilated by the hood exhaust system.

An exhaust system will be required for experimental hutches that use hazardous chemicals or gases. The requirements for this system need further evaluation. Alternatives that will be evaluated during detailed design include:

a) Provision of a central exhaust system with capability to connect to any beamline hutch, installed as part of the conventional facility construction.

b) Provision for separate and dedicated exhaust systems for beamlines that require exhaust, installed with each beamline construction.

Chemical and gas storage cabinets in the central chemical store will be exhausted directly to atmosphere.

Process exhaust ductwork materials of construction will be selected to be compatible with the chemicals or gases being exhausted and compliant with applicable codes and standards with regard to smoke and flame spread rating.

11.7.9 Noise

29 CFR 1910.95 (OSHA) has established permissible noise exposures for the workplace. Additional requirements by the American Conference of Governmental Industrial Hygienists (ACGIH) are also established which are generally more stringent than OSHA. This project will limit noise to the ACGIH TLVs or even more strict requirements.

Appropriate equipment performance criteria and/or sound attenuation will be specified for plant equipment, particularly air handling units and pumps, to ensure that these noise levels are not exceeded in the service buildings and other plant spaces.

The required noise criteria for experimental areas, offices, and laboratories for the purpose of personnel comfort are significantly lower than the OSHA or ACGIH criteria. These criteria are listed in Table 3.5.

Design criteria to achieve these NC levels will be further developed during detailed design. These include ductwork sizing and routing restrictions as well as proper equipment selection and application of acoustic treatments.

11.7.10 Confined Spaces

Confined spaces will be identified and managed in accordance with the requirements in OSHA 29 CFR 1910.146 – Permit-Required Confined Spaces and with BNL's confined space access program. Wherever practical, the need for a confined space will be avoided during design.

11.8 Biological Safety

11.8.1

Requirements and criteria for biological safety systems are derived from the following codes and orders

a) 10 CFR 851 – Worker Safety and Health Program

11.8.2 BSL-2 Laboratories

It is anticipated that theNSLS-II program will require fit-out of at least one Biosafety Level 2 (BSL-2) laboratory for biological experimentation. Design of the laboratory and ventilation systems will be in accordance with ANSI/AIHA Z9.5-2003 - Standard for Laboratory Ventilation. Provisions will be made to restrict access to personnel with the appropriate training or other qualifications. There is no requirement for directional inward air flow in a BSL-2 laboratory, except as may be required for chemical odor control; although the BSL-2 laboratories at NSLS-II will be designed to be negative to the surrounding spaces.

A fume hood or Class II, Type A biological safety cabinet will be provided in each BSL-2 laboratory.

Additional requirements for BSL-2 laboratories will be established during detailed design.

11.9 Electrical Safety

11.9.1 Requirements

Requirements and criteria for electrical system design are derived from the following codes and orders:

a) Building Code of New York State (2002)

b) DOE O 420.2B –Safety of Accelerator Facilities

c) 10 CFR 851 – Worker Safety and Health Program

d) OSHA 29 CFR 1910.147 – Control of Hazardous Energy (Lockout/Tagout)

Design mitigation strategies are also identified in the PHA under PHA-6 (Electrical Hazards)

11.9.2 Codes and Standards

The following codes and standards will apply to design of facilities and systems related to the hazard areas identified above.

a) Building Code of New York State (2002)

b) NFPA 70 – National Electrical Code (2005)

c) NFPA 70E – Standard for Electrical Safety in the Workplace (2004)

d) NFPA 780 – Standard for Installation of Lightning Protection Systems (2004)

11.9.3 Design Requirements

Specific requirements for implementation of applicable electrical codes and standards will be defined in the next phase of design. These requirements may include, but not be limited to, the following.

a) Specification of NRTL-approved devices.

b) Review of cable segregation, cable tray loadings, and cable stirrups.

c) Completion of an arc flash analysis for all electrical panels and disconnects.

d) Location of disconnects and provisions for lockout/tagout.

e) Provisions for adequate power distribution for beamline and experimental equipment, including allowances for future beamline installation.

f) Maintenance of proper clearances around distribution panels and other electrical equipment.

11.10 Other Environment, Safety And Health Issues

11.10.1 Experimental Operations

Most of the experimental hazards identified in the PHA are addressed in other sections of this chapter (e.g., chemical handling, ODH hazards resulting from use of cryogenic liquids).

PHA-10 describes the hazards associated with the generation of ozone when the unattenuated synchrotron beam passes through air. This hazard is most likely to occur at the experimental end stations. Several mitigation strategies are identified in the PHA, most of which are related to end station set-up. The need for conventional facilities such as extract or local air filtration will be further evaluated during detailed design.

11.10.2 Emissions to Air and Releases to Groundwater

PHA-3 describes the anticipated environmental hazards resulting in operation from the NSLS-II facility. BNL has also prepared an Environmental Assessment (EA) for the facility which describes anticipated environmental impacts in more detail.

Potential environmental hazards from NSLS-II include the potential for releasing, in amounts beyond regulatory limits, oils, solvents, chemicals, and radioactive material to the soil, groundwater, air, or sanitary

system as a result of the failure of equipment, impact from a natural phenomenon, fire, or a violation of established procedure.

Accelerator cooling water will be a closed-loop system with no anticipated discharges other than the potential rinsing of ion exchangers before they are brought on-line. While some accelerator components become locally activated as a result of operations, the levels are expected to be well below BNL's Accelerator Safety Subject Area guidelines for soil activation.. NSLS-II would not generate tritiated water above the BNL defined Action Level. Periodic sampling of the cooling water systems will assure that tritium levels remain below the Action Level.

Experiments using radioisotopes will be controlled by specific facility procedures, rendering remote the likelihood of these materials entering the sanitary or groundwater systems.

Roof and parking lot drains will empty into groundwater recharge basin 005 that lies southeast of the NSLS-II site. Cooling tower blowdown will be discharged to a separate stormwater collection basin. All other water discharges will be disposed of through the sanitary waste stream; there are no expected requirements to monitor this outflow's quantity or chemistry.

Exhaust emissions from laboratory fume hoods and experimental hutches are associated with research and development and, therefore, would be exempt from Federal and state permitting requirements. Fume hood exhaust systems will be designed to permit the installation of HEPA filters in the exhaust stream should experimental conditions warrant.

11.10.3 Equipment Protection

a) Leak detection will be provided where the potential for liquid leaks exist in areas that are not normally occupied (e.g., the tunnel), to provide remote indication of a potential piping or equipment system failure. An unobserved leak could result in equipment damage, injury to personnel, or both.

b) Access control requirements for protection of sensitive and/or hazardous spaces will be evaluated in the next phase of design.

12 CODE ANALYSIS

12.1 General

12.1.1 Introduction

This report serves as the Title One Phase Fire Protection Analysis Report for National Synchrotron Light Source II at Brookhaven National laboratories, Upton, New York. It is intended to identify minimum requirements for the building as mandated by the applicable codes and standards, user needs, or required operations as requested by BNL. This document will be used as a reference by the design team and BNL throughout subsequent phases of the project.

12.1.2 Purpose

The purpose of this report is to summarize the fire protection and life safety requirements contained in the codes and standards applicable to the project. This report identifies the minimum code requirements that will provide an acceptable level of fire/life safety. Measures, which result in an increased level of fire/life safety are not discussed. Requirements regarding accessibility for the disabled and other disciplines, except for fire alarm requirements, are outside the scope of this report and will be discussed elsewhere in future submissions.

This report is limited to the most restrictive requirements contained in the codes listed in this report. Throughout the report, code reference sections are provided in parenthesis following each requirement to facilitate review of the provisions in detail.

12.2 Applicable Codes and Standards

The facility design will be in accordance with the codes, standards and guidelines as listed the Architectural section. 3.1.3. Where there is a conflict between two or more codes, the most stringent requirement will be used.

12.3 Occupancy Classifications

12.3.1 Main Use

NYSBC section 304.1classifies the overall building occupancy as a Group B (Business) occupancy, this includes the Ring Building including the accelerator tunnel the experimental floor, the access corridor and the tunnel mezzanine, the Booster Ring/Linac and RF Buildings, the five Lab Office Buildings (LOB) three of which are in the base building scope and two are bid alternates, the five service buildings (SB) and the Operations Center Building. Other accessory use spaces within the NSLS-II will be classified as shown in Table 12.1 below.

Table 12.1 Building Classification.

Space	Code Ref.	Occupancy Classification
Ring Building, Central Lab Office Building, Lab Office Buildings, Linac, RF Building	NYSBC 304.1	Group B, Business
Breakout Rooms and Conference Rooms over 750sf	NYSBC 303.1	A-3, Assembly without fixed seats
Chemical and Gas Storage over the amount allowed per control area.	NYSBC 307.4 NYSBC 307.5	H2 or H-3 High Hazard Storage.

Per NYSBC Sec. 302.2, Accessory Use Areas are not required to have fire barrier separation if the accessory use area is < 10% of the area of the story in which it is located except as shown below in 12.3.2. Per NYSBC Table 302.3.3 note d. accessory assembly use A-3 area is not considered a separate occupancy from the main occupancy if the floor area of the given assembly use is less than 750sf. Per Section 303.1 an assembly area with less than 50 occupants will not be considered a separate occupancy from the main occupancy.

12.3.2 Separations between Occupancies

In accordance with table 302.3.3 of the NYSBC separations between occupancies shall be as follows:

- Between “B” Occupancy and A-3 Occupancy: Two hour fire barrier wall separation and 1 1/2 hour door separation, unless it is less than 10% of floor area, or less than 750sf, than no separation is required.
- Between “B” Occupancy and H-2 Occupancy: two hour fire separation and 1 ½” hour door separation.
- Between “B” Occupancy and H-3 Occupancy: one hour fire separation and ¾ hour door separation.

NYSBC section 302.3.3 exception (1) allows one hour rated separation deduction for a fully sprinklered building.

12.4 Construction

12.4.1 Type of Construction

The NSLS-II will be a Type IIB construction per NYSBC section 602.2, unprotected non-combustible. Type II-B also requires fully non-combustible (and therefore inorganic), construction which is also beneficial to a laboratory-use based project.

12.4.2 Allowable Area

The main building will be classified as a two story building and will have an unlimited fire area per NYSBC section 507.3 because it has a automatic fire sprinkler system and will be surrounded on all sides with a 60ft wide yard or public way..

The Operations Center Building (OPS Center) will two stories, the inside portion separated from the Ring Building with a two hour fire wall. The Operations Center allowable area will be a minimum of 46,000sf (23,000sf per floor) before area modifications. The maximum allowable height will be four stories and 55 feet (the actual height will be two stories with an optional third story) above grade plane. The following illustrates the maximum allowable individual floor and overall building gross square footage possible under Type II-B construction, if all of the additional area modifications are used, Per NYSBC Chapter 5:

The governing NYSBCC Sec. 503 area increase formula is:

$$A_a = A_f + \frac{A_t I_f}{100} + \frac{A_t I_s}{100}$$

where:

A_a = Allowable area/floor (sf)

A_t = Tabular area/floor in accordance w/ Table 503 (= 23,000 gsf for Type II-B)

I_f = Area increase due to frontage (%) as calculated in accordance w/ Sec. 506.2 (see calculation below; 80%)

I_s = Area increase due to sprinkler protection (%) as calculated in accord w/ Sec. 506.3 (200% for multi-story building)

The specific value for the frontage increase indicated by the "I_f" value in the area increase formula above is:

$I_f = 100((F/P)-0.25)(W/30)$;

$I_f = 100((50/100)-0.25)(30/30)$

$I_f = 100(.25)(1)$

I_f = 25% Area increase due to frontage

F = Bldg perimeter which fronts on a public way or open space w/ > 20ft open width (expressed as 50%.

P = Perimeter of entire bldg. (expressed as 100%)

W = Minimum width of public way or open space (based on the approximately 30ft of open space on two sides and 100' minimum of one side, but shall not exceed 1)

THEREFORE, the increased maximum allowed area per floor is :

$$A_a = (23{,}000) + \frac{(23{,}000)(25)}{100} + \frac{(23{,}000)(200)}{100}$$

(Type II-B construction):

A_a = 23,000 + 5750 + 46,000

A_a = 74,750 gsf/flr

Per NYSBC Sec. 506.4, the total building allowed area is (3x) the total single floor allowed area, therefore the total allowable building area based on Type II-B construction would be:

TOTAL ALLOWED BLDG.AREA = 74,750 gsf/flr x 2= 149,500 gsf.

If the alternate third floor is accepted the allowable square footage will increase to 224,250 gsf.

(Type II-B, "B" occupancy)

12.4.3 Allowable Height

Based on NYSBC section 504 The allowable height for the Operation Center Building can increase by one story and 20 feet because it is equipped throughout with an automatic sprinkler system. The height of the Operations Center can now be 5 stories and 75feet height.

12.4.4 Mezzanines – (NYSBC section 505)

Section 505.1: A mezzanine(s) in compliance with this section shall be considered a part of the floor below. Such mezzanines shall not contribute to the building area or number of stories regulated by Section 503.1. The area of the mezzanine shall be included in determining the fire area defined in Section 702. The clear height above and below the mezzanine floor shall be 7'-0" clear minimum.

Section 505.2 Area Limitations: The aggregate area of a mezzanine or mezzanines with in a room shall not exceed one–third of the area of the room in which it is located.

Section 505.3 Egress: There shall be two independent means of egress where the common path of travel does not exceed the limitations of 100 feet set forth in section 1004.2.5. exception 1. There will be exits from

the mezzanines based on exiting distance, there should be on exit every 600 feet minimum. The actual distance on the Tunnel Mezzanine will average 85 feet maximum.

Section 505.4 Openness: A mezzanine shall be open and unobstructed to the room within which it is located, except for walls not more than 42” high, columns and posts.

12.4.5 Control Areas – (NYSBC section 414.2)

Control Areas shall be areas within the building where quantities of hazardous materials not exceeding the maximum quantities allowed by this code are stored, dispensed, used or handled. See tables 12.3 and 12.4 for allowable chemical amounts per control area.

Wall Construction – NYSBC 414.2.1: The control areas need to be separated from each other with a 1 hour Fire barrier Wall (per section 706) or as called for in Table 414.2.2.

Floor construction – NYSBC 414.2.3: The floor construction and the construction supporting the floor shall have a 2 hour fire resistance rating.

Number of Control Areas per floor is governed by NYSBC Table 414.2.2 and is summarized below in Table 12.2.

Table 12.2 Control Areas per Floor.

Floor Level	Number of Control Areas
Below Grade	3
Above Grade First floor	4
Above Grade Second Floor	3
Third Floor	2

The Ring Building, the Booster Ring/Linac Building, the part of the OPS Center third floor above the Ring Building and The RF Building and the five service buildings (SB) will all be considered as part of one control area.

Each of the five LOBs will be designed to be a separate control area from the Ring Building with a one hour fire separation wall between the LOB and the Ring Building. It will then be up to the NSLS 2 administration to determine which of the three LOBs is designated a Control Area.

Since the Inner Ring Portion of the Operations Center is separated by a two hour fire wall then each floor can have control areas as shown in Table 12.2.

The current intent is to include the entire facility as a single control area at this time. With the construction separations described above, additional control areas can be administratively identified at a later time.

Table 12.3 Allowed Quantities of Hazardous Chemicals.

Maximum Allowable Quantities per Control Area		
Material	Allowed Storage(1)	Allowed Use (Open System)(2)
Flammable Class 1-A	120 gal	20 gal
Flammable Class I-B	240 gal	30 gal
Flammable Class I-C	360 gal	40 gal
Combined Flammables	480 gal	60 gal
Water Reactive Class 1	No limit	No limit
Water Reactive Class 2	200 lbs (3)	20 lbs (3)
Water Reactive Class 3	20 lbs	2 lbs
Oxidizer Class 1	800 gal	200 gal
Oxidizer Class 2	50 gal	10 gal
Oxidizer Class 3	4 gal	0.4 gal
Oxidizer Class 4	0.2 gal	0.02 gal
Unstable (Reactive) Class 1	No limit	No limit
Unstable (Reactive) Class 2	200 lbs	20 lbs
Unstable (Reactive) Class 3	20 lbs	2 lbs
Unstable (Reactive) Class 4	2 lbs	0.25 lbs
Toxic	500 lbs	125 lbs
Highly Toxic	40 lbs	3 gal
Corrosive	2,000 gal	200 gal

Notes:
1. Increased as allowed for automatically sprinklered spaces and use of approved storage cabinets.
2. Aggregate quantity of storage and in-use shall not exceed allowable quantity for storage.
3. Assumes sulfuric acid. Equivalent to 20 gallons in storage and 2 gallons in open use.

Table 12.4 Allowable Quantities of Hazardous Gases

Note: Quantities include all allowed increases for building automatic sprinkler system.

Maximum Allowable Quantities per Control Area		
Material	Allowed Storage(1)	Allowed Use (Closed System)(2)
Flammable	2,000 cf	2,000 cf
Pyrophoric	100 cf	20 cf
Highly Toxic	40 cf (3)	40 cf
Toxic	1,620 cf	1,620 cf
Oxidizing	3,000 cf	3,000 cf

Notes:
1. Increased as allowed for sprinklered spaces.
2. Aggregate quantity of storage and in-use shall not exceed allowable quantity for storage.
3. In approved gas cabinets only.

12.4.6 Minimum Fire Resistance Ratings for TYPE II-B

The minimum fire resistance ratings for Type II-B construction is given in NYSBC Tables 601 & 602. the applicable data is shown in Tables 12.8.5 and 12.8.6 below.

Table 12.5 (NYSBC 601 and 602) Fire Resistive Rating Requirements for Building Elements.

Building Element	(Hours)
Structural Frame (Including columns, girders, trusses)	0
Bearing Walls:	
Exterior	0
Interior	0
Nonbearing walls and partitions:	
Exterior	(SEE TABLE 12.4)
Nonbearing walls and partitions:	
Interior	0
Floor Construction (Including supporting beams and joists)	0
Roof Construction (Including supporting beams and joists)	0
Per NYSBC Section 707: Exit Enclosures – 707.4 (connecting less than 4 stories)	1
Shafts – at floor Penetrations	
• connecting no more than two floors	0
• Connecting less than four stories	1
• Connecting four stories or more	2
• The shaft enclosure shall not be less than the floor structure it penetrates but will not exceed 2-hours.	
• Shafts are not required from a mezzanine to the floor below	
Corridors – NYSBC Table 1004.3.2.1, greater than 30 Occupant Load With sprinklers	0
Control Areas – NYSBC 414.2, from each other	1

Table 12.6 (NYSBC Table 715.3) Fire-Resistive Rating Requirements for Exterior Walls based On Fire Separation Distance for unprotected openings.

Fire Separation Distance	Type of Construction	Rating (hours)
< 5ft	II-B	1
$\geq$ 5ft < 10ft	II-B	1
$\geq$ 10ft < 30ft	II-B	0
$\geq$ 30ft	II-B	0

12.4.6 Protection of Openings

General opening protective ratings in accordance with NYSBC Table 715.3 are as follows:

Table 12.7 (NYSBC Table 715.3) Protective Ratings of Openings.

Wall Type	Protective Rating
2-hour fire walls and fire barriers:	
Chemical storage rooms (NFPA 30-4-4.1.2)	1-1/2 hrs
1-hour fire barriers:	
Shaft exit enclosure and exit passageway walls	1
Other fire separation wall assemblies	3/4
Chemical storage rooms (NFPA 30-4-4.1.2)	3/4
Fire partitions:	
Corridor walls	1/3
Other fire partitions	3/4
Exterior Wall Openings: (NYSBC Table 704.8)	See Table 12.6

The maximum area of unprotected openings permitted in an exterior wall in any story may not exceed the following values. Note that per NYSBC Sec. 704.8.1, buildings that are fully sprinkled in accordance with Sec. 903.3.1.1, the “Unprotected” values are used in lieu of the “Protected” values. Fire separation distance is defined as the distance measured from the building face to the closest interior lot line, to the centerline of the street or public way of to an imaginary line between two buildings on the same property

Table 12.8 (NYSBC table 704.8) Unprotected Opening in Exterior Walls

Fire Separation Distance ft	Percentage of Exterior Wall Area (unprotected Values)	Percentage of Exterior Wall Area (Protected Values)
0 to 3	Not permitted	Not permitted
Greater than 3 to 5	Not permitted – unlimited in exterior walls not required to be fire rated.	15 %
Greater than 5 to 10	10 %– unlimited in exterior walls not required to be fire rated.	25 %
Greater than 10 to 15	15%– unlimited in exterior walls not required to be fire rated.	45%
Greater than 15 to 20	25 %– unlimited in exterior walls not required to be fire rated.	75 %
Greater than 20 to 25	45 %– unlimited in exterior walls not required to be fire rated.	Not limited
Greater than 25 to 30	70 %– unlimited in exterior walls not required to be fire rated.	Not limited
Greater than 30	Not limited	Not limited

NYSBC Section 714.3.2 Wired glass and NYSBC table 714.3.2 designate the amount of wired glass allowed in protected openings. The use of wired glass while still allowed for this occupancy and code is being

disallowed in most construction codes and occupancies. The desired glass for protected openings is a fire protection (ceramic) glass complying with NFPA 80 for size limitations.

Table 12.9 (NYSBC table 714.3.2) Limited Size of Wired Glass Panels

Fire Protection Rating	Maximum Area (square inches)	Maximum Height (Inches)	Maximum Width (Inches)
3-hours	0	0	0
1 1/2 hour in exterior doors	0	0	0
1 and 1 ½ hours	100	33	10
3/4 hour	1296	54	54
20 minutes	Not limited	Not limited	Not limited
Fire window assemblies	1296	54	54

Ducts and Air Transfer Openings will be protected in accordance with NYSBC section 715. Fire Dampers will be installed in accordance with NYSBC table 715.3.1

Table 12.10 (NYSBC table 715.3.1) Fire Damper Rating

Type of Penetration	Minimum Damper Rating (Hour)
Less than 3-hours fire resistive-rated assemblies	1.5 hours
3-hour or greater fire resistive-rated assemblies	3 hours

12.5 Interior Finishes

12.5.1 Interior Finish Flame Spread Ratings

Interior flame spread rating shall be established in accordance with NYSBC Sec. 803 & Table 803.4 - "Sprinkled" values

For "B" Occupancy

- Vertical exits and exit passageways: Use Group B Class B
- Exit access corridors and other exitways: Use Group B Class C
- Rooms and enclosed spaces: Use Group B Class C

For "A-3" Occupancy

- Vertical exits and exit passageways: Use Group B Class B
- Exit access corridors and other exitways: Use Group B Class B
- Rooms and enclosed spaces: Use Group B Class C

Other Requirements

- Plastics: Foam plastics installed as interior trim or finish shall comply with NYSBC Sec 2604.

- Acoustical Ceilings: Acoustical ceiling materials exposed within a plenum space shall have a flame spread rating of 25 or less and a smoke developed rating of 50 or less when tested in accordance with ASTM E84.
- Plenum Wire: All wiring within plenum spaces shall conform to Article 300.22 of NFPA 70, National Electrical Code.

12.5.2 Interior Floor Finish/Covering Classifications

Finished floors or floor covering materials of a traditional type, such as wood, vinyl, linoleum, terrazzo and other resilient floor covering materials are acceptable, and shall comply with NYSBC Sec. 804.5.

Carpeting and similar materials should comply with the DOC FF-1 "pill test" (CPSC 16 CFR, Part 1630).

Where building is equipped throughout with an automatic sprinkler system, class II are permitted where Class I materials are required.

12.6 Automatic Sprinkler System

A wet automatic sprinkler system will be install in accordance with NYSBC section 903 and NFPA 13.

12.6 Means of Egress

12.6.1 Exits

The minimum number of exits is based on occupancy in accordance with NYSBC Sec. 1005.2.1. All rooms and spaces within each story shall be provided with and have access to the minimum number of approved independent exits as required by Table 12.11.

Table 12.11 (NYSBC table 1005.2.1) Minimum Number of Exits for Occupant Load.

Occupancy	Minimum # of Exits
1 - 500	2
500 – 1,000	3
Over 1000	4

Buildings allowed to have one exit are as follows:

Table 12.12 (NYSBC table 1005.2.2) Building with one Exit

Occupancy	Maximum Height of Building above grade	Maximum Occupants per floor and travel distance
A-3	1 story	50 occupants and 75 feet travel distance
B	1 story	50 occupants and 75 feet travel distance
H-2, H-3	1 story	3 occupants and 25 feet travel distance

Exit Access is established by NYSBC Section 1004. Maximum Travel Distance shall be in accordance with NYSBC Sec. 1004.2.4 & Table 1004.2.4. The maximum length of exit access travel, measured from the most remote point in an area to an exit, should not exceed the values in Table 12.13.

Table 12.13 (NYSBC table 1005.2.1) Exit Access Travel Distance.

Occupancy	w/ Sprinkler System (feet)
Assembly (A), Storage (S-1)	250
Business (B)	300
High Hazard Storage (H2)	100
High Hazard Storage (H3)	150

Based on the above information and the circumference of approx. 2965 feet the number of exit access points into the Ring Building is 5 doors at a maximum of 600feet apart. However because of the maximum allowable common path of travel of 80 feet between the beamlines, from the ratchet wall door to the end of the hutch) an exit door has been provided at approx. 156 feet apart with a total number (including those into the LOBs) of 19 doors at 36” each. The two doors at each LOB (five total) are 72” doors.

Dead Ends are limited by NYSBC Sec 1008.8.5. The maximum dead-end distance shall not exceed 20 feet, except for “B” and “F” occupancies where the limit is 50 feet in a fully sprinkled building.

Common Path of Travel is limited by NYSBC Sec. 1004.2.5. The maximum common path of travel should not exceed the limits of Table 12.14.

Table 12.14 Maximum Common Path of Travel.

Occupancy	Common Path of Travel Allowed	Common Path of Travel Actual
Assembly (A)	75 ft	75 ft
Business (B), including Labs and Mechanical spaces	100 ft	80 ft
High Hazard H-2 or H-3	25 ft	25 ft

12.6.2 Egress Width

Egress Width is established by NYSBC Table 1003.2.3. Using the sprinkled building values, the required egress widths are as follows:

- Stairways: 0.2 inches/person
- Other Egress Components: 0.15 inches/person
- Exit Access Corridor Width Minimum: 44 inches (NYSBC Sec. 10043.2.2; 24 inches for access to electrical, mechanical or plumbing systems, 36 inches with a required occupant capacity of <50.)
- Doors shall not reduce the required width to less than one-half during the swing, and no more than 7 inches when fully open.

Exit or Exit Access Doorway Arrangement is governed by NYSBC Sec. 1014.2.1, Exception 2. Where a building is equipped throughout with an automatic sprinkler system in accordance with Sec. 903.3.1.1 or 903.3.1.2, the separation distance of the exit doors or exit access doorways shall not be less than one-third of the length of the maximum overall diagonal dimension of the area served.

Vertical Exit Enclosures must have fire ratings in accordance with NYSBC 707.4. Interior exit stairways and interior exit ramps shall be enclosed with fire barriers. Exit enclosures shall have a fire-resistance rating of not less than 2 hours where connecting four stories or more and not less than 1 hour where connecting less than four stories.

Horizontal Exits are governed by NYSBC Sec. 1005.3.5. A horizontal exit shall not serve as the only exit from a portion of the building, and not more than one-half of the total number of required exits from a portion of the building. The horizontal exit shall be separated by a fire wall complying with Sec 705 or a fire barrier

Exit Discharge requirements are established by NYSBC Sec. 1006. All exits should discharge directly to the exterior of the building. The exit discharge shall be at grade or shall provide direct access to grade. The exit discharge shall not re-enter a building. Exception #1 states that a maximum of 50 percent of the number and capacity of the exit enclosures is permitted to egress through areas on the level of exit discharge provided all of the following area met:

- Exits discharge to a free and unobstructed way to the exterior of the building, which is readily visible and identifiable from the point of termination of the exit enclosure.
- The entire area of the level of discharge is separated from areas below by construction conforming to the fire-resistance rating for the exit enclosure.

12.6.3 Egress Capacity and Width

The occupant load of a room, space or floor shall be determined using the occupant load factors from NYSBC Sec 1003.2.2 as shown in Table 12.15.

Table 12.15 (NYSBC table 1003.2.2.2) Maximum Floor Area Allowances per Occupant

Use	ft^2/person
Offices, Industrial (Labs)	100 gross
Conference Rooms (Tables & Chairs)	15 net
Loading Docks, Storage, Mechanical/Electrical Rm.	300 gross

12.8.6.4 Doors

Doors shall meet the requirements of NYSBC 1003.3.1 and 1005.3.1. Two exits or exit access doorways from any space shall be provided where one of the following conditions exists:

- The occupant load of the space exceeds the values in Table 12.16
- The common path of egress travel exceeds the limitations of Section 1004.2.5 shown in Table 12.14.
- Where required by NYSBC Table 1003.2.1

Table 12.16 Spaces with One Means of Egress

Occupancy	Maximum Occupant Load
Assembly (A) , Business (B)	50
High Hazard Storage (H2 and 3)	3

The minimum clear door width is 32 inches as established by NYSBC 1003.3.1.1 and 1005.3.1. Where a pair of doors are provided, at least one of the doors should provide a minimum clear width opening. The maximum width of a door leaf 48 inches.

Floor elevations at door openings are set by NYSBC Sec. 1003.1.4. The floor shall be the same elevation on both sides of the door, and level except for exterior landings, which are permitted a slope of 2%. Thresholds at doorways shall not exceed 1/2 inches. (NYSBC 1003.3.1.6)

Door Swing is specified by NYSBC section 1003.3.1.2. All means of egress doors regardless of occupancy shall swing in the direction of egress where serving a room with an occupant load of 50 or more persons, and for all H occupancy rooms. All egress doors shall be readily open-able from the side from which egress is made without the use of a key or special knowledge or effort (NYSBC Sec. 1003.3.1.8).

Latches and Panic Hardware are specified by NYSBC Sec 1003.3.1.8.3. A latch or other fastening device on a door should be provided with a knob, handle, exit device or other simple releasing device having an obvious method of operation under all lighting conditions. Doors shall be open-able with no more than one releasing operation. The releasing mechanism for any latch shall be installed between 34 inches and 48 inches above the finished floor.

12.6.4 Stairways

Stairways shall comply with NYSBC sections 1003.3.3.1 through 1003.3.3.12.1.

The minimum clear width of stairways is to be determined by Table NYSBC 1003.2.3 – Stairways, but not less than 44inches per 1003.3.3.1. Protruding Objects are limited by NYSBC sections 1003.2.5.1, 1003.5.4 and 1104.

Stair construction (NYSBC 1003.3.3.5) shall be of materials consistent with the construction type.

The minimum dimension of landings measured in the direction of travel shall be equal to the required width of the stairway. (NYSBC Sec 1003.3.3.4)

Minimum Headroom (NYSBC Sec. 1003.3.3.2): 80 inches.

Maximum Height between landings (NYSBC Sec. 1003.3.6): 12 feet.

Treads and Risers (NYSBC Sec. 1003.3.3.3):

- Maximum riser height - 7 in
- Minimum riser height - 4 in
- Minimum tread depth - 11 in

Stair Dimensions (NYSBC Sec. 1003.3.3.3.1): Stair dimensions should be uniform. Variation between treads or risers should not exceed 3/8 in.

12.7 Elevators

Elevators shall be designed in accordance with NYSBC section 1003.2.13.3. All passenger elevators shall be accessible in accordance with ADAAG, and ANSI A117.1.

12.8 Ramps

Ramps shall be designed in accordance with NYSBC section 1003.3.4.

13. ROOM DATA SHEETS

Program of Spaces - Net Area

Room #	Room Name	Room NSF	Qty	Total NSF
Injection				
BR-101	Booster Ring Tunnel	6,688	1	6,688
BR-102	Linac Room	1,715	1	1,715
BR-103	Booster Service Building - East	6,102	1	6,102
BR-104	Klystron Gallery	1,620	1	1,620
BR-105	Booster Service Building - Wes	1,568	1	1,568
		Injection Total Net Square Feet:		**17,693**
Lab Office Buildings				
LOB1-101	Private Office	110	48	5,280
LOB1-102	Open Office Space	90	24	2,160
LOB1-103	Laboratory - Wet	480	2	960
LOB1-103A	Laboratory - Dry	480	4	1,920
LOB1-104	Storage	110	1	110
LOB1-105	Conference Room	560	2	1,120
LOB1-105A	Conference Room	220	2	440
LOB1-106	Lobby & Interaction Space	150	4	600
LOB1-107	Break Room / Kitchen	240	2	480
LOB1-108	Ship-Receive & Storage	960	1	960
LOB1-109	Toilet / Shower	250	2	500
LOB1-110	Electrical / Data	153	1	153
LOB1-111	Janitor Closet	63	1	63
LOB1-112	Access Corridor Interface	2,090	1	2,090
LOB1-113	Machine Shop	270	1	270
LOB4-101	LOB #4 Shell	16,146	1	16,146
LOB5-101	Private Office	110	48	5,280
LOB5-102	Flexible Office Space	90	24	2,160
LOB5-103	Laboratory - Wet	480	2	960
LOB5-103A	Laboratory - Dry	480	4	1,920
LOB5-104	Storage	110	1	110
LOB5-105	Conference Room	560	2	1,120

Room #	Room Name	Room NSF	Qty	Total NSF
LOB5-105A	Conference Room	220	2	440
LOB5-106	Lobby & Interaction Space	150	4	600
LOB5-107	Break Room / Kitchen	240	2	480
LOB5-108	Ship-Receive & Storage	960	1	960
LOB5-109	Toilet / Shower	250	2	500
LOB5-110	Electrical / Data	153	1	153
LOB5-111	Janitor Closet	63	1	63
LOB5-112	Access Corridor Interface	2,090	1	2,090
LOB5-113	Machine Shop	270	1	270
	Lab Office Buildings Total Net Square Feet:			**50,358**

Operations Center

OPS-103	Control Conference Room	676	1	676
OPS-104	Control Room	1,547	1	1,547
OPS-105	Computer Room	976	1	976
OPS-106	2nd Floor Toilet & Shower	76	2	152
OPS-107	Entrance Lobby & Vestibule	2,415	1	2,415
OPS-108	Bridge & Viewing Gallery	1,450	1	1,450
OPS-109	Unisex Toilet	78	1	78
OPS-110	Break Room / Kitchenette	512	1	512
OPS-111	Telecom Room	409	1	409
OPS-118	Switchgear Room	655	1	655
OPS-120	Men's Locker Room	128	1	128
OPS-121	Women's Locker Room	126	1	126
OPS-122	Storage	108	1	108
	Operations Center Total Net Square Feet:			**9,232**

RF Building

RF-101	RF Cavity Room	9,756	1	9,756
RF-102	RF Test	426	1	426
	RF Building Total Net Square Feet:			**10,182**

Ring Building

RB-101	Accelerator Tunnel	37,300	1	37,300

Room #	Room Name	Room NSF	Qty	Total NSF
RB-102A	Experimental Hall	94,235	1	94,235
RB-102B	Access Corridor	33,018	1	33,018
RB-103	Tunnel Mezzanine	50,950	1	50,950
RB-104	Loading Dock	2,060	1	2,060
RB-105	Hazardous Materials Storage	450	1	450
RB-106	Stock Room	1,618	1	1,618
RB-107	Grille	257	1	257
		Ring Building Total Net Square Feet:		**219,888**

Service Buildings

SB-101	Service Building #1	9,626	1	9,626
SB-102	Service Building #2	9,626	1	9,626
SB-103	Service Building #3	9,626	1	9,626
SB-104	Service Building #4	9,626	1	9,626
SB-105	Service Building #5	9,626	1	9,626
		Service Buildings Total Net Square Feet:		**48,130**
		NSLS-II Net Square Feet:		**355,483**

ROOM DATA SHEET

Room Name: Booster Ring Tunnel **Room Number:** BR-101

Functional Area: Injection Ground Level **Space Type:** Accelerator

SPACE REQUIREMENT:

Allocated Space : 6,688 NSF x 1 Rooms Reqd. = **6,688** Total Net Square Feet

Function: House the Booster ring

Occupancy Class: B

General Notes: Radiation shielding required for tunnel walls and roof. Shielded doors or labyrinths required for entry.

STRUCTURAL DATA:

Floor Live Load: 350 psf Floor Capacity Load psf Vibration Requirements: None

Structural Notes: Minimize differential settlement

FINISHES:

Walls: Paint Floors: Sealed Concrete

Ceilings: Concrete Clg. Ht. 9'-0"

Finishes Notes:

ROOM ENVIRONMENT:

Temperature	78	F +/- 1.8	F	Cooling	78	F +/- 1.8	F	Heating
Humidity	50	RH +/- 10	RH	Cooling	30	RH +/- 10	RH	Heating

Room Pressure: Neutral Vibration Criteria: None

Acoustic Noise Level NC: None EMI Criteria: None

SPECIAL REQUIREMENTS:

- ☐ Storage Cabinet
- ☐ Casework
- ☐ Fume Hood
- ☐ Toxic / Hazardous Materials

Special Requirements Notes: Labyrinth entry required

FIRE PROTECTION:

Hazard Classification: Ordinary Hazard Group ☑ Wet System: ☐ Preaction System

Fire Protection Notes:

HVAC:

Air Changes / Hr

Recirc / Single Pass Airflow: Recirculated

HVAC Notes:

- ☐ General Exhaust:
- ☐ Heat Exhaust:
- ☐ Chemical Exhaust:
- ☑ Smoke Exhaust: by AHU

PLUMBING:

- ☐ Domestic Water H/C
- ☐ Eyewash / Safety Shower
- ☑ Floor / Trench Drain: Trench drain around perimeter

Plumbing Notes: Trench to have holding sump to allow testing prior to discharge to Sanitary Sewer.

PROCESS PIPING:

- ☑ Compressed Air
- ☑ Nitrogen: Possible replacement for compresse
- ☐ Liquid Nitrogen
- ☐ Other
- ☐ DI Water
- ☑ Process Cooling Water - Cu: Cu / Al by ASD
- ☐ Process Cooling Water - Al
- ☐ Chemical Drain

Piping Notes:

ELECTRICAL:

Lighting Fixture Type: Surface Mount

Lighting Lamp Type: Fluorescent

Lighting Direction: Direct

Light Switching: Low Voltage Switch

Lighting Level (FC): 30

Ground:

Electrical Notes:

Power Outlets:

No.	Voltage	Phase	Type	Location
20	120 v	1 ph	Normal	Wall
0				

Clean Power:

UPS:

Emergency Power: Lighting, life safety

TELECOMMUNICATION AND SPECIAL SYSTEMS:

- ☑ Phone / Voice
- ☐ PA System
- ☐ Gas Leak Detection
- ☐ Liquid Leak Detection
- ☑ Data Connections:
- ☑ Access Control:
- ☐ CCTV:
- ☑ Fire Detection Type: HSSD

Telecom Notes:

ROOM DATA SHEET

Room Name: Linac Room **Room Number:** BR-102

Functional Area: Injection Ground Level **Space Type:** Accelerator

SPACE REQUIREMENT:

Allocated Space : 1,715 NSF x 1 Rooms Reqd. = **1,715** Total Net Square Feet

Function: House the Linac

Occupancy Class: B

General Notes: Radiation shielding required for tunnel walls and roof. Shielded doors or labyrinths required for entry.

STRUCTURAL DATA:

Floor Live Load: 350 psf Floor Capacity Load psf Vibration Requirements: None

Structural Notes: Minimize differential settlement

FINISHES:

Walls: Paint Floors: Sealed Concrete

Ceilings: Concrete Clg. Ht. 9'-0"

Finishes Notes:

ROOM ENVIRONMENT:

Temperature	75	F +/-	5	F	Cooling	72	F +/- 5 F	Heating
Humidity	50	RH +/-	10	RH	Cooling	30	RH +/- 10 RH	Heating

Room Pressure: Positive Vibration Criteria: None

Acoustic Noise Level NC: None EMI Criteria: None

SPECIAL REQUIREMENTS:

- ☐ Storage Cabinet
- ☐ Casework
- ☐ Fume Hood
- ☐ Toxic / Hazardous Materials

Special Requirements Notes: Labyrinth entry required

FIRE PROTECTION:

Hazard Classification: Ordinary Hazard Group ☑ Wet System: ☐ Preaction System

Fire Protection Notes:

HVAC:

Air Changes / Hr

Recirc / Single Pass Airflow: Recirculated

HVAC Notes:

- ☐ General Exhaust:
- ☐ Heat Exhaust:
- ☐ Chemical Exhaust:
- ☑ Smoke Exhaust: by AHU

PLUMBING:

- ☐ Domestic Water H/C
- ☐ Eyewash / Safety Shower
- ☐ Floor / Trench Drain

Plumbing Notes:

PROCESS PIPING:

- ☑ Compressed Air
- ☐ Nitrogen
- ☐ Liquid Nitrogen
- ☐ Other
- ☐ DI Water
- ☑ Process Cooling Water - Cu: Cu / Al by ASD
- ☐ Process Cooling Water - Al
- ☐ Chemical Drain

Piping Notes:

ELECTRICAL:

Lighting Fixture Type: Pendant

Lighting Lamp Type: Fluorescent

Lighting Direction: Direct

Light Switching: Low Voltage Switch

Lighting Level (FC): 30

Ground:

Electrical Notes:

Power Outlets:

No.	Voltage	Phase	Type	Location
0	120 v	1 ph	Normal	Wall
0				

Clean Power:

UPS:

Emergency Power:

TELECOMMUNICATION AND SPECIAL SYSTEMS:

- ☑ Phone / Voice
- ☑ PA System
- ☐ Gas Leak Detection
- ☐ Liquid Leak Detection
- ☑ Data Connections:
- ☑ Access Control:
- ☐ CCTV:
- ☐ Fire Detection Type:

Telecom Notes:

ROOM DATA SHEET

Room Name: Booster Service Building - East **Room Number:** BR-103

Functional Area: Injection Ground Level **Space Type:** Accelerator

SPACE REQUIREMENT:

Allocated Space : 6,102 NSF x 1 Rooms Reqd. = **6,102** Total Net Square Feet

Function: House support functions for the Booster Ring

Occupancy Class: B

General Notes:

STRUCTURAL DATA:

Floor Live Load: 350 psf Floor Capacity Load psf Vibration Requirements: None

Structural Notes:

FINISHES:

Walls: Paint Floors: Sealed Concrete

Ceilings: No Ceiling Clg. Ht.

Finishes Notes:

ROOM ENVIRONMENT:

Temperature	75	F +/-	1	F	Cooling	72	F +/- 1 F	Heating
Humidity	50	RH +/-	10	RH	Cooling	30	RH +/- 10 RH	Heating

Room Pressure: Neutral Vibration Criteria: None

Acoustic Noise Level NC: Per ACGIH TLVs EMI Criteria: None

SPECIAL REQUIREMENTS:

- ☐ Storage Cabinet
- ☐ Casework
- ☐ Fume Hood
- ☐ Toxic / Hazardous Materials

Special Requirements Notes:

FIRE PROTECTION:

Hazard Classification: Ordinary Hazard Group ☑ Wet System: ☐ Preaction System

Fire Protection Notes:

HVAC:

Air Changes / Hr

Recirc / Single Pass Airflow: Recirculated

- ☐ General Exhaust:
- ☐ Heat Exhaust:
- ☐ Chemical Exhaust:
- ☑ Smoke Exhaust: by AHU

HVAC Notes:

PLUMBING:

- ☑ Domestic Water H/C
- ☑ Eyewash / Safety Shower
- ☑ Floor / Trench Drain: Provide floor drains to sanitary waste.

Plumbing Notes:

PROCESS PIPING:

- ☑ Compressed Air
- ☑ Nitrogen
- ☐ Liquid Nitrogen
- ☐ Other
- ☐ DI Water
- ☐ Process Cooling Water - Cu
- ☐ Process Cooling Water - Al
- ☐ Chemical Drain

Piping Notes:

ELECTRICAL:

Lighting Fixture Type: Pendant

Lighting Lamp Type: Fluorescent

Lighting Direction: Direct

Light Switching: Occupancy Sensor

Lighting Level (FC): 30

Ground:

Electrical Notes:

Power Outlets:

No.	Voltage	Phase	Type	Location
0	120 v	1 ph	Normal	Wall
0				

Clean Power:

UPS:

Emergency Power:

TELECOMMUNICATION AND SPECIAL SYSTEMS:

- ☑ Phone / Voice
- ☑ PA System
- ☐ Gas Leak Detection
- ☐ Liquid Leak Detection
- ☑ Data Connections:
- ☑ Access Control:
- ☐ CCTV:
- ☐ Fire Detection Type:

Telecom Notes:

ROOM DATA SHEET

Room Name: Klystron Gallery **Room Number:** BR-104

Functional Area: Injection Ground Level **Space Type:** Accelerator

SPACE REQUIREMENT:

Allocated Space : 1,620 NSF x 1 Rooms Reqd. = **1,620** Total Net Square Feet

Function: House klystrons and support equipment for the Linac

Occupancy Class: B

General Notes:

STRUCTURAL DATA:

Floor Live Load: 350 psf Floor Capacity Load psf Vibration Requirements: None

Structural Notes:

FINISHES:

Walls: Paint Floors: Sealed Concrete

Ceilings: No Ceiling Clg. Ht. 17'-0" clear

Finishes Notes:

ROOM ENVIRONMENT:

Temperature	75	F +/-	1	F	Cooling	72	F +/- 1 F	Heating
Humidity	50	RH +/-	10	RH	Cooling	30	RH +/- 10 RH	Heating

Room Pressure: Positive Vibration Criteria: None

Acoustic Noise Level NC: Per ACGIH TLVs EMI Criteria: None

SPECIAL REQUIREMENTS:

- ☐ Storage Cabinet
- ☐ Casework
- ☐ Fume Hood
- ☐ Toxic / Hazardous Materials

Special Requirements Notes:

FIRE PROTECTION:

Hazard Classification: Ordinary Hazard Group ☑ Wet System: ☐ Preaction System

Fire Protection Notes:

HVAC:

Air Changes / Hr

Recirc / Single Pass Airflow: Recirculated

HVAC Notes:

- ☐ General Exhaust:
- ☐ Heat Exhaust:
- ☐ Chemical Exhaust:
- ☑ Smoke Exhaust: by AHU

PLUMBING:

- ☐ Domestic Water H/C
- ☑ Eyewash / Safety Shower
- ☐ Floor / Trench Drain

Plumbing Notes:

PROCESS PIPING:

- ☑ Compressed Air
- ☐ Nitrogen
- ☐ Liquid Nitrogen
- ☐ Other
- ☐ DI Water
- ☑ Process Cooling Water - Cu: Cu / Al by ASD
- ☐ Process Cooling Water - Al
- ☐ Chemical Drain

Piping Notes:

ELECTRICAL:

Lighting Fixture Type: Pendant

Lighting Lamp Type: Fluorescent

Lighting Direction: Direct

Light Switching: Low Voltage Switch

Lighting Level (FC): 30

Ground:

Electrical Notes:

Power Outlets:

No.	Voltage	Phase	Type	Location
0	120 v	1 ph	Normal	Wall
0				

Clean Power:

UPS:

Emergency Power:

TELECOMMUNICATION AND SPECIAL SYSTEMS:

- ☑ Phone / Voice
- ☑ PA System
- ☐ Gas Leak Detection
- ☐ Liquid Leak Detection
- ☑ Data Connections:
- ☑ Access Control:
- ☐ CCTV:
- ☐ Fire Detection Type:

Telecom Notes:

ROOM DATA SHEET

Room Name: Booster Service Building - West **Room Number:** BR-105

Functional Area: Injection Ground Level **Space Type:** Accelerator

SPACE REQUIREMENT:

Allocated Space : 1,568 NSF x 1 Rooms Reqd. = **1,568** Total Net Square Feet

Function: Support functions and HVAC for the Booster Ring

Occupancy Class: B

General Notes:

STRUCTURAL DATA:

Floor Live Load: 350 psf Floor Capacity Load psf Vibration Requirements: None

Structural Notes:

FINISHES:

Walls: Paint Floors: Sealed Concrete

Ceilings: No Ceiling Clg. Ht.

Finishes Notes:

ROOM ENVIRONMENT:

Temperature 75 F +/- 5 F Cooling 72 F +/- 5 F Heating

Humidity 0 RH +/- 0 RH Cooling 0 RH +/- 0 RH Heating

Room Pressure Vibration Criteria

Acoustic Noise Level NC Per ACGIH TLVs EMI Criteria None

SPECIAL REQUIREMENTS:

- ☐ Storage Cabinet
- ☐ Casework
- ☐ Fume Hood
- ☐ Toxic / Hazardous Materials

Special Requirements Notes:

FIRE PROTECTION:

Hazard Classification: Ordinary Hazard Group ☑ Wet System: ☐ Preaction System

Fire Protection Notes:

HVAC:

Air Changes / Hr ☐ General Exhaust: ☐ Chemical Exhaust:

Recirc / Single Pass Airflow Recirculated ☐ Heat Exhaust: ☑ Smoke Exhaust: by AHU

HVAC Notes:

PLUMBING:

- ☑ Domestic Water H/C
- ☐ Eyewash / Safety Shower
- ☑ Floor / Trench Drain — Provide floor drains to sanitary waste.

Plumbing Notes:

PROCESS PIPING:

- ☐ Compressed Air
- ☐ Nitrogen
- ☐ Liquid Nitrogen
- ☐ Other
- ☐ DI Water
- ☐ Process Cooling Water - Cu
- ☐ Process Cooling Water - Al
- ☐ Chemical Drain

Piping Notes:

ELECTRICAL:

Lighting Fixture Type: Pendant

Lighting Lamp Type: Fluorescent

Lighting Direction: Direct

Light Switching: Occupancy Sensor

Lighting Level (FC): 30

Ground:

Electrical Notes:

Power Outlets:

No.	Voltage	Phase	Type	Location
0	120 v	1 ph	Normal	Wall
0				

Clean Power:

UPS:

Emergency Power:

TELECOMMUNICATION AND SPECIAL SYSTEMS:

- ☐ Phone / Voice
- ☐ PA System
- ☐ Gas Leak Detection
- ☐ Liquid Leak Detection
- ☐ Data Connections:
- ☑ Access Control:
- ☐ CCTV:
- ☐ Fire Detection Type:

Telecom Notes:

ROOM DATA SHEET

Room Name: Private Office **Room Number:** LOB1-101

Functional Area: Lab Office Buildings Ground Level **Space Type:** Office

SPACE REQUIREMENT:

Allocated Space : 110 NSF x 48 Rooms Reqd. = **5,280** Total Net Square Feet

Function: Enclosed private office space

Occupancy Class: B

General Notes:

STRUCTURAL DATA:

Floor Live Load: 100 psf Floor Capacity Load psf Vibration Requirements: None

Structural Notes:

FINISHES:

Walls: Painted Gypsum Board Floors: Carpet Tile

Ceilings: Acoustic Ceiling Tile Clg. Ht. 9'-0"

Finishes Notes:

ROOM ENVIRONMENT:

Temperature	75	F +/-	5	F	Cooling	72	F +/- 5 F	Heating
Humidity	50	RH +/-	10	RH	Cooling	30	RH +/- 10 RH	Heating

Room Pressure: Positive Vibration Criteria: None

Acoustic Noise Level NC: 35-40 EMI Criteria: None

SPECIAL REQUIREMENTS:

- ☐ Storage Cabinet
- ☐ Casework
- ☐ Fume Hood
- ☐ Toxic / Hazardous Materials

Special Requirements Notes:

FIRE PROTECTION:

Hazard Classification: Ordinary Hazard Group ☑ Wet System: ☐ Preaction System

Fire Protection Notes:

HVAC:

Air Changes / Hr: 20 CFM/Person ☐ General Exhaust: ☐ Chemical Exhaust:

Recirc / Single Pass Airflow: Recirculated ☐ Heat Exhaust: ☑ Smoke Exhaust: by AHU

HVAC Notes:

PLUMBING:

- ☐ Domestic Water H/C
- ☐ Eyewash / Safety Shower
- ☐ Floor / Trench Drain

Plumbing Notes:

PROCESS PIPING:

- ☐ Compressed Air
- ☐ Nitrogen
- ☐ Liquid Nitrogen
- ☐ Other
- ☐ DI Water
- ☐ Process Cooling Water - Cu
- ☐ Process Cooling Water - Al
- ☐ Chemical Drain

Piping Notes:

ELECTRICAL:

Lighting Fixture Type: Recessed Troffer

Lighting Lamp Type: Fluorescent

Lighting Direction: Direct

Light Switching: Occupancy Sensor

Lighting Level (FC): 30-50 (50 at work surface)

Ground:

Electrical Notes:

Power Outlets:

No.	Voltage	Phase	Type	Location
3	120 v	1 ph	Normal	Wall
0				

Clean Power:

UPS:

Emergency Power:

TELECOMMUNICATION AND SPECIAL SYSTEMS:

- ☑ Phone / Voice
- ☐ PA System
- ☐ Gas Leak Detection
- ☐ Liquid Leak Detection
- ☑ Data Connections:
- ☐ Access Control:
- ☐ CCTV:
- ☐ Fire Detection Type:

Telecom Notes:

ROOM DATA SHEET

Room Name: Open Office Space **Room Number:** LOB1-102

Functional Area: Lab Office Buildings Ground Level **Space Type:** Office

SPACE REQUIREMENT:

Allocated Space : 90 NSF x 24 Rooms Reqd. = **2,160** Total Net Square Feet

Function: Cubicle space

Occupancy Class: B

General Notes:

STRUCTURAL DATA:

Floor Live Load: 100 psf Floor Capacity Load psf Vibration Requirements: None

Structural Notes:

FINISHES:

Walls: Movable Partition Floors: Carpet Tile

Ceilings: No Ceiling Clg. Ht. 10'-0"

Finishes Notes:

ROOM ENVIRONMENT:

Temperature	75	F +/-	5	F	Cooling	72	F +/- 5 F	Heating
Humidity	50	RH +/-	10	RH	Cooling	30	RH +/- 10 RH	Heating

Room Pressure: Positive Vibration Criteria: None

Acoustic Noise Level NC: 35-40 EMI Criteria: None

SPECIAL REQUIREMENTS:

- ☐ Storage Cabinet
- ☐ Casework
- ☐ Fume Hood
- ☐ Toxic / Hazardous Materials

Special Requirements Notes:

FIRE PROTECTION:

Hazard Classification: Ordinary Hazard Group ☑ Wet System: ☐ Preaction System

Fire Protection Notes:

HVAC:

Air Changes / Hr: 20 CFM/Person ☐ General Exhaust: ☐ Chemical Exhaust:

Recirc / Single Pass Airflow: Recirculated ☐ Heat Exhaust: ☑ Smoke Exhaust: by AHU

HVAC Notes:

PLUMBING:

- ☐ Domestic Water H/C
- ☐ Eyewash / Safety Shower
- ☐ Floor / Trench Drain

Plumbing Notes:

PROCESS PIPING:

- ☐ Compressed Air
- ☐ Nitrogen
- ☐ Liquid Nitrogen
- ☐ Other
- ☐ DI Water
- ☐ Process Cooling Water - Cu
- ☐ Process Cooling Water - Al
- ☐ Chemical Drain

Piping Notes:

ELECTRICAL:

Lighting Fixture Type: Recessed Troffer

Lighting Lamp Type: Fluorescent

Lighting Direction: Direct

Light Switching: Occupancy Sensor

Lighting Level (FC): 30-50 (50 at work surface)

Ground:

Electrical Notes:

Power Outlets:

No.	Voltage	Phase	Type	Location
3	120 v	1 ph	Normal	Wall
0				

Clean Power:

UPS:

Emergency Power:

TELECOMMUNICATION AND SPECIAL SYSTEMS:

- ☑ Phone / Voice
- ☐ PA System
- ☐ Gas Leak Detection
- ☐ Liquid Leak Detection
- ☑ Data Connections:
- ☐ Access Control:
- ☐ CCTV:
- ☐ Fire Detection Type:

Telecom Notes:

ROOM DATA SHEET

Room Name: Laboratory - Wet **Room Number:** LOB1-103

Functional Area: Lab Office Buildings Ground Level **Space Type:** Laboratory

SPACE REQUIREMENT:

Allocated Space : 480 NSF x 2 Rooms Reqd. = **960** Total Net Square Feet

Function: General Purpose Wet Laboratory

Occupancy Class: B

General Notes: Laboratory equals two laboratory modules, each 240 SF.

STRUCTURAL DATA:

Floor Live Load: 350 psf Floor Capacity Load psf Vibration Requirements: None

Structural Notes:

FINISHES:

Walls: Epoxy Painted Floors: Linoleum Sheet

Ceilings: Acoustic Ceiling Tile Clg. Ht. 12'-0"

Finishes Notes:

ROOM ENVIRONMENT:

Temperature	75	F +/-	5	F	Cooling	72	F +/- 5 F	Heating
Humidity	50	RH +/-	10	RH	Cooling	30	RH +/- 10 RH	Heating

Room Pressure: Negative Vibration Criteria: None

Acoustic Noise Level NC: 45-50 EMI Criteria: None

SPECIAL REQUIREMENTS:

- [x] Storage Cabinet
- [x] Casework
- [x] Fume Hood — chemical storage cabinet below.
- [x] Toxic / Hazardous Materials — Fume Hood cabinet

Special Requirements Notes: Two labs per LOB require Fume Hoods. One Hood per LOB to have HEPA filtration

FIRE PROTECTION:

Hazard Classification: Ordinary Hazard Group

- [x] Wet System:
- [ ] Preaction System

Fire Protection Notes:

HVAC:

Air Changes / Hr: 100 %

Recirc / Single Pass Airflow: Single Pass

HVAC Notes: One fume hood with HEPA filtration on exhaust. Second to have capability to add HEPA filtration in the future.

- [x] General Exhaust: Room Exhaust
- [ ] Heat Exhaust:
- [x] Chemical Exhaust: Fume Hood
- [x] Smoke Exhaust: by AHU

PLUMBING:

- [x] Domestic Water H/C
- [x] Eyewash / Safety Shower
- [ ] Floor / Trench Drain

Plumbing Notes:

PROCESS PIPING:

- [x] Compressed Air — Lab Bench
- [x] Nitrogen — Lab Bench
- [ ] Liquid Nitrogen
- [ ] Other
- [x] DI Water
- [ ] Process Cooling Water - Cu
- [ ] Process Cooling Water - Al
- [ ] Chemical Drain

Piping Notes:

ELECTRICAL:

Lighting Fixture Type: Pendant

Lighting Lamp Type: Fluorescent

Lighting Direction: Direct/Indirect

Light Switching: Low Voltage Switch

Lighting Level (FC): 50-75 (75 at work surface)

Ground:

Electrical Notes:

Power Outlets:

No.	Voltage	Phase	Type	Location
2	120 v	1 ph	Normal	Wall
0	120 v	1 ph	Normal	Raceway

Clean Power:

UPS:

Emergency Power:

TELECOMMUNICATION AND SPECIAL SYSTEMS:

- [x] Phone / Voice
- [ ] PA System
- [ ] Gas Leak Detection
- [ ] Liquid Leak Detection
- [x] Data Connections:
- [x] Access Control:
- [ ] CCTV:
- [x] Fire Detection Type: Photoelectric Smoke Detectors

Telecom Notes:

ROOM DATA SHEET

Room Name: Laboratory - Dry **Room Number:** LOB1-103A

Functional Area: Lab Office Buildings Ground Level **Space Type:** Laboratory

SPACE REQUIREMENT:

Allocated Space : 480 NSF x 4 Rooms Reqd. = **1,920** Total Net Square Feet

Function: General Purpose Dry laboratory

Occupancy Class: B

General Notes: Laboratory equals two laboratory modules, each 240 SF.

STRUCTURAL DATA:

Floor Live Load: 350 psf Floor Capacity Load psf Vibration Requirements: None

Structural Notes:

FINISHES:

Walls: Paint Floors: Linoleum Sheet

Ceilings: Acoustic Ceiling Tile Clg. Ht. 12'-0"

Finishes Notes:

ROOM ENVIRONMENT:

Temperature	75	F +/-	5	F	Cooling	72	F +/- 5 F	Heating
Humidity	50	RH +/-	10	RH	Cooling	30	RH +/- 10 RH	Heating

Room Pressure: Negative Vibration Criteria: None

Acoustic Noise Level NC: 45-50 EMI Criteria: None

SPECIAL REQUIREMENTS:

- [x] Storage Cabinet
- [x] Casework
- [x] Fume Hood
- [ ] Toxic / Hazardous Materials

Special Requirements Notes:

FIRE PROTECTION:

Hazard Classification: Ordinary Hazard Group [x] Wet System: [ ] Preaction System

Fire Protection Notes:

HVAC:

Air Changes / Hr: 100 % [x] General Exhaust: Room Exhaust [ ] Chemical Exhaust:

Recirc / Single Pass Airflow: Single Pass [ ] Heat Exhaust: [x] Smoke Exhaust: by AHU

HVAC Notes:

PLUMBING:

- [ ] Domestic Water H/C
- [x] Eyewash / Safety Shower
- [ ] Floor / Trench Drain

Plumbing Notes:

PROCESS PIPING:

- [x] Compressed Air — Lab Bench
- [x] Nitrogen — Lab Bench
- [ ] Liquid Nitrogen
- [ ] Other
- [ ] DI Water
- [ ] Process Cooling Water - Cu
- [ ] Process Cooling Water - Al
- [ ] Chemical Drain

Piping Notes:

ELECTRICAL:

Lighting Fixture Type: Pendant

Lighting Lamp Type: Fluorescent

Lighting Direction: Direct/Indirect

Light Switching: Low Voltage Switch

Lighting Level (FC): 50-75 (75 at work surface)

Ground:

Electrical Notes:

Power Outlets:

No.	Voltage	Phase	Type	Location
2	120 v	1 ph	Normal	Wall
0	120 v	1 ph	Normal	Raceway

Clean Power:

UPS:

Emergency Power:

TELECOMMUNICATION AND SPECIAL SYSTEMS:

- [x] Phone / Voice
- [ ] PA System
- [ ] Gas Leak Detection
- [ ] Liquid Leak Detection
- [x] Data Connections:
- [x] Access Control:
- [ ] CCTV:
- [x] Fire Detection Type: Photoelectric Smoke Detectors

Telecom Notes:

ROOM DATA SHEET

Room Name: Storage **Room Number:** LOB1-104

Functional Area: Lab Office Buildings Ground Level **Space Type:** Lab Support

SPACE REQUIREMENT:

Allocated Space : 110 NSF x 1 Rooms Reqd. = **110** Total Net Square Feet

Function: Storage for Laboratory Equipment

Occupancy Class: B

General Notes:

STRUCTURAL DATA:

Floor Live Load: 125 psf Floor Capacity Load psf Vibration Requirements: None

Structural Notes:

FINISHES:

Walls: Paint Floors: Vinyl Tile

Ceilings: No Ceiling Clg. Ht.

Finishes Notes:

ROOM ENVIRONMENT:

Temperature	75	F +/-	5	F	Cooling	72	F +/- 5 F	Heating
Humidity	50	RH +/-	10	RH	Cooling	30	RH +/- 10 RH	Heating

Room Pressure: Negative Vibration Criteria: None

Acoustic Noise Level NC: 40-45 EMI Criteria: None

SPECIAL REQUIREMENTS:

☐ Storage Cabinet ☐ Fume Hood

☐ Casework ☐ Toxic / Hazardous Materials

Special Requirements Notes:

FIRE PROTECTION:

Hazard Classification: Ordinary Hazard Group ☑ Wet System: ☐ Preaction System

Fire Protection Notes:

HVAC:

Air Changes / Hr ☐ General Exhaust: ☐ Chemical Exhaust:

Recirc / Single Pass Airflow: Recirculated ☐ Heat Exhaust: ☑ Smoke Exhaust: by AHU

HVAC Notes:

PLUMBING:

☐ Domestic Water H/C ☐ Floor / Trench Drain

☐ Eyewash / Safety Shower

Plumbing Notes:

PROCESS PIPING:

☐ Compressed Air ☐ DI Water

☐ Nitrogen ☐ Process Cooling Water - Cu

☐ Liquid Nitrogen ☐ Process Cooling Water - Al

☐ Other ☐ Chemical Drain

Piping Notes:

ELECTRICAL:

Lighting Fixture Type: Pendant

Lighting Lamp Type: Fluorescent

Lighting Direction: Direct

Light Switching: Occupancy Sensor

Lighting Level (FC): 30

Ground:

Electrical Notes:

Power Outlets:

No.	Voltage	Phase	Type	Location
4	120 v	1 ph	Normal	Wall
0				

Clean Power:

UPS:

Emergency Power:

TELECOMMUNICATION AND SPECIAL SYSTEMS:

☐ Phone / Voice ☐ Data Connections:

☐ PA System ☐ Access Control:

☐ Gas Leak Detection ☐ CCTV:

☐ Liquid Leak Detection ☐ Fire Detection Type:

Telecom Notes:

ROOM DATA SHEET

Room Name: Conference Room **Room Number:** LOB1-105

Functional Area: Lab Office Buildings Ground Level **Space Type:** Interaction Area

SPACE REQUIREMENT:

Allocated Space : 560 NSF x 2 Rooms Reqd. = **1,120** Total Net Square Feet

Function: Conference Room

Occupancy Class: B

General Notes:

STRUCTURAL DATA:

Floor Live Load: 100 psf Floor Capacity Load psf Vibration Requirements: None

Structural Notes:

FINISHES:

Walls: Wall Coverings Floors: Carpet

Ceilings: Acoustic Ceiling Tile Clg. Ht. 10'-0"

Finishes Notes:

ROOM ENVIRONMENT:

Temperature	75	F +/-	5	F	Cooling	72	F +/- 5 F	Heating
Humidity	50	RH +/-	10	RH	Cooling	30	RH +/- 10 RH	Heating

Room Pressure: Neutral Vibration Criteria: None

Acoustic Noise Level NC: 30 EMI Criteria: None

SPECIAL REQUIREMENTS:

- ☐ Storage Cabinet
- ☐ Casework
- ☐ Fume Hood
- ☐ Toxic / Hazardous Materials

Special Requirements Notes:

FIRE PROTECTION:

Hazard Classification: Ordinary Hazard Group ☑ Wet System: ☐ Preaction System

Fire Protection Notes:

HVAC:

Air Changes / Hr: 20 CFM/Person ☐ General Exhaust: ☐ Chemical Exhaust:

Recirc / Single Pass Airflow: Recirculated ☐ Heat Exhaust: ☑ Smoke Exhaust: by AHU

HVAC Notes:

PLUMBING:

- ☐ Domestic Water H/C
- ☐ Eyewash / Safety Shower
- ☐ Floor / Trench Drain

Plumbing Notes:

PROCESS PIPING:

- ☐ Compressed Air
- ☐ Nitrogen
- ☐ Liquid Nitrogen
- ☐ Other
- ☐ DI Water
- ☐ Process Cooling Water - Cu
- ☐ Process Cooling Water - Al
- ☐ Chemical Drain

Piping Notes:

ELECTRICAL:

Lighting Fixture Type: Recessed Troffer

Lighting Lamp Type: Fluorescent

Lighting Direction: Direct/Indirect

Light Switching: Occupancy Sensor

Lighting Level (FC): 30

Ground:

Electrical Notes:

Power Outlets:

No.	Voltage	Phase	Type	Location
4	120 v	1 ph	Normal	Wall
0				

Clean Power:

UPS:

Emergency Power:

TELECOMMUNICATION AND SPECIAL SYSTEMS:

- ☑ Phone / Voice
- ☐ PA System
- ☐ Gas Leak Detection
- ☐ Liquid Leak Detection
- ☑ Data Connections:
- ☐ Access Control:
- ☐ CCTV:
- ☐ Fire Detection Type:

Telecom Notes:

ROOM DATA SHEET

Room Name: Conference Room **Room Number:** LOB1-105A

Functional Area: Lab Office Buildings Ground Level **Space Type:** Interaction Area

SPACE REQUIREMENT:

Allocated Space : 220 NSF x 2 Rooms Reqd. = **440** Total Net Square Feet

Function: Conference / Meeting Room

Occupancy Class: B

General Notes:

STRUCTURAL DATA:

Floor Live Load: 100 psf Floor Capacity Load psf Vibration Requirements: None

Structural Notes:

FINISHES:

Walls: Wall Coverings Floors: Carpet

Ceilings: Acoustic Ceiling Tile Clg. Ht. 10'-0"

Finishes Notes:

ROOM ENVIRONMENT:

Temperature	75	F +/-	5	F	Cooling	72	F +/- 5 F	Heating
Humidity	50	RH +/-	10	RH	Cooling	30	RH +/- 10 RH	Heating

Room Pressure: Neutral Vibration Criteria: None

Acoustic Noise Level NC: 30 EMI Criteria: None

SPECIAL REQUIREMENTS:

- ☐ Storage Cabinet
- ☐ Casework
- ☐ Fume Hood
- ☐ Toxic / Hazardous Materials

Special Requirements Notes:

FIRE PROTECTION:

Hazard Classification: Ordinary Hazard Group ☑ Wet System: ☐ Preaction System

Fire Protection Notes:

HVAC:

Air Changes / Hr: 20 CFM/Person ☐ General Exhaust: ☐ Chemical Exhaust:

Recirc / Single Pass Airflow: Recirculated ☐ Heat Exhaust: ☑ Smoke Exhaust: by AHU

HVAC Notes:

PLUMBING:

- ☐ Domestic Water H/C
- ☐ Eyewash / Safety Shower
- ☐ Floor / Trench Drain

Plumbing Notes:

PROCESS PIPING:

- ☐ Compressed Air
- ☐ Nitrogen
- ☐ Liquid Nitrogen
- ☐ Other
- ☐ DI Water
- ☐ Process Cooling Water - Cu
- ☐ Process Cooling Water - Al
- ☐ Chemical Drain

Piping Notes:

ELECTRICAL:

Lighting Fixture Type: Recessed Troffer

Lighting Lamp Type: Fluorescent

Lighting Direction: Direct/Indirect

Light Switching: Occupancy Sensor

Lighting Level (FC): 30

Ground:

Electrical Notes:

Power Outlets:

No.	Voltage	Phase	Type	Location
4	120 v	1 ph	Normal	Wall
0				

Clean Power:

UPS:

Emergency Power:

TELECOMMUNICATION AND SPECIAL SYSTEMS:

- ☑ Phone / Voice
- ☐ PA System
- ☐ Gas Leak Detection
- ☐ Liquid Leak Detection
- ☑ Data Connections:
- ☐ Access Control:
- ☐ CCTV:
- ☐ Fire Detection Type:

Telecom Notes:

ROOM DATA SHEET

Room Name: Lobby & Interaction Space **Room Number:** LOB1-106

Functional Area: Lab Office Buildings Ground Level **Space Type:** Interaction Area

SPACE REQUIREMENT:

Allocated Space : 150 NSF x 4 Rooms Reqd. = **600** Total Net Square Feet

Function: LOB Entrance

Occupancy Class: B

General Notes:

STRUCTURAL DATA:

Floor Live Load: 100 psf Floor Capacity Load psf Vibration Requirements: None

Structural Notes:

FINISHES:

Walls: Paint Floors: Carpet

Ceilings: Acoustic Ceiling Tile Clg. Ht. 12'-0"

Finishes Notes: Lobby floors to be ceramic tile.

ROOM ENVIRONMENT:

Temperature	75	F +/-	5	F	Cooling	72	F +/- 5 F	Heating
Humidity	50	RH +/-	10	RH	Cooling	30	RH +/- 10 RH	Heating

Room Pressure: Positive Vibration Criteria: None

Acoustic Noise Level NC: 40-45 EMI Criteria: None

SPECIAL REQUIREMENTS:

- ☐ Storage Cabinet
- ☐ Casework
- ☐ Fume Hood
- ☐ Toxic / Hazardous Materials

Special Requirements Notes:

FIRE PROTECTION:

Hazard Classification: Ordinary Hazard Group ☑ Wet System: ☐ Preaction System

Fire Protection Notes:

HVAC:

Air Changes / Hr: 20 CFM/Person ☐ General Exhaust: ☐ Chemical Exhaust:

Recirc / Single Pass Airflow: Recirculated ☐ Heat Exhaust: ☑ Smoke Exhaust: by AHU

HVAC Notes:

PLUMBING:

- ☑ Domestic Water H/C — Drinking Fountain
- ☐ Eyewash / Safety Shower
- ☐ Floor / Trench Drain

Plumbing Notes:

PROCESS PIPING:

- ☐ Compressed Air
- ☐ Nitrogen
- ☐ Liquid Nitrogen
- ☐ Other
- ☐ DI Water
- ☐ Process Cooling Water - Cu
- ☐ Process Cooling Water - Al
- ☐ Chemical Drain

Piping Notes:

ELECTRICAL:

Lighting Fixture Type: Recessed Troffer

Lighting Lamp Type: Fluorescent

Lighting Direction: Direct

Light Switching: Occupancy Sensor

Lighting Level (FC): 30

Ground:

Electrical Notes:

Power Outlets:

No.	Voltage	Phase	Type	Location
	120 v	1 ph	Normal	Wall
0				

Clean Power:

UPS:

Emergency Power:

TELECOMMUNICATION AND SPECIAL SYSTEMS:

- ☑ Phone / Voice
- ☑ PA System
- ☐ Gas Leak Detection
- ☐ Liquid Leak Detection
- ☑ Data Connections:
- ☑ Access Control:
- ☐ CCTV:
- ☐ Fire Detection Type:

Telecom Notes:

ROOM DATA SHEET

Room Name: Break Room / Kitchen **Room Number:** LOB1-107

Functional Area: Lab Office Buildings Ground Level **Space Type:** Interaction Area

SPACE REQUIREMENT:

Allocated Space : 240 NSF x 2 Rooms Reqd. = **480** Total Net Square Feet

Function: Seating and space for refrigerator, microwave, sink

Occupancy Class: B

General Notes:

STRUCTURAL DATA:

Floor Live Load: 100 psf Floor Capacity Load psf Vibration Requirements: None

Structural Notes:

FINISHES:

Walls: Paint Floors: Linoleum Sheet

Ceilings: Acoustic Ceiling Tile Clg. Ht. 10'-0"

Finishes Notes:

ROOM ENVIRONMENT:

Temperature	75	F +/-	5	F	Cooling	72	F +/- 5 F	Heating
Humidity	50	RH +/-	10	RH	Cooling	30	RH +/- 10 RH	Heating

Room Pressure: Negative Vibration Criteria: None

Acoustic Noise Level NC: 40 EMI Criteria: None

SPECIAL REQUIREMENTS:

- ☐ Storage Cabinet
- ☐ Casework
- ☐ Fume Hood
- ☐ Toxic / Hazardous Materials

Special Requirements Notes:

FIRE PROTECTION:

Hazard Classification: Ordinary Hazard Group ☑ Wet System: ☐ Preaction System

Fire Protection Notes:

HVAC:

Air Changes / Hr ☑ General Exhaust: ☐ Chemical Exhaust:

Recirc / Single Pass Airflow: Single Pass ☐ Heat Exhaust: ☑ Smoke Exhaust: by AHU

HVAC Notes:

PLUMBING:

- ☑ Domestic Water H/C — to sink
- ☐ Eyewash / Safety Shower
- ☑ Floor / Trench Drain — Provide floor drains to sanitary waste.

Plumbing Notes:

PROCESS PIPING:

- ☐ Compressed Air
- ☐ Nitrogen
- ☐ Liquid Nitrogen
- ☐ Other
- ☐ DI Water
- ☐ Process Cooling Water - Cu
- ☐ Process Cooling Water - Al
- ☐ Chemical Drain

Piping Notes:

ELECTRICAL:

Lighting Fixture Type: Recessed Troffer

Lighting Lamp Type: Fluorescent

Lighting Direction: Direct

Light Switching: Occupancy Sensor

Lighting Level (FC): 30

Ground:

Electrical Notes:

Power Outlets:

No.	Voltage	Phase	Type	Location
7	120 v	1 ph	Normal	Wall
0				

Clean Power:

UPS:

Emergency Power:

TELECOMMUNICATION AND SPECIAL SYSTEMS:

- ☑ Phone / Voice
- ☑ PA System
- ☐ Gas Leak Detection
- ☐ Liquid Leak Detection
- ☑ Data Connections:
- ☐ Access Control:
- ☐ CCTV:
- ☐ Fire Detection Type:

Telecom Notes:

ROOM DATA SHEET

Room Name: Ship-Receive & Storage **Room Number:** LOB1-108

Functional Area: Lab Office Buildings Ground Level **Space Type:** Building Support

SPACE REQUIREMENT:

Allocated Space : 960 NSF x 1 Rooms Reqd. = **960** Total Net Square Feet

Function: Shipping / Receiving loading platform and storage.

Occupancy Class: B

General Notes:

STRUCTURAL DATA:

Floor Live Load: 125 psf Floor Capacity Load psf Vibration Requirements: None

Structural Notes:

FINISHES:

Walls: Paint Floors: Sealed Concrete

Ceilings: No Ceiling Clg. Ht.

Finishes Notes:

ROOM ENVIRONMENT:

Temperature	75	F +/-	5	F	Cooling	75	F +/- 5 F	Heating
Humidity	50	RH +/-	10	RH	Cooling	30	RH +/- 10 RH	Heating

Room Pressure: Positive Vibration Criteria: None

Acoustic Noise Level NC: 45-50 EMI Criteria: None

SPECIAL REQUIREMENTS:

- ☐ Storage Cabinet
- ☐ Casework
- ☐ Fume Hood
- ☐ Toxic / Hazardous Materials

Special Requirements Notes: Overhead door

FIRE PROTECTION:

Hazard Classification: Ordinary Hazard Group ☑ Wet System: ☐ Preaction System

Fire Protection Notes:

HVAC:

Air Changes / Hr ☐ General Exhaust: ☐ Chemical Exhaust:

Recirc / Single Pass Airflow: Recirculation ☐ Heat Exhaust: ☑ Smoke Exhaust: by AHU

HVAC Notes: Air curtain at overhead door.

PLUMBING:

- ☐ Domestic Water H/C
- ☐ Eyewash / Safety Shower
- ☐ Floor / Trench Drain

Plumbing Notes:

PROCESS PIPING:

- ☑ Compressed Air
- ☐ Nitrogen
- ☑ Liquid Nitrogen — to Dewar fill station.
- ☐ Other
- ☐ DI Water
- ☐ Process Cooling Water - Cu
- ☐ Process Cooling Water - Al
- ☐ Chemical Drain

Piping Notes:

ELECTRICAL:

Lighting Fixture Type: Pendant

Lighting Lamp Type: Fluorescent

Lighting Direction: Direct

Light Switching: Occupancy Sensor

Lighting Level (FC): 30

Ground:

Electrical Notes:

Power Outlets:

No.	Voltage	Phase	Type	Location
11	120 v	1 ph	Normal	Wall
0				

Clean Power:

UPS:

Emergency Power:

TELECOMMUNICATION AND SPECIAL SYSTEMS:

- ☑ Phone / Voice
- ☑ PA System
- ☐ Gas Leak Detection
- ☐ Liquid Leak Detection
- ☑ Data Connections:
- ☑ Access Control:
- ☐ CCTV:
- ☐ Fire Detection Type:

Telecom Notes:

ROOM DATA SHEET

Room Name: Toilet / Shower **Room Number:** LOB1-109

Functional Area: Lab Office Buildings Ground Level **Space Type:** Building Support

SPACE REQUIREMENT:

Allocated Space : 250 NSF x 2 Rooms Reqd. = **500** Total Net Square Feet

Function: Restroom & shower

Occupancy Class: B

General Notes:

STRUCTURAL DATA:

Floor Live Load: 100 psf Floor Capacity Load psf Vibration Requirements: None

Structural Notes:

FINISHES:

Walls: Paint Floors: Vinyl Tile

Ceilings: Acoustic Ceiling Tile Clg. Ht. 9'-0"

Finishes Notes:

ROOM ENVIRONMENT:

Temperature F +/- F Cooling F +/- F Heating

Humidity RH +/- RH Cooling RH +/- RH Heating

Room Pressure Negative Vibration Criteria None

Acoustic Noise Level NC 40 EMI Criteria None

SPECIAL REQUIREMENTS:

☐ Storage Cabinet ☐ Fume Hood

☐ Casework ☐ Toxic / Hazardous Materials

Special Requirements Notes:

FIRE PROTECTION:

Hazard Classification: Ordinary Hazard Group ☑ Wet System: ☐ Preaction System

Fire Protection Notes:

HVAC:

Air Changes / Hr ☑ General Exhaust: ☐ Chemical Exhaust:

Recirc / Single Pass Airflow Single Pass ☐ Heat Exhaust: ☑ Smoke Exhaust: by AHU

HVAC Notes:

PLUMBING:

☑ Domestic Water H/C ☑ Floor / Trench Drain Provide floor drains to sanitary waste.

☐ Eyewash / Safety Shower

Plumbing Notes:

PROCESS PIPING:

☐ Compressed Air ☐ DI Water

☐ Nitrogen ☐ Process Cooling Water - Cu

☐ Liquid Nitrogen ☐ Process Cooling Water - Al

☐ Other ☐ Chemical Drain

Piping Notes:

ELECTRICAL:

Lighting Fixture Type: Surface Mount

Lighting Lamp Type: Fluorescent

Lighting Direction: Direct

Light Switching: Occupancy Sensor

Lighting Level (FC): 15

Ground:

Electrical Notes:

Power Outlets:

No.	Voltage	Phase	Type	Location
1	120 v	1 ph	Normal	Wall
0				

Clean Power:

UPS:

Emergency Power:

TELECOMMUNICATION AND SPECIAL SYSTEMS:

☐ Phone / Voice ☐ Data Connections:

☐ PA System ☐ Access Control:

☐ Gas Leak Detection ☐ CCTV:

☐ Liquid Leak Detection ☐ Fire Detection Type:

Telecom Notes:

ROOM DATA SHEET

Room Name: Electrical / Data **Room Number:** LOB1-110

Functional Area: Lab Office Buildings Ground Level **Space Type:** Building Support

SPACE REQUIREMENT:

Allocated Space : 153 NSF x 1 Rooms Reqd. = **153** Total Net Square Feet

Function:

Occupancy Class: B

General Notes:

STRUCTURAL DATA:

Floor Live Load: 125 psf Floor Capacity Load psf Vibration Requirements: None

Structural Notes:

FINISHES:

Walls: Movable Partition Floors: Sealed Concrete

Ceilings: No Ceiling Clg. Ht.

Finishes Notes:

ROOM ENVIRONMENT:

Temperature	75	F +/-	5	F	Cooling	72	F +/- 5 F	Heating
Humidity	50	RH +/-	10	RH	Cooling	30	RH +/- 10 RH	Heating

Room Pressure: Neutral Vibration Criteria: None

Acoustic Noise Level NC: Per ACGIH TLVs EMI Criteria: None

SPECIAL REQUIREMENTS:

- ☐ Storage Cabinet
- ☐ Casework
- ☐ Fume Hood
- ☐ Toxic / Hazardous Materials

Special Requirements Notes:

FIRE PROTECTION:

Hazard Classification: Ordinary Hazard Group ☑ Wet System: ☐ Preaction System

Fire Protection Notes:

HVAC:

Air Changes / Hr ☐ General Exhaust: ☐ Chemical Exhaust:

Recirc / Single Pass Airflow: Recirculated ☐ Heat Exhaust: ☑ Smoke Exhaust: by AHU

HVAC Notes:

PLUMBING:

- ☐ Domestic Water H/C
- ☐ Eyewash / Safety Shower
- ☐ Floor / Trench Drain

Plumbing Notes:

PROCESS PIPING:

- ☐ Compressed Air
- ☐ Nitrogen
- ☐ Liquid Nitrogen
- ☐ Other
- ☐ DI Water
- ☐ Process Cooling Water - Cu
- ☐ Process Cooling Water - Al
- ☐ Chemical Drain

Piping Notes:

ELECTRICAL:

Lighting Fixture Type: Pendant

Lighting Lamp Type: Fluorescent

Lighting Direction: Direct

Light Switching: Occupancy Sensor

Lighting Level (FC): 30

Ground:

Electrical Notes:

Power Outlets:

No.	Voltage	Phase	Type	Location
4	120 v	1 ph	Normal	Wall
0				

Clean Power:

UPS:

Emergency Power:

TELECOMMUNICATION AND SPECIAL SYSTEMS:

- ☑ Phone / Voice
- ☐ PA System
- ☐ Gas Leak Detection
- ☐ Liquid Leak Detection
- ☑ Data Connections:
- ☑ Access Control:
- ☐ CCTV:
- ☐ Fire Detection Type:

Telecom Notes:

ROOM DATA SHEET

Room Name: Janitor Closet **Room Number:** LOB1-111

Functional Area: Lab Office Buildings Ground Level **Space Type:** Building Support

SPACE REQUIREMENT:

Allocated Space : 63 NSF x 1 Rooms Reqd. = **63** Total Net Square Feet

Function: Maintenance space

Occupancy Class: B

General Notes:

STRUCTURAL DATA:

Floor Live Load: 100 psf Floor Capacity Load psf Vibration Requirements: None

Structural Notes:

FINISHES:

Walls: Paint Floors: Sealed Concrete

Ceilings: Acoustic Ceiling Tile Clg. Ht. 8'-0"

Finishes Notes:

ROOM ENVIRONMENT:

Temperature	0 F +/-	0 F	Cooling	0 F +/-	0 F	Heating
Humidity	0 RH +/-	0 RH	Cooling	0 RH +/-	0 RH	Heating
Room Pressure	Negative		Vibration Criteria	None		
Acoustic Noise Level NC	None		EMI Criteria	None		

SPECIAL REQUIREMENTS:

- ☐ Storage Cabinet
- ☐ Casework
- ☐ Fume Hood
- ☐ Toxic / Hazardous Materials

Special Requirements Notes:

FIRE PROTECTION:

Hazard Classification: Ordinary Hazard Group ☑ Wet System: ☐ Preaction System

Fire Protection Notes:

HVAC:

Air Changes / Hr ☑ General Exhaust: ☐ Chemical Exhaust:

Recirc / Single Pass Airflow Single Pass ☐ Heat Exhaust: ☑ Smoke Exhaust: by AHU

HVAC Notes:

PLUMBING:

- ☑ Domestic Water H/C
- ☐ Eyewash / Safety Shower
- ☑ Floor / Trench Drain — Provide floor drains to sanitary waste.

Plumbing Notes:

PROCESS PIPING:

- ☐ Compressed Air
- ☐ Nitrogen
- ☐ Liquid Nitrogen
- ☐ Other
- ☐ DI Water
- ☐ Process Cooling Water - Cu
- ☐ Process Cooling Water - Al
- ☐ Chemical Drain

Piping Notes:

ELECTRICAL:

Lighting Fixture Type: Pendant

Lighting Lamp Type: Fluorescent

Lighting Direction: Direct

Light Switching: Occupancy Sensor

Lighting Level (FC): 15

Ground:

Electrical Notes:

Power Outlets:

No.	Voltage	Phase	Type	Location
1	120 v	1 ph	Normal	Wall
0				

Clean Power:

UPS:

Emergency Power:

TELECOMMUNICATION AND SPECIAL SYSTEMS:

- ☑ Phone / Voice
- ☐ PA System
- ☐ Gas Leak Detection
- ☐ Liquid Leak Detection
- ☐ Data Connections:
- ☐ Access Control:
- ☐ CCTV:
- ☐ Fire Detection Type:

Telecom Notes:

ROOM DATA SHEET

Room Name: Access Corridor Interface **Room Number:** LOB1-112

Functional Area: Lab Office Buildings Ground Level **Space Type:** Circulation

SPACE REQUIREMENT:

Allocated Space : 2,090 NSF x 1 Rooms Reqd. = **2,090** Total Net Square Feet

Function: Extension of the Access Corridor into LOB

Occupancy Class: B

General Notes:

STRUCTURAL DATA:

Floor Live Load: 125 psf Floor Capacity Load psf Vibration Requirements: None

Structural Notes:

FINISHES:

Walls: Paint Floors: Sealed Concrete

Ceilings: No Ceiling Clg. Ht.

Finishes Notes:

ROOM ENVIRONMENT:

Temperature	75	F +/-	1	F	Cooling	75	F +/- 1 F	Heating
Humidity	50	RH +/-	10	RH	Cooling	30	RH +/- 10 RH	Heating

Room Pressure: Positive Vibration Criteria: None

Acoustic Noise Level NC: 55 or Better EMI Criteria: None

SPECIAL REQUIREMENTS:

- ☐ Storage Cabinet
- ☐ Casework
- ☐ Fume Hood
- ☐ Toxic / Hazardous Materials

Special Requirements Notes:

FIRE PROTECTION:

Hazard Classification: Ordinary Hazard Group ☑ Wet System: ☐ Preaction System

Fire Protection Notes:

HVAC:

Air Changes / Hr ☐ General Exhaust: ☐ Chemical Exhaust:

Recirc / Single Pass Airflow: Recirculated ☐ Heat Exhaust: ☑ Smoke Exhaust: by AHU

HVAC Notes:

PLUMBING:

- ☐ Domestic Water H/C
- ☐ Eyewash / Safety Shower
- ☐ Floor / Trench Drain

Plumbing Notes:

PROCESS PIPING:

- ☐ Compressed Air
- ☐ Nitrogen
- ☐ Liquid Nitrogen
- ☐ Other
- ☐ DI Water
- ☐ Process Cooling Water - Cu
- ☐ Process Cooling Water - Al
- ☐ Chemical Drain

Piping Notes:

ELECTRICAL:

Lighting Fixture Type: Pendant

Lighting Lamp Type: Fluorescent

Lighting Direction: Direct

Light Switching: Low Voltage Switch

Lighting Level (FC): 50

Ground:

Electrical Notes:

Power Outlets:

No.	Voltage	Phase	Type	Location
	120 v	1 ph	Normal	Wall
0				

Clean Power:

UPS:

Emergency Power:

TELECOMMUNICATION AND SPECIAL SYSTEMS:

- ☑ Phone / Voice
- ☑ PA System
- ☐ Gas Leak Detection
- ☐ Liquid Leak Detection
- ☑ Data Connections:
- ☐ Access Control:
- ☐ CCTV:
- ☐ Fire Detection Type:

Telecom Notes:

ROOM DATA SHEET

Room Name: Machine Shop **Room Number:** LOB1-113

Functional Area: Lab Office Buildings Ground Level **Space Type:** Lab Support

SPACE REQUIREMENT:

Allocated Space : 270 NSF x 1 Rooms Reqd. = **270** Total Net Square Feet

Function: Machine shop

Occupancy Class: B

General Notes:

STRUCTURAL DATA:

Floor Live Load: 125 psf Floor Capacity Load psf Vibration Requirements: None

Structural Notes:

FINISHES:

Walls: Paint Floors: Sealed Concrete

Ceilings: Acoustic Ceiling Tile Clg. Ht. 12'-0"

Finishes Notes:

ROOM ENVIRONMENT:

Temperature	75	F +/-	5	F	Cooling	72	F +/- 5 F	Heating
Humidity	50	RH +/-	10	RH	Cooling	30	RH +/- 10 RH	Heating

Room Pressure: Negative

Acoustic Noise Level NC: Per ACGIH TLVs

Vibration Criteria: None

EMI Criteria: None

SPECIAL REQUIREMENTS:

- ☐ Storage Cabinet
- ☐ Casework
- ☐ Fume Hood
- ☐ Toxic / Hazardous Materials

Special Requirements Notes:

FIRE PROTECTION:

Hazard Classification: Ordinary Hazard Group ☑ Wet System: ☐ Preaction System

Fire Protection Notes:

HVAC:

Air Changes / Hr: 20 CFM/Person

Recirc / Single Pass Airflow: Recirculated

- ☑ General Exhaust:
- ☐ Heat Exhaust:
- ☐ Chemical Exhaust:
- ☑ Smoke Exhaust: by AHU

HVAC Notes:

PLUMBING:

- ☐ Domestic Water H/C
- ☑ Eyewash / Safety Shower
- ☐ Floor / Trench Drain

Plumbing Notes:

PROCESS PIPING:

- ☑ Compressed Air
- ☐ Nitrogen
- ☐ Liquid Nitrogen
- ☐ Other
- ☐ DI Water
- ☐ Process Cooling Water - Cu
- ☐ Process Cooling Water - Al
- ☐ Chemical Drain

Piping Notes:

ELECTRICAL:

Lighting Fixture Type: Pendant

Lighting Lamp Type: Fluorescent

Lighting Direction: Direct

Light Switching: Occupancy Sensor

Lighting Level (FC): 50-75

Ground:

Electrical Notes:

Power Outlets:

No.	Voltage	Phase	Type	Location
2	120 v	1 ph	Normal	Wall
0				

Clean Power:

UPS:

Emergency Power:

TELECOMMUNICATION AND SPECIAL SYSTEMS:

- ☑ Phone / Voice
- ☐ PA System
- ☐ Gas Leak Detection
- ☐ Liquid Leak Detection
- ☑ Data Connections:
- ☐ Access Control:
- ☐ CCTV:
- ☐ Fire Detection Type:

Telecom Notes:

ROOM DATA SHEET

Room Name: LOB #4 Shell **Room Number:** LOB4-101

Functional Area: Lab Office Buildings Ground Level **Space Type:**

SPACE REQUIREMENT:

Allocated Space : 16,146 NSF x 1 Rooms Reqd. = **16,146** Total Net Square Feet

Function: Shelled space for future build-out of Lab Office Building

Occupancy Class:

General Notes:

STRUCTURAL DATA:

Floor Live Load: psf Floor Capacity Load psf Vibration Requirements:

Structural Notes:

FINISHES:

Walls: Floors: Concrete

Ceilings: No Ceiling Clg. Ht.

Finishes Notes: Unfinished space

ROOM ENVIRONMENT:

Temperature 0 F +/- 0 F Cooling 0 F +/- 0 F Heating

Humidity 0 RH +/- 0 RH Cooling 0 RH +/- 0 RH Heating

Room Pressure Vibration Criteria

Acoustic Noise Level NC EMI Criteria

SPECIAL REQUIREMENTS:

☐ Storage Cabinet ☐ Fume Hood

☐ Casework ☐ Toxic / Hazardous Materials

Special Requirements Notes:

FIRE PROTECTION:

Hazard Classification: Ordinary Hazard Group ☑ Wet System: ☐ Preaction System

Fire Protection Notes: Sprinklers to be installed.

HVAC:

Air Changes / Hr ☐ General Exhaust: ☐ Chemical Exhaust:

Recirc / Single Pass Airflow ☐ Heat Exhaust: ☐ Smoke Exhaust:

HVAC Notes: Freeze protection only.

PLUMBING:

☐ Domestic Water H/C ☐ Floor / Trench Drain

☐ Eyewash / Safety Shower

Plumbing Notes: Stub up for future plumbing in labs and toilets.

PROCESS PIPING:

☐ Compressed Air ☐ DI Water

☐ Nitrogen ☐ Process Cooling Water - Cu

☐ Liquid Nitrogen ☐ Process Cooling Water - Al

☐ Other ☐ Chemical Drain

Piping Notes: Process piping to be added when space fit-up

ELECTRICAL:

Lighting Fixture Type: Pendant

Lighting Lamp Type: Fluorescent

Lighting Direction: Direct

Light Switching: Occupancy Sensor

Lighting Level (FC): <10

Ground:

Electrical Notes: Exit lights and minimal lighting in space.

Power Outlets:

No.	Voltage	Phase	Type	Location
0				
0				

Clean Power:

UPS:

Emergency Power:

TELECOMMUNICATION AND SPECIAL SYSTEMS:

☐ Phone / Voice ☐ Data Connections:

☑ PA System Temporary speakers ☐ Access Control:

☐ Gas Leak Detection ☐ CCTV:

☐ Liquid Leak Detection ☐ Fire Detection Type:

Telecom Notes:

ROOM DATA SHEET

Room Name: Private Office **Room Number:** LOB5-101

Functional Area: Lab Office Buildings Ground Level **Space Type:** Office

SPACE REQUIREMENT:

Allocated Space : 110 NSF x 48 Rooms Reqd. = **5,280** Total Net Square Feet

Function: Enclosed private office space

Occupancy Class: B

General Notes:

STRUCTURAL DATA:

Floor Live Load: 100 psf Floor Capacity Load psf Vibration Requirements: None

Structural Notes:

FINISHES:

Walls: Painted Gypsum Board Floors: Carpet Tile

Ceilings: Acoustic Ceiling Tile Clg. Ht. 9'-0"

Finishes Notes:

ROOM ENVIRONMENT:

Temperature	75	F +/-	5	F	Cooling	72	F +/- 5 F	Heating
Humidity	50	RH +/-	10	RH	Cooling	30	RH +/- 10 RH	Heating

Room Pressure: Positive

Acoustic Noise Level NC: 35-40

Vibration Criteria:

EMI Criteria:

SPECIAL REQUIREMENTS:

- ☐ Storage Cabinet
- ☐ Casework
- ☐ Fume Hood
- ☐ Toxic / Hazardous Materials

Special Requirements Notes:

FIRE PROTECTION:

Hazard Classification: Ordinary Hazard Group ☑ Wet System: ☐ Preaction System

Fire Protection Notes:

HVAC:

Air Changes / Hr: 20 CFM/Person

Recirc / Single Pass Airflow: Recirculated

HVAC Notes:

- ☐ General Exhaust:
- ☐ Heat Exhaust:
- ☐ Chemical Exhaust:
- ☑ Smoke Exhaust: by AHU

PLUMBING:

- ☐ Domestic Water H/C
- ☐ Eyewash / Safety Shower
- ☐ Floor / Trench Drain

Plumbing Notes:

PROCESS PIPING:

- ☐ Compressed Air
- ☐ Nitrogen
- ☐ Liquid Nitrogen
- ☐ Other
- ☐ DI Water
- ☐ Process Cooling Water - Cu
- ☐ Process Cooling Water - Al
- ☐ Chemical Drain

Piping Notes:

ELECTRICAL:

Lighting Fixture Type: Recessed Troffer

Lighting Lamp Type: Fluorescent

Lighting Direction: Direct

Light Switching: Occupancy Sensor

Lighting Level (FC): 30-50 (50 at work surface)

Ground:

Electrical Notes:

Power Outlets:

No.	Voltage	Phase	Type	Location
3	120 v	1 ph	Normal	Wall
0				

Clean Power:

UPS:

Emergency Power:

TELECOMMUNICATION AND SPECIAL SYSTEMS:

- ☑ Phone / Voice
- ☐ PA System
- ☐ Gas Leak Detection
- ☐ Liquid Leak Detection
- ☑ Data Connections:
- ☐ Access Control:
- ☐ CCTV:
- ☐ Fire Detection Type:

Telecom Notes:

ROOM DATA SHEET

Room Name: Flexible Office Space **Room Number:** LOB5-102

Functional Area: Lab Office Buildings Ground Level **Space Type:** Office

SPACE REQUIREMENT:

Allocated Space : 90 NSF x 24 Rooms Reqd. = **2,160** Total Net Square Feet

Function: Cubicle space

Occupancy Class: B

General Notes:

STRUCTURAL DATA:

Floor Live Load: 100 psf Floor Capacity Load psf Vibration Requirements: None

Structural Notes:

FINISHES:

Walls: Movable Partition Floors: Carpet Tile

Ceilings: No Ceiling Clg. Ht. 10'-0"

Finishes Notes:

ROOM ENVIRONMENT:

Temperature	75	F +/-	5	F	Cooling	72	F +/- 5 F	Heating
Humidity	50	RH +/-	10	RH	Cooling	30	RH +/- 10 RH	Heating

Room Pressure: Positive

Acoustic Noise Level NC: 35-40

Vibration Criteria:

EMI Criteria:

SPECIAL REQUIREMENTS:

- ☐ Storage Cabinet
- ☐ Casework
- ☐ Fume Hood
- ☐ Toxic / Hazardous Materials

Special Requirements Notes:

FIRE PROTECTION:

Hazard Classification: Ordinary Hazard Group ☑ Wet System: ☐ Preaction System

Fire Protection Notes:

HVAC:

Air Changes / Hr: 20 CFM/Person

Recirc / Single Pass Airflow: Recirculated

HVAC Notes:

- ☐ General Exhaust:
- ☐ Heat Exhaust:
- ☐ Chemical Exhaust:
- ☑ Smoke Exhaust: by AHU

PLUMBING:

- ☐ Domestic Water H/C
- ☐ Eyewash / Safety Shower
- ☐ Floor / Trench Drain

Plumbing Notes:

PROCESS PIPING:

- ☐ Compressed Air
- ☐ Nitrogen
- ☐ Liquid Nitrogen
- ☐ Other
- ☐ DI Water
- ☐ Process Cooling Water - Cu
- ☐ Process Cooling Water - Al
- ☐ Chemical Drain

Piping Notes:

ELECTRICAL:

Lighting Fixture Type: Recessed Troffer

Lighting Lamp Type: Fluorescent

Lighting Direction: Direct

Light Switching: Occupancy Sensor

Lighting Level (FC): 30-50 (50 at work surface)

Ground:

Electrical Notes:

Power Outlets:

No.	Voltage	Phase	Type	Location
3	120 v	1 ph	Normal	Wall
0				

Clean Power:

UPS:

Emergency Power:

TELECOMMUNICATION AND SPECIAL SYSTEMS:

- ☑ Phone / Voice
- ☐ PA System
- ☐ Gas Leak Detection
- ☐ Liquid Leak Detection
- ☑ Data Connections:
- ☐ Access Control:
- ☐ CCTV:
- ☑ Fire Detection Type: Photoelectric Smoke Detectors

Telecom Notes:

ROOM DATA SHEET

Room Name: Laboratory - Wet **Room Number:** LOB5-103

Functional Area: Lab Office Buildings Ground Level **Space Type:** Laboratory

SPACE REQUIREMENT:

Allocated Space : 480 NSF x 2 Rooms Reqd. = **960** Total Net Square Feet

Function: General Purpose Wet Laboratory

Occupancy Class: B

General Notes:

STRUCTURAL DATA:

Floor Live Load: 350 psf Floor Capacity Load psf Vibration Requirements: None

Structural Notes:

FINISHES:

Walls: Epoxy Painted Floors: Linoleum Sheet

Ceilings: Acoustic Ceiling Tile Clg. Ht. 12'-0"

Finishes Notes:

ROOM ENVIRONMENT:

Temperature	75	F +/-	5	F	Cooling	72	F +/- 5 F	Heating
Humidity	50	RH +/-	10	RH	Cooling	30	RH +/- 10 RH	Heating

Room Pressure: Negative Vibration Criteria:

Acoustic Noise Level NC: 45-50 EMI Criteria:

SPECIAL REQUIREMENTS:

- [x] Storage Cabinet
- [ ] Casework
- [ ] Fume Hood — Chemical storage cabinet below
- [x] Toxic / Hazardous Materials — Fume Hood cabinet

Special Requirements Notes: Two labs per LOB require Fume Hoods. One Hood per LOB to have HEPA filtration

FIRE PROTECTION:

Hazard Classification: Ordinary Hazard Group [x] Wet System: [ ] Preaction System

Fire Protection Notes:

HVAC:

Air Changes / Hr: 100% [x] General Exhaust: Room Exhaust [x] Chemical Exhaust: Fume Hood

Recirc / Single Pass Airflow: Single Pass [ ] Heat Exhaust: [x] Smoke Exhaust: by AHU

HVAC Notes: One fume hood with HEPA filtration on exhaust. Second to have capability to add HEPA filtration in the future.

PLUMBING:

- [x] Domestic Water H/C
- [x] Eyewash / Safety Shower
- [ ] Floor / Trench Drain

Plumbing Notes:

PROCESS PIPING:

- [x] Compressed Air — Lab Bench
- [x] Nitrogen — Lab Bench
- [ ] Liquid Nitrogen
- [ ] Other
- [ ] DI Water
- [ ] Process Cooling Water - Cu
- [ ] Process Cooling Water - Al
- [ ] Chemical Drain

Piping Notes:

ELECTRICAL:

Lighting Fixture Type: Pendant

Lighting Lamp Type: Fluorescent

Lighting Direction: Direct/Indirect

Light Switching: Low Voltage Switch

Lighting Level (FC): 50-75 (75 at work surface)

Ground:

Electrical Notes:

Power Outlets:

No.	Voltage	Phase	Type	Location
2	120 v	1 ph	Normal	Wall
0	120 v	1 ph	Normal	Raceway

Clean Power:

UPS:

Emergency Power:

TELECOMMUNICATION AND SPECIAL SYSTEMS:

- [x] Phone / Voice
- [ ] PA System
- [ ] Gas Leak Detection
- [ ] Liquid Leak Detection
- [x] Data Connections:
- [ ] Access Control:
- [ ] CCTV:
- [x] Fire Detection Type: Photoelectric Smoke Detectors

Telecom Notes:

ROOM DATA SHEET

Room Name: Laboratory - Dry **Room Number:** LOB5-103A

Functional Area: Lab Office Buildings Ground Level **Space Type:** Laboratory

SPACE REQUIREMENT:

Allocated Space : 480 NSF x 4 Rooms Reqd. = **1,920** Total Net Square Feet

Function: General Purpose Dry laboratory

Occupancy Class: B

General Notes:

STRUCTURAL DATA:

Floor Live Load: 350 psf Floor Capacity Load psf Vibration Requirements: None

Structural Notes:

FINISHES:

Walls: Paint Floors: Linoleum Sheet

Ceilings: Acoustic Ceiling Tile Clg. Ht. 12'-0"

Finishes Notes:

ROOM ENVIRONMENT:

Temperature	75	F +/-	5	F	Cooling	72	F +/- 5 F	Heating
Humidity	50	RH +/-	10	RH	Cooling	30	RH +/- 10 RH	Heating

Room Pressure: Negative

Acoustic Noise Level NC: 45-50

Vibration Criteria:

EMI Criteria:

SPECIAL REQUIREMENTS:

- [x] Storage Cabinet
- [ ] Casework
- [ ] Fume Hood
- [ ] Toxic / Hazardous Materials

Special Requirements Notes:

FIRE PROTECTION:

Hazard Classification: Ordinary Hazard Group [x] Wet System: [ ] Preaction System

Fire Protection Notes:

HVAC:

Air Changes / Hr: 100% [x] General Exhaust: Room Exhaust [ ] Chemical Exhaust:

Recirc / Single Pass Airflow: Single Pass [ ] Heat Exhaust: [x] Smoke Exhaust: by AHU

HVAC Notes:

PLUMBING:

- [ ] Domestic Water H/C
- [x] Eyewash / Safety Shower
- [ ] Floor / Trench Drain

Plumbing Notes:

PROCESS PIPING:

- [x] Compressed Air — Lab Bench
- [x] Nitrogen — Lab Bench
- [ ] Liquid Nitrogen
- [ ] Other
- [ ] DI Water
- [ ] Process Cooling Water - Cu
- [ ] Process Cooling Water - Al
- [ ] Chemical Drain

Piping Notes:

ELECTRICAL:

Lighting Fixture Type: Pendant

Lighting Lamp Type: Fluorescent

Lighting Direction: Direct/Indirect

Light Switching: Low Voltage Switch

Lighting Level (FC): 50-75 (75 at work surface)

Ground:

Electrical Notes:

Power Outlets:

No.	Voltage	Phase	Type	Location
2	120 v	1 ph	Normal	Wall
0	120 v	1 ph	Normal	Raceway

Clean Power:

UPS:

Emergency Power:

TELECOMMUNICATION AND SPECIAL SYSTEMS:

- [x] Phone / Voice
- [ ] PA System
- [ ] Gas Leak Detection
- [ ] Liquid Leak Detection
- [x] Data Connections:
- [ ] Access Control:
- [ ] CCTV:
- [ ] Fire Detection Type:

Telecom Notes:

ROOM DATA SHEET

Room Name: Storage **Room Number:** LOB5-104

Functional Area: Lab Office Buildings Ground Level **Space Type:** Lab Support

SPACE REQUIREMENT:

Allocated Space : 110 NSF x 1 Rooms Reqd. = **110** Total Net Square Feet

Function: Storage for Laboratory Equipment

Occupancy Class: B

General Notes:

STRUCTURAL DATA:

Floor Live Load: 125 psf Floor Capacity Load psf Vibration Requirements: None

Structural Notes:

FINISHES:

Walls: Painted Gypsum Board Floors: Vinyl Tile

Ceilings: No Ceiling Clg. Ht.

Finishes Notes:

ROOM ENVIRONMENT:

Temperature	75	F +/-	5	F	Cooling	72	F +/- 5 F	Heating
Humidity	50	RH +/-	10	RH	Cooling	30	RH +/- 10 RH	Heating

Room Pressure: Negative Vibration Criteria:

Acoustic Noise Level NC: 40-45 EMI Criteria:

SPECIAL REQUIREMENTS:

- ☐ Storage Cabinet
- ☐ Casework
- ☐ Fume Hood
- ☐ Toxic / Hazardous Materials

Special Requirements Notes:

FIRE PROTECTION:

Hazard Classification: Ordinary Hazard Group ☑ Wet System: ☐ Preaction System

Fire Protection Notes:

HVAC:

Air Changes / Hr ☐ General Exhaust: ☐ Chemical Exhaust:

Recirc / Single Pass Airflow: Recirculated ☐ Heat Exhaust: ☑ Smoke Exhaust: by AHU

HVAC Notes:

PLUMBING:

- ☐ Domestic Water H/C
- ☐ Eyewash / Safety Shower
- ☐ Floor / Trench Drain

Plumbing Notes:

PROCESS PIPING:

- ☐ Compressed Air
- ☐ Nitrogen
- ☐ Liquid Nitrogen
- ☐ Other
- ☐ DI Water
- ☐ Process Cooling Water - Cu
- ☐ Process Cooling Water - Al
- ☐ Chemical Drain

Piping Notes:

ELECTRICAL:

Lighting Fixture Type: Pendant

Lighting Lamp Type: Fluorescent

Lighting Direction: Direct

Light Switching: Occupancy Sensor

Lighting Level (FC): 30

Ground:

Electrical Notes:

Power Outlets:

No.	Voltage	Phase	Type	Location
4	120 v	1 ph	Normal	Wall
0				

Clean Power:

UPS:

Emergency Power:

TELECOMMUNICATION AND SPECIAL SYSTEMS:

- ☐ Phone / Voice
- ☐ PA System
- ☐ Gas Leak Detection
- ☐ Liquid Leak Detection
- ☐ Data Connections:
- ☐ Access Control:
- ☐ CCTV:
- ☐ Fire Detection Type:

Telecom Notes:

ROOM DATA SHEET

Room Name: Conference Room **Room Number:** LOB5-105

Functional Area: Lab Office Buildings Ground Level **Space Type:** Interaction Area

SPACE REQUIREMENT:

Allocated Space : 560 NSF x 2 Rooms Reqd. = **1,120** Total Net Square Feet

Function: Conference Room

Occupancy Class: B

General Notes:

STRUCTURAL DATA:

Floor Live Load: 100 psf Floor Capacity Load psf Vibration Requirements: None

Structural Notes:

FINISHES:

Walls: Wall Coverings Floors: Carpet

Ceilings: Acoustic Ceiling Tile Clg. Ht. 10-0"

Finishes Notes:

ROOM ENVIRONMENT:

Temperature	75	F +/-	5	F	Cooling	72	F +/- 5 F	Heating
Humidity	50	RH +/-	10	RH	Cooling	30	RH +/- 10 RH	Heating

Room Pressure: Neutral

Acoustic Noise Level NC: 30

Vibration Criteria:

EMI Criteria:

SPECIAL REQUIREMENTS:

- ☐ Storage Cabinet
- ☐ Casework
- ☐ Fume Hood
- ☐ Toxic / Hazardous Materials

Special Requirements Notes:

FIRE PROTECTION:

Hazard Classification: Ordinary Hazard Group ☑ Wet System: ☐ Preaction System

Fire Protection Notes:

HVAC:

Air Changes / Hr: 20 CFM/Person

Recirc / Single Pass Airflow: Recirculated

HVAC Notes:

- ☐ General Exhaust:
- ☐ Heat Exhaust:
- ☐ Chemical Exhaust:
- ☑ Smoke Exhaust: by AHU

PLUMBING:

- ☐ Domestic Water H/C
- ☐ Eyewash / Safety Shower
- ☐ Floor / Trench Drain

Plumbing Notes:

PROCESS PIPING:

- ☐ Compressed Air
- ☐ Nitrogen
- ☐ Liquid Nitrogen
- ☐ Other
- ☐ DI Water
- ☐ Process Cooling Water - Cu
- ☐ Process Cooling Water - Al
- ☐ Chemical Drain

Piping Notes:

ELECTRICAL:

Lighting Fixture Type: Recessed Troffer

Lighting Lamp Type: Fluorescent

Lighting Direction: Direct/Indirect

Light Switching: Occupancy Sensor

Lighting Level (FC): 30

Ground:

Electrical Notes:

Power Outlets:

No.	Voltage	Phase	Type	Location
4	120 v	1 ph	Normal	Wall
0				

Clean Power:

UPS:

Emergency Power:

TELECOMMUNICATION AND SPECIAL SYSTEMS:

- ☑ Phone / Voice
- ☐ PA System
- ☐ Gas Leak Detection
- ☐ Liquid Leak Detection
- ☑ Data Connections:
- ☐ Access Control:
- ☐ CCTV:
- ☐ Fire Detection Type:

Telecom Notes:

ROOM DATA SHEET

Room Name: Conference Room **Room Number:** LOB5-105A

Functional Area: Lab Office Buildings Ground Level **Space Type:** Interaction Area

SPACE REQUIREMENT:

Allocated Space : 220 NSF x 2 Rooms Reqd. = **440** Total Net Square Feet

Function: Conference / Meeting Room

Occupancy Class: B

General Notes:

STRUCTURAL DATA:

Floor Live Load: 100 psf Floor Capacity Load psf Vibration Requirements: None

Structural Notes:

FINISHES:

Walls: Wall Coverings Floors: Carpet

Ceilings: Acoustic Ceiling Tile Clg. Ht. 10'-0"

Finishes Notes:

ROOM ENVIRONMENT:

Temperature	75	F +/-	5	F	Cooling	72	F +/- 5 F	Heating
Humidity	50	RH +/-	10	RH	Cooling	30	RH +/- 10 RH	Heating

Room Pressure: Neutral

Acoustic Noise Level NC: 30

Vibration Criteria:

EMI Criteria:

SPECIAL REQUIREMENTS:

☐ Storage Cabinet ☐ Fume Hood

☐ Casework ☐ Toxic / Hazardous Materials

Special Requirements Notes:

FIRE PROTECTION:

Hazard Classification: Ordinary Hazard Group ☑ Wet System: ☐ Preaction System

Fire Protection Notes:

HVAC:

Air Changes / Hr: 20 CFM/Person ☐ General Exhaust: ☐ Chemical Exhaust:

Recirc / Single Pass Airflow: Recirculated ☐ Heat Exhaust: ☑ Smoke Exhaust: by AHU

HVAC Notes:

PLUMBING:

☐ Domestic Water H/C ☐ Floor / Trench Drain

☐ Eyewash / Safety Shower

Plumbing Notes:

PROCESS PIPING:

☐ Compressed Air ☐ DI Water

☐ Nitrogen ☐ Process Cooling Water - Cu

☐ Liquid Nitrogen ☐ Process Cooling Water - Al

☐ Other ☐ Chemical Drain

Piping Notes:

ELECTRICAL:

Lighting Fixture Type: Recessed Troffer

Lighting Lamp Type: Fluorescent

Lighting Direction: Direct/Indirect

Light Switching: Occupancy Sensor

Lighting Level (FC): 30

Ground:

Electrical Notes:

Power Outlets:

No.	Voltage	Phase	Type	Location
4	120 v	1 ph	Normal	Wall
0				

Clean Power:

UPS:

Emergency Power:

TELECOMMUNICATION AND SPECIAL SYSTEMS:

☑ Phone / Voice ☑ Data Connections:

☐ PA System ☐ Access Control:

☐ Gas Leak Detection ☐ CCTV:

☐ Liquid Leak Detection ☐ Fire Detection Type:

Telecom Notes:

ROOM DATA SHEET

Room Name: Lobby & Interaction Space **Room Number:** LOB5-106

Functional Area: Lab Office Buildings Ground Level **Space Type:** Interaction Area

SPACE REQUIREMENT:

Allocated Space : 150 NSF x 4 Rooms Reqd. = **600** Total Net Square Feet

Function: LOB Entrance

Occupancy Class: B

General Notes:

STRUCTURAL DATA:

Floor Live Load: 100 psf Floor Capacity Load psf Vibration Requirements: None

Structural Notes:

FINISHES:

Walls: Paint Floors: Carpet

Ceilings: Acoustic Ceiling Tile Clg. Ht. 12'-0"

Finishes Notes:

ROOM ENVIRONMENT:

Temperature 75 F +/- 5 F Cooling 72 F +/- 5 F Heating

Humidity 50 RH +/- 10 RH Cooling 30 RH +/- 10 RH Heating

Room Pressure Positive Vibration Criteria

Acoustic Noise Level NC 40-45 EMI Criteria

SPECIAL REQUIREMENTS:

☐ Storage Cabinet ☐ Fume Hood

☐ Casework ☐ Toxic / Hazardous Materials

Special Requirements Notes:

FIRE PROTECTION:

Hazard Classification: Ordinary Hazard Group ☑ Wet System: ☐ Preaction System

Fire Protection Notes:

HVAC:

Air Changes / Hr 20 CFM/Person ☐ General Exhaust: ☐ Chemical Exhaust:

Recirc / Single Pass Airflow Recirculated ☐ Heat Exhaust: ☑ Smoke Exhaust: by AHU

HVAC Notes:

PLUMBING:

☐ Domestic Water H/C ☐ Floor / Trench Drain

☐ Eyewash / Safety Shower

Plumbing Notes:

PROCESS PIPING:

☐ Compressed Air ☐ DI Water

☐ Nitrogen ☐ Process Cooling Water - Cu

☐ Liquid Nitrogen ☐ Process Cooling Water - Al

☐ Other ☐ Chemical Drain

Piping Notes:

ELECTRICAL:

Lighting Fixture Type: Recessed Troffer

Lighting Lamp Type: Fluorescent

Lighting Direction: Direct

Light Switching: Occupancy Sensor

Lighting Level (FC): 30

Ground:

Electrical Notes:

Power Outlets:

No.	Voltage	Phase	Type	Location
	120 v	1 ph	Normal	Wall
0				

Clean Power:

UPS:

Emergency Power:

TELECOMMUNICATION AND SPECIAL SYSTEMS:

☑ Phone / Voice ☑ Data Connections:

☑ PA System ☑ Access Control:

☐ Gas Leak Detection ☐ CCTV:

☐ Liquid Leak Detection ☐ Fire Detection Type:

Telecom Notes:

ROOM DATA SHEET

Room Name: Break Room / Kitchen **Room Number:** LOB5-107

Functional Area: Lab Office Buildings Ground Level **Space Type:** Interaction Area

SPACE REQUIREMENT:

Allocated Space : 240 NSF x 2 Rooms Reqd. = **480** Total Net Square Feet

Function: Seating and space for refrigerator, microwave, sink

Occupancy Class: B

General Notes:

STRUCTURAL DATA:

Floor Live Load: 100 psf Floor Capacity Load psf Vibration Requirements: None

Structural Notes:

FINISHES:

Walls: Paint Floors: Linoleum Sheet

Ceilings: Acoustic Ceiling Tile Clg. Ht. 10'-0"

Finishes Notes:

ROOM ENVIRONMENT:

Temperature	75	F +/-	5	F	Cooling	72	F +/- 5 F	Heating
Humidity	50	RH +/-	10	RH	Cooling	30	RH +/- 10 RH	Heating

Room Pressure: Negative Vibration Criteria:

Acoustic Noise Level NC: 40 EMI Criteria:

SPECIAL REQUIREMENTS:

- ☐ Storage Cabinet
- ☐ Casework
- ☐ Fume Hood
- ☐ Toxic / Hazardous Materials

Special Requirements Notes: Overhead door

FIRE PROTECTION:

Hazard Classification: Ordinary Hazard Group ☑ Wet System: ☐ Preaction System

Fire Protection Notes:

HVAC:

Air Changes / Hr

Recirc / Single Pass Airflow: Single Pass

HVAC Notes:

- ☑ General Exhaust:
- ☐ Heat Exhaust:
- ☐ Chemical Exhaust:
- ☑ Smoke Exhaust: by AHU

PLUMBING:

- ☑ Domestic Water H/C
- ☐ Eyewash / Safety Shower
- ☑ Floor / Trench Drain: Provide floor drains to sanitary waste.

Plumbing Notes:

PROCESS PIPING:

- ☐ Compressed Air
- ☐ Nitrogen
- ☐ Liquid Nitrogen
- ☐ Other
- ☐ DI Water
- ☐ Process Cooling Water - Cu
- ☐ Process Cooling Water - Al
- ☐ Chemical Drain

Piping Notes:

ELECTRICAL:

Lighting Fixture Type: Recessed Troffer

Lighting Lamp Type: Fluorescent

Lighting Direction: Direct

Light Switching: Occupancy Sensor

Lighting Level (FC): 30

Ground:

Electrical Notes:

Power Outlets:

No.	Voltage	Phase	Type	Location
7	120 v	1 ph	Normal	Wall
0				

Clean Power:

UPS:

Emergency Power:

TELECOMMUNICATION AND SPECIAL SYSTEMS:

- ☑ Phone / Voice
- ☑ PA System
- ☐ Gas Leak Detection
- ☐ Liquid Leak Detection
- ☑ Data Connections:
- ☐ Access Control:
- ☐ CCTV:
- ☐ Fire Detection Type:

Telecom Notes:

ROOM DATA SHEET

Room Name: Ship-Receive & Storage **Room Number:** LOB5-108

Functional Area: Lab Office Buildings Ground Level **Space Type:** Building Support

SPACE REQUIREMENT:

Allocated Space : 960 NSF x 1 Rooms Reqd. = **960** Total Net Square Feet

Function: Shipping / Receiving loading platform and storage.

Occupancy Class: B

General Notes:

STRUCTURAL DATA:

Floor Live Load: 125 psf Floor Capacity Load psf Vibration Requirements: None

Structural Notes:

FINISHES:

Walls: Paint Floors: Sealed Concrete

Ceilings: No Ceiling Clg. Ht.

Finishes Notes:

ROOM ENVIRONMENT:

Temperature	75	F +/-	5	F	Cooling	72	F +/- 5 F	Heating
Humidity	50	RH +/-	10	RH	Cooling	30	RH +/- 10 RH	Heating

Room Pressure: Positive Vibration Criteria:

Acoustic Noise Level NC: 45-50 EMI Criteria:

SPECIAL REQUIREMENTS:

- ☐ Storage Cabinet
- ☐ Casework
- ☐ Fume Hood
- ☐ Toxic / Hazardous Materials

Special Requirements Notes:

FIRE PROTECTION:

Hazard Classification: Ordinary Hazard Group ☑ Wet System: ☐ Preaction System

Fire Protection Notes:

HVAC:

Air Changes / Hr ☐ General Exhaust: ☐ Chemical Exhaust:

Recirc / Single Pass Airflow: Recirculated ☐ Heat Exhaust: ☑ Smoke Exhaust: by AHU

HVAC Notes:

PLUMBING:

- ☐ Domestic Water H/C
- ☐ Eyewash / Safety Shower
- ☐ Floor / Trench Drain

Plumbing Notes:

PROCESS PIPING:

- ☑ Compressed Air
- ☐ Nitrogen
- ☑ Liquid Nitrogen: to Dewar fill station.
- ☐ Other
- ☐ DI Water
- ☐ Process Cooling Water - Cu
- ☐ Process Cooling Water - Al
- ☐ Chemical Drain

Piping Notes:

ELECTRICAL:

Lighting Fixture Type: Pendant

Lighting Lamp Type: Fluorescent

Lighting Direction: Direct

Light Switching: Occupancy Sensor

Lighting Level (FC): 30

Ground:

Electrical Notes:

Power Outlets:

No.	Voltage	Phase	Type	Location
11	120 v	1 ph	Normal	Wall
0				

Clean Power:

UPS:

Emergency Power:

TELECOMMUNICATION AND SPECIAL SYSTEMS:

- ☑ Phone / Voice
- ☑ PA System
- ☐ Gas Leak Detection
- ☐ Liquid Leak Detection
- ☑ Data Connections:
- ☑ Access Control:
- ☐ CCTV:
- ☐ Fire Detection Type:

Telecom Notes:

ROOM DATA SHEET

Room Name: Toilet / Shower **Room Number:** LOB5-109

Functional Area: Lab Office Buildings Ground Level **Space Type:** Building Support

SPACE REQUIREMENT:

Allocated Space : 250 NSF x 2 Rooms Reqd. = **500** Total Net Square Feet

Function: Restroom & shower

Occupancy Class: B

General Notes:

STRUCTURAL DATA:

Floor Live Load: 100 psf Floor Capacity Load psf Vibration Requirements: None

Structural Notes:

FINISHES:

Walls: Paint Floors: Vinyl Tile

Ceilings: Acoustic Ceiling Tile Clg. Ht. 9'-0"

Finishes Notes:

ROOM ENVIRONMENT:

Temperature 0 F +/- 0 F Cooling 0 F +/- 0 F Heating

Humidity 0 RH +/- 0 RH Cooling 0 RH +/- 0 RH Heating

Room Pressure Negative Vibration Criteria

Acoustic Noise Level NC 40 EMI Criteria

SPECIAL REQUIREMENTS:

☐ Storage Cabinet ☐ Fume Hood

☐ Casework ☐ Toxic / Hazardous Materials

Special Requirements Notes:

FIRE PROTECTION:

Hazard Classification: Ordinary Hazard Group ☑ Wet System: ☐ Preaction System

Fire Protection Notes:

HVAC:

Air Changes / Hr ☑ General Exhaust: ☐ Chemical Exhaust:

Recirc / Single Pass Airflow Single Pass ☐ Heat Exhaust: ☑ Smoke Exhaust: by AHU

HVAC Notes:

PLUMBING:

☑ Domestic Water H/C ☑ Floor / Trench Drain Provide floor drains to sanitary waste.

☐ Eyewash / Safety Shower

Plumbing Notes:

PROCESS PIPING:

☐ Compressed Air ☐ DI Water

☐ Nitrogen ☐ Process Cooling Water - Cu

☐ Liquid Nitrogen ☐ Process Cooling Water - Al

☐ Other ☐ Chemical Drain

Piping Notes:

ELECTRICAL:

Lighting Fixture Type: Surface Mount

Lighting Lamp Type: Fluorescent

Lighting Direction: Direct

Light Switching: Occupancy Sensor

Lighting Level (FC): 15

Ground:

Electrical Notes:

Power Outlets:

No.	Voltage	Phase	Type	Location
1	120 v	1 ph	Normal	Wall
0				

Clean Power:

UPS:

Emergency Power:

TELECOMMUNICATION AND SPECIAL SYSTEMS:

☐ Phone / Voice ☐ Data Connections:

☐ PA System ☐ Access Control:

☐ Gas Leak Detection ☐ CCTV:

☐ Liquid Leak Detection ☐ Fire Detection Type:

Telecom Notes:

ROOM DATA SHEET

Room Name: Electrical / Data **Room Number:** LOB5-110

Functional Area: Lab Office Buildings Ground Level **Space Type:** Building Support

SPACE REQUIREMENT:

Allocated Space : 153 NSF x 1 Rooms Reqd. = **153** Total Net Square Feet

Function:

Occupancy Class: B

General Notes:

STRUCTURAL DATA:

Floor Live Load: 125 psf Floor Capacity Load psf Vibration Requirements: None

Structural Notes:

FINISHES:

Walls: Paint Floors: Sealed Concrete

Ceilings: Acoustic Ceiling Tile Clg. Ht. 9'-0"

Finishes Notes:

ROOM ENVIRONMENT:

Temperature	75	F +/-	5	F	Cooling	72	F +/- 5 F	Heating
Humidity	50	RH +/-	10	RH	Cooling	30	RH +/- 10 RH	Heating

Room Pressure: Neutral Vibration Criteria:

Acoustic Noise Level NC: Per ACGIH TLVs EMI Criteria:

SPECIAL REQUIREMENTS:

☐ Storage Cabinet ☐ Fume Hood

☐ Casework ☐ Toxic / Hazardous Materials

Special Requirements Notes:

FIRE PROTECTION:

Hazard Classification: Ordinary Hazard Group ☑ Wet System: ☐ Preaction System

Fire Protection Notes:

HVAC:

Air Changes / Hr ☐ General Exhaust: ☐ Chemical Exhaust:

Recirc / Single Pass Airflow: Recirculated ☐ Heat Exhaust: ☑ Smoke Exhaust: by AHU

HVAC Notes:

PLUMBING:

☐ Domestic Water H/C ☐ Floor / Trench Drain

☐ Eyewash / Safety Shower

Plumbing Notes:

PROCESS PIPING:

☐ Compressed Air ☐ DI Water

☐ Nitrogen ☐ Process Cooling Water - Cu

☐ Liquid Nitrogen ☐ Process Cooling Water - Al

☐ Other ☐ Chemical Drain

Piping Notes:

ELECTRICAL:

Lighting Fixture Type: Pendant

Lighting Lamp Type: Fluorescent

Lighting Direction: Direct

Light Switching: Occupancy Sensor

Lighting Level (FC): 30

Ground:

Electrical Notes:

Power Outlets:

No.	Voltage	Phase	Type	Location
4	120 v	1 ph	Normal	Wall
0				

Clean Power:

UPS:

Emergency Power:

TELECOMMUNICATION AND SPECIAL SYSTEMS:

☐ Phone / Voice ☐ Data Connections:

☐ PA System ☑ Access Control:

☐ Gas Leak Detection ☐ CCTV:

☐ Liquid Leak Detection ☐ Fire Detection Type:

Telecom Notes:

ROOM DATA SHEET

Room Name: Janitor Closet **Room Number:** LOB5-111

Functional Area: Lab Office Buildings Ground Level **Space Type:** Building Support

SPACE REQUIREMENT:

Allocated Space : 63 NSF x 1 Rooms Reqd. = **63** Total Net Square Feet

Function: Maintenance space

Occupancy Class: B

General Notes:

STRUCTURAL DATA:

Floor Live Load: 100 psf Floor Capacity Load psf Vibration Requirements: None

Structural Notes:

FINISHES:

Walls: Paint Floors: Sealed Concrete

Ceilings: Acoustic Ceiling Tile Clg. Ht. 8'-0"

Finishes Notes:

ROOM ENVIRONMENT:

Temperature F +/- F Cooling F +/- F Heating

Humidity 0 RH +/- 0 RH Cooling 0 RH +/- 0 RH Heating

Room Pressure Negative Vibration Criteria

Acoustic Noise Level NC None EMI Criteria

SPECIAL REQUIREMENTS:

☐ Storage Cabinet ☐ Fume Hood

☐ Casework ☐ Toxic / Hazardous Materials

Special Requirements Notes:

FIRE PROTECTION:

Hazard Classification: Ordinary Hazard Group ☑ Wet System: ☐ Preaction System

Fire Protection Notes:

HVAC:

Air Changes / Hr ☑ General Exhaust: ☐ Chemical Exhaust:

Recirc / Single Pass Airflow Single Pass ☐ Heat Exhaust: ☑ Smoke Exhaust: by AHU

HVAC Notes:

PLUMBING:

☑ Domestic Water H/C ☑ Floor / Trench Drain Provide floor drains to sanitary waste.

☐ Eyewash / Safety Shower

Plumbing Notes:

PROCESS PIPING:

☐ Compressed Air ☐ DI Water

☐ Nitrogen ☐ Process Cooling Water - Cu

☐ Liquid Nitrogen ☐ Process Cooling Water - Al

☐ Other ☐ Chemical Drain

Piping Notes:

ELECTRICAL:

Lighting Fixture Type: Pendant

Lighting Lamp Type: Fluorescent

Lighting Direction: Direct

Light Switching: Occupancy Sensor

Lighting Level (FC): 15

Ground:

Electrical Notes:

Power Outlets:

No.	Voltage	Phase	Type	Location
1	120 v	1 ph	Normal	Wall
0				

Clean Power:

UPS:

Emergency Power:

TELECOMMUNICATION AND SPECIAL SYSTEMS:

☐ Phone / Voice ☐ Data Connections:

☐ PA System ☐ Access Control:

☐ Gas Leak Detection ☐ CCTV:

☐ Liquid Leak Detection ☐ Fire Detection Type:

Telecom Notes:

ROOM DATA SHEET

Room Name: Access Corridor Interface **Room Number:** LOB5-112

Functional Area: Lab Office Buildings Ground Level **Space Type:** Circulation

SPACE REQUIREMENT:

Allocated Space : 2,090 NSF x 1 Rooms Reqd. = **2,090** Total Net Square Feet

Function: Extension of the Access Corridor into LOB

Occupancy Class: B

General Notes:

STRUCTURAL DATA:

Floor Live Load: 125 psf Floor Capacity Load psf Vibration Requirements: None

Structural Notes:

FINISHES:

Walls: Floors:

Ceilings: Clg. Ht.

Finishes Notes:

ROOM ENVIRONMENT:

Temperature	75	F +/-	1	F	Cooling	72	F +/- 1 F	Heating
Humidity	50	RH +/-	10	RH	Cooling	30	RH +/- 10 RH	Heating

Room Pressure: Positive Vibration Criteria:

Acoustic Noise Level NC: 55 or Better EMI Criteria:

SPECIAL REQUIREMENTS:

☐ Storage Cabinet ☐ Fume Hood

☐ Casework ☐ Toxic / Hazardous Materials

Special Requirements Notes:

FIRE PROTECTION:

Hazard Classification: Ordinary Hazard Group ☑ Wet System: ☐ Preaction System

Fire Protection Notes:

HVAC:

Air Changes / Hr ☐ General Exhaust: ☐ Chemical Exhaust:

Recirc / Single Pass Airflow: Recirculated ☐ Heat Exhaust: ☑ Smoke Exhaust: by AHU

HVAC Notes:

PLUMBING:

☐ Domestic Water H/C ☐ Floor / Trench Drain

☐ Eyewash / Safety Shower

Plumbing Notes:

PROCESS PIPING:

☐ Compressed Air ☐ DI Water

☐ Nitrogen ☐ Process Cooling Water - Cu

☐ Liquid Nitrogen ☐ Process Cooling Water - Al

☐ Other ☐ Chemical Drain

Piping Notes:

ELECTRICAL:

Lighting Fixture Type: Pendant

Lighting Lamp Type: Fluorescent

Lighting Direction: Direct

Light Switching: Low Voltage Switch

Lighting Level (FC): 50

Ground:

Electrical Notes:

Power Outlets:

No.	Voltage	Phase	Type	Location
	120 v	1 ph	Normal	Wall
0				

Clean Power:

UPS:

Emergency Power:

TELECOMMUNICATION AND SPECIAL SYSTEMS:

☐ Phone / Voice ☐ Data Connections:

☑ PA System ☐ Access Control:

☐ Gas Leak Detection ☐ CCTV:

☐ Liquid Leak Detection ☐ Fire Detection Type:

Telecom Notes:

ROOM DATA SHEET

Room Name: Machine Shop **Room Number:** LOB5-113

Functional Area: Lab Office Buildings Ground Level **Space Type:** Lab Support

SPACE REQUIREMENT:

Allocated Space : 270 NSF x 1 Rooms Reqd. = **270** Total Net Square Feet

Function: Machine shop

Occupancy Class: B

General Notes:

STRUCTURAL DATA:

Floor Live Load: 125 psf Floor Capacity Load psf Vibration Requirements: None

Structural Notes:

FINISHES:

Walls: Paint Floors: Sealed Concrete

Ceilings: Acoustic Ceiling Tile Clg. Ht. 12'-0"

Finishes Notes:

ROOM ENVIRONMENT:

Temperature	75	F +/-	5	F	Cooling	72	F +/- 5 F	Heating
Humidity	50	RH +/-	10	RH	Cooling	30	RH +/- 10 RH	Heating

Room Pressure: Negative

Acoustic Noise Level NC: Per ACGIH TLVs

Vibration Criteria:

EMI Criteria:

SPECIAL REQUIREMENTS:

- ☐ Storage Cabinet
- ☐ Casework
- ☐ Fume Hood
- ☐ Toxic / Hazardous Materials

Special Requirements Notes:

FIRE PROTECTION:

Hazard Classification: Ordinary Hazard Group ☑ Wet System: ☐ Preaction System

Fire Protection Notes:

HVAC:

Air Changes / Hr: 20 CFM/Person

Recirc / Single Pass Airflow: Recirculated

- ☑ General Exhaust:
- ☐ Heat Exhaust:
- ☐ Chemical Exhaust:
- ☑ Smoke Exhaust: by AHU

HVAC Notes:

PLUMBING:

- ☐ Domestic Water H/C
- ☑ Eyewash / Safety Shower
- ☐ Floor / Trench Drain

Plumbing Notes:

PROCESS PIPING:

- ☑ Compressed Air
- ☐ Nitrogen
- ☐ Liquid Nitrogen
- ☐ Other
- ☐ DI Water
- ☐ Process Cooling Water - Cu
- ☐ Process Cooling Water - Al
- ☐ Chemical Drain

Piping Notes:

ELECTRICAL:

Lighting Fixture Type: Pendant

Lighting Lamp Type: Fluorescent

Lighting Direction: Direct

Light Switching: Occupancy Sensor

Lighting Level (FC): 50-75

Ground:

Electrical Notes:

Power Outlets:

No.	Voltage	Phase	Type	Location
2	120 v	1 ph	Normal	Wall
0				

Clean Power:

UPS:

Emergency Power:

TELECOMMUNICATION AND SPECIAL SYSTEMS:

- ☑ Phone / Voice
- ☐ PA System
- ☐ Gas Leak Detection
- ☐ Liquid Leak Detection
- ☑ Data Connections:
- ☐ Access Control:
- ☐ CCTV:
- ☐ Fire Detection Type:

Telecom Notes:

ROOM DATA SHEET

Room Name: Control Conference Room **Room Number:** OPS-103

Functional Area: Operations Center Level 2 **Space Type:** Laboratory

SPACE REQUIREMENT:

Allocated Space : 676 NSF x 1 Rooms Reqd. = **676** Total Net Square Feet

Function: Meeting space for control room operators

Occupancy Class: B

General Notes:

STRUCTURAL DATA:

Floor Live Load: 100 psf Floor Capacity Load psf Vibration Requirements: None

Structural Notes:

FINISHES:

Walls: Wall Coverings Floors: Carpet Tile

Ceilings: Acoustic Ceiling Tile Clg. Ht. 9'-0"

Finishes Notes:

ROOM ENVIRONMENT:

Temperature	75	F +/-	5	F	Cooling	72	F +/- 5 F	Heating
Humidity	50	RH +/-	10	RH	Cooling	30	RH +/- 10 RH	Heating

Room Pressure: Positive Vibration Criteria: None

Acoustic Noise Level NC: 30 EMI Criteria: None

SPECIAL REQUIREMENTS:

- ☐ Storage Cabinet
- ☐ Casework
- ☐ Fume Hood
- ☐ Toxic / Hazardous Materials

Special Requirements Notes:

FIRE PROTECTION:

Hazard Classification: Ordinary Hazard Group ☑ Wet System: ☐ Preaction System

Fire Protection Notes:

HVAC:

Air Changes / Hr: 20 CFM/Person ☐ General Exhaust: ☐ Chemical Exhaust:

Recirc / Single Pass Airflow: Recirculated ☐ Heat Exhaust: ☑ Smoke Exhaust: by AHU

HVAC Notes:

PLUMBING:

- ☐ Domestic Water H/C
- ☐ Eyewash / Safety Shower
- ☐ Floor / Trench Drain

Plumbing Notes:

PROCESS PIPING:

- ☐ Compressed Air
- ☐ Nitrogen
- ☐ Liquid Nitrogen
- ☐ Other
- ☐ DI Water
- ☐ Process Cooling Water - Cu
- ☐ Process Cooling Water - Al
- ☐ Chemical Drain

Piping Notes:

ELECTRICAL:

Lighting Fixture Type: Recessed Troffer

Lighting Lamp Type: Fluorescent

Lighting Direction: Direct/Indirect

Light Switching: Occupancy Sensor

Lighting Level (FC): 30

Ground:

Electrical Notes:

Power Outlets:

No.	Voltage	Phase	Type	Location
4	120 v	1 ph	Normal	Wall
0				

Clean Power:

UPS:

Emergency Power:

TELECOMMUNICATION AND SPECIAL SYSTEMS:

- ☑ Phone / Voice
- ☐ PA System
- ☐ Gas Leak Detection
- ☐ Liquid Leak Detection
- ☑ Data Connections:
- ☐ Access Control:
- ☐ CCTV:
- ☐ Fire Detection Type:

Telecom Notes:

ROOM DATA SHEET

Room Name: Control Room **Room Number:** OPS-104

Functional Area: Operations Center Level 2 **Space Type:** Accelerator

SPACE REQUIREMENT:

Allocated Space : 1,547 NSF x 1 Rooms Reqd. = **1,547** Total Net Square Feet

Function: House control panels for storage ring.

Occupancy Class: B

General Notes:

STRUCTURAL DATA:

Floor Live Load: 100 psf Floor Capacity Load psf Vibration Requirements: None

Structural Notes:

FINISHES:

Walls: Paint Floors: Raised Floor

Ceilings: Acoustic Ceiling Tile Clg. Ht. 9'-0"

Finishes Notes:

ROOM ENVIRONMENT:

Temperature	75	F +/-	5	F	Cooling	72	F +/- 5 F	Heating
Humidity	50	RH +/-	10	RH	Cooling	30	RH +/- 10 RH	Heating

Room Pressure: Positive

Acoustic Noise Level NC: 35-40

Vibration Criteria: None

EMI Criteria: None

SPECIAL REQUIREMENTS:

- ☐ Storage Cabinet
- ☐ Casework
- ☐ Fume Hood
- ☐ Toxic / Hazardous Materials

Special Requirements Notes:

FIRE PROTECTION:

Hazard Classification: Ordinary Hazard Group ☑ Wet System: ☐ Preaction System

Fire Protection Notes:

HVAC:

Air Changes / Hr: 20 CFM/Person

Recirc / Single Pass Airflow: Recirculated

- ☐ General Exhaust:
- ☐ Heat Exhaust:
- ☐ Chemical Exhaust:
- ☑ Smoke Exhaust: by AHU

HVAC Notes:

PLUMBING:

- ☐ Domestic Water H/C
- ☐ Eyewash / Safety Shower
- ☐ Floor / Trench Drain

Plumbing Notes:

PROCESS PIPING:

- ☐ Compressed Air
- ☐ Nitrogen
- ☐ Liquid Nitrogen
- ☐ Other
- ☐ DI Water
- ☐ Process Cooling Water - Cu
- ☐ Process Cooling Water - Al
- ☐ Chemical Drain

Piping Notes:

ELECTRICAL:

Lighting Fixture Type: Recessed Troffer

Lighting Lamp Type: Fluorescent

Lighting Direction: Indirect

Light Switching: Low Voltage Switch

Lighting Level (FC): 30-50

Ground:

Electrical Notes:

Power Outlets:

No.	Voltage	Phase	Type	Location
8	120 v	1	Normal	Wall
16	120 v	1 ph	Emergency	Floor

Clean Power:

UPS: 30 kVA for Control & Computer Rooms

Emergency Power: Floor receptacles for control stations

TELECOMMUNICATION AND SPECIAL SYSTEMS:

- ☑ Phone / Voice
- ☑ PA System
- ☐ Gas Leak Detection
- ☐ Liquid Leak Detection
- ☑ Data Connections:
- ☑ Access Control:
- ☑ CCTV:
- ☐ Fire Detection Type:

Telecom Notes:

ROOM DATA SHEET

Room Name: Computer Room **Room Number:** OPS-105

Functional Area: Operations Center Ground Level **Space Type:** Building Support

SPACE REQUIREMENT:

Allocated Space : 976 NSF x 1 Rooms Reqd. = **976** Total Net Square Feet

Function: House computers for storage ring control and monitoring

Occupancy Class: B

General Notes:

STRUCTURAL DATA:

Floor Live Load: 125 psf Floor Capacity Load psf Vibration Requirements: None

Structural Notes:

FINISHES:

Walls: Paint Floors: Raised Floor

Ceilings: Acoustic Ceiling Tile Clg. Ht. 9'-0"

Finishes Notes:

ROOM ENVIRONMENT:

Temperature	72 F +/-	5 F	Cooling	72 F +/-	5 F	Heating		
Humidity	50 RH +/-	10 RH	Cooling	30 RH +/-	10 RH	Heating		
Room Pressure	Positive			Vibration Criteria	None			
Acoustic Noise Level NC	45-50			EMI Criteria	None			

SPECIAL REQUIREMENTS:

- ☐ Storage Cabinet
- ☐ Casework
- ☐ Fume Hood
- ☐ Toxic / Hazardous Materials

Special Requirements Notes:

FIRE PROTECTION:

Hazard Classification: Ordinary Hazard Group ☑ Wet System: ☐ Preaction System

Fire Protection Notes:

HVAC:

Air Changes / Hr 20 CFM/Person ☐ General Exhaust: ☐ Chemical Exhaust:

Recirc / Single Pass Airflow Recirculated ☐ Heat Exhaust: ☑ Smoke Exhaust: by AHU

HVAC Notes:

PLUMBING:

- ☐ Domestic Water H/C
- ☐ Eyewash / Safety Shower
- ☐ Floor / Trench Drain

Plumbing Notes:

PROCESS PIPING:

- ☐ Compressed Air
- ☐ Nitrogen
- ☐ Liquid Nitrogen
- ☐ Other
- ☐ DI Water
- ☐ Process Cooling Water - Cu
- ☐ Process Cooling Water - Al
- ☐ Chemical Drain

Piping Notes:

ELECTRICAL:

Lighting Fixture Type: Pendant

Lighting Lamp Type: Fluorescent

Lighting Direction: Direct/Indirect

Light Switching: Occupancy Sensor

Lighting Level (FC): 50

Ground:

Electrical Notes:

Power Outlets:

No.	Voltage	Phase	Type	Location
4	120 v	1 ph	Normal	Wall
0				

Clean Power:

UPS: 30 kVA for Control & Computer Rooms

Emergency Power: for computers

TELECOMMUNICATION AND SPECIAL SYSTEMS:

- ☑ Phone / Voice
- ☑ PA System
- ☐ Gas Leak Detection
- ☐ Liquid Leak Detection
- ☑ Data Connections:
- ☑ Access Control:
- ☑ CCTV:
- ☐ Fire Detection Type:

Telecom Notes:

ROOM DATA SHEET

Room Name: 2nd Floor Toilet & Shower **Room Number:** OPS-106

Functional Area: Operations Center Level 2 **Space Type:** Building Support

SPACE REQUIREMENT:

Allocated Space : 76 NSF x 2 Rooms Reqd. = **152** Total Net Square Feet

Function:

Occupancy Class: B

General Notes:

STRUCTURAL DATA:

Floor Live Load: 100 psf Floor Capacity Load psf Vibration Requirements: None

Structural Notes:

FINISHES:

Walls: Paint Floors: Vinyl Tile

Ceilings: Acoustic Ceiling Tile Clg. Ht. 9'-0"

Finishes Notes:

ROOM ENVIRONMENT:

Temperature F +/- F Cooling F +/- F Heating

Humidity RH +/- RH Cooling RH +/- RH Heating

Room Pressure Negative Vibration Criteria None

Acoustic Noise Level NC None EMI Criteria None

SPECIAL REQUIREMENTS:

☐ Storage Cabinet ☐ Fume Hood

☐ Casework ☐ Toxic / Hazardous Materials

Special Requirements Notes:

FIRE PROTECTION:

Hazard Classification: Ordinary Hazard Group ☑ Wet System: ☐ Preaction System

Fire Protection Notes:

HVAC:

Air Changes / Hr ☑ General Exhaust: ☐ Chemical Exhaust:

Recirc / Single Pass Airflow Single Pass ☐ Heat Exhaust: ☑ Smoke Exhaust: by AHU

HVAC Notes:

PLUMBING:

☑ Domestic Water H/C ☑ Floor / Trench Drain Provide floor drains to sanitary waste.

☐ Eyewash / Safety Shower

Plumbing Notes:

PROCESS PIPING:

☐ Compressed Air ☐ DI Water

☐ Nitrogen ☐ Process Cooling Water - Cu

☐ Liquid Nitrogen ☐ Process Cooling Water - Al

☐ Other ☐ Chemical Drain

Piping Notes:

ELECTRICAL:

Lighting Fixture Type: Recessed Troffer

Lighting Lamp Type: Fluorescent

Lighting Direction: Direct

Light Switching: Occupancy Sensor

Lighting Level (FC): 10-15 (30 at sink)

Ground:

Electrical Notes:

Power Outlets:

No.	Voltage	Phase	Type	Location
1	120 v	1 ph	Normal	Wall
0				

Clean Power:

UPS:

Emergency Power:

TELECOMMUNICATION AND SPECIAL SYSTEMS:

☐ Phone / Voice ☐ Data Connections:

☐ PA System ☐ Access Control:

☐ Gas Leak Detection ☐ CCTV:

☐ Liquid Leak Detection ☑ Fire Detection Type: Photoelectric Smoke Detectors

Telecom Notes:

ROOM DATA SHEET

Room Name: Entrance Lobby & Vestibule **Room Number:** OPS-107

Functional Area: Operations Center Ground Level **Space Type:** Circulation

SPACE REQUIREMENT:

Allocated Space : 2,415 NSF x 1 Rooms Reqd. = **2,415** Total Net Square Feet

Function: Main entrance to NSLS-II and area for social gatherings

Occupancy Class: B

General Notes:

STRUCTURAL DATA:

Floor Live Load: 100 psf Floor Capacity Load psf Vibration Requirements: None

Structural Notes:

FINISHES:

Walls: Paint Floors: Ceramic Tile

Ceilings: No Ceiling Clg. Ht.

Finishes Notes:

ROOM ENVIRONMENT:

Temperature	75	F +/-	5	F	Cooling	72	F +/- 5 F	Heating
Humidity	50	RH +/-	10	RH	Cooling	30	RH +/- 10 RH	Heating

Room Pressure: Positive Vibration Criteria: None

Acoustic Noise Level NC: 40-45 EMI Criteria: None

SPECIAL REQUIREMENTS:

- ☐ Storage Cabinet
- ☐ Casework
- ☐ Fume Hood
- ☐ Toxic / Hazardous Materials

Special Requirements Notes:

FIRE PROTECTION:

Hazard Classification: Ordinary Hazard Group ☑ Wet System: ☐ Preaction System

Fire Protection Notes:

HVAC:

Air Changes / Hr: 20 CFM/Person ☐ General Exhaust: ☐ Chemical Exhaust:

Recirc / Single Pass Airflow: Recirculated ☐ Heat Exhaust: ☑ Smoke Exhaust: by AHU

HVAC Notes:

PLUMBING:

- ☑ Domestic Water H/C — Drinking Fountain
- ☐ Eyewash / Safety Shower
- ☐ Floor / Trench Drain

Plumbing Notes:

PROCESS PIPING:

- ☐ Compressed Air
- ☐ Nitrogen
- ☐ Liquid Nitrogen
- ☐ Other
- ☐ DI Water
- ☐ Process Cooling Water - Cu
- ☐ Process Cooling Water - Al
- ☐ Chemical Drain

Piping Notes:

ELECTRICAL:

Lighting Fixture Type: Recessed Troffer

Lighting Lamp Type: Fluorescent

Lighting Direction: Direct

Light Switching: Occupancy Sensor

Lighting Level (FC): 30

Ground:

Electrical Notes:

Power Outlets:

No.	Voltage	Phase	Type	Location
2	120 v	1 ph	Normal	Wall
0				

Clean Power:

UPS:

Emergency Power:

TELECOMMUNICATION AND SPECIAL SYSTEMS:

- ☑ Phone / Voice
- ☑ PA System
- ☐ Gas Leak Detection
- ☐ Liquid Leak Detection
- ☑ Data Connections:
- ☑ Access Control:
- ☐ CCTV:
- ☐ Fire Detection Type:

Telecom Notes:

ROOM DATA SHEET

Room Name: Bridge & Viewing Gallery **Room Number:** OPS-108

Functional Area: Operations Center Level 2 **Space Type:** Circulation

SPACE REQUIREMENT:

Allocated Space : 1,450 NSF x 1 Rooms Reqd. = **1,450** Total Net Square Feet

Function: Viewing area of Experimental Hall for tours.
Access to the Tunnel Mezzanine and Control Room

Occupancy Class: B

General Notes:

STRUCTURAL DATA:

Floor Live Load: 100 psf Floor Capacity Load psf Vibration Requirements: None

Structural Notes:

FINISHES:

Walls: Paint Floors: Vinyl Tile

Ceilings: No Ceiling Clg. Ht.

Finishes Notes:

ROOM ENVIRONMENT:

Temperature	75	F +/-	5	F	Cooling	72	F +/- 5 F	Heating
Humidity	50	RH +/-	10	RH	Cooling	30	RH +/- 10 RH	Heating

Room Pressure: Neutral Vibration Criteria: None

Acoustic Noise Level NC: 40-45 EMI Criteria: None

SPECIAL REQUIREMENTS:

- ☐ Storage Cabinet
- ☐ Casework
- ☐ Fume Hood
- ☐ Toxic / Hazardous Materials

Special Requirements Notes:

FIRE PROTECTION:

Hazard Classification: Ordinary Hazard Group ☑ Wet System: ☐ Preaction System

Fire Protection Notes:

HVAC:

Air Changes / Hr ☐ General Exhaust: ☐ Chemical Exhaust:

Recirc / Single Pass Airflow: Recirculated ☐ Heat Exhaust: ☑ Smoke Exhaust: by AHU

HVAC Notes:

PLUMBING:

- ☐ Domestic Water H/C
- ☐ Eyewash / Safety Shower
- ☐ Floor / Trench Drain

Plumbing Notes:

PROCESS PIPING:

- ☐ Compressed Air
- ☐ Nitrogen
- ☐ Liquid Nitrogen
- ☐ Other
- ☐ DI Water
- ☐ Process Cooling Water - Cu
- ☐ Process Cooling Water - Al
- ☐ Chemical Drain

Piping Notes:

ELECTRICAL:

Lighting Fixture Type: Pendant

Lighting Lamp Type: Fluorescent

Lighting Direction: Direct

Light Switching: Occupancy Sensor

Lighting Level (FC): 30

Ground:

Electrical Notes:

Power Outlets:

No.	Voltage	Phase	Type	Location
0	120 v	1 ph	Normal	Wall
0				

Clean Power:

UPS:

Emergency Power:

TELECOMMUNICATION AND SPECIAL SYSTEMS:

- ☑ Phone / Voice
- ☐ PA System
- ☐ Gas Leak Detection
- ☐ Liquid Leak Detection
- ☑ Data Connections:
- ☐ Access Control:
- ☐ CCTV:
- ☐ Fire Detection Type:

Telecom Notes:

ROOM DATA SHEET

Room Name: Unisex Toilet **Room Number:** OPS-109

Functional Area: Operations Center Ground Level **Space Type:** Building Support

SPACE REQUIREMENT:

Allocated Space : 78 NSF x 1 Rooms Reqd. = **78** Total Net Square Feet

Function: Restroom

Occupancy Class: B

General Notes:

STRUCTURAL DATA:

Floor Live Load: 100 psf Floor Capacity Load psf Vibration Requirements: None

Structural Notes:

FINISHES:

Walls: Paint Floors: Vinyl Tile

Ceilings: Acoustic Ceiling Tile Clg. Ht. 9'-0"

Finishes Notes:

ROOM ENVIRONMENT:

Temperature F +/- F Cooling F +/- F Heating

Humidity RH +/- 0 RH Cooling RH +/- RH Heating

Room Pressure Negative Vibration Criteria None

Acoustic Noise Level NC None EMI Criteria None

SPECIAL REQUIREMENTS:

☐ Storage Cabinet ☐ Fume Hood

☐ Casework ☐ Toxic / Hazardous Materials

Special Requirements Notes:

FIRE PROTECTION:

Hazard Classification: Ordinary Hazard Group ☑ Wet System: ☐ Preaction System

Fire Protection Notes:

HVAC:

Air Changes / Hr ☑ General Exhaust: ☐ Chemical Exhaust:

Recirc / Single Pass Airflow Single Pass ☐ Heat Exhaust: ☑ Smoke Exhaust: by AHU

HVAC Notes:

PLUMBING:

☑ Domestic Water H/C ☑ Floor / Trench Drain Provide floor drains to sanitary waste.

☐ Eyewash / Safety Shower

Plumbing Notes: Toilet and sink in each room

PROCESS PIPING:

☐ Compressed Air ☐ DI Water

☐ Nitrogen ☐ Process Cooling Water - Cu

☐ Liquid Nitrogen ☐ Process Cooling Water - Al

☐ Other ☐ Chemical Drain

Piping Notes:

ELECTRICAL:

Lighting Fixture Type: Surface Mount

Lighting Lamp Type: Fluorescent

Lighting Direction: Direct

Light Switching: Occupancy Sensor

Lighting Level (FC): 10-15 (30 at sink)

Ground:

Electrical Notes:

Power Outlets:

No.	Voltage	Phase	Type	Location
1	120 v	1 ph	Normal	Wall
0				

Clean Power:

UPS:

Emergency Power:

TELECOMMUNICATION AND SPECIAL SYSTEMS:

☐ Phone / Voice ☐ Data Connections:

☐ PA System ☐ Access Control:

☐ Gas Leak Detection ☐ CCTV:

☐ Liquid Leak Detection ☐ Fire Detection Type:

Telecom Notes:

ROOM DATA SHEET

Room Name: Break Room / Kitchenette **Room Number:** OPS-110

Functional Area: Operations Center Ground Level **Space Type:** Building Support

SPACE REQUIREMENT:

Allocated Space : 512 NSF x 1 Rooms Reqd. = **512** Total Net Square Feet

Function: Space to store and prepare personal meals

Occupancy Class: B

General Notes:

STRUCTURAL DATA:

Floor Live Load: 100 psf Floor Capacity Load psf Vibration Requirements: None

Structural Notes:

FINISHES:

Walls: Paint Floors: Linoleum Sheet

Ceilings: Acoustic Ceiling Tile Clg. Ht. 9'-0"

Finishes Notes:

ROOM ENVIRONMENT:

Temperature	75	F +/-	5	F	Cooling	72	F +/- 5 F	Heating
Humidity	50	RH +/-	10	RH	Cooling	30	RH +/- 10 RH	Heating

Room Pressure: Negative Vibration Criteria: None

Acoustic Noise Level NC: 40-45 EMI Criteria: None

SPECIAL REQUIREMENTS:

- ☐ Storage Cabinet
- ☑ Casework — Counter & cabinets
- ☐ Fume Hood
- ☐ Toxic / Hazardous Materials

Special Requirements Notes: Provide sink; space for refrigerator, microwave, vending machines.

FIRE PROTECTION:

Hazard Classification: Ordinary Hazard Group ☑ Wet System: ☐ Preaction System

Fire Protection Notes:

HVAC:

Air Changes / Hr

Recirc / Single Pass Airflow: Single Pass

HVAC Notes:

- ☑ General Exhaust:
- ☐ Heat Exhaust:
- ☐ Chemical Exhaust:
- ☑ Smoke Exhaust: by AHU

PLUMBING:

- ☑ Domestic Water H/C
- ☐ Eyewash / Safety Shower
- ☑ Floor / Trench Drain — Provide floor drains to sanitary waste.

Plumbing Notes: Kitchen sink

PROCESS PIPING:

- ☐ Compressed Air
- ☐ Nitrogen
- ☐ Liquid Nitrogen
- ☐ Other
- ☐ DI Water
- ☐ Process Cooling Water - Cu
- ☐ Process Cooling Water - Al
- ☐ Chemical Drain

Piping Notes:

ELECTRICAL:

Lighting Fixture Type: Recessed Troffer

Lighting Lamp Type: Fluorescent

Lighting Direction: Direct

Light Switching: Occupancy Sensor

Lighting Level (FC): 30

Ground:

Electrical Notes:

Power Outlets:

No.	Voltage	Phase	Type	Location
7	120 v	1 ph	Normal	Wall
0				

Clean Power:

UPS:

Emergency Power:

TELECOMMUNICATION AND SPECIAL SYSTEMS:

- ☑ Phone / Voice
- ☑ PA System
- ☐ Gas Leak Detection
- ☐ Liquid Leak Detection
- ☑ Data Connections:
- ☐ Access Control:
- ☐ CCTV:
- ☐ Fire Detection Type:

Telecom Notes:

ROOM DATA SHEET

Room Name: Telecom Room **Room Number:** OPS-111

Functional Area: Operations Center Ground Level **Space Type:** Building Support

SPACE REQUIREMENT:

Allocated Space : 409 NSF x 1 Rooms Reqd. = **409** Total Net Square Feet

Function: Electrical equipment room

Occupancy Class: B

General Notes:

STRUCTURAL DATA:

Floor Live Load: 125 psf Floor Capacity Load psf Vibration Requirements: None

Structural Notes:

FINISHES:

Walls: Paint Floors: Sealed Concrete

Ceilings: Acoustic Ceiling Tile Clg. Ht. 9'-0"

Finishes Notes:

ROOM ENVIRONMENT:

Temperature	78	F +/-	5	F	Cooling	72	F +/- 5 F	Heating
Humidity	0	RH +/-	0	RH	Cooling	0	RH +/- 0 RH	Heating

Room Pressure: Neutral Vibration Criteria: None

Acoustic Noise Level NC: 45-50 EMI Criteria: None

SPECIAL REQUIREMENTS:

☐ Storage Cabinet ☐ Fume Hood

☐ Casework ☐ Toxic / Hazardous Materials

Special Requirements Notes:

FIRE PROTECTION:

Hazard Classification: Ordinary Hazard Group ☑ Wet System: ☐ Preaction System

Fire Protection Notes:

HVAC:

Air Changes / Hr ☐ General Exhaust: ☐ Chemical Exhaust:

Recirc / Single Pass Airflow: Recirculated ☐ Heat Exhaust: ☑ Smoke Exhaust: by AHU

HVAC Notes:

PLUMBING:

☐ Domestic Water H/C ☐ Floor / Trench Drain

☐ Eyewash / Safety Shower

Plumbing Notes:

PROCESS PIPING:

☐ Compressed Air ☐ DI Water

☐ Nitrogen ☐ Process Cooling Water - Cu

☐ Liquid Nitrogen ☐ Process Cooling Water - Al

☐ Other ☐ Chemical Drain

Piping Notes:

ELECTRICAL:

Lighting Fixture Type: Pendant

Lighting Lamp Type: Fluorescent

Lighting Direction: Direct

Light Switching: Occupancy Sensor

Lighting Level (FC): 15

Ground:

Electrical Notes:

Power Outlets:

No.	Voltage	Phase	Type	Location
8	120 v	1 ph	Normal	Wall
0				

Clean Power:

UPS:

Emergency Power:

TELECOMMUNICATION AND SPECIAL SYSTEMS:

☑ Phone / Voice ☑ Data Connections:

☑ PA System ☑ Access Control:

☐ Gas Leak Detection ☐ CCTV:

☐ Liquid Leak Detection ☐ Fire Detection Type:

Telecom Notes:

ROOM DATA SHEET

Room Name: Switchgear Room **Room Number:** OPS-118

Functional Area: Operations Center Ground Level **Space Type:** Building Support

SPACE REQUIREMENT:

Allocated Space : 655 NSF x 1 Rooms Reqd. = **655** Total Net Square Feet

Function:

Occupancy Class: B

General Notes:

STRUCTURAL DATA:

Floor Live Load: 125 psf Floor Capacity Load psf Vibration Requirements: None

Structural Notes:

FINISHES:

Walls: Paint Floors: Sealed Concrete

Ceilings: Acoustic Ceiling Tile Clg. Ht. 9'-0"

Finishes Notes:

ROOM ENVIRONMENT:

Temperature	75	F +/-	5	F	Cooling	72	F +/-	5	F Heating
Humidity	50	RH +/-	10	RH	Cooling	30	RH +/-	10	RH Heating

Room Pressure: Neutral Vibration Criteria: None

Acoustic Noise Level NC: 45-50 EMI Criteria: None

SPECIAL REQUIREMENTS:

☐ Storage Cabinet ☐ Fume Hood

☐ Casework ☐ Toxic / Hazardous Materials

Special Requirements Notes:

FIRE PROTECTION:

Hazard Classification: Ordinary Hazard Group ☑ Wet System: ☐ Preaction System

Fire Protection Notes:

HVAC:

Air Changes / Hr ☐ General Exhaust: ☐ Chemical Exhaust:

Recirc / Single Pass Airflow: Recirculated ☐ Heat Exhaust: ☑ Smoke Exhaust: by AHU

HVAC Notes:

PLUMBING:

☐ Domestic Water H/C ☐ Floor / Trench Drain

☐ Eyewash / Safety Shower

Plumbing Notes:

PROCESS PIPING:

☐ Compressed Air ☐ DI Water

☐ Nitrogen ☐ Process Cooling Water - Cu

☐ Liquid Nitrogen ☐ Process Cooling Water - Al

☐ Other ☐ Chemical Drain

Piping Notes:

ELECTRICAL:

Lighting Fixture Type: Pendant

Lighting Lamp Type: Fluorescent

Lighting Direction: Direct

Light Switching: Occupancy Sensor

Lighting Level (FC): 15

Ground:

Electrical Notes:

Power Outlets:

No.	Voltage	Phase	Type	Location
4	120 v	1 ph	Normal	Wall
0				

Clean Power:

UPS:

Emergency Power:

TELECOMMUNICATION AND SPECIAL SYSTEMS:

☐ Phone / Voice ☐ Data Connections:

☐ PA System ☑ Access Control:

☐ Gas Leak Detection ☐ CCTV:

☐ Liquid Leak Detection ☐ Fire Detection Type:

Telecom Notes:

ROOM DATA SHEET

Room Name: Men's Locker Room **Room Number:** OPS-120

Functional Area: Operations Center Level 2 **Space Type:** Building Support

SPACE REQUIREMENT:

Allocated Space : 128 NSF x 1 Rooms Reqd. = **128** Total Net Square Feet

Function:

Occupancy Class: B

General Notes:

STRUCTURAL DATA:

Floor Live Load: 100 psf Floor Capacity Load psf Vibration Requirements: None

Structural Notes:

FINISHES:

Walls: Paint Floors: Vinyl Tile

Ceilings: Acoustic Ceiling Tile Clg. Ht. 9'-0"

Finishes Notes:

ROOM ENVIRONMENT:

Temperature F +/- F Cooling F +/- F Heating

Humidity RH +/- RH Cooling RH +/- RH Heating

Room Pressure Negative Vibration Criteria None

Acoustic Noise Level NC 40-45 EMI Criteria None

SPECIAL REQUIREMENTS:

☐ Storage Cabinet ☐ Fume Hood

☐ Casework ☐ Toxic / Hazardous Materials

Special Requirements Notes:

FIRE PROTECTION:

Hazard Classification: Ordinary Hazard Group ☑ Wet System: ☐ Preaction System

Fire Protection Notes:

HVAC:

Air Changes / Hr ☑ General Exhaust: ☐ Chemical Exhaust:

Recirc / Single Pass Airflow Single Pass ☐ Heat Exhaust: ☑ Smoke Exhaust: by AHU

HVAC Notes:

PLUMBING:

☑ Domestic Water H/C ☑ Floor / Trench Drain Provide floor drains to sanitary waste.

☐ Eyewash / Safety Shower

Plumbing Notes:

PROCESS PIPING:

☐ Compressed Air ☐ DI Water

☐ Nitrogen ☐ Process Cooling Water - Cu

☐ Liquid Nitrogen ☐ Process Cooling Water - Al

☐ Other ☐ Chemical Drain

Piping Notes:

ELECTRICAL:

Lighting Fixture Type: Surface Mount

Lighting Lamp Type: Fluorescent

Lighting Direction: Direct

Light Switching: Occupancy Sensor

Lighting Level (FC): 10-15

Ground:

Electrical Notes:

Power Outlets:

No.	Voltage	Phase	Type	Location
1	120 v	1 ph	Normal	Wall
0				

Clean Power:

UPS:

Emergency Power:

TELECOMMUNICATION AND SPECIAL SYSTEMS:

☐ Phone / Voice ☐ Data Connections:

☐ PA System ☐ Access Control:

☐ Gas Leak Detection ☐ CCTV:

☐ Liquid Leak Detection ☐ Fire Detection Type:

Telecom Notes:

ROOM DATA SHEET

Room Name: Women's Locker Room **Room Number:** OPS-121

Functional Area: Operations Center Level 2 **Space Type:** Building Support

SPACE REQUIREMENT:

Allocated Space : 126 NSF x 1 Rooms Reqd. = **126** Total Net Square Feet

Function:

Occupancy Class: B

General Notes:

STRUCTURAL DATA:

Floor Live Load: 100 psf Floor Capacity Load psf Vibration Requirements: None

Structural Notes:

FINISHES:

Walls: Paint Floors: Vinyl Tile

Ceilings: Acoustic Ceiling Tile Clg. Ht. 9'-0"

Finishes Notes:

ROOM ENVIRONMENT:

Temperature F +/- F Cooling F +/- F Heating

Humidity RH +/- RH Cooling RH +/- RH Heating

Room Pressure Negative Vibration Criteria None

Acoustic Noise Level NC 40-45 EMI Criteria None

SPECIAL REQUIREMENTS:

☐ Storage Cabinet ☐ Fume Hood

☐ Casework ☐ Toxic / Hazardous Materials

Special Requirements Notes:

FIRE PROTECTION:

Hazard Classification: Ordinary Hazard Group ☑ Wet System: ☐ Preaction System

Fire Protection Notes:

HVAC:

Air Changes / Hr ☑ General Exhaust: ☐ Chemical Exhaust:

Recirc / Single Pass Airflow Single Pass ☐ Heat Exhaust: ☑ Smoke Exhaust: by AHU

HVAC Notes:

PLUMBING:

☑ Domestic Water H/C ☑ Floor / Trench Drain Provide floor drains to sanitary waste.

☐ Eyewash / Safety Shower

Plumbing Notes:

PROCESS PIPING:

☐ Compressed Air ☐ DI Water

☐ Nitrogen ☐ Process Cooling Water - Cu

☐ Liquid Nitrogen ☐ Process Cooling Water - Al

☐ Other ☐ Chemical Drain

Piping Notes:

ELECTRICAL:

Lighting Fixture Type: Surface Mount

Lighting Lamp Type: Fluorescent

Lighting Direction: Direct

Light Switching: Occupancy Sensor

Lighting Level (FC): 10-15

Ground:

Electrical Notes:

Power Outlets:

No.	Voltage	Phase	Type	Location
1	120 v	1 ph	Normal	Wall
0				

Clean Power:

UPS:

Emergency Power:

TELECOMMUNICATION AND SPECIAL SYSTEMS:

☐ Phone / Voice ☐ Data Connections:

☐ PA System ☐ Access Control:

☐ Gas Leak Detection ☐ CCTV:

☐ Liquid Leak Detection ☐ Fire Detection Type:

Telecom Notes:

ROOM DATA SHEET

Room Name: Storage **Room Number:** OPS-122

Functional Area: Operations Center Level 2 **Space Type:** Building Support

SPACE REQUIREMENT:

Allocated Space : 108 NSF x 1 Rooms Reqd. = **108** Total Net Square Feet

Function:

Occupancy Class: B

General Notes:

STRUCTURAL DATA:

Floor Live Load: 125 psf Floor Capacity Load psf Vibration Requirements: None

Structural Notes:

FINISHES:

Walls: Paint Floors: Sealed Concrete

Ceilings: Acoustic Ceiling Tile Clg. Ht. 9'-0"

Finishes Notes:

ROOM ENVIRONMENT:

Temperature	75	F +/-	5	F	Cooling	72	F +/-	5	F Heating
Humidity	50	RH +/-	10	RH	Cooling	30	RH +/-	10	RH Heating

Room Pressure: Neutral Vibration Criteria: None

Acoustic Noise Level NC: 40-45 EMI Criteria: None

SPECIAL REQUIREMENTS:

☐ Storage Cabinet ☐ Fume Hood

☐ Casework ☐ Toxic / Hazardous Materials

Special Requirements Notes:

FIRE PROTECTION:

Hazard Classification: Ordinary Hazard Group ☑ Wet System: ☐ Preaction System

Fire Protection Notes:

HVAC:

Air Changes / Hr ☐ General Exhaust: ☐ Chemical Exhaust:

Recirc / Single Pass Airflow: Recirculated ☐ Heat Exhaust: ☑ Smoke Exhaust: by AHU

HVAC Notes:

PLUMBING:

☐ Domestic Water H/C ☐ Floor / Trench Drain

☐ Eyewash / Safety Shower

Plumbing Notes:

PROCESS PIPING:

☐ Compressed Air ☐ DI Water

☐ Nitrogen ☐ Process Cooling Water - Cu

☐ Liquid Nitrogen ☐ Process Cooling Water - Al

☐ Other ☐ Chemical Drain

Piping Notes:

ELECTRICAL:

Lighting Fixture Type: Pendant

Lighting Lamp Type: Fluorescent

Lighting Direction: Direct

Light Switching: Occupancy Sensor

Lighting Level (FC): 15

Ground:

Electrical Notes:

Power Outlets:

No.	Voltage	Phase	Type	Location
4	120 v	1 ph	Normal	Wall
0				

Clean Power:

UPS:

Emergency Power:

TELECOMMUNICATION AND SPECIAL SYSTEMS:

☐ Phone / Voice ☐ Data Connections:

☐ PA System ☐ Access Control:

☐ Gas Leak Detection ☐ CCTV:

☐ Liquid Leak Detection ☐ Fire Detection Type:

Telecom Notes:

ROOM DATA SHEET

Room Name: Accelerator Tunnel **Room Number:** RB-101

Functional Area: Ring Building Ground Level **Space Type:** Accelerator

SPACE REQUIREMENT:

Allocated Space : 37,300 NSF x 1 Rooms Reqd. = **37,300** Total Net Square Feet

Function: Houses the Storage Ring

Occupancy Class: B

General Notes: Radiation shielding required for tunnel walls and roof. Shielded doors required for entry. Equipment entry from infield

STRUCTURAL DATA:

Floor Live Load: 350 psf Floor Capacity Load 3000 psf Vibration Requirements: R = 25nm Power Spectral Density

Structural Notes: Minimize differential settlement

FINISHES:

Walls: Paint Floors: Sealed Concrete

Ceilings: Concrete Clg. Ht. 9'-0"

Finishes Notes:

ROOM ENVIRONMENT:

Temperature	78 F +/- 0.18 F	Cooling	78 F +/- 0.18 F	Heating
Humidity	50 RH +/- 10 RH	Cooling	30 RH +/- 10 RH	Heating
Room Pressure	Positive	Vibration Criteria	R<25 nm PSD
Acoustic Noise Level NC	None	EMI Criteria	No specific criteria established

SPECIAL REQUIREMENTS:

- ☐ Storage Cabinet
- ☐ Casework
- ☐ Fume Hood
- ☐ Toxic / Hazardous Materials

Special Requirements Notes: Shield doors required at ratchet wall for each beamline. Labyrinth entry require elsewhere.

FIRE PROTECTION:

Hazard Classification: Ordinary Hazard Group ☑ Wet System: ☐ Preaction System

Fire Protection Notes:

HVAC:

Air Changes / Hr ☐ General Exhaust: ☐ Chemical Exhaust:

Recirc / Single Pass Airflow Recirculated ☐ Heat Exhaust: ☑ Smoke Exhaust: by AHU

HVAC Notes:

PLUMBING:

- ☐ Domestic Water H/C
- ☐ Eyewash / Safety Shower
- ☑ Floor / Trench Drain — Trench drain around perimeter

Plumbing Notes: Trench drain to have holding sump to allow testing

PROCESS PIPING:

- ☑ Compressed Air
- ☑ Nitrogen — Possible replacement for compresse
- ☑ Liquid Nitrogen — TBD
- ☐ Other
- ☐ DI Water
- ☑ Process Cooling Water - Cu — Cu / Al by ASD
- ☐ Process Cooling Water - Al
- ☐ Chemical Drain

Piping Notes: Process Cooling Water and Process Chilled Water provided by ASD and coordinated by CFD.

ELECTRICAL:

Lighting Fixture Type: Surface Mount

Lighting Lamp Type: Fluorescent

Lighting Direction: Direct

Light Switching: Occupancy Sensor

Lighting Level (FC): 30

Ground:

Electrical Notes: Accelerator power fed from tunnel mezzanine thru tunnel roof.

Power Outlets:

No.	Voltage	Phase	Type	Location
0	120 v	1 ph	Normal	Wall
0				

Clean Power:

UPS:

Emergency Power: Lighting, life safety

TELECOMMUNICATION AND SPECIAL SYSTEMS:

- ☑ Phone / Voice
- ☐ PA System
- ☐ Gas Leak Detection
- ☑ Liquid Leak Detection — In Trench Drain
- ☑ Data Connections:
- ☑ Access Control:
- ☐ CCTV:
- ☑ Fire Detection Type: HSSD

Telecom Notes:

ROOM DATA SHEET

Room Name: Experimental Hall **Room Number:** RB-102A

Functional Area: Ring Building Ground Level **Space Type:** Laboratory

SPACE REQUIREMENT:

Allocated Space : 94,235 NSF x 1 Rooms Reqd. = **94,235** Total Net Square Feet

Function: House Beamlines and experimental hutches

Occupancy Class: B

General Notes: Occupants will be stationed in the LOBs although they will spend substantial time in the Experimental Hall. The Hall

STRUCTURAL DATA:

Floor Live Load: 350 psf Floor Capacity Load 2000 psf Vibration Requirements: VC-E

Structural Notes: Minimize differential settlement

FINISHES:

Walls: Pre-insulated Building Wall Panel Floors: Sealed Concrete

Ceilings: No Ceiling Clg. Ht.

Finishes Notes: Painted steel roof joists. Under side of roof to have acoustical treatment.

ROOM ENVIRONMENT:

Temperature	75	F +/-	1	F	Cooling	75	F +/- 1 F	Heating
Humidity	50	RH +/-	10	RH	Cooling	30	RH +/- 10 RH	Heating

Room Pressure: Positive Vibration Criteria: VC-E

Acoustic Noise Level NC: 55 or lower EMI Criteria: No specific criteria established

SPECIAL REQUIREMENTS:

- ☐ Storage Cabinet
- ☐ Casework
- ☐ Fume Hood
- ☑ Toxic / Hazardous Materials: unknown type

Special Requirements Notes:

FIRE PROTECTION:

Hazard Classification: Ordinary Hazard Group ☑ Wet System: ☐ Preaction System

Fire Protection Notes:

HVAC:

Air Changes / Hr ☐ General Exhaust: ☑ Chemical Exhaust: Hutch Exhaust

Recirc / Single Pass Airflow: Recirculated ☐ Heat Exhaust: ☑ Smoke Exhaust: by AHU

HVAC Notes:

PLUMBING:

- ☐ Domestic Water H/C
- ☐ Floor / Trench Drain
- ☑ Eyewash / Safety Shower: Distributed

Plumbing Notes:

PROCESS PIPING:

- ☑ Compressed Air: At tunnel mezzanine
- ☑ Nitrogen: At tunnel mezzanine
- ☑ Liquid Nitrogen: At tunnel mezzanine
- ☐ Other
- ☐ DI Water
- ☑ Process Cooling Water - Cu: Cu only/ by EF
- ☐ Process Cooling Water - Al
- ☐ Chemical Drain

Piping Notes:

ELECTRICAL:

Lighting Fixture Type: Pendant

Lighting Lamp Type: Metal Halide

Lighting Direction: Direct

Light Switching: Occupancy Sensor

Lighting Level (FC): 30

Ground: Instrument Reference Ground

Electrical Notes: Each panelboard for beamlines is served by a 75kVA transformer. Panelboards mounted on tunnel mezzanine.

Power Outlets:

No.	Voltage	Phase	Type	Location
60	120 v	1 ph	Normal	Wall
0				

Clean Power:

UPS:

Emergency Power:

TELECOMMUNICATION AND SPECIAL SYSTEMS:

- ☑ Phone / Voice
- ☑ PA System
- ☐ Gas Leak Detection
- ☐ Liquid Leak Detection
- ☑ Data Connections:
- ☑ Access Control:
- ☐ CCTV:
- ☑ Fire Detection Type: HSSD

Telecom Notes:

ROOM DATA SHEET

Room Name: Access Corridor **Room Number:** RB-102B

Functional Area: Ring Building Ground Level **Space Type:** Circulation

SPACE REQUIREMENT:

Allocated Space : 33,018 NSF x 1 Rooms Reqd. = **33,018** Total Net Square Feet

Function: Corridor around the outside of the Experimental Hall

Occupancy Class: B

General Notes:

STRUCTURAL DATA:

Floor Live Load: 350 psf Floor Capacity Load psf Vibration Requirements: None

Structural Notes:

FINISHES:

Walls: Pre-insulated Building Wall Panel Floors: Sealed Concrete

Ceilings: No Ceiling Clg. Ht.

Finishes Notes:

ROOM ENVIRONMENT:

Temperature	75	F +/-	1	F	Cooling	75	F +/-	1	F Heating
Humidity	50	RH +/-	10	RH	Cooling	30	RH +/-	10	RH Heating

Room Pressure: Positive Vibration Criteria: VC-E

Acoustic Noise Level NC: 55 or lower EMI Criteria: None

SPECIAL REQUIREMENTS:

- ☐ Storage Cabinet
- ☐ Casework
- ☐ Fume Hood
- ☐ Toxic / Hazardous Materials

Special Requirements Notes:

FIRE PROTECTION:

Hazard Classification: Ordinary Hazard Group ☑ Wet System: ☐ Preaction System

Fire Protection Notes:

HVAC:

Air Changes / Hr ☐ General Exhaust: ☐ Chemical Exhaust:

Recirc / Single Pass Airflow: Recirculated ☐ Heat Exhaust: ☑ Smoke Exhaust: by AHU

HVAC Notes:

PLUMBING:

- ☐ Domestic Water H/C
- ☐ Eyewash / Safety Shower
- ☑ Floor / Trench Drain: Trench drain around perimiter

Plumbing Notes:

PROCESS PIPING:

- ☑ Compressed Air
- ☐ Nitrogen
- ☐ Liquid Nitrogen
- ☐ Other
- ☐ DI Water
- ☐ Process Cooling Water - Cu
- ☐ Process Cooling Water - Al
- ☐ Chemical Drain

Piping Notes:

ELECTRICAL:

Lighting Fixture Type: Pendant

Lighting Lamp Type: Fluorescent

Lighting Direction: Direct

Light Switching: Low Voltage Switch

Lighting Level (FC): 30

Ground:

Electrical Notes:

Power Outlets:

No.	Voltage	Phase	Type	Location
60	120 v	1 ph	Normal	Wall
0				

Clean Power:

UPS:

Emergency Power:

TELECOMMUNICATION AND SPECIAL SYSTEMS:

- ☑ Phone / Voice
- ☑ PA System
- ☐ Gas Leak Detection
- ☐ Liquid Leak Detection
- ☐ Data Connections:
- ☑ Access Control:
- ☐ CCTV:
- ☑ Fire Detection Type: HSSD

Telecom Notes:

ROOM DATA SHEET

Room Name: Tunnel Mezzanine **Room Number:** RB-103

Functional Area: Ring Building Mezzanine **Space Type:** Accelerator

SPACE REQUIREMENT:

Allocated Space : 50,950 NSF x 1 Rooms Reqd. = **50,950** Total Net Square Feet

Function: Space for Electrical Gear supporting storage ring.

Occupancy Class: B

General Notes:

STRUCTURAL DATA:

Floor Live Load: 350 psf Floor Capacity Load psf Vibration Requirements: None

Structural Notes:

FINISHES:

Walls: Pre-insulated Building Wall Panel Floors: Sealed Concrete

Ceilings: No Ceiling Clg. Ht.

Finishes Notes:

ROOM ENVIRONMENT:

Temperature	75	F +/-	5	F	Cooling	75	F +/- 5 F	Heating
Humidity	50	RH +/-	10	RH	Cooling	30	RH +/- 10 RH	Heating

Room Pressure: Positive Vibration Criteria: None

Acoustic Noise Level NC: 55 or lower EMI Criteria: None

SPECIAL REQUIREMENTS:

- ☐ Storage Cabinet
- ☐ Casework
- ☐ Fume Hood
- ☐ Toxic / Hazardous Materials

Special Requirements Notes:

FIRE PROTECTION:

Hazard Classification: Ordinary Hazard Group ☑ Wet System: ☐ Preaction System

Fire Protection Notes:

HVAC:

Air Changes / Hr ☐ General Exhaust: ☐ Chemical Exhaust:

Recirc / Single Pass Airflow: Recirculated ☐ Heat Exhaust: ☑ Smoke Exhaust: by AHU

HVAC Notes:

PLUMBING:

- ☐ Domestic Water H/C
- ☐ Eyewash / Safety Shower
- ☑ Floor / Trench Drain: Floor drains

Plumbing Notes:

PROCESS PIPING:

- ☐ Compressed Air
- ☐ Nitrogen
- ☐ Liquid Nitrogen
- ☐ Other
- ☐ DI Water
- ☐ Process Cooling Water - Cu
- ☑ Process Cooling Water - Al: by ASD
- ☐ Chemical Drain

Piping Notes: Chilled Water supply and return for power supply cooling is required.

ELECTRICAL:

Lighting Fixture Type: Pendant

Lighting Lamp Type: Fluorescent

Lighting Direction: Direct

Light Switching: Low Voltage Switch

Lighting Level (FC): 30

Ground:

Electrical Notes:

Power Outlets:

No.	Voltage	Phase	Type	Location
60	120 v	1 ph	Normal	Wall
0				

Clean Power:

UPS:

Emergency Power:

TELECOMMUNICATION AND SPECIAL SYSTEMS:

- ☑ Phone / Voice
- ☑ PA System
- ☐ Gas Leak Detection
- ☐ Liquid Leak Detection
- ☑ Data Connections:
- ☐ Access Control:
- ☐ CCTV:
- ☑ Fire Detection Type: HSSD

Telecom Notes:

ROOM DATA SHEET

Room Name: Loading Dock **Room Number:** RB-104

Functional Area: Ring Building Ground Level **Space Type:** Building Support

SPACE REQUIREMENT:

Allocated Space : 2,060 NSF x 1 Rooms Reqd. = **2,060** Total Net Square Feet

Function: Loading Dock for NSLS-II facility

Occupancy Class: B

General Notes:

STRUCTURAL DATA:

Floor Live Load: 350 psf Floor Capacity Load psf Vibration Requirements: None

Structural Notes:

FINISHES:

Walls: Pre-insulated Building Wall Panel Floors: Sealed Concrete

Ceilings: No Ceiling Clg. Ht.

Finishes Notes:

ROOM ENVIRONMENT:

Temperature	75 F +/-	5 F	Cooling	75 F +/-	5 F	Heating
Humidity	0 RH +/-	0 RH	Cooling	0 RH +/-	0 RH	Heating

Room Pressure: Positive Vibration Criteria: None

Acoustic Noise Level NC: None EMI Criteria: None

SPECIAL REQUIREMENTS:

- ☐ Storage Cabinet
- ☐ Casework
- ☐ Fume Hood
- ☐ Toxic / Hazardous Materials

Special Requirements Notes:

FIRE PROTECTION:

Hazard Classification: Ordinary Hazard Group ☑ Wet System: ☐ Preaction System

Fire Protection Notes:

HVAC:

Air Changes / Hr ☐ General Exhaust: ☐ Chemical Exhaust:

Recirc / Single Pass Airflow: Recirculated ☐ Heat Exhaust: ☐ Smoke Exhaust: by AHU

HVAC Notes:

PLUMBING:

- ☐ Domestic Water H/C
- ☐ Eyewash / Safety Shower
- ☐ Floor / Trench Drain

Plumbing Notes:

PROCESS PIPING:

- ☑ Compressed Air
- ☐ Nitrogen
- ☐ Liquid Nitrogen
- ☐ Other
- ☐ DI Water
- ☐ Process Cooling Water - Cu
- ☐ Process Cooling Water - Al
- ☐ Chemical Drain

Piping Notes:

ELECTRICAL:

Lighting Fixture Type: Pendant

Lighting Lamp Type: Fluorescent

Lighting Direction: Direct

Light Switching: Occupancy Sensor

Lighting Level (FC): 30

Ground:

Electrical Notes:

Power Outlets:

No.	Voltage	Phase	Type	Location
8	120 v	1 ph	Normal	Wall
0				

Clean Power:

UPS:

Emergency Power:

TELECOMMUNICATION AND SPECIAL SYSTEMS:

- ☑ Phone / Voice
- ☑ PA System
- ☐ Gas Leak Detection
- ☐ Liquid Leak Detection
- ☑ Data Connections:
- ☑ Access Control:
- ☐ CCTV:
- ☐ Fire Detection Type:

Telecom Notes:

ROOM DATA SHEET

Room Name: Hazardous Materials Storage **Room Number:** RB-105

Functional Area: Ring Building Ground Level **Space Type:** Building Support

SPACE REQUIREMENT:

Allocated Space : 450 NSF x 1 Rooms Reqd. = **450** Total Net Square Feet

Function: Receipt and storage of hazardous materials

Occupancy Class: H-6

General Notes:

STRUCTURAL DATA:

Floor Live Load: 125 psf Floor Capacity Load psf Vibration Requirements: None

Structural Notes:

FINISHES:

Walls: Pre-insulated Building Wall Panel Floors: Sealed Concrete

Ceilings: No Ceiling Clg. Ht.

Finishes Notes:

ROOM ENVIRONMENT:

Temperature	75	F +/-	5	F	Cooling	75	F +/-	5	F Heating
Humidity	50	RH +/-	10	RH	Cooling	30	RH +/-	10	RH Heating

Room Pressure: Negative Vibration Criteria: None

Acoustic Noise Level NC: 45-50 EMI Criteria: None

SPECIAL REQUIREMENTS:

- ☐ Storage Cabinet
- ☐ Casework
- ☐ Fume Hood
- ☑ Toxic / Hazardous Materials

Special Requirements Notes:

FIRE PROTECTION:

Hazard Classification: Ordinary Hazard Group ☑ Wet System: ☐ Preaction System

Fire Protection Notes:

HVAC:

Air Changes / Hr

Recirc / Single Pass Airflow: Single Pass

HVAC Notes:

- ☐ General Exhaust:
- ☐ Heat Exhaust:
- ☑ Chemical Exhaust:
- ☑ Smoke Exhaust: by AHU

PLUMBING:

- ☐ Domestic Water H/C
- ☑ Eyewash / Safety Shower
- ☐ Floor / Trench Drain

Plumbing Notes:

PROCESS PIPING:

- ☐ Compressed Air
- ☐ Nitrogen
- ☐ Liquid Nitrogen
- ☐ Other
- ☐ DI Water
- ☐ Process Cooling Water - Cu
- ☐ Process Cooling Water - Al
- ☐ Chemical Drain

Piping Notes:

ELECTRICAL:

Lighting Fixture Type: Pendant

Lighting Lamp Type: Fluorescent

Lighting Direction: Direct

Light Switching: Occupancy Sensor

Lighting Level (FC): 30

Ground:

Electrical Notes: Wall outlets for standard power to be suitable for flammable / hazardous environment.

Power Outlets:

No.	Voltage	Phase	Type	Location
0	120 v	1 ph	Normal	Wall
0				

Clean Power:

UPS:

Emergency Power:

TELECOMMUNICATION AND SPECIAL SYSTEMS:

- ☑ Phone / Voice
- ☑ PA System
- ☑ Gas Leak Detection
- ☐ Liquid Leak Detection
- ☐ Data Connections:
- ☑ Access Control:
- ☐ CCTV:
- ☐ Fire Detection Type:

Telecom Notes:

ROOM DATA SHEET

Room Name: Stock Room **Room Number:** RB-106

Functional Area: Ring Building Ground Level **Space Type:** Building Support

SPACE REQUIREMENT:

Allocated Space : 1,618 NSF x 1 Rooms Reqd. = **1,618** Total Net Square Feet

Function: Receiving and storage for non-hazardous materials.

Occupancy Class: B

General Notes:

STRUCTURAL DATA:

Floor Live Load: 125 psf Floor Capacity Load psf Vibration Requirements: None

Structural Notes:

FINISHES:

Walls: Pre-insulated Building Wall Panel Floors: Sealed Concrete

Ceilings: No Ceiling Clg. Ht.

Finishes Notes:

ROOM ENVIRONMENT:

Temperature	75	F +/-	5	F	Cooling	75	F +/-	5	F Heating
Humidity	50	RH +/-	10	RH	Cooling	30	RH +/-	10	RH Heating

Room Pressure: Positive Vibration Criteria: None

Acoustic Noise Level NC: 40-45 EMI Criteria: None

SPECIAL REQUIREMENTS:

- ☐ Storage Cabinet
- ☐ Casework
- ☐ Fume Hood
- ☐ Toxic / Hazardous Materials

Special Requirements Notes:

FIRE PROTECTION:

Hazard Classification: Ordinary Hazard Group ☑ Wet System: ☐ Preaction System

Fire Protection Notes:

HVAC:

Air Changes / Hr ☐ General Exhaust: ☐ Chemical Exhaust:

Recirc / Single Pass Airflow: Recirculated ☐ Heat Exhaust: ☑ Smoke Exhaust: by AHU

HVAC Notes:

PLUMBING:

- ☐ Domestic Water H/C
- ☐ Eyewash / Safety Shower
- ☐ Floor / Trench Drain

Plumbing Notes:

PROCESS PIPING:

- ☐ Compressed Air
- ☐ Nitrogen
- ☐ Liquid Nitrogen
- ☐ Other
- ☐ DI Water
- ☐ Process Cooling Water - Cu
- ☐ Process Cooling Water - Al
- ☐ Chemical Drain

Piping Notes:

ELECTRICAL:

Lighting Fixture Type: Recessed Troffer

Lighting Lamp Type: Fluorescent

Lighting Direction: Direct

Light Switching: Occupancy Sensor

Lighting Level (FC): 30

Ground:

Electrical Notes:

Power Outlets:

No.	Voltage	Phase	Type	Location
4	120 v	1 ph	Normal	Wall
0				

Clean Power:

UPS:

Emergency Power:

TELECOMMUNICATION AND SPECIAL SYSTEMS:

- ☑ Phone / Voice
- ☑ PA System
- ☐ Gas Leak Detection
- ☐ Liquid Leak Detection
- ☑ Data Connections:
- ☑ Access Control:
- ☐ CCTV:
- ☐ Fire Detection Type:

Telecom Notes:

ROOM DATA SHEET

Room Name: Grille **Room Number:** RB-107

Functional Area: Ring Building Ground Level **Space Type:** Interaction Area

SPACE REQUIREMENT:

Allocated Space : 257 NSF x 1 Rooms Reqd. = **257** Total Net Square Feet
Function:
Occupancy Class: B
General Notes:

STRUCTURAL DATA:

Floor Live Load: 100 psf Floor Capacity Load psf Vibration Requirements: None
Structural Notes:

FINISHES:

Walls: Pre-insulated Building Wall Panel Floors: Linoleum Sheet
Ceilings: Acoustic Ceiling Tile Clg. Ht. 9'-0"
Finishes Notes:

ROOM ENVIRONMENT:

Temperature 75 F +/- 5 F Cooling 75 F +/- 5 F Heating
Humidity 50 RH +/- 10 RH Cooling 30 RH +/- 10 RH Heating
Room Pressure Negative Vibration Criteria None
Acoustic Noise Level NC 40-45 EMI Criteria None

SPECIAL REQUIREMENTS:

☐ Storage Cabinet ☐ Fume Hood
☐ Casework ☐ Toxic / Hazardous Materials
Special Requirements Notes:

FIRE PROTECTION:

Hazard Classification: Ordinary Hazard Group ☑ Wet System: ☐ Preaction System
Fire Protection Notes:

HVAC:

Air Changes / Hr ☑ General Exhaust: ☐ Chemical Exhaust:
Recirc / Single Pass Airflow Recirculated ☐ Heat Exhaust: ☑ Smoke Exhaust: by AHU
HVAC Notes:

PLUMBING:

☑ Domestic Water H/C ☑ Floor / Trench Drain Provide floor drains to sanitary waste.
☐ Eyewash / Safety Shower
Plumbing Notes:

PROCESS PIPING:

☐ Compressed Air ☐ DI Water
☐ Nitrogen ☐ Process Cooling Water - Cu
☐ Liquid Nitrogen ☐ Process Cooling Water - Al
☐ Other ☐ Chemical Drain
Piping Notes:

ELECTRICAL:

Lighting Fixture Type: Recessed Troffer
Lighting Lamp Type: Fluorescent
Lighting Direction: Direct
Light Switching: Occupancy Sensor
Lighting Level (FC): 30
Ground:
Electrical Notes:

Power Outlets:

No.	Voltage	Phase	Type	Location
8	120 v	1 ph	Normal	Wall
0				

Clean Power:
UPS:
Emergency Power:

TELECOMMUNICATION AND SPECIAL SYSTEMS:

☐ Phone / Voice ☐ Data Connections:
☐ PA System ☐ Access Control:
☐ Gas Leak Detection ☐ CCTV:
☐ Liquid Leak Detection ☐ Fire Detection Type:
Telecom Notes:

ROOM DATA SHEET

Room Name: RF Cavity Room **Room Number:** RF-101

Functional Area: RF Building Ground Level **Space Type:** Accelerator

SPACE REQUIREMENT:

Allocated Space : 9,756 NSF x 1 Rooms Reqd. = **9,756** Total Net Square Feet

Function: Location of RF cavities and support

Occupancy Class: B

General Notes:

STRUCTURAL DATA:

Floor Live Load: 350 psf Floor Capacity Load psf Vibration Requirements: None

Structural Notes:

FINISHES:

Walls: Paint Floors: Sealed Concrete

Ceilings: No Ceiling Clg. Ht. 20'-0" clear

Finishes Notes:

ROOM ENVIRONMENT:

Temperature	75	F +/-	1	F	Cooling	72	F +/- 1 F	Heating
Humidity	50	RH +/-	10	RH	Cooling	30	RH +/- 10 RH	Heating

Room Pressure: Neutral Vibration Criteria: None

Acoustic Noise Level NC: None EMI Criteria: None

SPECIAL REQUIREMENTS:

- ☐ Storage Cabinet
- ☐ Casework
- ☐ Fume Hood
- ☐ Toxic / Hazardous Materials

Special Requirements Notes:

FIRE PROTECTION:

Hazard Classification: Ordinary Hazard Group ☑ Wet System: ☐ Preaction System

Fire Protection Notes:

HVAC:

Air Changes / Hr

Recirc / Single Pass Airflow: Recirculated

- ☐ General Exhaust:
- ☐ Heat Exhaust:
- ☐ Chemical Exhaust:
- ☑ Smoke Exhaust: by AHU

HVAC Notes:

PLUMBING:

- ☐ Domestic Water H/C
- ☑ Eyewash / Safety Shower
- ☐ Floor / Trench Drain

Plumbing Notes:

PROCESS PIPING:

- ☑ Compressed Air
- ☐ Nitrogen
- ☐ Liquid Nitrogen
- ☐ Other
- ☐ DI Water
- ☐ Process Cooling Water - Cu
- ☐ Process Cooling Water - Al
- ☐ Chemical Drain

Piping Notes:

ELECTRICAL:

Lighting Fixture Type: Pendant

Lighting Lamp Type: Fluorescent

Lighting Direction: Direct

Light Switching: Occupancy Sensor

Lighting Level (FC): 30

Ground:

Electrical Notes:

Power Outlets:

No.	Voltage	Phase	Type	Location
12	120 v	1 ph	Normal	Wall
0				

Clean Power:

UPS:

Emergency Power:

TELECOMMUNICATION AND SPECIAL SYSTEMS:

- ☑ Phone / Voice
- ☑ PA System
- ☐ Gas Leak Detection
- ☐ Liquid Leak Detection
- ☑ Data Connections:
- ☑ Access Control:
- ☐ CCTV:
- ☐ Fire Detection Type:

Telecom Notes:

ROOM DATA SHEET

Room Name: RF Test **Room Number:** RF-102

Functional Area: RF Building Ground Level **Space Type:** Accelerator

SPACE REQUIREMENT:

Allocated Space : 426 NSF x 1 Rooms Reqd. = **426** Total Net Square Feet

Function: RF Test

Occupancy Class: B

General Notes: Radiation shielding required for walls and roof. Labyrinth for entrance to be provided.

STRUCTURAL DATA:

Floor Live Load: 350 psf Floor Capacity Load psf Vibration Requirements: None

Structural Notes:

FINISHES:

Walls: Paint Floors: Sealed Concrete

Ceilings: No Ceiling Clg. Ht. 20'-0" clear

Finishes Notes:

ROOM ENVIRONMENT:

Temperature	75	F +/-	1	F	Cooling	75	F +/- 1 F	Heating
Humidity	50	RH +/-	10	RH	Cooling	30	RH +/- 10 RH	Heating

Room Pressure: Positive Vibration Criteria: None

Acoustic Noise Level NC: None EMI Criteria: None

SPECIAL REQUIREMENTS:

- ☐ Storage Cabinet
- ☐ Casework
- ☐ Fume Hood
- ☐ Toxic / Hazardous Materials

Special Requirements Notes: Labyrinth entry required

FIRE PROTECTION:

Hazard Classification: Ordinary Hazard Group ☑ Wet System: ☐ Preaction System

Fire Protection Notes:

HVAC:

Air Changes / Hr

Recirc / Single Pass Airflow: Recirculated

- ☐ General Exhaust:
- ☐ Heat Exhaust:
- ☐ Chemical Exhaust:
- ☑ Smoke Exhaust: by AHU

HVAC Notes:

PLUMBING:

- ☐ Domestic Water H/C
- ☐ Eyewash / Safety Shower
- ☐ Floor / Trench Drain

Plumbing Notes:

PROCESS PIPING:

- ☑ Compressed Air
- ☐ Nitrogen
- ☑ Liquid Nitrogen
- ☐ Other
- ☐ DI Water
- ☐ Process Cooling Water - Cu
- ☐ Process Cooling Water - Al
- ☐ Chemical Drain

Piping Notes:

ELECTRICAL:

Lighting Fixture Type: Pendant

Lighting Lamp Type: Fluorescent

Lighting Direction: Direct

Light Switching: Dimmer

Lighting Level (FC): 30

Ground:

Electrical Notes:

Power Outlets:

No.	Voltage	Phase	Type	Location
4	120 v	1 ph	Normal	Wall
0				

Clean Power:

UPS:

Emergency Power:

TELECOMMUNICATION AND SPECIAL SYSTEMS:

- ☑ Phone / Voice
- ☑ PA System
- ☐ Gas Leak Detection
- ☐ Liquid Leak Detection
- ☑ Data Connections:
- ☐ Access Control:
- ☐ CCTV:
- ☐ Fire Detection Type:

Telecom Notes:

ROOM DATA SHEET

Room Name: Service Building #1 **Room Number:** SB-101

Functional Area: Service Buildings Ground Level **Space Type:** Building Support

SPACE REQUIREMENT:

Allocated Space : 9,626 NSF x 1 Rooms Reqd. = **9,626** Total Net Square Feet

Function: Mechanical and Electrical room

Occupancy Class: B

General Notes:

STRUCTURAL DATA:

Floor Live Load: 350/150 psf Floor Capacity Load psf Vibration Requirements: None

Structural Notes: 350 psf ground floor ; 150 psf second floor

FINISHES:

Walls: Paint Floors: Sealed Concrete

Ceilings: No Ceiling Clg. Ht.

Finishes Notes:

ROOM ENVIRONMENT:

Temperature	78	F +/-	5	F	Cooling	78	F +/- 5 F	Heating
Humidity		RH +/-	0	RH	Cooling	0	RH +/- 0 RH	Heating

Room Pressure: Neutral Vibration Criteria: None

Acoustic Noise Level NC: Per ACGIH TLVs EMI Criteria: None

SPECIAL REQUIREMENTS:

- ☐ Storage Cabinet
- ☐ Casework
- ☐ Fume Hood
- ☐ Toxic / Hazardous Materials

Special Requirements Notes:

FIRE PROTECTION:

Hazard Classification: Ordinary Hazard Group ☑ Wet System: ☐ Preaction System

Fire Protection Notes:

HVAC:

Air Changes / Hr: 6-10 AC/Hr ☐ General Exhaust: ☐ Chemical Exhaust:

Recirc / Single Pass Airflow: Single Pass ☑ Heat Exhaust: Summer Ventilatio ☑ Smoke Exhaust: Yes

HVAC Notes:

PLUMBING:

- ☑ Domestic Water H/C
- ☑ Eyewash / Safety Shower
- ☑ Floor / Trench Drain — Provide floor drains to sanitary waste.

Plumbing Notes:

PROCESS PIPING:

- ☑ Compressed Air
- ☐ Nitrogen
- ☐ Liquid Nitrogen
- ☐ Other
- ☐ DI Water
- ☐ Process Cooling Water - Cu
- ☐ Process Cooling Water - Al
- ☐ Chemical Drain

Piping Notes:

ELECTRICAL:

Lighting Fixture Type: Pendant

Lighting Lamp Type: Fluorescent

Lighting Direction: Direct

Light Switching: Occupancy Sensor

Lighting Level (FC): 15

Ground:

Electrical Notes:

Power Outlets:

No.	Voltage	Phase	Type	Location
24	120 v	1 ph	Normal	Wall
0				

Clean Power:

UPS:

Emergency Power:

TELECOMMUNICATION AND SPECIAL SYSTEMS:

- ☑ Phone / Voice
- ☑ PA System
- ☐ Gas Leak Detection
- ☐ Liquid Leak Detection
- ☑ Data Connections:
- ☑ Access Control:
- ☐ CCTV:
- ☐ Fire Detection Type:

Telecom Notes:

ROOM DATA SHEET

Room Name: Service Building #2 **Room Number:** SB-102

Functional Area: Service Buildings Ground Level **Space Type:** Building Support

SPACE REQUIREMENT:

Allocated Space : 9,626 NSF x 1 Rooms Reqd. = **9,626** Total Net Square Feet

Function: Mechanical and Electrical room

Occupancy Class: B

General Notes:

STRUCTURAL DATA:

Floor Live Load: 350/150 psf Floor Capacity Load psf Vibration Requirements: None

Structural Notes: 350 psf ground floor ; 150 psf second floor

FINISHES:

Walls: Paint Floors: Sealed Concrete

Ceilings: No Ceiling Clg. Ht.

Finishes Notes:

ROOM ENVIRONMENT:

Temperature	78 F +/-	5 F	Cooling	78 F +/-	5 F	Heating		
Humidity	0 RH +/-	0 RH	Cooling	0 RH +/-	0 RH	Heating		
Room Pressure	Neutral		Vibration Criteria	None				
Acoustic Noise Level NC	Per ACGIH TLVs		EMI Criteria	None				

SPECIAL REQUIREMENTS:

- ☐ Storage Cabinet
- ☐ Casework
- ☐ Fume Hood
- ☐ Toxic / Hazardous Materials

Special Requirements Notes:

FIRE PROTECTION:

Hazard Classification: Ordinary Hazard Group ☑ Wet System: ☐ Preaction System

Fire Protection Notes:

HVAC:

Air Changes / Hr 6-10 AC/Hr ☐ General Exhaust: ☐ Chemical Exhaust:

Recirc / Single Pass Airflow Single Pass ☑ Heat Exhaust: Summer Ventilatio ☑ Smoke Exhaust: Yes

HVAC Notes:

PLUMBING:

- ☑ Domestic Water H/C
- ☑ Eyewash / Safety Shower
- ☑ Floor / Trench Drain — Provide floor drains to sanitary waste.

Plumbing Notes:

PROCESS PIPING:

- ☑ Compressed Air
- ☐ Nitrogen
- ☐ Liquid Nitrogen
- ☐ Other
- ☐ DI Water
- ☐ Process Cooling Water - Cu
- ☐ Process Cooling Water - Al
- ☐ Chemical Drain

Piping Notes:

ELECTRICAL:

Lighting Fixture Type: Pendant

Lighting Lamp Type: Fluorescent

Lighting Direction: Direct

Light Switching: Occupancy Sensor

Lighting Level (FC): 15

Ground:

Electrical Notes:

Power Outlets:

No.	Voltage	Phase	Type	Location
24	120 v	1 ph	Normal	Wall
0				

Clean Power:

UPS:

Emergency Power:

TELECOMMUNICATION AND SPECIAL SYSTEMS:

- ☑ Phone / Voice
- ☑ PA System
- ☐ Gas Leak Detection
- ☐ Liquid Leak Detection
- ☑ Data Connections:
- ☑ Access Control:
- ☐ CCTV:
- ☐ Fire Detection Type:

Telecom Notes:

ROOM DATA SHEET

Room Name: Service Building #3 **Room Number:** SB-103

Functional Area: Service Buildings Ground Level **Space Type:** Building Support

SPACE REQUIREMENT:

Allocated Space : 9,626 NSF x 1 Rooms Reqd. = **9,626** Total Net Square Feet

Function: Mechanical and Electrical room

Occupancy Class: B

General Notes:

STRUCTURAL DATA:

Floor Live Load: 350/150 psf Floor Capacity Load psf Vibration Requirements: None

Structural Notes: 350 psf ground floor ; 150 psf second floor

FINISHES:

Walls: Paint Floors: Sealed Concrete

Ceilings: No Ceiling Clg. Ht.

Finishes Notes:

ROOM ENVIRONMENT:

Temperature	78 F +/-	5 F	Cooling	78 F +/-	5 F	Heating		
Humidity	0 RH +/-	0 RH	Cooling	0 RH +/-	0 RH	Heating		
Room Pressure	Neutral		Vibration Criteria	None				
Acoustic Noise Level NC	Per ACGIH TLVs		EMI Criteria	None				

SPECIAL REQUIREMENTS:

- ☐ Storage Cabinet
- ☐ Casework
- ☐ Fume Hood
- ☐ Toxic / Hazardous Materials

Special Requirements Notes:

FIRE PROTECTION:

Hazard Classification: Ordinary Hazard Group ☑ Wet System: ☐ Preaction System

Fire Protection Notes:

HVAC:

Air Changes / Hr 6-10 AC/Hr ☐ General Exhaust: ☐ Chemical Exhaust:

Recirc / Single Pass Airflow Single Pass ☑ Heat Exhaust: Summer Ventilatio ☑ Smoke Exhaust: Yes

HVAC Notes:

PLUMBING:

- ☑ Domestic Water H/C
- ☑ Eyewash / Safety Shower
- ☑ Floor / Trench Drain — Provide floor drains to sanitary waste.

Plumbing Notes:

PROCESS PIPING:

- ☑ Compressed Air
- ☐ Nitrogen
- ☐ Liquid Nitrogen
- ☐ Other
- ☐ DI Water
- ☐ Process Cooling Water - Cu
- ☐ Process Cooling Water - Al
- ☐ Chemical Drain

Piping Notes:

ELECTRICAL:

Lighting Fixture Type: Pendant

Lighting Lamp Type: Fluorescent

Lighting Direction: Direct

Light Switching: Occupancy Sensor

Lighting Level (FC): 15

Ground:

Electrical Notes:

Power Outlets:

No.	Voltage	Phase	Type	Location
24	120 v	1 ph	Normal	Wall
0				

Clean Power:

UPS:

Emergency Power:

TELECOMMUNICATION AND SPECIAL SYSTEMS:

- ☑ Phone / Voice
- ☑ PA System
- ☐ Gas Leak Detection
- ☐ Liquid Leak Detection
- ☑ Data Connections:
- ☑ Access Control:
- ☐ CCTV:
- ☐ Fire Detection Type:

Telecom Notes:

ROOM DATA SHEET

Room Name: Service Building #4 **Room Number:** SB-104

Functional Area: Service Buildings Ground Level **Space Type:** Building Support

SPACE REQUIREMENT:

Allocated Space : 9,626 NSF x 1 Rooms Reqd. = **9,626** Total Net Square Feet

Function: Mechanical and Electrical Room

Occupancy Class: B

General Notes:

STRUCTURAL DATA:

Floor Live Load: 350/150 psf Floor Capacity Load psf Vibration Requirements: None

Structural Notes: 350 psf ground floor ; 150 psf second floor

FINISHES:

Walls: Floors:

Ceilings: Clg. Ht.

Finishes Notes:

ROOM ENVIRONMENT:

Temperature	78	F +/-	5	F	Cooling	78	F +/- 5 F	Heating
Humidity	0	RH +/-	0	RH	Cooling	0	RH +/- 0 RH	Heating

Room Pressure: Neutral Vibration Criteria: None

Acoustic Noise Level NC: Per ACGIH TLVs EMI Criteria: None

SPECIAL REQUIREMENTS:

- ☐ Storage Cabinet
- ☐ Casework
- ☐ Fume Hood
- ☐ Toxic / Hazardous Materials

Special Requirements Notes:

FIRE PROTECTION:

Hazard Classification: ☐ Wet System: ☐ Preaction System

Fire Protection Notes:

HVAC:

Air Changes / Hr: 6-10 AC/Hr ☐ General Exhaust: ☐ Chemical Exhaust:

Recirc / Single Pass Airflow: Single Pass ☑ Heat Exhaust: Summer Ventilatio ☑ Smoke Exhaust: Yes

HVAC Notes:

PLUMBING:

- ☑ Domestic Water H/C
- ☐ Eyewash / Safety Shower
- ☑ Floor / Trench Drain: Provide floor drains to sanitary waste.

Plumbing Notes:

PROCESS PIPING:

- ☑ Compressed Air
- ☐ Nitrogen
- ☐ Liquid Nitrogen
- ☐ Other
- ☐ DI Water
- ☐ Process Cooling Water - Cu
- ☐ Process Cooling Water - Al
- ☐ Chemical Drain

Piping Notes:

ELECTRICAL:

Lighting Fixture Type: Pendant

Lighting Lamp Type: Fluorescent

Lighting Direction: Direct

Light Switching: Occupancy Sensor

Lighting Level (FC): 15

Ground:

Electrical Notes:

Power Outlets:

No.	Voltage	Phase	Type	Location
24	120 v	1 ph	Normal	Wall
0				

Clean Power:

UPS:

Emergency Power:

TELECOMMUNICATION AND SPECIAL SYSTEMS:

- ☑ Phone / Voice
- ☑ PA System
- ☐ Gas Leak Detection
- ☐ Liquid Leak Detection
- ☑ Data Connections:
- ☑ Access Control:
- ☐ CCTV:
- ☐ Fire Detection Type:

Telecom Notes:

ROOM DATA SHEET

Room Name: Service Building #5 **Room Number:** SB-105

Functional Area: Service Buildings Ground Level **Space Type:** Building Support

SPACE REQUIREMENT:

Allocated Space : 9,626 NSF x 1 Rooms Reqd. = **9,626** Total Net Square Feet

Function: Mechanical and Electrical Room

Occupancy Class: B

General Notes:

STRUCTURAL DATA:

Floor Live Load: 350/150 psf Floor Capacity Load psf Vibration Requirements: None

Structural Notes: 350 psf ground floor ; 150 psf second floor

FINISHES:

Walls: Floors:

Ceilings: Clg. Ht.

Finishes Notes:

ROOM ENVIRONMENT:

Temperature	78	F +/-	5	F	Cooling	78	F +/- 5 F	Heating
Humidity	0	RH +/-	0	RH	Cooling	0	RH +/- 0 RH	Heating

Room Pressure: Neutral Vibration Criteria: None

Acoustic Noise Level NC: Per ACGIH TLVs EMI Criteria: None

SPECIAL REQUIREMENTS:

- ☐ Storage Cabinet
- ☐ Casework
- ☐ Fume Hood
- ☐ Toxic / Hazardous Materials

Special Requirements Notes:

FIRE PROTECTION:

Hazard Classification: ☐ Wet System: ☐ Preaction System

Fire Protection Notes:

HVAC:

Air Changes / Hr: 6-10 AC/Hr ☐ General Exhaust: ☐ Chemical Exhaust:

Recirc / Single Pass Airflow: Single Pass ☑ Heat Exhaust: Summer Ventilatio ☑ Smoke Exhaust: Yes

HVAC Notes:

PLUMBING:

- ☑ Domestic Water H/C
- ☐ Eyewash / Safety Shower
- ☑ Floor / Trench Drain: Provide floor drains to sanitary waste.

Plumbing Notes:

PROCESS PIPING:

- ☑ Compressed Air
- ☐ Nitrogen
- ☐ Liquid Nitrogen
- ☐ Other
- ☐ DI Water
- ☐ Process Cooling Water - Cu
- ☐ Process Cooling Water - Al
- ☐ Chemical Drain

Piping Notes:

ELECTRICAL:

Lighting Fixture Type: Pendant

Lighting Lamp Type: Fluorescent

Lighting Direction: Direct

Light Switching: Occupancy Sensor

Lighting Level (FC): 15

Ground:

Electrical Notes:

Power Outlets:

No.	Voltage	Phase	Type	Location
24	120 v	1 ph	Normal	Wall
0				

Clean Power:

UPS:

Emergency Power:

TELECOMMUNICATION AND SPECIAL SYSTEMS:

- ☑ Phone / Voice
- ☑ PA System
- ☐ Gas Leak Detection
- ☐ Liquid Leak Detection
- ☑ Data Connections:
- ☑ Access Control:
- ☐ CCTV:
- ☐ Fire Detection Type:

Telecom Notes:

LEED-NC Version 2.2 Registered Project Checklist

BNL NSLS II Design Case

Yes	?	No			
5	**7**	**2**	**Sustainable Sites**		**14** Points
Y			Prereq 1	**Construction Activity Pollution Prevention**	Required
Y			Credit 1	**Site Selection**	1
		N	Credit 2	**Development Density & Community Connectivity**	1
		N	Credit 3	**Brownfield Redevelopment**	1
Y			Credit 4.1	**Alternative Transportation**, Public Transportation Access	1
Y			Credit 4.2	**Alternative Transportation**, Bicycle Storage & Changing Rooms	1
Y			Credit 4.3	**Alternative Transportation**, Low-Emitting and Fuel-Efficient Vehicles	1
	?		Credit 4.4	**Alternative Transportation**, Parking Capacity	1
	?		Credit 5.1	**Site Development,** Protect of Restore Habitat	1
Y			Credit 5.2	**Site Development,** Maximize Open Space	1
	?		Credit 6.1	**Stormwater Design,** Quantity Control	1
	?		Credit 6.2	**Stormwater Design,** Quality Control	1
	?		Credit 7.1	**Heat Island Effect,** Non-Roof	1
	?		Credit 7.2	**Heat Island Effect,** Roof	1
	?		Credit 8	**Light Pollution Reduction**	1

Yes	?	No			
3	**2**		**Water Efficiency**		**5** Points
Y			Credit 1.1	**Water Efficient Landscaping**, Reduce by 50%	1
Y			Credit 1.2	**Water Efficient Landscaping**, No Potable Use or No Irrigation	1
	?		Credit 2	**Innovative Wastewater Technologies**	1
Y			Credit 3.1	**Water Use Reduction**, 20% Reduction	1
	?		Credit 3.2	**Water Use Reduction**, 30% Reduction	1

Yes	?	No			
3	**1**	**13**	**Energy & Atmosphere**		**17** Points
Y			Prereq 1	**Fundamental Commissioning of the Building Energy Systems**	Required
Y			Prereq 2	**Minimum Energy Performance**	Required
Y			Prereq 3	**Fundamental Refrigerant Management**	Required
1	1	8	Credit 1	**Optimize Energy Performance** New Buildings / Existing Building Renovations: 10.5% / 3.5% = 1; 14% / 7% = 2; 17.5% / 10.5% = 3; 21% / 14% = 4; 24.5% / 17.5% = 5; 28% / 21% = 6; 31.5% / 24.5% = 7; 35% / 28% = 8; 38.5% / 31.5% = 9; 42% / 35% = 10	1 to 10
		3	Credit 2	**On-Site Renewable Energy** % Renewable / Energy Points: 2.5% = 1; 7.5% = 2; 12.5% = 3	1 to 3
Y			Credit 3	**Enhanced Commissioning**	1
Y			Credit 4	**Enhanced Refrigerant Management**	1
		N	Credit 5	**Measurement & Verification**	1
		N	Credit 6	**Green Power** Provide at least 35% of the building's electricity from renewable sources by engaging in at least a two-year renewable energy contract	1

Yes	?	No			
7		6	**Materials & Resources**		**13** Points
Y			Prereq 1	**Storage & Collection of Recyclables**	Required
		N	Credit 1.1	**Building Reuse**, Maintain 75% of Existing Walls, Floors & Roof	1
		N	Credit 1.2	**Building Reuse**, Maintain 100% of Existing Walls, Floors & Roof	1
		N	Credit 1.3	**Building Reuse**, Maintain 50% of Interior Non-Structural Elements	1
Y			Credit 2.1	**Construction Waste Management**, Divert 50% from Disposal	1
Y			Credit 2.2	**Construction Waste Management**, Divert 75% from Disposal	1
		N	Credit 3.1	**Materials Reuse**, 5%	1
		N	Credit 3.2	**Materials Reuse**,10%	1
Y			Credit 4.1	**Recycled Content**, 10% (post-consumer + ½ pre-consumer)	1
Y			Credit 4.2	**Recycled Content**, 20% (post-consumer + ½ pre-consumer)	1
Y			Credit 5.1	**Regional Materials**, 10% Extracted, Processed & Manufactured Regic	1
Y			Credit 5.2	**Regional Materials**, 20% Extracted, Processed & Manufactured Regic	1
		N	Credit 6	**Rapidly Renewable Materials**	1
Y			Credit 7	**Certified Wood**	1
Yes	?	No			
6	7	2	**Indoor Environmental Quality**		**15** Points
Y			Prereq 1	**Minimum IAQ Performance**	Required
Y			Prereq 2	**Environmental Tobacco Smoke** (ETS) **Control**	Required
Y			Credit 1	**Outdoor Air Delivery Monitoring**	1
		N	Credit 2	**Increased Ventilation**	1
Y			Credit 3.1	**Construction IAQ Management Plan**, During Construction	1
Y			Credit 3.2	**Construction IAQ Management Plan**, Before Occupancy	1
Y			Credit 4.1	**Low-Emitting Materials**, Adhesives & Sealants	1
Y			Credit 4.2	**Low-Emitting Materials**, Paints & Coatings	1
Y			Credit 4.3	**Low-Emitting Materials**, Carpet Systems	1
		N	Credit 4.4	**Low-Emitting Materials**, Composite Wood & Agrifiber Products	1
	?		Credit 5	**Indoor Chemical & Pollutant Source Control**	1
	?		Credit 6.1	**Controllability of Systems**, Lighting	1
	?		Credit 6.2	**Controllability of Systems**, Thermal Comfort	1
	?		Credit 7.1	**Thermal Comfort**, Design	1
	?		Credit 7.2	**Thermal Comfort**, Verification	1
	?		Credit 8.1	**Daylight & Views**, Daylight 75% of Spaces	1
	?		Credit 8.2	**Daylight & Views**, Views for 90% of Spaces	1
Yes	?	No			
4	1		**Innovation & Design Process**		**5** Points
Y			Credit 1.1	**Innovation in Design**: Recycled Content 30%	1
Y			Credit 1.2	**Innovation in Design**: Green Cleaning	1
Y			Credit 1.3	**Innovation in Design**: Sustainable Site Maintenance	1
	?		Credit 1.4	**Innovation in Design**: Provide Specific Title	1
Y			Credit 2	**LEED® Accredited Professional**	1
Yes	?	No			
28	18	23	**Project Totals** (pre-certification estimates)		**69** Points

Certified 26-32 points **Silver** 33-38 points **Gold** 39-51 points **Platinum** 52-69 points

APPENDICES

Appendix A1

Preliminary Geotechnical Report
May 25, 2007
GEI Consultants

Appendix A2

Preliminary Vibration and Acoustic Report
September 15, 2006
Colin Gordon & Associates, Inc.

Appendix A3

Preliminary EMI/RFI Site Assessment Study Report
September 1, 2006
VitaTech Engineering, LLC

Appendix A4

HVAC Calculations
Accelerator Ring Tunnel – one pentant
Experimental Hall – one pentant

Appendix A5

Hourly Whole Building Energy Analysis
September 10, 2007
EMO Energy Solutions

Appendix A1

Preliminary Geotechnical Report
May 25, 2007

GEI Consultants

GEI Consultants

Geotechnical
Environmental and
Water Resources
Engineering

Geotechnical Report

National Synchrotron Light Source II

Advanced Concept Design Phase
Brookhaven National Laboratory
Upton, New York

Submitted to:
HDR Architecture, Inc.
1101 King Street, Suite 400
Alexandria, VA 22314

Submitted by:
GEI Consultants, Inc.
455 Winding Brook Drive
Suite 201
Glastonbury, CT 06033
860-368-5300

May 25, 2007
Project 062152-*-1000

Nathan L. Whetten, P.E., C.G.
Senior Project Manager

Table of Contents

Table of Contents (cont.)

Figures

Appendices

H:\WPROC\Project\Brookhaven National Laboratory\062152 Advanced Concept Design\062152 ACD Report2.doc

1. Introduction

1.1 Introduction

Previously, we conducted subsurface explorations and geotechnical engineering evaluations for Conceptual Design, and prepared a summary report dated November 9, 2006. The proposed building location was subsequently shifted about 500 feet to the west. In April and May 2007, we conducted supplemental explorations and engineering evaluations within the western portion of the site, to update our conceptual design recommendations for the current building configuration.

This report summarizes the results of previous (conceptual design) and recent (advanced conceptual design) subsurface explorations, and our geotechnical design and construction recommendations for conceptual design of the proposed National Synchrotron Light Source II (NSLS II). This report supersedes our conceptual design phase geotechnical report dated November 9, 2006.

1.2 Summary

The subsurface explorations encountered up to about 9 feet of fill overlying a sand deposit that extends to more than 100 feet below ground surface (bgs). We recommend that foundations be designed as spread footing foundations with slab-on-grade floors. The existing fill should be removed within the building limits and replaced with compacted Structural Fill.

1.3 Scope of Work

GEI performed the following conceptual design tasks in 2006:

1. Engaged subsurface exploration contractors to conduct test borings and cone penetrometer tests.
2. Provided a full-time field representative to observe the explorations, and classify the soil samples in the borings.
3. Engaged a materials testing laboratory to perform mechanical gradation analyses on representatives soil samples from the borings.
4. Evaluated the subsurface conditions encountered in the conceptual design explorations and prepared a summary report dated November 9, 2006.

GEI performed the following advanced conceptual design tasks in 2007:

1. Engaged subsurface exploration contractors to conduct supplemental test borings and cone penetrometer tests.
2. Provided a full-time field representative to observe the explorations, and classify the soil samples in the borings.
3. Engaged a materials testing laboratory to perform mechanical gradation analyses on representatives soil samples from the borings.
4. Evaluated the subsurface conditions encountered in the conceptual design and advanced conceptual design explorations and prepared this summary report.

1.4 Project Personnel

The following personnel performed services for this project:

Steven Hawkins	Field Engineer
Nathan Whetten, P.E.	Senior Project Manger
Michael Paster, P.E.	Technical Review

1.5 Authorization

The 2006 work was completed in accordance with our agreement dated June 26, 2006. The 2007 Advanced Concept Design phase work was completed in accordance with our agreement dated April 6, 2007.

1.6 Project Vertical Datum

Elevations in this report are in feet. The vertical coordinate system is Brookhaven National Laboratory (BNL) ’94. We understand that BNL ’94 is substantially equivalent to National Geodetic Vertical Datum of 1929 (NGVD-29).

2. Site and Project Description

2.1 Site Description

The approximately 50-acre site is bounded by Brookhaven Avenue to the north, Grove Street to the west, Fifth Street to the east, and a former landfill to the southeast. Seventh Street runs through the middle of the site in a north-south direction, and divides the site roughly in half.

The eastern portion of the site is generally a lawn area or is wooded. The western portion is occupied by several buildings, adjacent parking areas, access roads with asphalt, concrete, or gravel pavement, concrete loading docks, at-grade concrete pads, two railroad tracks, and chain link fences. Existing site features are shown on Figure 2.

The ground surface slopes gently downward from east to west. Ground surface elevations range from about El. 83 along Fifth Street to about El. 63 along Grove Street.

2.2 Project Description

Brookhaven Science Associates is planning to replace the existing National Synchrotron Light Source with a new facility, referred to as NSLS II. The new facility will be located within the BNL, south and east of the existing NSLS building (Figure 1). NSLS II will be located south of Brookhaven Avenue and east of Grove Street. The proposed facility layout is shown in plan on Figure 2.

NSLS II will be a state-of-the-art research facility. The facility will include a Ring Building, Operations Center Building, lab/office buildings, and service buildings, totaling about 382,000 square feet. The facility will also include an approximately 50,000 square foot Joint Photon Science Institute (JPSI) building.

We understand that the lowest level floors will generally be at existing site grades, and no basement levels are planned. Proposed floor elevations for the various facility components, provided by HDR Architecture, Inc. (HDR), are indicated in the table below.

Structure	Proposed Floor El.	Ground Surface Elevation
Experimental Floor	El. 70	El. 68 (SW) to El. 77 (E)
Storage Ring Floor	El. 71.33	El. 68 (SW) to El. 77 (E)
Booster Ring	El. 71.33	El. 73
Lab/Office Buildings (LOB)	El. 70	El. 73 to 74 (N LOB) El. 73 to 77 (NE LOB) El. 70 to 77 (SE LOB) El. 66 to 68 (SW LOB) El. 68 to 73 (W LOB)
Operations Center Lower Floor	El. 71.33	El. 73
Service Buildings Lower Floor	El. 70	El. 73 (N Svc Bldg) El. 74 to 75 (NE Svc Bldg) El. 72 to 75 (SE Svc Bldg) El. 70 to 71 (SW Svc Bldg)
Joint Photon Science Institute	El. 70	El. 73 to 75

Comparing the proposed floor grades with the existing site grades, up to about 9 feet of excavation and up to 4 feet of fill will be required below floors.

We understand that the floor slab for the experimental hall will be 18 inches thick, and the adjacent tunnel ring slab will be 36 inches thick. These elements will be constructed as a monolithic slab. The design live load for the floor in these areas is 250 pounds per square foot (psf).

3. Subsurface Conditions

3.1 Previous Subsurface Explorations

1977 Explorations – In 1977, Stone & Webster conducted subsurface explorations for the existing NSLS facility. The explorations included six soil borings and four test pits. The borings were drilled to depths of 100 to 102 feet and the test pits were excavated to a depth of about 12 feet. Approximate exploration locations are shown on Figure 2, and logs of the test pits and borings are presented in Appendix A.

2003 Explorations – In 2003, we conducted eleven test borings for the nearby Center for Functional Nanomaterials (CFN) building. The test borings were advanced to depths of 7 to 62 feet bgs. Drilling activities were monitored by a GEI field technician. Test boring locations are shown on Figure 2, and boring logs prepared by the driller are provided in Appendix B.

3.2 Recent Subsurface Explorations

During the periods July 19 to 21, August 16, 2006, and April 23 to 26, 2007, we conducted ten test borings, (B101-B104 and B201-B206) and fifteen cone penetrometer soundings (CPT-1 to CPT-6, CPT-8, CPT-10 to CPT-14, and CPT-201 to CPT-203). Shear wave velocity measurements were made in CPT-3, -5A, -6, -12, -202, and -203 at 10-foot intervals within the sand. Explorations were monitored by a GEI engineer.

Test borings B101, B102, and B201-B204 were drilled to depths of 47 to 62 bgs. These borings were drilled using 3-inch-diameter driven casing, and Standard Penetration Tests were conducted at 5-foot intervals. Borings B101A and B102A were drilled a few feet away from borings B101 and B102, respectively, with continuous samples taken to a depth of 10 feet. Borings B103 and B104B were drilled to a depth of 32 feet using hollow-stem augers. B104 and B104A were terminated after encountering shallow refusals. Most of the borings included continuous or semi-continuous sampling within the upper 12 to 14 feet. Logs are presented in Appendix C.

The CPT soundings penetrated to depths typically ranging from 53 to 100 feet, and were terminated at refusal or at a maximum depth of 100 feet. Shallow refusals at depths less than 10 feet were encountered in CPT-5, -7, -13, and -13A. A second sounding (CPT-5A) was completed near CPT-5 to a depth of 83 feet; a second sounding (CPT-13A) near CPT-13 encountered shallow refusal and was terminated. CPT-9 was deleted from the exploration program. Logs of CPT soundings are presented in Appendix D.

3.3 Laboratory Testing

GeoTesting Express, of Boxborough, Massachusetts, performed 21 mechanical gradation analyses on soil samples recovered from the test borings. Sixteen gradation analyses were conducted on samples from borings B101 and B102, and five were conducted on samples from borings B202, B203, B204 and B206. Results are presented in Appendix E.

3.4 Subsurface Soil Conditions

Fill

Topsoil ranging in thickness from 2 to 12 inches was encountered in test borings that were drilled in landscaped areas. Topsoil was not encountered in B103, B104, B202, and B206, which were drilled in developed areas. Bituminous concrete approximately 4 inches thick was encountered in B202, which was drilled in an existing parking lot.

Each of the borings encountered fill typically described as silty sand (SM) or widely-graded sand (SW), and the thickness ranged from 2 to 9 feet. SPT N-Values ranged from 4 to 21 blows per foot (bpf), indicating the fill is loose to medium dense. Fill was also detected within the upper 1 to 10 feet in CPT soundings made near existing buildings and roadways. Explorations B104, B104A, CPT-13, and CPT-13A, located within the southern portion of the ring building, encountered refusals believed to represent buried objects, cobbles, or boulders within the fill.

Sand

A thick layer of stratified sand, sand with silt, and sand with gravel was encountered below the fill in all of the explorations. Subsurface explorations were terminated within the sand at maximum depths of about 100 feet. The sand is light brown to brown. SPT N-values ranged from about 15 bpf (medium dense) to greater than 50 bpf (very dense). The average corrected SPT N-value calculated from the CPTs within the upper 50 feet was about 30 bpf, The CPTs detected some localized zones with equivalent N-values between 10 and 20, 40 and 50, and over 50 bpf.

Shear wave velocity measurements made in CPT-3, -5A, -6, -12, -202, -203 indicate a uniform to slightly increasing shear wave velocity with depth. Velocities varied from 660 feet per second (fps) to 1,180 fps and typically ranged from 850 fps to 1,100 fps. The average of 54 shear wave velocity tests in these six CPTs was 946 fps.

A 1999 report on the stratigraphy and hydrogeologic conditions at the lab prepared by the United States Geologic Survey[1] refers to the sand as the "Upper Glacial Aquifer," and the thickness at BNL appears to be about 185 feet. Confining clay units and additional sand and gravel aquifers overlie bedrock, which reportedly occurs at a depth of about 1,500 feet.

3.5 Groundwater Conditions

Depths to groundwater range from about 21.5 (CPT-203) to 36.5 feet (B102) bgs, and vary with location at the site. Depths were measured in temporary wells and boreholes, and using a pore pressure transducer mounted on the cone probe. At the end of the cone probes, the excess pore water pressure was allowed to dissipate to measure the static water pressure. Groundwater level measurements represent conditions at the times and locations the measurements were made. Significantly different groundwater levels may occur at other times and locations.

1 "Stratigraphy and Hydrogeologic Conditions at the Brookhaven National Laboratory and Vicinity, Suffolk County, New York 1994-1997," prepared by the United States Geologic Survey, dated 1999.

4. Preliminary Foundation Recommendations

4.1 Foundation Design

We recommend that the proposed buildings be supported on spread footings bearing directly on the sand deposit, or on compacted structural fill placed after removal of existing fill. We recommend that footings be designed for a maximum allowable bearing pressure of 2.5 tons psf, and that footings be at least 3-feet wide.

Exterior footings should bear at least 4 feet below the adjacent finished grade for frost protection. Interior footings should be founded at least 18 inches below the bottom of the floor slab. The top of all footings should be at least 6 inches below the bottom of the overlying floor slab.

4.2 Floor Slab Design

Based on a comparison of proposed floor levels with existing site grades, the lowest level floors will range from 9 feet below to 4 feet above existing site grades. The lowest level floor may be designed as a slab-on-grade.

The existing fill is not considered suitable for support of floor slabs due to the low tolerance for settlement. Therefore, we recommend that all existing fill be removed from within the building limits, and replaced with compacted structural fill. A minimum of 6 inches of compacted structural fill should be placed below all floors.

Floors are above groundwater levels encountered in the explorations. Underslab drainage will not be required.

4.3 Settlement

Column and Wall Settlement

We estimate that total settlement of spread footings will be less than 1 inch, and differential settlements will be less than 0.75 inch. Settlement will occur as loads are applied. We understand that this settlement is acceptable for column and wall footings.

Floor Settlement

We understand that the floor slab within the experimental hall will support highly sensitive scientific equipment, and that settlement of the floor slab after the equipment has been installed and calibrated must be small. Based on discussions with HDR, we understand that post-construction total and differential settlement may need to be less than about 0.25 inch.

Soils beneath the floor slab will settle in response to dead and live loads. We anticipate that settlement will be complete within about one to two weeks after load application.

Settlement resulting from floor slab dead loads and fill required beneath the floor slab is expected to occur during construction, and therefore will not contribute to post-construction settlement. However, the 250 psf live load could cause minor post-construction settlement. We calculate the total and differential post-construction settlement from the live load to be less than 0.25 inch. Differential settlement will be less than the total settlement. For sensitive equipment, it may be desirable to allow a two to three week waiting period between installation and final calibration.

4.4 Seismic Design

The soil beneath the proposed buildings has an average shear wave velocity of 946 feet per second and is classified as a stiff soil profile for earthquake design purposes as defined by the New York State Building Code. The corresponding site class is D. The soil is not considered to be susceptible to liquefaction.

4.5 Reuse of Existing Fill

Based on the results of sieve analyses conducted on soil samples recovered from borings B101 and B102, we anticipate that the natural sand deposit will be suitable for reuse as compacted structural fill below building foundations. The existing fill has a relatively high percentage of fines (silt and clay size particles) and is not suitable for reuse as structural fill. The existing fill is suitable for reuse as common fill outside the building limits.

4.6 Subsurface Explorations for Final Design

Subsurface explorations conducted for the 2006 conceptual design and 2007 advanced concept design studies included a relatively small number of widely-spaced explorations. Most of these explorations penetrated to depths of 50 to 100 feet, to evaluate general subsurface conditions in the area of the facility.

We recommend that subsurface explorations for final design include additional test borings with continuous SPT sampling, to further evaluate the nature and thickness of fill materials.

Shallow refusals were encountered in B104, B104A, CPT-13 and -13A, and may indicate buried foundations or other objects within the fill. We recommend that test pits be excavated at locations where shallow refusal was encountered within the fill.

5. Final Design Services and Limitations

5.1 Final Design Engineering Services

We recommend that GEI be engaged during final design to:

- Conduct subsurface explorations, prepare a final geotechnical engineering report, and provide geotechnical consultation to the design team.
- Review plans and specifications to confirm that our recommendations have been interpreted and implemented as intended.

5.2 Limitations

This report was prepared for the exclusive use of HDR Architecture, Brookhaven Science Associates, and the NSLS II design team. Our recommendations are based on the project information provided to us at the time of this report and may require modification if there are any changes in the nature, design, or location of the proposed structure. We cannot accept responsibility for designs based on our recommendations unless we are engaged to review the final plans and specifications to determine whether any changes in the project affect the validity of our recommendations and whether our recommendations have been properly implemented in the design.

The recommendations in this report are based in part on the data obtained from the subsurface explorations. The nature and extent of variations between explorations may not become evident until construction. If variations from the anticipated conditions are encountered, it may be necessary to revise the recommendations in this report.

Our professional services for this project have been performed in accordance with generally accepted engineering practices. No warranty, express or implied, is made.

Figures

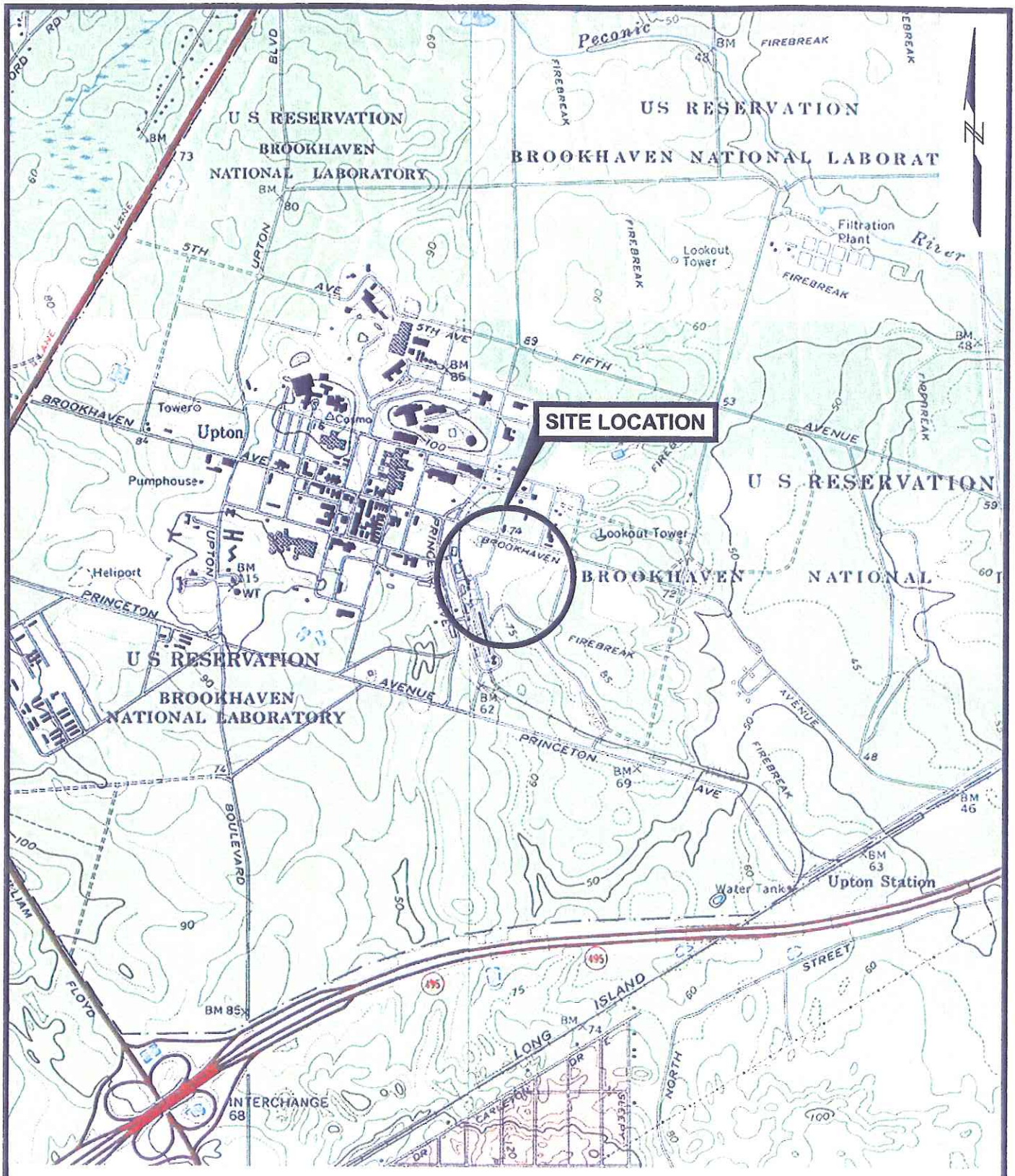

SOURCE: Map created with TOPO! ® ©2003 National Geographic (www.nationalgeographic.com/topo)

0 2000 4000

SCALE, FEET

PROPOSED NSLS II BROOKHAVEN NATIONAL LABORATORY UPTON, NEW YORK	GEI Consultants	SITE LOCATION MAP
HDR ARCHITECTURE, INC.	PROJECT 062150	August 2006 Figure 1

BROOKHAVEN NL\062150\BROOKHAVEN LOCATION MAP.CDR

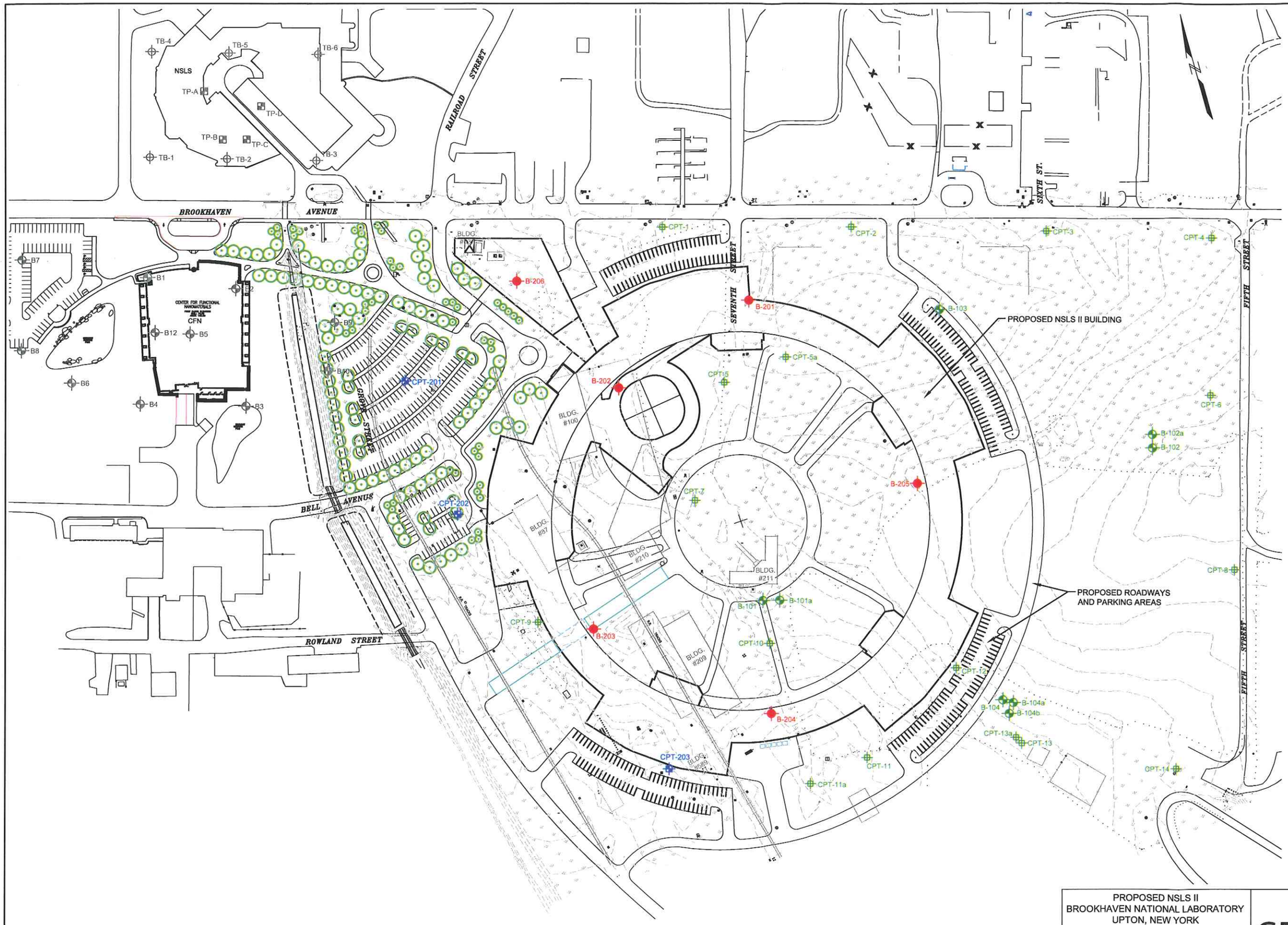

LEGEND:

ADC EXPLORATIONS:

- CPT-201 — APPROXIMATE LOCATION OF CONE PENETROMETER TEST MADE IN APRIL 2007
- B-201 — APPROXIMATE LOCATION OF TEST BORING DRILLED IN APRIL 2007

2006 EXPLORATIONS:

- B-101 — APPROXIMATE LOCATION OF TEST BORING DRILLED IN JULY AND AUGUST 2006
- CPT-1 — APPROXIMATE LOCATION OF CONE PENETROMETER TEST MADE IN JULY 2006

PREVIOUS EXPLORATIONS:

- TB-1 — APPROXIMATE LOCATION OF TEST BORING INSTALLED IN 1977
- TP-A — APPROXIMATE LOCATION OF TEST PIT INSTALLED IN 1977
- B1 — APPROXIMATE LOCATION OF TEST BORING INSTALLED IN 2003

NOTES:

1. PLAN BASED ON MAP TITLED ***TOPOGRAPHIC SURVEY, PROPOSED NSLS II SITE, SITUATED AT BNL,*** UPTON, NEW YORK, PREPARED BY MUNICIPAL LAND SURVEY P.C., 10 SYLVIA LANE, MIDDLE ISLAND, NEW YORK, 11953.
2. APPROXIMATE LOCATIONS OF 2006 AND 2007 EXPLORATIONS WERE PROVIDED BY BNL, AND WERE DETERMINED BY PACING FROM SITE FEATURES. LOCATIONS OF PREVIOUS EXPLORATIONS WERE ESTIMATED BASED ON RECORD DRAWINGS.
3. THE HORIZONTAL COORDINATE SYSTEM IS IN THE STATE PLANE COORDINATE SYSTEM, NEW YORK LONG ISLAND ZONE 3104, NAD '83, EXPRESSED IN US SURVEY FEET AS DEFINED BY BNL POINT COSMO RM3.
4. THE VERTICAL COORDINATE SYSTEM IS BNL '94 WHICH IS SUBSTANTIALLY EQUIVALENT TO THE NATIONAL GEODETIC VERTICAL DATUM OF 1929 (NGVD 1929), EXPRESSED IN US SURVEY FEET AS DEFINED BY BNL POINT COSMO RM3.
5. PROPOSED BUILDING LAYOUT REVISED BASED ON MAP PROVIDED BY HDR ARCHITECTURE, INC.

PROPOSED NSLS II
BROOKHAVEN NATIONAL LABORATORY
UPTON, NEW YORK

HDR ARCHITECTURE, INC.

PROJECT 062152-1000

GEI Consultants
455 WINDING BROOK DRIVE
SUITE 201
GLASTONBURY, CONNECTICUT 06033

ADC EXPLORATION LOCATIONS

May 2007 — Figure 2

I:\GEI\Brookhaven National Laboratory\614687\ BROOKHAVEN ADC EXPLORATION 5-07.dwg \May 23, 2007

Appendix A

1977 Test Boring and Test Pit Logs

SH 2 OF 2

SITE NATIONAL SYNCHROTRON LIGHT SOURCE J.O.No. 13011.01 BORING No. 1
TYPE OF BORING SS LOCATION BROOKHAVEN NATIONAL LABORATORY GROUND ELEV. 72.6
DATE DRILLED August 23, 1977 DRILLED BY V. ADAM LOGGED BY EBT
SUMMARY OF BORING

ELEV. FEET	DEPTH FEET	OVERALL WEATHERING AND RQD (0 25 50 75 100)	SAMPLE BLOWS/6" RECOV.	SAMPLE TYPE	GRAPHIC LOG	SOIL OR ROCK DESCRIPTION (FIELD AND LABORATORY TEST RESULTS OR OBSERVATIONS, REMARKS AND FAULTING; SOIL MINERALOGICAL DESCRIPTION; LITHOLOGY AND TEXTURE)
	0		28		SM	TOP SOIL, SILTY SAND, WIDELY GRADED, COARSE TO FINE, MOSTLY MEDIUM AND FINE, 12-20% NONPLASTIC FINES, LIGHT BROWN.
	5		36	SS #2	SP-SM	SAND, UNIFORM, MEDIUM TO FINE, MOSTLY MEDIUM, 8-10% NONPLASTIC FINES, LIGHT YELLOWISH BROWN.
	10		18	SS #3	SM	SILTY SAND, WIDELY GRADED, FINE TO VERY FINE, 20-25% NONPLASTIC FINES, GRAYISH BROWN.
	15		43	SS #4	SP	GRAVELLY SAND, POORLY GRADED, 10-15% ROUNDED GRAVEL TO 1.0 INCH MAXIMUM, COARSE TO FINE SAND, MOSTLY COARSE AND MEDIUM 3-5% NON-PLASTIC FINES, GRAYISH BROWN.
	20		18	SS #5	SP-SM	GRAVELLY SAND, 10-15% ROUNDED GRAVEL TO 0.25 INCH MAXIMUM, COARSE TO FINE SAND, MOSTLY COARSE AND MEDIUM, 8-10% NONPLASTIC FINES, BROWNISH GRAY.
	25		39	SS #6	SP	SAND, SIMILAR TO SS #4, EXCEPT GRAVEL TO 0.5 INCH MAXIMUM
	30		77	SS #7	SP	GRAVELLY SAND, POORLY GRADED, 18-20% ROUNDED GRAVEL TO 1.0 INCH MAXIMUM, COARSE TO FINE SAND, MOSTLY MEDIUM, 3-5% NONPLASTIC FINES, BROWNISH GRAY.
	35		65	SS #8	SP	SAND, POORLY GRADED, COARSE TO FINE, MOSTLY MEDIUM, 3-5% NONPLASTIC FINES, BROWNISH GRAY.
	40		35	SS #9	SP	SAND, POORLY GRADED, COARSE TO FINE, MOSTLY MEDIUM AND FINE, 2-3% NONPLASTIC FINES, BROWNISH GRAY.
	45		58	SS #10	SP	GRAVELLY SAND, POORLY GRADED, 20-25% GRAVEL TO 0.75 INCH MAXIMUM, COARSE TO FINE SAND, MOSTLY COARSE AND MEDIUM 0-3% NONPLASTIC FINES, BROWNISH GRAY.
	50		63	SS #11	SP	SAND, SAME AS SS #10.
	55		51	SS #12	SP	SAND, UNIFORM MEDIUM TO FINE, SOME COARSE PIECES, LESS THAN 3% NONPLASTIC FINES, GRAY.
	60		51	SS #13	SP	GRAVELLY SAND, POORLY GRADED, 12-15% ROUNDED GRAVEL TO 0.5 INCH MAXIMUM, COARSE TO FINE, MOSTLY COARSE AND MEDIUM, LESS THAN 3% FINES, GRAY.
	65		35	SS #14	SP	GRAVELLY SAND, SIMILAR TO SS #13, EXCEPT ROUNDED GRAVEL TO 0.3 INCH MAXIMUM.
			?		SP	SAND, POORLY GRADED, 3-5% GRAVEL TO 0.5 INCH MAXIMUM, COARSE TO FINE, MOSTLY MEDIUM 4-5% NONPLASTIC FINES, BROWNISH GRAY.

1. FIGURES IN BLOW OR RECOVERY COLUMN OPPOSITE SOIL SAMPLE DENOTE THE NUMBER OF BLOWS OF A 140 LB HAMMER FALLING 30" REQUIRED TO DRIVE A 2" OD SAMPLE SPOON 12" OR THE DISTANCE SHOWN. FIGURES SHOWN OPPOSITE ROCK CORES DENOTE THE PERCENT OF CORE RECOVERED.
2. ☒2 INDICATES LOCATION OF UNDISTURBED SAMPLE. ☒6 INDICATES LOCATION OF SPLIT-SPOON SAMPLE. ☐7 INDICATES LOCATION OF SAMPLING ATTEMPT WITH NO RECOVERY. SUBSCRIPT NEXT TO SYMBOL INDICATES SAMPLE NUMBER.
3. ⏚ INDICATES LOCATION OF NATURAL GROUND WATER TABLE.
4. RQD - ROCK QUALITY DESIGNATION.
5. ☐ INDICATES DEPTH & LENGTH OF NX COARING RUN
6. DATUM IS

NATIONAL SYNCHROTRON LIGHT SOURCE
BROOKHAVEN NATIONAL LABORATORY

STONE & WEBSTER ENGINEERING CORPORATION

SH 1 OF 2

SITE NATIONAL SYNCHROTRON LIGHT SOURCE J.O.No. 13011.10 BORING No. 1
TYPE OF BORING SS LOCATION BROOKHAVEN NATIONAL LABORATORY GROUND ELEV. 73.0
DATE DRILLED August 23, 1977 DRILLED BY V. ADAM LOGGED BY EBT
SUMMARY OF BORING

ELEV. FEET	DEPTH FEET	OVERALL WEATHERING AND RQD (0 25 50 75 100)	SAMPLE BLOWS/6" RECOV.	SAMPLE TYPE	GRAPHIC LOG	SOIL OR ROCK DESCRIPTION (FIELD AND LABORATORY TEST RESULTS OR OBSERVATIONS, REMARKS AND FAULTING; SOIL MINERALOGICAL DESCRIPTION; LITHOLOGY AND TEXTURE)
	75		56*	SS #15	SP	SAND, SAME AS SS #15.
	80		140	SS #17	SP	SAND, UNIFORM FINE, SOME COARSE PIECES, LESS THAN 3% NONPLASTIC FINES, LIGHT BROWNISH GRAY.
	85		58	SS #18	SP	GRAVELLY SAND, POORLY GRADED, 10-15% ROUNDED GRAVEL TO 0.5 INCH MAXIMUM, COARSE TO FINE SAND, MOSTLY MEDIUM 3-4% NONPLASTIC FINES, BROWNISH GRAY.
	90		58	SS #19	SP	SAND, UNIFORM MEDIUM, SOME COARSE PIECES, LESS THAN 5% NONPLASTIC FINES, LIGHT BROWNISH GRAY.
	95		58	SS #20	SP	SAND, SAME AS SS #19.
	100		59	SS #21	SP	SAND, SAME AS SS #19, [redacted] OF ROUNDED GRAVEL TO 0.3 INCH MAXIMUM.
		? TERMINATED				END OF BORING AT 101.9 FT.

1. FIGURES IN BLOW OR RECOVERY COLUMN OPPOSITE SOIL SAMPLE DENOTE THE NUMBER OF BLOWS OF A 140 LB HAMMER FALLING 30" REQUIRED TO DRIVE A 2" OD SAMPLE SPOON 12" OR THE DISTANCE SHOWN. FIGURES SHOWN OPPOSITE ROCK CORES DENOTE THE PERCENT OF CORE RECOVERED.
2. ☒2 INDICATES LOCATION OF UNDISTURBED SAMPLE. ☒6 INDICATES LOCATION OF SPLIT-SPOON SAMPLE. ☐7 INDICATES LOCATION OF SAMPLING ATTEMPT WITH NO RECOVERY. SUBSCRIPT NEXT TO SYMBOL INDICATES SAMPLE NUMBER.
3. ⏚ INDICATES LOCATION OF NATURAL GROUND WATER TABLE.
4. RQD - ROCK QUALITY DESIGNATION.
5. ☐ INDICATES DEPTH & LENGTH OF NX COARING RUN
6. DATUM IS

NATIONAL SYNCHROTRON LIGHT SOURCE
BROOKHAVEN NATIONAL LABORATORY

STONE & WEBSTER ENGINEERING CORPORATION

SH 1 OF 2

SITE NATIONAL SYNCHROTRON LIGHT SOURCE J.O. No. 13011.10 BORING No. 2
TYPE OF BORING SS LOCATION BROOKHAVEN NATIONAL LABORATORY GROUND ELEV. 71.4
DATE DRILLED AUGUST 27, 1977 DRILLED BY Y. AIMAR LOGGED BY RBT
SUMMARY OF BORING

ELEV. FEET	DEPTH FEET	OVERALL WEATHERING AND RQD	SAMPLE BLOWS PER 6"	SAMPLE NO.	SAMPLE TYPE	GRAPHIC LOG	SOIL OR ROCK DESCRIPTION (FIELD AND LABORATORY TEST RESULTS; IN-SITU TESTING, BEDDING AND FAULTING; SOIL STRATA DESCRIPTION; LITHOLOGY AND TEXTURE)
	0		13	SS 1	SM		SILTY SAND, WIDELY GRADED, COARSE TO FINE, MOSTLY FINE, 30-40% NONPLASTIC FINES, MOTTLED GRAY AND BROWN.
	5		15	SS 2	SP		SAND, UNIFORM; FINE, LESS THAN 5% NONPLASTIC FINES, LIGHT YELLOWISH GRAY.
	10		25	SS 3	SP		SAND, UNIFORM, MEDIUM TO FINE, MOSTLY FINE; LESS THAN 5% NONPLASTIC FINES, LIGHT YELLOWISH GRAY.
	15		23	SS 4	SP-SM		SAND, UNIFORM, MEDIUM TO FINE, MOSTLY FINE, 5-8% NONPLASTIC FINES, BROWNISH ORANGE.
	20		30	SS 5	SP		SAND, UNIFORM, MEDIUM TO FINE, MOSTLY FINE, LESS THAN 5% NONPLASTIC FINES, LIGHT YELLOWISH GRAY, SMALL BROWNISH ORANGE POCKETS OF SILTY SAND.
	25		39	SS 6	SP		GRAVELLY SAND, POORLY GRADED, 12-15% SUBROUNDED GRAVEL TO 0.25 INCH MAXIMUM, COARSE TO FINE, MOSTLY MEDIUM AND FINE, 3-5% NONPLASTIC FINES, YELLOWISH GRAY, SMALL LAYER OF BROWNISH GRAY VERY FINE SILTY SAND.
	30		38	SS 7	SP		GRAVELLY SAND, POORLY GRADED, 20-25% SUBROUNDED TO ROUNDED GRAVEL TO 1.0 INCH MAXIMUM, COARSE TO FINE, MOSTLY MEDIUM AND FINE, LESS THAN 5% NONPLASTIC FINES, YELLOWISH GRAY.
	35		104	SS 8	SM		SILTY SAND, UNIFORM, MEDIUM TO FINE, MOSTLY FINE, 35-40% NONPLASTIC FINES, BROWN.
	40		52	SS 9	SP-SM		SAND, POORLY GRADED, 1 PIECE OF SUBROUNDED GRAVEL 1.0 INCH MAXIMUM, COARSE TO FINE, MOSTLY MEDIUM AND FINE, 5-8% NONPLASTIC FINES, YELLOWISH GRAY.
	45		57	SS 10	SP		GRAVELLY SAND, POORLY GRADED, 10-15% ROUNDED GRAVEL TO 0.25 INCH MAXIMUM, COARSE TO FINE, MOSTLY MEDIUM AND FINE, LESS THAN 5% NONPLASTIC FINES, YELLOWISH GRAY.
	50		33	SS 11	SP		SAND, POORLY GRADED, LESS THAN 5% SUBROUNDED GRAVEL TO 0.25 INCH MAXIMUM, COARSE TO FINE SAND, MOSTLY MEDIUM, LESS THAN 5% NONPLASTIC FINES, YELLOWISH GRAY.
	55		64	SS 12	SP		SAND, POORLY GRADED, 3-5% SUBANGULAR GRAVEL TO 0.5 INCH MAXIMUM, COARSE TO FINE, MOSTLY MEDIUM, LESS THAN 5% NONPLASTIC FINES, YELLOWISH GRAY.
	60		44	SS 13	SP		SAND, SIMILAR TO SS #12 EXCEPT MOSTLY MEDIUM AND FINE SAND.
	65		50	SS 14	SP		SAND, POORLY GRADED, LESS THAN 3% SUBANGULAR GRAVEL TO 0.25 INCH MAXIMUM, COARSE TO FINE, MOSTLY MEDIUM, LESS THAN 3% NONPLASTIC FINES, YELLOWISH GRAY.
	70		116	SS 15	SP		GRAVELLY SAND, POORLY GRADED, 12-15% SUBROUNDED TO ROUNDED GRAVEL TO 0.75 INCH MAXIMUM, COARSE TO FINE SAND, MOSTLY MEDIUM AND FINE,

1. FIGURES IN BLOW OR RECOVERY COLUMN OPPOSITE SOIL SAMPLE DENOTE THE NUMBER OF BLOWS OF A 140 LB HAMMER FALLING 30" REQUIRED TO DRIVE A 2" OD SAMPLE SPOON 12" OR THE DISTANCE SHOWN. FIGURES SHOWN OPPOSITE ROCK CORES DENOTE THE PERCENT OF CORE RECOVERED.
2. ⊠2 INDICATES LOCATION OF UNDISTURBED SAMPLE. ⊠6 INDICATES LOCATION OF SPLIT-SPOON SAMPLE. ☐7 INDICATES LOCATION OF SAMPLING ATTEMPT WITH NO RECOVERY. SUBSCRIPT NEXT TO SYMBOL INDICATES SAMPLE NUMBER.
3. ⏚ INDICATES LOCATION OF NATURAL GROUND WATER TABLE.
4. RQD = ROCK QUALITY DESIGNATION.
5. ⊟ INDICATES DEPTH & LENGTH OF NX CORING RUN.
6. DATUM IS

NATIONAL SYNCHROTRON LIGHT SOURCE
BROOKHAVEN NATIONAL LABORATORY

STONE & WEBSTER ENGINEERING CORPORATION

SH 2 OF 2

SITE NATIONAL SYNCHROTRON LIGHT SOURCE J.O. No. 13011.10 BORING No. 2
TYPE OF BORING SS LOCATION BROOKHAVEN NATIONAL LABORATORY GROUND ELEV. 71.4
DATE DRILLED AUGUST 27, 1977 DRILLED BY Y. AIMAR LOGGED BY RBT
SUMMARY OF BORING

ELEV. FEET	DEPTH FEET	OVERALL WEATHERING AND RQD	SAMPLE BLOWS PER 6"	SAMPLE NO.	SAMPLE TYPE	GRAPHIC LOG	SOIL OR ROCK DESCRIPTION (FIELD AND LABORATORY TEST RESULTS; IN-SITU TESTING, BEDDING AND FAULTING; SOIL STRATA DESCRIPTION; LITHOLOGY AND TEXTURE)
							LESS THAN 5% NONPLASTIC FINES, YELLOWISH GRAY.
	75		85	SS 16	SP-SM		SAND, POORLY GRADED, LESS THAN 5% ROUNDED GRAVEL TO 0.75 INCH MAXIMUM, COARSE TO FINE SAND, MOSTLY MEDIUM, 5-8% NONPLASTIC FINES, YELLOWISH GRAY.
	80		52	SS 17	SP		SAND, POORLY GRADED, LESS THAN 3% SUBANGULAR GRAVEL TO 0.5 INCH MAXIMUM, COARSE TO FINE SAND, MOSTLY MEDIUM TO FINE; LESS THAN 5% NONPLASTIC FINES, YELLOWISH GRAY.
	85		54	SS 18	SP		GRAVELLY SAND, POORLY GRADED, 15-20% ROUNDED GRAVEL TO 0.5 INCH MAXIMUM, COARSE TO FINE SAND, MOSTLY COARSE AND FINE, LESS THAN 5% NONPLASTIC FINES, YELLOWISH GRAY.
	90		70	SS 19	SM-SW		SAND, POORLY GRADED, COARSE TO FINE, MOSTLY MEDIUM AND FINE, 5-8% NONPLASTIC FINES, YELLOWISH GRAY, SOME REDDISH BROWN STAINING AND A FEW PIECES OF GRAVEL TO 0.25 INCH MAXIMUM.
	95		80	SS 20	SP--		SAND, POORLY GRADED, LESS THAN 5% ROUNDED GRAVEL TO 0.5 INCH MAXIMUM, COARSE TO FINE SAND, MOSTLY MEDIUM AND FINE; LESS THAN 5% NONPLASTIC FINES, YELLOWISH GRAY.
	100		160	SS 21	SP-SM		SAND, POORLY GRADED, 5-8% SUBROUNDED GRAVEL TO 0.75 INCH MAXIMUM, COARSE TO FINE SAND, MOSTLY FINE, 5-8% NONPLASTIC FINES, LIGHT GRAY.
			CEMENTATED				
							END OF BORING AT 102.5 FT.

1. FIGURES IN BLOW OR RECOVERY COLUMN OPPOSITE SOIL SAMPLE DENOTE THE NUMBER OF BLOWS OF A 140 LB HAMMER FALLING 30" REQUIRED TO DRIVE A 2" OD SAMPLE SPOON 12" OR THE DISTANCE SHOWN. FIGURES SHOWN OPPOSITE ROCK CORES DENOTE THE PERCENT OF CORE RECOVERED.
2. ⊠2 INDICATES LOCATION OF UNDISTURBED SAMPLE. ⊠6 INDICATES LOCATION OF SPLIT-SPOON SAMPLE. ☐7 INDICATES LOCATION OF SAMPLING ATTEMPT WITH NO RECOVERY. SUBSCRIPT NEXT TO SYMBOL INDICATES SAMPLE NUMBER.
3. ⏚ INDICATES LOCATION OF NATURAL GROUND WATER TABLE.
4. RQD = ROCK QUALITY DESIGNATION.
5. ⊟ INDICATES DEPTH & LENGTH OF NX CORING RUN.
6. DATUM IS

NATIONAL SYNCHROTRON LIGHT SOURCE
BROOKHAVEN NATIONAL LABORATORY

STONE & WEBSTER ENGINEERING CORPORATION

SH 1 of 2

SITE NATIONAL SYNCHROTRON LIGHT SOURCE J.O. No. 13011.10 BORING No. 1

TYPE OF BORING SS LOCATION BROOKHAVEN NATIONAL LABORATORY GROUND ELEV. 72.3

DATE DRILLED AUGUST 24, 1977 DRILLED BY V. AINAR LOGGED BY [illegible]

SUMMARY OF BORING

ELEV. FEET	DEPTH FEET	OVERALL WEATHERING AND RQD	SAMPLE BLOWS/RECOV.	SAMPLE TYPE	GRAPHIC LOG	SOIL OR ROCK DESCRIPTION
						FIELD AND LABORATORY TEST RESULTS; OR IDENTIFICATION, BEDDING AND FAULTING DESCRIPTIONS — SOIL STRATA DESCRIPTION; LITHOLOGY AND TEXTURE
	0		18	SS 1	SM	TOP SOIL: SILTY SAND, WIDELY GRADED, 15-20% ANGULAR GRAVEL TO 0.7 INCH MAX. COARSE TO FINE, MOSTLY MEDIUM TO FINE SAND, 15-20% SLIGHTLY PLASTIC FINES, DARK BROWN MOTTLED WITH LIGHT BROWN, SOME ORGANIC MATERIAL
	5		36	SS 2	SW	SAND, POORLY GRADED, TRACE OF 0.4 INCH GRAVEL, COARSE TO FINE, MOSTLY MEDIUM SAND, <5% FINES, LIGHT BROWN
	10		30	SS 3	SW	GRAVELLY SAND, POORLY GRADED, 40-45% SUBANGULAR TO SUBROUNDED GRAVEL TO 0.8 INCH MAX. COARSE TO FINE, MOSTLY MEDIUM SAND, <5% FINES, LIGHT BROWN
	15		24	SS 4	SP-SM	SAND, POORLY GRADED, 3-8% GRAVEL TO 0.5 INCH MAX, COARSE TO FINE, MOSTLY MEDIUM SAND, 5-8% NONPLASTIC FINES, GRAYISH BROWN
	20		39	SS 5	SP-SM	GRAVELLY SAND, POORLY GRADED, 35-40% SUBROUNDED TO SUBANGULAR GRAVEL TO 0.7 [illegible] MAXIMUM COARSE TO FINE, MOSTLY MEDIUM SAND, 5-8% NONPLASTIC FINES, GRAYISH BROWN
	25		63	SS 6	SP-SM	GRAVELLY SAND, POORLY GRADED, 40-45% SUBANGULAR GRAVEL TO 0.9 INCH MAX. COARSE TO FINE, MOSTLY FINE SAND, 5-8% NONPLASTIC FINES, GRAYISH BROWN
	30		72	SS 7	SP	GRAVELLY SAND, POORLY GRADED, 15-20% SUBANGULAR GRAVEL TO 0.7 INCH MAX. COARSE TO FINE, MOSTLY MEDIUM SAND, <5% FINES GRAYISH BROWN
	35		74	SS 8	SP	GRAVELLY SAND, SIMILAR TO ABOVE, EXCEPT 30-35% GRAVEL
	40		96	SS 9	SP	SAND, POORLY GRADED, 3-5% GRAVEL TO 0.4 INCH MAX., COARSE TO FINE, MOSTLY FINE (VERY LITTLE COARSE) SAND, <5% FINES, GRAYISH BROWN
	45		29	SS 10	SP	GRAVELLY SAND, POORLY GRADED, 30-35% SUBROUNDED GRAVEL TO 0.7 INCH MAX. COARSE TO FINE, MOSTLY MEDIUM SAND, <5% FINES, GRAYISH BROWN
	50		43	SS 11	SP	GRAVELLY SAND, SIMILAR TO ABOVE
	55		AM	SS 12	SP	GRAVELLY SAND, SIMILAR TO ABOVE, EXCEPT 25-30% GRAVEL
	60		[illegible]	SS 13	SP	GRAVELLY SAND, POORLY GRADED, 40-45% SUBANGULAR TO SUBROUNDED GRAVEL TO 0.8 INCH MAX. COARSE TO FINE MOSTLY MEDIUM SAND, <5% FINES, GRAYISH BROWN
	65		69	SS 14	SP	GRAVELLY SAND, POORLY GRADED, 25-30% SUBANGULAR TO SUBROUNDED TO 0.7 INCH MAX. COARSE TO FINE, MOSTLY MEDIUM SAND, <5% FINES, GRAYISH BROWN
	70		65	SS 15	SP-SM	

1. FIGURES IN BLOW OR RECOVERY COLUMN OPPOSITE SOIL SAMPLE DENOTE THE NUMBER OF BLOWS OF A 140 LB HAMMER FALLING 30" REQUIRED TO DRIVE A 2" OD SAMPLE SPOON 12" OR THE DISTANCE SHOWN. FIGURES SHOWN OPPOSITE ROCK CORES DENOTE THE PERCENT OF CORE RECOVERED.
2. ▣2 INDICATES LOCATION OF UNDISTURBED SAMPLE. ▣6 INDICATES LOCATION OF SPLIT-SPOON SAMPLE. ▽7 INDICATES LOCATION OF SAMPLING ATTEMPT WITH NO RECOVERY. SUBSCRIPT NEXT TO SYMBOL INDICATES SAMPLE NUMBER.
3. ▼ INDICATES LOCATION OF NATURAL GROUND WATER TABLE.
4. RQD = ROCK QUALITY DESIGNATION.
5. [ ] INDICATES DEPTH & LENGTH OF NX CORING RUN.
6. DATUM IS

NATIONAL SYNCHROTRON LIGHT SOURCE
BROOKHAVEN NATIONAL LABORATORY

STONE & WEBSTER ENGINEERING CORPORATION

SH 2 of 2

SITE NATIONAL SYNCHROTRON LIGHT SOURCE J.O. No. 13011.10 BORING No. 1

TYPE OF BORING SS LOCATION BROOKHAVEN NATIONAL LABORATORY GROUND ELEV. 72.3

DATE DRILLED AUGUST 24, 1977 DRILLED BY V. AINAR LOGGED BY [illegible]

SUMMARY OF BORING

ELEV. FEET	DEPTH FEET	OVERALL WEATHERING AND RQD	SAMPLE BLOWS/RECOV.	SAMPLE TYPE	GRAPHIC LOG	SOIL OR ROCK DESCRIPTION
						FIELD AND LABORATORY TEST RESULTS; OR IDENTIFICATION, BEDDING AND FAULTING DESCRIPTIONS — SOIL STRATA DESCRIPTION; LITHOLOGY AND TEXTURE
	75		53	SS 16	SP-SM	SAND, POORLY GRADED, 3-5% GRAVEL, TO 0.5 INCH MAX. COARSE TO FINE, MOSTLY MEDIUM TO FINE SAND, 5-8% NONPLASTIC FINES, GRAYISH BROWN SAND, SIMILAR TO ABOVE
	80		63	SS 17	SP	GRAVELLY SAND, POORLY GRADED, 40-45% SUBANGULAR TO SUBROUNDED GRAVEL TO 0.7 INCH MAX. COARSE TO FINE, MOSTLY MEDIUM TO FINE SAND, <5% FINES, GRAYISH BROWN
	85		82	SS 18	SP	GRAVELLY SAND, SIMILAR TO ABOVE, EXCEPT 30-35% GRAVEL
	90		65	SS 19	SP	GRAVELLY SAND, SIMILAR TO ABOVE
	95		73	SS 20	SP	GRAVELLY SAND, POORLY GRADED, 10-15% SUBROUNDED GRAVEL TO 0.4 INCH MAX. COARSE TO FINE, MOSTLY MEDIUM SAND, <5% FINES, GRAYISH BROWN
	100		76	SS 21	SP	SAND, UNIFORM, MEDIUM TO FINE, TRACE OF COARSE SAND, <5% FINES, MEDIUM BROWN
		TERMINATED				END OF BORING AT 101.5 FT

1. FIGURES IN BLOW OR RECOVERY COLUMN OPPOSITE SOIL SAMPLE DENOTE THE NUMBER OF BLOWS OF A 140 LB HAMMER FALLING 30" REQUIRED TO DRIVE A 2" OD SAMPLE SPOON 12" OR THE DISTANCE SHOWN. FIGURES SHOWN OPPOSITE ROCK CORES DENOTE THE PERCENT OF CORE RECOVERED.
2. ▣2 INDICATES LOCATION OF UNDISTURBED SAMPLE. ▣6 INDICATES LOCATION OF SPLIT-SPOON SAMPLE. ▽7 INDICATES LOCATION OF SAMPLING ATTEMPT WITH NO RECOVERY. SUBSCRIPT NEXT TO SYMBOL INDICATES SAMPLE NUMBER.
3. ▼ INDICATES LOCATION OF NATURAL GROUND WATER TABLE.
4. RQD = ROCK QUALITY DESIGNATION.
5. [ ] INDICATES DEPTH & LENGTH OF NX CORING RUN.
6. DATUM IS

NATIONAL SYNCHROTRON LIGHT SOURCE
BROOKHAVEN NATIONAL LABORATORY

STONE & WEBSTER ENGINEERING CORPORATION

SH 1 OF 2

SITE NATIONAL SYNCHROTRON LIGHT SOURCE J.O. NO. ____ BORING NO. 1

TYPE OF BORING SS LOCATION BROOKHAVEN NATIONAL LABORATORY GROUND ELEV. 71.1

DATE DRILLED AUGUST 25, 1977 DRILLED BY V. ATMAR LOGGED BY MP

SUMMARY OF BORING ____

ELEV. FEET	DEPTH FEET	OVERALL WEATHERING AND RQD (0 25 50 75 100)	SAMPLE BLOWS/RECOV	SAMPLE TYPE	GRAPHIC LOG	SOIL OR ROCK DESCRIPTION (FIELD AND LABORATORY TEST RESULTS OR JOINTING, BEDDING AND FAULTING DESCRIPTIONS; SOIL STRATA DESCRIPTIONS; LITHOLOGY AND TEXTURE)
	0		17	SS	SM	TOP SOIL, SILTY SAND, TRACE GRAVEL, 10-12% SUBANGULAR GRAVEL TO 1.0 INCH MAXIMUM, COARSE TO FINE SAND, MOSTLY FINE, 20-30% NONPLASTIC FINES, BROWN, SOME ROOT PATTERNS, DRY MOIST, TRACE FRAGMENTS FILL
	5		24	SS	SM	SAND, UNIFORM FINE, LESS THAN 5% NONPLASTIC FINES, LIGHT GRAYISH BROWN.
	10		14	SS	SP	SAND, UNIFORM MEDIUM TO FINE, MOSTLY FINE, 5-8% NONPLASTIC FINES, YELLOWISH GRAY.
	15		54	SS	SP-SM	GRAVELLY SAND, POORLY GRADED 15-20% ROUNDED GRAVEL TO 0.5 INCH MAXIMUM, COARSE TO FINE SAND, MOSTLY COARSE AND MEDIUM, 5-8% NONPLASTIC FINES, YELLOWISH GRAY, ZONE POCKETS OF YELLOWISH GRAY SILTY SAND.
	20		97	SS	SP-SM	GRAVELLY SAND, POORLY GRADED, 15-20% SUBROUNDED GRAVEL TO 1.0 INCH MAXIMUM, COARSE TO FINE SAND, MOSTLY MEDIUM AND FINE, 10-12% NONPLASTIC FINES, BROWNISH GRAY.
	25		32	SS	SP	GRAVELLY SAND, POORLY GRADED, 15-20% ROUNDED GRAVEL TO 0.5 INCH MAXIMUM, COARSE TO FINE, MOSTLY MEDIUM AND FINE, LESS THAN 5% NONPLASTIC FINES, GRAY.
	30		45	SS	SP	SAND, UNIFORM MEDIUM TO FINE (TRACE OF COARSE), LESS THAN 5% NONPLASTIC FINES, GRAY, 3 PIECE OF GRAVEL TO 0.25 INCH MAXIMUM.
	35		75	SS	SP-SM	GRAVELLY SAND, POORLY GRADED, 15-18% SUBROUNDED GRAVEL TO 1.0 INCH MAXIMUM, COARSE TO FINE, MOSTLY COARSE AND MEDIUM, 10-12% NONPLASTIC FINES, YELLOWISH GRAY MOTTLED WITH DARK GRAY.
	40		47	SS	SP	GRAVELLY SAND, POORLY GRADED, 15-15% SUBROUNDED TO ROUNDED GRAVEL, TO 1.0 INCH, COARSE TO FINE MOSTLY MEDIUM AND FINE, LESS THAN 5% NONPLASTIC FINES, YELLOWISH GRAY.
	45		51	SS	SP	GRAVELLY SAND, POORLY GRADED, 20-30% SUBANGULAR TO SUBROUNDED GRAVEL TO 1.0 INCH MAXIMUM, COARSE TO FINE, MOSTLY MEDIUM AND FINE (VERY LITTLE COARSE), LESS THAN 5% NONPLASTIC FINES, YELLOWISH GRAY.
	50		93	SS	SP	GRAVELLY SAND, POORLY GRADED, 15-20% SUBROUNDED GRAVEL TO 0.5 INCH MAXIMUM, COARSE TO FINE, MOSTLY MEDIUM AND FINE, (VERY LITTLE COARSE) LESS THAN 5% NONPLASTIC FINES, YELLOWISH GRAY.
	55		124	SS	SP	GRAVELLY SAND, POORLY GRADED, 15-20% ROUNDED GRAVEL TO 0.5 INCH MAXIMUM, COARSE TO FINE, MOSTLY MEDIUM AND FINE, LESS THAN 5% NONPLASTIC FINES.
	60		124	SS	SP-SM	GRAVELLY SAND, POORLY GRADED, 20-30% SUBROUNDED GRAVEL TO 0.75 INCH MAXIMUM, COARSE TO FINE, MOSTLY MEDIUM AND FINE, 5-8% NONPLASTIC FINES, BROWNISH GRAY, WITH SOME BROWN STAINING.

1. FIGURES IN BLOW OR RECOVERY COLUMN OPPOSITE SOIL SAMPLE DENOTE THE NUMBER OF BLOWS OF A 140 LB HAMMER FALLING 30" REQUIRED TO DRIVE A 2" OD SAMPLE SPOON 12" OR THE DISTANCE SHOWN. FIGURES SHOWN OPPOSITE ROCK CORES DENOTE THE PERCENT OF CORE RECOVERED.
2. ⊠2 INDICATES LOCATION OF UNDISTURBED SAMPLE. ⊠6 INDICATES LOCATION OF SPLIT-SPOON SAMPLE. ⊠ INDICATES LOCATION OF SAMPLING ATTEMPT WITH NO RECOVERY. SUBSCRIPT NEXT TO SYMBOL INDICATES SAMPLE NUMBER.
3. ⊽ INDICATES LOCATION OF NATURAL GROUND WATER TABLE.
4. RQD - ROCK QUALITY DESIGNATION.
5. [INDICATES DEPTH & LENGTH OF NX CORING RUN.
6. DATUM IS

NATIONAL SYNCHROTRON LIGHT SOURCE
BROOKHAVEN NATIONAL LABORATORY

STONE & WEBSTER ENGINEERING CORPORATION

SH 2 OF 2

SITE NATIONAL SYNCHROTRON LIGHT SOURCE J.O. NO. ____ BORING NO. 2

TYPE OF BORING SS LOCATION BROOKHAVEN NATIONAL LABORATORY GROUND ELEV. 71.1

DATE DRILLED AUGUST 25, 1977 DRILLED BY V. ATMAR LOGGED BY MP

SUMMARY OF BORING ____

ELEV. FEET	DEPTH FEET	OVERALL WEATHERING AND RQD (0 25 50 75 100)	SAMPLE BLOWS/RECOV	SAMPLE TYPE	GRAPHIC LOG	SOIL OR ROCK DESCRIPTION (FIELD AND LABORATORY TEST RESULTS OR JOINTING, BEDDING AND FAULTING DESCRIPTIONS; SOIL STRATA DESCRIPTIONS; LITHOLOGY AND TEXTURE)
	75		#6	SS	SP	SAND, UNIFORM MEDIUM AND FINE, (TRACE OF ROUNDED GRAVEL TO 0.5 INCH MAXIMUM, (A TRACE OF COARSE SAND) LESS THAN 5% NONPLASTIC FINES, YELLOWISH GRAY.
	80		#6	SS	SP	GRAVELLY SAND, POORLY GRADED, 10-15% SUBANGULAR TO SUBROUNDED GRAVEL TO 0.5 INCH MAXIMUM, COARSE TO FINE, MOSTLY MEDIUM, LESS THAN 5% NONPLASTIC FINES, YELLOWISH GRAY.
	85		#6	SS	SP	GRAVELLY SAND, POORLY GRADED, 10-15% GRAVEL TO 0.5 INCH MAXIMUM, COARSE TO FINE SAND, MOSTLY MEDIUM AND FINE, (TRACE OF COARSE) LESS THAN 5% NONPLASTIC FINES, YELLOWISH GRAY.
	90		#5	SS	SP	SAND, UNIFORM MEDIUM AND FINE, (TRACE OF GRAVEL TO 0.25 INCH) MOSTLY FINE, LESS THAN 5% NONPLASTIC FINES, GRAY.
	95		#2	SS	SP	GRAVELLY SAND, POORLY GRADED 15-20% SUBROUNDED TO ROUNDED GRAVEL TO 0.5 INCH MAXIMUM, COARSE TO FINE SAND, MOSTLY MEDIUM AND FINE, LESS THAN 5% NONPLASTIC FINES, GRAY.
	100		#6	SS	SP	GRAVELLY SAND, POORLY GRADED, 15-20% SUBROUNDED GRAVEL, COARSE TO FINE, MOSTLY MEDIUM, LESS THAN 5% NONPLASTIC FINES, YELLOWISH GRAY.
	TERMINATED		#27	SS	SP	SAND, UNIFORM MEDIUM AND FINE, (TRACE OF GRAVEL TO 0.25 INCH), LESS THAN 5% NONPLASTIC FINES, GRAY.

END OF BORING AT 101.5 FT

1. FIGURES IN BLOW OR RECOVERY COLUMN OPPOSITE SOIL SAMPLE DENOTE THE NUMBER OF BLOWS OF A 140 LB HAMMER FALLING 30" REQUIRED TO DRIVE A 2" OD SAMPLE SPOON 12" OR THE DISTANCE SHOWN. FIGURES SHOWN OPPOSITE ROCK CORES DENOTE THE PERCENT OF CORE RECOVERED.
2. ⊠2 INDICATES LOCATION OF UNDISTURBED SAMPLE. ⊠6 INDICATES LOCATION OF SPLIT-SPOON SAMPLE. ⊠ INDICATES LOCATION OF SAMPLING ATTEMPT WITH NO RECOVERY. SUBSCRIPT NEXT TO SYMBOL INDICATES SAMPLE NUMBER.
3. ⊽ INDICATES LOCATION OF NATURAL GROUND WATER TABLE.
4. RQD - ROCK QUALITY DESIGNATION.
5. [INDICATES DEPTH & LENGTH OF NX CORING RUN.
6. DATUM IS

NATIONAL SYNCHROTRON LIGHT SOURCE
BROOKHAVEN NATIONAL LABORATORY

STONE & WEBSTER ENGINEERING CORPORATION

SH 1 OF 2

SITE NATIONAL SYNCHROTRON LIGHT SOURCE JO NO. 7011.01 BORING No. 1

TYPE OF BORING SS LOCATION BROOKHAVEN NATIONAL LABORATORY GROUND ELEV. 72.6

DATE DRILLED AUGUST 24, 1977 DRILLED BY TOMPKINS LOGGED BY RBP

SUMMARY OF BORING

ELEV. FEET	DEPTH FEET	OVERALL WEATHERING AND RQD	SAMPLE BLOWS/6" RECOV.	SAMPLE TYPE	GRAPHIC LOG	SOIL OR ROCK DESCRIPTION (FIELD AND LABORATORY TEST RESULTS; SOIL STRATA DESCRIPTIONS; LITHOLOGY; WEATHERING, BEDDING AND FRACTURING; SOIL TESTURE)
	0					
	5		55 1	SP		SAND, UNIFORM, FINE TO VERY FINE, MOSTLY FINE, < 5% NONPLASTIC FINES, GRAYISH YELLOW.
	10		22 33 2	SP		SAND, UNIFORM, MEDIUM TO FINE, MOSTLY FINE, < 5% NONPLASTIC FINES, GRAYISH YELLOW.
	15		24 33 3	SP		SAND, SIMILAR TO SS #2, [illegible] GRAY.
	20		42 55 4	SP		SAND, UNIFORM, MEDIUM TO FINE, MOSTLY FINE, < 5% NONPLASTIC FINES, YELLOWISH GRAY.
	25		67 55 5	SP		GRAVELLY SAND, POORLY GRADED, 15-20% SUBROUNDED TO ROUNDED, GRAVEL TO 1.0 INCH MAXIMUM, COARSE TO FINE, MOSTLY MEDIUM AND FINE, < 5% NONPLASTIC FINES, YELLOWISH GRAY.
	30		35 55 6	SP-SM		GRAVELLY SAND, POORLY GRADED, [illegible] SUBROUNDED GRAVEL TO 0.5 INCH MAXIMUM, COARSE TO FINE SAND, MOSTLY MEDIUM AND FINE, 5-8% NONPLASTIC FINES, YELLOWISH GRAY.
	35		55	SP-SM		SAND, SAME AS #6.
	40		4	SP-SM		GRAVELLY SAND, POORLY GRADED, [illegible] ROUNDED GRAVEL TO 0.5 INCH MAXIMUM, COARSE TO FINE SAND, MOSTLY SAND, 5-8% NONPLASTIC FINES, MOTTLED YELLOWISH GRAY AND LIGHT YELLOWISH BROWN.
	45		79 55 8	SP		SAND, POORLY GRADED, COARSE TO FINE, MOSTLY MEDIUM AND FINE, < 5% NONPLASTIC FINES, YELLOWISH GRAY.
	50		64 55 10	SP		SAND, [illegible], MEDIUM TO FINE, MOSTLY FINE (ONE PIECE OF GRAVEL TO 0.5 INCH) < 5% NONPLASTIC FINES, YELLOWISH GRAY.
	55		21 55 11	SP		SAND, SAME AS #10 (NO GRAVEL).
	60		57 55 12	SP		SAND, UNIFORM, MEDIUM TO FINE, MOSTLY FINE (TRACE OF COARSE AND ONE PIECE OF GRAVEL TO 0.25 INCH) < 5% NONPLASTIC FINES.
	65		50 55 13	SP		GRAVELLY SAND, GAP GRADED, 20-25% SUBROUNDED GRAVEL TO 1.0 INCH MAXIMUM, MOSTLY MEDIUM AND FINE, < 5% NONPLASTIC FINES, GRAYISH YELLOW.
	70		35 55 14	SP		SAND, UNIFORM, FINE TO MEDIUM (ONE PIECE OF GRAVEL TO 0.3 INCH) TRACE OF COARSE SAND, < 5% NONPLASTIC FINES, YELLOWISH GRAY.

1. FIGURES IN BLOW OR RECOVERY COLUMN OPPOSITE SOIL SAMPLE DENOTE THE NUMBER OF BLOWS OF A 140 LB HAMMER FALLING 30" REQUIRED TO DRIVE A 2" OD SAMPLE SPOON 12" OR THE DISTANCE SHOWN. FIGURES SHOWN OPPOSITE ROCK CORES DENOTE THE PERCENT OF CORE RECOVERED.
2. ■ INDICATES LOCATION OF UNDISTURBED SAMPLE. ▼ INDICATES LOCATION OF SPLIT-SPOON SAMPLE. ☐ INDICATES LOCATION OF SAMPLING ATTEMPT WITH NO RECOVERY. SUBSCRIPT NEXT TO SYMBOL INDICATES SAMPLE NUMBER.
3. ⏚ INDICATES LOCATION OF NATURAL GROUND WATER TABLE.
4. RQD - ROCK QUALITY DESIGNATION.
5. ☐ INDICATES DEPTH & LENGTH OF NX CORING RUN.
6. DATUM IS

NATIONAL SYNCHROTRON LIGHT SOURCE
BROOKHAVEN NATIONAL LABORATORY

STONE & WEBSTER ENGINEERING CORPORATION

SH 2 OF 2

SITE NATIONAL SYNCHROTRON LIGHT SOURCE JO NO. 7011.01 BORING No. 1

TYPE OF BORING SS LOCATION BROOKHAVEN NATIONAL LABORATORY GROUND ELEV. 72.6

DATE DRILLED AUGUST 24, 1977 DRILLED BY TOMPKINS LOGGED BY RBP

SUMMARY OF BORING

ELEV. FEET	DEPTH FEET	OVERALL WEATHERING AND RQD	SAMPLE BLOWS/6" RECOV.	SAMPLE TYPE	GRAPHIC LOG	SOIL OR ROCK DESCRIPTION (FIELD AND LABORATORY TEST RESULTS; SOIL STRATA DESCRIPTIONS; LITHOLOGY; WEATHERING, BEDDING AND FRACTURING; SOIL TESTURE)
	75		55 15	SP		GRAVELLY SAND, POORLY GRADED, 15-15% SUBROUNDED GRAVEL TO 1.0 INCH MAXIMUM, MEDIUM TO FINE, MOSTLY FINE, < 5% NONPLASTIC FINES, GRAYISH YELLOW - BROKEN JAR.
	80		109 55 16	SP		SAND, POORLY GRADED, 5-8% SUBANGULAR GRAVEL TO 0.25 INCH MAXIMUM, COARSE TO FINE SAND, MOSTLY MEDIUM TO FINE, < 5% NONPLASTIC FINES, YELLOWISH GRAY.
	85		121 55 17	SP		GRAVELLY SAND, POORLY GRADED, 15-20% GRAVEL TO 0.75 INCH MAXIMUM, COARSE TO FINE SAND, MOSTLY MEDIUM AND FINE, < 5% NONPLASTIC FINES, YELLOWISH GRAY, LAYER OF GRAY FINE TO VERY FINE SAND.
	90		253 55 18	SP		SAND, UNIFORM, MEDIUM TO FINE, MOSTLY FINE (TRACE OF COARSE) < 5% NONPLASTIC FINES, GRAYISH YELLOW.
	95		196 55 19	SP		SAND, POORLY GRADED, COARSE TO FINE, MOSTLY MEDIUM AND FINE, < 5% NONPLASTIC FINES, YELLOWISH GRAY WITH SOME REDDISH BROWN STAINING.
	100	Terminated	243 55 20	SP		SAND, UNIFORM, FINE TO VERY FINE (TRACE OF COARSE) < 5% NONPLASTIC FINES, YELLOWISH GRAY.
	105					END OF BORING AT 102.0 FT

1. FIGURES IN BLOW OR RECOVERY COLUMN OPPOSITE SOIL SAMPLE DENOTE THE NUMBER OF BLOWS OF A 140 LB HAMMER FALLING 30" REQUIRED TO DRIVE A 2" OD SAMPLE SPOON 12" OR THE DISTANCE SHOWN. FIGURES SHOWN OPPOSITE ROCK CORES DENOTE THE PERCENT OF CORE RECOVERED.
2. ■ INDICATES LOCATION OF UNDISTURBED SAMPLE. ▼ INDICATES LOCATION OF SPLIT-SPOON SAMPLE. ☐ INDICATES LOCATION OF SAMPLING ATTEMPT WITH NO RECOVERY. SUBSCRIPT NEXT TO SYMBOL INDICATES SAMPLE NUMBER.
3. ⏚ INDICATES LOCATION OF NATURAL GROUND WATER TABLE.
4. RQD - ROCK QUALITY DESIGNATION.
5. ☐ INDICATES DEPTH & LENGTH OF NX CORING RUN.
6. DATUM IS

NATIONAL SYNCHROTRON LIGHT SOURCE
BROOKHAVEN NATIONAL LABORATORY

STONE & WEBSTER ENGINEERING CORPORATION

SITE NATIONAL SYNCHROTRON LIGHT SOURCE J.O.No. 13011.01 BORING No. 6
TYPE OF BORING SS LOCATION BROOKHAVEN NATIONAL LABORATORY GROUND ELEV. 74±
DATE DRILLED AUGUST 25, 1977 DRILLED BY TOMKINS LOGGED BY DRM
SUMMARY OF BORING

ELEV. FEET	DEPTH FEET	OVERALL WEATHERING AND RQD (0 25 50 75 100)	SAMPLE BLOWS/6" RECOV.	SAMPLE TYPE	GRAPHIC LOG	SOIL OR ROCK DESCRIPTION (FIELD AND LABORATORY TEST RESULTS; BED./JOINTING, BEDDING AND FAULTING DESCRIPTIONS; SOIL STRATA DESCRIPTIONS; LITHOLOGY AND TEXTURE)
	0					
	5		4	SS	SM	SILTY SAND, UNIFORM MEDIUM TO FINE, MOSTLY FINE, 12-15% NONPLASTIC FINES, YELLOWISH BROWN
	10		14	SS	SM	SILTY SAND, WIDELY GRADED, 18-23% SUBANGULAR GRAVEL TO 0.7 INCH MAX. COARSE TO FINE, MOSTLY MEDIUM TO FINE SAND, 18-23% NONPLASTIC FINES, BROWN
	15		50	SS 3	SP	SAND, POORLY GRADED, 10-15% SUBANGULAR GRAVEL TO 0.6 INCH MAX. COARSE TO FINE, MOSTLY MEDIUM TO FINE SAND, <5% FINES, BROWN
	20		147	SS 4	GP	SANDY GRAVEL, POORLY GRADED, SUBANGULAR TO 0.8 INCH MAX. 43-47% COARSE TO FINE, MOSTLY MEDIUM TO FINE SAND, 3-5% FINES, GRAYISH BROWN
	25		126	SS 5	SP	GRAVELLY SAND, POORLY GRADED, 40-45% SUBANGULAR TO SUBROUNDED TO 0.7 INCH MAX. COARSE TO FINE, MOSTLY MEDIUM SAND, <5% FINES, GRAYISH BROWN
	30		149	SS 6	SP	GRAVELLY SAND, POORLY GRADED, 20-25% SUBANGULAR GRAVEL TO 0.8 INCH MAX. COARSE TO FINE, MOSTLY MEDIUM TO FINE SAND, <5% FINES, GRAYISH BROWN
	35		123	SS 7	SP	GRAVELLY SAND, POORLY GRADED, 40-45% SUBANGULAR GRAVEL TO 0.7 INCH MAX. COARSE TO FINE, MOSTLY MEDIUM TO FINE SAND, <5% FINES, GRAYISH BROWN
	40		83	SS 8	SP	GRAVELLY SAND, POORLY GRADED, 12-16% SUBROUNDED GRAVEL TO 0.5 INCH MAX. COARSE TO FINE, MOSTLY MEDIUM TO FINE SAND, <5% FINES, GRAYISH BROWN
	45		99	SS 9	SP	GRAVELLY SAND, SIMILAR TO ABOVE, EXCEPT 10-15% GRAVEL
	50		128	SS 10	SP	GRAVELLY SAND, SIMILAR TO ABOVE, EXCEPT 15-25% GRAVEL TO 0.6 INCH MAX.
	55		212	SS 11	SP-SM	SAND, POORLY GRADED, 5-8% GRAVEL TO 0.4 INCH MAX. COARSE TO FINE, MOSTLY MEDIUM TO FINE SAND, 5-8% NONPLASTIC FINES, GRAYISH BROWN
	60		40	SS 12	SP-SM	SAND, SIMILAR TO ABOVE
	65		72	SS 13	SP-SM	SAND, SIMILAR TO ABOVE
	70		57	SS 14	SP-SM	SAND, UNIFORM, MEDIUM TO FINE, TRACE OF 0.4 INCH GRAVEL, 5-8% NONPLASTIC FINES, GRAY

1. FIGURES IN BLOW OR RECOVERY COLUMN OPPOSITE SOIL SAMPLE DENOTE THE NUMBER OF BLOWS OF A 140 LB HAMMER FALLING 30" REQUIRED TO DRIVE A 2" OD SAMPLE SPOON 12" OR THE DISTANCE SHOWN. FIGURES SHOWN OPPOSITE ROCK CORES DENOTE THE PERCENT OF CORE RECOVERED.
2. ⊠2 INDICATES LOCATION OF UNDISTURBED SAMPLE. ⊠6 INDICATES LOCATION OF SPLIT-SPOON SAMPLE. ☒ INDICATES LOCATION OF SAMPLING ATTEMPT WITH NO RECOVERY. SUBSCRIPT NEXT TO SYMBOL INDICATES SAMPLE NUMBER.
3. ⏚ INDICATES LOCATION OF NATURAL GROUND WATER TABLE.
4. RQD = ROCK QUALITY DESIGNATION.
5. [INDICATES DEPTH & LENGTH OF NX CORING RUN.
6. DATUM IS

NATIONAL SYNCHROTRON LIGHT SOURCE
BROOKHAVEN NATIONAL LABORATORY

STONE & WEBSTER ENGINEERING CORPORATION

SITE NATIONAL SYNCHROTRON LIGHT SOURCE J.O No. 13011.01 BORING No. 6
TYPE OF BORING SS LOCATION BROOKHAVEN NATIONAL LABORATORY GROUND ELEV. 74±
DATE DRILLED AUGUST 25, 1977 DRILLED BY TOMKINS LOGGED BY DRM
SUMMARY OF BORING

ELEV. FEET	DEPTH FEET	OVERALL WEATHERING AND RQD (0 25 50 75 100)	SAMPLE BLOWS/6" RECOV.	SAMPLE TYPE	GRAPHIC LOG	SOIL OR ROCK DESCRIPTION (FIELD AND LABORATORY TEST RESULTS; BED./JOINTING, BEDDING AND FAULTING DESCRIPTIONS; SOIL STRATA DESCRIPTIONS; LITHOLOGY AND TEXTURE)
	75		132	SS 15	SP-SM	SAND, POORLY GRADED, 8-12% GRAVEL TO 0.5 INCH MAX., COARSE TO FINE, MOSTLY MEDIUM TO FINE SAND, 5-8% NONPLASTIC FINES, GRAYISH BROWN
	80		190/9"	SS 16	SP-SM	SAND, SIMILAR TO ABOVE
	85		206	SS 17	SP-SM	GRAVELLY SAND, POORLY GRADED, 10-15% SUBANGULAR GRAVEL TO 0.5 INCH MAX. COARSE TO FINE, MOSTLY MEDIUM TO FINE SAND, 5-8% NONPLASTIC FINES, GRAYISH BROWN
	90		90	SS 18	SP-SM	SAND, UNIFORM, MEDIUM TO FINE, TRACE OF 0.4 INCH GRAVEL, 5-8% NONPLASTIC FINES, GRAYISH BROWN
	95		136	SS 19	SP	GRAVELLY SAND, POORLY GRADED, 15-20% SUBANGULAR GRAVEL TO 0.6 INCH MAX. COARSE TO FINE, MOSTLY MEDIUM TO FINE SAND, <5% FINES, GRAYISH BROWN
	100		177	SS 20	SP	SAND, POORLY GRADED, 8-12% GRAVEL TO 0.5 INCH MAX. COARSE TO FINE, MOSTLY MEDIUM SAND, <5% FINES, GRAYISH BROWN
		TERMINATED				END OF BORING AT 102 FT

1. FIGURES IN BLOW OR RECOVERY COLUMN OPPOSITE SOIL SAMPLE DENOTE THE NUMBER OF BLOWS OF A 140 LB HAMMER FALLING 30" REQUIRED TO DRIVE A 2" OD SAMPLE SPOON 12" OR THE DISTANCE SHOWN. FIGURES SHOWN OPPOSITE ROCK CORES DENOTE THE PERCENT OF CORE RECOVERED.
2. ⊠2 INDICATES LOCATION OF UNDISTURBED SAMPLE. ⊠6 INDICATES LOCATION OF SPLIT-SPOON SAMPLE. ☒ INDICATES LOCATION OF SAMPLING ATTEMPT WITH NO RECOVERY. SUBSCRIPT NEXT TO SYMBOL INDICATES SAMPLE NUMBER.
3. ⏚ INDICATES LOCATION OF NATURAL GROUND WATER TABLE.
4. RQD = ROCK QUALITY DESIGNATION.
5. [INDICATES DEPTH & LENGTH OF NX CORING RUN.
6. DATUM IS

NATIONAL SYNCHROTRON LIGHT SOURCE
BROOKHAVEN NATIONAL LABORATORY

STONE & WEBSTER ENGINEERING CORPORATION

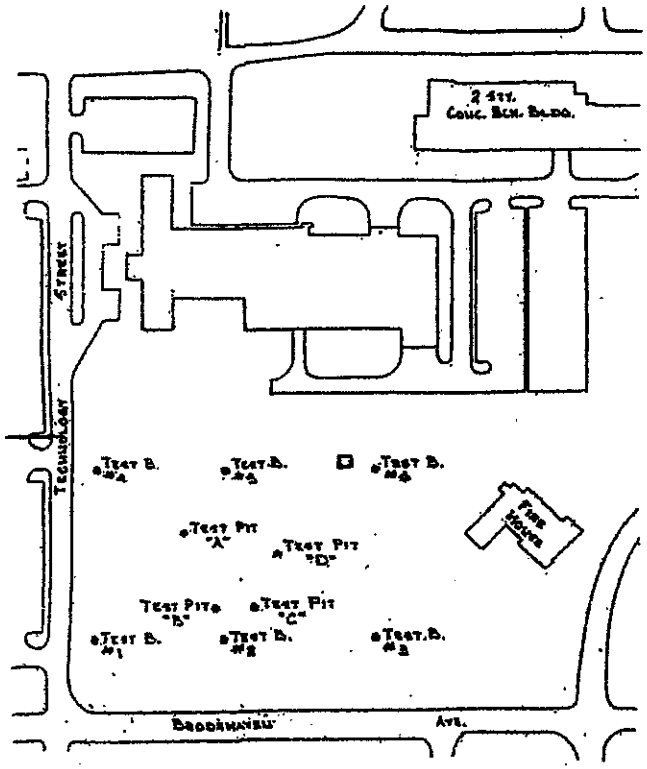

LOG OF TEST PITS

Test Pit "A"

East Wall

0 - 2'-6" Fill, Topsoil At Top
2'-6" - 4'-0" Sand, Silty, Fine Uniform, Compact, Medium Brown Weathered And Stained
4'-0" - 12'-0" Sand, Clean, Medium Fine, Uniform, Firm Well Rounded, Light Yellow Gray Shows Fore-Set Bedding Dipping South

West Wall

0 - 1'0" Fill, Sandy Topsoil
1'0" - 3'-3" Fill, Sandy
3'-3" - 5'-6" Sand, Silty, Fine, Uniform, Compact, Medium Brown, Weathered And Stained
5'-6" - 12'-0" Sand, Clean, Medium Fine, Uniform, Firm Well Rounded, Light Yellow-Gray Shows Fore-Set Bedding Dipping SW 20°

Test Pit "B"

0 - 3'-3" Topsoil (Fill?)
3'-3" - 8'-0" Sand, Silty, Fine, Uniform, Compact Medium Brown, Weathered And Stained
8'-0" - 12'-0" Sand, Clean, Medium Fine, Uniform Firm, Rounded, Light Yellow Gray Shows Fore-Set Bedding Dipping SW At 15°-20°

Note: Backfilled Trench Crosses Test Pit In East - West Direction - Bottom Depth Of 6-8 Ft. From Surface

Test Pit "C"

0 - 1'-5" Fill - Topsoil
1'-5" - 2'-4" Topsoil
2'-4" - 5'-7" Sand, Silty, Fine, Uniform, Compact Medium Brown, Weathered And Stained
5'-7" - 12'-0" Sand, Clean, Medium Fine, Uniform, Firm Rounded, Light Yellow Gray Shows Fore-Set Bedding Dipping W&W

Note: Backfilled Trench Crosses Test Pit In East - West Direction, Bottom Depth 6'-8"

Test Pit "D"

0 - 1'-0" Topsoil
1'-0" - 4'-10" Sand, Silty, Fine, Uniform, Compact Medium Brown, Weathered And Stained
4'-10" - 11'-0" Sand, Clean, Medium Fine, Uniform Firm, Rounded, Light Yellow-Gray Shows Fore-Set Bedding Dipping W&W At 20°

Location	Ground Elev.	Coordinates North	Coordinates East
Test Boring #1	72.8	100,100	100,350
" " #2	71.4	100,100	100,510
" " #3	72.3	100,100	100,700
" " #4	73.1	100,320	100,350
" " #5	72.6	100,320	100,510
" " #6	74.4	100,320	100,700
Test Pit A	71.7	100,240	100,460
" " B	71.5	100,140	100,500
" " C	71.7	100,140	100,350
" " D	71.7	100,210	100,580

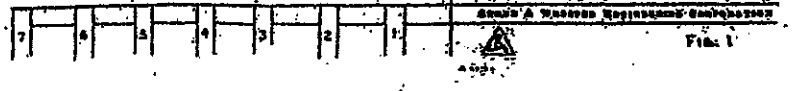

FOUNDATION INVESTIGATIONS
NATIONAL SYNCHROTRON LIGHT SOURCE
BROOKHAVEN NATIONAL LABORATORY

Fig. 1

Appendix B

2003 Test Boring Logs

CLIENT: GEI

PROJECT NAME: Brookhaven National Labs

LOCATION: Long Island, NY

DRILLER: T. Roe

INSPECTOR: A. Smart

DATE START: 10/28/03

DATE FINISH: 10/28/03

NEW ENGLAND BORING CONTRACTORS OF CT., INC.

129 KRIEGER LANE
GLASTONBURY, CT 06033
(860) 633-4649 – (413) 733-1232
FAX (860) 657-8046

BORING No. B-1

SHEET 1 OF 1

ARCHITECT/ ENGINEER

FILE NO. GEI-LongIsland, NY

SURFACE ELEV.

LINE & STATION

OFFSET

	Casing	Sampler	Core Barrel
TYPE	HSA	SS	
SIZE I.D.	3-1/4"	1-3/8"	
HAMMER WT.		140	
HAMMER FALL		30"	

SAMPLE No.	DEPTH RANGE IN FEET	BLOWS PER 6" ON SAMPLER 0-6	6-12	12-18	18-24	REC.	CASING BLOWS/ CORING TIMES PER FT.	FIELD CLASSIFICATION AND REMARKS	Well Cons.	Installation Details
S1	0'-2'	1	1	2	1	8"		8" Dark Brown Topsoil .6 Gray Brown Fine Sand, Some Silt, Trace of Roots - Fill 2.5		
S2	5'-7'	5	6	8	9	14"		Light Brown Fine Sand, Stratified		
S3	10'-12'	7	7	9	12	24"		Light Brown Fine Sand, Some Silt, Stratified		
S4	15'-17'	5	12	14	13	20"		Light Brown Fine Sand, Little Gravel, Stratified Cobble @ 19'-19'6"		
S5	20'-22'	5	7	7	9	24"		Brown Fine-Med. Sand, Trace of Gravel, Stratified		
S6	25'-27'	5	6	10	11	24"				
S7	30'-32'	9	11	13	17	20"		Brown Med.-Crs. Sand, Little Fine Sand 32.0 End of Boring @ 32' Water @ 31'		

NOTES: 1) The stratification lines represent the approximate boundary between soil types. Transitions may be gradual.

2) Water level readings have been made in the drill holes at times and under conditions stated on the boring logs. Fluctuations in the level of groundwater may occur due to factors other than those present at the time measurements were made.

REMARKS:

CLIENT: GEI

PROJECT NAME: Brookhaven National Labs

LOCATION: Long Island, NY

DRILLER: T. Roe

INSPECTOR: A. Smart

DATE START: 10/28/03

DATE FINISH: 10/28/03

NEW ENGLAND BORING CONTRACTORS OF CT., INC.

129 KRIEGER LANE
GLASTONBURY, CT 06033
(860) 633-4649 – (413) 733-1232
FAX (860) 657-8046

	Casing	Sampler	Core Barrel
TYPE	HSA	SS	
SIZE I.D.	3-1/4"	1-3/8"	
HAMMER WT.		140	
HAMMER FALL		30"	

BORING No. B-2

SHEET 1 OF 1

ARCHITECT/ ENGINEER

FILE NO. GEI-LongIsland, NY

SURFACE ELEV.

LINE & STATION

OFFSET

SAMPLE No.	DEPTH RANGE IN FEET	BLOWS PER 6" ON SAMPLER 0-6	6-12	12-18	18-24	REC.	CASING BLOWS/ CORING TIMES PER FT.	FIELD CLASSIFICATION AND REMARKS	Well Cons.	Installation Details
S1	0'-2'	2	2	2	2	20"		5" Dark brown Sandy Topsoil (.4)		
								Brown Fine Sand, Little Silt, Trace of Roots - Fill (3.0)		
S2	5'-7'	4	7	10	13	18"		Light Brown Fine Sand		
								Trace of Silt @ S6, Stratified		
S3	10'-12'	3	5	5	7	18"		Little Silt @ S7		
S4	15'-17'	3	4	5	5	16"				
S5	20'-22'	5	5	6	8	18"				
S6	25'-27'	6	8	10	10	20"				
S7	30'-32'	7	9	10	9	18"		(32.0)		
								End of Boring @ 32'		
								Water @ 29'		
								Water @ 28' Overnight		

NOTES: 1) The stratification lines represent the approximate boundary between soil types. Transitions may be gradual.

2) Water level readings have been made in the drill holes at times and under conditions stated on the boring logs. Fluctuations in the level of groundwater may occur due to factors other than those present at the time measurements were made.

REMARKS: *Note: Moved Hole 10' West Due to Overhead Branches*

CLIENT: GEI

PROJECT NAME: Brookhaven National Labs

LOCATION: Long Island, NY

DRILLER: T. Roe

INSPECTOR: A. Smart

DATE START: 10/28/03

DATE FINISH: 10/28/03

NEW ENGLAND BORING CONTRACTORS OF CT., INC.

129 KRIEGER LANE
GLASTONBURY, CT 06033
(860) 633-4649 – (413) 733-1232
FAX (860) 657-8046

BORING No. B-3

SHEET 1 OF 1

ARCHITECT/ ENGINEER

FILE NO. GEI-LongIsland, NY

SURFACE ELEV.

LINE & STATION

OFFSET

	Casing	Sampler	Core Barrel
TYPE	HSA	SS	
SIZE I.D.	3-1/4"	1-3/8"	
HAMMER WT.		140	
HAMMER FALL		30"	

SAMPLE No.	DEPTH RANGE IN FEET	BLOWS PER 6" ON SAMPLER 0-6	6-12	12-18	18-24	REC.	CASING BLOWS/ CORING TIMES PER FT.	FIELD CLASSIFICATION AND REMARKS	Well Cons.	Installation Details
S1	0'-2'	3	3	1	1	14"		1" Asphalt - 2" Dark Brown Topsoil. (2)		
								Brown Fine Sand, Trace of Silt, Possible Fill (2.5)		
S2	5'-7'	3	6	8	10	20"		Light Brown Fine Sand, Stratified		
S3	10'-12'	3	5	5	5	16"				
S4	15'-17'	3	2	3	4	24"				
S5	20'-22'	3	4	5	8	20"				
S6	25'-27'	4	6	6	9	24"				
S7	30'-32'	2	5	6	10	24"		(32.0) End of Boring @ 32'		
								Water @ 31'		
								Water @ 28' Overnight		

NOTES: 1) The stratification lines represent the approximate boundary between soil types. Transitions may be gradual.

2) Water level readings have been made in the drill holes at times and under conditions stated on the boring logs. Fluctuations in the level of groundwater may occur due to factors other than those present at the time measurements were made.

REMARKS:

CLIENT: GEI

PROJECT NAME: Brookhaven National Labs

LOCATION: Long Island, NY

DRILLER: T. Roe

INSPECTOR: A. Smart

DATE START: 10/27/03

DATE FINISH: 10/27/03

NEW ENGLAND BORING CONTRACTORS OF CT., INC.

129 KRIEGER LANE
GLASTONBURY, CT 06033
(860) 633-4649 – (413) 733-1232
FAX (860) 657-8046

	Casing	Sampler	Core Barrel
TYPE	NW	SS	
SIZE I.D.	3"	1-3/8"	
HAMMER WT.	300	140	
HAMMER FALL	24"	30"	

BORING No. B-4

SHEET 1 OF 2

ARCHITECT/ ENGINEER

FILE NO. GEI-LongIsland, NY

SURFACE ELEV.

LINE & STATION

OFFSET

SAMPLE No.	DEPTH RANGE IN FEET	BLOWS PER 6" ON SAMPLER 0-6	6-12	12-18	18-24	REC.	CASING BLOWS/ CORING TIMES PER FT.	FIELD CLASSIFICATION AND REMARKS	Well Cons.	Installation Details
S1	0'-2'	1	2	2	3	20"		Dark Brown Sandy Topsoil (1.0) / Gray Fine Sand, Little Silt, Trace of Roots - Fill (3.0) / Light Brown Fine-Med. Sand, Stratified		
S2	5'-7'	8	11	13	14	20"				
S3	10'-12'	9	10	9	8	18"				
S4	15'-17'	11	14	17	19	16"		Light Brown Fine-Crs. Sand, Trace of Fine Gravel, Stratified		
S5	20'-22'	3	4	6	9	12"		Light Brown Fine Sand, Some Med.-Crs. Sand, Trace of Fine-Crs. Gravel		
S6	25'-27'	14	16	26	28	12"				
S7	30'-32'	15	25	25	28	12"				
S8	35'-37'	9	12	15	22	14"				
S9	40'-42'	13	25	34	36	12"				
S10	45'-47'	9	22	22	25	14"				
S11	50'-52'	9	15	16	14	12"				
S12	55'-57'	10	14	10	9	12"				

NOTES: 1) The stratification lines represent the approximate boundary between soil types. Transitions may be gradual.

2) Water level readings have been made in the drill holes at times and under conditions stated on the boring logs. Fluctuations in the level of groundwater may occur due to factors other than those present at the time measurements were made.

REMARKS:

CLIENT: GEI

PROJECT NAME: Brookhaven National Labs

LOCATION: Long Island, NY

DRILLER: T. Roe

INSPECTOR: A. Smart

DATE START: 10/27/03

DATE FINISH: 10/27/03

NEW ENGLAND BORING CONTRACTORS OF CT., INC.

129 KRIEGER LANE
GLASTONBURY, CT 06033
(860) 633-4649 -- (413) 733-1232
FAX (860) 657-8046

	Casing	Sampler	Core Barrel
TYPE	NW	SS	
SIZE I.D.	3"	1-3/8"	
HAMMER WT.	300	140	
HAMMER FALL	24"	30"	

BORING No. B-4

SHEET 2 OF 2

ARCHITECT/ ENGINEER

FILE NO. GEI-LongIsland, NY

SURFACE ELEV.

LINE & STATION

OFFSET

SAMPLE No.	DEPTH RANGE IN FEET	BLOWS PER 6" ON SAMPLER 0-6	6-12	12-18	18-24	REC.	CASING BLOWS/ CORING TIMES PER FT.	FIELD CLASSIFICATION AND REMARKS	Well Cons.	Installation Details
S13	60'-62'	8	13	17	18	12"				
								62.0		
								End of Boring @ 62'		
								Water @ 18' Overnight		
								Water @ 23' After 60 Hours +/-		

CLIENT: GEI

PROJECT NAME: Brookhaven National Labs

LOCATION: Long Island, NY

DRILLER: T. Roe

INSPECTOR: A. Smart

DATE START: 10/30/03

DATE FINISH: 10/30/03

NEW ENGLAND BORING CONTRACTORS OF CT., INC.

129 KRIEGER LANE
GLASTONBURY, CT 06033
(860) 633-4649 – (413) 733-1232
FAX (860) 657-8046

	Casing	Sampler	Core Barrel
TYPE	HSA	SS	
SIZE I.D.	3-1/4"	1-3/8"	
HAMMER WT.		140	
HAMMER FALL		30"	

BORING No. B-5

SHEET 1 OF 1

ARCHITECT/ ENGINEER

FILE NO. GEI-LongIsland, NY

SURFACE ELEV.

LINE & STATION

OFFSET

SAMPLE No.	DEPTH RANGE IN FEET	BLOWS PER 6" ON SAMPLER 0-6	6-12	12-18	18-24	REC.	CASING BLOWS/ CORING TIMES PER FT.	FIELD CLASSIFICATION AND REMARKS	Well Cons.	Installation Details
S1	0'-2'	2	2	2	1	18"		6" Dark Brown Topsoil (.5)		
								Brown Fine Sand, Little Silt - Fill (3.0)		
S2	5'-7'	5	8	9	13	20"		Light Brown Fine Sand, Stratified		
S3	10'-12'	4	5	6	7	24"				
S4	15'-17'	4	4	4	6	20"				
S5	20'-22'	4	7	9	11	24"		Brown Fine Sand, Little Silt, Stratified		
S6	25'-27'	6	10	12	16	18"		Light Brown Fine Sand, Little Fine Gravel, Stratified		
S7	30'-32'	5	4	9	8	15"		Light Brown Fine-Med. Sand, Some Gravel, Stratified (32.0)		
								End of Boring @ 32'		
								Water @ 28' Overnight		

NOTES: 1) The stratification lines represent the approximate boundary between soil types. Transitions may be gradual.

2) Water level readings have been made in the drill holes at times and under conditions stated on the boring logs. Fluctuations in the level of groundwater may occur due to factors other than those present at the time measurements were made.

REMARKS:

CLIENT: GEI

PROJECT NAME: Brookhaven National Labs

LOCATION: Long Island, NY

DRILLER: T. Roe

INSPECTOR: A. Smart

DATE START: 10/29/03

DATE FINISH: 10/29/03

NEW ENGLAND BORING CONTRACTORS OF CT., INC.

129 KRIEGER LANE
GLASTONBURY, CT 06033
(860) 633-4649 -- (413) 733-1232
FAX (860) 657-8046

	Casing	Sampler	Core Barrel
TYPE	HSA	SS	
SIZE I.D.	3-1/4"	1-3/8"	
HAMMER WT.		140	
HAMMER FALL		30"	

BORING No. B-6

SHEET 1 OF 1

ARCHITECT/ ENGINEER

FILE NO. GEI-LongIsland, NY

SURFACE ELEV.

LINE & STATION

OFFSET

SAMPLE No.	DEPTH RANGE IN FEET	BLOWS PER 6" ON SAMPLER 0-6	6-12	12-18	18-24	REC.	CASING BLOWS/ CORING TIMES PER FT.	FIELD CLASSIFICATION AND REMARKS	Well Cons.	Installation Details
S1	0'-2'	2	7	4	2	24"		4" Dark Brown Topsoil - Fine Sand, Some Silt, Little Roots		
								.3 Brown Fine Sand, Some Silt, Stratified - Fill		
S2	5'-7'	9	11	12	19	20"		5.5 Light Brown Fine Sand, Stratified		
S3	10'-12'	9	10	12	15	24"		Trace of Gravel @ S3		
S4	15'-17'	4	9	6	7	24"				
S5	20'-22'	8	18	18	21	24"		Light Brown Fine Sand, Trace of Med.-Crs. Sand, Stratified		
S6	25'-27'	10	21	25	30	24"				
S7	30'-32'	16	27	25	22	24"		32.0 End of Boring @ 32' Water @ 30' +/-		

NOTES: 1) The stratification lines represent the approximate boundary between soil types. Transitions may be gradual.

2) Water level readings have been made in the drill holes at times and under conditions stated on the boring logs. Fluctuations in the level of groundwater may occur due to factors other than those present at the time measurements were made.

REMARKS:

CLIENT: GEI

PROJECT NAME: Brookhaven National Labs

LOCATION: Long Island, NY

DRILLER: T. Roe

INSPECTOR: A. Smart

DATE START: 10/29/03

DATE FINISH: 10/29/03

NEW ENGLAND BORING CONTRACTORS OF CT., INC.

129 KRIEGER LANE
GLASTONBURY, CT 06033
(860) 633-4649 – (413) 733-1232
FAX (860) 657-8046

	Casing	Sampler	Core Barrel
TYPE	SA	SS	
SIZE I.D.	4"	1-3/8"	
HAMMER WT.		140	
HAMMER FALL		30"	

BORING No. B-7

SHEET 1 OF 1

ARCHITECT/ ENGINEER

FILE NO. GEI-LongIsland, NY

SURFACE ELEV.

LINE & STATION

OFFSET

SAMPLE No.	DEPTH RANGE IN FEET	BLOWS PER 6" ON SAMPLER 0-6	6-12	12-18	18-24	REC.	CASING BLOWS/ CORING TIMES PER FT.	FIELD CLASSIFICATION AND REMARKS	Well Cons.	Installation Details
S1	0'-2'	1	2	1	1	24"		Dark Brown Topsoil		
								1.0 Brown Fine Sand, Some Silt - Fill		
								3.0 Light Brown Fine Sand, Stratified		
S2	5'-7'	5	8	10	12	24"		7.0 End of Boring @ 7' No Water		

NOTES: 1) The stratification lines represent the approximate boundary between soil types. Transitions may be gradual.

2) Water level readings have been made in the drill holes at times and under conditions stated on the boring logs. Fluctuations in the level of groundwater may occur due to factors other than those present at the time measurements were made.

REMARKS:

CLIENT: GEI

PROJECT NAME: Brookhaven National Labs

LOCATION: Long Island, NY

DRILLER: T. Roe

INSPECTOR: A. Smart

DATE START: 10/29/03

DATE FINISH: 10/29/03

NEW ENGLAND BORING CONTRACTORS OF CT., INC.

129 KRIEGER LANE
GLASTONBURY, CT 06033
(860) 633-4649 -- (413) 733-1232
FAX (860) 657-8046

	Casing	Sampler	Core Barrel
TYPE	SA	SS	
SIZE I.D.	4"	1-3/8"	
HAMMER WT.		140	
HAMMER FALL		30"	

BORING No. B-8

SHEET 1 OF 1

ARCHITECT/ ENGINEER

FILE NO. GEI-LongIsland, NY

SURFACE ELEV.

LINE & STATION

OFFSET

SAMPLE No.	DEPTH RANGE IN FEET	BLOWS PER 6" ON SAMPLER 0-6	6-12	12-18	18-24	REC.	CASING BLOWS/ CORING TIMES PER FT.	FIELD CLASSIFICATION AND REMARKS	Well Cons.	Installation Details
S1	0'-2'	3	2	3	2	18"		Brown Fine Sand, Little Silt - Fill		
								4.0		
S2	5'-7'	3	3	4	4	24"		Light Brown Fine Sand, Trace of Gravel, Stratified		
								7.0		
								End of Boring @ 7' No Water		

NOTES: 1) The stratification lines represent the approximate boundary between soil types. Transitions may be gradual.

2) Water level readings have been made in the drill holes at times and under conditions stated on the boring logs. Fluctuations in the level of groundwater may occur due to factors other than those present at the time measurements were made.

REMARKS:

CLIENT: GEI

PROJECT NAME: Brookhaven National Labs

LOCATION: Long Island, NY

DRILLER: T. Roe

INSPECTOR: A. Smart

DATE START: 10/29/03

DATE FINISH: 10/29/03

NEW ENGLAND BORING CONTRACTORS OF CT., INC.

129 KRIEGER LANE
GLASTONBURY, CT 06033
(860) 633-4649 -- (413) 733-1232
FAX (860) 657-8046

	Casing	Sampler	Core Barrel
TYPE	SA	SS	
SIZE I.D.	4"	1-3/8"	
HAMMER WT.		140	
HAMMER FALL		30"	

BORING No. B-9

SHEET 1 OF 1

ARCHITECT/ ENGINEER

FILE NO. GEI-LongIsland, NY

SURFACE ELEV.

LINE & STATION

OFFSET

SAMPLE No.	DEPTH RANGE IN FEET	BLOWS PER 6" ON SAMPLER 0-6	6-12	12-18	18-24	REC.	CASING BLOWS/ CORING TIMES PER FT.	FIELD CLASSIFICATION AND REMARKS	Well Cons.	Installation Details
S1	0'-2'	1	6	6	5	20"		8" Dark Brown Topsoil .6 Black Fine Sand, Trace of Roots, Ash, Brick		
S2	5'-7'	1	2	1	1	24"		Brown Fine Sand, Some Silt - Fill 7.0 Light Brown Fine Sand		
S3	10'-12'	5	5	4	7	18"		12.0 End of Boring @ 12' No Water		

NOTES: 1) The stratification lines represent the approximate boundary between soil types. Transitions may be gradual.

2) Water level readings have been made in the drill holes at times and under conditions stated on the boring logs. Fluctuations in the level of groundwater may occur due to factors other than those present at the time measurements were made.

REMARKS:

CLIENT: GEI

PROJECT NAME: Brookhaven National Labs

LOCATION: Long Island, NY

DRILLER: T. Roe

INSPECTOR: A. Smart

DATE START: 10/29/03

DATE FINISH: 10/29/03

NEW ENGLAND BORING CONTRACTORS OF CT., INC.

129 KRIEGER LANE
GLASTONBURY, CT 06033
(860) 633-4649 – (413) 733-1232
FAX (860) 657-8046

BORING No. B-10

SHEET 1 OF 1

ARCHITECT/ ENGINEER

FILE NO. GEI-LongIsland, NY

SURFACE ELEV.

LINE & STATION

OFFSET

	Casing	Sampler	Core Barrel
TYPE	SA	SS	
SIZE I.D.	4"	1-3/8"	
HAMMER WT.		140	
HAMMER FALL		30"	

SAMPLE No.	DEPTH RANGE IN FEET	BLOWS PER 6" ON SAMPLER 0-6	6-12	12-18	18-24	REC.	CASING BLOWS/ CORING TIMES PER FT.	FIELD CLASSIFICATION AND REMARKS	Well Cons.	Installation Details
S1	0'-2'	1	4	3	3	24"		Dark Brown Topsoil		
								1.0		
								Brown Fine Sand, Some Silt - Fill		
								5.0		
S2	5'-7'	2	4	6	5	24"		Light Brown Fine Sand, Trace of Gravel, Stratified		
								7.0		
								End of Boring @ 7'		
								No Water		

NOTES: 1) The stratification lines represent the approximate boundary between soil types. Transitions may be gradual.

2) Water level readings have been made in the drill holes at times and under conditions stated on the boring logs. Fluctuations in the level of groundwater may occur due to factors other than those present at the time measurements were made.

REMARKS:

CLIENT: GEI

PROJECT NAME: Brookhaven National Labs

LOCATION: Long Island, NY

DRILLER: T. Roe

INSPECTOR: A. Smart

DATE START: 10/29/03

DATE FINISH: 10/29/03

NEW ENGLAND BORING CONTRACTORS OF CT., INC.

129 KRIEGER LANE
GLASTONBURY, CT 06033
(860) 633-4649 – (413) 733-1232
FAX (860) 657-8046

	Casing	Sampler	Core Barrel
TYPE	HSA	SS	
SIZE I.D.	3-1/4"	1-3/8"	
HAMMER WT.		140	
HAMMER FALL		30"	

BORING No. B-12

SHEET 1 OF 1

ARCHITECT/ ENGINEER

FILE NO. GEI-LongIsland, NY

SURFACE ELEV.

LINE & STATION

OFFSET

SAMPLE No.	DEPTH RANGE IN FEET	BLOWS PER 6" ON SAMPLER 0-6	6-12	12-18	18-24	REC.	CASING BLOWS/ CORING TIMES PER FT.	FIELD CLASSIFICATION AND REMARKS	Well Cons.	Installation Details
S1	0'-2'	1	2	3	2	24"		8" Dark Brown Topsoil (.6) Brown Fine Sand, Little Silt - Fill (4.0)		
S2	5'-7'	2	5	8	8	24"		Brown Fine Sand, Stratified		
S3	10'-12'	5	9	9	11	24"				
S4	15'-17'	4	5	5	5	24"		Alternating 4"-10" Layers of Brown Fine Sand and Brown Fine Sand, Little Silt		
S5	20'-22'	7	11	18	19	24"		Light Brown Fine-Med. Sand, Trace of Gravel, Stratified		
S6	25'-27'	4	5	8	8	16"		Cobbles @ 22' to 24' Depth Light Brown Med. Sand, Little Gravel, Stratified		
S7	30'-32'	9	12	14	18	20"		(32.0) End of Boring @ 32' Water @ 30' +/-		

NOTES: 1) The stratification lines represent the approximate boundary between soil types. Transitions may be gradual.

2) Water level readings have been made in the drill holes at times and under conditions stated on the boring logs. Fluctuations in the level of groundwater may occur due to factors other than those present at the time measurements were made.

REMARKS: *Note: B-11 was Omitted*

GRAIN SIZE DISTRIBUTION TEST REPORT

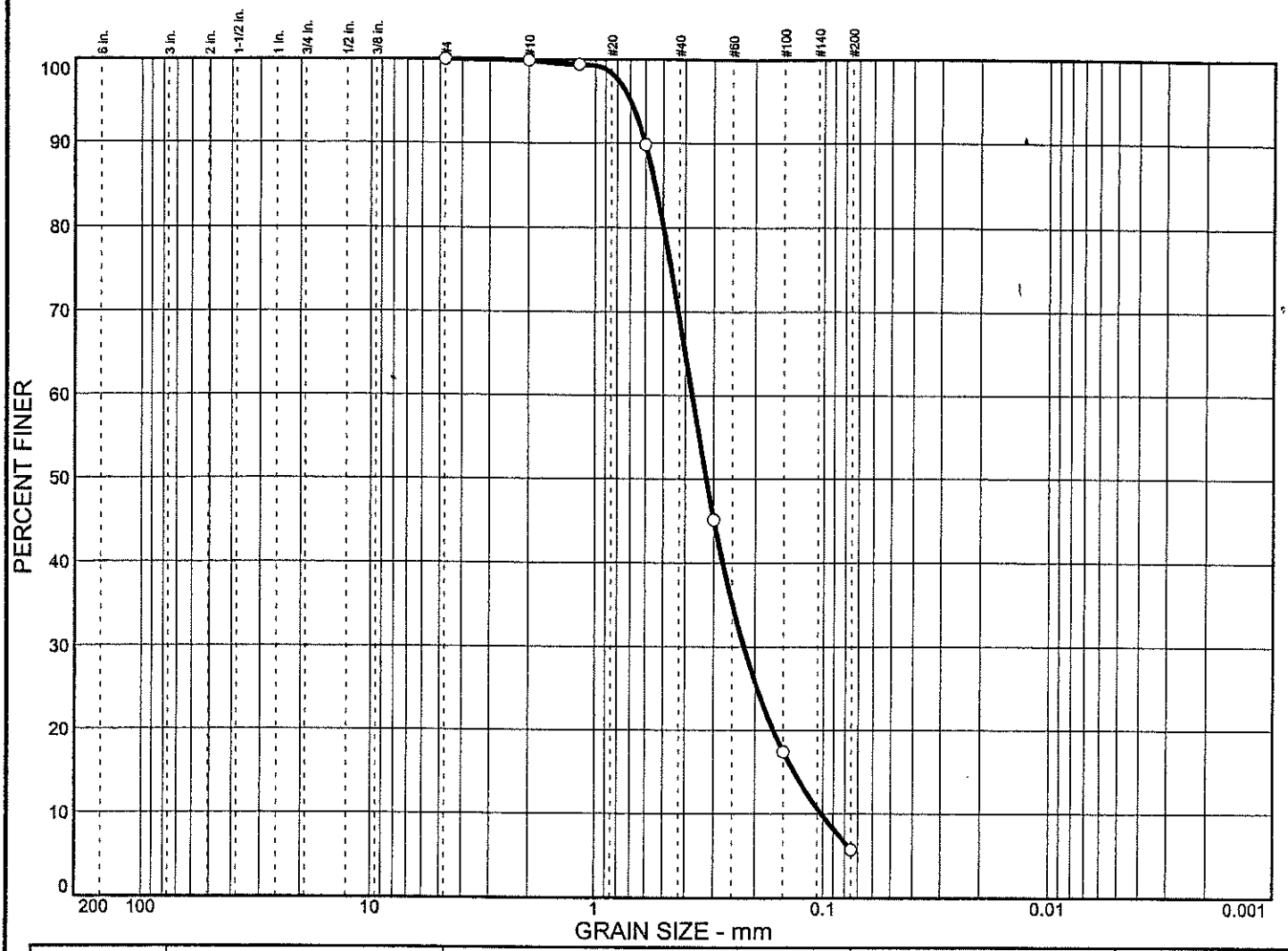

	% + 3"	% GRAVEL	% SAND	% SILT	% CLAY
○	0.0	0.0	94.3	5.7	

	LL	PL	D_{85}	D_{60}	D_{50}	D_{30}	D_{15}	D_{10}	C_c	C_u
○			0.544	0.374	0.324	0.223	0.135	0.102	1.31	3.67

MATERIAL DESCRIPTION	USCS	AASHTO
○ Narrowly graded SAND with Silt	SP-SM	

Project No. 03420 **Client:** HDR Architecture, Inc.

Project: Center for Functional Nanomaterials, Brookhaven National Laboratory

○ **Source:** B1 **Sample No.:** S2 **Elev./Depth:** 5 to 7 ft

Remarks:

○

GEI Consultants, Inc.

Fig.

GRAIN SIZE DISTRIBUTION TEST REPORT

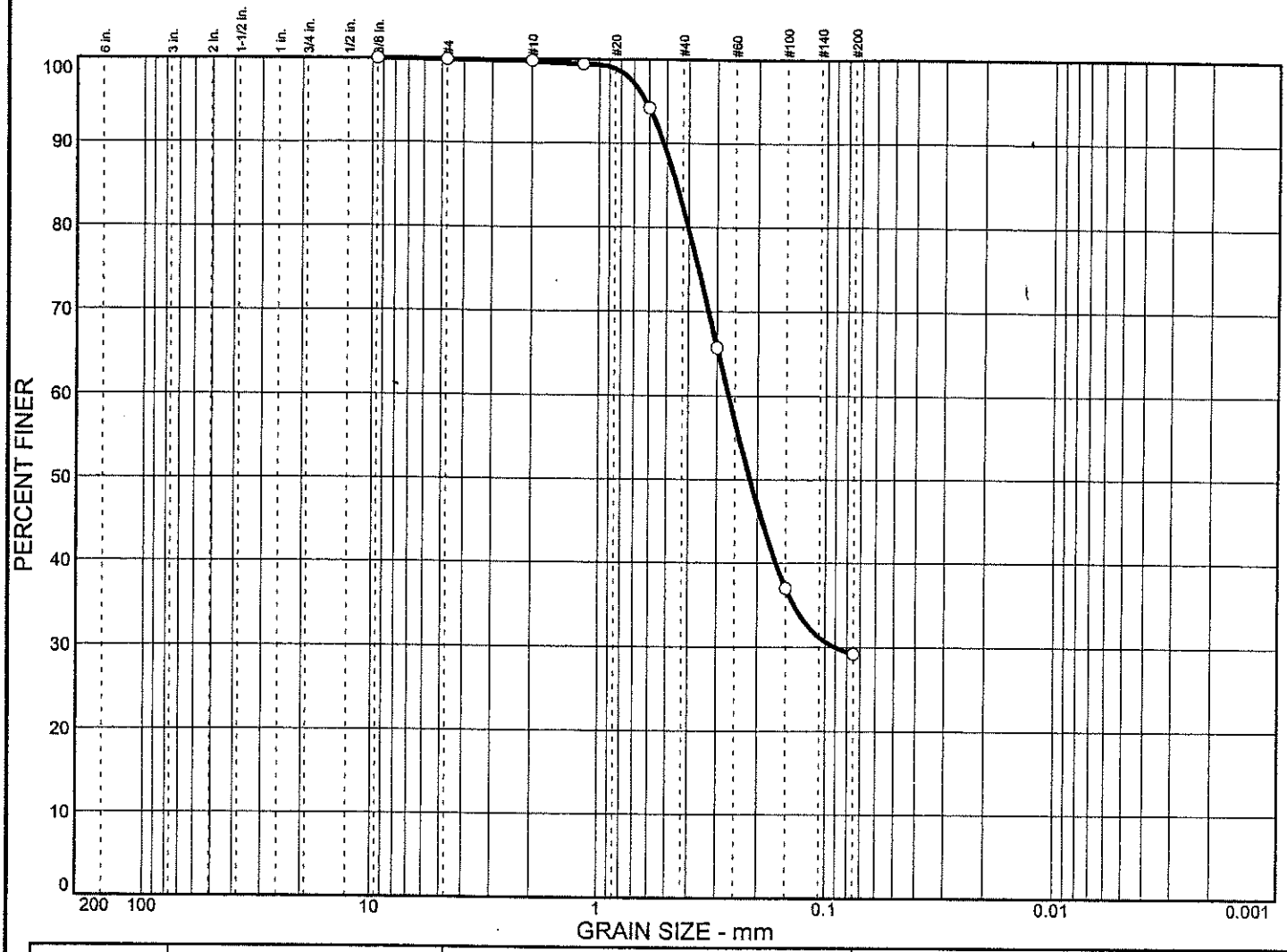

	% + 3"	% GRAVEL	% SAND	% SILT	% CLAY
○	0.0	0.1	70.7	29.2	

	LL	PL	D_{85}	D_{60}	D_{50}	D_{30}	D_{15}	D_{10}	C_c	C_u
○			0.454	0.267	0.215	0.0903				

MATERIAL DESCRIPTION	USCS	AASHTO
○ Silty SAND	SM	

Project No. 03420 **Client:** HDR Architecture, Inc.

Project: Center for Functional Nanomaterials, Brookhaven National Laboratory

○ **Source:** B2 **Sample No.:** S1 **Elev./Depth:** 5 to 7 ft

Remarks:

○

GEI Consultants, Inc.

Fig.

GRAIN SIZE DISTRIBUTION TEST REPORT

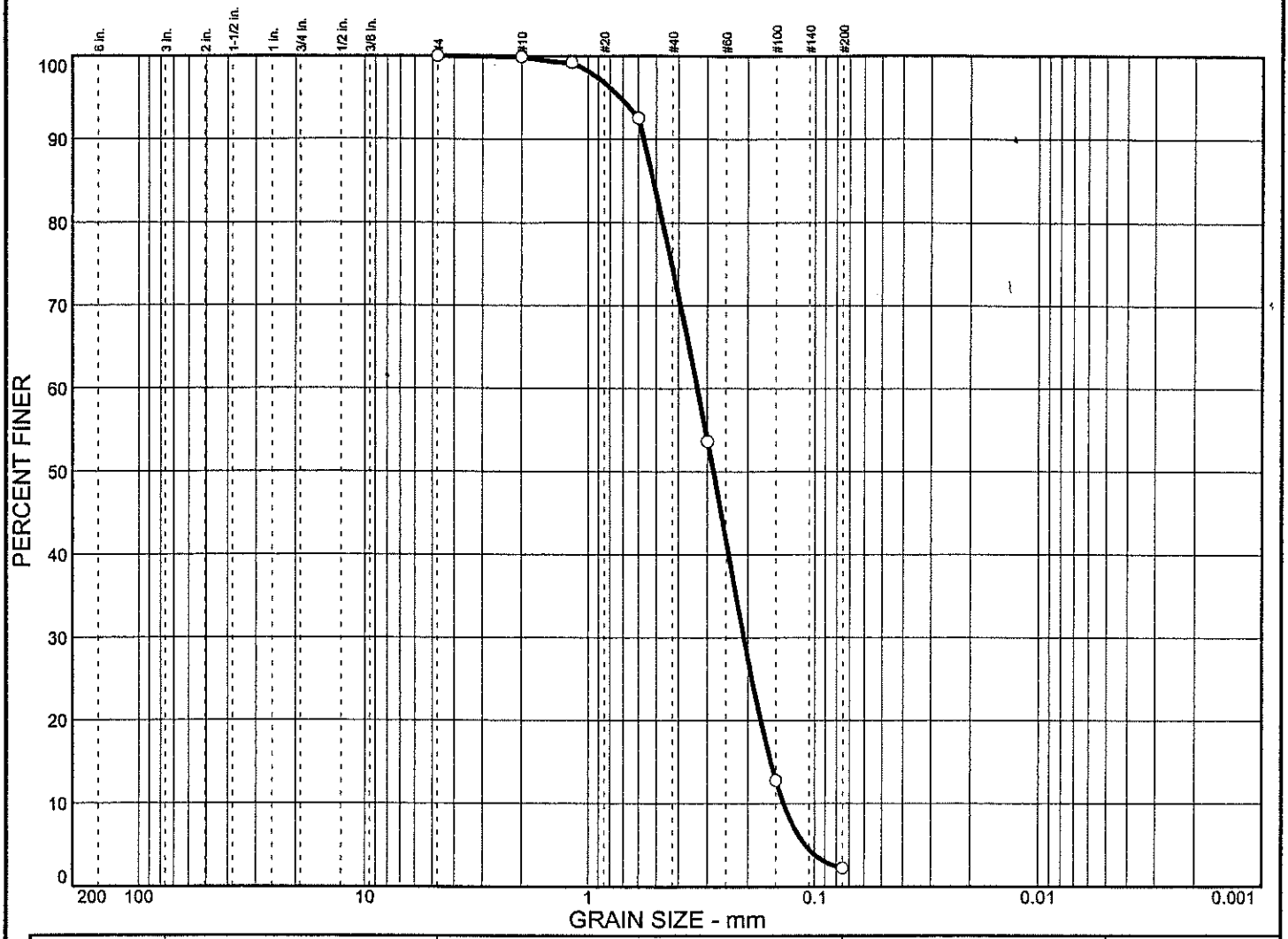

	% + 3"	% GRAVEL	% SAND	% SILT	% CLAY
○	0.0	0.0	97.8	2.2	

	LL	PL	D_{85}	D_{60}	D_{50}	D_{30}	D_{15}	D_{10}	C_c	C_u
○			0.518	0.332	0.284	0.209	0.158	0.138	0.95	2.40

MATERIAL DESCRIPTION	USCS	AASHTO
○ Narrowly graded SAND	SP	

Project No. 03420 **Client:** HDR Architecture, Inc.

Project: Center for Functional Nanomaterials, Brookhaven National Laboratory

○ **Source:** B3 **Sample No.:** S2 **Elev./Depth:** 5 to 7 ft

Remarks:

○

GEI Consultants, Inc.

Fig.

GRAIN SIZE DISTRIBUTION TEST REPORT

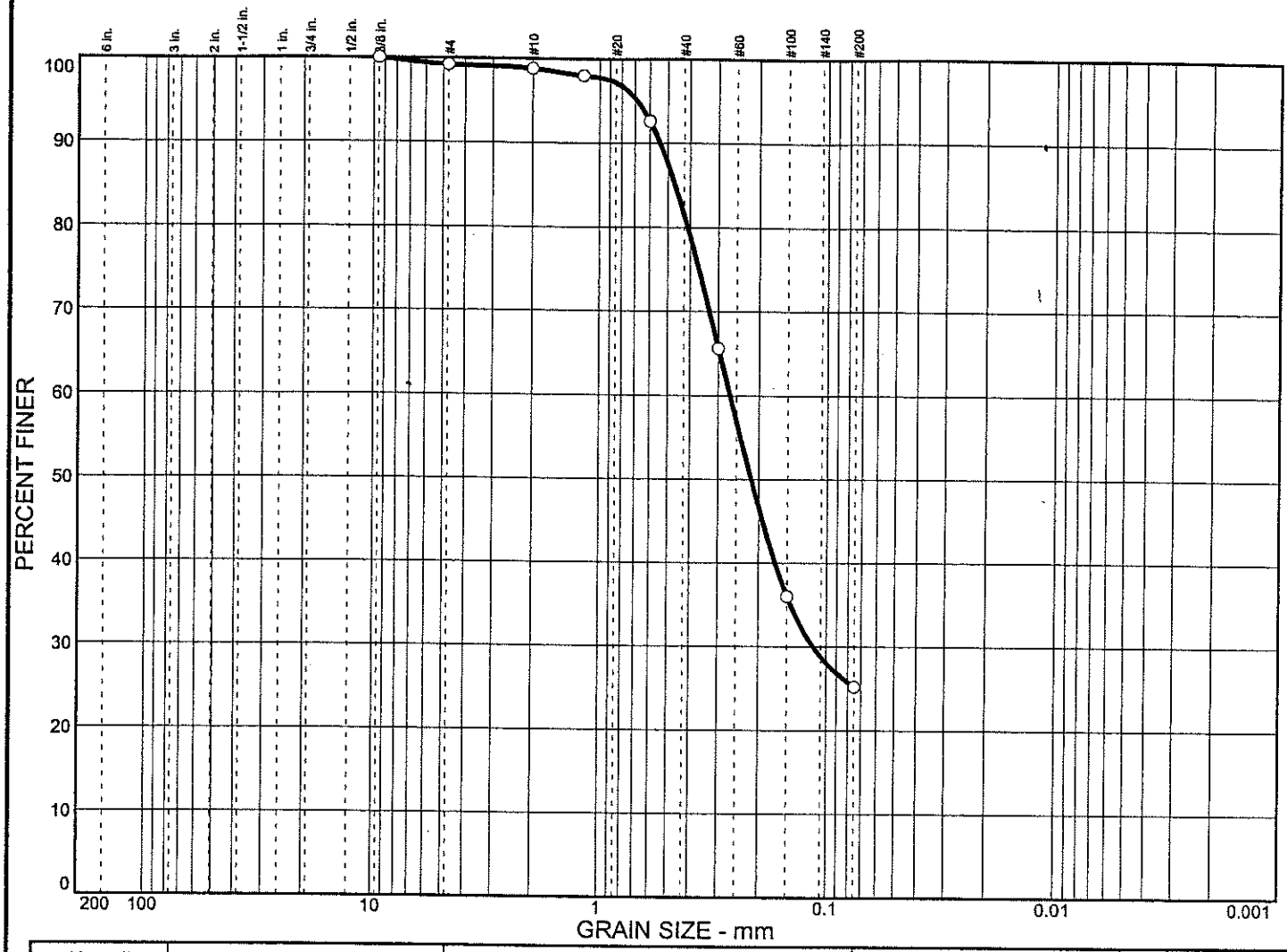

	% + 3"	% GRAVEL	% SAND	% SILT	% CLAY
○	0.0	0.8	74.0	25.2	

	LL	PL	D_{85}	D_{60}	D_{50}	D_{30}	D_{15}	D_{10}	C_c	C_u
○			0.467	0.267	0.216	0.115				

MATERIAL DESCRIPTION	USCS	AASHTO
○ Silty SAND	SM	

Project No. 03420 **Client:** HDR Architecture, Inc.

Project: Center for Functional Nanomaterials, Brookhaven National Laboratory

○ **Source:** B5 **Sample No.:** S1 **Elev./Depth:** 0 to 2 ft

Remarks:

○

GEI Consultants, Inc.

Fig.

GRAIN SIZE DISTRIBUTION TEST REPORT

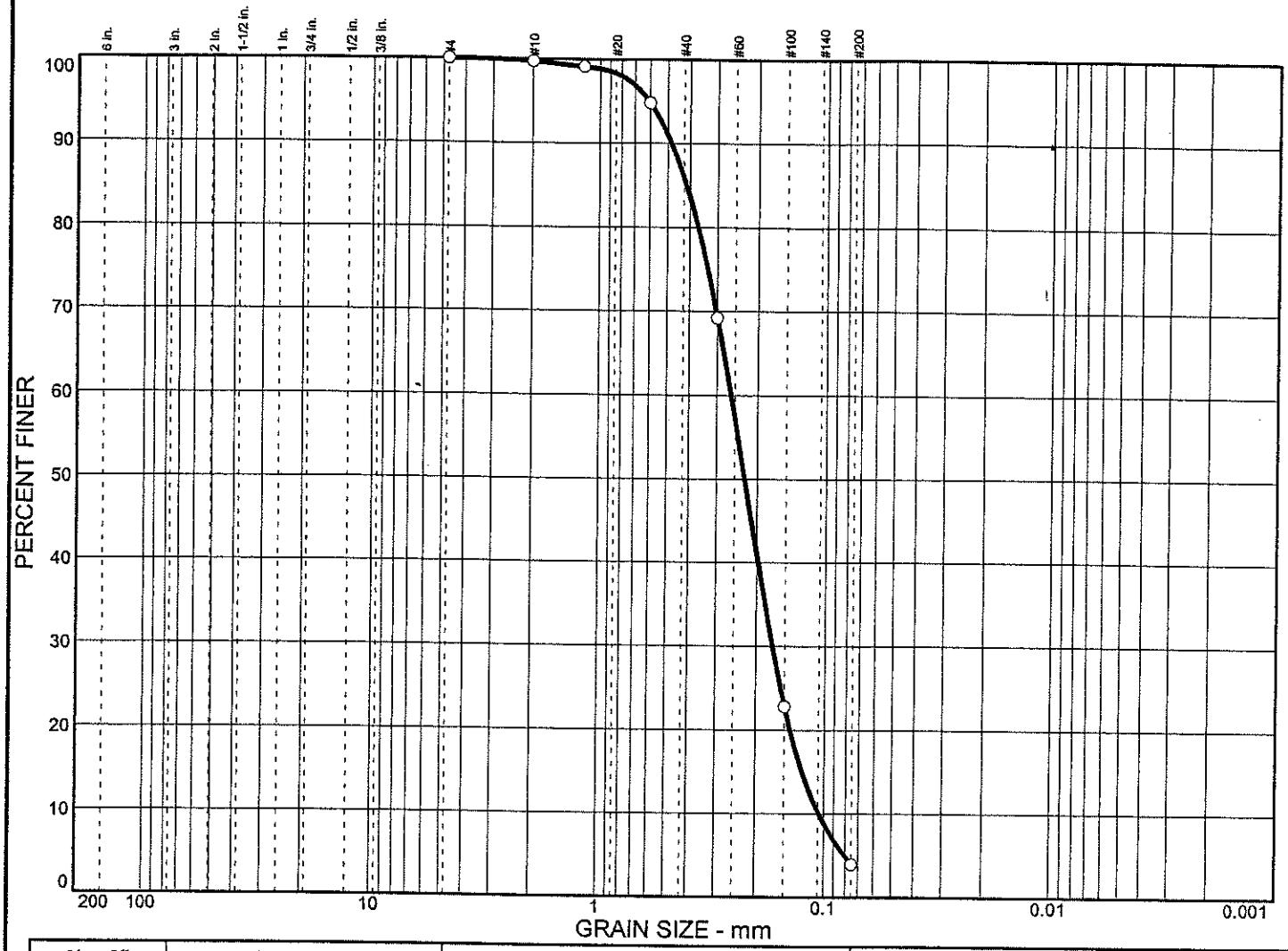

	% + 3"	% GRAVEL	% SAND	% SILT	% CLAY
○	0.0	0.0	96.1	3.9	

	LL	PL	D_{85}	D_{60}	D_{50}	D_{30}	D_{15}	D_{10}	C_c	C_u
○			0.415	0.261	0.227	0.170	0.125	0.105	1.05	2.48

MATERIAL DESCRIPTION	USCS	AASHTO
○ Narrowly graded SAND	SP	

Project No. 03420 **Client:** HDR Architecture, Inc.

Project: Center for Functional Nanomaterials, Brookhaven National Laboratory

○ **Source:** B5 **Sample No.:** S2 **Elev./Depth:** 5 to 7 ft

Remarks:

○

GEI Consultants, Inc.

Fig.

Appendix C

2006-2007 Test Boring Logs

Boring Location

NORTHING: _____ EASTING: _____ STATION: _____ OFFSET: _____
HORIZONTAL DATUM: NAD 83 STATION CENTERLINE: _____
VERTICAL DATUM: BNL 94 GROUND SURFACE ELEVATION (FT): 74.0
LOCATION: See Figure 2

BORING

B-101

Drilling Information

DATE START / END: 7/20/2006 - 7/20/2006 TOTAL DEPTH (FT): 52.0
CONTRACTOR: New England Boring DRILLER: Jeff Leavitt LOGGED BY: Steve Hawkins
EQUIPMENT: Mobile Drill B-53 Truck mounted Drill Rig BORING METHOD: Drive and Wash
AUGER ID/OD: N/A / N/A CASING ID/OD: N/A / 3 in CORE INFO: _____
HAMMER TYPE: Safety Hammer HAMMER WEIGHT (lbs): 140 HAMMER DROP (inch): 30
WATER LEVEL DEPTHS (ft): _____
GENERAL NOTES: Samples collected using a 2-in diameter split spoon

ABBREVIATIONS:
ID = Inside Diameter; OD = Outside Diameter; Pen. = Penetration Length; Rec. = Recovery Length
bpf = Blows per Foot; mpf = Minute per Foot; S = Split Spoon; DP = Direct Push Sample
U = Undistrubed Tube Sample; C = Rock Core; V = Field Vane Shear; SC = Sonic Core
WOR = Weight of Rods; WOH = Weight of Hammer; RQD = Rock Quality Designation; OVM = Organic Vapor Meter
Q_p = Pocket Penetrometer Strength; S_v = Pocket Torvane Shear Strength; F_v = Field Vane Shear Strength; NA, NM = Not Applicable, Not Measured

Elev. (ft)	Depth (ft)	Casing Pen. (bpf) or Core Rate (mpf)	Sample No.	Type	Depth (ft)	Pen./ Rec. (in)	Blows Count or RQD	Field Test Data	Graphic Log	Sample Description & Classification	H_2O Depth	Remarks
			1		0 to 2	24/18	4-6-9-9			SILTY SAND (SM); fine to coarse sand, 32% silty fines, 6% fine gravel, moist, dark brown, roots (TOPSOIL). Probable Fill, Silty Sand on auger cuttings.		
70												Strata change estimated at 3.5 feet
	5		2		5 to 7	24/12	21-25-27-30			WIDELY GRADED SAND WITH SILT (SW-SM); fine to coarse sand, 12% silty fines, 3% fine gravel, moist, light brown.		
65												
	10		3		10 to 12	24/10	4-8-8-9			WIDELY GRADED SAND (SW); fine to coarse sand, 8% fine gravel, 1% silty fines, wet, light brown.		
60												
	15		4		15 to 17	24/10	13-15-17-17			WIDELY GRADED SAND (SW); fine to coarse sand, 6% fine gravel, 3% silty fines, wet, light brown.		
55												
	20		5		20 to 22	24/12	20-25-32-41			WIDELY GRADED SAND (SW); fine to coarse sand, 5% fine gravel, 4% silty fines, wet, light brown.		

Stratification lines represent approximate boundary between soil types, transitions may be gradual. Water level readings have been made at times and under conditions stated. Fluctuations of groundwater may occur due to other factors than those present at the time measurements were made.

CLIENT: HDR Architecture, Inc.
PROJECT NAME: NSLS II Geotechnical Investigation
CITY/STATE: Upton, New York
GEI PROJECT NUMBER: 062150-*-1000

GEI Consultants
GEI Consultants, Inc.
455 Winding Brook Dr
Glastonbury, CT 06033
860.368.5408

GEOTECHNICAL BORING LOG 02 BNL NSLSII BORING LOGS.GPJ GEI DATA TEMPLATE.GDT 8/24/06

Boring Location

NORTHING: _____ EASTING: _____ STATION: _____ OFFSET: _____

HORIZONTAL DATUM: NAD 83 STATION CENTERLINE: _____

VERTICAL DATUM: BNL 94 GROUND SURFACE ELEVATION (FT): 74.0

LOCATION: See Figure 2

BORING

B-101

Elev. (ft)	Depth (ft)	Casing Pen. (bpf) or Core Rate (mpf)	SAMPLE INFORMATION: Sample No.	Type	Depth (ft)	Pen./ Rec. (in)	Blows Count or RQD	Field Test Data	GRAPHIC LOG	Sample Description & Classification	H_2O Depth	Remarks
45	25		6	X	25 to 27	24/12	25-27-29-31			WIDELY GRADED SAND WITH GRAVEL (SW); fine to coarse sand, 25% fine gravel, 5% silty fines, wet, light brown.		
40	30		7	X	30 to 32	24/10	18-22-24-29			WIDELY GRADED SAND WITH GRAVEL (SW); fine to coarse sand, ~30% fine gravel, <5% silty fines, wet, light brown.		
35	35		8	X	35 to 37	24/6	14-16-20-22			WIDELY GRADED SAND WITH GRAVEL (SW); fine to coarse sand, 27% fine to coarse gravel, 5% silty fines, wet, light brown.		
30	40		9	X	40 to 42	24/8	15-16-20-22			WIDELY GRADED SAND WITH GRAVEL (SW); fine to coarse sand, ~30% fine gravel, <5% silty fines, wet, light brown.		
25	45		10	X	45 to 47	24/8	20-26-35-47			WIDELY GRADED SAND WITH SILT (SW-SM); fine to coarse sand, 8% silty fines, 1% fine gravel, wet, light brown.		
20	50		11	X	50 to 52	24/12	29-30-31-28			WIDELY GRADED SAND WITH SILT (SW-SM); fine to coarse sand, ~10% silty fines, ~10% fine gravel, wet, brown.		
										End of Boring at 52 feet		

Stratification lines represent approximate boundary between soil types, transitions may be gradual. Water level readings have been made at times and under conditions stated. Fluctuations of groundwater may occur due to other factors than those present at the time measurements were made.

CLIENT: HDR Architecture, Inc.

PROJECT NAME: NSLS II Geotechnical Investigation

CITY/STATE: Upton, New York

GEI PROJECT NUMBER: 062150-*-1000

GEI Consultants, Inc.
455 Winding Brook Dr
Glastonbury, CT 06033
860.368.5408

GEOTECHNICAL BORING LOG 02 BNL NSLSII BORING LOGS.GPJ GEI DATA TEMPLATE.GDT 8/24/06

Boring Location

NORTHING: _____ EASTING: _____ STATION: _____ OFFSET: _____
HORIZONTAL DATUM: NAD 83 STATION CENTERLINE: _____
VERTICAL DATUM: BNL 94 GROUND SURFACE ELEVATION (FT): 74.0
LOCATION: See Figure 2

BORING

B-101a

Drilling Information

DATE START / END: 8/16/2006 - 8/16/2006 TOTAL DEPTH (FT): 10.0
CONTRACTOR: New England Borings DRILLER: Jeff Leavitt LOGGED BY: Steven Hawkins
EQUIPMENT: Mobile Drill B-53 truck mounted drill rig. BORING METHOD: Hollow Stem Auger
AUGER ID/OD: 4.25 in / N/A CASING ID/OD: N/A / N/A CORE INFO: _____
HAMMER TYPE: Safety Hammer HAMMER WEIGHT (lbs): 140 HAMMER DROP (inch): 30
WATER LEVEL DEPTHS (ft): _____
GENERAL NOTES: Samples collected using a 2-inch diameter split spoon.

ABBREVIATIONS:
ID = Inside Diameter; OD = Outside Diameter; Pen. = Penetration Length; Rec. = Recovery Length
bpf = Blows per Foot; mpf = Minute per Foot; S = Split Spoon; DP = Direct Push Sample
U = Undistrubed Tube Sample; C = Rock Core; V = Field Vane Shear; SC = Sonic Core
WOR = Weight of Rods; WOH = Weight of Hammer; RQD = Rock Quality Designation; OVM = Organic Vapor Meter
Q_v = Pocket Penetrometer Strength; S_v = Pocket Torvane Shear Strength; F_v = Field Vane Shear Strength; NA, NM = Not Applicable, Not Measured

Elev. (ft)	Depth (ft)	Casing Pen. (bpf) or Core Rate (mpf)	SAMPLE INFORMATION: Sample No.	Type	Depth (ft)	Pen./ Rec. (in)	Blows Count or RQD	Field Test Data	GRAPHIC LOG	Sample Description & Classification	H_2O Depth	Remarks
			S-1		0 to 2	24/14	3-3-4-4			SILTY SAND (SM); fine to coarse sand, ~25% silty fines, ~5% fine gravel, dry, brown, ~10% organics, 4 inches of topsoil.		
			S-2		2 to 4	24/20	4-9-9-10			SILTY SAND (SM); fine to coarse sand, ~25% silty fines, ~5% fine gravel, dry, brown, Bottom 5 inches consists of fine to coarse sand. FILL.		
70	5		S-3		4 to 6	24/12	9-10-10-12			WIDELY GRADED SAND WITH SILT (SW-SM); fine to coarse sand, ~10% silty fines, ~5% fine gravel, dry, brown.		Strata change estimated at 3.3 feet
			S-4		6 to 8	24/12	13-16-16-15			WIDELY GRADED SAND (SW); fine to coarse sand, ~5% silty fines, ~5% fine to coarse gravel, dry, brown.		
65	10		S-5		8 to 10	24/18	12-13-13-15			WIDELY GRADED SAND (SW); fine to coarse sand, ~5% silty fines, ~5% fine gravel, dry, brown.		
										End of Boring at 10 feet Fill with cuttings upon completion		
60	15											
55	20											

Stratification lines represent approximate boundary between soil types, transitions may be gradual. Water level readings have been made at times and under conditions stated. Fluctuations of groundwater may occur due to other factors than those present at the time measurements were made.

CLIENT: HDR Architechture, Inc.
PROJECT NAME: NSLS II Geotechnical Investigation
CITY/STATE: Upton, New York
GEI PROJECT NUMBER: 062150-*-1000

GEI Consultants
GEI Consultants, Inc.
455 Winding Brook Dr
Glastonbury, CT 06033
860.368.5408

GEOTECHNICAL BORING LOG 02 BNL NSLSII ADDITONAL BORING LOGS.GPJ GEI DATA TEMPLATE.GDT 8/24/06

Boring Location

NORTHING: _____ EASTING: _____ STATION: _____ OFFSET: _____
HORIZONTAL DATUM: NAD 83 STATION CENTERLINE: _____
VERTICAL DATUM: BNL 94 GROUND SURFACE ELEVATION (FT): 81.0
LOCATION: See Figure 2

BORING

B-102

Drilling Information

DATE START / END: 7/19/2006 - 7/20/2006 TOTAL DEPTH (FT): 62.0
CONTRACTOR: New England Boring DRILLER: Jeff Leavitt LOGGED BY: Steve Hawkins
EQUIPMENT: Mobile Drill B-53 Truck mounted Drill Rig BORING METHOD: Drive and Wash
AUGER ID/OD: N/A / N/A CASING ID/OD: N/A / 3 in CORE INFO: _____
HAMMER TYPE: Safety Hammer HAMMER WEIGHT (lbs): 140 HAMMER DROP (inch): 30
WATER LEVEL DEPTHS (ft): ▼ 36.50 7/20/2006 9:20 am ▼ 36.50 7/20/2006 1:55 pm
GENERAL NOTES: Samples collected using a 2-in diameter split spoon

ABBREVIATIONS:
ID = Inside Diameter; OD = Outside Diameter; Pen. = Penetration Length; Rec. = Recovery Length
bpf = Blows per Foot; mpf = Minute per Foot; S = Split Spoon; DP = Direct Push Sample
U = Undisturbed Tube Sample; C = Rock Core; V = Field Vane Shear; SC = Sonic Core
WOR = Weight of Rods; WOH = Weight of Hammer; RQD = Rock Quality Designation; OVM = Organic Vapor Meter
Q_v = Pocket Penetrometer Strength; S_v = Pocket Torvane Shear Strength; F_v = Field Vane Shear Strength
NA, NM = Not Applicable, Not Measured

Elev. (ft)	Depth (ft)	Casing Pen. (bpf) or Core Rate (mpf)	Sample No.	Type	Depth (ft)	Pen./ Rec. (in)	Blows Count or RQD	Field Test Data	GRAPHIC LOG	Sample Description & Classification	H_2O Depth	Remarks
80			1		0 to 2	24/8	3-13-5-4			SILTY SAND (SM); fine to coarse sand, 27% silty fines, 11% fine gravel, dry, brown, Contains roots, TOPSOIL.. Probable Fill, Silty Sand on auger cuttings.		
75	5		2		5 to 7	24/12	8-14-15-16			WIDELY GRADED SAND (SW); fine to coarse sand, 13% fine gravel, 5% silty fines, moist, light brown.		Strata change estimated at 5.0 feet
70	10		3		10 to 12	24/10	8-10-13-13			WIDELY GRADED SAND (SW); fine to coarse sand, 9% fine gravel, 3% silty fines, moist, light brown.		
65	15		4		15 to 17	24/12	4-9-18-18			WIDELY GRADED SAND WITH SILT (SW-SM); fine to coarse sand, 7% fine gravel, 7% silty fines, moist, light brown.		
60	20		5		20 to 22	24/12	12-18-24-22			WIDELY GRADED SAND WITH SILT (SW-SM); fine to medium sand, 6% silty fines, 1% fine gravel, moist, light brown.		

Stratification lines represent approximate boundary between soil types, transitions may be gradual. Water level readings have been made at times and under conditions stated. Fluctuations of groundwater may occur due to other factors than those present at the time measurements were made.

CLIENT: HDR Architecture, Inc.
PROJECT NAME: NSLS II Geotechnical Investigation
CITY/STATE: Upton, New York
GEI PROJECT NUMBER: 062150-*-1000

GEI Consultants
GEI Consultants, Inc.
455 Winding Brook Dr
Glastonbury, CT 06033
860.368.5408

GEOTECHNICAL BORING LOG 02 BNL NSLSII BORING LOGS.GPJ GEI DATA TEMPLATE.GDT 8/24/06

Boring Location

NORTHING: _____ EASTING: _____ STATION: _____ OFFSET: _____

HORIZONTAL DATUM: NAD 83 STATION CENTERLINE: _____

VERTICAL DATUM: BNL 94 GROUND SURFACE ELEVATION (FT): 81.0

LOCATION: See Figure 2

BORING

B-102

Elev. (ft)	Depth (ft)	Casing Pen. (bpf) or Core Rate (mpf)	SAMPLE INFORMATION: Sample No.	Type	Depth (ft)	Pen./ Rec. (in)	Blows Count or RQD	Field Test Data	GRAPHIC LOG	Sample Description & Classification	H_2O Depth	Remarks
55	25		6		25 to 27	24/12	27-36-46-45			WIDELY GRADED SAND WITH SILT (SW-SM); fine to medium sand, 10% silty fines, 3% fine gravel, moist, light brown.		Begins washing out ahead of casing advancement. Material too dense to drive casing.
50	30		7		30 to 32	24/10	37-45-47-61			WIDELY GRADED SAND (SW); fine to coarse sand, ~10% fine gravel, ~5% silty fines, wet, light brown.		
45	35		8		35 to 37	24/10	31-47-61-73			WIDELY GRADED SAND WITH SILT (SW-SM); fine to coarse sand, 7% silty fines, 5% fine gravel, wet, light brown.	▼	
40	40		9		40 to 41.5	18/10	39-62-100			WIDELY GRADED SAND (SW); fine to coarse sand, ~5% fine gravel, ~5% silty fines, wet, brown.		
35	45		10		45 to 47	24/12	31-42-49-55			WIDELY GRADED SAND WITH SILT (SW-SM); fine to coarse sand, 9% fine gravel, 8% silty fines, wet, brown.		
30	50		11		50 to 52	24/14	29-37-40-46			WIDELY GRADED SAND WITH GRAVEL (SW); fine to coarse sand, ~20% fine gravel, ~5% silty fines, wet, light brown.		

Stratification lines represent approximate boundary between soil types, transitions may be gradual. Water level readings have been made at times and under conditions stated. Fluctuations of groundwater may occur due to other factors than those present at the time measurements were made.

CLIENT: HDR Architecture, Inc.

PROJECT NAME: NSLS II Geotechnical Investigation

CITY/STATE: Upton, New York

GEI PROJECT NUMBER: 062150-*-1000

GEI Consultants

GEI Consultants, Inc.
455 Winding Brook Dr
Glastonbury, CT 06033
860.368.5408

GEOTECHNICAL BORING LOG 02 BNL NSLSII BORING LOGS.GPJ GEI DATA TEMPLATE.GDT 8/24/06

Boring Location

NORTHING: _____ EASTING: _____ STATION: _____ OFFSET: _____

HORIZONTAL DATUM: NAD 83 STATION CENTERLINE: _____

VERTICAL DATUM: BNL 94 GROUND SURFACE ELEVATION (FT): 81.0

LOCATION: See Figure 2

BORING

B-102

Elev. (ft)	Depth (ft)	Casing Pen. (bpf) or Core Rate (mpf)	SAMPLE INFORMATION: Sample No.	Type	Depth (ft)	Pen./ Rec. (in)	Blows Count or RQD	Field Test Data	GRAPHIC LOG	Sample Description & Classification	H_2O Depth	Remarks
25			12		55 to 57	24/14	27-32-39-48			WIDELY GRADED SAND WITH GRAVEL (SW); fine to coarse sand, ~20% fine gravel, ~5% silty fines, wet, light brown.		
	60		13		60 to 62	24/10	30-36-39-45			WIDELY GRADED SAND WITH GRAVEL (SW); fine to coarse sand, ~20% fine gravel, ~5% silty fines, wet, light brown.		
20										End of Boring at 62 feet		
	65											
15												
	70											
10												
	75											
5												
	80											
0												
	85											

Stratification lines represent approximate boundary between soil types, transitions may be gradual. Water level readings have been made at times and under conditions stated. Fluctuations of groundwater may occur due to other factors than those present at the time measurements were made.

CLIENT: HDR Architecture, Inc.

PROJECT NAME: NSLS II Geotechnical Investigation

CITY/STATE: Upton, New York

GEI PROJECT NUMBER: 062150-*-1000

GEI Consultants

GEI Consultants, Inc.
455 Winding Brook Dr
Glastonbury, CT 06033
860.368.5408

GEOTECHNICAL BORING LOG 02 BNL NSLSII BORING LOGS.GPJ GEI DATA TEMPLATE.GDT 8/24/06

Boring Location

NORTHING: _____ EASTING: _____ STATION: _____ OFFSET: _____
HORIZONTAL DATUM: NAD 83 STATION CENTERLINE: _____
VERTICAL DATUM: BNL 94 GROUND SURFACE ELEVATION (FT): 81.0
LOCATION: See Figure 2

BORING

B-102a

Drilling Information

DATE START / END: 8/16/2006 - 8/16/2006 TOTAL DEPTH (FT): 10.0
CONTRACTOR: New England Borings DRILLER: Jeff Leavitt LOGGED BY: Steven Hawkins
EQUIPMENT: Mobile Drill B-53 truck mounted drill rig. BORING METHOD: Hollow Stem Auger
AUGER ID/OD: 4.25 in / N/A CASING ID/OD: N/A / N/A CORE INFO: _____
HAMMER TYPE: Safety Hammer HAMMER WEIGHT (lbs): 140 HAMMER DROP (inch): 30
WATER LEVEL DEPTHS (ft): _____
GENERAL NOTES: Samples collected using a 2-inch diameter split spoon.

ABBREVIATIONS:
ID = Inside Diameter; OD = Outside Diameter; Pen. = Penetration Length; Rec. = Recovery Length
bpf = Blows per Foot; mpf = Minute per Foot; S = Split Spoon; DP = Direct Push Sample
U = Undistrubed Tube Sample; C = Rock Core; V = Field Vane Shear; SC = Sonic Core
WOR = Weight of Rods; WOH = Weight of Hammer; RQD = Rock Quality Designation; OVM = Organic Vapor Meter
Q_p = Pocket Penetrometer Strength; S_v = Pocket Torvane Shear Strength; F_v = Field Vane Shear Strength; NA, NM = Not Applicable, Not Measured

Elev. (ft)	Depth (ft)	Casing Pen. (bpf) or Core Rate (mpf)	Sample No.	Type	Depth (ft)	Pen./ Rec. (in)	Blows Count or RQD	Field Test Data	GRAPHIC LOG	Sample Description & Classification	H_2O Depth	Remarks
80			S-1		0 to 2	24/24	4-3-2-2			SILTY SAND (SM); fine to coarse sand, ~20% silty fines, ~10% fine to coarse gravel, dry, brown, Organics, 4 inches of Topsoil.		
			S-2		2 to 4	24/12	3-3-3-4			SILTY SAND (SM); fine to coarse sand, ~15% silty fines, ~5% fine to coarse gravel, dry, brown, FILL.		
	5		S-3		4 to 6	24/12	4-5-6-6			WIDELY GRADED SAND WITH SILT (SW-SM); fine to coarse sand, ~10% silty fines, ~5% fine gravel, dry, light brown.		Strata change estimated at 4 feet
75			S-4		6 to 8	24/13	8-10-11-6			WIDELY GRADED SAND WITH SILT (SW-SM); fine to coarse sand, ~10% silty fines, ~5% fine gravel, dry, light brown.		
			S-5		8 to 10	24/17	8-12-12-14			WIDELY GRADED SAND WITH SILT (SW-SM); fine to coarse sand, ~10% silty fines, ~5% fine gravel, dry, light brown.		
	10									End of Boring at 10 feet Fill with cuttings upon completion		
70												
	15											
65												
	20											
60												

Stratification lines represent approximate boundary between soil types, transitions may be gradual. Water level readings have been made at times and under conditions stated. Fluctuations of groundwater may occur due to other factors than those present at the time measurements were made.

CLIENT: HDR Architechture, Inc.
PROJECT NAME: NSLS II Geotechnical Investigation
CITY/STATE: Upton, New York
GEI PROJECT NUMBER: 062150-*-1000

GEI Consultants
GEI Consultants, Inc.
455 Winding Brook Dr
Glastonbury, CT 06033
860.368.5408

GEOTECHNICAL BORING LOG 02 BNL NSLSII ADDITONAL BORING LOGS.GPJ GEI DATA TEMPLATE.GDT 8/24/06

Boring Location

NORTHING: _____ EASTING: _____ STATION: _____ OFFSET: _____
HORIZONTAL DATUM: NAD 83 STATION CENTERLINE: _____
VERTICAL DATUM: BNL 94 GROUND SURFACE ELEVATION (FT): 73.0
LOCATION: See Figure 2

BORING

B-103

Drilling Information

DATE START / END: 8/16/2006 - 8/16/2006 TOTAL DEPTH (FT): 32.0
CONTRACTOR: New England Borings DRILLER: Jeff Leavitt LOGGED BY: Steven Hawkins
EQUIPMENT: Mobile Drill B-53 truck mounted drill rig. BORING METHOD: Hollow Stem Auger
AUGER ID/OD: 4.25 in / N/A CASING ID/OD: N/A / N/A CORE INFO: _____
HAMMER TYPE: Safety Hammer HAMMER WEIGHT (lbs): 140 HAMMER DROP (inch): 30
WATER LEVEL DEPTHS (ft): ▽ 28.00 8/16/2006 10:19 am
GENERAL NOTES: Samples collected using a 2-inch diameter split spoon.

ABBREVIATIONS:
ID = Inside Diameter; OD = Outside Diameter; Pen. = Penetration Length; Rec. = Recovery Length
bpf = Blows per Foot; mpf = Minute per Foot; S = Split Spoon; DP = Direct Push Sample
U = Undistrubed Tube Sample; C = Rock Core; V = Field Vane Shear; SC = Sonic Core
WOR = Weight of Rods; WOH = Weight of Hammer; RQD = Rock Quality Designation; OVM = Organic Vapor Meter
Q_u = Pocket Penetrometer Strength; S_v = Pocket Torvane Shear Strength; F_v = Field Vane Shear Strength; NA, NM = Not Applicable, Not Measured

Elev. (ft)	Depth (ft)	Casing Pen. (bpf) or Core Rate (mpf)	Sample No.	Type	Depth (ft)	Pen./ Rec. (in)	Blows Count or RQD	Field Test Data	GRAPHIC LOG	Sample Description & Classification	H_2O Depth	Remarks
			S-1		0 to 2	24/12	4-7-8-8			WIDELY GRADED SAND WITH SILT (SW-SM); fine to coarse sand, ~10% silty fines, ~5% fine gravel, dry, light brown, roots, topsoil, FILL.		
70			S-2		2 to 4	24/12	7-4-5-9			SILTY SAND (SM); fine to coarse sand, ~20% silty fines, ~5% fine gravel, moist, brown, FILL.		
										4-5 ft: Soil cuttings similar to material observed in S-2, FILL.		
	5		S-3		5 to 7	24/24	5-9-25-46			WIDELY GRADED SAND WITH SILT (SW-SM); fine to coarse sand, ~10% silty fines, ~10% fine gravel, moist, brown.		Strata change estimated at 5 feet
65			S-4		7 to 9	24/18	16-29-30-35			SILTY SAND (SM); fine to coarse sand, ~15% silty fines, ~5% fine gravel, moist, reddish brown.		
										9-10 ft: Soil cuttings similar to material observed in S-4.		
	10		S-5		10 to 12	24/20	13-16-16-17			WIDELY GRADED SAND WITH SILT (SW-SM); fine to coarse sand, ~10% silty fines, ~5% fine gravel, dry, brown.		
60			S-6		12 to 14	24/14	17-19-19-20			WIDELY GRADED SAND WITH SILT (SW-SM); fine to coarse sand, ~15% fine to coarse gravel, ~10% silty fines, dry, brown.		
	15		S-7		15 to 17	24/15	4-5-6-9			WIDELY GRADED SAND (SW); fine to coarse sand, ~5% silty fines, ~5% fine gravel, dry, tan.		
55												
	20		S-8		20 to 22	24/15	7-9-13-13			WIDELY GRADED SAND (SW); fine to coarse sand, ~10% fine to coarse gravel, ~5% silty fines, moist, tan.		
50												

Stratification lines represent approximate boundary between soil types, transitions may be gradual. Water level readings have been made at times and under conditions stated. Fluctuations of groundwater may occur due to other factors than those present at the time measurements were made.

CLIENT: HDR Architechture, Inc.
PROJECT NAME: NSLS II Geotechnical Investigation
CITY/STATE: Upton, New York
GEI PROJECT NUMBER: 062150-*-1000

GEI Consultants
GEI Consultants, Inc.
455 Winding Brook Dr
Glastonbury, CT 06033
860.368.5408

GEOTECHNICAL BORING LOG 02 BNL NSLSII ADDITONAL BORING LOGS.GPJ GEI DATA TEMPLATE.GDT 8/24/06

Boring Location

NORTHING: _____ EASTING: _____ STATION: _____ OFFSET: _____

HORIZONTAL DATUM: NAD 83 STATION CENTERLINE: _____

VERTICAL DATUM: BNL 94 GROUND SURFACE ELEVATION (FT): 73.0

LOCATION: See Figure 2

BORING

B-103

Elev. (ft)	Depth (ft)	Casing Pen. (bpf) or Core Rate (mpf)	SAMPLE INFORMATION: Sample No.	Type	Depth (ft)	Pen./ Rec. (in)	Blows Count or RQD	Field Test Data	GRAPHIC LOG	Sample Description & Classification	H_2O Depth	Remarks
45	25		S-9		25 to 27	24/15	9-12-16-17			WIDELY GRADED SAND (SW); fine to coarse sand, ~5% silty fines, ~5% fine gravel, moist, tan.	▽	
	30		S-10		30 to 32	24/18	13-16-19-39			WIDELY GRADED SAND (SW); fine to coarse sand, ~5% silty fines, wet, brown.		
										End of Boring at 32 feet Fill with cuttings upon completion		

40 35 35 40 30 45 25 50 20

Stratification lines represent approximate boundary between soil types, transitions may be gradual. Water level readings have been made at times and under conditions stated. Fluctuations of groundwater may occur due to other factors than those present at the time measurements were made.

CLIENT: HDR Architechture, Inc.

PROJECT NAME: NSLS II Geotechnical Investigation

CITY/STATE: Upton, New York

GEI PROJECT NUMBER: 062150-*-1000

GEI Consultants

GEI Consultants, Inc.
455 Winding Brook Dr
Glastonbury, CT 06033
860.368.5408

GEOTECHNICAL BORING LOG 02 BNL NSLSII ADDITONAL BORING LOGS.GPJ GEI DATA TEMPLATE.GDT 8/24/06

Boring Location

NORTHING: _____ EASTING: _____ STATION: _____ OFFSET: _____
HORIZONTAL DATUM: NAD 83 STATION CENTERLINE: _____
VERTICAL DATUM: BNL 94 GROUND SURFACE ELEVATION (FT): 76.0
LOCATION: See Figure 2

BORING

B-104

Drilling Information

DATE START / END: 8/16/2006 - 8/16/2006 TOTAL DEPTH (FT): 7.0
CONTRACTOR: New England Boring DRILLER: Jeff Leavitt LOGGED BY: Steve Hawkins
EQUIPMENT: Mobile Drill B-53 truck mounted drill rig. BORING METHOD: Hollow Stem Auger
AUGER ID/OD: 4.25 in / N/A CASING ID/OD: N/A / N/A CORE INFO: _____
HAMMER TYPE: Safety Hammer HAMMER WEIGHT (lbs): 140 HAMMER DROP (inch): 30
WATER LEVEL DEPTHS (ft): _____
GENERAL NOTES: Samples collected using a 2-inch diameter split spoon.

ABBREVIATIONS:
ID = Inside Diameter; OD = Outside Diameter; Pen. = Penetration Length; Rec. = Recovery Length
bpf = Blows per Foot; mpf = Minute per Foot; S = Split Spoon; DP = Direct Push Sample
U = Undistrubed Tube Sample; C = Rock Core; V = Field Vane Shear; SC = Sonic Core
WOR = Weight of Rods; WOH = Weight of Hammer; RQD = Rock Quality Designation; OVM = Organic Vapor Meter
Q_u = Pocket Penetrometer Strength; S_v = Pocket Torvane Shear Strength; F_v = Field Vane Shear Strength; NA, NM = Not Applicable, Not Measured

Elev. (ft)	Depth (ft)	Casing Pen. (bpf) or Core Rate (mpf)	SAMPLE INFORMATION: Sample No.	Type	Depth (ft)	Pen./ Rec. (in)	Blows Count or RQD	Field Test Data	GRAPHIC LOG	Sample Description & Classification	H_2O Depth	Remarks
75			S-1		0 to 2	24/12	3-4-4-3			SILTY SAND (SM); fine to coarse sand, ~25% silty fines, slight petroleum-like odor, moist, dark brown, organics, FILL.		
			S-2		2 to 4	24/15	3-4-6-16			SILTY SAND (SM); fine to coarse sand, ~30% silty fines, ~10% fine gravel, moist, brown, FILL.		
										4-5 ft: Soil cuttings similar to material observed in S-2, FILL.		
70	5		S-3		5 to 7	24/10	16-19-30-30			SILTY SAND (SM); fine to coarse sand, ~15% silty fines, ~5% fine gravel, dry, brown, Probable FILL.		
										Auger refusal encountered ~7-feet bgs. Fill with cuttings upon completion		
65	10											
60	15											
55	20											

Stratification lines represent approximate boundary between soil types, transitions may be gradual. Water level readings have been made at times and under conditions stated. Fluctuations of groundwater may occur due to other factors than those present at the time measurements were made.

CLIENT: HDR Architechture, Inc.
PROJECT NAME: NSLS II Geotechnical Investigation
CITY/STATE: Upton, New York
GEI PROJECT NUMBER: 062150-*-1000

GEI Consultants
GEI Consultants, Inc.
455 Winding Brook Dr
Glastonbury, CT 06033
860.368.5408

GEOTECHNICAL BORING LOG 02 BNL NSLSII ADDITONAL BORING LOGS.GPJ GEI DATA TEMPLATE.GDT 8/24/06

Boring Location

NORTHING: _____ EASTING: _____ STATION: _____ OFFSET: _____
HORIZONTAL DATUM: NAD 83 STATION CENTERLINE: _____
VERTICAL DATUM: BNL 94 GROUND SURFACE ELEVATION (FT): 76.0
LOCATION: ~5 feet North of B-104; See Figure 2

BORING

B-104a

Drilling Information

DATE START / END: 8/16/2006 - 8/16/2006 TOTAL DEPTH (FT): 3.0
CONTRACTOR: New England Boring DRILLER: Jeff Leavitt LOGGED BY: Steve Hawkins
EQUIPMENT: Mobile Drill B-53 truck mounted drill rig. BORING METHOD: Hollow Stem Auger
AUGER ID/OD: 4.25 in / N/A CASING ID/OD: N/A / N/A CORE INFO: _____
HAMMER TYPE: Safety Hammer HAMMER WEIGHT (lbs): 140 HAMMER DROP (inch): 30
WATER LEVEL DEPTHS (ft): _____
GENERAL NOTES: Samples collected using a 2-inch diameter split spoon.

ABBREVIATIONS:
ID = Inside Diameter; OD = Outside Diameter; Pen. = Penetration Length; Rec. = Recovery Length
bpf = Blows per Foot; mpf = Minute per Foot; S = Split Spoon; DP = Direct Push Sample
U = Undistrubed Tube Sample; C = Rock Core; V = Field Vane Shear; SC = Sonic Core
WOR = Weight of Rods; WOH = Weight of Hammer; RQD = Rock Quality Designation; OVM = Organic Vapor Meter
Q_v = Pocket Penetrometer Strength; S_v = Pocket Torvane Shear Strength; F_v = Field Vane Shear Strength
NA, NM = Not Applicable, Not Measured

Elev. (ft)	Depth (ft)	Casing Pen. (bpf) or Core Rate (mpf)	SAMPLE INFORMATION: Sample No.	Type	Depth (ft)	Pen./ Rec. (in)	Blows Count or RQD	Field Test Data	GRAPHIC LOG	Sample Description & Classification	H_2O Depth	Remarks
75										Soil cuttings similar to B-104a S-1, FILL.		
	5									Electrical wire encountered ~3-feet bgs. Auger refusal at ~3 feet bgs. Fill with cuttings upon completion		
70												
	10											
65												
	15											
60												
	20											
55												

Stratification lines represent approximate boundary between soil types, transitions may be gradual. Water level readings have been made at times and under conditions stated. Fluctuations of groundwater may occur due to other factors than those present at the time measurements were made.

CLIENT: HDR Architechture, Inc.
PROJECT NAME: NSLS II Geotechnical Investigation
CITY/STATE: Upton, New York
GEI PROJECT NUMBER: 062150-*-1000

GEI Consultants
GEI Consultants, Inc.
455 Winding Brook Dr
Glastonbury, CT 06033
860.368.5408

GEOTECHNICAL BORING LOG 02 BNL NSLSII ADDITONAL BORING LOGS.GPJ GEI DATA TEMPLATE.GDT 8/24/06

Boring Location

NORTHING: _____ EASTING: _____ STATION: _____ OFFSET: _____

HORIZONTAL DATUM: NAD 83 STATION CENTERLINE: _____

VERTICAL DATUM: BNL 94 GROUND SURFACE ELEVATION (FT): 76.0

LOCATION: ~5 feet West of B-104a; See Figure 2

BORING

B-104b

Drilling Information

DATE START / END: 8/16/2006 - 8/16/2006 TOTAL DEPTH (FT): 32.0

CONTRACTOR: New England Borings DRILLER: Jeff Leavitt LOGGED BY: Steven Hawkins

EQUIPMENT: Mobile Drill B-53 truck mounted drill rig. BORING METHOD: Hollow Stem Auger

AUGER ID/OD: 4.25 in / N/A CASING ID/OD: N/A / N/A CORE INFO: _____

HAMMER TYPE: Safety Hammer HAMMER WEIGHT (lbs): 140 HAMMER DROP (inch): 30

WATER LEVEL DEPTHS (ft): ▽ 31.00 8/16/2006 12:57 pm

GENERAL NOTES: Samples collected using a 2-inch diameter split spoon.

ABBREVIATIONS:

ID = Inside Diameter	bpf = Blows per Foot	U = Undistrubed Tube Sample	WOR = Weight of Rods	Q_u = Pocket Penetrometer Strength
OD = Outside Diameter	mpf = Minute per Foot	C = Rock Core	WOH = Weight of Hammer	S_v = Pocket Torvane Shear Strength
Pen. = Penetration Length	S = Split Spoon	V = Field Vane Shear	RQD = Rock Quality Designation	F_v = Field Vane Shear Strength
Rec. = Recovery Length	DP = Direct Push Sample	SC = Sonic Core	OVM = Organic Vapor Meter	NA, NM = Not Applicable, Not Measured

Elev. (ft)	Depth (ft)	Casing Pen. (bpf) or Core Rate (mpf)	SAMPLE INFORMATION: Sample No.	Type	Depth (ft)	Pen./ Rec. (in)	Blows Count or RQD	Field Test Data	GRAPHIC LOG	Sample Description & Classification	H_2O Depth	Remarks
75										See boring log B-104a for sample information and description of material from 0 to 7-feet bgs.		
	5											
70			S-1		7 to 9	24/6	15-22-27-39			SILTY SAND (SM); fine to coarse sand, ~15% silty fines, ~5% fine gravel, dry, brown.		
										9-10: Soil cuttings similar to material observed in S-4.		
	10		S-2		10 to 12	24/19	9-17-19-15			SILTY SAND (SM); fine to coarse sand, ~15% silty fines, ~5% fine gravel, moist, brown.		
65			S-3		12 to 14	24/20	13-14-16-16			WIDELY GRADED SAND (SW); fine to coarse sand, ~5% silty fines, ~5% fine gravel, moist, brown.		
	15		S-4		15 to 17	24/12	3-4-8-7			WIDELY GRADED SAND (SW); fine to coarse sand, ~10% fine to coarse gravel, ~5% silty fines, dry, tan.		
60												
	20		S-5		20 to 22	24/18	6-9-12-10			WIDELY GRADED SAND (SW); fine to coarse sand, ~10% fine to coarse gravel, ~5% silty fines, dry, tan.		
55												

Stratification lines represent approximate boundary between soil types, transitions may be gradual. Water level readings have been made at times and under conditions stated. Fluctuations of groundwater may occur due to other factors than those present at the time measurements were made.

CLIENT: HDR Architechture, Inc.

PROJECT NAME: NSLS II Geotechnical Investigation

CITY/STATE: Upton, New York

GEI PROJECT NUMBER: 062150-*-1000

GEI Consultants, Inc.
455 Winding Brook Dr
Glastonbury, CT 06033
860.368.5408

GEOTECHNICAL BORING LOG 02 BNL NSLSII ADDITONAL BORING LOGS.GPJ GEI DATA TEMPLATE.GDT 8/24/06

Boring Location

NORTHING: _____ EASTING: _____ STATION: _____ OFFSET: _____

HORIZONTAL DATUM: NAD 83 STATION CENTERLINE: _____

VERTICAL DATUM: BNL 94 GROUND SURFACE ELEVATION (FT): 76.0

LOCATION: ~5 feet West of B-104a; See Figure 2

BORING

B-104b

Elev. (ft)	Depth (ft)	Casing Pen. (bpf) or Core Rate (mpf)	SAMPLE INFORMATION: Sample No.	Type	Depth (ft)	Pen./ Rec. (in)	Blows Count or RQD	Field Test Data	GRAPHIC LOG	Sample Description & Classification	H_2O Depth	Remarks
50	25		S-6		25 to 27	24/12	10-15-19-17			WIDELY GRADED SAND WITH GRAVEL (SW); fine to coarse sand, ~15% fine to coarse gravel, ~5% silty fines, dry, tan.		
45	30		S-7		30 to 32	24/16	7-11-11-10			WIDELY GRADED SAND (SW); fine to coarse sand, ~10% fine to coarse gravel, ~5% silty fines, moist, tan.	▽	
										End of Boring at 32 feet Fill with cuttings upon completion		
40	35											
35	40											
30	45											
25	50											

Stratification lines represent approximate boundary between soil types, transitions may be gradual. Water level readings have been made at times and under conditions stated. Fluctuations of groundwater may occur due to other factors than those present at the time measurements were made.

CLIENT: HDR Architechture, Inc.

PROJECT NAME: NSLS II Geotechnical Investigation

CITY/STATE: Upton, New York

GEI PROJECT NUMBER: 062150-*-1000

GEI Consultants

GEI Consultants, Inc.
455 Winding Brook Dr
Glastonbury, CT 06033
860.368.5408

GEOTECHNICAL BORING LOG 02 BNL NSLSII ADDITONAL BORING LOGS.GPJ GEI DATA TEMPLATE.GDT 8/24/06

Boring Location

NORTHING: _____ EASTING: _____ STATION: _____ OFFSET: _____

HORIZONTAL DATUM: NAD83 CT STATION CENTERLINE: _____

VERTICAL DATUM: BNL 94 GROUND SURFACE ELEVATION (FT): 73.0

LOCATION: See Plan

BORING

B-201

Drilling Information

DATE START / END: 4/23/2007 - 4/23/2007 TOTAL DEPTH (FT): 47.0

CONTRACTOR: New England Borings DRILLER: Jeff Leavitt LOGGED BY: Steven Hawkins

EQUIPMENT: Truck BORING METHOD: Drive and Wash

AUGER ID/OD: N/A / N/A CASING ID/OD: 3 in / 3.25 in CORE INFO: _____

HAMMER TYPE: Safety Hammer HAMMER WEIGHT (lbs): 140 HAMMER DROP (inch): 30

WATER LEVEL DEPTHS (ft): ▼ 27.30 4/24/2007 7:26 am

GENERAL NOTES: _____

ABBREVIATIONS: ID = Inside Diameter; OD = Outside Diameter; Pen. = Penetration Length; Rec. = Recovery Length; bpf = Blows per Foot; mpf = Minute per Foot; S = Split Spoon; DP = Direct Push Sample; U = Undistrubed Tube Sample; C = Rock Core; V = Field Vane Shear; SC = Sonic Core; WOR = Weight of Rods; WOH = Weight of Hammer; RQD = Rock Quality Designation; OVM = Organic Vapor Meter; Q_v = Pocket Penetrometer Strength; S_v = Pocket Torvane Shear Strength; F_v = Field Vane Shear Strength; NA, NM = Not Applicable, Not Measured

Elev. (ft)	Depth (ft)	Casing Pen. (bpf) or Core Rate (mpf)	Sample No.	Type	Depth (ft)	Pen./ Rec. (in)	Blows Count or RQD	Field Test Data	GRAPHIC LOG	Sample Description & Classification	H_2O Depth	Remarks
			S-1		0 to 2	24/15	6-4-4-4			SILTY SAND (SM); ~75% sand, ~20% fines, ~5% gravel; moist, brown, F-M sand, roots, F gravel, 4" topsoil, FILL.		
70			S-2		2 to 4	24/16	11-13-27-30			WIDELY GRADED SAND (SW); ~90% sand, ~5% gravel, ~5% fines; fine to medium, dry, yellowish brown, F-C gravel max. 1in.		
	5		S-3		4 to 6	24/19	21-21-31-36			WIDELY GRADED SAND (SW); ~85% sand, ~10% gravel, ~5% fines; fine to medium, dry, light brown, F-C gravel max. 1in.		
			S-4		6 to 8	24/17	41-57-65-70			WIDELY GRADED SAND (SW); ~90% sand, ~5% gravel, ~5% fines; fine to medium, dry, light brown, F-C gravel max. 1in.		
65			S-5		8 to 10	24/19	22-27-31-37			WIDELY GRADED SAND WITH SILT (SW-SM); ~85% sand, ~10% fines, ~5% gravel; fine to medium, moist, brown, F-C gravel max. 1in.		
	10		S-6		10 to 12	24/14	40-41-42-40			WIDELY GRADED SAND WITH SILT (SW-SM); ~85% sand, ~10% fines, ~5% gravel; fine to medium, moist, brown, F-C gravel max. 3/4 in.		
60												
	15		S-7		15 to 17	24/9	14-10-10-11			WIDELY GRADED SAND (SW); ~90% sand, ~5% gravel, ~5% fines; fine to coarse, fine gravel, wet, light brown.		
55												
	20		S-8		20 to 22	24/10	19-17-22-34			WIDELY GRADED SAND (SW); ~90% sand, ~5% gravel, ~5% fines; fine to coarse, fine gravel, wet, light brown.		
50												

Stratification lines represent approximate boundary between soil types, transitions may be gradual. Water level readings have been made at times and under conditions stated. Fluctuations of groundwater may occur due to other factors than those present at the time measurements were made.

CLIENT: HDR Architechture, Inc.

PROJECT NAME: NSLS II - ACD

CITY/STATE: Upton, New York

GEI PROJECT NUMBER: 062152

GEI Consultants, Inc.
455 Winding Brook Dr
Glastonbury, CT 06033
860.368.5300

GEOTECHNICAL BORING LOG 02 ACD BORING LOGS.GPJ GEI DATA TEMPLATE.GDT 5/21/07

Boring Location

NORTHING: _____ EASTING: _____ STATION: _____ OFFSET: _____

HORIZONTAL DATUM: NAD83 CT STATION CENTERLINE: _____

VERTICAL DATUM: BNL 94 GROUND SURFACE ELEVATION (FT): 73.0

LOCATION: See Plan

BORING

B-201

Elev. (ft)	Depth (ft)	Casing Pen. (bpf) or Core Rate (mpf)	SAMPLE INFORMATION: Sample No.	Type	Depth (ft)	Pen./ Rec. (in)	Blows Count or RQD	Field Test Data	GRAPHIC LOG	Sample Description & Classification	H_2O Depth	Remarks
	25		S-9		25 to 27	24/11	20-21-37-29			WIDELY GRADED GRAVEL WITH SAND (GW); ~60% gravel, ~35% sand, ~5% fines; fine to coarse, rounded, wet, light brown.	▽	
45												
	30		S-10		30 to 32	24/10	20-25-30-35			WIDELY GRADED SAND (SW); ~95% sand, ~5% fines, ~0% gravel; fine to medium, wet, light brown.		
40												
	35		S-11		35 to 37	24/8	21-22-22-23			WIDELY GRADED SAND (SW); ~95% sand, ~5% fines, ~0% gravel; fine to medium, wet, light brown.		
35												
	40		S-12		40 to 42	24/8	17-21-25-39			WIDELY GRADED SAND (SW); ~90% sand, ~5% gravel, ~5% fines; fine to medium, coarse gravel, wet, light brown.		Drill Chatter
30												
	45		S-13		45 to 47	24/2	11-12-13-17			WIDELY GRADED SAND (SW); ~70% sand, ~25% gravel, ~5% fines; fine to coarse, fine to coarse gravel, wet, brown.		Running sands, rewash out casing.
25										End of Boring at 47 feet		
	50											
20												

Stratification lines represent approximate boundary between soil types, transitions may be gradual. Water level readings have been made at times and under conditions stated. Fluctuations of groundwater may occur due to other factors than those present at the time measurements were made.

CLIENT: HDR Architechture, Inc.
PROJECT NAME: NSLS II - ACD
CITY/STATE: Upton, New York
GEI PROJECT NUMBER: 062152

GEI Consultants, Inc.
455 Winding Brook Dr
Glastonbury, CT 06033
860.368.5300

GEOTECHNICAL BORING LOG 02 ACD BORING LOGS.GPJ GEI DATA TEMPLATE.GDT 5/21/07

Boring Location

NORTHING: _____ EASTING: _____ STATION: _____ OFFSET: _____

HORIZONTAL DATUM: NAD83 CT STATION CENTERLINE: _____

VERTICAL DATUM: BNL 94 GROUND SURFACE ELEVATION (FT): 73.5

LOCATION: See Plan

BORING

B-202

Drilling Information

DATE START / END: 4/25/2007 - 4/25/2007 TOTAL DEPTH (FT): 47.0

CONTRACTOR: New England Borings DRILLER: Jeff Leavitt LOGGED BY: Steven Hawkins

EQUIPMENT: Truck BORING METHOD: Drive and Wash

AUGER ID/OD: N/A / N/A CASING ID/OD: 3 in / 3.25 in CORE INFO: _____

HAMMER TYPE: Safety Hammer HAMMER WEIGHT (lbs): 140 HAMMER DROP (inch): 30

WATER LEVEL DEPTHS (ft): ▼ 31.30 4/25/2007 10:14 am

GENERAL NOTES: _____

ABBREVIATIONS: ID = Inside Diameter; OD = Outside Diameter; Pen. = Penetration Length; Rec. = Recovery Length; bpf = Blows per Foot; mpf = Minute per Foot; S = Split Spoon; DP = Direct Push Sample; U = Undistrubed Tube Sample; C = Rock Core; V = Field Vane Shear; SC = Sonic Core; WOR = Weight of Rods; WOH = Weight of Hammer; RQD = Rock Quality Designation; OVM = Organic Vapor Meter; Q_v = Pocket Penetrometer Strength; S_v = Pocket Torvane Shear Strength; F_v = Field Vane Shear Strength; NA, NM = Not Applicable, Not Measured

Elev. (ft)	Depth (ft)	Casing Pen. (bpf) or Core Rate (mpf)	SAMPLE INFORMATION: Sample No.	Type	Depth (ft)	Pen./ Rec. (in)	Blows Count or RQD	Field Test Data	GRAPHIC LOG	Sample Description & Classification	H_2O Depth	Remarks
										ASPHALT; 4" asphalt, 8" subbase.		
			S-1		1 to 3	24/14	3-2-2-2			SILTY SAND (SM); ~57% sand, ~35% fines, ~8% gravel; rounded, fine to coarse gravel, moist, dark brown to brown, FILL.		
70			S-2		3 to 4.5	18/11	3-3-3			SILTY SAND (SM); ~65% sand, ~30% fines, ~5% gravel; rounded, fine to coarse gravel, moist, brown, FILL.		
	5		S-3		5 to 7	24/21	8-13-21-28			SILTY SAND (SM); ~55% sand, ~40% fines, ~5% gravel; rounded, fine to coarse gravel, moist, brown, FILL.		Drilled through cobble. Move rig north ~2ft. in order to get casing past.
			S-4		7 to 9	24/13	27-28-30-33			WIDELY GRADED SAND (SW); ~90% sand, ~5% gravel, ~5% fines; fine to medium, fine gravel, moist, light brown.		
65										WIDELY GRADED SAND WITH SILT (SW-SM); ~85% sand, ~10% fines, ~5% gravel; fine to medium, fine gravel, moist, light brown.		
			S-5		9 to 11	24/16	25-30-31-23			WIDELY GRADED SAND (SW); ~85% sand, ~10% gravel, ~5% fines; fine to coarse, rounded, fine to coarse gravel, dry, light brown.		
	10											
60												
	15		S-6		15 to 17	24/11	17-20-20-21			WIDELY GRADED SAND (SW); ~90% sand, ~5% gravel, ~5% fines; fine to coarse, rounded, fine to coarse gravel, dry, light brown.		
55												
	20		S-7		20 to 22	24/12	14-12-12-16			WIDELY GRADED SAND (SW); ~85% sand, ~10% gravel, ~5% fines; fine to coarse, rounded, fine gravel, dry, light brown.		
50												

Stratification lines represent approximate boundary between soil types, transitions may be gradual. Water level readings have been made at times and under conditions stated. Fluctuations of groundwater may occur due to other factors than those present at the time measurements were made.

CLIENT: HDR Architechture, Inc.

PROJECT NAME: NSLS II - ACD

CITY/STATE: Upton, New York

GEI PROJECT NUMBER: 062152

GEI Consultants

GEI Consultants, Inc.
455 Winding Brook Dr
Glastonbury, CT 06033
860.368.5300

GEOTECHNICAL BORING LOG 02 ACD BORING LOGS.GPJ GEI DATA TEMPLATE.GDT 5/21/07

Boring Location

NORTHING: _____ EASTING: _____ STATION: _____ OFFSET: _____

HORIZONTAL DATUM: NAD83 CT STATION CENTERLINE: _____

VERTICAL DATUM: BNL 94 GROUND SURFACE ELEVATION (FT): 73.5

LOCATION: See Plan

BORING

B-202

Elev. (ft)	Depth (ft)	Casing Pen. (bpf) or Core Rate (mpf)	Sample No.	Type	Depth (ft)	Pen./ Rec. (in)	Blows Count or RQD	Field Test Data	GRAPHIC LOG	Sample Description & Classification	H_20 Depth	Remarks
45	25		S-8		25 to 27	24/10	20-21-17-17			WIDELY GRADED SAND (SW); ~80% sand, ~15% gravel, ~5% fines; fine to coarse, rounded, fine gravel, dry, light brown.		
40	30		S-9		30 to 32	24/14	17-16-12-16			WIDELY GRADED SAND (SW); ~75% sand, ~20% gravel, ~5% fines; fine to coarse, rounded, fine to coarse gravel, dry, light brown.	▼	
35	35		S-10		35 to 37	24/10	20-20-21-23			WIDELY GRADED SAND (SW); ~90% sand, ~5% gravel, ~5% fines; fine to coarse, rounded, fine gravel, dry, light brown.		
30	40		S-11		40 to 42	24/9	17-14-19-25			WIDELY GRADED SAND (SW); ~90% sand, ~5% gravel, ~5% fines; fine to coarse, rounded, fine gravel, dry, light brown.		
25	45		S-12		45 to 47	24/0	17-20-21-26			No recovery.		
20	50									End of Boring at 47 feet		

Stratification lines represent approximate boundary between soil types, transitions may be gradual. Water level readings have been made at times and under conditions stated. Fluctuations of groundwater may occur due to other factors than those present at the time measurements were made.

CLIENT: HDR Architechture, Inc.
PROJECT NAME: NSLS II - ACD
CITY/STATE: Upton, New York
GEI PROJECT NUMBER: 062152

GEI Consultants, Inc.
455 Winding Brook Dr
Glastonbury, CT 06033
860.368.5300

GEOTECHNICAL BORING LOG 02 ACD BORING LOGS.GPJ GEI DATA TEMPLATE.GDT 5/21/07

Boring Location

NORTHING: _____ EASTING: _____ STATION: _____ OFFSET: _____

HORIZONTAL DATUM: NAD83 CT STATION CENTERLINE: _____

VERTICAL DATUM: BNL 94 GROUND SURFACE ELEVATION (FT): 71.0

LOCATION: See Plan

BORING

B-203

Drilling Information

DATE START / END: 4/25/2007 - 4/25/2007 TOTAL DEPTH (FT): 47.0

CONTRACTOR: New England Borings DRILLER: Jeff Leavitt LOGGED BY: Steven Hawkins

EQUIPMENT: Truck BORING METHOD: Drive and Wash

AUGER ID/OD: N/A / N/A CASING ID/OD: 3 in / 3.25 in CORE INFO: _____

HAMMER TYPE: Safety Hammer HAMMER WEIGHT (lbs): 140 HAMMER DROP (inch): 30

WATER LEVEL DEPTHS (ft): ▼ 28.00 4/25/2007 2:07 pm

GENERAL NOTES: _____

ABBREVIATIONS: ID = Inside Diameter; OD = Outside Diameter; Pen. = Penetration Length; Rec. = Recovery Length; bpf = Blows per Foot; mpf = Minute per Foot; S = Split Spoon; DP = Direct Push Sample; U = Undistrubed Tube Sample; C = Rock Core; V = Field Vane Shear; SC = Sonic Core; WOR = Weight of Rods; WOH = Weight of Hammer; RQD = Rock Quality Designation; OVM = Organic Vapor Meter; Q_v = Pocket Penetrometer Strength; S_v = Pocket Torvane Shear Strength; F_v = Field Vane Shear Strength; NA, NM = Not Applicable, Not Measured

Elev. (ft)	Depth (ft)	Casing Pen. (bpf) or Core Rate (mpf)	Sample No.	Type	Depth (ft)	Pen./ Rec. (in)	Blows Count or RQD	Field Test Data	GRAPHIC LOG	Sample Description & Classification	H_2O Depth	Remarks
70			S-1		0 to 2	24/14	7-8-15-11			WIDELY GRADED SAND (SW); ~70% sand, ~20% gravel, ~10% fines; fine to coarse, coarse gravel, roots, moist, dark brown to gray, Top 8" topsoil, FILL.		
			S-2		2 to 2.5	6/0	6			No recovery.		Grind through cobble/debris
	5		S-3		4 to 6	24/12	8-12-14-16			WIDELY GRADED SAND WITH SILT (SW-SM); ~78% sand, ~13% fines, ~9% gravel; fine to coarse, rounded, fine to coarse gravel, dry, light brown.		
65			S-4		6 to 8	24/16	12-16-21-28			SILTY SAND (SM); ~80% sand, ~15% fines, ~5% gravel; fine to coarse, rounded, fine gravel, dry, light brown.		
			S-5		8 to 10	24/12	8-9-10-10			WIDELY GRADED SAND (SW); ~90% sand, ~5% gravel, ~5% fines; fine to coarse, rounded, fine to coarse gravel, dry, light brown.		
	10		S-6		10 to 12	24/17	10-8-8-11			WIDELY GRADED SAND (SW); ~90% sand, ~5% gravel, ~5% fines; fine to coarse, rounded, fine gravel, dry, light brown.		
60												
	15		S-7		15 to 17	24/10	11-12-13-14			WIDELY GRADED SAND (SW); ~90% sand, ~5% gravel, ~5% fines; fine to coarse, rounded, fine gravel, moist, light brown.		
55												
	20		S-8		20 to 22	24/10	23-25-26-31			WIDELY GRADED SAND (SW); ~90% sand, ~5% gravel, ~5% fines; fine to coarse, rounded, fine gravel, moist, light brown.		Drill chatter
50												

Stratification lines represent approximate boundary between soil types, transitions may be gradual. Water level readings have been made at times and under conditions stated. Fluctuations of groundwater may occur due to other factors than those present at the time measurements were made.

CLIENT: HDR Architechture, Inc.
PROJECT NAME: NSLS II - ACD
CITY/STATE: Upton, New York
GEI PROJECT NUMBER: 062152

GEI Consultants
GEI Consultants, Inc.
455 Winding Brook Dr
Glastonbury, CT 06033
860.368.5300

GEOTECHNICAL BORING LOG 02 ACD BORING LOGS.GPJ GEI DATA TEMPLATE.GDT 5/21/07

Boring Location

NORTHING: _____ EASTING: _____ STATION: _____ OFFSET: _____

HORIZONTAL DATUM: NAD83 CT STATION CENTERLINE: _____

VERTICAL DATUM: BNL 94 GROUND SURFACE ELEVATION (FT): 71.0

LOCATION: See Plan

BORING

B-203

Elev. (ft)	Depth (ft)	Casing Pen. (bpf) or Core Rate (mpf)	SAMPLE INFORMATION: Sample No.	Type	Depth (ft)	Pen./ Rec. (in)	Blows Count or RQD	Field Test Data	GRAPHIC LOG	Sample Description & Classification	H_2O Depth	Remarks
45	25		S-9		25 to 27	24/8	24-36-37-43			WIDELY GRADED SAND (SW); ~90% sand, ~5% gravel, ~5% fines; fine to coarse, rounded, fine gravel, moist, light brown.	▼	
40	30		S-10		30 to 32	24/11	16-14-12-10			WIDELY GRADED SAND (SW); ~90% sand, ~5% gravel, ~5% fines; fine to coarse, rounded, fine gravel, moist, light brown.		
35	35		S-11		35 to 37	24/8	16-16-16-20			WIDELY GRADED SAND (SW); ~90% sand, ~5% gravel, ~5% fines; fine to coarse, rounded, fine gravel, moist, light brown.		Rig chatter
30	40		S-12		40 to 42	24/7	11-10-9-9			WIDELY GRADED SAND (SW); ~75% sand, ~20% gravel, ~5% fines; fine to coarse, rounded, fine to coarse gravel, moist, light brown.		
25	45		S-13		45 to 47	24/0	11-15-12-14			No recovery.		
20	50									End of Boring at 47 feet		

Stratification lines represent approximate boundary between soil types, transitions may be gradual. Water level readings have been made at times and under conditions stated. Fluctuations of groundwater may occur due to other factors than those present at the time measurements were made.

CLIENT: HDR Architechture, Inc.
PROJECT NAME: NSLS II - ACD
CITY/STATE: Upton, New York
GEI PROJECT NUMBER: 062152

GEI Consultants

GEI Consultants, Inc.
455 Winding Brook Dr
Glastonbury, CT 06033
860.368.5300

GEOTECHNICAL BORING LOG 02 ACD BORING LOGS.GPJ GEI DATA TEMPLATE.GDT 5/21/07

Boring Location

NORTHING: _____ EASTING: _____ STATION: _____ OFFSET: _____

HORIZONTAL DATUM: NAD83 CT STATION CENTERLINE: _____

VERTICAL DATUM: BNL 94 GROUND SURFACE ELEVATION (FT): 68.0

LOCATION: See Plan

BORING

B-204

Drilling Information

DATE START / END: 4/25/2007 - 4/26/2007 TOTAL DEPTH (FT): 47.0

CONTRACTOR: New England Borings DRILLER: Jeff Leavitt LOGGED BY: Steven Hawkins

EQUIPMENT: Truck BORING METHOD: Drive and Wash

AUGER ID/OD: N/A / N/A CASING ID/OD: 3 in / 3.25 in CORE INFO: _____

HAMMER TYPE: Safety Hammer HAMMER WEIGHT (lbs): 140 HAMMER DROP (inch): 30

WATER LEVEL DEPTHS (ft): ▼ 26.00 4/26/2007 8:31 am

GENERAL NOTES: _____

ABBREVIATIONS:

ID = Inside Diameter	bpf = Blows per Foot	U = Undistrubed Tube Sample	WOR = Weight of Rods	Q_v = Pocket Penetrometer Strength
OD = Outside Diameter	mpf = Minute per Foot	C = Rock Core	WOH = Weight of Hammer	S_v = Pocket Torvane Shear Strength
Pen. = Penetration Length	S = Split Spoon	V = Field Vane Shear	RQD = Rock Quality Designation	F_v = Field Vane Shear Strength
Rec. = Recovery Length	DP = Direct Push Sample	SC = Sonic Core	OVM = Organic Vapor Meter	NA, NM = Not Applicable, Not Measured

Elev. (ft)	Depth (ft)	Casing Pen. (bpf) or Core Rate (mpf)	SAMPLE INFORMATION: Sample No.	Type	Depth (ft)	Pen./ Rec. (in)	Blows Count or RQD	Field Test Data	GRAPHIC LOG	Sample Description & Classification	H_2O Depth	Remarks
			S-1		0 to 2	24/19	2-3-5-7			WIDELY GRADED SAND WITH SILT (SM); ~83% sand, ~13% fines, ~4% gravel; fine to coarse, fine gravel, moist, dark brown to brown, Top 8" topsoil, FILL.		
65			S-2		2 to 4	24/16	7-5-2-4			SILTY SAND (SM); ~70% sand, ~25% fines, ~5% gravel; fine to coarse, fine gravel, dry, brown, FILL.		
	5		S-3		4 to 6	24/20	7-9-11-12			WIDELY GRADED SAND (SW); ~90% sand, ~5% gravel, ~5% fines; fine to coarse, fine gravel, dry, grayish brown, FILL.		
			S-4		6 to 8	24/18	15-25-37-41			WIDELY GRADED SAND WITH SILT (SW-SM); ~80% sand, ~10% gravel, ~10% fines; fine to coarse, fine to coarse gravel, moist, grayish brown.		
60			S-5		8 to 10	24/20	37-39-49-50			WIDELY GRADED SAND WITH SILT (SW-SM); ~71% sand, ~15% gravel, ~14% fines; fine to medium, fine gravel, moist, grayish brown.		
	10		S-6		10 to 12	24/20	17-21-28-27			WIDELY GRADED SAND WITH SILT (SW-SM); ~85% sand, ~10% fines, ~5% gravel; fine to medium, fine gravel, moist, grayish brown.		
55										WIDELY GRADED SAND (SW); ~90% sand, ~5% gravel, ~5% fines; fine to coarse, fine gravel, dry, light brown.		
	15		S-7		15 to 17	24/14	27-35-34-27			WIDELY GRADED SAND (SW); ~80% sand, ~15% gravel, ~5% fines; fine to coarse, subrounded, fine to coarse gravel, dry, light brown.		
50												
	20		S-8		20 to 22	24/13	20-22-24-20			WIDELY GRADED SAND (SW); ~85% sand, ~10% gravel, ~5% fines; fine to coarse, subrounded, fine gravel, dry, light brown.		
45												

Stratification lines represent approximate boundary between soil types, transitions may be gradual. Water level readings have been made at times and under conditions stated. Fluctuations of groundwater may occur due to other factors than those present at the time measurements were made.

CLIENT: HDR Architechture, Inc.

PROJECT NAME: NSLS II - ACD

CITY/STATE: Upton, New York

GEI PROJECT NUMBER: 062152

GEI Consultants

GEI Consultants, Inc.
455 Winding Brook Dr
Glastonbury, CT 06033
860.368.5300

GEOTECHNICAL BORING LOG 02 ACD BORING LOGS.GPJ GEI DATA TEMPLATE.GDT 5/21/07

Boring Location

NORTHING: _____ EASTING: _____ STATION: _____ OFFSET: _____

HORIZONTAL DATUM: NAD83 CT STATION CENTERLINE: _____

VERTICAL DATUM: BNL 94 GROUND SURFACE ELEVATION (FT): 68.0

LOCATION: See Plan

BORING

B-204

Elev. (ft)	Depth (ft)	Casing Pen. (bpf) or Core Rate (mpf)	SAMPLE INFORMATION: Sample No.	Type	Depth (ft)	Pen./ Rec. (in)	Blows Count or RQD	Field Test Data	GRAPHIC LOG	Sample Description & Classification	H_2O Depth	Remarks
	25		S-9		25 to 26.5	18/10	19-29-40			WIDELY GRADED SAND (SW); ~90% sand, ~5% gravel, ~5% fines; fine to coarse, subrounded, fine gravel, dry, light brown.	▼	Running sands
40												
	30		S-10		30 to 32	24/12	14-14-14-11			WIDELY GRADED SAND (SW); ~90% sand, ~5% gravel, ~5% fines; fine to coarse, subrounded, fine gravel, dry, light brown.		
35												
	35		S-11		35 to 37	24/7	9-9-7-13			WIDELY GRADED SAND (SW); ~90% sand, ~5% gravel, ~5% fines; fine to coarse, subrounded, fine to coarse gravel, dry, light brown.		
30												
	40		S-12		40 to 42	24/7	14-18-18-26			WIDELY GRADED SAND (SW); ~90% sand, ~5% gravel, ~5% fines; fine to medium, subrounded, coarse gravel, dry, light brown.		
25												
	45		S-13		45 to 47	24/12	20-29-35-37			WIDELY GRADED SAND (SW); ~90% sand, ~5% gravel, ~5% fines; fine to medium, subrounded, fine gravel, dry, light brown.		
										End of Boring at 47 feet		
20												
	50											
15												

Stratification lines represent approximate boundary between soil types, transitions may be gradual. Water level readings have been made at times and under conditions stated. Fluctuations of groundwater may occur due to other factors than those present at the time measurements were made.

CLIENT: HDR Architechture, Inc.
PROJECT NAME: NSLS II - ACD
CITY/STATE: Upton, New York
GEI PROJECT NUMBER: 062152

GEI Consultants
GEI Consultants, Inc.
455 Winding Brook Dr
Glastonbury, CT 06033
860.368.5300

GEOTECHNICAL BORING LOG 02 ACD BORING LOGS.GPJ GEI DATA TEMPLATE.GDT 5/21/07

Boring Location

NORTHING: _____ EASTING: _____ STATION: _____ OFFSET: _____

HORIZONTAL DATUM: NAD83 CT STATION CENTERLINE: _____

VERTICAL DATUM: BNL 94 GROUND SURFACE ELEVATION (FT): 77.0

LOCATION: See Plan

BORING

B-205

Drilling Information

DATE START / END: 4/24/2007 - 4/24/2007 TOTAL DEPTH (FT): 47.0

CONTRACTOR: New England Borings DRILLER: Jeff Leavitt LOGGED BY: Steven Hawkins

EQUIPMENT: Truck BORING METHOD: Drive and Wash

AUGER ID/OD: N/A / N/A CASING ID/OD: 3 in / 3.25 in CORE INFO: _____

HAMMER TYPE: Safety Hammer HAMMER WEIGHT (lbs): 140 HAMMER DROP (inch): 30

WATER LEVEL DEPTHS (ft): ▼ 32.00 4/24/2007 11:36 am

GENERAL NOTES: _____

ABBREVIATIONS: ID = Inside Diameter; OD = Outside Diameter; Pen. = Penetration Length; Rec. = Recovery Length; bpf = Blows per Foot; mpf = Minute per Foot; S = Split Spoon; DP = Direct Push Sample; U = Undistrubed Tube Sample; C = Rock Core; V = Field Vane Shear; SC = Sonic Core; WOR = Weight of Rods; WOH = Weight of Hammer; RQD = Rock Quality Designation; OVM = Organic Vapor Meter; Q_v = Pocket Penetrometer Strength; S_v = Pocket Torvane Shear Strength; F_v = Field Vane Shear Strength; NA, NM = Not Applicable, Not Measured

Elev. (ft)	Depth (ft)	Casing Pen. (bpf) or Core Rate (mpf)	SAMPLE INFORMATION: Sample No.	Type	Depth (ft)	Pen./ Rec. (in)	Blows Count or RQD	Field Test Data	GRAPHIC LOG	Sample Description & Classification	H_2O Depth	Remarks
			S-1		0 to 2	24/19	3-3-4-4			SILTY SAND (SM); ~75% sand, ~20% fines, ~5% gravel; roots, moist, dark brown, Top 8" topsoil, FILL.		
75			S-2		2 to 4	24/17	9-11-15-26			SILTY SAND (SM); ~80% sand, ~15% fines, ~5% gravel; fine to coarse gravel, dry, grayish brown.		
	5		S-3		4 to 6	24/20	21-41-40-29			WIDELY GRADED SAND (SW); ~90% sand, ~5% gravel, ~5% fines; fine to medium, fine to coarse gravel, dry, brown.		
70			S-4		6 to 8	24/15	21-22-25-21			WIDELY GRADED SAND (SW); ~90% sand, ~5% gravel, ~5% fines; fine to medium, fine to coarse gravel, dry, brown.		
			S-5		8 to 10	24/16	6-7-10-10			WIDELY GRADED SAND (SW); ~90% sand, ~10% gravel, ~0% fines; fine to medium, rounded, fine to coarse gravel, dry, light brown.		
	10		S-6		10 to 12	24/14	12-10-11-10			WIDELY GRADED SAND (SW); ~90% sand, ~10% gravel, ~0% fines; medium to coarse, rounded, fine to coarse gravel, dry, light brown.		
65												
	15		S-7		15 to 17	24/8	12-15-17-21			WIDELY GRADED SAND (SW); ~90% sand, ~5% gravel, ~5% fines; fine to coarse, rounded, fine to coarse gravel, wet, light brown.		
60												
	20		S-8		20 to 22	24/10	15-17-24-21			WIDELY GRADED SAND WITH GRAVEL (SW); ~70% sand, ~25% gravel, ~5% fines; fine to coarse, rounded, fine to coarse gravel, wet, light brown.		
55												

Stratification lines represent approximate boundary between soil types, transitions may be gradual. Water level readings have been made at times and under conditions stated. Fluctuations of groundwater may occur due to other factors than those present at the time measurements were made.

CLIENT: HDR Architechture, Inc.

PROJECT NAME: NSLS II - ACD

CITY/STATE: Upton, New York

GEI PROJECT NUMBER: 062152

GEI Consultants

GEI Consultants, Inc.
455 Winding Brook Dr
Glastonbury, CT 06033
860.368.5300

GEOTECHNICAL BORING LOG 02 ACD BORING LOGS.GPJ GEI DATA TEMPLATE.GDT 5/21/07

Boring Location

NORTHING: _____ EASTING: _____ STATION: _____ OFFSET: _____

HORIZONTAL DATUM: NAD83 CT STATION CENTERLINE: _____

VERTICAL DATUM: BNL 94 GROUND SURFACE ELEVATION (FT): 77.0

LOCATION: See Plan

BORING

B-205

Elev. (ft)	Depth (ft)	Casing Pen. (bpf) or Core Rate (mpf)	Sample No.	Type	Depth (ft)	Pen./ Rec. (in)	Blows Count or RQD	Field Test Data	GRAPHIC LOG	Sample Description & Classification	H_2O Depth	Remarks
50	25		S-9		25 to 27	24/9	36-25-22-34			WIDELY GRADED SAND WITH GRAVEL (SW); ~65% sand, ~30% gravel, ~5% fines; fine to coarse, rounded, fine gravel, wet, light brown.		
45	30		S-10		30 to 32	24/6	15-12-8-10			WIDELY GRADED SAND WITH GRAVEL (SW); ~65% sand, ~30% gravel, ~5% fines; fine to coarse, rounded, fine gravel, wet, light brown.	▼	
40	35		S-11		35 to 37	24/9	16-20-21-25			WIDELY GRADED SAND (SW); ~85% sand, ~10% gravel, ~5% fines; fine to coarse, rounded, fine gravel, wet, light brown.		
35	40		S-12		40 to 42	24/9	20-21-20-30			WIDELY GRADED SAND (SW); ~85% sand, ~10% gravel, ~5% fines; fine to coarse, rounded, fine gravel, wet, light brown.		
30	45		S-13		45 to 47	24/10	17-20-24-30			WIDELY GRADED SAND (SW); ~95% sand, ~5% fines, ~0% gravel; fine to coarse, wet, brown.		
25	50									End of Boring at 47 feet		

Stratification lines represent approximate boundary between soil types, transitions may be gradual. Water level readings have been made at times and under conditions stated. Fluctuations of groundwater may occur due to other factors than those present at the time measurements were made.

CLIENT: HDR Architechture, Inc.
PROJECT NAME: NSLS II - ACD
CITY/STATE: Upton, New York
GEI PROJECT NUMBER: 062152

GEI Consultants, Inc.
455 Winding Brook Dr
Glastonbury, CT 06033
860.368.5300

GEOTECHNICAL BORING LOG 02 ACD BORING LOGS.GPJ GEI DATA TEMPLATE.GDT 5/21/07

Boring Location

NORTHING: _____ EASTING: _____ STATION: _____ OFFSET: _____

HORIZONTAL DATUM: NAD83 CT STATION CENTERLINE: _____

VERTICAL DATUM: BNL 94 GROUND SURFACE ELEVATION (FT): 73.5

LOCATION: See Plan

BORING

B-206

Drilling Information

DATE START / END: 4/24/2007 - 4/24/2007 TOTAL DEPTH (FT): 47.0

CONTRACTOR: New England Borings DRILLER: Jeff Leavitt LOGGED BY: Steven Hawkins

EQUIPMENT: Truck BORING METHOD: Drive and Wash

AUGER ID/OD: N/A / N/A CASING ID/OD: 3 in / 3.25 in CORE INFO: _____

HAMMER TYPE: Safety Hammer HAMMER WEIGHT (lbs): 140 HAMMER DROP (inch): 30

WATER LEVEL DEPTHS (ft): ▼ 35.00 4/24/2007 4:06 pm

GENERAL NOTES: _____

ABBREVIATIONS: ID = Inside Diameter; OD = Outside Diameter; Pen. = Penetration Length; Rec. = Recovery Length; bpf = Blows per Foot; mpf = Minute per Foot; S = Split Spoon; DP = Direct Push Sample; U = Undistrubed Tube Sample; C = Rock Core; V = Field Vane Shear; SC = Sonic Core; WOR = Weight of Rods; WOH = Weight of Hammer; RQD = Rock Quality Designation; OVM = Organic Vapor Meter; Q_v = Pocket Penetrometer Strength; S_v = Pocket Torvane Shear Strength; F_v = Field Vane Shear Strength; NA, NM = Not Applicable, Not Measured

Elev. (ft)	Depth (ft)	Casing Pen. (bpf) or Core Rate (mpf)	SAMPLE INFORMATION: Sample No.	Type	Depth (ft)	Pen./ Rec. (in)	Blows Count or RQD	Field Test Data	GRAPHIC LOG	Sample Description & Classification	H_2O Depth	Remarks
70	0		S-1		0 to 2	24/20	6-5-5-5			SILTY SAND (SM); ~65% sand, ~30% fines, ~5% gravel; coal, dry, dark brown, FILL.		
			S-2		2 to 4	24/3	7-11-21-26			SILTY SAND (SM); ~80% sand, ~15% fines, ~5% gravel; roots, dry, dark brown, FILL.		
	5		S-3		4 to 6	24/18	15-21-28-39			WIDELY GRADED SAND (SW); ~85% sand, ~10% gravel, ~5% fines; fine to medium, rounded, fine gravel, dry, light brown, FILL.		
			S-4		6 to 8	24/14	26-29-31-33			SILTY SAND (SM); ~64% sand, ~26% fines, ~10% gravel; fine to coarse, rounded, dry, brown, FILL.		
65			S-5		8 to 10	24/23	12-13-13-16			SILTY SAND (SM); ~75% sand, ~20% fines, ~5% gravel; fine to coarse, rounded, dry, brown, FILL.		
	10		S-6		10 to 12	24/14	15-12-12-15			WIDELY GRADED SAND (SW); ~90% sand, ~5% gravel, ~5% fines; medium to coarse, fine gravel, moist, light brown. WIDELY GRADED SAND (SW); ~90% sand, ~5% gravel, ~5% fines; fine to medium, fine gravel, dry, white.		
60												
	15		S-7		15 to 17	24/9	9-10-11-15			WIDELY GRADED SAND (SW); ~90% sand, ~5% gravel, ~5% fines; fine to coarse, fine gravel, dry, light brown.		
55												
	20		S-8		20 to 22	24/14	14-18-20-25			WIDELY GRADED SAND (SW); ~90% sand, ~5% gravel, ~5% fines; fine to coarse, fine gravel, dry, light brown.		
50												

Stratification lines represent approximate boundary between soil types, transitions may be gradual. Water level readings have been made at times and under conditions stated. Fluctuations of groundwater may occur due to other factors than those present at the time measurements were made.

CLIENT: HDR Architechture, Inc.

PROJECT NAME: NSLS II - ACD

CITY/STATE: Upton, New York

GEI PROJECT NUMBER: 062152

GEI Consultants

GEI Consultants, Inc.
455 Winding Brook Dr
Glastonbury, CT 06033
860.368.5300

GEOTECHNICAL BORING LOG 02 ACD BORING LOGS.GPJ GEI DATA TEMPLATE.GDT 5/21/07

Boring Location

NORTHING: _____ EASTING: _____ STATION: _____ OFFSET: _____

HORIZONTAL DATUM: NAD83 CT STATION CENTERLINE: _____

VERTICAL DATUM: BNL 94 GROUND SURFACE ELEVATION (FT): 73.5

LOCATION: See Plan

BORING

B-206

Elev. (ft)	Depth (ft)	Casing Pen. (bpf) or Core Rate (mpf)	SAMPLE INFORMATION: Sample No.	Type	Depth (ft)	Pen./ Rec. (in)	Blows Count or RQD	Field Test Data	GRAPHIC LOG	Sample Description & Classification	H_2O Depth	Remarks
	25		S-9		25 to 27	24/12	26-25-25-25			WIDELY GRADED SAND (SW); ~90% sand, ~5% gravel, ~5% fines; fine to coarse, coarse gravel, dry, light brown, Max. gravel size 1.5".		
45												Rig chatter
	30		S-10		30 to 32	24/11	16-11-10-10			WIDELY GRADED SAND WITH GRAVEL (SW); ~80% sand, ~15% gravel, ~5% fines; fine to coarse, fine gravel, dry, light brown, Max. gravel size 1.5".		
40												
	35		S-11		35 to 37	24/8	17-23-23-26			WIDELY GRADED SAND WITH SILT (SW-SM); ~80% sand, ~10% gravel, ~10% fines; fine to coarse, fine gravel, dry, light brown, Max. gravel size 1.5".	▼	
35												
	40		S-12		40 to 42	24/6	15-16-20-23			WIDELY GRADED SAND WITH SILT (SW-SM); ~80% sand, ~10% gravel, ~10% fines; fine to coarse, fine gravel, dry, light brown, Max. gravel size 1.5".		
30												
	45		S-13		45 to 47	24/4	26-29-37-39			WIDELY GRADED SAND WITH SILT (SW-SM); ~80% sand, ~10% gravel, ~10% fines; fine to medium, fine gravel, dry, brown, Max. gravel size 1.5".		
										End of Boring at 47 feet		
25												
	50											
20												

Stratification lines represent approximate boundary between soil types, transitions may be gradual. Water level readings have been made at times and under conditions stated. Fluctuations of groundwater may occur due to other factors than those present at the time measurements were made.

CLIENT: HDR Architechture, Inc.
PROJECT NAME: NSLS II - ACD
CITY/STATE: Upton, New York
GEI PROJECT NUMBER: 062152

GEI Consultants, Inc.
455 Winding Brook Dr
Glastonbury, CT 06033
860.368.5300

GEOTECHNICAL BORING LOG 02 ACD BORING LOGS.GPJ GEI DATA TEMPLATE.GDT 5/21/07

Appendix D

2006-2007 Cone Penetrometer Test (CPT) Logs

TABLE 1 - SUMMARY OF CPTU SOUNDINGS

Job No.: 06-773
Location: Brookhaven National Labs
Client: GEI Consultants
Date: July 19, 20, 21, 2006

Date	CPTU Sounding	File Name	CPT Total Depth (ft)	Shear wave Velocity Tests	Comments
19-Jul-06	CPT-1	773cp01.cor	94.32		refusal
19-Jul-06	CPT-2	773cp02.cor	100.06		
20-Jul-06	CPT-3	773cp03.cor	86.12	9	refusal
19-Jul-06	CPT-4	773cp04.cor	95.14		refusal
20-Jul-06	CPT-5	773cp05.cor	7.87		refusal
20-Jul-06	CPT-5A	773cp05a.cor	82.68	9	refusal
20-Jul-06	CPT-6	773cp06.cor	100.06	10	
21-Jul-06	CPT-7	773cp07.cor	6.40		refusal
20-Jul-06	CPT-8	773cp08.cor	52.98		refusal
21-Jul-06	CPT-10	773cp10.cor	61.02		
21-Jul-06	CPT-11	773cp11.cor	73.49		
20-Jul-06	CPT-12	773cp12.cor	100.06	10	
20-Jul-06	CPT-13	773cp13.cor	6.73		refusal
20-Jul-06	CPT-13A	773cp13a.cor	5.58		refusal
21-Jul-06	CPT-14	773cp14.cor	95.80		refusal
Job Totals:		15	968.31	38	

CONETEC

GEI Consultants

Sounding:CPT-1
Site:National Labs

Piezocone:20 Ton AD164
Date:07:19:06 16:08

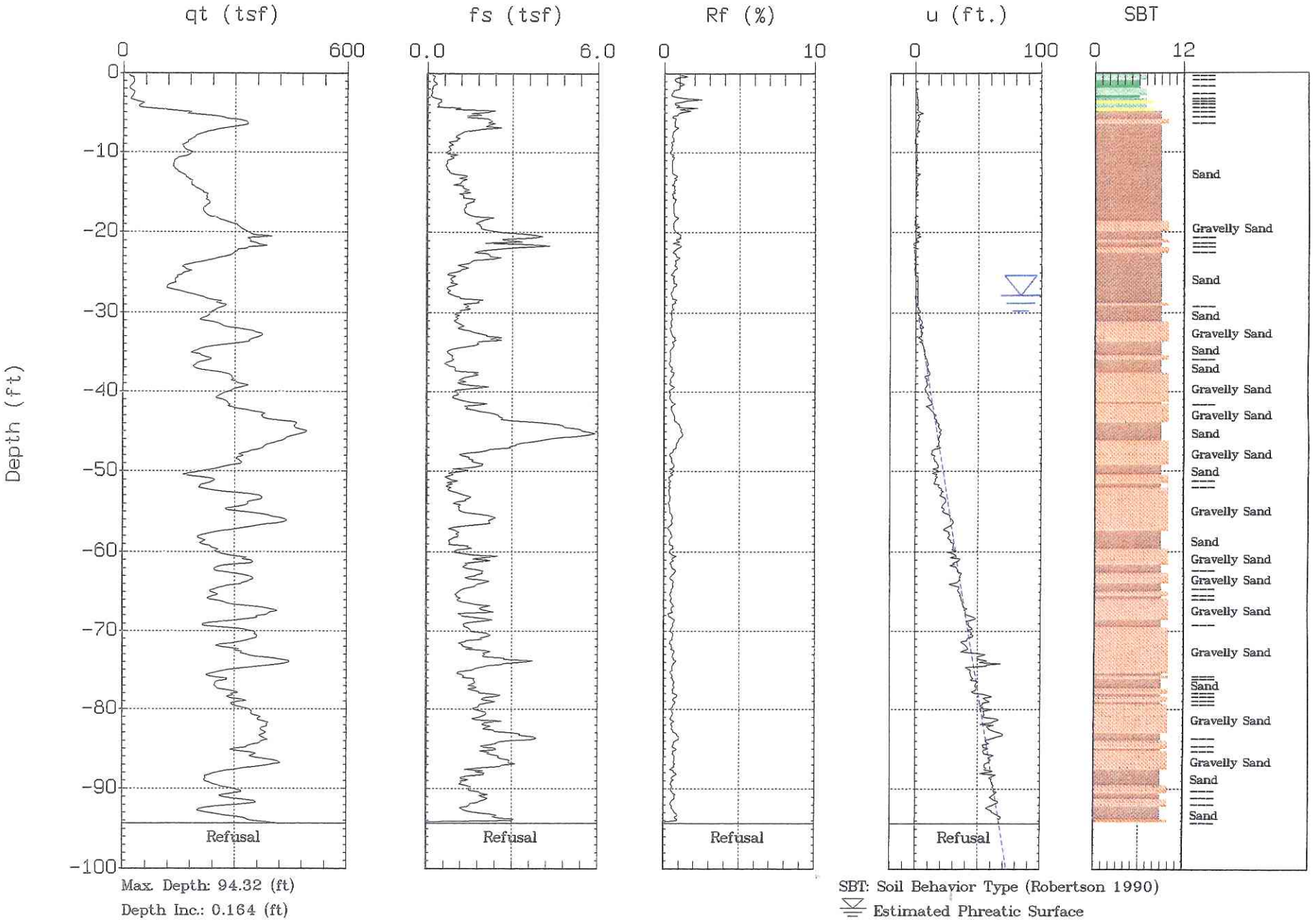

Max. Depth: 94.32 (ft)
Depth Inc.: 0.164 (ft)

SBT: Soil Behavior Type (Robertson 1990)
Estimated Phreatic Surface

CONETEC

GEI Consultants

Sounding:CPT-2
Site:National Labs

Piezocone:20 Ton AD164
Date:07:19:06 14:30

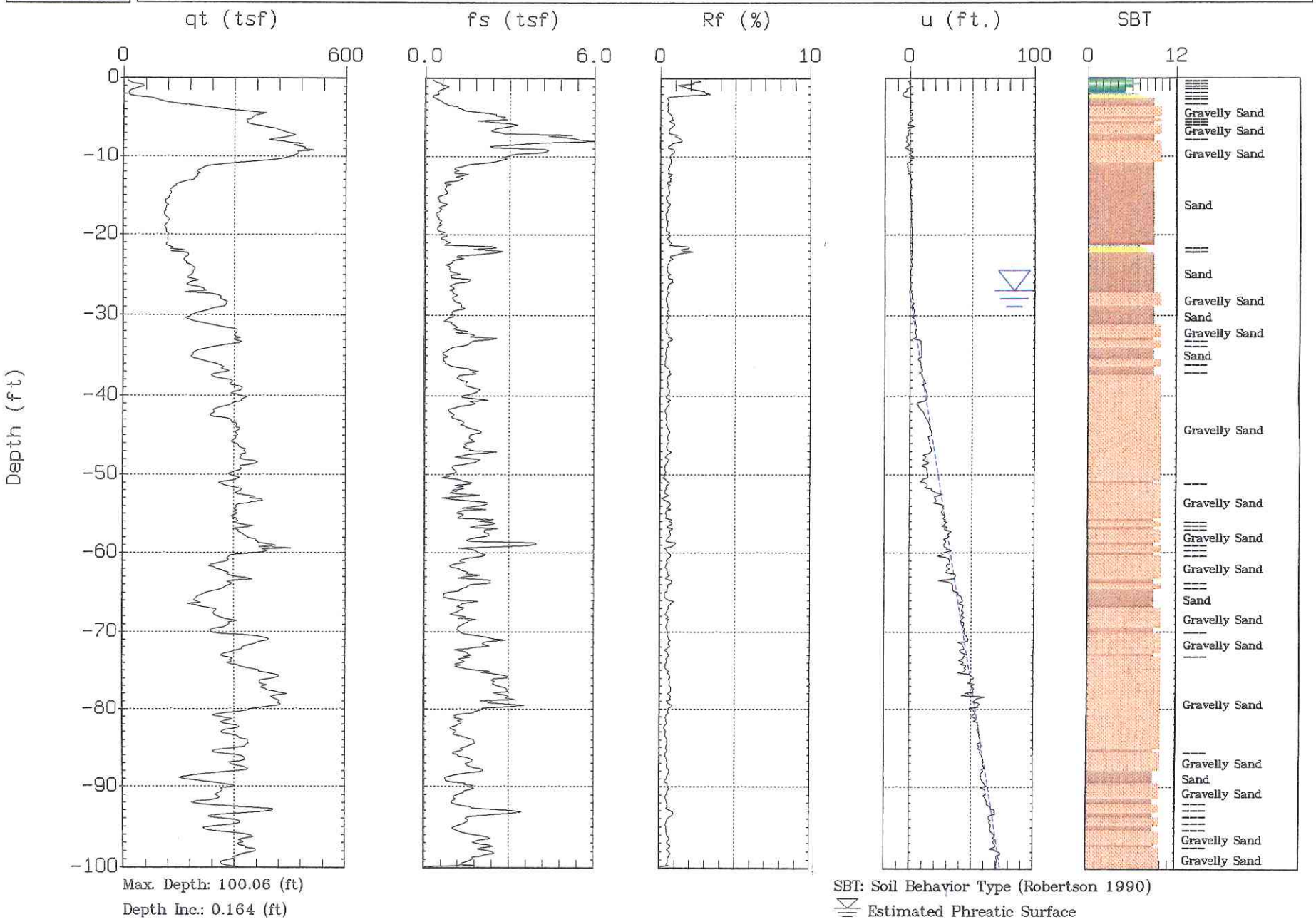

Max. Depth: 100.06 (ft)
Depth Inc.: 0.164 (ft)

SBT: Soil Behavior Type (Robertson 1990)
Estimated Phreatic Surface

CONETEC

GEI Consultants

Sounding:CPT-3
Site:National Labs

Piezocone:20 Ton AD164
Date:07:20:06 07:32

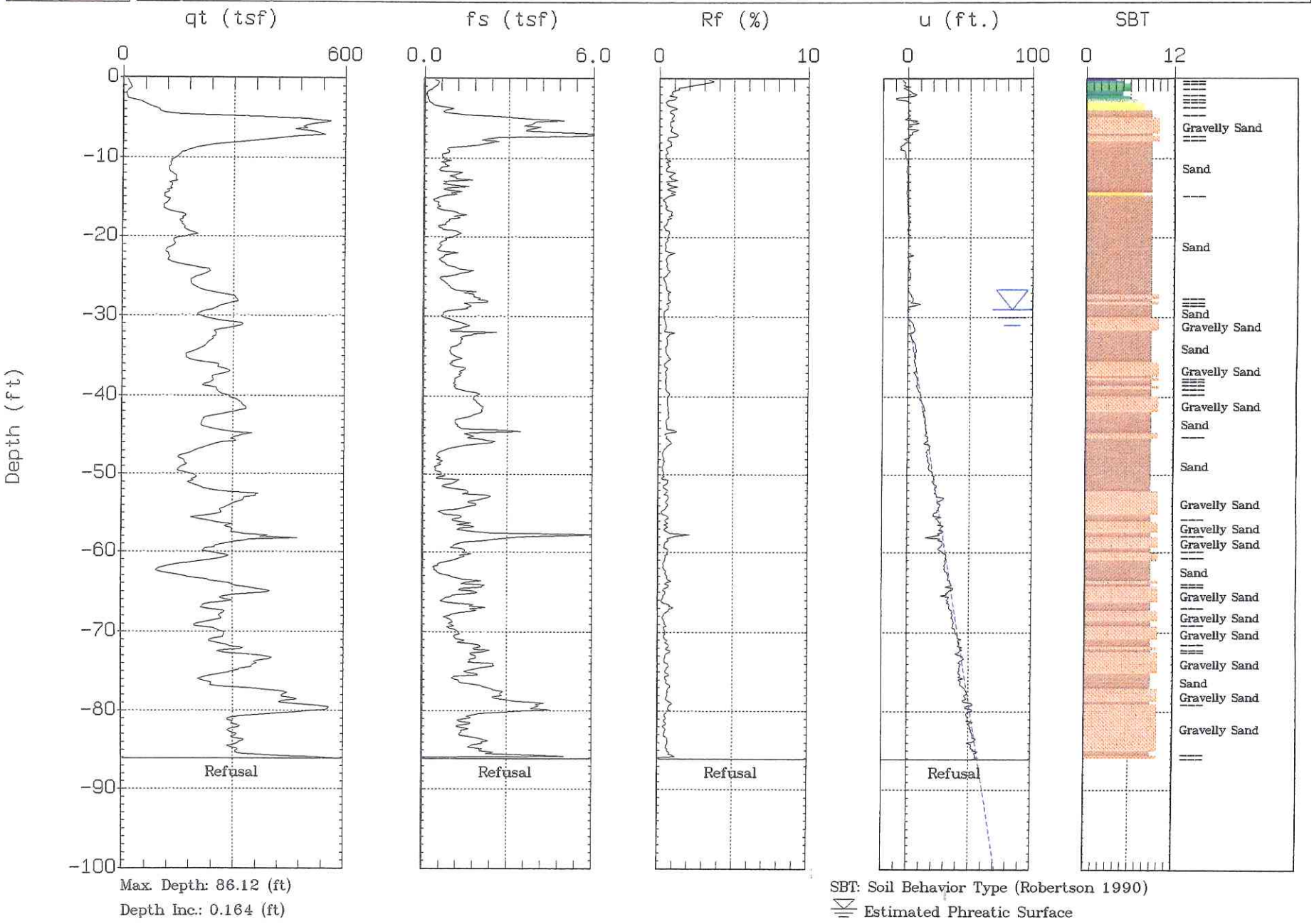

Max. Depth: 86.12 (ft)
Depth Inc.: 0.164 (ft)

SBT: Soil Behavior Type (Robertson 1990)
Estimated Phreatic Surface

CONETEC

GEI Consultants

Sounding:CPT-3
Site:National Labs

Piezocone:20 Ton AD164
Date:07:20:06 07:32

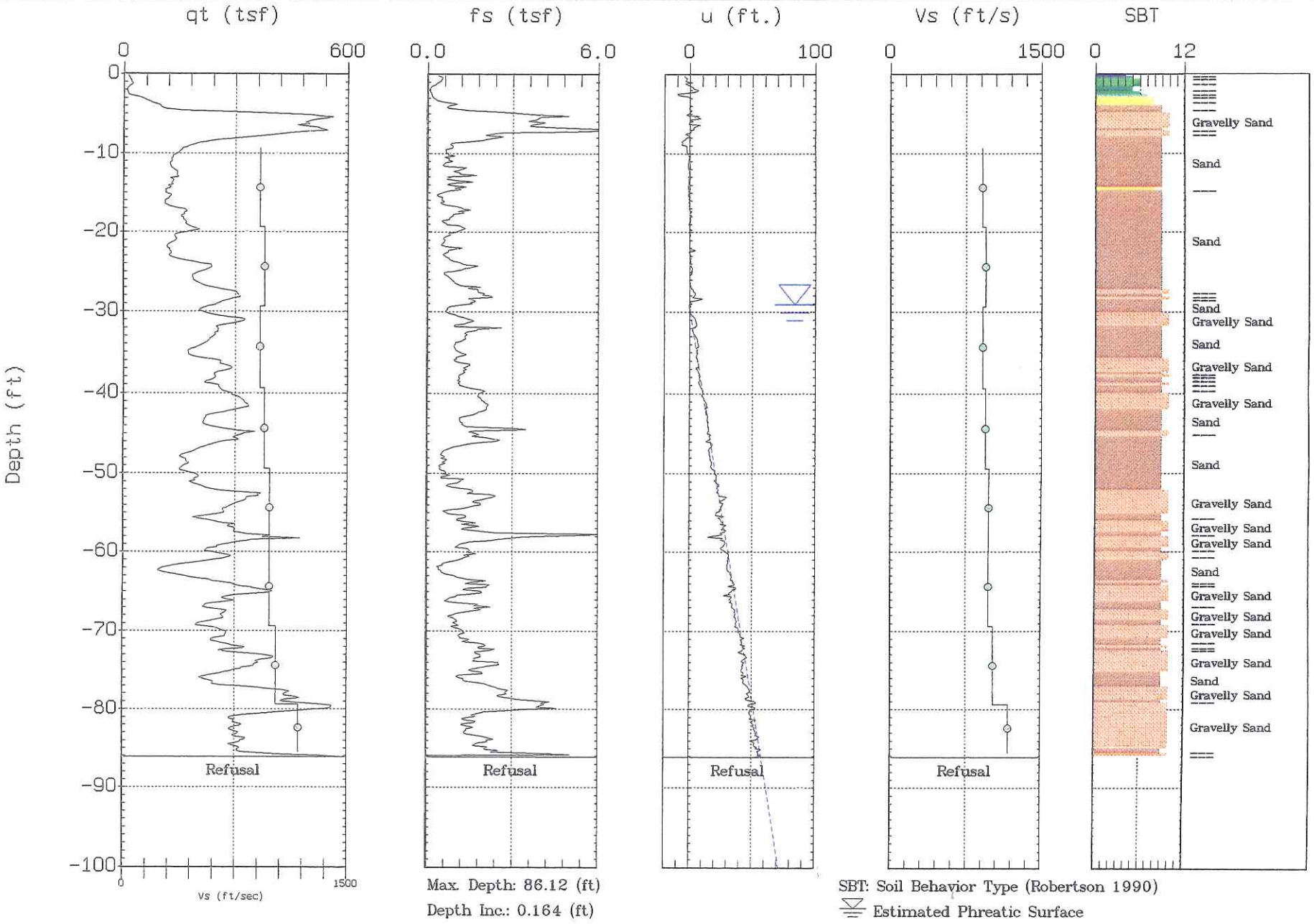

Max. Depth: 86.12 (ft)
Depth Inc.: 0.164 (ft)

SBT: Soil Behavior Type (Robertson 1990)

Estimated Phreatic Surface

Job No	06-773
Client	GEI Consultants
Project Title	National Labs
Hole	CPT-3
Site	Brookhaven, New York
Date	7/20/2006

Seismic Source:	Beam	
Source Offset:	1.97	(ft)
Source Depth:	0.00	(ft)
Geophone Offset:	0.66	(ft)

SEISMIC TEST RESULTS - Vs

Tip Depth (ft)	Geophone Depth (ft)	Ray Path (ft)	Depth Interval (ft)	Time Interval (ms)	Mid-layer Depth (ft)	Vs Interval Velocity (ft/s)
10.01	9.35	9.56				
20.01	19.35	19.45	9.89	10.84	14.35	913
30.02	29.36	29.43	9.98	10.57	24.36	944
40.03	39.37	39.42	9.99	10.93	34.37	914
50.03	49.37	49.41	9.99	10.57	44.37	945
60.04	59.38	59.42	10.00	10.20	54.38	981
70.05	69.39	69.42	10.01	10.20	64.39	981
80.05	79.39	79.42	10.00	9.75	74.39	1025
86.12	85.46	85.49	6.07	5.15	82.43	1178

Job No: 06-773
Client: GEI Consultants
Project: National Labs
Sounding: CPT-3
Date: July 20, 2006

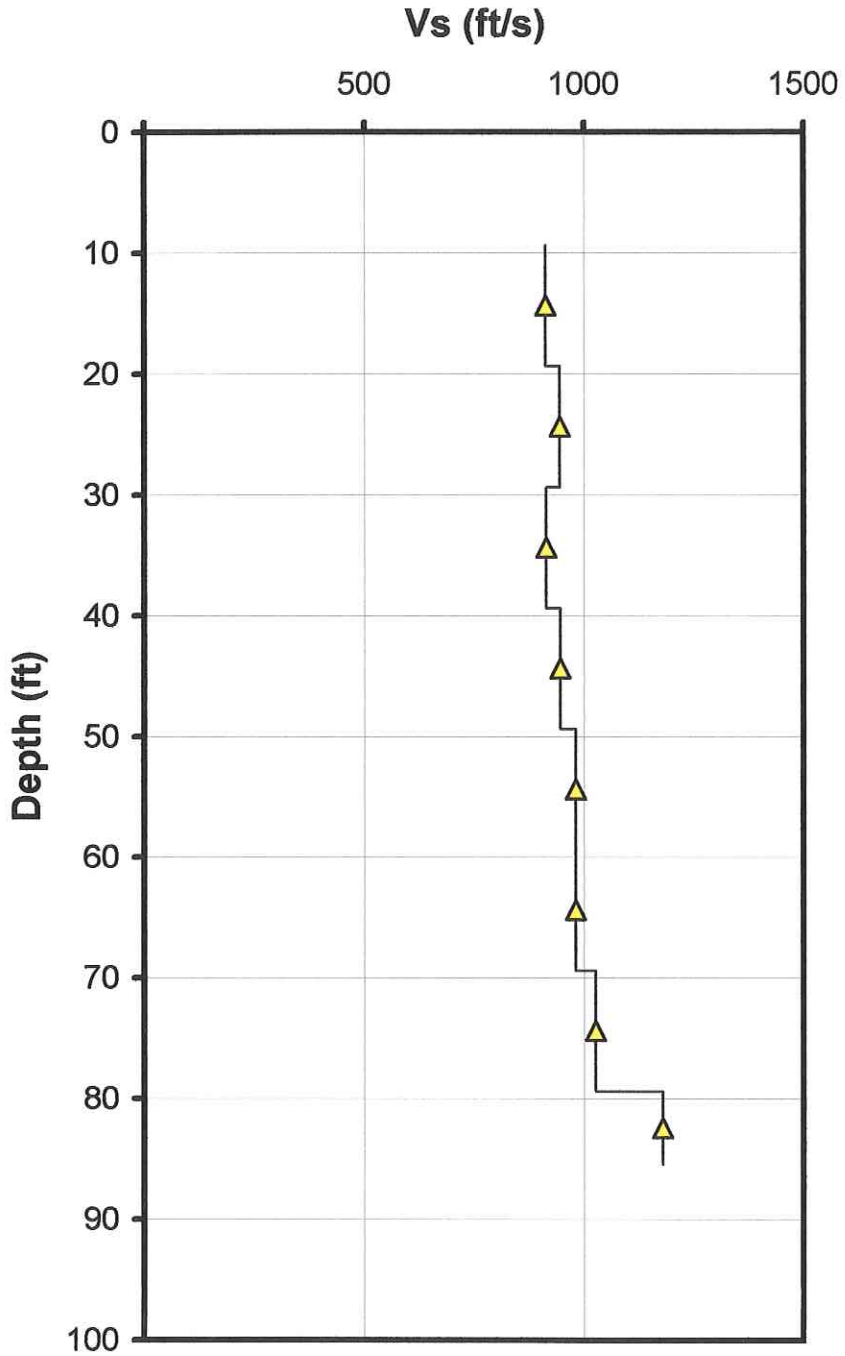

CONETEC

GEI Consultants

Sounding:CPT-4
Site:National Labs

Piezocone:20 Ton AD164
Date:07:19:06 13:13

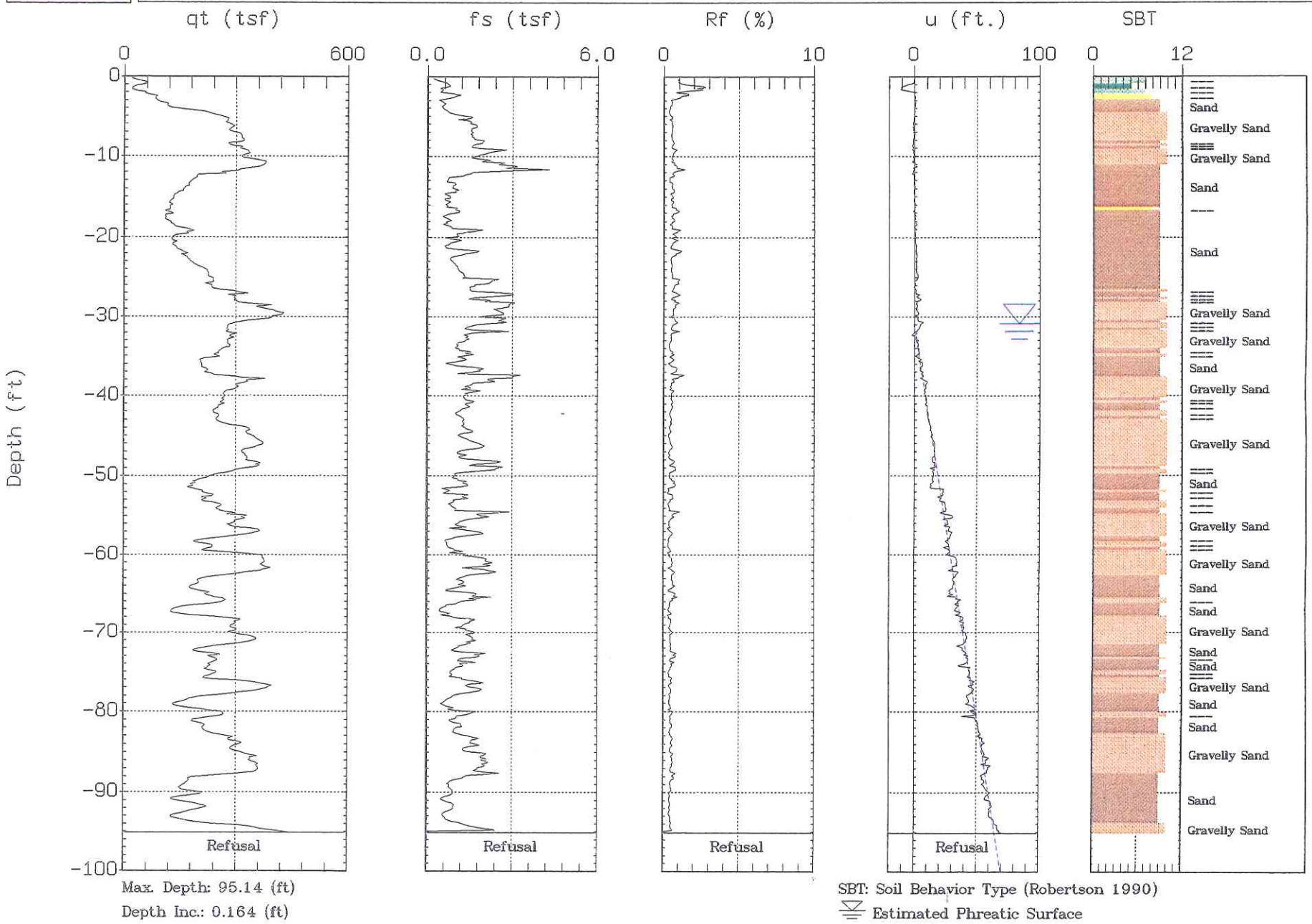

Max. Depth: 95.14 (ft)
Depth Inc.: 0.164 (ft)

SBT: Soil Behavior Type (Robertson 1990)

Estimated Phreatic Surface

CONETEC

GEI Consultants

Sounding:CPT-5
Site:National Labs

Piezocone:20 Ton AD164
Date:07:20:06 08:58

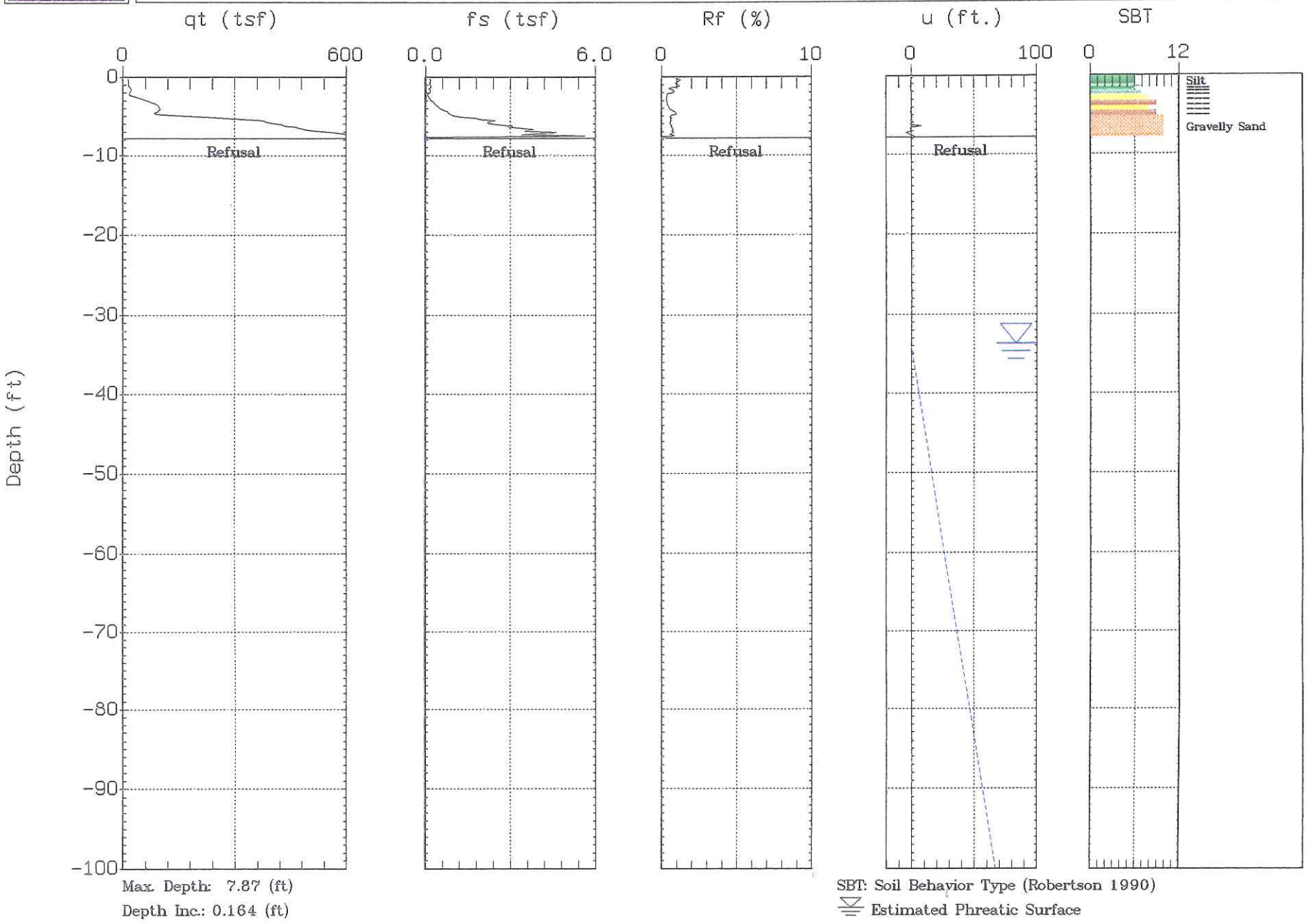

Max. Depth: 7.87 (ft)
Depth Inc.: 0.164 (ft)

SBT: Soil Behavior Type (Robertson 1990)

Estimated Phreatic Surface

CONETEC

GEI Consultants

Sounding:CPT-5A
Site:National Labs

Piezocone:20 Ton AD164
Date:07:20:06 09:27

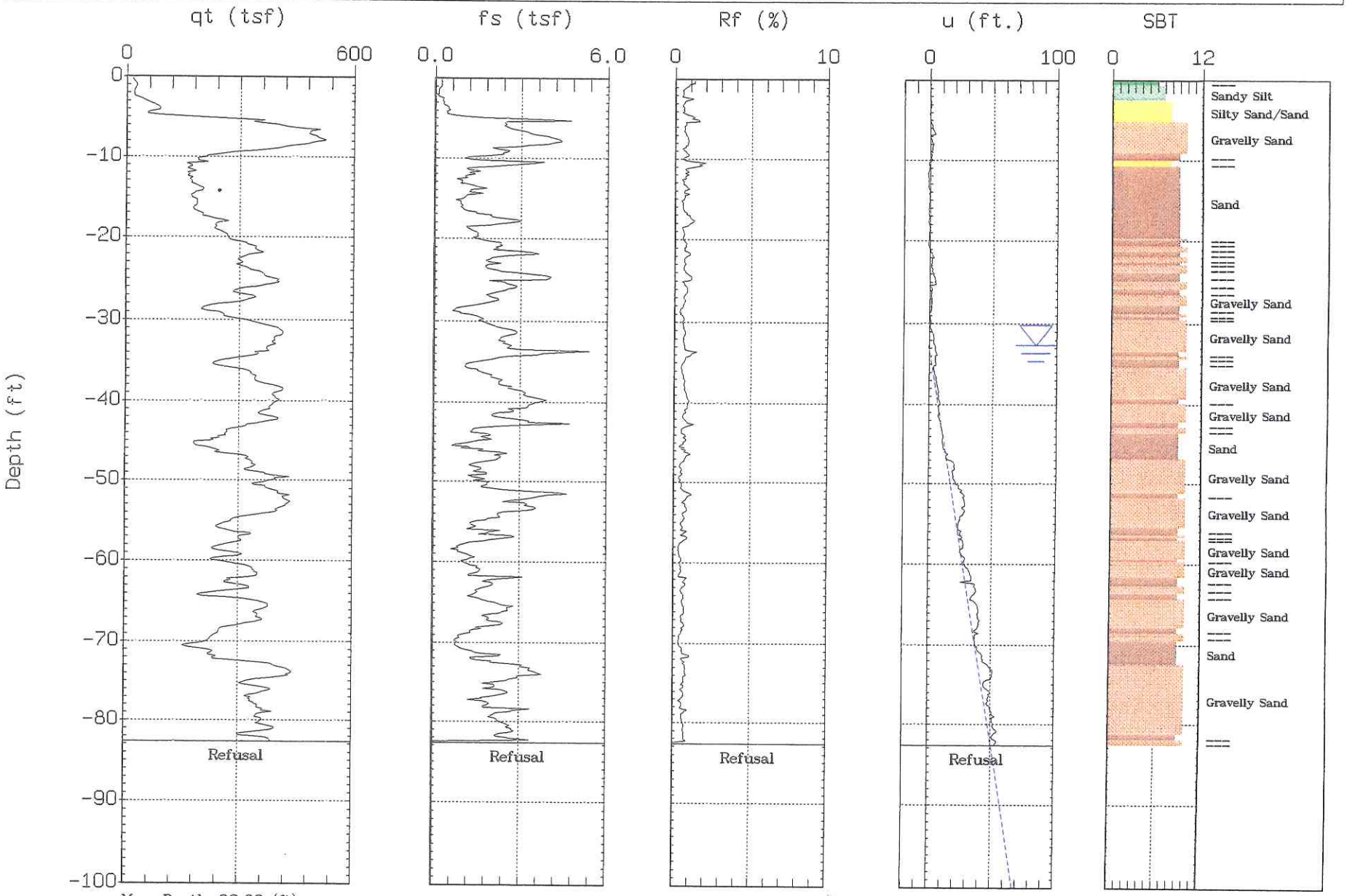

Max. Depth: 82.68 (ft)
Depth Inc.: 0.164 (ft)

SBT: Soil Behavior Type (Robertson 1990)
Estimated Phreatic Surface

CONETEC

GEI Consultants

Sounding:CPT-5A
Site:National Labs

Piezocone:20 Ton AD164
Date:07:20:06 09:27

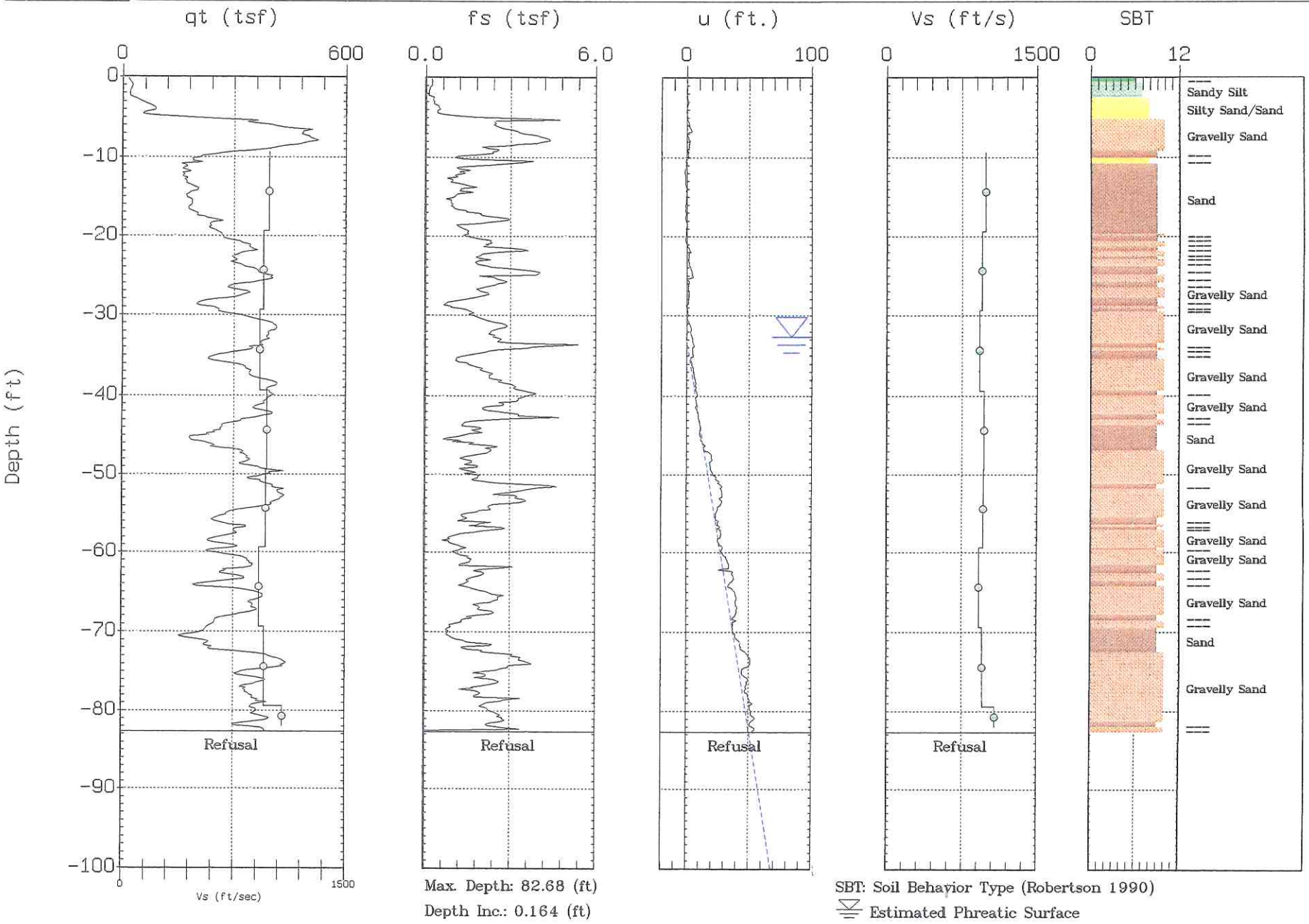

Max. Depth: 82.68 (ft)
Depth Inc.: 0.164 (ft)

SBT: Soil Behavior Type (Robertson 1990)

Estimated Phreatic Surface

Job No	06-773
Client	GEI Consultants
Project Title	National Labs
Hole	CPT-5A
Site	Brookhaven, New York
Date	7/20/2006

Seismic Source:	Beam	
Source Offset:	1.97	(ft)
Source Depth:	0.00	(ft)
Geophone Offset:	0.66	(ft)

SEISMIC TEST RESULTS - Vs

Tip Depth (ft)	Geophone Depth (ft)	Ray Path (ft)	Depth Interval (ft)	Time Interval (ms)	Mid-layer Depth (ft)	Vs Interval Velocity (ft/s)
10.01	9.35	9.56				
20.01	19.35	19.45	9.89	10.05	14.35	985
30.02	29.36	29.43	9.98	10.52	24.36	948
40.03	39.37	39.42	9.99	10.83	34.37	923
50.03	49.37	49.41	9.99	10.28	44.37	972
60.04	59.38	59.42	10.00	10.36	54.38	966
70.05	69.39	69.42	10.01	10.83	64.39	924
80.05	79.39	79.42	10.00	10.44	74.39	958
82.68	82.02	82.05	2.63	2.43	80.71	1082

Job No: 06-773
Client: GEI Consultants
Project: National Labs
Sounding: CPT-5A
Date: July 20, 2006

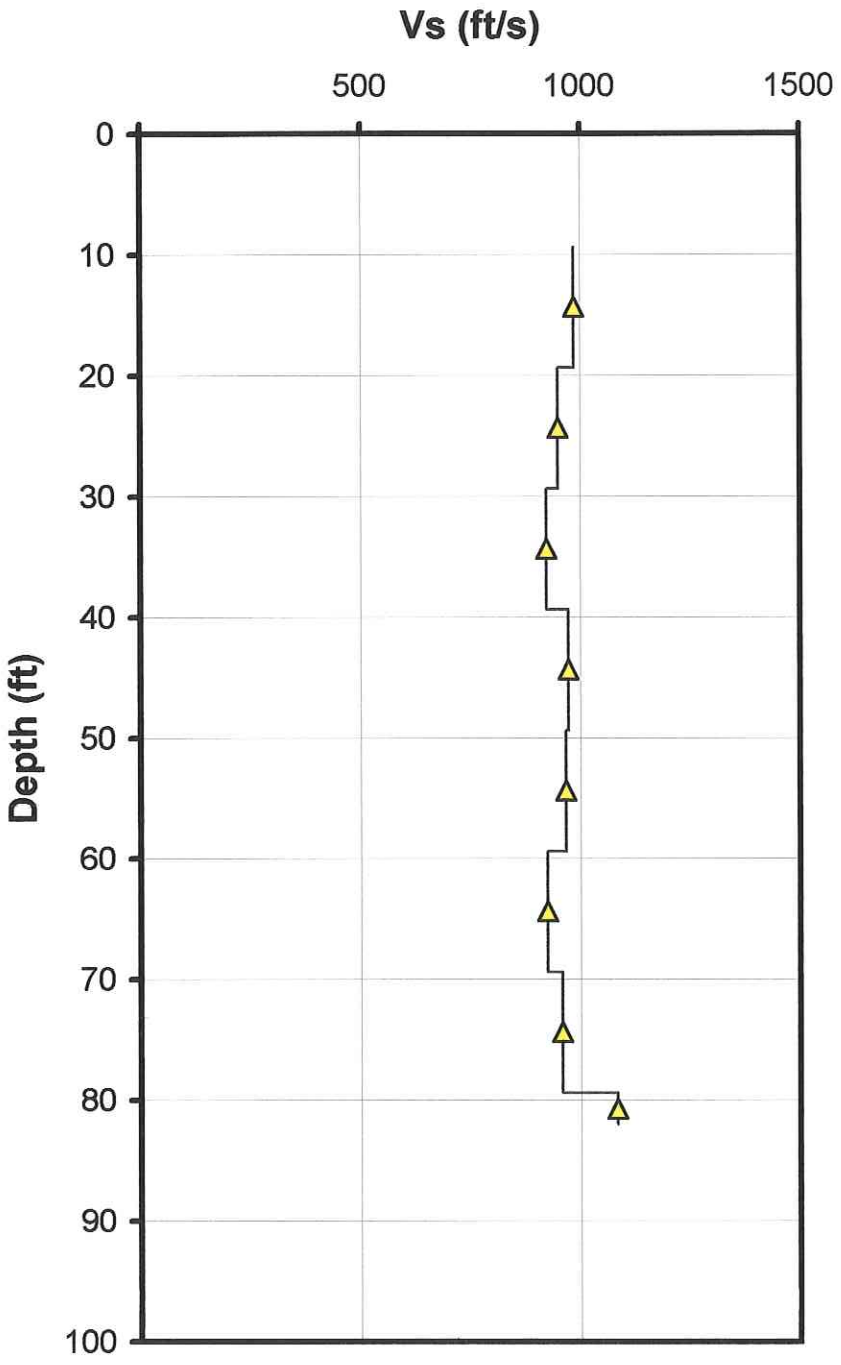

CONETEC

GEI Consultants

Sounding:CPT-6
Site:National Labs

Piezocone:20 Ton AD164
Date:07:20:06 10:46

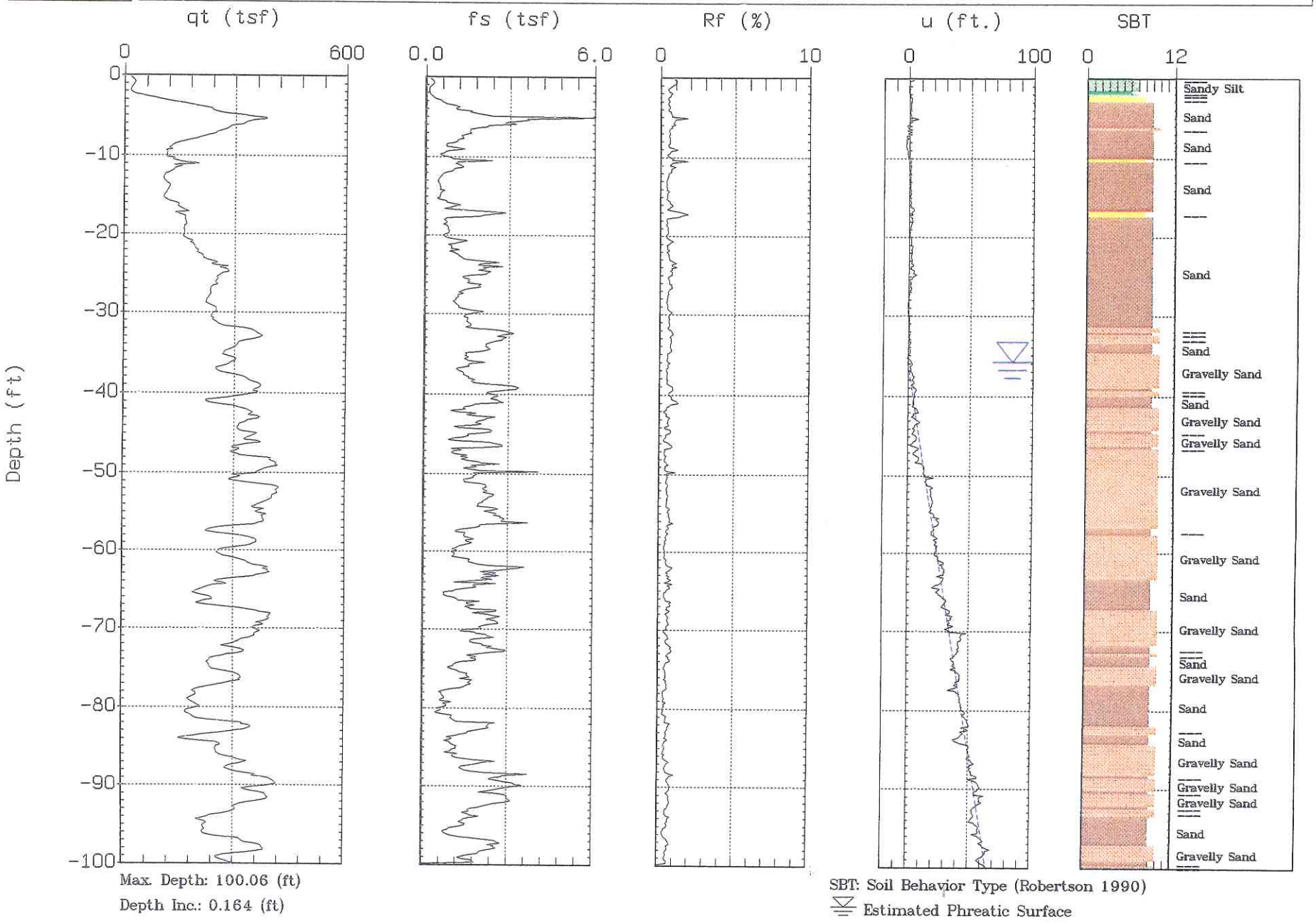

Max. Depth: 100.06 (ft)
Depth Inc.: 0.164 (ft)

SBT: Soil Behavior Type (Robertson 1990)
Estimated Phreatic Surface

CONETEC

GEI Consultants

Sounding:CPT-6
Site:National Labs

Piezocone:20 Ton AD164
Date:07:20:06 10:46

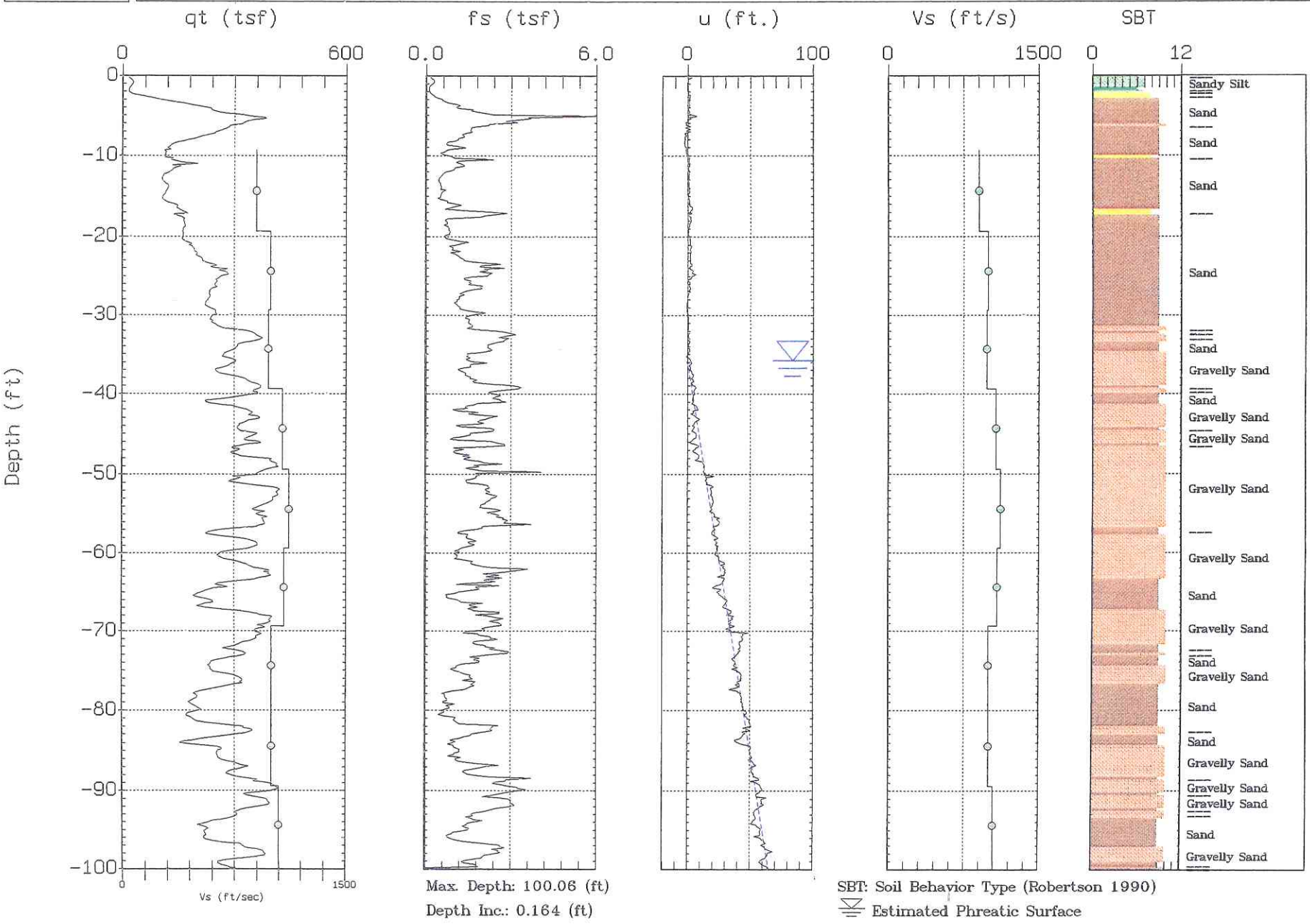

Max. Depth: 100.06 (ft)
Depth Inc.: 0.164 (ft)

SBT: Soil Behavior Type (Robertson 1990)

Estimated Phreatic Surface

Job No	06-773
Client	GEI Consultants
Project Title	National Labs
Hole	CPT-6
Site	Brookhaven, New York
Date	7/20/2006

Seismic Source:	Beam	
Source Offset:	1.97	(ft)
Source Depth:	0.00	(ft)
Geophone Offset:	0.66	(ft)

SEISMIC TEST RESULTS - Vs

Tip Depth (ft)	Geophone Depth (ft)	Ray Path (ft)	Depth Interval (ft)	Time Interval (ms)	Mid-layer Depth (ft)	Vs Interval Velocity (ft/s)
10.01	9.35	9.56				
20.01	19.35	19.45	9.89	11.00	14.35	900
30.02	29.36	29.43	9.98	10.02	24.36	996
40.03	39.37	39.42	9.99	10.20	34.37	980
50.03	49.37	49.41	9.99	9.30	44.37	1074
60.04	59.38	59.42	10.00	8.94	54.38	1119
70.05	69.39	69.42	10.01	9.21	64.39	1086
80.05	79.39	79.42	10.00	10.02	74.39	998
90.06	89.40	89.43	10.01	10.02	84.40	999
100.07	99.41	99.43	10.01	9.57	94.41	1046

Job No: 06-773
Client: GEI Consultants
Project: National Labs
Sounding: CPT-6
Date: July 20, 2006

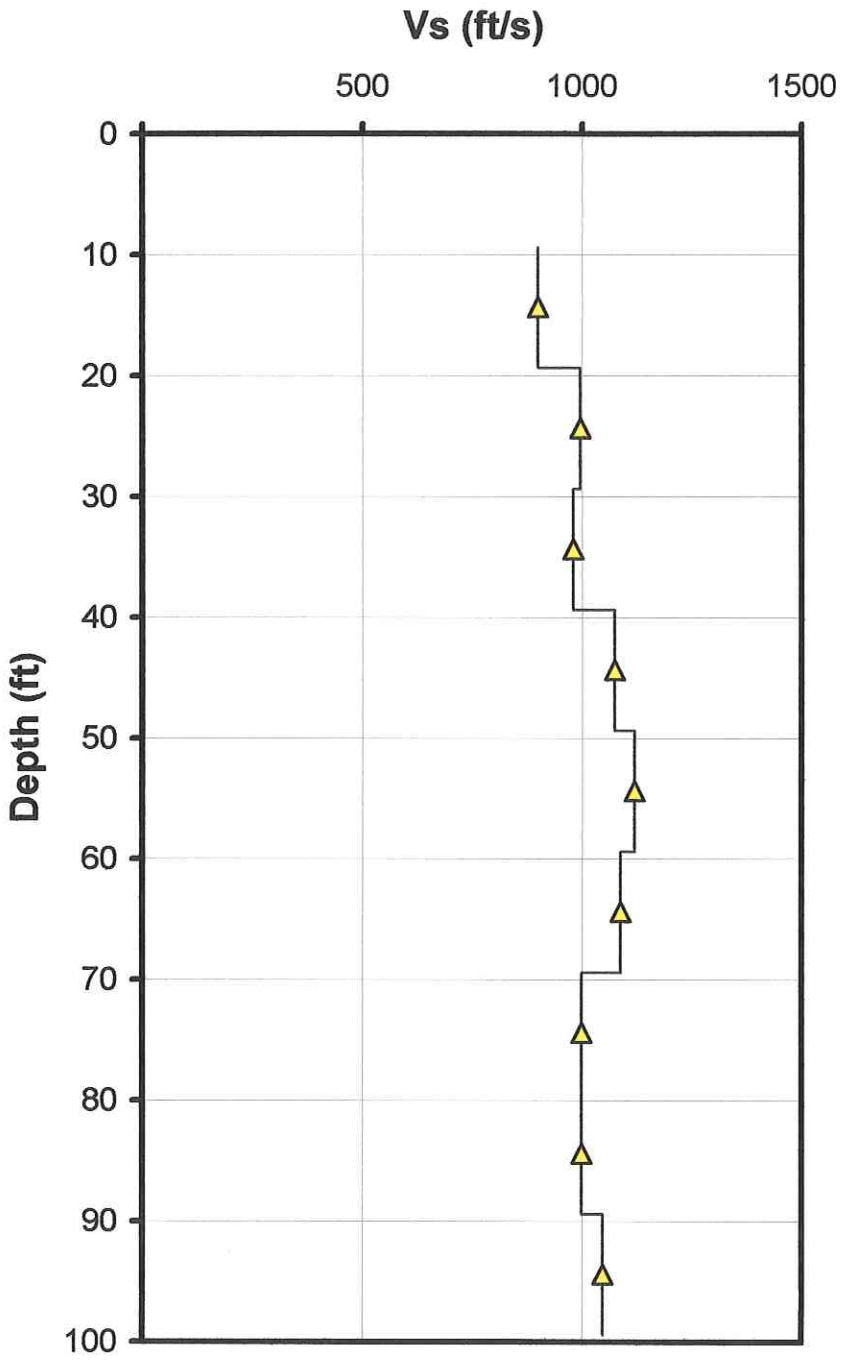

CONETEC

GEI Consultants

Sounding:CPT-7
Site:National Labs

Piezocone:20 Ton AD179
Date:07:21:06 12:03

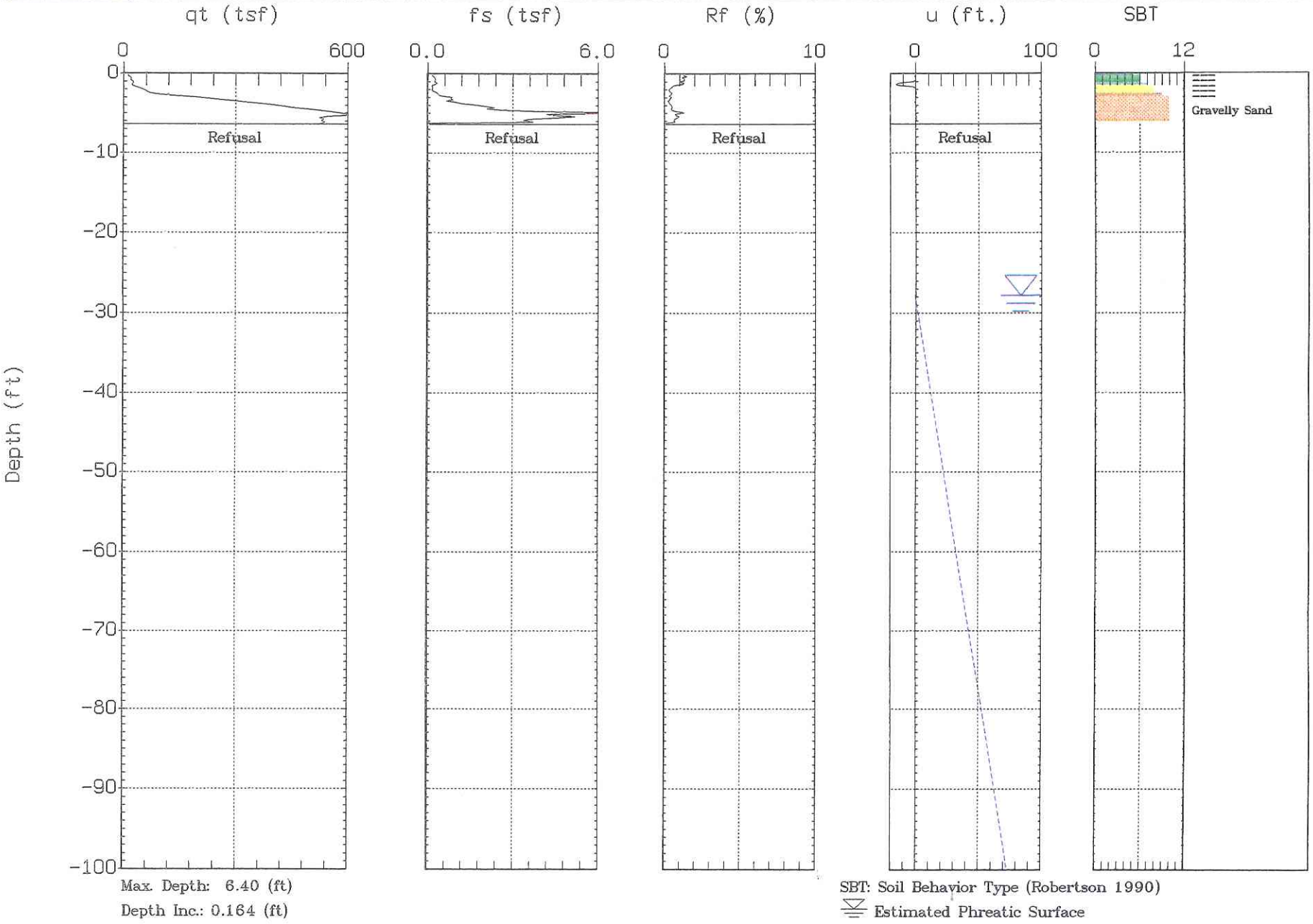

Max. Depth: 6.40 (ft)
Depth Inc.: 0.164 (ft)

SBT: Soil Behavior Type (Robertson 1990)
Estimated Phreatic Surface

CONETEC

GEI Consultants

Sounding:CPT-8
Site:National Labs

Piezocone:20 Ton AD164
Date:07:20:06 15:23

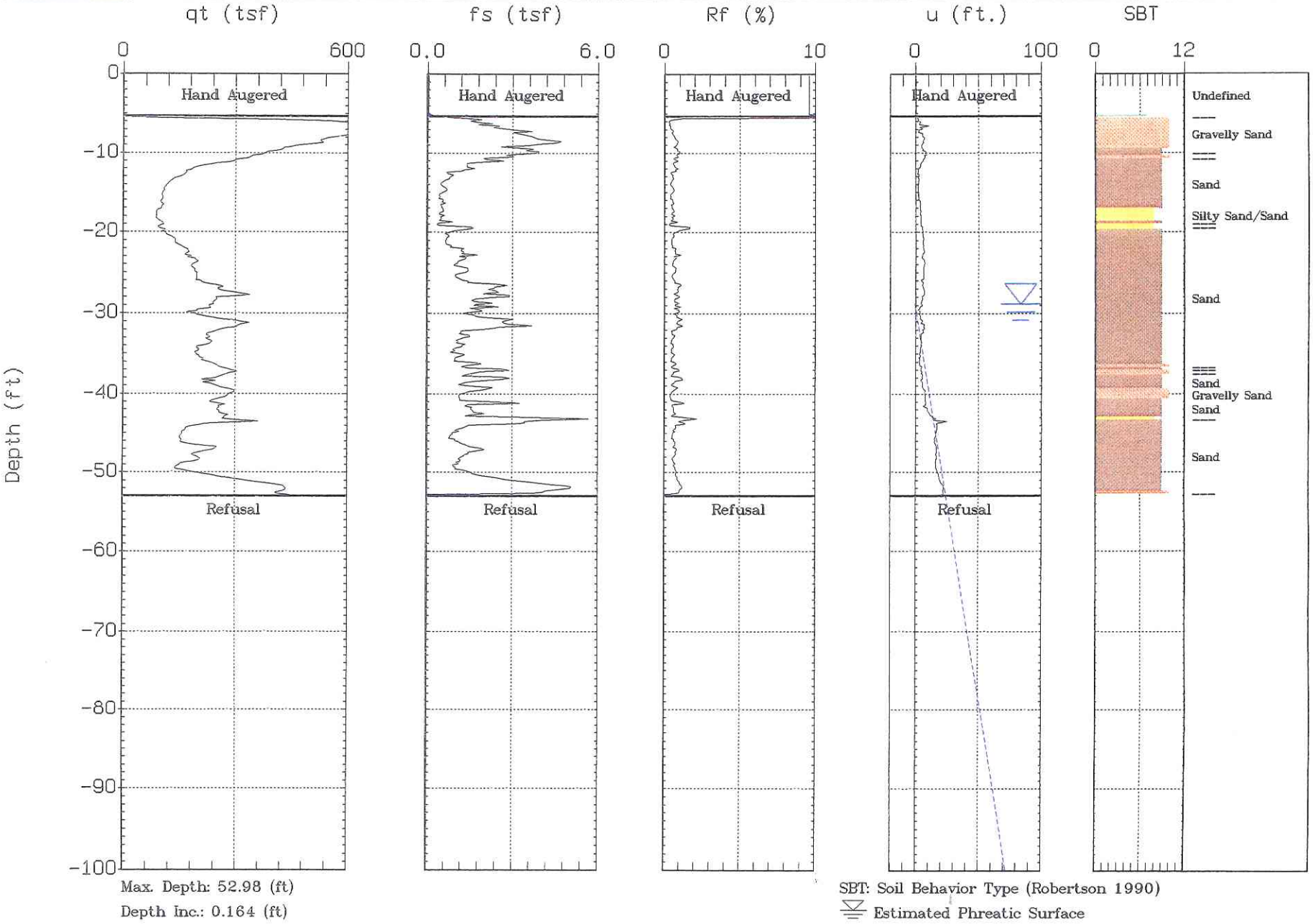

Max. Depth: 52.98 (ft)
Depth Inc.: 0.164 (ft)

SBT: Soil Behavior Type (Robertson 1990)
Estimated Phreatic Surface

CONETEC

GEI Consultants

Sounding:CPT-10
Site:National Labs

Piezocone:20 Ton AD179
Date:07:21:06 09:56

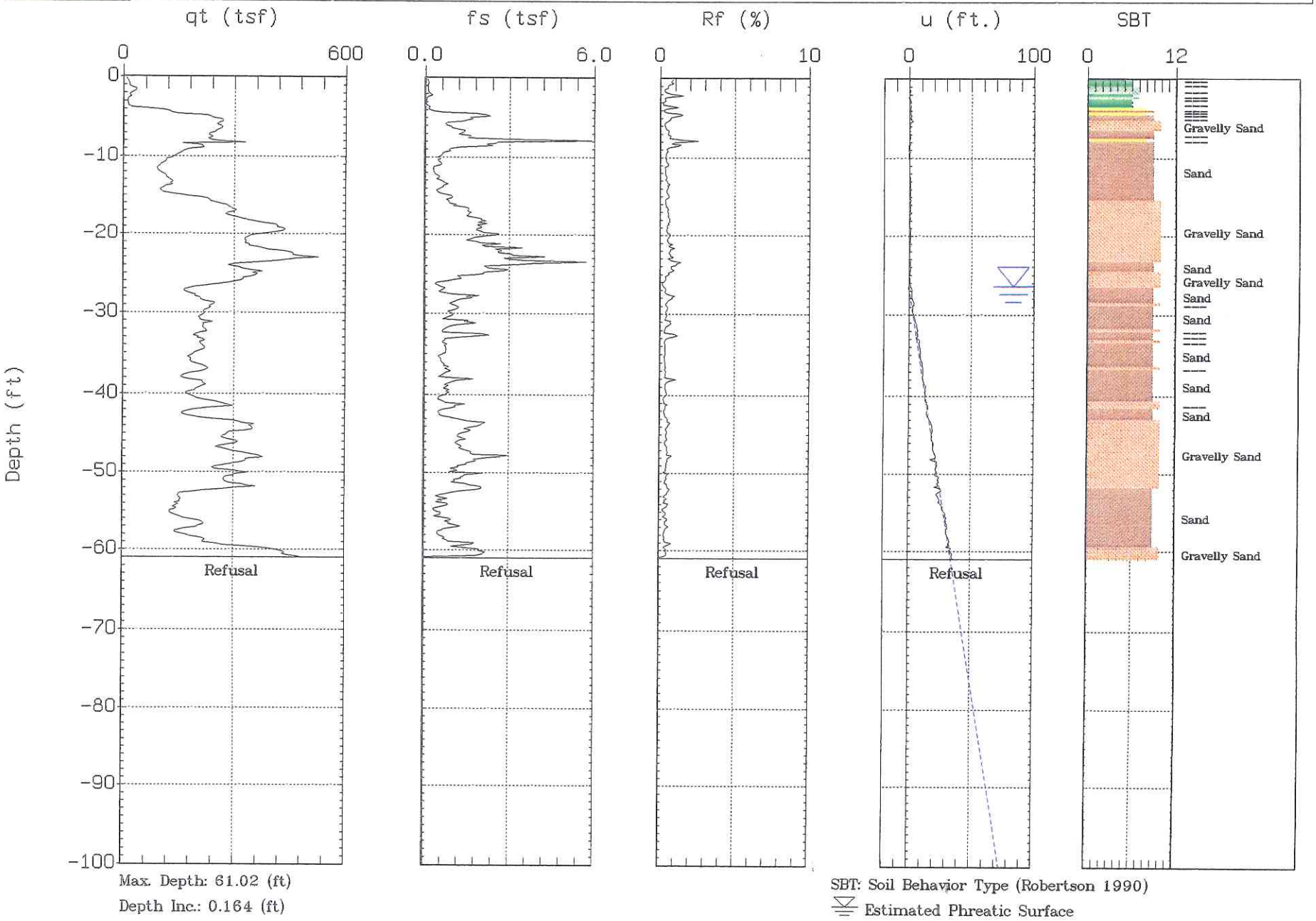

Max. Depth: 61.02 (ft)
Depth Inc.: 0.164 (ft)

SBT: Soil Behavior Type (Robertson 1990)

Estimated Phreatic Surface

CONETEC

GEI Consultants

Sounding:CPT-11
Site:National Labs

Piezocone:20 Ton AD179
Date:07:21:06 08:42

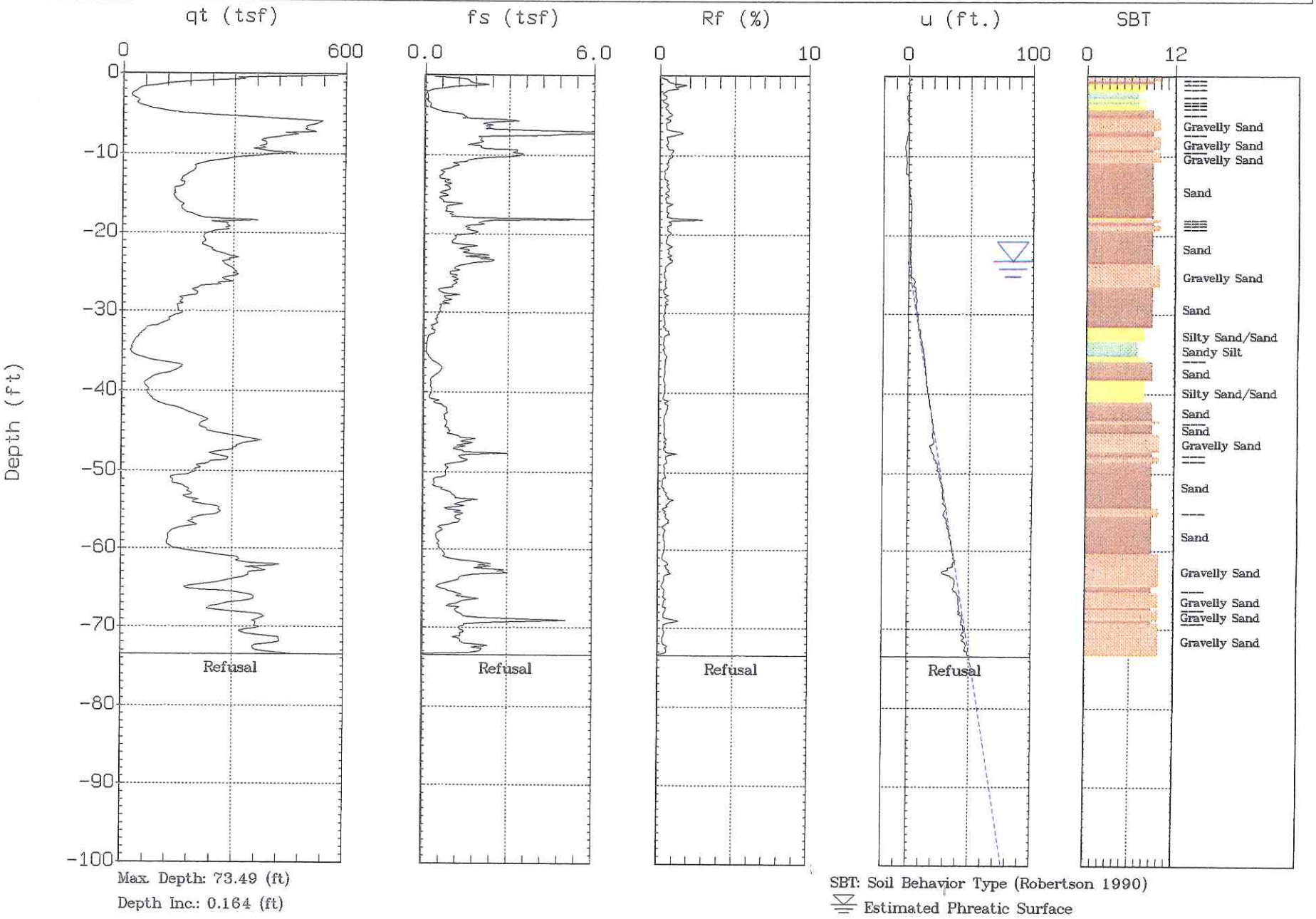

Max. Depth: 73.49 (ft)
Depth Inc.: 0.164 (ft)

SBT: Soil Behavior Type (Robertson 1990)

Estimated Phreatic Surface

CONETEC

GEI Consultants

Sounding:CPT-12
Site:National Labs

Piezocone:20 Ton AD164
Date:07:20:06 13:19

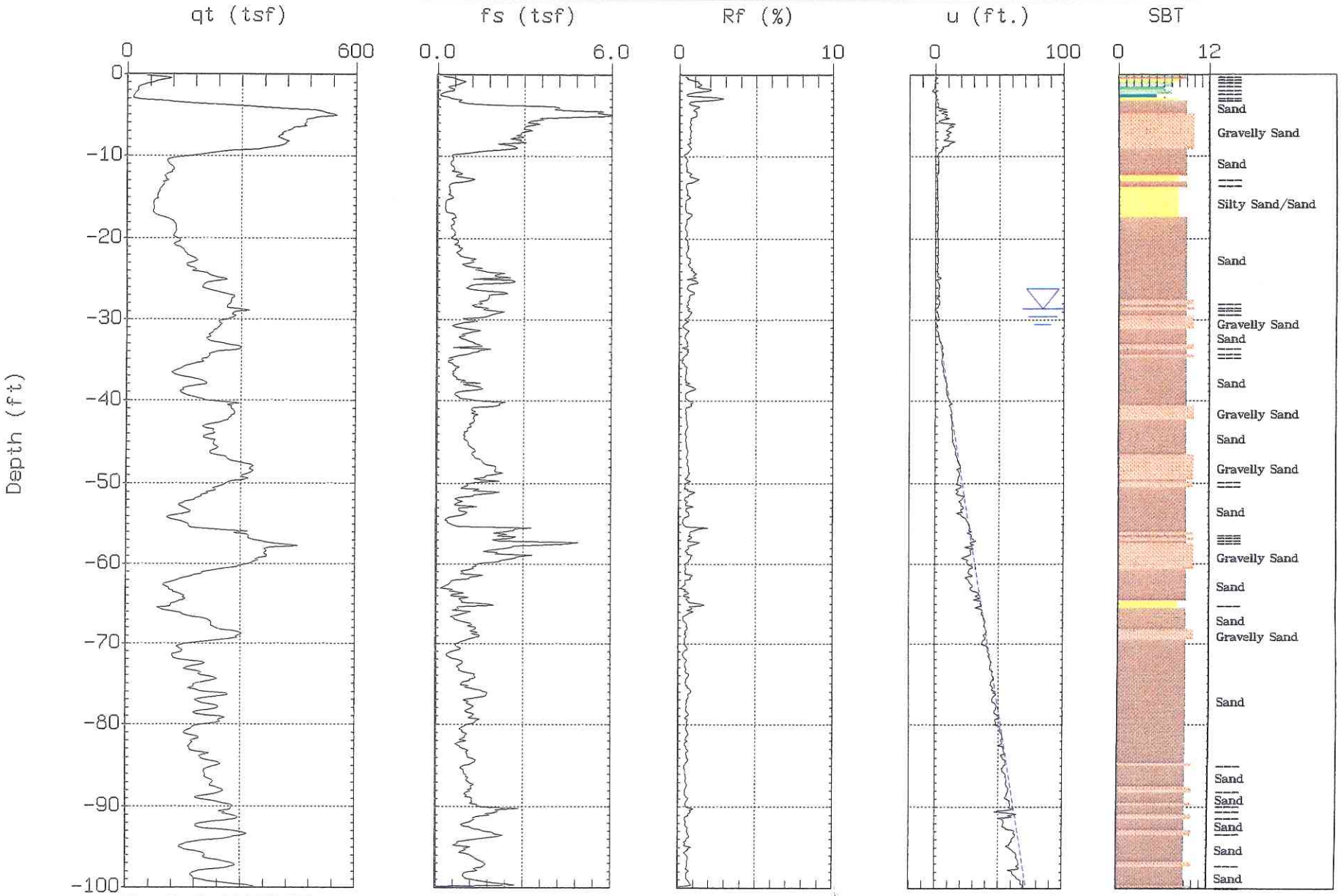

Max. Depth: 100.06 (ft)
Depth Inc.: 0.164 (ft)

SBT: Soil Behavior Type (Robertson 1990)

Estimated Phreatic Surface

CONETEC

GEI Consultants

Sounding:CPT-12
Site:National Labs

Piezocone:20 Ton AD164
Date:07:20:06 13:19

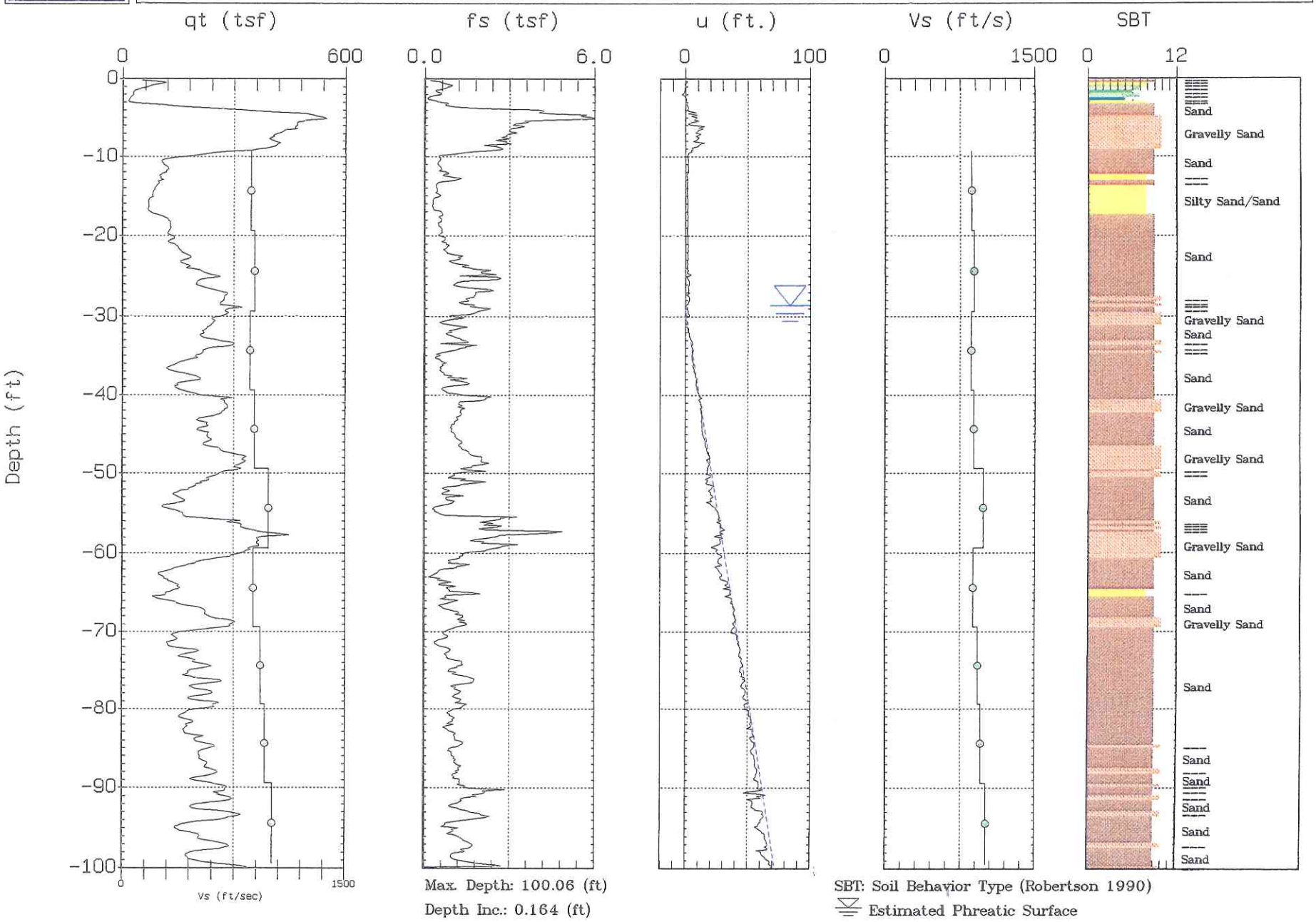

Max. Depth: 100.06 (ft)
Depth Inc.: 0.164 (ft)

SBT: Soil Behavior Type (Robertson 1990)
Estimated Phreatic Surface

Job No	06-773
Client	GEI Consultants
Project Title	National Labs
Hole	CPT-12
Site	Brookhaven, New York
Date	7/20/2006

Seismic Source:	Beam	
Source Offset:	1.97	(ft)
Source Depth:	0.00	(ft)
Geophone Offset:	0.66	(ft)

SEISMIC TEST RESULTS - Vs

Tip Depth (ft)	Geophone Depth (ft)	Ray Path (ft)	Depth Interval (ft)	Time Interval (ms)	Mid-layer Depth (ft)	Vs Interval Velocity (ft/s)
10.01	9.35	9.56				
20.01	19.35	19.45	9.89	11.44	14.35	865
30.02	29.36	29.43	9.98	11.24	24.36	888
40.03	39.37	39.42	9.99	11.64	34.37	859
50.03	49.37	49.41	9.99	11.24	44.37	889
60.04	59.38	59.42	10.00	10.15	54.38	986
70.05	69.39	69.42	10.01	11.34	64.39	882
80.05	79.39	79.42	10.00	10.74	74.39	931
90.06	89.40	89.43	10.01	10.45	84.40	958
100.07	99.41	99.43	10.01	9.95	94.41	1006

Job No: 06-773
Client: GEI Consultants
Project: National Labs
Sounding: CPT-12
Date: July 20, 2006

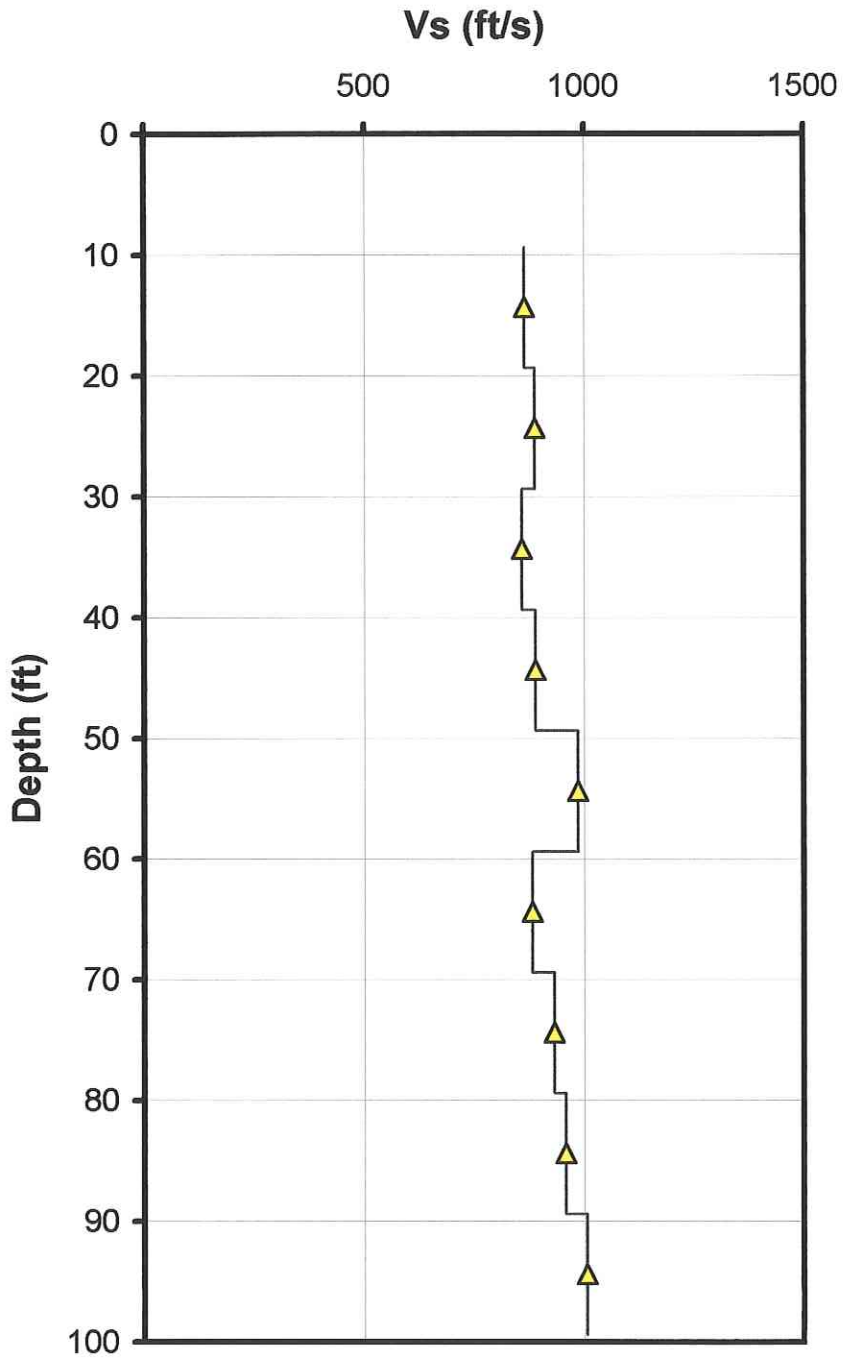

CONETEC

GEI Consultants

Sounding:CPT-13
Site:National Labs

Piezocone:20 Ton AD164
Date:07:20:06 12:23

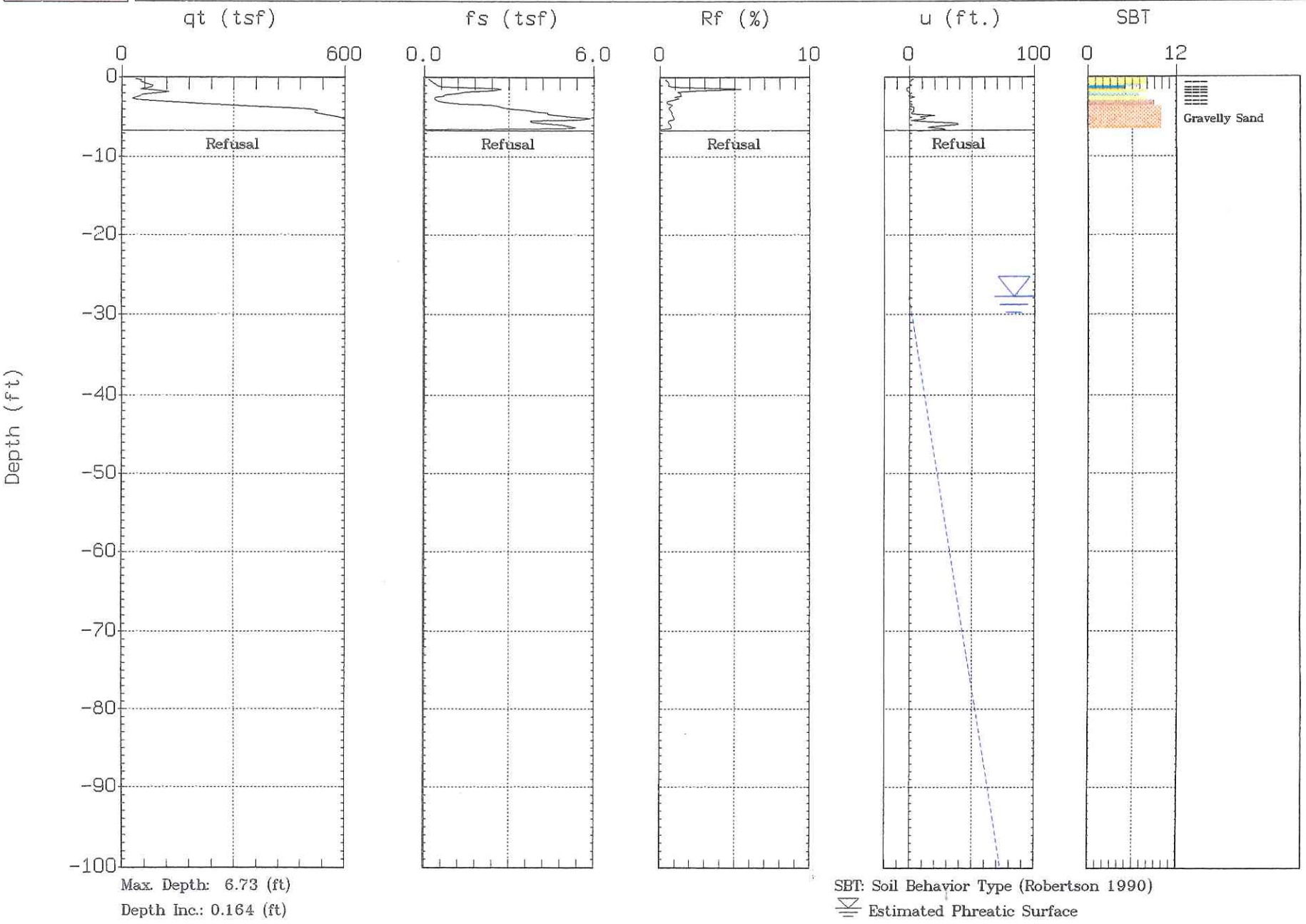

Max. Depth: 6.73 (ft)
Depth Inc.: 0.164 (ft)

SBT: Soil Behavior Type (Robertson 1990)
Estimated Phreatic Surface

CONETEC

GEI Consultants

Sounding:CPT-13A
Site:National Labs

Piezocone:20 Ton AD164
Date:07:20:06 12:50

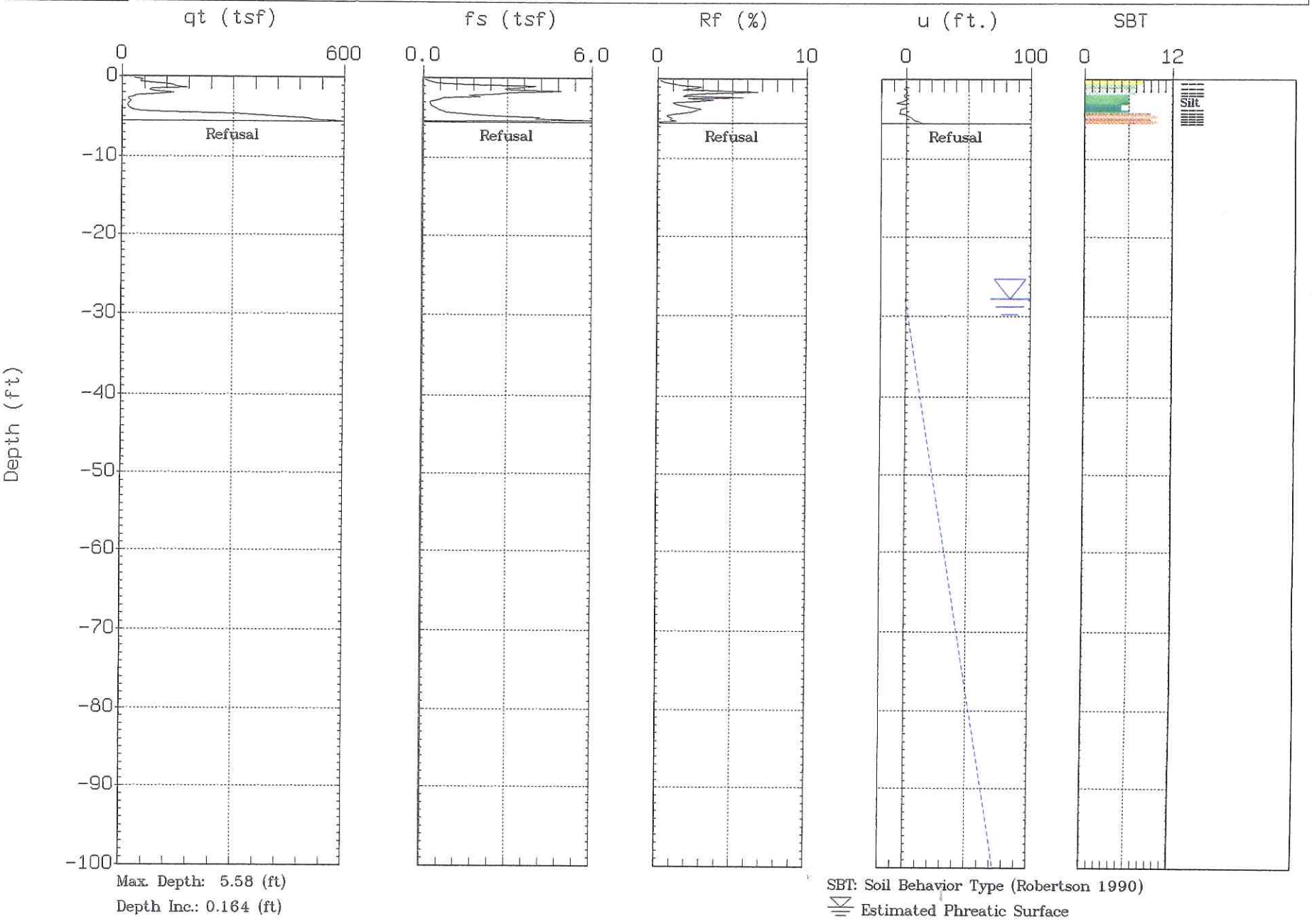

Max. Depth: 5.58 (ft)
Depth Inc.: 0.164 (ft)

SBT: Soil Behavior Type (Robertson 1990)

Estimated Phreatic Surface

CONETEC

GEI Consultants

Sounding:CPT-14
Site:National Labs

Piezocone:20 Ton AD179
Date:07:21:06 07:28

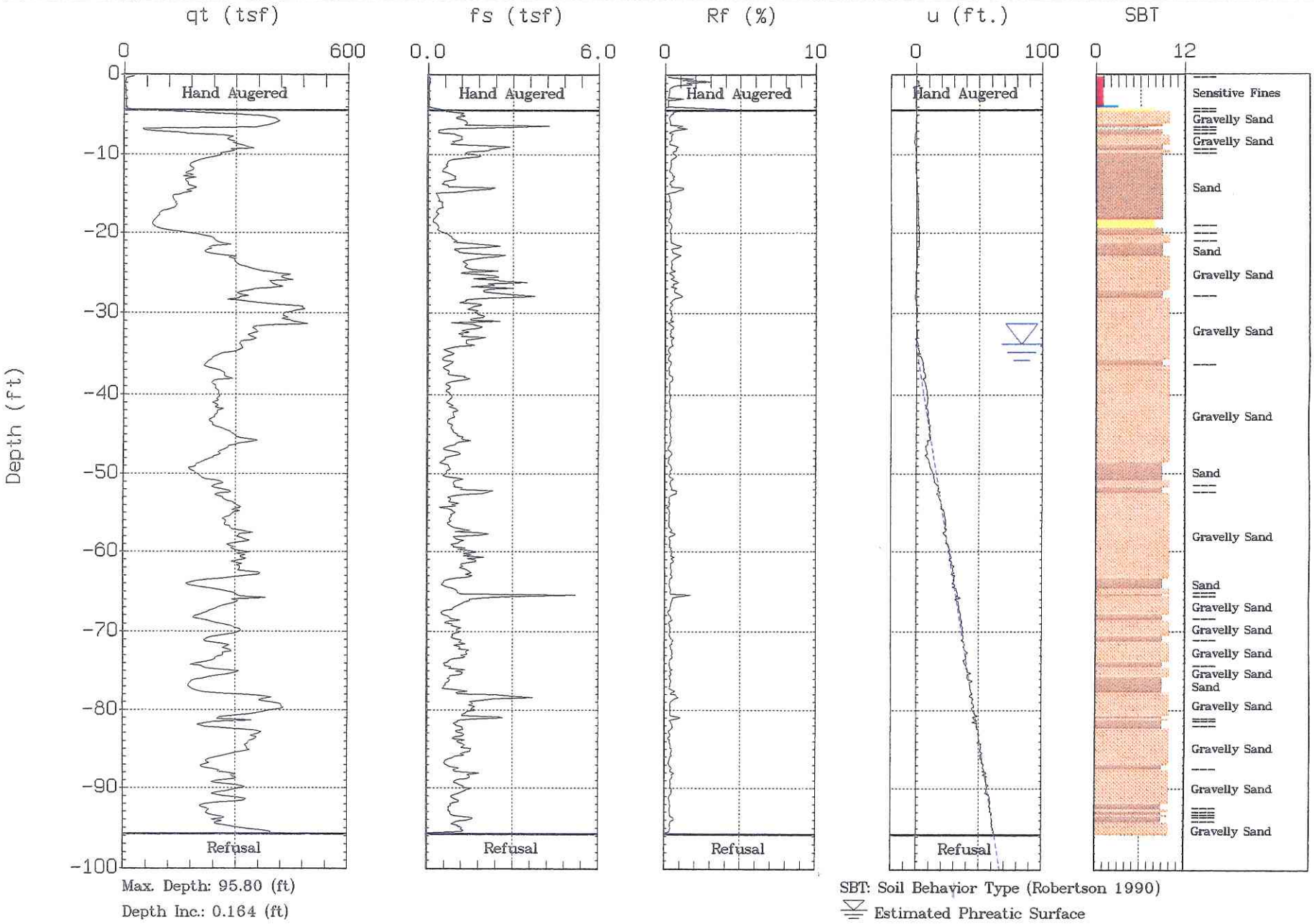

Max. Depth: 95.80 (ft)
Depth Inc.: 0.164 (ft)

SBT: Soil Behavior Type (Robertson 1990)
Estimated Phreatic Surface

CONETEC

GEI Consultants

Site: CPT-201
Location: Upton, NY

Cone:STD 20T AD179
Date:04:23:07 12:01

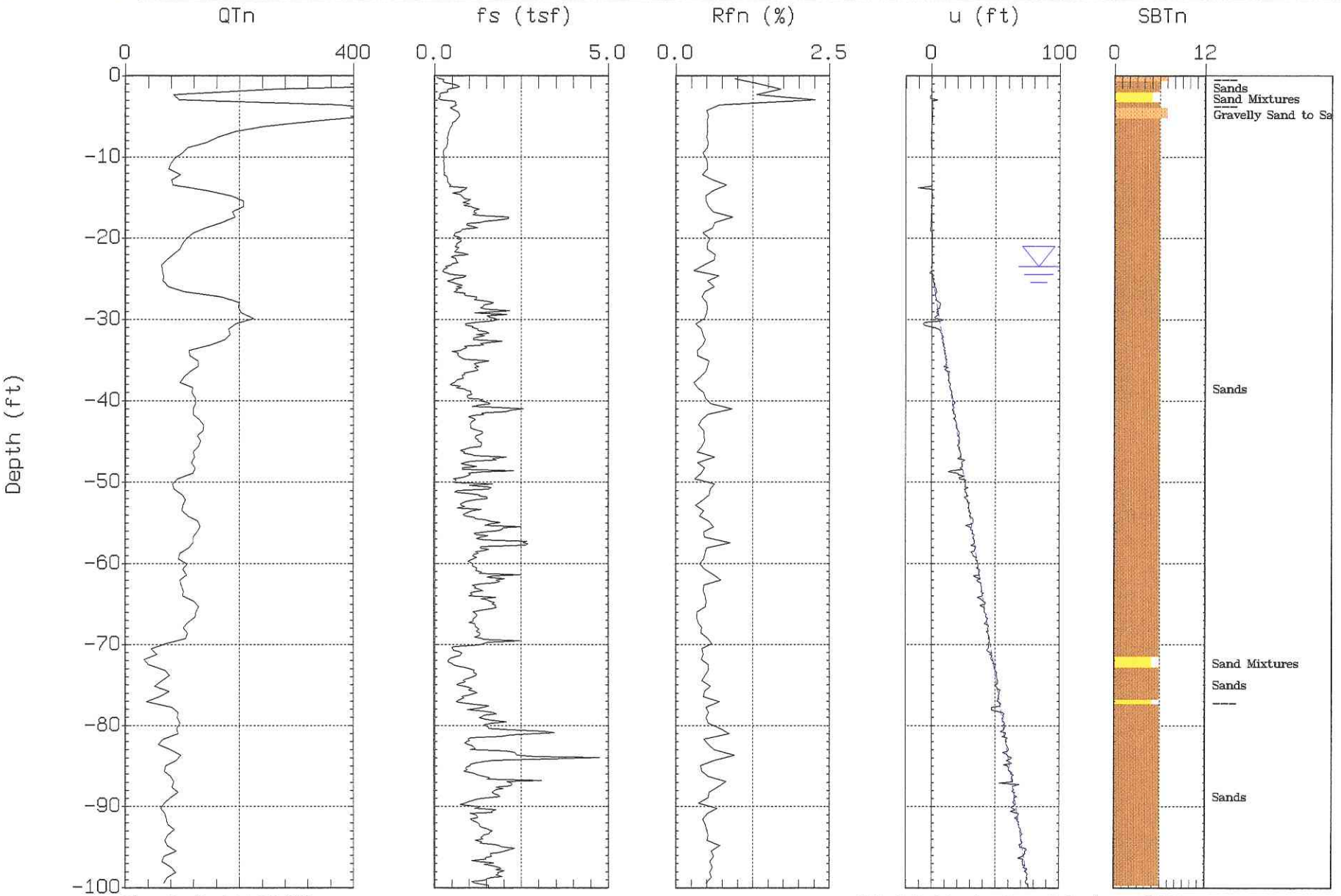

Max. Depth: 100.06 (ft)
Depth Inc.: 0.164 (ft)

SBT: Soil Behavior Type (Robertson 1990)
Estimated Phreatic Surface

CONETEC

GEI Consultants

Site: CPT-202
Location: Upton, NY

Cone:STD 20T AD179
Date:04:23:07 13:32

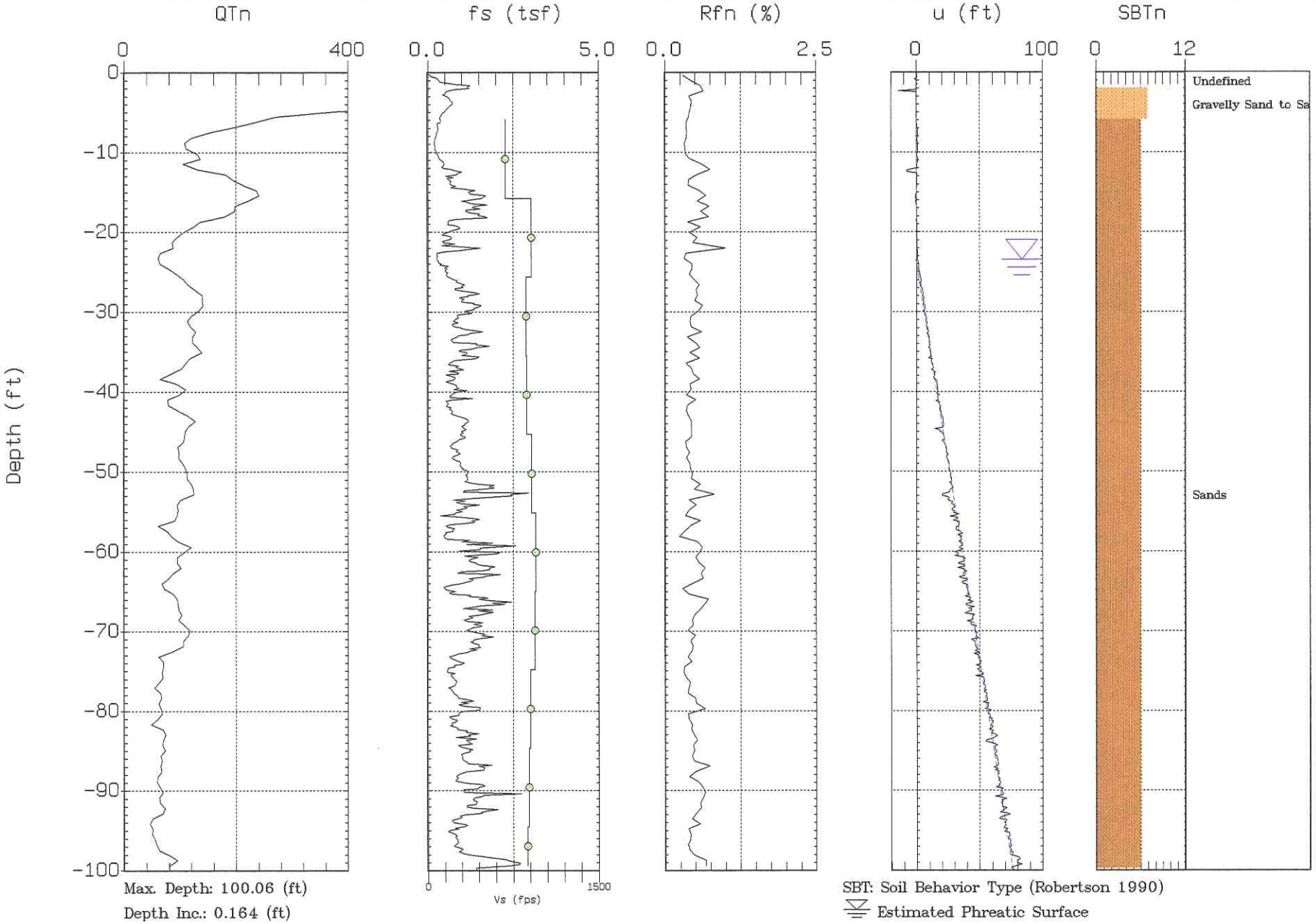

Max. Depth: 100.06 (ft)
Depth Inc.: 0.164 (ft)

SBT: Soil Behavior Type (Robertson 1990)
Estimated Phreatic Surface

CONETEC

Client: GEI Consultants
Project: Brookhaven National Laboratory, Upton, NY
Sounding: CPT-202
Date: April 23, 2007

Seismic Source: Beam
Source Offset (ft): 2.00
Source Depth (ft): 0.00
Geophone Offset (ft): 0.66

SEISMIC - Vs

Tip Depth (ft)	Geophone Depth (ft)	Ray Path (ft)	Depth Interval (ft)	Time Interval (ms)	Vs (ft/s)	Mid Layer (ft)
6.56	5.90	6.23				
16.40	15.74	15.87	9.64	14.24	677	10.82
26.25	25.59	25.66	9.79	10.82	905	20.67
36.09	35.43	35.49	9.82	11.41	861	30.51
45.93	45.27	45.32	9.83	11.35	866	40.35
55.77	55.11	55.15	9.83	10.80	911	50.19
65.62	64.96	64.99	9.84	10.39	947	60.04
75.46	74.80	74.83	9.84	10.49	938	69.88
85.30	84.64	84.67	9.84	10.93	900	79.72
95.14	94.48	94.51	9.84	11.08	888	89.56
100.07	99.41	99.43	4.92	5.63	874	96.94

Client: GEI Consultants
Location: Brookhaven National Laboratory, Upton, NY
CPT Sounding: CPT-202
Date: April 23, 2007

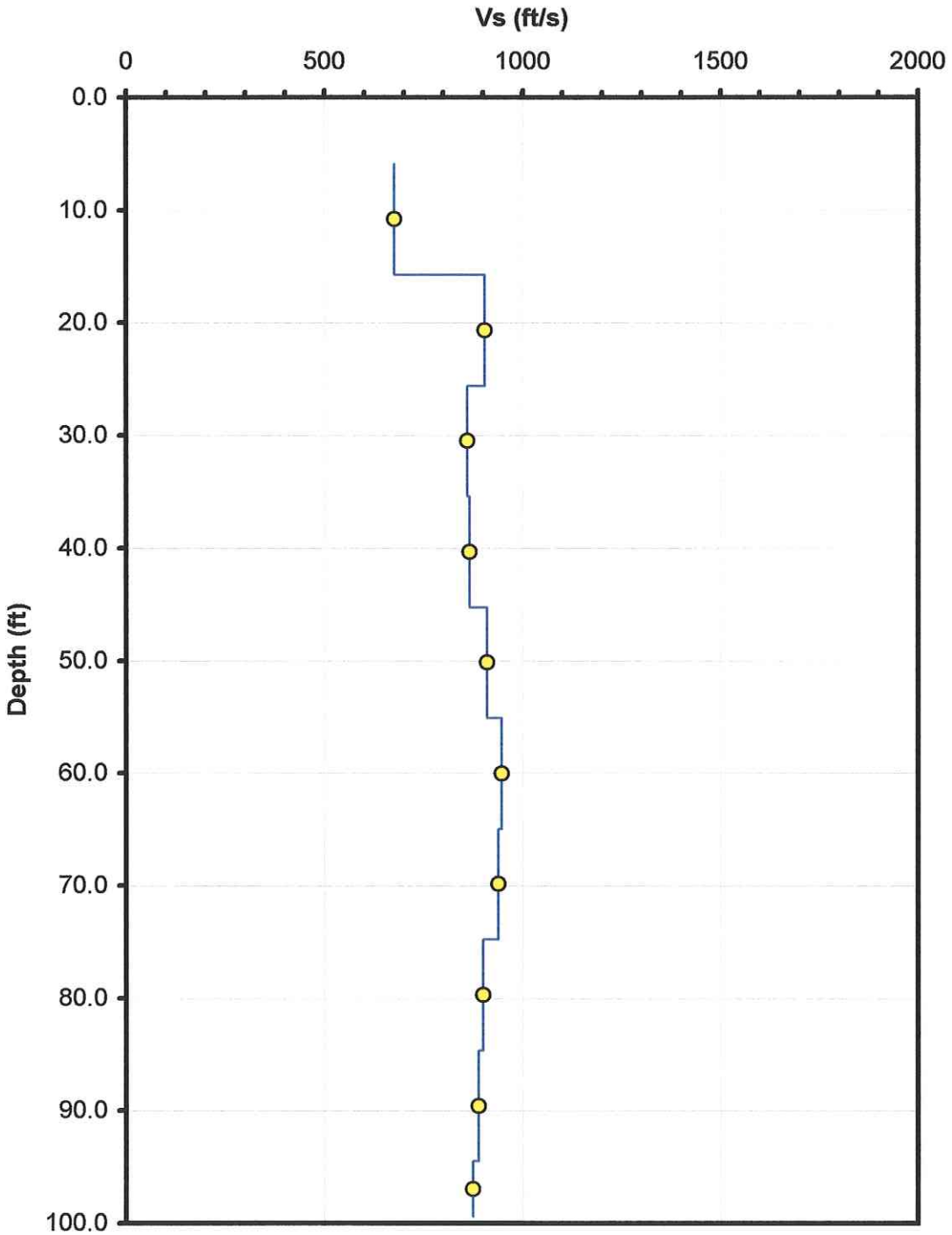

CONETEC

GEI Consultants

Site: CPT-203
Location: Upton, NY

Cone:STD 20T AD179
Date:04:23:07 15:16

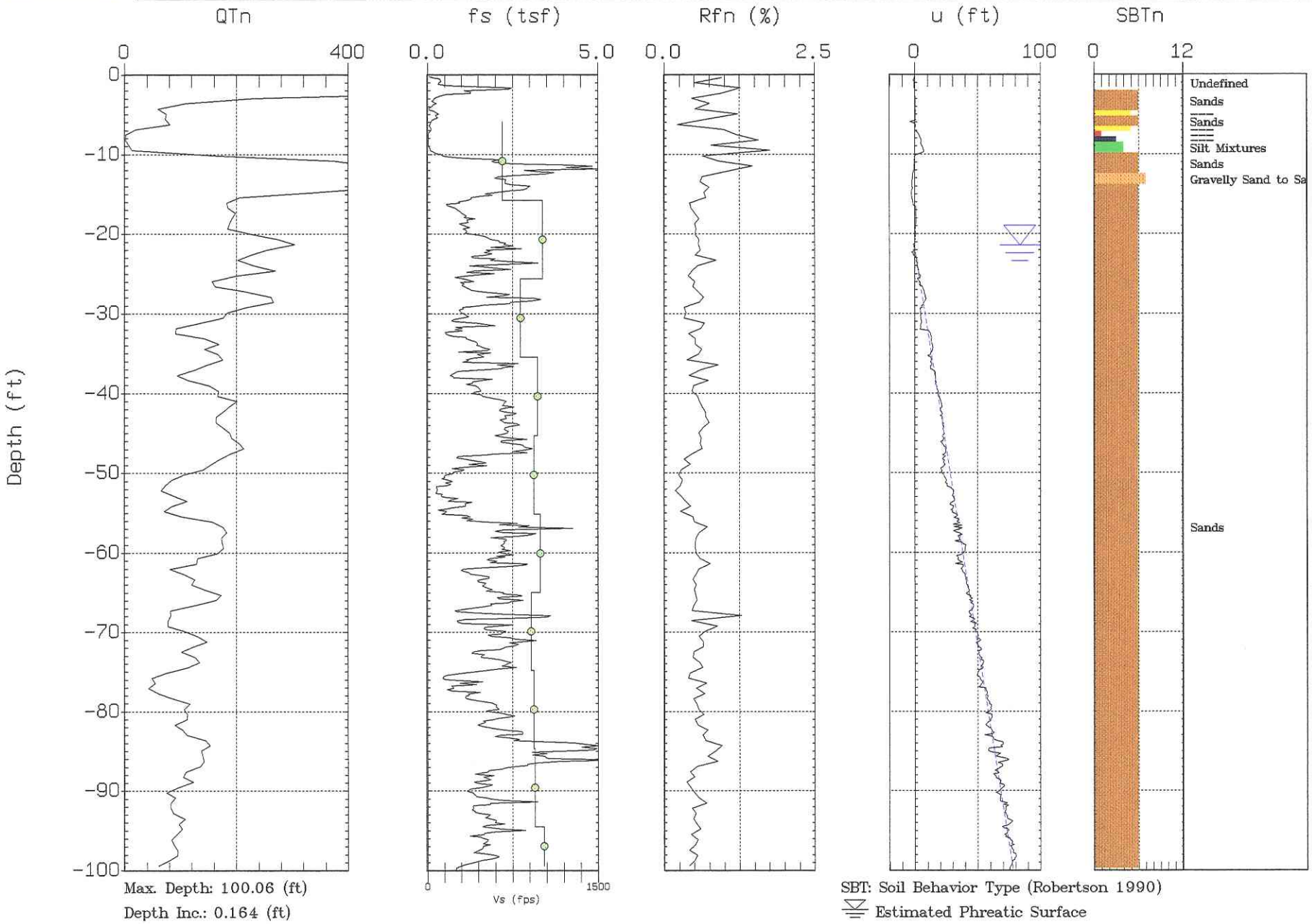

Max. Depth: 100.06 (ft)
Depth Inc.: 0.164 (ft)

SBT: Soil Behavior Type (Robertson 1990)

Estimated Phreatic Surface

CONETEC

Client: GEI Consultants
Project: Brookhaven National Laboratory, Upton, NY
Sounding: CPT-203
Date: April 23, 2007

Seismic Source: Beam
Source Offset (ft): 2.00
Source Depth (ft): 0.00
Geophone Offset (ft): 0.66

SEISMIC - Vs

Tip Depth (ft)	Geophone Depth (ft)	Ray Path (ft)	Depth Interval (ft)	Time Interval (ms)	Vs (ft/s)	Mid Layer (ft)
6.56	5.90	6.23				
16.40	15.74	15.87	9.64	14.63	659	10.82
26.25	25.59	25.66	9.79	9.68	1011	20.67
36.09	35.43	35.49	9.82	12.03	816	30.51
45.93	45.27	45.32	9.83	10.17	967	40.35
55.77	55.11	55.15	9.83	10.53	934	50.19
65.62	64.96	64.99	9.84	9.91	993	60.04
75.46	74.80	74.83	9.84	10.79	912	69.88
85.30	84.64	84.67	9.84	10.55	933	79.72
95.14	94.48	94.51	9.84	10.44	943	89.56
100.07	99.41	99.43	4.92	4.81	1024	96.94

Client: GEI Consultants
Location: Brookhaven National Laboratory, Upton, NY
CPT Sounding: CPT-203
Date: April 23, 2007

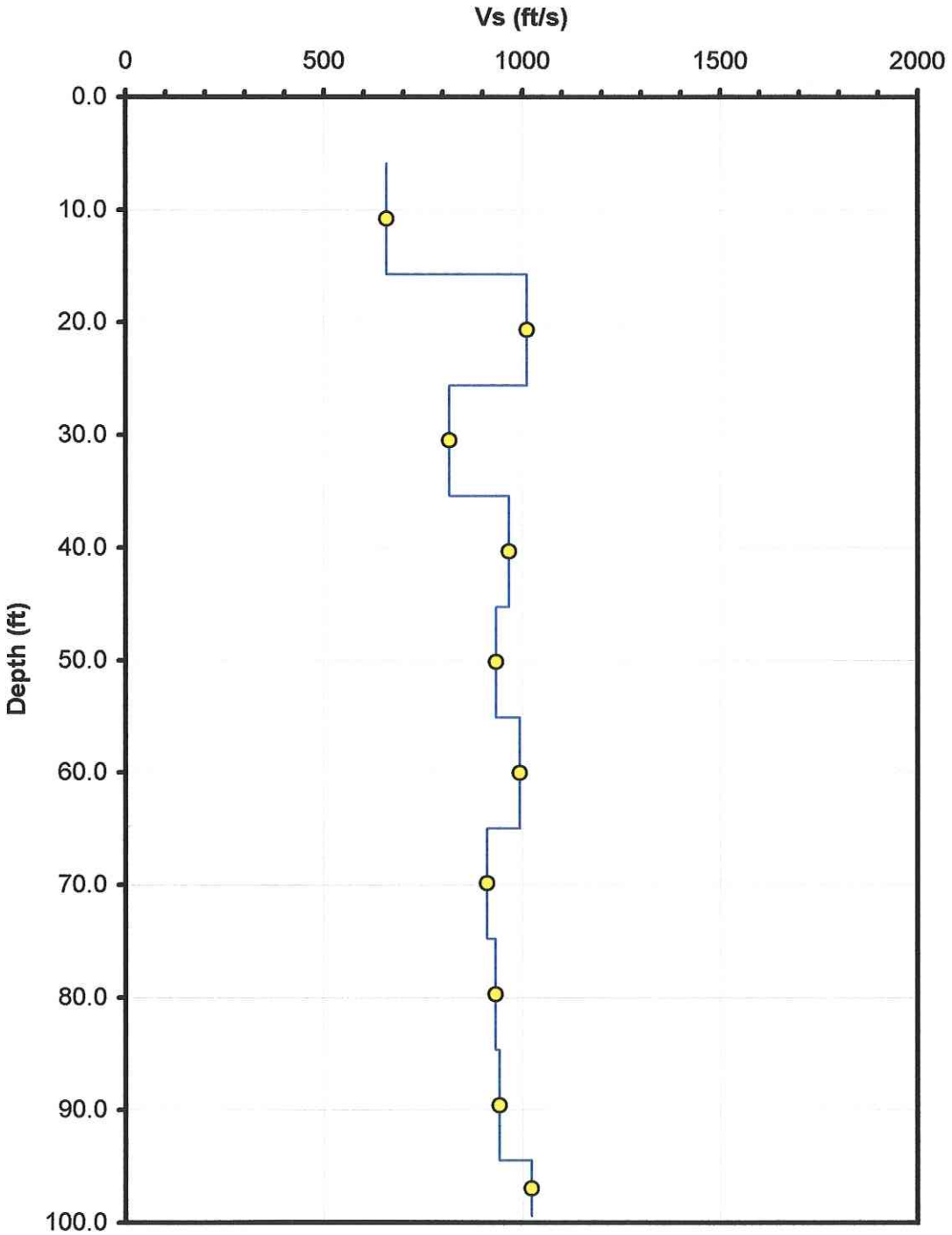

Appendix E

Laboratory Test Results

GeoTesting express
a subsidiary of Geocomp Corporation

Client:	GEI Consultants				
Project:	Brookhaven National Laboratory				
Location:	Upton, NY			Project No:	GTX-6864
Boring ID:	B-101	Sample Type:	jar	Tested By:	pcs
Sample ID:	S-1	Test Date:	08/04/06	Checked By:	jdt
Depth :	0-2 ft	Test Id:	94474		
Test Comment:	sieve stack 6				
Sample Description:	Moist, yellowish brown silty sand				
Sample Comment:	---				

Particle Size Analysis - ASTM D 422

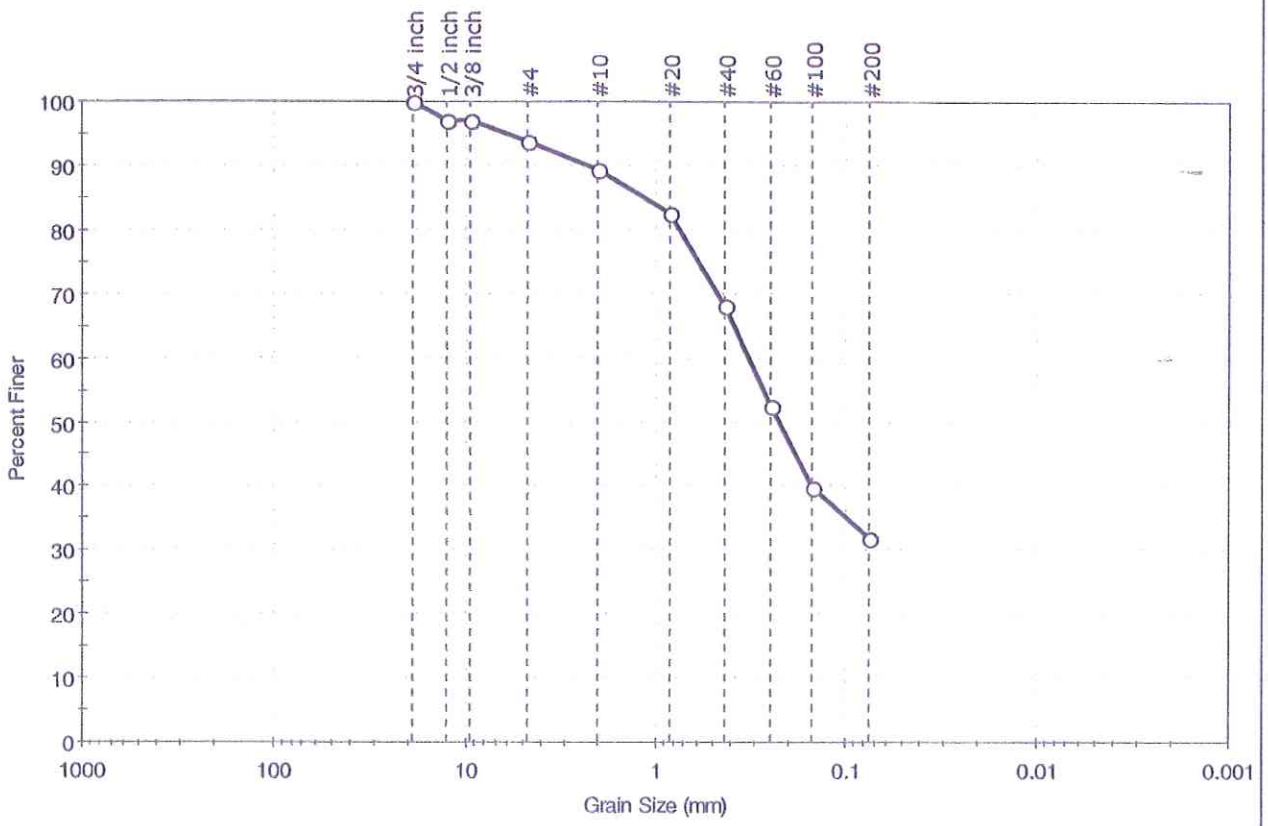

% Cobble	% Gravel	% Sand	% Silt & Clay Size
---	6.2	61.9	31.9

Sieve Name	Sieve Size, mm	Percent Finer	Spec. Percent	Complies
3/4 inch	19.00	100		
1/2 inch	12.70	97		
3/8 inch	9.51	97		
#4	4.75	94		
#10	2.00	89		
#20	0.84	83		
#40	0.42	68		
#60	0.25	52		
#100	0.15	40		
#200	0.075	32		

Coefficients

D_{85} = 1.1382 mm D_{30} = N/A
D_{60} = 0.3233 mm D_{15} = N/A
D_{50} = 0.2260 mm D_{10} = N/A
C_u = N/A C_c = N/A

Classification

ASTM N/A

AASHTO Silty Gravel and Sand (A-2-4 (0))

Sample/Test Description

Sand/Gravel Particle Shape : ROUNDED

Sand/Gravel Hardness : HARD

printed 8/4/2006 11:50:52 AM

GeoTesting express
a subsidiary of Geocomp Corporation

Client:	GEI Consultants				
Project:	Brookhaven National Laboratory				
Location:	Upton, NY			Project No:	GTX-6864
Boring ID:	B-101	Sample Type:	jar	Tested By:	pcs
Sample ID:	S-2	Test Date:	08/04/06	Checked By:	jdt
Depth :	5-7 ft	Test Id:	94475		
Test Comment:	sieve stack 6				
Sample Description:	Moist, light gray silty sand				
Sample Comment:	---				

Particle Size Analysis - ASTM D 422

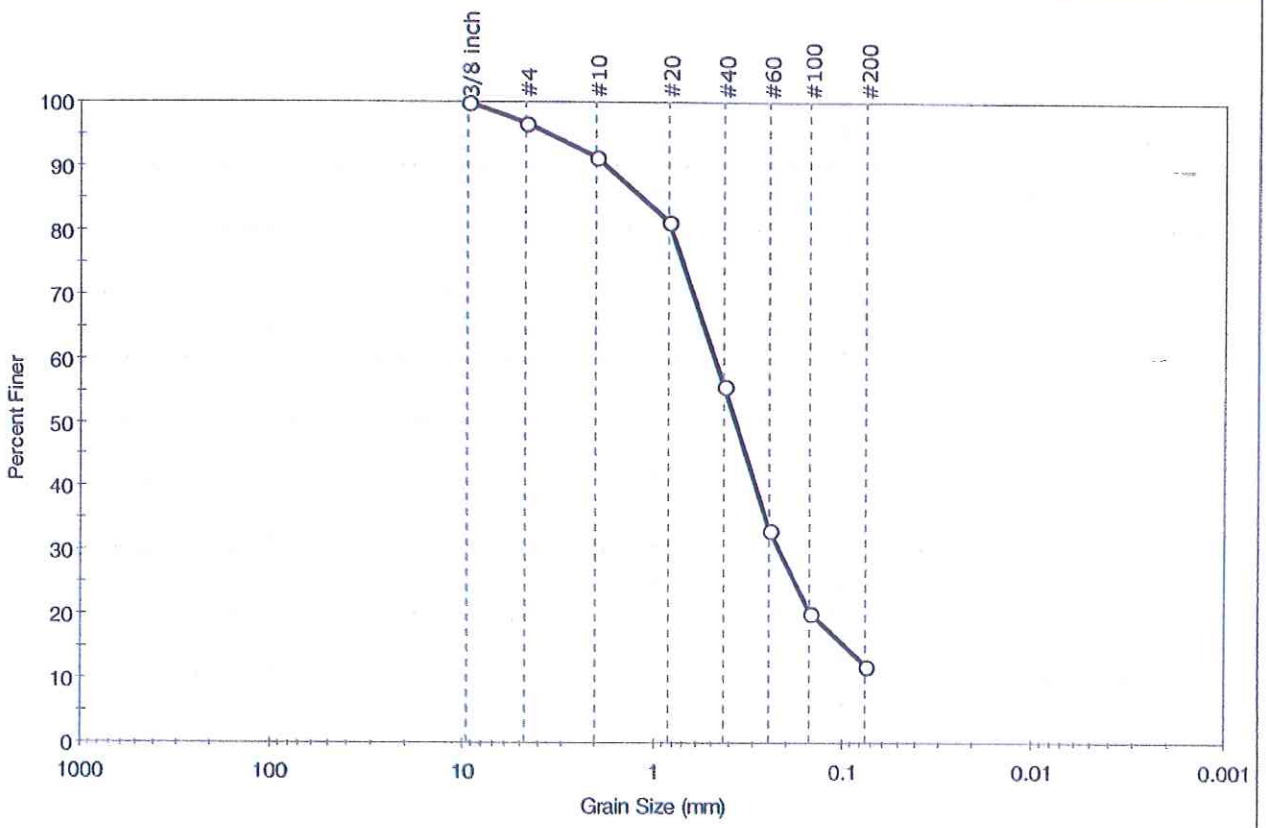

% Cobble	% Gravel	% Sand	% Silt & Clay Size
--	3.2	84.6	12.2

Sieve Name	Sieve Size, mm	Percent Finer	Spec. Percent	Complies
3/8 inch	9.51	100		
#4	4.75	97		
#10	2.00	91		
#20	0.84	81		
#40	0.42	56		
#60	0.25	33		
#100	0.15	20		
#200	0.075	12		

Coefficients

D_{85} = 1.1429 mm D_{30} = 0.2189 mm
D_{60} = 0.4753 mm D_{15} = 0.0949 mm
D_{50} = 0.3706 mm D_{10} = 0.0622 mm
C_u = 7.641 C_c = 1.621

Classification

ASTM N/A

AASHTO Silty Gravel and Sand (A-2-4 (0))

Sample/Test Description

Sand/Gravel Particle Shape : ANGULAR

Sand/Gravel Hardness : HARD

printed 8/4/2006 11:53:06 AM

GeoTesting express
a subsidiary of Geocomp Corporation

Client:	GEI Consultants				
Project:	Brookhaven National Laboratory				
Location:	Upton, NY			Project No:	GTX-6864
Boring ID:	B-101	Sample Type:	jar	Tested By:	pcs
Sample ID:	S-3	Test Date:	08/04/06	Checked By:	jdt
Depth :	10-12 ft	Test Id:	94476		
Test Comment:	sieve stack 6				
Sample Description:	Moist, light gray sand				
Sample Comment:	---				

Particle Size Analysis - ASTM D 422

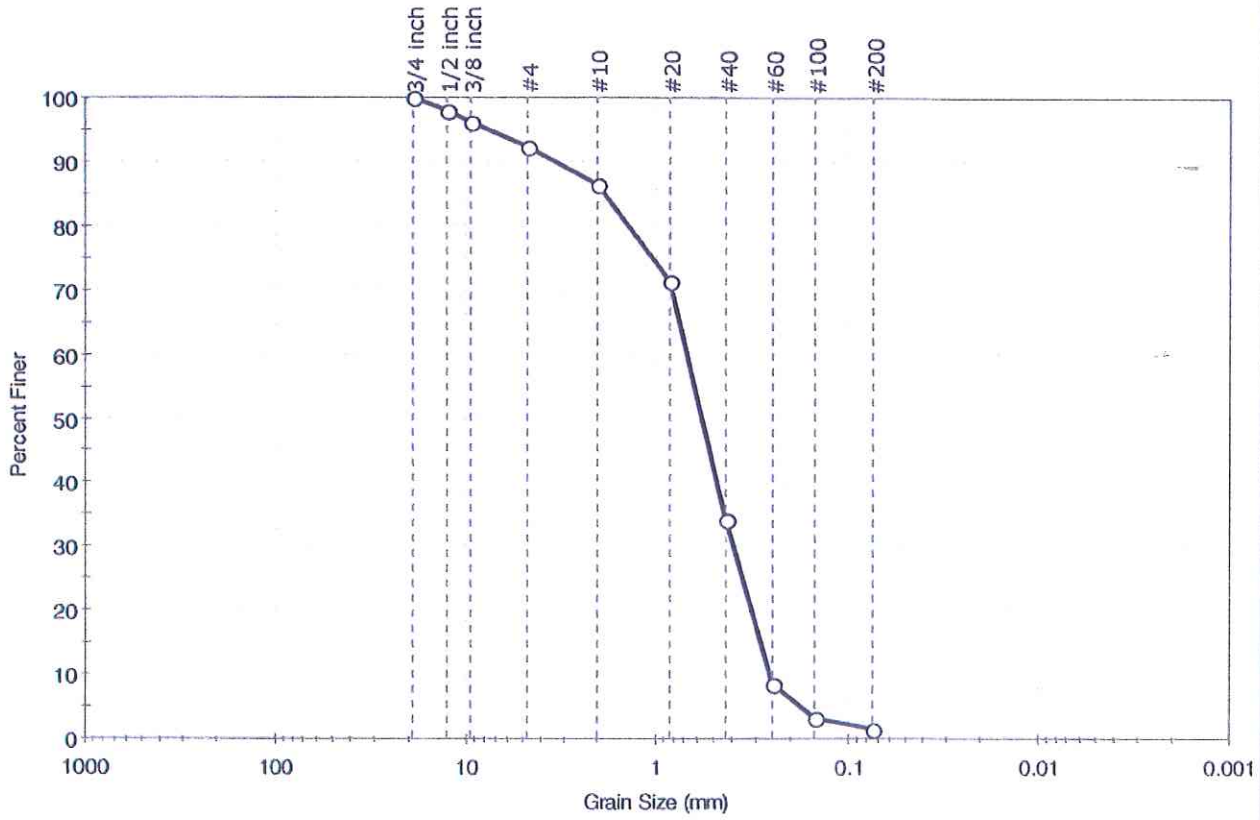

% Cobble	% Gravel	% Sand	% Silt & Clay Size
--	7.8	90.8	1.4

Sieve Name	Sieve Size, mm	Percent Finer	Spec. Percent	Complies
3/4 inch	19.00	100		
1/2 inch	12.70	98		
3/8 inch	9.51	96		
#4	4.75	92		
#10	2.00	86		
#20	0.84	71		
#40	0.42	34		
#60	0.25	9		
#100	0.15	3		
#200	0.075	1		

Coefficients

D_{85} = 1.8530 mm	D_{30} = 0.3886 mm
D_{60} = 0.6828 mm	D_{15} = 0.2854 mm
D_{50} = 0.5676 mm	D_{10} = 0.2575 mm
C_u = 2.652	C_c = 0.859

Classification

ASTM Poorly graded sand (SP)

AASHTO Stone Fragments, Gravel and Sand (A-1-b (0))

Sample/Test Description

Sand/Gravel Particle Shape : ANGULAR

Sand/Gravel Hardness : HARD

printed 8/4/2006 11:51:24 AM

GeoTesting express
a subsidiary of Geocomp Corporation

Client:	GEI Consultants				
Project:	Brookhaven National Laboratory				
Location:	Upton, NY			Project No:	GTX-6864
Boring ID:	B-101	Sample Type:	jar	Tested By:	pcs
Sample ID:	S-4	Test Date:	08/04/06	Checked By:	jdt
Depth :	15-17 ft	Test Id:	94477		
Test Comment:	sieve stack 1				
Sample Description:	Moist, light gray sand				
Sample Comment:	---				

Particle Size Analysis - ASTM D 422

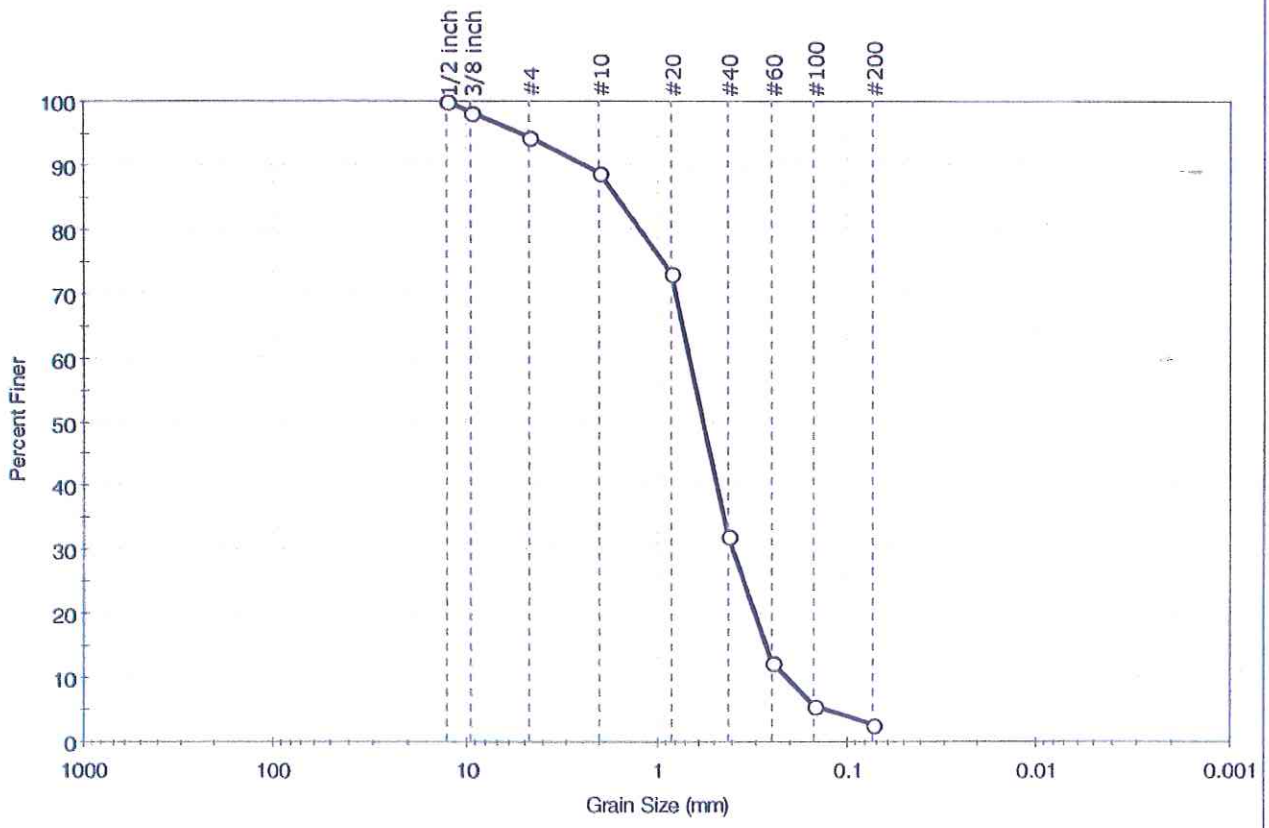

%Cobble	%Gravel	%Sand	%Silt & Clay Size
---	5.5	91.8	2.7

Sieve Name	Sieve Size, mm	Percent Finer	Spec. Percent	Complies
1/2 inch	12.70	100		
3/8 inch	9.51	98		
#4	4.75	95		
#10	2.00	89		
#20	0.84	73		
#40	0.42	32		
#60	0.25	12		
#100	0.15	6		
#200	0.074	3		

Coefficients

D_{85} = 1.6294 mm D_{30} = 0.3979 mm
D_{60} = 0.6737 mm D_{15} = 0.2672 mm
D_{50} = 0.5689 mm D_{10} = 0.2070 mm
C_u = 3.255 C_c = 1.135

Classification

ASTM Poorly graded sand (SP)

AASHTO Stone Fragments, Gravel and Sand (A-1-b (0))

Sample/Test Description

Sand/Gravel Particle Shape : ANGULAR

Sand/Gravel Hardness : HARD

printed 8/4/2006 11:49:05 AM

GeoTesting express
a subsidiary of Geocomp Corporation

Client:	GEI Consultants				
Project:	Brookhaven National Laboratory				
Location:	Upton, NY			Project No:	GTX-6864
Boring ID:	B-101	Sample Type:	jar	Tested By:	pcs
Sample ID:	S-5	Test Date:	08/02/06	Checked By:	jdt
Depth :	20-22 ft	Test Id:	94478		
Test Comment:	sieve stack 6				
Sample Description:	Moist, white sand				
Sample Comment:	---				

Particle Size Analysis - ASTM D 422

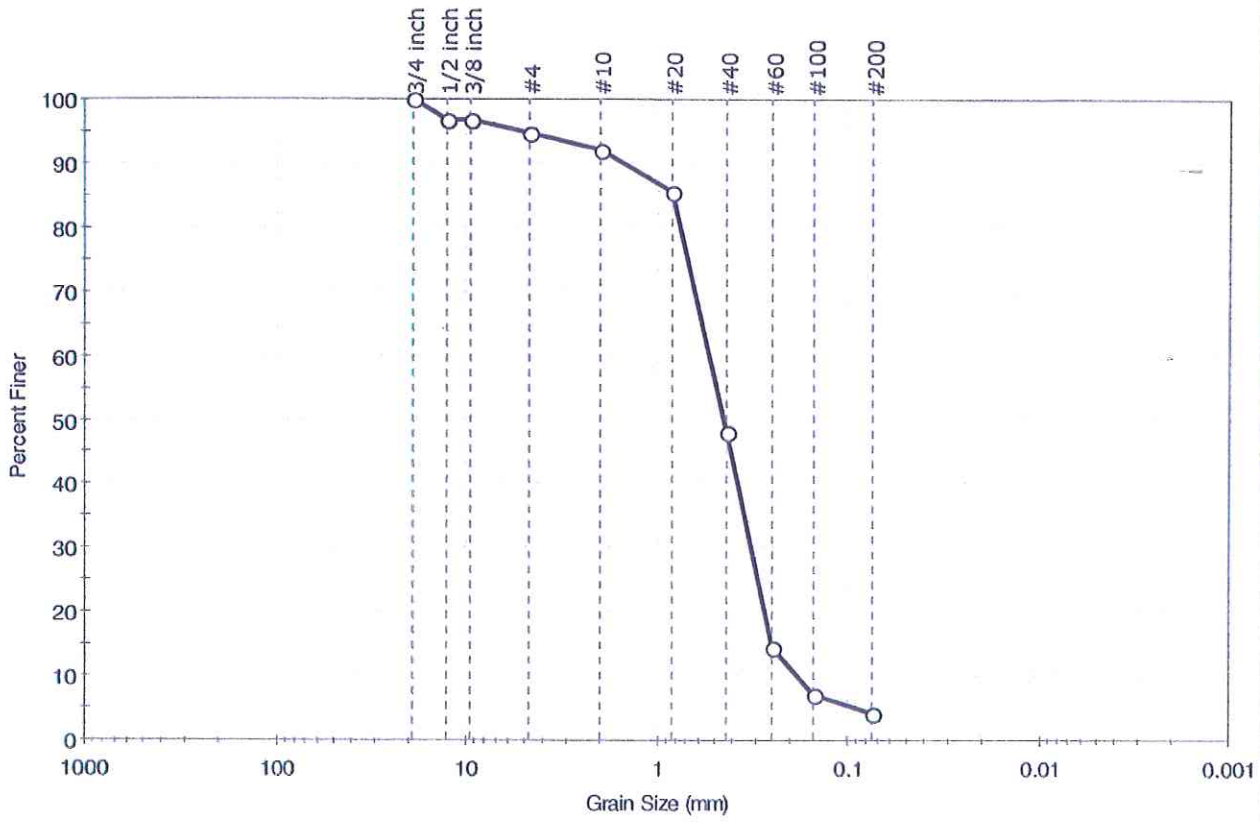

%Cobble	%Gravel	%Sand	%Silt & Clay Size
--	5.4	90.5	4.1

Sieve Name	Sieve Size, mm	Percent Finer	Spec. Percent	Complies
3/4 inch	19.00	100		
1/2 inch	12.70	97		
3/8 inch	9.51	97		
#4	4.75	95		
#10	2.00	92		
#20	0.84	86		
#40	0.42	48		
#60	0.25	15		
#100	0.15	7		
#200	0.075	4		

Coefficients

D_{85} = 0.8317 mm	D_{30} = 0.3192 mm
D_{60} = 0.5280 mm	D_{15} = 0.2516 mm
D_{50} = 0.4402 mm	D_{10} = 0.1818 mm
C_u = 2.904	C_c = 1.061

Classification

ASTM Poorly graded sand (SP)

AASHTO Stone Fragments, Gravel and Sand (A-1-b (0))

Sample/Test Description

Sand/Gravel Particle Shape : ANGULAR

Sand/Gravel Hardness : HARD

printed 8/4/2006 11:42:21 AM

GeoTesting express
a subsidiary of Geocomp Corporation

Client:	GEI Consultants				
Project:	Brookhaven National Laboratory				
Location:	Upton, NY			Project No:	GTX-6864
Boring ID:	B-101	Sample Type:	jar	Tested By:	pcs
Sample ID:	S-6	Test Date:	08/02/06	Checked By:	jdt
Depth :	25-27 ft	Test Id:	94479		
Test Comment:	sieve stack 1				
Sample Description:	Moist, very pale brown sand with silt and gravel				
Sample Comment:	---				

Particle Size Analysis - ASTM D 422

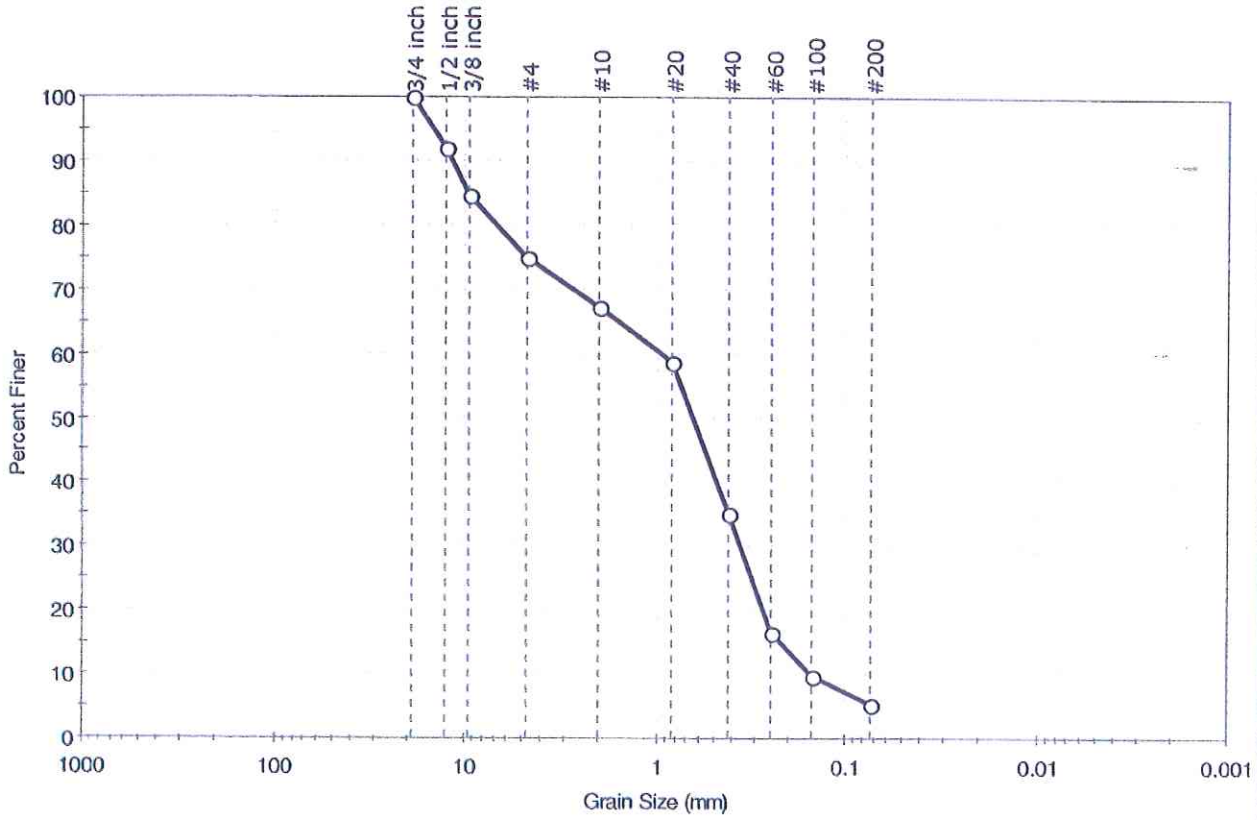

% Cobble	% Gravel	% Sand	% Silt & Clay Size
---	25.2	69.5	5.3

Sieve Name	Sieve Size, mm	Percent Finer	Spec. Percent	Complies
3/4 inch	19.00	100		
1/2 inch	12.70	92		
3/8 inch	9.51	85		
#4	4.75	75		
#10	2.00	67		
#20	0.84	59		
#40	0.42	35		
#60	0.25	17		
#100	0.15	10		
#200	0.074	5		

Coefficients

D_{85} =9.6327 mm	D_{30} =0.3633 mm
D_{60} =0.9539 mm	D_{15} =0.2209 mm
D_{50} =0.6500 mm	D_{10} =0.1520 mm
C_u =6.276	C_c =0.910

Classification

ASTM N/A

AASHTO Stone Fragments, Gravel and Sand (A-1-b (0))

Sample/Test Description

Sand/Gravel Particle Shape : ROUNDED

Sand/Gravel Hardness : HARD

printed 8/4/2006 11:44:43 AM

GeoTesting express
a subsidiary of Geocomp Corporation

Client:	GEI Consultants				
Project:	Brookhaven National Laboratory				
Location:	Upton, NY			Project No:	GTX-6864
Boring ID:	B-101	Sample Type:	jar	Tested By:	pcs
Sample ID:	S-8	Test Date:	08/04/06	Checked By:	jdt
Depth :	35-37 ft	Test Id:	94480		
Test Comment:	sieve stack 1				
Sample Description:	Moist, pale brown sand with gravel				
Sample Comment:	---				

Particle Size Analysis - ASTM D 422

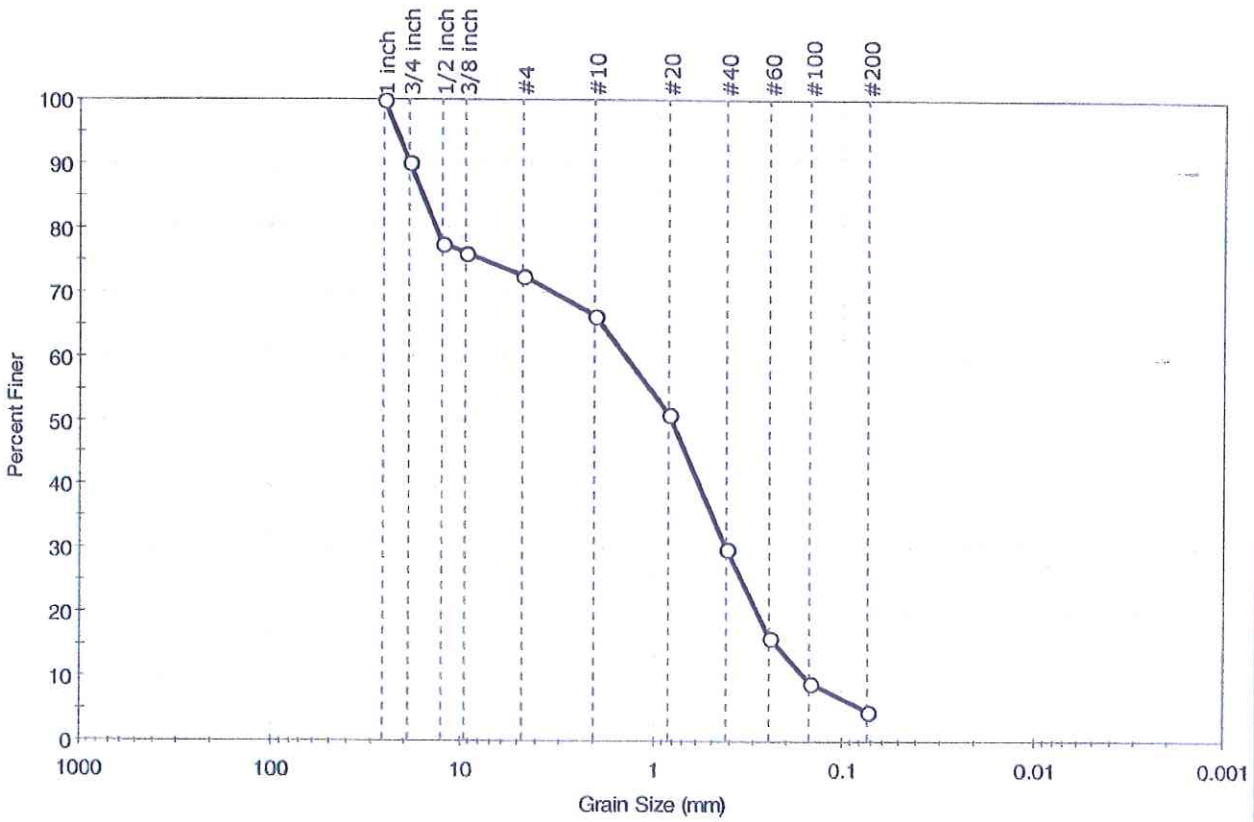

%Cobble	%Gravel	%Sand	%Silt & Clay Size
--	27.3	68.1	4.6

Sieve Name	Sieve Size, mm	Percent Finer	Spec. Percent	Complies
1 inch	25.70	100		
3/4 inch	19.00	90		
1/2 inch	12.70	78		
3/8 inch	9.51	76		
#4	4.75	73		
#10	2.00	66		
#20	0.84	51		
#40	0.42	30		
#60	0.25	16		
#100	0.15	9		
#200	0.074	5		

Coefficients

D_{85} = 16.0845 mm	D_{30} = 0.4168 mm
D_{60} = 1.3899 mm	D_{15} = 0.2294 mm
D_{50} = 0.8125 mm	D_{10} = 0.1594 mm
C_u = 8.720	C_c = 0.784

Classification

ASTM: Poorly graded sand with gravel (SP)

AASHTO: Stone Fragments, Gravel and Sand (A-1-b (0))

Sample/Test Description

Sand/Gravel Particle Shape : ANGULAR

Sand/Gravel Hardness : HARD

GeoTesting express
a subsidiary of Geocomp Corporation

Client:	GEI Consultants				
Project:	Brookhaven National Laboratory				
Location:	Upton, NY			Project No:	GTX-6864
Boring ID:	B-101	Sample Type:	jar	Tested By:	pcs
Sample ID:	S-10	Test Date:	08/04/06	Checked By:	jdt
Depth :	45-47 ft	Test Id:	94481		
Test Comment:	sieve stack 1				
Sample Description:	Moist, light yellowish brown sand with silt				
Sample Comment:	---				

Particle Size Analysis - ASTM D 422

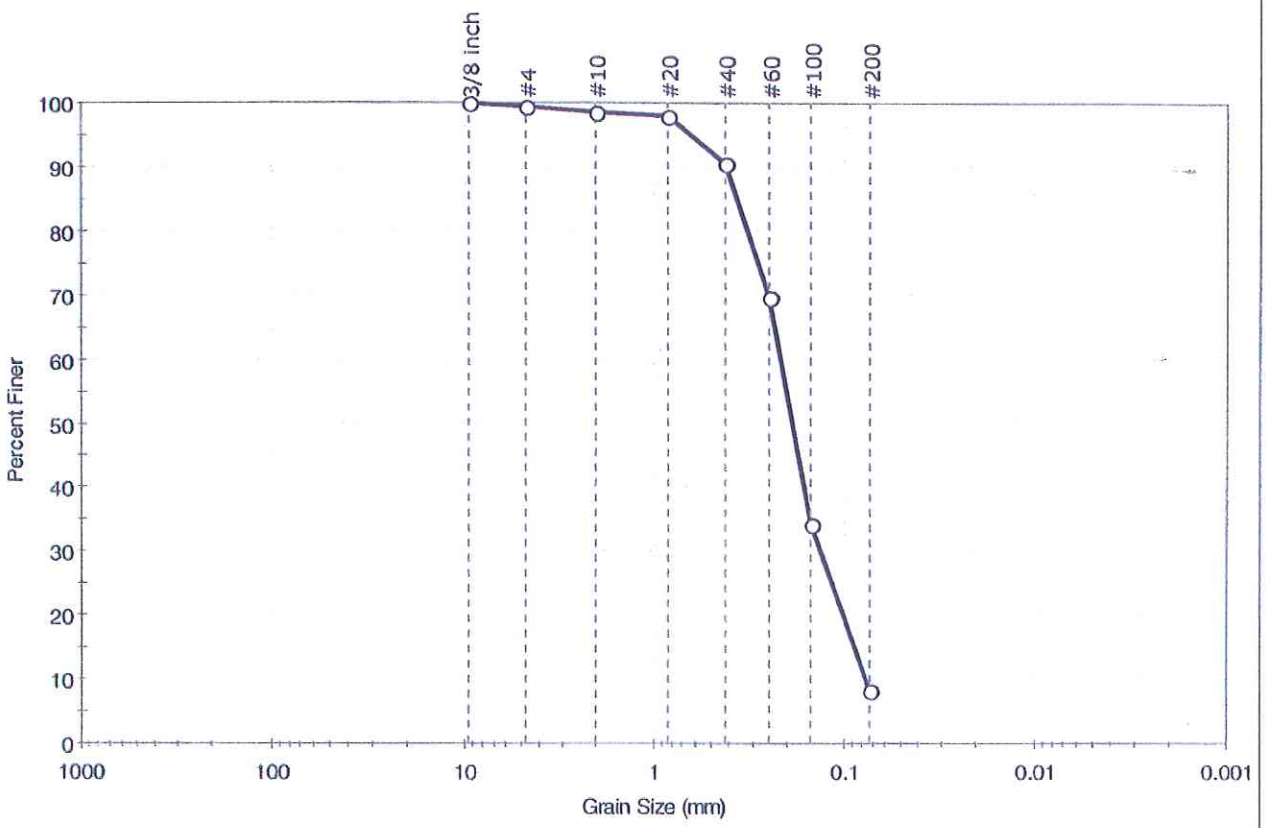

%Cobble	%Gravel	%Sand	%Silt & Clay Size
—	0.5	91.2	8.3

Sieve Name	Sieve Size, mm	Percent Finer	Spec. Percent	Complies
3/8 inch	9.51	100		
#4	4.75	99		
#10	2.00	99		
#20	0.84	98		
#40	0.42	90		
#60	0.25	70		
#100	0.15	34		
#200	0.074	8		

Coefficients

D_{85} = 0.3666 mm	D_{30} = 0.1332 mm
D_{60} = 0.2172 mm	D_{15} = 0.0888 mm
D_{50} = 0.1877 mm	D_{10} = 0.0775 mm
C_u = 2.803	C_c = 1.054

Classification

ASTM N/A

AASHTO Fine Sand (A-3 (0))

Sample/Test Description

Sand/Gravel Particle Shape : ---

Sand/Gravel Hardness : ---

printed 8/4/2006 11:50:20 AM

GeoTesting express
a subsidiary of Geocomp Corporation

Client:	GEI Consultants				
Project:	Brookhaven National Laboratory				
Location:	Upton, NY			Project No:	GTX-6864
Boring ID:	B-102	Sample Type:	jar	Tested By:	pcs
Sample ID:	S-1	Test Date:	08/04/06	Checked By:	jdt
Depth :	0-2 ft	Test Id:	94482		
Test Comment:	sieve stack 1				
Sample Description:	Moist, Dark yellowish brown silty sand				
Sample Comment:	---				

Particle Size Analysis - ASTM D 422

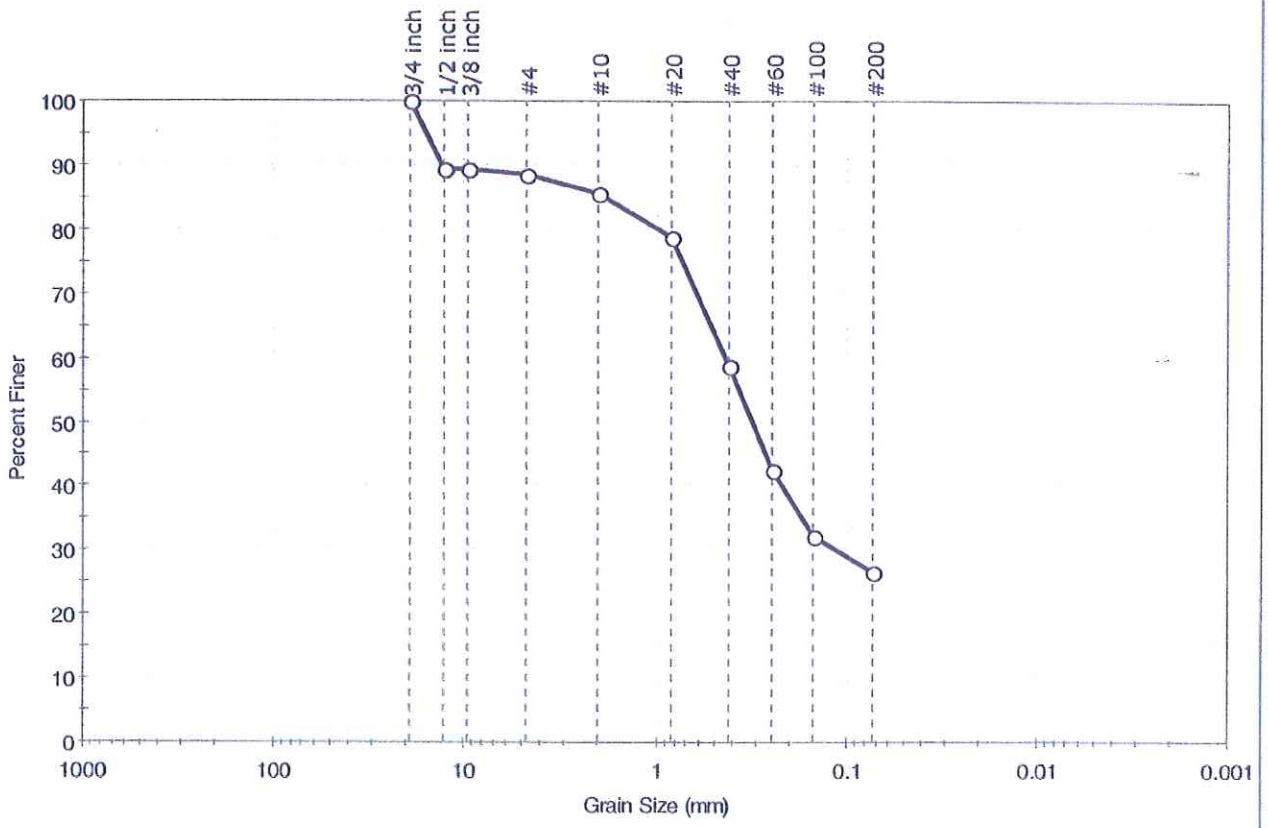

%Cobble	%Gravel	%Sand	%Silt & Clay Size
--	11.4	61.9	26.7

Sieve Name	Sieve Size, mm	Percent Finer	Spec. Percent	Complies
3/4 inch	19.00	100		
1/2 inch	12.70	89		
3/8 inch	9.51	89		
#4	4.75	89		
#10	2.00	86		
#20	0.84	79		
#40	0.42	59		
#60	0.25	42		
#100	0.15	32		
#200	0.074	27		

Coefficients

D_{85} = 1.8592 mm D_{30} = 0.1121 mm
D_{60} = 0.4377 mm D_{15} = N/A
D_{50} = 0.3177 mm D_{10} = N/A
C_u = N/A C_c = N/A

Classification

ASTM N/A

AASHTO Silty Gravel and Sand (A-2-4 (0))

Sample/Test Description

Sand/Gravel Particle Shape : ANGULAR

Sand/Gravel Hardness : HARD

printed 9/4/2006 11:52:05 AM

GeoTesting express
a subsidiary of Geocomp Corporation

Client:	GEI Consultants				
Project:	Brookhaven National Laboratory				
Location:	Upton, NY			Project No:	GTX-6864
Boring ID:	B-102	Sample Type:	jar	Tested By:	pcs
Sample ID:	S-2	Test Date:	08/04/06	Checked By:	jdt
Depth :	5-7 ft	Test Id:	94483		
Test Comment:	sieve stack 6				
Sample Description:	Moist, light olive brown sand				
Sample Comment:	---				

Particle Size Analysis - ASTM D 422

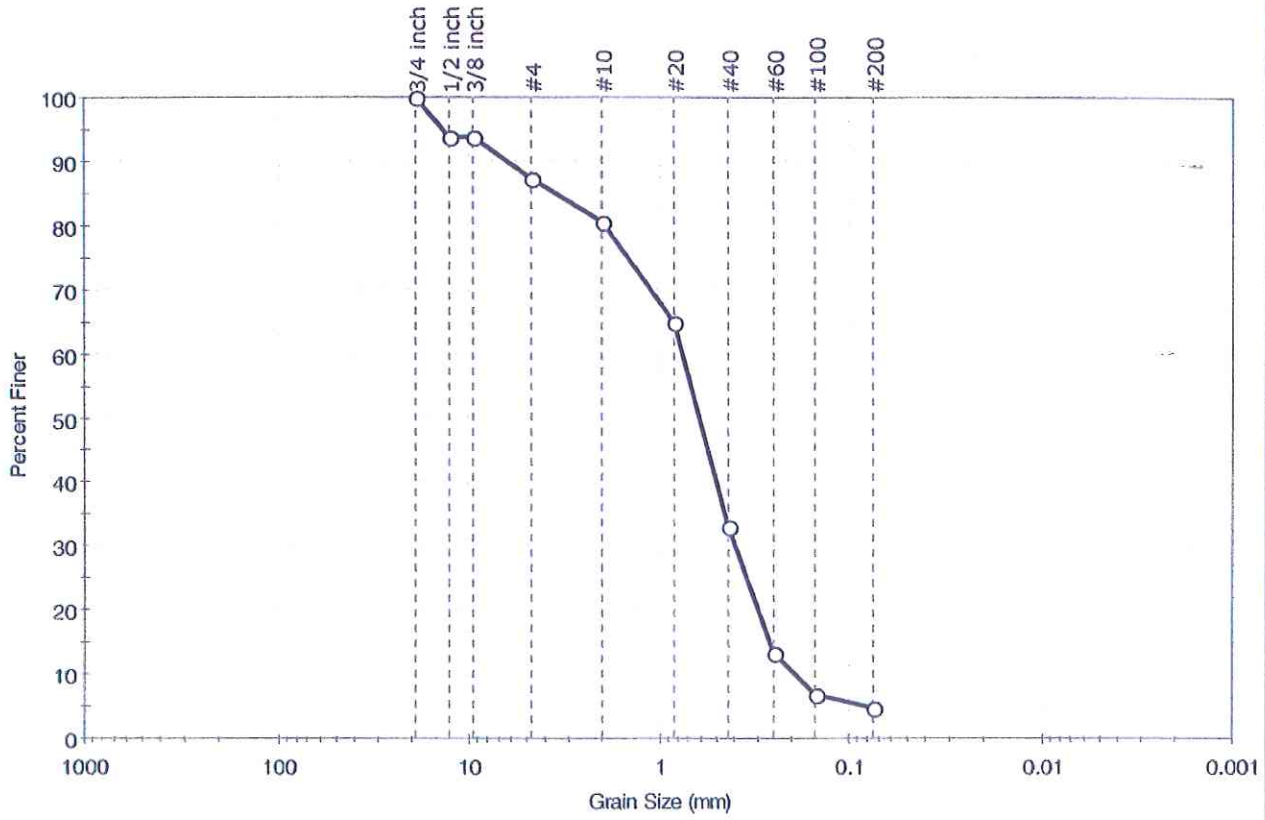

%Cobble	%Gravel	%Sand	%Silt & Clay Size
—	12.7	82.7	4.6

Sieve Name	Sieve Size, mm	Percent Finer	Spec. Percent	Complies
3/4 inch	19.00	100		
1/2 inch	12.70	94		
3/8 inch	9.51	94		
#4	4.75	87		
#10	2.00	81		
#20	0.84	65		
#40	0.42	33		
#60	0.25	13		
#100	0.15	7		
#200	0.075	5		

Coefficients

D_{85} = 3.5367 mm	D_{30} = 0.3920 mm
D_{60} = 0.7575 mm	D_{15} = 0.2627 mm
D_{50} = 0.6114 mm	D_{10} = 0.1938 mm
C_u = 3.909	C_c = 1.047

Classification

ASTM Poorly graded sand (SP)

AASHTO Stone Fragments, Gravel and Sand (A-1-b (0))

Sample/Test Description

Sand/Gravel Particle Shape : ANGULAR

Sand/Gravel Hardness : HARD

GeoTesting express
a subsidiary of Geocomp Corporation

Client:	GEI Consultants		
Project:	Brookhaven National Laboratory		
Location:	Upton, NY	Project No:	GTX-6864
Boring ID:	B-102	Sample Type: jar	Tested By: pcs
Sample ID:	S-3	Test Date: 08/04/06	Checked By: jdt
Depth :	10-12 ft	Test Id: 94484	
Test Comment:	sieve stack 6		
Sample Description:	Moist, light yellowish brown sand		
Sample Comment:	---		

Particle Size Analysis - ASTM D 422

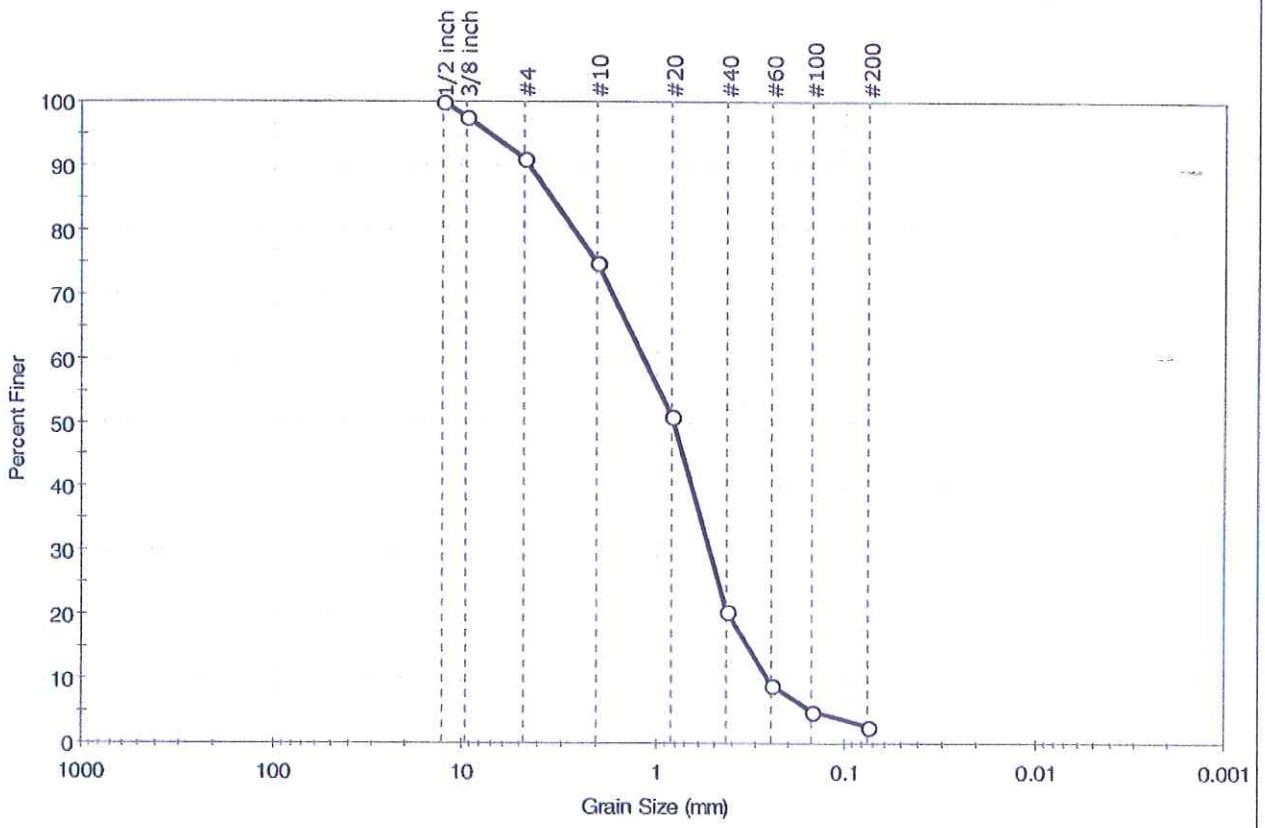

%Cobble	%Gravel	%Sand	%Silt & Clay Size
—	9.0	88.2	2.8

Sieve Name	Sieve Size, mm	Percent Finer	Spec. Percent	Complies
1/2 inch	12.70	100		
3/8 inch	9.51	98		
#4	4.75	91		
#10	2.00	75		
#20	0.84	51		
#40	0.42	21		
#60	0.25	9		
#100	0.15	5		
#200	0.075	3		

Coefficients

D_{85} =3.4384 mm	D_{30} =0.5240 mm
D_{60} =1.1657 mm	D_{15} =0.3278 mm
D_{50} =0.8227 mm	D_{10} =0.2611 mm
C_u =4.465	C_c =0.902

Classification

ASTM Poorly graded sand (SP)

AASHTO Stone Fragments, Gravel and Sand (A-1-b (0))

Sample/Test Description

Sand/Gravel Particle Shape :

Sand/Gravel Hardness :

printed 8/4/2006 11:47:59 AM

GeoTesting express
a subsidiary of Geocomp Corporation

Client:	GEI Consultants				
Project:	Brookhaven National Laboratory				
Location:	Upton, NY			Project No:	GTX-6864
Boring ID:	B-102	Sample Type:	jar	Tested By:	pcs
Sample ID:	S-4	Test Date:	08/02/06	Checked By:	jdt
Depth :	15-17 ft	Test Id:	94485		
Test Comment:	sieve stack 1				
Sample Description:	Moist, brown sand with silt				
Sample Comment:	---				

Particle Size Analysis - ASTM D 422

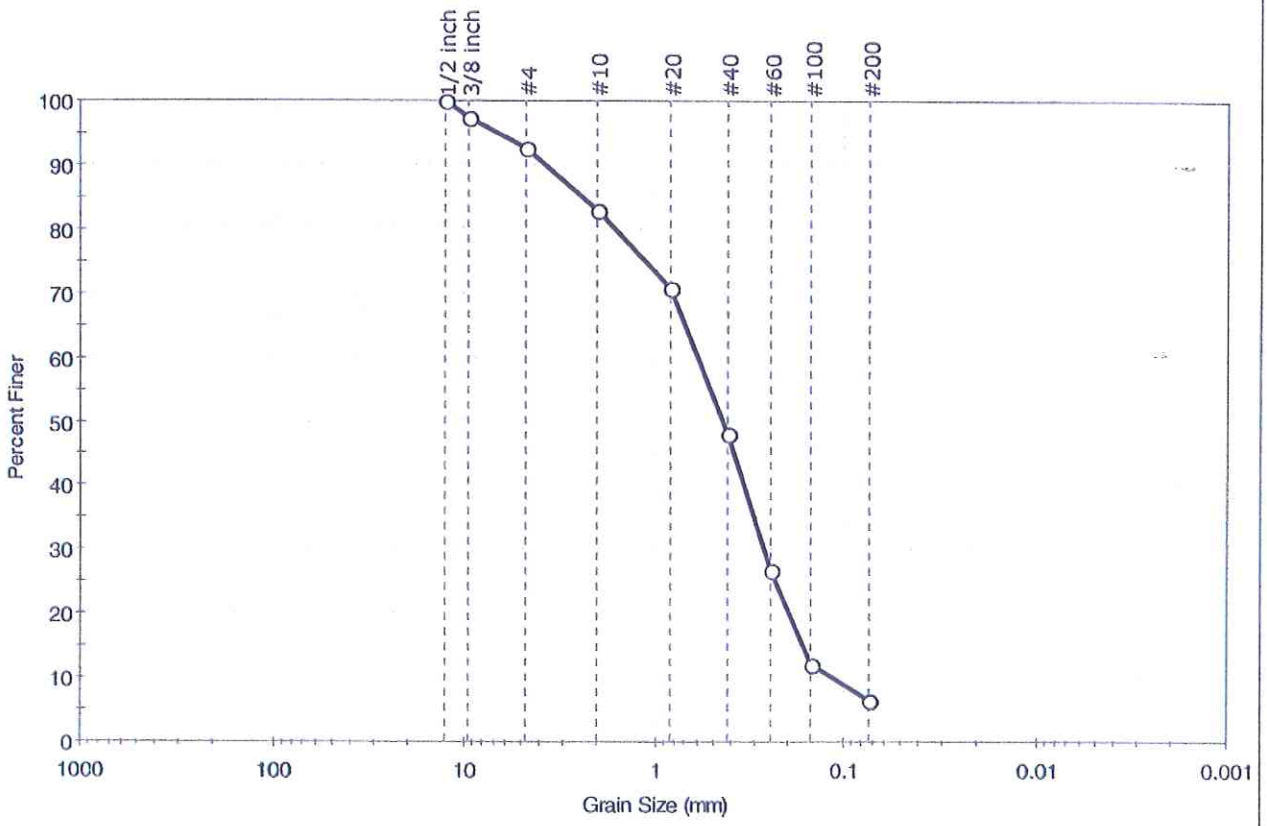

%Cobble	%Gravel	%Sand	%Silt & Clay Size
---	7.4	86.1	6.5

Sieve Name	Sieve Size, mm	Percent Finer	Spec. Percent	Complies
1/2 inch	12.70	100		
3/8 inch	9.51	97		
#4	4.75	93		
#10	2.00	83		
#20	0.84	71		
#40	0.42	48		
#60	0.25	27		
#100	0.15	12		
#200	0.074	7		

Coefficients

D_{85} = 2.4268 mm	D_{30} = 0.2707 mm
D_{60} = 0.6058 mm	D_{15} = 0.1657 mm
D_{50} = 0.4464 mm	D_{10} = 0.1157 mm
C_u = 5.236	C_c = 1.045

Classification

ASTM N/A

AASHTO Stone Fragments, Gravel and Sand (A-1-b (0))

Sample/Test Description

Sand/Gravel Particle Shape : ANGULAR

Sand/Gravel Hardness : HARD

printed 8/4/2006 11:48:25 AM

GeoTesting express
a subsidiary of Geocomp Corporation

Client:	GEI Consultants				
Project:	Brookhaven National Laboratory				
Location:	Upton, NY			Project No:	GTX-6864
Boring ID:	B-102	Sample Type:	jar	Tested By:	pcs
Sample ID:	S-5	Test Date:	08/02/06	Checked By:	jdt
Depth :	20-22 ft	Test Id:	94486		
Test Comment:	sieve stack 6				
Sample Description:	Moist, light brown sand with silt				
Sample Comment:	---				

Particle Size Analysis - ASTM D 422

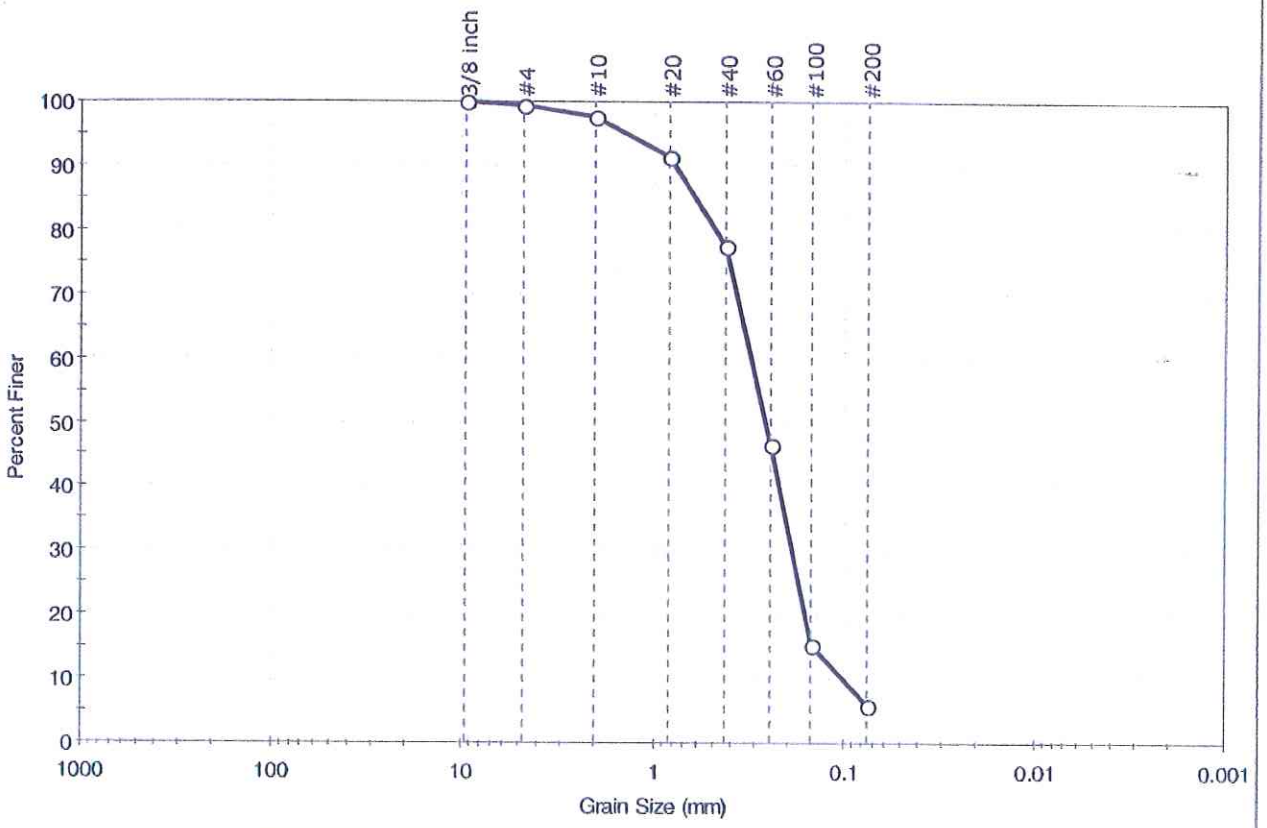

% Cobble	% Gravel	% Sand	% Silt & Clay Size
--	0.8	93.2	6.0

Sieve Name	Sieve Size, mm	Percent Finer	Spec. Percent	Complies
3/8 inch	9.51	100		
#4	4.75	99		
#10	2.00	98		
#20	0.84	92		
#40	0.42	78		
#60	0.25	47		
#100	0.15	15		
#200	0.075	6		

Coefficients

D_{85} =0.6113 mm	D_{30} =0.1901 mm
D_{60} =0.3148 mm	D_{15} =0.1455 mm
D_{50} =0.2653 mm	D_{10} =0.1005 mm
C_u =3.132	C_c =1.142

Classification

ASTM N/A

AASHTO Fine Sand (A-3 (0))

Sample/Test Description

Sand/Gravel Particle Shape : ---

Sand/Gravel Hardness : ---

GeoTesting express
a subsidiary of Geocomp Corporation

Client:	GEI Consultants		
Project:	Brookhaven National Laboratory		
Location:	Upton, NY	Project No:	GTX-6864
Boring ID:	B-102	Sample Type: jar	Tested By: pcs
Sample ID:	S-6	Test Date: 08/04/06	Checked By: jdt
Depth :	25-27 ft	Test Id: 94487	
Test Comment:	sieve stack 1		
Sample Description:	Moist, light yellowish brown sand with silt		
Sample Comment:	---		

Particle Size Analysis - ASTM D 422

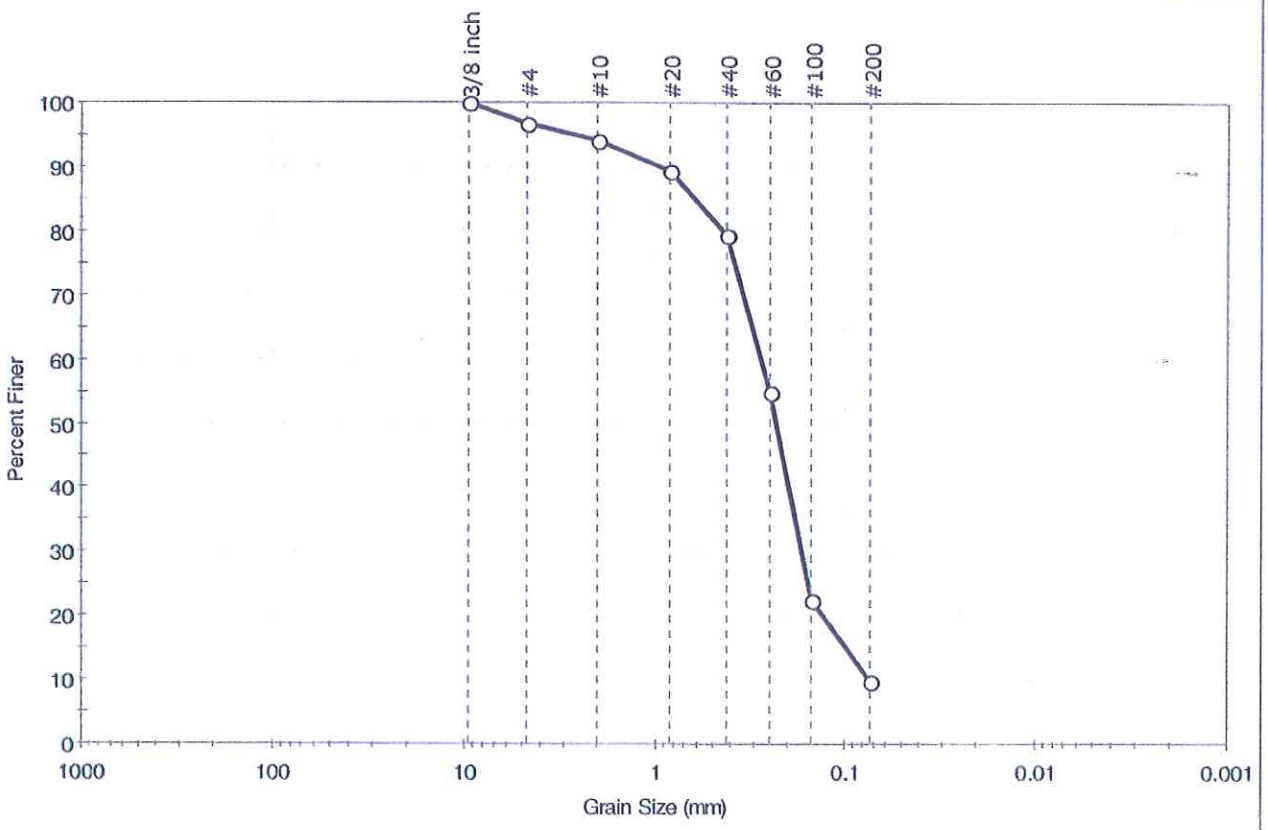

% Cobble	% Gravel	% Sand	% Silt & Clay Size
---	3.4	87.0	9.6

Sieve Name	Sieve Size, mm	Percent Finer	Spec. Percent	Complies
3/8 inch	9.51	100		
#4	4.75	97		
#10	2.00	94		
#20	0.84	89		
#40	0.42	79		
#60	0.25	55		
#100	0.15	22		
#200	0.074	10		

Coefficients

D_{85} = 0.6207 mm	D_{30} = 0.1681 mm
D_{60} = 0.2791 mm	D_{15} = 0.0992 mm
D_{50} = 0.2315 mm	D_{10} = 0.0756 mm
C_u = 3.692	C_c = 1.339

Classification

ASTM N/A

AASHTO Fine Sand (A-3 (0))

Sample/Test Description

Sand/Gravel Particle Shape : ---

Sand/Gravel Hardness : ---

printed 8/4/2006 11:52:38 AM

GeoTesting express
a subsidiary of Geocomp Corporation

Client:	GEI Consultants				
Project:	Brookhaven National Laboratory				
Location:	Upton, NY			Project No:	GTX-6864
Boring ID:	B-102	Sample Type:	jar	Tested By:	pcs
Sample ID:	S-8	Test Date:	08/04/06	Checked By:	jdt
Depth :	35-37 ft	Test Id:	94488		
Test Comment:	sieve stack 1				
Sample Description:	Moist, pale brown sand with silt				
Sample Comment:	---				

Particle Size Analysis - ASTM D 422

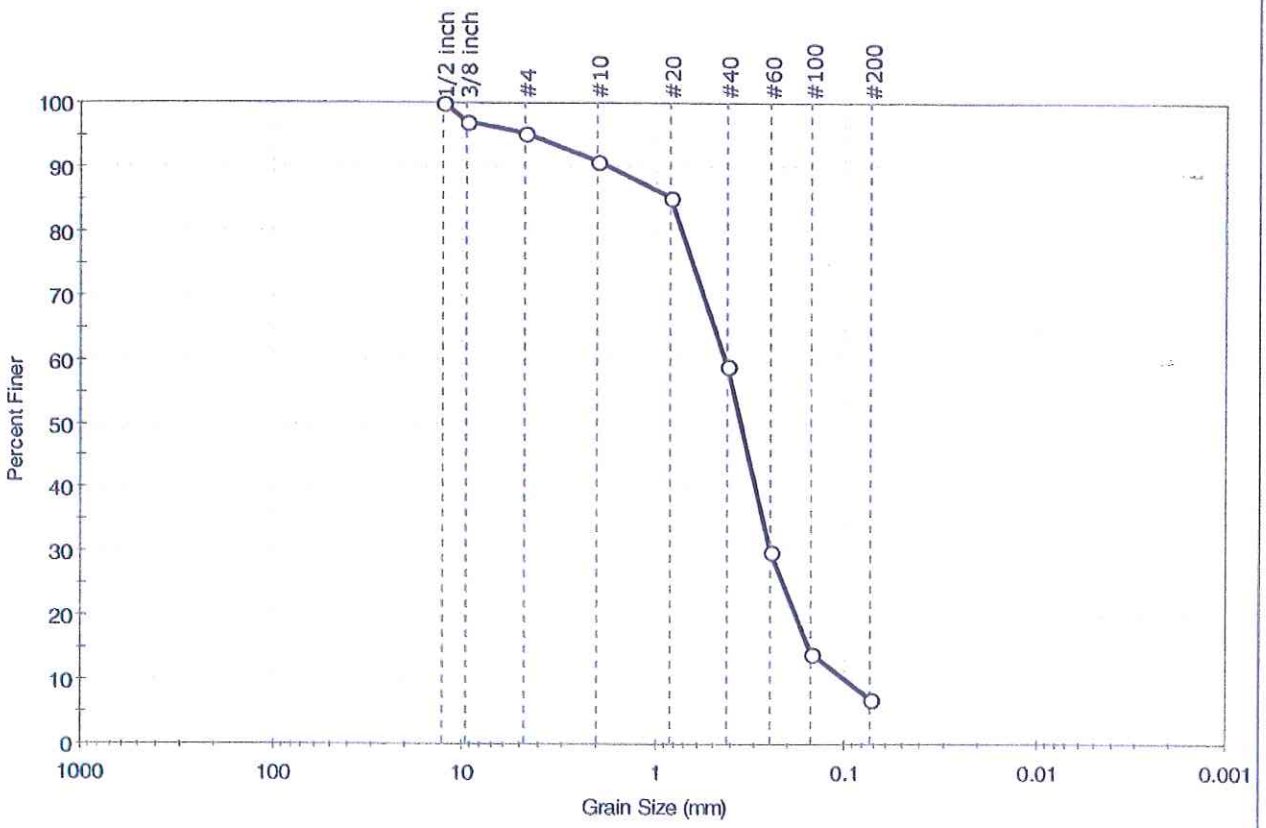

%Cobble	%Gravel	%Sand	%Silt & Clay Size
--	4.7	88.2	7.1

Sieve Name	Sieve Size, mm	Percent Finer	Spec. Percent	Complies
1/2 inch	12.70	100		
3/8 inch	9.51	97		
#4	4.75	95		
#10	2.00	91		
#20	0.84	85		
#40	0.42	59		
#60	0.25	30		
#100	0.15	14		
#200	0.074	7		

Coefficients

D_{85} = 0.8377 mm	D_{30} = 0.2499 mm
D_{60} = 0.4304 mm	D_{15} = 0.1533 mm
D_{50} = 0.3572 mm	D_{10} = 0.0988 mm
C_u = 4.356	C_c = 1.469

Classification

ASTM N/A

AASHTO Fine Sand (A-3 (0))

Sample/Test Description

Sand/Gravel Particle Shape : ANGULAR

Sand/Gravel Hardness : HARD

printed 8/4/2006 11:45:20 AM

GeoTesting express
a subsidiary of Geocomp Corporation

Client:	GEI Consultants				
Project:	Brookhaven National Laboratory				
Location:	Upton, NY			Project No:	GTX-6864
Boring ID:	B-102	Sample Type:	jar	Tested By:	pcs
Sample ID:	S-10	Test Date:	08/04/06	Checked By:	jdt
Depth :	45-47 ft	Test Id:	94489		
Test Comment:	sieve stack 6				
Sample Description:	Moist, light olive brown sand with silt				
Sample Comment:	---				

Particle Size Analysis - ASTM D 422

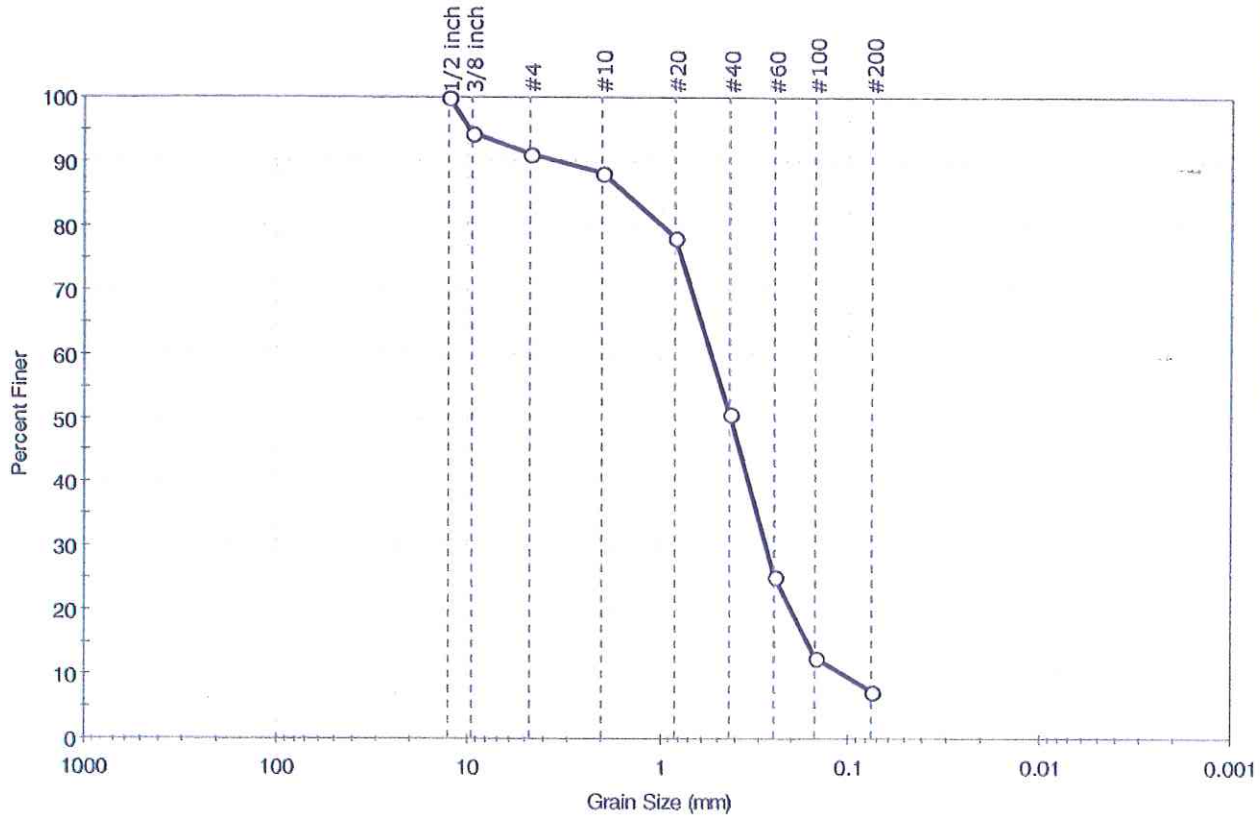

% Cobble	% Gravel	% Sand	% Silt & Clay Size
---	9.0	83.5	7.5

Sieve Name	Sieve Size, mm	Percent Finer	Spec. Percent	Complies
1/2 inch	12.70	100		
3/8 inch	9.51	94		
#4	4.75	91		
#10	2.00	88		
#20	0.84	78		
#40	0.42	51		
#60	0.25	25		
#100	0.15	13		
#200	0.075	7		

Coefficients

D_{85} = 1.5029 mm	D_{30} = 0.2758 mm
D_{60} = 0.5361 mm	D_{15} = 0.1639 mm
D_{50} = 0.4196 mm	D_{10} = 0.1047 mm
C_u = 5.120	C_c = 1.355

Classification

ASTM N/A

AASHTO Fine Sand (A-3 (0))

Sample/Test Description

Sand/Gravel Particle Shape : ANGULAR

Sand/Gravel Hardness : HARD

printed 8/4/2006 11:46:59 AM

GeoTesting express
a subsidiary of Geocomp Corporation

Client:	GEI Consultants				
Project:	Brookhaven National Laboratory				
Location:	Upton, NY			Project No:	GTX-6864
Boring ID:	B-202	Sample Type:	bag	Tested By:	mll
Sample ID:	S-1	Test Date:	05/14/07	Checked By:	jdt
Depth :	1-3 ft	Test Id:	111381		
Test Comment:	---				
Sample Description:	Moist, light olive brown clayey sand				
Sample Comment:	---				

Particle Size Analysis - ASTM D 422-63 (reapproved 2002)

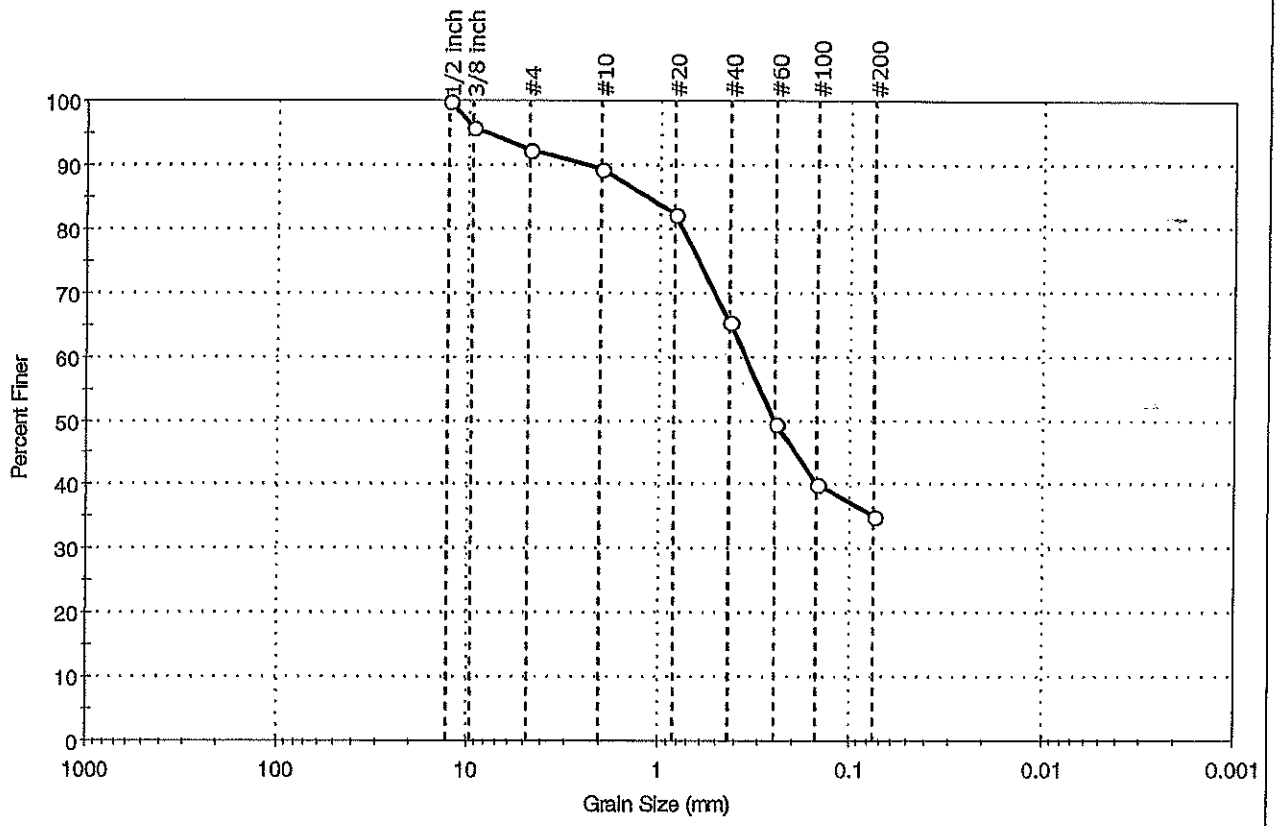

% Cobble	% Gravel	% Sand	% Silt & Clay Size
---	7.7	57.2	35.1

Sieve Name	Sieve Size, mm	Percent Finer	Spec. Percent	Complies
1/2 inch	12.70	100		
3/8 inch	9.51	96		
#4	4.75	92		
#10	2.00	89		
#20	0.84	82		
#40	0.42	65		
#60	0.25	49		
#100	0.15	40		
#200	0.075	35		

Coefficients

D_{85} = 1.1764 mm	D_{30} = N/A
D_{60} = 0.3555 mm	D_{15} = N/A
D_{50} = 0.2544 mm	D_{10} = N/A
C_u = N/A	C_c = N/A

Classification

ASTM N/A

AASHTO Silty Soils (A-4 (0))

Sample/Test Description

Sand/Gravel Particle Shape : ROUNDED

Sand/Gravel Hardness : HARD

printed 5/16/2007 11:49:10 AM

GeoTesting express
a subsidiary of Geocomp Corporation

Client:	GEI Consultants		
Project:	Brookhaven National Laboratory		
Location:	Upton, NY	Project No:	GTX-6864
Boring ID:	B-203	Sample Type: bag	Tested By: mll
Sample ID:	S-3	Test Date: 05/14/07	Checked By: jdt
Depth :	4-6 ft	Test Id: 111382	
Test Comment:	---		
Sample Description:	Moist, light yellowish brown silty sand		
Sample Comment:	---		

Particle Size Analysis - ASTM D 422-63 (reapproved 2002)

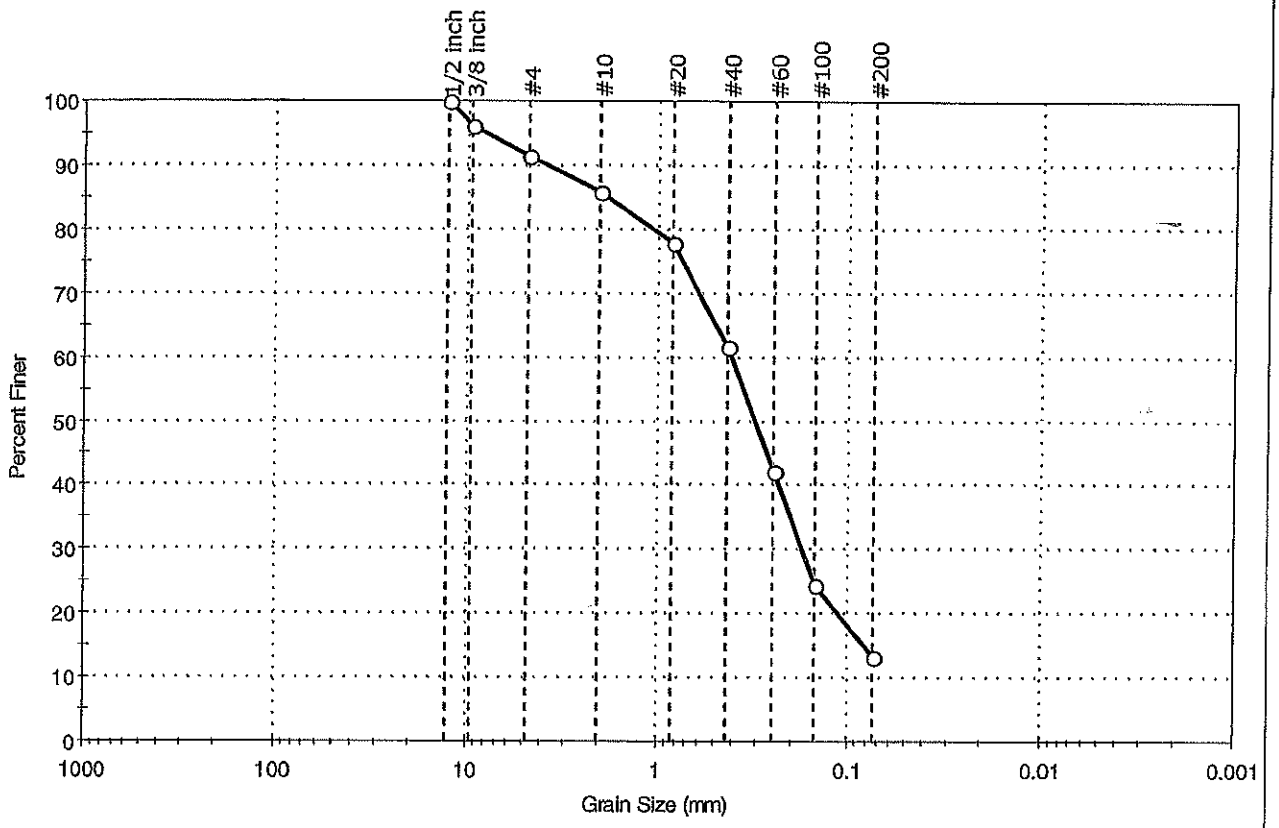

% Cobble	% Gravel	% Sand	% Silt & Clay Size
—	8.6	78.1	13.3

Sieve Name	Sieve Size, mm	Percent Finer	Spec. Percent	Complies
1/2 inch	12.70	100		
3/8 inch	9.51	96		
#4	4.75	91		
#10	2.00	86		
#20	0.84	78		
#40	0.42	62		
#60	0.25	42		
#100	0.15	25		
#200	0.074	13		

Coefficients

D_{85} =1.8062 mm D_{30} =0.1753 mm
D_{60} =0.4064 mm D_{15} =0.0822 mm
D_{50} =0.3087 mm D_{10} =0.0601 mm
C_u =N/A C_c =N/A

Classification

ASTM N/A

AASHTO Silty Gravel and Sand (A-2-4 (0))

Sample/Test Description

Sand/Gravel Particle Shape : ROUNDED

Sand/Gravel Hardness : HARD

printed 5/16/2007 11:49:31 AM

GeoTesting express
a subsidiary of Geocomp Corporation

Client:	GEI Consultants				
Project:	Brookhaven National Laboratory				
Location:	Upton, NY			Project No:	GTX-6864
Boring ID:	B-204	Sample Type:	bag	Tested By:	mll
Sample ID:	S-1	Test Date:	05/14/07	Checked By:	jdt
Depth :	0-2 ft	Test Id:	111383		
Test Comment:	---				
Sample Description:	Moist, olive brown silty sand				
Sample Comment:	---				

Particle Size Analysis - ASTM D 422-63 (reapproved 2002)

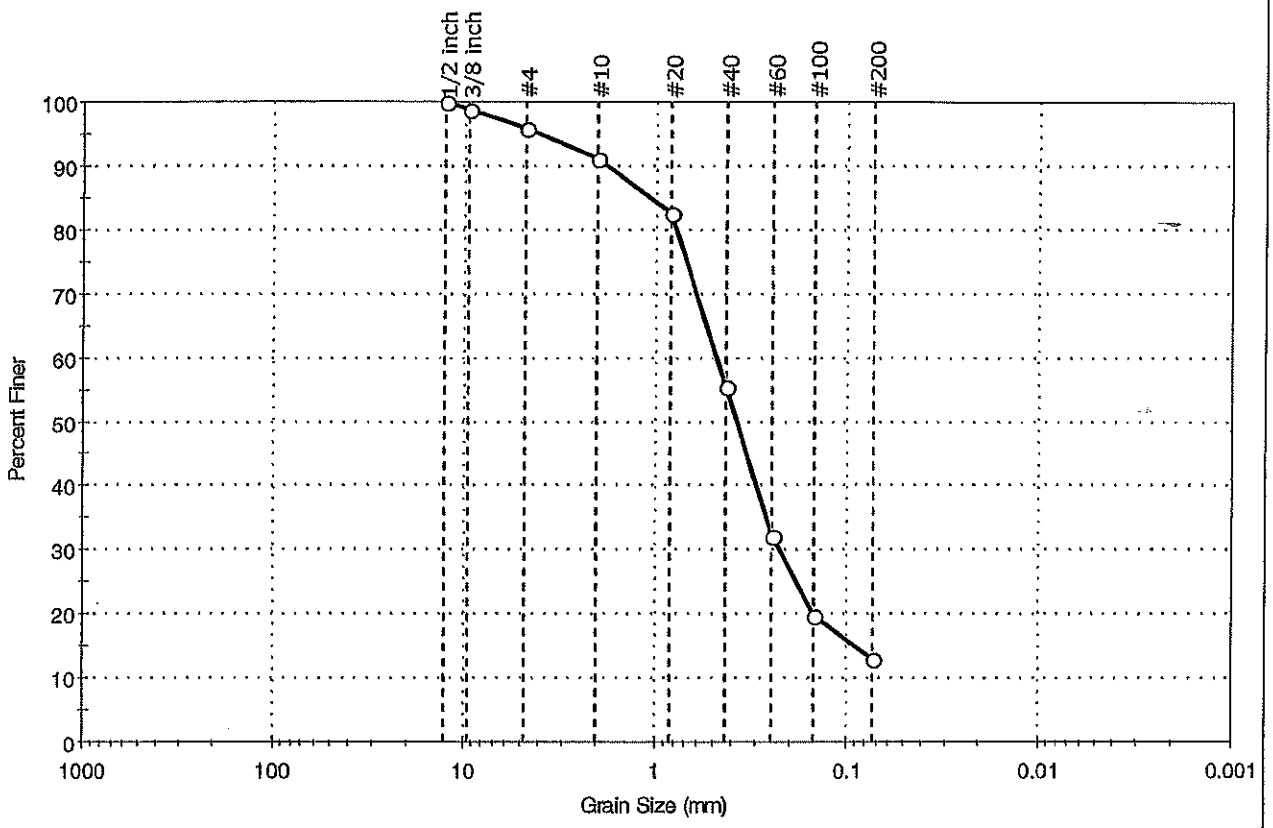

% Cobble	% Gravel	% Sand	% Silt & Clay Size
---	4.1	82.9	13.0

Sieve Name	Sieve Size, mm	Percent Finer	Spec. Percent	Complies
1/2 inch	12.70	100		
3/8 inch	9.51	99		
#4	4.75	96		
#10	2.00	91		
#20	0.84	83		
#40	0.42	55		
#60	0.25	32		
#100	0.15	20		
#200	0.074	13		

Coefficients

D_{85} = 1.0741 mm D_{30} = 0.2279 mm
D_{60} = 0.4772 mm D_{15} = 0.0912 mm
D_{50} = 0.3755 mm D_{10} = 0.0544 mm
C_u = N/A C_c = N/A

Classification

ASTM N/A

AASHTO Silty Gravel and Sand (A-2-4 (0))

Sample/Test Description

Sand/Gravel Particle Shape : ROUNDED

Sand/Gravel Hardness : HARD

printed 5/16/2007 11:49:50 AM

GeoTesting express
a subsidiary of Geocomp Corporation

Client:	GEI Consultants				
Project:	Brookhaven National Laboratory				
Location:	Upton, NY			Project No:	GTX-6864
Boring ID:	B-206	Sample Type:	bag	Tested By:	mll
Sample ID:	S-4	Test Date:	05/15/07	Checked By:	jdt
Depth :	6-8 ft	Test Id:	111385		
Test Comment:	---				
Sample Description:	Moist, reddish brown silty sand				
Sample Comment:	---				

Particle Size Analysis - ASTM D 422-63 (reapproved 2002)

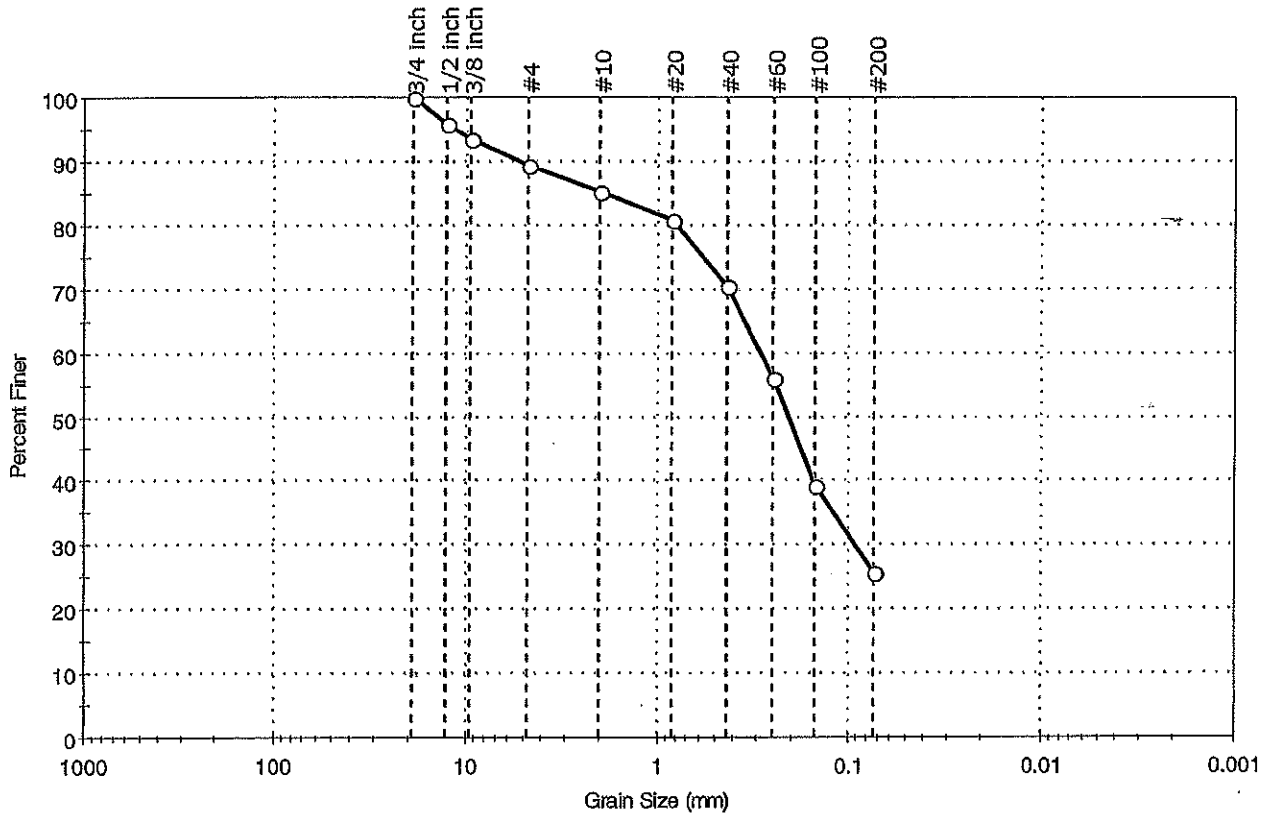

%Cobble	%Gravel	%Sand	%Silt & Clay Size
—	10.6	63.8	25.6

Sieve Name	Sieve Size, mm	Percent Finer	Spec. Percent	Compiles
3/4 inch	19.00	100		
1/2 inch	12.70	96		
3/8 inch	9.51	93		
#4	4.75	89		
#10	2.00	85		
#20	0.84	81		
#40	0.42	70		
#60	0.25	56		
#100	0.15	39		
#200	0.074	26		

Coefficients

D_{85} =1.8829 mm	D_{30} =0.0928 mm
D_{60} =0.2898 mm	D_{15} =N/A
D_{50} =0.2083 mm	D_{10} =N/A
C_u =N/A	C_c =N/A

Classification

ASTM N/A

AASHTO Silty Gravel and Sand (A-2-4 (0))

Sample/Test Description

Sand/Gravel Particle Shape : ROUNDED

Sand/Gravel Hardness : HARD

printed 5/16/2007 11:50:18 AM

GeoTesting express
a subsidiary of Geocomp Corporation

Client:	GEI Consultants		
Project:	Brookhaven National Laboratory		
Location:	Upton, NY	Project No:	GTX-6864
Boring ID:	B-204	Sample Type: bag	Tested By: mll
Sample ID:	S-5	Test Date: 05/14/07	Checked By: jdt
Depth :	8-10 ft	Test Id: 111384	
Test Comment:	---		
Sample Description:	Moist, light olive brown silty sand with gravel		
Sample Comment:	---		

Particle Size Analysis - ASTM D 422-63 (reapproved 2002)

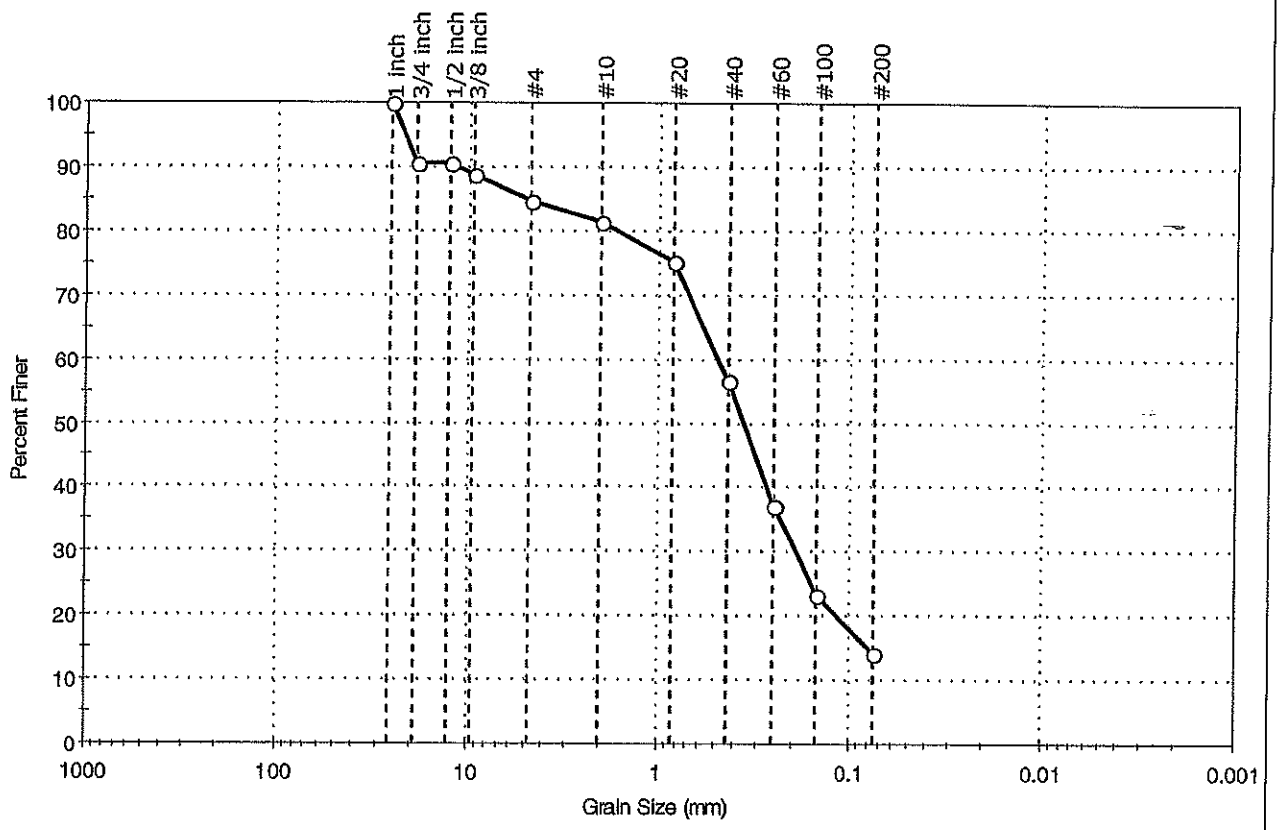

% Cobble	% Gravel	% Sand	% Silt & Clay Size
–	15.4	70.5	14.1

Sieve Name	Sieve Size, mm	Percent Finer	Spec. Percent	Complies
1 inch	25.70	100		
3/4 inch	19.00	91		
1/2 inch	12.70	91		
3/8 inch	9.51	89		
#4	4.75	85		
#10	2.00	81		
#20	0.84	75		
#40	0.42	57		
#60	0.25	37		
#100	0.15	23		
#200	0.075	14		

Coefficients

D_{85} =5.0799 mm	D_{30} =0.1913 mm
D_{60} =0.4813 mm	D_{15} =0.0804 mm
D_{50} =0.3543 mm	D_{10} =0.0552 mm
C_u =N/A	C_c =N/A

Classification

ASTM N/A

AASHTO Silty Gravel and Sand (A-2-4 (0))

Sample/Test Description

Sand/Gravel Particle Shape : ROUNDED

Sand/Gravel Hardness : HARD

printed 5/16/2007 12:11:01 PM

Appendix A2

Preliminary Vibration and Acoustic Report
September 15, 2006

Colin Gordon & Associates, Inc.

NSLS II Vibration and Acoustic Criteria

Vibration – Experiment Hall

The vibration limits of the experiment hall are those associated with the user-supplied research instruments, which are not well defined at this time. It may only be possible to represent the vibration requirements of this space using generic vibration criteria. The vibration needs of the vast majority of research equipment available today would be satisfied by a floor meeting vibration criterion VC-E or NIST-A.[1] At frequencies less than 20 Hz, the NIST-A criterion is more stringent than VC-E.

Vibration – Storage Ring

The vibration requirements for the storage ring have been provided in a much different manner. The RMS amplitude[2], *R*, is to be less than 20 to 30 nm, where *R* is defined as

$$R = \sqrt{\sum_{f=50}^{f=4} \Delta(f) \times \delta f}$$

where $\Delta(f)$ is the displacement power spectral density spectrum (in units such as m^2/Hz, where the frequency term in the denominator is the measurement bandwidth) and δf is the frequency resolution of the spectrum. The lower and upper bounds of the summation are 4 and 50 Hz, respectively. Frequency components outside this range may be neglected. The vibrations associated with fluid flow should meet the condition $R < 20$.

Acoustic Noise

The facility will have two primary groups of noise sources: (1) the facility's mechanical systems, such as air handlers, and (2) the user-provided research equipment. The noise control associated with the first group is within the purview of the NSLS II design team, but the ability to mitigate noise associated with the second group is somewhat limited. It can be anticipated via passive room noise control measures incorporated into the design, but it cannot be controlled via mechanical constraints such as airflow velocities, fan selection, or silencers, concepts typically employed for the first group.

Studies carried out during the design of the Advanced Photon Source determined that final operational room noise in the Experiment Hall would be a mix of sound from both groups of sources, and that NC-60 to NC-65 would be achievable from a combination of

---

[1] Vibration criteria VC-E and NIST-A are defined in **H. Amick**, M. Gendreau, T. Busch, and C. Gordon, "Evolving criteria for research facilities: vibration," *Proceedings of SPIE Conference 5933: Buildings for Nanoscale Research and Beyond*, San Diego, CA. Criterion VC-E has a one-third octave band rms velocity amplitude of 125 microinches/sec at frequencies between 1 and 100 Hz. Criterion NIST-A has a one-third octave band rms displacement amplitude of 1 microinch at frequencies between 1 and 20 Hz and a one-third octave band rms velocity amplitude of 125 microinches/sec at frequencies between 20 and 100 Hz.

[2] Simply stated, *R* is the area under the displacement PSD spectrum (m^2/Hz) between a lower and upper bound frequency.

mechanical system noise control measures on the proposed air handling system and room absorption made part of walls and ceiling.[3] This is the noise range found in many industrial cleanrooms. In the absence of absorptive material, the noise at APS was predicted to be on the order of NC-70. In order to achieve this, the recommended noise goal of the mechanical systems alone is NC-50 to NC-55.

[3] The results of the study were reported in "Acoustical Evaluation of Experiment Hall: Argonne National Laboratory", A. M. Yazdanniyaz & S. K. Bui, Acentech Report No. 56, January 1991. The noise from the experimental equipment was included in the model via sound power estimates based on measurements made at NSLS in 1989 by Acentech Incorporated as part of the APS design effort, reported in "Measurement of Noise and Vibration: National Synchrotron Light Source, Brookhaven National Laboratory", Hal Amick & Colin G. Gordon, Acentech Report No. 11, June 1989.

Site Vibration Study

Figure 1 shows an aerial photograph of the portion of the BNL complex containing the NSLS II site. Nearby are the site of the Center for Functional Nanomaterials (CFN), now under construction, and the existing NSLS. Vibrations were measured at all of these locations, as well as at Location 'A' and at a remote location to the north east of the indicated portion of the BNL campus.

Figure 2 shows a plan view of the proposed NSLS II, indicating Locations 1-6 at which ambient vibration measurements were made on the afternoon of 14 June 2006.[1] Vibrations were measured at each of these locations in each of three principal directions (vertical, north-south, and east-west). Each measurement lasted approximately two minutes, and produced an energy-averaged constant-bandwidth (FFT) rms velocity spectrum with 400 data points, 0-100 Hz frequency range, Hanning windowing, and 90% overlapping. The sensor, a seismic accelerometer, was supported on a 12" steel stake with a flat top, driven into the ground such that the flat top was flush with the ground.

The data were analyzed "live" and saved as spectra to the internal memory of the portable analyzer. The spectra were downloaded to a laptop computer and subsequently post-processed to obtain one-third octave band velocity spectra and 400-line displacement power spectral density (PSD) spectra. The PSD spectra, in turn, were processed to calculate RMS displacement amplitudes using numerical summing between a lower-frequency cutoff (CO) and 50 Hz. Nominally, the lower cutoff was 4 Hz for consistency with the particle ring criterion.

As noted previously, the nominal lower cutoff was 4 Hz for consistency with the particle ring criterion. However, in some cases the spectra below 6-7 Hz was contaminated by instrumentation noise floor. As a result, all of the RMS amplitudes are reported with low-frequency cutoff of 4, 6 and 8 Hz.

Figure 2(a) and (b) show a statistical representation of the vertical and horizontal vibrations, respectively, at the NSLS II site, in terms of one-third octave band rms velocity. These measurements were made during the mid-afternoon. Shown for reference are the VC-E and NIST-A criteria.

It should be noted in Figure 2 that the vibrations easily meet VC-E, but do not meet the NIST-A requirement. A similar observation was made at the time of the CFN vibration survey, and an additional study (using measurements at Location 'A') demonstrated that the low-frequency component which exceeds NIST-A disappears at night, and is thought to be due to traffic, probably on the Long Island Expressway.

The daytime and nighttime measurements at Location 'A' are represented in Figure 4 by open and closed triangles, respectively. At frequencies of 20 Hz and greater, the

[1] At the suggestion of BNL personnel, vibrations were not measured in the wooded areas, in order to avoid ticks.

difference is visible though not as significant as that observed at frequencies near 4 Hz. The log mean of the vertical vibrations at the NSLS II site, represented in Figure 4 using diamond symbols, lies between the two Location 'A' spectra at frequencies of 10 Hz and less.

The data from the NSLS II measurement locations, as well as from Location 'A', were taken with the sensor supported on a steel stake. It is known that a "free-field" measurement made in this manner produces a spectrum with a higher amplitude at most frequencies than one made on a slab of significant size or inside a building.[2] Discussions of this effect in the context of the NSLS II measurements suggested the desirability of carrying out vibrations inside a building with a similar thick slab, at night when the vibrations were at their least. The vertical spectrum obtained in this manner in the partially-completed microscopy suite in CFN is shown with circle symbols, and is thought to be representative of the performance of the eventual nighttime performance of the Experiment Hall slab in NSLS II.

The constant-bandwidth FFT velocity spectra saved to the portable analyzer and downloaded to a spreadsheet on a laptop were transformed to rms displacement spectra by dividing each point in a spectrum by 2π times the frequency of that point. The rms displacement spectra were then transformed to displacement PSD spectra by squaring the amplitude and dividing each squared amplitude by the measurement bandwidth (0.375 Hz). The statistical displacement PSD spectra are shown in Figure 5(a) and (b), for vertical and horizontal vibration, respectively. The log mean (the heavier red line) will be used for comparative purposes in a discussion that will follow.

As noted previously, the vibration criterion for the ring is defined in terms of R, the area beneath the PSD spectrum $\Delta(f)$ between cutoff frequencies f_1 and f_2, defined as 4 and 50 Hz, respectively. For the discrete spectra being used in this study, this may be defined as

$$R = \sqrt{\sum_{f_2=50}^{f_1=4} \Delta(f) \times \delta f}$$

where δf is the frequency resolution of 0.25 Hz. However, it was observed during post-processing that some of the spectra were contaminated by system noise at low frequencies (found after the fact to be due to connection noise in a cable), so values of R were calculated using additional f_1 frequencies of 6 and 8 Hz. The R values are summarized for the NSLS II site in Table 1. When the lower cutoff frequency f_1 is set to 4 Hz, the RMS quantities do not meet the criterion of 30 nm specified by BNL, but when f_1 is increased to 6 Hz, the quantity is within the prescribed limits. As noted previously, the PSD content at frequencies below 6 or 7 Hz is thought to be due to system noise, not actual vibration.

---

[2] H. Amick, T. Xu, and M. Gendreau, "The Role of Buildings and Slabs-on-Grade in the Suppression of Low-Amplitude Ambient Ground Vibrations," *Proc. 11th Intl. Conf. on Soil Dyn. & Earthquake Engng. (11th ICSDEE) & the 3rd Intl. Conf. on Earthquake Geotech. Engng. (3rd ICEGE)*, 7-9 January, 2004, Berkeley, CA.

Supplemental measurements were carried out on 31 Aug 2006 and 1 Sept 2006. The results of those measurements, along with some taken at Location 'A' for the CFN site study, are summarized in Table 2. The most important data are likely those taken in the microscopy lab at CFN, where the RMS amplitudes at both measurement times are 20 nm or less, in any direction. (The amplitudes calculated using 6 Hz and 8 Hz cutoff frequencies are shown for interest, but the CFN space meets the most stringent interpretation of the NSLS II criterion. This demonstrates that the building effect impacts the RMS amplitude, as well as the one-third octave band spectrum (shown in Figure 4).

Vibrations were measured on the floor at Beam Line X1 in NSLS, around midnight, to provide a comparison with the vibrations measured in CFN. These results are also shown in Table 2, as Location 9. The difference between the two is quite dramatic, 71 nm for NSLS compared to 20 nm in CFN. (The same low-noise setup was used in both cases.)

BNL provided collected PSD spectra measured at several other light source facilities. The log mean PSD for the NSLS II site are shown superimposed on these data in Figure 6. The arrow indicates the NSLS II spectrum. It should be noted that the data from other facilities represent several different quantities of data points (the present data containing 200 points between 0 and 50 Hz) and quantity of averages. Either a smaller number of data points or a greater number of averages (or both) will produce a smoother spectrum. (For example, the vertical PSD spectrum from ESRF (shown in red) contains a very large number of data points, but most likely resulted from less than five spectra being averaged.) However, it is the fundamental nature of PSD spectra that spectral amplitude of stationary random vibration is roughly independent of bandwidth.

The data in Figure 6 initially suggest a rather unfavorable comparison between the NSLS II site and the other light sources. This was one of the reasons that nighttime data were subsequently measured in NSLS and CFN, such that the presence of a building could be taken into consideration, and at a remote location on the BNL property, so that proximity to the campus energy sources could be removed from consideration.

Data measured at the following locations were used for comparison:

- Microscopy suite of CFN, under construction
- Foundation of a light standard near CFN, prior to installation of the pole; this may be considered a "free-field" location, unstiffened by the presence of the building
- The floor of NSLS, directly beneath Beam Line X1 in the Experiment Hall
- A remote location near the northeast corner of BNL campus, on a hard surface at the center of a fire access road

Figure 7 shows the vertical Log Mean of site vibrations at NSLS II site (red curve marked by red arrow), expressed as PSD, compared with similar data from ALS, ESRF and SPRING-8 (using data provided by BNL). Shown also are PSD spectra measured at NSLS Beam Line X1 just after midnight, the "free-field" location near CFN, and the microscopy suite at CFN (identified by the black arrow). The vertical red dashed line

indicates 4 Hz. The legend indicates the RMS amplitude using summation between 4 and 50 Hz, except for the NSLS II log mean, which is summed with a 6 Hz lower cutoff.

The vibrations near Beam Line X1 lie well above all the others, particularly at frequencies associated with rotating mechanical equipment, such as 18 Hz and 30 Hz. The data from the CFN microscopy suite lies below all the other BNL locations and ties with ALS for the -lowest RMS amplitude, at 20 nm.

Figure 8 compares the "best" BNL location—the CFN microscopy suite—with Location 'A' measured night using a stake and with the remote location simply measured on a road surface at noon. In this comparison, the remote location lies somewhat higher than the CFN spectrum at frequencies less than 8 Hz, but lies well below it at frequencies between 10 and 25 Hz. Recall from Figure 4 that there was a reduction factor of 3 to 5 times (in terms of amplitude) at frequencies below 8 Hz. In terms of power (i.e., PSD) this reduction factor becomes 9 to 25 times, which would suggest that the *surface* nighttime vibration at the remote location is less than that inside CFN, and would be lower yet inside a building at that location. Even though vibrations were not measured at night at the remote location, it is suggested that there is a cultural effect in the diurnal vibrations on the BNL campus, and that a remote site farther from the utility plant and the expressway might be worthy of consideration as design progresses.

The vibration study indicates that following the installation of the ring structure and experiment hall, which will significantly stiffen the site, the vibration environment will be comparable to that of other light source facilities. Additional modeling studies are recommended as the design progresses to examine the building and slab effect in greater detail, as much of the published experience deals with rectangular buildings, rather than toroidal. The dynamics are likely to differ to some extent.

Greater insight would be gained from carrying out a continuous vibration survey of 24 hours or more, in order to better document the diurnal variation of vibration at the site. This could be done at the ring site, using simultaneous multiple recording locations distributed around the ring. With data taken simultaneously, it may be possible to glean additional insight into the mechanism(s) and source(s) involved in the vibrations between 1 and 10 Hz.

The researchers may also benefit from a statistical representation of the temporal variation of vibration.[3]

[3] This is discussed at length in H. Amick, M. Gendreau, & N. Wongprasert, "Centile spectra, measurement times, and statistics of ground vibration," *Proceedings of the Second International Symposium on Environmental Vibrations: Prediction, Monitoring, Mitigation and Evaluation (ISEV2005)*, Okayama University, Okayama, Japan (20 to 22 September 2005)

Table 1. Summary of RMS amplitudes at NSLS II site, mid-afternoon

Location	Position		Vertical			North-South			East-West		
		f_1:	4 Hz	6 Hz	8 Hz	4 Hz	6 Hz	8 Hz	4 Hz	6 Hz	8 Hz
1	8 o'clock		69	29	23	45	23	19	35	24	21
2	10 o'clock		52	29	24	37	25	22	42	28	25
3	11 o'clock		43	26	20	30	20	17	29	19	16
4	1 o'clock		44	30	26	34	25	21	33	25	21
5	2 o'clock		36	26	22	30	23	21	46	36	33
6	7 o'clock		30	21	18	26	16	12	26	13	10

Table 2. Summary of RMS amplitudes at supplemental locations, various times

Location	Description	Time		Vertical			North-South			East-West		
			f_1:	4 Hz	6 Hz	8 Hz	4 Hz	6 Hz	8 Hz	4 Hz	6 Hz	8 Hz
7	Microscopy Lab in CFN	730pm		20	15	14	12	8	7	19	9	7
		1120pm		20	14	13	11	6	5	13	7	6
8	Free-Field, Foundation of Light Standard at CFN	1140pm		24	19	17	41	37	35	38	35	34
9	Beam Line X1 at NSLS	Midnight		71	48	42	12	9	8	13	9	7
10	Remote Site, on Wellhead	Noon		24	12	8	27	16	15	33	15	10
11	Remote Site, on Road	Noon		21	9	6	25	14	12	26	12	9
12	Location "A"	315pm		80	53	46						
		1030pm		35	29	27						

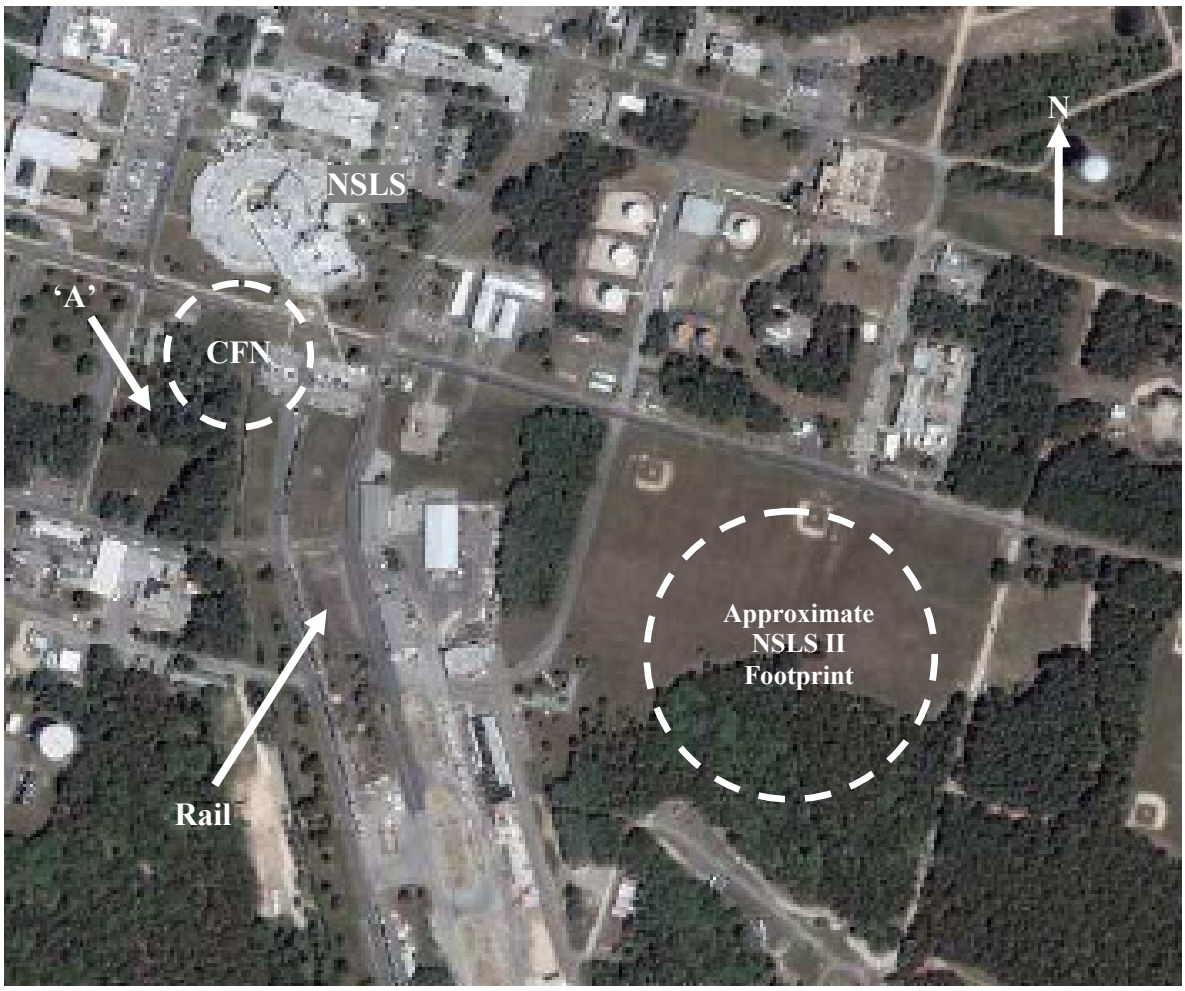

Figure 1. Aerial photograph of a portion of BNL showing approximate location for NSLS II and other relevant locations

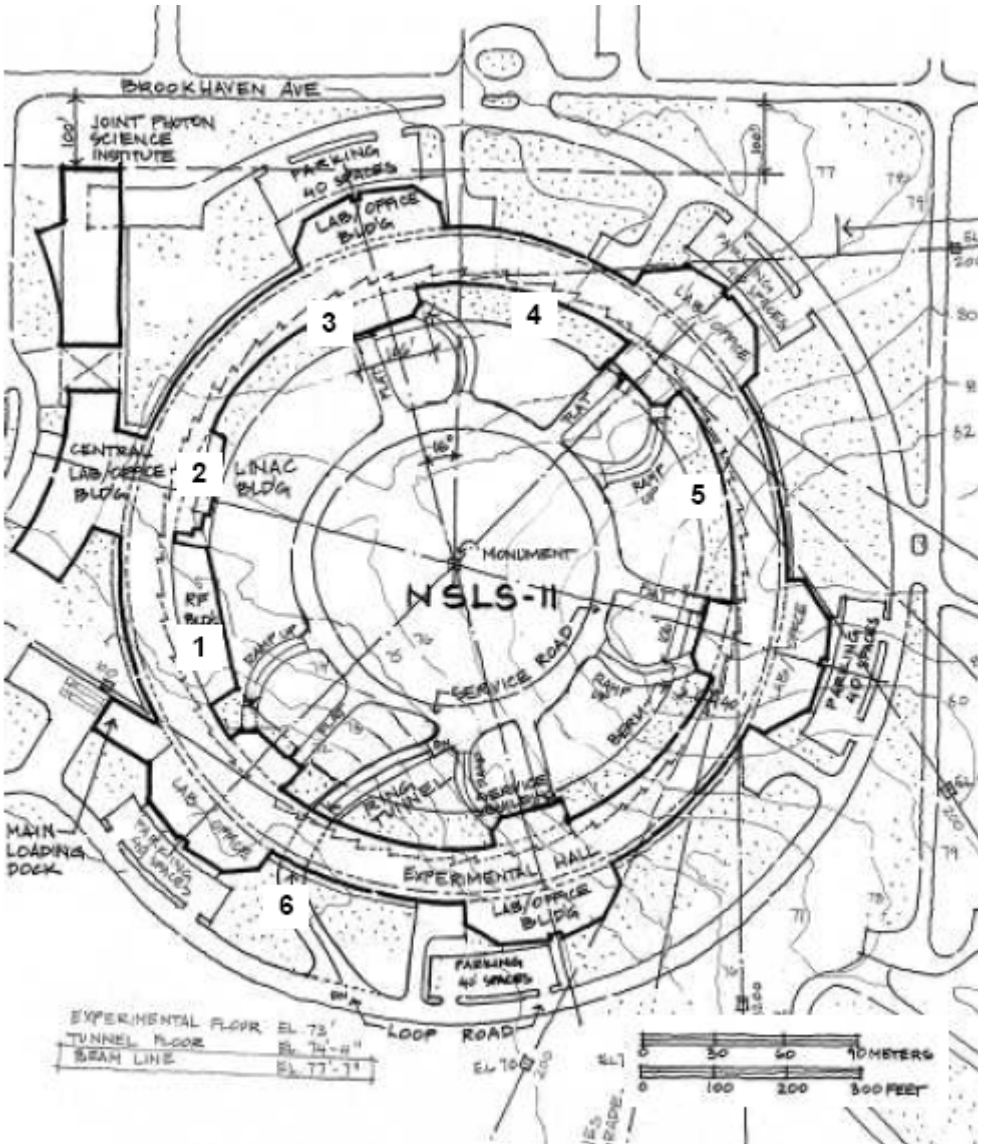

Figure 2. Site plan showing approximate location of NSLS II and the measurement locations used in this study

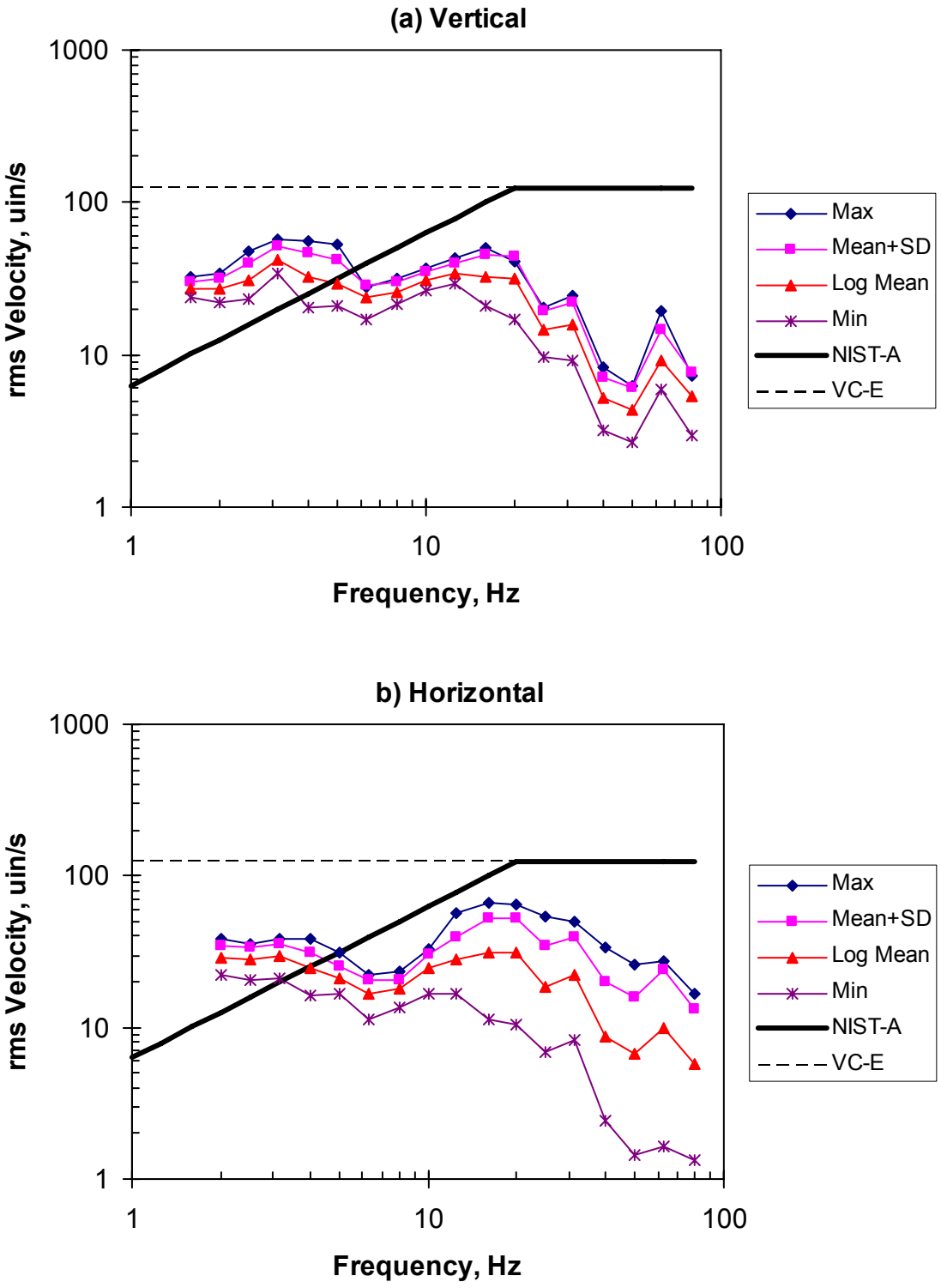

Figure 3. Statistical representation of daytime ambient site vibrations at Locations 1-6, NSLS II site

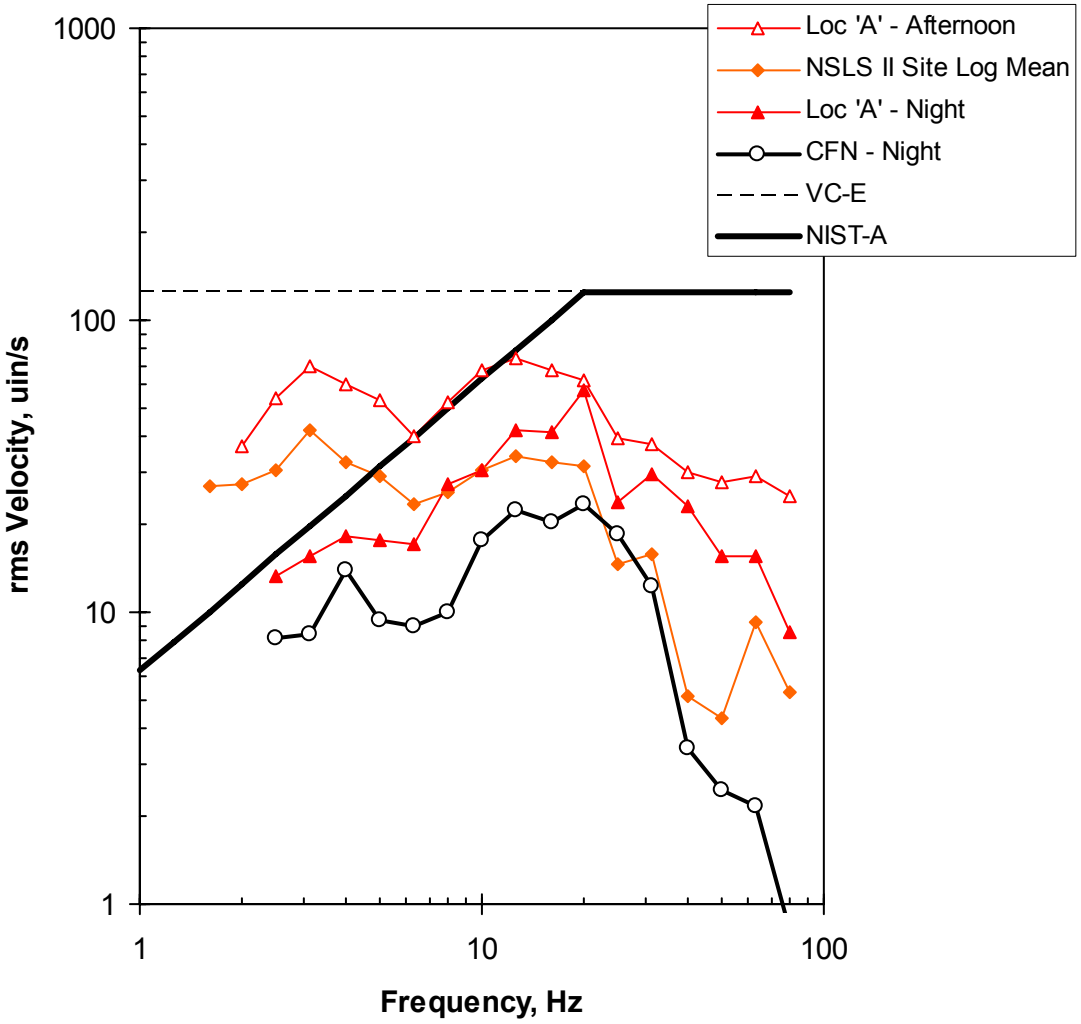

Figure 4. Comparison of one-third octave band vibrations at the NSLS II site, Location 'A', and at night in the CFN microscopy suite.

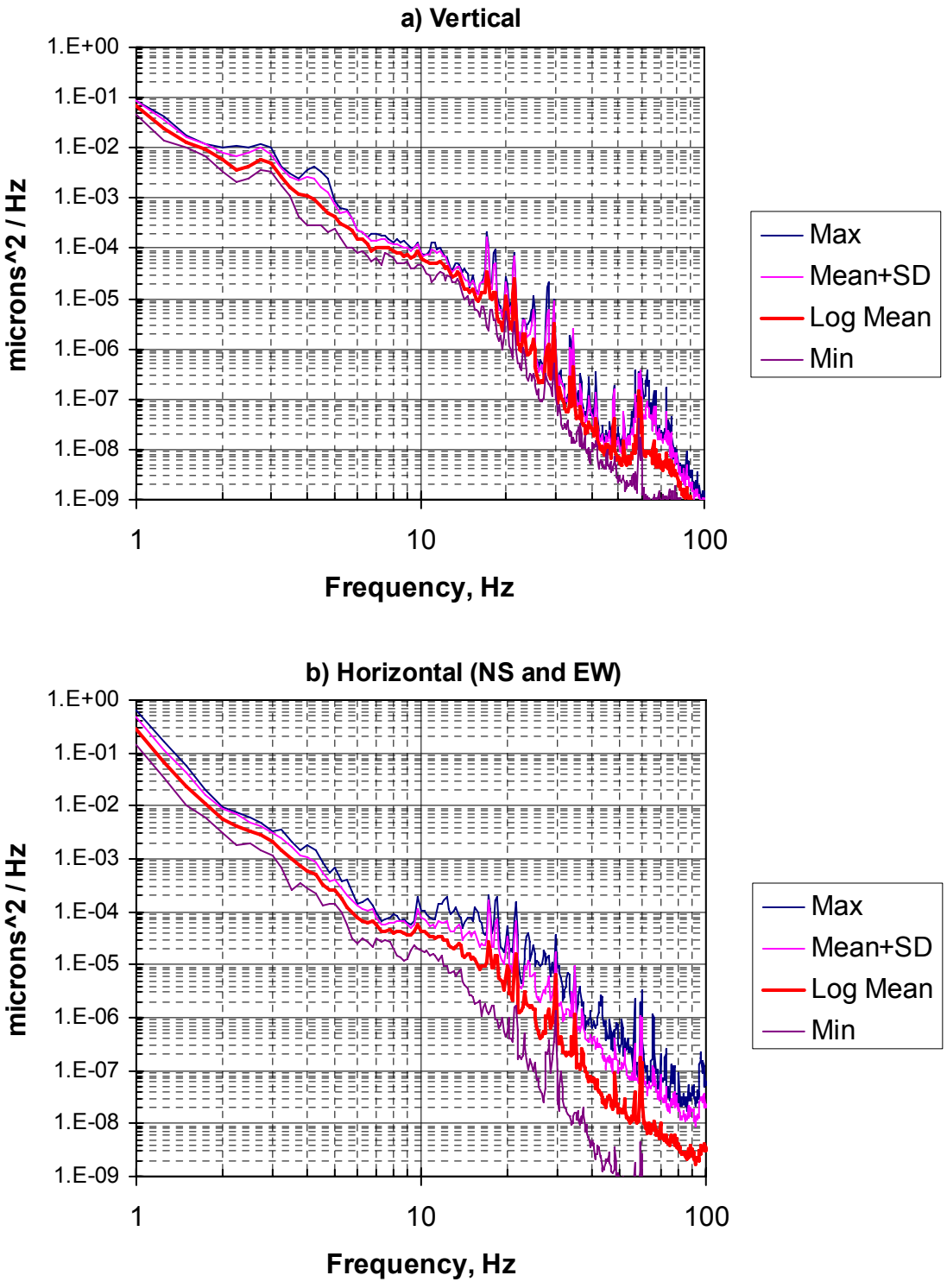

Figure 5. Statistical representation of daytime ambient site vibrations at Locations 1-6, NSLS II site, in terms of displacement power spectral density (PSD), 1-100 Hz

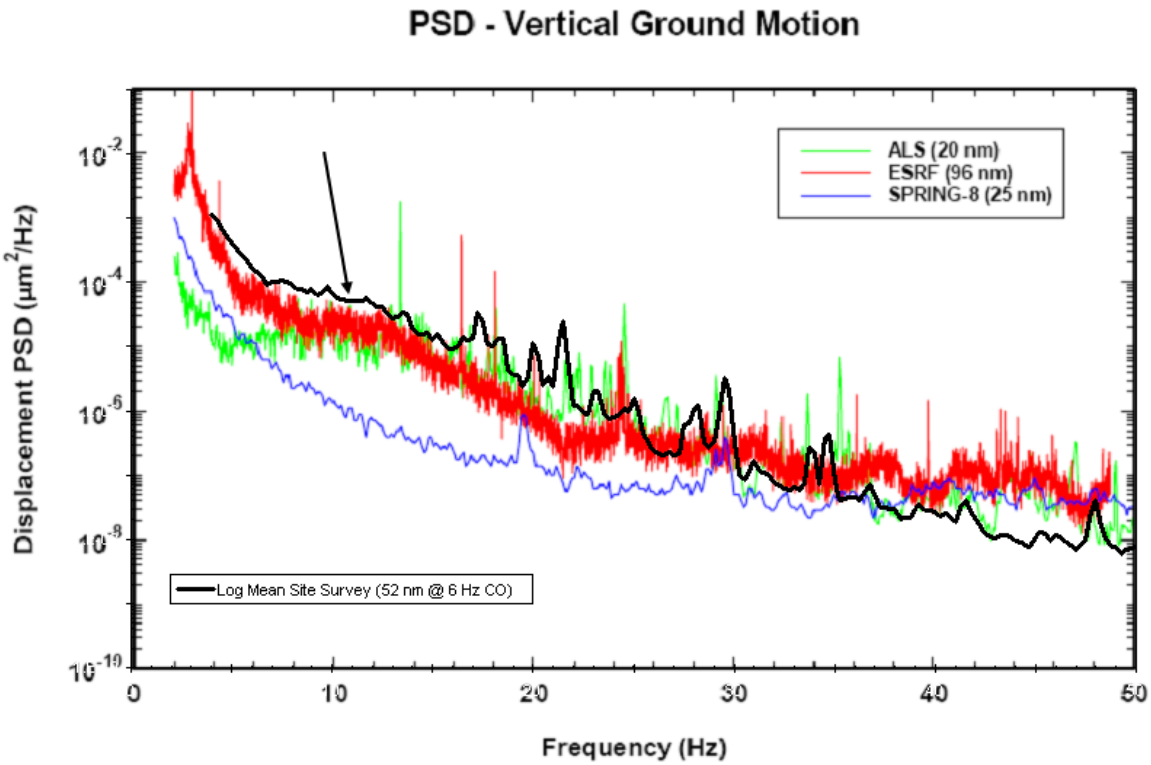

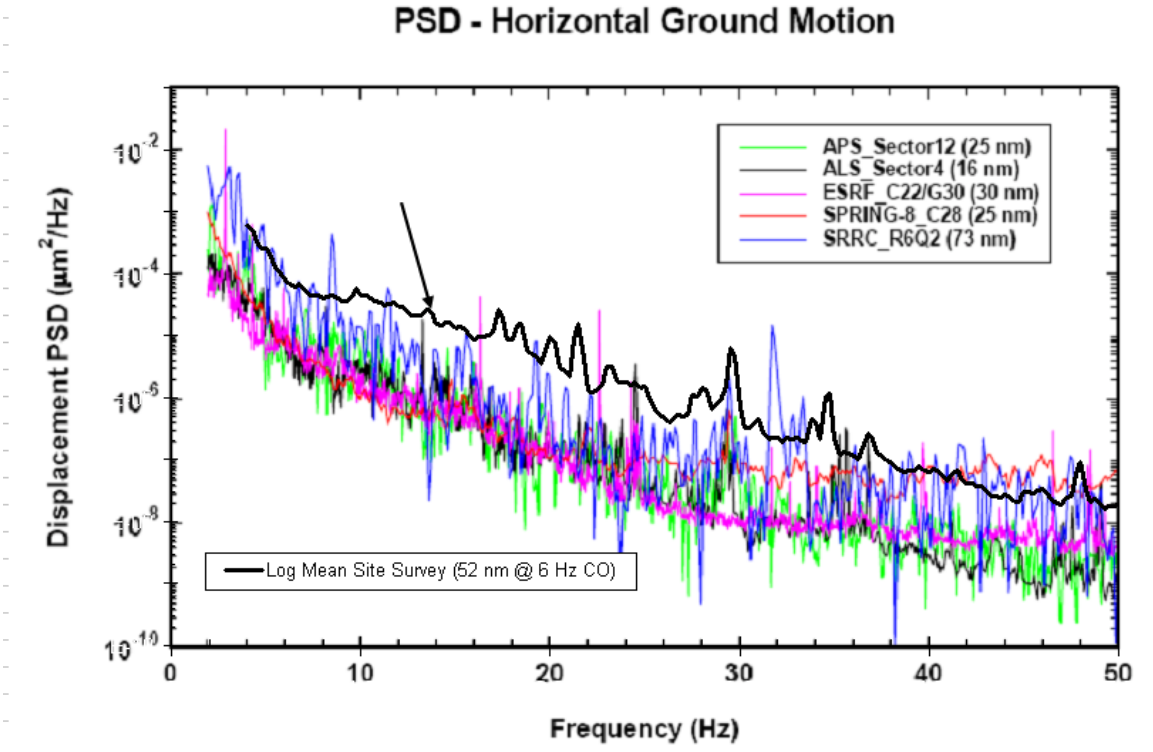

Figure 6. Log Mean of site vibrations at NSLS II site, expressed as PSD, compared with other sites (data for other sites provided by BNL)

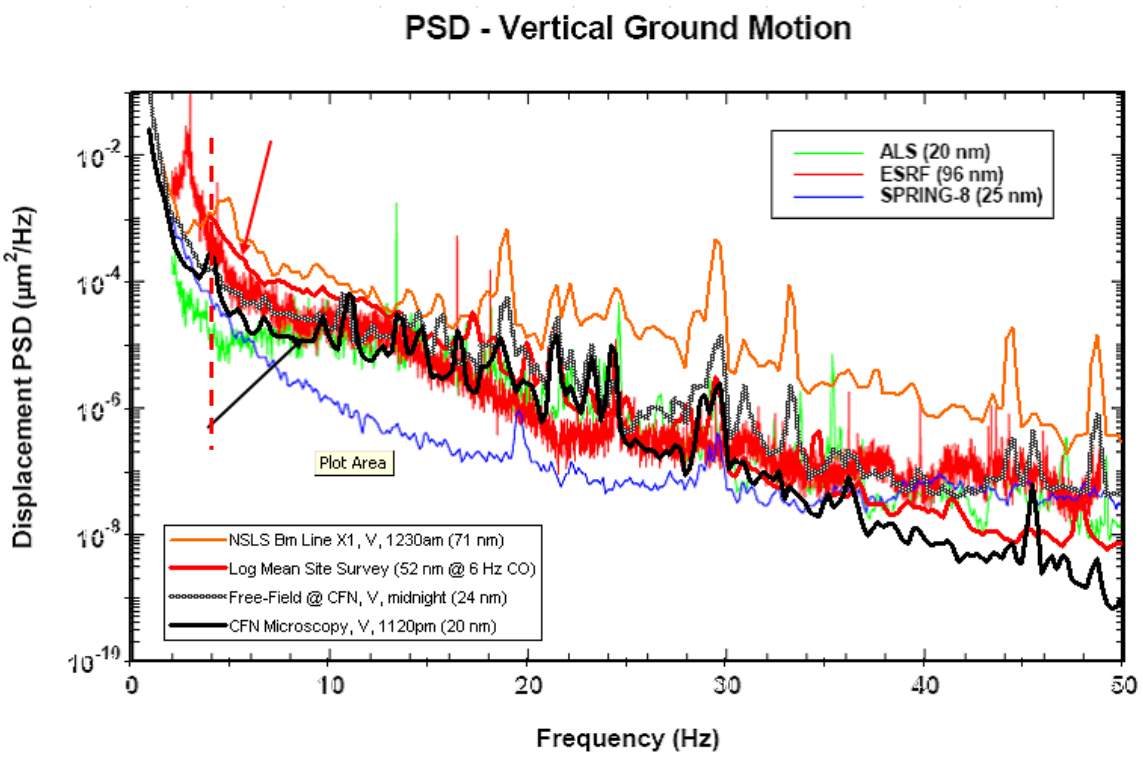

Figure 7. Log Mean of site vibrations at NSLS II site, expressed as PSD, compared with other sites (data for other sites provided by BNL) and with NSLS Beam Line X1, Free-Field at CFN, and the microscopy suite at CFN.

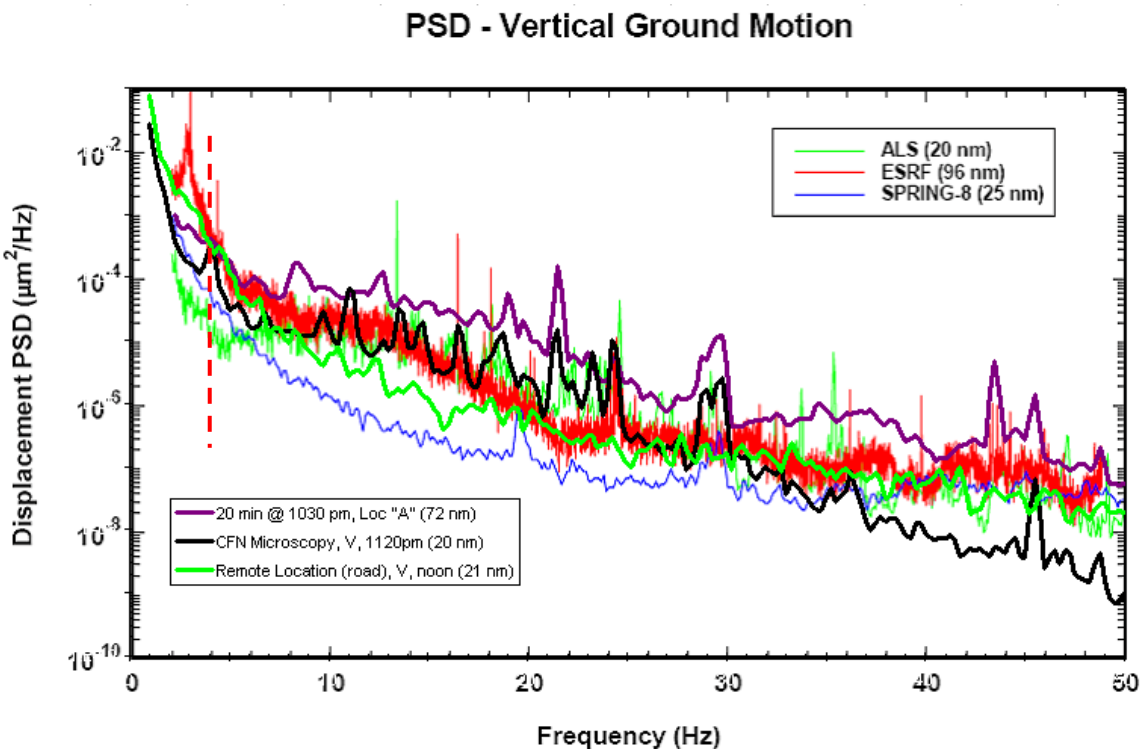

Figure 8. Comparison of PSD vibrations at three alternate reference locations, including Location 'A' and CFN Microscopy, both at night, and the remote location at noon.

Vibration and Acoustic Design Issues

Utility Distribution

Two utility concepts were examined during the course of this review. One was a distributed system along the lines of that used for APS, where the air handlers are placed at locations around the ring, perhaps along the outside of the experiment hall as at APS. The other concept was a centralized system, where the air handlers are placed at a central location and air distribution is via ducting. Each approach offers arguments pro and con, but examination of the issues specific to BNL philosophy and the proposed NSLS II layout led toward the centralized system.

From a vibration perspective, the difference between the two concepts lies in the amount of energy present in a concentrated area. (The distributed system works with a larger quantity of smaller air handlers, thus the maximum horsepower at any location near the ring is less, so there is a lower risk in placing the units closer to the ring.) However, a centralized system offers maintenance benefits, and the primary vibration control design issues become those of distance and conservative vibration isolation. It is important to maximize the distance between the air handlers themselves and the ring, though this will affect energy efficiency. A careful study of tradeoff between these two variables is recommended as design progresses.

A preference has been expressed to avoid vibration isolation on piping and ducting as much as possible. An important reason for this is that isolation works on the concept of exploiting a low resonance frequency of a sprung mass (the duct or pipe on a spring) and the random vibration energy in the duct or pipe is shifted to very low frequencies. Because the ring is sensitive to displacement, particularly at low frequencies, this is not a desirable feature. The alternatives for vibration control include low duct and pipe velocities (i.e., larger diameters) and long straight runs of mains. Both of these concepts can easily be incorporated as the design progresses.

Isolation of the Experiment Hall floor from the Ring tunnel floor

The outer corridor of the Experiment Hall will be separated from the floor slab of the Experiment Hall by means of a joint in the slab, following the APS model. This decouples the public corridor, which has pedestrian activities and deliveries, from the more vibration-sensitive Experiment Hall area.

Concerns have been expressed regarding the connectivity of the Tunnel and the floor of the Experiment Hall. This is not as simple a decision as that to decouple the outer corridor. The argument in favor of a joint is similar: it is desirable to mitigate "humming" and other vibration that might be generated by the equipment associated with the ring. The argument against a joint is that it introduces the risk of differential settlement between the Tunnel and Experiment Hall, which could cause a small, though quasi-static, beam misalignment.

The thick concrete slab of the Experiment Hall and Tunnel together will offer some improvement of the ground surface that might not be as dramatic if it is actually two ring slabs, one inside the other. This is an issue that can be addressed analytically as the design progresses.

An option worthy of consideration is the use of a damping admixture in the concrete beneath the ring. It would help to dissipate the high-frequency "humming" vibration. It could be placed as a topping on the concrete, as done in mechanical corridors at CFN. An unknown that would require evaluation is the severity of the radiation and how the polymer would respond to that radiation.

Acoustics of Experiment Hall

The Experiment Hall is a large open area which will have a vast quantity of user-supplied noise sources. A noise study was carried out in 1989 as part of the APS design effort, in part to develop a "typical" source sound power spectrum for design of the APS Experiment Hall.[1] At that time, the average noise level was found to be 69 dBA, though noise levels as high as 80 dBA were measured. It was assumed that the experiments themselves were not adversely affected (as noise protection could be built into the hutches), but the noise environment in the hall was a detriment to speech communication and contributed to researcher fatigue.

It might be worthwhile for BNL to consider imposing a limit on the allowable sound power associated with user-supplied equipment. However, the most proactive move is probably to use acoustically absorbent materials on walls and ceiling. The latter is relatively straightforward, by means of an acoustically absorbent roof deck. There are number of manufacturers of the product. Essentially it is a corrugated decking in which the grooves (as seen from above) are perforated and filled with acoustical material. The high spots are surfaces for supporting roofing or sheeting that supports concrete roof system. You can get very good performance from these systems. A facility with this kind of decking is the Experiment Hall at the Center for Advanced Microstructures and Devices (CAMD) at Louisiana State University. Some of the vendors of this product are Versa-Dek, United Steel Deck, and Vulcraft. A noise study should be carried out as the design progresses to the point that the mechanical system noise can be combined with the sound power for the research equipment.[2] That study can develop specific recommendations regarding the NRC of the decking and wall coverings and the optimal percentage of wall covering.

---

[1] Amick, H., and C. G. Gordon, "Measurement of Noise and Vibration, National Synchrotron Light Source, Brookhaven National Laboratory", Acentech Report 11 (June 1989).

[2] Sound power data for typical NSLS equipment were reported in "Acoustical Evaluation of Experiment Hall: Argonne National Laboratory", A. M. Yazdanniyaz & S. K. Bui, Acentech Report No. 56, January 1991. The noise from the experimental equipment was included in their noise model via sound power estimates based on measurements made at NSLS in 1989, see Acentech Report 11.

Appendix A3

Preliminary EMI/RFI Site Assessment Study Report
September 1, 2006

VitaTech Engineering, LLC

VitaTech Engineering, LLC

EMF Measurements, Surveys & Risk Assessment
EMF Mitigation - Shielding & Cancellation
E-mail: lvitale@vitatech.net
Homepage: www.vitatech.net

115 Juliad Court, Suite 105
Fredericksburg, VA 22406
(540) 286-1984
FAX: (540) 286-1865

September 1, 2006

Mark Jamison, P.E.
HDR One Company
8404 Indian Hills Drive
Omaha, NE 68114

Tel: (402) 399-4908

Subject: Future NSLS-II Brookhaven Labs EMI/RFI Site Assessment Study

Dear Mr. Jamison:

VitaTech Engineering was engaged by HDR to perform an EMI/RFI Site Assessment Study for the future NLSL-II building site located at Brookhaven Labs in Long Island, New York. The EMI/RFI data contained in this report was recorded on 14 June 2006 by the author of this report and Mr. Eric Friedlein of VitaTech Engineering. The proposed NSLS-II site has underground distribution circuits traveling east-west along Brookhaven Avenue and other electrical feeders west of Seventh Avenue running north-south. *VitaTech must return in late September to record additional RF data from the NEXRAD Dopper Radar 2200 ft. from the site.*

AC ELF Electromagnetic Interference (EMI)
Electron microscopes (SEMs, TEMs, STEMs), Focus Ion Beam (FIB) writers and E-Beam Writers are very susceptible to AC ELF (extremely low frequency) 3 Hz to 3000 Hz magnetic fields emanating from various electrical power sources outside of the NLSL-II building and within. VitaTech recommends a maximum of 1 mG Br (resultant) RMS AC ELF magnetic flux density emissions for NMRs and MRIs, 0.3 mG Br (resultant) RMS AC ELF magnetic flux density emissions for Cleanrooms and 0.1 mG Br (resultant) RMS AC ELF magnetic flux density emissions for SEMs, TEMs, STEMs, FIBs and E-Beam Writers as shown in the Chart #1 below:

EMI AC & DC Magnetic Field Performance Specs
NMR Maximum Requirement: 1 mG Br RMS (2.83 mG p-p)
Instrument & Quite Labs Maximum Requirement: 0.1 mG Br RMS (0.3 mG p-p)
Cleanrooms Maximum Requirement: 0.3 mG Br RMS (0.1 mG p-p)

Chart #1, Recommended EMI AC & DC Magnetic Performance Specs

Electromagnetic induction occurs when time-varying AC magnetic fields couple with any conductive object including wires, electronic equipment and people,

thereby inducing circulating currents and voltages. In unshielded (susceptible) electronic equipment (computers monitors, video projectors, computers, televisions, LANs, diagnostic instruments, magnetic media, etc.) and signal cables (audio, video, telephone & data), electromagnetic induction generates electromagnetic interference (EMI), which is manifested as visible screen jitter in displays, hum in analog telephone/audio equipment, lost sync in video equipment and data errors in magnetic media or digital signal cables.

Placement of each scientific tool and instrument depends on the actual EMI susceptibility under defined thresholds, which are often not easy to ascertain from the manufacturer's performance criteria. Magnetic flux density susceptibility can be specified in magnetic field strength (A/m) or in milligauss (mG) using one of three magnetic flux density terms: Brms, Bpeak-to-peak(Bp-p) and Bpeak (Bp) according to the following conversion formula below.

$$B_{rms} = \frac{Bp-p}{2\sqrt{2}} = \frac{Bp}{\sqrt{2}}$$

To convert magnetic field strength to units of milligauss (mG), simply multiple the magnetic field strength by 4π. For example, 3 A/m is equal to 37.7 mG (3 x 12.57 = 37.7 mG). Using simulated emission profiles and the correct conversion formula, it is possible to identify the appropriate levels acceptable for each tool *if the correct EMI susceptibility figure can be ascertained from the manufacturer's specifications. Therein, lies the real EMI challenge.*

Generally, for AC ELF sources the minimum EMI threshold is 10 mG in unshielded electronic equipment, especially 14" to 17" CRT color computer monitors and analog signal cables; however, the AC ELF EMI threshold for high-resolution 17" to 21" CRT color monitors is only 5 mG. *Analog audio/video equipment and cables are susceptible to EMI noise less than 5 mG including diagnostic medical instruments such as EEGs, EKGs, EMGs, ECGs, and other electrode contract devices.*

The semiconductor industry has specified AC EMI threshold performance requirements in SEMI E33-94, Specification For Semiconductor Manufacturing Facility Electromagnetic Compatibility, as shown below in Chart #2 - The AC ELF EMI Threshold Charts:

Chart #2 – AC ELF EMI Threshold Chart

AC ELF EMI Thresholds (screen jitter & noise)

10 mG for 12-15 inch computer monitors & audio/video equipment

5 mG for 17-21 inch CRT monitors & medical (i.e., EEGs, ECGs, EMGs,. etc.).

1.0 mG for standard scientific tools (STEMs, TEMs, FIB, I-Beam, etc.)

0.1- 0.3 mG high resolution Nanotech scientific tools

0.01 mG for optimum superhigh resolution STEM tools.

SEMI E33-94 AC ELF EMC Standards

Level A - less than 0.25 mG
Level B - less than 0.50 mG
Level C - less than 1.00 mG
Level D - less than 2.00 mG
Level E - 2.0 mG and greater

AC ELF EMI Recorded Data & Assessment

On 14 June 2006 VitaTech recorded lateral AC extremely low frequency (ELF) magnetic flux density levels at 1-meter above grade with a survey wheel and the FieldStar 1000 gaussmeter (see Test Instruments for details) within the proposed NLSL-II building site. The following is an AC ELF magnetic flux density assessment of the RMS recorded data:

Figure #1 shows five lateral Hatch Plots recorded across the proposed NLSL-II building site. Each lateral data path has four color hatch marks (0.1 mG, 0.25 mG, 1.0 mG and 5.0 mG) representing the threshold level recorded at each one-foot interval (no hatch marks indicate levels less the 0.1 mG). Figure #2 presents five Profile Plots of the Figure #1 Hatch Plots with resultant Br (black) levels and three Bx (red), By (green) and Bz (blue) components shown as a function of distance.

The three north-south laterals (records #1 - #3) in Figures #1 and #2 shows the recorded magnetic fields emanating from the east-west underground distribution lines on Brookhaven Avenue (peaks 1.5 to 3.4 mG). The three north-south laterals rapidly decay to less than 0.1 mG 75 to 100 feet from the Brookhaven Avenue south curb. The levels were also very low along the east-west lateral in the center of the field rapidly decaying to 0.00 mG between Seventh and Fifth Streets except within 75 feet south of Brookhaven Avenue. The proposed NLSL-II site has very low AC ELF magnetic flux density levels 75 feet south of Brookhaven Avenue, ranging from 0.1 mG to 0.00 mG as shown in the five Figure #2 Lateral Profile Plots.

Figure #3 shows the timed wideband 3 Hz to 3,000 Hz AC ELF magnetic flux density field levels at the proposed NLSL-II site recorded with the MultiWave System II three axis fluxgate magnetometer sampled at 15 second intervals for 42 minutes. The timed Br resultant peak was 0.192 mG with an average 0.18 mG over the 42 minute period: this is the noise floor of the MultiWave System II where the actual levels are below the recording range. Therefore, the actual timed levels are 0.0 mG at this distance (200 – 250 ft) south of Brookhaven Ave.

Conclusions: The recorded AC ELF magnetic flux density emissions were very low ranging from 0.1 mG at 75 to 100 feet south of Brookhaven Avenue rapidly decay to 0.00 mG at 100 feet all the way to the other side of the site including the wooded areas. The NSLS-II site complies with all four of the following AC ELF magnetic flux density performance requirements 100 feet south of Brookhaven Avenue between Seventh and Fifths Streets:

- ***0.01 to 0.1 mG EMI threshold for ultrahigh resolution STEMs;***
- ***0.1 to 0.3 mG EMI threshold for scientific tools (i.e., SEMs, TEMs, FIB, E-Beam Writers, etc.);***
- ***0.25 mG Level A SEMI E33-94 AC ELF EMF Standard; and,***
- ***10 mG long-term human exposures threshold recommended by the Swiss Bunderstat and NCRP Draft Report (see AC ELF Magnetic Field Health Issues, Standards & Guidelines)***

Ground/Net Current Issues

Ground and net currents are due to N.E.C. violations (i.e., grounded neutrals, wiring errors, etc.) in the electrical service, distribution and grounding systems of a building and N.E.S.C. violations (i.e., grounding problems, etc.) on distribution and transmission lines. Unbalanced phases on medium voltage distribution lines and 480V/208V low-voltage feeders generate zero-sequence currents, which return on the neutrals and grounding conductors. Most utilities maintain 5% and less unbalanced phases on high voltage transmission lines and 10-15% unbalanced phases on distribution lines (power quality issues) except in local neighborhoods where unbalanced phases may exceed 20%. A percentage of the zero-sequence neutral currents on distribution lines travel along other electrically conductive paths (i.e., underground water pipes, earth channels, grounded guy wires, building neutrals/grounding systems, etc.) back to the substation. If all the zero-sequence currents were to return via the multi-ground neutral system (MGN) wire mounted on the pole under the three phase conductors (sum of all phase and neutral currents are zero), then the magnetic fields would decay at the normal inverse square rate ($1/r^2$ in meters) from the single-circuit distribution line (same for transmission lines and low-voltage feeders). However, if only a fraction of the zero-sequence current returns on the MGN system or low-voltage neutral conductor, then there is a net current missing (amount of current returning via other paths) – this net current emanates a magnetic field similar to a ground current (electrical current of low voltage returning on a ground wire, water pipe or other conductive path) that decays at a linear 1/r (in meters) rate based upon the following formula:

$$\mathbf{B_{mG} = 2(I)/r}$$ where I is amps and r meters

Magnetic fields from ground and net (zero-sequence) currents decay at a slow, linear rate illustrated below, using a 5 amp ground/net current source: 10 mG is 1 m away, 1 mG is 10 m away, 0.5 mG is 20 m away and 0.1 m is 100 m away:

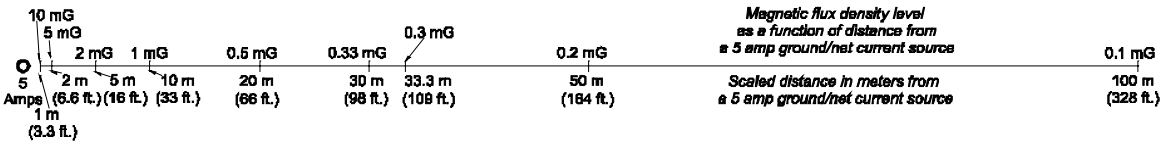

Since there is a proportional relationship between current load and magnetic flux density levels, the above chart can be used to predict the emission levels based upon ground/net current loads. Using 2.5 amps of ground/net current, the levels above the selected decay distance are calculated by dividing by 2, which is 50% of 5 amps. The ground/net current decay chart is indispensable in ascertaining the acceptable operating distance from ground and net (zero sequence) currents based upon a specified instrument performance criteria (i.e., 1 mG, 0.1 mG or 0.01 mG).

Ground and net current magnetic field emissions are difficult to shield using flat or L-shaped ferromagnetic and conductive shields -- the most effective shielding method for AC ELF ground/net current emissions requires a six-sided, seam welded aluminum plate shielding system with a waveguide entrance. *Finally, low ambient magnetic field levels can be achieved inside a research laboratory and imaging suite*

by adhering to the N.E.C. and good wiring practices. However, these low levels can only be achieved under the most pristine conditions and without any circulating ground/net currents present on the primary electrical distribution system outside of the building, low-voltage 480/208V distribution feeders and branch circuits inside the building systems and the grounding system.

DC Electromagnetic Interference (EMI)

Large and small ferromagnetic masses in motion such as elevators, cars, trucks, trains, subways and metal doors produce geomagnetic field perturbations in the sub-extremely low frequency (SELF) 0 - 3 Hz band that radiate (similar to throwing a pebble in a pond) from the source generating DC electromagnetic interference (EMI) in sensitive scientific tools and instruments. The magnitude of the geomagnetic field perturbation and radiated distance from the source depends on the size, mass and speed of the moving ferromagnetic object. Theoretically, DC magnetic emission sources (i.e., ferromagnetic objects, magnets, etc.) decay according to the inverse cube law, in practice the decay rates are not ideal. Other problematic DC EMI sources include traction currents from underground/surface electric DC trolleys/subways, electromagnetic pulse (EMP) devices with high-voltage discharge, and finally unshielded NMRs and MRIs.

Electron microscopes (SEMs, TEMs, STEMs), Focus Ion Beam (FIB) writers and E-Beam Writers are very susceptible to DC EMI emissions and require clean DC environments. VitaTech recommends a maximum of 1 mG dB/dt Br (resultant) RMS DC EMI for NMRs and MRIs, 0.3 mG dB/dt Br (resultant) RMS DC EMI for Cleanrooms and 0.1 mG dB/dt Br (resultant) RMS DC EMI for SEMs, TEMs, STEMs, FIBs and E-Beam Writers as shown in the Chart #1 below:

EMI AC & DC Magnetic Field Performance Specs
NMR Maximum Requirement: 1 mG Br RMS (2.83 mG p-p)
Instrument & Quite Labs Maximum Requirement: 0.1 mG Br RMS (0.3 mG p-p)
Cleanrooms Maximum Requirement: 0.3 mG Br RMS (0.1 mG p-p)

Chart #1, Recommended EMI AC & DC Magnetic Performance Specs

Placement of scientific tools depends on the actual DC EMI susceptibility under defined thresholds, which are often not easy to ascertain from the manufacturer's performance criteria. Electron microscopes are sensitive at 1 mG Brms from DC disturbances while SEMs and TEMs such as the TEM JOEL 2010 have 0.4 mG horizontal and 0.2 mG vertical performance requirements while next generation EM tools are less than 0.1 mG Brms and Super STEMs (also known as ultra-high resolution STEMs) have a 0.01 mG DC EMI threshold. DC susceptibility in typical 1.5 to 4 Tesla MRIs can range from 1 mG to over 0.5 Gauss depending on the

magnetic field strength, resolution and type (open vs. closed, active shielding, etc.). ***Furthermore, to ensure a safe working environment around MRIs and NMRs, adequate signage must be posted at 5 and 10 Gauss lines to warn staff and visitors with implantable devices and to minimize inadvertent data corruption (coercivity) of credit cards and other valuable magnetic media.*** Below is a list of DC EMI Thresholds in Gauss that will impact CRT displays, electronic instruments and magnetic media:

Chart #3 – DC EMI Threshold Chart

DC EMI Thresholds - CRT screen shift, noise & coercivity (data errors)
0.001 Gauss & Less SEMs, TEMs E-Beam/FIB Writers
0.75 Gauss CRT Monitors & Electronic Instruments
5 Gauss Cardiac Pacemakers & Implantable Devices Warning Sign
10 Gauss Credit Cards & Magnetic Media Warning Sign
300 Gauss Low Coercivity Mag-Stripe Cards
700 Gauss High Coercivity Mag-Sripe Cards & Video Tapes
1000 milligauss (mG) = 1 Gauss (G) & 1 mG = 0.001 G = 0.1 uT (microtesla)

According to the **National Geophysical Data Center (NGDC),** the average Br resultant DC magnetic flux density level at Brookhaven National Labs is 528.5 mG at 0 ft. elevation. Depending on the location and distance from ferromagnetic materials (pipes, steel beams, rebar, cars, etc.), the recorded average time DC Br resultant RMS levels at the site was 536.9 mG (see Figure #3), which is only a 8.4 mG differential.

Moving Vehicle DC EMI Emission Profiles & Impact

As discussed the DC EMI emissions from moving vehicles (cars, SUVs, VANs, trucks and busses), and trains can compromise sensitive research tools. Normally, VitaTech recommends adequate spacing between the proposed building site, roads with heavy traffic, parking garages, trains, subways and other DC EMI emission sources to minimize potential EMI problems with sensitive instruments and tools.

Figure #4 shows the timed (15 second interval) resultant (Br) and component (Bx, By and Bz) RMS DC data recorded with the MultiWave System II three-axis fluxgate magnetometer more than 200 feet from Brookhaven Avenue. The only noticeable DC dB/dt EMI data was generated from an SUV that drove up to our location (200 – 250 feet south of Brookhaven Avenue) within 10 feet of the fluxgate probe. The Br resultant chart shows a 4 mG dB/dt square pulse from the SUV vehicle as it approached the fluxgate probe.

VitaTech recorded timed DC EMI data from moving vehicles at the University of Florida several years ago as shown in Figure #5. Calculated car and bus vehicle profiles were generated by applying the decay data to Curve Fitting software – this data was overlaid on the NSLS-II site plan. Similarly, the vehicle decay chart should be used to evaluate the DC EMI impact from cars driving on Brookhaven Avenue and Seventh/Fifth Streets adjacent to the proposed site. It should be noted that in practice the magnetic fields decay more rapidly after 30 meters than the calculated levels indicate (see recorded data). Nevertheless, the calculated DC

differential dB/dt emissions from a moving bus at 40 meters would be 0.2 mG while in practice the actual bus levels will be less than 0.1 mG.

Conclusions: Standard resolution imaging tools with dB/dt differential DC EMI resultant RMS thresholds of 1 mG to 0.1 mG can be located between 12 meters (40 ft) to 40 m (131.2 ft) south of Brookhaven Avenue assuming cars and busses are moving east and west. High resolution imaging tools with differential dB/dt DC EMI resultant RMS thresholds of 0.1 to 0.01 mG can be located from 40 m (131.2 ft) to 60 m (197 ft.), which is the predicted 0.01 mG isoline) south of Brookhaven Avenue. Similar separation distances are required from the north-south Seventh and Fifth streets to ensure adequate DC EMI immunity for moving vehicles of similar mass.

Radiofrequency Interference (RFI)

The Federal Communications Commission (FCC), not the local municipal zoning authorities or law enforcement, has legal jurisdiction over radiofrequency interference (RFI). Simply stated RF devices (intentional and unintentional emitters) are not permitted to cause RFI with other radio services, electronic equipment and systems. At present, there are no mandated radiofrequency interference (RFI) susceptibility government standards in the United States. The only equipment susceptibility standards that exist are unique to equipment (quality control) internal standards written by equipment manufacturers based on radiated emission standards for intentional radiators set forth by the FCC. In other words, an equipment manufacturer in United States must design the equipment to function properly within a radiated emission field level from intentional radiators set forth by the FCC, Part 15. Like any other communications facility, wireless broadband facilities must comply with these FCC limits. The following FCC parts apply to electromagnetic interference (EMI) and radio frequency interference (RFI) conducted and radiated emissions (see below):

Radio Frequency Devices - Part 15
Multipoint Distribution Service - Part 21, subpart K
Paging and Radiotelephone Service - Part 22, subpart E
Cellular Radiotelephone Service - Part 22, subpart H
Personal Communications Services - Part 24
Satellite Communications - Part 25
General Wireless Communications Service - Part 26
Wireless Communications Service - Part 27
Radio Broadcast Services - Part 73
Experimental, auxiliary, and special broadcast and other program distributional services - Part 74
Experimental Radio Service - Part 5
Stations in the Maritime Service - Part 80
Private Land Mobile, Paging Operations - Part 90
Private Land Mobile, "Covered" Specialized Mobile Radio - Part 90
Amateur Radio Service - Part 97
Local Multipoint Distribution Service - Part 101, subpart L

Mobile and portable devices used as follows:

Cellular Radio Service
Personal Communications Service
Satellite Communications Branch
General Wireless Communications Service
Wireless Communications Service
Maritime Service
"Covered" Specialized Mobile Radio Service

In Europe, there are susceptibility (radiated immunity) standards, such as the EN 61000-6-1, that states 3 V/m level for residential electronic equipment, while 10 V/m is standard for industrial electronic equipment in the EN 61000-6-2. Engineers in the United States utilize the European susceptibility standards as a guideline. The SEMI E33-94 EMC Standard is 10 V/m and 3 V/m depending on frequency (see below):

Chart #4 – RFI Threshold Chart

Electric field strength RF levels were recorded in volts-per-meter (V/m) for 10 minutes sampled at 0.04-second intervals with a Narda ERM-300 electric field meter using a Probe 18 from 100 kHz to 3 Ghz (range of 0.2 to 320 V/m) and Probe 9C from 3 MHz to 18 GHz (range of 0.5 to 1000 V/m). The objective is to investigate sources of radio-frequency interference (RFI) over a wide bandwidth. It should be noted that 3 V/m is the industry standard RFI threshold and 1 V/m the medical/scientific instrument RFI threshold.

SEMI E33-94 RF Immunity Standards
Enclosure Ports
Radiated AM Immunity: 10 V/m 450-520 MHz and 800-950 MHz @ 80% AM
Radiated Pulse Modulated: 3 V/m 1.89 GHz 50% Duty cycle
Signal Line Ports & Ports for Process, Measurement & Control
RF Common Mode: 3 V/m 0.15 - 100 MHz @ 80% AM
Input/Output DC/AC Power Ports
RF Common Mode: 3 V/m 0.15 - 100 MHz @ 80% AM

RFI Electric Field Strength Site Assessments & Conclusions

Timed Wideband 100 kHz – 18 GHz RF Electric Field Strength Data

VitaTech recorded timed RF electric field strength data in volts-per-meter (V/m) was recorded at 1-meter above grade from 100 kHz to 3 GHz and 3 MHz to 18 GHz at 0.4 second intervals for two 10 minute periods on 14 June 2006 as shown in Figures #6 and #7. A summary of the 14 June 2006 recorded RF electric field strength levels are presented in Tables #1 and #2 below:

Table #1: 100KHz - 3GHz RF Data 14 June 2006

Site	Max (V/m)	Min (V/m)	Average (V/m)
NSLS-II	0.31	0.00	0.12

Table #2: 3MHz - 18GHz RF Data 14 June 2006

Site	Max (V/m)	Min (V/m)	Average (V/m)
NSLS-II	0.25	0.0	0.12

Tables #1 and #2 present 20 minutes of recorded RF electric field strength at the NSLS-II site as shown in Figure #6. These are very low RF electric field strength levels considering the NEXRAD Doppler Weather Radar is only 2200 ft. away from the site, therefore the radar was not operational or under low power during data collection. Figure #7 shows the maximum electric field strength thresholds recorded during two ten minute sampling periods. Again, very low maximum peak

threshold levels were recorded from 100 kHz to 3 GHz and from 3 MHz to 18 GHz indicating the radar was not operational or under low power during the testing.

The NEXRAD Doppler Radar transmitter frequency range is 2.7 to 3.0 GHz with a peak output power of 750 kW (pulse width - short at 1.57 microsecond and 4.5 microsecond wide) from an S-Band center-feed parabolic dish (28 ft. outside-diameter) with a 0.95 degree pencil beam, 6 RPM azimuth rate and -1 to +20 degree elevation. VitaTech will return in late September 2006 with our new spectrum analyzer, the Narda SRM-3000 Selective Radiation Meter, to record the electric field strength and FCC Bulletin 65 (MPE) maximum permissible exposure levels at the proposed NSLS-II site with the NEXRAD Doppler Radar at maximum power (must be scheduled with the NEXRAD engineers and operators).

VitaTech previously recorded electric field strength levels for the Center for Functional Nanomaterials on the roof of the existing LightSpeed building. The RF emission levels around scientific tools such as the E-Beam Writers, NMRs, and Mass Spectrometers should be 20 mV/m or less. *Based upon the previously recorded RF emission levels at that site, RF shielding was recommended on the façade of the Center for Functional Nanomaterials, but budgetary issues deleted the RF shielding. Nevertheless, the existing LightSource building had RFI problems from the NEXRAD Dopper Radar, and RF shielding was installed around selected laboratory and research areas to reduce the RFI problems.*

<u>Center for Functional Nanomaterials RF Shielding Assessment/Mitigation Options</u>
The following section was extracted from the Center For Functional Nanomaterials report on RFI shielding options. It should be noted that the estimated prices are not accurate and should be increased by 30% for budgetary reasons:

> The nearby NEXTRAD Doppler Radar operates between the 2.7 to 3 GHz frequency range with up to 750 kW of effective radiated power (ERP) depending resolution and weather conditions. Building materials will provide natural shielding attenuation based upon frequency and distance from the façade facing the RF emission source. At 3 GHz the aluminum metal building façade (0.04 inches thick) would provide 50 dB to 60 dB of attenuation due to the high reflection and absorption characteristics of the exterior interlocking aluminum siding/roofing. The second floor heavy gage steel floor pans (0.034 inches thick) would add another 50 dB to 60 dB of attenuation (i.e., reflection and absorption) to the roof figures for a total of 100 to 120 dB attenuation in the vertical plane. If the east façade windows and walls were not shielded the natural horizontal attenuation factor would be 25 dB at 5 meters inside the exterior wall, over 35 dB at 10 meters, and over 60 dB at 20 meters deep inside the building. Although the east façade exterior wall is covered with aluminum panels providing at least 50 to 60 dB of attenuation, the large unshielded windows provide an open portal allowing the Doppler RF energy to penetrate deep into the building. ***Therefore, RF shielding the windows is necessary to minimize potential RFI problems in the adjacent ground floor laboratories.***

VitaTech presents two RF window shielding options: transparent conductive RF film that can be applied to the windows when needed and conductive RF shielded glass with conductive gaskets and aluminum window frames. The best conductive RF film available is from 3M and sold under the Scotchtint trademark providing from 26 to 36 dB of attenuation depending on the type of film purchased (i.e., tint, conductivity, UV block and other parameters). When installed by professionals, the 3M Scotchtint has a 10 year warranty. It is supplied in 100 ft. by 5 ft. wide rolls costing from $1,200 to $1,500 per roll (not including installation) depending on the tint, shielding performance and energy rating. VitaTech provided samples of the P-18AR High Performance Silver (26 dB at 2.5 GHz) and RE35AMARL (36 dB at 2.5 GHz) to HDR several week ago. *It would cost $40,000 - $60,000 to install 3M RF film on 2,380 sq. ft. of windows including labor, expenses and profit.*

The other option is to use recently developed RF shielded glass "DATASTOP" sold by Pilkington and Tempest Security Systems, Inc. of Troy, OH. Shielding performance of the sealed double glazed DATASTOP windows ranged from 62 dB for the D50 with neutral tint up to 78 dB for the D60 with gold tint as shown below:

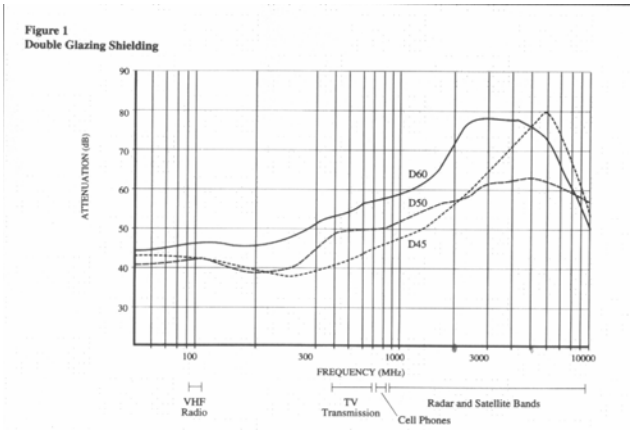

The DATASTOP double glazed windows are typically two layers of ¼-inch thick glass separated by a ½-inch air gap mounted with conductive gaskets in an aluminum window frame shown below:

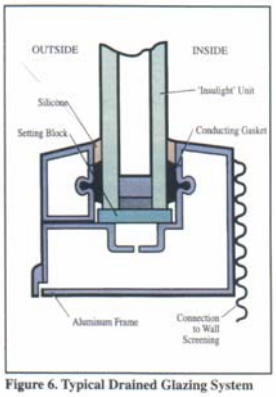

Figure 6. Typical Drained Glazing System

The basic no tint double glazed DATASTOP window costs $60 per square foot (not including installation). It has a 10 year warranty and would provide an average of 60 dB of attenuation, which is similar in attenuation to the exterior aluminum façade and aluminum roof. RF energy may penetrate into the building interior through various holes, openings, and mechanical seams in the aluminum exterior east façade wall: any space more than a 1/2λ of 3 GHz, which is 1.95 inches in diameter (see mesh section for formula). Since the DATASTOP aluminum window frames will not be conductively bonded and/or RF sealed to the exterior east aluminum wall panels, RF penetration through any 2 inch and large space will occur around the windows, doors and other separation joints between the conductive and metallic surfaces. *It would cost $290,000 - $325,000 to install 2,380 sq. ft. of DATASTOP D50 double glazed windows with no tint, fames and conductive gaskets including labor, expenses and profit.*

Shielding the east building façade with wire mesh behind the aluminum exterior panels would significantly attenuate any RF energy leakage into thorough holes and penetrations the research laboratories while providing an extra layer of RF protection. First, the wavelength of 3 GHz must be calculated using $C = \lambda f$ where C is the speed of light (2.997×10^8 m/s) and f is frequency of attenuation (3.0×10^9 in cycles per second). The wavelength λ of 3 GHz is 0.0999 meters (99.9 mm or 3.9 inches) while any wavelength greater than 1/2 λ (1.95 inches) is attenuated (i.e., lower the frequency the longer the wavelength).

Next, the ideal shielding effectiveness (SE) in decibels for wire mesh is calculated where λ (lamda) is the wavelength of the incident Doppler microwave in meters and g is the airgap in meters: $(SE)_{dB} = 20 \log_{10} (0.5 \lambda/g)$

Assuming 60 dB of attenuation is the objective, than the calculated wire mesh spacing (airgap g) is 0.04995 mm (0.002 inches), which is equivalent to a 270 mesh. Only stainless steel fine mesh wire cloth is available in a 270 mesh size and is not used in RF shielding because of the difficulty in seam bonding and grounding. There are two other reasonable alternatives: 100 Mesh copper or aluminum screening. The calculated SE for 100 Mesh (0.0045 copper) with a 0.14 mm airgap is 51 dB while the measured SE is 47 dB as shown in the diagram below:

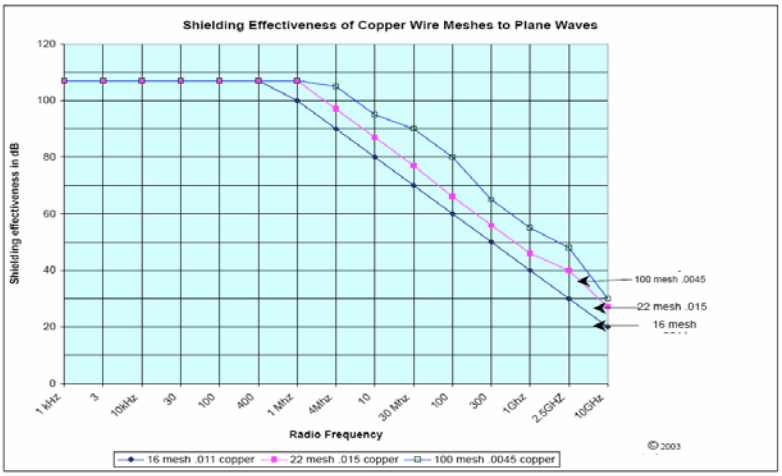

The 100 Mesh copper comes in 100 ft. rolls, 48 inches wide, and costs $1.30 to $1.50 per square foot (F.O.B). Aluminum 100 Mesh of the same length and width is a custom weave (must be an alloy with lower conductivity because of the needed tensile strength during the weaving process) costs $1.50 to $1.75 per square foot (F.O.B). The 100 Mesh copper and aluminum screens are easy to apply (staples, screws and adhesives) to the outside wall, can be mechanically bonded to the aluminum window frames using screws, and seam bonded (overlap edges and soldered) and grounded. Therefore, 47 dB of attenuation is available using the 100 Mesh copper and 40 dB using 100 Mesh aluminum alloy RF screening. *It would cost $55,000 - $80,000 to install 5,660 sq. ft. of aluminum 100 Mesh on the exterior walls beneath the aluminum panels and mechanically bonded to the aluminum window frames including labor, expenses and profit.*

VitaTech does not recommend applying copper and aluminum tapes with conductive adhesive backings over wire mesh seams, on window frames or other conductive structures because overall shielding performance will seriously degrade over time due to weathering and temperature variations. If wire mesh RF shielding is used on the east façade wall behind the exterior aluminum panels, it must be mechanically bonded to the window frames and all other metallic surfaces to ensure long-term performance with minimal failure (warning to avoid galvanic reactions only aluminum can be mechanically bonded to aluminum window/door frames).

<u>RF Shielding Options & Estimated Costs</u>

VitaTech presents the following RF shielding options with costs to minimize RFI interference from the nearby Doppler radar inside the new Center for Functional Nanomaterials building laboratories and offices:

Option 1: Additional RF shielding is not installed because the aluminum exterior east wall and roof building surfaces will provide at least 50 to 60 dB of attenuation coupled with the interior attenuation characteristics of the building. It should be noted that the east side 1st floor windows will provide open portals to the Doppler RF energy with only the office doors and walls to absorb and reflect the microwave energy. If RFI problems are identified and

measured in specific laboratories, localized RF shielding should be applied to the area of concern to mitigate the problem, where practical. However, two alternative RF solutions are offered below with Option 1 where improved RF shielding is required:

Alternative #1: apply 3M conductive film to 1st floor windows for additional 36 dB of attenuation for an estimated cost of $40,000 - $60,000 including labor, expenses and profit. Shielding performance will be marginal because the edge between the conductive window film and window frame is difficult to bond (ground). Therefore, RF leakage around the inside glass window frames will present a serious problem.

Alternative #2: to reduce RF leakage through holes and seams along windows, doors and other openings apply 5,600 sq. ft. of aluminum 100 Mesh for an estimated costs of $55,000 - $80,000 including labor, expenses and profit. Special Note: aluminum 100 Mesh can not be applied after exterior aluminum wall panels are installed.

Option 2: Install DATASTOP RF shielded windows, conductive gaskets and frames in ground and 2nd floor east wall façade (2,380 sq. ft. area) as shown in Figure #11. Assume conductivity with aluminum exterior wall and roof to provide a reasonable RF shielding system of 60 dB and higher. Estimated cost: $290,000 - $325,000 for windows, frames, gaskets including labor, expenses and profit. Additional RF shielding is required to minimize RF leakage and improve overall shielding performance:

Alternative #3: seams with minimal electrical conductivity between DATASTOP aluminum window frames and exterior east aluminum walls will cause RF leakage penetrating into the interior building laboratories – install 100 Mesh aluminum screen to ground and 2nd floor walls behind aluminum panels and mechanically couple to the DATASTOP window frames RF sealing the east side of the building. Estimated cost: $55,000 - $80,000 for *5,660 sq. ft. of aluminum 100 Mesh includes labor, expense and profit.*

VitaTech recommends shielding the east exterior wall with the DATASTOP windows and 100 Mesh aluminum screen presented in Option 2 and Alternative #3 to provide the maximum RF shielding attenuation especially with close proximity to the ground floor research labs just several feet from the east side offices. Unfortunately, the Option 1 RF shielding solutions with Alternatives #1 and #2 will be marginally effective.

Conclusions: The four ambient timed recorded 100 kHz to 18 GHz electric field strength average and maximum peak data does not reflect the actual conditions since the Doppler Radar was probably not operational or at very low power. VitaTech will return in late September 2006 to record additional RF data with a spectrum analyzer (coordinate with engineers).

AC ELF, DC & RF Test Instruments

FieldStar 1000 Gaussmeter - AC ELF Magnetic Flux Density

VitaTech recorded the AC ELF magnetic flux density data using a FieldStar 1000 gaussmeter with a NIST traceable calibration certificate manufactured by Dexsil Corporation. The FieldStar 1000 has a resolution of 0.04 mG in the 0 - 10 mG range, 1% full-scale accuracy to 1000 mG and a frequency response of 60 Hz (55 - 65 Hz @ 3dB). Three orthogonal powdered-iron core coils are oriented to reduce interference to less than 0.25% over the full dynamic range. The three coils are arranged inside the unit holding horizontal with the display forward: Bx horizontal coil points forward, By horizontal coil points to the right side, and Bz vertical coil points upward. The microprocessor instantly converts the magnetic field to true RMS magnetic flux density (milligauss) readings of each axis (Bx, By, Bz) and simultaneously calculates the resultant R_{rms} (root-means-square) vector according to the following formula:

$$R_{rms} = \sqrt{Bx^2 + By^2 + Bz^2}$$

When collecting contour path data, a nonmetallic survey wheel is attached to the FieldStar 1000 gaussmeter and the unit is programmed to record mapped magnetic flux density data at selected (1-ft., 5-ft., 10-ft. etc.) intervals. The FieldStar 1000 is exactly 39.37 inches (1 meter) above the ground with the survey wheel attached. Along each path the distance is logged by the survey wheel and the relative direction (turns) entered on the keyboard. Up to 22,000 spot, mapped and timed data points can be stored, each containing three components (Bx, By & Bz), event markers and turn information. After completing the path surveys, magnetic flux density data is uploaded and processed. All plots display a title, time/date stamp, ID path number, and the following statistical data (in milligauss) defined below:

Peak - maximum magnetic field (flux) value measured in group.
Mean - arithmetic average of all magnetic field (flux) values collected.

The following is a quick description of the Hatch, Profile and 3-D Contour plots presented in the figures of this report:

Hatch Plot - data is represented by four difference hatch marks (0.1 mG, 0.25 mG, 0.5 mG and 1.0 mG thresholds) based on width and color as a function of distance along the survey path that shows 90 and 45 degree turns. Note: the site drawing and all Hatch Plots were scaled in feet to verify actual recorded distances and correct survey locations.

Profile Plot - data shows each recorded component (Bx, By, Bz) axis and the resultant (Br) levels as a function of distance: Bx (red) is the horizontal component parallel to the survey path, By (green) is the horizontal component normal (perpendicular) to the survey path, and Bz (blue) is the vertical component with the computed Br resultant RMS (root-means-square) summation of the three components.

EMR-300 RF Meter - Electric Field Strength Data 100 kHz - 18 GHz

The EMR-300 is an radiofrequency (RF) electric field strength meter for broadband measuring and monitoring from 100 kHz to 18 GHz. The isotropic non-directional field probe with high sensitivity records average, maximum, peak and timed data in electric fields strength volts-per-meter (V/m), magnetic field strength amps-per-meter (A/m) and power levels. Ten minute timed data was sampled at 0.4 seconds intervals from 100 kHz – 3 GHz with a Probe 18 (range 0.2 V/m to 320 V/m) and from 3 MHz to 18 GHz with Probe 9C (range 0.5 V/m to 1000 V/m) at each location.

MultiWave System II – Magnetic Flux Density 0 Hz – 3000 Hz

Geomagnetic and static DC magnetic emission measurements were recorded with a fluxgate triple-axis MultiWave System II magnetometer (serial #1045). The MultiWave System II consists of a hand-held LCD display and keyboard controller unit, wideband 10 Gauss (G) peak (DC – 3 kHz) tri-axial fluxgate magnetometer, data acquisition and processing unit with 3.5" floppy disk drive unit and 0 to 10 Gauss range, 1% accuracy, 0.1 mG resolution.

AC ELF Magnetic Field Health Issues, Standards & Guidelines

Currently, there are no Federal standards for AC ELF electric and magnetic field levels. The National Energy Policy Act of 1992 authorized the Secretary of the Department of Energy (DOE) to establish a five-year, $65 million EMF Research and Public Information Dissemination (RAPID) Program to ascertain the affects of ELF EMF on human health, develop magnetic field mitigation technologies, and provide information to the public. In May 1999, the NIEHS Director Kenneth Olden, Ph.D. delivered his final report, *Health Effects from Exposure to Power-Line Frequency Electric and Magnetic Fields*, to Congress that stated the following in the Cover Letter and Executive Summary below:

> *The scientific evidence suggesting that ELF-EMF exposures pose any health risk is weak. The strongest evidence for health effects comes from associations observed in human populations with two forms of cancer: childhood leukemia and* ***chronic lymphocytic leukemia in occupationally exposed adults... The NIEHS concludes that ELF-EMI exposure cannot be recognized at this time as entirely safe because of weak scientific evidence that exposure may pose a leukemia hazard.***

U.S. & International Organizational AC ELF EMF Standards

The International Commission on Non-Ionizing Radiation Protection (IRPA/INIRC) have established 833 mG maximum human exposure limit over 24 hours for the general public and 4,167 mG for occupational workers. Whereas The American Conference of Governmental Industrial Hygienists (ACGIH) recommends a 10,000 mG (10 Gauss) exposure limit over 24 hours for occupational workers, but specifies only 1,000 mG (1 Gauss) as a maximum exposure for workers with cardiac pacemakers.

New York State Public Service Commission AC ELF EMF Standards

Effective September 1990, the State of New York Public Service Commission (PSC) "began a process looking toward the adoption of an interim magnetic field standard for future major electric transmission facilities". The Commission concludes that a prudent approach should be taken that will avoid unnecessary increases in existing levels of magnetic field exposure. Therefore, future transmission circuits shall be designed, constructed and operated such that magnetic fields at the edges of their rights-of-way will not exceed 200 mG when the circuit phase currents are equal to the winter-normal conductor rating. They also established an electric field strength interim standard of 1.6 kV/m electric transmission facilities.

IARC June 2002 Report

In June 2002, the International Agency for Research on Cancer (IARC) issued a 400+ page report formally classifying extremely low frequency magnetic fields as ***possibly carcinogenic to humans*** based on studies of EMF and childhood leukemia. **This is the first time that a recognized public health organization has formally classified EMF as a possible cause of human cancer**. IARC found that, while selection bias in the childhood leukemia studies could not be ruled out, pooled analyses of data from a number of well-conducted studies show a fairly consistent statistical association between childhood leukemia and power-frequency residential magnetic fields above 4 milliGauss (mG), with an approximately two-fold increase in risk that is unlikely to be due to chance.

IARC is a branch of the World Health Organization. The IARC classification of EMF was made by a panel of scientists from the U.S. National Institute of Environmental Health Sciences, the U.S. Environmental Protection Agency, the U.K. National Radiological Protection Board, the California Department of Health Services, EPRI, and other institutions around the world.

Switzerland's February 2000 AC ELF Standard

The Swiss Bundersrat in February 2000 set by law an emission control limit of 10 mG from overhead and underground transmission lines, substations, transformer vaults and all electrical power sources.

VitaTech's & NCRP Draft Recommended 10 mG Standard

Section 8.4.1.3 option 3 in the National Council of Radiation Protection and Measurements (NCRP) draft report published in the July/August 1995 issue of *Microwave News* (visit the Microwave News Homepage <www.microwavenews.com> for the entire draft report) recommended the following:

> ***8.4.1.3 Option 3:*** *An exposure guideline of 1 μT (10 mG) and 100 V/m: A considerable body of observations has documented bioeffects of fields at these strengths across the gamut from isolated cells to animals, and in man. Although the majority of these reported effects do not fall directly in the category of hazards, many may be regarded as potentially hazardous. Since epidemiological studies point to increased cancer risks at even lower levels, a case can be made for recommending 1 μT (10 mG) and 100 V/m as levels not*

to be exceeded in prolonged human exposures. Most homes and occupational environments are within these values, but it would be prudent to assume that higher levels may constitute a health risk. In the short term, a safety guideline set at this level would have significant consequences, particularly in occupational settings and close to high voltage transmission and distribution systems, but it is unlikely to disrupt the present pattern of electricity usage. These levels may be exceeded in homes close to transmission lines, distribution lines and transformer substations, in some occupational environments, and for users of devices that operate close to the body, such as hair dryers and electric blankets. From a different perspective, adoption of such a guideline would serve a dual purpose: first, as a vehicle for public instruction on potential health hazards of existing systems that generate fields above these levels, as a basis for "prudent avoidance"; and second, as a point of departure in planning for acceptable field levels in future developments in housing, schooling, and the workplace, and in transportation systems, both public and private, that will be increasingly dependent on electric propulsion.

RF Human Exposure Standards

Presently, four major RF standards are used in the United States: IEEE, ACGIH (American Conference of Governmental Industrial Hygienists), NCRP (National Council on Radiation Protection and Measurements) and the ICNIRP (International Commissions of Non-Ionizing Radiation Protection). In 1991, the IEEE released a revised RF human exposure standard IEEE C95.1-1991, *Standard for Safety Levels with Respect to Human Exposure to Radio Frequency Electromagnetic Fields, 3 kHz to 300 GHZ*. However, in August 1997 the Federal Communications Commission (FCC) Office of Engineering & Technology (OTE) released Bulletin 65 *Evaluating Compliance with FCC Guidelines for Human Exposure to Radiofrequency Electromagnetic Fields*, which became the defacto RF exposure standard in the United States. Both standards are very similar for Occupational/Controlled and General Population/Uncontrolled maximum permissible exposure (MPE), except for some minor differences -- the FCC standard is more restrictive and used in RF Safety & Exposure Testing.

The FCC's Bulletin 65 specifies separate maximum permissible exposure (MPE) limits for Occupational/Controlled and General Population/Uncontrolled exposure over a 0.3 MHz to 100 GHz bandwidth as shown below:

LIMITS FOR MAXIMUM PERMISSIBLE EXPOSURE (MPE)

(A) Limits for Occupational/Controlled Exposure

Frequency Range (MHz)	Electric Field Strength (E) (V/m)	Magnetic Field Strength (H) (A/m)	Power Density (S) (mW/cm^2)	Averaging Time $\|E\|^2$, $\|H\|^2$ or S (minutes)
0.3-3.0	614	1.63	(100)*	6

3.0-30	1842/f	4.89/f	(900/f²)*	6
30-300	61.4	0.163	1.0	6
300-1500	--	--	f/300	6
1500-100,000	--	--	5	6

Occupational/controlled limits apply in situations in which persons are exposed as a consequence of their employment provided those persons are fully aware of the potential for exposure and can exercise control over their exposure. Limits for occupational/controlled exposure also apply in situations when an individual is transient through a location where occupational/controlled limits apply provided he or she is made aware of the potential for exposure.

(B) Limits for General Population/Uncontrolled Exposure

Frequency Range (MHz)	Electric Field Strength (E) (V/m)	Magnetic Field Strength (H) (A/m)	Power Density (S) (mW/cm²)	Averaging Time |E|², |H|² or S (minutes)
0.3-1.34	614	1.63	(100)*	30
1.34-30	824/f	2.19/f	(180/f²)*	30
30-300	27.5	0.073	0.2	30
300-1500	--	--	f/1500	30
1500-100,000	--	--	1.0	30

f = frequency in MHz *Plane-wave equivalent power density

General population/uncontrolled exposures apply in situations in which the general public may be exposed, or in which persons that are exposed as a consequence of their employment may not be fully aware of the potential for exposure or can not exercise control over their exposure.

Specific Absorption Rate (SAR) is the basis of most safety standards, when applied in the far-field, plane-wave conditions. It is the rate of energy absorption per unit of body mass. When the human body is exposed to the RF field, the SAR experienced is proportional to the squared value of the electric field strength induced in the body. At an absorption level of 4 W/kg, reversible behavioral disruption is noted. Levels above 5 W/kg can result in permanent adverse affects. Therefore, most standards have been based on SAR's of 0.4 W/kg to conservatively limit exposures to 1/10th of the levels to account for biological uncertainty and to add an additional safety factor.

Unfortunately, the Occupational Safety & Health Administration (OSHA) has not revised the standard since 1978 (see OSHA Regulations Standards - 29 CFR, Non-ionizing Radiation - 1910.97), but has already cited and fined organizations for exceeding the new standards. OSHA has the right to enforce based on consensus of scientifically-based standards under its general duty clause. **Nevertheless, OSHA uses 10 mW/cm² as the maximum SAR exposure over an averaged period of 6 minutes from continuous or intermittent RF sources between 10 MHz and 100 GHz.**

Figure 1, below presents the FCC Limits for Maximum Permissible Exposure (MPE) in units of Power Density (mW/cm^2):

Figure 1. **FCC Limits for Maximum Permissible Exposure (MPE)**

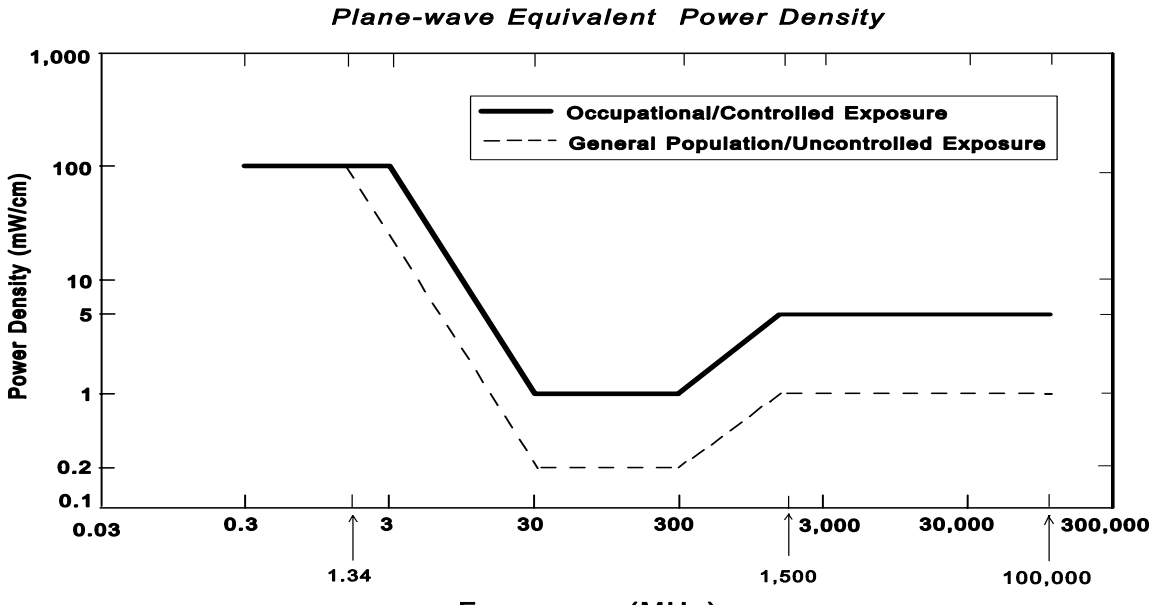

This completes the *Future NSLS-II Brookhaven Labs EMI/RFI Site Assessment Study.*

Best regards,

Louis S. Vitale, Jr.
President & Chief Engineer

Attachments: Figures #1 - #7.

Figure #1, NSLS-II Brookhaven National Labs Proposed Site Hatch Plots AC ELF Magnetic Flux Density Levels @ 1-meter - Upton, Long Island, New York

Refer To Figure #2 for Profile Plots of Hatch Data

VitaTech Engineering, LLC
(540) 286-1984
Fredericksburg, Va

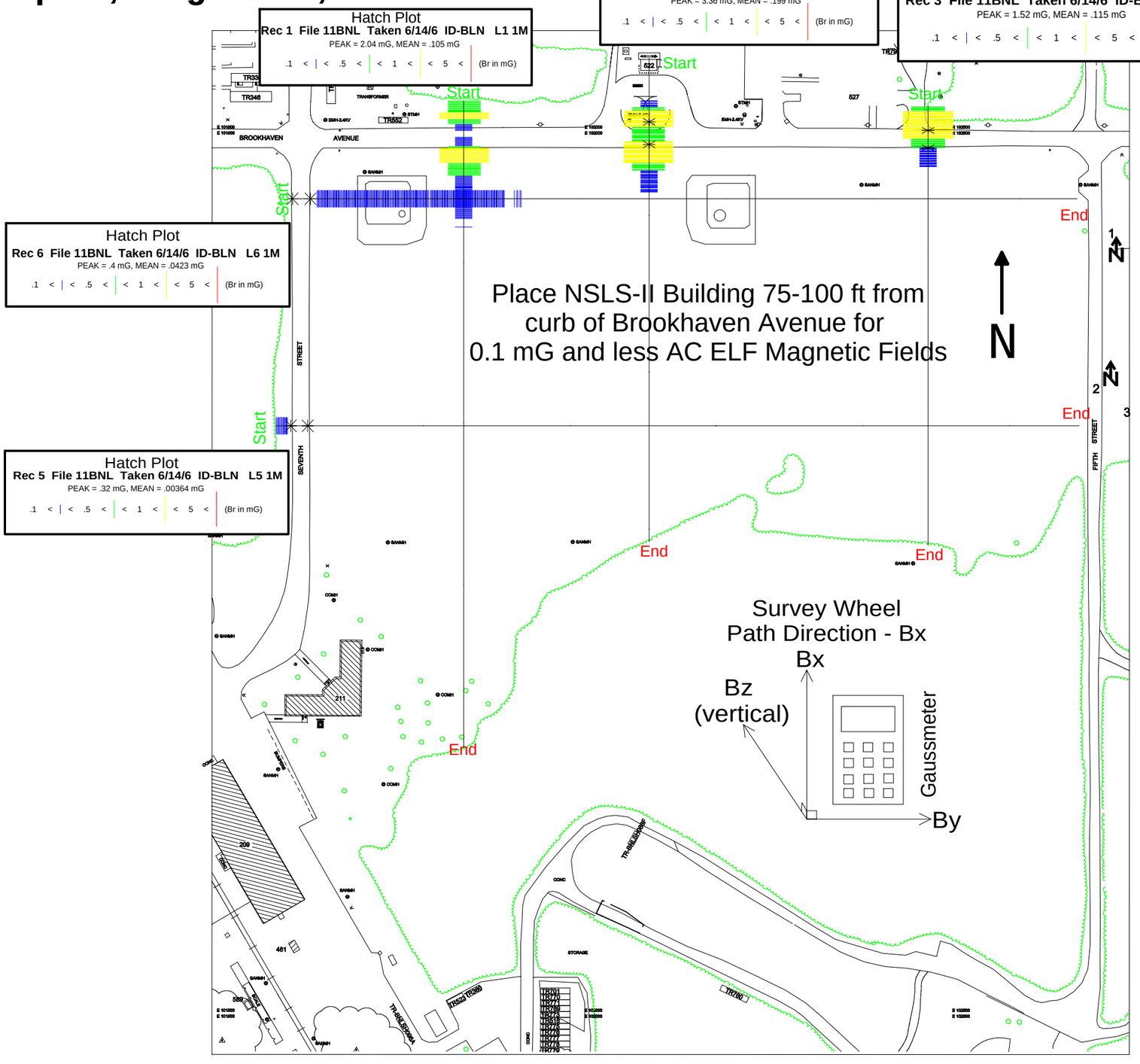

EMI AC & DC Magnetic Field Performance Specs
NMR Maximum Requirement:
1 mG Br RMS (2.83 mG p-p)

Instrument & Quite Labs Maximum Requirement:
0.1 mG Br RMS (0.3 mG p-p)

Cleanrooms Maximum Requirement:
0.3 mG Br RMS (0.1 mG p-p)

AC ELF Magnetic Field Human Exposure Standards

NYS Public Service Commission
200 mG @ 1-meter on Edge -ROW
or 50 ft. from 69 kV poles

IRPA/INIRC
833 mG over 24 hours
General Public Exposure

ACGIH
1000 mG general public
& workers with cardia pacemakers

Swiss Bunderstat
NCRP Draft Report
10 mG from overhead/underground transmission/distribution lines, substations, etc.

All magnetic flux density data recorded with a FieldStar 1000 gaussmeter and survey wheel.

AC ELF EMI Thresholds (screen jitter & noise)

10 mG for 12-15 inch CRT computer monitors & audio/video equipment
5 mG for 17-21 inch CRT monitors & medical (i.e., EEGs, ECGs, EMGs,. etc.).
1.0 mG for standard scientific tools (STEMs, TEMs, FIB, I-Beam, etc.)
0.1- 0.3 mG for high resolution Nanotech scientific tools
0.01 mG for optimum superhigh resolution STEM tools

SEMI E33-94 AC ELF EMC Standards
Level A - less than 0.25 mG
Level B - less than 0.50 mG
Level C - less than 1.00 mG
Level D - less than 2.00 mG
Level E - 2.0 mG and greater

Figure #2, NSLS-II Brookhaven National Labs Proposed Site Profile Plots of Hatch Data AC ELF Magnetic Flux Density Levels @ 1-meter - Upton, Long Island, New York

Refer To Figure #1 for Hatch Plots of Profile Data

VitaTech Engineering, LLC
(540) 286-1984
Fredericksburg, Va

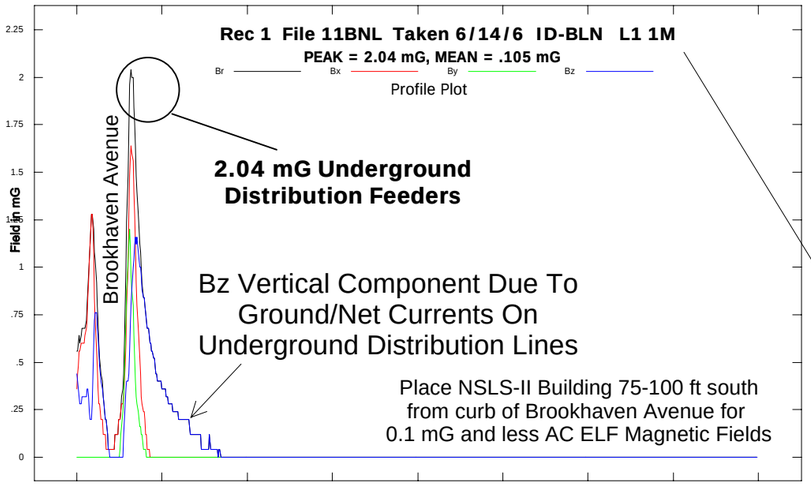

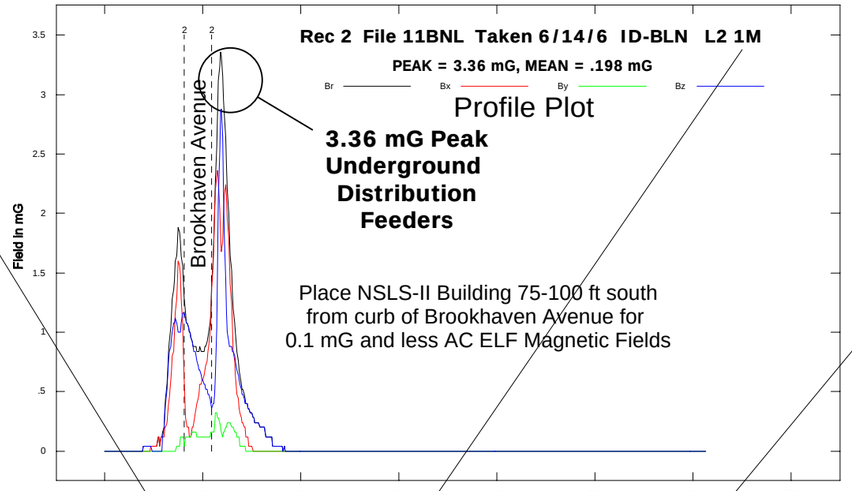

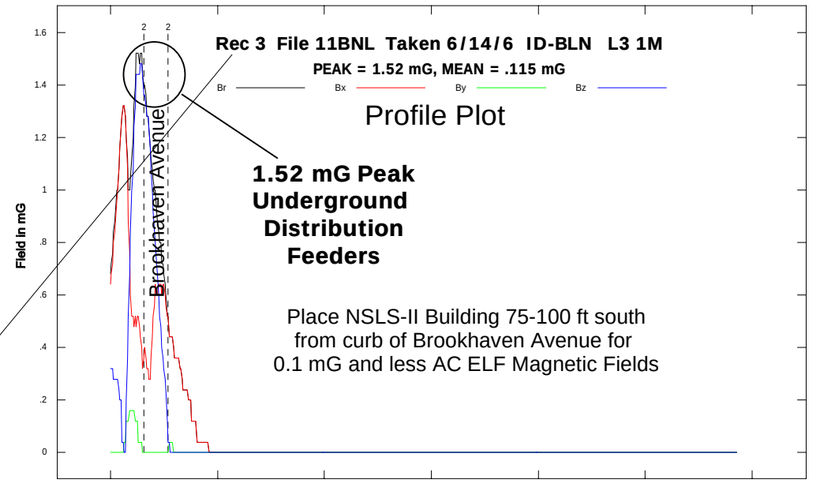

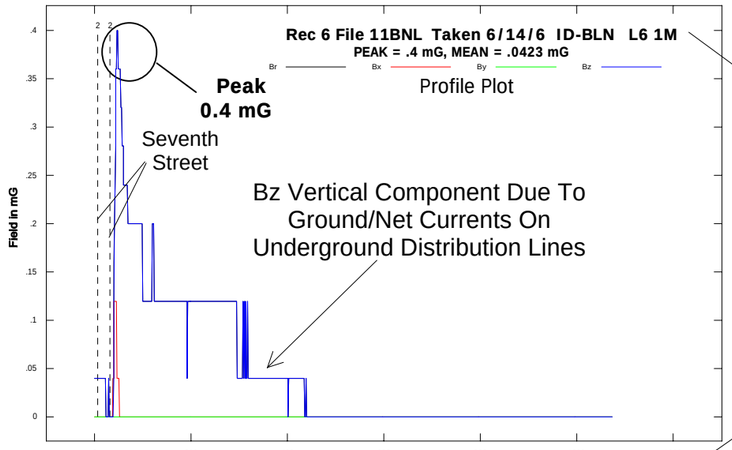

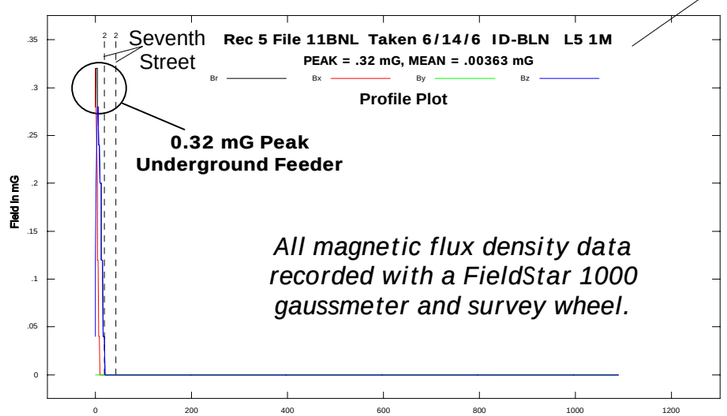

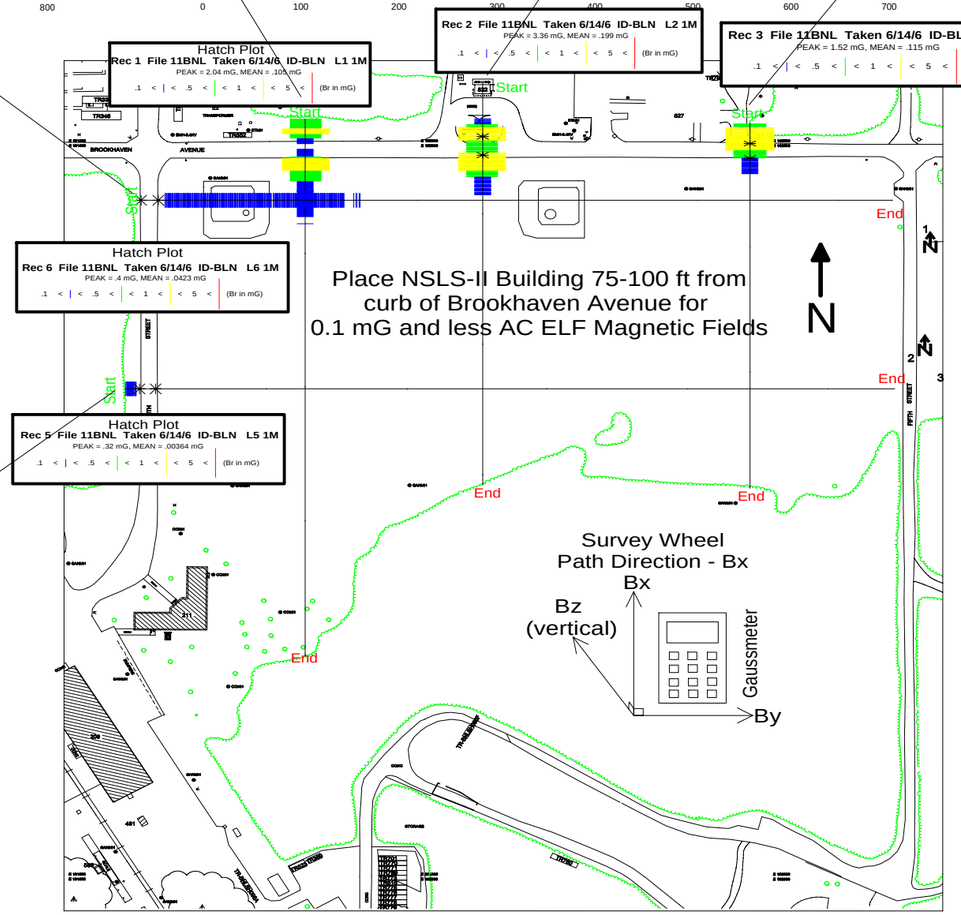

EMI AC & DC Magnetic Field Performance Specs

NMR Maximum Requirement: 1 mG Br RMS (2.83 mG p-p)

Instrument & Quite Labs Maximum Requirement: 0.1 mG Br RMS (0.3 mG p-p)

Cleanrooms Maximum Requirement: 0.3 mG Br RMS (0.1 mG p-p)

AC ELF Magnetic Field Human Exposure Standards

NYS Public Service Commission
200 mG @ 1-meter on Edge -ROW
or 50 ft. from 69 kV poles

IRPA/INIRC
833 mG over 24 hours
General Public Exposure

ACGIH
1000 mG general public
& workers with cardia pacemakers

Swiss Bunderstat
NCRP Draft Report
10 mG from overhead/underground transmission/distribution lines, substations, etc.

AC ELF EMI Thresholds (screen jitter & noise)

10 mG for 12-15 inch CRT computer monitors & audio/video equipment
5 mG for 17-21 inch CRT monitors & medical (i.e., EEGs, ECGs, EMGs,. etc.).
1.0 mG for standard scientific tools (STEMs, TEMs, FIB, I-Beam, etc.)
0.1- 0.3 mG for high resolution Nanotech scientific tools
0.01 mG for optimum superhigh resolution STEM tools

SEMI E33-94 AC ELF EMC Standards
Level A - less than 0.25 mG
Level B - less than 0.50 mG
Level C - less than 1.00 mG
Level D - less than 2.00 mG
Level E - 2.0 mG and greater

Figure #3, NSLS-II Brookhaven National Labs Proposed Site
Timed AC ELF (0.3 Hz - 3,000 Hz) Magnetic Flux Density Levels @ 1-meter
Upton, Long Island, New York

VitaTech Engineering, LLC
(540) 286-1984
Fredericksburg, Va

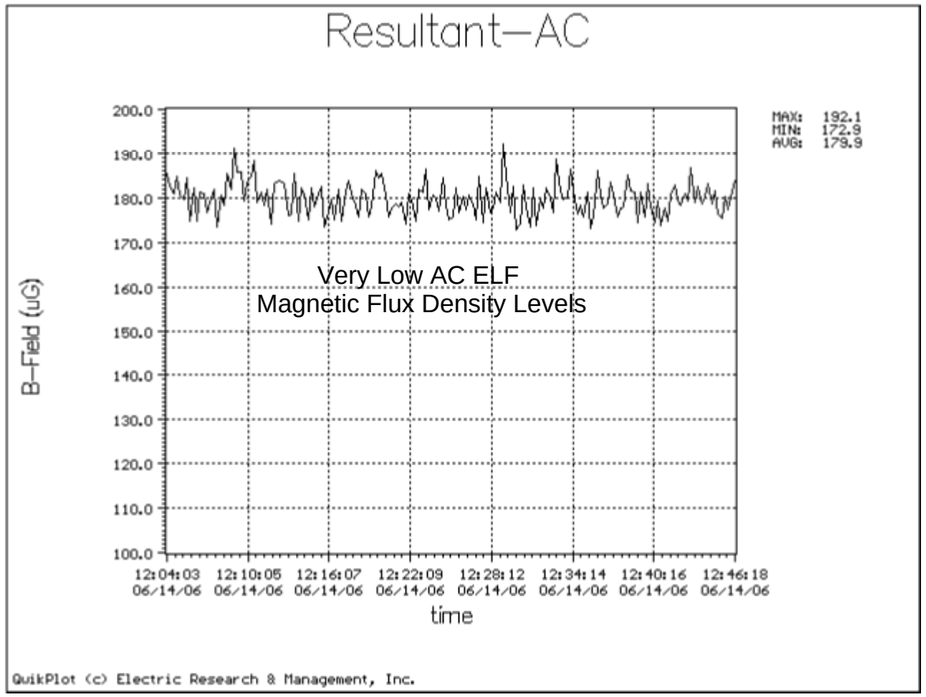

AC ELF Magnetic Field Human Exposure Standards

NYS Public Service Commission
200 mG @ 1-meter on Edge -ROW
or 50 ft. from 69 kV poles

IRPA/INIRC
833 mG over 24 hours
General Public Exposure

ACGIH
1000 mG general public
& workers with cardia pacemakers

Swiss Bunderstat
NCRP Draft Report
10 mG from overhead/underground
transmission/distribution lines,
substations, etc.

EMI AC & DC Magnetic Field Performance Specs
NMR Maximum Requirement:
1 mG Br RMS (2.83 mG p-p)

Instrument & Quite Labs
Maximum Requirement:
0.1 mG Br RMS (0.3 mG p-p)

Cleanrooms
Maximum Requirement:
0.3 mG Br RMS (0.1 mG p-p)

AC ELF EMI Thresholds (screen jitter & noise)

10 mG for 12-15 inch CRT computer monitors & audio/video equipment
5 mG for 17-21 inch CRT monitors & medical (i.e., EEGs, ECGs, EMGs,. etc.).
1.0 mG for standard scientific tools (STEMs, TEMs, FIB, I-Beam, etc.)
0.1- 0.3 mG for high resolution Nanotech scientific tools
0.01 mG for optimum superhigh resolution STEM tools

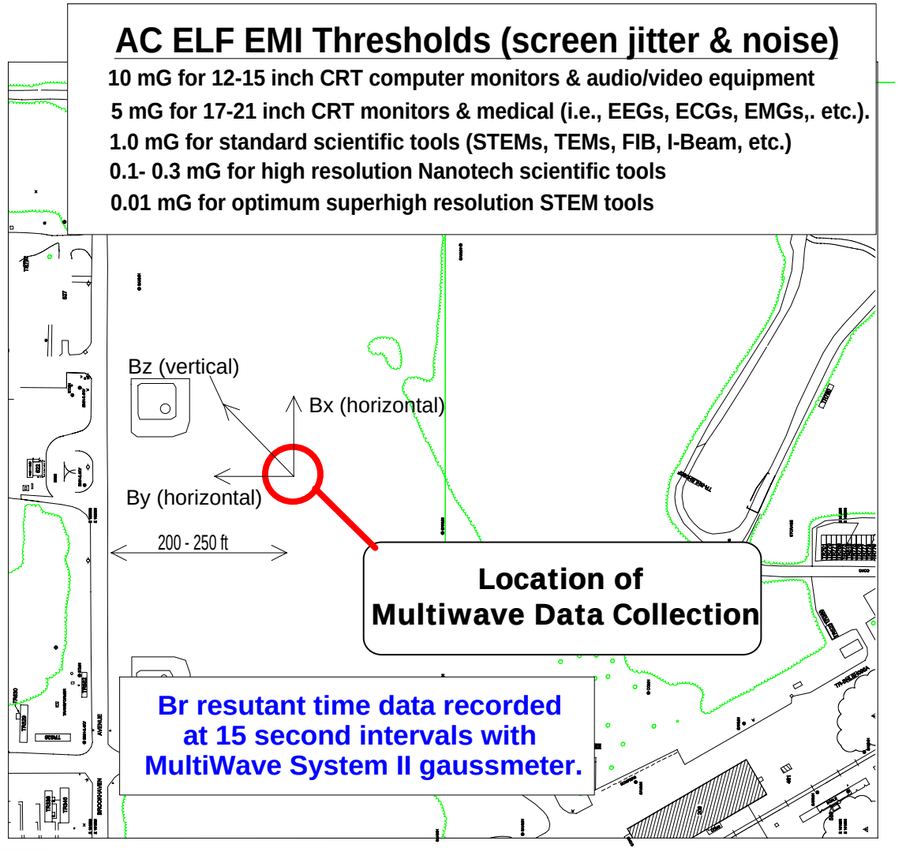

Br resutant time data recorded at 15 second intervals with MultiWave System II gaussmeter.

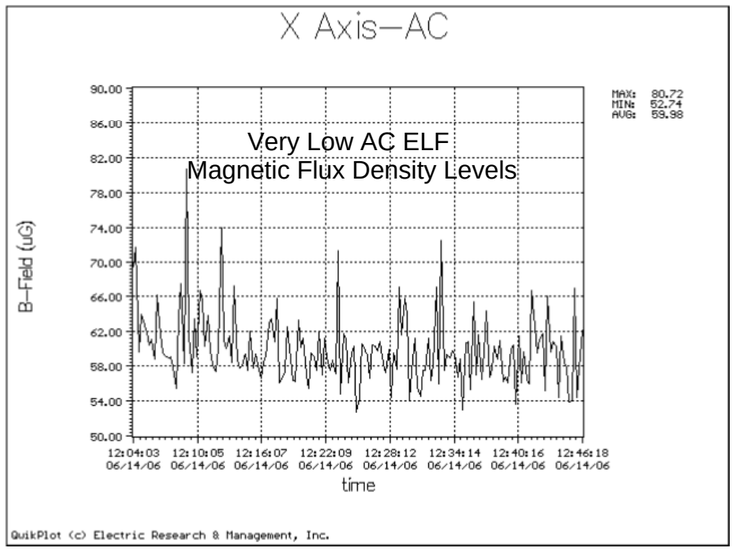

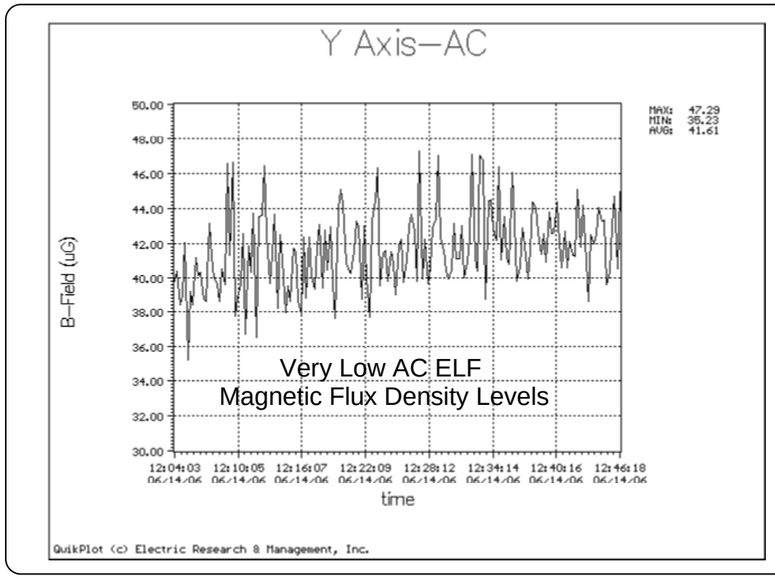

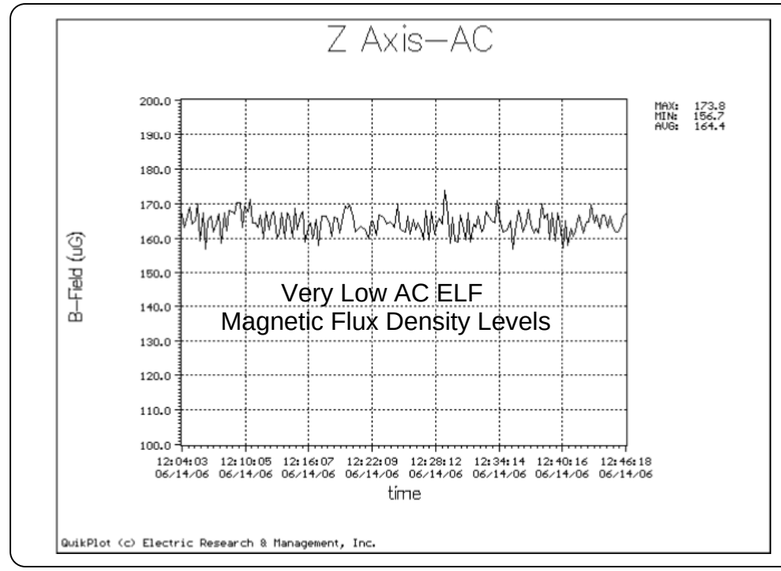

Figure #4, NSLS-II Brookhaven National Labs Proposed Site
Timed DC (0 Hz - 0.3 Hz) Magnetic Flux Density Levels @ 1-meter
Upton, Long Island, New York

VitaTech Engineering, LLC
(540) 286-1984
Fredericksburg, Va

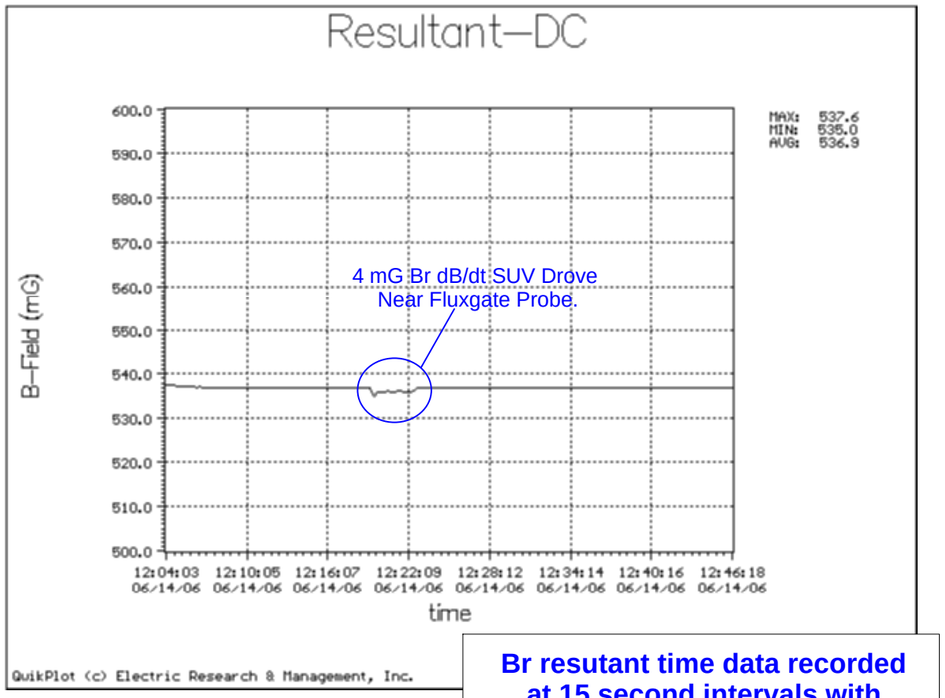

Br resutant time data recorded at 15 second intervals with MultiWave System II gaussmeter.

DC EMI Thresholds - CRT screen shift, noise & coercivity (data errors)

0.001 Gauss & Less SEMs, TEMs E-Beam/FIB Writers
0.75 Gauss CRT Monitors & Electronic Instruments
5 Gauss Cardiac Pacemakers & Implantable Devices Warning Sign
10 Gauss Credit Cards & Magnetic Media Warning Sign
300 Gauss Low Coercivity Mag-Stripe Cards
700 Gauss High Coercivity Mag-Sripe Cards & Video Tapes

1000 milligauss (mG) = 1 Gauss (G) & 1 mG = 0.001 G = 0.1 uT (microtesla)

EMI AC & DC Magnetic Field Performance Specs
NMR Maximum Requirement: 1 mG Br RMS (2.83 mG p-p)

Instrument & Quite Labs Maximum Requirement: 0.1 mG Br RMS (0.3 mG p-p)

Cleanrooms Maximum Requirement: 0.3 mG Br RMS (0.1 mG p-p)

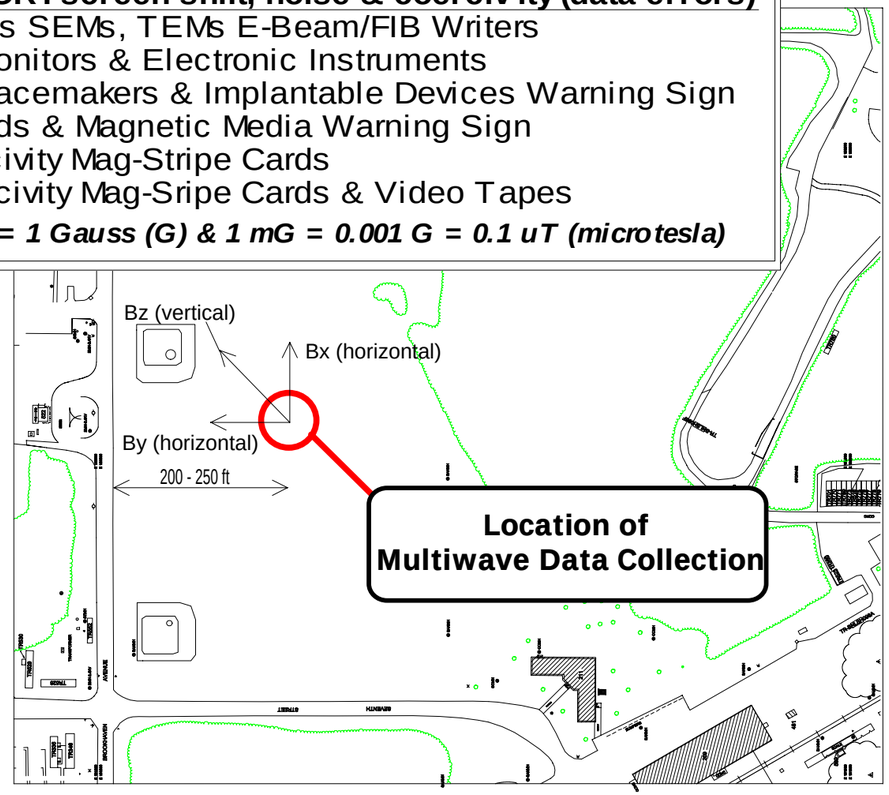

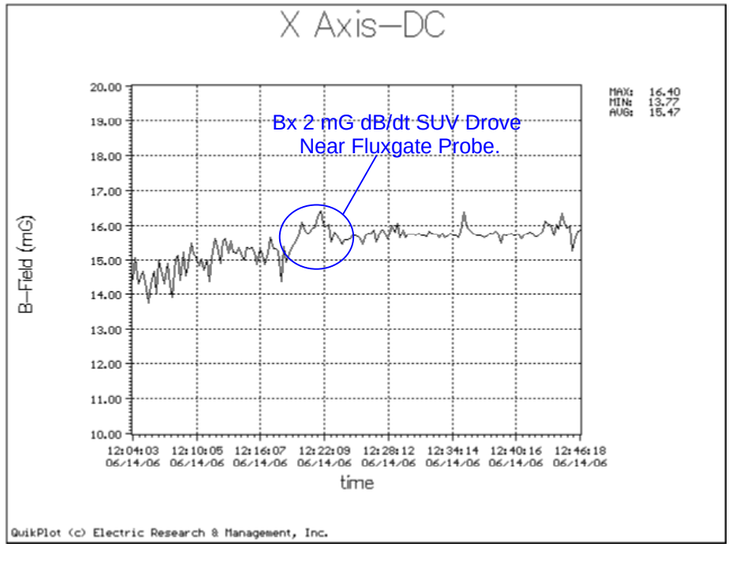

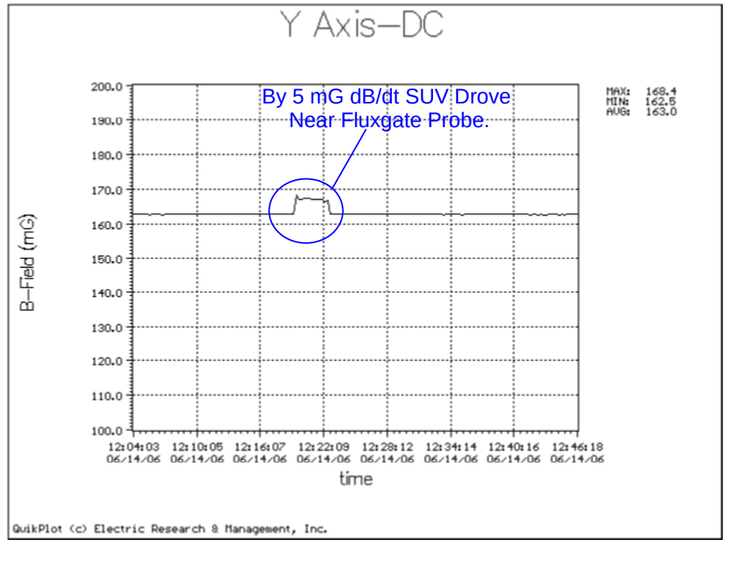

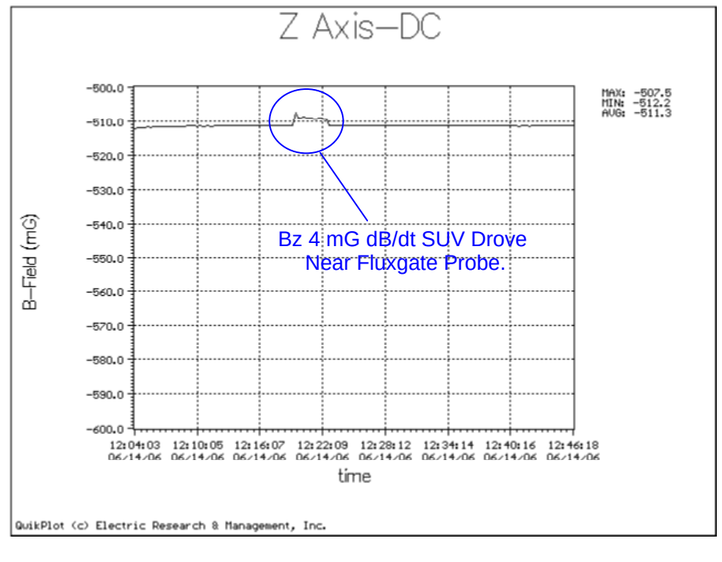

Timed DC magnetic flux density levels recorded with MEDA FVM-400 three-axis fluxgate magnetometer (bandwidth DC - 5 Hz and 0.01 mG resolution, 1200 mG maximum) Data recorded on October 6, 2004

Figure #5, Comparison Recorded & Predicted Moving Vehicle DC Magnetic Emissions

DC magnetic flux density data recorded at 0.2 second intervals
University of Florida DC EMI Data
Nanoscience Institute for Medical & Engineering Technology (NIMET)
Nanoscale Research Facility (NRF), University of Florida
Overlayed on NSLS-II Brookhaven National Labs Proposed Site

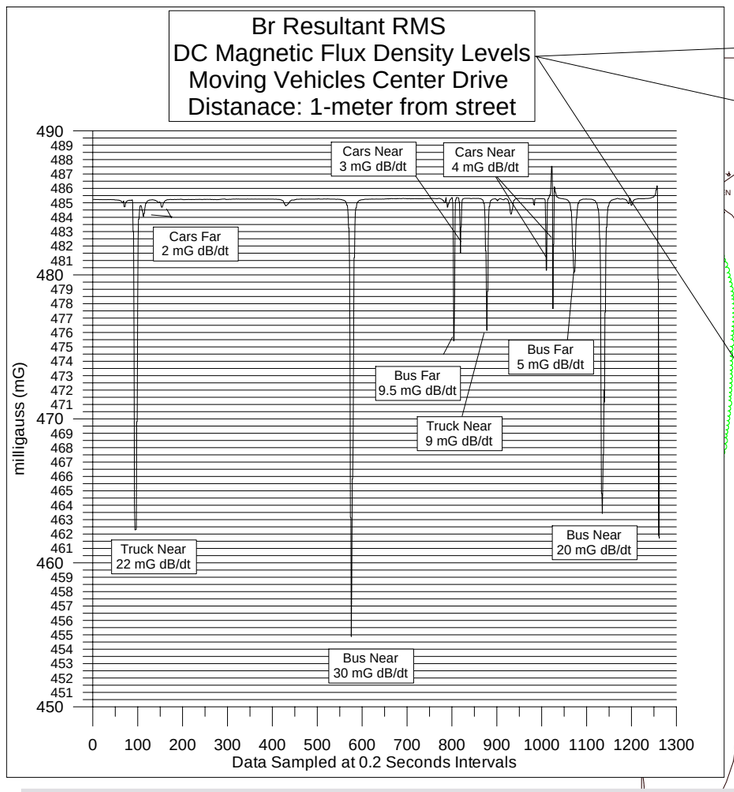

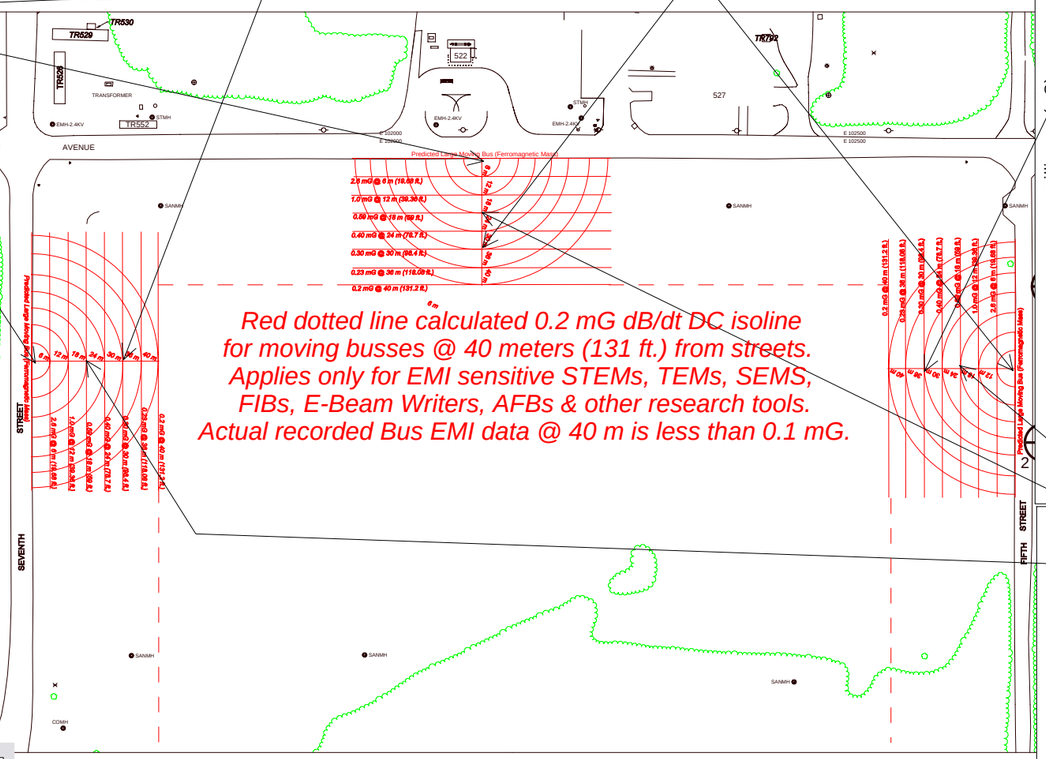

Red dotted line calculated 0.2 mG dB/dt DC isoline for moving busses @ 40 meters (131 ft.) from streets. Applies only for EMI sensitive STEMs, TEMs, SEMS, FIBs, E-Beam Writers, AFBs & other research tools. Actual recorded Bus EMI data @ 40 m is less than 0.1 mG.

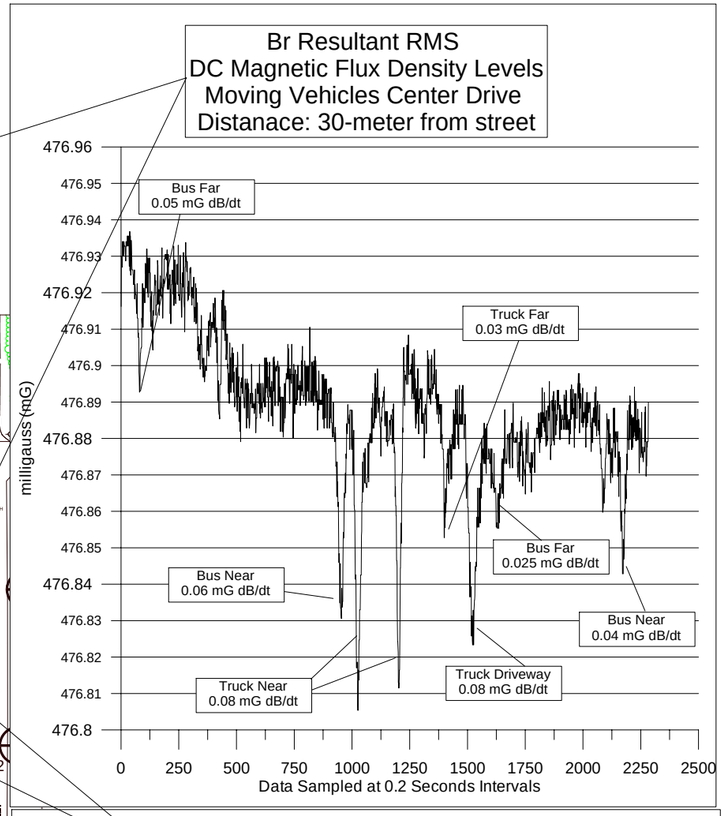

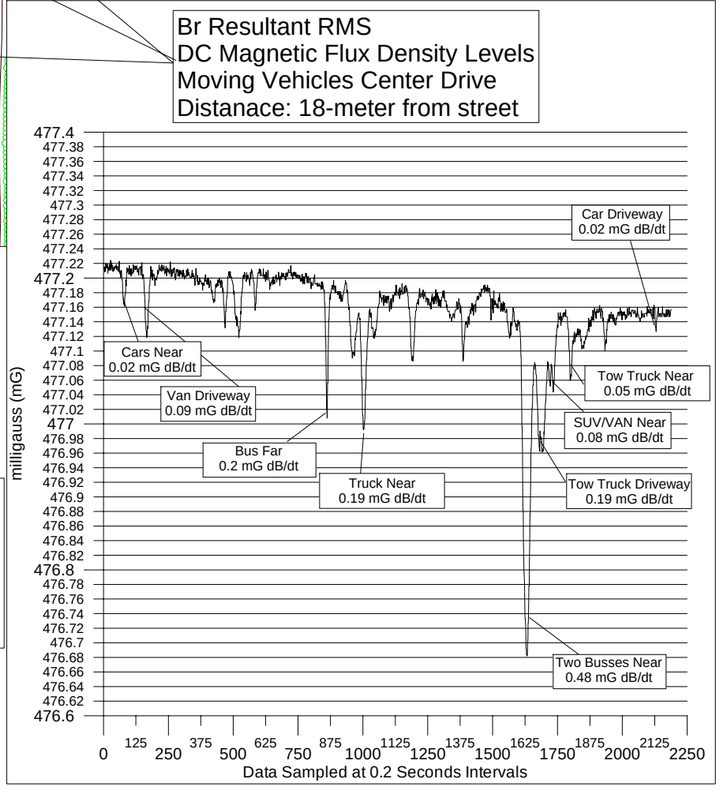

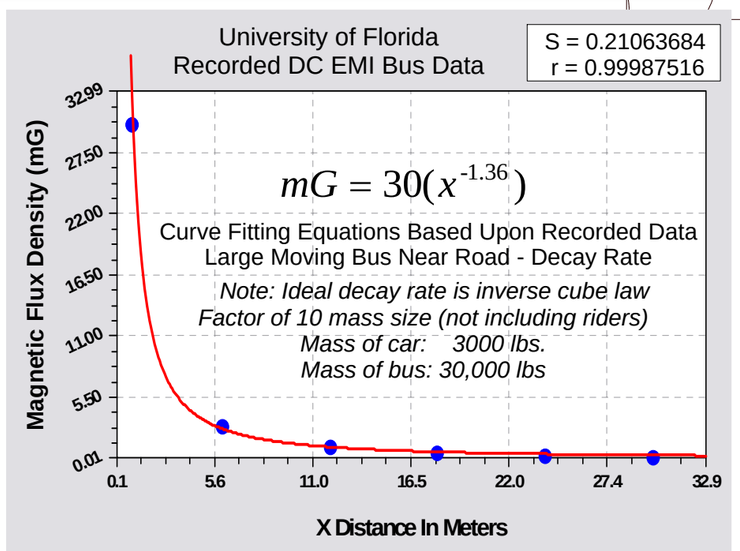

Calculated Vehicle Profiles

Distance	Car	Bus
1 m	3.50 mG	30.0 mG
6 m	0.48 mG	2.6 mG
12 m	0.22 mG	1.0 mG
18 m	0.15 mG	0.59 mG
24 m	0.11 mG	0.40 mG
30 m	0.08 mG	0.30 mG
36 m	0.07 mG	0.23 mG
40 m	0.06 mG	0.20 mG

Special Note: magnetic fields decay more rapidly after 30 meters than the calculated levels indicate.

DC EMI Thresholds - CRTscreen shift, noise & coerciv ity (data errors)
0.001 Gauss & Less SEMs, TEMs E-Beam/FIB Writers
0.75 Gauss CRT Monitors & Electronic Instruments
5 Gauss Cardiac Pacemakers & Implantable Devices Warning Sign
10 Gauss Credit Cards & Magnetic Media Warning Sign
300 Gauss Low Coercivity Mag-Stripe Cards
700 Gauss High Coercivity Mag-Sripe Cards & Video Tapes
1000 milligauss (mG) = 1 Gauss (G) & 1 mG = 0.001 G = 0.1 uT (microtesla)

VitaTech Engineering, LLC
Fredericksburg, VA
July 20, 2006

Figure #6, NSLS-II Brookhaven National Labs Proposed Site 100 kHz to 18 GHz Timed RF Electric Field Strength Data Upton, Long Island, New York

VitaTech Engineering, LLC
(540) 286-1984
Fredericksburg, Va

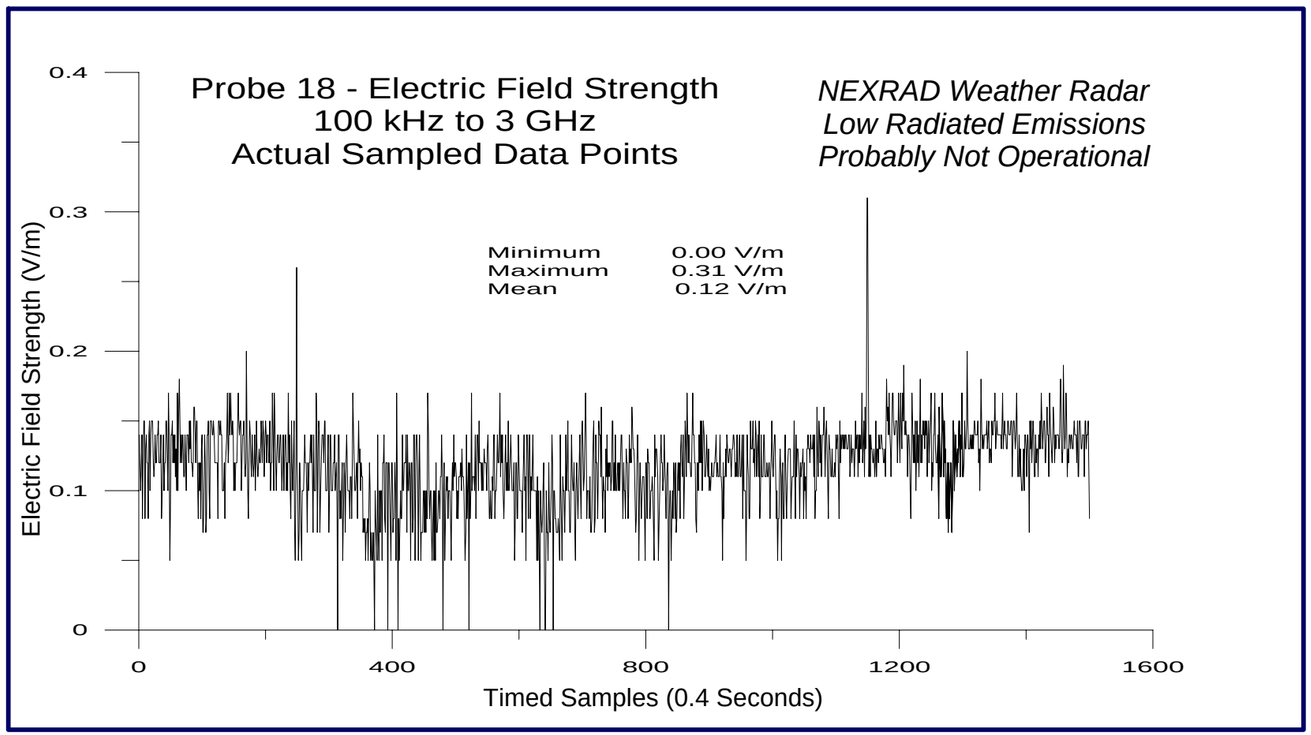

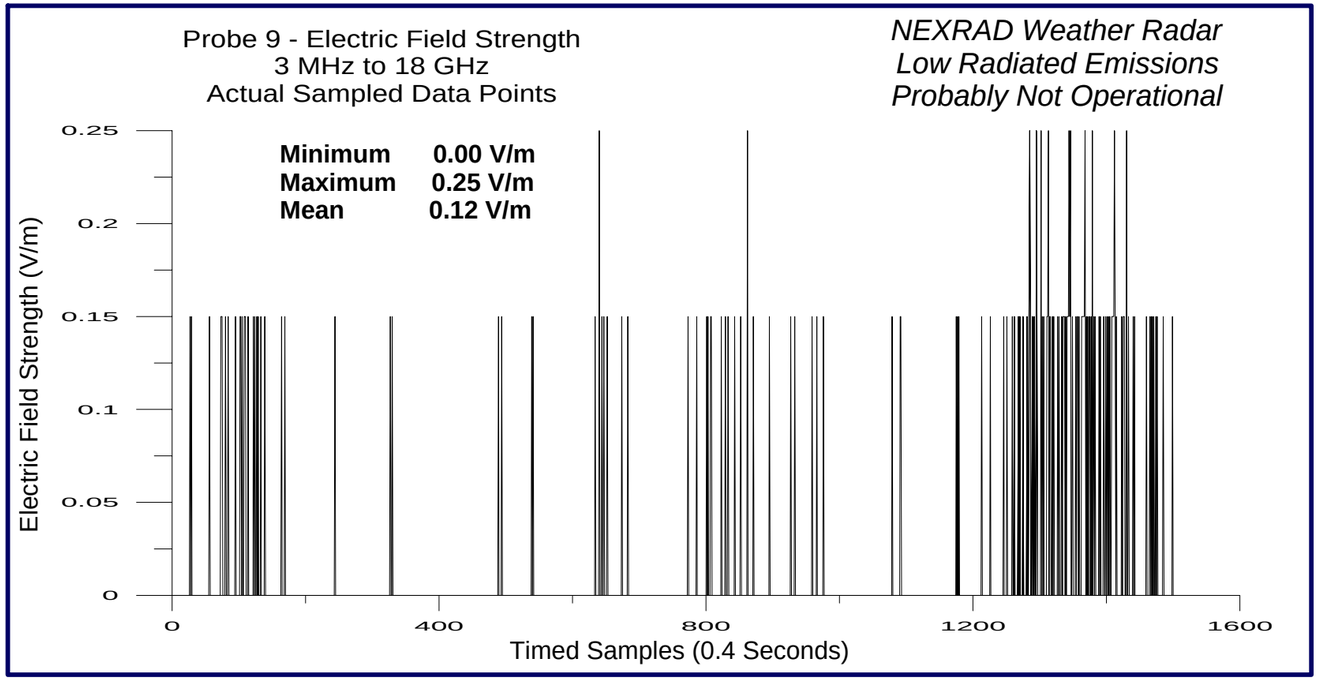

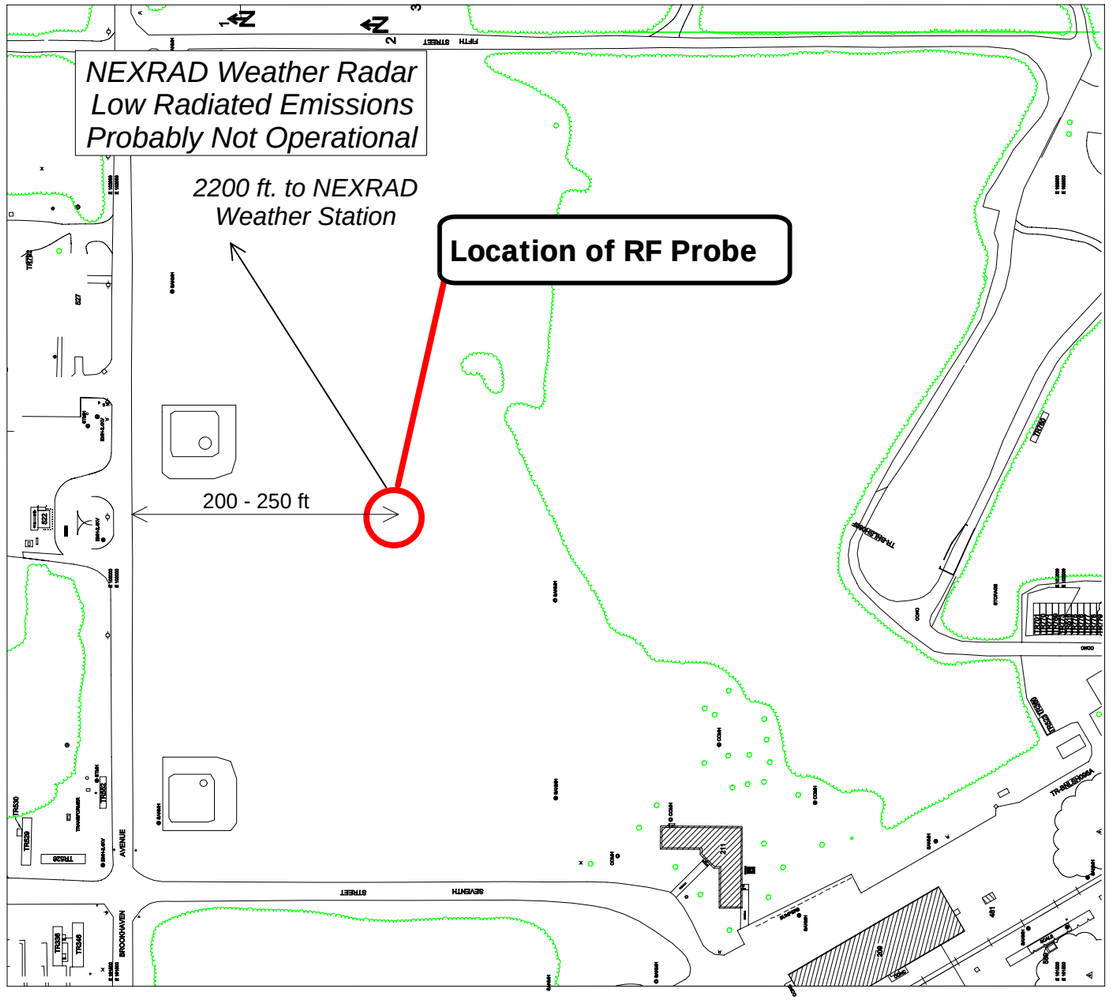

Electric field strength RF levels were recorded in volts-per-meter (V/m) for 10 minutes sampled at 0.04-second intervals with a Narda ERM-300 electric field meter using a Probe 18 from 100 kHz to 3 Ghz (range of 0.2 to 320 V/m) and Probe 9C from 3 MHz to 18 GHz (range of 0.5 to 1000 V/m). The objective is to investigate sources of radio-frequency interference (RFI) over a wide bandwidth. It should be noted that 3 V/m is the industry standard RFI threshold and 1 V/m the medical/scientific instrument RFI threshold.

Figure #7, NSLS-II Brookhaven National Labs Proposed Site
100 kHz to 18 GHz Timed RF Maximum Electric Field Strength Data
Upton, Long Island, New York

VitaTech Engineering, LLC
(540) 286-1984
Fredericksburg, Va

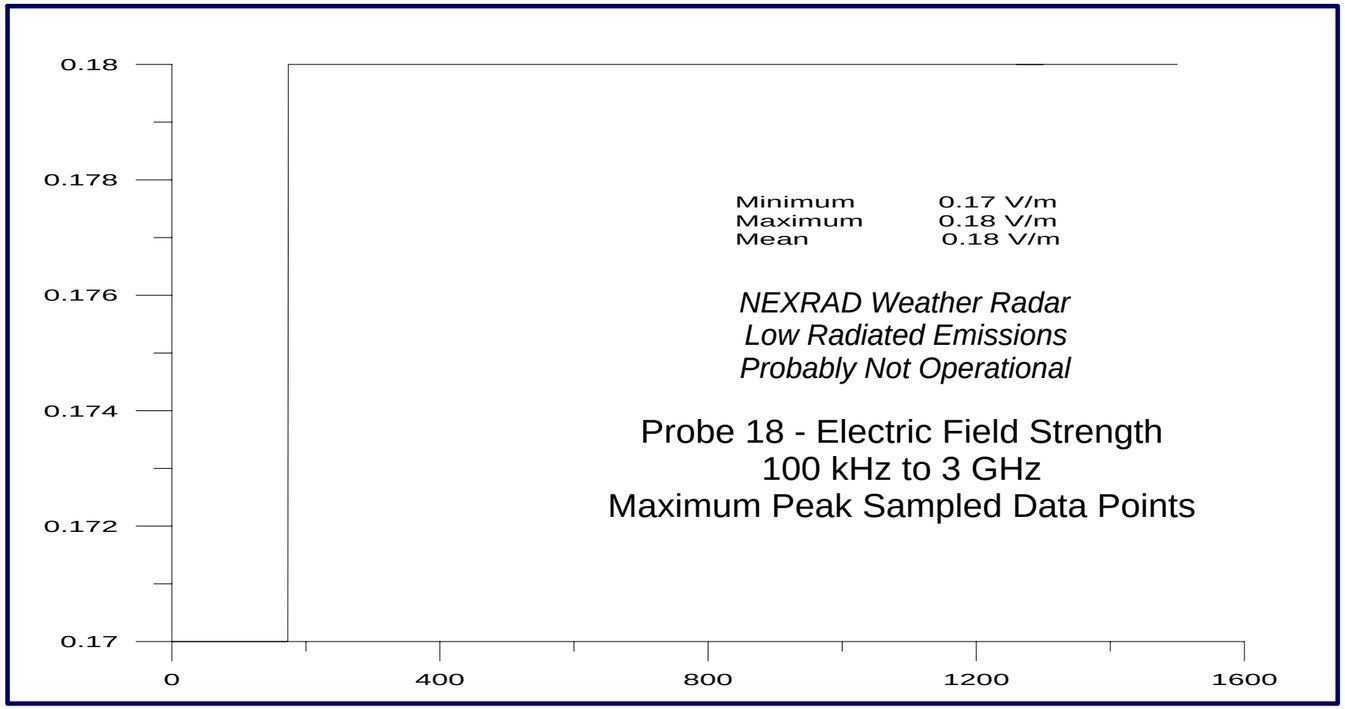

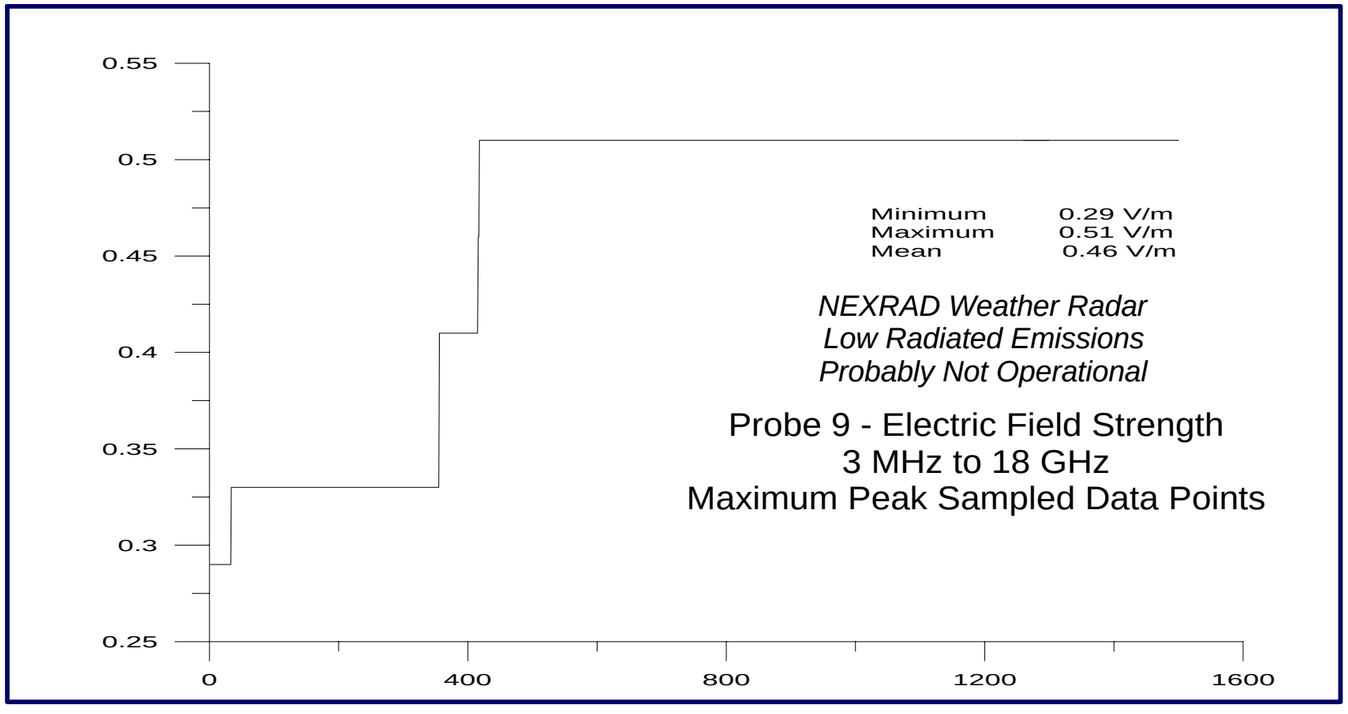

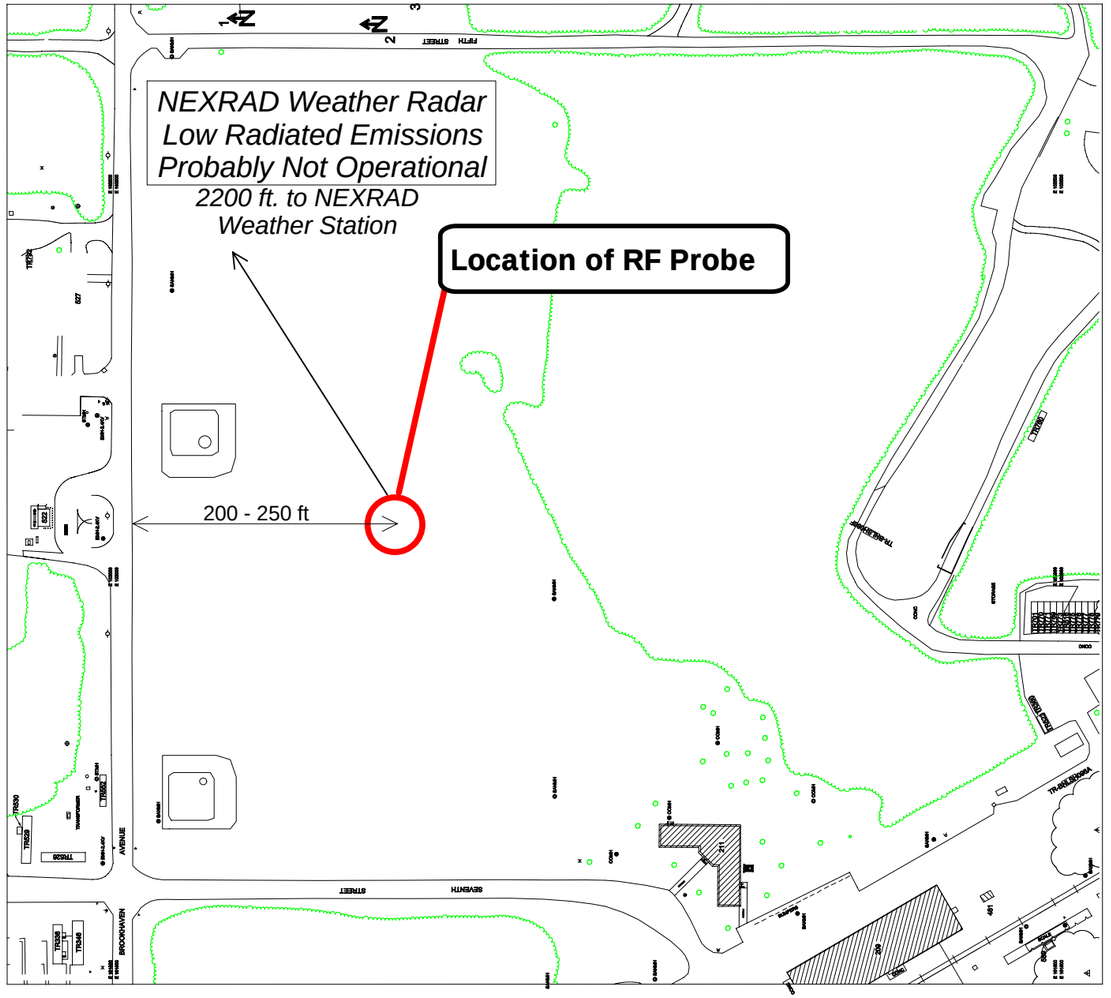

Electric field strength RF levels were recorded in volts-per-meter (V/m) for 10 minutes sampled at 0.04-second intervals with a Narda ERM-300 electric field meter using a Probe 18 from 100 kHz to 3 Ghz (range of 0.2 to 320 V/m) and Probe 9C from 3 MHz to 18 GHz (range of 0.5 to 1000 V/m). The objective is to investigate sources of radio-frequency interference (RFI) over a wide bandwidth. It should be noted that 3 V/m is the industry standard RFI threshold and 1 V/m the medical/scientific instrument RFI threshold.

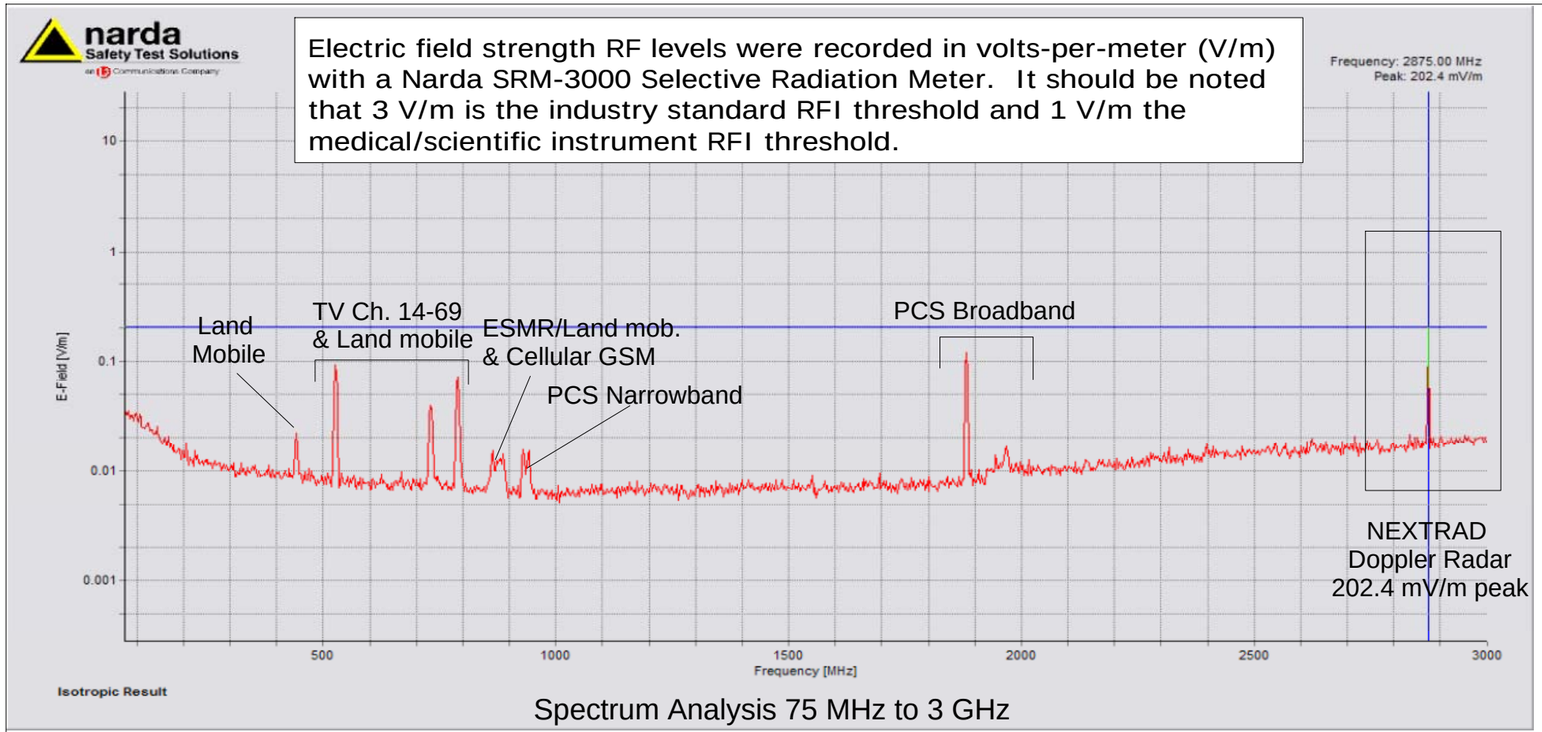

Spectrum Analysis 75 MHz to 3 GHz

Figure #2 - RF Spectrum 75 MHz - 3 GHz @ 1-meter
NSLS-II Brookhaven National Labs Proposed Site

Peak Chart By Frequency & Level

Index	Frequency	Level
1	2875.00 MHz	202.4 mV/m
2	1882.32 MHz	120.5 mV/m
3	525.70 MHz	97.07 mV/m
4	789.27 MHz	73.45 mV/m
5	730.69 MHz	39.49 mV/m
6	82.26 MHz	35.32 mV/m
7	97.02 MHz	33.77 mV/m
8	105.52 MHz	33.09 mV/m
9	88.52 MHz	32.23 mV/m
10	123.96 MHz	27.72 mV/m
11	142.63 MHz	25.48 mV/m
12	114.28 MHz	24.84 mV/m
13	130.42 MHz	23.77 mV/m
14	137.95 MHz	21.93 mV/m
15	442.51 MHz	21.88 mV/m
16	2835.09 MHz	21.26 mV/m
17	2952.94 MHz	20.85 mV/m
18	2715.16 MHz	20.76 mV/m
19	2902.43 MHz	20.65 mV/m
20	2960.11 MHz	20.62 mV/m

Dataset Type	SPEC
Store Mode	MAN
Date	09/19/2006
Time	10:02:18
Minimum Frequency [Hz]	75 MHz
Maximum Frequency [Hz]	3 GHz
Resolution Bandwidth [Hz]	5 MHz
Measurement Range [V/m]	2.5 V/m
Unit	V/m
Result Type	MAX
Number of Averages	64
Average Flag	OK
Overdrive Flag	OK
Threshold [V/m]	25 µV/m
Y-Scale Reference [V/m]	28 V/m
Y-Scale Range [dB]	100
Axis	RSS
Standard Name	ICNIRP GP
Comment	G4
Device Serial No.	J-0016
Device Calibration Date	05/15/2006
Device Firmware Version	V1.4.10
Cable Name	
Cable Serial No.	
Cable Calibration Date	
Antenna Name	3AX 75M-3G
Antenna Serial No.	G-0147
Antenna Calibration Date	05/18/2006

RF Data Recorded
9/19/2006

VitaTech Engineering, LLC
(540) 286-1984
Fredericksburg, Va

Power Spectrum Chart By Service, Level & Frequency Band

RF Data Recorded
9/19/2006

Service	Value	Lower Frequency	Upper Frequency	
FM Radio	375.5 pW/cm²	88.000 MHz	108.000 MHz	
Paging	56.83 pW/cm²	152.000 MHz	159.000 MHz	
TV Ch. 7-13	166.3 pW/cm²	174.000 MHz	216.000 MHz	
TV Ch. 14-69	2.169 nW/cm²	470.000 MHz	806.000 MHz	
SMR Tx	14.06 pW/cm²	806.000 MHz	821.000 MHz	
Privat lnd mob	3.397 pW/cm²	821.000 MHz	824.000 MHz	
Cellular AMPS	21.99 pW/cm²	824.000 MHz	849.000 MHz	
ESMR/Land mob.	48.83 pW/cm²	849.000 MHz	869.000 MHz	
Cellular AMPS	82.96 pW/cm²	869.000 MHz	894.000 MHz	
aerontical mobl	2.285 pW/cm²	894.000 MHz	896.000 MHz	
private lnd mob	4.556 pW/cm²	896.000 MHz	901.000 MHz	
pcs narrowband	1.013 pW/cm²	901.000 MHz	902.000 MHz	
land mobile&Ham	57.99 pW/cm²	902.000 MHz	930.000 MHz	
pcs narrowband	2.817 pW/cm²	930.000 MHz	931.000 MHz	
Paging	26.71 pW/cm²	931.000 MHz	932.000 MHz	
pcs narrowband	21.94 pW/cm²	940.000 MHz	941.000 MHz	
public land mob	14.88 pW/cm²	941.000 MHz	960.000 MHz	
PCS Broadband	283.3 pW/cm²	1850.000 MHz	1990.000 MHz	
NEXTRAD Dopple	972.4 pW/cm²	2700.000 MHz	2900.000 MHz	
Others	3.874 nW/cm²			
Total	8.201 nW/cm²	88.000 MHz	2900.000 MHz	

Electric field strength RF levels were recorded in volts-per-meter (V/m) with a Narda SRM-3000 Selective Radiation Meter. It should be noted that 3 V/m is the industry standard RFI threshold and 1 V/m the medical/scientific instrument RFI threshold.

Service Chart By Level & Frequency Band

Service	Value	Lower Frequency	Upper Frequency
FM Radio	37.63 mV/m	88.000 MHz	108.000 MHz
Paging	14.64 mV/m	152.000 MHz	159.000 MHz
TV Ch. 7-13	25.04 mV/m	174.000 MHz	216.000 MHz
TV Ch. 14-69	90.43 mV/m	470.000 MHz	806.000 MHz
SMR Tx	7.281 mV/m	806.000 MHz	821.000 MHz
Privat lnd mob	3.579 mV/m	821.000 MHz	824.000 MHz
Cellular AMPS	9.105 mV/m	824.000 MHz	849.000 MHz
ESMR/Land mob.	13.57 mV/m	849.000 MHz	869.000 MHz
Cellular AMPS	17.68 mV/m	869.000 MHz	894.000 MHz
aerontical mobl	2.935 mV/m	894.000 MHz	896.000 MHz
private lnd mob	4.144 mV/m	896.000 MHz	901.000 MHz
pcs narrowband	1.954 mV/m	901.000 MHz	902.000 MHz
land mobile&Ham	14.79 mV/m	902.000 MHz	930.000 MHz
pcs narrowband	3.259 mV/m	930.000 MHz	931.000 MHz
Paging	10.03 mV/m	931.000 MHz	932.000 MHz
pcs narrowband	9.094 mV/m	940.000 MHz	941.000 MHz
public land mob	7.489 mV/m	941.000 MHz	960.000 MHz
PCS Broadband	32.68 mV/m	1850.000 MHz	1990.000 MHz
NEXTRAD Dopple	60.55 mV/m	2700.000 MHz	2900.000 MHz
Others	120.8 mV/m		
Total	175.8 mV/m	88.000 MHz	2900.000 MHz

Figure #2A - FCC Spectrum 75 MHz - 3 GHz @ 1-meter
NSLS-II Brookhaven National Labs Proposed Site

Dataset Type	TAB
Store Mode	MAN
Date	09/19/2006
Time	10:06:25
Minimum Frequency [Hz]	88 MHz
Maximum Frequency [Hz]	2.9 GHz
Measurement Range [V/m]	2.5 V/m
Unit	V/m
Result Type	MAX
Number of Averages	4
Average Flag	OK
Overdrive Flag	OK
Threshold [V/m]	25 µV/m
Display	DETAIL
Axis	RSS
Standard Name	ICNIRP GP
Service Table Name	FCC STD
Comment	G5
Device Serial No.	J-0016
Device Calibration Date	05/15/2006
Device Firmware Version	V1.4.10
Cable Name	
Cable Serial No.	
Cable Calibration Date	
Antenna Name	3AX 75M-3G
Antenna Serial No.	G-0147
Antenna Calibration Date	05/18/2006

VitaTech Engineering, LLC
(540) 286-1984
Fredericksburg, Va

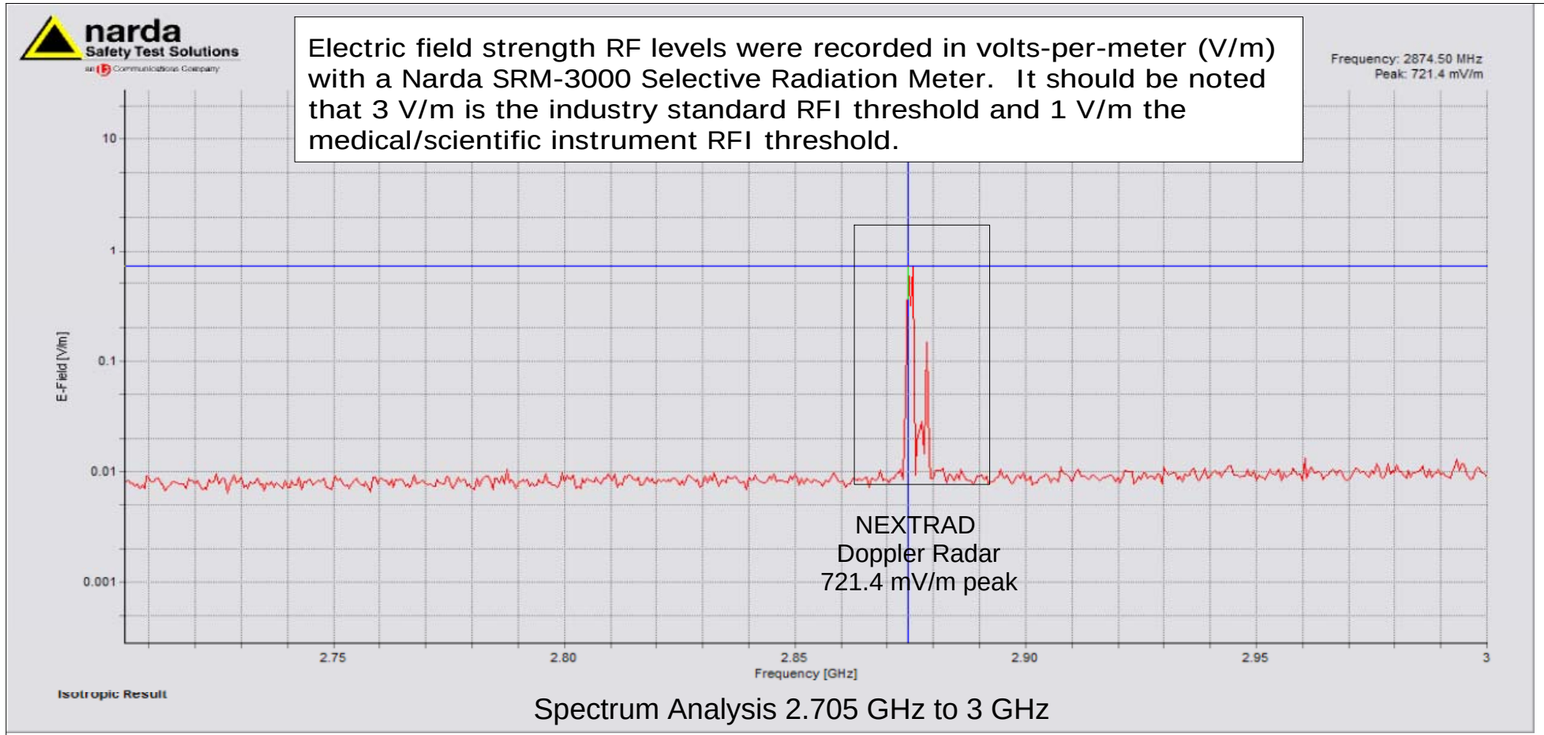

Spectrum Analysis 2.705 GHz to 3 GHz

Peak Chart By Frequency & Level

Index	Frequency	Level
1	2874.50 MHz	721.4 mV/m
2	2875.50 MHz	698.0 mV/m
3	2878.50 MHz	146.6 mV/m
4	2877.37 MHz	29.03 mV/m
5	2960.51 MHz	13.30 mV/m
6	2993.46 MHz	12.80 mV/m
7	2994.64 MHz	11.95 mV/m
8	2976.09 MHz	11.78 mV/m
9	2978.51 MHz	11.62 mV/m
10	2980.52 MHz	11.37 mV/m
11	2944.16 MHz	11.36 mV/m
12	2985.95 MHz	11.29 mV/m
13	2930.14 MHz	11.14 mV/m
14	2997.95 MHz	11.05 mV/m
15	2907.64 MHz	11.03 mV/m
16	2961.96 MHz	10.96 mV/m
17	2936.35 MHz	10.72 mV/m
18	2938.88 MHz	10.69 mV/m
19	2881.86 MHz	10.68 mV/m
20	2971.65 MHz	10.66 mV/m

Dataset Type	SPEC
Store Mode	MAN
Date	09/19/2006
Time	09:52:16
Minimum Frequency [Hz]	2.705 GHz
Maximum Frequency [Hz]	3 GHz
Resolution Bandwidth [Hz]	1 MHz
Measurement Range [V/m]	2.5 V/m
Unit	V/m
Result Type	MAX
Number of Averages	64
Average Flag	OK
Overdrive Flag	OK
Threshold [V/m]	25 µV/m
Y-Scale Reference [V/m]	28 V/m
Y-Scale Range [dB]	100
Axis	RSS
Standard Name	ICNIRP GP
Comment	G1
Device Serial No.	J-0016
Device Calibration Date	05/15/2006
Device Firmware Version	V1.4.10
Cable Name	
Cable Serial No.	
Cable Calibration Date	
Antenna Name	3AX 75M-3G
Antenna Serial No.	G-0147
Antenna Calibration Date	05/18/2006

Figure #1 - RF Spectrum 2.7 - 3 GHz NEXTRAD Doppler Radar @ 1-meter
NSLS-II Brookhaven National Labs Proposed Site

RF Data Recorded
9/19/2006

VitaTech Engineering, LLC
(540) 286-1984
Fredericksburg, Va

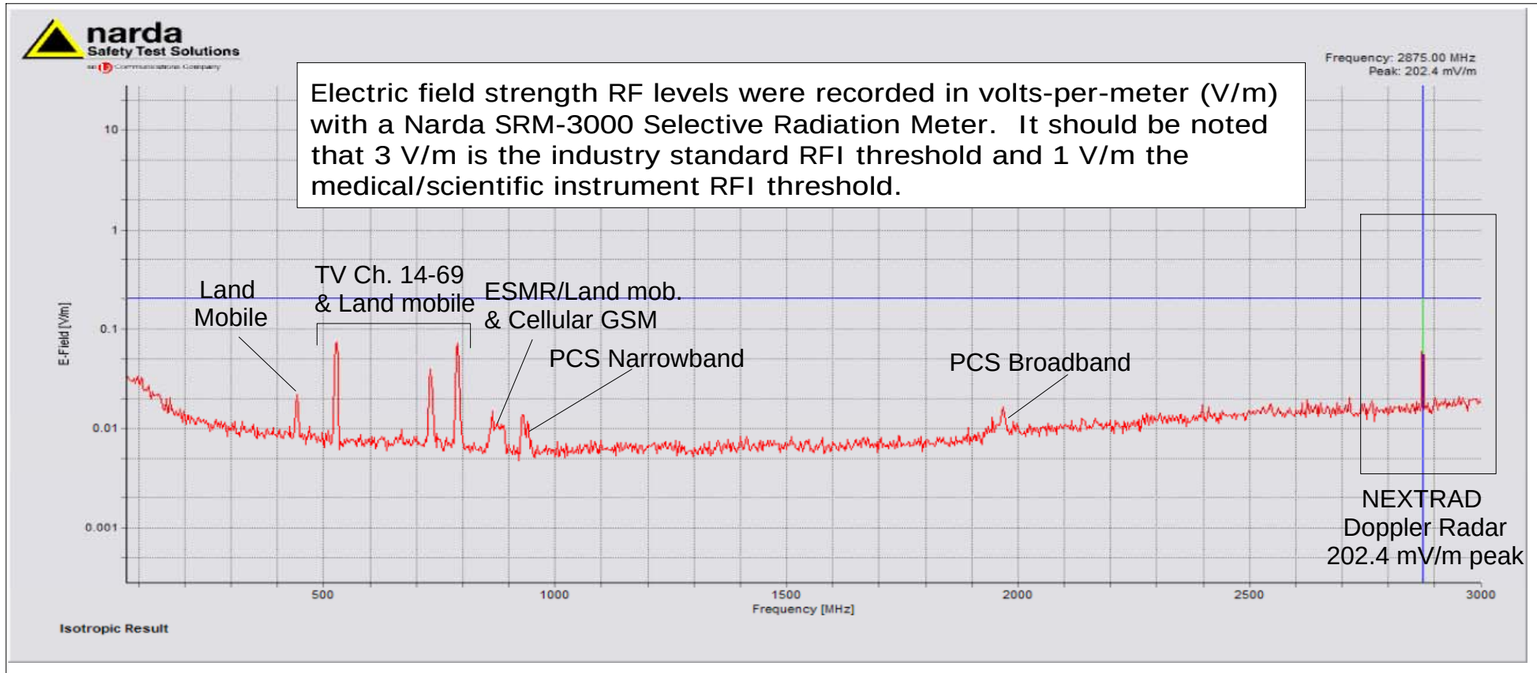

Figure #1A - RF Spectrum 75 Mz - 3 GHz @ 1-meter
NSLS-II Brookhaven National Labs Proposed Site

Peak Chart By Frequency & Level

Index	Frequency	Level
1	2875.00 MHz	202.4 mV/m
2	526.38 MHz	76.24 mV/m
3	789.27 MHz	73.45 mV/m
4	730.05 MHz	39.06 mV/m
5	77.28 MHz	33.71 mV/m
6	96.96 MHz	33.43 mV/m
7	105.52 MHz	33.09 mV/m
8	89.69 MHz	31.85 mV/m
9	121.75 MHz	27.17 mV/m
10	114.79 MHz	24.80 mV/m
11	130.33 MHz	23.81 mV/m
12	143.68 MHz	22.49 mV/m
13	138.11 MHz	21.94 mV/m
14	442.51 MHz	21.88 mV/m
15	2952.42 MHz	20.77 mV/m
16	2715.16 MHz	20.76 mV/m
17	2902.43 MHz	20.65 mV/m
18	2960.28 MHz	20.65 mV/m
19	167.63 MHz	20.56 mV/m
20	2988.98 MHz	20.52 mV/m

Dataset Type	SPEC
Store Mode	MAN
Date	09/19/2006
Time	10:00:21
Minimum Frequency [Hz]	75 MHz
Maximum Frequency [Hz]	3 GHz
Resolution Bandwidth [Hz]	5 MHz
Measurement Range [V/m]	2.5 V/m
Unit	V/m
Result Type	MAX
Number of Averages	64
Average Flag	OK
Overdrive Flag	OK
Threshold [V/m]	25 µV/m
Y-Scale Reference [V/m]	28 V/m
Y-Scale Range [dB]	100
Axis	RSS
Standard Name	
Comment	
Device Serial No.	J-0016
Device Calibration Date	05/15/2006
Device Firmware Version	V1.4.10
Cable Name	
Cable Serial No.	
Cable Calibration Date	
Antenna Name	3AX 75M-3G
Antenna Serial No.	G-0147
Antenna Calibration Date	05/18/2006

RF Data Recorded
9/19/2006

VitaTech Engineering, LLC
(540) 286-1984
Fredericksburg, Va

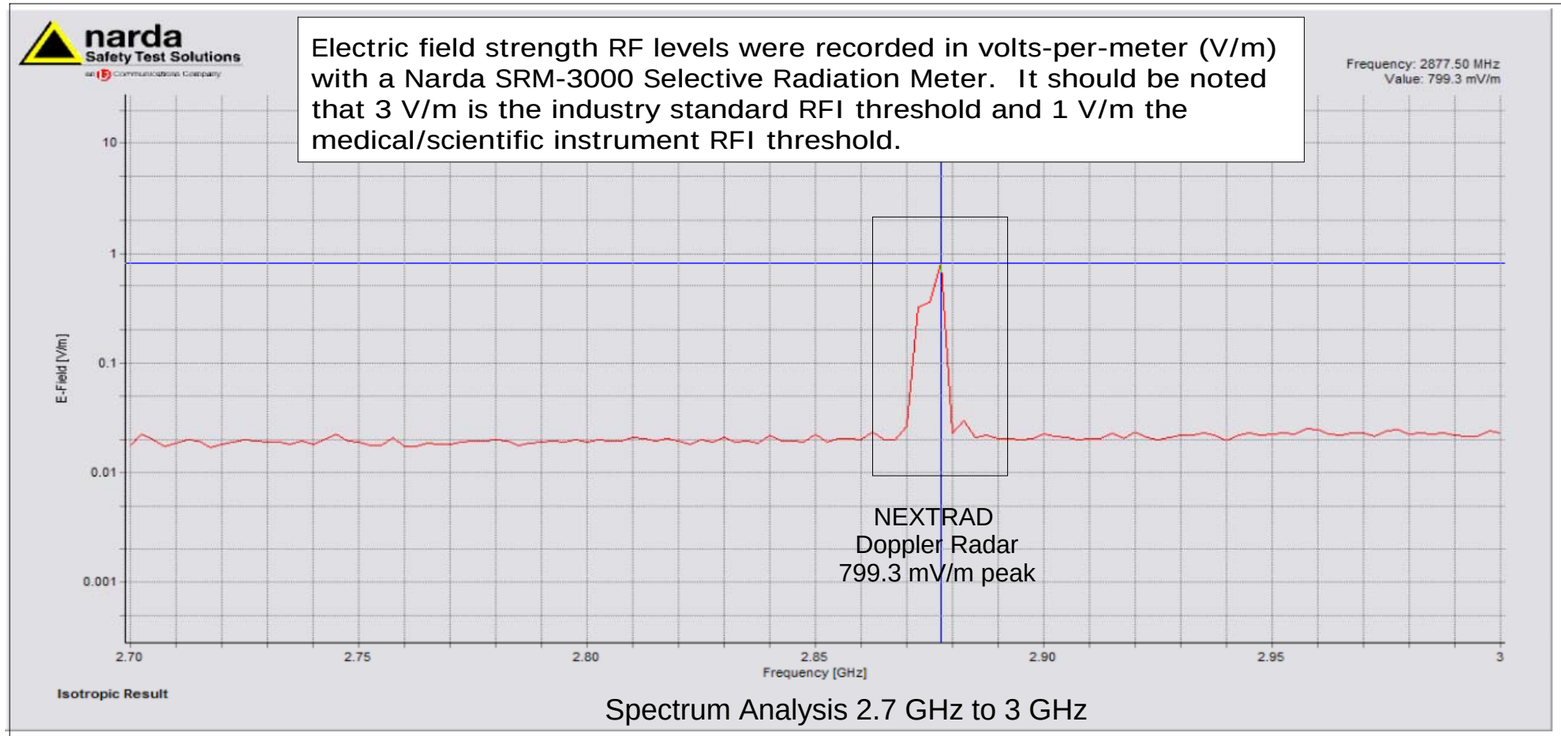

Spectrum Analysis 2.7 GHz to 3 GHz

Peak Chart By Frequency & Level

Index	Frequency	Level
1	2877.50 MHz	799.3 mV/m
2	2882.33 MHz	29.75 mV/m
3	2958.57 MHz	25.45 mV/m
4	2976.75 MHz	24.74 mV/m
5	2998.20 MHz	24.10 mV/m
6	2920.20 MHz	23.58 mV/m
7	2969.14 MHz	23.33 mV/m
8	2862.48 MHz	23.32 mV/m
9	2987.01 MHz	23.30 mV/m
10	2982.76 MHz	23.07 mV/m
11	2944.80 MHz	22.96 mV/m
12	2952.63 MHz	22.96 mV/m
13	2702.93 MHz	22.82 mV/m
14	2935.21 MHz	22.82 mV/m
15	2914.99 MHz	22.79 mV/m
16	2744.92 MHz	22.69 mV/m
17	2900.43 MHz	22.65 mV/m
18	2849.97 MHz	22.51 mV/m
19	2887.17 MHz	21.96 mV/m
20	2840.23 MHz	21.96 mV/m

Dataset Type	SPEC	
Store Mode	MAN	
Date	09/19/2006	
Time	10:41:34	
Minimum Frequency [Hz]		2.7 GHz
Maximum Frequency [Hz]		3 GHz
Resolution Bandwidth [Hz]		5 MHz
Measurement Range [V/m]		2.5 V/m
Unit	V/m	
Result Type	MAX	
Number of Averages		64
Average Flag	OK	
Overdrive Flag	OK	
Threshold [V/m]	25 µV/m	
Y-Scale Reference [V/m]		28 V/m
Y-Scale Range [dB]	100	
Axis	RSS	
Standard Name		
Comment		
Device Serial No.	J-0016	
Device Calibration Date		05/15/2006
Device Firmware Version		V1.4.10
Cable Name		
Cable Serial No.		
Cable Calibration Date		
Antenna Name	3AX 75M-3G	
Antenna Serial No.	G-0147	
Antenna Calibration Date		05/18/2006

Figure #3 - RF Spectrum 75 MHz - 3 GHz @ 15.2 m (50 ft)
NSLS-II Brookhaven National Labs Proposed Site

RF Data Recorded From Cherry-Picker 9/19/2006

VitaTech Engineering, LLC
(540) 286-1984
Fredericksburg, Va

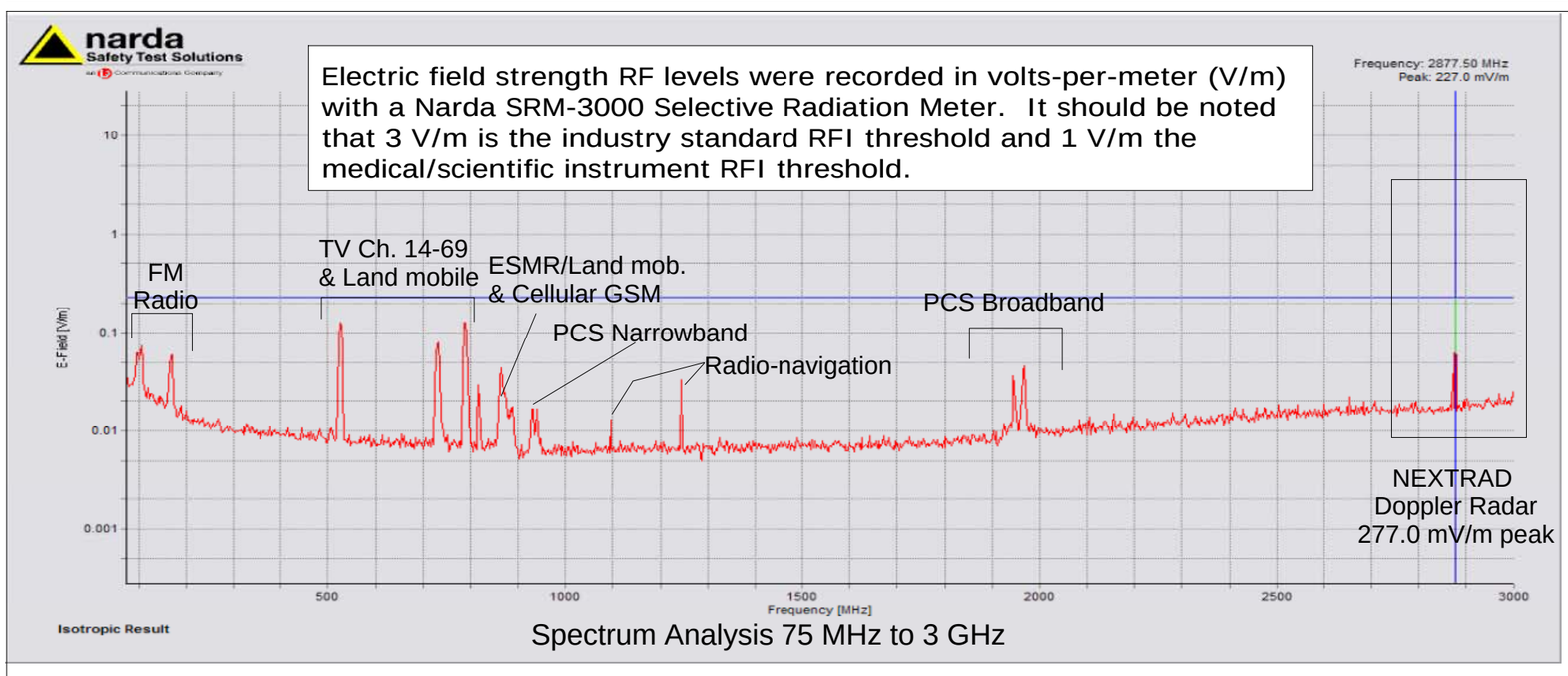

Spectrum Analysis 75 MHz to 3 GHz

Peak Chart By Frequency & Level

Index	Frequency	Level
1	2877.50 MHz	227.0 mV/m
2	788.89 MHz	130.6 mV/m
3	526.03 MHz	129.3 mV/m
4	731.52 MHz	83.46 mV/m
5	104.60 MHz	73.53 mV/m
6	168.81 MHz	67.70 mV/m
7	96.37 MHz	64.39 mV/m
8	1966.71 MHz	47.85 mV/m
9	865.03 MHz	42.70 mV/m
10	2872.50 MHz	37.88 mV/m
11	1945.85 MHz	37.86 mV/m
12	1245.00 MHz	32.78 mV/m
13	84.61 MHz	29.72 mV/m
14	817.50 MHz	29.29 mV/m
15	119.93 MHz	26.91 mV/m
16	2997.38 MHz	24.93 mV/m
17	871.60 MHz	24.34 mV/m
18	126.17 MHz	23.81 mV/m
19	2970.19 MHz	23.73 mV/m
20	142.21 MHz	22.54 mV/m

Dataset Type	SPEC	
Store Mode	MAN	
Date	09/19/2006	
Time	10:46:07	
Minimum Frequency [Hz]		75 MHz
Maximum Frequency [Hz]		3 GHz
Resolution Bandwidth [Hz]		5 MHz
Measurement Range [V/m]		2.5 V/m
Unit	V/m	
Result Type	MAX	
Number of Averages		64
Average Flag	OK	
Overdrive Flag	OK	
Threshold [V/m]	25 µV/m	
Y-Scale Reference [V/m]		28 V/m
Y-Scale Range [dB]	100	
Axis	RSS	
Standard Name		
Comment		
Device Serial No.	J-0016	
Device Calibration Date		05/15/2006
Device Firmware Version		V1.4.10
Cable Name		
Cable Serial No.		
Cable Calibration Date		
Antenna Name	3AX 75M-3G	
Antenna Serial No.	G-0147	
Antenna Calibration Date		05/18/2006

Figure #3A - RF Spectrum 75 Mz - 3 GHz @ 15.2 m (50 ft.)
NSLS-II Brookhaven National Labs Proposed Site

RF Data Recorded From Cherry-Picker 9/19/2006

VitaTech Engineering, LLC
(540) 286-1984
Fredericksburg, Va

Appendix A4

HVAC Calculations
Accelerator Ring Tunnel – one pentant
Experimental Hall – one pentant

HVAC

CALCULATIONS

HVAC Load Calculations for:

- One Accelerator Ring Tunnel Pentant AHU-101
- One Experimental Hall Pentant AHU – 201A and AHU-201B

HDR MECHANICAL SECTION

HEATING/COOLING LOAD CALCULATIONS

1.000 ROOM TYPES

ROOM DATA

0 CFM

PROJECT: BNL

UNIT: AHU-101

DATE: 05-Sep-07

ENGINEER: ATIENZA

ROOM NO:	T1		PEOPLE (NO EA):	15
ROOM NAME:	TUNNEL 1		LIGHTS (WATTS):	1.5
AREA (SQFT):	6393		MISC SENS (BTUH):	216000
HEIGHT (FT):	9		MISC LAT (BTUH):	
DESIGN AC:	6		RA=0/EA=1	0
RM TEMP (DEG F):	78	78	CFM/SQFT:	
PEOPLE SENS (BTUH):	450		PRESS (CFM):	0
PEOPLE LAT (BTUH):	450		NO OF RMS:	1

	WALL AREA (SQFT)	WINDOW AREA (SQFT)
N:	0	0
E:	0	0
S:	0	0
W:	0	0

ROOF AREA (SQFT):	
WALL BELOW GRADE (SQFT):	6841
SLAB ON GRADE (SQFT):	6393

HDR MECHANICAL SECTION

HEATING/COOLING LOAD CALCULATIONS

1.000 ROOM TYPES
0 CFM

ROOM DATA

PROJECT: BNL
DATE: 05-Sep-07

UNIT: AHU-201-A
ENGINEER: ATIENZA

ROOM NO:	P1A	
ROOM NAME:	PENTANT 1A	
AREA (SQFT):	19762	
HEIGHT (FT):	12	
DESIGN AC:	6	
RM TEMP (DEG F):	75	75
PEOPLE SENS (BTUH):	450	
PEOPLE LAT (BTUH):	450	

PEOPLE (NO EA):	38
LIGHTS (WATTS):	2.0
MISC SENS (BTUH):	118000
MISC LAT (BTUH):	
RA=0/EA=1	0
CFM/SQFT:	
PRESS (CFM):	0
NO OF RMS:	1

	WALL AREA (SQFT)	WINDOW AREA (SQFT)
N:	6411	1188
E:	0	0
S:	6295	0
W:	0	0

ROOF AREA (SQFT):	19762
WALL BELOW GRADE (SQFT):	
SLAB ON GRADE (SQFT):	19762

HDR MECHANICAL SECTION

HEATING/COOLING LOAD CALCULATIONS

1.000 ROOM TYPES

ROOM DATA

0 CFM

PROJECT: BNL

UNIT: AHU-201-B

DATE: 05-Sep-07

ENGINEER: ATIENZA

ROOM NO:	P1B		PEOPLE (NO EA):	38
ROOM NAME:	PENTANT 1B		LIGHTS (WATTS):	2.8
AREA (SQFT):	19762		MISC SENS (BTUH):	118000
HEIGHT (FT):	12		MISC LAT (BTUH):	
DESIGN AC:	6		RA=0/EA=1	0
RM TEMP (DEG F):	75	75	CFM/SQFT:	
PEOPLE SENS (BTUH):	450		PRESS (CFM):	0
PEOPLE LAT (BTUH):	450		NO OF RMS:	1

	WALL AREA (SQFT)	WINDOW AREA (SQFT)
N:	6411	1188
E:	0	0
S:	6295	0
W:	0	0

ROOF AREA (SQFT):	19762
WALL BELOW GRADE (SQFT):	
SLAB ON GRADE (SQFT):	19762

HEATING/COOLING LOAD CALCULATIONS

ROOM DATA SUMMARY

PROJECT: BNL
DATE: 05-Sep-07

UNIT: AHU-101
PAGE: 1

ROOM NO	ROOM NAME	SA (CFM)	RA (CFM)	EA (CFM)	SQFT	)ES/SQFT AC	COOL AC	DT HTG
T1	TUNNEL 1	10280	10280	0	6393	6	11	4
		10280	10280	0	6393			

HEATING/COOLING LOAD CALCULATIONS

ROOM DATA SUMMARY

PROJECT: BNL
DATE: 05-Sep-07

UNIT: AHU-101
PAGE: 2

COOLING (BTUH)

ROOM NO	ROOM	TOTAL SENS	EXT SENS	INTERNAL SENSIBLE LIGHTS	PEOPLE	MISC	TOTAL LATENT	HTG (BTUH)	HTG (BTUH/FT)
T1	TUNNEL 1	255354	0	32604	6750	216000	6750	39702	
		255354	0	32604	6750	216000	6750	39702	

HEATING/COOLING LOAD CALCULATIONS

AHU DATA SUMMARY

PROJECT: BNL
DATE: 05-Sep-07

UNIT: AHU-101
PAGE: 3

	COOLING LOAD SENSIBLE (BTUH)						HTG (BTUH)		
BTUH	8	10	12	2	4	6			
TOTAL SENSIBLE	255354	255354	255354	255354	255354	255354	39702		
TOTAL LATENT	6750	6750	6750	6750	6750	6750	0		
GRAND TOTAL	262104	262104	262104	262104	262104	262104			
							AC	SQFT	HTG
AVG DT	23	23	23	23	23		CFM	CFM	CFM
SA (CFM)	10280	10280	10280	10280	10280	10280	5754	0	106387
RA (CFM)	10280	10280	10280	10280	10280	10280			
EA (CFM)	0	0	0	0	0	0			
TOTAL SA (CFM)	10280								
TOTAL RA (CFM)	10280								
TOTAL EA (CFM)	0								
	0	0	0	0	0	0	0	0	
SENSIBLE COOLING	0	0	0	0	0	0	0	0	
	255354	255354	255354	255354	255354	255354	39702		
	255354	255354	255354	255354	255354	255354	39702	0	0
LATENT COOLING	0	0	0	0	0	0	0	0	
	6750	6750	6750	6750	6750	6750	0		
	6750	6750	6750	6750	6750	6750	0	0	0
SUPPLY AIR	0	0	0	0	0	0	0	0	
	10280	10280	10280	10280	10280	10280	5754	0	106387
	10280	10280	10280	10280	10280	10280	5754	0	106387
RETURN AIR	0	0	0	0	0	0	0	0	
	10280	10280	10280	10280	10280	10280	5754	0	60193
	10280	10280	10280	10280	10280	10280	5754	0	60193
EXHAUST AIR	0	0	0	0	0	0	0	0	
	0	0	0	0	0	0	0	0	51610
	0	0	0	0	0	0	0	0	51610

9 10 9 9 9 9 9 9 9 9 9 100

HEATING/COOLING LOAD CALCULATIONS

GLOBAL DATA

PROJECT: BNL
DATE: 05-Sep-07
ENGINEER: ATIENZA

AHU-101
PAGE: 4.00 4.00

Uwall:	0.05	20.00	PEOPLE SENS (BTUH	250.00
Uwindow s:	0.30		PEOPLE LAT (BTUH):	200.00
Uwindow w:	0.29		OAT WINT (DEG F):	0.00
Uroof:	0.04		SA TEMP (DEG F):	55.00
SHADE FC:	0.44		DT HTG (DEG F):	40.00
WALL CONST:	3.00	(BELOW GRADE)		
FLOOR CONST:	3.00	(BELOW GRADE)		

Factors Corrected for Latitude-Month

Time of Day	08:00 AM	10:00 AM	12:00 PM	02:00 PM	04:00 PM	06:00 PM
CLTDroof:	22	23	26.00	31.00	36.00	39.00
CLTDwall: TYPE B						
N:	9	8	7.64	8.47	9.30	23.00
E:	13	13	16.77	19.26	21.75	32.00
S:	12	10	10.13	10.96	13.45	43.00
W:	17	15	13.45	12.62	13.45	43.00
CLTDwindow:	3	7	12.00	16.00	17.00	12.00
SHGF:						
N:	130	130	130	130	130	130
E:	216	216	216	216	216	216
S:	205	205	205	205	205	205
W:	216	216	216	216	216	216
CLFwindow:						
N:	0.65	0.80	0.89	0.86	0.75	0.70
E:	0.80	0.62	0.27	0.22	0.17	0.16
S:	0.23	0.58	0.83	0.68	0.35	0.33
W:	0.11	0.15	0.17	0.53	0.82	0.67

Time of Day	08:00 AM	10:00 AM	12:00 PM	02:00 PM	04:00 PM	06:00 PM

Raw Factors

CLTDroof		20	21.00	24.00	29.00	34.00	38.00
CLTDwall	TYPE E						
N:		4	6	9.00	13.00	17.00	20.00
E:		11	26	36.00	37.00	34.00	32.00
S:		3	5.00	13.00	24.00	32.00	33.00
W:		6	6.00	9.00	14.00	27.00	43.00

CLTD Correction Factor (LM)	
Roof:	1
Walls:	
N	3
E	0
S	10
W	0

HEATING/COOLING LOAD CALCULATIONS

ROOM DATA SUMMARY

PROJECT: BNL
DATE: 05-Sep-07

UNIT: AHU-201-A
PAGE: 1

ROOM NO	ROOM NAME	SA (CFM)	RA (CFM)	EA (CFM)	SQFT	)ES/SQFT AC	COOL AC	DT HTG
P1A	PENTANT 1A	23710	23710	0	19762	6	4	8
		23710	23710	0	19762			

HEATING/COOLING LOAD CALCULATIONS

ROOM DATA SUMMARY

PROJECT: BNL
DATE: 05-Sep-07

UNIT: AHU-201-A
PAGE: 2

COOLING (BTUH)

ROOM NO	ROOM	TOTAL SENS	EXT SENS	INTERNAL SENSIBLE LIGHTS	PEOPLE	MISC	TOTAL LATENT	HTG (BTUH)	HTG (BTUH/FT)
P1A	PENTANT 1A	378408	108926	134382	17100	118000	17100	192059	
		378408	108926	134382	17100	118000	17100	192059	

HEATING/COOLING LOAD CALCULATIONS

AHU DATA SUMMARY

PROJECT: BNL
DATE: 05-Sep-07

UNIT: AHU-201-A
PAGE: 3

	COOLING LOAD SENSIBLE (BTUH)						HTG (BTUH)		
BTUH	8	10	12	2	4	6			
TOTAL SENSIBLE	344150	355770	365774	369640	367524	378408	192059		
TOTAL LATENT	17100	17100	17100	17100	17100	17100	0		
GRAND TOTAL	361250	372870	382874	386740	384624	395508			
							AC	SQFT	HTG
AVG DT	20	20	20	20	20		CFM	CFM	CFM
SA (CFM)	15933	16471	16934	17113	17015	17519	23714	0	149622
RA (CFM)	15933	16471	16934	17113	17015	17519			
EA (CFM)	0	0	0	0	0	0			

TOTAL SA (CFM)	23710
TOTAL RA (CFM)	23710
TOTAL EA (CFM)	0

	0	0	0	0	0	0	0	0		
SENSIBLE COOLING	0	0	0	0	0	0	0	0		
	344150	355770	365774	369640	367524	378408	192059			
	344150	355770	365774	369640	367524	378408	192059	0	0	
LATENT COOLING	0	0	0	0	0	0	0	0		
	17100	17100	17100	17100	17100	17100	0			
	17100	17100	17100	17100	17100	17100	0	0	0	
SUPPLY AIR	0	0	0	0	0	0	0	0		
	15933	16471	16934	17113	17015	17519	23714	0	149622	
	15933	16471	16934	17113	17015	17519	23714	0	149622	
RETURN AIR	0	0	0	0	0	0	0	0		
	15933	16471	16934	17113	17015	17519	23714	0	103427	
	15933	16471	16934	17113	17015	17519	23714	0	103427	
EXHAUST AIR	0	0	0	0	0	0	0	0		
	0	0	0	0	0	0	0	0	51610	
	0	0	0	0	0	0	0	0	51610	

9	10	9	9	9	9	9	9	9	9	9	100

HEATING/COOLING LOAD CALCULATIONS

GLOBAL DATA

PROJECT: BNL
DATE: 05-Sep-07
ENGINEER: ATIENZA

AHU-201-A
PAGE: 4.00 4.00

Uwall:	0.05	20.00	PEOPLE SENS (BTUH	250.00
Uwindow s:	0.30		PEOPLE LAT (BTUH):	200.00
Uwindow w:	0.29		OAT WINT (DEG F):	0.00
Uroof:	0.04		SA TEMP (DEG F):	55.00
SHADE FC:	0.44		DT HTG (DEG F):	40.00
WALL CONST:	3.00	(BELOW GRADE)		
FLOOR CONST:	3.00	(BELOW GRADE)		

Factors Corrected for Latitude-Month

Time of Day	08:00 AM	10:00 AM	12:00 PM	02:00 PM	04:00 PM	06:00 PM
CLTDroof:	22	23	26.00	31.00	36.00	39.00
CLTDwall: TYPE B						
N:	9	8	7.64	8.47	9.30	23.00
E:	13	13	16.77	19.26	21.75	32.00
S:	12	10	10.13	10.96	13.45	43.00
W:	17	15	13.45	12.62	13.45	43.00
CLTDwindow:	3	7	12.00	16.00	17.00	12.00
SHGF:						
N:	130	130	130	130	130	130
E:	216	216	216	216	216	216
S:	205	205	205	205	205	205
W:	216	216	216	216	216	216
CLFwindow:						
N:	0.65	0.80	0.89	0.86	0.75	0.70
E:	0.80	0.62	0.27	0.22	0.17	0.16
S:	0.23	0.58	0.83	0.68	0.35	0.33
W:	0.11	0.15	0.17	0.53	0.82	0.67

Time of Day	08:00 AM	10:00 AM	12:00 PM	02:00 PM	04:00 PM	06:00 PM

Raw Factors

CLTDroof		20	21.00	24.00	29.00	34.00	38.00
CLTDwall	TYPE E						
N:		4	6	9.00	13.00	17.00	20.00
E:		11	26	36.00	37.00	34.00	32.00
S:		3	5.00	13.00	24.00	32.00	33.00
W:		6	6.00	9.00	14.00	27.00	43.00

CLTD Correction Factor (LM)	
Roof:	1
Walls:	
N	3
E	0
S	10
W	0

HEATING/COOLING LOAD CALCULATIONS

ROOM DATA SUMMARY

PROJECT: BNL
DATE: 05-Sep-07

UNIT: AHU-201-B
PAGE: 1

ROOM NO	ROOM NAME	SA (CFM)	RA (CFM)	EA (CFM)	SQFT	)ES/SQFT AC	COOL AC	DT HTG
P1B	PENTANT 1B	23710	23710	0	19762	6	5	8
		23710	23710	0	19762			

HEATING/COOLING LOAD CALCULATIONS

ROOM DATA SUMMARY

PROJECT: BNL
DATE: 05-Sep-07

UNIT: AHU-201-B
PAGE: 2

COOLING (BTUH)

ROOM NO	ROOM	TOTAL SENS	EXT SENS	INTERNAL SENSIBLE LIGHTS	PEOPLE	MISC	TOTAL LATENT	HTG (BTUH)	HTG (BTUH/FT)
P1B	PENTANT 1B	432161	108926	188134	17100	118000	17100	192059	
		432161	108926	188134	17100	118000	17100	192059	

HEATING/COOLING LOAD CALCULATIONS

AHU DATA SUMMARY

PROJECT: BNL
DATE: 05-Sep-07

UNIT: AHU-201-B
PAGE: 3

	COOLING LOAD SENSIBLE (BTUH)						HTG (BTUH)		
BTUH	8	10	12	2	4	6			
TOTAL SENSIBLE	397902	409523	419526	423393	421277	432161	192059		
TOTAL LATENT	17100	17100	17100	17100	17100	17100	0		
GRAND TOTAL	415002	426623	436626	440493	438377	449261			
							AC CFM	SQFT CFM	HTG CFM
AVG DT	20	20	20	20	20				
SA (CFM)	18421	18959	19423	19602	19504	20007	23714	0	113799
RA (CFM)	18421	18959	19423	19602	19504	20007			
EA (CFM)	0	0	0	0	0	0			
TOTAL SA (CFM)	23710								
TOTAL RA (CFM)	23710								
TOTAL EA (CFM)	0								
	0	0	0	0	0	0	0	0	
SENSIBLE COOLING	0	0	0	0	0	0	0	0	
	397902	409523	419526	423393	421277	432161	192059		
	397902	409523	419526	423393	421277	432161	192059	0	0
LATENT COOLING	0	0	0	0	0	0	0	0	
	17100	17100	17100	17100	17100	17100	0		
	17100	17100	17100	17100	17100	17100	0	0	0
SUPPLY AIR	0	0	0	0	0	0	0	0	
	18421	18959	19423	19602	19504	20007	23714	0	113799
	18421	18959	19423	19602	19504	20007	23714	0	113799
RETURN AIR	0	0	0	0	0	0	0	0	
	18421	18959	19423	19602	19504	20007	23714	0	67604
	18421	18959	19423	19602	19504	20007	23714	0	67604
EXHAUST AIR	0	0	0	0	0	0	0	0	
	0	0	0	0	0	0	0	0	51610
	0	0	0	0	0	0	0	0	51610

9	10	9	9	9	9	9	9	9	9	9	100

HEATING/COOLING LOAD CALCULATIONS

GLOBAL DATA

PROJECT: BNL AHU-201-B
DATE: 05-Sep-07 PAGE: 4.00 4.00
ENGINEER: ATIENZA

Uwall:	0.05	20.00	PEOPLE SENS (BTUH	250.00
Uwindow s:	0.30		PEOPLE LAT (BTUH):	200.00
Uwindow w:	0.29		OAT WINT (DEG F):	0.00
Uroof:	0.04		SA TEMP (DEG F):	55.00
SHADE FC:	0.44		DT HTG (DEG F):	40.00
WALL CONST:	3.00	(BELOW GRADE)		
FLOOR CONST:	3.00	(BELOW GRADE)		

Factors Corrected for Latitude-Month

Time of Day	08:00 AM	10:00 AM	12:00 PM	02:00 PM	04:00 PM	06:00 PM
CLTDroof:	22	23	26.00	31.00	36.00	39.00
CLTDwall: TYPE B						
N:	9	8	7.64	8.47	9.30	23.00
E:	13	13	16.77	19.26	21.75	32.00
S:	12	10	10.13	10.96	13.45	43.00
W:	17	15	13.45	12.62	13.45	43.00
CLTDwindow:	3	7	12.00	16.00	17.00	12.00
SHGF:						
N:	130	130	130	130	130	130
E:	216	216	216	216	216	216
S:	205	205	205	205	205	205
W:	216	216	216	216	216	216
CLFwindow:						
N:	0.65	0.80	0.89	0.86	0.75	0.70
E:	0.80	0.62	0.27	0.22	0.17	0.16
S:	0.23	0.58	0.83	0.68	0.35	0.33
W:	0.11	0.15	0.17	0.53	0.82	0.67

Time of Day	08:00 AM	10:00 AM	12:00 PM	02:00 PM	04:00 PM	06:00 PM

Raw Factors

CLTDroof		20	21.00	24.00	29.00	34.00	38.00
CLTDwall	TYPE E						
N:		4	6	9.00	13.00	17.00	20.00
E:		11	26	36.00	37.00	34.00	32.00
S:		3	5.00	13.00	24.00	32.00	33.00
W:		6	6.00	9.00	14.00	27.00	43.00

CLTD Correction Factor (LM)	
Roof:	1
Walls:	
N	3
E	0
S	10
W	0

HEATING/COOLING LOAD CALCULATIONS

ROOM DATA SUMMARY

PROJECT: BNL
DATE: 08-AUG-07

UNIT: AHU-101
PAGE: 1

ROOM NO	ROOM NAME	SA (CFM)	RA (CFM)	EA (CFM)	SQFT	DES/SQFT AC	COOL AC	DT HTG	OA	%OA
T1	TUNNEL 1	10280	10280		6393	6	11	4	540	5.25%
		10280	10280		6393				540	5.25%

AIR FLOW W/DIVERSITY	10280	CFM		
SF AIR FLOW	11822	CFM		
RF AIR FLOW	11822	CFM		
EA=SF-RF		CFM		
OA	540	CFM	5%	
OA CHECK		CFM		
RELIEF	540	CFM		

OA MAX	540	CFM
OA BY %	540	CFM
Y	5.25%	<<<<<<<<<<
X	5.25%	
Z	5.25%	

HEATING/COOLING LOAD CALCULATIONS

ROOM DATA SUMMARY

PROJECT: BNL
DATE: 08-AUG-07

UNIT: \HU-201-A
PAGE: 1

ROOM NO	ROOM NAME	SA (CFM)	RA (CFM)	EA (CFM)	SQFT	DES/SQFT AC	COOL AC	DT HTG	OA	%OA
P1A	PENTANT 1A	23710	23710		19762	6	4	8	1368	5.77%
		23710	23710		19762				1368	5.77%

AIR FLOW W/DIVERSITY	23714	CFM		
SF AIR FLOW	27272	CFM		
RF AIR FLOW	27272	CFM		
EA=SF-RF		CFM		
OA	1368	CFM	6%	
OA CHECK		CFM		
RELIEF	1368	CFM		

OA MAX	1368	CFM
OA BY %	1368	CFM
Y	5.77%	<<<<<<<<<<
X	5.77%	
Z	5.77%	

HEATING/COOLING LOAD CALCULATIONS

ROOM DATA SUMMARY

PROJECT: BNL
DATE: 08-AUG-07

UNIT: \HU-201-B
PAGE: 1

ROOM NO	ROOM NAME	SA (CFM)	RA (CFM)	EA (CFM)	SQFT	DES/SQFT AC	COOL AC	DT HTG	OA	%OA
P1B	PENTANT 1B	23710	23710		19762	6	5	8	1368	5.77%
		23710	23710		19762				1368	5.77%

AIR FLOW W/DIVERSITY	20007	CFM		
SF AIR FLOW	23009	CFM		
RF AIR FLOW	23009	CFM		
EA=SF-RF		CFM		
OA	1368	CFM	7%	
OA CHECK		CFM		
RELIEF	1368	CFM		

OA MAX	1368	CFM
OA BY %	1368	CFM
Y	5.77%	<<<<<<<<<<
X	5.77%	
Z	5.77%	

BNL NSLS II
05-Sep-07

AIR HANDLING UNIT PSYCHROMETRICS
CV

AHU-101 <<<<<<<<< ENGINEER: ATIENZA <<<<<<<<<

OUTSIDE DESIGN CONDITIONS

	SUMMER		WINTER
OA DB	95 DEG F	<<<<<<<<<	0 DEG F<<<<<
OA WB	76 DEG F	<<<<<<<<<	
OA ENT	39.3 BTU/LB OF DRY AIR		

AIR FLOW			HEAT GAIN			HEAT LOSS		
SA	11822	CFM<<<<<	SENSIBLE	255354	BTUH<<<<<	63839 BTUH<<<<<	18776	W
RA	11282	CFM	PLENUM	0	BTUH<<<<<<<			
OA	540	CFM<<<<<	LATENT	1000	BTUH<<<<<			

FAN TOTAL PRESSURE		FAN TEMP RISE	FAN ENT RISE
SUPPLY	4 IN WG <<<	3.1 DEG F	0.74 BTU/LB OF DRY AIR
RETURN	1.5 IN WG <<<	1.4 DEG F	0.35 BTU/LB OF DRY AIR
LIGHTS TO PLENUM		0.0 DEG F	0.00 BTU/LB OF DRY AIR

AHU LAT

LAT DB	56 DEG F	<<<<<<<<<
LAT WB	53.0 DEG F	
LAT ENT	22.61 BTU/LB OF DRY AIR	

ROOM CONDITIONS

SRMTEMP DB	78.0 DEG F<<<<<<<	WRMTEMP DB	68 DEG F<<<<<<<
SRMTEMP WB	60.0 DEG F		
RMENT	27.91 BTU/LB OF DRY AIR		

RETURN AIR

RA DB	79.4 DEG F
RA WB	60.4 DEG F
RA ENT	28.26 BTU/LB OF DRY AIR

COOLING COIL

EAT DB	80.2 DEG F
EAT WB	61.2 DEG F
EA ENT	28.76 BTU/LB OF DRY AIR
LAT DB	52.9 DEG F
LAT WB	52.8 DEG F
LA ENT	21.88 BTU/LB OF DRY AIR
CAPACITY	31 TONS

PREHEAT COIL AT NORMAL OPERATION			REHEAT COILS	HEAT LOSS	TOTAL HEATING
SA WINTER	11822	CFM <<<<<<<<<			
EAT DB	64.9	DEG F	65 DEG F EAT		
LAT DB	52.9	DEG F			
HTG CAP	0	BTUH	39658 BTUH	63839 BTUH	103496 BTUH
HTG CAP	0	KW	12 KW		
HTG CAP	0	LBS/HR STEAM	42 LBS/HR STEAM		

HUMIDIFIER

WRMTEMP DB	68.0 DEG F		0	
REL HUM	30 %	<<<<<<<<<		
HUM RAT	30 GR/LB OF DRY AIR			
CAPACITY	72 LBS/HR STEAM		ECON OA	4244 CFM
			MIN OA	540 CFM

PREHEAT COIL AT 100% OA

EAT DB	0 DEG F
LAT DB	52.9 DEG F
HTG CAP	675757 BTUH
HTG CAP	199 KW
HTG CAP	711 LBS/HR STEAM

BNL NSLS II
05-Sep-07

AIR HANDLING UNIT PSYCHROMETRICS
VVR

AHU-201-A <<<<<<<<< ENGINEER: ATIENZA <<<<<<<<<

OUTSIDE DESIGN CONDITIONS

	SUMMER		WINTER
OA DB	95	DEG F <<<<<<<<<	0 DEG F<<<<<
OA WB	76	DEG F <<<<<<<<<	
OA ENT	39.3	BTU/LB OF DRY AIR	

AIR FLOW			HEAT GAIN		HEAT LOSS	
SA	27272	CFM<<<<<	SENSIBLE	589066 BTUH<<<<<	147266 BTUH<<<<	43314 W
RA	25904	CFM	PLENUM	0 BTUH<<<<<<<		
OA	1368	CFM<<<<<	LATENT	1000 BTUH<<<<<		

FAN TOTAL PRESSURE		FAN TEMP RISE	FAN ENT RISE
SUPPLY	6 IN WG <<<	4.6 DEG F	1.11 BTU/LB OF DRY AIR
RETURN	1.5 IN WG <<<	1.4 DEG F	0.35 BTU/LB OF DRY AIR
LIGHTS TO PLENUM		0.0 DEG F	0.00 BTU/LB OF DRY AIR

AHU LAT

LAT DB	56	DEG F <<<<<<<<<
LAT WB	53.0	DEG F
LAT ENT	22.09	BTU/LB OF DRY AIR

ROOM CONDITIONS

SRMTEMP DB	75.0	DEG F<<<<<<<	WRMTEMP DB	68 DEG F<<<<<<<
SRMTEMP WB	60.0	DEG F		
RMENT	26.66	BTU/LB OF DRY AIR		

RETURN AIR

RA DB	76.4	DEG F
RA WB	60.4	DEG F
RA ENT	27.01	BTU/LB OF DRY AIR

COOLING COIL

EAT DB	77.4	DEG F
EAT WB	61.2	DEG F
EA ENT	27.62	BTU/LB OF DRY AIR
LAT DB	51.4	DEG F
LAT WB	51.3	DEG F
LA ENT	20.99	BTU/LB OF DRY AIR
CAPACITY	68	TONS

PREHEAT COIL AT NORMAL OPERATION			REHEAT COILS	HEAT LOSS	TOTAL HEATING
SA WINTER	27272	CFM <<<<<<<<<			
EAT DB	64.6	DEG F	65 DEG F EAT		
LAT DB	51.4	DEG F			
HTG CAP	0	BTUH	100466 BTUH	147266 BTUH	247732 BTUH
HTG CAP	0	KW	30 KW		
HTG CAP	0	LBS/HR STEAM	106 LBS/HR STEAM		

HUMIDIFIER

WRMTEMP DB	68.0	DEG F	0	
REL HUM	30	% <<<<<<<<<		
HUM RAT	30	GR/LB OF DRY AIR		
CAPACITY	154	LBS/HR STEAM	ECON OA	9091 CFM
			MIN OA	1368 CFM

PREHEAT COIL AT 100% OA

EAT DB	0	DEG F
LAT DB	51.4	DEG F
HTG CAP	1513618	BTUH
HTG CAP	445	KW
HTG CAP	1593	LBS/HR STEAM

BNL NSLS II
05-Sep-07

AIR HANDLING UNIT PSYCHROMETRICS
VVR

AHU-201-B <<<<<<<<< ENGINEER: ATIENZA <<<<<<<<<

OUTSIDE DESIGN CONDITIONS

	SUMMER		WINTER
OA DB	95	DEG F <<<<<<<<<	0 DEG F<<<<<
OA WB	76	DEG F <<<<<<<<<	
OA ENT	39.3	BTU/LB OF DRY AIR	

AIR FLOW			HEAT GAIN			HEAT LOSS		
SA	23009	CFM<<<<<	SENSIBLE	496985	BTUH<<<<<	124246	BTUH<<<<	36543 W
RA	21641	CFM	PLENUM	0	BTUH<<<<<<<			
OA	1368	CFM<<<<<	LATENT	1000	BTUH<<<<<			

FAN TOTAL PRESSURE		FAN TEMP RISE	FAN ENT RISE
SUPPLY	6 IN WG <<<	4.6 DEG F	1.11 BTU/LB OF DRY AIR
RETURN	1.5 IN WG <<<	1.4 DEG F	0.35 BTU/LB OF DRY AIR
LIGHTS TO PLENUM		0.0 DEG F	0.00 BTU/LB OF DRY AIR

AHU LAT

LAT DB	56	DEG F <<<<<<<<<
LAT WB	53.0	DEG F
LAT ENT	22.09	BTU/LB OF DRY AIR

ROOM CONDITIONS

SRMTEMP DB	75.0	DEG F<<<<<<<	WRMTEMP DB	68 DEG F<<<<<<<
SRMTEMP WB	60.0	DEG F		
RMENT	26.66	BTU/LB OF DRY AIR		

RETURN AIR

RA DB	76.4	DEG F
RA WB	60.4	DEG F
RA ENT	27.01	BTU/LB OF DRY AIR

COOLING COIL

EAT DB	77.5	DEG F
EAT WB	61.4	DEG F
EA ENT	27.74	BTU/LB OF DRY AIR
LAT DB	51.4	DEG F
LAT WB	51.3	DEG F
LA ENT	20.99	BTU/LB OF DRY AIR
CAPACITY	58	TONS

PREHEAT COIL AT NORMAL OPERATION			REHEAT COILS		HEAT LOSS	TOTAL HEATING
SA WINTER	23009	CFM <<<<<<<<<				
EAT DB	64.0	DEG F	64	DEG F EAT		
LAT DB	51.4	DEG F				
HTG CAP	0	BTUH	100466	BTUH	124246 BTUH	224712 BTUH
HTG CAP	0	KW	30	KW		
HTG CAP	0	LBS/HR STEAM	106	LBS/HR STEAM		

HUMIDIFIER

WRMTEMP DB	68.0	DEG F	0	
REL HUM	30	% <<<<<<<<<		
HUM RAT	30	GR/LB OF DRY AIR		
CAPACITY	130	LBS/HR STEAM	ECON OA	7670 CFM
			MIN OA	1368 CFM

PREHEAT COIL AT 100% OA

EAT DB	0	DEG F
LAT DB	51.4	DEG F
HTG CAP	1277014	BTUH
HTG CAP	376	KW
HTG CAP	1344	LBS/HR STEAM

========== ========== ========== ========== ========== ========== ========== ========== ==========

Appendix A5

Hourly Whole Building Energy Analysis
September 10, 2007

EMO Energy Solutions

EMO Energy Solutions
Energy Efficiency & Sustainable Design Consulting

September 10th, 2007

BROOKHAVEN NSLS II – UPTON, NEW YORK: SCHEMATIC DESIGN ENERGY ANALYSIS
HOURLY WHOLE BUILDING ENERGY ANALYSIS AND LEED®-NC V2.2 EA CR.1 OPTIMIZATION

U.S. DEPARTMENT OF ENERGY | BROOKHAVEN NATIONAL LABORATORY | HDR

Purpose & Scope:

The United States Department of Energy (DOE) has contracted HDR Architecture, Inc. (HDR) and for the design and implementation of sustainable design strategies and features for the new Brookhaven National Laboratory – National Synchrotron Light Source II (NSLS II) in Upton, New York. This project is intended to incorporate environmentally sensitive materials and technologies along with the principals of sustainable design and the integrated whole building design approach. To this end, HDR has contracted EMO Energy Solutions, LLC (EMO) to perform a comprehensive whole building energy simulation, energy analysis, and general sustainable design and green engineering assistance.

This project will be applying for Leadership in Energy and Environmental Design, New Construction (LEED®-NC) version 2.2 with the goal of a "Gold" level of certification. As part of this certification process, EMO will simulate the annual energy use of the building as-designed / Design Energy Cost (DEC) model and the building as if it were designed to meet ASHRAE 90.1-2004 minimum specifications / Performance Rating Method (PRM) model. The difference in consumption between the two models is used to determine the final point total for Credit-1 of the LEED®-NC Energy and Atmosphere category.

Given this stage (Schematic) in design, this energy analysis report is intended to cover the following for the design team:

- Preliminary hourly building energy analysis
- Energy performance as compared to ASHRAE 90.1-2004 baseline (*initial – performance expected to change with more refined building*)
- Provide the design team feedback with regards to energy cost savings expectations going forward into the Design Development phase
- Itemize some of the energy cost savings for different energy efficiency opportunities
- Highlight some key ASHRAE 90.1-2004 Appendix G requirements
- Provide the design team information regarding energy utilization in the proposed facility and how to improve LEED®-NC EA Cr.1 performance

For this "SD Level" energy analysis, EMO has incorporated the estimated envelope, building design, and HVAC system options for the SD phase as well as all other parameters and components as represented in the documents (dated 27 January 2007), the "Title I Preliminary Design Report – 50% Review Submittal" and conversations with HDR.

Methodology:

The standard sustainable design approach employed by EMO is based upon and optimized by the interactive design approach. Sustainable improvements are defined as modifications that will reduce the negative environmental impact of the building for future generations by minimizing the energy and water consumption, minimizing pollution emissions, and increasing the useful life of the building by improving the quality of the occupied spaces. This process incorporates four distinct, but fluid processes that work with the design team through the course of the design:

- **Generate the Baseline** - Generate a DOE-2.2 energy model of the current design of the facility, of which include all proposed building systems including the ASHRAE 90.1 guidelines for new construction where applicable.
- **Evaluate the Baseline** - Compare to ASHRAE or existing building code and PRM for LEED® ; determine energy goals and targets
- **Generate and Evaluate ECMs** - Generate parametric runs for any and all applicable ECMs to account for any associated savings that would add any LEED® credits in the Energy & Atmosphere category of the LEED® Rating System
- **Final Design** - Present the packaged ECMs, highlighting the energy savings, the overall Energy Usage Intensity (EUI-kBtu/sf) reduction, and the potential LEED® credits awarded.

The process of identifying energy efficiency and conservation measures relies on the following three step strategy. This strategy is applied to optimize and fully capitalize on the associated savings and emphasis on reduction of waste:

- **Minimize Building Loads** - Improve the building envelope, reduce lighting power densities and usage, incorporate suitable day lighting techniques, reduce equipment power densities and usage, and reduce water consumption flow rates.
- **Improve System Effectiveness** – Improve HVAC system design, increase motor efficiencies, utilize solar heating technologies, incorporate energy recovery technologies, and utilize applicable controls strategies.
- **Optimize Resource Delivery** – Provide renewable energy generation, incorporate energy storage techniques, increase the efficiency of the plant, review utility rate options, and investigate district heating and cooling options.

The method of evaluation closely followed the guidelines stipulated by the US Green Building Council's LEED® design approach and the ASHRAE/IESNA 90.1-2004 interactive calculation method.

All project energy modeling used eQUEST 3.61e, a program that utilizes DOE-2.2 to simulate the hourly energy consumption and demand load shapes for a given facility. To develop a model, the user creates a graphic representation of the building, using floor plans, floor heights, and window configurations. Specifics of the central plant, air-handling units, and building envelope are included along with the operating parameters such as lighting power density, occupancy, building schedules, and airflow rates. The simulation uses 30-year average hourly weather data to accurately estimate the energy consumption of the building for each hour of the year.

Results Summary:

With the assumptions and strategies represented in the design drawings and implementation of all listed measures this project is expected to save ~**$492,908/yr (~21.8%)** in total energy costs when compared to the ASHRAE baseline **meeting EA Prerequisite 2** and equating to **(3-4) LEED®-NC v2.2 E&A Credit 1 (New Construction) points.**

It is important to note that the quoted performance will change once the design is developed further. However, it gives the project team an idea of the expectation following an aggressive design. [Review section "Energy Performance Issues"]

Brief Modeling Description:

The following is a list, in no particular order, of some of the major modeling parameters accounted for at this stage. A more detailed line-by-line description of the differences between the "As-designed (DEC)" and "Initial Baseline (PRM)" energy simulations is shown in Figure 1.

- DOE Energy Information Administration published blended utility rates for New York State ($0.1543/kWh)
- Assumed a district steam rate of $25.00/MMBtu-delivered
- Utilizing typical meteorological year TMY2 hourly weather file for New York City, NY
- Utilized Title 24 approved diversity schedules for lighting, occupancy, plugs, process, etc.
- All envelop parameters (layer-by-layer assemblies, vertical glazings, programming, etc.)
- All internal loads (lighting, equipment "plugs", domestic hot water, occupancy, etc.)
- All external loads (climate zone, infiltration, solar transmitted, ground conductance, etc.)
- Photocells, occupancy sensors, CO_2, etc. / where anticipated
- All HVAC components (Chillers – ASHRAE 90.1, district steam, air-side equipment, controls, circulation loop infrastructure, settings, thermal zones, etc)
- Assumed on-site ASHRAE 90.1-2004 compliant chillers (per requirement for district system)
- All unknown parameters assumed to be ASHRAE 90.1-2004 Appendix G minimally compliant
- Water-cooled Synchrotron cooling neglected (i.e. ~2400 tons cooling, etc.); only energy uses of which can be controlled are included in addition to the LEED®-NC requirement for process energy
- Others…

DEC – "As-Designed"

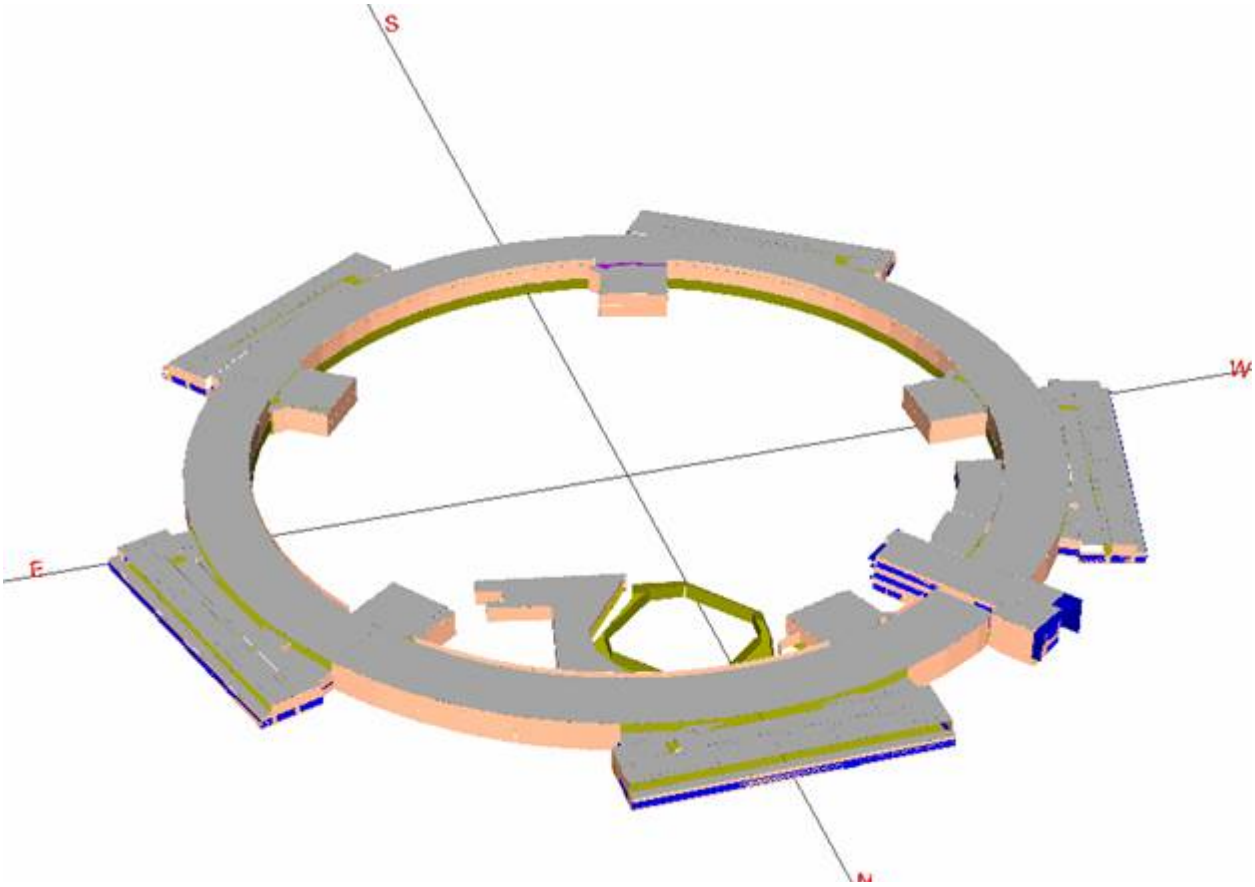

Figure 1: 3-D Energy Model Renderings of the Design Energy Cost

Energy Performance Issues:

This section of the memo is intended to highlight some of the energy performance "highlights" and energy "hogs" of which will work either for or against optimizing total energy cost savings for LEED®-NC v2.2 Energy & Atmosphere Credit 1. The following, in no particular order, is a list of key parameters that are both improving and reducing our energy performance related to the ASHRAE 90.1-2004 Appendix G Performance Rating Method:

Improved Energy Cost Performance

- Having high process energy and tight indoor thermal requirements (i.e. 1°F) enables the project to do rather well when compared to ASHRAE 90.1-2004 compliance
- Long Island is one of the only areas in New York that doesn't require air-side economizers. Including economizers at a facility with high internal heat gains will pay huge dividends. If the site was located elsewhere the annual energy cost savings would be significantly less (see "Energy Efficiency Opportunities")
- Outside air economizers (N.R. per ASHRAE climate zone 4a)
- Having tight thermal requirements for the Experimental Hall provides significant opportunity (more so than most projects) for energy cost savings with a significantly improved envelope

  Centria® Formawall®: U-value = 0.045
  (see "Appendix A")

  Metal Deck Roof: U-value = 0.054
  (High Albedo white roof w/ low absorptance)

  High Performance Glazing:
  U-value = 0.311 | SHGC =
  (BOD: Viracon VE 1-2M)
- High efficiency lighting for Experimental Hall (0.8 W/sf), Offices (0.9 W/sf), and Laboratories (1.0 W/sf)
- Daylighting and photocell control for perimeter LOB offices (N.R. per ASHRAE 90.1)

Reduced Energy Cost Performance

- Stringent requirement for Total Fan Power. Assumed ASHRAE 90.1-2004 Appendix G fan power (very important to confirm) – Designers should review the following:

  Appendix G Table G3.1.2.9
  Section G31.2.9
  Appendix G User's Manual (Pgs G-28, G-29)
- District steam does not provide the opportunity to generate plant level heating savings given no site level heating source (Appendix G3.1.1.1)
- District chilled water does not provide the opportunity to generate plant level heating savings given no site level heating source (Appendix G3.1.3.7)
- Constant volume AHUs for Laboratory spaces
- Other parameters are unknown and a judgment cannot be made either way as to their impact at this time

Energy Efficiency Opportunities:

Variable Air Volume AHUs for Laboratories: Currently, the proposed facility is utilizing constant volume AHUs for the laboratories. If this is the case then the project cannot claim the energy cost savings associated with the sensible heat recovery since it will be required per ASHRAE 90.1-2004 G3.1.2.10. If VAV AHUs are utilized then the savings for ventilation energy or heat recovery can be claimed. Table 1 illustrates the savings associated with VAV AHUs equipped with variable speed drives.

Table 1. Savings Summary for EEO-1

EEO No.	Description	Electricity Savings (kWh)	Annual Steam Savings (MMBtu)	Annual Energy Cost Savings	Total % Cost Savings
1	VAV for Laboratories	129,777	-1	$19,977	1.1%

High Performance Glazings: As mentioned earlier, having tight thermal conditions in a large space volume opens up the opportunity for significant energy cost savings with improvements in the building envelope. The Experimental Hall is required to be maintained at 75°F year round with a 1.0°F tolerance. Therefore, there will be a significant amount of off-peak heating required and as such improving the glazing will generate energy cost savings. The basis-of-design for the "As-Designed" glazing is Viracon VE 1-2M or equivalent with improved conduction and reduced solar heat gain coefficient compared to that required by ASHRAE 90.1-2004 Climate Zone 4a. Table 2 illustrates the savings associated with VAV AHUs equipped with variable speed drives.

Table 2. Savings Summary for EEO-2

EEO No.	Description	Electricity Savings (kWh)	Annual Steam Savings (MMBtu)	Annual Energy Cost Savings	Total % Cost Savings
2	High Performance Glazings	45,439	764	$26,089	1.5%

Daylighting Control: Currently, the proposed design shows several photocells in the commons areas, laboratories, classrooms, and main stairwell. EMO has elected to itemize the energy cost savings associated with turning off electrical lighting for the perimeter LOB office space only where adequate natural light is sufficient in supporting the specific space's primary function. Table 3 illustrates the savings associated with a typical LOB perimeter office employing photocell control based on natural light.

Table 3. Brief Daylighting Statistics

Space	Percentage Lighting controlled	Foot Candle photocell setpoint	Peak Energy Reduction (Daylit hours)	Percentage Runtime Reduction (All hours)
LOB Perimeter Office	100%	50	79.0%	46.0%

Table 4 of this report illustrates the energy cost savings associated with this measure.

Table 4. Savings Summary for EEO-3

EEO No.	Description	Electricity Savings (kWh)	Annual Steam Savings (MMBtu)	Annual Energy Cost Savings	Total % Cost Savings
3	Daylighting (Perimeter Offices Only)	39,953	-37	$5,232	0.3%

Improved Building Envelope: Similar to that of EEO-2 an improved envelope will generate substantial savings at this site. EMO has itemized the savings with the improved wall assembly, roof assembly, and roof absorptance proposed for this project to illustrate the importance of the measure. Table 5 of this report illustrates the energy cost savings associated with this measure.

Table 5. Savings Summary for EEO-4

EEO No.	Description	Electricity Savings (kWh)	Annual Steam Savings (MMBtu)	Annual Energy Cost Savings	Total % Cost Savings
4	Improved Building Envelope	99,318	1,757	$59,231	3.2%

Air-side Economizers: Upton, New York is one of the only regions in New York State of which air-side economizers are not required (Climate Zone 4a). The savings for this measure are much higher than in a typical building given the high internal heat gains, substantial exterior surface area, and only 75°F cooling requirement. Table 6 of this report illustrates the energy cost savings associated with this measure.

Table 6. Savings Summary for EEO-5

EEO No.	Description	Electricity Savings (kWh)	Annual Steam Savings (MMBtu)	Annual Energy Cost Savings	Total % Cost Savings
5	Air-side Economizer	1,826,471	-354	$272,952	13.4%

Improved Lighting Efficiency: HDR is expecting to have low peak power densities for a significant portion of the building. The majority of the electrical lighting in this facility is that of the Experimental Hall. The ASHRAE Table 9.6.1 requirement for this Laboratory type space is a lighting power density (LPD-W/sf) of 1.40 W/sf. HDR has indicated that the Experimental Hall will be designed to an LPD of 0.80 W/sf (43% improvement). This will require an aggressive lighting design most likely including 5-lamp T5HO technology in lieu of HID or T8 lighting technologies. Furthermore, HDR is designing to 0.90 W/sf in the Offices and 1.00 W/sf in the LOB laboratories. Table 7 of this report illustrates the energy cost savings associated with improving the lighting as indicated.

Table 7. Savings Summary for EEO-6

EEO No.	Description	Electricity Savings (kWh)	Annual Steam Savings (MMBtu)	Annual Energy Cost Savings	Total % Cost Savings
6	Improved Lighting Efficiency	632,559	-871	$75,810	4.1%

Figure 2 and Figure 3 provide energy and cost by building end-use for the “Initial PRM” and “All EEOs” simulations.

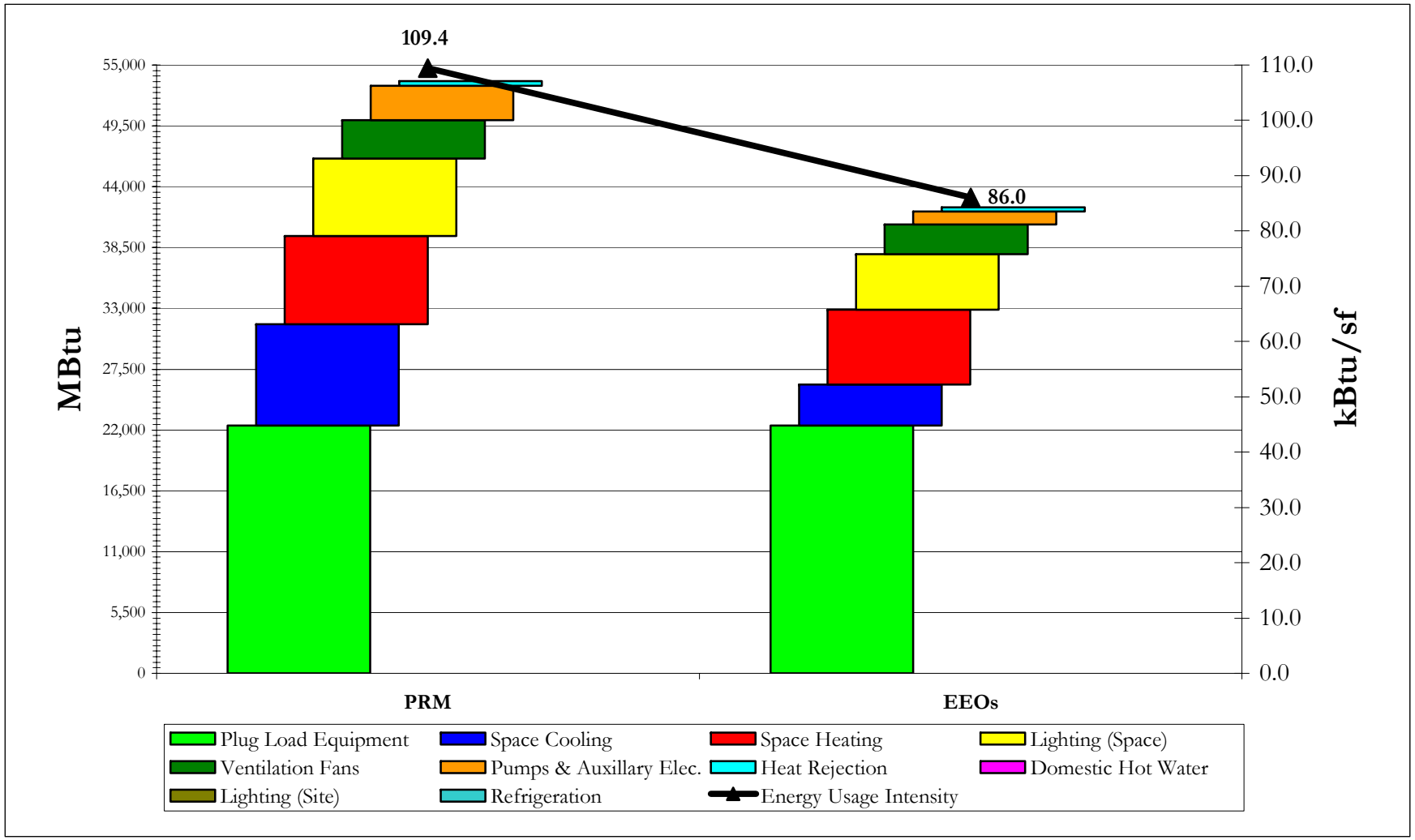

Figure 2: Energy End-Use Breakdown and Energy Usage Intensity

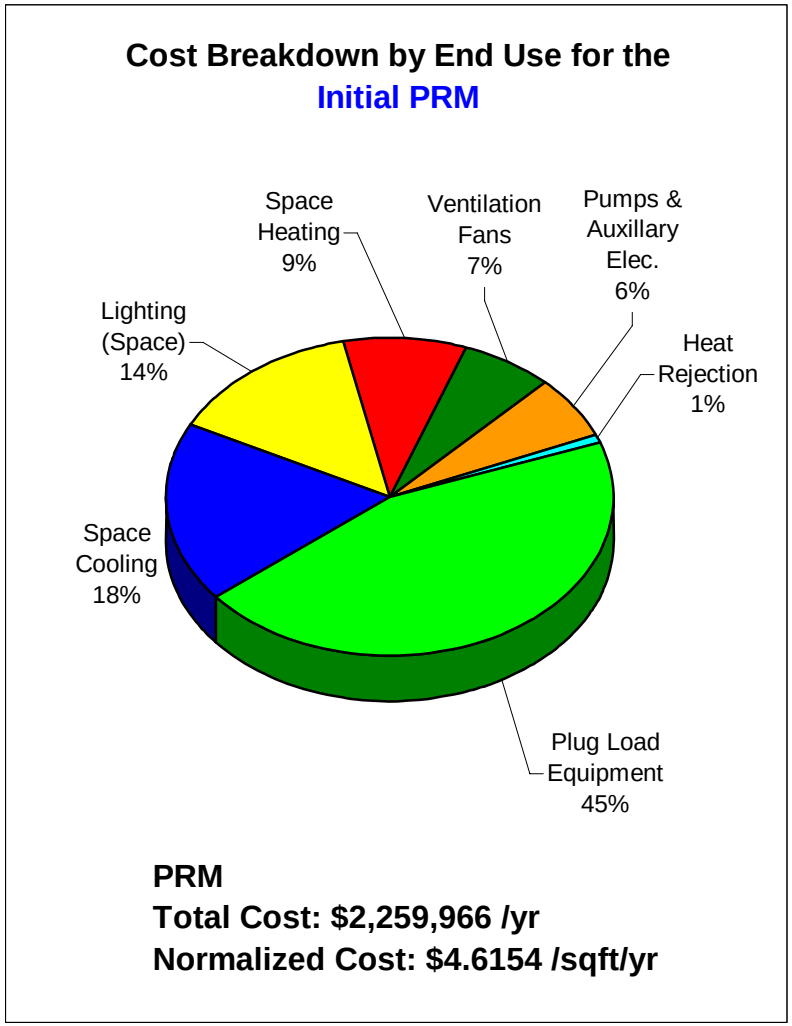

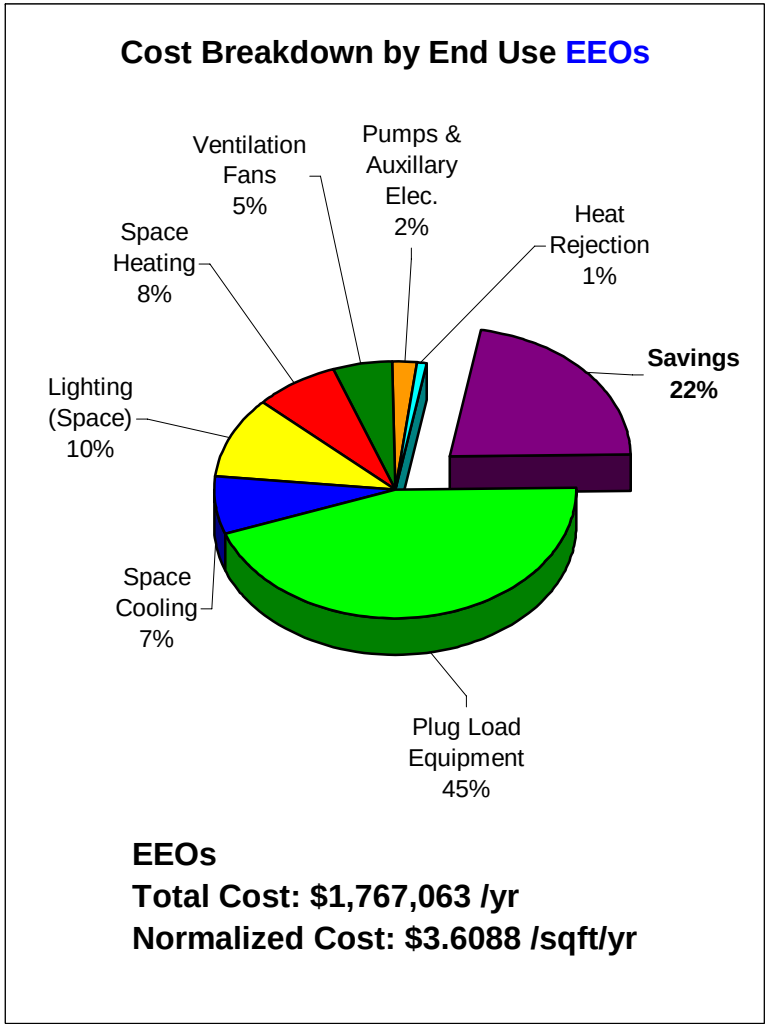

Figure 3: Energy Cost Breakdown by End-Use and Annual Utility Budgets

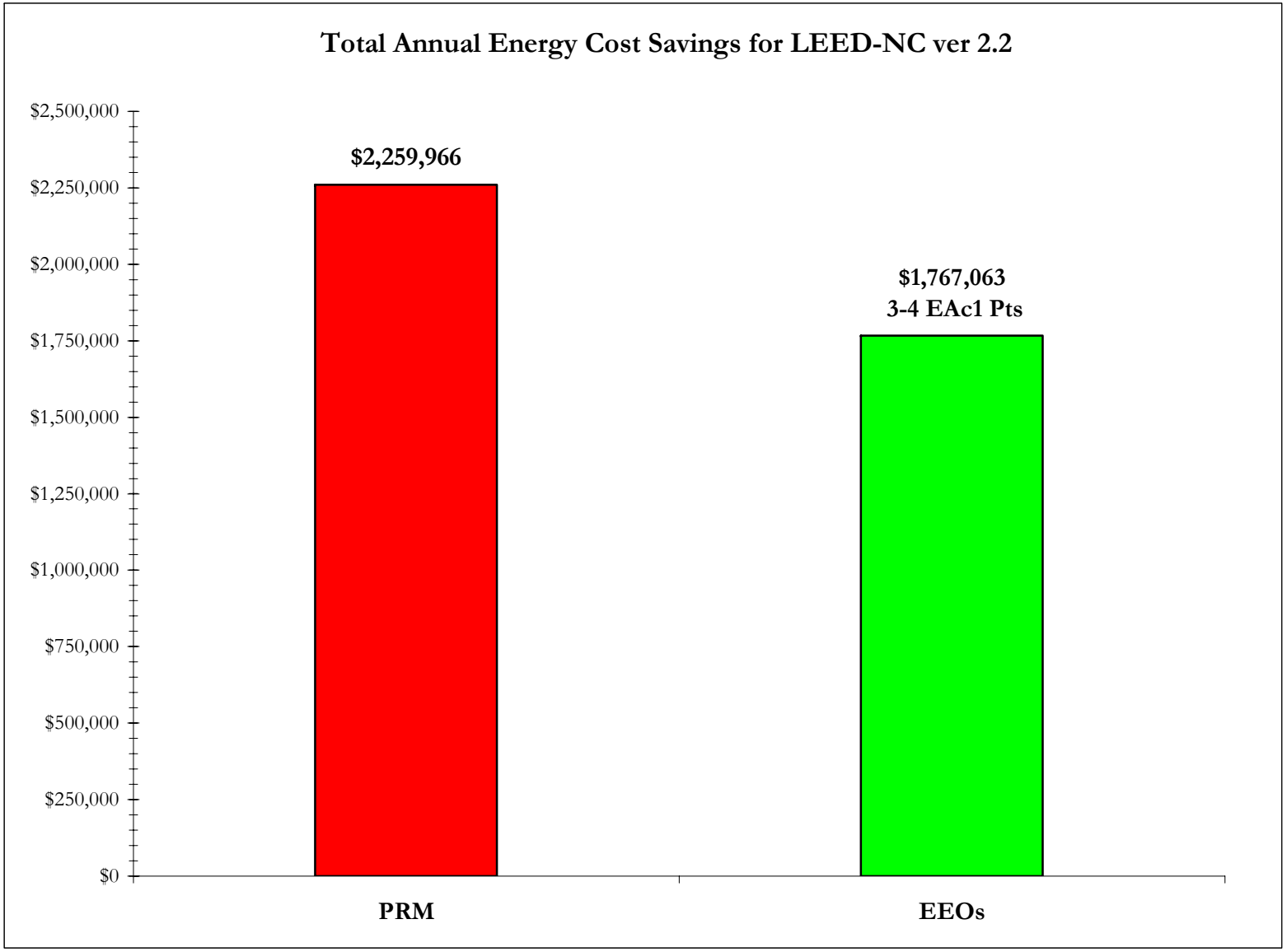

Figure 4: Annual Energy Cost and LEED-NC ver 2.2 Points

Appendix A: Centria® Formawall™

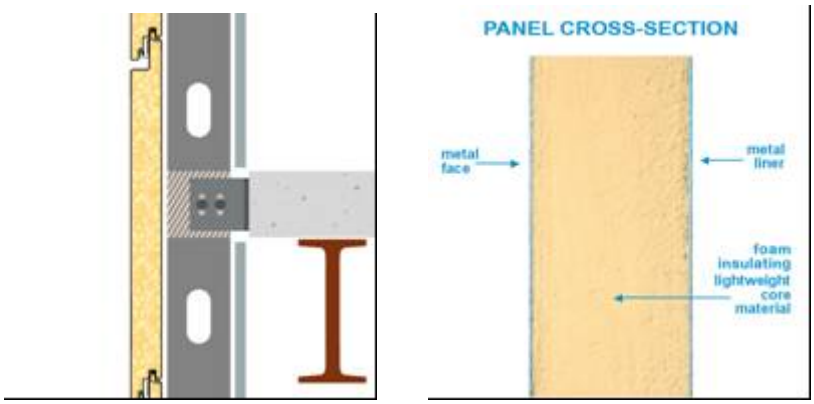

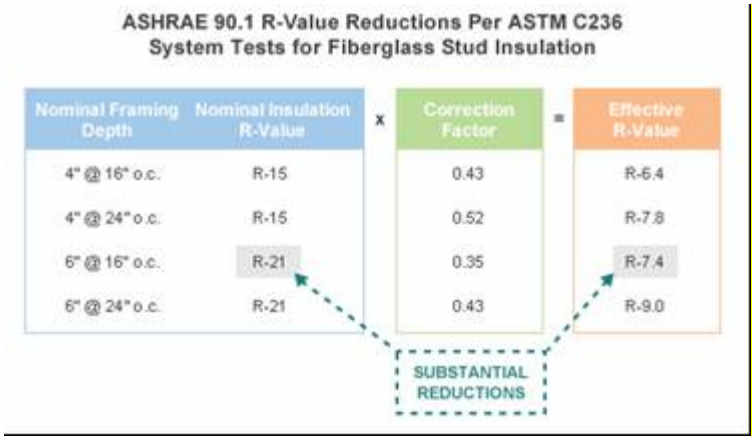

LEED® Quick Hits

- Significantly reduces thermal bridging from outside-to-inside and conduction for drastically improved envelope assembly (**Total wall = R-22.2 | AHSRAE 90.1-2004 = R-8.1**). [LEED®-NC EA Cr.1]
- Opportunity for earning **LEED® Innovation Credit for utilizing a "Cradle-to-Cradle" certified building material**
- Formawall™ panels contain an average of at least **16% post-consumer and 6% post-industrial recycled content**. [LEED®-NC MR Cr 4.1 & 4.2]
- **Panels have a VOC content of 180 grams/liter**, which is less than the maximum limit of 250 grams/liter established by this regulation for architectural sealants. [LEED®-NC EQ Cr. 4.1]
- **No VOC's are generated at the jobsite** from field-painting operations. [LEED®-NC EQ Cr 4.2]

1 ENVIRONMENT, SAFETY, & HEALTH, AND QUALITY ASSURANCE

1.1 INTRODUCTION

Brookhaven National Laboratory is committed to the success of the mission objectives of the National Synchrotron Light Source II and to the safety of its users, staff, and the public. The NSLS-II Project Director is responsible for achieving this objective. The NSLS-II Environmental Safety and Health Manager is responsible for ensuring that an ES&H system is established, implemented, and maintained in accordance with requirements. The ES&H Manager will provide oversight and support to the project participants to ensure a consistent ES&H program.

It is our vision to provide a "Best in Class" safety program. We view such a program as essential to the safety of the workers as well as the successful completion of the project. We will seek to provide an injury free work environment and will measure our performance by comparison with only those who have achieved recognition as "Best in Class." To achieve this vision, safe working conditions and practices are an absolute requirement for all staff and contractors. We expect all design and work to be performed with this goal in mind. We will not be satisfied unless our ES&H program as well as our new facility are both recognized as "Best in Class." To accomplish this vision, it is essential that ES&H be fully integrated into the project and be-managed as tightly as quality, cost and schedule.

An ES&H Program Plan [1.1] with this vision in mind has been prepared by the ES&H Manager and approved by the NSLS-II Project Director. This plan specifies that the program implemented for NSLS-II shall satisfy its ES&H commitments by:

1. Establishing an Integrated Safety Management Program that implements the DOE Policy, DOE P 450.4, "Safety Management System Policy," the BNL Subject-Based Management System topic areas, and the requirements of the DOE "Accelerator Safety Order." The program will protect the environment and the safety of workers and the general public by assuring that:
    a. Facilities, systems, and components needed to meet mission requirements are fully defined and are designed, constructed, and operated in accordance with applicable BNL and DOE requirements
    b. Potential hazards to personnel associated with all NSLS-II systems, structures, and components are identified and controlled through the timely preparation of safety assessment documents
    c. Potential risks to the environment are addressed through the timely and comprehensive preparation of appropriate National Environmental Protection Act documentation
    d. ISO 14001 and OHSAS 18001 criteria are implemented to assure that all ES&H risks are identified and addressed
    e. Requirements in 10 CFR Part 835, part 850, and Part 851 are fully implemented to protect worker safety and health
2. Implementing a QA program that follows DOE Order 414.1-2A, "Quality Assurance Management System Guide," and incorporates quality requirements from BNL's SBMS subject area Graded Approach for Quality Requirements.
3. Implementing an effective construction safety programs to ensure worker safety on the NSLS-II site during construction. All work performed on the NSLS-II site will be conducted in accordance with the NSLS-II Environmental, Safety, and Health Plan.

4. Performing Independent Design Reviews on systems, structures, and components designated as "safety significant" or "safety class" in the SAD or as defined through QA classifications described in the NSLS-II QA Plan.
5. Providing appropriate training to ensure that project staff are adequately trained and qualified to perform their assigned work safely. Job training assessments will be conducted for all staff to ensure knowledge of job-related hazards and their controls. All project staff are responsible for ensuring that their training and qualification requirements are fulfilled, including continuing training to maintain proficiency and qualifications.
6. Developing and implementing operating procedures to control work on NSLS-II technical systems.
7. Performing and documenting safety inspections of all project facilities and work areas, and ensuring prompt correction of any issues identified in the inspection.
8. Reporting and investigating occurrences and incidents in accordance with the BNL Occurrence Reporting Policies and Procedures as defined in the BNL SBMS. Any incident, accident, or other abnormal event will be properly communicated and investigated via established procedures.

Policies and requirements to ensure implementation of these expectations will be established and communicated to all staff, contractors, and vendors.

1.2 FINAL HAZARD ANALYSIS (FHA)

A principal component of an effective ES&H program is to ensure that all hazards have been properly identified and controlled through design and procedure. To ensure that these issues are understood at the preliminary design phase, a Final Hazard Analysis [1.4] has been conducted to identify the hazards that will be encountered during the project's construction and operational phases. This analysis is an update of the Preliminary Hazard Analysis developed during the Conceptual Design. No new significant issues were identified in this update, and it was re-confirmed that the NSLS-II will be classified as an "Accelerator Facility," as defined in DOE Order 420.2B, "Safety of Accelerator Facilities."

Generally, all the hazards and their risks anticipated to be encountered at NSLS-II as identified in the FHA are well known to the accelerator community. Years of experience with such facilities at BNL and within the DOE complex have generated well-defined design criteria and controls to eliminate and/or control these risks. Table 1.1 below summarizes the hazards that have been considered, and the codes and standards that apply to the reduction of risk associated with each hazard.

This Hazard Analysis process began concurrent with the conceptual design, to ensure that all significant hazards were identified and adequately addressed in the early design work. Each of these issues will be followed as design advances and as construction and installation work commence. A Baseline Hazards List [1.2] was developed as the first step in identifying the potential hazards. This list utilized the best available information, encompassing data from the NSLS-II conceptual design, existing NSLS safety-basis documentation, subject-matter expertise (with conventional facilities, accelerator systems, and ES&H) and lessons-learned from the DOE's accelerator community covering design criteria, regulatory requirements, and related occurrences. It also included preliminary (pre-mitigation) risk assessments that identified risk categories before incorporating the ES&H-related design and operational controls that are postulated to mitigate those risks. The identified hazards then were further developed in the PHA [1.3] issued in December 2006, where the proposed ES&H design enhancements were taken into consideration. The FHA re-analyzed the risks, including these enhancements and, in certain cases, operational controls, to establish a post-mitigation risk category. The FHA was supported by extensive discussions and review of hazards with personnel responsible for the design of all major systems associated with NSLS-II. This process provides a realistic assessment of the residual ES&H risks posed by the NSLS-II facility and is input to the preliminary design.

Fifteen of the hazards reviewed in the FHA are mitigated to Low risk or below and one hazard remains at a Moderate level, Construction. While the FHA adequately addresses all risks and their design as well as operational controls, the Construction category will be given a high level of attention during the Title 1 and subsequent design processes to ensure that its risks are adequately controlled.

A brief review of each hazard and the means of mitigating risks are provided in the following sections.

Table 1.1 Hazards Considered in FHA and Applicable Codes and Standards.

FHA Identifier	Hazard List	Applicable NSLS-II ES&H Regulations, Standards, Codes, Order
NSLS-II – FHA-1	Construction hazards Site clearing Excavation Work at elevations (steel, roofing) Material handling Utility interfaces, (electrical, steam, chilled water, compressed air) Miscellaneous finishing work Weather-related conditions Transition to Operations	BNL SBMS Construction Safety subject area 29 CFR 1926, Safety and Health Regulations for Construction 10 CFR Part 851, Appendix A, Functional Area 1, Construction Safety
NSLS-II – FHA-2	Natural phenomena hazards Seismic Flooding Wind Snow & Ice Lightning	DOE Order 420.2B Safety of Accelerator Facilities DOE Guide 420.2-1 Accelerator Facility Safety Implementation Guide DOE Order 420.1B Facility Safety DOE STD 1020-2002 Natural Phenomena Hazards Design and Evaluation Criteria for Department of Energy Facilities DOE STD 1021-93 Natural Phenomena Hazards Performance Categorization Guidelines for Structures, Systems and Components. DOE STD 1022-94 Natural Phenomena Hazards Site Characterization Criteria. DOE STD 1023-95 Natural Phenomena Hazards Assessment Criteria. New York State Building Code
NSLS-II – FHA-3	Environmental hazards Construction impacts Storm-water discharge (construction and operations) Operations impacts Soil & groundwater activation Air activation Cooling-water activation (HVAC and machine) Oils/chemical/biological leaks Discharge/emission points (atmospheric, ground and sanitary system)	BNL SBMS National Environmental Policy Act (NEPA) and Cultural Resources Evaluations subject area. NYSDEC Petroleum bulk storage, SCDHS Article 12 40 CFR 61 - Subpart A, National Emissions Standards for Hazardous Air Pollutants (NESHAPS) 6 NYCRR 200 – 234 – NYSDEC Prevention and Control of Air contamination and Air Pollution National Environmental Policy Act (NEPA) of 1969, as amended (42 USC 4321-4347) Council on Environmental Quality (CEQ) regulations for implementing NEPA (40 CFR 1500-1508) DOE NEPA Regulations (10 CFR 1021)

FHA Identifier	Hazard List	Applicable NSLS-II ES&H Regulations, Standards, Codes, Order
NSLS-II – FHA-4	Waste hazards Construction phase Facility maintenance Experimental operations Industrial Hazardous Radiological Biological/Medical	BNL SBMS Biosafety in Research subject area BNL SBMS Hazardous Waste Management subject area BNL SBMS Industrial Waste and Radioactive Waste Management subject area BNL SBMS Interim Procedure 2006-001 Approach to Nano-material ESH. 6 NYCRR Part 371, Identification and Listing of Hazardous Wastes 6 NYCRR Part 374.3, Standards for Universal Waste 40 CFR 262.11, Hazardous Waste Determination (EPA 1987) 40 CFR 273, Standard for Universal Waste Management 6 NYCRR Part 374-2 and 225-2, Used Oil Specifications 10 CFR Part 851, Appendix A, Functional Area 8, Occupational Medicine
NSLS-II – FHA-5	Fire Hazards Construction materials Storage/Housekeeping Flammable/combustible solids/ liquids Flammable gasses Egress/access Electrical Lightning	BNL SBMS Fire Safety subject area NFPA 101 Life Safety Code NFPA 45 Fire Protection for Laboratories Using Chemicals Elevator Std DOE Standard 1066-99 10 CFR Part 851, Appendix A, Functional Area 2, Fire Protection
NSLS-II – FHA-6	Electrical hazards Low voltage/high current High voltage/high power Non-NRTL certified equipment Arc flash Electrical shock Cable tray overloading/mixed utilities Mechanical damage to cables	BNL SBMS Electrical Safety subject area NFPA 70 National Electrical Code NFPA 70 E Standard for Electrical Safety in the Workplace NFPA 70 B Recommended Practice for Electrical Equipment Maintenance 10 CFR Part 851, Appendix A, Functional Area 10, Electrical Safety
NSLS-II – FHA-7	Noise Equipment exceeding ACGIH noise limits	BNL SBMS Noise and Hearing subject area OSHA 29 CFR 1910.95 Occupational Noise Exposure
NSLS-II – FHA-8	Cryogenic and Pressure hazards Oxygen deficiency Thermal Pressure	BNL SBMS Cryogenics Safety subject area American Society of Mechanical Engineers (ASME) Boilers and Pressure Vessel Code, sections I through XII including applicable Code Cases, (2004). * ASME B31 (ASME Code for Pressure Piping) as follows: (i) B31.1—2001—Power Piping, and B31.1a—2002—Addenda to ASME B31.1—2001; (ii) B31.2—1968—Fuel Gas Piping; (iii) B31.3—2002—Process Piping; (iv) B31.4—2002—Pipeline Transportation Systems for Liquid Hydrocarbons and Other Liquids; (v) B31.5—2001—Refrigeration Piping and Heat Transfer Components, and B31.5a—2004, Addenda to 29 CFR 1910.134, OSHA Respiratory Protection Standard 10 CFR Part 851, Appendix A, Functional Area 4, Pressure Safety
NSLS-II – FHA-9	Confined space hazards Asphyxiation Impact with mechanical systems	BNL SBMS Confined Space subject area 29 CFR 1910.146, Permit-required confined spaces

FHA Identifier	Hazard List	Applicable NSLS-II ES&H Regulations, Standards, Codes, Order
NSLS-II – FHA-10	Ozone hazards Breathing impairment Tissue damage	BNL Subject Areas DOE G 420.2-1, Accelerator Facility Implementation Guide OSHA Permissible Exposure Limit (PEL) NIOSH Recommended Exposure Limit (REL)
NSLS-II – FHA-11	Chemical/hazardous materials, nanomaterials, biological materials Toxic Extremely toxic Compressed gas Carcinogens, mutagens, teratogens, reproductive Nanomaterials Biological/medical materials Combustibles Explosives Flammable gases/liquids/solids Lead (shielding) Beryllium articles	BNL SBMS Working with Chemicals subject area BNL SBMS Biosafety in Research subject area BNL SBMS Approach to Nanomaterial ESH interim procedure 49 CFR Department of Transportation ANSI Z358.1-2004 Emergency Eyewash and Shower Equipment OSHA 1910 10 CFR Part 851, Appendix A, Functional Areas 6, Industrial Hygiene; 7, Biological Safety; and 8, Occupational Medicine
NSLS-II – FHA-12	Accelerator/Beamline hazards Vacuum/Pressure Over-heating High pressure heating (bake-out) water Compressed gas Electrical Heavy equipment handling Static magnetic Cryogenic Mechanical (moving shutters, valves and actuators) Radiological	BNL SBMS Subject Areas DOE Order 420.2B Safety of Accelerator Facilities DOE G 420.2-1, Accelerator Facility Implementation Guide 10 CFR Part 851, Appendix A
NSLS-II – FHA-13	Ionizing radiation hazards Prompt radiation (synchrotron radiation scatter, neutrons, bremsstrahlung) Radioactive contamination Activation (equipment) Radioactive material (dispersibles, sealed sources, storage, surface contamination)	BNL SBMS Radiological Safety subject areas BNL Radiological Control Manual 10 CFR Part 835, Occupational Radiation Protection
NSLS-II – FHA-14	Lasers and other non-ionizing radiation hazards Lasers RF & microwave Static magnetic fields Visible light Infrared Ultraviolet	BNL SBMS Laser Safety subject area BNL SBMS Static Magnetic Fields subject area RF and Microwave Safety subject area ANSI Z136.1-2000 Safe Use of Lasers
NSLS-II – FHA-15	Material handling hazards Overhead cranes/hoists Fork trucks Manual material handling Delivery area distribution Manual movement of materials Suspect/counterfeit equipment	BNL SBMS Lifting Safety subject area ASTM B30 Overhead Cranes 10 CFR Part 851, Appendix A, Functional Area 9, Motor Vehicle Safety

FHA Identifier	Hazard List	Applicable NSLS-II ES&H Regulations, Standards, Codes, Order
NSLS-II – FHA-16	Experimental operations Electrical equipment Transportation of hazardous materials Biological/Medical materials Chemicals (corrosive, reactive, toxic, flammable) Nanomaterials (particulates) Falls from elevations Ionizing radiation Ozone production Slips, trips, falls Machine & hand tools Stray static magnetic fields Research gasses (corrosive, reactive, toxic, flammable)	BNL SBMS Work Planning and Control For Experiments and Operations subject area and other related subject areas 10 CFR Part 851, Appendix A, Functional Areas 2, Fire Protection; 3, Explosives Safety; 4, Pressure Safety; 6, Industrial Hygiene; 7, Biological Safety; 8, Occupational Medicine; 10, Electrical Safety

1.2.1 Construction Hazards (NSLS-II FHA – 1)

BNL has a mature construction safety program, with recent experience in constructing the Research Support Building (64,000 sq ft) and the Center for Functional Nanomaterials (94,500 sq feet). Lessons-learned from these two projects, as well as from other construction projects in the DOE complex, coupled with the existing program, will control risk at the NSLS-II facility. Typical construction hazards anticipated at the NSLS-II construction site include the following:

- Site clearing
- Excavation
- Work at elevations (steel, roofing)
- Utility interfaces, (electrical, steam, chilled water, compressed air)
- Material handling
- Miscellaneous finishing work
- Weather-related conditions
- Transition to Operations

1.2.1.1 Construction Hazards – Mitigating Factors (Design)

- Engineered and approved excavation systems
- Engineered and approved fall-protection systems
- Permanent fall-protection systems incorporated into facility's roof systems (for future maintenance)
- Modern code-compliant construction equipment with the required safety controls

1.2.1.2 Construction Hazards – Mitigating Factors (Operational)

- Strict adherence to 29 CFR 1926, OSHA Construction Standard
- Integrated Safety Management (contractually flowed down to subcontractors)
- Contractor-Required Health and Safety Plan (flowed down to subcontractors)
- NSLS-II Construction Safety Plan
- Construction Safety Professional on staff
- Pre-qualification of contractors and subcontractors based on their Experience Modification Rate; Days Away, Restricted, Transfer rate; and Total Recordable Case rate
- Independent third-party inspections of construction safety program
- Dedicated onsite construction safety professionals
- Phase hazards analysis for high-risk activities (e.g., site clearing, work at elevations)
- Pre-excavation search for utilities and other legacy systems
- Contractor-safety incentive program
- Frequent ES&H communication with contractor and subcontractors at plan-of-day, "tool box" meetings
- Major construction equipment inspected before arriving on site

1.2.2 Natural Phenomena Hazards (NSLS-II FHA-2)

Natural Phenomena Events, include high winds, floods, and earthquakes. The NSLS-II design will be governed by the Building Code of the State of New York (BCNY). The BCNY specifies design criteria for wind loading, snow loading, and seismic events. NSLS-II was determined to be a Performance Category 1 facility per DOE STD-1021-93. It will contain only small quantities of activated, radioactive, and hazardous chemical materials. If a NPH were to cause significant damage, the impact would be mission related and would not pose a hazard to the public or the environment.

1.2.2.1 NPE Mitigating Factors (Design)

- Performance Classification designation PC-1
- Strict conformance to Building Codes State of New York
- Snow-loading criteria: 45 psf ground, 30 psf+ drift where applicable
- Wind design: 120 mph (with 3-second gust)
- Seismic design: to 0.25g acceleration velocity
- Lateral load building design
- Lightning-protection system per NFPA (National Fire Protection Association) 780
- Pitched roofs on structures to preclude localized flooding/roof leaks
- Site drainage designed to shed water

1.2.2.2 NPE Mitigating Factors (Operational)

- Limited and controlled quantities of hazardous materials
- BNL Site Emergency Plan
- NSLS-II site emergency plan
- Emergency drills
- NEXRAD facility on BNL site for early notification of severe weather

1.2.3 Environmental Hazards (NSLS-II FHA 3)

Environmental hazards from NSLS-II include the potential for releasing, in amounts beyond regulatory limits, oils, solvents, chemicals, and radioactive material to the soil, groundwater, air, or sanitary system. The principal initiators for such a release would be the failure of equipment, impact from a natural phenomenon, fire, or a violation of procedures/processes.

The NSLS-II facility established a goal of obtaining Leadership in Energy and Environmental Design (LEED) certification that contains requirements for sustainable design principles, pollution prevention, and waste minimization during construction and operations.

1.2.3.1 Environmental Hazards – Mitigating Factors (Design)

- Closed-loop cooling systems
- Minimal need for the regeneration of filter beds and the use of water-treatment chemicals
- Handling and storage facility for control of waste water
- Design to Suffolk County Article 12 (secondary containment) requirements
- Radiation loss points evaluated to determine shielding requirements to protect environment from soil activation
- NSLS-II will include sustainable design principles with the goal of obtaining LEED certification

1.2.3.2 Environmental Hazards – Mitigating Factors (Operational)

Implementation of an environmental management program designed to international standards (ISO 14001), where chemical use is minimized through review, and less hazardous chemicals and processes are substituted where possible. Controls are based on the following:

- Environmental Management System manual
- Environmental Compliance Representative input
- Significant Environmental Aspect matrix
- Chemical Management System database
- Process Assessments

- ES&H Committee, Beamline Review Committee, design reviews
- Work Planning, Experimental Safety Reviews, Tier I inspections
- Training/qualification
- NSLS-II NEPA Environmental Assessment and Finding of No Significant Impact
- NESHAP evaluation
- Soil and water sampling
- Use of oil-less pumps and synthetic oils
- HEPA-filtered hoods

1.2.4 Waste Hazards (NSLS-II FHA-4)

Waste-related hazards from NSLS-II include the potential for releasing waste materials (oils, solvents, chemicals, and radioactive material) to the environment, injury of personnel, and a possible reactive or explosive event. Typical initiators would be transportation accidents, incompatible materials, insufficient packaging/labeling, failure of the packaging, a natural phenomenon or a procedural violation.

The types and volume of wastes that will be generated by NSLS-II are not anticipated to differ markedly from those generated by the existing NSLS. During a typical year of operation, NSLS-II will generate 3,000 to 5,000 pounds (1,400 to 2,300 kilograms) of waste.

1.2.4.1 Waste Hazards – Mitigating Factors (Design)

- Two 90-day waste accumulation areas on opposite sides of ring
- 90-day areas are designed with 2-hr fire rating, independent exhaust ventilation, fire detection, alarm pull box, communications (phone) system, access control (card reader), and secondary containment

1.2.4.2 Waste Hazards – Mitigating Factors (Operational)

- NSLS-II chemical use and waste production will be minimized through review; less hazardous chemical and processes will be substituted where possible
- Local Satellite Accumulation Areas in laboratories or at beamlines
- 90-day weekly inspections
- Periodic New York State Department of Environmental Conservation inspections of the 90-day areas and Satellite Accumulation Areas
- Hazardous Waste Generator training
- Experimental Safety Review process
- Work planning and control
- Facility-Specific safety orientation
- Tier I inspections
- Process Assessment Forms
- Tritium sampling program for accelerator's cooling-water systems
- Waste reduction, pollution prevention, and recycling
- HazMat transportation procedures per DOT

1.2.5 Fire Hazards (NSLS-II FHA – 5)

Operational experience at accelerators throughout the DOE complex has demonstrated that most fires in accelerator facilities are electrically initiated, typically by component failure. However, other sources of fire are considered in the design of the NSLS-II facility. They include the combustibility of building construction materials, the accumulation of combustible materials by occupants, the use of pyrophoric or reactive materials, improper storage or use of flammable materials, lightning storms, and static discharge.

1.2.5.1 Fire Hazards – Mitigating Factors (Design)

- Design to Business Occupancy BCNY and appropriate NFPA standards
- Preliminary Fire Hazards Analysis
- Noncombustible construction throughout facility
- Early-warning fire-detection systems (e.g., HSSD, smoke detectors, rate of rise detectors, pre-alarm)
- Fully sprinklered, including a fire department standpipe service (except hutches)
- Draft curtains and manually activated exhausts around ring to limit spread of heat and smoke
- Redundant Water Supplies
    - Two feeds to NSLS-II
    - Well gridded water supply system
    - Supply for three days without electric power
- Emergency power supply for essential systems
- Hazardous material storage areas: rated, vented, alarmed
- Lightning protection system for facilities
- Adequate grounding systems

1.2.5.2 Fire Hazards – Mitigating Factors (Operational)

- Manual fire suppression provided by sufficient portable fire-extinguishers
- Alarm systems to alert occupants and summon fire department (e.g., fire alarm bells/strobes, manual pull stations, connected to on-site fire department)
- Full-time, BNL Fire/Rescue Group with mutual aid arrangements with local fire departments
- Ongoing Tier I inspection program to minimize combustibles and ignition sources
- Ignition-source control programs (cutting/welding permits, no smoking policy)
- Experimental Safety Review and Work Planning to minimize fire hazards of experiments and other work within the facility
- Fire evacuation drills

1.2.6 Electrical Hazards (NSLS-II FHA – 6)

The NSLS-II will have a large amount of facility-related and experimental electrical equipment. Electrical hazards from NSLS-II include the potential for serious injury, death, and equipment damage. Electrical shock and arc flash can be caused by exposed conductors, defective and substandard equipment, lack of adequate training, or improper procedures.

1.2.6.1 Electrical Hazards – Mitigating Factors (Design)

- Design to NFPA 70 and 70 E National Electric Code
- Provide adequate power distribution (beamlines and laboratories) to reduce need for extension cords
- Provide segregated power and utility distribution; no over-loading (cable/utility trays)
- Electrical and mechanical equipment rooms adequately sized and accessible from outside of ring
- Electrical distribution/disconnect equipment located in unobstructed areas (physically marked to provide clear access)
- Protect equipment and cables from mechanical and other hazards
- NRTL-certified equipment if available, all non-NRTL certified by BNL EEI program
- Conduct arc flash calculations, determining PPE requirement, and label all electrical panels and switches
- Assess need and feasibility for remote operation of high voltage switches and breakers to prevent human contact during opening and closing
- Implement Lockout/Tagout capability into design of energized equipment

1.2.6.2 Electrical Hazards – Mitigating Factors (Operational)

- Non NRTL-certified equipment inspected and certified by an Electrical Equipment Inspector
- Engineering and beamline design reviews
- Operation of equipment at <50 volts where feasible
- SBMS procedures for electrical safety
- Electrical safety training
- Operational procedures to keep electrical equipment unobstructed
- Tier I inspection program

1.2.7 Noise Hazards (NSLS-II FHA – 7)

Hazards from noise include overexposure of personnel to ACGIH and OSHA occupational exposure limits and permanent hearing loss, also known as Permanent Threshold Shift. NSLS-II will incorporate a wide variety of equipment that will produce a range of noise. Support equipment (e.g., pumps, motors, fans, machine shops, and general HVAC) all contribute to point source- and overall ambient-noise levels. While noise will typically be below the ACGIH 8-hr time-weighted average, certain areas with mechanical equipment could exceed that criterion and will require periodic monitoring, posting, and the use of Personal Protective Equipment. Ambient background noise is of a greater concern from the standpoint of users' comfort, stress level, and fatigue. Background noise in the accelerator and experimental areas at the existing NSLS is a common quality-of-life complaint and may be distracting and tiring.

1.2.7.1 Noise – Mitigating Factors (Design)

- Use low noise equipment (fans) in HVAC systems
- Incorporate sound-absorbing materials into structure (wall and ceilings) and around equipment
- Use of water or whisper fan cooling for equipment
- Achieve Noise Criterion of 60 or better

1.2.7.2 Noise – Mitigating Factors (Operational)

- Baseline and periodic area noise surveys, and postings
- Personnel noise dosimetry
- Noise-exposure medical protocol where required
- New equipment reviews for noise levels as part of procurement and installation process
- Local sound proofing, if needed
- Personal protective equipment

1.2.8 Cryogenic, Including Pressure Hazards (NSLS-II FHA – 8)

Cryogenic hazards at NSLS-II will include the potential for oxygen-deficient atmospheres due to catastrophic failure of the cryogenic systems, thermal hazards (cold burns) from cryogenic components, and pressure hazards. Initiators could include the failure or rupture of cryogenic systems from overpressure, failure of insulating vacuum jackets, mechanical damage or failure, deficient maintenance, or improper procedures.

Large volumes of liquid nitrogen will be piped into and around the NSLS-II facility from a centralized distribution point located outside of the ring building. In addition, dewar vessels (typically up to 500 liters) will be used locally in experiments.

Liquid nitrogen and liquid helium will be used for cooling experimental samples such as protein crystals, and also to cool beamline equipment, such as detectors, for enhanced sensitivity. Similarly, liquid coolants will chill accelerator components such as magnetic insertion devices, to make them superconducting (i.e., have zero resistance to electrical current) as well as equipment located within beamline front end optical enclosures.

Other pressurized systems include the facility compressed air distribution system providing air pressurized to 100 psig, the facility compressed nitrogen system pressurized to 100 psig used within the experimental program and compressed as cylinders (typically 2000 psig) used for the experimental program. Pressurized systems present hazards of asphyxiation, fire, injury from fragments or missiles or contact with toxic gases produced by system failure.

1.2.8.1 Cryogenic and Pressure Hazards – Mitigating Factors (Design)

- Design cryogenic and other pressure systems per ASME and ANSI codes or equivalent
- Evaluate failure scenarios and provide PDH sensors and alarms as required
- Provide interlocks and automatic exhaust system/quench installed
- Provide relief mechanisms in all piping and dewar systems
- Design review process
- Initial system pressure testing
- Major systems reviewed by BNL Cryogenic and Pressure Safety sub-committee and testing completed as required by SBMS

1.2.8.2 Cryogenic and Pressure Hazards – Mitigating Factors (Operational)

- NSLS-II facility-specific access training
- Compressed-gas safety training
- Cryogen safety awareness training
- Oxygen Deficiency Hazard training
- ODH classification and controls
- System-specific training
- Personal protective equipment

1.2.9 Confined Space Hazards (NSLS-II FHA – 9)

Hazards from confined spaces could result in death or injury due to asphyxiation, compressive asphyxiation, smoke inhalation, or impact with mechanical systems. Initiators would include failure of cryogenic systems releasing gas, fire, or the failure of mechanical systems or chemical spills.

Two types of confined spaces should be considered for the NSLS-II facility. The first are those associated with the facility's support/maintenance and typically include sump pits and HVAC plenums that would only be accessed by Plant Engineering's maintenance personnel or vendor personnel. NSL:S-II staff and users would not have access to these spaces. The second category is those confined spaces created by the experimental programs and may include pits for support equipment or large tanks installed to recover inert gases.

1.2.9.1 Confined-Space Hazards – Mitigating Factors (Design)

- Definition of confined space criteria for designers – "design out," where possible
- Design of multiple means of egress, where possible
- Adequately size mechanical enclosures to provide for maintenance

1.2.9.2 Confined-Space Hazards – Mitigating Factors (Operational)

- Identification and posting of all confined spaces
- Facility-specific safety orientation to identify spaces
- Work Planning and Control program
- Interface with site's maintenance personnel identify their confined spaces

1.2.10 Ozone Hazards (NSLS-II FHA-10)

Synchrotron radiation produced by the storage ring dipole bending magnets and insertion devices can generate significant levels of ozone when the unattenuated beam passes through air. Experience at the current NSLS demonstrated that in some instances, ozone concentrations may approach or exceed the ACGIH Threshold Limit Values and precautions are needed to control potential exposures.

1.2.10.1 Ozone Hazards – Mitigating Factors (Design)

- Direct the beam path through evacuated or inert gas atmosphere containing pipes
- Minimize beam's horizontal and vertical dimensions
- Minimize beam path's length
- Filter beam to eliminate lower photon energies
- Scrub air round beam path with ozone filters
- Install ozone monitoring at potential problem areas

1.2.10.2 Ozone Hazards – Mitigating Factors (Operational)

- Experimental and beamline review program
- Delay personnel entry time to allow ozone to degrade

1.2.11 Chemicals and Hazardous Materials, Including Nano-materials and Biological Materials (NSLS-II FHA – 11)

The use of chemical and hazardous materials (HazMat) at NSLS-II could result in injury and death, or in exposures that exceed regulatory limits. Initiators could be experimental operations, transfer of material, failure of packaging, improper marking/labeling, failure of fume hood or glove box, reactive or explosive event, improper selection (or lack) of personal protective equipment, or a natural phenomenon.

1.2.11.1 Chemical and HazMat Hazards – Mitigating Factors (Design)

- Dedicated Chemical Storage Area with segregation, ventilation, fire-protection system, flammable, and O_2 monitors and access control
- Chemical delivery area located adjacent to loading dock
- Each lab designed based on anticipated use and future use (user input in design process, historical inventories/hazards considered)
- Labs designed for Biosafety Level 2 materials
- Vented chemical storage cabinets in laboratories and at beamlines as determined
- Gas cabinets for toxic and highly toxic gasses, individual venting and purging capacity and exterior access
- Double-wall stainless tubing for toxic and highly toxic gas distribution
- Dedicated storage for biological and infectious materials
- Bulk gas piped in, (Liquid Nitrogen, Gaseous Nitrogen, Air); limit number of individual cylinders

- Exhausted fume hoods in laboratories meeting industry consensus standards (specialized hoods such as HEPA filters for nanomaterials and radioactive materials, where necessary)
- Covered centralized location for storing gas. Satellite locations due to size of ring.
- Safety showers and eyewashes in each wet laboratory (tepid water)
- Loading dock with leveling system to reduce material handling
- All lead material encapsulated/painted
- Hutches with exhaust ventilation to exterior of building

1.2.11.2 Chemical and HazMat Hazards – Mitigating Factors (Operational)

- Experimental safety review to determine type and use of chemicals, nanomaterials and biologicals; minimize quantities in use and in storage
- Compliance with BNL Subject Area and part 851 requirements for handling chemicals, including nano and biological materials
- Chemical Inventory control system (barcode); Chemical Management System (CMS)
- Lab Standard/Hazcom or other required training
- Transport of materials per DOT and BNL Hazardous Material Transportation Manual (HMTM)
- Assess needs for exposure monitoring
- Safety protocols for workers using or machining lead

1.2.12 Accelerator/Beamline Hazards (NSLS-II FHA – 12)

Hazards from the accelerator and beamlines include the loss of vacuum and cooling water system control, compressed air and gas, electrical, material handling, and static magnetic, cryogenic, mechanical and also scattered radiation.

The accelerator and beamlines will have various types of electrical equipment and associated power supplies. High-power equipment includes vacuum pumps, vacuum gauges, detectors and beam-position monitors (higher voltage-biased system).

Two important hazards are synchrotron scatter from beamline optics and bremsstrahlung radiation from loss of high-energy electrons from the orbit. Both hazards are found along the beamline. Synchrotron scatter will mostly be from the first optical elements. Bremsstrahlung radiation is confined to the beamline vacuum chamber with lead collimators until it can be directed into a beam stop. On many beamlines, the synchrotron light is offset from the bremsstrahlung cone at the monochromator and can be stopped there. For lines that have insufficient offset, a backstop is placed in the hutch behind the endstation.

1.2.12.1 Accelerator/Beamline Hazards – Mitigating Factors (Design)

- Engineered safety-systems in place will protect the ring and beamlines from vacuum, cooling-water flow, extreme temperatures, and compressed air faults
- Vacuum faults will cause the accelerator's interlock systems to close the sector and front-end valves, thus dumping beam; beamline interlocks will close a beamline valve and/or a front-end valve; insertion device beamline interlocks will close the fast valve and dump RF
- Reduced cooling water flow or loss of temperature control is sensed, causing the accelerator's interlocks to dump RF and causes beamline interlocks to close the safety shutters
- Elevated magnet temperature would turn off the magnet's power supply; if sensed on ring components, would dump RF; if sensed in the pump room water, would dump RF and magnet power supplies.
- Loss of primary compressed air supply from the Central Chilled Water Facility alerts the control room
- Loss of backup compressed air supply (affecting operation of front-end masks, safety shutters, and fast valves) alerts the control room

1.2.12.2 Accelerator/Beamline Hazards – Mitigating Factors (Operational)

- Safety Analysis Document and Accelerator Safety Envelope
- Operational procedures
- Systems design review

1.2.13 Ionizing Radiation Hazards (NSLS-II FHA – 13)

Potential hazards from ionizing radiation include prompt radiation (x-rays, neutrons, bremsstrahlung) produced during machine operation, induced activity in machine components, and experimental radioactive material (use, storage). Typical initiators of radiation exposure would include operating machines, maintenance work, and use of radioactive materials. Accidental exposure could result from failure of an interlock or other protective system, inadequate design or control of shielding, or an inadequate procedure.

Management and control of ionizing radiation hazards will follow the requirements in 10 CFR 835, Occupational Radiation Protection, the BNL SBMS Radiological Safety subject areas, and the BNL Radiological Control Manual. The facility will be designed and operated in a manner to maintain radiation exposure to staff, users, and the general public personnel within DOE and BNL dose limits and control levels [1.6]–[1.11].

A full discussion of radiation shielding at NSLS-II is given in Chapter 15.

1.2.13.1 Ionizing Radiation – Mitigating Factors (Design)

- Well designed shielding for accelerators (including roof) and hutches to reduce dose to administrative levels
- Interlock systems, e.g. beam dumps if interlock broken, emergency stop capability, audible/visual alarms
- Redundant interlock systems for accelerator enclosures and beamline hutches
- Redundantly monitored radiation safety critical devices (e.g., transfer line beam stops, beamline safety shutters) with reach back to upstream devices if there is a failure
- Real-time beam loss monitoring system for injection and storage-ring operation
- Shielding around penetrations to minimize leakage, e.g. single-block concrete construction wherever possible, tongue-and-groove to eliminate line of sight, shielding labyrinths and chicanes
- Office areas/staff lounges and other public areas, e.g. walkways, should not be exposed to significant radiation fields produced by machine operators or by equipment

1.2.13.2 Ionizing Radiation – Mitigating Factors (Operational)

- Radiological protection program incorporating requirements of 10 CFR 830 and 835, and BNL SBMS subject areas and BNL Radiological Control Manual
- Strict configuration control of shield and interlock systems
- Routine area monitoring of dose levels by passive dosimeters for neutrons and gammas on the experimental floor (and other occupied areas subject to radiation)
- Radiological safety training, e.g. GERT, Radiation Worker I
- Facility-specific Safety Orientation and ES&H Orientations
- Work planning and control procedures for work in radiation areas or with radioactive materials
- ALARA designs and committee reviews
- Administrative control levels and limits specified in Accelerator Safety Envelope

1.2.14 Lasers and other Non-Ionizing Radiation Hazards (NSLS-II FHA – 14)

Anticipated non-ionizing radiation hazards at NSLS-II include radio frequency, microwave, static magnetic, visible light, infrared, ultraviolet and laser hazards. The NSLS-II accelerators and storage rings will depend on the reliable operation of pulsed klystrons and continuous-wave high-power radio-frequency (RF)

systems for injecting electrons and maintaining the stored beam. Both of these devices generate electromagnetic radiation within the RF and microwave energy ranges of 500 MHz to 3 GHz) and, in addition, pose significant electrical hazards. The devices typically are operated and maintained such that these energies will be shielded and, therefore, will not thermally or electrically expose nearby personnel.

The NSLS-II operations and experimental programs will use Class 1, 2, 3a, 3b, and 4 lasers. Some lasers will occupy permanent locations, while others will be part of short-term beamline experiments, in place for just days to weeks at a time. Lasers, particularly those in Class 3b and 4, will require written laser controlled area standard operation procedures for each device to control exposure, and associated electrical and industrial hygiene hazards, e.g. exposure to solvents, dyes, and halogen gases.

1.2.14.1 Lasers and other Non-Ionizing Radiation Hazards – Mitigating Factors (Design)

- Commercial equipment designed with integral enclosure shielding and interlock systems
- Laser labs will address ANSI design requirements, including control of exposed beams and interlock systems
- Use of gas cabinets for lasers using halogens (fluorine gas) vented exterior to the building

1.2.14.2 Lasers and other Non-Ionizing Radiation Hazards – Mitigating Factors (Operational)

- Baseline and routine surveys for stray static magnetic fields, RF, and microwave
- Training for static magnetic fields, RF, microwave hazards
- Laser safety training
- Equipment ES&H review
- Laser Safety Officer reviews, especially of written procedures for Class 3b and 4 lasers
- Experiment safety reviews
- Personnel protective equipment

1.2.15 Material-Handling Hazards (NSLS-II – FHA – 15)

The consequences of hazards encountered in material handling include serous injury or death to equipment operators and bystanders, damage to equipment, and interruption of the program. These hazards could be initiated by a dropped or shifted load, equipment failure such as from suspect/counterfeit bolts and rigging equipment, improper procedures, or insufficient training or qualification of operators.

1.2.15.1 Material-Handling Hazards – Mitigating Factors (Design)

- Hoists and attach points designed to ASTM/ANSI standards
- Gases piped in to reduce handling of cylinders
- Adequate aisle space for maneuvering loads

1.2.15.2 Material-Handling Hazards – Mitigating Factors (Operational)

- Hoists and lifts proof tested after installation and any modification
- Routine inspection and maintenance of hoists and forklifts and rigging equipment
- Only trained and qualified personnel allowed to use hoists and fork trucks
- Hoists and forklifts are locked to prevent unauthorized use
- Inspection before each use as required by SBMS to assure proper operating conditions
- Ensure areas are adequately protected from the forklifts and other traffic

1.2.16 Experimental Hazards (NSLS-II – FHA – 16)

The consequences from experimental operation hazards range from minor to severe injuries, possible death, and danger to the experimental, accelerator, or facility equipment, as well as a programmatic impact. Initiators would include the release or unexpected reaction of hazardous material, the failure of protective systems, the use of radioactive materials and of biological materials, operators' error, lack of training, poorly designed/installed equipment, failure of equipment, unexpected chemical reactions, and undefined hazards or risks from material not considered in experimental safety reviews. Many of the anticipated hazards are discussed in the specific hazard-analysis sections, e.g., ozone, non-ionizing radiation.

Inert and other research gases will be used in experiments; inert gases include nitrogen, helium, and argon. Small amounts of flammable gases, such as hydrogen, propane, and butane, may be required. Various toxic gases, such as hydrogen sulfide, carbon monoxide, or nitrogen oxides might also be used in liter quantities. Small-scale use of oxygen and the halogens also is anticipated. Liquid nitrogen and liquid helium will be used to cool experimental samples such as protein crystals.

The NSLS-II team continues to work with the DOE "nano" community to share the latest information on the hazards of nanoparticles and to fully implement the Secretarial Policy Statement on Nanoscale Safety (DOE P 456.1). Future changes in design guidance and equipment/systems may be necessary due to emerging information.

1.2.16.1 Experimental Hazards – Mitigating Factors (Design)

- Each laboratory designed based on its anticipated use and future use (user input in design process, historical inventories/hazards considered).
- Facility designed for Bio-safety Level 2.
- Chemical fume hoods installed in laboratories will be appropriate to experimental activity conducted, HEPA filtered hoods for nanomaterial particulate and radiological dispersible work (once through systems)..
- An adequate power designed into laboratory to support equipment/future growth (GFCI protected).
- Equipment bonding system installed.
- Adequate chemical storage.
- Vented storage cabinets for flammable gases in laboratories
- Laboratories designed for easy access/egress, process flow, ease of cleaning
- Laboratories located in proximity to beamlines reducing travel with experimental materials
- Facility and laboratories designed to meet OSHA 1910 (walkways, stairs, egress)
- Safety shower and eye wash in each chemical laboratory (hands-free, tepid water)

1.2.16.2 Experimental Hazards – Mitigating Factors (Operational)

- Experimental safety review program
- Control of hazardous materials (inventory, storage)
- ES&H support staff (subject-matter experts, monitoring technicians)
- Principal Investigator's R2A2 and training
- Adequate beamline staffing

1.3 NEPA COMPLIANCE

In compliance with the National Environmental Protection Act (NEPA) and its implementing regulations (10 CFR 1021 and 40 CFR 1500-1508) and in accordance with the requirements of DOE Order 451.1B, an Environmental Assessment (EA) was prepared to evaluate the potential environmental consequences of

constructing and operating NSLS-II at DOE's preferred site (BNL) has been carried out [1.11]. The EA analyzed the potential environmental consequences of the facility and compared them to the consequences of a No Action alternative. The assessment included detailed analysis of all potential environmental, safety, and health hazards anticipated as the design, construction, and operation of the facility progresses. The EA determined that there would be no significant impact from the construction and operation of the proposed facility and that an Environmental Impact Statement (EIS) was not required. A Finding of No Significant Impact (FONSI) was approved by the DOE Brookhaven Site Office (BHSO) Manager and made available to the general public and project stakeholders [1.12].

1.4 QUALITY ASSURANCE

NSLS-II management will design and build a world-class user facility for scientific research with the assistance of a fully involved Quality Assurance (QA) Program.

The NSLS-II Project Director is responsible for achieving performance goals. The NSLS-II Quality Assurance Manager is responsible for ensuring that a quality system is established, implemented, and maintained in accordance with requirements. The QAM will provide oversight and support to the project participants to ensure a consistent quality program.

A QA Program Plan [1.13] has been prepared by the QA Manager and approved by the NSLS-II Project Director. This plan specifies the program requirements that apply to all NSLS-II work. The primary objective of the QA program is to implement quality assurance criteria in a way that achieves adequate protection of the workers, the public, and the environment, taking into account the work to be performed and the associated hazards. The objectives include:

- "Designing in" quality and reliability
- Assuring that all personnel involved in the project uphold the NSLS-II Quality Assurance Plan
- Promoting early detection of problems to minimize failure costs and impact on schedule
- Developing appropriate documentation to support construction and operational requirements
- Assuring that personnel have the necessary training as needed before performing critical activities, especially activities that have environmental, safety, security, or health consequences.
- Defining the general requirements for design and readiness reviews, including environmental, safety, security, and health issues related to NSLS-II and contractor hardware, software, and processes.

References

[1.1] NSLS-II Environment, Safety, and Health Plan.
[1.2] NSLS-II Baseline Hazards List, March 2006
[1.3] NSLS-II Preliminary Hazards Analysis; December 2006
[1.4] NSLS-II Final Hazard Analysis (currently under review by DOE/BHSO)
[1.5] NSLS-II Technical Note 00012; "Preliminary Radiological Considerations for the Design and Operation of NSLS-II Linac"; PK Job and WR Casey July25, 2006.
[1.6] NSLS-II Technical Note 00013; "Preliminary Radiological Considerations for the Design and Operation of NSLS-II storage Ring and Booster Synchrotron; PK Job and WR Casey July25, 2006.
[1.7] NSLS-II Technical Note 00014; "Preliminary Shielding Estimates for NSLS-II Beamlines and Front Ends"; PK Job and WR Casey July 25, 2006.
[1.8] J. Panakkal, W.R. Casey, "Preliminary Activation Analysis of Accelerator Components and Beam Stops at the NSLS-II"; NSLS-II Technical Note 00015; August 1, 2006.
[1.9] NSLS-II Technical Note 00016; "Preliminary Activation Analysis of Soil, Air and Water near the NSLS-II Accelerator Enclosures"; PK Job and WR Casey August 15, 2006.

[1.10] NSLS-II Technical Note 00021; "Shadow Shields in the Storage Ring of NSLS II"; PK Job and WR Casey September , 2006
[1.11] NSLS-II Technical Note 00032; "Preliminary Material Requirement for the Supplementary Shielding at NSLS-II"; PK Job and WR Casey July 18, 2007
[1.12] NSLS-II Environmental Assessment.
[1.13] Finding of No Significant Impact for NSLS-II Project, approved by BHSO, September 27, 2006.
[1.14] NSLS-II Quality Assurance Plan.

2 RADIATION SAFETY AND SHIELDING

2.1 SHIELDING OBJECTIVES

NSLS-II is subject to DOE radiation protection standards. The primary document that defines the DOE radiation protection standard is the Code of Federal Regulations, 10 CFR 835. In addition, the accelerator-specific safety requirements are set by DOE Order 420.2b, Safety of Accelerator Facilities. All radiation protection policies and guidelines at NSLS-II must be in compliance with these regulations along with the BNL Radiation Control Manual and other pertinent documents in the BNL Standards Based Management System.

The maximum annual exposure limits to radiation workers and members of the public are limited in 10 CFR Part 835 to 5,000 mrem and 100 mrem, respectively. To keep radiation exposures well below regulatory limits, BNL maintains an annual administrative control level of 1,250 mrem for its workers and 5 mrem per year from any single facility to the public off-site. An additional control level of 25 mrem/year from NSLS-II operations is established for personnel working in non-NSLS-II facilities on site and for visitors and minors within the NSLS-II building.

The dose to workers and beamline scientists from NSLS-II operations will be kept well below federal limits and within BNL administrative levels through shielding, operational procedures, and administrative controls. Shielding will be provided to reduce radiation levels during normal operation to less than 0.5 mrem/h and as low as reasonably achievable. Assuming an occupancy of 2,000 hours per year, this will reduce annual exposure to 1,000 mrem or less, in accordance with 10 CFR 835.1001. Because of higher occupancy compared to accelerator enclosure walls, beamline enclosures will be shielded during normal operations to 0.25 mrem/h or less.

Shielding will also be evaluated for abnormal operating conditions. Additional shielding or engineering controls will be provided to reduce the potential severity of an abnormal operating condition. The controls will be considered acceptable if exposures in excess of 100 mrem per incident are considered unlikely and exposures above 2,000 mrem are considered extremely remote. Based on the current experience at NSLS and other synchrotron radiation facilities, we expect annual radiation exposures <<100 mrem/year to NSLS-II staff and users.

Effectiveness of the shielding will be actively monitored by radiation instruments located on the experimental floor and other locations and by frequent area-surveys performed by the health physics personnel. Additional local shielding will be provided to reduce the radiation field as needed. Passive area monitors will also be used to integrate doses in various areas. The results will be analyzed for trends, and shielding will be improved in the form of supplementary shielding as appropriate.

2.2 SHIELDING ESTIMATES FOR THE ACCELERATOR ENCLOSURES

Radiological conditions for the design and operation of the NSLS-II linac, booster, and storage ring have been analyzed using the preliminary design parameters. The booster synchrotron will be housed in a separate tunnel from the storage ring at NSLS-II. Calculations of the resulting radiation fields and required shielding have been made for normal loss of stored beam and loss of beam during injection at the septum/extraction magnets. The shielding estimates are based on conservative assumptions, including several modes of operations that involve normal beam loss mechanisms as well as certain abnormal beam loss scenarios. The

conservative factors used in the calculations are conservative beam loss assumptions, conservative radiation attenuation factors, storage ring beam life time of 2 hours, radiation dose equivalent factors derived from the thick target approximation and the dose rates calculated on contact at the shield walls.

The beam loss scenarios are drawn from experiences and assumptions used at existing accelerator and synchrotron radiation facilities. Shielding requirements for the storage ring and booster synchrotron are based on maintaining exposure to personnel to less than 1,000 mrem/year assuming an occupancy of 2,000 hours per year for a worker at NSLS-II. The calculated shielding for the occupied regions during operation is for a dose rate of <0.5 mrem/h, at the exterior of the accelerator enclosures on contact. Sufficiently conservative factors are included in these estimates to provide additional margin of safety.

2.2.1 Sources of Radiation Hazard at the Electron Accelerators

For the radiological analysis of NSLS-II accelerator enclosures, the following radiation components were considered:

- bremsstrahlung radiation created during electron beam loss
- neutron production by high-energy bremsstrahlung
- synchrotron radiation from the insertion devices

High-energy electrons produce bremsstrahlung [2.1] when intercepted by the accelerator components or residual gas molecules in the vacuum chamber. Bremsstrahlung, or "breaking radiation," is emitted by a high-energy electron as it decelerates due to inelastic radiative interaction with the coulomb field of atomic nuclei of the medium it traverses. Subsequent pair production and bremsstrahlung production can generate an electromagnetic shower. The radiation originating in the shower is highly forward-peaked in the forward direction of the electron beam. However the transverse component is significant and cannot be ignored. The lateral shielding for the accelerator enclosures is designed to protect personnel from the transverse component of the electromagnetic shower. In addition to bremsstrahlung radiation, two other radiation components need to be considered. These are Giant Resonance Neutrons and High Energy Neutrons originating from the interaction of bremsstrahlung with heavy metals [2.2]. GRN are produced by photonuclear interactions when the photon energy is above the threshold energy of 7 to 20 MeV. This component has an average effective energy of about 2 MeV and is emitted isotropically. If the photon energy is above 50 MeV, high-energy neutrons (>25 MeV) are also emitted. The high-energy neutron component is slightly forward peaked and not isotropic. To estimate the shielding and other requirements for the NSLS-II accelerator enclosures, these sources of radiation have been considered, across a range of possible conditions.

2.2.2 Shielding Design Methodology for the Accelerators

2.2.2.1 Radiation Attenuation Factors for the Shielding Materials

The radiation attenuation factors used for the materials in the current shielding calculations are given in Table 2.2.1. These data have been obtained from various sources in the literature [2.3–2.6]. A number of references which discuss these attenuation factors have been reviewed. We have chosen conservative values for these factors to provide an additional safety margin for the shielding calculations.

Table 2.2.1 Radiation Attenuation Factors of Shielding Materials.

Radiation Component	Shielding Material	Density [g/cm^3]	Attenuation Length [g/cm^2]
Bremsstrahlung	Concrete	2.35	49
	Heavy Concrete	3.70	50
	Lead	11.34	25
	Iron	7.80	37
	Earth	1.60	70
	Polyethylene	1.01	70
Giant Resonance Neutrons	Concrete	2.35	40
(E <25 MeV)	Heavy Concrete	3.70	45
	Lead	11.34	161
	Iron	7.80	100
	Earth	1.60	33
	Polyethylene	1.01	6.3
High-Energy Neutrons	Concrete	2.35	65 (<100 MeV) 115(>100 MeV)
	Heavy Concrete	3.70	125(>100 MeV)
	Lead	11.34	191
	Iron	7.80	138
	Earth	1.60	90
	Polyethylene	1.01	62

2.2.2.2 Shielding Calculations for NSLS-II Accelerator Enclosures

The bulk shielding for the accelerator enclosures has been calculated using the following expression [2.9]:

$$H = \sum_i \frac{F_i J}{R^2} e^{-t/\lambda_i} \tag{5-1}$$

where H = Dose Equivalent Rate summed over all components, in mrem/h, F_i = Radiation Dose Equivalent Factors for the corresponding radiation component (i^{th} component), J = electron energy dissipation in joules/hour, R = total distance of the dose point from the source in meters, t = thickness of bulk shielding in g/cm^2, and λ_i = attenuation length of the i^{th} radiation component in g/cm^2.

The equation is solved using a parameter search for the thickness of the bulk shielding (concrete), such that H <0.5 mrem/h. The shielding strategy employed is to use concrete as bulk shielding, to provide global shielding of accelerator enclosures for distributed losses in the system. This shielding needs to be supplemented by additional local shielding, employing lead for bremsstrahlung or polyethylene for neutrons, to reduce radiation fields from the high loss points to acceptable limits of <0.5 mrem/h (1,000 mrem per 2,000-hour work year).

2.2.2.3 Dose Equivalent Factors of Radiation Components

Effective Dose Equivalent factors for the unshielded source terms at 1 meter in the transverse direction (90 degrees) from a 3.0 GeV electron beam interaction on a thick copper or iron target are given in Table 2.2.2. The data are taken from Sullivan [2.7]. Note that the dose equivalent factors in the transverse direction (90 degrees) are independent of the electron beam energy, but dependent on the beam power.

Table 2.2.2 Dose Equivalent Factors (Fi) Used for Shielding Calculations.

Radiation Component	Dose Equivalent Factor [mrem-m^2/Joule]
Bremsstrahlung	1.39
Giant Resonance Neutrons	0.27
High-Energy Neutrons	0.043

In the absence of any shielding, the bremsstrahlung component will include low-energy particle component (e^- and e^+), which can be disregarded, since shielding for bremsstrahlung will ensure attenuation of the particle component. In the forward direction with respect to the electron beam (zero degrees), the dose equivalent factor for bremsstrahlung [2.8] is 8.3 × E mrem-m^2/J, where E is the electron energy in MeV. The bremsstrahlung dose rate at 1 m near zero degrees, but not within the forward spike [2.8], is taken as 850 mrem-m^2/J. The GRN component is assumed to be isotropic from the loss point. These forward dose equivalent components are important for the design of ratchet wall shielding of the storage ring in the forward direction.

2.2.3. Shielding Estimates for the Linac Enclosure

2.2.3.1 Linac Parameters

For NSLS-II, a linac will be providing 200-MeV (injection energy) electrons into the booster synchrotron. In the current calculations the linac tunnel is assumed to be 60 meters long, 4 meters wide, and 3 meters high. The salient features of the linac system are as follows:

beam energy	200 MeV
beam current	15 nA
frequency	1 Hz
tunnel length	40 m
tunnel width x height	4 m x 3 m
position of beam from floor	1 m
power	2.96 W

2.2.3.2 Bulk Shielding for the Linac Tunnel

For the linac system, the bulk shielding computations are based upon normal operation beam losses of certain fractions of beam power. Table 2.2.3. gives the estimated losses of beam energy in the linac system components.

Table 2.2.3 Estimated Losses in the Linac System Components.

Component	Charge [nC/s]	Loss [%]	Energy [MeV]	Power Loss [W]
Accelerator system	15	10% distributed	200	0.30
Injection septum	7.5	50%	200	1.48
Linac beam stop	15	100%	200	2.96

To estimate the bulk shielding for the linac tunnel, a distributed loss of 10% of the beam energy is assumed along the length of the tunnel. The shielding requirements for the lateral walls and the roof of the linac tunnel are calculated based on this beam loss scenario and are shielded for a dose rate of 0.5 mrem/h.

The distance of the lateral wall at the klystron gallery side is at 3.0 m and the roof is taken as at 2 m from the beam center line.

The bulk shielding estimates of the concrete thickness for the linac tunnel are given in Table 2.2.4. 100 cm-thick standard concrete with a density of 2.35 g/cm^3 will limit the dose rate to <0.5 mrem/h at the exterior of the lateral wall, for an assumed 10% distributed beam loss scenario.

The injection septum for the linac injection to the booster synchrotron is covered in the next section.

Table 2.2.4 Bulk Shielding Estimates for the Linac Tunnel.

Component	Lateral wall Concrete Equivalent[1] Thickness [cm]	Roof Concrete Equivalent[1] Thickness [cm]
Non-injection region	100	110
Linac downstream wall	220	110
	100 cm + 15 cm (Pb)	

[1] A density of 2.35 g/cm^3 is considered standard for concrete.

The bulk shielding estimates in the forward direction of the linac should be estimated, because an occupiable region exists in the forward direction of the bend magnet in the booster ring. The calculations are based on the forward direction bremsstrahlung and neutron dose equivalent rates provided by Sullivan [2.7]. These estimates are given in Table 2.2.4. The estimated concrete equivalent thickness for bulk shielding in the forward direction is 220 cm. Local shielding of lead in the forward direction can be provided to save on the concrete bulk shielding. A factor of 7 with respect to standard concrete can be applied to calculate the equivalent thickness of lead. Local shielding by the equivalent thickness of lead may replace concrete in the forward direction at the extraction region of the linac.

2.2.4 Design of the Linac Beam Dump

When the linac is not injecting into the booster, the beam is dumped at the linac beam stop. This beam stop will be located at the end of the linac accelerator tunnel closer to the bending magnet. Since the detailed layout of the building is not currently available, it is assumed that the concrete bulk shield, which separates the occupiable regions, is 2 m away in all directions from the beam stop. 100% of the ~3-W electron beam is dissipated on the beam stop. The shielding strategy in this case will be to shield the stop locally in addition to the linac concrete bulk shielding available at the injection/extraction region.

When 200-MeV electrons interact with the material of the beam stop, an electromagnetic shower will be generated within the material, due to successive bremsstrahlung and pair-production interactions. A shower is developed in the material when the primary electron energy is much greater than the critical energy of the material. The critical energy, E_c, is the electron energy for a given element at which the average energy loss from bremsstrahlung production is equal that from ionization. The lateral and longitudinal shower dimensions within the material are determined by the Moliere radius and the radiation length of the material [2.10]. Table 2.2.5 gives the shower parameters for various shielding materials that are also used for beam stops.

Table 2.2.5 Electromagnetic Shower Parameters for Various Materials.

Material	Density [gm/cm^3]	Critical Energy [MeV]	Radiation Length [cm]	Moliere Radius [cm]
Aluminum	2.70	51.0	8.89	3.70
Iron	7.87	27.4	1.76	1.40
Copper	8.96	24.8	1.43	1.22
Tungsten	19.3	10.2	0.33	0.73
Lead	11.35	9.5	0.56	1.25
Concrete	2.35	51.0	10.9	4.5

The material considered for the linac stop is iron, for various qualities such as sturdiness, thermal stability, conductivity, and relative compactness of shower dimensions. Iron being a low Z material, the photo-neutron yield and the resulting activation will also be minimal.

The theory of electromagnetic showers stipulates that material of dimensions of approximately 20 radiation lengths in longitudinal and 3 Moliere radii in transverse will contain 99.99% of the electromagnetic shower [2.10]. Thus, an iron cylinder of 35 cm length and 8.5 cm diameter will be sufficient to effectively contain the electromagnetic shower in the linac stop. The scattered low-energy photon radiation will require additional lead shielding, but will be well below the critical energy and photospallation reaction threshold. The neutrons created in the shower will escape isotropically from the stop and require additional shielding.

Table 2.2.6 shows the dose rate due to various radiation components around the linac beam stop at the exterior of the 1m concrete shield wall without local shielding. This table also provides the dose rates on the exterior of the concrete shield wall with a local shielding of 15 cm of Pb and 20 cm of polyethylene (density = 1 g/cm^3). The local shielding limits the dose rate at the exterior of the concrete bulk shielding to <0.5 mrem/h. The stop will be in the linac enclosure; personnel will have no access to the enclosure when there is the potential for beam acceleration.

Table 2.2.6 Dose Rates at the Exterior of the Concrete Shield Wall around the Linac Beam Stop.

Radiation Component	Unshielded Dose Rates [mrem/h]	Dose Rates with 15 cm Pb and 20 cm Poly [mrem/h]
Bremsstrahlung	18.37	0.0142
Giant Resonance Neutrons	1.21	0.0079
High Energy Neutrons	1.85	0.2172
Total Dose Rate	21.43	0.2393

2.2.5 Bulk Shielding Estimates for the Booster Enclosure

At NSLS-II, the compact booster synchrotron will be housed in a separate enclosure. A top-off injection from the linac to the booster synchrotron will take place approximately every minute. The injected beam energy is 200 MeV and the injected charge is 15 nC. These electrons are accelerated to 3.0 GeV and injected into the storage ring. There may be a higher rate of injection during other modes of operation, such as accelerator performance evaluation or during injection to fill the storage ring from zero current. Assuming that top-off is the prevailing mode of operation, shielding calculations are performed for an average injection frequency of one in every minute and 2% of the beam energy at 3.0 GeV being dissipated at any single point in the booster synchrotron during acceleration. A 50% beam loss at the booster injection septum at 200 MeV is assumed. The salient features of the booster synchrotron are given below.

beam energy	3.0 GeV
repetition rate	1 Hz
ring circumference	158.4 m
accelerated charge	15 nC
no of electrons per fill	9.36×10^{10}
total energy in the booster	43.75 J

The lateral wall at the occupied regions and the roof are each assumed to be 2 meters from the center line of the booster vacuum chamber. Bulk shielding for the booster synchrotron is calculated based on the algorithm given in Section 2.2.2.2 and given in Table 2.2.7. It must be emphasized that the distance from the source to the bulk shielding is critical in determining dose rates outside the shielding. The stated distances in the current calculations need to be maintained in the civil construction design, and any change warrants rescaling of the bulk shielding thickness. No credit has been given to the shielding provided by the magnet iron in the booster ring. Supplementary shielding is also provided around the injection septum for possible higher injection rates. The area above the injection region is potentially occupiable and will be shielded with Pb supplementary shielding.

Table 2.2.7 Bulk Shielding Estimates of the Booster Enclosure.

	Lateral wall concrete equivalent (cm)	Roof concrete equivalent (cm)
Booster	70	70

2.2.6 Booster Beam Dump

When the booster is not injecting into the storage ring, the beam is dumped at the booster beam Dump. This beam dump will be located on the floor of the booster ring closer to the beam extraction region. It is assumed that the concrete bulk shield, which separates the occupiable regions, is 1 meter away at the storage ring side and 2 meters away from the roof.

The electromagnetic shower parameters for various materials considered for the booster beam stop are given in Table 2.2.5. Iron is the preferred material for the dump, due to various qualities such as sturdiness, thermal stability, conductivity, and relative compactness of shower dimensions. As iron is a relatively low-Z material, the photo-neutron yield and the resulting activation will also be minimal.

The theory of electromagnetic showers (Table 2.2.5) stipulates that material approximately 20 radiation lengths long and 3 Moliere radii in the transverse direction will contain 99.99% of the electromagnetic shower [2.10]. Thus, an iron cylinder 35 cm long and 8.5 cm in diameter will be sufficient to effectively contain the electromagnetic shower in the booster beam stop. The scattered low-energy photon radiation will require additional lead shielding, but will be well below the critical energy to further propagate the shower and the photospallation reaction threshold. The neutrons created in the shower will escape isotropically from the stop and require additional shielding.

Table 2.2.8 shows the dose rates at the concrete bulk shielding wall due to various radiation components around the booster beam stop with no supplementary shielding in place other than the concrete bulk shielding. This table also provides the dose rates on the exterior of the concrete shield wall with a local shielding of 10 cm of Pb and 10 cm of polyethylene ($1 g/cm^3$). It can be seen that the dose rates after local shielding are primarily due to high-energy neutrons. With the proposed local shielding, the dose rates come down to <0.5 mrem/h on contact at the exterior of the concrete shield walls. The stop is inside the booster enclosure, and

personnel have no access when the beam is in the storage ring. Additional supplementary shielding is required for possible higher rate of injection [2.11].

Table 2.2.8 Dose Rates on Contact : Exterior Concrete Shield Walls near the Booster Beam Stop.

	Dose Rate on Lateral wall [mrem/h]		Dose Rate on Roof [mrem/h]		Dose Rate on Inboard Wall [mrem/h]	
Radiation Component	No local shielding	Pb+Poly 10+10 cm	No local shielding	Pb+Poly 10+10 cm	No local shielding	Pb+Poly 10+10 cm
Bremsstrahlung	0.3011	0.0028	2.2600	0.0208	4.0189	0.0369
Giant Resonance Neutrons	0.0104	0.0010	0.1493	0.0151	0.2653	0.0268
High Energy Neutrons	0.0616	0.0178	0.2277	0.0660	0.4048	0.1174
Total Dose Rate	0.3731	0.0216	2.6370	0.1019	4.6890	0.1811

2.3 SHIELDING ESTIMATES FOR THE STORAGE RING

2.3.1 Storage Ring Parameters

The operations goal for the NSLS-II storage ring is to store a 500 mA current of 3.0 GeV electrons injected by the booster synchrotron. The conservatively estimated lifetime of the beam in the storage ring is 2 hours. In the current calculations, the storage ring tunnel is assumed to be 791 meters in circumference. The maximum assumed operating parameters of the storage ring system are shown below.

beam energy	3.0 GeV
beam current	500 mA
beam lifetime	2 hr
tunnel circumference	791 m
stored charge	1.3 μC
stored electrons	8.1×10^{12}
stored energy	3898 J

2.3.2 Storage Ring Beam Loss Assumptions

In the beam loss scenario perceived for these calculations, we considered the use of four scrapers in the injection region (two vertical and two horizontal), to intercept injected electrons that enter the storage ring at the wrong trajectory. The scrapers intercept incorrectly positioned electrons and prevent loss at other locations in the ring (e.g., at undulators). It is believed that it will be possible to intercept essentially all electrons that might be lost during injection on the scrapers and septum. The scrapers are likely to intercept a significant fraction of stored beam losses, as well. The bulk shielding calculations of the storage ring are performed with the following beam loss scenario. Assuming a conservative 2-hour lifetime and 80% injection efficiency, 18 nC of charge will be injected into the storage ring every minute to replenish the 14 nC of stored beam lost the previous minute (assuming 2 hours lifetime). Of the 18 nC injected, 4 nC (~20%) is lost during injection. We assume that 50% of the particles lost during injection (2 nC/min), will be lost at the injection septum and the remaining 50% will be intercepted at two horizontal injection scrapers (1 nC/min each) in the storage ring.

The 14 nC of stored beam will eventually be lost in the next minute. It is further assumed that out of ~14 nC/min lost from the stored beam:

- 30% is lost at the two horizontal scrapers (2.1 nC/min each)
- 15% is lost at the septum (2.8 nC/min)
- The remaining 55% is lost at vertical apertures, assumed to be at the two vertical scrapers and arbitrarily at five other limiting apertures (1.1 nC/min each)

Taking into account all the loss assumptions, in the present calculations, a 13 nC/min loss is assumed at any point in the injection region of the booster to storage ring injection (combined loss at the septum and the scrapers) and 1.1 nC/min loss is assumed at any given location in the non-injection region of the storage ring.

2.3.2.1 Bulk Shielding for the Storage Ring Enclosure

With two hours of beam lifetime in the storage ring, ~50% of the 1.3 μC of the stored beam loss occurs in one hour. 1.1 nC/min of this beam loss is assumed to occur at any one location of the storage ring. The shielding requirements for the storage ring at regions other than the injection/extraction region are calculated based on this beam loss scenario: The lateral wall of the storage ring on the experimental floor side is assumed to be 1 meter from the storage ring vacuum chamber center line. The roof and the inboard walls are assumed to be 2 meters from the vacuum chamber. The ratchet wall in the forward direction is assumed to be at 20 meters from the middle of the insertion device straight section. The ratchet wall shielding thickness is calculated using the forward-peaking component of the Dose Equivalent Factors available in the literature [2.8]. The occupied regions on the experimental floor side of the storage ring are shielded for a dose limit of <0.5 mrem/h for 2,000 hours of occupancy per year. The roof and inboard wall are also considered as fully occupied regions, in the current calculations.

The bulk shielding estimates in terms of concrete thickness for the storage ring are given in Table 2.3.1. Shielding wall thickness in standard concrete equivalent is given for the lateral wall and roof. The ratchet wall shielding thicknesses at the FOE side of the beamlines are also given in that table. These walls are assumed to be 20 meters from the center of the straight section of the insertion devices.

Table 2.3.1 Bulk Shielding Estimates for the Storage Ring.

Component	Expt. Floor Wall Concrete Equivalent Thickness [cm]	Roof Concrete Equivalent Thickness [cm]	Inboard Wall Concrete Equivalent Thickness [cm]
Storage ring non-injection region	101	81.5	81.5
Booster to storage ring injection region	141	116	116
Storage ring ratchet wall (forward direction)	137	---	---

2.3.3 Bulk Shielding: Booster-to-Storage Ring Injection/Extraction Region

Injection from the booster synchrotron to the storage ring takes place approximately every 1 minute. Taking into account the storage ring lifetime as 2 hours, 0.83% of the beam is lost in 1 minute. In 1 hour, 49.77% of the beam is lost and an equivalent amount is injected into the storage ring to keep the ring current at 500 mA. During injection, 20% injection efficiency is assumed. Also, beam loss takes place on the scrapers. The shielding requirements at the injection/extraction region are calculated taking into account this beam loss scenario. There may be a higher rate of injection during other modes of operation, such as accelerator performance evaluation or during injection to fill the storage ring from zero current. Assuming that top-off is the prevailing mode of operation in the long run, shielding calculations are performed for an average injection frequency of once every minute.

The bulk shielding estimates in terms of concrete thickness for the storage ring enclosure at the booster-to-storage-ring injection region are given in Table 2.3.1. 141 cm-thick standard concrete with a density of

2.35 g/cm^3 will limit the dose rate to <0.5 mrem/h at the exterior of the lateral wall of the storage ring. 116 cm of concrete on the roof will limit the dose rate to the same level at the exterior on contact. It may be possible to replace the additional concrete shielding by lead supplementary shielding at the roof and inboard wall side of the storage ring. Additional supplementary shielding is also required for possible higher point beam losses and higher rates of injection (greater than 1 injection per minute).

2.4 SHIELDING ESTIMATES FOR BEAMLINES AND FRONT ENDS

2.4.1 Sources of Radiation Hazard in the Beamlines

The radiation present on the experimental floor can be separated into sources that come through the ratchet wall penetration and those that come through the ratchet wall itself.

2.4.1.1 Radiation through the Ratchet Wall

In the process of operating the storage ring, as well as producing the desired synchrotron radiation [2.11], there is considerable generation of other radiation behind the storage ring wall. The shielding for this parasitic radiation is achieved by the concrete shield wall and the local shielding at various locations inside the storage ring. During the commissioning of the storage ring, surveys will be made to determine if any "hot spots" exist and, if so, additional local shielding will be employed to reduce the dose rates on the experimental floor to acceptable levels.

2.4.1.2 Radiation through the Ratchet Wall Penetration

The radiation through the ratchet wall penetration falls into the following categories:

- radiation from electron beam hitting storage ring components
- gas bremsstrahlung created from electron interaction with the residual gas molecules in the vacuum chamber straight section
- synchrotron radiation created by the bending magnets and the insertion devices [2.11]

To estimate the shielding and other requirements for NSLS-II beamlines, these sources of radiation have been considered across a range of possible conditions. The neutron dose estimates done by the PICA neutron shield program [2.12] and confirmed by measurements in other synchrotron radiation facilities [2.13] determined that neutron dose hazard on the experiment floor is insignificant for all credible scenarios. Therefore, neutron shielding on the experiment floor for the beamlines has not been recommended other than for specific instances.

2.4.1.3 Interaction of Stored Beam with Storage Ring Components

If the stored electron beam collides with any storage ring component, a bremsstrahlung shower will be produced. Only a small portion of this radiation makes it through the synchrotron radiation apertures. In addition, bremsstrahlung collimators in the front end will severely limit the line of sight through the ratchet wall penetration. These collimators allow only radiation scattered in small angles to the beam path to exit onto the experimental floor. The beamline shielding present to account for other radiation sources will be more than sufficient to stop the radiation from beam losses inside the storage ring components.

Initial operations at NSLS-II will require that the beamline safety shutters (located inside the ratchet wall) be closed during injection. The closed shutters will keep any radiation that might come through the ratchet wall penetration. When NSLS-II begins operating in the top-off mode, in which the safety shutters are left

open, the additional radiation due to this mode of operation needs to be addressed. Preliminary analysis and experience at other facilities indicates that it is not expected to be a problem [2.14].

2.4.2 Shielding Design Simulations

Bremsstrahlung dose scattering calculations for NSLS-II ID, BM, and 3PW beamlines were carried out using the EGS4 electron-gamma shower simulation program [2.15]. This implementation is part of the CALOR program package distributed by the Radiation Shielding Information Center (RSIC) of Oak Ridge National Laboratory. EGS4 simulates the coupled interactions of photons and electrons with materials over an energy range from a few keV to several TeV. It also includes a standalone program, PEGS4, which creates parameterized cross sections to be used by EGS4. Physical processes simulated by this program include bremsstrahlung production, positron annihilation at rest and in flight, Moliere multiple scattering, Moller and Bhabha scattering, Compton scattering, pair production, photoelectric effect, and continuous energy loss by Bethe-Bloch formalism. The photoneutron production and transport are not simulated by EGS4, but measurements at other third-generation light source facilities have confirmed that photoneutrons are not a radiation hazard at the synchrotron radiation beamlines.

The synchrotron radiation scattering calculations for NSLS-II beamlines have been performed using the STAC8 program [2.16]. STAC8 was developed at the SPring8 facility and has been used extensively at other third-generation synchrotron radiation facilities during design and operation. STAC8 generates insertion device radiation spectra and monochromatic beams with a fixed band width. The program simulates photon transport by Compton scattering (with anisotropy), Rayleigh scattering, and photo-absorption. It calculates scattered photon flux as a function of energy and angle, and converts photon flux to dose rates. Build-up factors in the shielding materials are taken into account, but the effect of polarization has not been considered.

2.4.3 Bremsstrahlung Source Estimates in the Beamlines

Gas bremsstrahlung is produced by interaction of the storage ring electron beam with residual gas molecules in the ring vacuum chamber. Such interactions are sources of stored beam loss, which results in beam decay and occurs continuously during storage ring operation. Gas bremsstrahlung interactions take place all around the storage ring, but are a particular concern in the straight sections for the insertion devices. Gas bremsstrahlung is produced in a very narrow beam in the straight path and sums up for the entire straight path in the line of sight of the beamlines. The NSLS-II straight beam paths in the line of sight of the beamlines are 12.5 m for the insertion device straight sections and 6.6 meters for the BM/3PW beamlines.

The total beam integrated bremsstrahlung dose rate D (rem/h) from the straight particle trajectory in the vacuum chamber of the storage ring at a distance L from the straight path is usually approximated by semi-empirical equations. The semi-empirical equation proposed by Frank [2.17] had been successfully utilized at the Advanced Photon Source and other similar facilities. Using the equation developed by Frank, the dose rate due to primary bremsstrahlung is described at a distance L from the end of the straight path as

$$\text{dose rate (rem/h)} = \frac{3.0\times10^{-4}}{\pi\times X_0}\ \frac{E^2}{0.511^2}\ \frac{l\times I}{L(L+l)}\ , \qquad (5\text{-}2)$$

where X_0 = radiation length of air at 10^{-9} Torr = 2.34×10^{16} cm, l = effective length of the straight path (15.5/6.6 meters), I = beam current in e/s (3.1×10^{18} electrons/s for 500 mA), and E = electron beam energy in MeV. L is nominally taken as 20 meters. This equation yields a primary bremsstrahlung dose rate of 240 rem/hour for the insertion device beamlines and 100 rem/h for the BM/3PW beamlines.

2.4.4 Design of Bremsstrahlung Shutters/Stops

2.4.4.1 Geometry Used for the Calculations

The primary bremsstrahlung dose rates at the insertion device beamlines determine the thickness of bremsstrahlung shutters, stops, and collimators in the beamlines and front ends. Figure 2.4.1 shows the geometry used in the EGS4 simulations to calculate the thickness of lead and tungsten required to attenuate the dose rate <0.5 mrem/h at the downstream side of the stop/shutter on contact. These shutters will be located inside the shielded enclosures. The primary bremsstrahlung source term was estimated using the empirical formulae from Table 2.4.1 to scale the dose rate results. The bremsstrahlung beam from the NSLS-II straight section is incident on a lead or tungsten block with transverse dimensions of 20 x 20 cm^2. The heavy metal is followed by the ICRU tissue [2.20] of 30 cm-thick to score the dose at the downstream side of the shutter/stop. The ICRU tissue is binned into 1 cm^3 bins for scoring the dose, and the maximum dose is taken as the dose index.

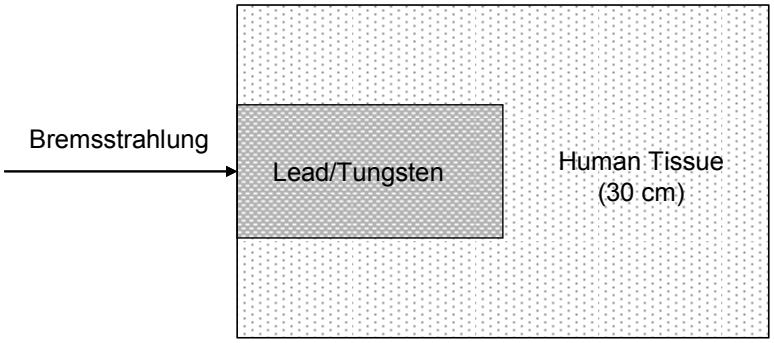

Figure 2.4.1 Simulated EGS4 geometry of the NSLS-II safety shutters.

2.4.4.2 Thickness of Shutters/Stops

Table 2.4.1 shows the primary bremsstrahlung dose rates predicted and the thickness of lead or tungsten required to reduce the radiation dose rate at the back of the shutter/collimator to less than 0.5 mrem/h (<5.0 μSv/h). The dose rates at the downstream surface in the ICRU tissue were calculated as a function of lead or tungsten thickness and fitted using an effective exponential attenuation factor. The results are also plotted in Figure 2.4.2. Note that a lead thickness of >30 cm or a tungsten thickness of >20 cm are required as stops/shutters at NSLS-II beamlines to reduce the dose rate to less than 0.5 mrem/h (<5.0 μSv/h). Therefore a uniform lead thickness of 30 cm and a tungsten thickness of 20 cm are recommended for bremsstrahlung shutters or stops for insertion device and bending magnet beamlines.

Table 2.4.1 Calculated Thickness of Bremsstrahlung Shutters and Stops.

	Insertion Device Beamlines	3PW and BM Beamlines
Bremsstrahlung dose rate at 1 nT (rem/h)	240 rem/h	100 rem/h
Lead thickness required (cm)	28.9 cm	26.4
Tungsten thickness required (cm)	19.6 cm	17.8
Dose rate behind the stop/shutter (mrem/h)	0.5 mrem/h	0.5 mrem/h

For all beamlines, a lead thickness of 30 cm and tungsten thickness of 20 cm are recommended for the bremsstrahlung stops/shutters.

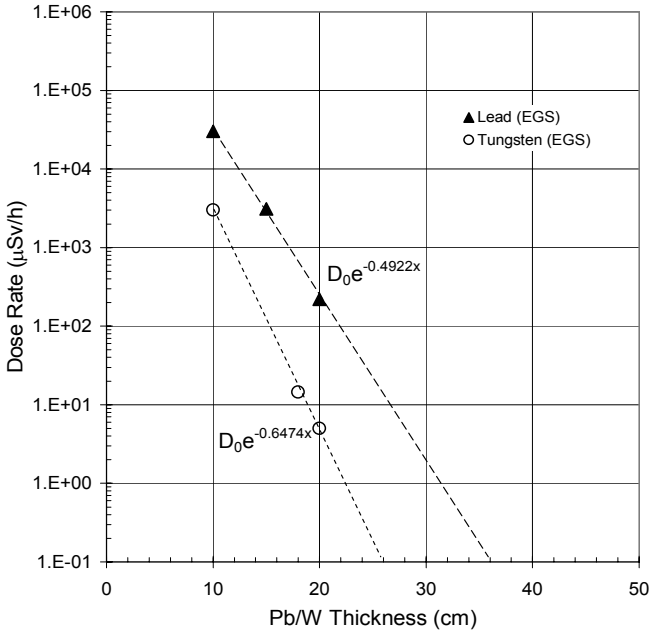

Figure 2.4.2
Contact dose rates at the downstream surface of the shutters/stops. Bremsstrahlung source was calculated by method 1.

2.4.5 Shielding Estimates for Experimental Stations

2.4.5.1 Computation for Bremsstrahlung and Synchrotron Radiation Scattering

The synchrotron radiation and bremsstrahlung can be scattered from any potential component in the beamlines and front ends. Such components include windows, slits, monochromators, mirrors, and so forth, and vary from beamline to beamline. Therefore, calculations were performed with a worst-case potential scatterer upstream of the FOE (Figure 2.4.3), of typical dimensions (2.0 m wide, 3 m high, and 10 m long). Figure 2.4.4 shows the results of the calculations. Typically, the worst-case potential scatterer for bremsstrahlung is 3 cm-thick copper, and for synchrotron radiation is 1 cm-thick aluminum with small transverse dimensions. The EGS4 calculations were performed for bremsstrahlung, and STAC8 calculations were performed for synchrotron radiation.

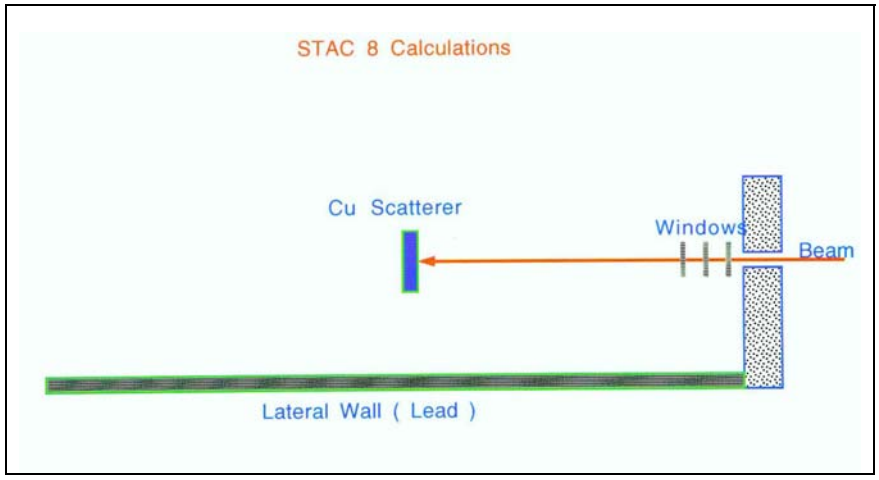

Figure 2.4.3 EGS4 and STAC8 geometry for bremsstrahlung and synchrotron radiation scattering calculations.

2.4.5.2 Shielding Estimates for the First Optics Enclosures

Preliminary shielding estimates for the NSLS-II First Optics Enclosures (FOEs) are calculated using the available beamline and insertion device parameters. For each shielding situation, the synchrotron and bremsstrahlung shielding have been calculated for the representative station geometry. The shielding simulations for bremsstrahlung were done using the EGS4 program and for synchrotron radiation using the STAC8 program. In most cases, one of the sources (bremsstrahlung or synchrotron radiation) dominates for the shielding requirement and the contribution of the other becomes negligible; thus, the calculated shielding for the dominant source can be implemented. All bremsstrahlung and synchrotron radiation calculations for the beamlines were done at 500 mA of beam current, at 3.6 GeV electron beam energy. Also, all the doses are scored in the ICRU tissue on contact. Shielding of these areas is designed to maintain individual exposures when in contact with the hutch wall as <0.25 mrem/h for 2,000 hours of exposure per year. Station shielding is designed to meet this criterion to ensure that occupational radiation doses are ALARA.

2.4.5.3 Shielding Estimates for Secondary Bremsstrahlung

Bremsstrahlung scattering calculations for the representative geometry of the NSLS-II FOE were performed using EGS4. The computational geometry given in Figure 2.4.1 was used. The EGS4 program calculates integral energy deposition per particle at various regions of the geometry. The radiation dose (energy deposited per unit mass) at any given location per particle was calculated from the 3D energy deposition profile in the standard ICRU tissue placed at the location, taking the maximum energy deposition per unit mass**.** Once energy deposition per particle at each region is available, the absolute dose rate at any region can be scaled, using the primary bremsstrahlung dose rate provided by the empirical formulae.

Figure 2.4.4 gives the scattered bremsstrahlung dose rates 1 meter away from a 3 cm-thick copper scatterer in terms of μSv/h (× 0.1 mrem/h) for the NSLS-II insertion device beamlines. The bremsstrahlung forward-beam direction in this figure is 90 degrees. The transverse directions are 0 degrees and 180 degrees. Calculations are for a 240 rem/h (2.4 Sv/h) primary bremsstrahlung dose rate. Note that the scattered bremsstrahlung beam is highly forward peaked.

To calculate the shielding requirements for the downstream wall of the insertion device FOE, the calculated dose rates (DR) from Figure 2.4.4 were used. The minimum distance from the copper scattering target to the downstream wall is taken as 10 meters. For small angles, a constant distance of 10 m to the wall is assumed, and the distance-adjusted dose factor is taken as 10^2. The required lead thickness for the downstream wall of the FOE, as a function of the scattering angle to achieve the design dose limit of <0.25 mrem/h, is calculated using the expression

$$\text{lead thickness (cm)} = [\ln (0.01 \times DR) - \ln 0.25\ ] / 0.473. \quad (5\text{-}3)$$

The minimum attenuation coefficient of 0.473 cm^{-1} for lead, calculated by EGS4, has been used in these calculations for bremsstrahlung attenuation. The same methodology is also used for the Bending Magnet (BM) and 3-Pole Wiggler (3PW) beamlines.

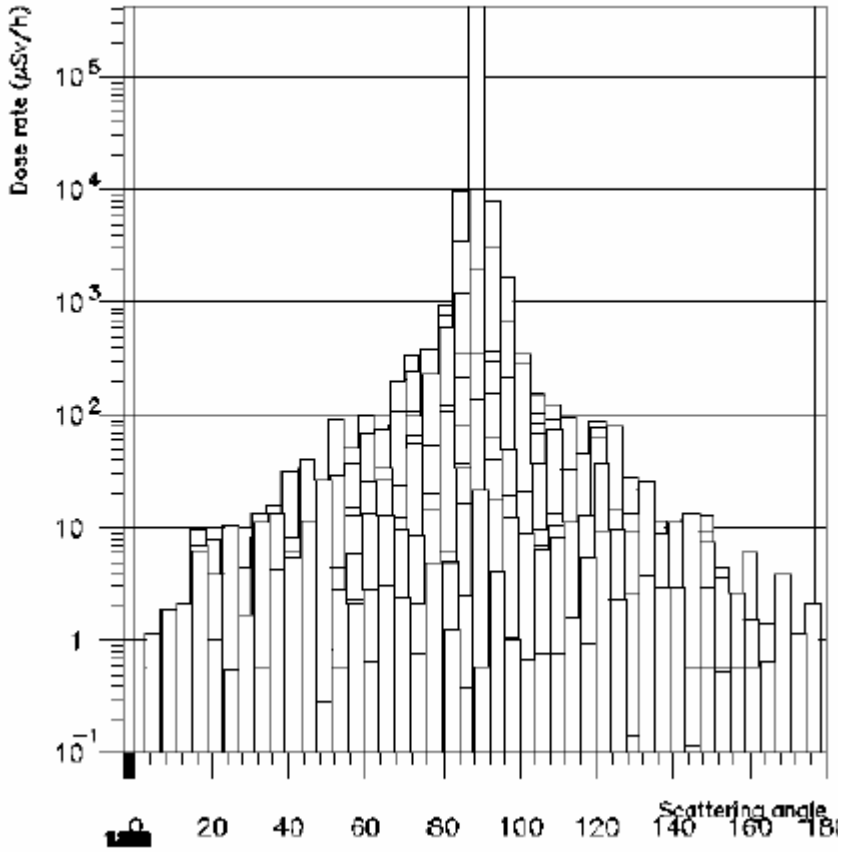

Figure 2.4.4
Scattered bremsstrahlung dose rates for the NSLS-II ID beamlines. (Primary bremsstrahlung scattered from a Cu target of 3 cm thickness with small transverse dimensions.)

Tables 2.4.2 and 2.4.3 provide the calculated lead thickness for the downstream panels of the FOE for ID and BM/3PW beamlines as a function of the scattering angle to achieve the design dose limit of <0.25 mrem/h. Because of the forward-peaking nature of the high-energy bremsstrahlung scattering, the lead shielding thickness required at small angles along the beam direction is large. In practice, this will be satisfied by the presence of collimators or bremsstrahlung stops approximately from 0 to 2 degrees. Considering a uniform downstream wall thickness of 5 cm, additional shielding will be required for scattering angles <4 degrees. This can be satisfied by placing the appropriate lead local shielding around the beam transport pipe penetrations. The exact transverse dimensions of these local shields can be calculated once the station dimensions are available. Currently, a uniform downstream wall thickness of 50 mm of lead is recommended for the insertion device beamlines and 35 mm of lead is recommended for the BM/3PW beamlines.

Table 2.4.2 Bremsstrahlung Shielding for the Downstream Panel of the First Optics Enclosures of the Insertion Device Beamlines.

Angle [deg.]	Dose Rate [mrem/m^2·h]	Pb to shield < 0.25 mrem/h [mm]
1	5.0 x 10^3	108
2	1.5 x 10^3	84
3	7.0 x 10^2	68
4	4.0 x 10^2	56
5	2.2 x 10^2	44
6	1.5 x 10^2	37
8	1.0 x 10^2	28
10	7.0 x 10^1	21

Table 2.4.3 Bremsstrahlung Shielding for the Downstream Panel of the First Optics Enclosures of the BM and 3PW Beamlines.

Angle [deg.]	Dose Rate [mrem/m^2·h]	Pb to shield < 0.25 mrem/h [mm]
1	2.1 x 10^3	90
2	6.2 x 10^2	66
3	2.9 x 10^2	50
4	1.6 x 10^2	38
5	9.1 x 10^1	26
6	6.2 x 10^1	19
8	4.1 x 10^1	10
10	2.8 x 10^1	6

The lateral wall (side wall) and roof shielding for the FOE can also be calculated using the same equation. DR is designated as the scattered secondary bremsstrahlung dose rate in the transverse direction:

$$\text{lead thickness (cm)} = [\ln DR - \ln 0.25] / 0.473. \quad (5\text{-}4)$$

Tables 2.4.4 and 2.4.5 show the calculated lead thickness for the lateral panels of the FOE for ID and BM/3PW beamlines. For comparison, it also shows the thickness of Pb for lateral panels required to shield for the dose rates <0.05 mrem/h.

It must also be emphasized that the bremsstrahlung production is linear with respect to the pressure in the vacuum chamber. In the current calculations for primary bremsstrahlung source term, a vacuum chamber pressure of 1 nTorr is assumed. A higher vacuum chamber pressure might result in requirements for safety shutters to be closed until vacuum is restored.

Table 2.4.4 Bremsstrahlung Shielding for the Lateral Panel of the First Optics Enclosures of the Insertion Device Beamlines.

Angle [deg.]	Dose Rate [mrem/m^2·h]	Pb to shield [<0.25 mrem/h]	Pb to shield [<0.05 mrem/h]
90	0.15	None	23

Table 2.4.5 Bremsstrahlung Shielding for the Lateral Panel of the First Optics Enclosures of the BM and 3PW Beamlines.

Angle [deg.]	Dose Rate [mrem/m^2·h]	Pb to shield [<0.25 mrem/h]	Pb to shield [<0.05 mrem/h]
90	0.062	None	5

2.5 SYNCHROTRON RADIATION SCATTERING CALCULATIONS WITH STAC8

Synchrotron radiation scattering calculations to estimate the shielding requirements for the NSLS-II FOE were performed using the STAC8 shield program. The worst-case scatterer, typically 10 mm aluminum, is used as the potential scatterer upstream of the station. The source spectrum for the NSLS-II insertion devices and BM for this calculation was generated by the STAC8 program. Five sources are considered for the NSLS-II beamline station shielding design. The salient features of these sources, calculated by the STAC8 program, are given in Table 2.5.1. The source parameters in this section are calculated for the beamlines at a beam energy of 3.6 GeV and a beam current of 500 mA.

The lateral walls of the experimental stations are assumed to be at a distance of 1 meter and the roof at 1.5 meter from the beam center line. Shielding for these areas was calculated to maintain individual exposures, when in contact with the experimental station wall, at less than 0.25 mrem/h at the occupiable areas.

Table 2.5.1 Source Parameters for the NSLS-II Beamlines.

Source	Source opening angle (mrad-Hori.) FOE Aperture	No. of Periods	B_{eff} [T]	Period [mm]	Length [m]	E_c [KeV]	Total Power [KW]
DW	3.0 mrad-H (60 x 5 mm^2)	70	1.8	100	7 m	15.5	58.75
EPU45 L.Mode	1.0 mrad-H (14 x 4 mm^2)	89	1.03	45	4 m	8.87	19.89
U19	1.0 mrad-H (4 x 4 mm^2)	158	1.14	19	3 m	9.05	16.54
BM	10.0 mrad-H (200 x 5mm^2)	1	0.4		2.6 m	3.44	0.321
3PW	4.0 mrad-H (80 x 5 mm^2)	1	1.1		0.15 m	9.24	0.671

2.5.1 Shielding Recommendations for the First Optics Enclosures

Table 2.5.2 gives the combined results of the STAC8 and EGS4 calculations for the shielding requirements of the lateral panel and the roof for the five sources. The shielding requirements for the downstream panels of the FOEs are dominated by bremsstrahlung and therefore the recommendation in Section 2.4.5.3 applies. For comparison, shielding requirements for the annual dose rate of 0.05 mrem/h mrem are also given.

The station dimensions are taken as 2 m wide, 3 m high and 10 m long. The lateral panel is at a distance of 1 m and the roof is at a distance of 1.5 m from the beamline. If the stations are narrower, the shielding estimates need to be re-evaluated.

Table 2.5.2 Shielding Thickness in Pb for NSLS-II First Optics Enclosures.

Beamline Source	Lateral Panel Pb to shield <0.25 mrem/h [mm]	Lateral Panel Pb to shield <0.05 mrem/h [mm]	Roof Pb to shield <0.25 mrem/h [mm]	Roof Pb to shield <0.05 mrem/h [mm]
DW	12	23	11	11
EPU45	8	23	7	7
U19	9	23	8	8
BM	6 (Fe)	5	4(Fe)	4 (Fe)
3PW	5	5	5	5

2.5.2 Shielding Calculations for Monochromatic Experimental Enclosures

The shielding calculations for the monochromatic experimental stations are carried out by the STAC8 program. Since bremsstrahlung is stopped in the FOEs, no EGS4 simulations are necessary to estimate the shielding thickness of the side, roof and downstream panels. Five reflections (111, 333, 444, 555, and 777) with corresponding bandwidths are considered for these calculations. One of the energies (88 KeV) corresponds to the K-edge energy of lead. The five energies and their corresponding bandwidths used for the monochromatic experimental station shielding calculations are given in Table 2.5.3.

Table 2.5.3 Monochromatic Beam Energies and Bandwidths used for STAC8 Calculations.

Energy (KeV)	Band Width (%)
22	5×10^{-4}
66	4×10^{-5}
88	3×10^{-5}
110	6×10^{-6}
154	1.5×10^{-6}

All calculations are done for the beam energy of 3.6 GeV at 500 mA. The dimensions of monochromatic experimental station are assumed to be 2 m (W) x 3 m (H). Side panels are at a distance of 1.0 m from the roof and 1.5 m away from the beamline. Buildup factors for lead and iron are taken into account.

2.5.3 Shielding Thickness for the Monochromatic Experimental Enclosures

The results of these calculations are provided in Table 2.5.4. The recommended shielding thickness for the side panels, roof and upstream/downstream panels are given. In most cases thickness in Pb is given and in some cases the lead panels can be replaced by steel (Fe). An appropriate monochromatic stop can be provided in the line of sight of the beam in the monochromatic experimental station. The monochromatic experimental stations with a vicinity of higher occupancy by non-radiation workers is shielded for an annual dose rate of 100 mrem per year.

Table 2.5.4 Shielding Thickness for NSLS-II Monochromatic Experimental Stations.

Beamline Source	Lateral Panels Pb to shield <0.05 mrem/h [mm]	Roof Pb to shield <0.05 mrem/h [mm]	US & DS Panels Pb to shield <0.05 mrem/h [mm]
DW	6	5	6
EPU45	3 16 (Fe)	3 14 (Fe)	3 16 (Fe)
U19	4	3	4
BM	2 (Fe)	2 (Fe)	2 (Fe)
3PW	1.5 8 (Fe)	1.5 6 (Fe)	1.5 8 (Fe)

a. All calculations are done for beam energy of 3.6 GeV at 500 mA
b. Station dimensions are assumed to be 2 m (W) x 3 m (H)
c. Side panels are at a distance of 1.0 m and roof at 1.5 m away from the beamline

2.6 SHIELDING FOR THE PINK BEAM EXPERIMENTAL ENCLOSURES

In most cases, the pink beam experimental stations (assuming 30 to 50 KeV cut-off) have the same shielding requirements as the monochromatic experimental stations because of the absence of higher energy synchrotron radiation component in the pink beam. However, bremsstrahlung needs to be completely stopped in the upstream station.

2.7 RADIOLOGICAL CONSEQUENCES OF ACCIDENTAL BEAM LOSS

2.7.1 Consequences of Accidental Linac Beam Losses

Shielding calculations for the linac enclosure have been carried out assuming a 10% distributed beam loss during beam acceleration (6.6% at any given point). Shielding thickness has been calculated for a dose rate of <0.5 mrem/h, at the exterior of the concrete bulk shielding. In the unlikely event of 100% linac beam loss during beam acceleration at any given point of the accelerator system, the dose rate on contact at the exterior shielding wall will be ~15 times more than the limiting value. The dose rate will be <7.5 mrem/h at the exterior of the concrete bulk shielding of the enclosure due to this beam loss event.

2.7.2 Consequences of Booster-to-Storage Ring Injection Losses

The shielding calculations for the booster to storage ring injection assume an average injection frequency of once per minute. A scenario was developed where 15 nC/s, the capacity of the linac, was injected continuously into the booster and the storage ring, and all of it was lost at the injection septum. The total charge lost in this case in an hour would be 5.4×10^4 nC/h. Assuming 13 nC/min loss of injected beam at the injection/extraction region, 780 nC/h would be lost at the region for which the shielding design calculations were carried out. The shielding for the accelerators is designed for a dose rate of <0.5 mrem/h at the occupiable regions, on the exterior of the bulk shielding. Therefore, the dose rate at the occupiable regions during this accident scenario would be 35 mrem/h at the exterior of the shield wall on contact.

2.7.3 Consequences of Loss of Vacuum in the Straight Section

Loss of vacuum in the insertion device straight path is another credible incident that can cause higher dose rates around the beamline FOEs. In the bremsstrahlung source calculations in Section 2.4.3, a straight section pressure of 10 to 9 Torr is assumed. A sudden loss of vacuum to 1 Torr in the straight section would increase bremsstrahlung production by a factor of 109. We further assumed that this scenario would last for <1 millisecond (approximately 1,000 revolutions of the beam) before the beam would be completely absorbed. No credit was given to the engineering controls that trip the beam at vacuum loss. The FOEs are designed for a dose rate of <0.25 mrem/h on contact at the exterior of the shield panels. The dose rate during this accident scenario would be higher by a factor of 109, but would last for only a millisecond. The total dose commitment to an individual beamline scientist due to one such incident can be estimated as $<(0.25 \times 10^9) / (3.6 \times 10^6) = 70$ mrem.

2.7.4 Consequences of Linac-to-Booster Injection Losses

The shielding calculations for the booster enclosure assume an average charge of 15 nC/min injected to the booster system with a frequency of once per minute. A scenario is developed where 15 nC/s, the maximum capacity of the linac, is injected continuously into the booster, and all of it is lost at some location in the booster structure. The total charge lost in this case in an hour would be 5.4×10^4 nC/h. Assuming 2% (0.3 nC/min) loss of injected beam at any location in the booster system, 18 nC/h would be lost at the location for which the shielding design calculations are carried out. The shielding for the accelerators is designed for a dose rate of <0.5 mrem/h at the occupiable regions, on the exterior of the bulk shielding. Therefore, the dose rate at the occupiable regions during this accident scenario would be <1,500 mrem/h at the exterior of the shield wall on contact.

2.8 ACTIVATION ANALYSIS OF ACCELERATOR COMPONENTS

Bremsstrahlung is generated in accelerator systems of synchrotron radiation facilities by the radiative interaction of the circulating electron beam with accelerator components and with residual gas molecules in the vacuum chamber. The photoneutron interaction of bremsstrahlung with materials leads to the radioactivation of accelerator components through neutron emission and the production of radioisotopes. However, this activation interaction is a second-order effect, because it involves the intermediate process of bremsstrahlung production. Photoneutron interaction takes place above the threshold bremsstrahlung energy of 7–20 MeV; the cross section for photoneutron interactions is in millibarns. Therefore the electron beam activation of materials is not as abundant as the proton beam activation, because electrons do not cause direct spallation interaction with the nuclei.

Photospallation is another process (with comparable cross sections) by which radioisotopes are produced. The particular radionuclides produced in a material will depend on (γ, n), (γ, 2n), and photospallation cross sections of the material. These interactions can potentially activate various accelerator components. Isotopes and their saturation activities are listed in IAEA 188 [2.21]. The materials of interest for NSLS-II operations are aluminum, iron (in steel), copper, tungsten, and lead.

Radioactivity builds up during the operation of accelerator systems. When operations cease, there is an initial rapid decay of shorter-lived isotopes; after a waiting period, only the longer-lived isotopes remain. For routine operations of NSLS-II, short-lived isotopes will be of interest, because residual activity in the accelerator components and beam stops may be high enough to limit access time to the area.

2.8.1 Residual Activity Estimates of Accelerator Components

2.8.1.1 Methodology for Estimating Activation in Materials

The methodology of estimating activity of a radionuclide formed by (γ,n) reaction is to assume that the yield of neutrons is also the yield of radionuclide atoms [5.9]. The neutron yield in the accelerator components and in the beam stops is based on the equation from Swanson:

$$Y^1 = 1.21 \times 10^8 \, Z_1^{0.66} \text{ neutrons/joule,} \tag{5-5}$$

where Z1 = atomic number of the element. The equation can be modified for a given isotope as

$$Y = F(1.21 \times 10^8 \, Z^{0.66}) \text{ n/J,} \tag{5-6}$$

where F is the fractional abundance of a given isotope with atomic number Z. Therefore, the change in the number of radioactive nuclides (N) due to (γ,n) interactions per unit time is given by

$$dN/dt = WYf - \lambda_R N \text{ atoms/sec,} \tag{5-7}$$

where W = dissipated electron beam power in watts, f = fraction of electron beam power which converts to bremsstrahlung, and λR = radioactive decay constant of the radionuclide in s-1. By solving the equation and applying the initial boundary condition N = 0 for t = 0,

$$N = \frac{WYf}{\lambda_R} (1 - e^{-\lambda R t}) \text{ atoms.} \tag{5-8}$$

Since the activity is λRN

$$\text{Activity} = WYf (1 - e^{-\lambda R t}) \text{ disintegrations/sec,} \tag{5-9}$$

the saturation activity of the radionuclide, as t tends to be large, is

$$A = WYf \text{ disintegrations/sec} \tag{5-10}$$

This is the saturation activity of a radionuclide with a given half life if the continuous operation time of the accelerator system is about three times the half life of the radionuclide formed. For each of the potential activated materials, Swanson (IAEA 188) has prepared tables listing the saturation activities of the (γ,n), (γ,2n) and photospallation products in (Ci/kW), and the exposure rate in (R/h) at 1 meter from the saturation activity.

The data in these tables have been used to estimate the saturation activity and the radiation fields following certain operation periods and the residual radiation field after shutdown.

2.8.1.2 Radioactivation of the Linac Iron Beam Stop

Approximately 3 watts of electron beam power at 200 MeV are dissipated in the linac beam stop during the continuous beam dump on the stop. The radioactive materials formed in the iron beam stop have a range of half lives from a few seconds to a few years. Continuous operation for 1 hour of the iron beam stop results in about 90% of the saturation exposure rate. The main activities are due to 52Mn(m), 56Mn, 54Mn, 52Fe, and 53Fe. The estimated combined exposure rate at 1 meter from the beam stop for a power dissipation of 4 watts is about 2.21 mR/h, contributed mainly by 52Mn (m) (half life 21.1 min) and 53Fe (half life 8.51 min). After about an hour of shutdown, the exposure rate would be ~0.046 mR/h at 1 meter. 54Mn, the long-living isotope formed in the iron beam stop with a half life of 303 days, will not attain saturation activity until about three years of continuous operation. After 200 hours of continuous operation of the beam stop, the activity due to 54Mn in iron would be 0.05 mR/h. 55Fe, produced from 54Fe, will not pose any substantial exposure hazard, due to the low-energy x-ray emission of 5.95 keV. Activation of the linac beam stop during NSLS-II operations is not a serious radiological hazard.

2.8.1.3 Radioactivation of the Booster Iron Beam Stop

Approximately 0.73 watts of electron beam power at 3.0 GeV is dissipated in the booster beam stop during a continuous beam dump on the stop. Continuous operation of 1 hour of the iron beam stop results in about 90% of the saturation exposure rate. The main activities are due to 52Mn(m), 56Mn, 54Mn, 52Fe, and 53Fe. The estimated combined exposure rate at 1 meter from the beam stop is about 0.48 mR/h, contributed mainly by 52Mn(m) (half life 21.1 min) and 53Fe (half life 8.51 min). After about an hour the exposure rate would be ~0.01 mR/h at 1 meter. 54Mn, the long-living isotope formed in the iron beam stop with a half life of 303 days, will not attain saturation activity until about three years of continuous operation. After 200 hours of continuous operation of the beam stop, the activity due to 54Mn in iron would be 0.01 mR/h. 55Fe, produced from 54Fe, will not pose any substantial exposure hazard, due to the low-energy x-ray emission of 5.95 keV. Activation of the booster beam stop during NSLS-II operations is not a serious radiological hazard.

Saturation activity and the resulting radiation field, due to the activation of iron in the storage ring septum magnet from injection losses, will be comparable to or less than at the booster beam stop.

2.8.1.4 Radioactivation of Copper at the Injection Septum

The injection septum in the storage ring also consists of copper conductor with iron. As the septum is a high beam-loss point, the copper in the injection septum can become activated during continuous operation, as happens during top-off. Most of the isotopes formed during this process are short-lived except 60Co (half life 5.26 years) and 63Ni (half life 93 years). Other short-lived isotopes produced are 58Co (half life 71.3

days), 58Co(m) (half life 9.2 h), 61Cu (half life 3.32 h), 62Cu (half life 9 min), and 64Cu (half life 12.8 h). After 100 hours of continuous operation, these isotopes will attain saturation activity. After shutdown, the initial activity will be mainly due to 62Cu. The initial combined activity after 100 hours of continuous operation is estimated <5.8 mR/h at 1 m from the septum. After 200 hours of operation, 60Co will achieve only 0.3% of the saturation value. The radiation field attributable to this isotope will be negligible. After about an hour of waiting time, the activity from short-lived isotopes will decay, and the corresponding radiation field will be <0.09 mR/h.at 1 meter from the septum.

2.8.1.5 Radioactivation of Lead at the Injection Septum

The injection septum is a high beam-loss point. This region is heavily shielded with lead, which becomes activated and results in the production of 206Tl, 207Tl, 207Tl(m), 202Pb(m), 203Pb(m), and 204Pb(m). Most of these isotopes are relatively short lived and attain saturation activity in a few hours of continuous operation of the septum. After prolonged operation of the septum, the estimated initial radiation field from lead activation at 1 meter from the septum shielding will be 1.6 mR/h. After a few minutes of waiting time, the activity will be 0.36 mR/h, mainly from 204Pb(m), which has a half life of 67 minutes.

Lead is also used as bremsstrahlung beam stops and collimators in the beamlines and front ends. These stops and collimators intercept the bremsstrahlung beam from the straight section coming along the beamlines. The bremsstrahlung power incident on these stops/collimators consists of a few microwatts. This bremsstrahlung energy will not create any detectable activation of the safety stops and collimators in the beamlines and front ends.

2.8.1.6 Radioactivation of the Aluminum Vacuum Chambers

The vacuum chambers of the accelerator system are made of aluminum. Stored beam loss occurs continuously during storage ring operations. For shielding calculations of the storage ring, a stored beam loss of 1.1 nC/min is assumed to take place at any given location of the storage ring. Part of his beam loss energy will dissipate on the aluminum vacuum chamber, possibly activating it. The main activation products are ^{11}C, ^{13}N, ^{15}O, ^{24}Ne, ^{25}Al, and $^{26}Al(m)$. The isotopes will attain saturation activity after a few hours of operation. ^{22}Na, the long-living isotope produced by activation, will not attain saturation activity until about seven years. After a few hours of operation, the combined exposure rate due to saturation activity is estimated as <0.2 mR/h, at 1 meter from the vacuum chamber. The major contribution is from $^{26}Al(m)$ (half life 6.37 s). After a few minutes, the exposure rate will come down to less than 0.02 mR/h at 1 meter from the vacuum chamber. After 200 hours of continuous operation, ^{22}Na will attain only 0.5% of the saturation value and the corresponding radiation field will be <0.1 mR/h at 1 m from the vacuum chamber.

Table 2.8.1 summarizes the results of the activation analysis for various accelerator components that can be potentially activated at NSLS-II. For each component, activity and the resulting exposure rates have been calculated for the assumed beam loss scenario.

Table 2.8.1 Activation Results for Various Accelerator Components at NSLS-II.

Accelerator Components	Activity after 200 hours of operation [mCi]	Immediately after shutdown, exposure rate at 1 m [mR/h]	1 hour after shutdown, exposure rate at 1 m [mR/h]
Linac iron beam stop	3.45	2.21	0.05
Booster iron beam stop	0.75	0.48	0.01
Copper at injection septum	11.0	5.8	0.09
Lead at the septum shielding	4.28	1.6	0.44
Storage ring aluminum vacuum chamber	0.56	0.20	0.05

The foregoing analysis shows that the activation of accelerator and beamline components is not a serious radiation hazard during NSLS-II operations, although it is good practice to conduct a complete radiation survey of each accelerator enclosure prior to permitting access after prolonged operation. Based on this survey, access requirements are to be specified at various locations inside the accelerator enclosures.

2.8.2 Activation of the Soil

The potential for soil activation is limited at the electron accelerators, since the main radiation component, bremsstrahlung, is mainly in the forward direction of the electron beam and gets absorbed by machine components such as magnets, absorbers, and so forth. The soil berms are generally at very large angles (almost at right angles) to the forward direction of the electron beam. However, there exists a potential for the high-energy neutron component to penetrate through the transverse concrete shield and produce radioisotopes in the soil. These isotopes can migrate to the groundwater systems. Therefore, it is desirable to assess this risk in detail at a large installation like NSLS-II to reassure the staff and the public.

The soil activation analysis for the NSLS-II design has been carried out at three distinct locations of the accelerator enclosures where the probability for beam loss is significant. These are at the linac beam stop, booster beam stop, and booster-to-storage-ring injection septum.

2.8.2.1 Results of Soil Activation Calculations for NSLS-II

Table 2.8.2 gives the activity in the soil created by 3H and ^{22}Na at various beam-loss locations, for 5,000 hours of NSLS-II operation. The potential activity created by leachables in the groundwater is also shown. Leachability rates of 100% and 7.5% are assumed for 3H and ^{22}Na, respectively. A water concentration factor of 1.1 is used. Although the average annual local rainfall is 55 cm, the soil beneath the concrete floor is not exposed to rainfall and the potential leachability of radioactive isotopes from the soil to the water table at these locations is minimal.

Table 2.8.2 Activity in the Berm Created by ^{3}H and ^{22}Na at Various Beam Loss Locations.

Beam Loss Location	Average HEN Flux in soil [Φ_{av}]	^{3}H Soil Activity [Ci/cm^3]	^{3}H Leachable to water [pCi/liter]	^{22}Na Soil Activity [Ci/cm^3]	^{22}Na Leachable to water [pCi/liter]
Linac beam stop (floor berm)	0.22×10^{2}	2.77×10^{-15}	2.97	2.47×10^{-14}	2.04
Linac beam stop (inboard berm)	0.39×10^{2}	4.91×10^{-15}	5.40	4.38×10^{-14}	3.61
Booster beam stop (floor berm)	0.05×10^{2}	0.62×10^{-15}	0.68	0.56×10^{-14}	0.46
Booster beam stop (inboard berm)	0.08×10^{2}	1.00×10^{-15}	1.10	0.90×10^{-14}	0.74
Storage ring septum (floor berm)	0.04×10^{2}	0.50×10^{-15}	0.55	0.45×10^{-14}	0.37
Storage ring septum (inboard berm)	0.06×10^{2}	0.76×10^{-15}	0.84	0.67×10^{-14}	0.55

2.8.3 Activation of Air in the Accelerator Enclosures

Routine accelerator operations at NSLS-II would generate small amounts of air activation at high beam-loss locations, due to photospallation reactions of bremsstrahlung in air. The isotopes produced by air activation are ^{13}N (half life 10 min), ^{11}C (half life 20 min), and ^{15}O (half life 2.1 min). These isotopes would be produced within the accelerator enclosure and would attain saturation activity within hours of operation, but would decay quickly because of their short half lives and would remain primarily within the confines of the enclosure.

The air activation analysis for NSLS-II has been carried out at three distinct locations of the accelerator enclosures where the probability for beam loss is significant. These are at the linac beam stop, booster beam stop, and booster-to-storage-ring injection septum.

2.8.3.1 Results of Air Activation Calculations for the Accelerator Enclosures

Table 2.8.3 gives the activity in air at various beam-loss locations inside the accelerator enclosures of NSLS-II. For the linac tunnel, an effective bremsstrahlung straight path of 30 m is assumed. The linac tunnel volume is taken as $3\times3\times60 = 540$ m^3. A half chord length of 23 meters from the source inside the storage ring tunnel is considered as the maximum bremsstrahlung path length inside the tunnel. For the purpose of calculating activity per unit volume, a corresponding volume of air $3\times3\times46$ m^3 = 414 m^3 is assumed inside the storage ring.

Table 2.8.3 Saturation Activity in Air at Various Beam Loss Locations.

Beam Loss Location	Beam Loss [Watts]	Volume of air [m^3]	^{13}N [pCi/cm^3]	^{15}O [pCi/cm^3]	^{11}C [pCi/cm^3]
Linac beam stop	3.0	540	0.083	0.009	0.002
Booster Beam stop	0.73	414	0.019	0.002	0.0004
Storage ring septum	0.63	414	0.484	0.052	0.010

The computed concentration of radionuclides in air at various beam loss locations inside the accelerator enclosures is orders of magnitude smaller than the derived air concentration for environmental exposure in DOE Order 5400.5. Once the operation is shut down, this concentration will rapidly decrease, due to both radioactive decay and air ventilation.

2.8.4 Activation of Cooling Water

Activation of water for cooling the magnets and the other accelerator components may be estimated by the similar method as the estimation of air activation inside the accelerator enclosures. The primary reactions leading to the activation of cooling water are the bremsstrahlung interactions with ^{16}O in water. The most abundant of the radionuclide produced by this process is ^{15}O. Other activation products that are formed include ^{11}C (4.4% of ^{15}O), 3H (at saturation, 2.2% of ^{15}O) and ^{13}N (about 1% of ^{15}O). ^{15}O has a radioactive half life of 2.05 minutes and attains saturation during a short period of operation. 3H will not attain saturation until several decades of accelerator operation.

2.8.4.1 Results of Cooling Water Activation Estimates

Among the accelerator components which require cooling, the storage ring septum is a maximum beam loss location. The saturation activity of radionuclides in the cooling water is estimated at the storage ring septum. A closed-loop inventory of 100,000 gallons (3.785×108 cm^3) of water is assumed in the system. Table 2.8.4 provides the saturation concentrations of the radionuclides in the cooling water of the storage ring septum. As mentioned earlier, 3H will attain saturation only after decades of operation. After 5,000 hours of continuous operation, the concentration of 3H will be only 3% of the saturation value.

Table 2.8.4 Saturation Activities of Radionuclides in the Cooling Water at the Storage Ring Septum.

Beam loss [Watts]	^{15}O [pCi/cm^3]	^{11}C [pCi/cm^3]	^{13}N [pCi/cm^3]	3H [pCi/cm^3]
0.20	0.24	0.01	0.002	0.005

The computed concentration of radionuclides in cooling water of the storage ring septum is orders of magnitude smaller than the derived concentration for environmental discharge limits in the DOE Order 5400.5. Once the operation is shut down, concentration of all nuclides, except that of 3H, will rapidly decrease, due to radioactive decay of the short-lived isotopes.

2.9 SKYSHINE ESTIMATES AND SITE BOUNDARY DOSES

The term *skyshine* refers to the radiation that is initially directed skyward from a source but, due to scattering reactions with air nuclei, then is directed back to the earth. The neutron component of the radiation will be the major contributing factor to the skyshine dose. Any location in the accelerator where there is a probability for potential beam loss can be a source of skyshine. However, the potential beam loss and the resultant photo-neutron production at any given location in the accelerator system is small. The neutron component is well shielded at NSLS-II for personnel protection. Therefore, most beam losses do not cause significant skyshine.

2.9.1 Estimates of Skyshine Created at the Linac Beam Stop

Some skyshine radiation will be produced at the linac beam stop, where approximately 3 watts of electron beam power will be dissipated. For the skyshine calculations, it is assumed that the linac beam stop is completely unshielded locally, aside from the 1 meter of concrete shielding on the roof.

The skyshine dose rates due to neutron radiation are calculated using the method developed by Rindi and Thomas [2.22]. The unshielded neutron dose at the concrete roof is taken as the source term. The skyshine at a given distance is calculated by the following algorithm.

$$\text{skyshine dose rate} = (a \times H / r^2)\, e^{-r/\lambda} \qquad (5\text{-}11)$$

Where a = 7 (constant), H = unshielded dose rate on the concrete roof (source term), r = distance of the dose point from the source in meters, and λ = 3300 meters, effective air attenuation factor.

Table 2.9.1 gives the calculated skyshine estimates for the linac beam stop at 100 meters and 1 mile (1,600 meters) from the linac stop. For a conservative operational period of the linac, 5,000 hours a year, the annual skyshine dose estimates are well within the acceptable limits. With the additional local shielding of the linac stop, the skyshine doses will be comparable to background levels.

Table 2.9.1 Estimates of Skyshine Created at the NSLS-II Linac Beam Stop.

	Skyshine Dose at 100 m		Skyshine Dose at 1 mile	
Neutron source component	[mrem/h]	[mrem/year]	[mrem/h]	[mrem/year]
Giant resonance neutrons	8.2×10^{-4}	4.1	2.0×10^{-6}	0.010
High-energy neutrons	1.3×10^{-3}	6.3	3.0×10^{-6}	0.015
Total skyshine dose	2.1×10^{-3}	10.4	5.0×10^{-6}	0.025

2.9.2 Estimates of Skyshine Created at the Booster Beam Stop

Some skyshine radiation will be created at the booster beam stop. However, these dose rates will be lower than the skyshine dose rates produced at the linac beam stop because only 0.73 watts of electron power are dissipated routinely at the booster beam stop, versus 3 watts at the linac beam stop. For the booster beam stop skyshine calculations, it was assumed to be unshielded locally, except for the 70 cm concrete bulk shielding.

Table 2.9.2 gives the calculated skyshine estimates for the booster beam stop using the same algorithm as in the previous section. The skyshine estimates at 100 meters and 1 mile (1,600 meters) from the beam stop have been calculated. For a conservative operational period of 5,000 hours a year, the annual skyshine dose estimates are well within the acceptable limits. With the additional local shielding of the booster beam stop, the skyshine doses will be comparable to background levels.

All other skyshine dose rates that result from beam losses in the accelerator systems will be comparable to background dose rates.

Table 2.9.2 Estimates of Skyshine Created at the NSLS-II Booster Beam Stop.

	Skyshine Dose at 100 m		Skyshine Dose at 1 mile	
Neutron Source component	[mrem/h]	[mrem/year]	[mrem/h]	[mrem/year]
Giant Resonance Neutrons	1.0×10^{-4}	0.5	2.5×10^{-7}	0.001
High Energy Neutrons	1.6×10^{-4}	0.8	3.7×10^{-7}	0.002
Total Skyshine Dose	2.6×10^{-4}	1.3	6.2×10^{-7}	0.003

References

[2.1] Perkins, D.H., *Introduction to High Energy Physics*, Third Edition, Addison-Wesley Publishing (1984).

[2.2] J.S. Levinger, "Theories of photonuclear reactions," *Ann. Rev. of Nucl. Sci*., 4 (1954).

[2.3] Hubbel, J.H., Photon Cross Sections and Attenuation Coefficients from 10 keV to 100 GeV, NSRDS-NBS 29 (1969).

[2.4] Schaeffer, N.M., Reactor Shielding for Nuclear Engineers, NTIS, Springfield, VA (1973).

[2.5] R.G. Alsmiller, and J. Barish, "Shielding against neutrons produced when 400 MeV electrons are incident on thick copper target," *Particle Accelerators*, **5** (1973).

[2.6] Fasso, A., et al., Radiation Problems in the Design of LEP Collider, CERN 84-02 (1984).

[2.7] Sullivan, A.H., *A Guide to Radiation near High Energy Particle Accelerators*, Nucl. Tech. Publishing (1992).

[2.8] Swanson, W.P., et al. Aladdin Upgrade Design Study, University of Wisconsin Report, AUS14 (1985).

[2.9] Moe, H., Advanced Photon Source - Radiological Design Considerations, APS-LS-141 (1991).

[2.10] Basic Aspects of High Energy Particle Interactions and Radiation Dosimetry, ICRU -28 (1978).

[2.11 Job, P.K. and W.R. Casey, Supplementary shielding Estimates for NSLS-II, NSLS-II Technical Note 32.

[2.11] Schwinger, J., "Classical radiation of accelerated electrons," *Phys. Rev.* **75** (1949).

[2.12] Gabriel, T. A., PICA, Intra-nuclear Cascade Calculations, ORNL 4687 (1971).

[2.13] M. Pisharody et al., "Dose measurements of Bremsstrahlung produced neutrons," *Nucl. Instr.& Meth.* A230 (1999) p 542.

[2.14] H. Moe, et al., Radiological Considerations for TopUp at APS, APS-LS 276 (1998).

[2.15] EGS4 Code System, User's Manual, SLAC265 (1985).

[2.16] STAC8 Program Manual, Y.Asano, SPring-8 Publication (1998).

[2.17] Frank, J.C., LURE EP 88-01 (1988).

[2.18] Ferrari, et al., Estimation of gas bremsstrahlung, *Health Physics*, 68 (1995).

[2.19] Tromba, G., and A. Rindi, "Gas bremsstrahlung from electron storage ring," *Nucl. Instr. & Meth*., A292 (1990).

[2.20] Photon, Electron, Proton and Neutron Interaction Data in Body Tissues, ICRU Report 46 (1992).

[2.21] Swanson, W.P., *Radiological Safety Aspects of Electron Linear Accelerators*, IAEA 188 (1979).

[2.22] Rindi, A., and R.H. Thomas, "Skyshine - A paper tiger," *Particle Accelerators* **7** (1975).